

BRIGHAM YOUNG UNIVERSITY

GEOLOGY

S T U D I E S

GEOLOGICAL SOCIETY OF AMERICA



FIELD TRIP GUIDE BOOK



1997 ANNUAL MEETING • SALT LAKE CITY, UTAH



EDITED BY PAUL KARL LINK AND BART J. KOWALLIS

V O L U M E 4 2 • 1 9 9 7

PART **2** TWO

MESOZOIC TO RECENT GEOLOGY OF UTAH

Edited by

Paul Karl Link and Bart J. Kowallis

BRIGHAM YOUNG UNIVERSITY GEOLOGY STUDIES

Volume 42, Part II, 1997

CONTENTS

Triassic and Jurassic Macroinvertebrate Faunas of Utah: Field Relationships and Paleobiologic Significance	Carol M. Tang and David J. Bottjer	1
Part 2: Trace fossils, hardgrounds and ostreoliths in the Carmel Formation (Middle Jurassic) of southwestern Utah	Mark A. Wilson	6
Part 3: Low-diversity faunas of the Middle Jurassic Carmel Formation and their paleobiological implications	Carol M. Tang and David J. Bottjer	10
Part 4: Paleoecology of Lower Triassic marine carbonates in the southwestern USA	David J. Bottjer and Jennifer K. Schubert	15
Structure and Kinematics of a Complex Impact Crater, Upheaval Dome, Southeast Utah	Bryan J. Kriens, Eugene M. Shoemaker, and Ken E. Herkenhoff	19
Stratigraphy, and structure of the Sevier thrust belt, and proximal foreland-basin system in central Utah: A transect from the Sevier Desert to the Wasatch Plateau	T. F. Lawton, D. A. Sprinkel, P. G. DeCelles, G. Mitra, A. J. Sussman,, and M. P. Weiss	33
Lower to Middle Cretaceous Dinosaur Faunas of the Central Colorado Plateau: A Key to Understanding 35 Million Years of Tectonics, Sedimentology, Evolution, and Biogeography	James I. Kirkland, Brooks Britt, Donald L. Burge, Ken Carpenter, Richard Cifelli, Frank DeCourten, Jeffrey Eaton, Steve Hasiotis, and Tim Lawton	69
Sequence Architecture, and Stacking Patterns in the Cretaceous Foreland Basin, Utah: Tectonism versus Eustasy	P. Schwans, K. M. Campion	105
Fluvial-Deltaic Sedimentation, and Stratigraphy of the Ferron Sandstone	Paul B. Anderson, Thomas C. Chidsey, Jr., and Thomas A. Ryer	135
Depositional Sequence Stratigraphy and Architecture of the Cretaceous Ferron Sandstone: Implications for Coal and Coalbed Methane Resources—A Field Excursion	James R. Garrison Jr., T. C. V. van den Bergh, Charles E. Barker, and David E. Tabet	155

Extensional Faulting, Footwall Deformation and Plutonism in the Mineral Mountains, Southern Sevier Desert	Drew S. Coleman, John M. Bartley, J. Douglas Walker, David E. Price, and Anke M. Friedrich	203
Neotectonics, Fault segmentation, and seismic hazards along the Hurricane fault in Utah and Arizona: An overview of environmental factors	Meg E. Stewart, Wanda J. Taylor, Philip A. Pearthree, Barry J. Solomon, and Hugh A. Hurlow	235
Part 2: Geologic hazards in the region of the Hurricane fault	William R. Lund	255
Part 3: Field Guide to Neotectonics, fault segmentation, and seismic hazards along the Hurricane fault in southwestern Utah and northwestern Arizona	Meg E. Stewart, Wanda J. Taylor, Philip A. Pearthree, Barry J. Solomon, and Hugh A. Hurlow	261
Fault-Related Rocks of the Wasatch Normal Fault	James P. Evans, W. Adolph Yonkee, William T. Parry, and Ronald L. Bruhn	279
Geologic Hazards of the Wasatch Front, Utah	Michael D. Hylland, Bill D. Black, and Mike Lowe	299
Bedrock Geology of Snyderville Basin: Structural Geology Techniques Applied to Understanding the Hydrogeology of a Rapidly Developing Region, Summit County, Utah	Kelly E. Keighley, W. Adolph Yonkee, Frank X. Ashland, and James P. Evans	325
New explorations along the northern shores of Lake Bonneville	Charles G. (Jack) Oviatt, David M. Miller, Dorothy Sack, and Darrell Kaufman	345
Quaternary Geology and Geomorphology, Northern Henry Mountains Region	Benjamin L. Everitt, Andrew F. Godfrey, Robert S. Anderson, and Alan D. Howard	373
Part 2: Wind Erosion of Mancos Shale Badlands	Andrew E. Godfrey	384
Part 3: Long-Term Measurements of Soil Creep Rates on Mancos Shale Badland Slopes	Andrew E. Godfrey	386
Part 4: Vegetation and Geomorphology on the Fremont River	Ben Everitt	388
Part 5: Gravel Deposits North of Mount Ellen, Henry Mountains, Utah	Andrew E. Godfrey	390
Part 6: Monitoring flash floods in the Upper Blue Hills badlands, southern Utah	Gregory S. Dick, Robert S. Anderson, and Daniel E. Sampson	392
Part 7: Dating the Fremont River Terraces	James L. Repka, Robert S. Anderson, Greg S. Dick, and Robert C. Finkel	398

A Publication of the
Department of Geology
Brigham Young University
Provo, Utah 84602

Editor

Bart J. Kowallis

Brigham Young University Geology Studies is published by the Department of Geology. This publication consists of graduate student and faculty research within the department as well as papers submitted by outside contributors. Each article submitted is externally reviewed by at least two qualified persons.

Cover photos taken by Paul Karl Link.

Top: Upheaval Dome, southeastern Utah.

Middle: Lake Bonneville shorelines west of Brigham City, Utah.

Bottom: Bryce Canyon National Park, Utah.

ISSN 0068-1016
9-97 700 23870/24290

Preface

Guidebooks have been part of the exploration of the American West since Oregon Trail days. Geologic guidebooks with maps and photographs are an especially graphic tool for school teachers, University classes, and visiting geologists to become familiar with the territory, the geologic issues and the available references.

It was in this spirit that we set out to compile this two-volume set of field trip descriptions for the Annual Meeting of the Geological Society of America in Salt Lake City in October 1997. We were seeking to produce a quality product, with fully peer-reviewed papers, and user-friendly field trip logs. We found we were bucking a tide in our profession which de-emphasizes guidebooks and paper products. If this tide continues we wish to be on record as producing "The Last Best Geologic Guidebook."

We thank all the authors who met our strict deadlines and contributed this outstanding set of papers. We hope this work will stand for years to come as a lasting introduction to the complex geology of the Colorado Plateau, Basin and Range, Wasatch Front, and Snake River Plain in the vicinity of Salt Lake City. Index maps to the field trips contained in each volume are on the back covers.

Part 1 "Proterozoic to Recent Stratigraphy, Tectonics and Volcanology: Utah, Nevada, Southern Idaho and Central Mexico" contains a number of papers of exceptional interest for their geologic synthesis. Part 2 "Mesozoic to Recent Geology of Utah" concentrates on the Colorado Plateau and the Wasatch Front.

Paul Link read all the papers and coordinated the review process. Bart Kowallis copy edited the manuscripts and coordinated the publication via Brigham Young University Geology Studies. We would like to thank all the reviewers, who were generally prompt and helpful in meeting our tight schedule. These included: Lee Allison, Genevieve Atwood, Gary Axen, Jim Beget, Myron Best, David Bice, Phyllis Camilleri, Marjorie Chan, Nick Christie-Blick, Gary Christenson, Dan Chure, Mary Droser, Ernie Duebendorfer, Tony Ekdale, Todd Ehlers, Ben Everitt, Geoff Freethy, Hugh Hurlow, Jim Garrison, Denny Geist, Jeff Geslin, Ron Greeley, Gus Gustason, Bill Hackett, Kimm Harty, Grant Heiken, Lehi Hintze, Peter Huntoon, Peter Isaacson, Jeff Keaton, Keith Ketner, Guy King, Mel Kuntz, Tim Lawton, Spencer Lucas, Lon McCarley, Meghan Miller, Gautam Mitra, Kathy Nichols, Robert Q. Oaks, Susan Olig, Jack Oviatt, Bill Perry, Andy Pulham, Dick Robison, Rube Ross, Rich Schweickert, Peter Sheehan, Norm Silberling, Dick Smith, Barry Solomon, K.O. Stanley, Kevin Stewart, Wanda Taylor, Glenn Thackray and Adolph Yonkee. In addition, we wish to thank all the dedicated workers at Brigham Young University Print Services and in the Department of Geology who contributed many long hours of work to these volumes.

Paul Karl Link and Bart J. Kowallis, Editors

Triassic and Jurassic macroinvertebrate faunas of Utah: Field relationships and paleobiologic significances

CAROL M. TANG

Department of Geology, Arizona State University, Tempe, Arizona 85287-1404

DAVID J. BOTTJER

*Department of Earth Sciences, University of Southern California,
Los Angeles, California 90089-0740*

ABSTRACT

Analysis of marine faunas from understudied strata of the Triassic and Jurassic of the western United States have made contributions to our understanding of the Mesozoic, a critical time period in the history of life on earth. Paleobiological study of the Lower Triassic Sinbad and Virgin Members of the Moenkopi Formation have provided significant information on the pace and style of ecological recovery after the Permian-Triassic mass extinction. The Middle Jurassic Carmel Formation has yielded some unique hard-substrate assemblages as well as low-diversity soft-substrate paleocommunities which have been used to evaluate paleocommunity evolution in the Jurassic western interior seaway. This field trip will allow participants to visit several significant exposures of marine Triassic and Jurassic strata in southern Utah.

INTRODUCTION

The Mesozoic is considered to be a critical transitional period in the history of life on Earth as faunas recovered and proliferated after the Permian-Triassic mass extinction, the largest extinction in Earth history when 90% of marine genera were estimated to have gone extinct (Erwin, 1993). Many globally significant oceanographic and biological events occurred through the Mesozoic. Biologically, the Mesozoic was a time of rapidly increasing faunal diversity which occurred with the origination of many major groups of organisms (e.g., heart urchins, planktonic foraminifera, 1981). During this time interval, organisms of the "Modern Fauna" (i.e., bivalves, gastropods) replaced the "Archaic Fauna" of the Paleozoic (i.e., crinoids, bryozoans) (Sepkoski, 1981). These ecological changes have been referred to as the "Mesozoic Marine Revolution" which was brought on by escalation of the "arms race" between predators and prey (Vermeij, 1977).

While Cretaceous marine strata of the western United States have received a great deal of paleontological research, marine Triassic and Jurassic faunas of the U.S. have been largely neglected. Thus, recently renewed paleoecological and paleobiological research on these faunas provides much insight into the recovery after the Permian-Triassic extinction as well as evolutionary patterns during the Mesozoic Marine Revolution.

GEOLOGICAL SETTING

Mesozoic rocks in the southwestern United States generally overlie the Late Permian Kaibab Formation unconformably. During intervals of Triassic and Jurassic time, the western interior was the site of marine, marginal marine, and non-marine deposition; at times, southwestern Utah was the site of marine deposition along the edge of the epicontinental seaways (Caputo et al., 1994). Strata deposited in this region include shallow normal-marine, marginal-marine, sabhka, erg, and fluvial facies. Although the Triassic and Jurassic western interior seaways were mixed carbonate-siliciclastic depositional systems, the Lower Triassic and Middle Jurassic fossiliferous strata examined during this field trip will all be limestones which were deposited during times of major transgressions within the seaway; however Triassic and Jurassic siliciclastic fluvial and erg deposits will be seen in Zion and Capitol Reef National Parks as well as surrounding areas.

PALEOBIOLOGY AND PALEOECOLOGY

Both the Early Triassic and Middle Jurassic benthic marine faunas in southern Utah are characterized by low diversities and fairly simple paleoecological structure. The depauperate nature of the faunas within the Lower Triassic Moenkopi Formation is thought to reflect the slow, pro-

longed faunal recovery after the Permian-Triassic mass extinction (see Bottjer and Schubert, this volume). The Sinbad Member contains predominantly bivalves and gastropods while the younger Virgin Member exhibits a slightly more diverse and complex association with the addition of regular echinoids and the oldest known articulate crinoid.

In the Middle and Upper Jurassic of the western interior seaway, the regional (gamma) diversity of trace fossils and benthic marine organisms is low compared to other Jurassic faunas (Wilson and Palmer, 1994; Tang, 1996). In addition, both hard- and soft-substrate assemblages exhibit fairly low diversities within paleocommunities (alpha diversity) and between paleocommunities (beta diversity, i.e., low differentiation between communities) (Tang, 1996; Tang and Bottjer, 1996). The faunas are heavily dominated by bivalves although gastropods, crinoids, echinoids, bryozoans, corals, and serpulids are present as well.

The low-diversity nature of some level-bottom paleocommunities within the Middle Jurassic Carmel Formation may reflect their deposition within marginal marine environments. For example, the Carmel Formation hardground associations found near Gunlock Reservoir exhibit much lower diversities and complexities than do those from comparable hardgrounds in other parts of the world, possibly due to their deposition under marginal marine conditions (Wilson and Palmer, 1994; Wilson, this volume). However, the presence of crinoids and other echinoderms associated with other low-diversity assemblages—such as those found at Mount Carmel Junction—indicate that low-diversity paleocommunities were common in normal marine settings as well (see Tang and Bottjer, this volume). Thus, the low-diversity of Middle Jurassic marine faunas of southern Utah is probably the result of many factors including biogeography, oceanographic conditions, the level of environmental disturbance, the restricted nature of the seaway, and the abundance/patchiness of suitable environments for colonization.

ROAD LOG

This field trip will go south out of Salt Lake City to St. George before heading northeast to Green River through Zion, Bryce Canyon, and Capitol Reef National Parks (fig. 1). There will be a total of nine geological stops of which five will be paleontological in nature.

<u>Stops</u>	<u>Mileage</u>	<u>Mileage</u>	<u>Description and directions</u>
	<u>(cumul)</u>	<u>interval</u>	
Day 1			
	0		Salt Lake City. Junction of Interstates 15 and 215. Go south on 15.
	84.4	84.4	Third Nephi exit.

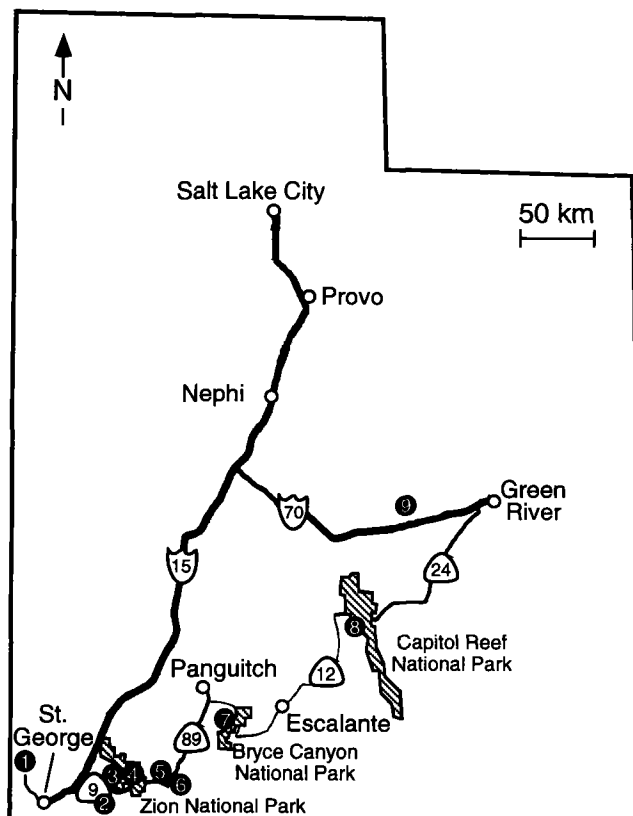


Figure 1. Route of this field trip through Utah. Stop 1: Gunlock reservoir—Carmel Formation. Stop 2: Hurricane Cliffs—Virgin Limestone Member of Moenkopi Formation. Stop 3: Zion National Park. Stop 4: Checkerboard Mesa—Navajo Formation. Stop 5: Mount Carmel Junction, west—Carmel Formation. Stop 6: Mount Carmel Junction, east—Carmel Formation. Stop 7: Bryce Canyon National Park—Clarion Formation. Stop 8: Capitol Reef National Park. Stop 9: San Rafael Swell—Sinbad Member of Moenkopi Formation.

119.1	34.7	(Exit for Scipio and US Highway 50.)
160.5	41.4	(Interstate 70.)
166	5.5	Rest Area.
205.1	39.1	Rest Area.
248.7	43.6	Rest Area.
253.3	4.6	(Kolob Canyon entrance of Zion National Park.)
284.8	31.5	St. George Boulevard exit. Exit and proceed northwest.

Day 2

0		Intersection between Bluff Street and St. George Boulevard. Go northeast on Bluff Street. Zero odometer.
1	1	Sunset Boulevard. Turn left.

	6	5	(Highway 300)		113.4	0.7	(Zion National Park east entrance booth.)
	12	6	Crossroad. <i>Turn right toward Gunlock Reservoir.</i>		113.6	0.2	(Zion National Park boundary.)
	19.4	7.4	BLM dirt road. <i>Turn left and cross Santa Clara River.</i>	Stop 5	126.1	12.5	Mount Carmel Junction between Highways 9 and 89. Carmel Formation encrinite is located on the northwest corner of the junction. <i>Pull into RV parking lot or gas station parking lot. Outcrop is located across small gully.</i>
Stop 1	20.1	0.7	Large gully on left side. <i>Pull into gully and turn around. Walk along gully to find Carmel hard-ground surface. Trace fossils and ostreoliths found in exposures of Carmel on right side of gully.</i>				<i>Pull out of parking lot onto Highways 9 and 89 east. Go straight through intersection on Highway 89 south east past Thunderbird resort and golf course.</i>
	20.1		<i>Pull out of gully and turn right on dirt road.</i>		126.1		
	20.7	0.6	Santa Clara River. <i>Cross river.</i>				
	20.8	0.1	Intersection with paved road. <i>Turn right.</i>				
	28.2	7.4	Intersection. <i>Turn left.</i>		126.5	0.4	Dirt road leading to highway maintenance yard and gravel pit. <i>Turn left and cross Virgin River.</i>
	39.2	11	Bluff Street. <i>Turn right.</i>				
	40.2	1	St. George Boulevard. <i>Turn left.</i>				
	42.2	2	Interstate Highway 15. <i>Take 15 north-east.</i>		126.6	0.1	Maintennance yard and gravel pit. <i>Turn left at the end onto paved road.</i>
	49.6	7.4	Highway 9. <i>Take 9 east.</i>				
	59.3	9.7	Junction with Highways 17 and 59. <i>Take 59 east.</i>	Stop 6	126.7	0.1	Extensive outcrop of Carmel Formation. <i>Turn vans around and park near end of paved road near river.</i>
	62.7	3.4	BLM dirt road. <i>Turn right.</i>				
	63.7	1	(Cattleguard.)				
	64.8	1.1	(Ostrich Farm.)		126.8	0.1	<i>Turn right off paved road onto dirt road.</i>
	65.8	1	Fork in road. <i>Bear right toward Arizona border.</i>		126.9	0.1	Highway 89. <i>Take 89 Northwest by turning right.</i>
Stop 2	68.7	2.9	Virgin Limestone Member is exposed in cliff along right side of road. Road is on a bedding plane full of bivalves and occasional crinoid stems. <i>Turn around and park along the road.</i>		127.5	0.6	Mount Carmel Junction. <i>Continue on Highway 89 north by taking a right turn.</i>
					150.1	22.6	(Intersection with Highway 14.)
					170.8	20.7	(Intersection with Highway 12.)
	71.6	2.9	Fork in road. <i>Bear to the left.</i>		177.8	7	Panguitch.
	74.7	3.1	End of dirt road onto highway 59. <i>Turn left on 59.</i>	Day 3	0	0	Panguitch.
					7	7	Highway 12. <i>Take 12 East by turning left.</i>
	78.1	3.4	Junction between Highways 9, 59, and 17. <i>Go north on Highways 17 and 9 by turning right.</i>		20.7	13.7	State Road 63 to Bryce Canyon National Park. <i>Turn right to go south on 63.</i>
	80.8	2.7	Crossroads. <i>Continue east on 17 and 9 toward Zion.</i>	Stop 7	26.2	5.5	Fairyland viewpoint. <i>Park.</i>
	100.8	20	(Entering Zion National Park.)		31.7	5.5	Highway 12. <i>Turn left.</i>
Stop 3	102.1	1.3	Zion National Park visitors' center. <i>Park.</i>		43.9	12.2	(Turnoff to Kodachrome Basin State Park.)
	103.1	1	Intersection with Zion Canyon Road. <i>Bear right to continue east on Zion-Mt. Carmel Highway.</i>		76.3	32.4	(Escalante Petrified Forest State Park.)
					78.6	2.3	(Escalante.)
	106.6	3.5	(Zion Tunnel.)		101.9	23.3	(Intersection with Hell's Backbone Road.)
	107.6	1	(Exit Zion Tunnel.)				
Stop 4	112.7	5.1	Checkerboard Mesa Viewpoint. <i>Park in parking lot.</i>		105.7	3.8	(Anasazi Indian Village State Park.)

	141.9	36.2	Intersection with Highway 24. <i>Turn right to go east on 24.</i>
Stop 8	151.9	10	Capitol Reef National Park Visitors' Center. <i>Park and view exhibits, book store, and the Castle.</i>
	160.9	9	Exiting Capitol Reef National Park.
	189.5	28.6	Hanksville. Intersection with Highway 95. <i>Turn left and continue north on 24.</i>
	233.5	44	Junction with Interstate Highway 70. <i>Take 70 west.</i>
	235.3	1.8	(Pass over San Rafael River.)
	236.7	1.4	(Rest Area. Note San Rafael Swell flatirons/hogbacks.)
	251.3	14.6	Exit #129, Farm Road. <i>Exit highway, bear right (north) onto Frontage Road, a graded BLM road.</i>
	253.7	2.4	(Cattleguard.)
	255.2	1.5	(Dirt road to Hyde Draw.)
	257.4	2.2	(Dirt road to Jackass Benches.)
Stop 9	264.1	6.7	Outcrop of Sinbad Member on east side of graded road. <i>Turn around, pull off road, and stop.</i>
	276.9	12.8	Interstate Highway 70. <i>Take 70 west.</i>
	291.9	15	Rest Area at Exit 114.
	351.9	60	Highway 50. <i>Exit freeway, go north on 50.</i>
	356.4	4.5	(Salina.)
	383	26.6	Junction with Interstate Highway 15. <i>Take 15 north.</i>
	502.1	119.1	Junction between Interstate Highways 15 and 215.

BRIEF DESCRIPTIONS OF FIELD TRIP STOPS

Detailed descriptions of the stratigraphy, sedimentology, fauna and paleobiological significances of Stops 1, 2, 4, 5, and 8 are found in the following chapters in this volume. Several good references for Mesozoic depositional systems within the western interior can be found within Caputo et al., (1994).

Stop 1 Carmel Formation—Gunlock Reservoir Locality

We will examine outcrops of the marine and marginal-marine strata of the Middle Jurassic Carmel Formation with emphasis on (1) a horizon of extensive hardground development with abundant *Liostrea strigilecula* encrusters and *Gastrochaenolites* borings; (2) facies with abundant

trace fossils, especially those of *Gyrochorte* and *Neonereites*; and (3) ostreoliths ("oyster balls") which are spherical accumulations of free-rolling *Liostrea* colonies. Wilson (this volume) provides a more detailed account of the facies and faunas found in this section of the Carmel Formation ("Member D").

Stop 2 Virgin Limestone Member Hurricane Cliffs Locality

We will examine one laterally-extensive outcrop and bedding plane of the Early Triassic Virgin Limestone Member of the Moenkopi Formation which contains numerous bivalves and occasional crinoid stems from *Holocrinus? smithi*, the oldest-known articulate crinoid. This deposit represents the one of the first examples of the re-development of relatively complex paleocommunities following the Permian-Triassic mass extinction. A more detailed discussion is contained within Bottjer and Schubert (this volume).

Stop 3 Zion National Park Visitors' Center

In addition to several natural history displays, the visitors' center affords a good view of some of the Mesozoic sandstone formations such as the Kayenta and Navajo Formations which make up Zion and which will be visible during our drive through the park. The fossil-bearing marine and marginal marine Carmel Formation can also be seen capping some of the taller structures in the park.

Stop 4 Checkerboard Mesa Viewpoint

Excellent view of Checkerboard Mesa which exhibits jointing, cross-bedding, and trough cross-bedding in Lower Jurassic erg sandstones of the Navajo Formation.

Stop 5 Carmel Formation—Mount Carmel Junction Locality, northwest

An outcrop of shallow-water, nearshore carbonates of the Co-op Creek Member of the Carmel Formation contains one of the youngest crinoidal limestones in the fossil record. The encrinite is composed of partially-articulated stems of *Isocrinus nicoleti*, the first non-endemic crinoid identified in the Jurassic western interior (Tang et al., in prep). Fairly abundant and well-preserved examples of the bryozoan *Eurystrotos duoflulina* can be found from units just above the encrinite. More information is included in Tang and Bottjer (this volume).

Stop 6 Carmel Formation—Mount Carmel Junction, northeast

A laterally-extensive exposure of the Carmel Formation underlain by the Temple Cap Member of the Navajo For-

mation can be found along the northside of Highway 89. The dominant fossils are bivalves which can be well-preserved and include *Liostrea*, *Lina*, and *Camptonectes*, but a number of other rare taxa such as gastropods, echinoids, serpulids, and crinoids can be found as well. The trace fossil *Gyrochorte* can be found on bedding planes. Details about this locality are provided in Tang and Bottjer (this volume).

Stop 7 Bryce Canyon National Park Fairyland Viewpoint

Fairyland Viewpoint is the northernmost viewpoint within the park and offers a view of the Pink Cliffs and the Aquarius Plateau in the distance. Bryce Canyon is not a canyon but a series of amphitheaters eroded from the Paunsaugunt Plateau. The colorful hoodoos and spires are a result of erosion of the Paleogene Claron Formation (formerly referred to as the Wasatch Formation).

Stop 8 Capitol Reef National Park Visitors' Center

The visitors' center contains a small geological display and offers a picturesque view of "The Castle" eroded from the Triassic Wingate Formation (fig. 2). Other Mesozoic formations exposed through the park in the Waterpocket Fold include the Moenkopi, Chinle, Kayenta, Navajo, Carmel, Entrada, and Curtis Formations.

Stop 9 Sinbad Member—San Rafael Swell Locality

We will examine Early Triassic gastropods and bivalves from the Sinbad Limestone Member of the Moenkopi Formation. The gastropods, originally described by Batten and Stokes (1987), are good examples of Early Triassic "Lazarus taxa." More information can be found in Bottjer and Schubert (this volume).

ACKNOWLEDGMENTS

We would like to thank Drs. J. Schubert, M.A. Wilson, GSA Field Trip Coordinator Edna Collis, and 1997 GSA



Figure 2. "The Castle," eroded from the Triassic Wingate Formation, can be viewed from the Capitol Reef National Park visitor's center (Stop 8).

Field Trip Co-chairs P. K. Link and B. J. Kowallis for their assistance.

REFERENCES CITED

- Batten, R.L., and Stokes, W.M.L., 1987, Early Triassic gastropods from the Sinbad Member of the Moenkopi Formation, San Rafael Swell, Utah: *American Museum Novitates*, v. 164, p. 1–33.
- Caputo, M.V., Peterson, J.A., and Franczyk, K.J. (eds.), 1994, *Mesozoic systems of the Rocky Mountain region, USA: Rocky Mountain Section of SEPM*, Denver, 536 p.
- Erwin, D.H., 1993, *The Great Paleozoic Crisis: Columbia University Press*, New York, 327 p.
- Sepkoski, J.J., Jr., 1981, A factor analytic description of the marine fossil record: *Paleobiology*, v. 7, p. 36–53.
- Tang, C.M., and Bottjer, D.J., 1996, Long-term faunal stasis without evolutionary coordination: Jurassic benthic marine paleocommunities, western interior, U.S.A.: *Geology*, v. 24, p. 815–818.
- Tang, C.M., Bottjer, D.J., and Simms, M.J., in prep, Stalked crinoids in a North American Middle Jurassic tidal deposit.
- Vermeij, G.J., 1977, The Mesozoic marine revolution: evidence from snails, predators and grazers: *Paleobiology*, v. 3, p. 245–258.
- Wilson, M.A., and Palmer, T.J., 1994, A carbonate hardground in the Carmel Formation (Middle Jurassic, SW Utah, USA) and its associated encrusters, borers and nestlers: *Ichnos*, v. 3, p. 79–87.

Trace fossils, hardgrounds and ostreoliths in the Carmel Formation (Middle Jurassic) of southwestern Utah

MARK A. WILSON

Department of Geology, The College of Wooster, Wooster, Ohio 44691 USA

INTRODUCTION

The Middle Jurassic Carmel Formation in southwestern Utah is a diverse unit with a fascinating array of sedimentary facies. It is approximately 250 meters thick in the area north of St. George, and is particularly well exposed just north of the Gunlock Reservoir. Here the most paleontologically and stratigraphically interesting portion is "Member D" (*sensu* Nielson, 1990), which is a shallowing-upward sequence of ooid-rich carbonate shoal deposits, lagoonal muds, and intertidal and supratidal carbonate and siliciclastic sands, silts and clays. The low diversity, mollusk-rich fossil assemblage in Member D supports the hypothesis that this area was a marginal marine environment at the southern end of the Carmel-Twin Creek Seaway in the Middle Jurassic (Imlay, 1980; Nielson, 1990). These restricted conditions led to the development of a unique and diverse set of trace fossils, along with extensive carbonate hardgrounds and unusual free-rolling oyster assemblages termed ostreoliths, or colloquially as "oyster balls." This contribution introduces these elements of the marine portion of the Carmel Formation and places them within a stratigraphic and regional context.

TRACE FOSSILS

Trace fossils are abundant and diverse in the carbonates and fine-grained siliciclastic units in Member D of the Carmel Formation in southwestern Utah. Only a few geologists have examined this ichnofauna. Blakey et al., (1983) and Nielson (1990) briefly noted some of the prominent soft-sediment burrow systems, and Wilson and Palmer (1992, 1994) described the bivalve and phoronid borings in the carbonate hardgrounds and their associated shelly fauna. Smail and Wilson (1993) presented the most extensive analysis of the ichnofauna in a study which continues.

The ichnogenera identified in Member D of the Carmel Formation include, in alphabetical order: *Asteriacites* (Fig. 3), *Chondrites*, *Gastrochaenolites*, *Gyrochorte*, *Lockeia*, *Monocraterion*, *Neonereites*, *Palaeophycus*, *Planolites*, *Skolithos*, *Taenidium*, *Talpina*, and *Teichichnus*. These traces are for the most part very well preserved, especially as

hypichnia on the soles of thin-bedded carbonate units. The most prominent ichnofossil is *Gyrochorte comosa* Heer (1865), which is a sinuous, bilobate intrastratal trackway preserved as both convex epichnia and concave hypichnia in oolitic and peloidal siltstones and grainstones formed in a shallow lagoon. Heinberg (1970, 1973) interpreted *Gyrochorte* as the product of an elongate worm, such as a polychaete, which tunneled obliquely through the sediment. Fürsich (1974) considered *Gyrochorte* to be a tunnel produced by a burrowing amphipod. *Gyrochorte* is common to abundant in Jurassic shallow-water carbonate and siliciclastic sequences around the world, including west-central India (Howard and Singh, 1985; Kulkarni & Ghare, 1991; Fürsich et al., 1991), eastern Greenland (Heinberg & Birkelund, 1984), and western Europe (Fürsich, 1974, 1975).

The marine facies in Member D of the Carmel Formation have distinct ichnological assemblages. The oolitic shoal deposits represent the highest environmental energy in the member. These coarse grainstones and packstones contain relatively few trace fossils, which is probably a function of preservation. The trace fossils present in this facies include *Lockeia*, *Palaeophycus* and *Taenidium*. The lagoonal sediments (mostly peloidal and ooid-rich siltstones and grainstones) have the highest diversity and abundance of trace fossils, including *Asteriacites*, *Chondrites*, *Palaeophycus*, *Monocraterion*, *Teichichnus*, and the especially abundant *Gyrochorte* and *Neonereites*. The carbonate hardgrounds are most common in this facies; their trace fossils are covered below. The subtidal and intertidal facies (represented primarily by calcareous mudstones) contain *Planolites*, *Chondrites* and *Skolithos*. No trace fossils have been found in the supratidal sediments (siltstones and mudstones with desiccation cracks, anhydrite nodules and halite crystal casts), almost certainly because these evaporative conditions did not support much life.

Smail and Wilson (1993) suggested that the more basinward facies of Member D, include the seaward sides of the lagoons, contained ichnogenera generally larger in size and deposit feeders usually working the strata parallel to bedding. More vertically-oriented and domichnial forms characterize the landward lagoonal and intertidal environments.

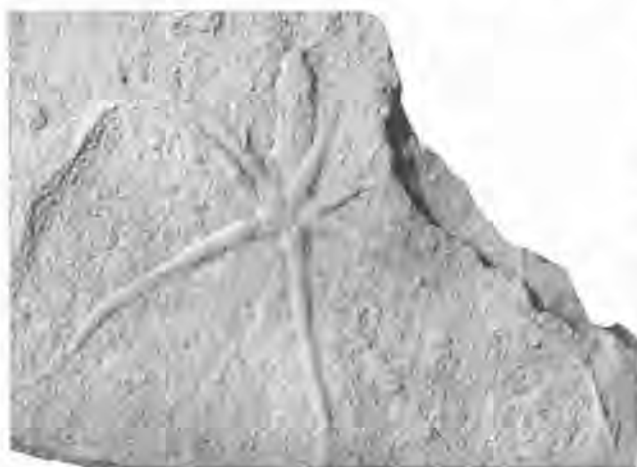


Figure 3. *Asteriacites lumbricalis* von Schlotheim, 1820. Trace fossil of a burrowing ophiuroid echinoderm from Member D, Carmel Formation, near Gunlock, Utah. Natural size.

HARDGROUNDS

Carbonate hardgrounds and their associated fossils are prominent in the lagoonal facies of the Carmel Formation's Member D. Hardgrounds are syndimentarily lithified carbonate sea-floors that became hardened *in situ* by the precipitation of a carbonate cement in the primary pore spaces (Wilson and Palmer, 1992, p. 3). They are found in the rock record from the Cambrian through the Recent, most abundantly in the Cambrian and Jurassic (Palmer, 1982; Wilson and Palmer, 1992). The intervals of common hardground formation coincide with the "Calcite Seas" postulated by Sandberg (1975, 1983). During Calcite Sea times, low magnesium calcite was the primary inorganic precipitate from seawater, and hence the most common hardground cement.

Several hardground horizons are present in Member D of the Carmel, but one described in detail by Wilson and Palmer (1994) is very extensive and seen over several kilometers. It is between 110 and 120 meters above the base of the Carmel in the Gunlock area. The hardground is at the base of a regressive sequence; it probably formed during a brief sea level highstand. This hardground varies in its composition from an interbedded silty micrite and sandy oolitic grainstone, with only occasional mollusk shell fragments and micritic intraclasts, to a packstone with thin intraclasts of silty micrite and abundant ooids and bioclastic debris. The hardground was formed in a lagoonal complex, from ooid-rich shoals seaward to a subtidal shelly facies landward.

The most extensive Carmel hardground in the Gunlock area is often heavily encrusted by the oyster *Liostrea strigilecula* (White, 1877), with minor numbers of the cementing bivalve *Plicatula* sp. The boring *Gastrochaenolites lapi-*

dicus Kelly and Bromley (1984) is very common in the hardground upper surfaces. The mytilid bivalve *Lithophaga* is sometimes preserved inside the *Gastrochaenolites* excavations, which it apparently produced. The mytilid bivalve *Modiolus subimbricatus* (Meek, 1873) is also occasionally found in the borings, most likely as a nestler. Wilson and Palmer (1994) also described a rare bioimmuration of the soft-bodied bryozoan *Arachnidium* which encrusted the hardground upper surface and was covered by oysters. Some Carmel hardgrounds were undermined by currents while on the seafloor, producing shallow cavities beneath the cemented horizon as uncemented sediments below were removed. These small caves had their own cryptic hardground fauna, including the common *Gastrochaenolites*, thecidean brachiopods, cyclostome bryozoans, and serpulid worm tubes.

The Carmel hardgrounds resemble most other carbonate hardgrounds in the Jurassic, especially those of western Europe. For example, a Bathonian hardground in England described by Palmer and Fürsich (1974) is very similar; from the carbonate petrography to the differences between the exposed fauna on the upper surfaces to the cryptic faunas below. The Carmel hardgrounds are unusual, though, in their lack of encrusting echinoderms and cementing foraminiferans. This may be due to the restricted marine conditions under which the Carmel hardgrounds formed.

OSTREOLITHS

Two horizons in Member D of the Carmel Formation in the Gunlock area contain some unusual fossils which are worth special notice. They are radial accumulations of oysters which formed around a nucleus and rolled freely on the seafloor (Fig. 4). Nielson (1990) was the first to describe them, calling them "oyster colonies" and "oyster boundstones." Wilson et al., (1997) prefer the term "ostreolith," and have interpreted their formation in detail. Ostreoliths such as these have not been described from anywhere else.

The Carmel ostreoliths are made primarily of left valves of the oyster *Liostrea strigilecula*, the same species which is the most common encruster on the Carmel hardgrounds. The most common ostreoliths average about 15 cm in diameter and have a calcite-filled cast of a formerly aragonitic bivalve (such as *Isognomon* or *Astarte*) as a nucleus, and then sequential layers of *Liostrea*. Other encrusters are rare, but they include *Plicatula*, and the cyclostome bryozoan *Eurystrotois duofluwina* (Cuffey and Ehleiter, 1984). The oyster framework is frequently penetrated by *Gastrochaenolites lapidicus*, sometimes with the nestler *Modiolus subimbricatus* in place. A less common but larger group of ostreoliths (up to 50 cm in diameter) has similar borers and encrusters (along with the inarticulate brachiopod *Disciniscia*), but has pieces of carbonate hardground as the nuclei.



Figure 4. *Ostreolith* made primarily of left valves of the oyster *Liostrea strigilecula* (White, 1877). From Member D, Carmel Formation, near Gunlock, Utah. Natural size.

In the interpretation of Wilson et al., (1997), the Carmel ostreoliths formed in two ways. The smaller ostreoliths formed on a soft, ooid-rich substrate as oysters encrusted loose mollusk valves. The larger ostreoliths developed as oysters accumulated on dislodged blocks of carbonate hardground. *Liostrea* preferred the upward-facing, exposed surfaces of the nuclei, and *Plicatula*, *Eurystrotos* and *Gastrochaenolites* accumulated on the cryptic undersurfaces. The ostreoliths were frequently overturned, allowing the framework oyster *Liostrea* to cover all surfaces, producing the nearly-spherical objects. The form of these ostreoliths is a direct function of the morphology of *Liostrea strigilecula*, especially its rapid growth, deep left valve, and calcitic composition.

The Carmel ostreoliths are found in two laterally extensive horizons in the top half of Member D. Like the hardgrounds, these horizons cross facies boundaries from ooid-rich sediments to otherwise unfossiliferous muds. It appears that the ostreoliths formed in oolitic shoal environments and were later washed into muddy lagoons by large storms.

ACKNOWLEDGMENTS

Steve Smail, Colin Ozanne and Andy Buddenhagen were College of Wooster students who worked on the Carmel Formation as part of their Independent Study requirements; they contributed much to the ideas and evidence presented in this review. Bob Varga also played an important role in the early fieldwork, and Gloria Wilson critically read the manuscript. Dru Nielson and the Geology Department at Brigham Young University provided important information and specimens. Our studies of the Carmel Formation have been supported by The Howard Hughes Medical Institute

and the Faculty Development and Moke and Ver Steeg Funds at The College of Wooster.

REFERENCES CITED

- Blakey, R.C., Peterson, E., Caputo, M.V., Geesaman, R.C., and Voorhes, B.J., 1983, Paleogeography of Middle Jurassic continental, shoreline, and shallow-marine sedimentation, southern Utah, in Reynolds, M.W., and Dolly, E.D., eds., Mesozoic paleogeography of west central United States: Society of Economic Paleontologists and Mineralogists, Rocky Mountain Section, p. 77-100.
- Cuffey, R.J., and Ehleiter, J.E., 1984, New bryozoan species from the Mid-Jurassic Twin Creek and Carmel Formations of Wyoming and Utah: *Journal of Paleontology*, v. 58, p. 668-682.
- Fürsich, F.T., 1974, Corallian (Upper Jurassic) trace fossils from England and Normandy: *Stuttgarter Beiträge zur Naturkunde, Serie B (Geologie und Paläontologie)*, v. 13, p. 1-51.
- Fürsich, F.T., 1975, Trace fossils as environmental indicators in the Corallian of England and Normandy: *Lethaia*, v. 8, p. 151-172.
- Fürsich, F.T., Oschmann, W., Jaitly, A.K., and Singh, I.B., 1991, Faunal response to transgressive-regressive cycles: example from the Jurassic of western India: *Paleogeography, Paleoclimatology, Paleoecology*, v. 85, p. 149-159.
- Heer, O., 1865, *Flora Tetiaria Helvetiae* I, 117 p. J. Würster and Company, Zürich.
- Heinberg, C., 1970, Some Jurassic trace fossils from Jameson Land (East Greenland), in Crimes, T.P., and Harper, J.C., eds., *Trace Fossils: Geological Journal Special Issue No. 3*, The Seel House Press, Liverpool, p. 227-234.
- Heinberg, C., 1973, The internal structure of the trace fossils *Gyrochorte* and *Curculithus*: *Lethaia*, v. 6, p. 227-238.
- Heinberg, C., and Birkelund, T., 1984, Trace-fossil assemblages and basin evolution of the Vardekloft Formation (Middle Jurassic, Central East Greenland): *Journal of Paleontology*, v. 58, p. 362-397.
- Howard, J.D., and Singh, I.B., 1985, Trace fossils in the Mesozoic sediments of the Kachchh, western India: *Paleogeography, Paleoclimatology, Paleoecology*, v. 52, p. 99-122.
- Imlay, R.W., 1980, Jurassic paleobiogeography of the conterminous United States and its continental setting: U.S. Geological Survey Professional Paper 1062, 134 p.
- Kelly, S.R.A. and Bromley, R.G., 1984, Ichnological nomenclature of clavate borings: *Paleontology*, v. 27, p. 793-807.
- Kulkarni, K.G., and Ghare, M.A., 1991, Locomotory traces (Repichnia) from the Jurassic sequence of Kutch, Gujarat: *Journal of the Geological Society of India*, v. 37, p. 374-387.
- Meek, F.B., 1873, Preliminary paleontological report, consisting of lists and descriptions of fossils, with remarks on the ages of the rocks in which they were found, etc., etc. United States Geological Survey Territories (Hayden), 6th Annual Report, 1872, p. 431-518.
- Nielson, D.R., 1990, Stratigraphy and Sedimentology of the Middle Jurassic Carmel Formation in the Gunlock area, Washington County, Utah: *Brigham Young University Geology Studies*, v. 36, p. 153-192.
- Palmer, T.J., 1982, Cambrian to Cretaceous changes in hardground communities: *Lethaia*, v. 15, p. 309-323.
- Palmer, T.J., and Fürsich, F.T., 1974, The ecology of a Middle Jurassic hardground and crevice fauna: *Paleontology*, v. 17, p. 507-524.
- Sandberg, E.A., 1975, New interpretations of Great Salt lake ooids and of ancient non-skeletal carbonate mineralogy: *Sedimentology*, v. 22, p. 497-538.
- Sandberg, E.A., 1983, An oscillating trend in Phanerozoic non-skeletal carbonate mineralogy: *Nature*, v. 305, p. 19-22.
- Smail, S.E., and Wilson, M.A., 1993, Detailed ichnology of a Middle Jurassic shallowing-upward marine sequence in the Carmel Formation,

- southwestern Utah, USA: *Geological Society of America Abstracts with Programs*, v. 25(6), p. 270
- White, C.A., 1877, Report upon the invertebrate fossils collected in portions of Nevada, Utah, Colorado, New Mexico, and Arizona. *United States Geographical Surveys West of 100th Meridian (Wheeler)*, v. 4, part 1, p. 1–219.
- Wilson, M.A., and Palmer, T.J., 1992, Hardgrounds and hardground faunas. *University of Wales, Aberystwyth, Institute of Earth Studies Publications*, v. 9, p. 1–131.
- Wilson, M.A., and Palmer, T.J., 1994, A carbonate hardground in the Carmel Formation (Middle Jurassic, SW Utah, USA) and its associated encrusters, borers and nestlers. *Ichnos*, v. 3, p. 79–87.
- Wilson, M.A., Ozanne, C.R., and Palmer, T.J., 1997, Origin and paleoecology of free-rolling oyster accumulations (ostreoliths) in the Middle Jurassic of southwestern Utah, USA: *Palaios* (in press).

Low-diversity faunas of the Middle Jurassic Carmel Formation and their paleobiological implications

CAROL M. TANG

Department of Geology, Arizona State University, Tempe, Arizona 8527-1404

DAVID J. BOTTJER

*Department of Earth Sciences, University of Southern California,
Los Angeles, California 90089-0740*

ABSTRACT

Laterally-extensive outcrops of Middle Jurassic normal marine carbonate strata are present at Mount Carmel Junction in southwestern Utah. These fossil-bearing limestones are part of the Co-op Creek Member of the Carmel Formation and include ooid grainstones, crinoidal grainstones, peloidal packstones, and bivalve-dominated packstones. These facies are interpreted to represent deposition in a nearshore, shallow-water lagoon-shoal setting.

The paleocommunities found in this southern end of the Middle Jurassic North American epicontinental seaway are low-diversity and exhibit low levels of complexity and tiering. Soft-bottom macrofossil assemblages are heavily dominated by oysters, limids, and pectens although serpulids, crinoids, echinoids, bryozoans, gastropods, possible stromatolites, and the trace fossil *Gyrochorte* can be found as well. One paleobiologically significant deposit is a crinoidal limestone composed of partially-articulated stems of *Isocrinus nicoleti*, the first non-endemic crinoid reported in the western interior. This deposit represents one of the youngest shallow-water encrinites in the fossil record and may provide evidence for unique conditions in this seaway.

INTRODUCTION

The Jurassic is a time of many significant global changes in the lithosphere, hydrosphere, atmosphere, and biosphere. For example, the breakup of Pangaea and the opening of the Atlantic Ocean first occurred during Jurassic times and greatly influenced oceanographic and climatic patterns. In the biosphere, the Jurassic saw the origination of many significant groups of modern taxa, the rapid increase in familial diversity (Sepkoski, 1981), and many ecological changes of the Mesozoic Marine Revolution (Vermeij, 1977). Thus, the study of the evolutionary paleoecological changes which occurred through this critical time interval may shed light on the response of the biota to global change processes. Surprisingly, despite centuries of intense study of Jurassic fossils in Europe (especially in England) (see Arkell, 1933), the Jurassic marine fauna of North America has been largely ignored. After the initial discovery and identification of Jurassic fossils by federal surveys in the 1800's, most modern paleontological work on this fauna was conducted by Ralph Imlay of the U.S. Geological Survey. Even many of

the theses and dissertations which included paleontological aspects were conducted in consultation with Imlay.

One possible reason for the lack of attention to these faunas may be that these Jurassic marine strata are not highly fossiliferous and are low-diversity in comparison to other Jurassic faunas around the world. In addition, the Jurassic seaway which covered the U.S. western interior was a unique biological province with its own succession of ammonites (Taylor et al., 1984), thus making biostratigraphy and global correlation difficult. Even regional stratigraphic correlations across short distances are difficult due to the general lack of good biostratigraphic fossils and the large variability of rock lithologies resulting from such things as local changes in terrestrial sediment input, sea levels, and topography (Brenner and Peterson, 1994; Peterson, 1994).

PALEOGEOGRAPHIC SETTING

During the Jurassic in the U.S. western interior, a series of marine and marginal marine rocks were deposited in a

shallow seaway during a 20 million year interval from Middle to Late Jurassic times (Imlay, 1980). The seaway was very shallow, probably never deeper than 100 meters, had many topographic highs, and had only one restricted opening to the open ocean in the north (Imlay, 1980) (Fig. 5). The seaway experienced several major sea level changes (reviewed by Brenner and Peterson, 1994; Peterson, 1994). Although much of the strata is fully marine, there are also many deposits indicative of terrestrial, brackish, high salinity, and marginal marine conditions (Brenner and Peterson, 1994; Peterson, 1994). Thus, the Jurassic western interior seaway is a unique system in which to examine ecological and evolutionary changes through the Mesozoic Marine Revolution.

STRATIGRAPHY OF CARMEL FORMATION

The Carmel Formation was first formally described by Gregory and Moore (1931). It was deposited in and adjacent to an epicontinental seaway which formed during a Middle Jurassic transgression across the western interior of the United States (Imlay, 1980). A stratigraphic column is shown in Figure 6. The Carmel Formation overlies Unconformity J-1 and Navajo Formation. In the type area near Mount Carmel Junction where this field trip will stop, the Temple Cap Member of the Navajo Formation underlies the Carmel Formation. The Carmel Formation is laterally equivalent with the Twin Creek Formation of northern Utah, Idaho, and Wyoming and the Arapien Shale of central Utah (Imlay, 1980).

The nomenclature of the members within the Carmel Formation has changed many times and differs among regions; for example, Wilson (this volume) adopts the informal member names used by Nielson (1990). The unit we will examine at Mount Carmel Junction is the limestone unit in the lower section of the Carmel Formation. In the literature, it has been referred to as the lower limestone member (Cashion, 1967), Kolob Limestone (Thompson and Stokes, 1970), Judd Hollow Member (Wright and Dickey, 1962), and most recently, the Co-op Creek Member (Doelling and Davis, 1989). In this discussion, I have adopted the terminology of Doelling and Davis (1989).

The Co-op Creek Member consists of a thin lower unit of non-marine pink and green clastics and a sequence of marine and marginal marine carbonates which are interpreted to have been deposited during a transgression (Peterson, 1994; Taylor, 1981). The Co-op Creek Member has been interpreted to have been deposited in subtidal to supratidal conditions in low- to moderate-energy regimes (Taylor, 1981). The lower Co-op Creek carbonates are composed of thin beds which have been interpreted as possible stromatolites (Taylor, 1981). Most of the fossils found from the Carmel Formation come from the middle carbonate

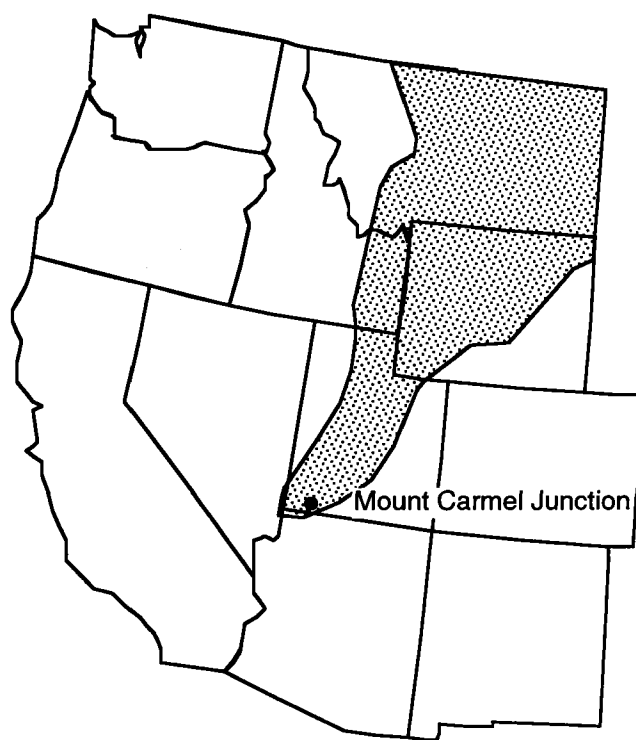


Figure 5. Stippled region represents the extent of the Middle Jurassic western interior epicontinental seaway during deposition of the Carmel Formation. Mount Carmel Junction is the site of Field Trip Stops 5 and 6 on Day 2 where we will examine an encrinite and low-diversity bivalve communities in the Co-op Creek Member of the Carmel Formation. (Modified from Nielson, 1990)

unit of the Co-op Creek Member which is composed of interbedded ooidal grainstones, peloidal packstones, and bivalve packstones representing deposition within a lagoonal-ooid shoal environment. The presence of echinoids and abundant crinoids indicate that these fossiliferous beds were most likely deposited under normal marine salinities.

PALEOBIOLOGY AND PALEOECOLOGY

Mount Carmel Junction (northwest corner):

On the west side of Mount Carmel Junction, there is an outcrop of the Co-op Creek middle limestone unit which includes a dense accumulation of partially-articulated crinoid stems measuring about 1 meter in thickness with a restricted lateral extent of about 100 meters. Crinoid columnals identified as *Pentacrinus asteriscus* Meek and Hayden were reported by John Wesley Powell from Jurassic deposits of southern Utah as early as 1876 and by Gregory and Moore in their original descriptions of the type locality of the Carmel Formation (1931). However, current work indicates that the crinoid at Mount Carmel Junction is *Isocrinus nicoleti*, a species described from

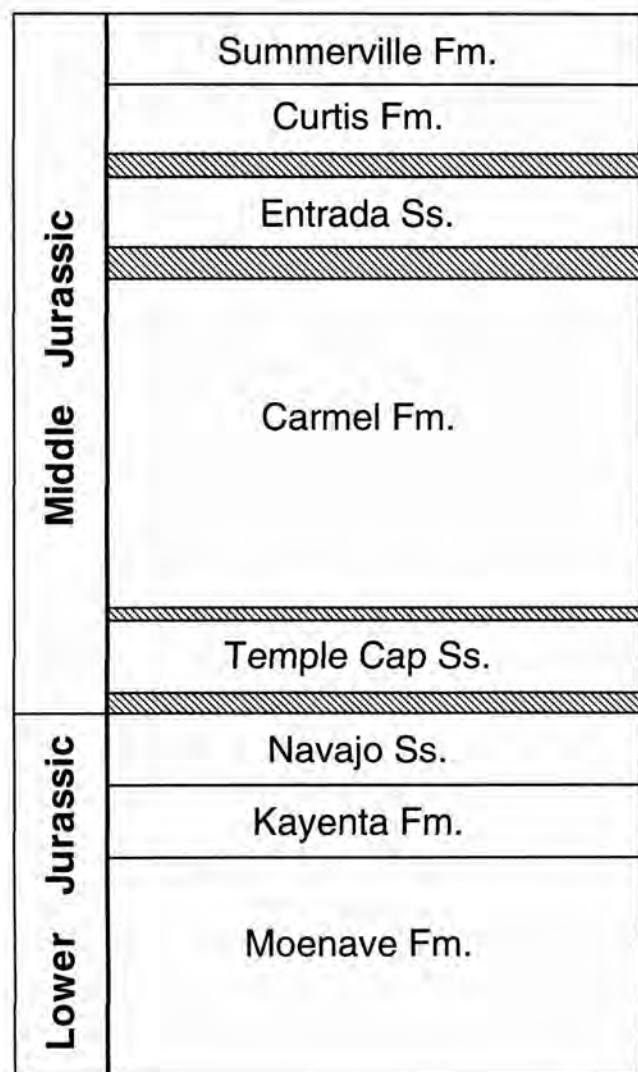


Figure 6. Schematic stratigraphic column depicting the Lower and Middle Jurassic formations of southern Utah.

European Jurassic strata (Tang et al., in prep). This crinoid occurrence in the Carmel Formation would represent the first non-endemic species described from the Jurassic of the U.S. western interior.

Based on sedimentological evidence at outcrop and thin-section scales, the crinoidal limestone has been interpreted as a tidally-influenced deposit, possibly representing accumulation in a tidal channel (Tang et al., 1994; Tang, 1996). The articulated nature of stems (Fig. 7) and some arms indicates that the crinoids experienced little transport after death and were buried fairly rapidly; it appears that these crinoids were living either in a tidal channel or on a tidal bar and used taphonomic feedback mechanisms to colonize a shifting sand-gravel sea floor which excluded most other

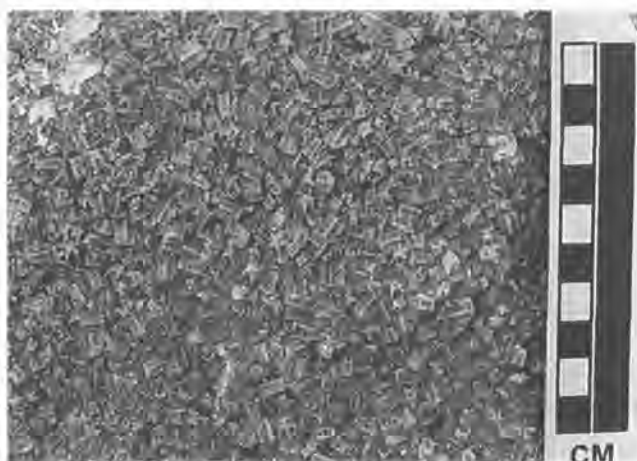


Figure 7. Well-preserved, partially-articulated crinoid columns are exposed on a bedding plane within the Carmel Formation crinoidal limestone (encrinite) at Mount Carmel Junction (Stop 5). Scale is in centimeters.

organisms. This crinoid accumulation is one of the youngest shallow-water crinoidal limestones (encrinites) in the fossil record. Thus, it represents one of the last "stands" of stalked crinoids in shallow-water environments and may suggest unusual oceanographic and ecological conditions leading to the development of a refugium. If crinoids were excluded from shallow-water environments due to increases in predatory pressures during the Mesozoic Marine Revolution as suggested by Meyer and Macurda (1983), the presence of this encrinite suggests that predatory pressures may not have been intense in this southernmost extent of the Jurassic epicontinental seaway (Tang et al., 1994).

Well-preserved specimens of the cyclostome *Eurystotos duofluvina*—one of a handful of bryozoans described from the Jurassic of the western interior—can be found in wackestones overlying the encrinite. This species was originally described as *Berenicea duofluvina* by Cuffey and Ehleiter (1984) based on rare specimens from the Twin Creek Formation near Kemmerer, Wyoming. They can also be found on Carmel Formation ostreoliths from Gunlock, UT (Wilson, this volume).

Mount Carmel Junction (northeast):

At this locality, we will focus on the two lowermost ledge-forming carbonate units of the Co-op Creek Member (Fig. 8). The lowest resistant unit is composed of thin beds which have been interpreted as stromatolites (Taylor, 1981). However, without detailed study, this interpretation remains unsubstantiated.

Above this first ledge is a talus slope which is capped by a second resistant carbonate unit which is interpreted to have been deposited within a lagoonal-oid shoal environ-



Figure 8. Outcrop of lower section of the Co-op Creek Member of the Carmel Formation at Mount Carmel Junction (Stop 6). At the base, interbedded pink and green siltstones are overlain by the first ledge-forming limestone unit. Fossil-bearing carbonate beds are seen at the top of the photograph.

ment. While most of the beds in this unit are not highly fossiliferous, echinoderm fragments, algae, ostracodes and molluscan fragments can be identified in thin section. Rare spherical colonies of polychaete worms are about 20 cm in diameter and appear to be composed of radially-arranged smooth polychaete worm tubes with diameters of about 1 cm. One bed contains many good examples of the trace fossil *Gyrochorte* which is also found at the Gunlock locality of the Carmel Formation (Wilson, this volume) and in other parts of the world.

In this limestone unit, one bed does contain abundant well-preserved fossils and is interpreted to have been deposited in much quieter waters than the other horizons as evidenced by the presence of large amounts of micrite, very large and complete bivalves, unoriented valves, and

other sedimentological, petrological, and taphonomic evidence (Tang, 1996). Based on this information, the fossils are interpreted to represent a para-autochthonous (disturbed neighborhood) assemblage. In this fossiliferous unit, common body fossils are *Liostrea strigilecula*, *Camptonectes stygius*, and *Lima occidentalis*. Less common fossils include *Modiolus*, *Vaugonia*, *Isognomon* and others listed by Imlay (1964).

Paleoecologically, the fauna at Mount Carmel Junction exhibits low within-community (alpha) diversity and low between-community (beta) diversity similar to faunas across the entire Jurassic western interior seaway (Tang, 1996). The trophic nuclei of the Carmel Formation paleocommunities—the taxa which make up 80% of the assemblage—were usually composed of only two species, *Liostrea strigilecula* along with either *Lima occidentalis* or less commonly, *Camptonectes stygius*. However, numerically, *Liostrea strigilecula* individuals dominated almost all soft-bottom assemblages. Non-bivalve taxa are rarely found associated with the bivalve paleocommunities: rare encrusters can be found on bivalve shells and very rare crinoid and echinoid fragments can be present. Thus, these assemblages are heavily dominated by epifaunal suspension-feeding bivalves. Not only are these faunas low-diversity in nature, they also exhibit very low levels of trophic and tiering complexity. The Carmel Formation taxa have been interpreted as being generalists since they do not appear to be greatly partitioning their resources nor exhibiting habitat specialization (Tang, 1996). In this sense, the Carmel Formation fauna is congruent with low-diversity generalist faunas found throughout the entire western interior seaway from Middle to Late Jurassic times (Tang and Bottjer, 1996).

DISCUSSION

Fossiliferous limestones of the Co-op Creek Member of the Carmel Formation provide a glimpse into the paleoecological conditions which existed in the southern end of the Middle Jurassic western-interior epicontinental seaway. The presence of one of the youngest examples of an encrinite in the fossil record suggests that there may have been unique conditions in this area which may have created a short-lived refugium for Mesozoic stalked crinoids.

Paleoecological analyses of soft-bottom, para-autochthonous fossil assemblages indicate that the Co-op Creek Member fauna was heavily dominated by epifaunal suspension-feeding bivalves which formed very low-diversity paleocommunities. The Carmel Formation fauna provides a dramatic example of the generalist nature of the fauna found throughout the entire Jurassic western interior seaway and suggests that this seaway may be a unique laboratory in which to examine the development and evolution of low-diversity generalist taxa and their paleocommunities.

ACKNOWLEDGMENTS

This work was conducted as part of a doctoral dissertation by CMT at the University of Southern California. Funding was provided by the National Geographic Society (to DJB) and grants to CMT from the USC Department of Geological Sciences, Sigma Xi, Geological Society of America, American Museum of Natural History, Paleontological Society, ARCS Foundation, and the American Association of University Women. Helpful insights were provided by Drs. M.L. Droser, A.G. Fischer, M.J. Simms, and M.A. Wilson.

REFERENCES CITED

- Arkell, W.J., 1933, *The Jurassic System in Great Britain*. Oxford, Clarendon Press, 681 p.
- Brenner, R.L., and Peterson, J.A., 1994, Jurassic sedimentary history of the northern portion of the western interior seaway, USA, in Caputo, M.V., Peterson, J.A., and Franczyk, K.J., eds., *Mesozoic Systems of the Rocky Mountain Region, USA*: Denver, Colorado, Rocky Mountain Section-SEPM, p. 217–232.
- Cashion, W.B., 1967, Carmel Formation of the Zion Park Region, southwestern Utah—a review. U.S. Geological Survey Professional Paper 1244-J, 9 p.
- Cuffey, R.J., and Ehleiter, J.E., 1984, New bryozoan species from the mid-Jurassic Twin Creek and Carmel Formations of Wyoming and Utah. *Journal of Paleontology*, v. 58, p. 668–682.
- Doelling, H.H., and Davis, F.D., 1989, The geology of Kane County, Utah, geology, mineral resources, geologic hazards. *Utah Geological and Mineralogical Survey Bulletin*, v. 124, p. 194.
- Gregory, H.E., and Moore, R.C., 1931, The Kaiparowits region: a geographic and geologic reconnaissance of parts of Utah and Arizona. U.S. Geological Survey Professional Paper 164, 161 p.
- Imlay, R.W., 1964, Marine Jurassic pelecypods from central and southern Utah, United States Geological Survey Professional Paper 483C, 42 p.
- Imlay, R.W., 1980, Jurassic paleobiogeography of the conterminous United States in its continental setting. United States Geological Survey Professional Paper 1062, 121 p.
- Meyer, D.L., and Macurda, D.B., Jr., 1983, Adaptive radiation of the comatulid crinoids. *Paleobiology*, v. 3, p. 74–82.
- Nelson, D.R., 1990, Stratigraphy and sedimentology of the Middle Jurassic Carmel Formation in the Gunlock Area, Washington County, Utah: Brigham Young University Geology Studies, v. 36, p. 153–191.
- Peterson, F., 1994, Sand dunes, sabkhas, streams, and shallow seas: Jurassic paleogeography in the southern part of the western interior basin, in Caputo, M.V., Peterson, J.A., and Franczyk, K.J., eds., *Mesozoic Systems of the Rocky Mountain Region, USA*. Denver, Colorado, Rocky Mountain Section-SEPM, p. 233–272.
- Powell, J.W., 1876, Report on the Geology of the Eastern Portion of the Uinta Mountains and a region of country adjacent thereto: Washington D.C., U.S. Government Printing Office, p.
- Sepkoski, J.J., Jr., 1981, A factor analytic description of the marine fossil record. *Paleobiology*, v. 7, p. 36–53.
- Tang, C.M., 1996, Evolutionary paleoecology of Jurassic marine invertebrate assemblages of the western interior, U.S.A. University of Southern California, unpublished dissertation, 235 p.
- Tang, Carol M., and Bottjer, David J., 1996, Long-term faunal stasis without evolutionary coordination. Jurassic benthic marine paleocommunities, western interior, U.S.A. *Geology*, v. 24, p. 815–818.
- Tang, Carol M., Bottjer, David J., and Simms, Michael, 1994, Paleocology of a Middle Jurassic shallow-water encrinite (Carmel Formation, southern Utah). Implications for the retreat of stalked crinoids to the deep-sea. *Geological Society of America Abstracts with Programs*, v. 26, p. A428.
- Tang, Carol M., Bottjer, David J., and Simms, Michael, in prep. Stalked crinoid accumulation in a North American Middle Jurassic tidal deposit.
- Taylor, D.G., Callomon, J.H., Hall, R., Smith, P.L., Tipper, H.W., and Westermann, G.E.G., 1984, Jurassic ammonite biogeography of western North America: the tectonic implications, in Westermann, G.E.G., ed., *Jurassic-Cretaceous biochronology and paleogeography of North America*: Geological Association of Canada Special Paper 27, p. 121–141.
- Taylor, D.W., 1981, Carbonate petrology and depositional environments of the limestone member of the Carmel Formation, near Carmel Junction, Kane County, Utah. Brigham Young University Geology Studies, v. 28, p. 117–133.
- Thompson, S.E., and Stokes, W.L., 1970, Stratigraphy of the San Rafael Group, southwest and south central Utah. *Utah Geological and Mineral Survey Bulletin*, v. 87, p. 53.
- Vermeij, G.J., 1977, The Mesozoic marine revolution: evidence from snails, predators and grazers. *Paleobiology*, v. 3, p. 245–258.
- Wright, J.C., and Dickey, D.D., 1962, Relations of the Navajo and Carmel Formations in southwest Utah and adjoining Arizona: Short Papers in Geology, Hydrology, and Topography, USGS Professional Paper 450-E, p. E63–E72.

Paleoecology of Lower Triassic marine carbonates in the southwestern USA

DAVID J. BOTTJER

JENNIFER K. SCHUBERT

*Department of Earth Sciences, University of Southern California,
Los Angeles, California 90089-0740*

ABSTRACT

Paleoecologic study of benthic invertebrate faunas from successive Early Triassic seaways reveals that biotic recovery from the end-Permian mass extinction event was slow, and that full recovery did not occur until after the Early Triassic. Simple, cosmopolitan, opportunistic generalists, and low-diversity, low-complexity paleocommunities were characteristic of the entire Early Triassic in the southwestern USA. An increase in guild and taxonomic diversity is observed with the addition of several new higher taxa in the late Early Triassic (Spathian), to the almost exclusively molluscan faunas of the earlier early Triassic (Nammalian). Comparison with data on faunas from the Permian and Triassic suggests that, worldwide, even the most diverse Early Triassic faunas (in the Spathian) were rather low in guild diversity and species richness. These characteristics of genera and paleocommunities in the Early Triassic may be typical of mass extinction aftermaths.

INTRODUCTION

The mass extinction at the Permian-Triassic boundary constitutes the most devastating biotic crisis of the Phanerozoic, and punctuates the transition from Paleozoic to Mesozoic life. Overall, marine families experienced a 49% reduction (Erwin, 1993, 1994), and an estimated 90% of the marine genera present in the late Permian disappeared (Erwin, 1993). A spectrum of causal mechanisms for the Permian/Triassic mass extinction has been proposed, from extensive flood basalt volcanism to abrupt extraterrestrial phenomena, with effects ranging from prolonged climate deterioration, to changes in ocean stratification, circulation and cycling (Erwin, 1993). However, the aftermath of this mass extinction is virtually unknown. Although comprehensive biostratigraphic work has been done, paleoecologic studies examining faunas as a whole are just beginning. This study (first reported in Schubert, 1993; Schubert and Bottjer, 1995) of benthic invertebrate recovery in the Early Triassic of the western USA has as a fundamental goal the identification of characteristics of this post-extinction fauna and its ecology that might be distinctive of mass extinction aftermaths.

STRATIGRAPHIC AND PALEOENVIRONMENTAL CONTEXT

The latest Permian and earliest Triassic are times of emergence and non-deposition in much of the western USA,

with a significant time gap of 1–6 m.y. commonly accepted for the Paleozoic-Mesozoic boundary (Paull and Paull, 1986). In the Early Triassic, both subsidence of the area and global sea level increases caused transgressive pulses from the northwest, bringing marine conditions recorded by fossiliferous limestones (Paull and Paull, 1986). The first of these (Griesbachian) transgressive events is recorded in the north by the Dinwoody Formation (Carr and Paull, 1983) (Fig. 9). The second (Nammalian) transgression is marked by a widespread marine carbonate unit containing ammonoids (*Meekoceras*), which defines the base of the Thaynes Formation (Kummel, 1954) (Fig. 9). This Nammalian transgression was geographically more extensive, and is recorded in south-central Utah by the Sinbad Limestone Member of the Moenkopi Formation (Fig. 9). The third (Spathian) transgression in the Early Triassic is recorded by thick sequences in the field area of the Virgin Limestone member of the Moenkopi (Paull et al., 1989) (Fig. 9).

The Moenkopi Formation in southeastern Nevada and southwestern Utah contains three limestone members (Fig. 9). The lower limestone member, the Timpoweap, is only very sparsely fossiliferous and is primarily a marginal marine deposit (Larson, 1966). The middle Virgin Limestone Member contains limestone units (Fig. 10) deposited under normal marine conditions during the Spathian transgression, intercalated with fine-grained siliciclastics and less common sandstones, representing marginal and subtidal environments (Larson, 1966; Rief and Slatt, 1979). The upper

Age	SE Nevada SW Utah	SE-central Utah	W & N-central Utah, Idaho, Montana & Wyoming
241 SPATHIAN	MOENKOPI FM		THAYNES FM
	Upper Red		
	Schnabkaib	Moody Canyon	
	Middle Red		
	Virgin Limestone	Torrey	upper limestone
	Lower Red		
242 NAMMALIAN	Timpoweap	Sinbad Limestone	
		Black Dragon	
243.5 GRIESBACHIAN			DINWOODY FM
245			

Figure 9. Stratigraphy of the Lower Triassic in the Western USA, compiled and simplified from Larson (1966) and Hintze (1973); modified from Schubert and Bottjer (1995).

limestone, the Schnabkaib Limestone, is unfossiliferous and mainly evaporitic.

The Moenkopi changes in both lithology and nomenclature from southwestern Utah to the southeast-central part of the state, where the Lower Triassic section is dominated by terrigenous red and yellow siliciclastics (Blakey, 1974; Dean, 1981). Four members are recognized (Fig. 9), the Black Dragon, the Sinbad Limestone, the Torrey Member, and the Moody Canyon Member, which represent a range of environments, including bar, beach, delta, lagoon and shallow subtidal (Blakey, 1974; Dean, 1981). The Sinbad Limestone, deposited during the Nammalian transgression, is considered to be a major southern tongue of the lower Thaynes Formation (Kummel, 1954). The Sinbad Limestone is a thin yellow silty fossiliferous marine limestone and dolomite (Blakey, 1974; Dean, 1981). Sinbad depositional environments produced evaporitic tidal flat deposits, intertidal oolites, and subtidal and lagoonal pelletal mudstones as well as bioturbated skeletal wackestones from lagoon, tidal channel, and sub-wave-base shelf settings (Dean, 1981).

METHODS OF STUDY

Paleoecologic and paleoenvironmental data were collected at selected sites of the Lower Triassic in the south-



Figure 10. The Virgin Limestone Member is exposed at the top of a cliff near Hurricane, Utah (Stop 2). Person is standing on the bedding plane pictured in Figure 11. (Photo by C. Tang)

western United States (Schubert and Bottjer, 1996). In particular, study was made of localities of the Virgin Limestone in the Hurricane Cliffs area (Figs. 10,11), as well as localities of the Sinbad in the San Rafael Swell area, the two stops to be visited during this field trip. Collection of bulk sample faunal data involved removal of about 8000 cm³ of rock from intervals 15 cm or less in thickness. Fossils freed from the matrix and exposed on broken surfaces were identified and counted. Paleocommunities were defined from tallies of generic abundance of Virgin and Sinbad samples based upon cluster analysis (Schubert and Bottjer, 1996). Paleoecologic studies also included an analysis of the adaptive strategies of organisms in these paleocommunities. Bambach (1983) introduced this approach, and each of the major adaptive strategies that he defined have been termed "Bambachian megaguilds" (Droser et al., 1997).

PALEOCOMMUNITY ANALYSIS

Characteristics of the paleocommunities in these Lower Triassic strata indicate that ecologic recovery from this mass extinction was not achieved in the Early Triassic (e.g., Schubert and Bottjer, 1995; Bottjer et al., 1996). Diversity at high taxonomic levels is very low; only bivalves, crinoids, plus in some cases, echinoids, gastropods, and brachiopods, are represented. Diversity at low taxonomic levels is low as well; most of these groups are represented by only one species (e.g., crinoids and echinoids) or a few species (e.g., brachiopods). Bambachian megaguild diversity is relatively low and few taxa are represented in each megaguild. Examination of the nature and timing of recovery throughout the Early Triassic of the western USA reveals that it was slow and uneven.



Figure 11. A bedding plane of the Virgin Limestone with numerous cross-sections of bivalves and occasional columnals of the crinoid *H. smithi* (Stop 2, near Hurricane, Utah). (Photo by C. Tang)

Nammalian Sinbad Limestone paleocommunities exhibit a greater diversity at higher and lower taxonomic levels than the older Dinwoody Formation to the north (Schubert and Bottjer, 1995); a larger variety of bivalves and several species of microgastropod are typically present. The increase in taxic diversity also signals an increase in megaguild diversity, particularly the addition of grazing/detritovore and predatory life habits represented by the gastropods. However, relatively few tiers (e.g., Bottjer and Ausich, 1986), or levels of vertical space, are occupied in these Sinbad paleocommunities. Suspension-feeding bivalves, as well as the microgastropods, lived at the sediment surface, semi-infaunally, and as shallow burrowers (*Arenicolites*, observed in the Sinbad, also records shallow burrowing). None of the organisms represented by body fossils found in these paleocommunities lived elevated above the sediment surface, or burrowed deeply within it.

Sinbad paleocommunities can be very high in dominance, with one or two species of microgastropod or bivalve extraordinarily numerous, and a relatively small number of individuals of other species present. These microgastropods are typical of and limited to the Nammalian Sinbad Limestone (Batten and Stokes, 1987), and are neither abundant nor diverse in faunas of the Spathian Virgin Limestone. This waxing and waning of microgastropods may represent volatility in the process of ecologic recovery. Possibly, ecologic rebound cannot be described as an increasing linear function, but is in part a fitful unpredictable process. The boom/bust behavior exhibited by the microgastropods, which were extremely abundant in the Sinbad, but almost unknown from seemingly similar environments of the Virgin, could also be a function of the kinds of genera that are characteristic of mass extinction aftermaths: opportunists known for blooms and crashes in their population dynamics.

Although bivalves remain dominant in Spathian Virgin paleocommunities (Fig. 11), different bivalve genera occur in different relative abundances than in Nammalian Sinbad paleocommunities. A more diverse assemblage of higher taxa is known from the Spathian. For example, Virgin paleocommunities are characterized by the first appearance (in the western USA) of representatives of important Mesozoic clades, *Holocrinus* (?) *smithi* (crinoids) and *Miocidaris utahensis* (echinoids). *H. smithi* is the earliest known member of its clade and served as the stem group for all post-Paleozoic crinoids. Representing the brachiopods is one terebratulid genus. Because the terebratulids and rhychonellids are the only articulate orders to persist into the present, these two genera are important as a link between Permian and Triassic brachiopods, and as potential ancestral stock for post-Paleozoic brachiopods.

The presence of these taxa in the Spathian of the western USA is also of ecologic significance, since it represents the re-appearance of life habits previously absent from the dominantly molluscan paleocommunities of earlier Triassic settings. Shallow infaunal, semi-infaunal, and epifaunal suspension-feeding bivalves were prominent members of Griesbachian, Nammalian, and Spathian invertebrate paleocommunities in the western USA (Schubert and Bottjer, 1995). The stemmed crinoid represents the addition in the Spathian of not only a new guild but also a new tier in the vertical space partitioning of the community, since its feeding activity occurs above the substrate at the raised calyx. As a mobile epifaunal grazer and detritovore, the Spathian echinoid also belongs to a different guild. Though more complex than paleocommunities in the Sinbad, these Spathian paleocommunities are still simple in structure and vary little in terms of dominant genera over the vast geographic area of the Early Triassic Virgin seaway; the same handful of bivalves and a single crinoid species recur in paleocommunities throughout the western USA (Schubert and Bottjer, 1995).

CONCLUSIONS

Paleoecologic study of invertebrate faunas from successive Early Triassic seaways in the southwestern USA reveals that biotic recovery from the end-Permian mass extinction event was slow and incomplete. Simple, cosmopolitan, opportunistic generalists, and low-diversity, low-complexity paleocommunities were characteristic of the entire Early Triassic throughout this region (Schubert and Bottjer, 1995). An increase in guild and taxonomic diversity was observed with the addition of other higher taxa in the late Early Triassic (Spathian) to the almost exclusively molluscan faunas of the earlier Early Triassic (Nammalian). Comparison with data on faunas from the Permian and Triassic suggest that even the most diverse Early Triassic faunas (in the Spathian)

were rather low in megaguild diversity and species richness (Schubert and Bottjer, 1995).

A remarkable aspect of the ecology and biota of the Early Triassic aftermath is the apparent small part played by radiation during this 4–5 m.y. time period. Groups such as crinoids, echinoids, and articulate brachiopods that eventually appeared in Spathian paleocommunities probably did not evolve there. Rather, this most probably simply reflects their migration into the area, and does not represent much evolutionary innovation. These Spathian taxa, like the Lazarus taxa for which the Triassic is so noted (e.g., Hallam, 1991), are groups that vanish from the fossil record of the western USA during the mass extinction interval and reappear later in the Triassic without being much (if at all) different from those in the Paleozoic. They must have persisted, or originated from very similar forms, in unknown refuges. What we see here is a slow trickling back of survivors, scattered over megaguilds and taxa, that would serve as the basis for radiations that occurred, not in the Early Triassic, but much later in the Triassic and Jurassic.

ACKNOWLEDGEMENTS

Supported by grants to DJB from the University of Southern California Faculty Research and Innovation Fund, the National Geographic Society and the National Science Foundation (EAR-90-04547), as well as grants to JKS from the Paleontological Society, the Geological Society of America, the American Association of Petroleum Geologists, Sigma Xi, the Theodore Roosevelt Memorial Fund of the American Museum of Natural History, and the University of Southern California Department of Earth Sciences. We thank D.H. Erwin, P.B. Wignall, A. Hallam, M.L. Droser, and A.G. Fischer for advice and encouragement during the course of this study.

REFERENCES CITED

- Bambach, R.K., 1983, Ecospace utilization and guilds in marine communities through the Phanerozoic, in Tevesz, M.J.S., and McCall, P.L., eds., *Biotic interactions in recent and fossil benthic communities*. New York, New York, Plenum, p. 719–746.
- Batten, R.L., and Stokes, W.M.L., 1987, Early Triassic gastropods from the Sinbad Member of the Moenkopi Formation, San Rafael Swell, Utah: *American Museum Novitates*, v. 1864, p. 1–33.
- Blakey, R.V., 1974, Stratigraphic and depositional analysis of the Moenkopi Formation, southeastern Utah: *Utah Geological and Mineralogical Survey Bulletin*, v.104, p. 1–81.
- Bottjer, D.J., and Ausich, W.I., 1986, Phanerozoic development of tiering in soft substrata suspension-feeding communities: *Paleobiology*, v. 12, p. 400–412.
- Bottjer, D.J., Schubert, J.K., and Droser, M.L., 1996, Comparative evolutionary palaeoecology. Assessing the changing ecology of the past, in Hart, M.B., ed., *Biotic recovery from mass extinction events: Geological Society Special Publication 102*, p. 1–13.
- Carr, T.R., and Paull, R.K., 1983, Early Triassic stratigraphy and paleogeography of the Cordillera miogeocline, in Reynolds, M.W., and Dolly, E.D., eds., *Mesozoic paleogeography of the west-central United States*, Rocky Mountain Paleogeography Symposium 2: Denver, Colorado, Society of Economic Paleontologists and Mineralogists, Rocky Mountain Section, p. 39–55.
- Dean, J.S., 1981, Carbonate petrology and depositional environments of the Sinbad Limestone Member of the Moenkopi Formation in the Teasdale Dome area, Wayne and Garfield Counties, Utah. *Brigham Young University Geology Series*, v. 28, p. 19–51.
- Droser, M.L., Bottjer, D.J., and Sheehan, P.M., 1997, Evaluating the ecological architecture of major events in the Phanerozoic history of marine invertebrate life. *Geology*, v. 25, p. 167–170.
- Erwin, D.H., 1993, *The great Paleozoic crisis. life and death in the Permian*. New York, New York, Columbia University Press, 327 p.
- Erwin, D.H., 1994, The Permian-Triassic extinction. *Nature*, v. 367, p. 231–236.
- Hallam, A., 1991, Why was there a delayed radiation after the end-Paleozoic extinctions? *Historical Biology*, v. 5, p. 257–262.
- Hintze, L.F., 1973, Geological history of Utah. *Brigham Young University Geology Studies* 20, 181p.
- Kummel, B., 1954, Triassic stratigraphy of southeastern Idaho and adjacent areas. *United States Geological Survey Professional Paper*, v. 254-H, p. 164–194.
- Larson, A.R., 1966, *Stratigraphy and paleontology of the Moenkopi Formation in southern Nevada* [Ph.D. thesis]. Los Angeles, University of California at Los Angeles, 257 p.
- Paull, R.K., Paull, R.A., and Kraemer, B.R., 1989, Depositional history of Lower Triassic rocks in southwestern Montana and adjacent parts of Wyoming and Idaho, in French, D.E., and Grabb, R.F., ed., *Montana Centennial Edition: Field Conference Guidebook*. Montana Geological Society, p. 69–90.
- Paull, R.K., and Paull, R.A., 1986, Epilogue for the Permian in the western Cordillera—a retrospective view from the Triassic. *Contributions to Geology*, University of Wyoming, v. 24, p. 243–252.
- Rief, D.M.K., and Slatt, R.M., 1979, Red bed members of the Lower Triassic Moenkopi Formation, southern Nevada, sedimentology and paleogeography of muddy tidal deposits. *Journal of Sedimentary Petrology*, v. 49, p. 869–889.
- Schubert, J.K., 1993, Rebound from the Permian-Triassic mass extinction event: paleoecology of Lower Triassic carbonates in the western U.S. [Ph.D. thesis]: Los Angeles, University of Southern California, 396 p.
- Schubert, J.K., and Bottjer, D.J., 1995, Aftermath of the Permian-Triassic mass extinction event: paleoecology of Lower Triassic carbonates in the western USA. *Palaeogeography, Palaeoclimatology, Palaeoecology*, v. 116, p. 1–39.

Structure and Kinematics of a Complex Impact Crater, Upheaval Dome, Southeast Utah

BRYAN J. KRIENS

*Department of Earth Sciences, California State University, Dominguez Hills,
Carson, California 90747*

EUGENE M. SHOEMAKER

U.S. Geological Survey and Lowell Observatory, Flagstaff, Arizona 86001

KEN E. HERKENHOFF

Jet Propulsion Laboratory, MS 183-501, Pasadena, California 91109

ABSTRACT

Two vastly different phenomena, impact and salt diapirism, have been proposed for the origin of Upheaval Dome, southeast Utah. Detailed geologic mapping, seismic refraction data, and the presence of shock metamorphosed rocks indicate that the dome originated by collapse of a transient cavity formed by impact. Evidence is: (1) the occurrence of a lag deposit of rare impactites, (2) fan-tailed fracture surfaces (shatter surfaces) and rare shatter cones are present near the center of the structure, (3) the top of the underlying salt horizon is at least 500 m below the surface at the center of the dome and there are no exposures of salt or associated rocks of the Paradox Formation in the dome to support the possibility that a salt diapir has ascended through it, (4) sedimentary strata in the center of the structure are pervasively imbricated by top-toward-the-center thrust faulting and are complexly folded as well, (5) top-toward-the-center normal faults are found at the perimeter of the structure, and (6) clastic dikes are widespread.

We show that the dome formed mainly by centerward motion of rock units along listric faults. Outcrop-scale folding and upturning of beds, especially common in the center, are largely a consequence of this motion. We have also detected some centerward motion of fault-bounded wedges resulting from displacements on subhorizontal faults that conjoin and die out within horizontal bedding near the perimeter of the structure. The observed deformation corresponds to the central uplift and the encircling ring structural depression seen in complex impact craters.

INTRODUCTION

Upheaval Dome, located in Canyonlands National Park, southeast Utah, is a structure that has stimulated controversy regarding its origin (Bucher, 1936; Boon and Albritton, 1938; McKnight, 1940; Shoemaker and Herkenhoff, 1983, 1984; Schultz-Ela et al., 1994). Although considered by many to be the result of salt diapirism, our study shows Upheaval Dome to be an eroded impact crater. It is the best-exposed complex crater in the world and thus one of the best places to study impact mechanics. Much of the three dimensional structure of Upheaval Dome is revealed in the deep canyons that have been cut into it. This field trip guide presents data

and interpretations resulting from our study, and a brief discussion of the development of complex craters.

Field studies of terrestrial impact structures and the morphology of craters on the other terrestrial planets and on the Moon has led to the recognition of a variety of structural classes of craters. Small impact craters typically have a simple bowl-shape, and the rocks of their walls preserve much of the structure developed during passage of the shockwave and opening of an initial or transient cavity (Shoemaker, 1960). Above a certain threshold size, the transient cavity collapses, and a complex crater is formed. Rocks of the walls and rim of the transient cavity subside

and are transported inward, generally along listric faults. The convergent flow forces the rocks underlying the transient cavity floor to rise in a structurally complex central uplift. The amplitude of this structural uplift, SU , is given approximately by $SU = 0.06 D^{1.1}$, where D is the final crater diameter in km (Grieve et al., 1981; Grieve, 1991). For a crater with the diameter of the Upheaval Dome structure, the expected uplift is approximately 350 m. On Earth, the transition from simple to complex craters occurs at crater diameters of about 2 km in sedimentary rocks and about 4 km in strong crystalline rocks (Grieve, 1991). Upheaval Dome is an example of a complex crater somewhat above the transition size. The dome and surrounding ring structural depression provide a particularly clear example of the deformation that accompanies transient cavity collapse.

GEOLOGIC BACKGROUND

Upheaval Dome is located in the canyon lands region of the Colorado Plateau in southeast Utah (fig. 1). Most of the region is underlain by nearly flat-lying to gently deformed sedimentary strata of Pennsylvanian to Cretaceous age. Salt anticlines occur within the Paradox depositional basin of Pennsylvanian and Permian age (e.g. Doelling et al., 1988). Normal faults and small salt diapirs (300–400 m across) are found in The Grabens area at the south end of Canyonlands National Park (Huntoon et al., 1982). Upheaval Dome, a 2.5 km-diameter complex structural uplift surrounded by a 5-km diameter annular structural depression lies near the north end of the park (fig. 2). The dome is located near the western margin of the Paradox Basin. The presence of known salt structures in the region influenced early interpretations that Upheaval Dome resulted from salt diapirism, although cryptovolcanic and impact origins were also considered (Bucher, 1936; Boon and Albritton, 1938; McKnight, 1940).

Rock units exposed in the dome range from the uppermost formation of the Cutler Group (the White Rim Sandstone) of Permian age to the middle of the Navajo Sandstone of Jurassic age (fig. 3). Strata shown in figure 3 older than the White Rim Sandstone have been penetrated by drilling. On the basis of subsurface strata encountered in a drill hole in the eastern part of the ring structural depression, the top of the highest salt lies more than 500 m below the lowest exposed surface outcrops (D.L. Baars, written communication, 1984). A recent seismic refraction experiment confirmed that no salt is present within 500 m of the surface in the central area of the dome (Louie et al., 1995). No trace of salt or associated rocks of the Paradox Formation has been found among the complexly faulted rocks in the center of the dome to support the suggestion that a salt diapir has ascended through the dome.

STRUCTURAL GEOLOGY OF UPHEAVAL DOME

With the exception of the talus slopes below the Wingate Sandstone, quality of exposure at Upheaval Dome is roughly 75–90% bedrock. Along canyon walls, the exposure of structural features is remarkably complete. Faults, folds, and clastic dikes are conspicuous, and were mapped at a scale of 1:6,000. A highly simplified map is presented in figure 2.

In general, the structure of Upheaval Dome is marked by a complexly faulted and folded central uplift in which the Moenkopi Formation and White Rim Sandstone have been raised approximately 350 m in elevation compared to outcrops in the undeformed perimeter of the dome. The White Rim Sandstone occurs as beds and clastic dikes. Proceeding outward from the central uplift to the vicinity of a major syncline that encircles the uplift (the ring structural depression), there are circular outcrop bands of Chinle, Wingate, Kayenta, and Navajo units, respectively. In these outcrops, the Chinle and Kayenta formations are primarily folded and thrust faulted, whereas the Wingate and Navajo sandstones are mainly folded. Clastic dikes derived from Navajo to Wingate units are found in these outcrops, and some of the Wingate Sandstone appears to have flowed as tongue-shaped masses into or overlapping the Chinle Formation. All rock units for the most part dip away from the central uplift until the axis of the syncline is reached. Outward from the syncline axis, rock units of the Navajo Sandstone to the Moenkopi Formation are exposed and dip toward the central uplift. In this vicinity there are faults that omit stratigraphic section. A few clastic dikes presumably derived from Navajo Sandstone are found in the Navajo and Kayenta units here. Further outward, the rock units flatten at the axis of a regional encircling monocline. This monocline is the outermost structure associated with Upheaval Dome. The region outward from the monocline is characterized by essentially flat-lying strata.

Our map data agree with that reported by Schultz-Ela et al., (1994), who interpret their data to support the passage of a salt diapir through the dome. However, the structures seen in the dome are remarkably similar to those found in known complex impact craters (e.g. Wilshire et al., 1972; Offield and Pohn, 1979). Below, we describe the structural features of Upheaval Dome in more detail.

Faults

The pattern of faulting at Upheaval Dome is characterized by low-angle normal faults in the perimeter and thrust faults in the central area (fig. 2). Owing to limitations of scale, only about a third of the faults near the center are shown in figure 2. Kinematic data from offset bedding, drag folds, and slickensides indicate top-toward-the-center vergence on both normal and thrust faults (fig. 4). Some thrust

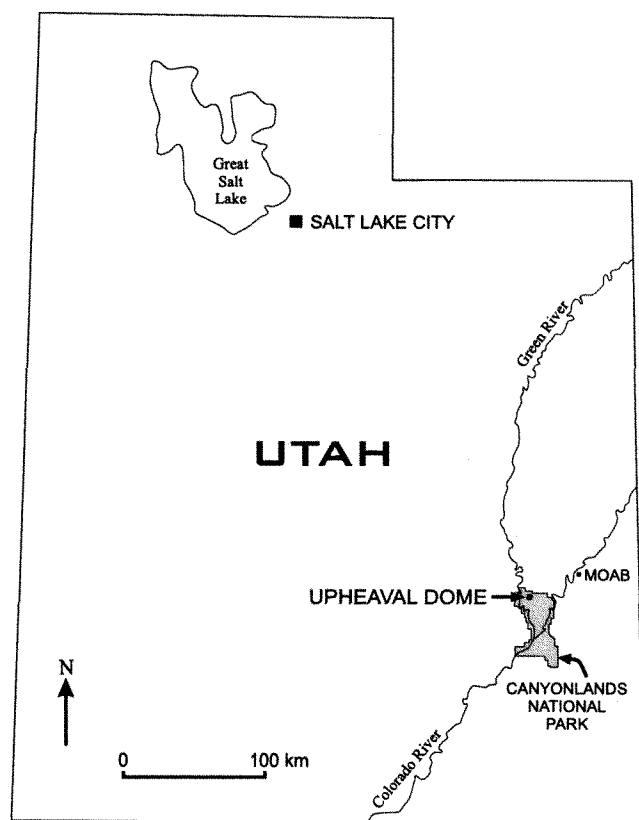


Figure 1. Map of Utah, showing location of Upheaval Dome.

faults display top-away-from-the-center vergence, however. Along Upheaval Canyon (the breach west of the dome center), listric normal faults can be traced into rising thrust faults on the flank of the central uplift. Near the perimeter, some faults have facilitated omission of strata, but die out along bedding planes rather than ramp up section as they are traced into undeformed rocks. Rock units generally are structurally thickened by repetition along faults in the central area and structurally thinned in the outer area. A high density of faults in the central area has led to thickening mainly by thrusting.

Folds

Folds of many scales and orientations are expressed throughout Upheaval Dome (fig. 2). Half-wavelengths vary from 0.5 cm to 1 km, and fold axis orientations are generally circumferential (parallel to circumferential segments drawn around the center) or radial (parallel to radii drawn outward from the center). The largest folds have circumferential axial traces and are: (1) a monocline which delimits the boundary between Upheaval Dome and the surrounding nearly flat-lying strata around most of the structure, and (2) a syncline lying in the region of transition between normal and thrust

faulted areas. Smaller folds with half-wavelengths on the order of tens of meters are well exposed in the Wingate Sandstone cliff and are dominantly closed, upright folds of radial orientation (fig. 5). Outcrop-scale folds are common in the Kayenta Formation, and are present to a lesser extent in the Chinle and Moenkopi Formations. These folds are open to isoclinal, upright to inclined, and are approximately circumferential or radial in orientation. Circumferential folds in the Kayenta Formation in places are asymmetric or show drag where related to faults. Where discernible, top-toward-the-center vergence is usually indicated, but a few folds record top-away-from-center vergence.

Clastic dikes

Clastic dikes are found throughout Upheaval Dome in all rock units and comprise roughly 5–25% of the outcrops. High percentages of dikes are found in the center of the structure and their number decreases radially outward. In most cases, the dikes have intruded along faults and tensional fractures, and range in thickness from less than a centimeter to several meters. A few appear to have flowed into the host rock without the aid of a fracture. These dikes have contacts that are lobate or resemble flame structures, suggesting local plastic behavior of the host rock during intrusion. Cross-cutting relations show that at least some of the dike injection preceded faulting (fig. 6), but the occurrence of dikes along fault planes indicates synkinematic to post-kinematic injection. No systematic orientation of dikes is apparent.

The dikes are composed of orange, red, or white quartzose sandstone. White dikes are found mainly in the center of the dome and the orange and red dikes occur near the center to the perimeter of the dome. Some show contorted flow structure in outcrop (fig. 6). In thin section, samples show a broad range of grain fracturing. The most highly fractured grains are seen in samples from the center of the dome.

Orange-colored dikes in the Chinle Formation have been physically traced to a source at the base of the Wingate Sandstone, but in general, protoliths for the clastic dikes must be inferred on the basis of color, mineralogy, and the assumption that they are not far-traveled. White dikes in the center were derived from the White Rim Sandstone (top of the Cutler Group); orange dikes in the Kayenta Formation are from the Wingate Sandstone or Navajo Sandstone, and the orange dikes in the Navajo Sandstone and red dikes in the Kayenta Formation are derived from the formations in which they occur.

Interpretation of Structural Features

Displacement along normal faults and structural thinning of strata in the perimeter, and occurrence of thrust

by Bryan Kriens, Eugene Shoemaker, and Ken Herkenhoff 1997

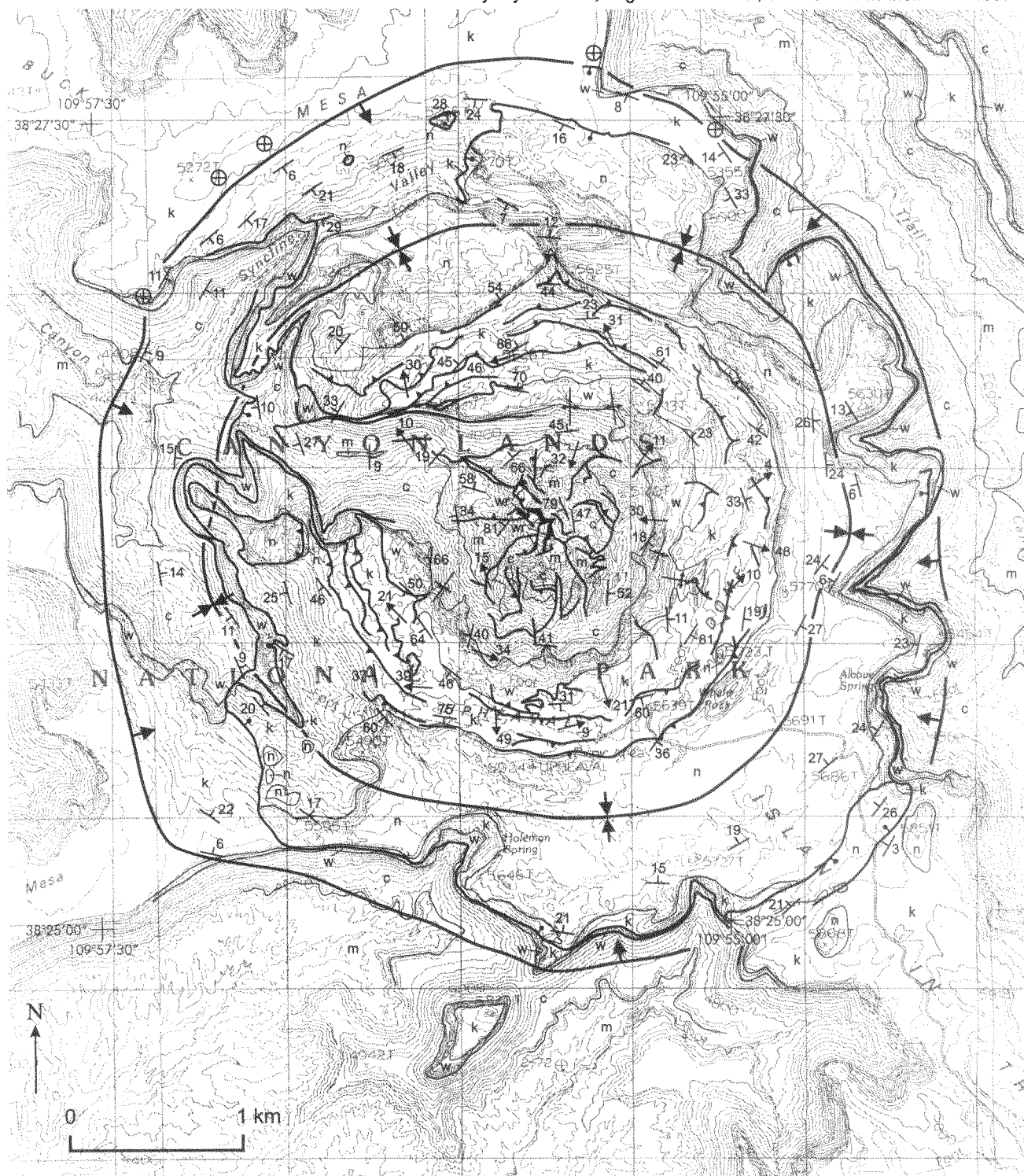
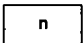
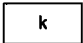
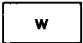
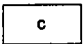
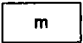














Figure 2. Simplified geologic map of Upheaval Dome, compiled from mapping at 1:6,000.

LEGEND

	Jurassic Navajo Sandstone
	Jurassic Kayenta Formation
	Jurassic to Triassic Wingate Sandstone
	Triassic Chinle Formation
	Triassic Moenkopi Formation
	Permian White Rim Sandstone beds and clastic dikes
	depositional contact
	fault
	normal fault, bar and ball on downthrown side
	thrust or reverse fault, teeth on hanging wall
	axial trace of syncline, 1/2 wavelength on the order of tens of meters
	axial trace of anticline, 1/2 wavelength on the order of tens of meters
	axial trace of regional syncline
	axial trace of regional monocline
	strike and dip of bedding
	horizontal bedding
	trend and plunge of outcrop-scale fold axes

faults, radial folds, and structurally thickened strata in the center all demonstrate motion of rock from the perimeter toward the center of the structure (fig. 7). As shown by continuous exposure in Upheaval Canyon, the normal and thrust faults are coeval and connected components of a listric fault system that facilitated gravitational sliding of rocks toward the center (fig. 8). Some centerward motion of fault-bound wedges evidently also occurred on subhorizontal faults that conjoin and die out within horizontal bedding near the perimeter of the structure. The large-scale circumferential syncline and monocline were formed chiefly by the removal of underlying rock units of the Kayenta to Moenkopi formations from the axial region of the syncline. Some of the synclinal folding could also be due to relatively minor flow of salt at depth (fig. 8). This syncline is interpreted to be the ring structural depression of a complex crater.

The prevalence of faults in the dome illustrates that the rocks largely behaved brittly during impact and subsequent

gravitational sliding, but the occurrence of folds and clastic dikes indicates some fluid to plastic behavior. Massive to thick-bedded relatively homogeneous sandstone formations such as the Wingate Sandstone and Navajo Sandstone are relatively free of faults within each formation, whereas thinner-bedded, lithologically heterogeneous formations are cut by numerous faults. Local plastic to fluid behavior of the Wingate and, to a lesser extent, other units may be due to the presence of fluids and/or a low degree of lithification, since the deformation in many places resembles that seen in soft-sediment landslides.

In summary, the development of Upheaval Dome began with fracture and local fluidization (clastic diking) of rocks during impact, followed by convergent flow of brittle to plastic material toward the center and some continued emplacement of clastic dikes. This convergent flow formed the central uplift and ring structural depression.

IMPACTITES

A lag deposit of resistant quartzose impactites occurs in patches and as individual fragments scattered along a minor drainage within the ring structural depression, near its eastern margin. The impactites rest on the Navajo Sandstone and on colluvium and wind-blown sand derived from the Navajo.

Much of the impactite material is in the form of rounded cobbles 5 to 15 cm in diameter, but many angular fragments and broken cobbles are also present. Where they are broken open, the large cobbles are found to be stream-worn or wind-abraded vesicular bombs with nonvesicular to weakly vesicular quenched rims (fig. 9). Although they are now largely crystalline, these objects appear to have been once partly and perhaps largely molten. A few bombs have stubby tails formed in the process of pull apart and break up of the impact melt. Some impactites are dense or have few vesicles, and some of the dense specimens are strongly flow-banded. All of the impactites that we have examined so far are composed predominantly of quartz and evidently are derived from quartzose sandstone protoliths. The vesicles are lined with tiny quartz crystals. Curiously, the impactites seem to be entirely or almost entirely recrystallized. Thin sections that we have examined revealed little or no glass, although some of the rock is sufficiently fine grained to impede easy identification under the microscope (fig. 9).

SHATTER SURFACES AND
SHATTER CONES

Shatter cones are conical fracture surfaces decorated with "fan-tailed" patterns of ridges and grooves that diverge away from the apices of the cones. They were first described from the Steinheim Basin, Germany (Branco and Fraas, 1905) and have been found at many other, but not all,

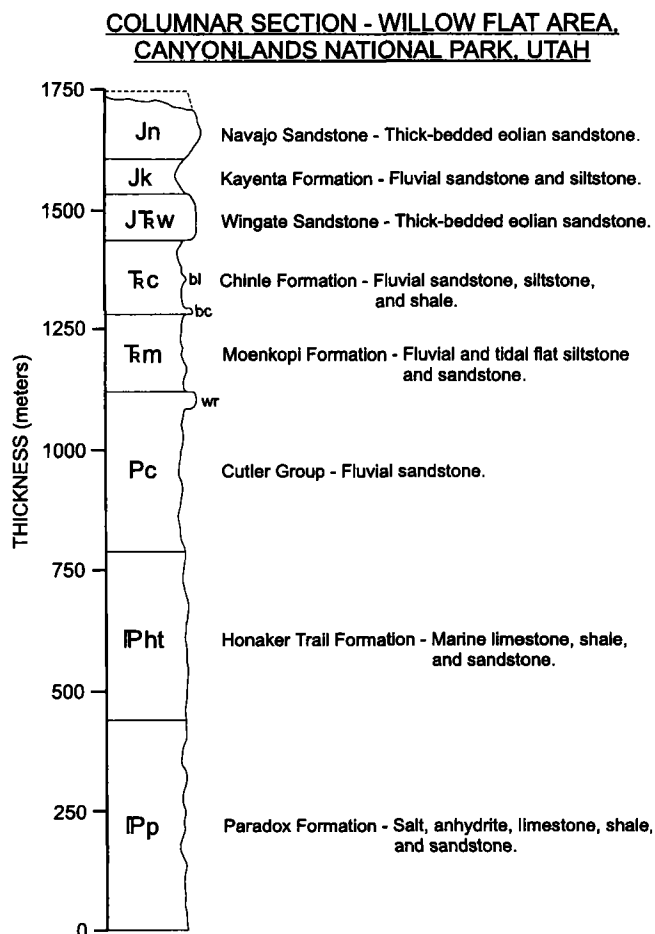


Figure 3. Stratigraphic column showing rock units and their thicknesses from an undeformed area near the perimeter of Upheaval Dome. Column was constructed primarily from a gamma log located near Willow Flat campground, approximately 5 km southeast of Upheaval Dome, and published stratigraphic field studies of undeformed rocks at other localities near the perimeter of the dome (McKnight, 1940; Stewart et al., 1972a; Stewart et al., 1972b; D.L. Baars, written communication, 1984). Older Paleozoic rocks and pre-Cambrian crystalline basement lie below the Paradox Formation but are not shown here. Ledge-former shown at top of Cutler Group (labeled wr) is the White Rim Sandstone, the lowest stratigraphic unit exposed at Upheaval Dome. Ledge-former shown at base of Chinle Formation (bc) is a conspicuous gray conglomeratic sandstone. Resistant unit in the middle of the Chinle Formation (bl) is the Black Ledge Member. The top of the Navajo Sandstone is not exposed in or around Upheaval Dome, but estimated thickness based on the closest exposure is shown as a dashed line.

impact structures (Dietz, 1963, 1968). They also have been produced by high speed impact experiments and by detonation of chemical and nuclear explosives (Shoemaker et al., 1961; Bunch and Quaide, 1968; Schneider and Wagner, 1976; Roddy and Davis, 1977). Milton (1977) estimates that shatter cones may be formed over a range of shock pressures from about 2.5 to 25 gigapascals.

Shatter cones were reported by Shoemaker et al., (1993) from thin sandstone beds of the Moenkopi Formation near the center of Upheaval Dome. These cones are rare and not as finely decorated and grooved as shatter cones found at many other impact structures (fig. 10). In places on the central uplift, however, thin beds of siltstone and very fine sandstone of the Moenkopi are pervasively cut by roughly planar fractures decorated with fan-tailed patterns of grooves and ridges. We refer to these fractures as shatter surfaces. Generally, the shatter surfaces are inclined at angles of about 45° to 60° to the bedding. Multiple sets of shatter surfaces are present in individual beds. Locally, shatter surfaces can be traced with varying strike over arcs with radii of curvature of tens of centimeters. The shatter surfaces along these arcs appear to be segments of large cones whose apices point in the stratigraphically up direction. We suggest that the shatter surfaces observed at Upheaval Dome have been formed in response to shock pressures within part of the range over which typical shatter cones are formed.

DISCUSSION AND CONCLUSION

Detailed geologic mapping at Upheaval Dome has yielded several lines of evidence for an impact origin. The structure of Upheaval Dome corresponds to that expected for a complex crater. The pattern of faulting, folding, and clastic dike injection at Upheaval Dome resembles that seen in other known impact structures, such as the Sierra Madera structure of southwest Texas (Wilshire et al., 1972). Shock effects include shatter cones and shatter surfaces and impactite fragments and bombs.

Figure 4. (A) Thrust fault in Kayenta Formation. Outcrop is located in NNE area of the circular band of Kayenta outcrops shown on figure 2. View is looking west at top-toward-the-center vergence. On a smaller scale, some top-away-from-the-center vergence is also visible above the main fault. (B) Low-angle normal fault exposed in SW perimeter of the dome. View is to the NW, center of the dome lies to the right of the photo. Fault can be seen just right of photo center, dipping NE and cutting down through the Wingate Sandstone cliff. Note Kayenta-Wingate contact near top of cliff (bedded Kayenta above, massive Wingate below) is offset by top-toward-the-center vergence. Although difficult to see here, the Kayenta Formation has been significantly thinned.





Figure 5. Looking NNE at radial folds in basal Wingate Sandstone. Width of view is approximately 300 m.

Shoemaker and Herkenhoff (1984) suggested that, since the time of impact, one to two km of strata might have been removed from the vicinity of Upheaval Dome and that the crater likely was formed in late Cretaceous or Paleogene time. Their suggestion implied that the crater-like head of Upheaval Canyon, located in the center of Upheaval Dome, is strictly the result of differential erosion long after the impact structure was formed. Our subsequent discovery of an impactite lag deposit and reexamination of unusual lobes of Wingate Sandstone along the walls of Upheaval Canyon now lead us to a rather different perspective on the depth of erosion and age of the impact structure.

The discovery of eroded impactite bombs resting on Navajo Sandstone within the ring structural depression was a complete surprise. Even though these quartzose cobble-size objects are much more resistant to weathering than the Navajo Sandstone or other higher sandstone formations that might have been present at the time of impact, it is difficult to imagine that the land surface where they are found could have been denuded more than 100 or 200 m before the

impactites were entirely washed away. Indeed, the impactites may have been initially deposited on a surface directly underlain by the Navajo Sandstone.

Lobate or tongue-like structurally coherent masses of Wingate Sandstone and adjacent beds of the upper Chinle Formation occur low on the wall of the crater-like topographic feature at the head of Upheaval Canyon (see fig. 2). At least one of these masses is displaced down the wall across lower beds of the Chinle along a contact that is roughly parallel with the wall. Elsewhere, one of the Wingate lobes penetrates into the underlying Chinle. We suggest that these lobes may represent partly fluidized sandstone that slumped along the walls of the initial transient cavity. If so, the walls of the present topographic crater must be close to the final position of the transient cavity walls after their inward migration during crater collapse. This inner, constricted crater has been breached on the west side and all strongly shocked rocks evidently have been removed from the center by erosion. The total erosion of the center, however, might be no more than a few hundred meters,



sufficient to remove any deposits filling the initial crater and any strongly shocked material and to produce the highly dissected central topography we see today.

The deep canyons in the landscape surrounding Upheaval Dome and incised into the impact structure have been cut subsequent to impact. This episode of canyon cutting is no older than integration of the upper with the lower Colorado River drainage at about 5 Ma and the cutting of the lower Grand Canyon (Lucchitta, 1972). Recent work suggests that deep canyon cutting in the center of the Colorado Plateau, upstream from the Grand Canyon, has occurred chiefly in the last half million years (Lucchitta et al., 1994). Upheaval Dome probably has been formed late in the history of denudation of the central Colorado Plateau, possibly as late as a few million years ago. It is also possible, but in our view much less likely, that impact occurred in the Jurassic not long after deposition of the Navajo Sandstone. Isotopic studies of the impactites at the U.S. Geological Survey and fission-track investigations at the University of Pennsylvania of shocked apatite from the center of the Dome are currently underway to further constrain the age of Upheaval Dome.

Our field study of Upheaval Dome has permitted us to examine the mechanical behavior of rocks and the kinematics of structures associated with collision and subsequent formation of the central uplift and ring structural depression in sedimentary target bodies. It appears that even at relatively shallow depth below the transient crater and zone of impact



Figure 6. (A) Outcrop from perimeter of Upheaval Dome, looking east. West-dipping normal fault at top truncates near-vertical sandstone dike. At some other localities, dikes intrude faults. (B) Looking NW at clastic dike in Kayenta Formation. Hammer rests on country rock, dike is to the right. Note contorted flow structure, and lobate contact with country rock. (C) Looking down at sandstone dike with sandstone clasts and flow structure. Contact is at hammer, light-colored host rock at lower right is Kayenta Formation.

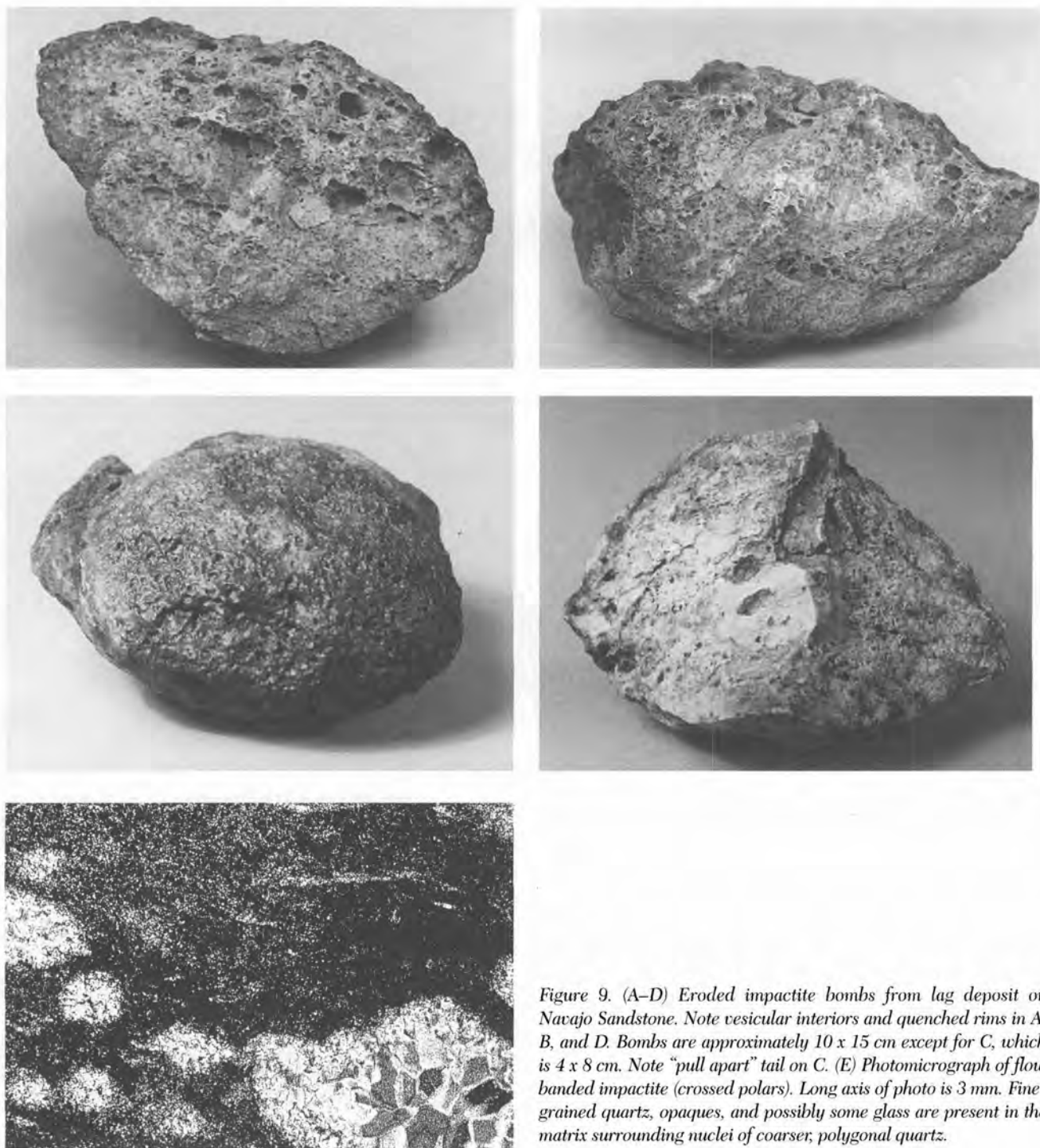


Figure 9. (A–D) Eroded impactite bombs from lag deposit on Navajo Sandstone. Note vesicular interiors and quenched rims in A, B, and D. Bombs are approximately 10 x 15 cm except for C, which is 4 x 8 cm. Note “pull apart” tail on C. (E) Photomicrograph of flow banded impactite (crossed polars). Long axis of photo is 3 mm. Fine-grained quartz, opaques, and possibly some glass are present in the matrix surrounding nuclei of coarser, polygonal quartz.



Figure 10. Shatter cone in sandstone of the Moenkopi Formation. Scale is in centimeters.

such a way as to create tongue-shaped outcrops which extend into or overlap the Chinle Formation.

Locality 1-2. Looking north at the upper cliff face, we can see thrust faults in the Kayenta Formation and upper Wingate Sandstone. Motion is top-toward-the-center based on this exposure and two outcrop-scale drag folds found 100 m north of the cliff.

Locality 1-3. We are now located in the undeformed zone outside of Upheaval Dome. Looking WNW, we see part of the monocline and, further right, a low-angle normal fault which shows top-toward-the-center offset (same cliff face is also shown in figure 4B). The Kayenta-Wingate contact is at the top of the lower massive cliff and provides the best offset marker. The Navajo Sandstone, exposed in the upper massive cliff, is also in fault contact with the Kayenta Formation. Although difficult to see from here, the Navajo Sandstone displays reverse drag of bedding at its southern end (or left end of outcrop).

Day 2

Locality 2-1. In this general area there are faults, folds, and clastic dikes to observe closehand. The largest fold in this area is a radial anticline which has a reverse fault on its southern limb. Other faults are found in the north limb and further north. Many of these faults are nearly parallel to bedding and have drag folds associated with them, but some of the folds are disharmonic and thus yield ambiguous sense-of-shear. Some drag folds indicate top-away-from-the-center vergence.

Continuing north along the trail, we come to an outcrop of clastic dikes. Note that clasts are either angular rock fragments or blebs and stringers with flow structure. This illustrates the local fluid behavior of the sandstones.

Locality 2-2. To the north we see two low-angle faults dipping west. One cuts out the top of the Wingate Sand-



Figure 11. Field trip localities.

stone and is analogous to the normal fault seen at locality 1-3. The other fault is at the base of the Wingate cliff and truncates the top of the Chinle Formation. Although the exposures here do not show this, the lower fault in most places never ramps up-section in the hanging wall but instead dies out in the Wingate-Chinle contact or within the Chinle Formation as it is traced away from the center of the dome. Bedding cutoffs in basal Wingate and upper Chinle elsewhere indicate that a wedge-shaped fault block has been removed by centerward lateral extrusion in this lower fault zone.

ACKNOWLEDGMENTS

We are grateful to David Bice, Peter Huntoon, and Paul Link for reviewing the paper and providing helpful comments. The work was funded by the NASA planetary geology and geophysics program.

REFERENCES CITED

- Boon, J.D., and Albritton, C.C., Jr., 1938, Established and supposed examples of meteoritic craters and structures: *Field and Laboratory*, v. 6, p. 44-56.
- Branco, W., and Fraas, E., 1905, Das kryptovulkanische Becken von Steinheim: *Akademie der Wissenschaften Berlin, Phys.-math. Kl., Abh.* 1, 64 p.

- Bucher, W.H., 1936, Cryptovolcanic structures in the United States: International Geological Congress, 16th, Washington, D.C., 1933, Report, v. 2, p. 1055-1084.
- Bunch, T.E., and Quaide, W.L., 1968, Shatter cones in the Danny Boy nuclear crater. *in* French, B.M., and Short, N.M., eds., Shock metamorphism of natural materials, Mono Book Corp., Baltimore, p. 285.
- Dietz, R.S., 1963, Astroblemes. ancient meteorite-impact structures on the Earth: *in* Middlehurst, B.M., and Kuiper, G.P., eds., The Moon, meteorites and comets. University of Chicago Press, Chicago, p. 285-300.
- Dietz, R.S., 1968, Shatter cones in cryptoexplosion structures: *in* French, B.M., and Short, N.M., eds., Shock metamorphism of natural materials. Mono Book Corp., Baltimore, p. 267-285.
- Doelling, H.H., Oviatt, C.G., and Huntoon, P.W., 1988, Salt deformation in the Paradox region: Utah Department of Natural Resources Bulletin 122, 93 p.
- Grieve, R.A.F., Robertson, P.B., and Dence, M.R., 1981, Constraints on the formation of ring impact structures, based on terrestrial data. *in* Schultz, P.H., and Merrill, R.B., eds., Multi-ring basins, Pergamon Press, New York, p. 37-57.
- Grieve, R.A.F., 1991, Terrestrial impact: the record in the rocks: *Meteoritics*, v. 26, p. 175-194.
- Huntoon, P.W., Billingsley, G.H., Jr., and Breed, W.J., 1982, Geologic map of Canyonlands National Park and vicinity, Utah: Canyonlands Natural History Association, Moab, Utah.
- Louie, J.N., Chavez-Perez, S., and Plank, G., 1995, Impact deformation at Upheaval Dome, Canyonlands National Park, Utah, revealed by seismic profiles [abs.]: EOS (Transactions, American Geophysical Union), v. 76, p. 337.
- Lucchitta, I., 1972, Early history of the Colorado River in the Basin and Range province: Geological Society of America Bulletin, v. 83, p. 1933-1948.
- Lucchitta, I., Caffee, M., Finkel, R.C., Curtis, G., Davis, M., Davis, S., Hanks, T.C., and Turrin, B.D., 1994, Quaternary alluvial chronology in the eastern Grand Canyon-Lake Powell region, Arizona and Utah: Geological Society of America Abstracts with Programs, v. 26, no. 7, p. A-258.
- McKnight, E.T., 1940, Geology of area between Green and Colorado Rivers, Grand and San Juan Counties, Utah: U.S. Geological Survey Bulletin 908, 147 p.
- Milton, D.J., 1977, Shatter cones—An outstanding problem in shock mechanics: *in* Roddy, D.J., Pepin, R.O., and Merrill, R.B., eds., Impact and explosion cratering, Pergamon Press, New York, p. 703-714.
- Offield, T.W., and Pohn, H.A., 1979, Geology of the Decaturville impact structure, Missouri: U.S. Geological Survey Professional Paper 1042, 48 p.
- Roddy, D.J., and Davis, L.K., 1977, Shatter cones formed in large-scale experimental explosion craters. *in* Roddy, D.J., Pepin, R.O., and Merrill, R.B., eds., Impact and explosion cratering, Pergamon Press, New York, p. 715-750.
- Schneider, E., and Wagner, G.A., 1976, Shatter cones produced experimentally by impacts in limestone targets. *Earth and Planetary Science Letters*, v. 32, p. 40-44.
- Schultz-Ela, D.D., Jackson, M.P.A., Hudec, M.R., Fletcher, R.C., Porter, M.L., and Watson, I.A., 1994, Structures formed by radial contraction at Upheaval Dome, Utah. Geological Society of America Abstracts with Programs, v. 26, no. 7, p. A-72.
- Shoemaker, E.M., 1960, Penetration mechanics of high velocity meteorites, illustrated by Meteor Crater, Arizona. International Geological Congress, 21st, Copenhagen, 1960, Report, pt. 18, p. 418-434.
- Shoemaker, E.M., Gault, D.E., and Lugin, R.V., 1961, Shatter cones formed by high speed impact in dolomite. U.S. Geological Survey Professional Paper 424-D, p. 365-368.
- Shoemaker, E.M., and Herkenhoff, K.E., 1983, Impact origin of Upheaval Dome, Utah [abs.]: EOS (Transactions, American Geophysical Union), v. 64, p. 747.
- Shoemaker, E.M., and Herkenhoff, K.E., 1984, Upheaval Dome impact structure [extended abs.]: Lunar and Planetary Science XV, p. 778-779.
- Shoemaker, E.M., Herkenhoff, K.E., and Gostin, V.A., 1993, Impact origin of Upheaval Dome, Utah [abs.]: EOS (Transactions, American Geophysical Union), v. 74, October 26, 1993 Supplement, p. 388.
- Stewart, J.H., Poole, F.G., and Wilson, R.F., 1972a, Stratigraphy and origin of the Chinle Formation and related Upper Triassic strata in the Colorado Plateau region. U.S. Geological Survey Professional Paper 690, 336p.
- Stewart, J.H., Poole, F.G., and Wilson, R.F., 1972b, Stratigraphy and origin of the Triassic Moenkopi Formation and related strata in the Colorado Plateau region: U.S. Geological Survey Professional Paper 691, 195 p.
- Wilshire, H.G., Offield, T.W., Howard, K.A., and Cummings, D., 1972, Geology of the Sierra Madera cryptoexplosion structure, Pecos County, Texas: U.S. Geological Survey Professional Paper 599-H, 42 p.

Stratigraphy and structure of the Sevier thrust belt and proximal foreland-basin system in central Utah: A transect from the Sevier Desert to the Wasatch Plateau

T.F. LAWTON

*Department of Geological Sciences, New Mexico State University,
Las Cruces, New Mexico 88003*

D.A. SPRINKEL

Utah Geological Survey, 1594 W. North Temple, Suite 3110, Salt Lake City, Utah 84114

P.G. DECELLES

Department of Geosciences, University of Arizona, Tucson, Arizona 85721

G. MITRA

A.J. SUSSMAN

*Department of Earth and Environmental Sciences, University of Rochester,
Rochester, New York 14627*

M.P. WEISS

*Department of Geological Sciences, Preston Cloud Research Laboratory,
University of California, Santa Barbara, California 93106*

ABSTRACT

The Sevier orogenic belt in central Utah comprises four north-northwest trending thrust plates and two structural culminations that record crustal shortening and uplift in late Mesozoic and early Tertiary time. Synorogenic clastic rocks, mostly conglomerate and sandstone, exposed within the thrust belt were deposited in wedge-top and foredeep depozones within the proximal part of the foreland-basin system. The geologic relations preserved between thrust structures and synorogenic deposits demonstrate a foreland-breaking sequence of thrust deformation that was modified by minor out-of-sequence thrust displacement. Structural culminations in the interior part of the thrust belt deformed and uplifted some of the thrust sheets following their emplacement.

Strata in the foreland basin indicate that the thrust sheets of central Utah were emplaced between latest Jurassic and Eocene time. The oldest strata of the foredeep depozone (Cedar Mountain Formation) are Neocomian and were derived from the hanging wall of the Canyon Range thrust. The foredeep depozone subsided most rapidly during Albian through Santonian or early Campanian time and accumulated about 2.5 km of conglomeratic strata (Indianola Group). The overlying North Horn Formation accumulated in a wedge-top basin from the Campanian to the Eocene and records propagation of the Gunnison thrust beneath the former foredeep. The Canyon Range Conglomerate of the Canyon Mountains, equivalent to the Indianola Group and the North Horn Formation, was deposited exclusively in a wedge-top setting on the Canyon Range and Pavant thrust sheets.

This field trip, a three day, west-to-east traverse of the Sevier orogenic belt in central Utah, visits localities where timing of thrust structures is demonstrated by geometry of cross-cutting relations, growth strata associated with faults and folds, or deformation of foredeep deposits. Stops in the Canyon Mountains emphasize geometry of late structural culminations and relationships of the Canyon Range thrust to growth strata deposited in

the wedge-top depozone. Stops in the San Pitch Mountains illustrate deposits of the foredeep depozone and younger, superjacent wedge-top depozone. Stops in the Sanpete Valley and western part of the Wasatch Plateau examine the evolution of the foreland-basin system from foredeep to wedge-top during growth of a triangle zone near the front of the Gunnison thrust.

INTRODUCTION

The Sevier orogenic belt is part of a linear zone of late Mesozoic thin-skinned deformation that extends northward from the vicinity of Las Vegas, Nevada, through the Canadian Rocky Mountains, and into northern Alaska. Although the term, Sevier orogenic belt, has been applied to fold-and-thrust deformation as far north as Montana (e.g., Schmitt et al., 1995), the name was originally proposed by Armstrong (1968) for that part of the deformed belt, consisting of thrust faults and related folds, that lies between southern Nevada and the northern boundary of Utah. Armstrong (1968, p. 451) recognized that the thin-skinned deformation was primarily a Cretaceous event and therefore older than basement uplifts of the Laramide orogeny that began to form near the end of the Cretaceous. He intended that the term discriminate, both temporally and kinematically, the thrust-related deformation at the eastern edge of the Basin and Range from the basement-involved structures of the central Rocky Mountains. The exact timing of initiation of thrusting remains somewhat controversial (e.g., Heller et al., 1986; DeCelles and Currie, 1996), and there is significant overlap in age of late thrust movement and Laramide basement uplift to the east (e.g., Lawton and Trexler, 1991; Lawton et al., 1993); however, the Sevier orogeny was a major, distinct episode of crustal shortening recorded both by its structural geometry and by the stratigraphic record of the Cretaceous foreland (e.g., Kauffman, 1977).

Since the general geologic community's most recent visit to the Sevier orogenic belt in central Utah in 1982 (Nielson, 1982 and papers therein), a tremendous amount of field research has taken place in central Utah. In addition, thrust belts and foreland basins have enjoyed a scientific renaissance; general concepts have blossomed and advanced greatly in the last 17 years. Tools and concepts applied universally today that were nascent or nonexistent in the early 1980s include balanced cross sections (e.g., Dahlstrom, 1969; Woodward and Boyer, 1985), geometric models for thrust belts (e.g., Bally et al., 1966; Boyer and Elliott, 1982), critical-wedge theory (Davis et al., 1983), provenance modeling (Graham et al., 1986; DeCelles, 1988), subsidence of foreland basins as a result of flexure (Beaumont, 1981; Jordan, 1981), and growth-stratal analysis (Riba, 1976; Suppe et al., 1992). Application of these tools has advanced our understanding of thrust timing and foreland-basin origins, both in the Cordilleran fold-and-thrust belt and elsewhere in the world. The trip through the central Utah part of the Sevier

orogen will examine some aspects of the thrust belt and proximal foreland basin that were unknown in 1982.

Geologic Setting

Four thrust sheets and two structural culminations, the Sevier and Canyon Range culminations, are presently defined in the central Utah segment of the Sevier orogenic belt (fig. 1.). The thrust belt to be visited on the field trip represents only a frontal zone of imbricate thrusts that lies cratonward of the Sevier culmination. The Sevier culmination is a stack of basement blocks inferred to lie mostly in the subsurface of the Sevier Desert beneath a Miocene basin, although it is partly exposed in the House and Confusion ranges (DeCelles et al., 1995; Coogan and DeCelles, 1996). In the Late Cretaceous, the Sevier culmination constituted a strong wedge of competent Precambrian crystalline basement and Proterozoic strata, dominantly quartzite, at the rear of the orogen (fig. 1; DeCelles et al., 1995; Mitra, in press). The upper part of the culmination that was available for erosion during the Cretaceous probably consisted of Paleozoic and Mesozoic strata. The Canyon Range culmination lies roughly 5–10 km to the west of the frontal trace of the Canyon Range thrust and caused uplift and stripping of much of the frontal part of the Canyon Range thrust plate (fig. 2; Sussman and Mitra, 1995).

Three exposed thrust plates overlie the Canyon Range, Pavant, and Gunnison thrusts, from west to east. The Canyon Range thrust emplaces Proterozoic sedimentary rocks above Cambrian through Devonian strata and the Cretaceous Canyon Range Conglomerate (Christiansen, 1952; Millard, 1983; Holladay, 1984). The Pavant thrust structurally underlies the Canyon Range thrust and emplaces Cambrian through Ordovician strata over Jurassic strata (Burchfiel and Hickox, 1972; Millard, 1983; Hintze, 1991a). The Gunnison thrust is a frontal detachment in Jurassic evaporite east of a ramp that emplaces Paleozoic over lower Mesozoic strata (Standlee, 1982; Lawton, 1985; Coogan et al., 1995). A wedge-top or piggyback basin developed on the Gunnison thrust sheet during latest Cretaceous and Paleogene time (Lawton and Trexler, 1991). Some workers infer the presence of an additional thrust, the Paxton thrust, in the subsurface based on analysis of stratigraphy and structure in boreholes (fig. 1; Royse, 1993; Coogan et al., 1995; Mitra, in press). The thrust structure of the central Utah part of the Sevier orogenic belt terminates at a structural cross-strike discontinuity at Leamington Canyon (Morris, 1983). North

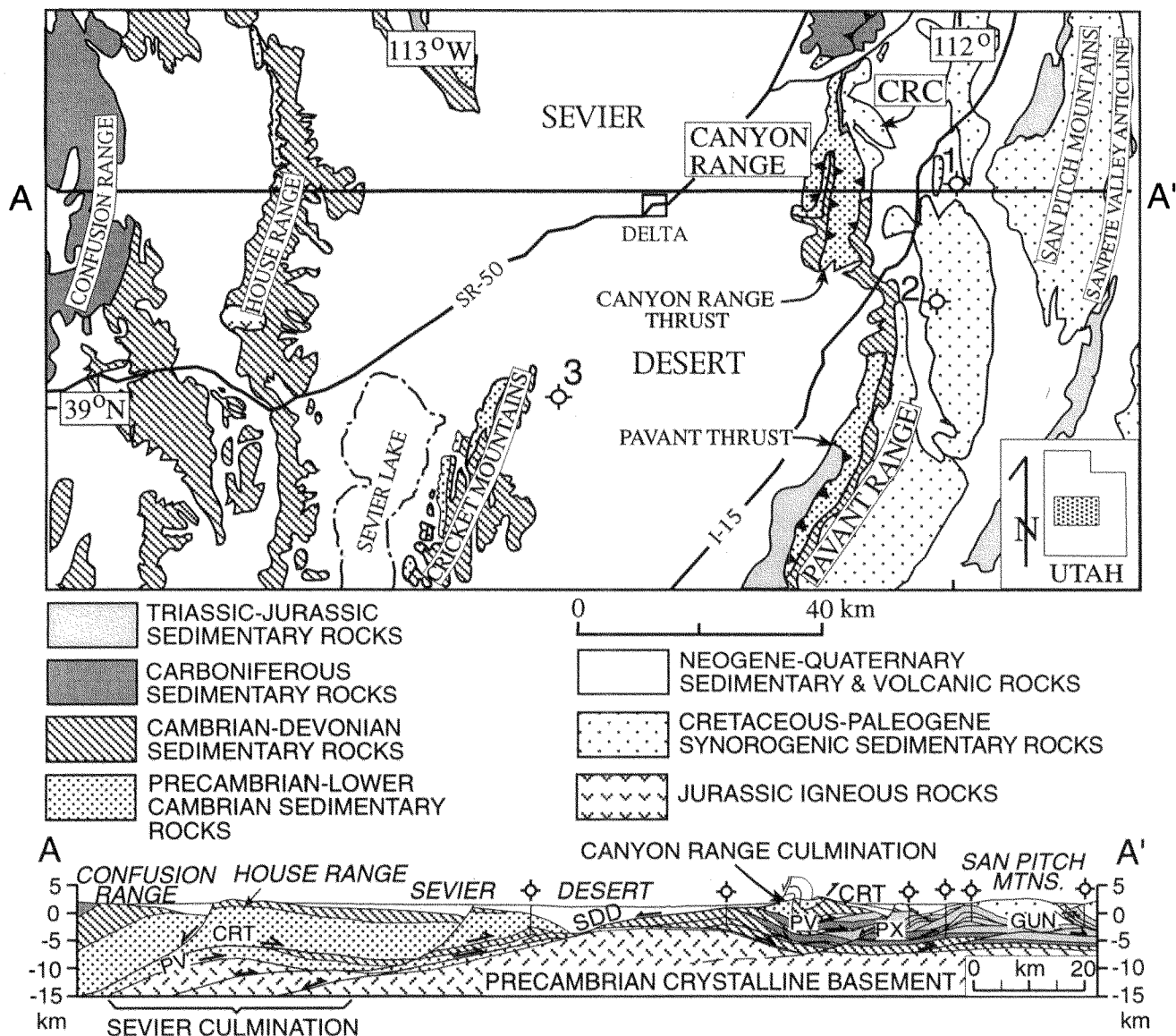


Figure 1. Generalized geologic map of central Utah, after Hintze (1980) and cross section through Sevier orogenic belt (Coogan et al., 1995). Boreholes: 1, Placid WXC Barton1; 2, Placid WXC USA 1-2; 3, Cominco American #2 Beaver River. CRC indicates Canyon Range Conglomerate. Major structures: CRT, Canyon Range thrust; PV, Pavant thrust; SDD, Sevier Desert detachment fault; PX, Paxton thrust; GUN, Gunnison thrust. The Leamington structural cross-strike discontinuity parallels the highway at the north end of the Canyon Range (Canyon Mountains of this text). From Decelles et al., (1995).

of the Leamington cross-strike discontinuity are thrust plates with different hanging-wall stratigraphies and kinematic histories (Mitra, in press).

Thrust faulting is generally believed to have followed a foreland-breaking progression (fig. 4; Lawton, 1986; DeCelles et al., 1995; Mitra, in press), although alternative scenarios have been proposed (Villien and Kligfield, 1986; Schwans, 1995). Recent detailed work on proximal foreland-basin stratigraphy and consideration of cross-cutting and refolding relationships among thrusts has shown that minor out-

of-sequence thrusting was common (DeCelles et al., 1995; Mitra and Sussman, 1997; Mitra, in press). For example, the Canyon Range Conglomerate rests unconformably on both the Canyon Range and Pavant thrust sheets along the east flank of the Canyon Mountains and in the Pavant Range (fig. 1; Millard, 1983; Holladay, 1984; Hintze, 1991a). Prior to deposition of the Canyon Range Conglomerate, significant uplift of the Canyon Range sheet was caused by displacement on underlying thrusts, including the Pavant thrust (fig. 1; Lawton 1986). The Canyon Range Conglomerate was

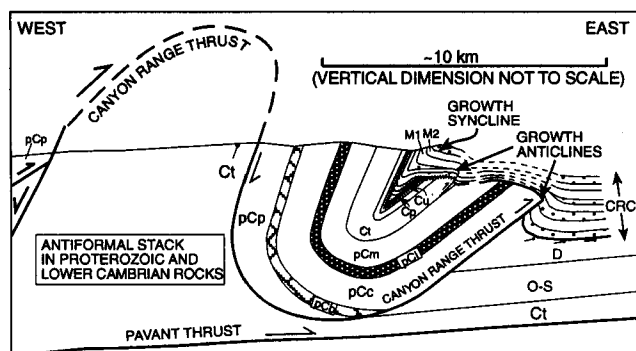


Figure 2. Schematic, generalized cross section through northern Canyon Mountains, showing relationships of Canyon Range thrust, Canyon Range culmination (antiformal stack exposed beneath thrust), and Canyon Range conglomerate (CRC). Stippled units in conglomerate are quartzite petrofacies; unpatterned units are carbonate and mixed (M1, M2) petrofacies. Stratigraphic units: pCp, Pocatello Group; pCb, Black Rock Canyon Limestone; PCc, Caddy Canyon Quartzite; pCi, Indom Formation; pCm, Mutual Formation; Ct, Tintic Quartzite; Cp, Pioche Formation; Cu, Cambrian undifferentiated (limestone, shale and dolostone); O-S, Ordovician and Silurian carbonates and siliciclastics; D, Devonian carbonates.

deposited on the Canyon Range and Pavant thrust sheets and subsequently was overthrust several hundred meters by the Canyon Range thrust sheet, although the amount of thrust displacement was minor compared with initial displacement of the Canyon Range thrust that emplaced Precambrian strata over Devonian strata (see additional discussion in text at stop 3). Thus, the Canyon Range thrust experienced a small amount of out-of-sequence displacement following emplacement of the Pavant thrust (Villien and Kligfield, 1986; DeCelles et al., 1995).

Thrust-related uplift contributed detritus to a foreland basin that lay immediately east of the orogen. Even before the structural characteristics of the Sevier belt were understood, the presence of coarse-grained Cretaceous deposits west of the Wasatch Plateau lead early workers to postulate the presence of orogenic uplift to the west. On the evidence of conglomeratic deposits and angular unconformities, Spieker (1946) defined three orogenic events in western Utah during Cretaceous and early Tertiary time. He termed these orogenic episodes the mid-Cretaceous movement of early Late Cretaceous age, the early Laramide movement of latest Cretaceous age, and the pre-Flagstaff movement of Paleocene age. In defining these events, he recognized the temporal separation of Sevier and Laramide deformation. Spieker (1949; p. 21) was also first to recognize an unroofing sequence, consisting of abundant Paleozoic limestone clasts in the lower part of the conglomeratic section and abundant quartzite clasts in the upper part, in the stratigraphy of the foreland basin. The source of the clasts in west-

ern Utah was delineated by Harris (1959), who recognized that Mesozoic and some Paleozoic formations corresponding to clast types in the conglomerate are absent beneath Tertiary volcanic strata of the Basin and Range. He termed this uplifted terrane the Sevier arch (Harris, 1959), the source of the term subsequently employed by Armstrong (1968).

The stratigraphic record of thrusting in the proximal part of the foreland basin, or that part of the basin lying between the Canyon Mountains and the Wasatch Plateau (fig. 5), consists primarily of conglomeratic strata that range in age from Neocomian through Paleocene (figs. 5, 6). Synorogenic strata of the foreland basin include five major stratigraphic units (fig. 6): The Cedar Mountain Formation; the Indianola Group; the South Flat Formation, a fine-grained unit of sandstone, shale, and minor conglomerate generally excluded from the Indianola Group (Hunt, 1954); the Price River Formation; the North Horn Formation. Based on physical correlation and unpublished palynomorph data (G.L. Waanders, written communications, 1981, 1982, 1983, 1991, 1992, 1993, 1994), the Canyon Range Conglomerate of the Canyon Mountains is interpreted as equivalent to all or part of these units (e.g., Stolle, 1978). Ages of these units are interpreted primarily from a few localities where palynomorphs have been recovered, coupled with regional correlation. Correlation is difficult and involves interpretations of physical stratigraphic sequence and clast population (e.g., DeCelles et al., 1995; Schwans, 1995). Recent regional work on the proximal stratigraphy has yielded a preliminary correlation of units in the foreland basin between the Canyon Mountains and Castle Valley, east of the Wasatch Plateau (fig. 6). Considered in terms of the foreland-basin system of DeCelles and Giles (1996), these rocks were deposited in the wedge-top and foredeep depozones. The wedge-top depozone includes basins, such as piggyback basins, formed on thrust sheets of the orogen. The foredeep depozone represents the thick deposits of the basin immediately adjacent to the tip of the thrust wedge. The Canyon Range Conglomerate, deposited directly on the Canyon Range and Pavant sheets, represents deposits of the wedge-top depozone. Strata of the Indianola Group in the San Pitch Mountains were deposited in the foredeep depozone, whereas strata of the North Horn Formation at the same locality are wedge-top deposits that accumulated on the hanging wall of the Gunnison thrust after it propagated beneath the former foredeep. Correct interpretation of the relationships among these proximal strata and the thrust faults is essential to understanding the evolution of the thrust belt, both in terms of kinematics and timing.

Each thrust sheet of the Sevier orogenic belt contains a stratigraphic section originally deposited in the Proterozoic-early Mesozoic Cordilleran miogeocline. Although parts of the miogeoclinal stratigraphy are common to all thrust

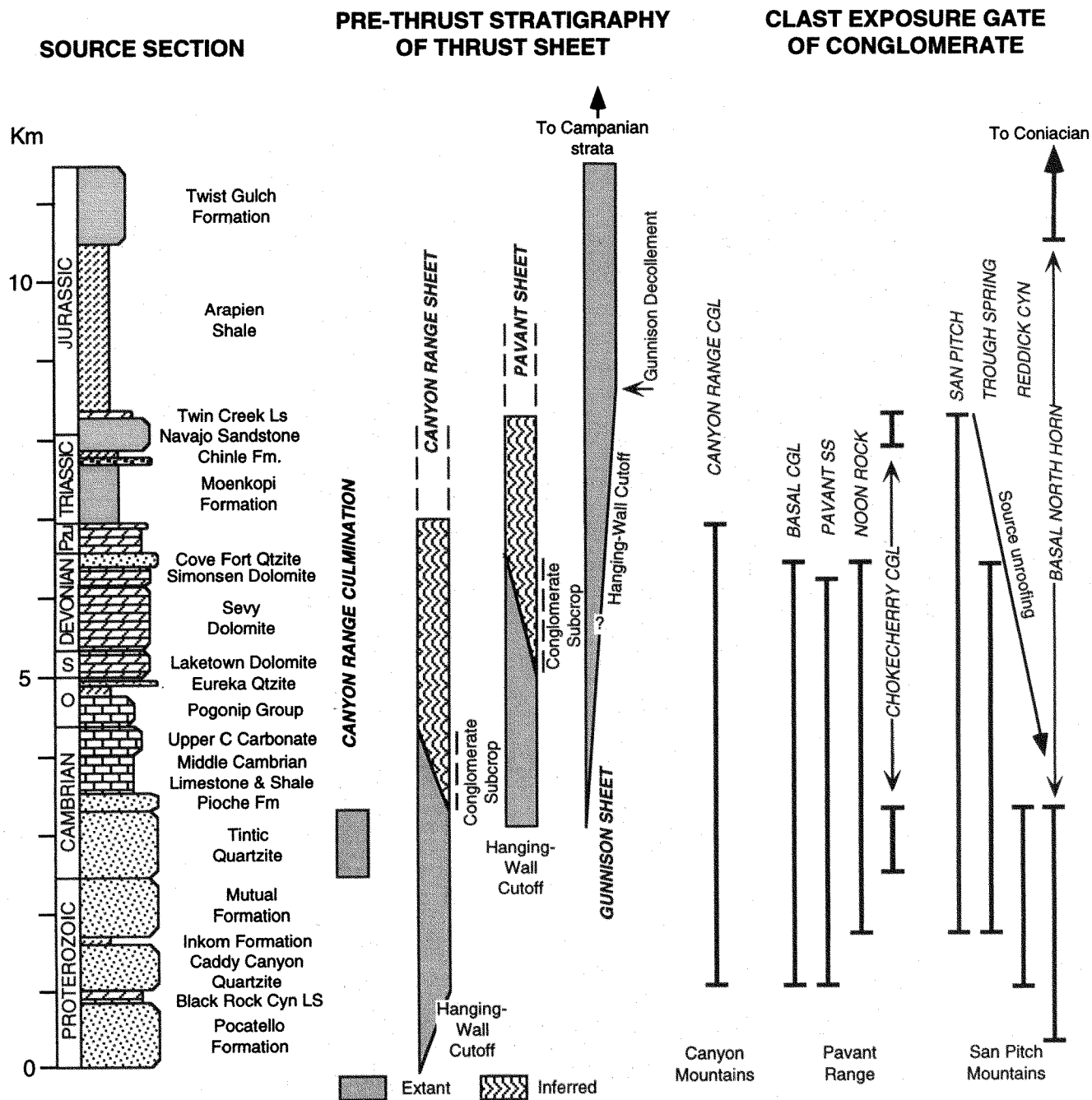


Figure 3. Stratigraphic section present in thrust sheets of the Sevier orogenic belt in central Utah and its relationship to clast populations in synorogenic conglomerate of the proximal foreland-basin system. Left column depicts stratigraphic section present in thrust belt (after Hintze, 1988). Central bars indicate ranges of formations that are present (extant) and postulated to have been present in the Cretaceous (inferred) in each of the three exposed thrust sheets and the Canyon Range culmination. At the initiation of its displacement, the Gunnison sheet included strata as young as Campanian. Vertical lines on right indicate range of clasts present in selected conglomeratic formations of the Canyon Mountains, Pavant Range, and San Pitch Mountains. The range of clasts indicates the exposure gate, or stratigraphic interval available for erosion, during deposition of a particular conglomeratic formation (Graham et al., 1986; DeCelles, 1988). Successively younger conglomeratic units of the San Pitch Mountains (names explained in figure 17) record progressive unroofing of the source section (Lawton, 1986). In the San Pitch Mountains, the basal member of the North Horn Formation contains clasts with a bimodal age distribution because it was derived from both thrust sheets to the west and the rising Sevier-Sanpete Valley antiform above the tip of the Gunnison thrust (Lawton et al., 1993).

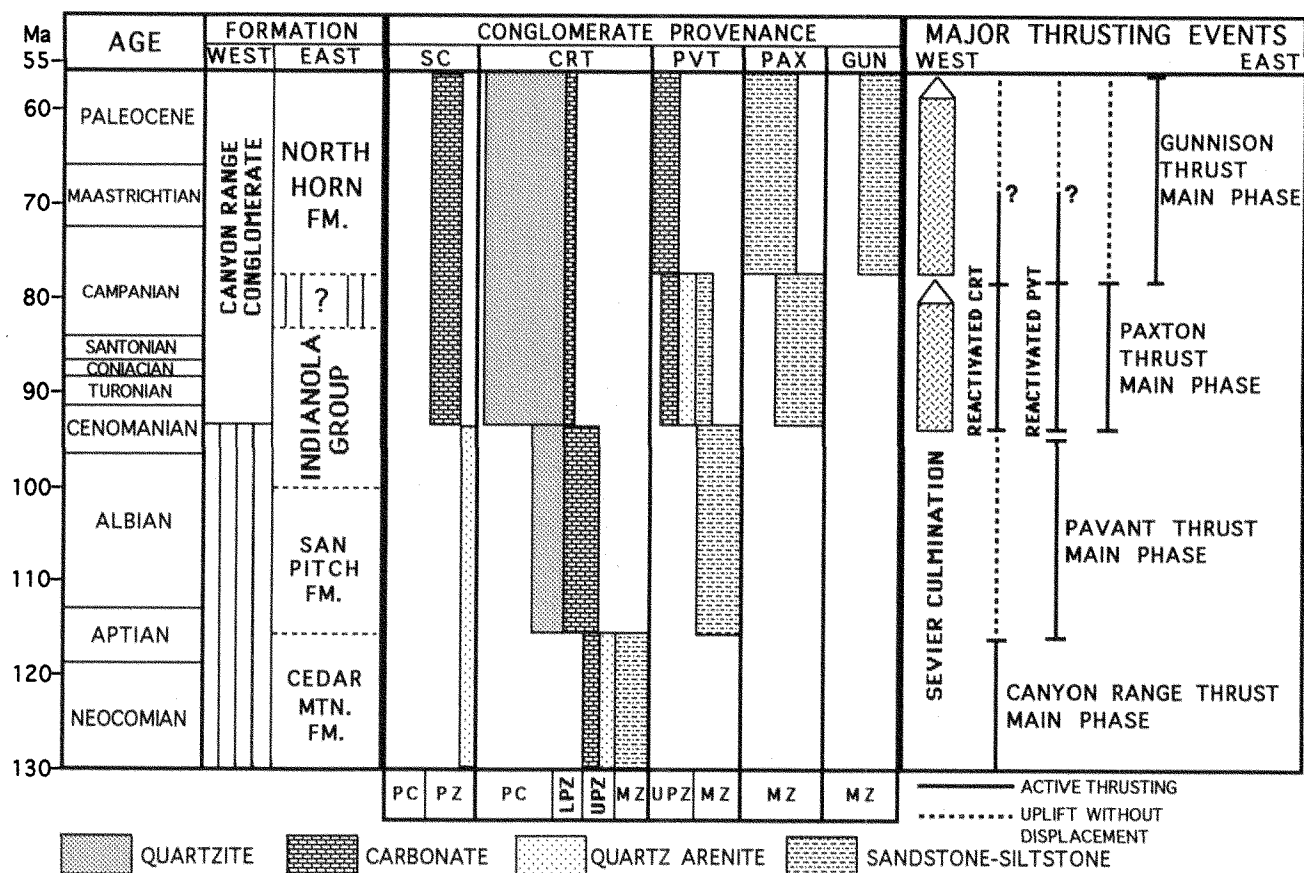


Figure 4. Provenance of Cretaceous-Paleocene conglomeratic units and proposed sequence of Sevier thrust faulting in central Utah (DeCelles et al., 1995). Conglomerate provenance panel shows likely source stratigraphic units (ages of units are along bottom of panel) and lithologies, indicated by patterns, divided among five principal source terranes: SC, Sevier culmination; CRT, Canyon Range sheet; PVT, Pavant sheet; PAX, Paxton sheet; GUN, Gunnison sheet. Ages of conglomerate source-rock units: PC, Proterozoic; PZ, Paleozoic; LPZ, lower Paleozoic; UPZ, upper Paleozoic; MZ, Mesozoic.

sheets, some parts are unique to a given thrust plate (figs. 3, 4). This is particularly true if the stratigraphy is considered in terms of what parts of each sheet were exposed in the Cretaceous and early Tertiary during thrusting. Stratigraphic units still extant in some thrust plates never produced detritus for synorogenic deposits of the foreland basin, whereas they were prodigious contributors from other thrust sheets. For example, lower Paleozoic strata of the Canyon Range sheet in the House Range and in the Canyon Mountains south of Leamington Canyon contributed abundant clasts (DeCelles et al., 1995); on the other hand, the lower Paleozoic section of the Pavant sheet was never exposed to erosion (figs. 1, 3). In addition, only the Canyon Range sheet contains Precambrian strata that were ever exposed to erosion (fig. 1); therefore, essentially all first-cycle Proterozoic quartzite clasts and lower Paleozoic quartzite clasts in the central Utah part of the proximal foreland basin were derived from the hanging wall of the Canyon Range thrust.

Field Trip Road Log and Stops

The field trip traverses the central Utah part of the Sevier orogenic belt from west to east, beginning in the Canyon Mountains and proceeding to the San Pitch Mountains and Sanpete Valley (fig. 5). Stops in the Canyon Mountains illustrate the structure of the Canyon Range culmination and thrust sheet, superb examples of growth strata deposited during folding (e.g., Suppe et al., 1982), depositional facies in the proximal conglomerate and the nature of the Leamington cross-strike discontinuity where the Sevier River crosses between the Gilson and Canyon mountains (fig. 5). Stops in the western San Pitch Mountains illustrate deposits of the foredeep depozone and the temporal transition between foredeep and wedge-top depozones. Stops in and near the Sanpete Valley illustrate early foreland-basin stratigraphy and interaction of syntectonic foreland-basin deposition with an actively growing frontal triangle zone.

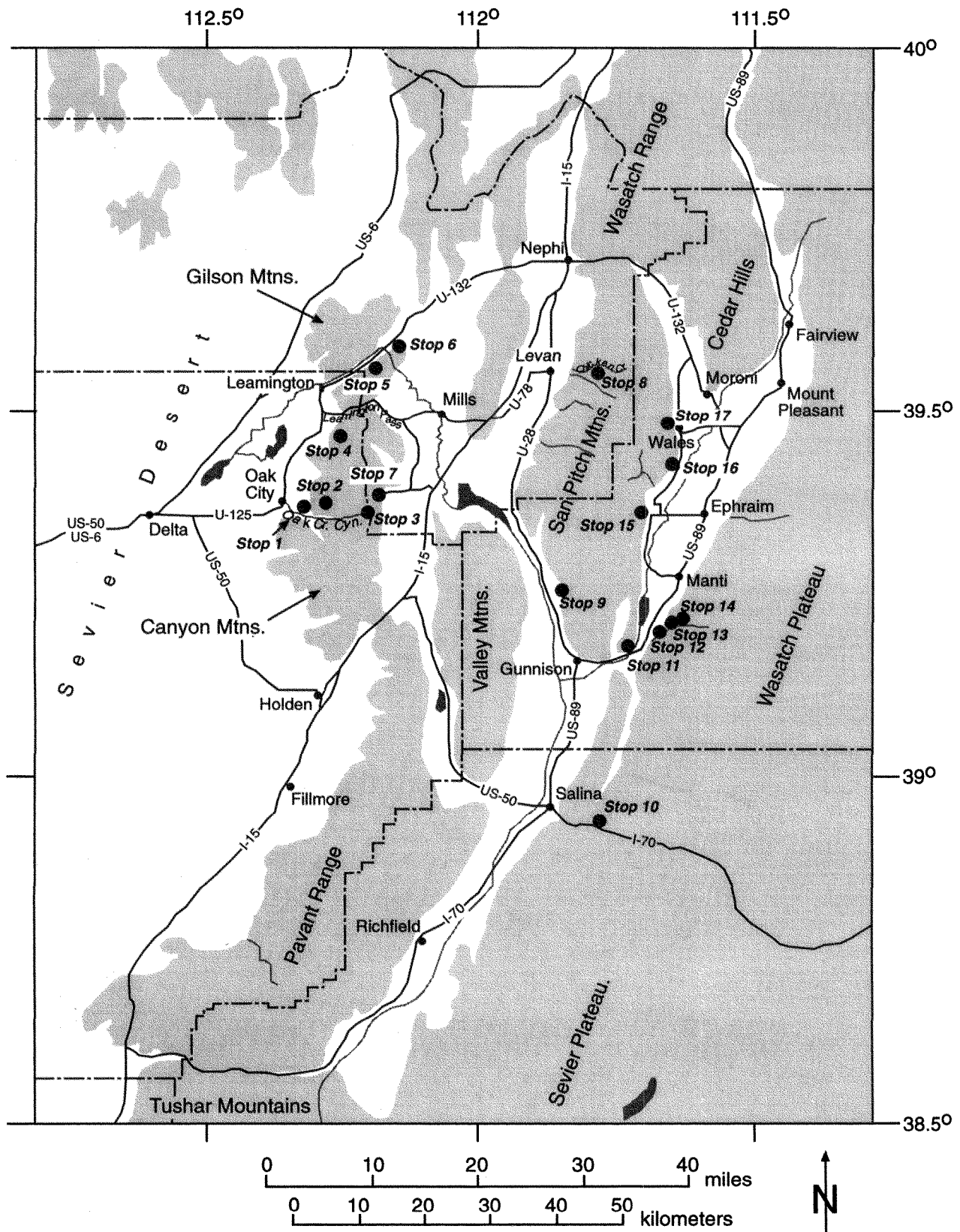


Figure 5. Location map of central Utah, showing field trip stops.

ment. Apatite fission-track data from the western part of the range suggest rapid uplift and denudation of the Canyon Mountains at 18 Ma, possibly as a result of exhumation by a major low-angle detachment (Stockli and Linn, 1996).

Closer to the mouth of Oak Creek Canyon and north of the road, the front of the range is defined by fault scarps, expressed as small triangular facets, that represent segments of a steeply west-dipping normal fault system (Otton, 1995; Sussman and Mitra, 1996). The normal faults have downdropped the folded Canyon Range thrust so that it is not exposed anywhere along the western flank of the range (figs. 7, 8; Sussman and Mitra, 1995). Gently dipping Proterozoic Pocatello Formation in the hanging wall of the Canyon Range thrust is exposed on low hills west of the normal fault trace. Beyond and east of the break in slope, the footwall of the normal fault preserves a connecting splay duplex antiformal stack that developed in the footwall of the Canyon Range thrust and resulted in folding of the thrust (Mitra and Sussman, 1997). The duplex contains repeated slices of Proterozoic Mutual through Cambrian carbonate rocks; some repeated slices of the Cambrian Tintic Formation can be seen from here. Also visible near the top of the ridge is the western end of Paul's Meadow, the location of Stop 2.

- (15.8, 2.3) Cattleguard, not far beyond Fishlake National Forest sign on right, marks entrance to National Forest.
- (17.4, 1.6) Limekiln Canyon. Turn left (north) on Forest Road 419. This road requires high clearance and four-wheel drive. It is narrow, locally rough, and turnaround spots are few after the first half-mile.
- (19.4, 2.0) **Stop 2. Canyon Range culmination and Canyon Range syncline.** Two mile strenuous walk uphill, approximately 3 hours round trip.

From the end of the road, climb northward (up the valley) to Paul's Meadow at the gap between the Cambrian Tintic quartzite ridge to the west and the Cambrian carbonate ridge to the east. From Paul's Meadow, climb to the top of the carbonate ridge to the east. Here we are in the footwall of the folded Canyon Range thrust.

The knob immediately east of this point along the east-west ridge is made up of Proterozoic Pocatello Formation in the hanging wall of the Canyon Range thrust. The thrust dips to the east here, and hanging-wall rocks have been transported to the east. The eastward dips are seen in the west limb of the Canyon Range syncline which has folded the entire Canyon Range thrust sheet; Proterozoic Pocatello through Cambrian Tintic formations are exposed on the west limb. The far end of the east-west ridge is Fool

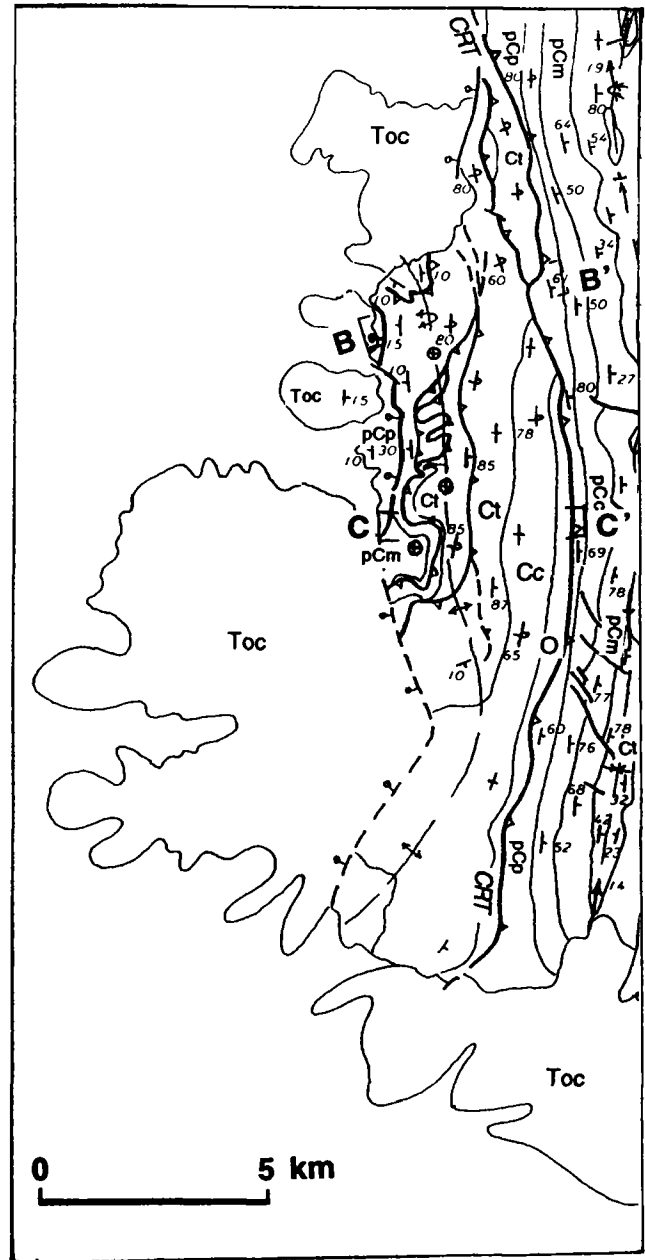


Figure 7. Map of part of west flank of Canyon Mountains, showing thrust slices that form the antiformal stack in the footwall of the Canyon Range thrust. Explanation: pCp, Pocatello Formation; pCm, Mutual Formation; Ct, Tintic Quartzite, Cc, Cambrian carbonate rocks, undifferentiated, O, Ordovician rocks, Toc, Oak City Formation. CRT, Canyon Range thrust.

Creek Peak whose west face is a dip slope composed of Canyon Range Conglomerate overlying Cambrian Tintic Formation in the east limb of the Canyon Range syncline.

Looking north, we see that the west limb of the syncline becomes progressively steeper and eventually overturned

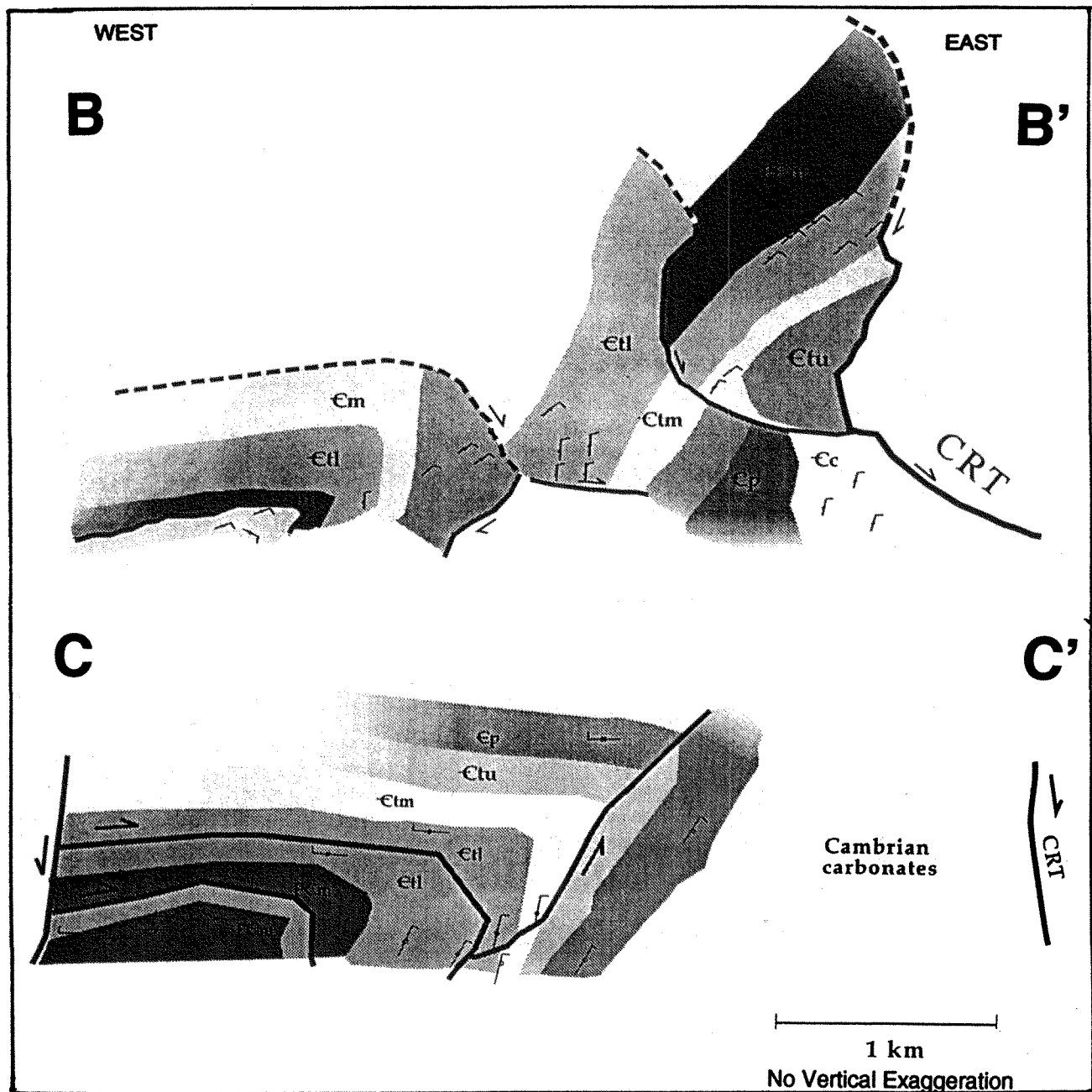


Figure 8. Down-plunge projections through the antiformal stack in the footwall of the Canyon Range thrust exposed on the west side of the Canyon Mountains. Explanation: PCm, Mutual Formation; Ct, Tintic Quartzite, divided into lower (CtI), middle (Ctm), and upper (Ctu) members; Cp, Pioche Formation. CRT, Canyon Range thrust.

(fig. 9a). At the northern end of the range, bedding strike swings northeastward at Leamington Canyon, which separates the Canyon Mountains from the Gilson Mountains. The east limb of the syncline has uniform dips, shown by dip slopes of the Caddy Canyon, Mutual and Tintic quartzites. The core of the syncline exposes folded Canyon Range

Conglomerate, which we will visit at Stop 4. The west limb of the syncline also exposes the east-dipping Canyon Range thrust and its footwall. The footwall exposes the core of the Canyon Range anticlinal culmination made up of an antiformal stack that repeats Proterozoic and Cambrian quartzites (fig. 7); one of the faults repeating the Cambrian Tintic

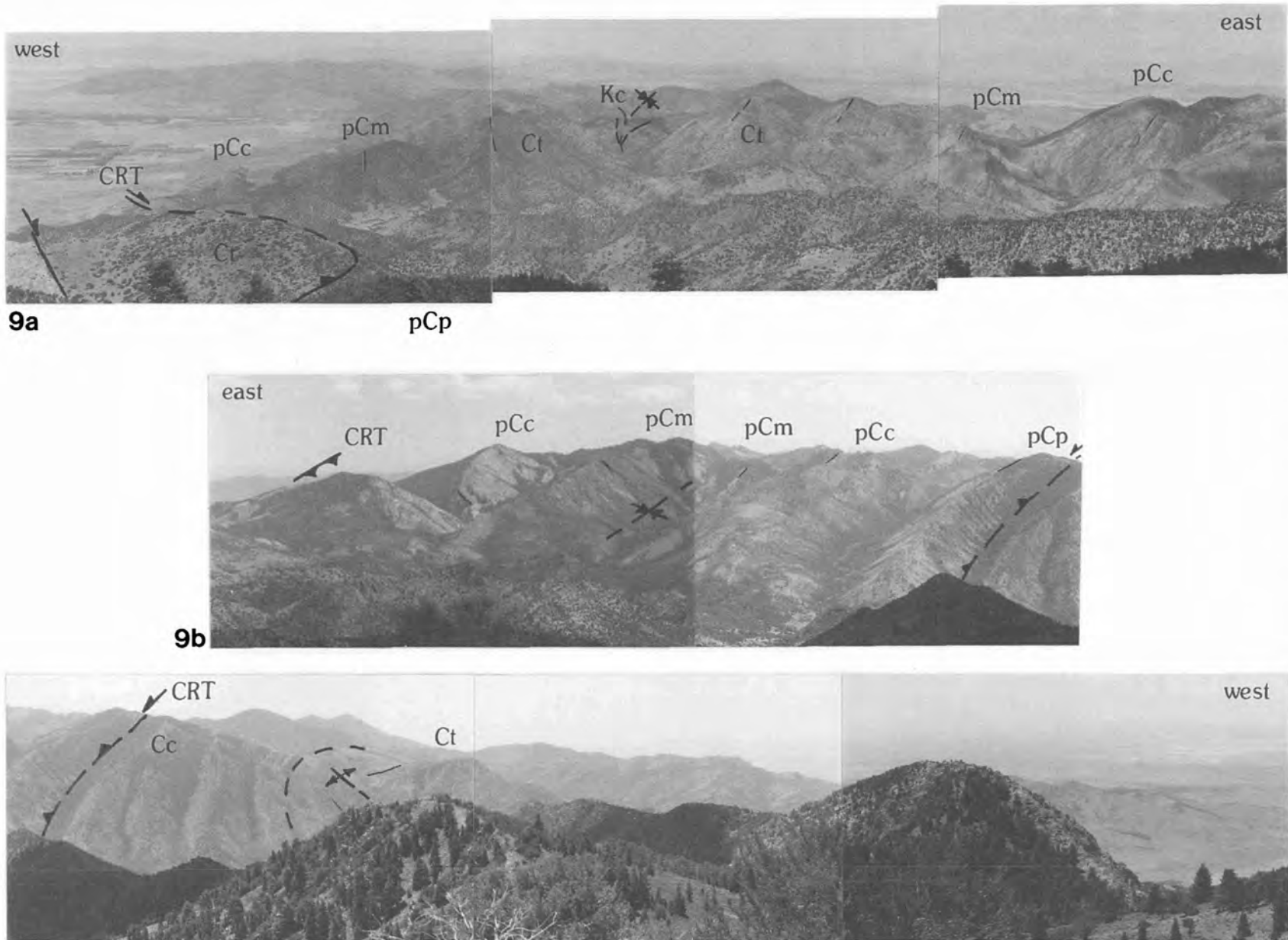


Figure 9. Panoramas from Paul's Meadow of Canyon Range thrust, Canyon Range culmination, and Canyon Range syncline. A. View north. B. View south. Symbols as in figure 7 with following additions: pCc, Caddy Canyon Quartzite; Kc, Canyon Range Conglomerate. Lower two panels overlap at Canyon Range thrust, which is duplicated on adjacent photos.

stratigraphy is clearly visible on the east-west ridge immediately north of here (fig. 9a).

Looking south (fig. 9b), we see the southward-plunging closure of the antiformal culmination defined by the Limestone Canyon slice of the antiformal stack, on which we are standing. The underlying slices of the stack are all exposed west of the Tintic ridge to our right (west). East of the anticline is the Canyon Range syncline made up of hanging-wall rocks of the Canyon Range thrust. The west limb of the syncline exposes Proterozoic Pocatello through Mutual formations. The east limb of the syncline contains Proterozoic Blackrock Canyon through Mutual formations, with the Blackrock Canyon and Caddy Canyon formations emplaced above Devonian rocks and Cretaceous conglomerate along the Canyon Range thrust, which we will visit at Stop 3.

Return to road in Oak Creek Canyon.

- (21.4, 2.0) Turn left (east).
- (22.8, 1.4) South Walker Canyon on right. Cross western exposure of Canyon Range thrust, which emplaces Proterozoic Pocatello Formation of the hanging wall on Ordovician Pogonip Group of the footwall (fig. 10; Millard, 1983).
- (23.0, 0.2) Contact of Proterozoic Caddy Canyon Quartzite and Proterozoic Blackrock Canyon Limestone exposed on north side of canyon.
- (23.3, 0.3) Picnic area. Proterozoic Inkorn Formation, a shale unit above the Caddy Canyon Quartzite, crosses the canyon here.
- (24.1, 0.8) Dark red exposures are of Proterozoic Mutual Formation in core of syncline in hanging wall of Canyon Range thrust.
- (24.4, 0.3) Inkorn strike valley at Lyman Creek (south of road). Canyon Range Conglomerate caps Fool Creek Peak to the north (9:00), where it overlies Cambrian Tintic Quartzite in the core of the syncline.
- (24.6, 0.2) End of road.

Stop 3. Canyon Range thrust and Canyon Range Conglomerate. Three mile walk (round trip). The first part is leisurely on good trails to Oak Creek summit where views are available; after that the walk is moderately strenuous south to a vantage point on a sloping meadow in the Blackrock Canyon Limestone, where views are extraordinary. Approximately 2.5 hours.

The view northward from the high meadow at stop 3 (fig. 11) encompasses the entire Canyon Range syncline, the frontal trace of the Canyon Range thrust, and growth structures in the Canyon Range Conglomerate. The summit of Fool Creek Peak is located near the axis of the syncline and is occupied by a quartzite-boulder conglomerate facies of the Canyon Range Conglomerate resting in angular unconformity upon gently west-dipping beds of the Lower

Cambrian Tintic Quartzite. A minor out-of-the syncline thrust cuts the Tintic Quartzite and the conglomerate (fig. 10), but the conglomerate also overlaps the thrust. This thrust thus developed during deposition of the conglomerate. East of Fool Creek Peak, the 30° west-dipping eastern limb of the Canyon Range syncline comprises the Tintic, Mutual, Inkorn and Caddy Canyon formations. The eastern limb of the folded Canyon Range thrust is visible in the foreground, where it places Caddy Canyon Quartzite on top of the Canyon Range Conglomerate. Beds in the lower part of the conglomerate are tightly folded beneath the thrust, but stratigraphically higher beds overlap the thrust. Several hundred meters of eastward displacement is visible along the thrust. A closer inspection of the conglomerate above the thrust tip reveals a prominent growth anticline in the east limb of which bedding dip decreases progressively upsection. This is an example of a "progressive syntectonic unconformity" (Riba, 1976). These relationships indicate that the Canyon Range Conglomerate was deposited during late-stage reactivation of the Canyon Range thrust; however, it is important to remember that the conglomerate in the footwall rests on Devonian strata. This means that the Canyon Range thrust must have had an earlier, major phase of displacement that juxtaposed Proterozoic strata with Paleozoic strata at this location. Subsequently, both the hanging wall and footwall must have been deeply eroded. The footwall alone must have been stripped of several kilometers of middle Paleozoic to Jurassic strata (Royse, 1993; DeCelles et al., 1995). The uplift needed to sustain this major erosional event probably took place during the emplacement of underlying thrust sheets such as the Pavant, Paxton, and Gunnison thrusts. Although we have no firm handle on when the Canyon Range thrust sheet was initially emplaced, regional provenance data from the Cedar Mountain Formation (figs. 4, 6) indicate that lower Paleozoic and upper Proterozoic rocks were exposed by Early Cretaceous time. J.K. Linn (personal communication, 1996) recently reported an apatite fission-track age of 146 Ma from the Tintic Formation in the hanging wall of the Canyon Range thrust at the north end of the Canyon Mountains, near stop 6. Thus, the relationships in the Canyon Mountains in combination with regional stratigraphic data suggest that the Canyon Range thrust experienced its main phase of displacement during Early Cretaceous or latest Jurassic time and was subsequently folded and reactivated during emplacement of younger, underlying thrusts during Late Cretaceous-Paleocene time (fig. 4).

A west-trending oblique ramp in the Pavant thrust, termed here the Oak Creek ramp, crosses the range at this point. South of the ramp, Proterozoic rocks in the hanging wall structurally overlie Devonian dolostones of the footwall (Millard, 1983). Northward from the ramp, the Canyon Range Conglomerate is preserved beneath Proterozoic

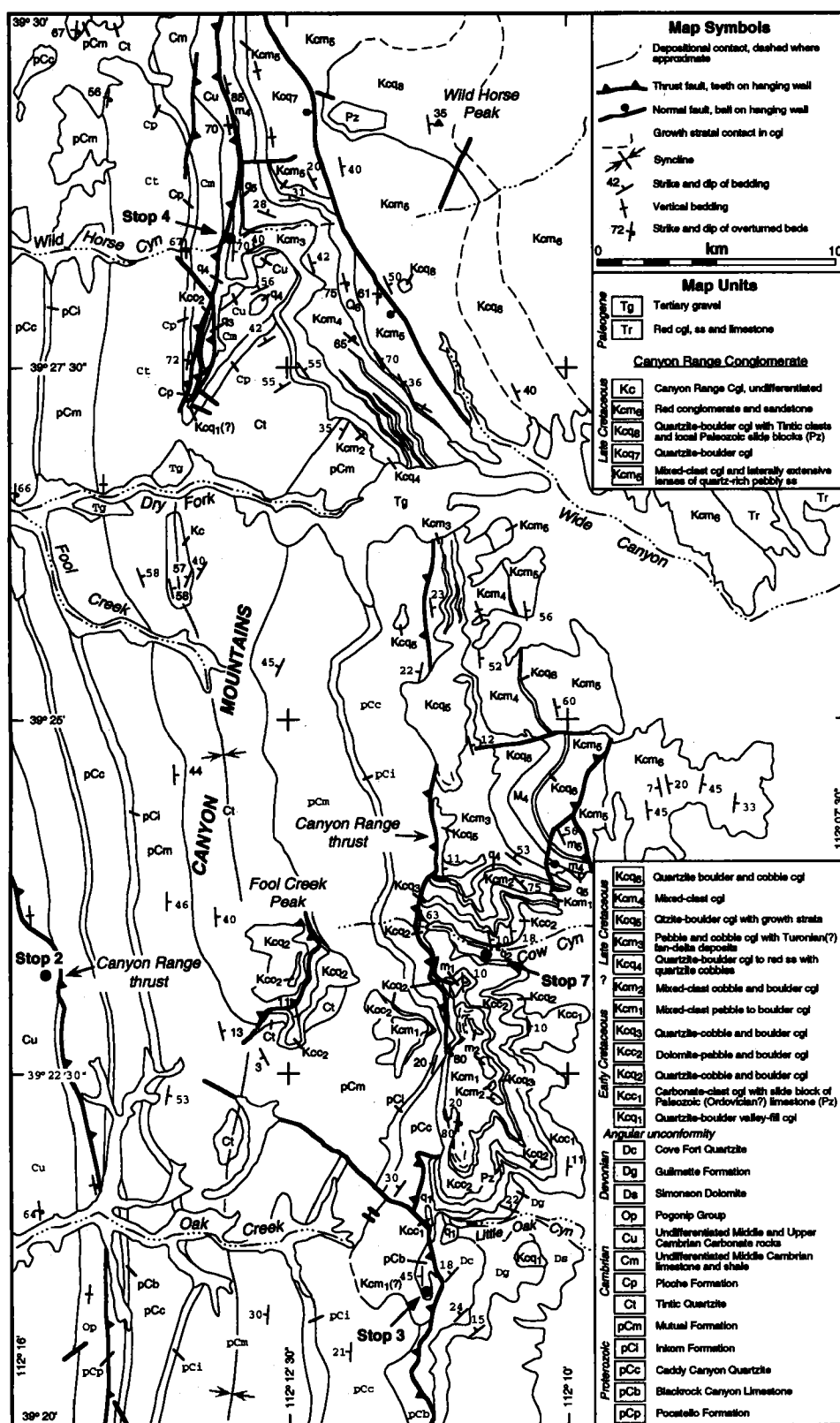
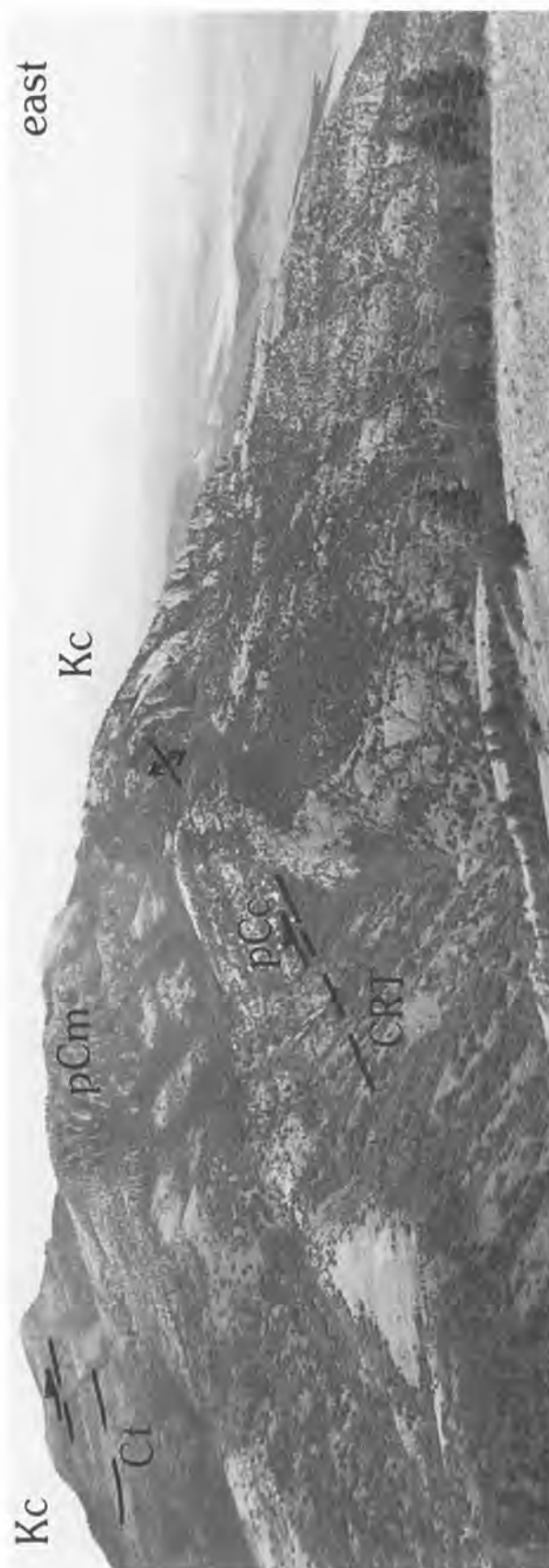


Figure 10. Geologic map of the northern part of the Canyon Mountains. Pre-Cretaceous geology modified from Millard (1983), Holladay (1984) and Hintze (1991 b, c).



hanging-wall rocks and unconformably overlies Devonian strata in the footwall (Millard, 1983). The leading edge of the Canyon Range thrust descends in elevation from south to north, but is less deformed than footwall rocks, which dip north as much as 60° at the ramp. Structural relationships thus indicate the ramp formed prior to late emplacement of the Canyon Range thrust over the conglomerate.

Retrace route to vehicle and return west down Oak Creek Canyon.

- (32.7, 8.1) Center and Main (Utah Route 125) Streets, Oak City. Turn right (north) on Utah Route 125.
- (37.5, 4.8) Intermountain Power Plant in the Sevier Desert at 9:00 (west). The flats in near distance are Pleistocene Lake Bonneville beds dotted with partially vegetated dunes.
- (39.6, 2.1) Low hills at 3:00 (east) are underlain by Oak City Formation (Miocene).
- (40.3, 0.7) Dirt road to Fool Creek Canyon on right.
- (42.1, 1.8) Leamington Pass road (gravel). Turn right (east). Red strata of Mutual Formation form the base of the Canyon Mountains north of Pass Canyon.
- (43.3, 1.2) Cattle guard at entrance to Fishlake National Forest (Forest Road 086). Strike ridge at 3:00 (south) is Proterozoic Caddy Canyon Quartzite. A gravel pit is present to the southwest in the alluvial fan at the mouth of Pass Canyon. All clasts in this fan are Precambrian and Paleozoic lithic types derived from the nearby Canyon Mountains, demonstrating that the Sevier River, which transports volcanic clasts, has never flowed through Leamington Pass.
- (43.6, 0.3) Turn right on Forest Road 425 (dirt) and proceed south along the strike valley in Inkom Formation.
- (44.1, 0.5) Bear left (south) at Y intersection formed by power line road.

Figure 11. Panorama of Canyon Range thrust (CRT) and progressive syntectonic unconformity in Canyon Range conglomerate (Kc) at stop 3, Little Oak Canyon. Thrust, carrying Caddy Canyon Quartzite (pCc) in its hanging wall, cuts lower part of conglomerate in center of photo, but younger part of conglomerate is folded to form a tip anticline over thrust (center skyline). Canyon Range conglomerate on Fool Creek Peak (upper left) unconformably overlies Tintic Quartzite (Ct) in core of Canyon Range syncline. Conglomerate on Fool Creek Peak is duplicated by a minor out-of-the-syncline thrust (fig. 10). Mutual Formation (pCm) is in east flank of Canyon Range syncline.

- (45.2, 1.1) Bear right (south) at small side canyon. Passing outcrops of the Mutual Formation on the left (east).
- (45.7, 0.5) Left at T intersection at mouth of Wild Horse Canyon. Proceed east.
- (46.4, 0.7) Gate. Crossing contact between Proterozoic Mutual Formation and Cambrian Tintic Quartzite.
- (47.0, 0.6) Contact of Tintic Quartzite and Lower Cambrian Pioche Formation is exposed in the saddle on the right. In the next 0.3 mile, ridges of Middle Cambrian limestone formations alternate with strike valleys composed of eroded, poorly exposed shale formations. Beds are vertical, with stratigraphic tops to the east. The succession above the Pioche Formation is Howell Limestone, Chisholm Formation, Dome Limestone, Whirlwind Formation, and Swasey Limestone (fig. 12). The Paleozoic section on the west limb of the Canyon Range syncline in the main drainage of Wild Horse Canyon is truncated above the Swasey Limestone where it is thrust over the Canyon Range Conglomerate (figs. 10, 12). North of the the main drainage, the Middle Cambrian Wheeler and Pierson Cove formations are present in the hanging wall of the thrust (fig. 12).
- (47.3, 0.3) **Stop 4. Canyon Range syncline, Wild Horse Canyon.** Moderately strenuous one-half mile walk up ridge to south, approximately 1 hour.

Units of the Canyon Range Conglomerate at stop 4 are compositionally distinct with sharp contacts, making it possible to confidently differentiate units according to their clast populations (fig. 12). Red-weathering, quartzite-cobble conglomerate (Kcq4) dominated by Tintic and Pioche clasts forms the basal conglomerate of the Canyon Range Conglomerate at the stop. Pioche clasts are purplish-red and contain muscovite and glauconite; Tintic clasts are tan and white. The overlying conglomerate (Kcm3) contains limestone and dolostone pebbles mostly from Devonian and Mississippian formations, but Cambrian units of mottled gray and tan limestone are present as well. This unit forms an upward-coarsening succession with wave ripples and hummocky cross stratification interpreted by DeCelles et al., (1995) as a fan-delta deposit. This unit is postulated to represent deposits of the Turonian sea-level high stand in the Western Interior, an interpretation supported by physical correlation with Cenomanian-Turonian strata present in the subsurface of the Valley Mountains and Pavant Range to the southeast of this locality (figs. 5, 6). Follow the carbonate

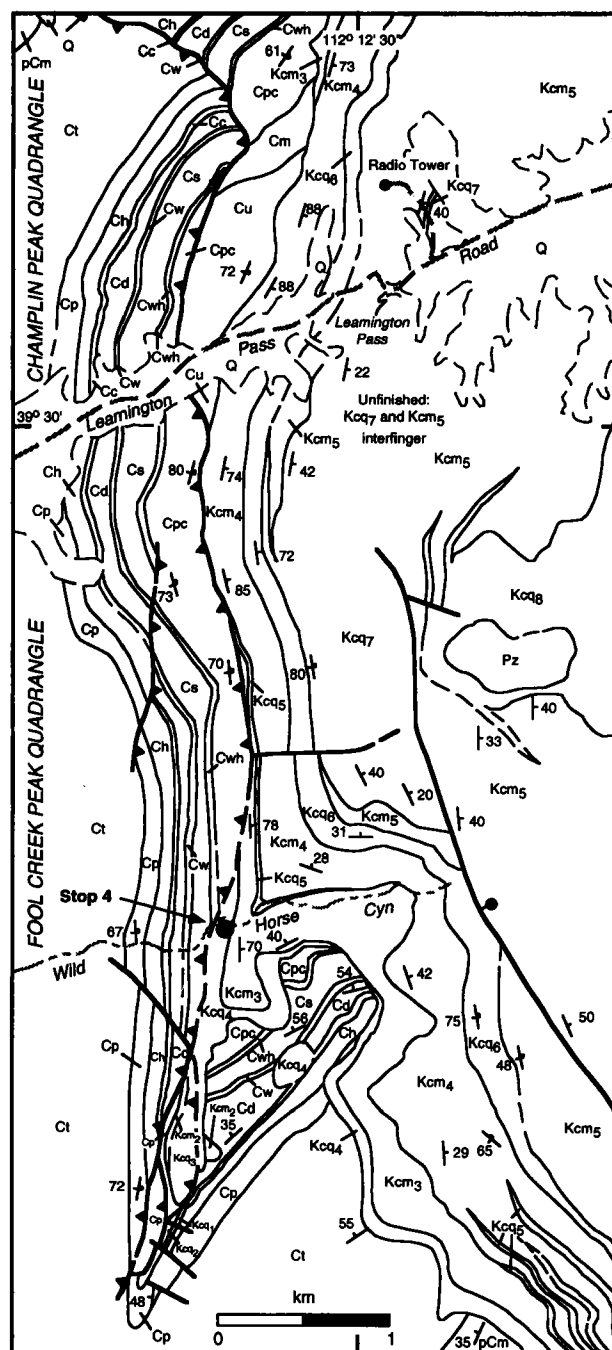


Figure 12. Geologic map of Canyon Mountains in vicinity of stop 4, Wild Horse Canyon to Pass Canyon. Explanation; pCm, Mutual Formation; Ct, Tintic Quartzite; Cp, Pioche Formation; Ch, Howell Limestone; Cc, Chisholm Formation; Cd, Dome Limestone; Cu, Whirlwind Formation; Cs, Swasey Limestone; Cwh, Wheeler Formation; Cpc, Pierson Cove Formation; Cm, undifferentiated Middle Cambrian rocks; Cu, undifferentiated Upper Cambrian rocks. Pz, undifferentiated rock-avalanche deposits composed of lower Paleozoic rocks; Q, undifferentiated surficial deposits. Units of Canyon Range Conglomerate are in figure 10 explanation. Geology of Paleozoic units modified from Holladay (1984) and Hintze (1991b).

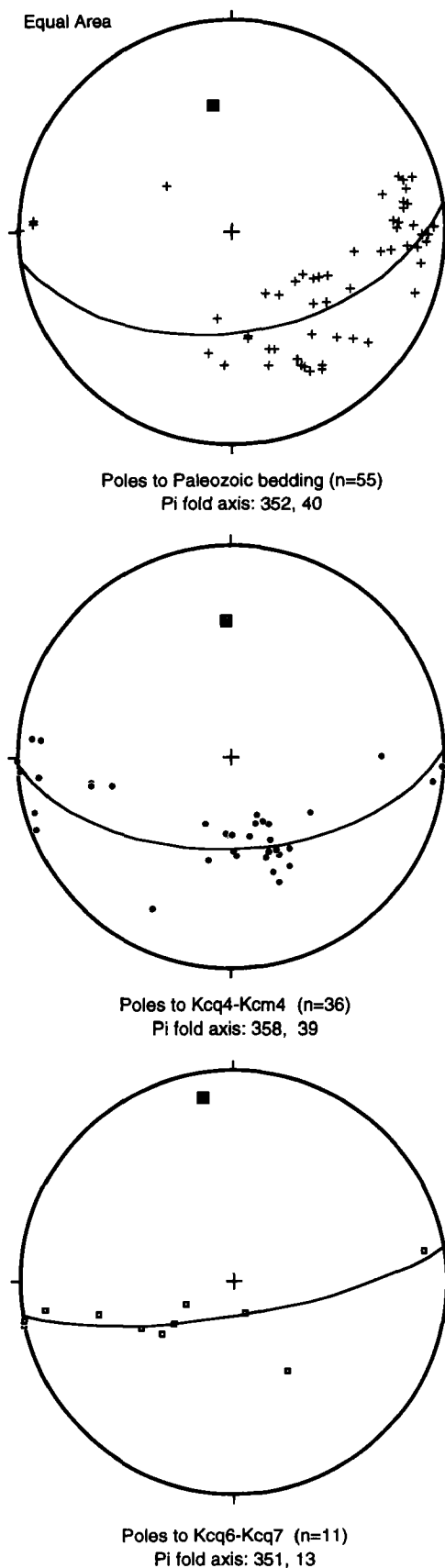
conglomerate exposures upslope to a saddle for views of the Canyon Range syncline.

The syncline at this locality consists of a vertical to overturned west limb and a moderately dipping east limb. Older conglomerate beds are more deformed than younger beds; on the ridge north of Wild Horse Canyon, bedding dips decrease within a quartzite-boulder conglomerate (Kcq7) in the hinge of the syncline (fig. 12). These features indicate that conglomerate was deposited during tightening of the syncline. The fold in the Canyon Range Conglomerate plunges northward at Wild Horse Canyon, with plunges decreasing in progressively younger units (fig. 13). The plunge is inferred to result from an oblique ramp in the Canyon Range thrust (Pequera et al., 1994), termed the Wild Horse ramp. At this point, the Canyon Range and Pavant thrusts apparently dip northward, resulting in preservation of progressively younger strata northward in the hanging wall of the Canyon Range thrust. As a result of the northward dip of the thrusts, the region between here and Leamington Canyon to the north was the structurally lowest part of the thrust belt. Fluvial conglomerate was transported through this zone from the interior part of the thrust belt (Lawton et al., 1994; DeCelles et al., 1995). Imbrication in fluvial facies of the Canyon Range Conglomerate indicates southeast dispersal in this region (Lawton, unpublished data).

Retrace route to Utah Route 125.

- (52.4, 5.1) Right (north) on Utah Route 125. For the next 1.2 miles, the road traverses Fool Creek Flats, a surface on Pleistocene Lake Bonneville beds.
- (53.6, 1.2) Descending terrace into valley of Sevier River cut to post-Pleistocene level of Sevier Lake.
- (54.9, 1.3) Turn right (west) on Utah Route 132, pass through downtown Leamington, and return to Delta via Lynndyl, approximately 21 miles. End of Day 1 road log.

Figure 13. Equal area stereonet plots of bedding poles and pi axes of stratigraphic units in syncline at Wild Horse Canyon. Pi axes are coincident for upper two plots that summarize poles to bedding for Paleozoic strata and lower four conglomerate units exposed in Wildhorse Canyon. Pi axis for younger conglomerate beds (bottom plot) has approximately 20° shallower plunge, indicating that ramp affected Paleozoic strata and older conglomerate equally, whereas younger conglomerate was affected less, probably as a result of deposition during ramp formation.



Day 2. Leamington cross-strike discontinuity, Cow Canyon, Western San Pitch Mountains. Road log begins at junction of Utah Routes 132 and 125 immediately east of Leamington.

- (0.0) Depart junction with Utah Route 125, heading east on Utah Route 132.
- (0.9, 0.9) Steeply dipping Caddy Canyon Quartzite at 9:00 (north of Sevier River) is in hanging wall of the Canyon Range thrust.
- (1.4, 0.5) Charcoal-making ovens on left side of road.
- (2.0, 0.6) Saddle at 4:00 contains Inkorn Formation; brown hill on left is Caddy Canyon Quartzite. Exposures of the Mutual Formation are on the left (red exposures).
- (3.3, 1.3) Millard County line. Lake Bonneville beds in roadcut on right. On right immediately ahead, bedding surfaces of vertical Tintic beds and Mutual-Tintic contact are exposed.
- (4.5, 1.2) Passing under cement conveyor. Ash Grove Cement Company quarries Swasey Limestone from vertical beds to the south.
- (5.5, 1.0) Pull over on right onto old highway right-of-way. Vertical beds of Tintic Quartzite face south.

Stop 5. Canyon Range Conglomerate at Leamington Canyon. Easy one-half mile climb up hillside. Approximately 1 hour.

Boulder conglomerate with abundant Caddy Canyon, Mutual, Tintic, and Pioche clasts overlies Tintic Quartzite at this locality (fig. 14). This clast assemblage is typical of conglomerate derived from the hanging wall of the Canyon Range thrust, which contains the only nearby exposures of Proterozoic strata. Angular unconformities within the conglomerate cause northward thinning here and nearer the cement plant, and suggest that these are growth strata. These quartzite-clast conglomerates rest on Paleozoic strata at this locality, but lateral equivalents of these units overlie mixed-clast conglomerate west of the cement plant (fig. 14), nearer the axis of the Canyon Range syncline. The boulder conglomerate represents alluvial-fan deposits locally sourced from rocks in the hanging wall of the Canyon Range thrust. The alluvial-fan deposits interfinger westward with imbricated pebble conglomerate composed of lower Paleozoic limestone and dolostone clasts derived from the strata now exposed in the House Range to the west (DeCelles et al., 1995). Large slide blocks and debris-avalanche deposits of Cambrian limestone are present in the zone of interfingering with the fluvial strata. We tentatively correlate one of these units (Kcq4; fig. 14) with the Dakota Sandstone of the Colorado Plateau (fig. 6). Angular unconformities between conglomerate beds, coarse grain size of the conglomerate

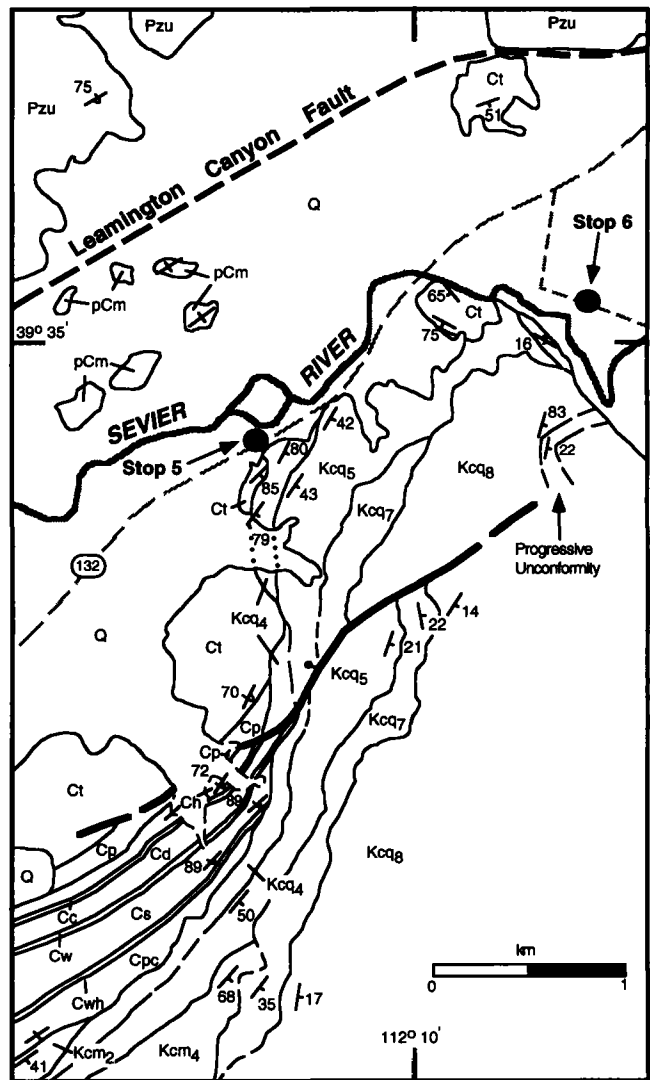


Figure 14. Geologic map of Leamington Canyon area, vicinity of stops 5 and 6. Pre-Cretaceous units and surficial deposits modified from Higgins (1982). See figure 12 for explanation of map units. Additional unit: Pzu, upper Paleozoic sedimentary rocks.

facies, and slide blocks in conglomerate along strike indicate that the steep attitudes associated with the Leamington cross-strike discontinuity began to form early in the depositional history of the Canyon Range Conglomerate, perhaps at the beginning of the Late Cretaceous; therefore, this cross-strike discontinuity is not a late feature in the history of thrust kinematics in central Utah. We infer that folding associated with the formation of the Leamington cross-strike structural discontinuity took place during the deposition of the quartzite-clast conglomerate at Stop 5.

The Leamington cross-strike discontinuity is probably the Canyon Range thrust folded to a near-vertical attitude.

The structural discontinuity is expressed as a juxtaposition of northeast-striking Proterozoic and Cambrian strata with Upper Paleozoic strata of the Gilson Mountains (fig. 14). North of stop 5, across the Sevier River, vertical, south-facing beds of the Mutual Formation are in fault contact with Pennsylvanian Oquirrh Group strata (Higgins, 1982). The fault has a steep southward dip in Leamington Canyon (Higgins, 1982). This structure was interpreted as a transcurrent fault by Morris (1983); however, Precambrian, Cambrian, and Cretaceous strata south of the fault change strike to north-south near the western flank of the Canyon Mountains, and are continuous with strata in the hanging wall of the Canyon Range thrust throughout the Canyon Mountains, indicating the likelihood that this fault is contiguous with the Canyon Range thrust. If one accepts that the fault in Leamington Canyon is indeed the Canyon Range thrust, three conclusions may be drawn: 1) The Leamington cross-strike discontinuity is a folded hanging-wall ramp in the Canyon Range thrust that cuts upsection eastward from the Caddy Canyon Quartzite (west of figure 14) to the Tintic Quartzite (fig. 14); 2) there is a footwall ramp north of Wild Horse Canyon on which the Canyon Range thrust rises from Precambrian to Pennsylvanian strata; 3) the Canyon Range thrust was folded and uplifted by propagation of a deeper thrust during deposition of the alluvial-fan deposits at stop 5.

Continue east on Utah Route 132.

- (6.6, 1.1) Bridge over Sevier River. Quarry on south bank in vertical beds of Tintic Quartzite, facing west. J.K. Linn (personal communication, 1996) reported an apatite fission-track age of 146 Ma from the quartzite at this locality.
- (6.9, 0.3) Turn right (south) on dirt road. Bear left after 0.3 mile and proceed upstream for 0.2 mile.

Stop 6. Progressive unconformity at Sevier River.

Northeast-dipping and -thickening beds of conglomerate are present across the river at this point (fig. 15). Similar features consisting of wedge-shaped, unconformity-bounded bodies of conglomerate that thin onto the flanks of folds or basement uplifts in the Ebro basin of Spain were termed progressive syntectonic unconformities by Riba (1976) and interpreted by him to have formed as a result of deposition during on-going deformation and uplift. These conglomerate beds are part of the youngest coarse quartzite-clast conglomerate lithosome (Kcq8) in the the Canyon Mountains (fig. 14). At Leamington Pass to the south, near the axis of the Canyon Range syncline, Kcq8 overlies a very thick interval of mixed-clast conglomerate (Kcm5) of fluvial origin (figs. 10, 12, 14). The base of Kcq8 cuts down section to the northeast, causing this distinctive, orange-weathering, Tintic-clast conglomerate to rest on somewhat older conglomerate (Kcq7) at Leamington Canyon (fig. 14). The de-



Figure 15. Progressive unconformity in the Canyon Range Conglomerate along the Sevier River, north end of the Canyon Mountains at stop 6. Conglomerate beds on light-gray face in center of photo dip steeply toward viewer; beds on left thin onto older conglomerate and decrease in dip upsection.

formation that caused this angular discordance was likely displacement of the leading edge of the Canyon Range thrust or a related splay. North of the progressive unconformity, overturned mixed-clast conglomerate dips shallowly westward, and appears to be beneath Tintic Quartzite exposed northward along the river and at the quarry near the highway bridge (fig. 14). We interpret these exposures as Tintic thrust above overturned conglomerate and overlapped by younger conglomerate (Kcq5) derived from the hanging wall of the Canyon Range thrust. This may be the northernmost exposure of the leading edge of the Canyon Range thrust. Similar relationships are better exposed at the next stop.

Return to highway and retrace route westward to Utah Route 125 at Leamington.

- (13.8, 6.9) Turn left (south) on State Route 125.
- (16.3, 2.5) Turn left (east) at Leamington Pass road (gravel).
- (17.4, 1.1) West-vergent, out-of-syncline reverse fault at 3:00 (south) emplaces Howell Limestone over Pioche Formation.
- (18.9, 1.5) Leamington Pass. Leaving Fishlake National Forest. The road descends a valley north of Wild Horse Peak, which is underlain by Tintic-clast conglomerate (Kcq8) of Stop 6. Red conglomeratic beds on the east flank of Wild Horse Peak have been assigned to the upper member of the Canyon Range Formation (Holladay, 1984). The road winds through Flagstaff Limestone beveled by a pediment surface that was graded to the Sevier River when it flowed into Pleistocene Lake Bonneville.
- (26.2, 7.3) Cuesta straight ahead to the northeast is underlain by North Horn Formation (red) and Flag-

staff Limestone (white). Mt. Nebo, composed of Paleozoic strata, is slightly to the left and beyond the cuesta.

- (27.6, 1.4) Intersection with road to Mills, Utah. Proceed straight (south).
- (28.4, 0.8) Ascend grade through Sevier River delta of Lake Bonneville highstand. Top of grade at elevation 1520 m. Pebbles of this gravel accumulation include silicic welded tuffs, intermediate volcanic rocks, subordinate dark gray chert, sandstone, and oolitic chert. Provenance is Tertiary Marysvalde volcanic field and Mesozoic and Tertiary strata exposed in the upper drainage basin of the Sevier River to the south.
- (29.1, 0.7) Pass road to Wide Canyon on right (west). Continue straight.
- (33.1, 4.0) Turn right (west) at fenceline.
- (33.6, 0.5) Crossing from Lake Bonneville deposits to alluvial-fan deposits. The lake beds form bottomless dust or mud, depending upon time of year. Quaternary fans are graded to this level. In wet years in the spring, this grassland is a vast expanse of green. It is common to see Ferruginous Hawks and Long-Billed Curlews migrating through.
- (33.7, 0.1) Bear left (west). Road to right goes to Wide Canyon, by way of a gate that is nearly impossible to close. A gate is also present on the field trip route in 0.1 mile. Be sure to leave gates as they are found, whether open or closed.
- (35.8, 2.1) Gate at Fishlake National Forest Boundary. Folded Canyon Range Conglomerate on ridge to north. Road becomes increasingly steep as it climbs the proximal part of the Cow Canyon alluvial fan.
- (36.9, 1.1) Turn right at 3-way intersection deep in Gambel Oak thicket.
- (37.2, 0.3) Park at watering trough on left (south side of road).

Stop 7. Cow Canyon: Footwall Canyon Range Conglomerate, Canyon Range thrust. Walk uphill to the north, approximately 1 mile. 2 hours.

At Cow Canyon (fig. 10), quartzite-boulder conglomerate derived from the the Canyon Range sheet is interbedded with mixed-clast conglomerate of interior thrust belt provenance. Conglomerate lithosomes are easily differentiated by composition, and paleosols are developed on the tops of most lithosomes, particularly on the mixed-clast conglomerates at this locality. Alluvial-fan lithosomes, represented by the quartzite-boulder units, can be traced to paleovalleys eroded into the hanging wall. These paleoval-

leys were backfilled with conglomerate, and folded over the tip of the thrust during its late phases of displacement (fig. 10). The alluvial-fan lithosomes have along-strike dimensions of 5–10 km; their edges break up and interfinger to the north with the more distal, fluvial conglomerates. To the northwest, Caddy Canyon Quartzite of the hanging wall overrides the quartzite-clast lithosomes, and mixed-clast units thin toward the thrust (fig. 16). Each of three folded alluvial-fan deposits on the north side of Cow Canyon has a separate, distinct axial surface, indicating that fold growth was spatially discontinuous and may have involved both kink-band migration and progressive limb rotation.

From a vantage point on the ridge north of Cow Canyon, the conglomerate on the south side of the canyon can be seen to steepen from 10° east dips to form a fold that probably represents a tip anticline, possibly on a splay of the Canyon Range thrust. As discussed at stop 3, the impressive exposures here record only late and minor (several hundred meters) displacement on the Canyon Range thrust. Prior to deposition of the Canyon Range Conglomerate, Proterozoic rocks were emplaced on strata as young as Devonian, and both the hanging wall and the footwall of the Canyon Range thrust (the latter being also the hanging wall of the Pavant thrust) were deeply eroded. Conglomerate was then deposited on Devonian strata of the footwall. The conglomerate in the footwall is approximately 600 m thick on the ridge north of Cow Canyon. We tentatively correlate this conglomerate with middle to late Albian beds, also unconformable on Devonian strata of the hanging wall of the Pavant thrust, that were encountered in drill holes, including the Placid WXC USA 1-2 (fig. 1), on the west side of the Valley Mountains, visible to the southeast. The late Albian age of these subsurface beds is inferred from their stratigraphic position beneath strata that contain Cenomanian to Turonian palynomorphs (Pavant Sandstone of figure 6; G.L. Waanders, written communications, 1982, 1993). These stratigraphic relations indicate that much of the hanging wall of the Pavant thrust was buried by the end of the Albian and probably did not subsequently serve as an important source of first-cycle detritus.

Return to vehicles and proceed back down Cow Canyon road.

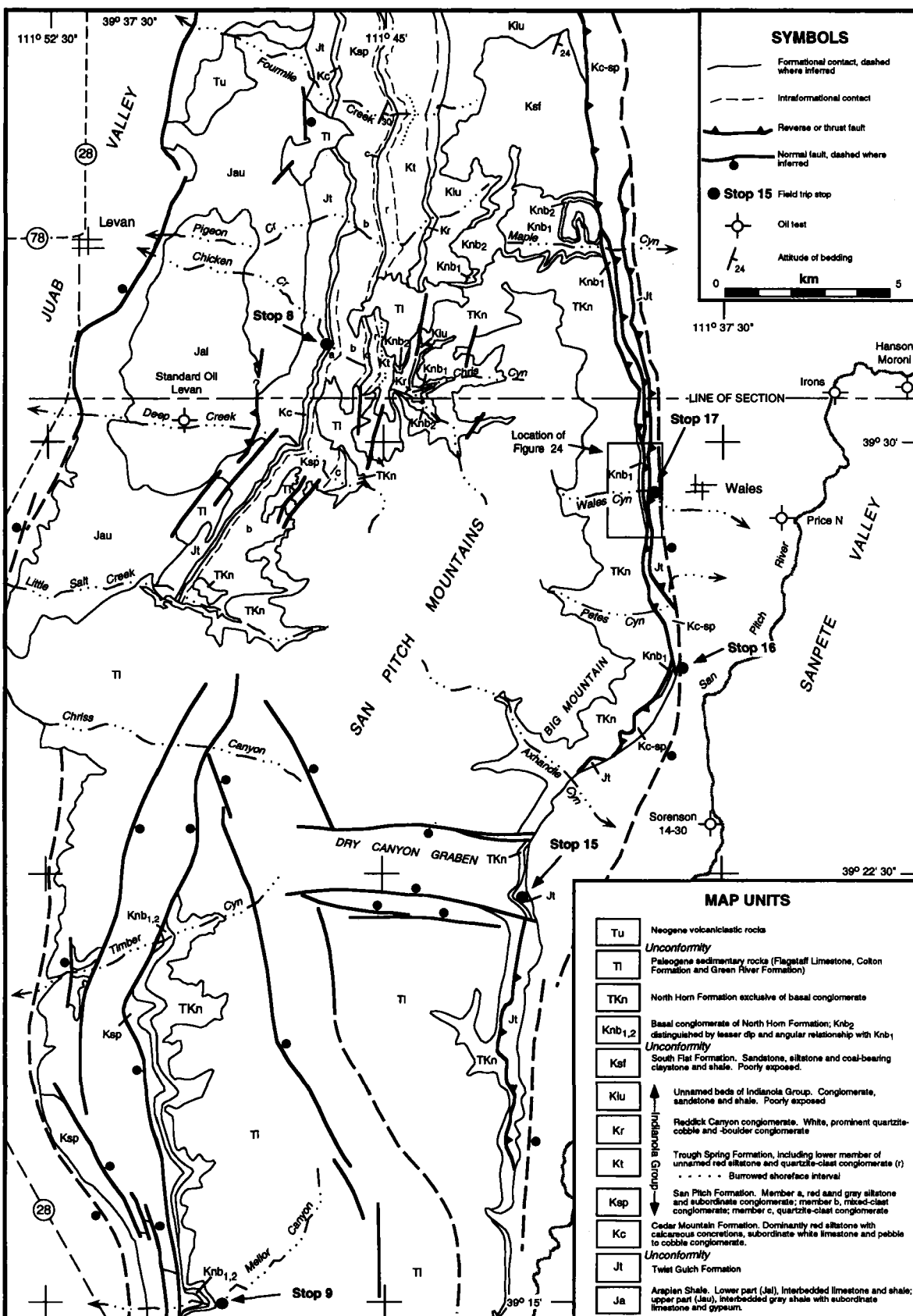
- (37.5, 0.3) Turn right at 3-way intersection in oak thicket. High clearance required for the next mile.
- (38.8, 1.3) Bear left at junction. Road to right ends in 0.9 mile at a flagstone quarry in a lacustrine fan-delta unit at the base of a carbonate-clast conglomerate (Kcc2 of figure 10). Footwall conglomerate, dipping homoclinally 11 degrees east, is exposed to the west along the front of Canyon Mountains. Flatirons on upper slopes

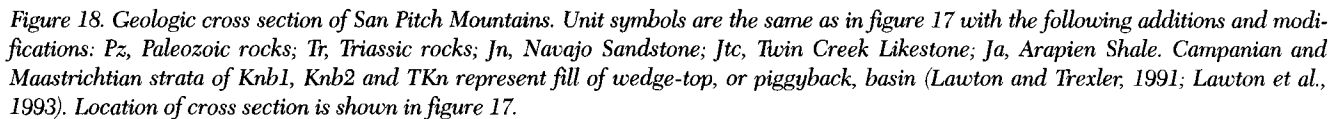


Figure 16. View of north wall of Cow Canyon, looking north. Homoclinal, east-dipping conglomerate is folded beneath Canyon Range thrust (arrow). Thrust emplaces Caddy Canyon Quartzite (pCc) over alluvial-fan lithosomes Kcq2 through Kcq5 of the Canyon Range Conglomerate (fig. 10).

- are the same beds folded over the front of the Canyon Range thrust.
- (39.7, 0.9) Gate at east boundary of Fishlake National Forest. The road descends the gentle slope of a sage brush-covered grassland, home of Lark and Vesper Sparrows, Horned Larks, Sage Thrashers and Western Meadowlarks.
- (43.8, 4.1) Gate at frontage road, west side of I-15. Turn left (north) on frontage road. You should have passed four gates since leaving the National Forest. From here, there is a view westward of the Oak Canyon lateral ramp in the hanging wall of the Pavant thrust (fig. 10). On the south side of the ramp, the Canyon Range thrust emplaces Proterozoic over Devonian strata, which dip steeply northward at the ramp. The Canyon Range thrust descends from south to north as well, but not as steeply as footwall beds. North of the ramp, the Canyon Range thrust overrides footwall Canyon Range Conglomerate. Basal conglomerate (Kcq1) also dips steeply northward at the ramp to form discontinuous exposures on Devonian beds south of Little Oak Creek Canyon. These relationships show that late movement of the Canyon Range thrust largely postdates development of the ramp in the hanging wall of Pavant thrust.
- (50.5, 6,7) Cross overpass (Interchange 202, Yuba Lake) to east side of I-15 and enter interstate heading north. Views of Canyon Mountains to the west. Highest point is Fool Creek Peak, composed of Tintic Quartzite overlain by Canyon Range Conglomerate.
- (54.4, 3.9) Exit I-15 at Interchange 207. Turn right (east) on Utah Route 78 toward Levan.
- (63.3, 8.9) Junction Utah Routes 78 and 28. Turn right (south) on Utah Route 28.
- (63.5, 0.2) Turn left (east) on First South Street in Levan. Directly ahead are outcrops of Jurassic Arapien Shale that forms the western foothills of the San Pitch Mountains. The Arapien is folded and faulted, and oil wells drilled in this belt to the south indicate that the Jurassic Navajo Sandstone beneath the Arapien is duplicated (figs. 17, 18; Ritzma, 1972). This belt of deformation has been interpreted as a duplex zone associated with a ramp in the Gunnison thrust (Standlee, 1982; Lawton, 1985) and as an anti-formal stack or triangle zone above the tip of the Paxton thrust (Coogan et al., 1995).

Figure 17. Geologic map of the San Pitch Mountains. Geology modified from Mattox (1987), Witkind et al., (1987), Auby (1991), Witkind and Weiss (1991), Fong (1995), and Lawton and Weiss (in press).





- thick here and range in age from Neocomian(?)–late Albian. This represents the maximum thickness of Lower Cretaceous strata in the region and marks the foredeep depozone of the foreland-basin system at that time. Beds low in the San Pitch Formation within 50 m of the Cedar Mountain Formation are middle Albian (G.L. Waanders, written communication, 1992). Clasts of Paleozoic limestone and dolostone and Mesozoic sandstone were derived primarily from the hanging wall of the Pavant thrust, whose tip lay only a few km to the west; subordinate quartzite clasts were derived from the hanging wall of the Canyon Range thrust.

(69.7, 0.6) Beds of cobble conglomerate of the San Pitch Formation alternate with red sandy siltstone beds as much as several tens of meters thick. Furrows on the bases of beds indicate northeast or southwest sediment dispersal, parallel to the foredeep. Although the thick parts of foreland basins are commonly referred to as foredeeps (e.g., DeCelles and Giles, 1995), this stratigraphic section, composed entirely of fluvial deposits, illustrates that foredeeps need not be bathymetrically deep.

(70.6, 0.9) Higher in the section, shallow-marine deposits of probable Turonian age are exposed along the road. These deposits represent the maximum transgression into the region of the San Pitch Mountains and probably correlate with the fan-delta deposits in the Canyon Range syncline at Stop 4.

(71.0, 0.4) Massive boulder conglomerate of the Reddick Canyon Conglomerate (Santonian?) at Reddick Canyon represents the initial incursion of alluvial-fan deposits into this part of the basin. Although the conglomerate is primarily clast supported, abundant boulder clusters adja-

cent to boulder-filled channels are interpreted as debris-flow levees. Sediment dispersal was eastward, indicated by measured orientations of channels filled with sandy siltstone and furrows on bases of conglomerate beds. The Red-dick Canyon Conglomerate pinches out gradually to the north. There is no apparent angularity at the basal contact; in fact, the unit appears to coarsen upward from wave-rippled conglomerate and sandstone, and may have begun as a fan delta. This unit also has been interpreted as an incised valley-fill succession (Schwans, 1995). We regard it instead as a major alluvial-fan lithosome.

- (71.3, 0.3) At Chris Canyon, quartzite-boulder conglomerate overlies a series of paleosols and shows a progressive decrease in dip upsection. Massive conglomerate contains fluid-escape and slump structures. The angular discordance at this point in the section causes removal of Campanian and Santonian beds from north to south along the range (fig. 17). Schwans (1995) has termed this unit the Chris Canyon Conglomerate. We consider it equivalent to beds recently assigned to the basal North Horn on the east side of the range (fig. 17; Lawton et al., 1993). The changing dip upsection and slump features indicate that this interval is a progressive unconformity formed by deposition concomitant deposition with growth of the fault-bend fold in the western San Pitch Mountains. Progressive unconformities are also present on the east side of the range in the basal North Horn Formation (Lawton and Trexler, 1991; Lawton et al., 1993), associated with west-vergent thrusting above the decollement of the Gunnison thrust. These features record the initiation of the Axhandle basin, a wedge-top basin filled with fluvial and lacustrine deposits above the Gunnison thrust in middle to late Campanian time (Lawton et al., 1993). The Axhandle basin occupies most of the San Pitch Mountains, and is flanked by an antiformal duplex or fault-bend fold on the west side of the range and a west-vergent fault-propagation fold on the east side.

Retrace route to Levan.

- (79.1, 7.8) Turn left, (south) on Utah Route 28.
 (80.1, 1.0) Utah Route 28 runs along the east side of Juab Valley, paralleling the Levan segment of the Wasatch fault system.
 (80.8, 0.7) Fanhead fault scarp (just below Juniper trees) in small alluvial fan on left (east). Scarps are

also exposed on the heads of alluvial fans for the next few miles. Tan-weathering beds of the Eocene Green River Formation are exposed low along the flank of the range

- (82.0, 1.2) Deep Creek Canyon on left (east). The Standard Oil of California Levan well was drilled in this canyon in 1959. It spudded in the Jurassic Arapien Shale, penetrated an upright section of the Jurassic Navajo Sandstone and Triassic redbeds, and bottomed in the Navajo Sandstone (fig. 18; Ritzma, 1972).
 (88.6, 6.6) Skinner Peaks at 10:00 (southeast). Caprock dipping WSW is Green River Formation. Arapien Shale underlies the Green River Formation and forms the lower slopes. This is probably a diapiric piercement structure, circular in plan view, but the Green River Formation is depositional on the Arapien Shale. Red, white, and orange beds in the vicinity are volcanoclastic Goldens Ranch Formation (Oligocene)
 (91.9, 3.3) Golden's Ranch Formation (Oligocene volcanoclastics) form the hills to west of highway. These strata are in the hanging wall of the Wasatch normal fault system
 (92.9, 1.0) Sanpete County Line; begin descent into Sevier Valley.
 (96.6, 3.7) Craggs at 9:00 (east) are San Pitch Formation of the Indianola Group, dipping west, in vicinity of Hells Kitchen Canyon (fig. 17). The north-trending Chriss-Mellor graben system of Mattox (1987) separates the west-dipping strata from east-dipping strata on the east side of graben. The graben system marks the crest of a fault-bend fold in the hanging wall of the Gunnison thrust system. Exposures of the San Pitch Formation continue for 3.5 mi along range front. West of the conglomerate exposures, the Fayette segment of Wasatch fault zone is expressed as scarps in dissected alluvium.
 (102.5, 5.9) Mellor Canyon road. Turn left (east) at gate.
 (103.0, 0.5) Cross Fayette fault. First exposures along mountain front are west-dipping panels of Flagstaff Limestone (Paleocene-Eocene).
 (103.5, 0.5) Entering Chriss-Mellor graben system. Conglomerate of the Indianola Group is exposed on both sides of road.
 (104.2, 0.7) White-weathering exposures of Mellor Canyon Conglomerate on left (north).

Stop 9. Progressive unconformity in Mellor Canyon Conglomerate. One-half mile walk up hillside to the north. Approximately one hour.

The Mellor Canyon Conglomerate, dominated by Tintic clasts, is exposed in Mellor Canyon east of the Chriss-Mellor graben system (fig. 17). The conglomerate contains dewatering and slump structures related to deformation coeval with deposition (Balcer, 1992). Concurrence of sedimentation and folding here is also indicated by progressive decrease in bed dip upsection through the unit; bed dips continue to shallow upsection through the red-weathering North Horn Formation and Flagstaff Limestone. The Mellor Canyon Conglomerate rests unconformably on conglomeratic strata equivalent to the San Pitch Formation (fig. 17). The subjacent conglomerate contains a population of mixed carbonate and quartzite clasts. The San Pitch Formation was lithified prior to deposition of the Mellor Canyon, indicated by fissures extending downward from the contact and steep-walled segments of the unconformity. The Mellor Canyon Conglomerate is equivalent to the conglomerates at Stop 8 in Chris Canyon. The soft-sediment deformation here signifies development of the fault-bend fold on the west side of the San Pitch Mountains as the Gunnison thrust propagated beneath this locality in the Campanian, the same event recorded by soft-sediment deformation at Chris Canyon.

Flat-bedded sandstone at the top of the main conglomerate unit bevels and fills in topography developed on the underlying conglomerate by slumping. Pebbly sandstone above the main part of the formation is capped by a major rootlet horizon formed during uplift. The Mellor Canyon Conglomerate thins westward and pinches out adjacent to the crest of the fault-bend fold. This relationship is consistent for 13 km northward to Timber Canyon, where the formation is covered by Tertiary strata (fig. 17). Paleocurrents are generally southeastward, down structural dip.

Retrace route to Utah Route 28.

- (105.9, 1.7) Turn left (south) at Utah Route 28.
- (112.4, 6.5) Intersection of Utah Route 28 and U.S. Highway 89. Entering Gunnison. Continue straight (south) on U.S. Highway 89.
- (113.9, 1.5) Entering Centerfield. Valley Mountains are to the west, with the Pavant Range forming the southwestern skyline behind them. Sevier Plateau looms over the southeast flank of Sevier Valley. Tushar Mountains (fig. 5) of the Tertiary Marysvale volcanic field are to the far south.
- (120.0, 6.1) Steeply dipping hogbacks at 10:00–11:00 composed of Eocene Green River Formation, depositional on Eocene Colton Formation, or locally, Arapien Shale in core of anticline.
- (121.3, 1.3) Sevier County line.
- (123.2, 1.9) Redmond Hills are composed of Quaternary sediment on the Arapien Shale, with salt mines locally, at 3:00 (west). Hills of the Arapien

Shale to the south are capped by dark gray Oligocene volcanic rocks.

- (126.4, 3.2) Entering Salina. End day 2 road log.

Day 3. Salina Canyon and Sanpete Valley: Structure and sedimentation associated with Sevier-Sanpete Valley antiform. Road log begins at Mom's Cafe, at Center and Main Streets in downtown Salina.

- (0.0) Proceed east on Main Street.
- (0.2, 0.2) Turn right on 300 East. Proceed south.
- (0.7, 0.5) Hills of member E of Arapien Shale of Hardy (1952) on both sides of road.
- (2.6, 1.9) Member D of Arapien Shale overlain by volcanoclastics of formation of Black Cap Mountain (late Oligocene) and Osiris Tuff (early Miocene) at 9:00 (north) (Willis, 1986).
- (3.0, 0.4) Pavement becomes intermittent, continue straight on gravel road.
- (3.4, 0.4) Arapien Shale on left (north) overlain by Green River Formation dipping west on flank of Wasatch monocline.
- (3.7, 0.3) Steep beds of Twist Gulch Formation on the left are overlain by gently west-dipping red-beds of the Eocene Flagstaff and Colton formations (Willis, 1986).
- (3.8, 0.1) Bear left onto spur road just west of underpass beneath I-70.
- (4.0, 0.2) Pass gate and take first right at fork of dirt road. Angular unconformity above vertical beds of the Twist Gulch Formation is exposed to north.
- (4.2, 0.2) Park at base of slope where tan sandstone is exposed in a steep road cut up the slope. This sandstone is in the Twist Gulch Formation and is equivalent to the base of the Jurassic Curtis Formation of the Colorado Plateau (Willis, 1986; Lawton and Willis, 1987).

Stop 10. Salina Canyon. Early foreland basin stratigraphy at tip of thrust belt. Two mile round-trip walk, east along base of hillslope. Approximately 1.5 hour. This traverse is described in detail by Lawton and Willis (1987).

Jurassic and Cretaceous strata beneath the unconformity with Tertiary strata in Salina Canyon are the most accessible and most eastern exposures of late Mesozoic strata in the thrust belt. This locality is an important link between thrust belt and Colorado Plateau stratigraphy (fig. 6). Steep dips here represent the east flank of the Sevier-Sanpete Valley antiform, a fold in the hanging wall of the Gunnison thrust formed above a decollement in shale and salt of the Arapien Shale (Standlee, 1982; Lawton, 1985).

Beds of the Twist Gulch Formation to the north are recognizable as the upper part of the San Rafael Group, including the Entrada Sandstone, Curtis Formation and

Summerville Formation (Imlay, 1980; Lawton and Willis, 1987). The Summerville Formation is overlain by gray mudstone from which Doug Sprinkel has recently recovered Late Jurassic pollen. Above the mudstone is a chert-pebble conglomerate that contains poorly rounded clasts of silicified wood. Above the conglomerate are white sandstone with crossbeds and gray mudstone beneath drab smectitic mudstone of the Cedar Mountain Formation. The nonmarine section between the Twist Gulch Formation and overlying Lower Cretaceous strata is on the order of 15 m thick and may be the Morrison Formation. Overlying strata are correlative with the Cedar Mountain Formation, indicated by Albian to Cenomanian zircon and apatite fission-track ages (ranging from 85 ± 5 to 105 ± 10 Ma; Willis, 1986; Willis and Kowallis, 1988). The steeply dipping beds crop out as ribs of conglomeratic sandstone and pink and gray siltstone with micrite nodules. The Cedar Mountain Formation is 188 m thick and is overlain by 84 m of conglomeratic strata of the San Pitch Formation, earlier assigned to the upper member of the Pigeon Creek Formation by Schwans (1988). A prominent chert-pebble conglomerate forms the base of the San Pitch Formation (fig. 20). Palynomorphs collected from the top of the San Pitch Formation at this locality include *Tigrisporites scurrandus*, with a middle to late Albian range (G.L. Waanders, written communication, 1992).

The base of the Upper Cretaceous section is a prominent, white-weathering quartzite-clast conglomerate about 10 m thick (fig. 20). It is exposed on both the north and south sides of Salina Canyon. The clast assemblage consists of Tintic Quartzite (70%), very fine grained white quartzite that may be Proterozoic Caddy Canyon Quartzite (25%), red pebbly quartzite of the Mutual Formation (5%), and a trace of pale green quartz arenite with glauconite (Pioche Formation). This conglomerate locally forms the base of the Sanpete Formation, which is equivalent to the Dakota Formation of the Colorado Plateau (Lawton and Willis, 1987; Schwans, 1995). A retrogradational succession overlies a flooding surface on top of the conglomerate. A fine-grained, mottled white sandstone with vertical and horizontal burrows above the conglomerate is overlain by very fine grained tan sandstone with ripples and in turn by brown mudstone. The succeeding three sandstone bodies are 2–3 m thick, with cross beds and burrowed tops, and may be estuarine deposits. The overlying part of the Sanpete Formation consists of tan-weathering sandstone beds with pebble lags that include quartzite, carbonate and chert clasts. Interbedded siltstone is poorly exposed. The uppermost part of the Sanpete Formation consists of an assemblage of burrowed, upward-coarsening shoreface deposits, channelform sandstone beds, and oyster-bearing sandstone. The Sanpete Formation is 380 m thick in Salina Canyon. Overlying the Sanpete is the Allen Valley Shale, composed of gray shale and siltstone beds that contain the middle Turonian ammonite,

Collignonicerias woollgari (Lawton, 1982). The Sanpete Formation and Allen Valley Shale correlate with the Dakota Formation and Tununk Member of the Mancos Shale, respectively, on the east side of the Wasatch Plateau (fig. 6). The lower member of the Funk Valley Formation, equivalent to the Ferron Sandstone to the east (fig. 6), crops out beneath Tertiary strata south of Interstate 70.

These Lower to Upper Cretaceous strata constitute the relatively distal equivalents of the coarse conglomerates exposed in the Canyon Mountains and San Pitch Mountains. Unlike their western, more proximal counterparts, these distal facies lack any evidence of syndepositional, progressive deformation. This absence of progressive deformation distinguishes these rocks as foredeep deposits, in contrast to the wedge-top deposits visited during Days 1 and 2.

Retrace route to vehicles. If you choose to walk along the interstate, be careful of coal trucks descending the grade. Retrace route to downtown Salina.

- (8.4, 4.2) Corner of Main and Center Streets, Salina. Turn right (north) onto U.S. Highway 89.
- (22.4, 14.0) Turn right (east) on U.S. Highway 89 just north of Gunnison. Colored beds to the right are the upper Eocene Crazy Hollow Formation resting on the Green River Formation.
- (23.3, 0.9) Light gray exposures at 2:00–3:00 are outcrops of Arapien Shale in core of Sevier-Sanpete antiform.
- (25.1, 1.8) Pass cuesta of upper Green River Formation on left (north). The strike valley to the northeast is underlain by Colton Formation (Eocene), which is stratigraphically beneath the Green River.
- (26.1, 1.0) Pickup truck on light gray cuesta of Flagstaff Limestone on left.
- (26.9, 0.8) Stop at milepost 213, U.S. Highway 89.

Stop 11. Christianburg. Lower Cretaceous foredeep stratigraphy.

This locality is on the west flank of a large boxlike anticline with faulted flanks and core that underlies Sanpete Valley. Although the base of the Cretaceous section is faulted (figs. 21, 22), this is one of the most complete exposures of the Cedar Mountain and San Pitch formations in the southern part of the San Pitch Mountains (fig. 5). A west-vergent syncline in Cretaceous units is overlapped from the west by Tertiary beds of the North Horn Formation, which forms a progressive unconformity on the flank of the anticline in Sanpete Valley.

Here, beds assigned to the Cedar Mountain (Witkind et al., 1986) or lower member of the Pigeon Creek Formation (Schwans, 1988) consist dominantly of mudstone with abundant calcareous nodules and subordinate sandstone and light gray limestone. The mudstone represents flood-

plain deposits, the calcareous nodules represent paleosol carbonate, and the limestones with oncolites were deposited in freshwater ponds (Schwans, 1988). Soil horizons within the section appear to be composite or stacked, and thus suggest slow deposition punctuated by unconformities.

The base of the upper member of the Pigeon Creek Formation (Schwans, 1988) is at the lowermost conglomerate in the section. Sprinkel and coworkers (in review) suggest the term San Pitch Formation for this section of Lower Cretaceous conglomerate (fig. 22). Conglomerate beds are on the order of 10 m thick and broadly lenticular. They are interbedded with red siltstone and mudstone. Clasts within the lower 57 m include green quartzite clasts of the Proterozoic Dutch Peak Formation, as well as sandstone clasts derived from Jurassic and Triassic Formations. The Dutch Peak Formation is exposed in the Sheeprock Mountains northwest of the San Pitch Mountains, and the Mesozoic clasts were presumably derived from the Pavant thrust sheet to the west. These diverse lithologies were contributed in part by a large Early Cretaceous drainage network that departed the thrust belt at an embayment in the mountain front (Lawton et al., 1994). Overlying conglomerate beds in an interval 96 m thick contain boulders and cobbles of both quartzite and carbonate (mostly dolostone). Interbedded mudstone is reddish orange and silty. The upper 44 m consists of reddish-brown to gray silty mudstone (fig. 22). It is unconformably overlain by a striking quartzite-boulder conglomerate that marks the base of the Sanpete Formation, which is equivalent to the Dakota Sandstone (fig. 6).

Continue north on U.S. Highway 89.

- (27.9, 1.0) Overturned, east-dipping beds of Arapien Shale at 9:00 (north). Ridge is formed by member C, the middle of five members in the Arapien Shale (Weiss, 1994). Member C consists of thin-bedded calcareous shale and mudstone with subordinate thin beds of fossiliferous micrite. Member B, bluish gray and red gypsiferous shale with local halite, is exposed to the right of the highway and on the east flank of the ridge. Exposures of the Arapien Shale are continuous from here southward past Salina and form the core of the Sevier-Sanpete Valley antiform. Two kilometers to the south, all members of the Arapien Shale are exposed in a zone of imbricate reverse faults with west vergence. The decollement of the Gunnison thrust system (fig. 1) apparently lies in evaporite and shale near the base of member A, which is above a Jurassic limestone succession equivalent to the Twin Creek Limestone of northern Utah (Sprinkel, 1982). Member A overlies some thrust faults

Explanation of Symbols used for the measured sections

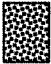

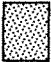
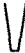
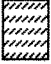

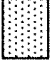

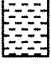




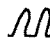



Lithology Type	Sedimentary Structures
 quartzite dominant	 concretion
 carbonate dominant	 burrows
 mixed clast	 roots
 quartzarenite	 trough crossbeds
 mudstone	 wedge crossbeds
 covered	 planar crossbeds
	 wavy crossbeds
	 convoluted beds
	 Fc flute cast
	 tool and groove
	 ripples

Figure 19. Explanation of symbols for measured sections in figures 20 and 22.

in the structural culmination of the Sevier-Sanpete Valley antiform, but older limestone is not exposed.

- (30.2, 2.3) Entering Sterling, Utah.
 (30.9, 0.7) Turn right (east) on road to Palisade Lake State Park.
 (31.6, 0.7) Stop at turnout on left (north side of road), directly east of dirt road to the north.

Stop 12. Overview of type Indianola Group. Fifteen minutes

North-striking strata of the Indianola Group form ridges and valleys to the north of the road. This is the locality at which formations of the group were first defined (Spieker, 1946). These rocks were determined to be Late Cretaceous in age on the basis of marine fossils present in the section here (Spieker and Reeside, 1926; Spieker, 1946). Spieker (1946, 1949) also recognized that these strata coarsen westward to conglomeratic equivalents in the western part of the San Pitch Mountains and postulated a western source

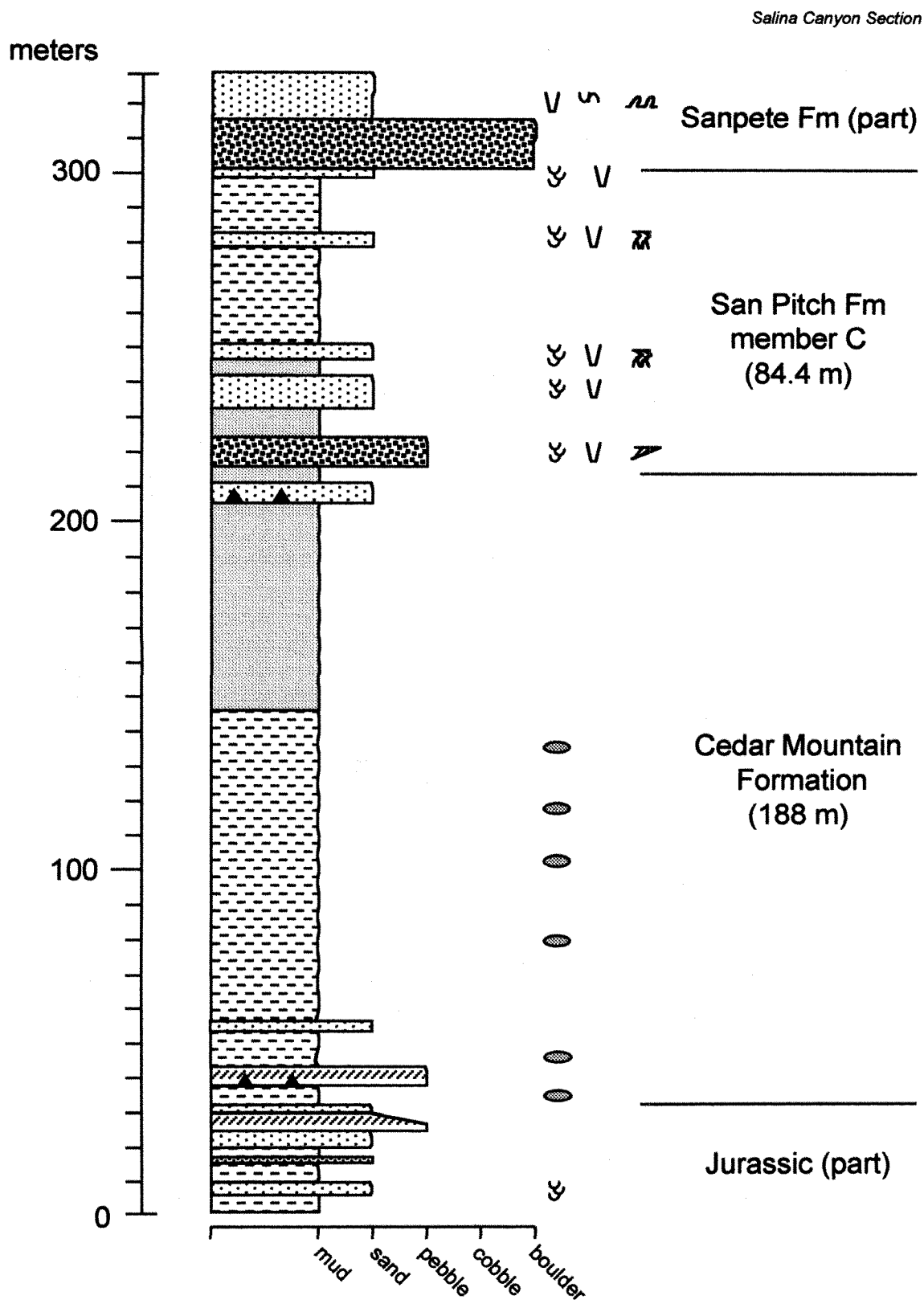


Figure 20. Measured section of Lower Cretaceous strata in Salina Canyon. Base of Cedar Mountain Formation is an unconformity with Jurassic strata, possibly Morrison Formation. See figure 19 for explanation of symbols.

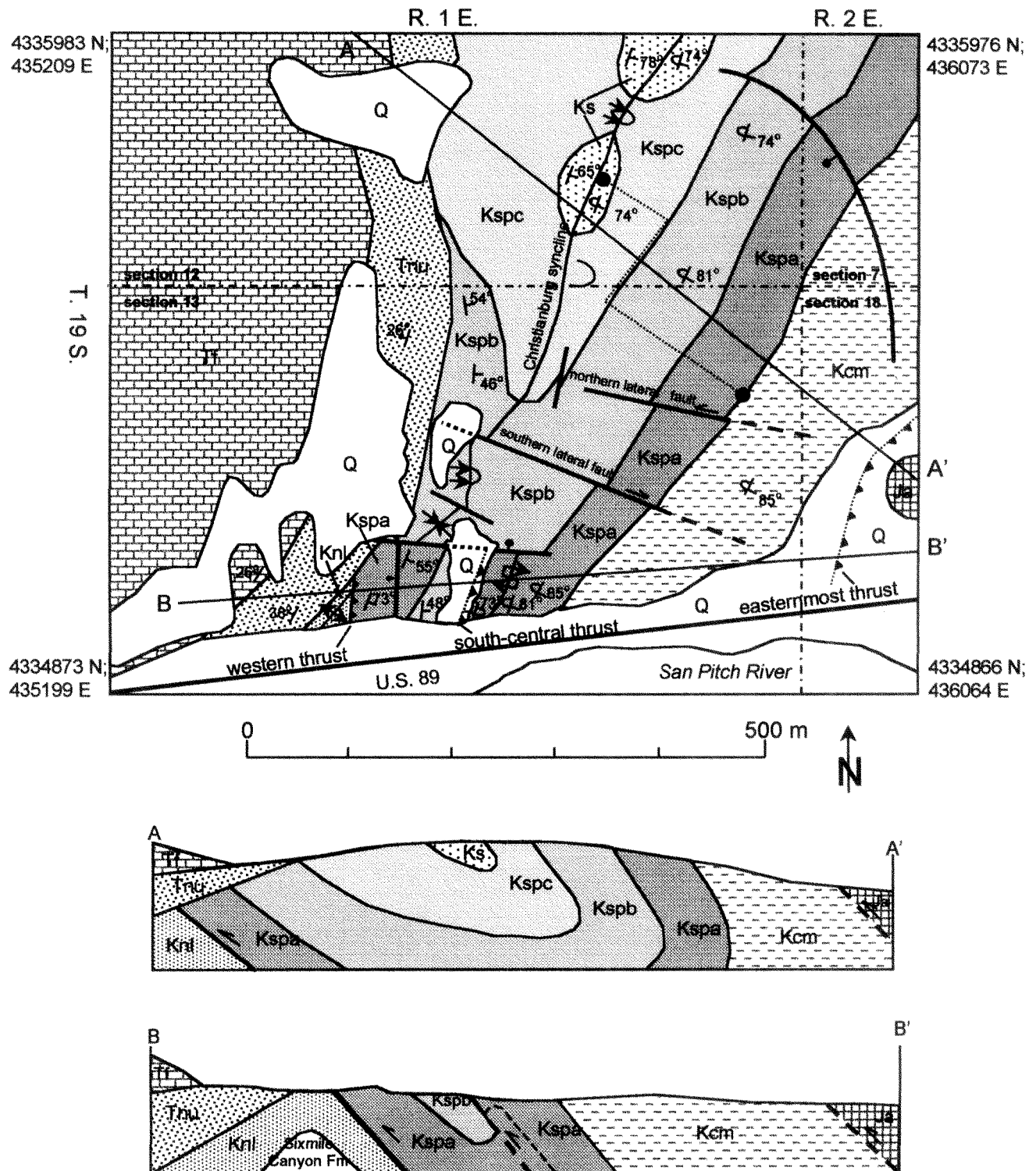


Figure 21. Generalized geologic map and diagrammatic cross sections of the Christianburg area.

Christianburg Section

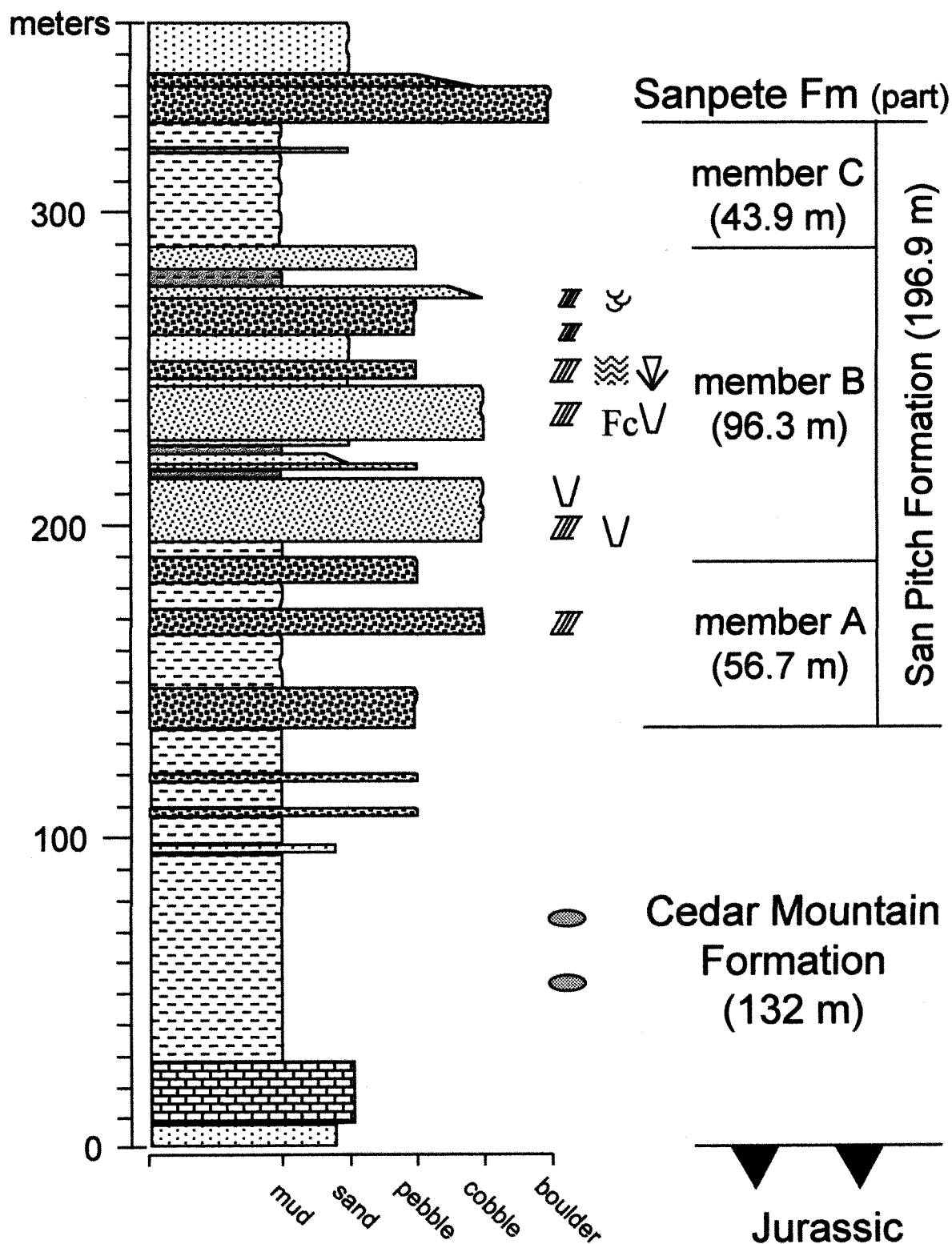


Figure 22. Measured section of Lower Cretaceous strata at Christianburg. Base of the Cedar Mountain Formation is a thrust fault with Jurassic Arapien Shale. See figure 19 for explanation of symbols.

for the clastic material. Ridge to the north is underlain by Sanpete Formation (Cenomanian-Turonian); strike valley mostly covered with alfalfa fields is underlain by the Allen Valley Shale (middle Turonian). Shoreface deposits of lower Funk Valley Formation (Turonian) are exposed in ridge to the east of Allen Valley Shale.

- (33.1, 1.5) Park in golf course parking lot at end of paved road.

Stop 13. Indianola-Flagstaff angular unconformity.
Fifteen minutes.

Excellent views to the north of steeply dipping shoreface deposits in upper part of Funk Valley Formation (Coniacian) overlain by flat-lying Flagstaff Limestone (Paleocene), which postdates local shortening. Prior to onlap by the Flagstaff Limestone, the Mesozoic rocks formed an island in Eocene Lake Flagstaff, termed Sterling Island by Weiss (1994). Comparison of the Funk Valley section with wells to north in Sanpete Valley indicates that much of the unit is missing from here, apparently cut out by a thrust fault near the east flank of the ridge west of the golf course. Along this trend, upright, east-dipping beds are thrust over steeply west-dipping, overturned beds.

- (33.9, 0.8) Retrace route on paved road to Sixmile Canyon road (dirt). Turn left.
- (34.3, 0.4) Flagstaff Limestone unconformably overlies the lower member of the Campanian Sixmile Canyon Formation at 9:00 (north). The Sixmile Canyon Formation is the uppermost unit of the Indianola Group (Spieker, 1946). Light gray, thick pebbly sandstone beds of the lower member are unconformable on the Funk Valley Formation.
- (35.6, 1.3) Road to Manti on left (north). Continue east up Sixmile Creek.
- (35.7, 0.1) Turn right, downhill into turnoff and park. **Do not** attempt to drive over bridge. Walk across bridge and climb trail 5095 to a bench for a view of the north wall of Sixmile Canyon (approximately 150 meters from bridge).

Stop 14. Progressive unconformity in Campanian strata, Sixmile Canyon.

Fluvial strata on north side of Sixmile Canyon (fig. 5) contain several unconformities that converge in a westward direction, causing the stratigraphic section to thicken to the east. Unconformity-bounded successions of sandstone are discordant in the west, but become concordant in a short distance eastward. The most obvious truncation is beneath beds assigned to the Price River Formation (Spieker, 1946; Lawton, 1982; Weiss, 1994). From its westernmost exposure, the Price River Formation may be traced eastward

from an angular unconformity with underlying beds of the upper member of the Sixmile Canyon into an apparently concordant succession of strata (fig. 23). With a little imagination, one can also make out subtle truncations in the underlying Sixmile Canyon Formation. Bedding dip decreases upsection through the unconformity-bounded successions. Campanian pollen have been reported from the middle member of the Sixmile Canyon Formation at the coal prospect to the west (Schwans, 1995) and late Campanian pollen were found in the Price River Formation to the east in the southwest corner of section 30, where it is traversed by the Sixmile Canyon road (Fouch et al., 1983). These strata, which appear to be genetically related, were deposited during incremental rotation in a short period of time during the Campanian.

This progressive unconformity lies on the east flank of the Sevier-Sanpete Valley antiform and indicates that growth of the antiform, and thus movement on the Gunnison thrust, took place late in the Campanian. Lawton et al., (1993) have reported similar relations in Campanian strata on the west flank of the structure; therefore, equivalent growth strata on both sides of Sanpete Valley record structural growth.

West-dipping Tertiary strata on the west flank of the Wasatch Plateau are also visible from this vantage point. This structure is termed the Wasatch monocline (Spieker, 1946). Beds of the lower to middle Eocene Green River Formation are folded, indicating that the monocline is a late Eocene-early Oligocene structure (Weiss, 1994).

Retrace route down Sixmile Canyon and proceed west on paved road toward Sterling.

- (37.5, 1.8) Turn right (north) on dirt road. After 0.8 mile this road merges with a north-trending paved road that parallels a strike ridge of Sanpete Formation. After 1.4 miles on the pavement, the road crosses the strike ridge and the contact of the Sanpete and Allen Valley formations. Shoreface deposits of the Lower Funk Valley Formation are exposed at 3:00 (east) beyond the alfalfa field.
- (40.3, 2.8) Turn right (northeast) on U.S. Highway 89.
- (43.1, 2.8) Turn left (west) on 5th North Street on the north side of Manti, across from the Mormon temple, which is built of limestone blocks quarried from the upper part of the Green River Formation just east of the Temple. Temple Hill is a synclinal forebay block composed of Green River and Crazy Hollow (late Eocene) formations emplaced over a cuesta of limestone in the Green River Formation.
- (45.8, 2.7) Cross San Pitch River. River knolls on left (southwest) are composed of late Tertiary



Figure 23. Panorama of Campanian strata in upper part of Sixmile Canyon. Upper Member of Sixmile Canyon Formation (Ks) is truncated by unconformity beneath Price River Formation (Kp). North Horn Formation (T:n) thins to the west above Price River Formation and beneath Flagstaff Limestone (Tf). Late Campanian pollen were reported by Fouch et al., (1983) from the Price River Formation at the east end of the panel (asterisk).

gravels that dip 50° west. These gravel deposits were tilted by diapirism of Arapien Shale, which also deflected the course of the river to the east.

(49.7, 3.9) On east side of the San Pitch Mountains, vertical conglomerate beds of the North Horn Formation rest depositionally on overturned, east-dipping Twist Gulch Formation. The vertical beds form the east limb of a broad, asymmetric syncline in the footwall of a thrust that carries Arapien Shale in its hanging wall. West-vergent folds and reverse faults are exposed discontinuously along the base of the eastern part of the San Pitch Mountains (fig. 17). This zone of reverse faulting is part of the faulted forelimb of a west-vergent fault-propagation fold that underlies Sanpete Valley (fig. 18; Lawton and Weiss, in press).

(53.0, 3.3) Turn left (west) at T intersection. Proceed west 1.3 mile to a sharp right (north) turn. West-vergent structures are visible in Big Mountain to the north. After 0.4 mile, turn left (west) and proceed toward mouth of Dry Canyon. Proceed straight 0.5 mile, then bear left on dirt road. Road ends in another 0.2 mi.

(55.4, 2.4) End of road in Dry Canyon.

Stop 15 (optional). Fold in Flagstaff Limestone. Walk up the canyon several hundred meters to the fold.

At Dry Canyon (fig. 17), a west-vergent anticline-syncline pair in the Paleocene-Eocene Flagstaff Limestone indicates that some shortening took place following early Eocene time. The Flagstaff is unconformable on overturned, east-dipping Twist Gulch Formation; folding appears to be related to reverse faults that propagated along bedding in the Twist Gulch Formation.

Retrace route to main dirt road on west side of Sanpete Valley.

(57.8, 2.4) Proceed straight (east) at T intersection.

(58.2, 0.4) At ranch buildings, turn left (north) on west-side road (dirt).

(58.8, 0.6) Sharp left turn.

(58.9, 0.1) Sharp right turn (north) to follow main road.

(61.4, 2.5) On the left (9:00–11:00) west-vergent reverse faults in Cretaceous strata are visible at foot of range in the vicinity of Coal Canyon. Chevron fold in upper San Pitch and Sanpete formations is present north of Coal Canyon. Beds of the North Horn Formation in the footwall of the reverse faults occupy a growth syncline and were deposited intermittently during shortening.

(63.3, 1.9) Sheep pens on left. Pull off road on left (west).

Stop 16. Progressive unconformity in basal North Horn (Upper Cretaceous), Lambs Canyon. Fifteen minutes.

Beds in the basal part of the North Horn Formation visible on the south side of Lambs Canyon form several unconformity-bound sequences that are truncated eastward by convergence of the unconformities. Bedding attitudes decrease upsection. Clasts within the conglomerate record an unroofing sequence derived from the rising structure to the east: Indianola clasts in the middle part of the section are overlain in succession by conglomerate, limestone, and sandstone clasts derived from Lower Cretaceous and Jurassic beds (Lawton et al., 1993). The basal North Horn Formation here is late Campanian in age (Talling et al., 1994) and correlates with the Sixmile Canyon and Price River formations at stop 14.

- (63.8, 0.5) Cottonwoods at 10:00 (west) grow at springs on the main normal fault at the foot of the range. Stratigraphic offset on this fault is about 640 m (Lawton and Weiss, in press). The fault reactivated an older west-vergent thrust fault (Standlee, 1982).
- (66.6, 2.8) Entering Wales, Utah.
- (67.3, 0.7) Left (west) on Wales Canyon Road.
- (68.2, 0.9) Park on right (north) side of road, east of prominent hogback.

Stop 17. Wales Gap. Axhandle wedge-top basin and Wales thrust system.

Vertical and overturned strata exposed at the narrow portal called Wales Gap display discordant relationships created by both thrust faults and angular unconformities (fig. 24). The prominent hogback consists of cobble to boulder conglomerate that dips 90° and faces west. It represents the lowermost unit in the fill of the Axhandle piggyback, or wedge-top basin, which contains as much as 1100 m of strata in its thickest part (Lawton et al., 1993). The strata of the basin, comprising the North Horn Formation and Flagstaff Limestone, thin eastward onto the belt of folding and faulting, known informally as the Wales thrust system, along the eastern base of the San Pitch Mountains. The prominent conglomerate was considered by Spieker (1946, 1949) as Price River Formation, but Lawton et al., (1993) termed it the basal conglomerate member of the North Horn Formation to emphasize its genetic link with overlying North Horn strata of the wedge-top basin. This conglomerate correlates with conglomeratic strata seen yesterday at Chris Canyon on the other side of the range, west northwest of here. On the south side of the creek, the basal conglomerate overlies overturned, east-dipping Sanpete Formation with angular discordance. Beds of the Sanpete Formation depositionally overlying the San Pitch Formation are also exposed on the south side of the creek. To the east, a reverse fault emplaces Jurassic Twist Gulch Formation

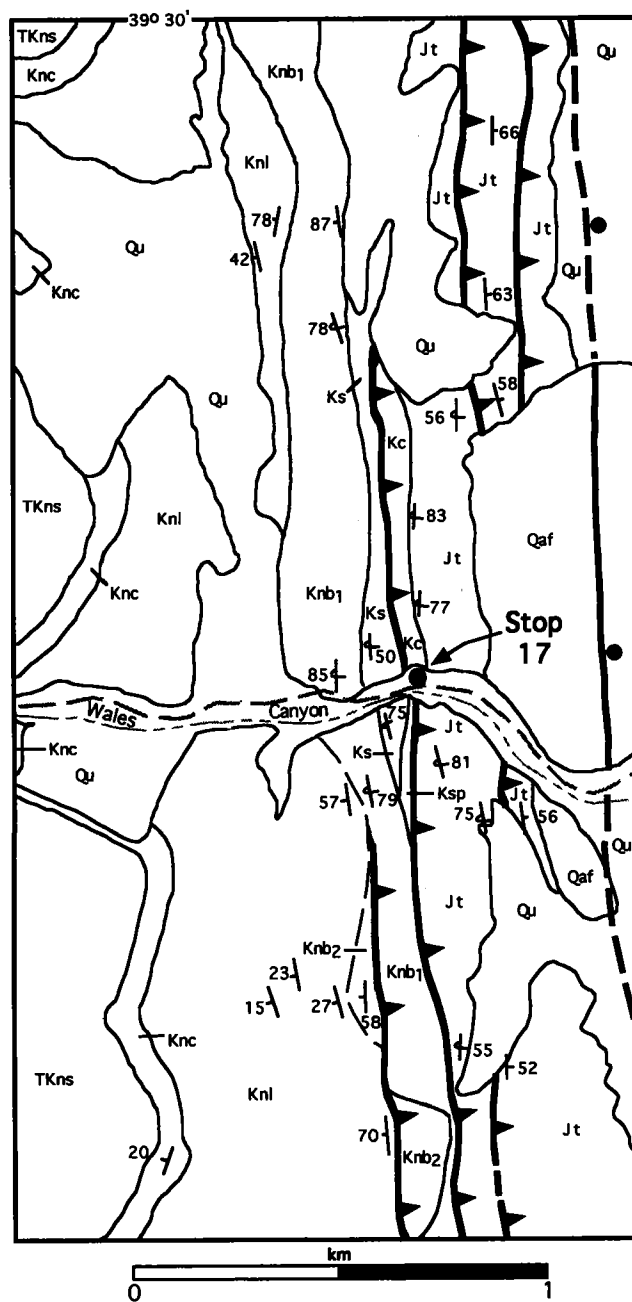


Figure 24. Geologic map of Wales Gap and vicinity of stop 17 on the east flank of the San Pitch Mountains (Lawton and Weiss, in press). Explanation: Jt, Twist Gulch Formation; Kc, Cedar Mountain Formation; Ksp, San Pitch Formation; Knb1, Knb2, basal members of North Horn Formation; Knl, lower redbed member of North Horn Formation; Knc, coal-bearing member of North Horn Formation; TKns, upper siltstone member of North Horn Formation; Qaf, alluvial-fan deposits; Qu, undifferentiated surficial deposits. Location of map is shown on figure 17.

above the San Pitch Formation. To the north, the thrust cuts upsection in the hanging wall and footwall, juxtaposing the Cedar Mountain Formation with the Sanpete Formation north of Wales Creek (fig. 24). Beds within the North Horn Formation west of the hogback have progressively lower dips upsection, partly as a result of the geometry of the syncline and partly a result of angular unconformities in the lower part of the section.

Wales gap displays structures typical of the Wales thrust system. The steep western forelimb of the Sevier-Sanpete Valley antiform formed the structural margin of the Axhandle basin in which the North Horn Formation was deposited (Lawton and Trexler, 1991; Lawton et al., 1993; Talling et al., 1995). The late Campanian onset of deposition in the piggyback, or wedge-top, basin marks major movement of the Gunnison thrust.

End road log. Retrace route to Wales, turn left (north) at Wales Ward Chapel and proceed north on Utah Route 177 to Fountain Green (12 miles). Then turn left on Utah Route 132 to Nephi and Interstate 15.

ACKNOWLEDGMENTS

We thank Lehi Hintze for careful review of the Canyon Range map and for discussions of both Paleozoic and Cretaceous stratigraphy, Phyllis Camilleri and Paul Link for constructive reviews of the manuscript, and Tommy Delgado for help with drafting. Partially supported by National Science Foundation grants EAR-9316700 (to DeCelles) and EAR-9205411 (to Lawton), and by a grant from the Donors of the Petroleum Research Fund (ACS-PRF #25163-AC2) administered by the American Chemical Society (to Mitra).

REFERENCES CITED

- Allmendinger, R.W., Sharp, J.W., Von Tish, D., Serpa, L., Brown, L., Kaufman, S., and Oliver, J., 1983, Cenozoic and Mesozoic structure of the eastern Basin and Range province, Utah, from COCORP seismic-reflection data: *Geology*, v. 11, p. 537–541.
- Anders, M.H., and Christie-Blick, 1994, Is the Sevier Desert reflection of west-central Utah a normal fault?: *Geology*, v. 22, p. 771–774.
- Armstrong, R.L., 1968, Sevier orogenic belt in Nevada and Utah. *Geological Society of America Bulletin*, v. 79, p. 429–458.
- Auby, W.L., 1991, Provisional geologic map of the Levan quadrangle, Juab County, Utah. Utah Geological Survey Map 135, scale 1:24,000, 13 p.
- Balcer, D.M., 1992, Lateral facies variability, nomenclature, and depositional environments of a syntectonic conglomerate in the southwest San Pitch Mountains, central Utah (M.S. thesis): Las Cruces, New Mexico State University, 121 p.
- Bally, A.W., Gordy, P.L., and Stewart, G.A., 1966, Structure, seismic data, and orogenic evolution of the southern Canadian Rocky Mountains. *Canadian Petroleum Geology Bulletin*, v. 14, p. 337–381.
- Beaumont, C., 1981, Foreland basins: *Geophysical Journal of the Royal Astronomical Society*, v. 65, p. 291–329.
- Boyer, S.E., and Elliott, D., 1982, Thrust systems. *American Association of Petroleum Geologists Bulletin*, v. 66, p. 1196–1230.
- Burchfiel, B.C., and Hickox, C.W., 1972, Structural development of central Utah, in Baer, J.L., and Callaghan, E., eds., *Plateau-Basin and Range Transition Zone, Central Utah, 1972: Utah Geological Association Publication 2*, p. 55–66.
- Christiansen, F.W., 1952, Structure and stratigraphy of the Canyon Range, central Utah. *Geological Society of America Bulletin*, v. 63, p. 717–740.
- Coogan, J.C., and DeCelles, P.G., 1996, Extensional collapse along the Sevier Desert reflection, northern Sevier Desert basin, western United States: *Geology*, v. 24, p. 933–936.
- Coogan, J.C., DeCelles, P.G., Mitra, G., and Sussman, A.J., 1995, New regional balanced cross section across the Sevier Desert region and the central Utah thrust belt: *Geological Society of America Abstracts with Programs*, v. 27, no. 4, p. 7.
- Dahlstrom, C.D.A., 1969, Balanced cross sections: *Canadian Journal of Earth Sciences*, v. 6, p. 743–757.
- Davis, D., Suppe, J., and Dahlen, F.A., 1983, Mechanics of fold-and-thrust belts and accretionary wedges. *Journal of Geophysical Research*, v. 88, p. 1153–1172.
- DeCelles, P.G., 1988, Lithologic provenance modeling applied to the Late Cretaceous synorogenic Echo Canyon Conglomerate, Utah: A case of multiple source areas. *Geology*, v. 16, p. 1039–1043.
- DeCelles, P.G., and Currie, B.S., 1996, Long-term sediment accumulation in the Middle Jurassic-early Eocene Cordilleran retroarc foreland-basin system. *Geology*, v. 24, p. 591–594.
- DeCelles, P.G., and Giles, K.A., 1996, Foreland basin systems. *Basin Research*, v. 8, p. 105–123.
- DeCelles, P.G., Lawton, T.F., and Mitra, G., 1995, Thrust timing, growth of structural culminations, and synorogenic sedimentation in the type Sevier orogenic belt, western United States. *Geology*, v. 23, p. 699–702.
- Fong, A., 1995, Geologic map of the Fountain Green South quadrangle. Utah Geological Survey Open File Report, Scale 1:24,000, 18 p.
- Fouch, T.D., Lawton, T.F., Nichols, D.J., Cashon, W.B., and Cobban, W.A., 1983, Patterns and timing of synorogenic sedimentation in Upper Cretaceous rocks of central and northeast Utah, in Reynolds, M.W., and Dolly, E.D., eds., *Symposium 2—Mesozoic paleogeography of west-central United States*. Society of Economic Paleontologists and Mineralogists, Rocky Mountain Section, p. 305–336.
- Graham, S.A., Tolson, R.B., DeCelles, P.G., Ingersoll, R.V., Bargar, E., Caldwell, M., Cavazza, W., Edwards, D.P., Folio, M.F., Handschy, J.R., Lemke, L., Moxon, I., Rice, R., Smith, G.A., and White, J., 1986, Provenance modelling as a technique for analysing source terrane evolution and controls on foreland sedimentation, in Allen, P.A., and Home-wood, P., eds., *Foreland basins*. International Association of Sedimentologists Special Publication 8, p. 141–152.
- Hardy, C.T., 1952, Eastern Sevier Valley, Sevier and Sanpete Counties, Utah, with reference to formations of Jurassic age. Utah Geological and Mineralogical Survey Bulletin 43, 98 p.
- Harris, H.D., 1959, Late Mesozoic positive area in western Utah. *American Association of Petroleum Geologists Bulletin*, v. 43, p. 2636–2652.
- Heller, P.L., Bowdler, S.S., Chambers, H.P., Coogan, J.C., Hagen, E.S., Shuster, M.W., Winslow, N.S., and Lawton, T.F., 1986, Time of initial thrusting in the Sevier orogenic belt, Idaho-Wyoming and Utah. *Geology*, v. 14, p. 388–392.
- Higgins, J.M., 1982, Geology of the Champlin Peak quadrangle, Juab and Millard Counties, Utah: Brigham Young University Geology Studies, v. 29, part 2, p. 40–58.
- Hintze, L.F., 1980, Geologic map of Utah. Utah Geological and Mineral Survey, scale 1:500,000.
- Hintze, L.F., 1988, Geologic history of Utah. Brigham Young University Geology Studies Special Publication 7, 202 p.
- Hintze, L.F., 1991a, Interim geologic map of the Scipio Pass quadrangle, Millard County, Utah. Utah Geological Survey Open File Report 222, scale 1:24,000.
- Hintze, L.F., 1991b, Interim geologic map of the Fool Creek Peak quadrangle, Juab and Millard Counties, Utah. Utah Geological Survey Open File Report 220, Scale 1:24,000.

- Hintze, L.F., 1991c, Interim geologic map of the Williams Peak quadrangle, Juab and Millard Counties, Utah. Utah Geological Survey Open File Report 223, scale 1:24,000.
- Holladay, J.C., 1984, Geology of the northern Canyon Range, Millard and Juab counties, Utah. Brigham Young University Geology Studies, v. 31, p. 1-28.
- Hunt, R.E., 1954, South Flat Formation, new Upper Cretaceous Formation of central Utah. American Association of Petroleum Geologists Bulletin, v. 38, p. 118-128.
- Imlay, R.W., 1980, Jurassic paleobiogeography of the conterminous United States in its continental setting. U.S. Geological Survey Professional Paper 1062, 134 p.
- Jordan, T.E., 1981, Thrust loads and foreland basin evolution, Cretaceous, western United States. American Association of Petroleum Geologists Bulletin, v. 65, p. 2506-2520.
- Kauffman, E.G., 1977, Geological and biological overview Western Interior Cretaceous basin. Mountain Geologist, v. 14, p. 75-99.
- Lawton, T.F., 1982, Lithofacies correlations within the Upper Cretaceous Indianola Group, central Utah, in Nielson, D.L., ed., Overthrust belt of Utah. Salt Lake City, Utah Geological Association Publication 10, p. 199-213.
- Lawton, T.F., 1985, Style and timing of frontal structures, thrust belt, central Utah. American Association of Petroleum Geologists Bulletin, v. 69, p. 1145-1159.
- Lawton, T.F., 1986, Compositional trends within a clastic wedge adjacent to a fold-thrust belt. Indianola Group, central Utah, U.S.A., in Allen, P.A., and Homewood, P., eds., International Association of Sedimentologists Special Publication 8, p. 411-423.
- Lawton, T.F., and Trexler, J.H., Jr., 1991, Piggyback basin in the Sevier orogenic belt, Utah—Implications for development of the thrust wedge. Geology, v. 19, p. 827-830.
- Lawton, T.F., and Weiss, M.P., in press, Geological map of the Wales quadrangle, Juab and Sanpete counties, Utah. Utah Geological Survey Map, Scale 1:24,000.
- Lawton, T.F., and Willis, G.C., 1987, The geology of Salina Canyon, Utah, in Beus, S.S., ed., Rocky Mountain Section of the Geological Society of America. Geological Society of America Centennial Field Guide Volume 2, p. 265-268.
- Lawton, T.F., Boyer, S.E., and Schmitt, J.G., 1994, Influence of inherited taper on structural variability and conglomerate distribution, Cordilleran fold and thrust belt, western United States. Geology, v. 22, p. 339-342.
- Lawton, T.F., Talling, P.J., Hobbs, R.S., Trexler, J.H., Jr., Weiss, M.P., and Burbank, D.W., 1993, Structure and stratigraphy of Upper Cretaceous and Paleogene strata (North Horn Formation), eastern San Pitch Mountains, Utah—Sedimentation at the front of the Sevier orogenic belt. U.S. Geological Survey Bulletin 1787-II, 33 p.
- Mattox, S.R., 1987, Provisional geologic map of the Hells Kitchen Canyon SE quadrangle, Sanpete County, Utah. Utah Geological and Mineral Survey Map 98, scale 1:24,000.
- Millard, A.W., 1983, Geology of the southwest quarter of Scipio North quadrangle, Millard and Juab counties, Utah. Brigham Young University Geology Studies, v. 30, p. 59-81.
- Mitra, G., in press, Evolution of salients in a fold-and-thrust belt. The effects of sedimentary basin geometry, strain distribution and critical taper, in Sengupta, S., ed., Evolution of geologic structures from macro- and micro-scales. London, Chapman and Hall.
- Mitra, G., and Sussman, A.J., 1997, Structural evolution of connecting splay duplexes and their implications for critical taper. An example based on geometry and kinematics of the Canyon Range culmination, Sevier belt, central Utah. Journal of Structural Geology, v. 19, p. 503-521.
- Morris, H.T., 1983, Interrelations of thrust and transcurrent faults in the central Sevier orogenic belt near Leamington, Utah, in Miller, D.M., Todd, V.R., and Howard, K.A., eds., Tectonic and stratigraphic studies in the eastern Great Basin. Geological Society of America Memoir 157, p. 75-81.
- Nielson, D.L., (ed.), 1982, Overthrust belt of Utah. Utah Geological Association Publication 10, 335 p.
- Ottom, J.K., 1995, Western frontal fault of the Canyon Range: Is it the breakaway zone of the Sevier Desert detachment? Geology, v. 23, p. 547-550.
- Pequera, N., Mitra, G., and Sussman, A.J., 1994, The Canyon Range thrust sheet in the Sevier fold-and-thrust belt of central Utah. Deformation history based on structural analysis. Geological Society of America Abstracts With Programs, v. 26, no. 6, p. 58.
- Riba, O., 1976, Syntectonic unconformities of the Alto Cardener, Spanish Pyrenees. A genetic interpretation. Sedimentary Geology, v. 15, p. 213-233.
- Ritzma, H.R., 1972, Six Utah "hinge-line" wells, in Baer, J.L., and Callaghan, E., eds., Plateau-Basin and Range transition zone, central Utah, 1972. Utah Geological Association Publication 2, p. 75-80.
- Royse, F., Jr., 1993, Case of the phantom foredeep. Early Cretaceous in west-central Utah. Geology, v. 21, p. 133-136.
- Schmitt, J.G., Haley, J.C., Lageson, D.R., Horton, B.K., and Azevedo, P.A., 1995, Sedimentology and tectonics of the Bannack-McKnight Canyon-Red Butte area, southwest Montana. New Perspectives on the Beaverhead Group and Sevier orogenic belt. Northwest Geology, v. 24, p. 245-313.
- Schwans, P., 1988, Depositional response of Pigeon Creek Formation, Utah, to initial fold-thrust deformation in a differentially subsiding foreland basin, in Schmidt, C.J., and Perry, W.J., eds., Interaction of the Rocky Mountain foreland and the Cordilleran thrust belt. Geological Society of America Memoir 171, p. 531-556.
- Schwans, P., 1995, Controls on sequence stacking and fluvial to shallow-marine architecture in a foreland basin, in Van Wagoner, J.C., and Bertram, G.T., eds., Sequence stratigraphy of foreland basin deposits, outcrop and subsurface examples from the Cretaceous of North America. American Association of Petroleum Geologists Memoir 64, p. 55-102.
- Spieker, E.M., 1946, Late Mesozoic and early Cenozoic history of central Utah. U.S. Geological Survey Professional Paper 205-D, p. 117-161.
- Spieker, E.M., 1949, The transition between the Colorado Plateaus and the Great Basin in central Utah. Utah Geological Society, Guidebook to the Geology of Utah, no. 4, 106 p.
- Spieker, E.M., and Reeside, J.B., Jr., 1926, Upper Cretaceous shore line in Utah. Geological Society of America Bulletin, v. 37, p. 429-438.
- Spieker, E.M., and Reeside, J.B., Jr., 1926, Upper Cretaceous shore line in Utah. Geological Society of America Bulletin, v. 37, p. 432-435.
- Sprinkel, D.A., 1982, Twin Creek Limestone-Arapien Shale relations in central Utah, in Nielson, D.L., ed., Overthrust belt of Utah. Utah Geological Association Special Publication 10, v. 1, p. 169-179.
- Sprinkel, D.A., Weiss, M.P., Fleming, R.W., and Waanders, G.L., in review, Redefining the Lower Cretaceous stratigraphy of central Utah and an example of the structural development with the foreland basin, in Lageson, D.A., and Schmitt, J.A., eds., Geological Society of America Memoir.
- Standlee, L.A., 1982, Structure and stratigraphy of Jurassic rocks in central Utah. Their influence on tectonic development of the Cordilleran foreland thrust belt, in Powers, R.B., ed., Geologic studies of the Cordilleran thrust belt. Denver, Rocky Mountain Association of Geologists, v. 1, p. 357-382.
- Stockh, D.F., and Linn, J.K., 1996, Apatite fission-track thermochronology of the Canyon Range, Utah. Exhumation of the breakaway zone of the Sevier Desert detachment. Geological Society of America Abstracts With Programs, v. 28, no. 7, p. A-116.

- Stolle, J.M., 1978, Stratigraphy of the lower Tertiary and Upper Cretaceous(?) continental strata in the Canyon Range, Juab County, Utah. *Brigham Young University Geology Studies*, v. 25, pt. 3, p. 117–139.
- Suppe, J., Chou, G.T., and Hook, S.C., 1992, Rates of folding and faulting determined from growth strata, in McClay, K.R., ed., *Thrust tectonics* New York, Chapman and Hall, v. , p. 105–122.
- Sussman, A.J., and Mitra, G., 1995, Deformation patterns in the footwall of the Canyon Range thrust, central Utah. Implications for Sevier fold-and-thrust belt development. *Geological Society of America Abstracts with Programs*, v. 27, no. 4, p. 57.
- Talling, P.J., Burbank, D.W., Hobbs, R.S., Lawton, T.F., and Lund, S.P., 1994, Magnetostratigraphic chronology of Cretaceous to Eocene thrust belt evolution, central Utah: *Journal of Geology*, v. 102, p. 181–196.
- Talling, P.J., Lawton, T.F., Burbank, D.W., and Hobbs, R.S., 1995, Evolution of latest Cretaceous-Eocene nonmarine deposystems in the Axhandle piggyback basin of central Utah. *Geological Society of America Bulletin*, v. 107, p. 297–315.
- Villien, A., and Kligfield, R.M., 1986, Thrusting and synorogenic sedimentation in central Utah, in Peterson, J.A., ed., *Paleotectonics and sedimentation in the Rocky Mountain region, United States*. American Association of Petroleum Geologists Memoir 41, p. 281–308.
- Weiss, M.P., 1994, Geologic map of the Sterling quadrangle, Sanpete County, Utah. *Utah Geological Survey Map 159*, scale 1:24,000, 26 p.
- Willis, G.C., 1986, Geologic Map of the Salina Quadrangle, Sevier County, Utah. *Utah Geological and Mineral Survey Map Series no. 83*, scale 1:24,000, 16 p.
- Willis, G.C., and Kowallis, B.J., 1988, Newly recognized Cedar Mountain Formation in Salina Canyon, Sevier County, Utah. *Brigham Young University Geology Studies*, v. 35, p. 57–61.
- Witkind, I.J., and Weiss, M.P., 1991, Geologic map of the Nephi 30' x 60' quadrangle, Carbon, Emery, Juab, Sanpete, Utah, and Wasatch counties, Utah. *U.S. Geological Survey Map I-1937*, Scale 1:100,000.
- Witkind, I.J., Standlee, L.A., and Maley, K.F., 1986, Age and correlation of Cretaceous rocks previously assigned to the Morrison(?) Formation, Sanpete-Sevier Valley area, central Utah. *U.S. Geological Survey Bulletin* 1584, 9 p.
- Witkind, I.J., Weiss, M.P., and Brown, T.L., 1987, Geologic map of the Manti 30' x 60' quadrangle, Carbon, Emery, Juab, Sanpete, and Sevier counties, Utah. *U.S. Geological Survey Map I-1631*, scale 1:100,000.
- Woodward, N.B., and Boyer, S.E., 1985, An outline of balanced cross-sections. Knoxville, University of Tennessee, Department of Geological Sciences Studies in Geology 11, 123 p.

Lower to Middle Cretaceous Dinosaur Faunas of the Central Colorado Plateau: A Key to Understanding 35 Million Years of Tectonics, Sedimentology, Evolution and Biogeography

JAMES I. KIRKLAND

Dinamation International Society, 550 Jurassic Court, Fruita, Colorado 81521

BROOKS BRITT

Museum of Western Colorado, P.O. Box 25000, Grand Junction, Colorado 80102

DONALD L. BURGE

College of Eastern Utah, Prehistoric Museum, 451 E. 400 N., Price, Utah 84501

KEN CARPENTER

Dept. of Earth Sciences, Denver Museum of Natural History, 2001 Colorado Blvd., Denver, Colorado 80205

RICHARD CIFELLI

Oklahoma Museum of Natural History, University of Oklahoma, Norman, Oklahoma 73019

FRANK DECOURTEN

Geology/Earth Science, Sierra College, 5000 Rocklin Road, Rocklin, California 95677

JEFFREY EATON

Department of Geology, Weber State University, Ogden, Utah 84408-2507

STEVE HASIOTIS

Department of Geological Sciences, University of Colorado, Boulder, Colorado 80309-0250

TIM LAWTON

Dept. of Earth Sciences, New Mexico State University, Los Cruces, New Mexico 88003

ABSTRACT

Three distinct dinosaur faunas separated by unconformities representing about 10 my each are present in the Cedar Mountain Formation of east-central Utah. These biostratigraphic relationships compliment the lithostratigraphic relationships present in the Cedar Mountain Formation resulting in the recognition of five members to be recognized. These members are a basal Buckhorn Conglomerate and four new members defined herein. In ascending order these are the Yellow Cat Member, Poison Strip Sandstone, Ruby Ranch Member, and Mussentuchit Member.

The Buckhorn Conglomerate is a trough cross-bedded pebble conglomerate present at the base of the Cedar Mountain Formation on the west and north sides of the San Rafael Swell. It is unfossiliferous. The oldest fauna

preserved is in the largely fine grained deposits of basal Yellow Cat Member east of the San Rafael Swell. The dinosaurs include abundant polacanthids, cf. *Polacanthus* n. gen., *Iguanodon ottingeri*, a sail-backed iguanodontid (= *I. ottingeri* ?), camarasaurid and titanosaurid sauropods, a small maniraptoran theropod, cf. *Ornitholestes* n. gen., and the giant dromaeosaurid *Utahraptor ostrommaysorum*. The ankylosaurs, iguanodontids, and sauropods indicate close temporal and geographic ties to the Barremian of Europe.

The cliff forming Poison Strip Sandstone outcrops across central Utah east of the San Rafael Swell. Dinosaurs present in this member are limited to the nodosaurid ankylosaur *Sauropelta*, and isolated theropod and sauropod bones. The overlying Ruby Ranch Member is characterized by largely illitic mudstones and an abundance of calcareous nodules. It preserves a dinosaur fauna including the nodosaurid *Sauropelta*, the primitive iguanodontian *Tenontosaurus*?, sauropods assigned to *Pleurocoelus*, dromaeosaurid teeth, an unidentified large theropod, and *Acrocanthosaurus*. This fauna compares well with those documented from the Cloverly Formation, Arundel Formation, and Trinity Group characteristic of North America's apparently endemic Aptian-Albian dinosaur fauna.

A sharp break from carbonate nodule bearing, non-smectitic strata to carbonaceous, highly smectitic strata marks the base of the Mussentuchit Member in the western San Rafael Swell region. It is dated as spanning the Albian/Cenomanian boundary based on palynology and radiometric dates. This youngest dinosaur fauna includes a small nodosaurid, cf. *Pawpawsaurus* n. gen., a small ornithomimid, a primitive lambeosaurid hadrosaur, ceratopsian teeth, pachycephalosaur teeth, tiny sauropod teeth, a dromaeosaurid, cf. *Richardoestesia* teeth, cf. *Paronychodon* teeth, and an early tyrannosaurid. This dinosaur fauna is remarkably similar to those of the Campanian and Maastrichtian of western North America. As the most likely ancestors of the tyrannosaurid, hadrosaur and ceratopsian are from the Early Cretaceous of Asia, the dramatic shift to faunas typical of the North American Late Cretaceous is interpreted to result from opening migration corridors to and from Asia through Alaska at the end of the Early Cretaceous, when migration to eastern North America was still possible. The middle to upper Cenomanian Dakota Formation preserves a dinosaur fauna much like that of the Mussentuchit fauna with the notable absence of sauropods.

The fossil record in east-central Utah indicates that a Barremian iguanodont-polacanthid fauna with European affinities predating common flowering plants was replaced by an Aptian-middle Albian *Tenontosaurus*-*Pleurocoelus* fauna, perhaps representing an impoverished recovery fauna following a Early Cretaceous extinction event (endemic to North America). In turn, this was followed by a latest Albian-earliest Cenomanian hadrosaur dominated fauna with Asian affinities when flowering plants were co-dominant, which continued until the end of the Cretaceous.

INTRODUCTION

Approximately 50 million years of Earth's history is represented between the final deposition of the Late Jurassic Morrison Formation and the first transgression of the Late Cretaceous Western Interior Seaway across the Colorado Plateau. The Cedar Mountain and Dakota Formations record part of this history. Historically, these terrestrial strata have been considered to be largely unfossiliferous (Stokes, 1944, 1952; Young, 1960). Age relationships of the terrestrial Dakota Formation have been based on overlying latest Cenomanian marine fossils (Cobban, 1976; Eaton, Kirkland, and Kauffman, 1990). The uppermost Cedar Mountain Formation in the western San Rafael Swell had been dated as late Albian based on palynomorphs by Tschudy and others (1984). Dates based on freshwater bivalves, ostracodes, charophytes, and plants, while not as accurate, are compati-

ble (Mitchell, 1956; Stokes, 1952; Young, 1960). Thus, it has been accepted that a broadly Albian Cedar Mountain Formation was overlain by a largely Cenomanian Dakota Formation. The Cedar Mountain Formation has subsequently been considered as a homogenous Aptian-Albian unit in most regional studies (ex. Lawton, 1985; 1986; Heller, et al., 1986; Baars, 1988).

Additionally, the North American terrestrial vertebrate record is very poor overall for the "middle" Cretaceous; a the notable exception being the Aptian-Albian fauna from the Cloverly Formation of northern Wyoming and southern Montana (Ostrom, 1970). Largely correlative faunas are known from the Antlers Formation of Oklahoma, Arkansas, and west Texas (Stovall and Langston, 1950; Langston, 1974), the Pauluxy and Twin Mountains formations of central Texas (Langston, 1974; Winkler et al., 1989; 1990), and the

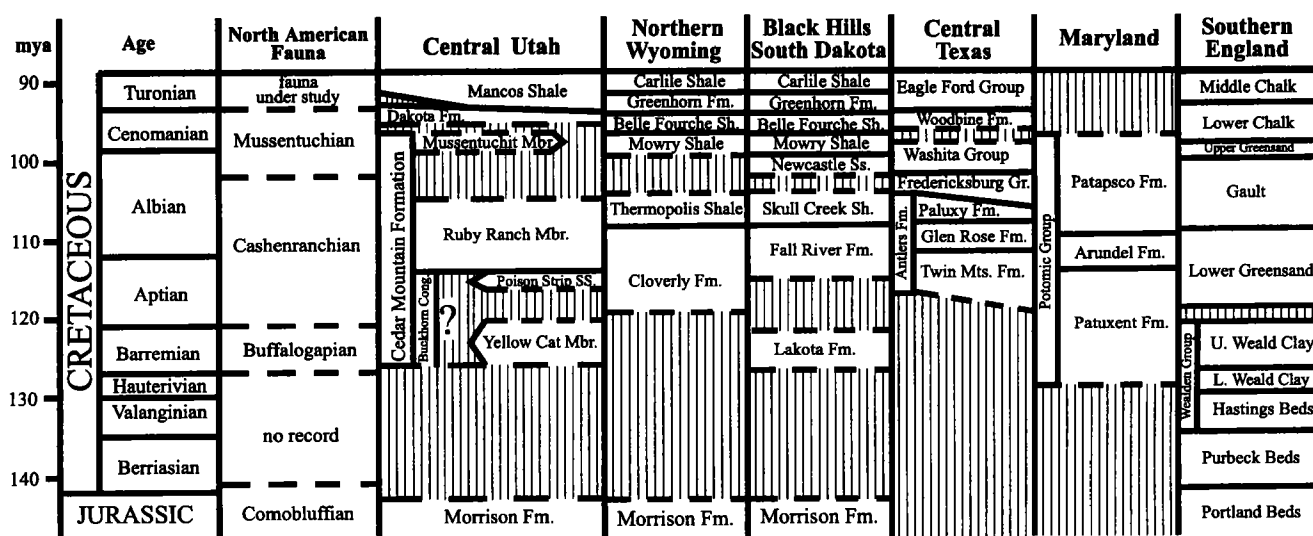


Figure 1. Correlation chart showing age relationships of stratigraphic units discussed in text. Vertical lines denote unconformities. Time scale from Obradovich (1993). North American faunas ages after Lucas (1993) and this paper. Data from Dyman et al., (1994), Winkler et al., (1995), Hancock et al., (1993), Kranz (1989), and Benton and Spencer (1995).

Arundel Formation of Maryland (Gilmore, 1921; Kranz, 1989, 1996) (Fig. 1).

Recent research has indicated that there are three distinct dinosaur faunas separated by unconformities representing about 10 my each in the Cedar Mountain Fm. of east-central Utah (ex. Kirkland, 1996b). In addition to the well known Aptian-Albian fauna, there are distinct earlier and later faunas preserved in the Cedar Mountain Formation. A diverse fauna has also been recovered from the overlying Dakota Formation in southern Utah and from a small site in the western San Rafael Swell (Eaton, 1987, 1993a, b; Eaton et al., 1997). Improved biostratigraphic resolution within this time interval indicates a more complex regional history during the Early to "middle" Cretaceous and will lead to refinements in our geological interpretations.

Significant localities demonstrating this three-fold division of the Cedar Mountain Formation will be visited, as will a pertinent outcrop of the Dakota Formation during the course of this field trip (Fig. 2). Additionally, each of the proposed members of the Cedar Mountain Formation will be examined.

Detailed descriptions as to how to get to the fossil localities described in this guidebook are not provided as these are sensitive sites of ongoing research by many institutions. This information is on file at these institutions (listed below) and will be provided to qualified researchers. It is hoped that this field trip and guidebook will provide ample explanation as to why our fossil resources should be protected so that they can continue provide data to better understand the Earth's geological, biological and climatic history.

Lower Cretaceous Strata in the Thrust Belt.

Lower Cretaceous strata of the central Utah thrust belt were deposited near the tip of the advancing thrust wedge west of the Wasatch Plateau in the axis of a foreland basin created by the load of the thrust faults. The section thickens very rapidly to the northwest from the vicinity of Salina, Utah, achieving a maximum thickness of 1160 m at Chicken Creek in the west central San Pitch Mountains (Sprinkel et al., written commun., 1996). From that point westward, correlative strata thin by onlap onto the hanging wall of the Pavant thrust. Clasts in conglomerate of the Lower Cretaceous section were derived from hanging wall rocks of both the Canyon Range and Pavant thrusts, coeval with movement of the Pavant Thrust (Lawton, 1985; DeCelles, et al., 1995). Paleocurrent data and clast composition trends indicate that the conglomeratic part of the section was at times distributed southeastward away from the thrust belt, reaching the latitude of Salina as toes of large fans, and at other times dispersed northeast longitudinally along the axis of foredeep of the foreland basin by large braided rivers. The robust river systems that occupied the rapidly subsiding axis of the basin were probably poorly represented or even completely absent from equivalent depositional systems of more slowly subsiding regions further from the thrust belt. It is not surprising that correlation of this interval through the subsurface of the Wasatch Plateau has proven challenging. The Lower Cretaceous section in the central Utah part of the thrust belt is characterized by a quartzite-cobble and boulder conglomerate that is generally regarded as correla-

tive with the base of the Dakota Formation (Schwans, 1995; Lawton et al., in press; Sprinkel et al., written commun., 1996).

Strata in the central Utah part of the Sevier orogenic belt equivalent to the Cedar Mountain Formation of the Colorado Plateau have a varied history of nomenclature (Fig. 3). They were tentatively identified as Morrison Formation based on stratigraphic position (Spieker and Reeside, 1926). Spieker (1946, 1949) later hedged his correlation with a query as he learned more about regional relations of the continental interval above the San Rafael Group. Although Stokes (1972) questioned the Morrison assignment on the basis of polished chert pebbles or gastroliths in the beds of the thrustbelt, it was not until a succession of studies in the 1980's that the Early Cretaceous age of these strata was established. Standlee (1982), Witkind et al., (1986), and Weiss and Roche (1988) recommended use of the term Cedar Mountain for redbeds exposed in the San Pitch Mountains, although there was some confusion among some workers about how to handle an interval of red conglomerate lying above the gastrolith shales and beneath the Indianola Group. Schwans (1988a, b) reassigned the Lower Cretaceous section to the Pigeon Creek Formation, assigning the lower shale-rich part to a lower member and about a kilometer of conglomerate on the west side of the San Pitch Mountains to an upper member. Weiss (1994) included the lower mudstone interval in the Cedar Mountain Formation and overlying conglomerate in an unnamed basal formation of the Indianola Group. Based on ongoing, detailed biostratigraphic and structural studies Sprinkel et al., (1992;

written commun., 1996) recommended assignment of the lower shale-rich interval to the Cedar Mountain Formation, and the upper conglomeratic interval to a new formation, the "San Pitch Formation," to be included in the Indianola Group.

Palynomorph biostratigraphy indicates that both the shale-rich and conglomerate rich intervals of the thrust belt correlate with the Cedar Mountain Formation exposed east of the Wasatch Plateau. The base of the conglomerate is middle to late Albian in the San Pitch Mountains based on concurrent range zones of palynomorph collections (Sprinkel et al., written commun., 1996). The Cedar Mountain Formation of the San Pitch Mountains is probably Aptian-lower Albian by comparison with similar lithologies rich in carbonate nodules associated with the Ruby Ranch Member of the Cedar Mountain on the Colorado Plateau. Both the Cedar Mountain and the overlying conglomerate beds are therefore equivalent to the Cedar Mountain of the Colorado Plateau, although the conglomerate beds appears rather inconveniently to correspond to an unconformity between the Ruby Ranch and Mussentuchit members of the plateau.

The Cedar Mountain Formation.

The term Cedar Mountain Shale was designated by Stokes (1944) for the drab variegated slope-forming sediments lying between the Buckhorn Conglomerate and the Dakota Formation (Fig. 4); the type section lies on the southwest flank of Cedar Mountain, Emery County, Utah. It was characterized as having slopes covered with abundant carbonate nodules that were often septarized with agate, barite, and other fillings. Stokes noted an abundance of elongate sandstone lenses (ribbon sandstones) that represented abandoned river channels. The presence of polished chert pebbles "gastroliths" was also noted.

Stokes (1952) renamed the unit the Cedar Mountain Formation and included the Buckhorn Conglomerate as its basal member (Fig. 4). His measured type section (Sec. 9, T18S, R10E) is 123.6 meters thick. He recognized that the Burro Canyon Formation of western Colorado (Stokes and Phoenix, 1948) is largely equivalent to the Cedar Mountain Formation and recommended using the Colorado River as the dividing line between these formations (Stokes, 1952).

Young (1960), recognizing the continuity of the two formations, proposed that the term Burro Canyon be abandoned in favor of Cedar Mountain Formation. This proposal has been ignored by subsequent authors (ex. Craig, 1981). Young (1960) recognized several regionally extensive sandstones in the Cedar Mountain that were useful for correlation (Fig. 4).

Based on correlations of regionally persistent sandstone units, Young (1960) proposed that, toward the east, calcareous mudstones assigned to the Cedar Mountain passed into

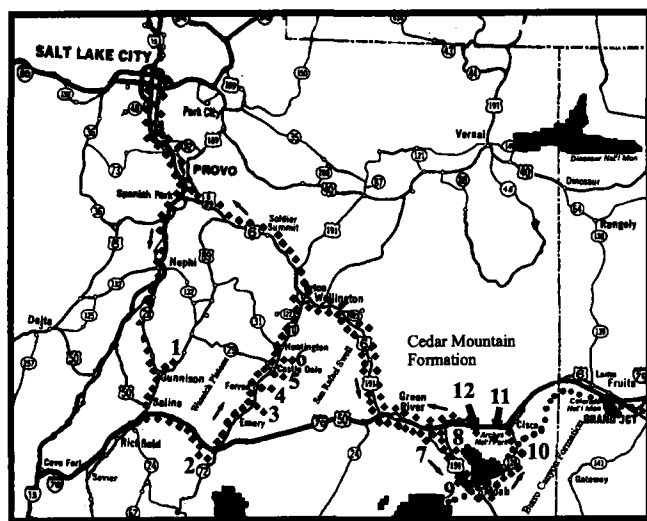


Figure 2. Map showing route of field trip (diamonds). Field trip stops listed by number. Line of dots indicates geographic boundary between Cedar Mountain and Burro Canyon Formations.

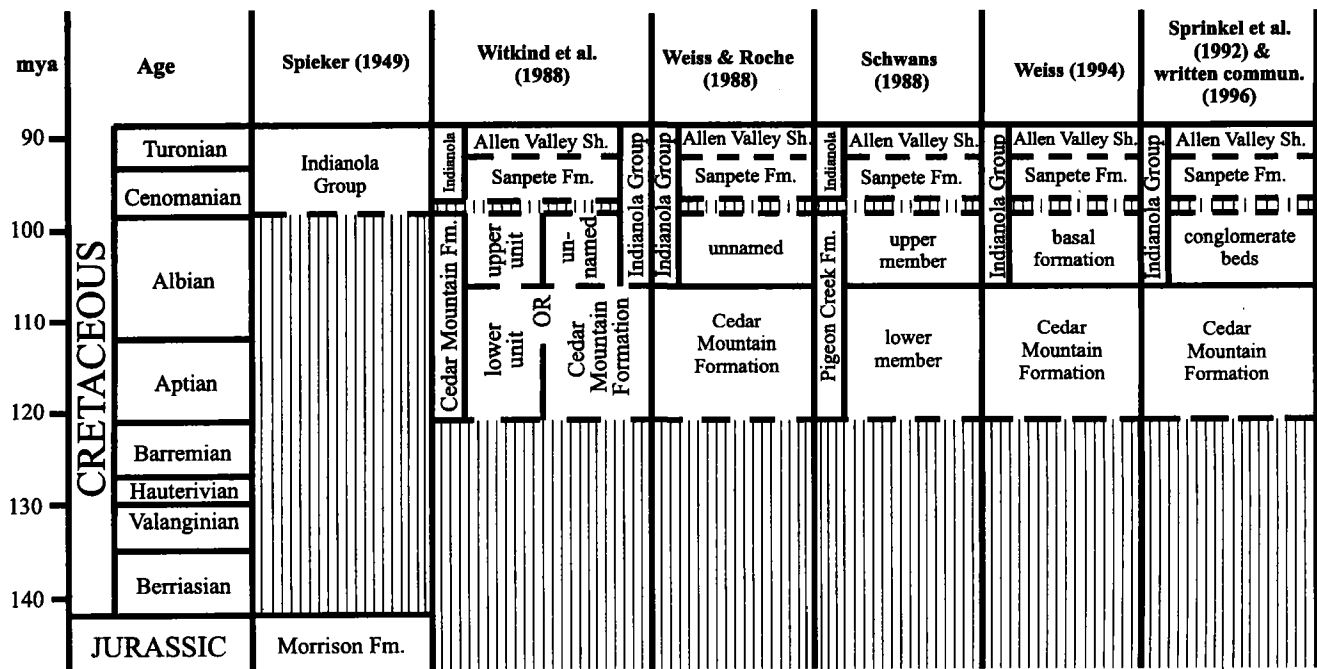


Figure 3. History of nomenclature for "middle" Cretaceous strata in the San Pete Valley. Time scale from Obradovich (1993).

the carbonaceous sandstones and shales of his Naturita Formation (Fig. 4). Although the more refined biostratigraphy developed herein precludes such a rapid facies change, Molenaar and Cobban (1991) and correlations presented here indicate that the upper Cedar Mountain Formation correlates with the upper Dakota Formation northwestward across the Uinta Basin. Young's (1960) sandstone correlations suffered from this lack of biostratigraphic control, but these units mark major breaks in sedimentation as indicated by the dramatic faunal changes documented herein. Thus Young's (1960) recognition of these units represented a significant, if belatedly utilized, breakthrough in our understanding of the Cedar Mountain Formation.

In addition to the basal Buckhorn Conglomerate of the western San Rafael Swell, four additional members are newly proposed herein. In ascending order, based on stratigraphic and biostratigraphic relationships, these are; Yellow Cat Member, Poison Strip Sandstone, Ruby Ranch Member, and Mussentuchit Member (Figs. 1, 3).

The Buckhorn Conglomerate.

The Buckhorn Conglomerate was defined by Stokes (1944) for exposures below the dam at Buckhorn Reservoir on the southwest flank of Cedar Mountain, where its exposed thickness is 7.5 m. At the type locality, the pebbles have an average diameter of 3 cm and are composed mostly of black chert. Trough crossbedding indicate flow direc-

tions to the northeast. It is best developed in the northern San Rafael Swell area (Fig. 5). Because of its discontinuous nature, Stokes (1952) subsequently included it as the lower member of the Cedar Mountain Formation. Young (1960) also noted that the member was discontinuous and found that it could not be correlated with any specific sandstone east of the San Rafael Swell. Aubrey (1996, in press) has proposed that the Buckhorn intertongues with the Morrison Formation and should be considered Late Jurassic (Fig. 4). Beyond reworked late Paleozoic invertebrates, no primary fossils have been recovered from the Buckhorn Conglomerate.

The Yellow Cat Member.

We propose that the mudstone interval at the base of the Cedar Mountain Formation in the region around Arches National Park be designated the Yellow Cat Member of the Cedar Mountain Formation, with its type section near the Gaston Quarry west of the Yellow Cat Road (Fig. 6, Stop 12). At this site (NE1/4, SE1/4, NE1/4, SW1/4, Sec. 35, T22S, R21E on the Mollie Hogans, Utah, U.S.G.S. 1:24,000 Quad.), the member measures 24 m thick. It begins at the top of a 2–3 meter thick calcrete marking the top of the Morrison Formation and consists primarily of mauve mudstone with thin (5–30 cm thick) sandstone beds. At 17.3 m above the base, there is an interval of interbedded limestone and shale that preserves mudcracks, dinosaur tracks,

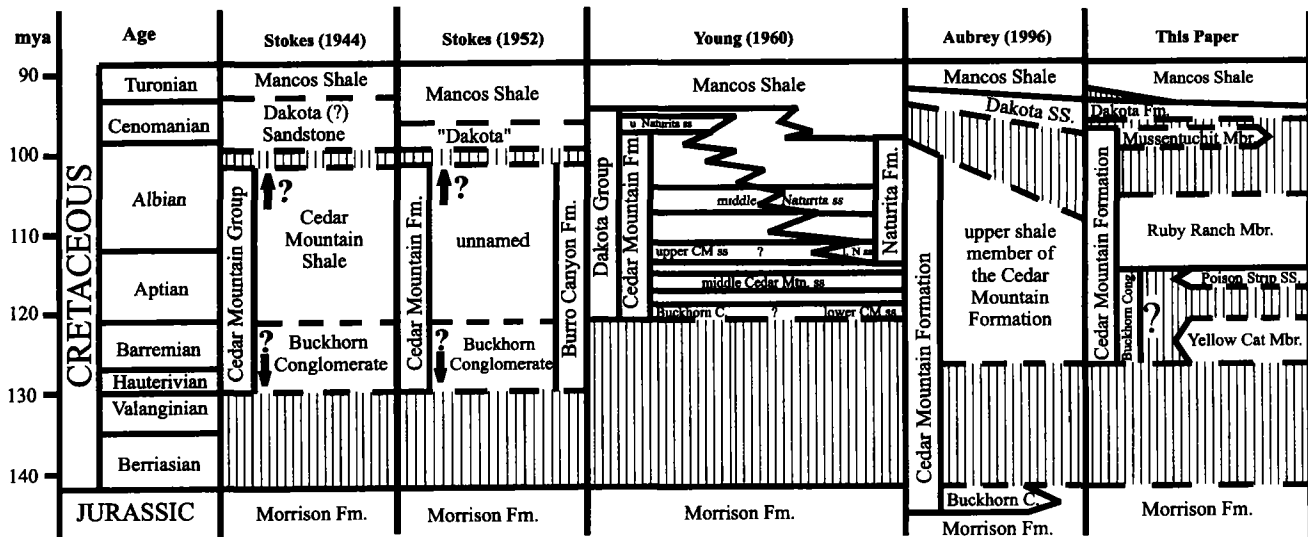


Figure 4. History of nomenclature for "middle" Cretaceous strata on the central Colorado Plateau. Time scale from Obradovich (1993).

and barite crystal clusters. The sharp upper contact with this slope forming unit is at the base of the sandstone ledge formed by the Poison Strip Sandstone.

The interval of interbedded limestone and shale toward the top of the member in the type section marks the base of the Cedar Mountain Formation in this area as described by Young (1960, Fig. 6, sec. 37). Thus, the Cedar Mountain Formation properly includes strata older than was recognized by Young (1960) in region around Arches National Park.

The newly proposed Yellow Cat Member is known to occur in a belt extending from the west side of the ancestral Uncompahgre Uplift west of Dewey Bridge, Utah, to the east side of the San Rafael Swell (Fig. 5). At most exposures, it extends from a basal calcrete (Aubrey, 1996; in press) up to the base of a regionally extensive sandstone ledge, (middle sandstone of Young, 1960; Poison Strip Sandstone, herein). Typically the member is 20–30 meters thick, but locally may thicken to 50–100 meters thick. To both the east and west the member pinches out between the Morrison Formation and the overlying sandstone. These thickness variations, together with the observed differences in its basal contact, may reflect the topography of the early Cretaceous erosional surface formed on the upper Jurassic strata. It is probable that as much as 20 million years of geological time may not be represented by sediments between Morrison and Cedar Mountain deposition (Obradovich, 1993; Kowallis et al., in press).

These sediments consist mostly of interbedded mudstone, with interbeds of sandstone and limestone. These mudstones tend to be mauve toward the base and pale green toward the top. They differ from those of the Morrison Formation

in being drabber and less strongly variegated. In addition, the mudstones in the Yellow Cat Member do not appear to be smectitic based on weathering expression, in stark contrast to the underlying mudstones in the Brushy Basin Member the Morrison Formation.

The basal calcrete is not always present, and at some sites there is a shale on shale contact, although common polished chert pebbles (referred to as "gastroliths") are generally found at the probable contact (Stokes, 1944, 1952) suggesting a deflation surface. At other sites, there may be several calcretes and the contact is picked at the top of the lowest calcrete above smectitic mudstones of the Brushy Basin Member of the Morrison Formation. Examination of the basal calcrete indicates that locally it is a complex of superimposed calcretes. Aubrey (1996, in press) utilized the base of the calcrete as the base of the Cedar Mountain; however, the basal surface is often gradational. It is assumed that this calcrete represents a soil horizon developed on the Morrison paleosurface. The uppermost Morrison below the calcrete is often nonsmectitic, rooted, and a brick red color, perhaps reflecting a long period of exposure and oxidation between deposition of the Morrison Formation and the onset of Cedar Mountain deposition.

The distribution of these sediments provides an important constraint on the beginning of Sevier thrusting. Aubrey (1996, in press) has postulated that thrusting may have begun in the Barremian, based on the recognition of this basal Cedar Mountain fauna (Kirkland, 1992). However, as these sediments pinch out to the west, they would seem to preclude the onset of Sevier thrusting until at least the Aptian as there is no evidence the development of a foreland basin proximal to the thrust belt. These data provide

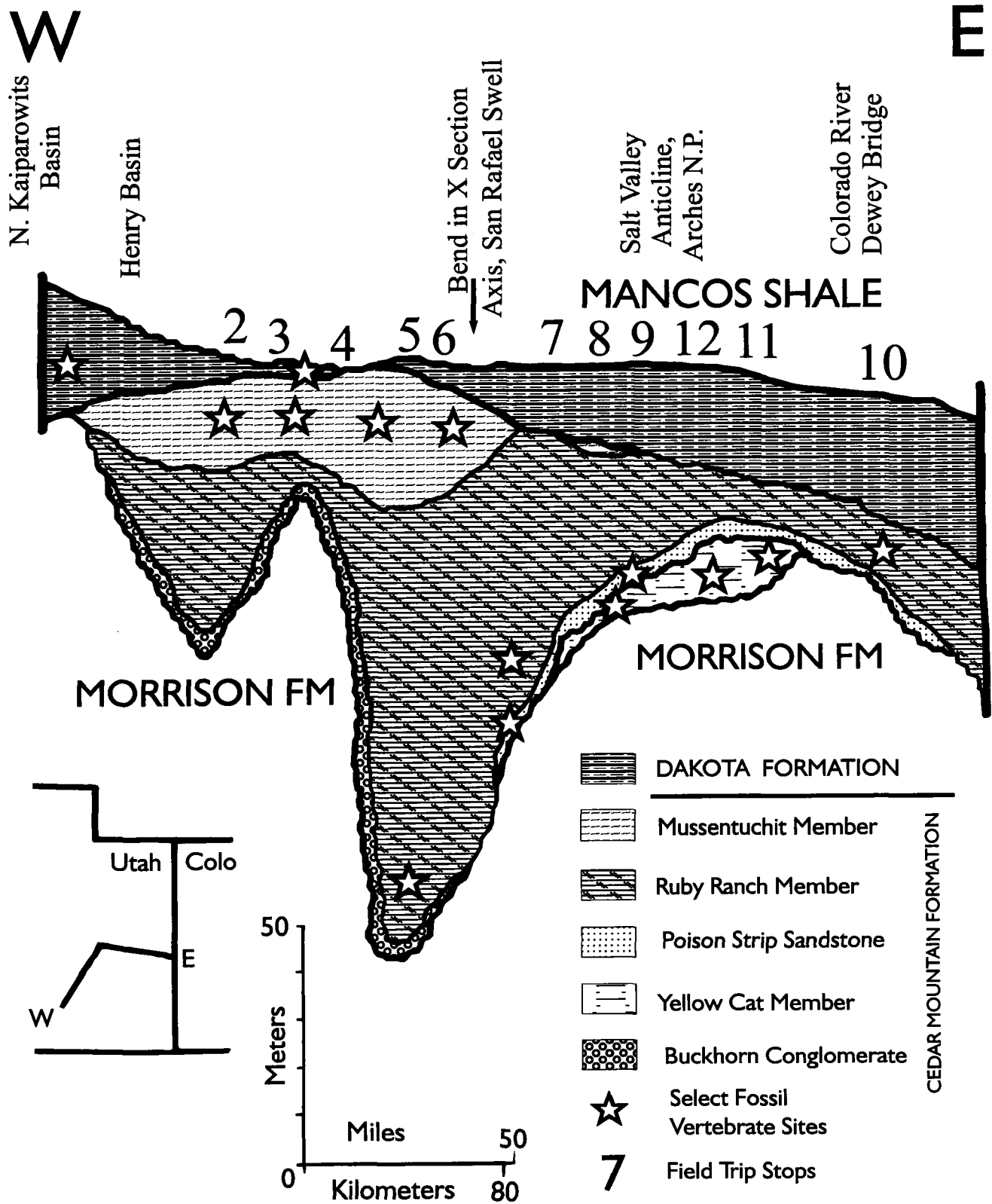


Figure 5. Cross-section showing the distribution of "middle" Cretaceous units discussed in text. Field trip stops are numbered (Fig. 2).

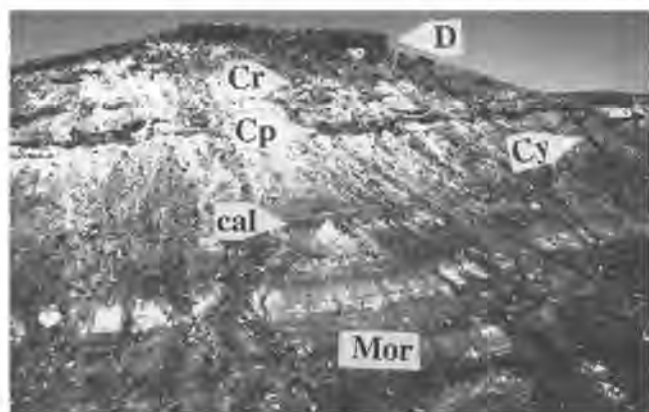


Figure 6. Type section of Yellow Cat Member of the Cedar Mountain Formation above Yellow Cat Flat near the Gaston Quarry. Arrow points to position of Gaston Quarry. Abbr. cal = calcrete; Cp = Poison Strip Sandstone; Cr = Ruby Ranch Member; Cy = Yellow Cat Member; D = Dakota Formation; Mor = Morrison Formation.

additional support to previously published Aptian-Albian dates for the onset of thrusting (Lawton, 1985, 1986; Heller et al., 1986).

The distribution of the Yellow Cat Member from the Uncompahgre Uplift to the San Rafael Swell is compatible with the proposal by Doelling (1988) and Aubrey (1996); that the distribution of Barremian age sediments in eastern Utah was controlled by salt tectonics during the Early Cretaceous. This might help explain the rapid thinning and thickening of the Yellow Cat Member in this region.

The Yellow Cat fauna as preserved at numerous sites (Stops 8, 9, 11, 12) includes abundant polacanthid specimens cf. *Polacanthus* n. gen., *Iguanodon ottingeri* (Galton and Jensen, 1979), perhaps a distinct sail-backed iguanodontid (= *I. ottingeri*, Britt and Scheetz, personal commun., 1997), titanosaurid and camarasaurid sauropods, a small maniraptoran theropod cf. *Ornitholestes* n. gen., and the giant dromaeosaurid *Utahraptor ostrommaysorum* (Kirkland et al., 1993a, 1993b, 1995; Britt et al., 1996). In addition, fish, turtles, crocodilians, and a sphenodontid have been recognized (Table 1). Significant collections of these fossils are housed at the Earth Science Museum, Brigham Young University, College of Eastern Utah (CEU) Prehistoric Museum, Denver Museum of Natural History, and the Oklahoma Museum, of Natural History. The polacanthid ankylosaur, iguanodontids, and sauropods indicate close temporal and geographic ties to the Barremian of Europe (Blows, 1993; Norman, 1988). This correlation is also supported by charophyte data (Shudack, written commun., 1997). Furthermore, they indicate a close correlation with the Lakota Formation at Buffalo Gap, South Dakota (Fig. 1) (Kirkland, 1992; Kirkland et al., 1993; Lucas, 1993). Lucas

Table 1. Yellow Cat Fauna

Class Chondrichthyes
Order Hybodontoidae
<i>Hybodus</i> sp.
Class Osteichthyes
Subclass Dipnoi
<i>Ceratodus</i> n. sp.
Subclass Actinopterygia
cf. <i>Semionotus</i> ? sp.
cf. <i>Amia</i> sp.
Class Reptilia
Order Chelonio
cf. <i>Glyptops</i> sp.
Order Rhynchocephalia
cf. <i>Toxolophosaurus</i> sp.
Order Crocodilia
indet. teeth
Order Theropoda
Family Dromaeosauridae
<i>Utahraptor ostrommaysorum</i>
? Family
small maniraptoran n. gen.
Order Sauropoda
Family Camarasauridae
n. gen.
Family Titanosauridae
n. gen.
Order Ornithopoda
Family Iguanodontidae
<i>Iguanodon ottingeri</i>
n. gen. "with very high neural spines"
(= <i>I. ottingeri</i> ?)
Order Ankylosauria
Family "Polacanthidae"
n. gen. cf. <i>Polacanthus</i> sp.

(1993) has proposed that faunas of this composition be referred to as Buffalogapian for Buffalo Gap, South Dakota, where this fauna is relatively well developed in the Lakota Formation.

The presence of numerous calcareous nodules representing paleosols indicates that the Yellow Cat Member was deposited under a semiarid, monsoonal climate similar to that interpreted for the underlying Morrison Formation (Dodson et al., 1980; Wing and Sues, 1992). The widespread occurrence of fish, freshwater turtles, and crocodilians suggest it may have been somewhat wetter than indicated for the Late Jurassic of the Colorado Plateau. The floras recorded for the Barremian are generally devoid of

angiosperms, suggesting a flora much like that of the Jurassic (Wing and Sues, 1992).

The Poison Strip Sandstone

We propose the Poison Strip Sandstone as the official designation for the middle sandstone unit of Young (1960) at the top of the Yellow Cat Member in eastern Utah (Fig. 4). The name comes from the typical exposures of this unit along the Poison Strip. The type section forms the sandstone cliff holding up the escarpment on the southwest end of the Poison Strip (SW1/4, NE1/4, NW1/4, Sec. 31, T22S, R22E on the Mollie Hogans, Utah, U.S.G.S. 1:24,000 Quad.) east northeast of the Ringtail Mine (Fig. 7). The type section measures 5.4 m thick and is fine to medium grained with floating black, gray, and white chert pebbles. It is trough crossbedded and becoming slabby, with pale greenish mudstone partings toward the top.

Laterally, the Poison Strip Sandstone contains minor conglomeratic lenses and stringers of gray and white chert pebbles. In places there are as many as three crossbedded sandstones that are probably genetically related, and locally there is only a thin crevasse splay or no sandstone at all. This persistent sandstone interval holds up the escarpment exposing the upper Morrison Formation throughout the area from Green River to the Utah/Colorado border. It forms one of the most persistent and distinctive stratigraphic intervals in the entire Cedar Mountain Formation of eastern Utah. At some sites along the Poison Strip escarpment (Stop 11), large scale (5 m +) epsilon cross-bedding indicates that a large meandering river system was mostly responsible for its deposition. Sedimentologically, the sandstone is clearly distinct from the trough-crossbedded conglomerate of the Buckhorn Member of the Cedar Mountain Formation in the San Rafael Swell area. The middle sandstone unit as used by Young (1960) in the western San Rafael Swell area is well up within the Aptian-Lower Albian portion of the Cedar Mountain and appears to be an unrelated sandstone of more limited extent.

Although both the Buckhorn Conglomerate and the Poison Strip Sandstone lie below the Ruby Ranch Member (Fig. 5), there is no means of correlation between these two units and areas (Young, 1960). In the western San Rafael Swell area, no fossils have been found in the Buckhorn Conglomerate at the base of the Cedar Mountain Formation, so it is impossible as yet to date the Buckhorn. However, DeCourten (1991) has recognized an Aptian-Albian fauna from just above the base of the Cedar Mountain Formation in one of the thickest sections near Castledale, Utah (Stop 5).

On the northeast side of Arches (Stop 8) Bodily (1969) described a large ankylosaur from the Poison Strip Sandstone. Coombs (1969) referred the taxon to the Cloverly Formation nodosaurid ankylosaur, *Sauropelta*. Just north of this



Figure 7. Type section of Poison Strip Sandstone Member of the Cedar Mountain Formation on the west end of the Poison Strip. Abbr. Cp = Poison Strip Sandstone; Cy = Yellow Cat Member; Mor = Morrison Formation

site a second specimen of *Sauropelta* was recently discovered by researchers from the Denver Museum of Natural History. These fossils indicated the Poison Strip Sandstone is close to the same age as the overlying Ruby Ranch Member. The CEU Prehistoric Museum has recovered parts of an ornithomimid from a conglomeratic sandstone at the base of the Cedar Mountain Formation, southeast of Wellington, Utah (Burge, 1996). This specimen appears to represent *Tenontosaurus* (also characteristic of the Cloverly Formation) and suggests this sandstone may approximately correlate to the Poison Strip Sandstone. The sparse, small, black, gray, and white chert pebbles are similar to those in the Poison Strip Sandstone. Large conifer logs and cycads are present locally within this sandstone in the area around Arches National Park.

The Ruby Ranch Member

We propose a type section (Fig. 5) for the Ruby Ranch Member north of the Ruby Ranch site (NW1/4, NW1/4, SW1/4, Sec. 31, T22S, R18E on the Dee Pass, Utah, U.S.G.S. 1:24,000 Quad.). The basal contact is with the Poison Strip Sandstone, and the upper contact is at the base of the Dakota Formation. The type section is 33.1 m thick and consists primarily of drab green and mauve variegated mudstone with abundant irregular carbonate nodules that literally cover the slope. At 2.1, 14, and 16.6 m above the base there are ribbon sandstones 2–3 meters thick, whose thalweg and crossbed directions indicate that they represent eastward flowing rivers. Overall the drab variegated mudstones have a pale mauve surface expression. The upper 8.5 m is a pale greenish gray with fewer, but larger carbonate nodules.

The Ruby Ranch Member extends across the entire outcrop belt of the Cedar Mountain Formation and eastward into sediments currently assigned to the Burro Canyon

Formation east of the Colorado River. Its basal contact is with the Poison Strip Member of the Cedar Mountain Formation from at least the Utah/Colorado border region westward to the eastern San Rafael Swell. The upper contact of the Ruby Ranch is clearly with the base of the coals, carbonaceous shales, and sandstones of the Dakota Formation from Colorado westward to the eastern San Rafael Swell. On the west side of the San Rafael Swell, a sharp break from carbonate-nodule-bearing, non-smectitic strata to carbonaceous, highly smectitic strata marks the upper contact. A conglomerate unit rich in quartzite pebbles, that is equivalent for the most part to Young's (1960) middle Naturita sandstone, lies at this position along the northeastern side of the San Rafael Swell (Kirschbaum, written commun., 1997).

Locally, on the west side of Arches National Park a smectitic interval is present at the top of the Cedar Mountain Formation. Potentially, this interval correlates with the Mussentuchit Member of the western San Rafael Swell. The report of a hadrosaur femur from this area may lend support to that correlation (Galton and Jensen, 1979). In this area and to the east, weathering profiles of the Ruby Ranch Member indicated the some of the clays may be partially smectitic, but not to the degree observed in smectitic interval at the top of the Cedar Mountain Formation.

Throughout its extent, the Ruby Ranch Member consists of drab, variegated mudstones with minor sandstone and limestone layers. Perhaps most characteristic of this member are the abundant carbonate nodules that often are so abundant as to form a pavement covering the exposed slopes. The abundance of these nodules makes prospecting for fossils in this interval difficult. The Ruby Ranch Member contains ribbon sandstone bodies that often hold up ridges that may extend for a mile or more (ex. Young, 1960, DeCourten, 1991). A good portion of the northwestward thickening observed in the Cedar Mountain across the San Rafael Swell (ex. Stokes, 1952, Young, 1960) is represented by the Ruby Ranch Member. There is also a good deal of rapid thinning and thickening of this interval south to north along the west side of the San Rafael Swell.

The Ruby Ranch fauna (Table 2) includes the primitive iguanodontid *Tenontosaurus*?, the large nodosaurid *Sauropelta*, sauropods assigned to *Pleurocoelus* (= *Astrodon*), dromaeosaurid teeth, an unidentified large theropod, and *Acrocanthosaurus* (Weishampel and Weishampel, 1983; DeCourten, 1991; Kirkland, 1996b). This is the least well known of the Cedar Mountain faunas. Important collections of these fossils are housed at the University of Utah, CEU Prehistoric Museum, and the Oklahoma Museum of Natural History. This fauna compares well with those documented from the Cloverly Formation, Arundel Formation, and Trinity Group characteristic of North America's apparently endemic Aptian-Lower Albian dinosaur fauna (Kirk-

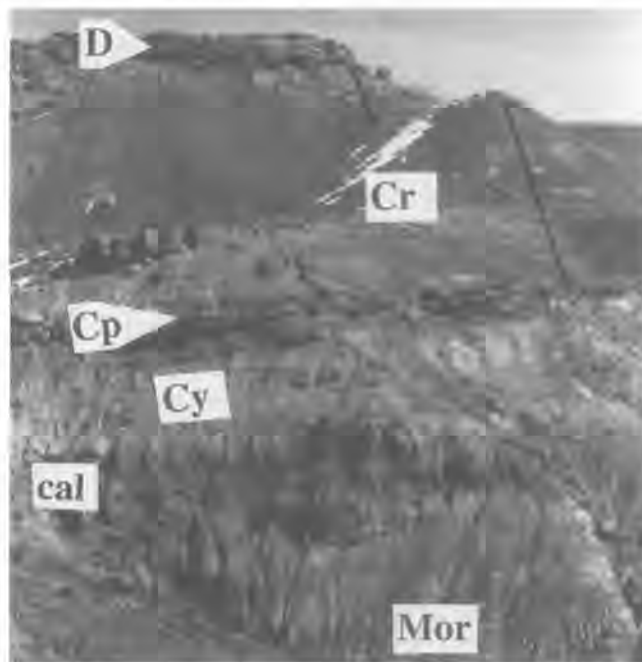


Figure 8. Type section of Ruby Ranch Member of the Cedar Mountain Formation north of the Ruby Ranch homestead site; Abbr: cal = calcrete; Cp = Poison Strip Sandstone; Cr = Ruby Ranch Member; Cy = Yellow Cat Member; D = Dakota Formation; Mor = Morrison Formation.

land, 1996b). Lucas (1993) has proposed referring to faunas with these characteristic taxa as Cashenranchian for the Cashen Ranch, in southern Montana, where this fauna is well developed in the Cloverly Formation (Fig. 1).

The presence of very abundant calcareous nodules representing paleosols indicate that the Ruby Ranch Member was deposited under a semiarid monsoonal climate similar to that interpreted for the underlying Morrison Formation (Dodson et al., 1980, Wing and Sues, 1992). The abundance of paleosols suggests the time involved in deposition of the entire Ruby Ranch Member was significant, as each paleosol represents a hiatus in deposition (Kraus and Bown, 1986). The pollen record indicates that angiosperms were becoming a part of Western Interior floras at this time (Wing and Sues, 1992).

The Mussentuchit Member.

We proposed that upper Cedar Mountain Formation along the west side of the San Rafael Swell be designated the Mussentuchit Member (Fig. 9, Stop 2), with its type section south of Mussentuchit Wash (SW1/4, NW1/4, SE1/4, Sec. 4, T25S, R6E on the Willow Springs, Utah, U.S.G.S. 1:24,000 Quad). At the type section, the member measures 25 m thick and is predominantly composed of drab, gray highly smectitic mudstone. A thin discontinuous sandstone

Table 2. Ruby Ranch Fauna

Class Chondrichthyes
Order Hybodontidae
<i>Hybodus</i> sp.
Class Reptilia
Order Crocodilia
very large blunt teeth and small teeth
Order Theropoda
Family Dromaeosauridae
cf. <i>Deinonychus</i> sp.
Family Allosauridae ?
new large theropod
cf. <i>Acrocanthosaurus</i> sp.
Order Sauropoda
Family Brachiosauridae
<i>Pleurocoelus</i> sp. = <i>Astrodon</i> sp.
Order Ornithopoda
Family Iguanodontidae
<i>Tenontosaurus</i> sp.
Order Ankylosauria
Family Nodosauridae
cf. <i>Sauropelta</i> sp.

marks, the base, where the nonsmectitic mudstone rich in carbonate nodules is replaced by smectitic mudstone as determined by its characteristic "popcorn" weathering. Several thin lenticular sandstones and lignitic horizons are present. It is dated as straddling the Albian-Cenomanian boundary on palynology (Nichols and Sweet, 1993) and subsurface correlations (Molenaar and Cobban, 1994). The top of the member is marked by a thick buff sandstone representing the base of the Dakota Formation.

This member clearly was intended to be included by Stokes (1944, pl. 4, Fig. 2; 1952, p. 1773) in the Cedar Mountain Shale as is illustrated by his picture of the type section capped by a laterally extensive ledge of sandstone at the base of the Dakota Formation. However, he described the Cedar Mountain as having abundant carbonate nodules and does not mention that at the top it may lack such nodules. Locally, in the area of the southwestern San Rafael Swell south of Interstate 70, sandstone lenses near the top of this interval compare well with the more extensive sandstone ledge typically used to define the base of the Dakota Formation (ex. Stokes, 1944). This suggests that this interval may represent nearly continuous sedimentation with the more carbonaceous overlying Dakota Formation. In fact, Young (1960) included this interval in the Dakota Formation. The dramatic shift in the sedimentology and paleontology at the base of this interval suggests that perhaps this interval would be better included as a basal member of the



Figure 9. Type Section of Mussentuchit Member of the Cedar Mountain Formation near Mussentuchit Wash. Abbr. Cb = Buckhorn Conglomerate; Cm = Mussentuchit Member; Cr = Ruby Ranch Member; D = Dakota Formation.

Dakota Formation. This would mean, however, that nearly every fossiliferous horizon in the area of the western San Rafael Swell attributed to the Cedar Mountain Formation would have to be placed in the Dakota Formation (Kitch, 1951; Stokes, 1952; Thayne, et al., 1983; 1985; Thayne and Tidwell, 1984; Tidwell and Thayne, 1985; Jensen, 1970; Eaton and Nelson, 1991; Cifelli, 1993; Kirkland and Burge, 1994; Cifelli et al., in press a, b).

The preserved dinosaur fauna (Table 3) includes a small nodosaurid cf. *Pauciposaurus* (= *Texasites*) n. sp., a small iguanodontian grade ornithomimid, a primitive lambeosaurine hadrosaur, ceratopsian teeth, pachycephalosaur teeth, tiny sauropod teeth, a dromaeosaurid, cf. *Richardoestesia* teeth, cf. *Paronychodon* teeth, and an early tyrannosaurid (Kirkland and Burge, 1994; Kirkland and Parrish, 1995; Burge, 1996). Teeth of a very small sauropod similar in morphology to those described as *Astrodon* are also present marking the last occurrence of sauropods in North America prior to their reintroduction from South America in the Late Maastrichtian (Lucas and Hunt, 1989). At the family level, this fauna is remarkably similar to those of the Campanian and Maastrichtian of western North America (Kirkland, 1996b). Important collections of these fossils are housed at the Oklahoma Museum of Natural History and the CEU Prehistoric Museum.

As the only likely ancestors of the hadrosaur, ceratopsian, and perhaps the tyrannosaurid are from the Early Cretaceous of Asia, the dramatic shift to faunas typical of the North American Late Cretaceous is interpreted to be the result of opening migration corridors to and from Asia through Alaska at the end of the Early Cretaceous, when migration to eastern North America was still possible (Kirkland, 1996b; Cifelli et al., in press a). Following an extensive screen washing operation by the University of Oklahoma, that resulted in thousands of catalogued specimens representing nearly 80 vertebrate taxa, Cifelli et al., (in press b) characterized this fauna as the Mussentuchit Local Fauna

Table 3. *Mussentuchit Fauna*
(after Cifelli et al., in press a, b)

Class Chondrichthyes

Order Hybodontidea

Polyacrodus sp.

Lissodus sp.

Order Orectolobiformes

2 genera

Order Batoidea

cf. *Baibisha* n. sp.

Rhinobatus sp.

Ischyrrhiza sp.

Class Osteichthyes

Subclass Dipnoi

Ceratodus sp.

Subclass Actinopteria

cf. *Semionotus* 2 n. gen.

Lepisosteiformes

Pycnodontiformes

Amiiformes

Class Amphibia

Inc. sedis

Albanerpetodontidae

2 genera

Order Caudata

2 genera

Order Anura

4 genera

Class Reptilia

Order Chelonia

Naomichelys sp.

Glyptops sp.

ident. gen. & sp.

Order Squamata

cf. *Peneteius* sp.

6 n. gen. n. sp.

Order Serpentes

Coniophis sp.

Order Crocodillia

Bernissartia sp.

cf. *Dakotasuchus* sp.

Polydectes sp.

Machimosaurus sp.

3 indet. gen. sp.

Order Theropoda

Family Dromaeosauridae

new cf. *Deinonychus* sp. large

Family Troodontidae

cf. *Troodon* sp.

Family Tyrannosauridae

cf. *Alectrosaurus* sp.

Family indet.

cf. *Paronychodon* sp.

cf. *Richardoestesia* sp.

Order Sauropoda

Family Brachiosauridae

? cf. *Astrodon* sp.

Order Ornithopoda

Family Hypsilophodontidae

cf. *Zephrosaurus* sp.

2 indet. gen. sp.

Family Iguanodontidae ?

cf. *Tenontosaurus* sp.

Family Hadrosauridae

n. gen. n. sp.

Order Ankylosauria

Family Nodosauridae

cf. *Pawpawsaurus* n. sp.

Order Pachcephalosauria

indet. gen. sp.

Order Ceratopsia

indet. gen. sp.

Class Aves

Order Hesperornithiformes

sp. indet.

Order indet.

Class Mammalia

Order Triconodonta

Astroconodon n. sp.

2 n. gen. sp.

Order Docodonta

indet. gen. sp.

Order Multituberculata

Paracimexomys robisoni

? *Paracimexomys bestia*

2 *P.* n. sp.

2 ? *p.* n. sp..

2 n. gen. sp.

Order Symmetrodontia

Spalacotheroides sp.

Spalacotheridium n. sp.

n. gen. sp.

Order Tribotheria

indet. gen. sp.

3 n. gen. sp.

Order Marsupialia

Kokopellia juddi

2 n. gen.

for Mussentuchit Wash, where many of the best vertebrate sites are located. Perhaps following traditional land-animal ages begun in the middle Mesozoic by Lucas (1993), faunas preserving these taxa should be referred to as Mussentuchitian.

The most common animal from the upper fauna is a primitive hadrosaur (Kirkland and Burge, 1994). Common hadrosaur teeth from Cedar Mountain sites on the west side of the San Rafael Swell were first noted by Parrish (1991). At present, the Cedar Mountain hadrosaur has been determined to be a primitive hadrosaur somewhat like *Telmatosaurus* (Weishampel et al., 1993) from the Upper Cretaceous of eastern Europe and a bit more advanced than the iguanodont *Probaetosauros* (Rozhdestvensky, 1967; Norman, 1990) from the Lower Cretaceous of central Asia. More research is needed to determine its systematic position relative to the Hadrosaurinae and Lambeosaurinae (Seren, 1986; Horner, 1990; Weishampel and Horner, 1990). However, the material discovered to date suggest lambeosaur affinities. Further research will be needed to see if this determination is based on primitive characters lost in later mainline hadrosaurines.

It is important to note that Molenaar and Cobban (1991) have concluded that subsurface relationships indicate the uppermost Cedar Mountain Formation may correlate to the Mowry Shale to the northeast and thus be of basal Cenomanian age. The Albian-Cenomanian boundary on the basis of non-marine palynomorphs has been placed at the first occurrence of tricolporates (ie. *Nyssapollenites*, rare in marine rocks) and obligate tetrads (Singh, 1975; Nichols and Sweet, 1993). Tschudy et al., (1984) did not encounter these palynomorphs in their samples from the upper Cedar Mountain Formation near Castledale, Utah. Their occurrence is diachronous across Alberta (Nichols and Sweet, 1993, p. 559). In addition, with the older placement of the Albian-Cenomanian boundary by Cobban and Kennedy (1989, by ammonite correlations to the type areas in Europe), it is likely that this datum is above the base of the Cenomanian (Nichols and Sweet, 1993, p. 578).

The critical thing is that the palynology and lithostratigraphy support a correlation with the Latest Albian-Basal Cenomanian Mowry Shale to the northeast (Nichols and Sweet, 1993; Molenaar and Cobban, 1991). The classic Cloverly-Pauluxy fauna occurs at the beginning of the Kiowa-Skull Creek second order cyclothem (ex. Kauffman and Caldwell, 1993). The thin sandy interval below the Mussentuchit Member probably correlates to the base level draw down (i.e. unconformity) that occurs between these two cyclothem. Many geologists would prefer to see the unconformity at the base of the Dakota Formation to represent this unconformity and the authors of this volume are not in agreement relative to retaining the Mussentuchit

Member at part of the Cedar Mountain Formation. A compromise view is to retain it as part of the Cedar Mountain Formation following Stokes' (1944, 1952) original definition.

The absence of calcareous nodules representing paleosols indicates that the Mussentuchit Member was deposited under a significantly wetter environment than were the lower members of the Cedar Mountain Formation, in part due to the transgression of the Mowry Sea into the area of the northwestern Uinta Basin (Wing and Sues, 1992). The plant record indicates that angiosperms were becoming a more important part of Western Interior floras at this time (Wing and Sues, 1992) and some of the earliest records of some angiosperm wood types are from this member (Thayne et al., 1983, 1985; Tidwell, 1996). Finally, the dramatic increase in the volume of volcanic ash preserved in the Mussentuchit Member indicates a significant increase in volcanic activity to west.

A dramatic shift in faunal composition between Albian and middle Cenomanian has been noted in Texas (Lee, 1995; Winkler et al., 1995). The new dates for the Mussentuchit Member indicate that this faunal turnover was even more dramatic than was previously thought, with a nearly complete turnover of the dinosaur fauna during the late Albian. Recognition of the Mussentuchit Local Fauna indicates that instead of a two fold zonation of Cedar Mountain Formation based on dinosaurs (Kirkland, 1992; Lucas, 1993) there are three distinct faunas (Kirkland, 1996b). These are: (1) a basal Barremian iguanodont-polarcanthid fauna with European affinities predating common flowering plants found in the Yellow Cat Member, (2) a middle Aptian-middle Albian *Tenontosaurus-Pleurocoelus* fauna perhaps representing an impoverished recovery fauna following a major Lower Cretaceous extinction event (endemic to North America) found in the Poison Strip Sandstone and Ruby Ranch Member, and (3) an upper latest Albian-lowest Cenomanian hadrosaur fauna with Asian affinities when flowering plants were co-dominant found in the Mussentuchit Member. The replacement of North American taxa by taxa with Asia origins indicates that biogeography rather than the rise of angiosperms account for most of the extinction of dinosaurs recorded within the upper Cedar Mountain Formation (Kirkland, 1996b; Cifelli et al., in press b).

The Dakota Formation.

The carbonaceous strata between the Cedar Mountain and Burro Canyon Formations and the overlying Mancos Shale have been called the Dakota Sandstone or Dakota Formation. The term "Dakota (?)" has also been used (Fig. 4) because of the uncertainty of the relationship of these rocks on the Colorado Plateau with the type area of the

Table 4. *Dakota Fauna*
(after Eaton et al., 1997)

Order Hybodontoidae	Order Crocodillia
Class Chondrichthyes	Bernissartidae
Order Hybodontoidae	<i>Goniopholis</i> sp.
<i>Hybodus</i> sp.	<i>Telorhinus</i> sp.
<i>Lissodus</i> sp.	indet. gen. sp.
Order Batoidea	Order Theropoda
n. gen. sp. cf. <i>Myledaphus</i>	Family Dromaeosauridae
<i>Ischyrrhiza</i> sp. cf. <i>I. avonicola</i>	2 indet. gen. sp.
Class Osteichthyes	Family Troodontidae
Subclass Dipnoi	cf. <i>Troodon</i> sp.
<i>Ceratodus gustasoni</i>	Family Tyrannosauridae
Subclass Actinoptergiria	indet. gen. sp.
cf. <i>Semionotus</i> 2 n. gen.	Family indet.
<i>Lepidotes</i> sp.	cf. <i>Paronychodon</i> sp.
cf. <i>Dapedius</i> sp.	cf. <i>Richardoestesia</i> sp.
Pycnodontiformes	Order Ornithopoda
Lepisosteidae	Family Hypsilophodontidae
Amiiformes	indet. gen. sp.
Class Amphibia	Family Hadrosauridae
Inc. sedis	indet. gen. n. sp.
Albanerpetodontidae	Order Ankylosauria
1 genus	Family Nodosauridae
Order Caudata	indet. gen. sp.
Batrachosauridae	Family Ankylosauridae
cf. <i>Batrachosauroides</i> sp.	indet. gen. sp.
Class Reptilia	Class Mammalia
Order Chelonia	Order Multituberculata
cf. <i>Deinonychys</i> sp.	<i>Cimolodon</i> sp. cf. <i>C. similis</i>
<i>Naomichelys</i> 3 sp.	<i>Paracimexomys</i> sp. cf. <i>P. robisoni</i>
<i>Glyptops</i> sp.	<i>Dakotamys malcolmi</i>
Order Squamata.	Order Symmetrodonta
cf. <i>Saurillodon</i> sp.	indet. gen. sp.
6 indet. gen. sp.	Order Tribotheria
	<i>Dakotadens morrowi</i>
	Order Marsupialia
	<i>Alphadon clemensi</i>
	<i>Alphadon lilligraveni</i>
	<i>Protalphadon</i> sp.
	<i>Pariadens kirklandi</i>

Dakota Sandstone on the Missouri River near Dakota, Nebraska (Meek and Hayden, 1862). Recognizing this problem, Young (1960) referred these strata to the Naturita Formation, with a type area near Naturita, western Colorado. Additionally, he joined the Cedar Mountain and Naturita into a Dakota Group providing continuity with the terminology being employed in the Colorado Front Range (Fig. 4). Young (1960) reported extensive intertonguing of the Cedar Mountain with his Naturita Formation from west to east. Craig et al., (1961) emphasized the unconformable nature of the contact between the Cedar Mountain and

"Naturita" Formation. The term Naturita Formation has largely been ignored by subsequent authors.

The Dakota Formation on the Colorado Plateau has generally been divided into three informal members (ex. Katich, 1956; Eaton, 1987): (1) a lower 0–20 m thick basal sandstone or conglomerate; (2) a middle 0–24 m thick interval of sandy carbonaceous shales, channel sandstones with coal; and (3) an upper 0–25 m thick interval of transgressive marine shale and sandstone. The Dakota Formation is generally thin and highly variable throughout the central Colorado Plateau. Locally it may pinch out completely (ex. Eaton

et al., 1990) or where sandstones are largely absent it forms a continuous slope between the upper Cedar Mountain Formation and Mancos Shale.

Most terrestrial vertebrate remains from the Dakota Formation are from the middle carbonaceous member. No radiometric dates exist as yet for this interval but assuming the coals were deposited proximal to the Mancos Sea, these units can be approximately dated from marine fossils capping the sequence (Cobban, 1976; Eaton et al., 1990) and lateral relationships with marine strata (Elder and Kirkland, 1993, 1994). These relationships provide dates of middle to early late Cenomanian for these strata, which is supported by macrofloral and palynological studies summarized by Tidwell (1996).

The dinosaur fauna from the Dakota Formation is based on the wet screenwashing of microvertebrate sites (Parrish, 1991; Eaton et al., 1997) and includes teeth of dromaeosaurids, troodontids, cf. *Richardoestesia* sp., cf. *Paronychodon* sp., tyrannosaurids, nodosaurids, ankylosaurids, hypsilophodontids, and hadrosaurids. Most noticeably absent, but represented in all the earlier faunas, are sauropods, recording the base of the North American mid-Cretaceous sauropod hiatus (Table 4). Rushforth (1971) speculated that the carbonaceous units were deposited in a lush swampy mudflat near the edge of the Mancos Sea. The floras are dominated by ferns and horsetails; various gymnosperms and angiosperms grew along streams and adjoining upland areas.

STOP 1. Christianburg locality, southeastern San Pitch Mountains. T. Lawton

Stop at milepost 213 on US Highway 89, 4.5 miles east of Gunnison, Utah. We will hike across a section of slope-forming mudstones (Cedar Mountain Formation) and overlying conglomerate beds. At Christianburg, the Lower Cretaceous section is well studied and generally representative of the section of the San Pitch Mountains; the Cedar Mountain is 132 m thick (Witkind et al., 1986); the overlying conglomeratic section is 197 m thick (Sprinkel et al., written commun. 1996). The beds here dip steeply and overturned to the east. They are in fault contact with the Jurassic Arapien Formation to the east (Weiss, 1994), contain a number of east dipping thrust faults, and are overlapped by Paleocene (?) beds of the North Horn Formation on the southwest and west (Weiss, 1994; Sprinkel et al., written commun. 1996). This structure represents the faulted west flank of a box fold or popup cored by Jurassic shale and evaporite of the Sanpete Valley. The entire Cretaceous section is detached from Jurassic and older strata beneath this location at a decollement, termed the Gunnison thrust, in the evaporite beds (Standlee, 1982; Lawton, 1985).

Beds assigned to the Cedar Mountain here consist of

mudstone with abundant calcareous nodules and subordinate sandstone and light gray limestone. The mudstone represents flood-plain deposits, the calcareous nodules represent paleosols, and the limestones were deposited in freshwater ponds (Schwans, 1988b). Soil horizons within the section appear to be composite or stacked, and thus indicate slow deposition punctuated by unconformities.

The base of the San Pitch Formation is at the lowermost conglomerate in the section. Beds of the conglomeratic section above the Cedar Mountain are on the order of 10 m thick and have a broadly lenticular or channel form. They are interbedded with red siltstone and mudstone. Clasts within the lower 57 m include green quartzite clasts of the Proterozoic Dutch Peak Formation, as well as sandstone clasts derived from Jurassic and Triassic formations. The Dutch Peak Formation is now exposed in the Sheeprock Mountains northwest of the San Pitch Mountains, and the Mesozoic clasts were presumably derived from the Pavant thrust plate to the west. These diverse lithologies were contributed in part by a large Early Cretaceous drainage network that departed the thrust belt at the Leamington cross-strike discontinuity (Lawton et al., 1994). Conglomerate beds of the overlying 96 m contain boulders and cobbles of both quartzite and carbonate, mostly dolostone. Interbedded mudstone is reddish orange and silty. The uppermost part of the section consists of 44 m of reddish-brown to gray silty mudstone (Sprinkel et al., written commun. 1996). It is unconformably overlain by a striking quartzite-boulder conglomerate that marks the base of the Sanpete Formation, which is equivalent to the Dakota Sandstone.

STOP 2. The Mussentuchit Member of the Cedar Mountain Formation along Mussentuchit Wash. R. Cifelli & J. Kirkland

At this stop (Figs. 2, 5), we will have an opportunity to examine the type section of the Mussentuchit Member described above. Over the past several years discoveries in the upper Cedar Mountain along Mussentuchit Wash by field crews from the Oklahoma Museum of Natural History have revealed a diversity of vertebrate sites in the Mussentuchit Member. Extensive quarry operations and wet screen washing have revealed an extraordinary diversity of vertebrate taxa rivaling the most productive sites in North America. Of nearly 80 taxa recorded in this area, many record the first or last occurrences for their particular families. Among the freshwater elasmobranchs these include the first occurrence of freshwater oreotolobids and sclerorhynchids. Among the Squamata, there are early occurrences of helodermatids and snakes. The dinosaurs include many first occurrences including those of the tyrannosaurids, the enigmatic tooth form "*Paronychodon*," hadrosaurids (Fig. 10), pachycephalosaurids, and the neoceratopsids. There are



Figure 10. Skull elements of juvenile specimen of early hadrosaur from one of the OMNH's Mussentuchit sites. Scale in cm.

also first North American occurrences of birds (ex. herperornithiformes) and mammals (ex. marsupials) (Cifelli, 1993; Cifelli et al., in press a, b).

The basal Buckhorn Conglomerate member of the Cedar Mountain Formation in this area forms a distinct ledge 1–3 meters thick (Fig. 12). The overlying Ruby Ranch Member forms a mauve slope 25 m thick covered by carbonate nodules. No fossils have been found in the Ruby Ranch Member in this area. The Ruby Ranch Member is overlain by 25 m of drab smectitic mudstone of the Mussentuchit Member. About midway up in the Mussentuchit Member, a thin lignitic layer preserves abundant plant debris and a volcanic ash (or ashes) associated with several of the OMNH localities (Fig. 11), for which Radiometric Dating is now in progress. The basal Dakota Formation consists of a thick buff sandstone that weathers into large blocks that cover much of the Cedar Mountain slope (Fig. 11).

STOP 3. The Mussentuchit Member of the Cedar Mountain Along the Moore Cutoff Road. R. Cifelli and J. Kirkland.

At this stop (Figs. 2, 5), we will examine a microvertebrate site with abundant dinosaur egg fragments in the Mussentuchit Member. The Cedar Mountain Formation along the Moore Cutoff Road is thinner than that observed either to the south or to the north. The Buckhorn Conglomerate is well developed here, but the Ruby Ranch is very thin. In fact, if it were not for carbonate nodules weathered out on the bench formed by the Buckhorn, it would be hard to demonstrate its presence at all. The Mussentuchit Member is well developed and is on the order of 20 m thick.

In this area, we will examine a significant OMNH microvertebrate site that is characterized by abundant dinosaur egg shell fragments. Jensen (1970) first reported eggshell in

the Cedar Mountain Formation from the Castledale area. The eggshell at this site (Fig. 12) appears to have been transported and mixed with microvertebrate remains, however the large volume of eggshell appears to indicate a nesting site was nearby.

Transported eggshell that may pertain to the *Mussentuchit* hadrosaur is abundant at this site together with isolated teeth. This egg shell has a reticulate surface pattern and is about 3 mm thick. In fact, some of the eggshell described from the Cedar Mountain Formation by Jensen (1970) may pertain to this animal (Karl Hirsch, pers. commun.) as they certainly came from the same stratigraphic level. Part of an embryonic maxilla has also been identified. The presence of embryonic, juvenile, and adult material indicates that the entire growth history of this common new dinosaur will eventually be documented.

STOP 4. The Cedar Mountain and Dakota Formations East of Ferron. J. Eaton and J. Kirkland.

At this stop (Figs. 2, 5) we will examine field evidence documenting local uplift unroofing of the Buckhorn Conglomerate in the basal Turonian.

The diverse fauna found in the Mussentuchit Member in the area of Mussentuchit Wash and the Moore Cutoff Road have been found in the area east of Ferron and Castledale, Utah including the Rough Road Quarry and Robison's Eggshell Quarry (Nelson and Crooks, 1987; Pomes, 1988; Eaton and Nelson, 1991). Important collections from these sites are housed at the Sternberg Museum, Hays, Kansas, University of Colorado Museum, University of California at Berkeley, Paleontological Museum, Brigham Young University Geological Museum, and the Oklahoma Museum of Natural History.

The specimens of *Tenontosaurus* from the Cedar Mountain Formation noted by Weishampel and Weishampel (1983) are from somewhere in this area. The nodular carbonate matrix on many of the bones suggests that these specimens are from the Ruby Ranch Member.

Perhaps most significantly, a terrestrial vertebrate fauna was recovered by Eaton (1987) from the Dakota Formation in this area, (University of Colorado, UCM Loc. 83275). In regard to dinosaurs, this site produced hadrosaurid, iguanodontid, and theropod teeth. It has also produced fishes, turtles, crocodilians, and a multituberculate mammal tooth. A much more diverse fauna of 50 taxa has been recovered in correlative units of the Dakota Formation in southern Utah (Eaton, 1987, 1993a, 1993b; Eaton et al., 1997; Kirkland, 1987) that can be dated as middle to very basal upper Cenomanian based on intertonguing relationships with overlying and laterally adjacent marine rocks (Eaton, 1987; Elder and Kirkland, 1993, 1994). Dinosaurs include veloceraptorine and dromaeosaurine dromaeosaurs, cf. *Troodon*



Figure 11. Arrow points to one of the most productive OMNH microvertebrate sites in Mussentuchit Member. Basal sandstone Dakota Formation caps exposure and litters slope with large blocks of sandstone.

sp., tyrannosaurids, cf. *Richardoestesia* sp., cf. "*Paronychodon*" sp., nodosaurids, ankylosaurids, hypsilophodontids, and hadrosaurids. Taxa from this fauna also includes four freshwater elasmobranchs, eight osteichthians, two amphibians, six turtles, seven lizards, three crocodilians and ten mammals (Table 4). The Dakota fauna is most significant in that it records the last occurrence of many freshwater taxa such as lungfish, semionotids, and the turtle, *Glyptops* (Kirkland, 1987; Eaton et al., 1997). However, while this records a major extinction of freshwater taxa, terrestrial faunas show no extinctions to speak of.

The Dakota Formation ranges from 0–60 meters thick in the area. Marine and mixed brackish water invertebrate fossils from the top of the Dakota Formation from south of the Moore Road date the strata to the latest Cenomanian *Neocardioceras juddii* Zone. In this area, the Dakota coarsens up section to the top of the formation, where there are abundant isolated chert pebbles. Eaton et al., (1990) recognized that the basal Tununk Shale of the Mancos Shale throughout this area is characterized by a pebble-to-cobble,

mud/clay supported conglomerate (Fig. 13) that weathers back, leaving a broad surface at the top of the Dakota Formation covered in dark chert pebbles and cobbles (Fig. 14). Small pebbles are often found nestled in the shells of the abundant gryphaeoid oyster, *Pycnodonte newberryi umbonatus*, a subspecies characteristic of the basal Turonian (Kirkland, 1996c). Shales above this conglomerate can be best dated as late early Turonian (Eaton, 1987; Eaton et al., 1990). The Dakota Formation pinches out locally between Ferron and Castledale, whereas the conglomerate at the base of the Tununk extends throughout the area.

As the chert pebbles resemble those preserved in the Buckhorn Conglomerate, it was proposed that the presence of these along the Dakota/Tununk contact represents local tectonic activity (Eaton et al., 1990). Shortly following the marine transgression into the area during the latest Cenomanian, local uplift, perhaps of the San Rafael Swell, led to unroofing and erosion of the Buckhorn Conglomerate. With continued sealevel rise during the earliest Turonian, the locally derived chert pebbles and conglomerate were re-



Figure 12. Arrow points to OMNH's egg and microvertebrate site near Moore Road.

worked over a wide area. The area was fully submerged below wave base by the late early Turonian (Elder and Kirkland, 1993, 1994).

A local source for the chert pebbles, rather than one in the Sevier thrust belt, is supported by the fact that the correlative Indianola Group conglomerates are rich in Precambrian clasts and are poor in chert (Sprinkel et al., written commun. 1996). Secondly poorly dated Cretaceous faulting on the west side of the San Rafael Swell has been documented (Neuhauser, 1988). At present, recycling of Lower Cretaceous conglomerate seems to be the simplest explanation for the basal Tununk conglomerate.

STOP 5. The Long Walk Quarry, Ruby Ranch Member. F. DeCourten

At this stop (Figs. 2, 5), we will examine the Long Walk Quarry in western Emery County, Utah, that was opened by the Utah Museum of Natural History in 1987. Following the initial collection of surface material, excavations at the site were conducted during three consecutive field seasons

and resulted in the removal of 16 large blocks of the bone-bearing matrix. Quarrying operations were suspended after the 1990 field season to avoid an excessive backlog of unprepared material. Preparation of the material collected from 1987–1990 is still under way, due in part to the hard limestone matrix present at the site. However, the material thus far available clearly documents no less than three individual dinosaurs representing at least two taxa.

In the vicinity of the Long Walk Quarry, the Cedar Mountain Formation is 130 m thick (Fig. 15). The lower contact of the Cedar Mountain Formation is marked by the abrupt, vertical transition from red pebbly mudstones of the Brushy Basin Member of the Morrison Formation to nodular, calcareous mudstone. No Buckhorn Conglomerate is present and the lowermost beds of the Cedar Mountain Formation are the Ruby Ranch Member at the Long Walk Quarry. The Morrison-Cedar Mountain contact is clearly unconformable as indicated by a scoured surface, with up to 1 meter of relief, which separates the two formations. In addition, well developed root traces in the uppermost Morrison mud-



Figure 13. Conglomerate filled scour surface between Tununk Member of Mancos Shale and underlying Dakota Formation.



Figure 14. Lag of black chert pebbles and cobbles on bench formed by Dakota Formation.

stones are locally truncated along this contact, confirming the interpretation of the boundary as an omission surface. The regional extent and temporal significance of this Cedar Mountain/Morrison disconformity remain uncertain, but it may represent a profound pre-Barremian-Aptian period of erosion. The upper contact of the Cedar Mountain Formation with the thin and discontinuous "Dakota" Formation is obscure, but can be defined by the first occurrence of well-sorted, yellow-gray, arenitic to subarenitic sandstone which exhibits small-scale tabular and trough cross-stratification. This sandstone, where present, is from 1 to 3.5 meters thick and grades vertically into the overlying gray marine shale of the Tununk Member of the Mancos Shale. While the sandstone representing the "Dakota" Formation at the Long Walk Quarry serves as a convenient horizon marking the top of the Cedar Mountain Formation, its correlation with the Dakota Formation, as that term is used by other workers in other areas, is uncertain.

The Ruby Ranch Member of the Cedar Mountain Formation is dominantly composed of calcareous mudstone which contains abundant carbonate nodules. The calcareous mudstones are associated with several thin, lenticular, and commonly conglomeratic sandstones. Approximately 135 ft (45 m) above the base of the Cedar Mountain Formation, a ribbon of channel sandstone, similar to those in the Ruby Ranch Member on the east of the San Rafael Swell (Young, 1960; Harris, 1980), is exposed and can be traced for several hundred meters along its generally west-east course.

The base of the Mussentuchit Member is picked where mudstone rich in carbonate nodules are replaced by smectitic mudstone. The Mussentuchit Member makes up the upper 30 meters of the Cedar Mountain Formation at the Long Walk Quarry. It is composed dominantly of carbonaceous, rather than calcareous, mudstone in association with numerous thin, lenticular sandstone bodies. One of these

sandstone units, about 10 meters below the "Dakota" Formation, yields numerous isolated dinosaur tracks. These tracks are assigned to ornithopods (Fig. 16) and ankylosaurs (Lockley et al., in press). Toward the top of the Mussentuchit Member is an important palaeobotanical site (Katich, 1951; Stokes, 1952; Tschudy et al., 1984) that has long been used to date the Cedar Mountain Formation (Fig. 15).

The bone bed forming the Long Walk Quarry occurs in a nodular limestone layer, approximately 0.6 meters thick, overlain and underlain by softer calcareous mudstone typical of the lower portion of the Cedar Mountain Formation. The quarry horizon is approximately 15 meters above the Cedar Mountain-Morrison contact. The nodular limestone may represent a mature calichified surface developed between fluvial channels, though other evidence of pedogenic origin is weak. The preserved bones are completely disarticulated, and each fossil has no direct anatomical association with adjacent material. The long axes of the elongate elements exhibit a preferred orientation in a northeast-southwest direction. This orientation, coupled with previous studies documents a northeastward pattern of sediment dispersal in central Utah during the Early Cretaceous (Heller and Paola, 1989; Harris, 1980). It suggests that the bones were transported to the point of accumulation by streams flowing from a source to the southwest. This inferred northwest paleodrainage is consistent with a source in the southern Sevier Orogenic Belt, as proposed by Fillmore (1993).

The articular surfaces of elongate elements from the Long Walk Quarry exhibit varying degrees of abrasion and most fossils bear small fractures on the outer surfaces that are filled by carbonate material identical to the enclosing matrix. These features suggest at least some pre-burial transportation of the fossils from the Long Walk Quarry. The primary preservational mode of bone is carbonate per-

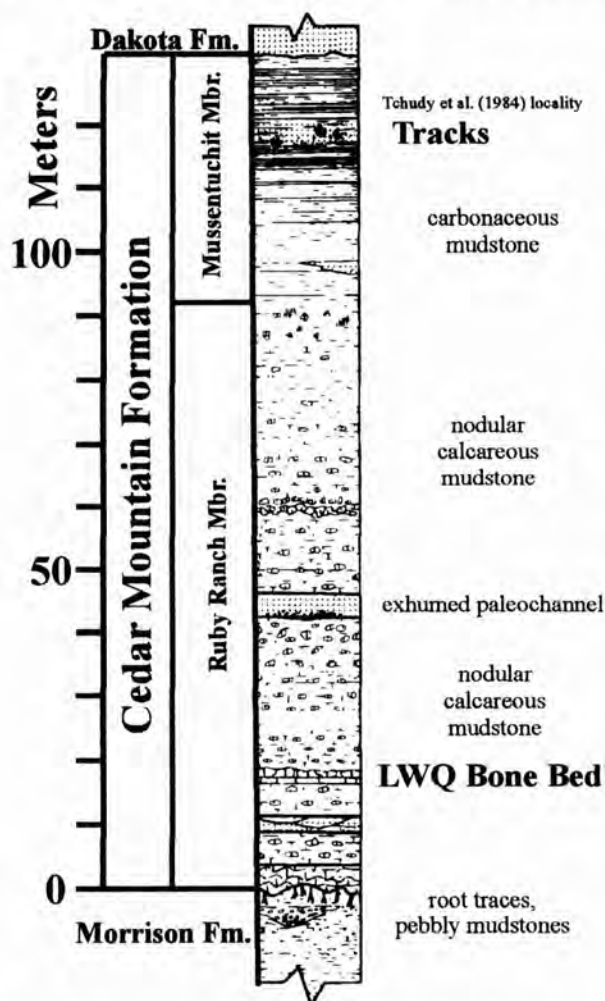


Figure 15. Measured section of the Cedar Mountain Formation at the UMNH's Long Walk Quarry (LWQ), Emery County, Utah (from DeCourten, 1991).

mineralization, which may reflect both depositional and diagenetic events. For additional details concerning the nature of the fossil accumulation at the Long Walk Quarry, see the review of DeCourten (1991).

The Long Walk Quarry is significant because it represents the largest known concentration of dinosaur material in the Ruby Ranch Member of the Cedar Mountain Formation. In spite of the discovery of numerous vertebrate localities in the Cedar Mountain Formation in recent years, very few fossils had been found in the middle portions of the formation. The majority of the elements thus far recovered from the Long Walk Quarry can be tentatively identified as belonging to a *Pleurocoelus*-like sauropod. Sauropod material thus far recovered includes several isolated teeth, a dentary fragment, caudal and dorsal vertebrae, ribs, and fragmentary limb elements. Though current knowledge of the



Figure 16. Ornithopod track from Long Walk track site near top of Cedar Mountain Formation in Mussentuchit Member.



Figure 17. Close up of teeth in early lambeosaurine hadrosaurid jaw from CEU's Carol Site.

osteology of *Pleurocoelus* is incomplete, the Long Walk Quarry material is nearly identical to the type material for this genus from the Arundel Formation in Maryland and to the fossils referred to this genus from the Cloverly Formation of Wyoming and Montana. Several dorsal vertebrae have now been recovered that have the deep pleurocoels and rugose neural suture typical of *Pleurocoelus* (Marsh, 1888). The identification of a *Pleurocoelus*-like animal at the Long Walk Quarry represents the first published account of sauropod dinosaurs in the Lower Cretaceous of the Colorado Plateau region. Some of the sauropod elements evidently represent a juvenile specimen, indicating that the remains of at least two individual sauropods are preserved at the Long Walk Quarry.

In addition to the *Pleurocoelus*-like material, two nearly complete teeth, several partial teeth, and an ilium presently

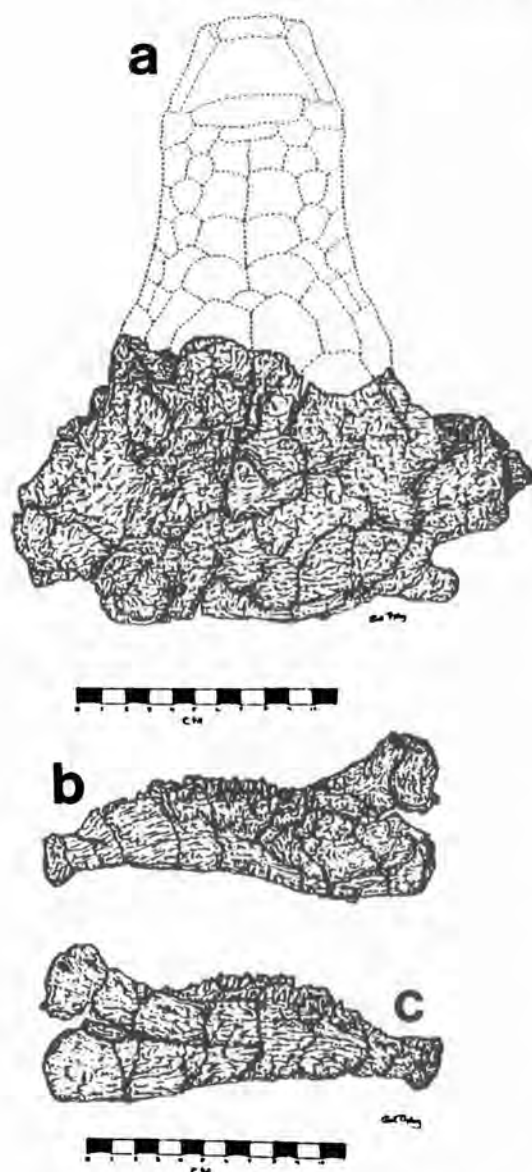


Figure 18. Skull and jaws of cf. *Pawpawsaurus* n. gen. & n. sp. a. dorsal view of skull, b. medial view of jaw, c. lateral view of jaw (from Burge, 1996).

undergoing preparation document the presence of at least one large theropod dinosaur at the Long Walk Quarry. The teeth are of typical theropod form, with coarse serrated edges and a curved anterior margin. The two complete teeth are 84 mm and 99 mm long, comparable in size to the teeth of *Allosaurus*, a well-known large theropod from the Upper Jurassic of east-central Utah. The ilium is at least 40 cm long and appears to belong to a bipedal predator of about average *Allosaurus* size as well. The only known Early Cretaceous theropod similar in size to the Long Walk Quarry



Figure 19. Assorted postcranial elements cf. *Pawpawsaurus* n. gen. & n. sp. skeleton.

specimen is *Acrocanthosaurus* (Stovall and Langston, 1950) from the Comanchean Series of Texas and Oklahoma. However, Kirkland and Parrish (1995) suggested that the teeth of the Long Walk Quarry theropod are distinct from *Acrocanthosaurus* in that they are much more coarsely serrated.

The Long Walk Quarry, and about 6 hectares (15 acres) of surrounding land, has been deeded to the Utah Museum of Natural History at the University of Utah. Plans for the future development of the quarry are being formulated at the present time. Only an estimated 3–5% of the bone bed has been excavated, and even less of it has been thoroughly processed in the preparation laboratory. It is anticipated that between 5000 and 10,000 elements may eventually be recovered at the Long Walk Quarry. This material will provide much needed data on dinosaur fauna from the main body of the Cedar Mountain Formation. The Long Walk Quarry clearly has the potential to develop into one of the most significant fossil localities of the Colorado Plateau region.

STOP 6. The Carol Site, The Ruby Ranch/Mussentuchit Contact. D. Burge and J. Kirkland

At this stop (Figs. 2, 5), we will examine the Carol Site, just above the contact between the Ruby Ranch and Mussentuchit members. This locality was discovered by Carol and Ramon Jones of Salt Lake City, Utah. Material collected so far is from near the surface in a highly rooted interval. As such, portions of some of the bones were completely destroyed by roots. However, careful preparation by John Bird of the CEU Prehistoric Museum in Price, Utah has resulted in a very significant specimen being made available for study. Initial excavations revealed an associated adult hadrosaur skeleton with a disarticulated skull (Fig. 17).

A radiological technician at the University of Utah, Ramon Jones developed a specially shielded device to care-



Figure 20. CEU Prehistoric Museum's Carol Site indicated by arrow northwest of Castledale, Utah. Arrow indicates Carol Site. Abbr. Cb = Buckhorn Conglomerate, Cr/Cm = contact between Ruby Ranch and Mussentuchit Members, D = Dakota Formation.

fully record radiation levels in the shallow subsurface (Jones and Burge, 1995). This resulted in the discovery of a small nodosaurid ankylosaur (Figs. 18, 19) related to *Paupawsaurus* (= *Texasetes*) from the Late Albian of Texas (Coombs, 1995; Lee, 1996). The greatest significance of this discovery, beyond it being a new species of nodosaurid, is that it is the first dinosaur skeleton ever discovered solely using a remote sensing instrument. Additionally, this specimen will be useful in resolving the *Paupawsaurus*/*Texasetes* question, as *Paupawsaurus* is based on a skull (Lee, 1996) and *Texasetes* is based mainly on a postcranial skeleton (Coombs, 1995) and the new Cedar Mountain specimen preserves both (Figs. 18, 19).

A 3–4 m thick section of Buckhorn Conglomerate marks the base of the Cedar Mountain section at this site. It forms a broad northwest sloping bench about a mile. It has abundant black and white chert and limestone clasts up to 10 cm in diameter. Crossbeds indicate a transport direction of N 75 E in this area. The Ruby Ranch Member is 18.3 meters thick, with a prominent ribbon sandstone 0.7 m thick and 100 m across about 10 m above its base. A pebble conglomerate 60 cm thick with a mudstone matrix is replaced by a greenish sandstone to the west just below the Carol site (Fig. 20). The Carol site lies at the base of the Mussentuchit Member, which is 12.3 m thick. It is remarkable that the Cedar Mountain section is only 27% as thick as it is a few kilometers south at the Long Walk Quarry and so close to the type area at Cedar Mountain.

STOP 7. Cedar Mountain Formation at Ruby Ranch. J. Kirkland and S. Hasiotis

At this stop (Figs. 2, 5), we will examine the type section of the Ruby Ranch Member of the Cedar Mountain Formation. The Cedar Mountain Formation has a total thickness of 46.2 m at Ruby Ranch (Fig. 8). The Yellow Cat Member is 11.1 meters thick, with a 0.5–1.5 meter thick algal lime-



Figure 21. Bluff held up by massive calcrete at top of Morrison Formation.

stone 6.8 m above the base locally. The overlying Poison Strip Member is 3–4 meters thick and consists of trough-crossbedded gravely sandstone with interbeds of pale greenish mudstone. The overlying type section of the Ruby Ranch Member described above is 31.1 m thick below its contact with the basal sandstone of the Dakota Formation.

The base of the Cedar Mountain at the Ruby Ranch section is remarkable. Locally, it is at the top of a 8–10 m thick calcrete bed (Fig. 21) (Aubrey, 1996, in press). Laterally, this calcrete grades into an 8 m thick interval rich in carbonate nodules at the base of the Yellow Cat Member. Coincidentally, where the calcrete is best developed, there is a silicified algal limestone bed developed within the overlying Yellow Cat Member of the Cedar Mountain Formation. This suggests post-burial diagenesis may have played a role forming this thick carbonate unit.

No vertebrate body fossils have been found at the Ruby Ranch site, but ornithopod tracks have been recognized (Lockley et al., in press) in a fluvial sandstone 2.1 meters above the base of the Ruby Ranch Member (Fig. 22). Additional invertebrate trace fossils of the *Scoyenia* assemblage are common in many sandstone units in the Cedar Mountain Formation. These include traces produced by ants, termites, and crayfish.

STOP 8. Cedar Mountain Formation Sites on the West side of Arches. J. Kirkland and K. Carpenter

At this stop (Figs. 2, 5), we will examine Denver Museum of Natural History (DMNH) localities in the Yellow Cat Member and Poison Strip Sandstone. There are several important dinosaur sites in the Cedar Mountain Formation on the west side of Arches National Park. The Bodily (1969) nodosaurid site (Fig. 23) was discovered in the early 1960s by Lin Ottinger of Moab, Utah, who reported it to Jim Jensen of Brigham Young University. Bodily (1969) described this large nodosaurid ankylosaur as *Hoplitosaurus* sp. In his review of the Ankylosauria, Coombs (1969) referred the



Figure 22. Ornithopod track from fluvial sandstone from near base of Ruby Ranch Member.

specimen to *Sauropelta* sp. In 1996, field crews with the Denver Museum of Natural History began to excavate a second specimen of *Sauropelta* a few kilometers north of the Bodily site. This specimen is clearly preserved within the Poison Strip Sandstone. Further examination of the Bodily site suggests that it too may lie within the Poison Strip Sandstone. Vertebrae and ribs of a sauropod were excavated from about six meters above the base of the Yellow Cat Member just north of the DMNH nodosaurid site.

Galton and Jensen (1981) reported on a highly eroded hadrosaur femur 112–117 cm long from a few kilometers south of these sites. Although, the exact horizon of this specimen is not known, smectitic mudstones at the top of the Cedar Mountain Formation in this area suggest it may have been recovered from strata equivalent to the Mussentuchit Member of the San Rafael Swell. This is the first report of a hadrosaur in the Cedar Mountain Formation.

STOP 9. Dalton Wells, Yellow Cat Member. **Brooks Britt**

At this stop (Figs. 2, 5), we will examine the extraordinarily rich deposit of dinosaur remains at the Dalton Wells Quarry (Fig. 24). It is rich not only in the number of bones, but in the number of different types of dinosaurs preserved, several of which are new to science. This Cedar Mountain Formation locality is in the Yellow Cat Member and is par-

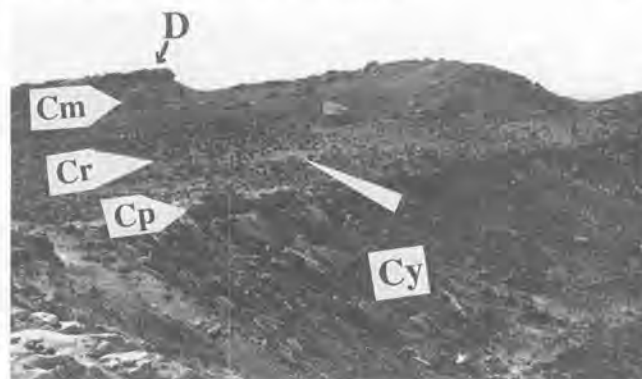


Figure 23. Brigham Young University's Bodily's Nodosaur Site indicated by arrow on west of Arches National Park. Arrow points to quarry. Abbr. Cm = Mussentuchit Member, Cp = Poison Strip Sandstone, Cr = Ruby Ranch Member, Cy = Yellow Cat Member, D = Dakota Formation.



Figure 24. Brigham Young University's Dalton Wells Quarry indicated by D and brackets. Abbr. Cp = Poison Strip Sandstone, Mor = Morrison Formation.

ticularly important because it is one of the best samples of Early Cretaceous dinosaurs in North America. The quarry is being developed in a joint project of Brigham Young University's Earth Science Museum and the Museum of Western Colorado.

The Dalton Wells quarry takes its name from a homestead established by Earl Dalton. In the early 1930's, the federal government erected a Civilian Conservation Corps (CCC) camp on the homestead. During World War II, following a 15 month closure, the site was converted to a Japanese internment camp, complete with high watch towers, for male Japanese-Americans vocal in their opposition to the imprisonment of American citizens. Today, a grove of cottonwood trees and concrete foundation slabs are all that remain of the camps, but crews working the quarry use the site as a campground.



Figure 25. Holotype maxilla fragment with two teeth of *Iguanodon ottingeri* (Galton and Jensen (1979) from the Dalton Wells Quarry. Darker *Iguanodon* tooth resting on top from the Gaston Quarry (Stop 11).

The quarry area has been known to casual collectors for decades but until Lin Ottinger showed James A. Jensen a small maxilla with teeth in 1968, the significance of the site was not recognized (Fig. 22). Ottinger's find revealed that the formation was Early Cretaceous in age, and the skull fragment was later designated as the holotype of *Iguanodon ottingeri* (Galton and Jensen, 1979). Jensen and Stadtman of BYU conducted a preliminary excavation in 1975, and a quarry was opened in 1978. The quarry remained dormant until 1994, when BYU and MWC joined forces to systematically collect the site and prepare recovered elements for study. At the time of this writing nearly 1400 bones have been recovered and are being analyzed.

In the immediate area of the quarry, the boundary between the Yellow Cat Member of the Cedar Mountain Formation and the underlying Morrison Formation remains to be determined. Calcrete and conglomerate horizons used in other areas to differentiate the formations are discontinuous in the area. Doelling (1988) and Aubrey (1996) noted that, during the deposition of the Cedar Mountain Formation, salt diapirs in the underlying Permian Paradox Formation were actively flowing, resulting in the formation of small depositional centers. This hypothesis accounts for the discontinuity of marker beds in the Cedar Mountain Formation.

In the Dalton Wells, quarry bones occur in the basal meter of a 4 meter thick, conglomeratic, silty, mudstone lithosome (Fig. 26). This fossiliferous horizon extends for some 400 meters but is nearly devoid of internal sedimentary structures. The largest clasts are bones (up to 1.5 m long) and 10 cm in diameter, well rounded, chert pebbles. With the exception of the larger bones, the clasts are matrix supported. Mud drapes in the middle of the conglomeratic

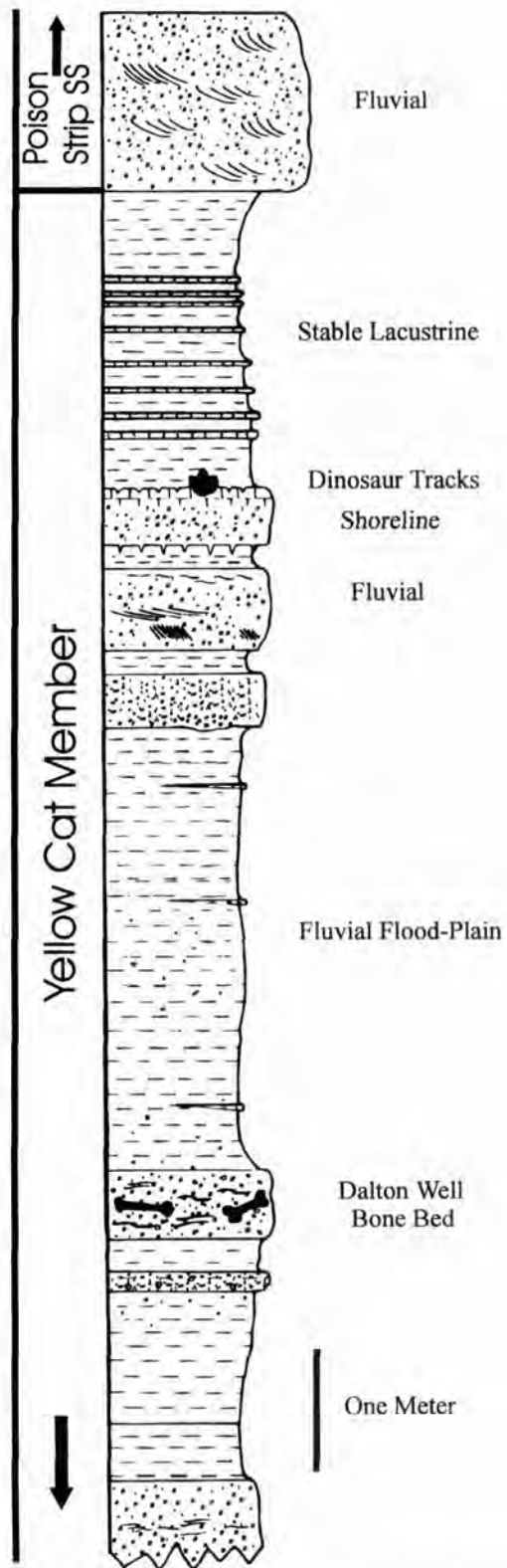


Figure 26. Detailed stratigraphic section of the upper Yellow Cat Member at Dalton Wells Quarry. Sandstone at top, base of Poison Strip Sandstone. Scale bar equals one meter.



Figure 27. Brooks Britt holding dorsal vertebra of high spined iguanodontid at Dalton Wells Quarry.



Figure 28. Oklahoma Museum of Natural History's Hotel Mesa Site indicated by arrow looking east across the Colorado River. Abbr. Cp = Poison Strip Sandstone, D = Dakota Formation.

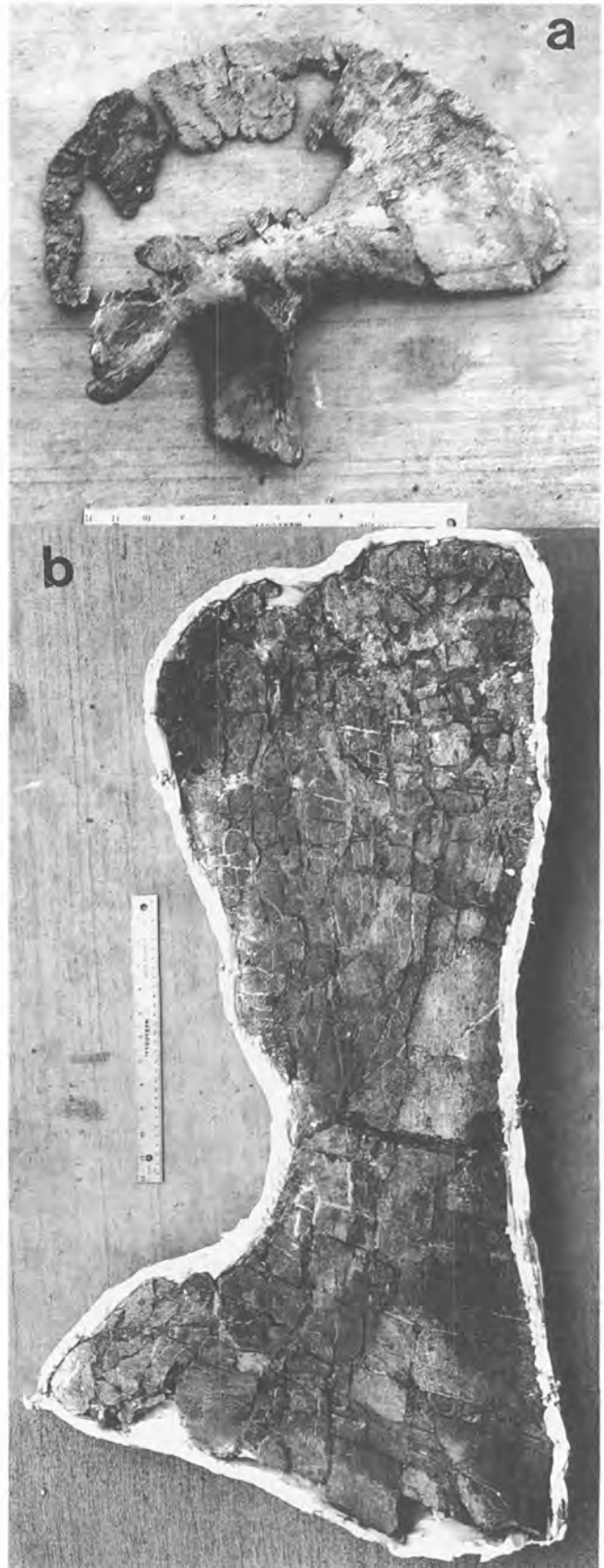


Figure 29. Pleurocoelus bones from OMNH's Hotel Mesa Quarry. a. ilia of juvenile specimen, b. scapula of adult specimen. Scale is one foot (30 cm).



Figure 30. Bone bed at CEU's Gaston Quarry. Bones include, polacanthid ankylosaur ribs, sacrum, caudal vertebrae, femur, and abundant armor and *Utahraptor* tibia and premaxilla.

mudstone indicate at least two flow events are preserved. The bone-bearing lithosome is interpreted to have originated as viscous crevasse splay(s) deposited into a broad, topographic low. Thin sandstones overlying the conglomeratic mudstone represent more normal, continuous flow events. Desiccation-cracked marl with sauropod and ornithomimid tracks overlie the sandstones and represent a fluctuating, lacustrine shoreline. Thin micritic limestone beds indicate the lake was relatively shallow but stable for some period of time before fluvial conditions again dominated the area.

Although articulated bones are rare, several spectacular specimens have been recovered, including three partial cervical sets. Two of the sets are of sauropods, with one cervical set still in articulation with the cranium. A partial cervical series of a nodosaurid was also found. Most bones are disarticulated, but clusters of associated bones make it possible to recognize individuals. Preserved bones range from pristine, delicate cervical vertebrae of sauropods to badly fractured, 1.5 meter long limb bones. Preliminary investigations suggest that most of the bones were broken by fluvial action. Taxonomic diversity and the range of growth stages represented in the quarry suggest a catastrophic event led to the demise of a large number of animals. Later, the bones were picked up and concentrated by a fluvial event. The rarity of articulated bones, the presence of tooth marks on some bones indicate the skeletons were subaerially exposed prior to being entrained in a fluvial system. The rare articulated bones represent portions of skeletons entombed while flesh still bound them together.

The Dalton Wells fauna is diverse, with six dinosaur genera currently recognized. Sauropod elements dominate excavated areas and account for about three-quarters of the 1400 recovered bones. Rare turtle shell fragments are the only non-dinosaurian remains. Few theropod elements have been recovered, but they represent at least two taxa. *Utah-*



Figure 31. *Utahraptor* bones, top, premaxilla; middle, first manus ungual (claw); bottom second pedal ungual (sickle-claw). Swiss army knife for scale.



Figure 32. Skull of new genus of polacanthid ankylosaur.



Figure 33. Interbedded limestones and shales at CEU's Gaston Quarry. Arrow indicates level of bone pavement.



Figure 34. Sauropod tracks (round shadowed depressions in foreground) at base of bone bed CEU's Gaston Quarry. Rob Gaston standing in background.

raptor, a large dromaeosaurid, is the most common and largest theropod at the site. A relatively small, maniraptoran theropod is also present but remains to be described. A minimum of six juvenile and adult sauropods have been identified, representing two genera; a camarasaurid and a titanosaurid. The adults are of medium size, but several elements indicate the presence of a large individual 21+ meters long. The tentative identification of the camarasaurid is based on unusually large, spatulate teeth set in vertically deep mandibular and maxillary elements, and delicate, thin-walled, cervical vertebrae with bifurcated neural spines. A cranium was found in articulation with the atlas and axis, which in turn were closely associated with several succeeding vertebrae. The caudal vertebrae are amphicoelous. The robustness of the skull elements, cranial and tooth morphology, and the cleft spines in the mid-cervicals suggest a camarasaurid affinity. A titanosaurid is recognized based on the presence of strongly procoelous cau-

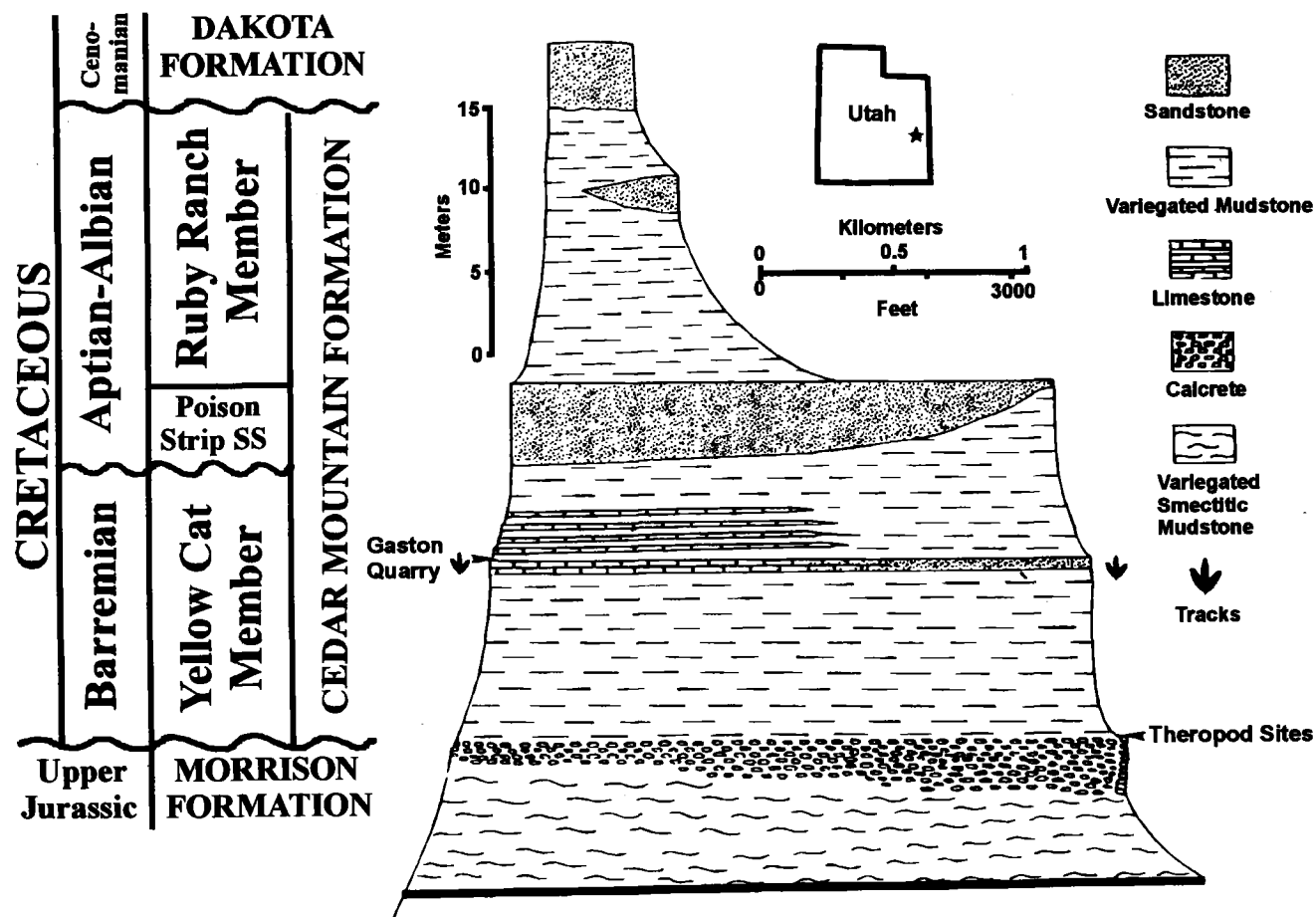


Figure 35. Cross-section of butte at Gaston Quarry showing relationships of sites on western and eastern sides.

dal vertebrae. Vertebrae from all vertebral regions have been recovered. All postaxial presacral vertebrae are pneumatic but are of the underived, camerate form with large camerae surrounded by thick bone. Neural spines of the cervical, dorsal, and caudal vertebrae are short and non-bifid, and the neural arches of the dorsal vertebrae are markedly tall. A partial skull is tentatively assigned to this taxon. The hypothesized Barremian age of this fauna make this the oldest titanosaurid in North America.

A large iguanodontid, with an estimated length of 8 meters, is represented by a minimum of three individuals. The type specimen of *Iguanodon ottingeri*, (Galton & Jensen, 1979), a partial maxilla of a juvenile, is currently designated *nomen dubium* by Weishampel and Bjork (1989). However, the taxon is now known from an array of cranial and post-cranial elements. The North American *Iguanodon lakotaensis* from the Lakota Formation of South Dakota is correlated in relative geographic and stratigraphic context. The broad neural spine of the dorsal vertebrae from Dalton Wells is longer than any other iguanodont (Fig. 27) except the

African form, *Ouranosaurus nigeriensis* (Taquet, 1976). Two small (2.5 m) polacanthid ankylosaur specimens are represented by femora, vertebrae, numerous scutes and spikes, and fragmentary pectoral and pelvic elements.

In summary, the Dalton Wells quarry is yielding a significant fauna that will contribute to an understanding of the Early Cretaceous dinosaurs of North America and to biogeography.

Stop 10. The Hotel Mesa, Ruby Ranch Member of the Burro Canyon Formation. Jim Kirkland

At this short stop (Figs. 2, 5) we will look at the Hotel Mesa site in the Ruby Ranch Member just to the east across the Colorado River (Fig. 28). It can be considered to be the first productive dinosaur quarry in the Burro Canyon Formation as the formation names traditionally change at the Colorado River (Stokes, 1952; Craig, 1981). Discovered by Ralph Pavonka of Grand Junction, Colorado, it was first reported to paleontologists by William Hawes of Grand



Figure 36. Loose ornithopod tracks formed at base of crevasse splay near Yellow Cat Road east of Gaston Quarry.



Figure 37. CEU Prehistoric Museum's small theropod sites indicated by dots just to the east of the Gaston Quarry. Abbr. Cp = Poison Strip Sandstone, Cy = Yellow Cat Member, cal = calcrete.

Junction. In this area, the Cedar Mountain and correlative Burro Canyon formations are relatively thin. The Yellow Cat Member has not been recognized in this area, and only the Poison Strip Sandstone and Ruby Ranch Member are present and thus clearly can be recognized in the Burro Canyon Formation east of The Colorado River. The Hotel Mesa site is located just a few meters below the base of the Dakota Formation.

To date, the Hotel Mesa site has only undergone preliminary salvage excavations by the Oklahoma Museum of Natural History, but the materials so far discovered are interesting. Most of the fossils pertain to a sauropod comparable to *Pleurocoelus* (Fig. 29). These include elements of both a large and a young individual and include numerous ribs, a caudal vertebra, an ilium, and most of a broad scapula. Additionally, microvertebrate material is also present including teeth of a hybodont shark, large and small crocodilian teeth, turtle shell fragments, a small theropod claw, and teeth possibly referable to the dromaeosaurid *Deinonychus*.

This site is significant in being the easternmost Lower Cretaceous dinosaur quarry sampled to date on the Colorado Plateau. Fossil vertebrates are known further to the east in Colorado, but the material discovered so far has been very scrappy and indeterminate.

STOP 11. The lower Cedar Mountain Formation along the Poison Strip. J. Kirkland and R. Cifelli.

At this stop (Figs. 2, 5) and we will examine the Yellow Cat Member and Poison Strip Sandstone south of Cisco, Utah on the eastern end of the Poison Strip. A number of small vertebrate sites have been discovered in the Yellow Cat Member in this area. These sites have been investigated by field crews from the Oklahoma Museum of Natural History. Surface material collected includes a number of partial turtles similar to *Glyptops*, ganoid fish scales and

teeth, a partial jaw of an eilenodontine sphenodontid, teeth of a small theropod and ankylosaur, and fragments from a polacanthid ankylosaur. The sphenodontid jaw is significant in that together with a specimen from the Kootenai Formation (Lower Cretaceous) it represents one of the youngest occurrences of this family outside of New Zealand (Throckmorton et al., 1981). Some small fragments of eggshell were also recovered that have been examined by Karl Hirsch and are currently under study by Emily Bray of the University of Colorado. The greater abundance of turtles and fishes suggest that these sites in the Yellow Cat Member may represent a wetter environment than sites farther west. An attempt was made to wet screenwash one productive layer, but it did not break down readily. However, this sample did produce numerous charophytes.

The presence of the charophyte, *Nodosoclavator bradleyi* (Harris) suggests an age of no younger than Barremian for the lower Cedar Mountain Formation in this area (Michael Schudack in a report to Fred Peterson). The only report suggesting a younger age (Aptian) for this taxon is by Peck (1957), who described this form as *Clavator nodosus* from the lower half of the Lakota Formation in South Dakota. In an examination of the Ostracoda, Sohn (1979) subsequently considered these strata to be pre-Aptian. Thus the limited data from charophytes supports the Barremian age suggested by the dinosaur fauna.

Along the southern side of the escarpment held up by the Poison Strip Sandstone (Fig. 7) various aspects of the Poison Strip Sandstone can be observed. These include thinning and thickening of the member, the lateral relationships of individual sandstone units in the member, and large scale epsilon crossbeds supporting the interpretation of the Poison Strip Sandstone as representing a complex meandering river system. Pale brown to white petrified wood is present at a number of localities along this escarpment and in addition to conifers includes the cycads, *Cyca-*



Figure 38. Foot of juvenile specimen of small maniraptoran theropod, top proximal view of metatarsals, bottom overview of foot.

deioidea and *Monanthesia* (Tidwell; personal commun. 1997). The Poison Strip Sandstone is of economic significance in this area, as it is the primary target in the Cisco Oil and Gas Field to the northeast (Moyer, pers. commun.). Detailed sedimentology has never been done for the Poison Strip Sandstone, but the quality of exposures in this area make an interesting study of this sequence boundary very feasible.

STOP 12. Gaston Quarry. J. Kirkland and D. Burge

At this stop (Figs. 2, 5) we will examine the Gaston Quarry and type section of the Yellow Cat Member of the Cedar Mountain Formation. The Gaston Quarry was discovered by Robert Gaston in the winter of 1990 near the top of a 100 meter butte held up by the Poison Strip Sandstone Member. To date, over 1100 completely disarticulated bones have been recovered from approximately 30 square meters (Burge, 1996), forming a literal pavement of bones (Fig. 30). Most of the bones represent a new, undescribed polacanthid ankylosaur represented by a minimum of four individuals (Kirkland et al., 1991; Kirkland, 1993, 1996; Carpenter et al., 1996). Additionally the type material of *Utahraptor ostrommaysorum* (Fig. 31) (Kirkland et al., 1993) and an iguanodont tentatively assigned to *Iguanodon ottingeri* Galton and Jensen (1979) have been recovered from the site. It is thought that rather than representing the "sail-backed" iguanodont as proposed by Britt et al., (1996; this paper), that *Iguanodon ottingeri* (Fig. 25) may prove to be a conservative iguanodont perhaps synonymous with *Iguanodon lakotaensis* (Weishampel and Bjork, 1989).

The polacanthid ankylosaur compares closely to *Polacanthus foxi* from the Wealden of England and *Polacanthus marshi* from the Lakota Formation of South Dakota on the basis of possessing a sacral shield of fused armor; asymmetric, hollow-based lateral plates; hollow-based, laterally directed, shoulder spines with a long posterior groove; and in having an additional set of large erect, solid-based, shoulder spines (Blows, 1987; Pereda-Suberbiola, 1993, 1994; Kirkland, 1993, 1996a). It differs from *Polacanthus* in not having a free lesser trochanter on the femur, not having diverging lateral margins of ilia, and a more massively constructed ulna (Kirkland, 1993; 1996). It has the only well preserved skull known for any polacanthid ankylosaur (Fig. 32), which suggests a close relationship with the Ankylosauridae and not the Nodosauridae (Kirkland, 1993; in manuscript; Carpenter et al., 1996). It also appears to be closely related to ankylosaurs recently discovered in the Morrison Formation (Kirkland and Carpenter, 1994; Carpenter, et al., 1996).

The bones are preserved in an interval of alternating limestone and silty shale (Fig. 33) 6.5 m below the top of the Yellow Cat Member of the Cedar Mountain Formation. Bones preserved in the limestone are beautifully three dimensional, while those preserved in the underlying silty shale are badly crushed. Isolated barite roses are present in association with these beds, suggesting the site may represent an ephemeral alkaline pond and that the limestone is largely diagenetic. The limestone at the base of the bone-bearing interval was found to be a sauropod tracksite (Fig. 34), with the next limestone layer up preserving ornithopod tracks. This interval of alternating limestone and shale was thought to mark the base of the Cedar Mountain Formation

in this area (Young, 1960, Fig. 6, sec. 37). In redefining the base of the Cedar Mountain, Aubrey (1996; in press) lowered the boundary to the calcrete 7 m down section.

On the other side of the butte toward the Yellow Cat Road, the quarry horizon correlates with a dark brown crevasse splay (Fig. 35). Ornithopod tracks have been found at the base of this splay (Fig. 36). Immediately above the calcrete (Fig. 37) at the base of the Yellow Cat Member, three partial skeletons of a small maniraptoran theropod (Fig. 38) have been excavated (Kirkland et al., 1995). Other fossils from this area include a lungfish tooth plate and a small crocodilian tooth fragment. Also, there have been spiral concretions filled with ganoid fish scales found at approximately this level. These are thought to represent enterospines of a hybodont shark, for which a fragment of a dorsal fin spine has been found. Additionally, fragments of the polacanthid ankylosaur have been found just below the Poison Strip Sandstone on this side of the butte also.

The Yellow Cat Member measures 24 meters thick in its type area as described above (Fig. 3). The overlying Poison Strip Sandstone measures as much as five meters thick near the Gaston Quarry but pinches out at the Yellow Cat Road 1.5 miles to the east (Fig. 34). It reappears again just to the east of the road and the type section is visible a short distance to the south. The Ruby Ranch Member is 17 meters thick in this area and has a prominent east trending ribbon sandstone 2–3 meters thick, 10 meters above its base. The overlying Dakota Formation has a chert pebble-to-cobble conglomerate at its base locally. A section of *Tempskya* log was found within this conglomerate.

ACKNOWLEDGMENTS

We thank the many people too numerous to count who have helped in the field, including many from the Utah Friends of Paleontology, Uncompahgre Plateau Paleontological Society, and the Western Interior Paleontological Society. Special thanks are extended to the Judd family of Castledale, Utah; the Jones family of Salt Lake City, Utah; the Gaston family of Knoxville, Tennessee; and the Corbett family of Raleigh, North Carolina. Robert Young of Grand Junction, Colorado is gratefully acknowledged for providing copies of his extensive field notes on the Cedar Mountain and Dakota Formations. Excavations were all undertaken under permits issued by the Bureau of Land Management and the Utah Division of State Lands. Partial funding in support of this research was provided by the National Geographic Society (grants 4761-91 and 5021-92 to RLC; 5263-94 to JIK) and the National Science Foundation (grants BSR 8906992 and DEB 941094 to RLC). Special thanks are due to John Bird and Carl Limone, CEU Prehistoric Museum, Harold Bollen, Dinamation International Society, Robert Gaston, Gaston Design, Fruita, Colorado; Randy Nydam,

Oklahoma Museum of Natural History, Rod Scheetz, Museum of Western Colorado, Ken Stadtman and Dee Hall, Brigham Young University, and Scott Madsen, Dinosaur National Monument for their skilled field assistance and preparation skills. Mike Parrish, Northern Illinois University is thanked for his help in the analysis of the theropod teeth. We thank Leo Hintzi, Spencer Lucas and Paul Link for their helpful reviews. Innumerable colleagues throughout our professions have also aided this research with their knowledge, advice, encouragement, and camaraderie.

REFERENCES CITED

- Aubrey, W.M., 1996, Stratigraphic architecture and deformational history of Early Cretaceous Foreland Basin, eastern Utah and southwestern Colorado, in Huffman, A.C., Jr., Lund, W.R., and Godwin, L.H., (eds.), *Geology and Resources of the Paradox Basin: Utah Geological Association Gudebook 25*, p. 211–220.
- Aubrey, W.M., in press, A newly discovered, widespread fluvial facies and unconformity marking the Upper Jurassic/Lower Cretaceous boundary, Colorado Plateau, in Carpenter, K., Chure, D., and Kirkland, J.I., eds., *The Morrison Formation—An integrated study: Modern Geology*.
- Baars, D.L., and 15 others, 1988, Basins of the Rocky Mountain region, in Sloss, L.L., (ed.), *Sedimentary Cover—North American Craton; U.S. Geological Society of America, The Geology of North America*, v. D-2, p. 109–220.
- Benton, M.J., and Spencer, P.S., 1995, *Fossil Reptiles of Great Britain: Chapman Hall Inc, New York*, 386 p.
- Blows, W.T., 1987, The armored dinosaur *Polacanthus foxi* from the Lower Cretaceous of the Isle of Wight: *Palaeontology*, v. 30, p. 557–580.
- Blows, W.T., 1993, William Fox (1813–1881), a neglected dinosaur collector on the Isle of Wight. *Archives of Natural History*, v. 11, no. 2, 299–313.
- Bodily, N.M., 1969, An Armored dinosaur from the Lower Cretaceous of Utah. *Brigham Young University Studies*, v. 16, no. 3, p. 557–580.
- Britt, B.B., Stadtman, K.L., and Scheetz, R.D., 1996, The Early Cretaceous Dalton Wells dinosaur fauna and the earliest North American titanosaund sauropod: *Journal of Vertebrate Paleontology*, v. 17, sup to no. 3 [Abstracts], p. 24A.
- Burge, D.L., 1996, New dinosaur discoveries in the Lower Cretaceous of southeastern Utah: *Fossils of Arizona*, v. 4, Southwest Paleontological Society and Mesa Southwest Museum, Mesa, Arizona, p. 85–105.
- Carpenter, K., Kirkland, J.I., Miles, C., Cloward, K., and Burge, D., 1996, Evolutionary significance of new ankylosaurs (Dinosauria) from the Upper Jurassic and Lower Cretaceous, western Interior: *Journal of Vertebrate Paleontology*, v. 17, sup. to no. 3 [Abstracts], p. 25A.
- Cifelli, R.L., 1993, Early Cretaceous mammal from North America and the evolution of marsupial dental characters, *Proceedings of the National Academy of Science*, v. 90, p. 9413–9416.
- Cifelli, R.L., Kirkland, J.I., Weil, A., Deinos, A.R., and Kowallis, B.J., in press, High-precision $^{40}\text{Ar}/^{39}\text{Ar}$ geochronology and the advent of North America's Late Cretaceous terrestrial fauna: *Proceedings of the National Academy of Science*.
- Cifelli, R.L., Nydam, R.L., Weil, A., Gardner, J.D., Eaton, J.G., Kirkland, J.I., and Madsen, S.K., in press, Medial Cretaceous vertebrates from the Cedar Mountain Formation, Emery County: The Mussentuchit local fauna, in Gillette, D., ed., *Fossil Vertebrates of Utah*, Utah Geological Survey.
- Cobban, W.A., 1976, Ammonite record from the Mancos Shale of the Castle Valley-Price-Woodside area, east-central Utah. *Brigham Young University Geological Studies*, v. 22, p. 117–126.

- Cobban, W.A., and Kennedy, W.J., 1989, The ammonite *Metengonoceras* Hyatt, 1903, from the Mowry Shale (Cretaceous) of Montana and Wyoming. U.S. Geological Survey Bulletin 1787L, p. L1-L11
- Coombs, W.P., Jr., 1971, The Ankylosauria. unpub. Ph.D. dissertation, Columbia University, New York, 487 p.
- Coombs, W.P., Jr., 1995, A nodosaurid ankylosaur (Dinosauria, Ornithischia) from the Lower Cretaceous of Texas: Journal of Vertebrate Paleontology, v. 15, p. 298-312.
- Craig, L.C., 1981, Lower Cretaceous rocks, southwestern Colorado and southeastern Utah. Rocky Mountain Association of Geologists, 1981 Field Conference, p. 195-200.
- Craig, L.C., Ekren, E.B., Housen, F.N., Shawe, D.R., Simmons, G.C., and Katich, P.J., Jr., 1961, Dakota Group of the Colorado Plateau, discussion: American Association of Petroleum Geologists Bulletin, v. 45, p. 1582-1592.
- DeCelles, P.G., Lawton, T.F., and Mitra, G., 1995, Thrust timing, growth of structural culminations, and synorogenic sedimentation in the type Sevier orogenic belt, western United States: Geology, v. 23, p. 699-702.
- DeCourten, F.L., 1991, New data on Early Cretaceous dinosaurs from Long Walk Quarry and Tracksite, Emery County, Utah, in Chidsey, T.C., Jr., ed., Geology of East-Central Utah. Utah Geological Association Publication v. 19, p. 311-324.
- Dodson, P.A., Behrensmeyer, A.K., Bakker, R.T., and McIntosh, J.S., 1980, Taphonomy and paleoecology of dinosaur beds of the Jurassic Morrison Formation. Paleobiology, v. 6, p. 1567-1578.
- Doelling, H.H., 1988, Geology of Salt Valley Anticline and Arches National Park, in Doelling, H.H., Oviatt, C.G., Huntoon, P.W., eds., Salt Deformation in the Paradox Region. Utah Geological and Mineral Survey, Bulletin 122, p. 1-60
- Dyman, T.S., Merewether, E.A., Molenaar, C.M., Cobban, W.A., Obradovich, J.D., Weimer, R.J., and Bryant, W.A., 1994, Stratigraphic transects for Cretaceous rocks, Rocky Mountain and Great Plains regions, in Caputo, M.V., Peterson, J.A., and Franczyk, K.J., eds., Mesozoic Systems of the Rocky Mountain region, USA: Rocky Mountain Section, Society for Sedimentary Geology, Denver, Colorado, p. 365-391.
- Eaton, J.G., 1987, Stratigraphy, Depositional Environments, and age of Cretaceous mammal-bearing rocks in Utah, and Systematics of the Multituberculata. unpub. Ph.D. dissertation, University of Colorado, Boulder, 308 p.
- Eaton, J.G., 1993a, Therian mammals from the Cenomanian (Upper Cretaceous) Dakota Formation, southwest Utah. Journal of Vertebrate Paleontology, v. 13, p. 105-124.
- Eaton, J.G., 1993b, Marsupial dispersal, National Geographic Research and Exploration, v. 9, no. 4, p. 436-443.
- Eaton, J.G., and Nelson, M.E., 1991, Multituberculate mammals from the Lower Cretaceous Cedar Mountain Formation, San Rafael Swell, Utah: Contributions to Geology, University of Wyoming, v. 29, p. 1-12.
- Eaton, J.G., Kirkland, J.I., and Kauffman, E.G., 1990, Evidence and dating of mid-Cretaceous tectonic activity in the San Rafael Swell, Emery County, Utah. The Mountain Geologist, v. 27, no. 2, p. 39-45.
- Eaton, J.G., Kirkland, J.I., Hutchison, J.H., Denton, R., O'Niell, R.C., and Parrish, J.M., 1997, Nonmarine extinction across the Cenomanian-Turonian (C-T) boundary, southwestern Utah, with a comparison to the Cretaceous-Tertiary (K-T) extinction event. Geological Society of America Bulletin, v. 109, no. 5, p. 560-567.
- Elder, W.P., and Kirkland, J.I., 1993, Cretaceous paleogeography of the Colorado Plateau and adjacent areas, in Morales, M., ed., Aspects of Mesozoic geology and paleontology of the Colorado Plateau. Museum of Northern Arizona Bulletin, v. 59, p. 129-151
- Elder, W.P., and Kirkland, J.I., 1994, Cretaceous paleogeography of the southern Western Interior region, in Caputo, M.V., Peterson, J.A., and Franczyk, K.J., eds., Mesozoic Systems of the Rocky Mountain region, USA: Rocky Mountain Section, Society for Sedimentary Geology, Denver, Colorado, p. 415-440.
- Fillmore, R.P., 1993, Late Cretaceous paleogeography of the southern Sevier foreland, southwest Utah, southern Nevada, and northwest Arizona, in Dunn, G., and McDougall, K., eds., 1993, Mesozoic Paleogeography of the Western United States-II, Pacific Section, Society of Economic Paleontologists and Mineralogists, Book 71, p. 417-432.
- Galton, P.M., and Jensen, J.A., 1975, *Hypsilophodon* and *Iguanodon* from the Lower Cretaceous of North America. Nature, v. 257, p. 668-669.
- Galton, P.M., and Jensen, J.A., 1979, Remains of ornithomimid dinosaurs from the Lower Cretaceous of North America. Brigham Young University Geology Studies, v. 25, no. 1, p. 1-10.
- Gilmore, C.W., 1921, The fauna of the Arundel Formation of Maryland, Proceedings of the United States National Museum, v. 59, p. 581-594.
- Gradstein, F.M., Agterberg, F.P., Ogg, J.G., Hardenbol, J., van Veen, P., Thierry, J., Huang, Z., 1994, A Mesozoic time scale: Journal of Geophysical Research, v. 99, no. B12, p. 24,051-24,074
- Hancock, J.M., Kennedy, W.J., and Cobban, W.A., 1993, A correlation of the Upper Albian to basal Coniacian sequences of northwest Europe, Texas and the United States Western Interior, in Caldwell, W.G.E., and Kauffman, E.G., eds., Evolution of the Western Interior Basin. Geological Association of Canada Special Paper 39, p. 453-476
- Harris, D.R., 1980, Exhumed paleochannels in the Lower Cretaceous Cedar Mountain Formation near Green River, Utah: Brigham Young University Geology Studies, v. 27, no. 1, p. 51-66
- Heller, P.L., and Paola, C., 1989, The paradox of Lower Cretaceous gravels and the initiation of thrusting in the Sevier Orogenic belt, United States Western Interior. Geological Society of America Bulletin, v. 101, no. 6, p. 864-975.
- Heller, P.L., Bowdler, S.S., Chambers, H.P., Coogan, J.C., Hagen, E.S., Shuster, M.W., and Winslow, N.S., 1986, Time of initial thrusting in the Sevier orogenic belt: Geology, v. 14, p. 388-391.
- Horner, J.R., 1990, Evidence of diphyletic origination of the hadrosaurian (Reptilia: Ornithischia) dinosaurs, in Dinosaur Systematics: Perspectives and Approaches, Carpenter, K., and Currie, P.J., eds., Cambridge University Press, p. 179-187
- Jensen, J.A., 1970, Fossil eggs from the Lower Cretaceous of Utah. Brigham Young University Geology Studies, v. 17, no. 1, p. 51-66.
- Jones, R., and Burge, D., 1995, Radiological surveying as a method for mapping dinosaur bone sites: Journal of Vertebrate Paleontology, v. 15, sup. to no. 3, [Abstracts], 38A.
- Katich, P.J., 1951, Occurrence of *Tempskya* in the Lower Cretaceous of the Western Interior, Journal of Paleontology, v. 26, no. 4, p. 677
- Katich, P.J., 1956, Some notes on the Cretaceous faunas of eastern Utah and western Colorado, in Peterson, J.A., ed., Geology and economic deposits of east central Utah. Intermountain Association of Petroleum Geologists, Seventh Annual Field Conference, p. 116-119.
- Kauffman, E.G., and Caldwell, W.G.E., 1993, The Western Interior Basin in space and time, in Caldwell, W.G.E., and Kauffman, E.G., eds., Evolution of the Western Interior Basin. Geological Association of Canada Special Paper 39, p. 1-30.
- Kirkland, J.I., 1987, Upper Jurassic and Cretaceous Lungfish Tooth Plates from the Western Interior of North America. Hunteria, Vol. 2, No. 2, University of Colorado Museum, Boulder, Colorado, 16 p
- Kirkland, J.I., 1992, Dinosaurs define a two-fold Lower Cretaceous zonation of the Cedar Mountain Formation, central Utah. Geological Society of America Abstracts with Programs, v. 24, no. 6, p. 22.
- Kirkland, J.I., 1993, Polacanthid nodosaurs from the Upper Jurassic and Lower Cretaceous of the east-central Colorado Plateau. Journal of Vertebrate Paleontology, Vol. 13, sup. to no. 3, [Abstracts], 44A-45A.
- Kirkland, J.I., 1996a, Reconstruction of Polacanthid Ankylosaurs based on new discoveries from the Late Jurassic and Early Cretaceous. Dinofest

- International Symposium, April 18–21, 1996, Wolberg, D.L., and Stump, E., eds., Arizona State University, p. 67.
- Kirkland, J.I., 1996b, Biogeography of North America's Mid-Cretaceous Dinosaur faunas—Losing European ties and the first great Asian-North American Interchange: *Journal of Vertebrate Paleontology*, v. 16, sup. to no. 3 [Abstracts], p. 45A.
- Kirkland, J.I., 1996c, Paleontology of the Greenhorn Cyclothem (Cretaceous; Late Cenomanian to Middle Turonian) at Black Mesa, north-eastern Arizona: *New Mexico Museum of Natural History and Science Bulletin* 9, 131 p., 50 pl.
- Kirkland, J.I., and Burge, D., 1994, A large primitive hadrosaur from the Lower Cretaceous of Utah: *Journal of Vertebrate Paleontology*, v. 14, sup. to no. 3 [Abstracts], p. 32A.
- Kirkland, J.I., and Carpenter, K., 1994, North America's First pre-Cretaceous Ankylosaur (Dinosauria) from the Upper Jurassic Morrison Formation of Western Colorado. *Brigham Young University Geology Studies*, v. 40, p. 25–42.
- Kirkland, J.I., and Parrish, J.M., 1995, Theropod teeth from the lower and middle Cretaceous of Utah: *Journal of Vertebrate Paleontology*, v. 15, sup. to no. 3, [Abstracts], p. 39A.
- Kirkland, J.I., Burge, D., and Gaston, R., 1993a, A large dromaeosaur (Theropoda) from the Lower Cretaceous of Utah: *Hunteria*, v. 2, no. 10, p. 1–16.
- Kirkland, J.I., Carpenter, K., and Burge, D., 1991, A nodosaur with a distinct sacral shield of fused armor from the lower Cretaceous of east-central Utah: *Journal of Vertebrate Paleontology*, v. 11, sup. to no. 3, [Abstracts], p. 40A.
- Kirkland, J.I., Burge, D., Britt, B.B., and Blows, W.T., 1993b, The Earliest Cretaceous (Barremian?) Dinosaur Fauna Found to date on the Colorado Plateau. *Journal of Vertebrate Paleontology*, v. 13, sup. to no. 3, [Abstracts], p. 45A.
- Kirkland, J.I., Britt, B.B., Madsen, S., and Burge, D., 1995, A small theropod from the basal Cedar Mountain Formation (Lower Cretaceous, Barremian) of eastern Utah: *Journal of Vertebrate Paleontology*, v. 15, sup. to no. 3, [Abstracts], p. 39A.
- Kowallis, B., Deino, A.R., Peterson, F., and Turner-Peterson, C., in press, High precision radiometric dating of the Morrison Formation, in Carpenter, K., Chure, D., and Kirkland, J.I., (eds.), *The Morrison Formation—An integrated study: Modern Geology*.
- Kranz, P.M., 1989, Dinosaurs in Maryland: Maryland Geological Survey Educational Series no. 6, 34 p.
- Kranz, P.M., 1996, Notes on sedimentary iron ores of Maryland and their dinosaurian fauna: Maryland Geological Survey, Special Publication, no. 3, p. 87–115.
- Kraus, M.J., and Bown, T.M., 1986, Paleosols and time resolution in alluvial stratigraphy, in Wright, V.P., ed., *Paleosols: Their recognition and interpretation*: Princeton University Press, Princeton, New Jersey, p. 180–207.
- Langston, W., 1974, Nonmammalian Comanchean tetrapods: *Geoscience and Man*, v. 3, p. 77–102.
- Lawton, T.F., 1985, Style and timing of frontal structures, thrust belt, central Utah: *American Association of Petroleum Geologists Bulletin*, v. 69, p. 1145–1159.
- Lawton, T.F., 1986, Compositional trends within a clastic wedge adjacent to a fold-thrust belt: Indianola Group, central Utah, U.S.A., Special Publications International Association of Sedimentologists, v. 8, p. 411–423.
- Lawton, T.F., Boyer, S.E., and Schmitt, J.G., 1994, Influence of inherited taper on structural variability and conglomerate distribution, Cordilleran fold and thrust belt, western United States: *Geology*, v. 22, p. 339–342.
- Lee, Y.-N., 1995, Mid-Cretaceous archosaur faunal changes in Texas, in Ailing, S., and Yauquig, W., (eds.) *Sixth Symposium on Mesozoic Terrestrial Ecosystems and Biota, Short Papers*. China Ocean Press, Beijing, p. 175–177.
- Lee, Y.-N., 1996, A new nodosaurid ankylosaur (Dinosauria: Ornithischia) from the Paw Paw Formation (Late Albian) of Texas: *Journal of Vertebrate Paleontology*, v. 16, no. 2, p. 232–245.
- Lockley, M., Kirkland, J.I., DeCourtin, F., Hasiotis, S., in press, Dinosaur tracks from the Cedar Mountain Formation of eastern Utah; a preliminary report, in Gillette, D., ed., *Fossil Vertebrates of Utah: Utah Geological Survey*.
- Lucas, S.G., 1993, Vertebrate biochronology of the Jurassic-Cretaceous boundary, North American western interior: *Modern Geology* v. 18, p. 371–390.
- Lucas, S.G., and Hunt, A.P., 1989, *Alamosaurus* and the sauropod hiatus in the Cretaceous of the North American western interior, in Farlow, J.O., ed., *Paleobiology of the Dinosaurs*, Geological Society of America Special Paper, no. 238, p. 75–86.
- Marsh, O.C., 1888, Notice of a new genus of Sauropoda and other new dinosaurs from the Potomac Formation: *American Journal of Science*, v. 35, no. 3, p. 85–94.
- Meek, F.B., and Hayden, F.V., 1862, Description of new lower Silurian (Primordial), Jurassic, Cretaceous and Tertiary fossils collected in Nebraska Territory. . . . With some remarks on the rocks from which they were obtained: *Proceedings Academy of Natural Sciences Philadelphia*, v. 13, p. 415–447.
- Mitchell, J.G., 1956, Charophytes as a guide to distinguishing between Lower Cretaceous and Upper Jurassic continental sediments in the subsurface, in Peterson, J.A., ed., *Geology and economic deposits of east-central Utah*. Intermountain Association of Petroleum Geologists, Seventh annual Field Conference, p. 105–112.
- Molenaar, C.M., and Cobban, W.A., 1991, Middle Cretaceous stratigraphy on the south and east sides of the Uinta Basin, northeastern Utah and northwestern Colorado: *U.S. Geological Survey Bulletin* 1787, p. P1–P34.
- Nelson, M.E., and Crooks, D.M., 1987, Stratigraphy and paleontology of the Cedar Mountain Formation (Lower Cretaceous), eastern Emery County, Utah. in Averett, W.R., ed., *Paleontology of the Dinosaur Triangle—guidebook for 1987 field trip*, Museum of Western Colorado, Grand Junction, Colorado, p. 55–63.
- Neuhaus, K.R., 1988, Sevier-age ramp-style thrust faults at Cedar Mountain, northwestern San Rafael swell (Colorado Plateau), Emery County, Utah: *Geology*, v. 16, p. 299–302.
- Nichols, D.J., and Sweet, A.R., 1993, Biostratigraphy of Upper Cretaceous non-marine palynofloras in a north-south transect of the Western Interior Basin. in Caldwell, W.G.E., and Kauffman, E.G., eds., *Evolution of the Western Interior Basin*. Geological Association of Canada Special Paper 39, p. 539–584.
- Norman, D.B., 1988, Wealden dinosaur biostratigraphy. In Currie, P.J., and Koster, E.H., eds., *Fourth Symposium on Mesozoic Ecosystems, Short Papers*, p. 165–170.
- Norman, D.B., 1990, A review of *Vectisaurus valdensis*, with comments on the family Iguanodontidae, in Carpenter, K., and Currie, P.J., eds., *Dinosaur Systematics: Perspectives and Approaches*: Cambridge University Press, p. 147–161.
- Obradovich, J., 1993, A Cretaceous time scale, in Caldwell, W.G.E., and Kauffman, E.G., eds., *Evolution of the Western Interior Basin*. Geological Association of Canada Special Paper 39, p. 379–396.
- Ostrom, J.H., 1970, Stratigraphy and Paleontology of the Cloverly Formation (Lower Cretaceous) of the Bighorn Basin area, Wyoming and Montana. Yale University, Peabody Museum of Natural History Bulletin v. 350, 234 p.
- Parrish, J.M., 1991, Diversity and evolution of dinosaurs in the Cretaceous of the Kaiparowits Plateau, Utah. *Journal of Vertebrate Paleontology*, v. 11, sup. to no. 3, (Abstracts) p. 50A.

- Peck, R.E., 1957, North American Mesozoic Charophyta: U.S. Geological Survey Professional Paper 294-A, 44 p. 8 pl.
- Pereda-Suberbiola, J., 1993, *Hylaosaurus*, *Polacanthus* and the systematics and stratigraphy of Wealden armored dinosaurs: Geological Magazine, v. 130, p. 767-781.
- Pereda-Suberbiola, J., 1994, *Polacanthus* (Ornithischia, Ankylosauria), a transatlantic armored dinosaur from the Early Cretaceous of Europe and North America: *Palaeontographica Abteilung A*, v. 232, p. 133-159.
- Pomes, M.L., 1988, Stratigraphy, paleontology, and paleogeography of lower vertebrates from the Cedar Mountain Formation (Lower Cretaceous), Emery County, Utah. M.S. Thesis, Fort Hays State University, Hays, Kansas, 87 p.
- Rozhdestvensky, A.K., 1967, New Iguanodonts from central Asia: *International Geology Review* v. 9, no. 4, p. 556-566.
- Rushforth, S.R., 1971, A flora from the Dakota Sandstone Formation (Cenomanian) near Westwater, Grand County, Utah: *Brigham Young University Science Bulletin*, v. 14, p. 1-44.
- Schwans, P., 1988a, Stratal packages at the subsiding margin of the Cretaceous foreland basin, unpub. Ph.D. dissertation, Columbus, Ohio, The Ohio State University, 447 p.
- Schwans, P., 1988b, Depositional response of Pigeon Creek Formation, Utah to initial fold-thrust deformation in a differentially subsiding foreland basin, in Schmidt, C.J., and Perry, W.J., eds., *Interaction of the Rocky Mountain foreland and the Cordilleran thrust belt*: Geological Society of America Memoir 171, p. 531-556.
- Schwans, P., 1995, Controls on sequence stacking and fluvial to shallow-marine architecture in a foreland basin, in Van Wagoner, J.C., and Bertram, G.T., eds., *Sequence stratigraphy of foreland basin deposits; outcrop and subsurface examples from the Cretaceous of North America*: American Association of Petroleum Geologists Memoir 64, p. 55-102.
- Sereno, P.C., 1986, *Phylogeny of the bird-hipped dinosaurs (Order Ornithischia)*: National Geographic Research, v. 2, p. 234-256.
- Singh, C., 1975, Stratigraphic significance of early angiosperm pollen in the mid-Cretaceous strata of Alberta, in Caldwell, W.G.E., ed., *The Cretaceous System in the Western Interior of North America*. Geological Association of Canada Special Paper, v. 13, p. 365-389.
- Sohn, I.G., 1979, Nonmarine ostracodes in the Lakota Formation (Lower Cretaceous) from South Dakota and Wyoming: U.S. Geological Survey Professional Paper 1069, 24 p., 8 pl.
- Spieker, E.M., 1946, Late Mesozoic and early Cenozoic history of central Utah: U.S. Geological Survey Professional Paper 205-D, p. 117-161.
- Spieker, E.M., 1949, The transition between the Colorado Plateau and the great Basin in central Utah. Utah Geological Society, Guidebook to the Geology of Utah, no. 4, 106 p.
- Spieker, E.M., and Reeside, J.B., Jr., 1926, Upper Cretaceous shoreline in Utah: *Geological Society of America Bulletin*, v. 37, p. 429-438.
- Sprinkel, D.A., Weiss, M.P., and Fleming, R.W., 1992, Stratigraphic reinterpretation of a synorogenic unit of late Early Cretaceous age, Sevier Orogenic belt, central Utah: *Geological Society of America Abstracts with Programs*, v. 24, no. 6, p. 63.
- Standlee, L.A., 1982, Structure and stratigraphy of Jurassic rocks in central Utah; Their influence on tectonic development with the foreland thrust belt, in Powers, R.B., ed., *Geological studies of the Cordilleran thrust belt*. Denver Rocky Mountain Association of Geologists, p. 357-382.
- Stokes, W.L., 1944, Morrison and related deposits in the Colorado Plateau. Geological Society of America Bulletin, v. 55, p. 951-992.
- Stokes, W.L., 1952, Lower Cretaceous in Colorado Plateau: American Association of Petroleum Geologists Bulletin, v. 36, p. 1766-1776.
- Stokes, W.L., 1972, Stratigraphic problems of Triassic and Jurassic sedimentary rocks of central Utah, in Baer, L.L., and Callaghan, E., eds., Plateau-Basin and Range transition zone. Utah Geological Association Publication 2, p. 21-28.
- Stokes, W.L., and Phoenix, D.A., 1948, *Geology of the Egnar-Cypsum Valley area*, San Miguel and Montrose Counties, Colorado: U.S. Geological Survey Preliminary Map 93, Oil and Gas Inventory Survey.
- Stovall, J.W., and Langston, W., Jr., 1950, *Acrocanthosaurus atokensis*, a new genus and species of Lower Cretaceous Theropoda from Oklahoma: *The American Midland Naturalist*, v. 43, no. 3, p. 696-728.
- Taquet, P., 1976, *Geologie et paleontologie du gisement du Gadoufaoua (Aptien du Niger)*: Centre National de la Recherche Scientifique, *Cashiers de Paleontologie*, Paris, 191 p.
- Thayne, G.F., and Tidwell, W.D., 1984, Flora of the Lower Cretaceous Cedar Mountain Formation of Utah and Colorado, Part II. *Mesembrioxylon stokesi*: *Great Basin Naturalist*, v. 44, no. 2, p. 257-262.
- Thayne, G.F., Tidwell, W.D., and Stokes, W.L., 1983, Flora of the Lower Cretaceous Cedar Mountain Formation of Utah and Colorado, Part I *Paraphyllanthoxylon utahense*: *Great Basin Naturalist*, v. 43, no. 3, p. 394-402.
- Thayne, G.F., Tidwell, W.D., and Stokes, W.L., 1985, Flora of the Lower Cretaceous Cedar Mountain Formation of Utah and Colorado, Part III. *Icacinoxylon pittense* n. sp.: *American Journal of Botany*, v. 72, no. 2, p. 175-180.
- Throckmorton, G.S., Hopson, J.A., and Parks, P., 1981, A redescription of *Toxolophosaurus cloudi* Olson, a Lower Cretaceous herbivorous sphenodontid reptile: *Journal of Paleontology*, v. 55, no. 3, p. 586-597.
- Tidwell, W.D., 1996, Cretaceous floras of east-central Utah and western Colorado—a review, in Herendeen, P.S., Johnson, K., Tidwell, W.D., and Ash S.R., eds., *Guidebook for Paleozoic, Mesozoic, and Cenozoic excursion of Utah and Colorado: The Fifth Annual Paleobotanical Conference*, p. 57-72.
- Tidwell, W.D., and Thayne, G.F., 1985, Flora of the Lower Cretaceous Cedar Mountain Formation of Utah and Colorado, Part IV. *Palaeopiceoxylon thinosus* (Protopinaceae). *The Southwestern Naturalist*, v. 30, no. 4, p. 525-532.
- Tschudy, R.H., Tschudy, B.D., and Craig, L.C., 1984, Palynological evaluation of Cedar Mountain and Burro Canyon Formations, Colorado Plateau. U.S. Geological Survey Professional Paper 1281, p. 1-21.
- Weishampel, D.B., and Bjork, P.R., 1989, The first indisputable remains of Iguanodon (Ornithischia: Ornithopoda) from North America. *Iguanodon lakotaensis*, sp. nov. *Journal of Vertebrate Paleontology*, v. 9, no. 1, p. 56-66.
- Weishampel, D.B., and Horner, J.R., 1990, Hadrosauridae, in Weishampel, D.B., Dodson, P., and Osmolska, H., eds., *The Dinosauria*: University of California Press. Berkeley p. 534-561.
- Weishampel, D.B., and Weishampel, J.B., 1983, Annotated localities of ornithopod dinosaurs; implications to Mesozoic paleobiogeography Mosasaur, v. 1, p. 43-87.
- Weishampel, D.B., Norman, D.B., Grigorescu, D., 1993, *Telmatosaurus transsylvanicus* from the Late Cretaceous of Romania. the most Basal hadrosaurid dinosaur. *Palaeontology*, v. 36, no. 2, p. 361-385.
- Weiss, M.P., 1994, *Geological map of the Sterling quadrangle*, Sanpete County, Utah: Utah Geological Survey, Map 159, 2 plates, 26 p.
- Weiss, M.P., and Roche, M.G., 1988, The Cedar Mountain Formation (Lower Cretaceous) in the Gunnison Plateau, central Utah, in Schmidt, C.J., and Perry, W.J., eds., *Interaction of the Rocky Mountain foreland and the Cordilleran thrust belt*: Geological Society of America Memoir 171, p. 557-569.
- Wing, S.L., and Sues, H.-D., 1992, Mesozoic and early Cenozoic terrestrial ecosystems, in Behrensmeyer, A.K., Damuth, J.D., DiMichele, W.A., Potts, R., Sues, H.-D., and Wing, S.L., eds., *Terrestrial ecosystems through time; Evolutionary paleoecology of terrestrial plants and animals*: The University of Chicago Press, Chicago, Illinois, p. 327-416.

- Winkler, D.A., Murry, P.A., and Jacobs, L.L., 1989, Vertebrate paleontology of the Trinity Group, Lower Cretaceous of central Texas, *in* Winkler, D.A., Murry, P.A., and Jacobs, L.L., eds., *Field Guide to the Vertebrate Paleontology of the Trinity Group, Lower Cretaceous of Central Texas*: (Dallas Institute for the Study of the Earth and Man, Southern Methodist University, p. 1–22.
- Winkler, D.A., Murry, P.A., and Jacobs, L.L., 1990, Early Cretaceous (Comanchean) vertebrates of central Texas: *Journal of Vertebrate Paleontology*, v. 10, no. 1, p. 95–116.
- Winkler, D.A., Jacobs, L.L., Lee, Y.-N., and Murry, P., 1995, Sea level fluctuations and terrestrial faunal change in north-central Texas, *in* Ailing, S., and Yaunquig, W., eds., *Sixth Symposium on Mesozoic Terrestrial Ecosystems and Biota, Short Papers*. China Ocean Press, Beijing, p. 175–177.
- Witkind, I.J., Standlee, L.A., and Maley, K.F., 1986, Age and correlation of Cretaceous rocks previously assigned to the Morrison Formation, Sanpete-Sevier Valley area, central Utah: *U.S. Geological Survey Bulletin* 1584, 9 p.
- Young, R.G., 1960, Dakota Group of the Colorado Plateau: *American Association of Petroleum Geologists Bulletin*, v. 44, no. 2, p. 156–194.

Sequence Architecture and Stacking Patterns in the Cretaceous Foreland Basin, Utah: Tectonism versus Eustasy

P. SCHWANS

Exxon Exploration Company, P.O. Box 4778, Houston, Texas 77060-4778

K.M. CAMPION

Exxon Production Research Company, P.O. Box 2189, Houston, Texas 99252-2189

ABSTRACT

The field trip examines the variations in depositional architecture, stacking patterns, and unconformity expression in strata deposited at the Cretaceous foreland basin margin in central Utah. Two sediment accommodation zones are identified. A zone proximal to the thrust front (<150 km distance) with high basin subsidence and sediment accommodation features predominantly alluvial deposits and sequences bounded by merged 3rd-order and angular unconformities; airy-isostatic subsidence dominated here. In a second zone located farther basinward (>150 km distance) basin subsidence and sediment accommodation decrease to the east and the basin fill is predominantly transitional alluvial to shallow-marine. Sequences are bounded by higher frequency unconformities and their correlative conformities; flexural subsidence dominates here and defines a ramp. Sequence expression and stacking patterns are explained within an accommodation cycle of basin subsidence and sea level change. This can be used to better understand the influence of structuring versus eustasy on depositional architecture.

INTRODUCTION

Sequence stratigraphy concepts were originally developed from shallow-marine successions along passive margins where subsidence increases basinward, shelf edges separate shallow-water from deep-water environments, and tectonic events are muted (Vail et al., 1977, 1984; Haq et al., 1987, 1988, Jervey, 1988; Posamentier and Vail, 1988; Posamentier et al., 1988). Over the last several years sequence-stratigraphy has been increasingly applied and tested in foreland basins, where basin subsidence increases toward an active fold belt, strata are deposited across a ramp of uniform dip, and deep-water environments are absent. Consequently, the applicability of sequence stratigraphy concepts in foreland basins and the impact of tectonism on stratal patterns have been scrutinized; examples, among others, are the work by Weimer (1984), Jervey (1988), Jordan and Flemings (1991), Schwans (1990, 1991, 1995), Walker and Eyles (1991), Posamentier et al., (1992), Devlin et al., (1993), Gardner (1993), Martinsen, et. al., (1993), and Leithold (1994).

PREVIOUS WORK

Previous stratigraphic work on the transitional alluvial to shallow-marine foreland basin strata in central Utah, commonly referred to as Indianola Group, utilized formational attributes and sparse biostratigraphic strata. Pioneering studies are those of Spieker and Reeside (1925) and Spieker (1946, 1949). More recent examples are the works of Hale and Van De Graff (1964), Gill and Hail (1975), Cobban (1976), Lawton (1982, 1983, 1985), Ryer (1981), Ryer and McPhillips (1983), Fouch et al., (1983), and more recently Franczyk et al., (1992), among others. A different approach was taken by Schwans (1988a, 1988b, 1995), who placed facies and similarities in stratal successions and stacking patterns into a biostratigraphic and sequence-stratigraphic framework; Figure 1 shows the resulting chronostratigraphy. The hiatus of the unconformities and the age of sequences in the chart are based on biostratigraphic and absolute age data discussed in detail in Schwans (1985a, 1986a, 1988a, 1988b, 1995); discussed are also the relationship between the sequence framework (Fig. 1) and the existing formation

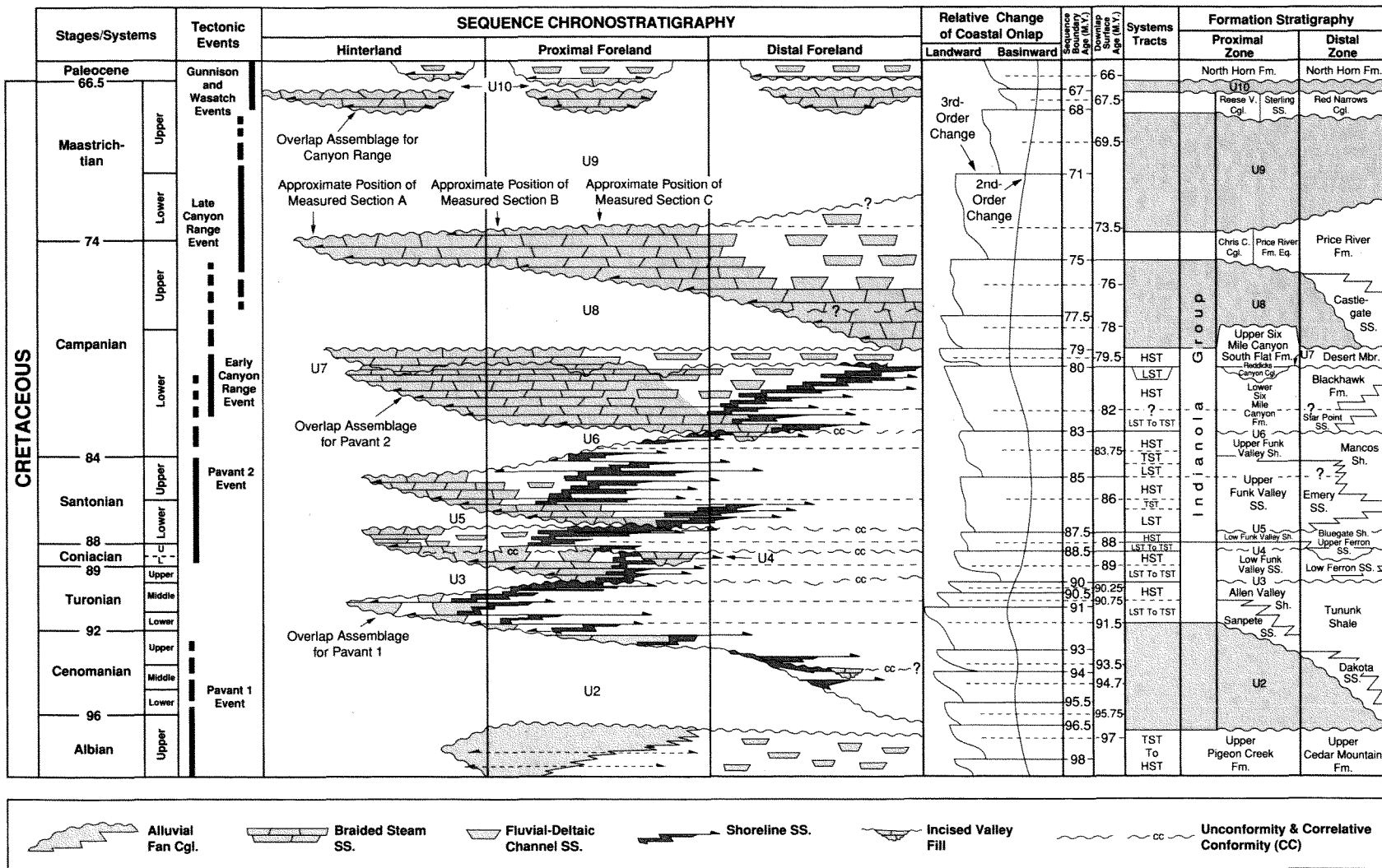


Figure 1. Sequence chronostratigraphy of the Cretaceous foreland basin in Utah with formations and interpreted tectonic events indicated. Ages of formations and timing of tectonic events are based on biostratigraphic and other age data discussed in Schwans (1988a, 1988b, 1995). The curves of relative change of coastal onlap are after Haq et al., (1987, 1988). LST—Lowstand systems tract; HST—Highstand systems tract; TST—Transgressive systems tract.

stratigraphy. The curve of coastal onlap and the ages of sequence boundaries and downlap surfaces from Haq et al., (1987) are included to provide comparison between the cyclicities observed in the foreland basin and at passive margin worldwide. Other studies on Cretaceous sequence stratigraphy in the foreland basin include, among others, Schwans (1986b, 1989, 1995), Vail and Bowman (1987), Aubrey (1989), Shanley and McCabe (1991, 1995), Van Wagoner (1991a, 1991b, 1995), and Van Wagoner et al., (1990). Figure 2 is a location map of the field trip area with the stops indicated.

STRUCTURE AND FORELAND BASIN ZONATION

Structure

The field trip area straddles a major structural transition zone the *Cordilleran hingeline*. Picha (1986) describes the *hingeline* as a zone that separates thick cratonic crust to the east from thinned, late Proterozoic-rifted crust in the west. Paleozoic miogeoclinal strata above basement thicken westward of the *hingeline* from 1000 m beneath the Wasatch Plateau to 11,000 m at the Utah-Nevada border (Standlee, 1982). The western portion of the Cretaceous foreland basin lies within this *hinge zone* (Schwans, 1988a, 1988b, 1995). Figure 3 shows the structural elements that influenced the configuration of the foreland basin in Utah; these are: (1) Proterozoic-rifted basement structures, (2) basement lineaments, and (3) Cretaceous-Tertiary thrust-fold structures.

Basement highs defined the position of the Mesozoic thrust ramps and the Cenozoic thrust-cored anticlines (Allmendinger et al., 1986, 1987; Lawton et al., 1994; Schwans, 1987a, 1987b, 1995). Intervening basement lows influenced the geographic configuration and position of alluvial to lacustrine Cenozoic basins. The eastern margin of the *hinge zone* is defined by the *Ephraim Fault* (EF in Fig. 3); basement is downthrown to the west to 9 km depth (Allmendinger et al., 1987).

Three basement lineaments or transverse faults cross the field trip area. The lineaments originated during Proterozoic rifting and were reactivated during Cretaceous-Tertiary compression as tear faults or right-lateral ramps to the eastward propagating thrusts (Fig. 3). In addition, the lineament acted as sediments conduits, linking the alluvial basins in the thrust belt to the marine foreland basin. Figure 4 is an interpreted seismic line across the field trip area; the interpretation is tied to measured section B (Stops 3.3, 3.4 in Fig. 2) and C (Stops 2.4, 2.5, 2.6 in Fig. 2) and two wells. Together, the figures illustrate the configuration of the thrust systems. The Pavant 1 (P1), Pavant 2 (P2), and the Canyon Range (C) thrust are Mesozoic thrusts, while the

Gunnison (G) and Wasatch (W) thrusts are of early Cenozoic age; the latter terminate as blind thrusts in Jurassic strata underneath the Wasatch Plateau (Standlee, 1982; Lawton, 1985; Villien and Kligfield, 1986). Figure 5 shows the interpreted structural and stratigraphic history of the fold-thrust belt in central Utah by Schwans (1988b, 1995). Alternate views and an expanded discussions are by Lawton and Trexler (1991), Royse (1993), Lawton et al., (1994), DeCelles et al., (1995), and Talling et al., (1995).

Zonation

Schwans (1995) discussed in detail the structural and stratigraphic zonation of the Cretaceous foreland basin. A zone proximal to the thrust front (<150 km distance) exhibits high sediment accommodation and tectonic subsidence, probably due to Airy isostasy. In contrast, tectonic subsidence and sediment accommodation in a second zone located farther basinward (>150 km distance) decreases to the east, probably due to flexural subsidence across the ramp. The different subsidence modes significantly influenced stratal stacking and sequence boundary character throughout the history of foreland basin infilling. The U2-U3 (96.5-90 Ma) sequence in Figure 1 is an example of a composite sequence that formed due to regional loading and crustal relaxation. The U2 unconformity defines the top of the Lower Cretaceous basin fill (Stop 3.2 in Fig. 2). Overlying 3rd-order sequences of Late Cretaceous age are stacked into retrograding, aggrading, and prograding sequence sets (Stops 3.4, 3.5 in Fig. 2).

Thrust-loading also impacted short-term sediment accommodation and stratal patterns during final shortening in the latest Campanian, Maastrichtian, and early Paleocene (Schwans, 1987b; Lawton and Trexler, 1991; Talling et al., 1995). Movement along the foreland thrust systems (G and W in Fig. 3) caused segmentation of the proximal zone into a series of north-south elongate, thrust-cored anticlines (*see* Maastrichtian-Paleocene in Fig. 5). The history of the anticlinal uplifts is manifested in the basin fill of adjacent synclines in a series of unconformity-bounded, clastic wedges (U8-U9 and U9-U10 sequences in Fig. 1) that onlap the anticlinal structures (Stops 1.1, 1.2, 1.3, and 3.1 in Fig. 2).

LOWER CRETACEOUS BASIN FILL

Sequence Stratigraphy and Zonation

Figure 6 is a measured section of the earliest foreland basin deposits in the proximal zone (Stop 3.1 in Fig. 2). Schwans (1985a, 1986b, 1988a, 1988b) discusses the facies, demonstrates the character and regional extent of the bounding unconformities, and suggests a Barremian(?) through late Albian age for the U1-U2 sequence; Figure 1 shows only the upper portion of the sequence and unconformity U2. The

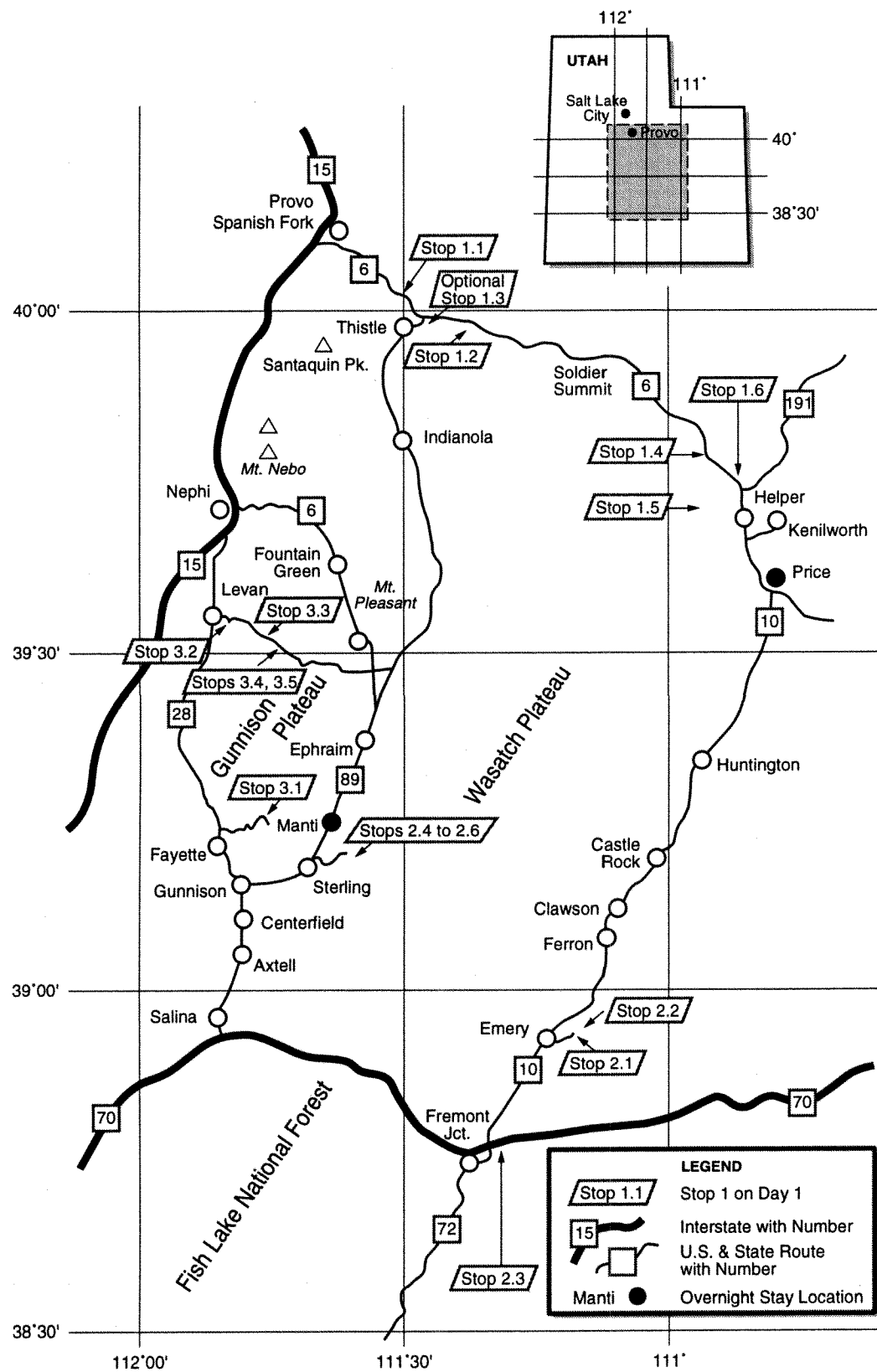


Figure 2. Location map of field trip area with stops and overnight stay locations indicated.

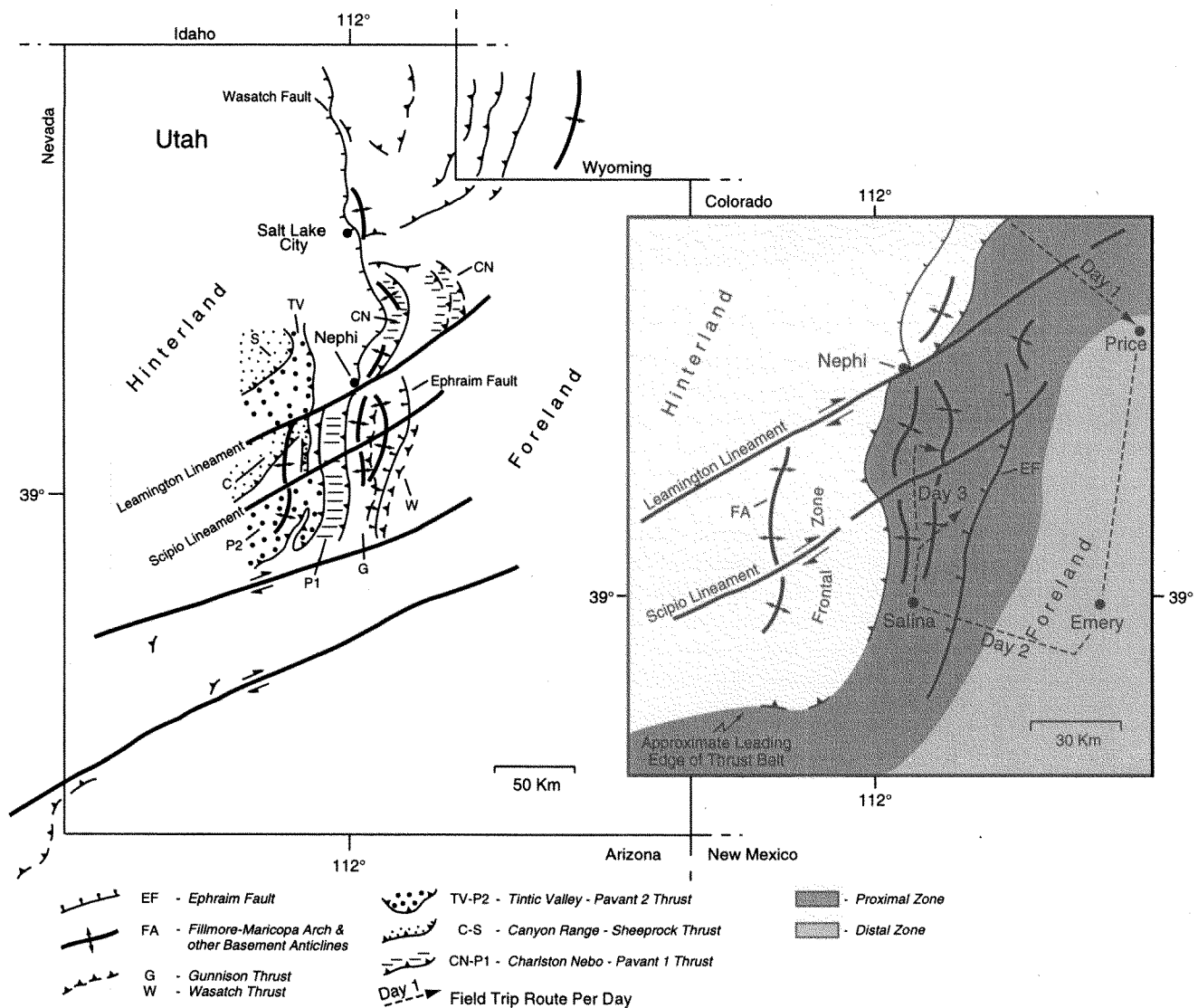


Figure 3. Map of the structural elements pertinent to foreland basin evolution in Utah. Modified after Allmendinger et al., (1986) and Picha (1986). The two shaded areas in the inset delineate the proximal and distal subsidence zones in the foreland basin; the approximate route of the field trip is shown for reference.

name Pigeon Creek Formation was suggested by Schwans (1988a) for the proximal clastics with the measured section in Figure 6 as the type section. Correlative formations are the Cedar Mountain and Burro Canyon formations in the distal zone in eastern Utah and western Colorado (Schwans, 1988b), which range in age from Barremian[?] through latest Albian (116.5-96 MA) (Heller and Paola, 1989; Yingling and Heller, 1992).

Proximal Zone Architecture

Initial sedimentation in the proximal zone and onset of thrusting occurred during Barremian through lower to mid-

dle? Aptian time and was marked by the deposition of *thin lacustrine limestones*, *flood plain mudstones*, and *intercalated channel-form sandstones* (see Lower Mbr. in Fig. 6). Flood-plain-dominated systems were overwhelmed by *sheet-flood fan conglomerates* (Upper Mbr. in Fig. 6) during the middle? Aptian through late Albian. Fans were sourced by the emergent Pavant 1 allochthon and shed eastward and later southward into the subsiding foredeep (Schwans, 1986b, 1988a, 1988b). In the outcrop (Stop 3.1 in Fig. 2), earliest sheet-flood fan deposits are made up of thin sheets of *chert-pebble conglomerates and sandstones* set within thick sections of *variegated mudstones*. Later, fan deposits form a

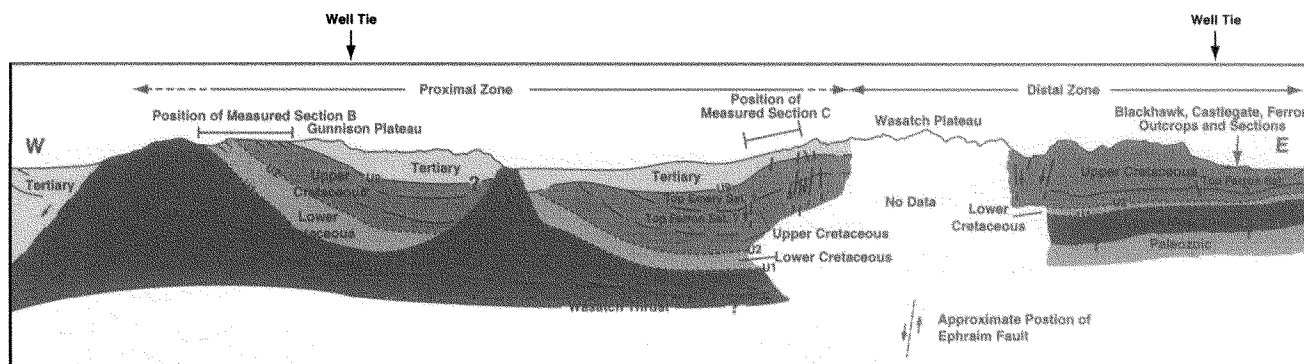


Figure 4. Interpreted seismic line and structural-stratigraphic cross section across the proximal and distal zones of the foreland basin margin. The interpretations are based on seismic tied to wells (see Well Tie), well-log correlations of Schwans (1988b, 1995), and outcrop data (see Position of measured section B, Blackhawk, Castlegate, Ferron Outcrops and Sections). No Data, refers to poor seismic data and no visible geometries.

thick succession of quartzite- and carbonate-clast *sheet-flood conglomerates* stacked into vertically amalgamated and laterally overlapping sheets separated by thin, *red mudstones* (Fig. 7). The succession of clast lithologies, clast sizes, and facies reflects hanging wall emergence and erosion of the Pavant 1 allochthon, resulting in an inverted clast-lithology stratigraphy (Schwans, 1998a).

Sediment thicknesses of the initial basin fill (e.g., Barremian through early to middle? Aptian) range from >300 m at the thrust front to 100 m along the eastern edge of the proximal zone (see dark grey area west of left dashed line, e.g. LPC, in Fig. 8). Sheet-flood fan accumulation was most pronounced in areas located basinward of the intersection point between the Leamington lineament and the frontal zone. The latter acted as a lateral ramp between the Charleston-Nebo thrust sheet to the north and the Pavant 1 thrust sheet in the south; the resulting tear fault zone between the thrust sheets formed a paleovalley and acted as sediment conduit. In contrast, sediment thicknesses during the middle? Aptian through late Albian range from >600 m at the thrust front to 300 m along the eastern edge of the proximal zone (see darkest grey area west of left dashed line, e.g. UPC, in Fig. 9) (Heller and Paola, 1989).

Distal Zone Architecture

Initial deposition in the distal zone in eastern Utah and western Colorado during the Barremian through lower-middle? Aptian consisted of chert- to quartzite-pebble conglomerates and sandstones transported in braided to low-sinuosity, multi-channel systems. Early drainages seem restricted to northwest-southeast oriented, broadly incised paleovalleys located in southeastern and eastern Utah (see light gray area, e.g. LBC and LCM, in Fig. 8) (Yingling and Heller, 1992). Well logs indicate that sediment thicknesses

in the paleovalleys do not exceed 60 m (Schwans, 1986b, 1988b).

The coarse-clastic paleovalley fills are overlain by extensive *flood plain mudstones* with thin intercalated *lacustrine limestones*, *paleosols*, zones of calcrete nodules, and partially to completely exhumed, *highly sinuous, channel-form sandstones* with laterally attached *sheet sandstones*. The flood plain-dominated successions are of Albian-age and were deposited across a wide area of minor topographic relief that experienced little or no subsidence (see light and lightest grey area east of left dashed line, e.g. UCM and UBC in Fig. 9). Well logs indicate that sediment thickness does not exceed 300 m (Schwans, 1986b, 1988b).

Implications for Basin Subsidence

Initial basin subsidence in the proximal zone allowed the accumulation of 1000 m of strata within a narrow subsiding trough defined by the Pavant 1 thrust front in the west and the Ephraim Fault in the east. Conversely, sediment accommodation in the distal zone during the same time interval was more or less insignificant across a wide basin area. Schwans (1986b, 1987a) interpreted this difference in sediment accommodation patterns to indicate that tectonic subsidence in the proximal zone was predominantly an Airy isostatic subsidence of basement blocks beneath and near the thrust load and decoupled or detached from subsidence of the stable, unbroken craton of the distal zone. A comparison of Figures 8 and 9 shows that net aggradation and net subsidence accelerated during the late Aptian through Albian, involving most of eastern Utah. This change is interpreted to reflect the change from laterally restricted, Airy isostatic subsidence near the load to larger scale, flexural subsidence.

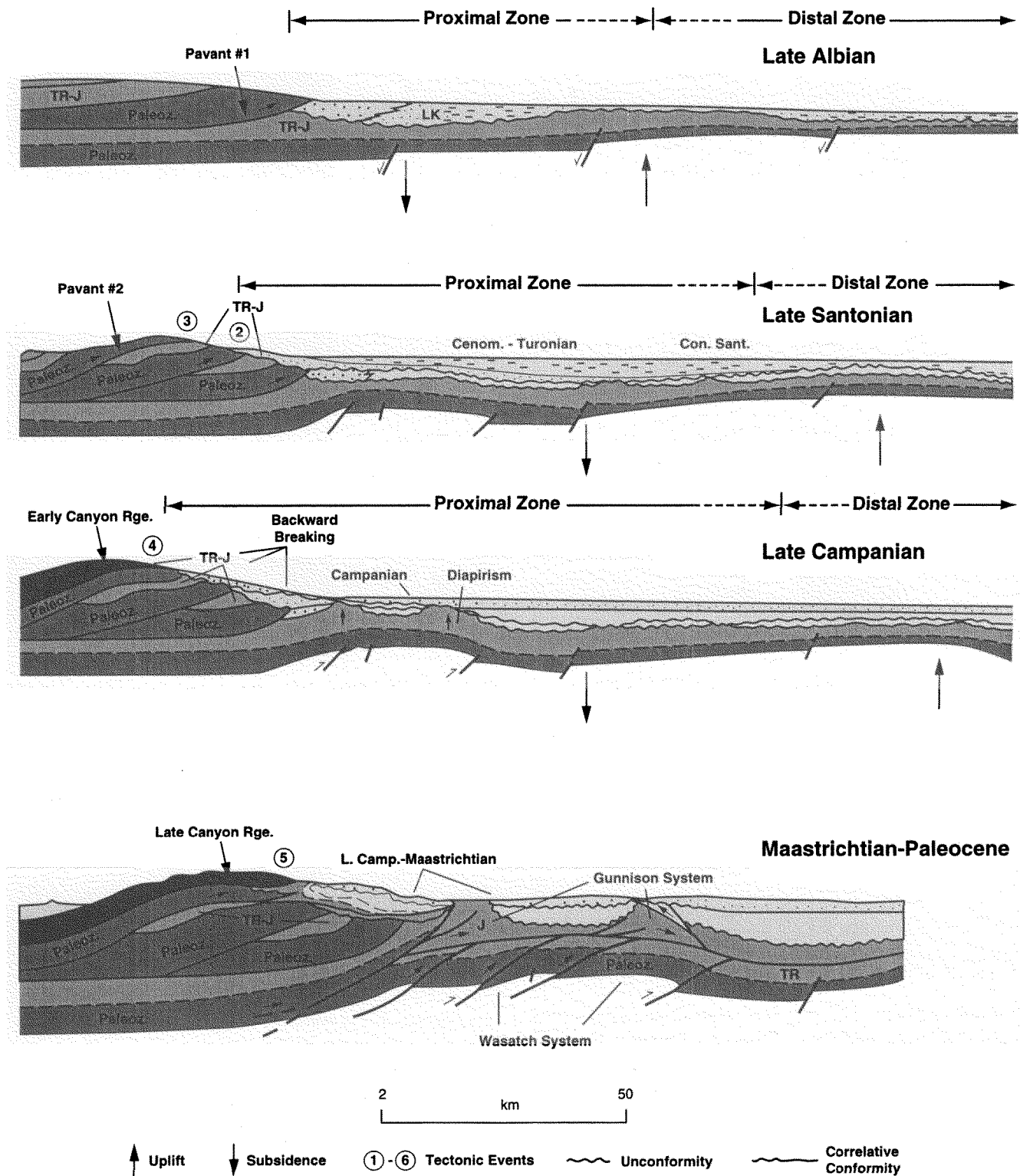


Figure 5. Interpreted compressional history of the Cretaceous fold-thrust belt in central Utah. Structural relationships and timing after Villien and Kligfield (1986) and Schwans (1988a, 1988b).

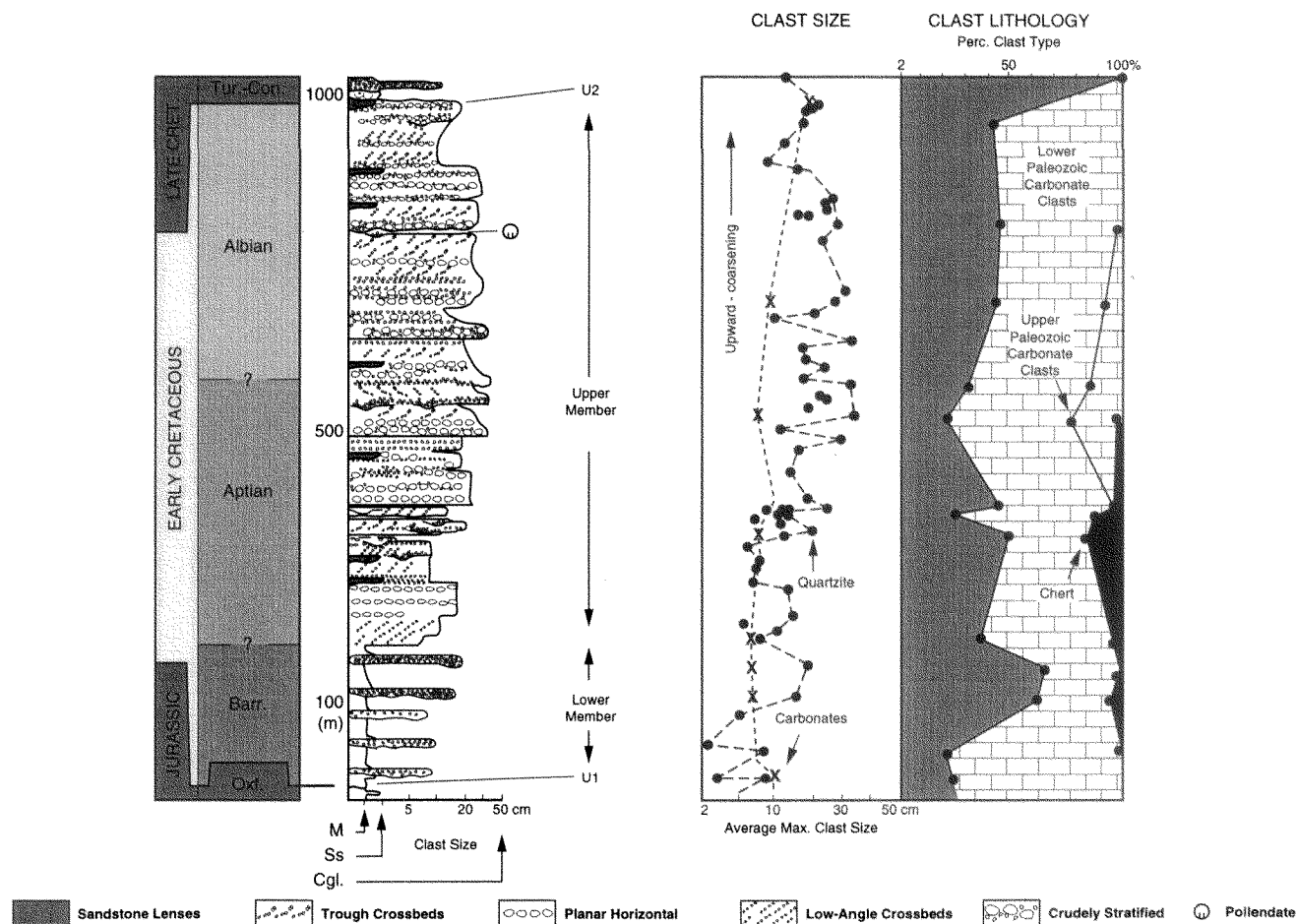


Figure 6. Measured section of the Lower Cretaceous portion of Indianola Group (Undifferentiated) of Spieker (1946, 1949) in Chicken Creek Canyon (Sec. 12, T. 15S, R. 1E), east of Levan, Utah (Stop 3.2 in Fig. 2). The section shows the age, grain size distribution, bedding types, maximum clast size distribution, and clast type distribution for the Pigeon Creek Formation of Schwans (1988a, 1988b). The section defines the U1-U2 sequence of Figure 1.

UPPER CRETACEOUS SEQUENCE BASIN FILL

Sequence Stratigraphy and Zonation

Spieker (1946, 1949) defined the Upper Cretaceous Indianola Group and its members (*see* Proximal Foreland column in Fig. 1). Lawton (1982, 1983) presented an updated lithostratigraphic framework and facies scheme. Schwans (1985b, 1986a, 1988b, 1989, 1990, 1991, 1995) revised the biostratigraphy and proposed a sequence-stratigraphic framework for the Upper Cretaceous Indianola Group (*see* Proximal Zone in Formation Stratigraphy column in Fig. 1) and associated time-equivalent units, including conglomerates to the west in the Gunnison Plateau (*e.g.*, Indianola Group [Undifferentiated] of Spieker [1946, 1949]), the Canyon Range, and in the Pavant Range (*e.g.*, Hinterland

column in Fig. 1), as well as shallow-marine strata in the east in the Wasatch Plateau and Book Cliffs (Distal Foreland column in Fig. 1).

Nine unconformities and ten depositional sequences (U2 through U10 in Fig. 1) are identified in the basin fill. Within each depositional sequence alluvial fan conglomerates and braided stream sandstones located at the thrust front (Figs. 10, 11) grade down-depositional dip and eastward into braided stream and overbank successions (Figs. 12, 13) (Stops 3.1, 3.4, 3.5 in Fig. 2); the latter may be cut by conglomeratic valley fills several kilometers wide and up to 300 m thick (*see* conglomerates in measured sections Figs. 11, 12, 14) (Stops 3.4, 3.5, and Optional Stop 1.3 in Fig. 2). The nonmarine strata give way to shoreline and open-marine facies via wave-dominated shorelines (Stop 1.5 in Fig. 2), fluvial-dominated deltas (Stop 2.1, 2.2 in Fig. 2), and braid-deltas (Figs. 15, 16) (Stops 2.4, 2.5, 2.6 in Fig. 2).



Figure 7. Photograph of sheet-flood conglomerates with intercalated thin, red mudstones at Stop 3.2 (Fig. 2). The strata are part of the Upper Pigeon Creek Member of Schwans (1988a).

Three types of sequences and sequence boundaries are observed: (1) high-frequency sequences and unconformities with probable cyclicities of 100,000–200,000 years; (2) third-order sequences and unconformities with cyclicities of about 1–3 MY.; and (3) composite sequences and unconformities with cyclicities greater than 3 MY.; composite unconformities consist of several, merged higher frequency surfaces. Examples for the first type are the high-frequency sequences and unconformities observed in the Dakota Formation and the U4 surface in Figure 1, which separates the upper and lower Ferron Sandstone of Schwans (1988b, 1995) (Stop 2.3 in Fig. 2). The surfaces and strata record the numerous changes in relative sea level during the gradual westward shift of shoreline facies across Utah with the incursion of the seaway in the late Albian through early Turonian. Likely examples of third-order sequences and unconformities and probably the direct result of eustasy in the marine foreland basin and (Type-1 sequences *in sensu* Van Wagoner et al., 1990) are the surfaces U3 and U6 in Figure 1 (Stop 2.3, 2.6, respectively in Fig. 2). The third type, composite sequences and unconformities, seem to be most common in the foreland basin fill; examples are the surfaces U2 (Stop 3.2 in Fig. 2) and U8 through U10 (Stops 3.1, 3.4, and 1.4 in Fig. 2). These types of unconformities are marked angular toward the tectonic belt and exhibit a variable hiatus (Figs. 4, 10, 12). An example is the U2 surface and its associated hiatus, which may span as much as 5 MY. at the thrust front and as little as 0.25–3 MY. in the distal zone. This variation is interpreted as the combined result of erosion and sediment bypass, following thrust emergence and westward directed onlap with basin subsidence

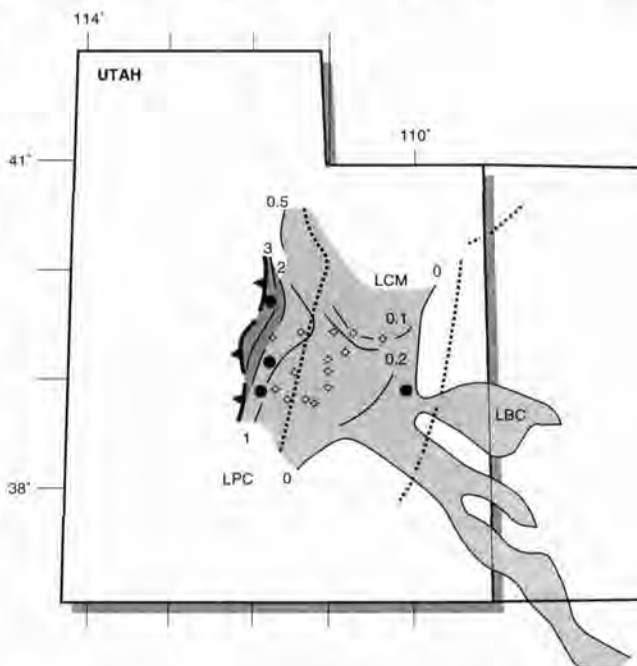


Figure 8. Thickness distribution of Barremian through middle Aptian strata in Utah. Thicknesses are in hundreds of meters and based on measured sections (heavy dots) and interpreted well logs (well symbols) from Schwans (1988b). The shading highlights the thickness variations. Dashed line between LPC (Lower Pigeon Creek Formation) and LCM (Lower Cedar Mountain Formation) depicts the eastern limit of the proximal zone; dashed line between LCM and LBC (Lower Burro Canyon Formation) depicts approximate eastern limit of distal zone.

and seaway expansion. Figure 17 (Stop 3.1 in Fig. 2) is an example of a composite surface associated with local uplift and infilling of the adjacent sub basin; the hiatus associated with this surface may range from < 5 MY. in the basin to > 10 MY. on structure (Schwans, 1987b, Talling et al., 1995).

Proximal Zone Architecture

Individual depositional sequences in the proximal zone are defined by a spectrum of depositional environments, which includes, arranged from up-dip to down-depositional dip, alluvial fan deposits, conglomeratic paleovalley fills, and braided stream deposits. Table 1 summarizes the lithofacies and interpreted depositional environments in the proximal zone.

Alluvial fan elastics are the most proximal deposits found in the Upper Cretaceous basin fill (Figs. 10, 11). Figure 11 shows crudely stratified *block and boulder conglomerates* and cross bedded *scour-based boulder- to cobble-conglomerates* forming 20 m to 30 m-thick, upward-fining successions. The successions in turn stack to form 500 m to 1000 m

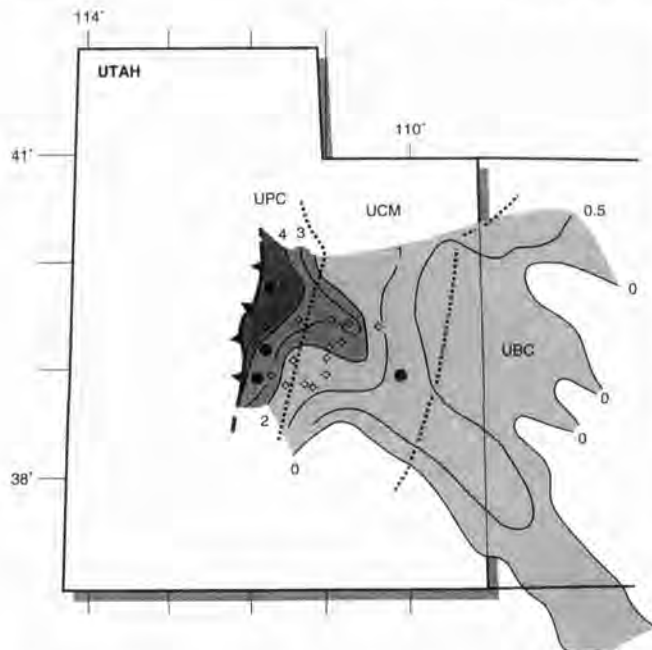


Figure 9. Thickness distribution of Middle Aptian through late Albian age strata in the foreland basin in Utah. Thicknesses are in hundreds of meters and based on measured sections (heavy dots) and interpreted well logs (well symbols) from Schwans (1988b). The shading highlights the thickness variations. Dashed line between UPC (Lower Pigeon Creek Formation) and UCM (Upper Cedar Mountain Formation) depicts eastern limits of proximal zone; dashed line between UCM and UBC (Upper Burro Canyon Formation) depicts approximate eastern limit of distal zone.

wide, wedge-shaped stratal bodies. The *block and boulder conglomerates* occur at the thrust front in the Canyon and Pavant ranges and are interpreted by Schwans (1988b) to represent alluvial fan deposition by catastrophic, bedload-concentrated flows transported during episodic flood discharges under a humid-tropical climate; overlying finer grained *cross bedded pebbly sandstones* represent low-energy deposition on the fan surface, possibly during lower water stage in small channels and bars. The measured section shown in Figure 11 is located west of the field trip area in the Canyon Range (Figs. 3) and will not be visited; it is shown here to provide a more complete depositional spectrum.

The *scour-based boulder-cobble-conglomerate* and *gravelly sandstone* facies association is the coarsest in the field trip area and forms discrete paleovalley fills that are several kilometers wide and 50–250 m deep (Stops 1.2, 3.4 in Fig. 2). Examples are the strata above U7 in Figures 12 and 14 (Stop 3.4 in Fig. 2) and the incised valley fill above U3 in Figure 16 (Optional Stop 1.3 in Fig. 2). The strata are part of the Indianola Group (Undifferentiated) of Spieker (1946, 1949) and correspond to the Reddicks Canyon Conglom-



Figure 10. Photograph of alluvial fan conglomerates and braided stream sandstones located at the thrust front in Oak Creek Canyon in the Canyon Range (see measured section A in Fig. 11). Canyon Range thrust (arrow) and position of unconformities are indicated. ET-erosional truncation; ON-onlap.

erate and the Lower Funk Valley Sandstone of Schwans (1988b) in Figure 1. Transportation and deposition of conglomerates occurred in shallow bars under a perennial and seasonally wet-tropical climate; interbedded lenses of gravelly sandstones are the fills of small channels.

The bedload to mixed load braided stream deposits comprise the bulk of the Upper Cretaceous coarse-clastics, formerly called Indianola Group (Undifferentiated), in the proximal foreland zone. Lithofacies of these deposits are arranged into 150–300 m-thick upward-fining, sheet-like bodies that parallel the structural strike of the frontal zone for 10 km to > 100 km. In the measured section in Figure 12, the lower, coarse-clastic portion of individual upward-fining units are trough cross-bedded, *scour-based, cobble-pebble conglomerates* of sheet geometry grading upward into cross bedded, *pebbly sandstones* and *sandstones* (e.g., strata immediately above U3, U4, U5, and U6 in Fig. 12) (Stop 3.3 in Fig. 2). Conglomerates and sandstones were transported and deposited in mixed gravelly and sandy bars in a braided stream. The coarse clastics of individual upward-fining units are overlain along a sharp surface by a thick section of *overbank siltstones* and *detrital carbonates* with a wide variety of ripple cross-stratification, an abundance of secondary sedimentary structures, and numerous angiosperm leaf impressions (Schwans, 1988b). Intercalated are trough cross bedded, *pebbly channel-form sandstones* (Stop 3.3 in Fig. 2). This facies association is interpreted to represent mixed sand-mud deposition by low-sinuosity channels located in a ponded flood plain.

Figure 13 is a composite photo of a portion of the measured section in Figure 12. Figure 18 is a block diagram

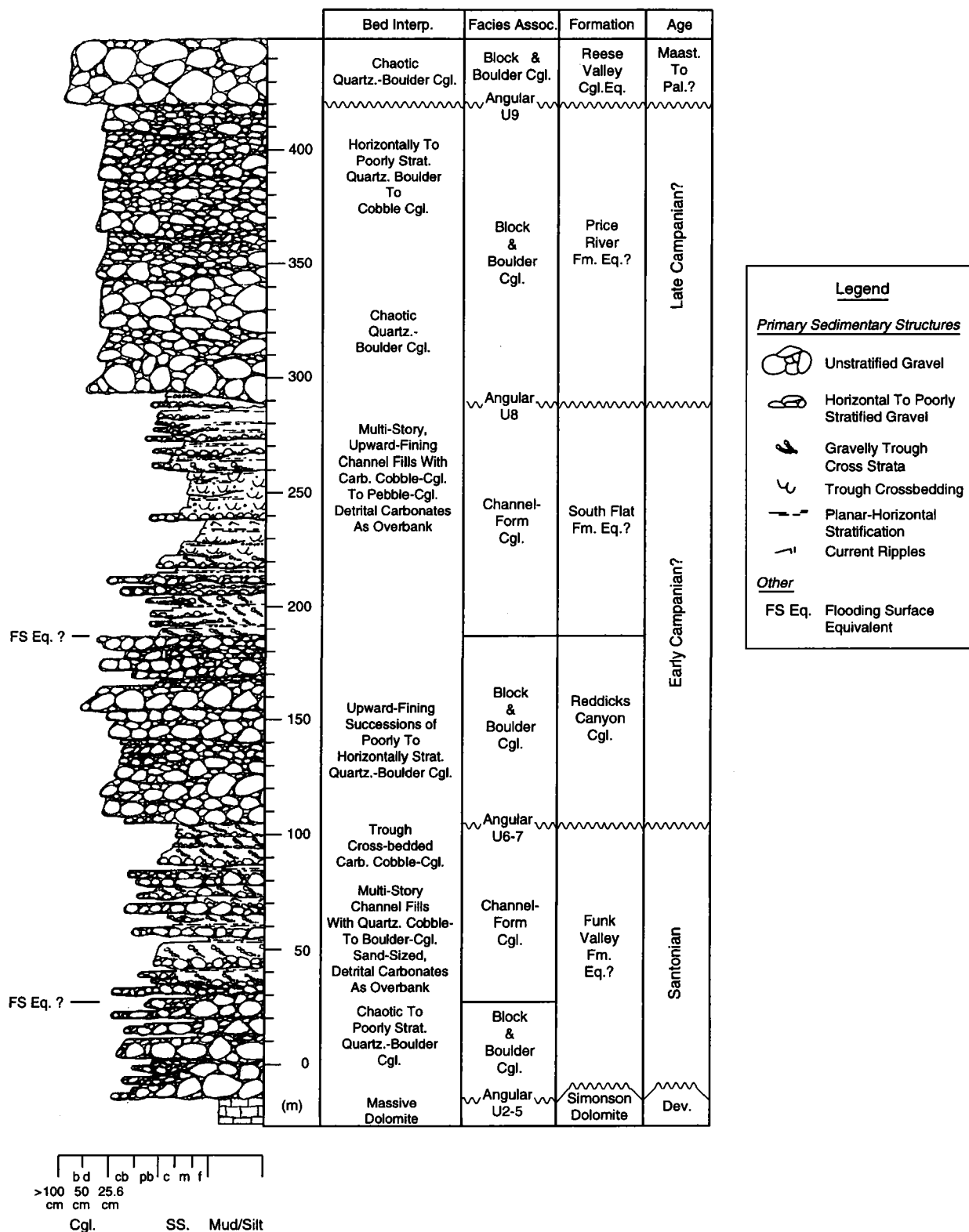


Figure 11. Measured section A of alluvial fan conglomerates shown in Figure 10. Section was measured in Oak Creek Canyon (Sec. 10, T. 17S., R. 2W.), Canyon Range, Utah. Lithofacies include crudely stratified block and boulder conglomerates, cross bedded scour-based boulder- to cobble-conglomerates, and cross bedded pebbly sandstones arranged into 20 m to 30 m-thick, upward-fining successions.

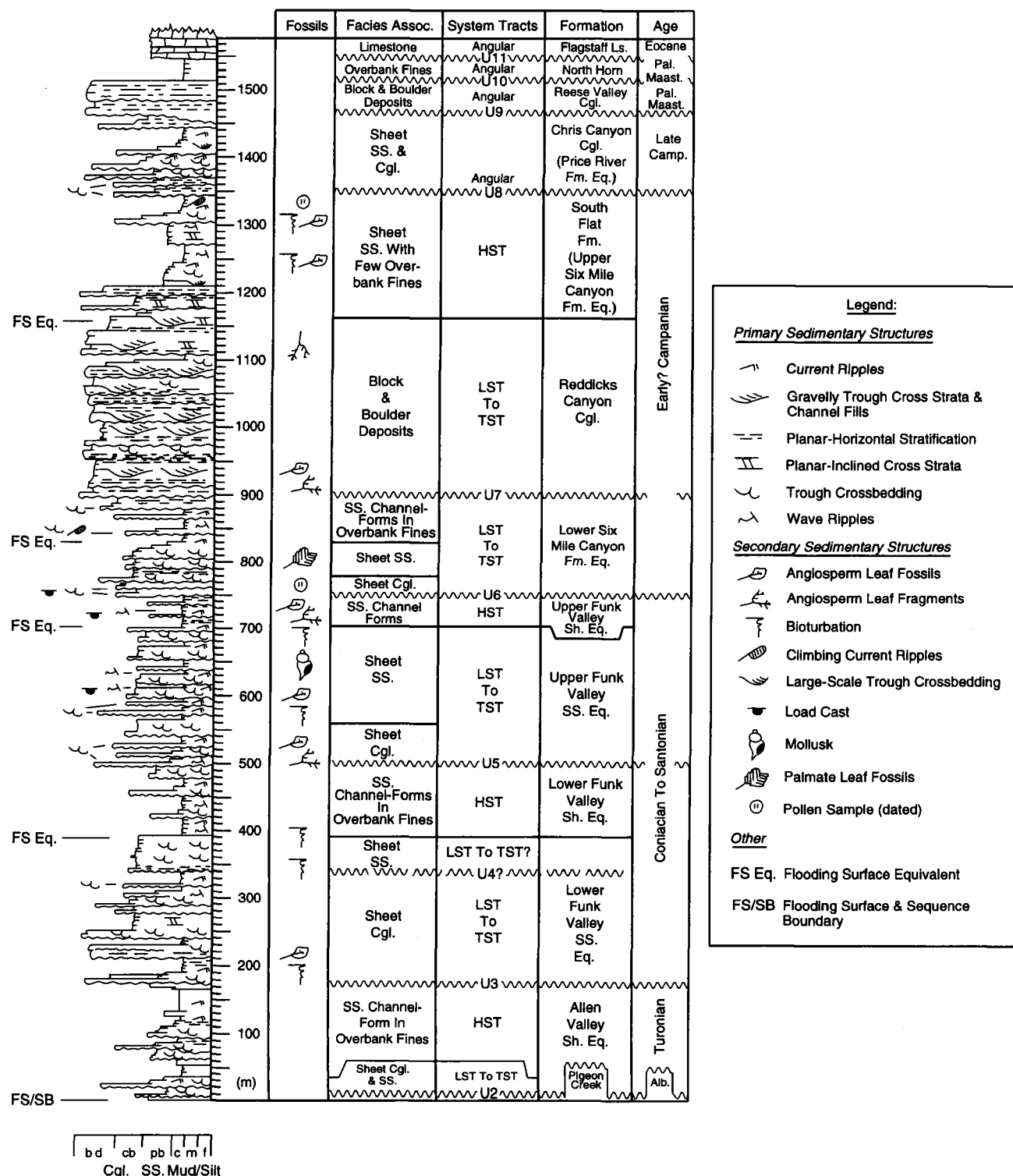


Figure 12. Measured section B (see Figs. 1 and 4) of the Upper Cretaceous portion of the Indianola Group (Undifferentiated) of Spieker (1946, 1949) in Chicken Creek Canyon (Sec. 12, T. 15S, R. 1E), east of Levan, Utah (Stops 3.2 through 3.5 in Fig. 2). The section illustrates the alluvial architecture of ten depositional sequences of Schwans (1988b, 1995).



Figure 13. Composite photograph of three depositional sequences shown in Figure 12 (Stops 3.4, 3.5 in Fig. 2). Within each sequence the coarse-clastic braided stream deposits represent the lowstand to transgressive systems tract (LST-TST), while overlying overbank fines with intercalated single-channels forms are the highstand systems tract (HST). Strata dip to the left and east, view is to the south. ET—erosional truncation; ON—onlap.

that illustrates sequence architecture and sequence stacking for nonmarine strata in the proximal zone. According to Schwans (1995), each large-scale, upward-fining unit is a depositional sequence bounded by unconformities. Within each sequence the coarse-clastic braided stream deposits represent the lowstand to transgressive systems tract (LST-TST in Figs. 1, 12), while overlying overbank fines with intercalated channels form the highstand systems tract (HST in Figs. 1, 12). The systems tracts in the proximal zone are thus defined by a change in depositional architecture from a bedload-dominated, fluvial systems with vertically amalgamated channels to a suspended-load dominated system with isolated channel-forms set in overbank fines.

Distal Zone Lithofacies And Architecture

Individual depositional sequences in the distal zone include a range of depositional environments; these are fluvial-dominated shoreline deposits, wave-dominated shoreline deposits, and open-marine deposits. Table 2 summarizes the lithofacies and interpreted depositional environments in the distal zone.

Fluvial-dominated shoreline deposits are exposed along the western (Stops 2.4, 2.5, 2.6 in Fig. 2) and eastern margins (Stops 2.1, 2.2, 2.3 in Fig. 2) of the Wasatch Plateau, or proximal and distal zones, respectively, and feature coarse-grained *tabular sandstones* and finer grained *lenticular sandstones* separated by thick *mudstones with thin beds of siltstones and muddy sandstones*. In the measured section in Figure 15, *tabular sandstones* exhibit low-amplitude cross

beds, numerous reactivation and internal scour surfaces, and abundant shelly debris. This 50 m-thick section above unconformity U3 is part of the Lower Funk Valley Formation of Schwans (1988b) and reflects braid-delta progradation into a shallow-marine, estuarine embayment and shallow-incised paleovalley. The sandstone bodies onlap U3 along depositional strike (Fig. 19) and form a part of the lowstand to transgressive systems tract above U3 (LST to TST in Figs. 1, 15). The shales beneath U3 are part of a highstand systems tract (HST in Figs. 1, 15) and form the Allen Valley Shale of Spieker (1946, 1949) (Stop 2.4 in Fig. 2).

The *tabular sandstones* are sharply overlain along a flooding surface (first FS above U3 in Fig. 15) by a 250 m-thick interval of *mudstones with thin beds of wave- and flaser-rippled siltstones and muddy sandstones* organized into 10–15 m-thick, coarsening-upward parasequence sets; the latter are crevasse splays and small deltas that shed into brackish-water bays. Parasequences feature mudstones and siltstones coarsening upward into rippled, often soft-sediment deformed, bioturbated, muddy sandstones with lags of mollusks. The deposition of the mudstone-dominated interval occurred in response to a rise in relative sea level during early highstand systems tract (Schwans, 1995) (HST above U3 in Figs. 1, 15).

Lenticular sandstones, shelly banks, and mudstones are common in the distal zone at the eastern margin of the Wasatch Plateau (Stops 2.1, 2.2, 2.3 in Fig. 2). Mudstone-siltstone intervals feature a variety of ripple cross strata (see Table 2), normal-graded beds, and burrows, and coarsen



Figure 14. Photograph of the incised paleovalley fill located above U7 in Figures 12 and 13 (Stop 3.4 in Fig. 2). The paleovalley fill is the Reddicks Canyon Cgl. of Schwans 1988b (see Figs. 1, 12). Strata are dipping to the east (top of photo). Note the flat lying Tertiary strata above U9 and U10.

upward into sandstones with low-angle inclined laminae sets (Stop 2.1). In places, zones with tightly packed shell fragments and whole pelecypod valves occur. Symmetrical channel scours up to 4 m wide and 2 m deep are cut into the tops of the sandstone bodies. The lithofacies stack to form a series of deltaic parasequences and parasequence sets of the inner and outer stream-mouth bar. Figures 20 and 21 show an example of two such deltas (Stop 2.3 in Fig. 2). The photos show the Coniacian-age, Upper Ferron Sandstone of Schwans (1988b, 1995) and Cotter (1971, 1975) and represent fluvial-deltaic progradation in the distal zone during the lowstand to transgressive systems tract above unconformity U4 (Fig. 1). The Coniacian age designation and formation interpretation is contrary to that of Gardner (1993), Ryer (1981) and Ryer and McPhillips (1983). Schwans (1988b, 1995) offers a detailed discussion of the biostratigraphy, well-log correlations, and paleogeographic reconstructions. Figure 22 is an outcrop and well-log cross section excerpted from Schwans (1995) and illustrates the stratal relationships between the Lower Funk Valley Sandstone exposed in measured section C (Stop 2.4 and Fig. 15) in the proximal zone and the Upper Ferron Sandstone exposed in Stops 2.1 through 2.3 in the distal zone (Fig. 2). In the cross section the unconformity U4 truncates most of the underlying Lower Ferron Sandstone of Turonian age toward the east and superposes Coniacian-age, fluvial-deltaic strata of the Upper Ferron onto pro delta and offshore mudstones of the Turonian-age Lower Ferron, indicating a significant basinward shift in facies and the presence of U4 in Stop 2.3 (Fig. 2). The parasequence set stacking pattern observed in said stops is also present in the nearby wells. For example, the lower flooding surface (e.g.,

FS above U4 in Figs. 20, 21) that separates the two stacked deltas and parasequence sets in the outcrop can be correlated to the flooding surface that separates the upper and lower sand above U4 in wells #3 through #5 in Figure 22. The delta-front clinoforms beneath the lower FS in the outcrop are truncated along their tops by channels of the inner stream-mouth bar, suggesting a high-frequency unconformity; the latter surface is marked also in the well-log cross section.

Wave-dominated shoreline deposits are found in the proximal zone at the western margin of the Wasatch Plateau (Stops 2.5, 2.6 in Fig. 2), where they form the Upper Funk Valley Sandstone of Schwans (1988b, 1995) (see strata above and below U5 in Figs. 15, 23), and in the distal zone at the eastern margin of the plateau, where they form the stacked shoreface units of the Blackhawk Formation (Stops 1.5, 1.6 in Fig. 2). Shoreline parasequences consist of *wave-rippled mudstones, siltstones, and sandstones* at their base that represent deposition at shelfal depth. These grade upward into *hummocky cross-stratified* and bioturbated, *trough cross-bedded sandstones* deposited by traction currents in the lower and upper shoreface; burrows are of the *Skolithos* ichnofacies. Parasequences in the proximal zone may exhibit *scour-based, pebbly sandstones* at their tops that have cut into underlying cross strata (for example, at 1390 m in Fig. 15).

Open-marine, fine-grained deposits are found in the proximal zone at the western margin of the Wasatch Plateau (Stops 2.4, 2.5, 2.6 in Fig. 2), where they form the Allen Valley Shale, the Lower Funk Valley Shale, and the Upper Funk Valley Shale of Schwans (1988b, 1995) (Figs. 1, 15, 19, and 23), and in the distal zone at the eastern margin of the plateau, where they form the Tununk and Bluegate tongues of the Mancos Shale (Stops 2.1, 2.2, 2.3 in Fig. 2). Open-marine deposits comprise thick intervals of massive to *horizontal-planar bedded, carbonaceous mudstones* with thin beds of *wave-rippled sandstones and flaser bedded siltstones to very fine sandstones*. Less common are thin, dark gray, foraminifer-bearing *micritic limestones*. Bioturbate structures indicate low species diversity and include small burrow of *Teichichnus* sp. and *Planolites* sp. Mudstones represent deposition in a distal pro-delta and shelfal setting at water depths below effective wave base and are deposited during the highstand systems tract of individual sequences (HST's in Fig. 1). The micritic limestones in the same interval are rare and probably reflect maximum water depth. Schwans (1988b) offers a detailed discussion of the fauna and biostratigraphy of the various Mancos tongues shown in Figure 1.

In the measured section in Figure 15, the deltaic and estuarine sandstones of the lowstand to transgressive systems tracts above U2 and U3 are abruptly overlain along a maximum flooding surfaces (MFS) by open-marine mud-

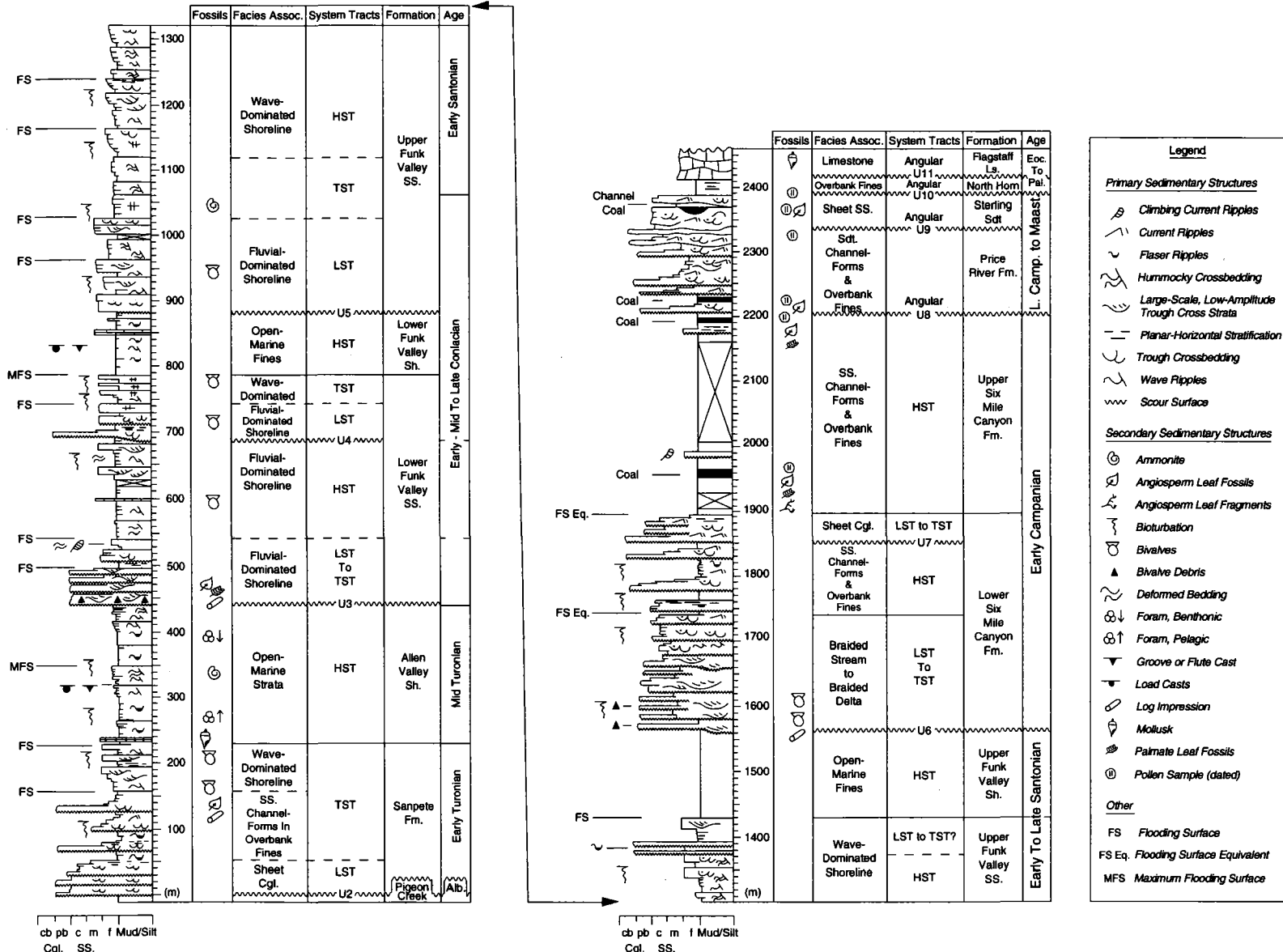


Figure 15. Measured section C (see Figs. 1, 4) of the Upper Cretaceous portion of the Indianola Group of Spieker (1946, 1949) at Palisade Lake State Park (Secs. 36-36-25, T. 18S., R. 2E.), east of Sterling, Utah (Stops 2.4 through 2.6 in Fig. 2). The section illustrates the alluvial to nearshore-marine architecture of ten depositional sequences of Schwans (1988b, 1995).

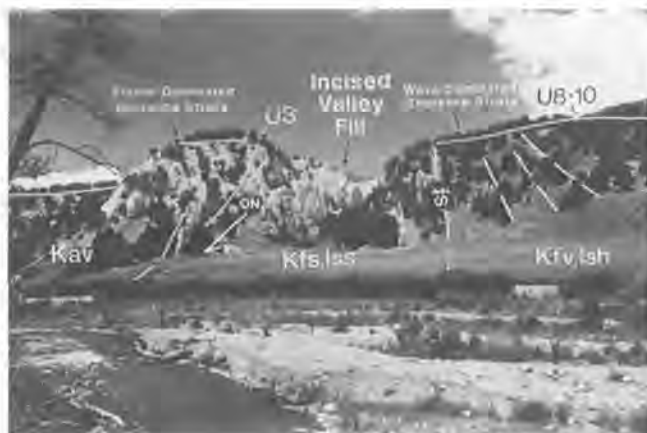


Figure 16. Photograph of an incised paleovalley fill (Optional Stop 1.3 in Fig. 2) equivalent to the Lower Funk Valley Sandstone (Fig. 1) at Lake Fork (Sec. 2, T. 9S., R. 4E.); strata are vertical and unconformably overlain along U8-10 by Paleocene-age Red Narrows Conglomerate (Fig. 1). Fluvial-dominated shoreline strata beneath U3 (e.g. to the left) are Early Turonian and equivalent to the Allen Valley Shale (Fig. 1). They are sharply overlain along a flooding surface (FS) by wave-dominated shoreline strata of the transgressive systems tract of middle-late Turonian age, based on mollusks described in Schwacs (1988b).

stones of the corresponding highstand systems tract. The highstand strata are truncated by the sequence boundaries, which are overlain by fluvial-deltaic, incised-valley deposits of the next lowstand systems tract (*see* strata above U3 through U6 in Figs. 19, 23), indicating repeated relative shallowing of the basin and a basinward shift in facies. Figure 24 is an example of a significant basinward shift in facies across U6 (Fig. 15), superposing braided-stream conglomerates of the lowstand systems tract onto open-marine mudstones of a highstand systems tract.

CONCLUSIONS

The facies architecture and the associated parasequence and sequence stacking patterns across the foreland basin margin occur within an accommodation cycle of subsidence and sea level change. Case I in Figure 25 shows the architecture and stacking patterns for a period marked by high tectonic subsidence (e.g., proximal zone), multiple higher frequency changes in relative sea level, and abundant sediment supply. The fluvial architecture of a highstand systems tract in the sea level cycle shown (1 and 3 in case I of Fig. 25) is marked by overbank-dominated systems with well-defined, single-channel geometries. Correlative nearshore-marine strata show an aggradational parasequence stacking pattern. The associated lowstand systems tract (2 in Case I) is characterized by a change in parasequence stacking pattern from aggradational to progradational and a minor



Figure 17. Photo of an uppermost Maastrichtian to Eocene piggy-back basin fill in Mellor Canyon (Stop 3.1 in Fig. 2), near the town of Fayette (Sec. 17, T. 18S., R. 1E.), southwestern Gunnison Plateau. The Tertiary-age, deformed conglomerates and overbank mudstones of the North Horn Formation and the lacustrine limestones of the Flagstaff Limestone onlap probably Campanian-age, east-dipping (e.g. to the right), braided stream deposits of the Six Mile canyon Formation along composite surface U8-9. View is to the north. ET—erosional truncation; ON—onlap.

basinward shift in facies. At the same time, fluvial architecture in the up-dip shows increased channel clustering to lateral coalescing of single-channel geometries. Examples for Case I stacking patterns and architecture are the Emery Sandstone and the correlative Upper Funk Valley Sandstone (U5-U6 sequence in Fig. 1).

Case II in Figure 25 shows the architecture and stacking patterns for a period marked by low tectonic subsidence (e.g., distal zone) and multiple higher frequency changes in relative sea level under an abundant supply of sediment. As was previously the case, the fluvial architecture of a highstand systems tract (1 and 3 in case II of Fig. 25) is marked by overbank-dominated systems with single-channel geometries and correlative nearshore-marine strata are essentially aggradationally stacked. The associated lowstand systems tract, however, is marked by an abrupt change in parasequence stacking pattern from aggradational to progradational, a major basinward shift in facies, subaerial erosion of marine strata, and formation of incised valley systems. Correlative fluvial architecture in the up-dip shows formation of bedload-dominated systems and valley incision. Examples for Case II stacking patterns and architecture are the Ferron Sandstones and the correlative Lower Funk Valley Sandstone (U3-U4 and U4-U5 sequence in Fig. 1) and the Blackhawk and Six Mile Canyon formations (U6-U7 sequence in Fig. 1).

The described accommodation cycle of subsidence and sea level change can be applied to characterize and predict depositional architecture per basin zone and sequence.

Table 1: Lithofacies and depositional environments in the proximal zone

Environment	Lithofacies & Bedding Types
Alluvial Fan	<i>Block and boulder conglomerates</i> <ul style="list-style-type: none"> • chaotic to crude-horizontal stratification <i>Scour-based, boulder-cobble-pebble conglomerates and gravely sandstones</i> <ul style="list-style-type: none"> • trough cross beds, horizontal planar beds, ripple cross beds
Paleovalley Fills	<i>Scour-based, boulder-cobble conglomerates and gravely sandstones</i> <ul style="list-style-type: none"> • low-angle, planar-inclined cross beds, trough cross beds, horizontal planar beds
Bedload to Mixed-Load Braided Stream	<i>Scour-based, cobble-pebble conglomerates, pebbly sandstones, and sandstones</i> <ul style="list-style-type: none"> • trough cross beds
Mixed to Suspended Load Fixed-Channel Stream and Floodplain	<i>Pebbly, channel-form sandstones</i> <ul style="list-style-type: none"> • trough cross beds <i>Overbank siltstones, mudstones, and detrital carbonates</i> <ul style="list-style-type: none"> • trough cross beds, ripple cross beds, contorted beds, load and flute casts, rizoliths, biogenic traces of <i>Scoyenia</i> ichnofacies, angiosperm leaf impressions

Facies successions are thus not only specific to either foreland basin zone, but are also definitive with respect to the changes in the position of relative sea level and can be grouped into the three component systems tract.

ROAD LOG

(Refer to Figure 2 for Stops, town names, and landmarks)

Day 1

Key Topics: Thrust systems and basin-fill overview; alluvial fan facies, braided stream facies (Flagstaff Ls., Red Narrows Cgl., North Horn Fm., Price River Fm., Castlegate Sdst.) wave-dominated shoreline facies (Blackhawk Fm.); parasequence expression and stacking patterns; unconformity types.

Miles

- 0.0** Travel south on I-15 from Salt Lake City to Provo. Interstate runs parallel to the Wasatch Mountains. The Wasatch Fault, a major down-to-the-west normal fault, lies at the base of the foothills of the Wasatch Range.
- 50.0** Exit I-15 onto Routes 89 and 6 proceed on Route 6 toward Price.

- 56.0** The road approaches the Wasatch Mountains and passes through Pennsylvanian to Permian marine sedimentary rocks.

64.0 **Stop 1.1—Charlston-Nebo Thrust at summit at Lake Fork.**

Jurassic Navajo Sandstone of the Charlston-Nebo thrust allochthon is exposed on north side of highway cut. Individual trough cross sets are up to 50 m thick. The Navajo Sandstone is conformably overlain by the Jurassic Twin Creek Limestone. The rocks are part of the platform assemblage deposited prior to Cretaceous thrusting and foredeep development.

65.0 **Stop 1.2—Red Narrows Conglomerate, Late Maastrichtian?-Paleocene, Lake Fork**

The Red Narrows conglomerates form the basal portion of a piggy-back basin fill; the basin formed and detached along the Gunnison and Wasatch thrusts during the latest Maastrichtian (Fig. 2). Conglomerates are part of the *scour-based, boulder-cobble conglomerates and gravely sandstones* facies association (see Table 1) and are sourced from the Triassic-Jurassic strata exposed in the Charlston-Nebo allochthon to the west. Conglomerates are in unconformably overlain and onlapped along unconformity U10 by the Paleocene North Horn Forma-

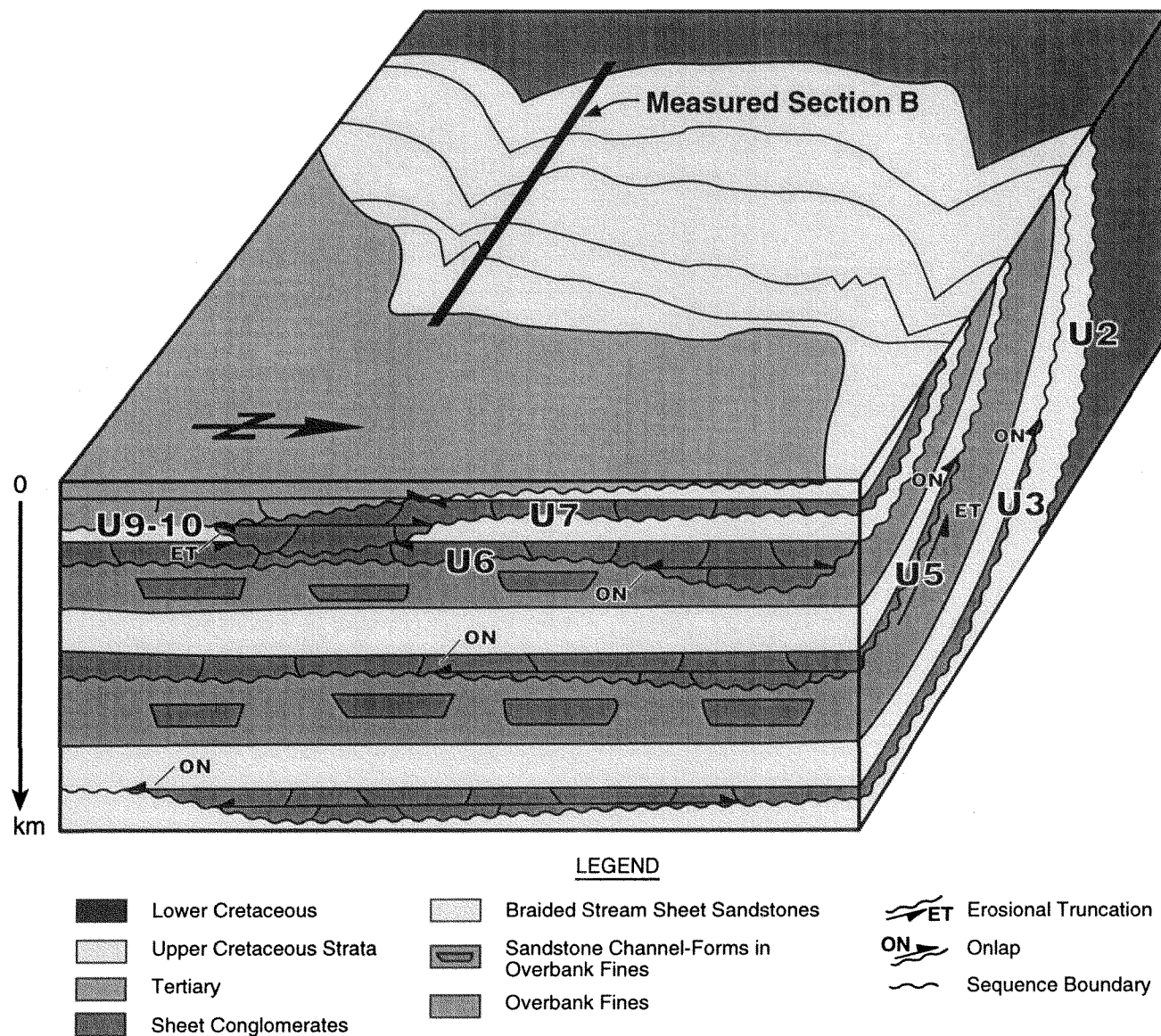


Figure 18. Block diagram and reconstruction of the three-dimensional, depositional sequence architecture in the proximal zone at measured section B (Fig. 12). The block diagram is based on combining facies association identified in the outcrop with geometries observed in aerial photographs.

tion (Fig. 1). North Horn architecture comprises laterally isolated channel forms and occasional lacustrine limestones set in thick red flood plain mudstones.

67.0 Optional Stop 1.3—Angular Unconformity between Red Narrows Conglomerate and Albion through Turonian Cretaceous Strata, Lake Fork
To get there retrace U.S. Hwy. 6 for 1.5 miles toward the west. Turn south onto State Route 89 and cross rail road tracks; take first dust road on left at end of

concrete barrier. Proceed east on dust road parallel to Hwy. 6 on south side of valley. Take first fork into small side valley to the right; follow road for about 500 yards into valley. Figure 16 shows a portion of the outcrops located on the east side of the side valley. Horizontal Red Narrows Conglomerate unconformably overlies steeply dipping Cretaceous strata. Fluvial-dominated shoreline deposits beneath U3 are unconformably overlain by quartzite conglomerates and paleovalley fill. A parasequences

Table 2: Lithofacies and depositional environments in the distal zone

Environment	Lithofacies & Bedding Type
Fluvial-dominated Shoreline Deposits	<p><i>Tabular sandstones</i></p> <ul style="list-style-type: none"> low-amplitude crossbeds and trough cross beds with reactivation surfaces, internal scours lined with ripped up shale clasts, shell debris, and log impressions <p><i>Mudstones with thin beds of siltstones and muddy sandstones</i></p> <ul style="list-style-type: none"> wave ripples, wave-form and current flaser ripples, soft-sediment deformation, lags of mollusks, burrows of <i>Planolites</i>, <i>Palaeophycus</i>, and <i>Skolithos</i> <p><i>Lenticular sandstones, shelly banks, and mudstones</i></p> <ul style="list-style-type: none"> low-angle inclined cross strata, trough cross beds, horizontal planar normal-graded beds, current ripples, wave-form flaser and lenticular ripples, shelly beds, burrows of <i>Planolites</i>, <i>Palaeophycus</i>, <i>Thalassinoides</i>, and <i>Ophiomorpha</i>
Wave-dominated Shoreline Deposits	<p><i>Rippled mudstones and siltstones</i></p> <ul style="list-style-type: none"> wave-form flaser ripples, wave ripples, small hummocky cross <p><i>Hummocky cross-stratified sandstones</i></p> <ul style="list-style-type: none"> hummocky cross strata, wave ripples, shelly lags, few burrows of <i>Ophiomorpha</i> <p><i>Trough cross-bedded sandstones</i></p> <ul style="list-style-type: none"> large-scale, low-amplitude trough cross beds, burrows of <i>Planolites</i>, <i>Palaeophycus</i>, <i>Thalassinoides</i>, <i>Ophiomorpha</i>, and <i>Skolithos</i> <p><i>Scour-based, pebbly sandstones</i></p> <ul style="list-style-type: none"> trough cross beds
Open-Marine Fine-grained Deposits	<p><i>Mudstones with thin beds of wave-rippled sandstones and flaser bedded siltstones to very fine sandstones.</i></p> <ul style="list-style-type: none"> massive, horizontal-planar bedded, carbonaceous <p><i>Micritic limestones</i></p>

- set of wave-dominated shoreline deposits sharply overlies the valley fill along a flooding surface.
- 68.0** Return to U.S. Hwy. 6 and proceed east through Red Narrows toward Price.
- 75.0** Approximate contact between the red flood plain and fluvial deposits of the North Horn Formation and the variegated lake plain mudstones of the Eocene Flagstaff Formation.
- 76.0** Approximate contact between Flagstaff Formation and the lake-margin to lacustrine limestones and gray to green mudstones of the Green River Formation. Time correlative red-colored, lake plain mudstones with well-defined fluvial channel-forms and small deltas are considered part of the Colton Formation of Early Eocene age.
- 94.0** Soldiers Summit
- 106.0** Price River Recreation Area. Paleocene North Horn unconformably overlies Price River Formation of

latest Campanian and Maastrichtian age along unconformity U8 (Fig. 1).

108.0 Stop 1.4—Contact between Price River Formation and Castlegate Sandstone

The Price River Formation outcrops north of the road and comprises *pebbly, channel-form sandstones* and *overbank mudstones and siltstones* deposited in a mixed to suspended-load dominated braided stream and flood plain. In contrast, the underlying, cliff-forming Castlegate Sandstone (*see* cliffs down road toward east) consists of *scour-based, cobble-pebble conglomerates, pebbly sandstones, and sandstones* transported and deposited in laterally coalesced barforms in a bedload-dominated braided stream systems and channel complex. This contrast in depositional architecture is interpreted to reflect a significant acceleration in sediment accommoda-



Figure 19. Photo of tabular sandstones onlapping (ON) unconformity U3. Sandstones are part of the Upper Turonian Lower Fink Valley Sandstone and strike north-south (left-right). U3 erosionally truncates (ET) underlying open-marine mudstones of the lower to mid Turonian Allen Valley Shale, which rests with sharp contact and flooding surface (FS) of wave-dominated shoreline sandstones of the Sanpete Formation (in lower right).

tion and subsidence patterns within the foreland basin, probably due to foreland basin segmentation during the Late Campanian.

111.0 Highway 6 Road Cut, just west of Power Plant, Castlegate Sandstone-Blackhawk Fm. Contact, Helper

The tall sandstone cliffs on both sides of the road are the Castlegate Sandstone. The coal-bearing strata beneath the sandstone cliffs are the shoreline and coastal plain deposits are part of the Blackhawk Formation of mid-late Campanian age. The Castlegate Sandstone unconformably overlies the Blackhawk Formation along unconformities U7-U8 (Fig. 1).

112.0 Stop 1.5—Wave-Dominated Shoreline Facies in Gentile Wash Canyon, Blackhawk Fm., Helper

Turn right into second side canyon; the turn-off is across from a large, gravel strewn pull-out area located on the east side of the road, just down from the Power Plant. The Blackhawk Formation represents a series of stacked, prograding shoreline parasequences or parasequence sets. Individual parasequence sets overlie each other along high-frequency unconformities. Pioneering studies on the regional stratigraphy and depositional settings are by Young (1952, 1955). More recent studies on the parasequence expression and high-frequency parasequence set stacking patterns include, among others, those of Kamola and Van Wagoner (1995), O'Byrne and Flint (1995), and Taylor and Lovell

(1995). Six sandstone and coal-bearing members are recognized in the Blackhawk Formation; these are in ascending stratigraphic order, from oldest to youngest, the Spring Canyon Member, Aberdeen Member, Kenilworth Member, Sunnyside Member, and Desert Member. The Spring Canyon and Aberdeen members are exposed in Gentile Wash, while overlying members are truncated by the composite U7-U8 unconformity at the base of the Castlegate Sandstone. The lower Spring Canyon Member in Gentile Wash comprises 4 or possibly 5 parasequences; these are stacked to form a progradational parasequence set. The overlying Aberdeen Member consists of 4 parasequences stacked into a progradational parasequence set. Component depositional facies include *rippled mudstones and siltstones, hummocky cross-stratified sandstones, and trough cross-bedded sandstones* deposited in the open-marine and distal lower to lower shoreface environments. Upper shoreface and foreshore sandstones overlain by coastal plain fines and coals comprise the Aberdeen Member.

113.0 Stop 1.6—Stacking Patterns Summary at the Power Plant, Blackhawk Fm., Helper

Review of parasequence concepts, summarize the day, and proceed on Route 6 to Price. The top of the Aberdeen Sandstone and progradational parasequence set is exposed in the road cut of Route 6 above the Power Plant. The outcrop is an excellent example of the rapid lateral facies changes that are predicted by the parasequence sedimentology and stacking patterns examined in Gentile Wash.

124.0 Price City Limits

Day 2

Key Topics: Fluvial-dominated shoreline facies (Ferron Sandstone.); parasequence expression, stacking patterns and unconformity types in the distal zone; Upper and Lower Ferron Sandstone; systems tract architecture and sequence expression in the Indianola Group and proximal zone (Sanpete Fm., Allen Valley Shale, Funk Valley Fm., Six Mile Canyon Fm.).

0.0 Leave hotel and proceed south on Route 6

1.0 Exit right onto Hwy. 10 South.

10.0 Emery County Line. The highway runs along the eastern edge of the Wasatch Plateau and descends down-stratigraphic section through the distal deltaic siltstones and parasequences that are equivalent to the Star Point Sandstone (Fig.1). The strata exposed in the slopes of the Wasatch Plateau to the west are, listed in from top to base, the Castlegate Sand-



Figure 20. Photo of the lowstand delta complex of the Coniacian Upper Ferron Sandstone at I-70 (Stop 2.3 in Fig. 2). Deposits of the inner and outer stream-mouth bar above U4 downlap onto pro delta and open-marine mudstones low U4. The dashed line indicates the approximate position of the correlative conformity (CC) of U3, based on correlations shown in Figure 22. View is to the north. FS—Flooding surface, here parasequence set boundary.



Figure 21. Photo of the same lowstand delta complex. View is to the east into the basin. The coastal plain fines of the lowstand systems tract are abruptly overlain by the open-marine mudstones of the Bluegate Shale.

stone, the Blackhawk Formation, the Masuk tongue of the Mancos Shale, the Emery Sandstone, and the Bluegate tongue of the Mancos Shale.

30.0 Castle Dale, Utah

41.1 Ferron, Utah

47.0 Road to Moore, Utah, on left

52.2 Another road to Moore, Utah, on left

55.4 Turn left onto paved road just after the sign for the town of Emery, Utah; bear left at fork and stay on paved road

60.0 Stop 2.1—Fluvial-Dominated Shoreline Deposits in Upper Ferron Sandstone, Jim Miller Canyon

The sandstone cliffs exposed in the canyon are part of the Coniacian-age Ferron delta complex. Mudstones with thin, ripple-laminated and horizontally laminated siltstones, sharp-based, and very fine sandstones with normal-graded, horizontal laminations and current ripples form the base of the outcrop and represent deposition in the pro delta, distal delta front, and proximal delta front. Overlying thickly bedded to massive sandstones with intercutting scours and trough cross beds were deposited in the stream mouth bar. Together these form the *lenticular sandstone*, *shelly bank*, and *mudstone* facies association and stack to form a progradational parasequence set or lowstand systems tract.

61.0 Stop 2.2—Transgressive Systems Tract of the Upper Ferron Sandstone and Bluegate Shale, Jim Miller Canyon

Turn around and proceed west out of the canyon. As the road leaves the canyon, strata exposed on either side include a range of coastal plain sub environments and lithologies, such as flood plain mudstones, coals, crevasse-splay sandstones and siltstones, and channel-form sandstones. These are in turn abruptly overlain by *open-marine mudstones* of the Bluegate Shale; a few thin tidal parasequences and sandstones are exposed on the north side of the road. As the road traverses the crest and descends the west-dipping backslope of the Ferron hogback, two or possibly three shoreline parasequences are visible in the distance to the west where they form shallow north-south oriented ridges. Together with the tidal parasequences above the Ferron coastal plain, these form the transgressive systems tract to the Ferron lowstand delta complex.

64.6 Return to the main road at the town of Emery, Utah. Turn left onto Hwy. 10 and proceed south.

74.0 Fremont Junction and intersection of Hwy. 10 with I-70. Turn left and get onto I-70 east.

76.5 Stop 2.3—Lowstand Delta and Incised Valley Fill, Upper Ferron Sandstone, I-70 Road Cut

Exposures of the Ferron delta complex and coastal plain are found north and south of the Interstate 70 road cut (Figs. 20, 21). *Wave-rippled mudstones, siltstones, and sandstones* at the base are part of the Turonian Tinunk Shale. These are abruptly overlain *hummocky cross-stratified* and bioturbated sandstones, which in turn are overlain by delta-front clinoforms. Figure 22 shows U4 at the base of

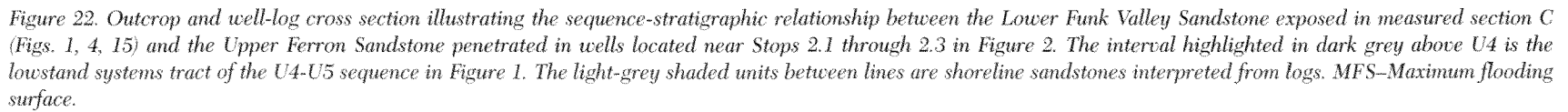


Figure 22. Outcrop and well-log cross section illustrating the sequence-stratigraphic relationship between the Lower Funk Valley Sandstone exposed in measured section C (Figs. 1, 4, 15) and the Upper Ferron Sandstone penetrated in wells located near Stops 2.1 through 2.3 in Figure 2. The interval highlighted in dark grey above U4 is the lowstand systems tract of the U4-U5 sequence in Figure 1. The light-grey shaded units between lines are shoreline sandstones interpreted from logs. MFS—Maximum flooding surface.

the Ferron Sandstone in well #3. The delta-front clinoforms are truncated along their tops by channels of the inner stream-mouth bar, suggesting a high-frequency unconformity; the latter surface is marked also in the well-log cross section. The surface U4 is also exposed in outcrops located on the west side of the plateau.

- 76.5** Turn around and return to Fremont Junction; proceed west on I-7 toward Salina, Utah.
- 81.0** Entering the Wasatch Plateau and Fishlake National Forest. Exposures on either side of the interstate are, in order of older to younger, the deltaic and wave-dominated shoreline sandstones of the Emery Sandstone (Late Coniacian through Santonian), the coal-bearing Blackhawk Formation (Campanian), and the Castlegate Sandstone forming the cliffs within the plateau.
- 91.0** Joe's Graben. Varied-colored mudstones and channel sandstones of the Colton Formation have been faulted down along a series of normal faults. Castlegate Sandstone forms the cliff on along the western edge of the graben.
- 108.0** Approximate contact between the horizontal red mudstones and siltstones of the Eocene Flagstaff and east-dipping Cretaceous strata. The contact is a composite and angular unconformity consisting of surfaces U5 through U11. The east-dipping Cretaceous strata beneath the angular unconformity are Turonian in age and part to the Lower Ferron Sandstone in Figure 1.
- 110.0** Exit I-70 and proceed north on Route 28 to the town of Gunnison. Overturned to steeply east-dipping sections of the Jurassic Arapien Shale are exposed to the right (east) of the road in the foothills of the Wasatch Plateau. The valley and the Jurassic strata along the edges form the core to the completely eroded, Tertiary-age Sevier Valley anticline. Cretaceous strata are exposed in respective limbs of the anticline along the edges of the valley and dip to the east and west. They are in turn overlapped by Maastrichtian to Paleocene units similar in facies to the Red Narrows Conglomerate examined in Stops 1.2 and 1.3.
- 127.0** Gunnison, Utah. Turn right onto U.S. 89 at the north end of town toward Manti, Utah.
- 133.0** Road cuts through two small hogbacks or blocks of Green River strata, turns northward, and crosses the San Pitch River. The blocks are autochthonous and detached from the underlying Jurassic Arapien Shale via reverse thrusts; movement was down to the west, due to gravity sliding down the west-dipping limb of the Wasatch Monocline. The varied-



Figure 23. Photo of open-marine mudstones of the transgressive and highstand systems tracts of the U4-U5 sequence in measured section C (Fig. 15) at Palisade Lake. The shales are the Lower Funk Valley Shale and form the highstand systems tract (Stop 2.6 in Fig. 2), which overlies the transgressive systems tract (Stop 2.5 in Fig. 2) or top of the Lower Funk Valley Sandstone along the flooding surface FS on the right. Wave-dominated shoreline strata on the left are the base of the Upper Funk Valley Sandstone. View is to the south; strata are vertical and strike north-south. Up-section is to the left (east).

colored mudstones in the valley and along the base of the Wasatch Plateau on the right are Jurassic Arapien Shale.

- 136.0** Gunnison Reservoir on right
- 137.0** Sterling, Utah. Turn right at northern end of town and proceed on Six Mile Canyon Road toward the plateau and Palisade Lake State Park.
- 137.5** **Stop 2.4—Systems Tracts, Sequences, and Facies in the Proximal Zone, Indianola Group at Palisade Lake Reservoir**
Pull-over on left side of road at second dust road. Two ridges separated by a valley are visible 500 yards north of the paved road. The lower ridge on the left is the Sanpete Formation and the basal unit of the Indianola Group of Spieker (1946, 1949); strata are vertical and strike north-south in the ridge. The braided stream and wave-dominated shoreline sandstones of the Sanpete Formation are sharply overlain along a flooding surface by open-marine mudstones of the Allen Valley Shale. The Sanpete Formation and the Allen Valley Shale form the U2-U3 sequence (Figs. 1, 15). The ridge to the right is the Lower Ferron Sandstone of Schwans (1988b), which unconformably overlies the shale along U3 (Fig. 19). The associated hiatus spans the Late Turonian (Fig. 1). The section in Figure 15 was measured across the ridges and valley toward



Figure 24. Photo of braided-stream conglomerates of the Six Mile Canyon Formation (Fig. 1) and the U6-U7 lowstand systems tract unconformably overlying the open-marine mudstones of the Upper Funk Valley Shale and U5-U6 highstand systems tract along U6. The outcrop is part of measured section C (Fig. 15); Tertiary strata above U8-11 (upper left) are flat lying and drape over the east-dipping Cretaceous strata. View is to the east. FS—Flooding surface; ON—Onlap.

the plateau. Proceed on road and enter Palisade Lake State Park.

138.5 Stop 2.5—Lowstand-Transgressive Systems Tract of the U4-U5 Sequence, Lower Funk Valley Sandstone and Shale, Palisade Lake Reservoir, Sterling

The strata exposed at the west side of Palisade Lake and the golf course are part of the Upper Funk Valley Sandstone of Schwans (1988b) (Fig. 1) and correlative to the Ferron outcrops seen in previous Stops 2.1, 2.2, and 2.3. Lithofacies include *mudstones with thin beds of wave- and flaser-rippled siltstones and muddy sandstones* overlain by pebbly to coarse grained, *tabular sandstones* with trough cross bedding and low-angle cross bedding; scours overlain by pebble stringers can be found. The sandstones and mudstones are interpreted as braid-delta deposits, possibly deposited within an estuary, and form a progradational parasequence set or lowstand systems tract of the U4-U5 sequence (Figs. 15, 23). They are overlain by a retrogradational stack of wave-dominated parasequences. The valley and golf course at Palisade Lake lie within the open-marine shales of the Lower Funk Valley Shale of Coniacian age (Fig. 1) and are abruptly overlain along unconformity U5 by sandstones of the Upper Funk Valley Sandstone exposed east of the golf course (Fig. 23). The basinward shift in facies across U5 is minor.

139.0 Stop 2.6—Highstand Systems Tracts of the U4-U5 Sequence and the U6 Unconformity, Upper Funk Valley Sandstone and Shale and Six Mile Canyon Fm., Six Mile Canyon, Sterling

Leave palisade Lake Park, turn left golf course and park. The Upper Funk Valley Sandstone exposed along the east side of the golf course were deposited along a wave-dominated shoreline. Lithofacies *wave-rippled mudstones, siltstones, and sandstones, hummocky cross-stratified, bioturbated, trough crossbedded sandstones, and few scour-based, pebbly sandstones*. The sandstones and mudstones are laterally continuous and form parasequences stacked in an aggradational to minor progradational pattern. The strata are late Coniacian through Santonian in age, based on ammonites and pelecypods (Fig. 1).

Leave parking lot and turn left onto first dust road on the left past entrance to state park; proceed up the dust road into grassy valley below rim of Flagstaff Limestone. Figure 15 shows that in the valley the wave-dominated shoreline sandstones of the Upper Funk Valley Formation are sharply overlain by open-marine mudstones of the Upper Funk Valley Shale of Schwans (1988b). Palynomorphs recovered from the same unit in a nearby well indicate a Santonian age (Villien and Kligfield, 1986). The marine mudstones are sharply overlain along unconformity U6 (see east side of valley) by the coarse-grained sandstones of the Lower Six Mile Canyon Formation of the Indianola Group. Basal sandstones are of the *tabular sandstone* lithofacies and exhibit large-scale, trough cross bedding, numerous scours, and impressions and casts of rafted logs. The sedimentary structures and the presence of abundant *Inoceramus* debris in the sandstones are interpreted to reflect deposition in a braid delta. The hiatus associated with U6 incorporates the latest Santonian through possibly Early Campanian (Schwans, 1988b).

140.0 Return to U.S. 89 and the town of Sterling.

Day 3

Key Topics: Piggy-back basin fill and composite unconformities (North Horn Fm., Flagstaff Limestone); Lower Cretaceous basin fill (Pigeon Creek Fm.); Upper Cretaceous basin fill in the proximal zone (Indianola Group Undifferentiated); non-marine systems tract architecture and sequence expression.

0.0 Leave Sterling on U.S. 89 south.

10.0 Gunnison, Utah. Turn right onto Route 28 north. Road cuts across the southern end of the Gunnison

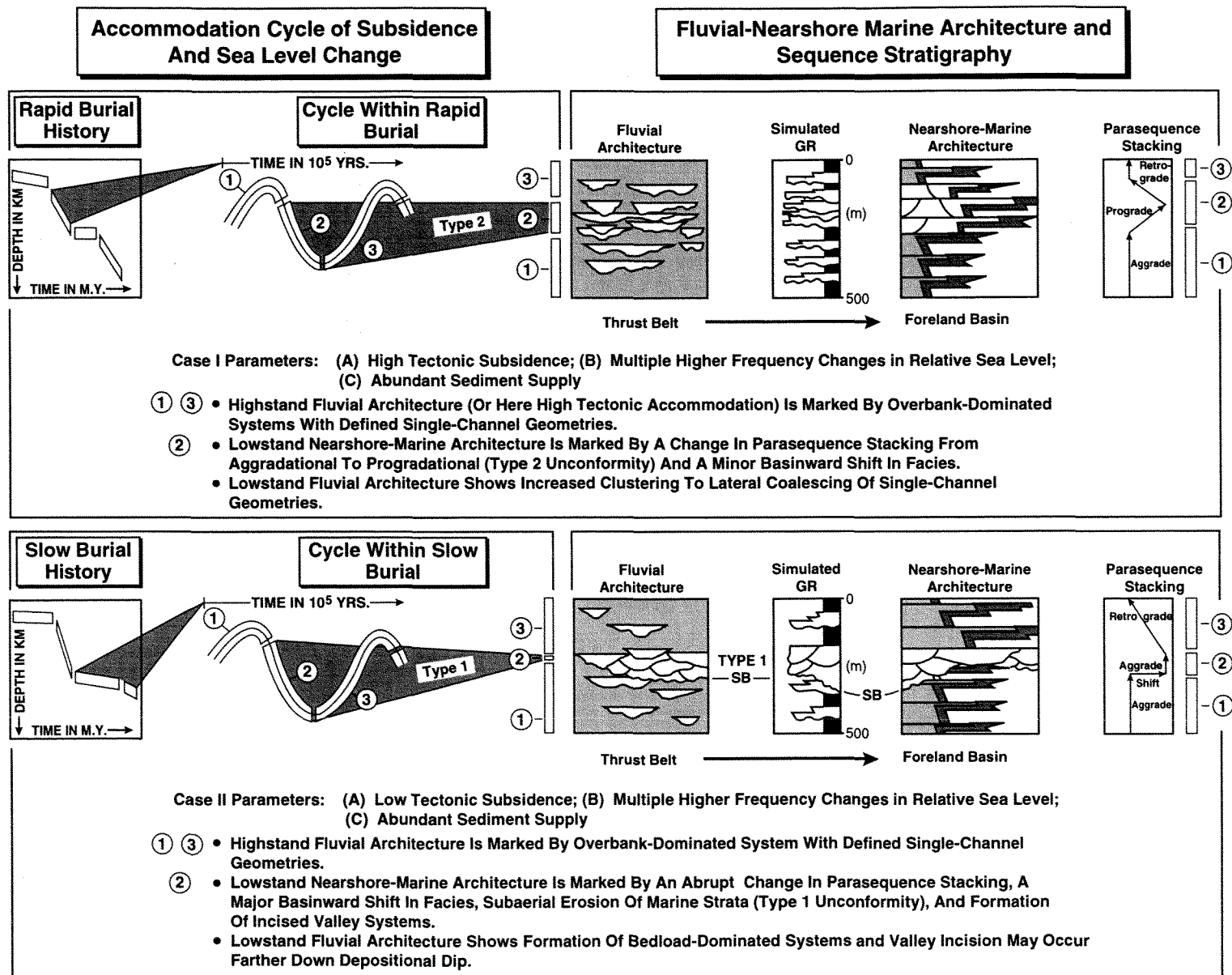


Figure 25. Fluvial and nearshore-marine architecture and parasequence stacking patterns in the accommodation cycle of subsidence and sea level change. The sea level cycle of approximately 10^5 Yr. duration resides on the longer term signal of basin subsidence. Two cases are illustrated.

- Plateau; outcrops on the right are lacustrine limestones of the Green River Formation.
- 17.0** Sevier Bridge Reservoir on left in valley; sign for town of Fayette, Utah. The floor of the valley consists of Jurassic Arapien Shale, which constitute the core of the collapsed Sevier Valley Anticline.
- 18.0** Turn right behind the town of Fayette onto dust road that leads into Mellor Canyon. The road is marked by a cattle guard and runs straight toward the cliffs.
- 19.0** **Stop 3.1—Piggy-back Basin Fill and Composite Unconformities, North Horn Fm., Mellor Canyon, Fayette**
The east—dipping conglomerates and sandstones in Mellor Canyon are equivalent to the Campanian Six Mile Canyon Formation examined in Stop 2.6 (Fig. 17). Lithofacies include trough cross-bedded, *scour-based*, *cobble-pebble conglomerates* grading upward into cross bedded, *pebbly sandstones* and *sandstones*; both represent deposition in gravely and sandy bars on a low-relief alluvial fan. The clastics form the eastern flank of the Sevier Anticline, a thrust-cored uplift of Maastrichtian through Eocene age, and are onlapped along composite surface U8-U9 by folded, *scour-based boulder-cobble-conglomerates*. The latter constitute a paleo-valley fill probably age-equivalent to the Red Narrows Conglomerate and record the onset of Sevier Anticline uplift. They are in turn onlapped along U10 by the red *overbank siltstones* and *mudstones* of the North Horn Formation. Conglomerate-filled channels at the base of the North Horn have scoured into the underlying deformed conglomerate unit along U10. The North Horn is onlapped along U11 by the lacustrine mudstones and limestones of the Flagstaff, which eventually overlap the flank of the anticline. For a detailed discussion of piggy back basin formation and the fill see Lawton and Trexler (1991) and Talling et al., (1995).
- 20.0** Leave Mellor Canyon and return to Route 28; turn right and proceed north.
As the road drops out of the foothills of the Gunnison Plateau a few miles north of Juba Lake, the mountain range visible in the distance to the west (left) is the Canyon Range. The jagged peaks of the range comprise the Precambrian to Cambrian quartzites of the Canyon Range allochthon.
- 44.0** Levan, Utah. Turn right onto paved road toward Wales and Chester and the Gunnison Plateau.
- 45.0** Bear right at fork and enter Chicken Creek Canyon. The strata exposed on either side of the canyon are part of the Arapien Shale and include open-marine shales, evaporites, such as gypsum, and thin bedded limestones.
- 48.0** Uinta National Forest sign
- 48.5** **Stop 3.2—Facies and Depositional Architecture in the Lower Cretaceous Pigeon Creek Fm. and U1-U2 Sequence, Chicken Creek Campground, Levan**
Turn right into campground located at foot of cliff and park; walk up-canyon on road to where pavement ends. Exposed is the Albian-age upper member of the Pigeon Formation. It forms the cliff and western flank of the Gunnison Plateau (Figs. 6, 7) and consists of stacked and laterally overlapping sheets of horizontally bedded, minor trough cross bedded, pebble-cobble conglomerates with thin, intercalated mudstones. Schwans (1988a) interpreted these as sheetflood fan deposits. Strata of the Barremian to Aptian-age lower member are exposed in the foothills beneath the cliff and consist of stacks of thickbedded, variegated mudstones with intercalated silty-sandy zones, sheets of horizontally-bedded, pebble-sandstones, and sheets of horizontally bedded, chert-pebble and mixed quartzite-carbonate cobble conglomerates. Deposition occurred under a wet-dry, ephemeral climate on gravely sheet-flood fans terminating in a ponded flood plain. The lower member unconformably overlies marginal-marine tidal-flat deposits of the Twist Gulch Formation of Late Jurassic age along unconformity U1.
- 50.0** **Stop 3.3—Expression of Unconformity U2, Chicken Creek Canyon, Levan**
Return to campground and drive up-canyon past previously visited outcrops. The unconformity U2 separates Lower and Upper Cretaceous strata and is located in the outcrop next to the dust road where reddish colored mudstones and quartzite-carbonate pebble sandstones are overlain by brown to tan-colored, quartzite-pebble to cobble conglomerates. Conglomerates exposed below the surface are of sheet geometry and exhibit mostly horizontal stratification, a red sandstone matrix, few intercalated red mudstones and crossbedded sandstones, and an average maximum clast size of 10 cm. In contrast, conglomerates above U2 overlie well-defined scours, are large-scale lenticular in cross section, and exhibit trough cross bedding, a tan-colored sandstone matrix, and an average maximum clast size of 6 cm. The conglomerate clast composition changes significantly across the surface, indicating a vastly different provenance.

The U2 surface is thus expressed in the measured section (Fig. 12) by (1) a loss in labile clast components, (2) an increase in stable clast types, (3) a significant reduction in maximum clast size, and (4) a change in depositional architecture. Regional correlations show that U2 is onlapped from east to west; the associated hiatus in Chicken Creek Canyon probably spans the latest Albian through Early-Mid? Turonian.

51.5 Stop 3.4—Facies, Systems Tracts, and Sequence Architecture in the Upper Cretaceous Indianola Group, Upper Chicken Creek Canyon, Levan

Continue up-canyon and stop at ponds; walk back 100 yards and view outcrops above U6. The measured section in Figure 12 shows five unconformity-bounded and upward fining packages. Lithofacies in the outcrop include *scour-based, cobble-pebble conglomerates* grading upward into cross bedded, *pebbly sandstones* and *sandstones* and reflect traction transport and deposition in gravely and sandy bars in a mixed-load dominated braided stream. The scour-based coarse-clastics are overlain along a sharp surface by *overbank siltstones* and *detrital carbonates* with intercalated trough cross bedded, *pebbly channel-form sandstones*; climbing ripple lamina sets, wedge-planar cross-stratification, trough cross-stratification, contorted bedding, and micro cross-stratified sets, together with an abundance of preserved secondary structures, such as contorted bedding, load and flute casts, rhizoliths, plant impressions, and biogenic traces are ubiquitous. Feeding and foraging traces belong to the *Scoyenia* ichnofacies. Deposition occurred via low-sinuosity, mixed-to suspended-load dominated channels set in a ponded flood plain.

In terms of the foreland accommodation model of Schwans (1995), this change in depositional architecture per sequences reflects the up-dip response of fluvial systems located in the proximal zone to base level changes occurring at the shoreline in the distal zone. In this example, the unconformity U6 is expressed by erosion of underlying strata, a basinward shift in facies across the surface, and onlap against the surface.

53.0 Stop 3.5—Cretaceous-Tertiary Transition and U8 to U9 Sequence Boundaries in Chris Canyon, uppermost Chicken Creek Canyon, Levan

Continue on dust road past cliffs with quartzite-boulder conglomerates; these are the paleo-valley fill facies shown in Figure 16. Stop at mouth of Chris Canyon or second dust road branching off to

the right. Quartzite-boulder conglomerates identical to those previously encountered in Mellor Canyon (Stop 3.1) and in the Red Narrows (Stop 1.2) occur beneath and above the angular unconformity U9 at the mouth of the canyon. The transition from the Cretaceous to the Tertiary is expressed as a series of angular unconformity, including U8 through U11, that merge on structure toward the emergent anticlines in the Sanpete Valley to the east and the Sevier Valley in the west. In all localities, the conglomerates above U9 show a pronounced angular relationship to those beneath the surface, indicating that erosion and redeposition occurred during uplift and basin subsidence. Pollen recovered from channel coals in Six Mile Canyon (strata above U6 or Stop 2.6) indicate a Late Maastrichtian age for these. The quartzite-boulder conglomerates are onlapped along surface U10 by the red mudstones of the Paleocene North Horn Formation.

59.0 Return to Levan and turn right onto State Route 28 toward Nephi. Turn right onto I-15 North toward Salt Lake City.

ACKNOWLEDGMENTS

We are grateful to M.H. Feeley, Exxon Exploration Company, and A.S. Reeckmann, Exxon Production Research Company, for sponsoring and supporting this field trip. Over the past decades numerous Exxon, Ohio State, and USGS geologists have worked this area. E.M. Spieker and his student from The Ohio State University were true pioneers and visionaries of their time and defined much of the stratigraphy. Their work serves as an inspiration and is the foundation for the sequence stratigraphy presented herein. A.R. Sprague, C. Rossen, and M. Jervey are among many that have worked on the Ferron; their work contributed much to our present understanding of the Ferron. J.C. Van Wagoner defined the sequence stratigraphy of the Blackhawk and the Castlegate. Tom. H. Mooney and Barbara L. Faulkner provided portions of the road log. Last but not least, many thanks to Caroline Peacock for her tireless pursuit of seemingly never-ending logistical problems.

REFERENCES CITED

- Allmendinger, R.W., et al., 1986, Phanerozoic tectonics of the Basin and range-Colorado Plateau transition from COCORP data and geologic data. A review, in Barazangi, M., and Brown, L., eds., *Reflection seismology. The continental crust: Am. Geophys. Union Geodyn. Ser. 14*, p. 257-267.
- Allmendinger, R.W., et al., 1987, Overview of the COCORP 40 degree N transect, western United States: The fabric of an orogenic belt. *Geological Society of America Bulletin*, v. 98, p. 308-319.

- Aubrey, W.M., 1989, Mid-Cretaceous alluvial-plain incision related to eustasy, southeastern Colorado Plateau. *Geological Society of America Bulletin*, v. 101, p. 443-449.
- Cobban, W.A., 1976, Ammonite record from Mancos Shale of the Castle Valley-Price-Woodside area, east-central Utah. *Brigham Young University Geology Studies*, v. 22, p. 117-126.
- Cotter, E., 1971, Paleoflow characteristics of a Late Cretaceous river in Utah from analysis of sedimentary structures in the Ferron Sandstone. *Journal Sedimentary Petrology*, v. 41, p. 129-138.
- Cotter, E., 1975, Late Cretaceous sedimentation in a low-energy coastal zone. The Ferron Sandstone of Utah, in *Deltas, Models for Exploration*, Broussard, M.L.S., ed., Houston Geological Society Publication, p. 471-484.
- DeCelles, P.G., Lawton, T.F., and Mitra, G., 1995, Thrust timing, growth of structural culminations, and synorogenic sedimentation in the type Sevier orogenic belt, western United States. *geology*, v. 23, p. 699-702.
- Devlin, W.J., Rudolph, K.W., Ehmann, K.H., and Shaw, C.A., 1993, The effect of tectonic and eustatic cycles on accommodation and sequence-stratigraphic framework in the Upper Cretaceous foreland basin of southeastern Wyoming, in *Summerhayes, C.P., Haq, B.U., and Allen, G.P., eds., Stratigraphy and facies associations in a sequence stratigraphic framework*. International Association of Sedimentologists Special Publication 18, p. 501-520.
- Fouch, T.D., et al., 1983, Patterns and timing of synorogenic sedimentation in Upper Cretaceous rocks of central and northeast Utah, in *Reynolds, M.W., and Dolly, E.D., eds., Mesozoic paleogeography of the west-central United States*, Rocky Mountain Paleogeography Symposium 2 Rocky Mountain Sect. of S.E.P.M., Denver, CO, p. 305-336.
- Franczyk, K.J., Fouch, T.D., Jonson, R.C., Molenaar, C.M., and Cobban, W.A., 1992, Cretaceous and Tertiary paleogeographic reconstructions for the Uinta-Piceance Basin study area, Colorado and Utah, *US Geological Survey Bulletin* 1787, 37 p.
- Gardner, M.H., 1993, Sequence stratigraphy of the Ferron sandstone (upper Turonian) of east-central Utah: Ph.D. Dissertation, Department of Geology and Geological Engineering, Colorado School of Mines, Golden Colorado, 405 p.
- Gill, J.R., and Hail, W.J., Jr., 1975, Stratigraphic sections across Upper Cretaceous Mancos Shale-Mesa Verde Group boundary, eastern Utah and western Colorado. *USGS Oil and Gas Investigations Chart* OC-68.
- Hale, L.A., and Van De Graaf, F.R., 1964, Cretaceous stratigraphy and facies patterns-northeastern Utah and adjacent areas. *Intermountain Association of Petroleum Geologists 13th Annual Field Conference, Guidebook to the geology and mineral resources of the Uinta Basin-Utah's hydrocarbon storehouse*, p. 115-138.
- Haq, B.U., Hardenbol, J., and Vail, P.R., 1987, Chronology of fluctuating sea levels since the Triassic: *Science*, v. 235, p. 1156-1167.
- Haq, B.U., Hardenbol, J., and Vail, P.R., 1988, Mesozoic and Cenozoic chronostratigraphy and cycles of sea-level change, in *Wilgus, C.K., Hastings, B.J., Posamentier, H.W., Van Wagoner, J.C., and Ross, C.A., and Kendall, C.G. St. C., eds., Sea level change. An integrated approach: Society of Economic Paleontologists and Mineralogists Special Publication 42*, p. 71-108.
- Heller, P.L., and Paola, C., 1989, The paradox of Lower Cretaceous gravels and the initiation of thrusting in the Sevier orogenic belt, United States Western Interior: *GSA Bulletin*, v. 101, p. 864-875.
- Jervy, M.T., 1988, Quantitative geological modeling of siliciclastic rock sequences and their seismic expression, in *Wilgus, C.K., et al., eds., Sea-level changes: An integrated approach*. Society of Economic Paleontologists and Mineralogists Special Publication 42, p. 47-69.
- Jordan, T.E., and Flemings, P.B., Large-scale stratigraphic architecture, eustatic variation, and unsteady tectonism. A theoretical evaluation: *Journal of Geophysical Research*, v.96, p. 6681-6699.
- Kauffman, E.G., 1977a, Geological and biological overview Western Interior Cretaceous basin. *The Mountain Geologist*, v. 14, p. 75-99.
- Kauffman, E.G., 1977b, Illustrated guide to the biostratigraphically important Cretaceous macro fossils, Western Interior Basin, U.S.A. *The Mountain Geologist*, v. 14, p. 225-274.
- Komola, D.L., and Van Wagoner, J.C., 1995, Stratigraphy and facies architecture of with examples from the Spring Canyon Member, Blackhawk Formation, Utah, in *Van Wagoner, J.C., and Bertram, G.T., eds., Sequence stratigraphy of foreland basin deposits*. AAPG Memoir 64, p. 11-26.
- Lawton, T.F., 1982, Lithofacies correlations within the Upper Cretaceous Indianola Group, central Utah, in *Nielson, D.L., ed., Overthrust Belt of Utah*. Utah Geological Association Publication 10, p. 199-214.
- Lawton, T.F., 1983, Late Cretaceous fluvial systems and the age of foreland uplifts in central Utah, in *Lowell, J.D., ed., Rocky Mountain Foreland Basins and Uplifts, Guidebook to Field Conference*, Steamboat Springs, Colorado. Rocky Mountain Association of Geologists, Denver, Colorado, p. 181-199.
- Lawton, T.F., 1985, Style and timing of frontal structures, thrust belt, central Utah. *American Association of Petroleum Geologists*, v. 69, p. 1145-1159.
- Lawton, T.F., and Trexler, J.H., Jr., 1991, Piggy-back basin in the Sevier orogenic belt, Utah: Implications for the development of the thrust wedge: *Geology*, v. 19, p. 827-830.
- Lawton, T.F., Boyer, S.E., and Schmitt, J.G., 1994, Influence of inherited taper on structural variability and conglomerate distribution, Cordilleran fold and thrust belt, western United States. *Geology*, v. 22, p. 339-342.
- Leithold, E.L., 1994, Stratigraphic architecture at the muddy margin of the Cretaceous Western Interior Seaway, southern Utah, *Sedimentology*, v. 41, p. 521-542.
- Martinsen, O.J., Martinsen, R.S., and Steidtmann, J.R., 1993, Mesaverde Group (Upper Cretaceous), Southeastern Wyoming. Allostratigraphy versus sequence stratigraphy in a tectonically active area. *American Association of Petroleum Geologists*, v. 77, p. 1351-1373.
- O'Byrne, C.J., and Flint, S., 1995, Sequence, parasequence, and intrasequence architecture of the Grassy Member, Blackhawk Formation, Book Cliffs, Utah, U.S.A., in *Van Wagoner, J.C., and Bertram, G.T., eds., Sequence stratigraphy of foreland basin deposits*. AAPG Memoir 64, p. 225-256.
- Picha, F., 1986, The influence of pre-existing tectonic trends on geometries of the Sevier orogenic belt and its foreland in Utah, in *Peterson, J.A., ed., Paleotectonics and sedimentation*. A.A.P.G. Memoir 41, p. 309-320.
- Posamentier, H.W., and Vail, P.R., 1988, Eustatic controls on clastic deposition II—Sequence and systems tract models, in *Wilgus, C.K., et al., eds., Sea-level changes. An integrated approach*. Society of Economic Paleontologists and Mineralogists Special Publication 42, p. 125-154.
- Posamentier, H.W., Jervy, M.T., and Vail, P.R., 1988, Eustatic controls on clastic deposition I—Conceptual framework, in *Wilgus, C.K., et al., eds., Sea-level changes: An integrated approach*. Society of Economic Paleontologists and Mineralogists Special Publication 42, p. 110-124.
- Posamentier, H.W., Allen, G.P., James, D.P., and Tesson, M., 1992, Forced regression in a sequence-stratigraphic framework: concepts, examples, and exploration significance. *American Association of Petroleum Geologists*, v. 76, p. 1687-1709.
- Royce, F., Jr., (1993), Case of the phantom foredeep. Early Cretaceous in west-central Utah. *Geology*, v. 21, p. 133-136.
- Ryer, T.A., 1981, Deltaic coals of Ferron Sandstone Member of Mancos Shale. Predictive model for Cretaceous coal-bearing strata of Western Interior. *American Association of Petroleum Geologists*, v. 65, p. 2323-23240.
- Ryer, T.A., and McPhillips, M., 1983, Early late Cretaceous paleogeography of east-central Utah, in *M.W., and Dolly, E.D., eds., Mesozoic*

- paleogeography of the west-central United States, Rocky Mountain Paleogeography Symp. 2: Rocky Mountain Sect. of S.E.P.M., Denver, CO, p. 253–272.
- Schwans, P., 1985a, Fonglomerate deposition in the foreland of the Sevier overthrust belt, control, facies, and timing of earliest syntectonic deposition in Utah, western U.S. [abs.] in *Proceedings of the 3rd International Fluvial Sedimentology Conference (IFSC)*, Ft. Collins, Colorado, p. 34.
- Schwans, P., 1985b, Depositional controls in the alluvial hinterland of the Cretaceous Interior Seaway: Tectonics, eustasy, and syntectonic sedimentation in central Utah, western U.S.A. [abs.] in *Programme and Abstracts of Proceedings of International Symposium on Foreland Basins*, Fribourg, Switzerland, p. 116.
- Schwans, P., 1986a, Late Cretaceous depositional sequence evolution as a result of tectonism, basin subsidence, and sea level change, Turonian to Santonian, west-central Utah [abs.]: *American Association of Petroleum Geologists Bulletin*, v. 70, p. 1055.
- Schwans, P., 1986b, Early Cretaceous depositional sequence evolution in the foreland of the Sevier overthrust belt in west-central Utah [abs.]: *Geological Society of America Abstracts with Programs*, v. 18, p. 411.
- Schwans, P., 1987a, Initial foreland flexure and sedimentation, Early Cretaceous, central Utah [abs.]: *Geological Society Abstracts with Programs*, v. 19, p. 835.
- Schwans, P., 1987b, Sedimentological effects of the tectonic transition from fold-thrust deformation to thrust-cored uplift, proximal Sevier foreland (Six Mile Canyon-Price River-North Horn interval), Campanian-Paleogene of Utah [abs.]: *Geological Society of America Abstracts with Programs*, v. 19, p. 332.
- Schwans, P., 1988a, Depositional response of Pigeon Creek Formation, Utah, to initial fold-thrust deformation in a differentially subsiding foreland basin, in Schmidt, C.J., and Perry, W.J., eds., *Interaction of the Rocky Mountain Foreland and the Cordilleran Thrust Belt*: Geological Society of America Memoir 171, p. 531–556.
- Schwans, P., 1988b, Stratal packages at the subsiding foreland basin margin of the Cretaceous foreland basin, Utah, Ph.D. Dissertation, Department of Geology and Mineralogy, The Ohio State University, Columbus, Ohio (Vol. I and II): University Microfilms International, 447 p.
- Schwans, P., 1989, Alluvial-marine sequence architecture at a foreland basin margin, Turonian-Santonian, central Utah [abs.], in *Proceedings to International Conference of Fluvial Sedimentology*, Barcelona, Sitges, Spain, p. 215.
- Schwans, P., 1990, Sequence stacking and architecture, Cretaceous foreland basin, Utah [abs.]: *American Association of Petroleum Geologists Bulletin*, v. 74, p. 759.
- Schwans, P., 1991, Forcing factors and stratal stacking in the thrust-belt to foreland basin accommodation profile: Late Cretaceous Indianola Group, west-central Utah [abs.]: *Geological Society of America Abstracts with Programs*, v. 23, p. 95.
- Schwans, P., 1995, Controls on sequence stacking and fluvial to shallow-marine architecture in a foreland basin, in Van Wagoner, J.C., and Bertram, G.T., eds., *Sequence stratigraphy of foreland basin deposits*: AAPG Memoir 64, p. 55–102.
- Shanley, K.W., and McCabe, P.J., 1991, Predicting facies architecture through sequence stratigraphy—An example from the Kaiparowits Plateau, Utah: *Geology*, v. 19, p. 742–745.
- Spieker, E.M., 1946, Late Mesozoic and Early Cenozoic history of central Utah: U.S. Geological Society Professional Paper 205-D, p. 117–161.
- Spieker, E.M., 1949, Sedimentary facies and associated diastrophism in the Upper Cretaceous of central and eastern Utah, in Longwell, C.R., ed., *Sedimentary facies in geologic history*: Geological Society of America Memoir, v. 39, p. 55–81.
- Spieker, E.M., and Reeside, J.B., 192, Cretaceous and Tertiary formations of the Wasatch Plateau, Utah: *GSA Bulletin*, v. 36, p. 435–454.
- Standlee, L.A., 1982, Structure and stratigraphy of Jurassic rocks in central Utah: their influence on tectonic development of the Cordilleran foreland thrust belt, in Powers, B., ed., *Geologic studies of the Cordilleran thrust belt*, volume 1: R.M.A.G., Denver, Colorado, p. 357–382.
- Talling, P.J., Lawton, T.F., Burbank, D.W., and Hobbs, R.S., 1995, Evolution of latest Cretaceous-Eocene nonmarine deposystems in the Axhandle piggyback basin of central Utah: *Geological Society of America Bulletin*, v. 107, p. 297–315.
- Taylor, D.R., and Lovell, R.W.W., 1995, High-frequency sequence stratigraphy and paleogeography of the Kenilworth Member, Blackhawk Formation, Book Cliffs, Utah, U.S.A., in Van Wagoner, J.C., and Bertram, G.T., eds., *Sequence stratigraphy of foreland basin deposits*: AAPG Memoir 64, p. 257–276.
- Vail, P., Mitchum, R.M., Thompson, S., III, 1977, Global cycles of relative changes of sea level, in Payton, C.E., ed., *Seismic stratigraphy—Applications to Hydrocarbon Exploration*: A.A.P.G. Memoir 26, p. 83–98.
- Vail, P.R., Hardenbol, J., and Todd, R.G., 1984, Jurassic unconformities, chronostratigraphy, and sea-level changes from seismic stratigraphy and biostratigraphy, in Schlee, J.S., ed., *Interregional unconformities and hydrocarbon accumulations*: A.A.P.G. Memoir 36, p. 129–144.
- Vail, P.R., and Bowman, S.A., 1987, Sequence stratigraphic concepts applied to stratal patterns in the Cretaceous seaway, western interior of North America [abs.]: *Geological Society of America Abstracts with Program*, v. 19, p. 875.
- Van Wagoner, J.C., 1991a, High-frequency sequence-stratigraphy and facies architecture of the Sego sandstone in the Book Cliffs of western Colorado and eastern Utah, in Van Wagoner, Nummedal, D., Jones, C.R., Taylor, D.R., Jennette, D.C., and Riley, G.W., 1991, *Sequence stratigraphy applications to shelf sandstone reservoirs: Outcrop to subsurface examples*: Field Guide to American Association of Petroleum Geologists Field Conference, September 21–28, 1991.
- Van Wagoner, J.C., 1991b, Sequence stratigraphy and facies architecture of the Desert Member of the Blackhawk Formation and the Castlegate Formation in the Book Cliffs of eastern Colorado and western Utah, in Van Wagoner, Nummedal, D., Jones, C.R., Taylor, D.R., Jennette, D.C., and Riley, G.W., 1991, *Sequence stratigraphy applications to shelf sandstone reservoirs: Outcrop to subsurface examples*: Field Guide to American Association of Petroleum Geologists Field Conference, September 21–28, 1991.
- Van Wagoner, J.C., Mitchum, R.M., Campion, K.M., and Rahmanian, V.D., 1990, Siliclastic sequence stratigraphy in well logs, cores, and outcrops: Concepts for high-resolution correlation of time and facies: *American Association of Petroleum Geologists Methods in Exploration Series #7*, 55 p.
- Van Wagoner, J.C., 1995, Sequence stratigraphy and marine to nonmarine facies architecture of foreland basins, in Van Wagoner, J.C., and Bertram, G.T., eds., *Sequence stratigraphy of foreland basin deposits*: AAPG Memoir 64, p. 137–223.
- Villien, A., and Kligfield, R.M., 1986, Thrusting and synorogenic sedimentation in central Utah, in Peterson, J.A., ed., *Paleotectonics and sedimentation*: A.A.P.G. Memoir 41, p. 281–307.
- Walker, R.G., and Eyles, C.H., 1991, Topography and significance of basin-wide sequence-bounding erosions surfaces in the Cretaceous Cardium Formation, Alberta, Canada: *Journal of Sedimentary Petrology*, v. 61, p. 473–496.
- Weimer, R.J., 1984, Relations of unconformities, tectonics, and sea-level changes, Cretaceous of Western Interior, U.S.A., in Schlee, J.S., ed., *Interregional unconformities and hydrocarbon accumulation*: A.A.P.G. Memoir 36, p. 7–36.
- Yingling, V.L., and Heller, P.L., 1992, Timing and record of foreland sedimentation during the initiation of the Sevier orogenic belt in central Utah: *Basin research*, v. 4, p. 279–290.

- Young, R.G., 1952, *Stratigraphic relations in the Upper Cretaceous of the Book Cliffs, Utah-Colorado*: Ph.D. Dissertation, Ohio State University, Columbus, Ohio, 147 p.
- Young, R.G., 1955, *Sedimentary facies and inter tonguing in the Upper Cretaceous of the Book Cliffs, Utah-Colorado*, G.S.A. Bulletin, v. 66, p. 177-202.

Fluvial-deltaic Sedimentation and Stratigraphy of the Ferron Sandstone

PAUL B. ANDERSON

Geological Consultant, Salt Lake City, Utah 84102

THOMAS C. CHIDSEY, JR.

Utah Geological Survey, Salt Lake City, Utah 84114

THOMAS A. RYER

The ARIES Group, Louisville, Colorado 80027

ABSTRACT

East-central Utah has world-class outcrops of dominantly fluvial-deltaic Turonian to Coniacian aged strata deposited in the Cretaceous foreland basin. The Ferron Sandstone Member of the Mancos Shale records the influences of both tidal and wave energy on fluvial-dominated deltas on the western margin of the Cretaceous western interior seaway. Revisions of the stratigraphy are proposed for the Ferron Sandstone. Facies representing a variety of environments of deposition are well exposed, including delta-front, strandline, marginal marine, and coastal-plain. Some of these facies are described in detail for use in petroleum reservoir characterization and include permeability structure.

INTRODUCTION

The Ferron Sandstone Member of the Cretaceous Mancos Shale is well exposed along the west flank of the San Rafael Swell of east-central Utah (fig. 1). The Ferron Sandstone is a fluvial-deltaic deposit with excellent exposures of a variety of delta facies deposited along the margins of a rapidly subsiding basin. The Ferron Sandstone has been interpreted as an analog for many of the highly productive oil and gas reservoirs in the Alaskan North Slope, Gulf Coast, and Rocky Mountain regions.

The Ferron Sandstone is an eastward-thinning clastic wedge deposited during Turonian-Coniacian (Late Cretaceous) time. The Ferron and equivalent portions of the Frontier Formation in northern Utah and Wyoming record a pronounced and widespread regression of the Cretaceous western interior seaway. In east-central Utah, these deposits accumulated on a deltaic shoreline in a rapidly subsiding portion of the Cretaceous foreland basin. The Ferron consists of a series of stacked, transgressive-regressive cycles which are well displayed in outcrop. Eleven stratigraphic units have been mapped: Clawson, Washboard, Last Chance, and numbers 1 through 8 (in ascending order). These various units define a pattern of seaward-stepping, vertically-stacked, and landward-stepping depositional geometries. This architecture indicates an initial strong supply of sedi-

ment relative to available space where sediment could accumulate, followed by near-balance, and then a relative decrease in sediment supply. Each unit contains in outcrop all, or portions of, the complex of facies that make up a typical fluvial-dominated deltaic deposit. Such facies include deposits of: (1) meandering, distributary, and tidal channels; (2) wave-modified strandlines and fluvial deltas; and (3) transgressive events, bays, lagoons, and flood basins.

The excellent exposures and accessibility of the three stacking patterns and associated complex facies make the Ferron Sandstone an excellent outcrop analog for petroleum reservoirs in fluvial-dominated deltas. The Ferron Sandstone is an excellent model for, and is correlative to, the Cretaceous Frontier Formation, which produces petroleum throughout Wyoming. The Ferron facies are also a good analog for the Tertiary Green River and Wasatch Formations, the major oil and gas producing reservoirs in the Uinta Basin, Utah. In addition to its value as a reservoir analog, sands and coalbeds of the Ferron Sandstone produce gas north of the field trip area in the Wasatch Plateau and along the west-northwest flank of the San Rafael uplift, currently the most active gas play in Utah.

Petroleum industry and U.S. Department of Energy (DOE) analysis of the Ferron Sandstone is also motivated by the need to deal with complex reservoir heterogeneities

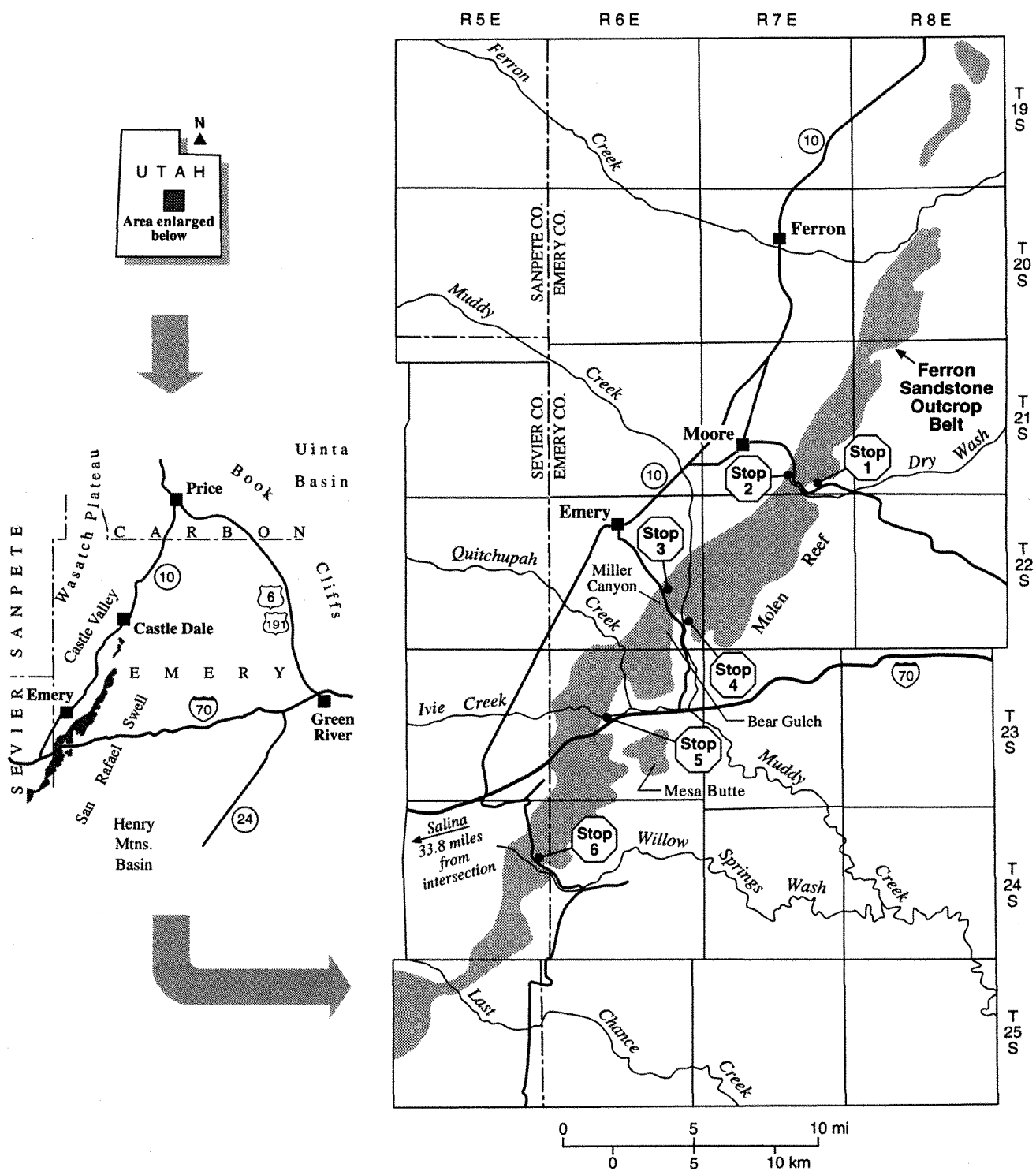


Figure 1. Index map of the Ferron Sandstone outcrop belt (shaded) showing locations of field trip stops.

on an interwell to field scale. These scales are difficult to resolve in reservoir exploration and development activities. Standard industry approaches to field development rely on generic depositional models constrained primarily by data obtained in petrophysical (logging and coring) evaluations of exploration and development wells. The quantity, quality, and distribution of these data are typically insufficient to adequately model the reservoir. Work on the Ferron Sandstone has been predicated on the assumption that detailed outcrop mapping of petrophysical and geological properties of this analog reservoir will provide an additional database for reservoir characteristics used in model simulations.

REGIONAL STRATIGRAPHY

Ferron Sandstone is recognized as a member of the Mancos Shale. No type section has been designated. The name is derived from the town of Ferron, Utah, but it is clear from Lupton's work (1916) that he would have chosen the outcrops southeast of the town of Emery (fig. 1) as representative of the member where it is most typically developed. The name Ferron Sandstone is presently used on outcrops around the San Rafael Swell, in the Henry Mountains basin, and beneath Castle Valley and the Wasatch Plateau.

During middle Turonian time, the relatively straight, north-trending western shoreline of the western interior seaway had reached about half way across Utah (Williams and Stelek, 1975). The shoreline configuration changed as it prograded eastward. The rate of progradation was more rapid in northern and southern Utah, less rapid in central Utah, because of geographical variations in subsidence rates and volumes of sediment arriving from the Sevier orogenic belt to the west. The result was a shoreline bend to the west in the Castle Valley area of east-central Utah. Ryer and Lovekin (1986) concluded that this embayment was caused primarily by very rapid subsidence.

We have divided the Ferron Sandstone into mappable units or bodies of rock. Most of these units would be members of the Ferron, if it were elevated to formation status. Eleven mappable units have been recognized on outcrop (fig. 2). We have used a hierarchical system of abbreviations to designate each mappable body of rock. Kf designates Cretaceous Ferron Sandstone. The first dash designates the next hierarchical subdivision, e.g. Kf-2, which is comparable to a member or informal "tongue." Most of these "members" are separated by major flooding surfaces and include smaller-scale progradational units that display distinctive stacking patterns; in essence they are parasequence sets, as defined by Van Wagoner et al., (1990). The lowest two units, Kf-Clawson and Kf-Washboard (fig. 2), have been separated and together informally designated "lower Ferron Sandstone" by Ryer and McPhillips (1983). Ryer and McPhillips' "upper Ferron Sandstone" consists of delta-front units 1–7

(our Kf-1 through 7). We have divided their delta-front unit 1 into Kf-Last Chance (Kf-LC) below and Kf-1 above; in addition, a Kf-8 unit is recognized above Kf-7.

The next dash in our hierarchical scheme designates a higher frequency stratigraphic unit which is mappable and is separated from the rocks above and below by a flooding surface and/or transgressive surface of erosion, and makes up the highest frequency unit mapped within each larger stratigraphic unit or parasequence set (e.g. Kf-2-Muddy Canyon). In most cases these units would fit the definition of a parasequence (Van Wagner et al., 1990), but in some cases, in our opinion, these units do not strictly fit Van Wagner's definition. With these qualifications, we have chosen to use the term parasequence to designate the highest frequency stratigraphic unit recognized and mapped. (For a discussion of earlier Ferron Sandstone stratigraphic nomenclature, see Garrison et al., this volume.)

Other recent studies (Gardner, 1991, 1993, 1995; Barton and Angle, 1995) have not distinguished parasequences in Kf-Clawson, Kf-Washboard, and Kf-7 and 8, although they may exist. Kf-LC contains several parasequences, but it is arguable whether or not a "major" flooding surface is present between it and Kf-1. Internal morphology of Kf-LC indicates it is more aggradational than Kf-1. It is possible for the stacking pattern of a group of parasequences to change from aggradational to progradational without a "major flooding surface." Other characteristics of Kf-LC are distinctive from Kf-1 and discussed later, hence its hierarchical designation. Kf-1 through 7 have associated coal beds, which carry letter designations originally assigned by Lupton (1916).

The oldest unit exposed on the Ferron outcrop belt in Castle Valley is Kf-LC. Kf-LC contains parasequences that are relatively short in overall dip length (1.3 to 0.75 miles [2.1–1.2 km]), rapidly thickening (0 to 60 feet [0–18 m]) with steeply seaward-inclined bed sets (about 5°). The contact with the underlying Tununk Shale, which has a characteristic brown iron stain, is sharp. Kf-LC was deposited in a steeper gradient shoreline topography with abundant sediment supply.

Progradation of Kf-1 and Kf-2 was characterized by an abundant supply of sediment compared to the creation of accommodation space (Gardner, 1995). A relatively small amount of sediment was required to aggrade the coastal plain and a considerable proportion passed north and east through the fluvial systems to reach the shoreline. Rapid supply of sediment at the river mouths promoted the building of fluvial-dominated deltas, the deposits of which are conspicuously more abundant in Kf-1 and Kf-2 than they are in Kf-4 through Kf-7 (Gardner, 1993). It is highly probable that relative sea level rise caused either by eustatic fluctuations or by pulses of basin subsidence, continually affected the area and are the underlying mechanism for inducing both parasequence-set and parasequence-level transgres-

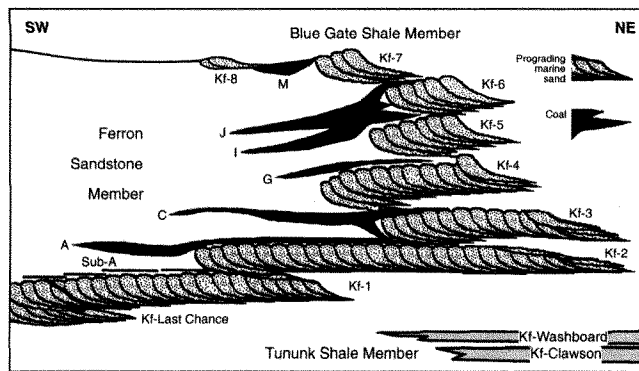


Figure 2. Diagrammatic cross section of the Ferron Sandstone and adjacent members of the Mancos Shale showing the numbering and stacking of the deltaic-front units. Coal zones (black) are designated by letters.

sions and regressions. A delta is very much “at risk” should even a minor rise of relative sea level occur. Transgression of the coast adjacent to a delta diminishes the river’s already inefficient gradient, leading inevitably to avulsion of the river, abandonment of the delta, and rapid transgression across the delta plain. Many such transgressions are recognizable in Kf-LC, Kf-1, and Kf-2.

The earliest, proximal part of each parasequence set consists of parasequences deposited on wave-dominated coasts. The relative sea level rise that brought about the parasequence-level transgressions caused reduction of sediment supply to the coast. As the rise slowed and the balance shifted back to progradation, the supply of sediment to the coast increased. Initially, the supply was low, allowing extensive wave reworking. This also explains the pronounced seaward stratigraphic rise of many parasequences just seaward of their pinchouts. The younger, more distal parasequences of Kf-1 and Kf-2 commonly contain more fluvial-dominated deltaic deposits. At these times, the rate of rise of relative sea level was slower and the amount of sediment delivered to the shoreline was correspondingly greater. The supply was great enough to allow progradation of recognizable deltas.

FIELD TRIP OVERVIEW

Geological, physiographical, and cultural features along the field trip route are noted in the road log. The main Ferron Sandstone cliffs and its deeply incised canyons together provide a three-dimensional view of facies variations and transitions. The Ferron Sandstone has excellent exposures along depositional strike; numerous canyons that cut perpendicular to strike offer excellent exposures along the depositional dip direction.

The field trip has two parts, each with a different emphasis: (1) a review of regional stratigraphy and (2) detailed analysis of depositional environments and permeability trends. The primary objective of **Day One** will be to provide a detailed interpretation of the regional stratigraphy of the Ferron Sandstone outcrop belt from Dry Wash to Last Chance Creek (fig. 1). Parasequence designations are based on flooding surfaces which separate notable coarsening-upward depositional sequences. In many cases, landward pinchouts of the marine facies can be observed enclosed within the coastal-plain facies. In Ferron deltaic deposits, parasequence sets/stratigraphic units may be considered as large-scale reservoir blocks because marine and/or delta-plain shales that separate stratigraphic units may act as laterally extensive permeability barriers. The dimensions and depositional environments of selected parasequence sets and the nature of the contacts between parasequences and facies are well displayed at various stops. Bounding surfaces (fluid-flow barriers or baffles), geometries, and depositional environments of these rocks characterize the variability of fluvial-dominated deltaic oil and gas reservoirs. The regional morphological framework can be incorporated into model simulations at the oil and gas field scale.

The primary objective of **Day Two** will be to develop a detailed sedimentological characterization of the facies in the Ivie Creek area just north of Interstate 70 (I-70) (fig. 1). The Ivie Creek area was selected because it contains abrupt facies changes in Kf-1 and Kf-2. Access to the area is excellent because of the close proximity to I-70. Kf-1 in the Ivie Creek area is represented by a fluvial-dominated delta deposit consisting of two stacked parasequences preliminarily identified as Kf-1-Ivie Creek-a and Kf-1-Ivie Creek-c (Kf-1-Iv-a and Kf-1-Iv-c). Kf-1-Iv-a changes from proximal to distal from east to west and is the focus of geologic and permeability characterization. Kf-2 in the Ivie Creek area represents a wave-modified deltaic deposit consisting of lower, middle, and upper shoreface, foreshore, and mouth-bar environments of deposition. Facies of this type are typically found in deltaic reservoirs worldwide. Using a combination of recent drill hole and outcrop data a deterministic three-dimensional view of the rocks within the Ivie Creek area was developed. Detailed stratigraphic sections and cliff-face mapping of rock units on a photomosaic base, combined with petrophysics and outcrop/core permeability data, are the basis for a three-dimensional characterization of these rocks. An evaluation will be presented of how variations in facies influence both compartmentalization and permeability structure. The field trip participants will examine the major reservoir types (mouth-bar complex, wave-modified and fluvial-dominated delta front, distributary channel, and tidal deposits) associated with the Ferron Sandstone.

Much of the information presented on this field trip was gathered by the Utah Geological Survey and associated contractors, who conducted a major DOE-funded study of the Ferron Sandstone from 1993 through 1997. Preliminary findings from the study have been presented by the following: Adams, 1995; Adams et al., 1995a, 1995b; Allison, 1995; Anderson and Ryer, 1995; Dewey et al., 1995; Hucka et al., 1995a, 1995b; Chidsey, 1995; Ryer and Anderson, 1995; Ryer et al., 1995; Snelgrove et al., 1995; Anderson et al., 1996; Chidsey and Allison, 1996; Mattson and Chan, 1996; Snelgrove et al., 1996; and Chidsey, 1997.

ROAD LOG

First Day

MILEAGE
Cumulative Interval

0.0	0.0	Enter eastbound I-70 at junction with U.S. Highway 89, Salina, Utah. Follow road logs of Rigby et al., (1974).
31.7	31.7	View to the east of the San Rafael Swell and Upper Cretaceous Ferron Sandstone Member of the Mancos Shale. Pinnacles of Jurassic Navajo Sandstone on the skyline.
33.8	2.1	Junction of I-70 with Utah Highway 10 (fig. 1). Turn off I-70 and proceed north (left) on Highway 10 towards Emery through Castle Valley. Highway 10 lies on the Blue Gate Shale Member of the Mancos Shale. Boulders of Miocene basalt are strewn over adjacent slopes (Bunnell, 1991). These boulders were eroded from flows to the southwest in the Thousand Lake Mountain area.
35.5	1.7	Ivie Creek. Wasatch Plateau in the distance to the west. Ledge-forming sandstone represents shoreface deposits of the Upper Cretaceous Star Point Sandstone of the Mesa Verde Group (Bunnell, 1991). The Star Point intertongues with the overlying delta- and alluvial-plain deposits of the Blackhawk Formation, the major coal-bearing formation in the Wasatch Plateau and Book Cliffs coal fields. The Masuk Shale Member of the Mancos Shale forms the slopes beneath the Star Point. The Masuk Shale overlies the Emery Sandstone Member in the immediate foreground.

38.5	2.8	Pass by junction of Utah Highway 10 with Hidden Valley coal mine access road to the east.
41.5	3.0	Sevier-Emery County line. Joe's Valley graben fault system to the north on the eastern edge of the Wasatch Plateau.
42.4	0.9	Quitcupah Creek. Browning coal mine in the distance to the east (right).
46.1	3.7	Town of Emery. Continue north on Utah Highway 10.
48.4	2.3	To the left is the site of Texaco's A.L. Jensen 27-9 Ferron coalbed methane well (SE1/4SE1/4 section 27, T. 21 S., R. 06 E., Salt Lake Base Line) drilled in 1995 to a depth of approximately 2,100 feet (640 m). The operator is still evaluating the well.
49.7	1.3	Muddy Creek.
49.9	0.2	Junction with County Road 1612. Turn right onto County Road 1612 toward Moore.
50.5	0.6	Road to Rochester rock art panel to the right.
52.3	1.8	Moore.
52.6	0.3	Turn right toward Dry Wash and continue on county road to the east.
53.1	0.5	Continue straight (east) off pavement towards I-70 at bend in the road (becomes graveled road at this point). Cross the Spanish Trail, a transportation route from 1800 to 1850.
55.5	2.4	Contact between Blue Gate Shale and top of the Ferron Sandstone.
57.2	1.7	STOP 1. Mouth of Dry Wash: overview of Kf-Clawson and Kf-Washboard, and Kf-2 (fig. 3). Kf-Clawson of the Ferron, first described by Cotter (1975a, b), extends from the northern part of San Rafael Swell southward along its western flank, through Molen Reef, finally feathering out westward toward Muddy Canyon. Kf-Washboard (fig. 2) (Cotter, 1975a, b) extends from the northern part of San Rafael Swell southward to Mesa Butte (just south of I-70), slightly farther than does the underlying Kf-Clawson. These units consist of silty, very fine-grained sandstone; they are interpreted as shelf sand bodies with a northern source deposited 10 miles (16 km) or more off-

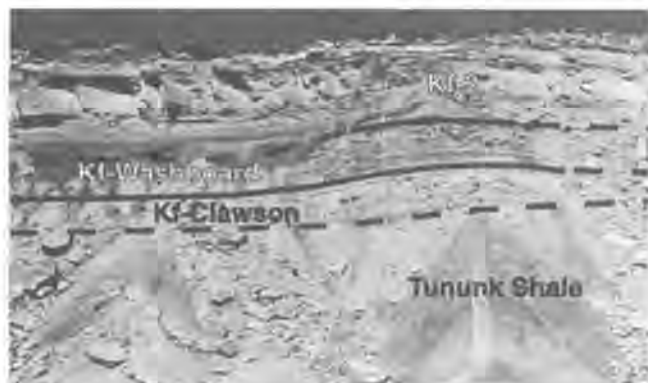


Figure 3. Coal Cliffs (view to the west) near the mouth of Dry Wash at Stop 1 (mile 57.2) with, in ascending order, Kf-Clawson, Kf-Washboard, and Kf-2 outcropping. The upward-coarsening Kf-Clawson and Kf-Washboard are interpreted as two still-stands separated by a relative rise of sea level. Kf-2 consists of interbedded fine-grained sandstone and mudstone, abruptly overlain by cross-bedded, fine- to medium-grained mouth-bar sandstone.

shore, at depths near fair-weather wave base. Extensive burrowing and the presence of large concretions suggest that rates of sedimentation were slow. Lowering of sea level prior to Kf-Clawson and Kf-Washboard deposition facilitated southward transport of very-fine- and fine-grained sand onto a shoal area that marks the eastern hinge of the foredeep developed in front of the Sevier orogenic belt. The shoal may represent a peripheral bulge. The two distinct, upward-coarsening sandstone units suggests that there were two still-stands separated by a relative rise of sea level. In addition to feathering out southward, both Kf-Clawson and Kf-Washboard become less sandy and disappear toward the west. A gentle structural flexure has been recognized in this area, suggesting the presence of a down-to-the-west basement fault. The fact that Cretaceous rocks were flexed but not broken by movement on the proposed fault (unlike the younger faults associated with Tertiary extension) suggests that this fault moved during Cretaceous time in response to thrust loading. The westward loss of sand in Kf-Clawson and Kf-Washboard suggests that it was active during lower Ferron deposition.

Kf-2 at Dry Wash is composed of two parasequences. The lower parasequence is all delta-front facies and displays upward-coarsening grain size. The lower part of the parasequence consists of interbedded fine-grained sandstone and mudstone; it is abruptly overlain by cross-bedded, fine- to medium-grained sandstone of the upper part. The upper part has a decided fluvial appearance, but lacks the mudstone intraclasts commonly associated with fluvial channel deposits. The top of Kf-2 consists of a series of lenses or pods, the younger lenses cutting out and replacing the older ones. These are interpreted to be mouth-bar and distributary channel deposits of a fluvial-dominated delta.

The younger and overlying parasequence consists of an upward-coarsening sequence of sandy mudstone and sandstone containing a brackish-water fauna representing a bay. The bay-fill sequence is capped by carbonaceous mudstone, carbonaceous sandstone, and a minor amount of coal. These rocks represent the lower split of the C-coal zone (fig. 2). It, in turn, is abruptly overlain by a thin, transgressive lag and lower delta-front deposits of Kf-3. This parasequence is defined on the basis of a shoreline sandstone unit whose landward pinchout of the marine facies crosses the northern edge of the cliffs of the Molen Reef south of Dry Wash and intercepts the cliffs on the north side of the wash, defining a northwest shoreline trend. The pinchout is less distinct than most others, possibly because of development of a flood-tidal delta in this area. A large lagoon/bay complex lies landward of the pinchout and can be traced for several miles southward in the Molen Reef outcrops and westward to the limit of Kf-2 outcrops in Dry Wash. Numerous channel deposits, including three large, lenticular channel bodies in Dry Wash and several in the Molen Reef cliffs appear to belong to Kf-2. The facies content of this shoreline unit is wave-modified, probably strand plain in its proximal part.

Turn around and head towards Moore.

- 58.1 0.9 Kf-Clawson at road level.
 58.3 0.2 Kf-2 at bend in the road to the left.
 58.5 0.2 **STOP 2. Dry Wash: depositional environments of Kf-3 (fig. 4).** Cross road and walk up wash to the left.

Kf-3 contains more storm layers than does Kf-2. It also displays hummocky cross-stratification in many places. Like Kf-2, it includes trough cross-bedded sandstone in its upper part. Kf-3, however, includes a sandstone body that has a much more clearly defined erosional base, is coarser grained, contains a variety of burrow types, the most conspicuous of which is *Ophiomorpha*, and displays lateral accretion surfaces inclined toward the northwest. This inclined sandstone body is interpreted to be an inlet or a point-bar deposit on a tidal channel immediately behind the inlet. On the north side of the wash, it is apparent that the inclined, laterally accreted sandstone beds are truncated at their tops by what was originally a horizontal surface. The erosional surface is a transgressive unconformity. It is underlain by a transgressive lag of bioturbated sandstone. The lag, in turn, is overlain by a southward-thinning tongue of offshore-marine shale that separates Kf-3 and Kf-4.

- 58.6 0.1 Ferron Sandstone Kf-4 and Kf-6 (Barton and Angle, 1995) include only prodelta and lower- to middle-delta-front deposits; the shoreline never prograded this far seaward. From a vantage point on top of Kf-4, the gradational seaward termination of Kf-6 can be observed toward the north, where the road crosses the outcrop. Kf-6 sandstone is overlain by the Blue Gate Shale Member of the Mancos Shale. The seaward termination of Kf-4 is only a short distance north of Dry Wash. The seaward feather edge of Kf-5 is present a short distance away on the wall of the canyon visible to the south.
 59.0 0.4 Kf-6. Continue towards Moore.
 61.2 2.2 Return to pavement, continue straight to Moore.
 61.7 0.5 **Moore. Turn left towards Emery at stop sign.**
 64.4 2.7 **Junction with Utah Highway 10, turn left (south) towards Emery.**



Figure 4. Kf-3 in Dry Wash (view to the west from south side of the road) at Stop 2 (mile 58.5) containing hummocky and trough cross-stratification, and bioturbated beds. The thicker bedded sandstones with inclined bedsets to the right are tidal-channel deposits.

- 67.6 3.2 **Enter Emery, turn left on to 300 East.**
 68.0 0.4 Continue south past 400 South in Emery. TRC Minerals to the right processes carbonaceous shale from the Ferron Sandstone for use as potting soil and health tonics.
 68.4 0.4 **Turn left onto Miller Canyon Road toward I-70.** Thousand Lake Mountain and Boulder Mountain can be seen on the skyline to the south.
 70.9 2.5 Enter Miller Canyon. Channel sands and overbank deposits of Kf-5 and shoreface sandstone of Kf-7 are exposed at the head of the canyon.
 71.1 0.2 Access road to one of several carbonaceous shale mines in the G-coal zone on the right.
 71.4 0.3 **STOP 3. Miller Canyon: stratigraphy of Kf-4 and Kf-2 (fig. 5).** Walk southeast along the sandstone bench at road level, north side of the canyon.

The Miller Canyon road descends through the stratigraphic section, hence, the description of the stratigraphy moves from top to bottom.

Compared to the stratigraphic units that preceded it, Kf-4 thickens very rapidly seaward, indicating a high rate of relative sea-level rise during its deposition (Ryer, 1981; 1982). Regionally, two parasequences are recognizable within this unit. The overlying G-coal zone only locally contains more than a few feet of coal,

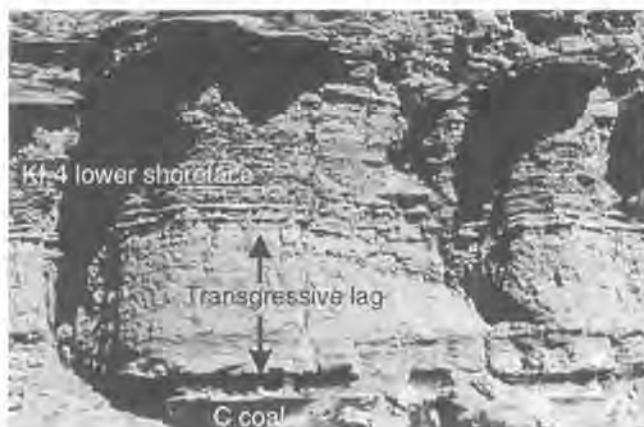


Figure 5. Transgressive deposits above the C-coal zone of Kf-4 in Miller Canyon near the Christensen mine on the east side of the Miller Canyon road at Stop 3 (mile 71.4).

probably because peat accumulation could not keep up with the rapid relative rise of sea level that characterized this unit. For about 20 years carbonaceous mudstones of the G-coal zone have been mined in Miller Canyon to produce a soil conditioner, locally referred to by the trade name "Live Earth."

Only the older parasequence of Kf-4 is represented by marine facies in Miller Canyon. The lower parasequence is a wave-modified shoreline sandstone body and forms high cliffs. The landward pinchout of the main facies of this parasequence is located about 0.5 mile (0.8 km) south of Bear Gulch (fig. 1), but is somewhat obscured because the upper part of the unit is scoured into by a younger meanderbelt deposit. This meanderbelt deposit is very widespread, being recognized for several square miles around the Miller-Muddy Creek Canyon area and east to the eastern limit of the outcrop. It is relatively coarse-grained, being made up of medium- to coarse-grained sandstone that locally includes granules and, rarely, pebbles. The landward-most part of the lower parasequence is strongly wave modified and this is probably true of the unit as a whole, although it is difficult to tell with the upper part of the unit removed. The basic facies content is wave-modified shoreline-strand plain proximally to wave-modified delta distally.

Marine facies of Kf-3 are not present in this area, the landward pinchout of the marine facies is located to the east.

At this locality Kf-2 contains four parasequences. We will use the nomenclature established by Anderson (1993), Gustason (1993), and Ryer (1993). The top parasequence is Kf-2-Muddy Canyon-b (Kf-2-MC-b). Kf-2-MC-b is defined on the basis of a shoreline sandstone unit that has a distinctive white color. The landward pinchout of Kf-2-MC-b marine facies is present in the southern Coal Cliffs just north of Bear Gulch, and south of the mouth of Miller Canyon. Near the pinchout, the unit is characterized by large-scale, inclined surfaces that dip to the north, essentially parallel to the trend of the pinchout (strike of inclined surfaces perpendicular to shoreline trend). The surfaces are interpreted to represent a series of tidal inlets that were driven northward by longshore drift. Equivalent flood-tidal delta and lagoonal deposits have been tentatively identified in Miller Canyon and Bear Gulch. Kf-2-MC-b thickens rapidly eastward, to more than 75 feet (23 m). It extends eastward into Molen Reef, where it is a major cliff former, and northward to Dry Wash (about 9 miles [14.5 km]). This unit is widely distributed compared to most Ferron parasequences. The facies content of this shoreline unit is a wave-modified coast proximally, probably strand plain; and deltaic deposits distally. A thin A-coal zone lies above this unit. This coal zone pinches out just northeast of Miller Canyon.

Kf-2-Muddy Canyon-a (Kf-2-MC-a) forms ledges and lesser cliffs above the higher cliffs formed by Kf-2-Miller Canyon-b (Kf-2-Mi-b) throughout most of the lower part of Muddy Creek Canyon and into the southern Coal Cliffs to the south. Most of the delta facies of Kf-2-MC-a has been cut out by meanderbelt deposits. Although very sandy in some areas, much of the meanderbelt deposits consist of laterally accreted sands with minor siltstone and mudstone. Two distinct meanderbelt units are distinguished on the basis of paleocurrent directions. The landward pinchout of marine facies of Kf-2-MC-a is

located south of Miller Canyon near the southern termination of the Coal Cliffs. In the Miller-Muddy Canyon area there can be no question that the surface that separates Kf-2-MC-a from the underlying Kf-2-Mi-b is a transgressive surface: it places offshore, marine shale directly upon upper shoreface sandstone and, locally, has planed off small channels within the top of Kf-2-Mi-b. The facies content of this shoreline unit is a fluvial-dominated delta and probably represents a low-wave-energy delta that prograded into a protected bay.

Kf-2-Mi-b includes the shoreline sandstone that forms the massive cliffs in the lower parts of Miller and Muddy Creek Canyons (Anderson, 1993; Gustason, 1993; Ryer, 1993). It appears to be a very strongly wave-modified unit. It thins toward the northwest, finally disappearing into marine shale in the southern part of Molen Reef along with overlying Kf-2-MC-a parasequence. In Muddy Creek Canyon (but not yet elsewhere), it is possible to subdivide Kf-2-Mi-b into two subunits bounded by a distinctive surface. The southern subunit is wave modified, the northern one very strongly wave modified. The surface that separates these subunits could be a transgressive surface, but the overlying transgressive surface beneath Kf-2-MC-a has removed any direct evidence. In the absence of compelling evidence to the contrary, it is assumed the surface marks some change of autocyclic origin. The facies content of this shoreline unit is wave-modified, probably strand plain in proximal part.

The bottom parasequence in Kf-2 in this area is Kf-2-Miller Canyon-a (Kf-2-Mi-a). The boundary between this unit and the overlying Kf-2-Mi-b is difficult to recognize in many places, but is very apparent where rotated slump blocks, which are generally restricted to Kf-2-Mi-a in this area, are present. The transgressive surface is apparent where it has beveled the tops of the rotated blocks, which are common enough to facilitate tracing the contact throughout the area. Its seaward feather-edge can be approximately located in Miller Canyon and in

the lower part of Muddy Creek Canyon. It has a general northeast trend, suggesting that this parasequence built northwestward, probably as a deltaic lobe.

Kf-2 in Miller Canyon (fig. 6) view to east but west of Muddy Creek.

Junction of Muddy Creek with Miller Canyon.

STOP 4. Lunch.

From the lunch stop, dramatic seaward (eastward) thickening of the top parasequence of Kf-2 can be observed. On the west the thin white-capping sandstone is visible, while this same sand is nearly 30-feet (9-m) thick on the east wall of the canyon. The underlying meanderbelt-dominated facies of Kf-2-MC-a is well exposed in all cliff faces. Some Kf-2-MC-a-aged channels have cut across the top of the underlying shoreface of Kf-2-Mi-b and deep into these deposits. Note how much thicker Kf-2 is in this area compared to our earlier stop at Dry Wash.

Kf-2 is fertile ground for a classic problem in sequence stratigraphy. The scours into delta-front and wave-dominated shoreface deposits observed here can be traced intermittently for tens of miles to the south and several miles to the north along the outcrop. Does this represent a drop in relative sea level? Similar "cannibalization" of shoreline sands is present in Kf-1, 3, 4, and 5. During normal progradation of a shoreline some scouring into older shoreline deposits is expected as fluvial systems feeding the seaward prograding shoreline move across a low-gradient delta-plain. Evidence of emergence, such as rooted coal in the bottom of mud-filled channels, or part way up in a channel-fill sequence; low-angle slopes to the edge of "valley-fill" deposits; regionally correlatable transgressive deposits within the "incised valley" would indicate a drop in sea level as the agent for channel incision. Some workers in the Ferron feel they have observed sufficient evidence to call upon a relative sea-level drop within Kf-2 (Garrison, personal communication, 1996) and Barton (1997) implies more frequent occurrence of minor sea-level drops during Ferron deposition.

72.0	0.6
72.4	0.4
72.8	0.4



Figure 6. View down Miller Canyon (north side) near the junction with Muddy Creek showing Kf-2 and its four parasequences between Stops 3 and 4 (mile 72.0).

76.5	3.7	Junction with I-70. Turn right (west) on I-70 towards Salina.
77.8	1.3	Mesa Butte to the south, capped chiefly by Kf-1 and Kf-2. There is a very limited area of C-coal zone on the mesa. The lowest ledge-forming unit in the east-facing cliffs is Kf-Washboard.
78.3	0.5	Quitichupah Canyon to the north.
78.8	0.5	STOP 5. Ivie Creek Amphitheater: the fluvial-dominated Kf-1 and wave-modified Kf-2 (fig. 7). Turn off I-70, drive down slight embankment, and park along the right-of-way fence. We will examine the Kf-1 and Kf-2 today and walk through the outcrop tomorrow.

Kf-1 is represented by two parasequences in the Ivie Creek area. Kf-1-Ivie-a (Kf-1-Iv-a) is characterized locally by distinctive, steeply inclined bedsets (clinoforms) that accumulated on a prograding lobe of the delta. This deltaic lobe has an arcuate shape based on mapping of clinoforms in the Ivie Creek area. The lobe prograded toward the south (just south of I-70), toward the west in the amphitheater north of Ivie Creek, and toward the north in the southern part of Quitichupah Canyon. It is possible that the odd characteristics of Kf-1-Iv-a can be attributed to its location at the flexure described for Kf-Clawson. If this flexure marks the hinge of the foredeep, flexure of strata caused by movement of a basement fault may have created the deep-

water bay into which Kf-1-Iv-a prograded (fig. 8); the distributary system from which its feeder channel came was situated on the high side of the flexure. The seaward limit of Kf-1-Iv-a is mapped in mid-Quitichupah Canyon. This fluvial-dominated deltaic deposit changes from proximal to distal east to west across the amphitheater in the Ivie Creek area. Clinoforms in the delta front dip 10° to 15° and pinchout laterally within a mile (1.6 km) down depositional dip (fig. 9).

The overlying sand-rich and coarsening-upward facies of the Kf-1-Ivie Creek-c (Kf-1-Iv-c) also vary in thickness within the area. In contrast to Kf-1-Iv-a, delta-front deposits of this parasequence dip less than 5°. Kf-1-Iv-c laps onto the more distal parts of Kf-1-Iv-a in the western part of the Ivie Creek area and represents the distal portion of another delta lobe, probably originating from the southwest. The upper section of Kf-1-Iv-c is continuous across the entire Ivie Creek area and represents a fluvial-dominated delta. Kf-1-Iv-c contains loading features near the mouth of Ivie Creek. It thickens to the north as Kf-1-Iv-a pinches out. As with most parasequences, small channels cut into the top of Kf-1-Iv-c. A consistent zone of brackish-water-rich fossils is found above the marine delta-front sandstones of Kf-1-Iv-c. These deposits often grade to *Crassostrea coquinas* which sometimes split the sub-A coal. A flooding surface has been identified at the top of the sub-A coal. The boundary with the overlying Kf-2 is drawn at the change from delta plain to lower shoreface deposits.

Kf-2 contains three parasequences at Ivie Creek: Kf-2-Ivie Creek-a, b, and c (Kf-2-Iv-a, Kf-2-Iv-b, and Kf-2-Iv-c). These parasequences show less lateral variation in facies than Kf-1 parasequences, possibly because wave processes were dominant. Kf-2-Iv-a is the oldest parasequence in Kf-2 and grades from proximal facies of a shoreface on the west to its pinch out before reaching Quitichupah Creek on the east. Kf-2-Iv-b has a similar west to east variation in facies. This parasequence has distinctive seaward inclined beds near Quitichupah Canyon and appears to have

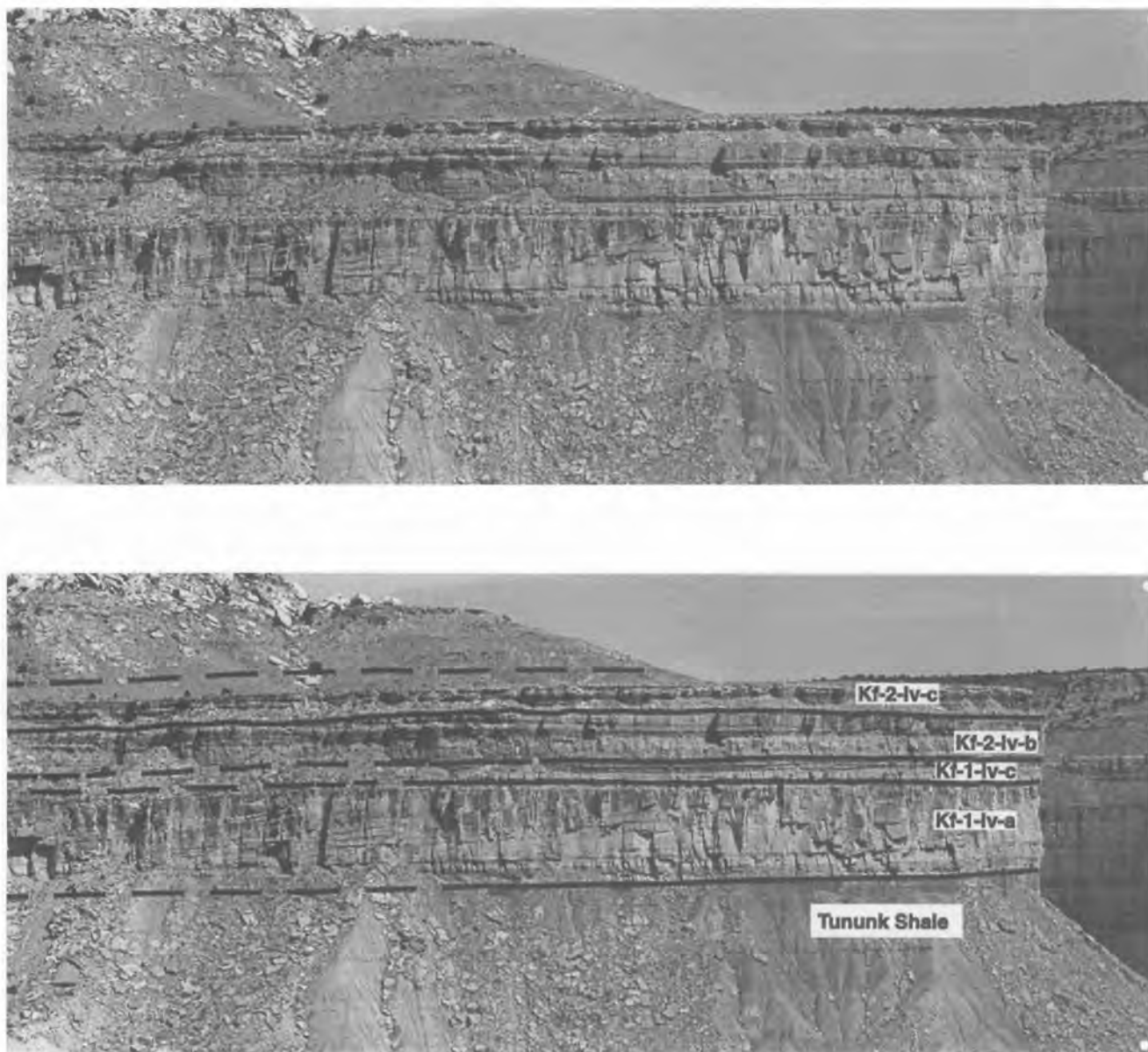


Figure 7. Photomosaics (view to the north near I-70), unannotated (top) and annotated (bottom), of the Ivie Creek area at Stop 5 (mile 78.8) displaying contrasting delta-front architectural styles. On the annotated photomosaic black lines separate the parasequences of Kf-1 and Kf-2, designated with letters. Kf-1-iv-a has steeply inclined (10 to 15°) clinoforms representing fluvial-dominated deposition. Kf-2-iv-b has gently inclined ($< 3^\circ$) clinoforms representing wave-modified deposition.

considerable lateral continuity along the strike of the outcrop. Kf-2-iv-c has the landward pinchout of its marine facies well exposed in the I-70 road cut and upper Ivie Creek Canyon. Connecting these two points indicates a more north-south trend for the shoreline. A remarkable transition from shoreface to bay deposits is also well exposed in this area.

In the Ivie Creek area, deposition of sandstones in Kf-1-iv-a was from the south-southeast to north-northwest, whereas the general coarsening in grain size of Kf-2 to the west and the presence of a landward pinchout of the marine facies in Kf-2-iv-c suggests that this unit was deposited from west to east. Kf-2 contains more and cleaner sand, indicat-

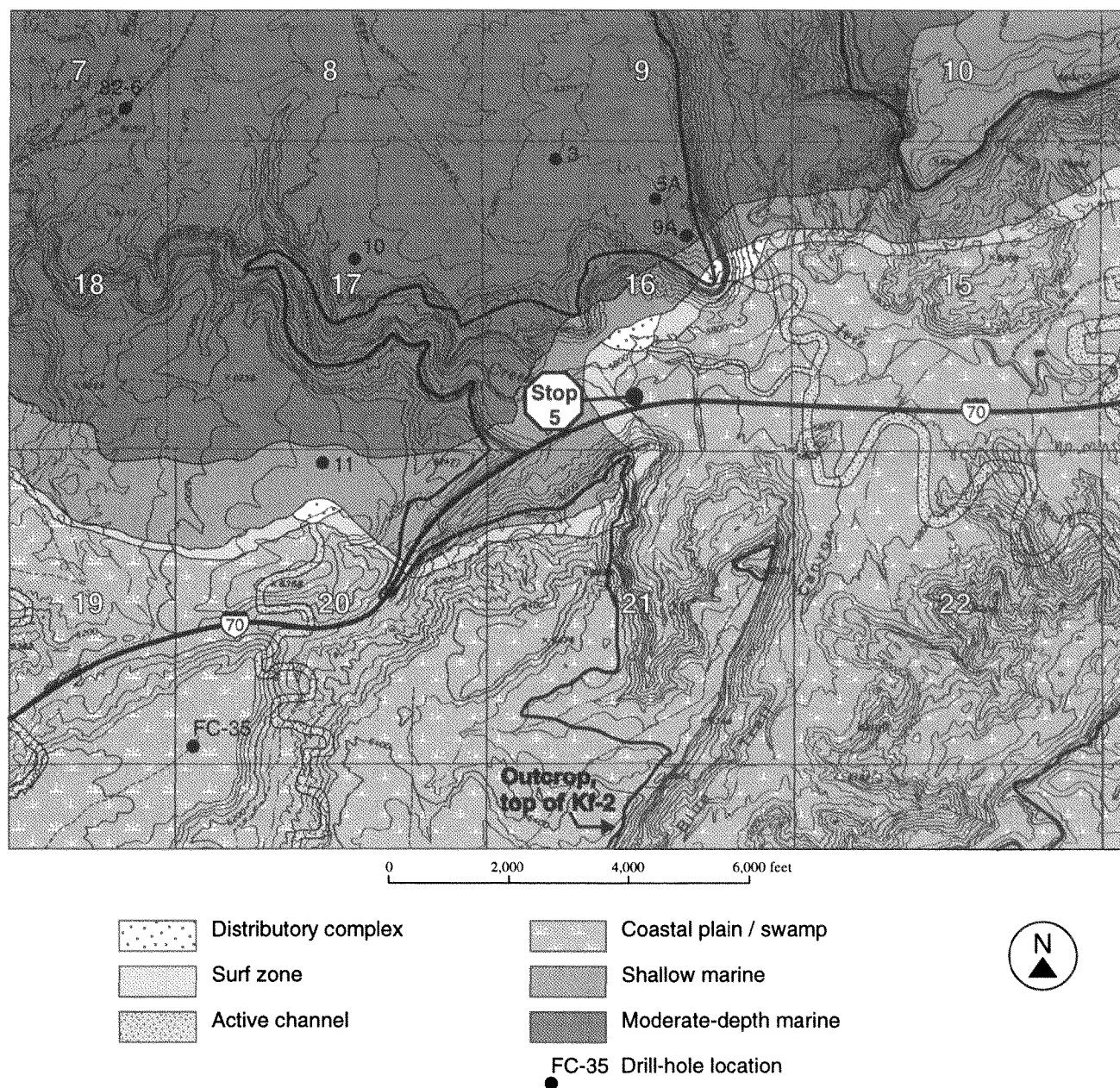


Figure 8. Paleogeographic interpretation of the third of five time steps of Kf-1-Iv-a parasequence in the Ivie Creek area. River channels flowing from the south and southeast deposited sands into a protected embayment in the northwest part of the area.

		ing a more wave-modified environment of deposition. Kf-1 is more heterolithic, indicating a fluvial-dominated environment of deposition.	
79.1	0.3	I-70 roadcut, Kf-1 (fig. 10)	
79.5	0.4	I-70 roadcut, sub-A coal, and Kf-2/Kf-1 contact on right.	
79.8	0.3	Note the landward pinchout of the marine	

		facies of Kf-2-Iv-c. By looking back toward the east, one can trace the rapid thickening of marine shoreface facies as the unit prograded to the east. Also note that the marine sandstone pinches out into coastal-plain facies of the A-coal zone C-coal zone with Kf-4 alluvial-plain facies above.	
79.9	0.1		



Figure 9. An east-west oriented photomosaic of the Ivie Creek amphitheater viewed from Stop 5 (view to the north), showing typical clinoform geometries in Kf-1-iv-a.



Figure 10. Photomosaic near I-70 at Stop 5, view to the south, showing both Kf-1 and Kf-2. A major distributary channel (center of photo) has cut down to near the base of Kf-2.

80.2	0.3	Large channel sandstone which created a split in I-coal zone on south side of I-70 (see Ryer and Langer, 1980).
80.7	0.5	Carbonaceous shale of the Ferron Sandstone and overlying Blue Gate Shale in roadcut on south side of I-70.
81.8	1.1	Sevier/Emery County line.
82.5	0.7	Walker Flat.
84.4	1.9	Deep roadcut in Blue Gate Shale.
84.9	0.5	Junction with Utah Highway 10. Leave I-70 and turn left (south).
85.0	0.1	Continue south off pavement towards Willow Springs.
86.9	1.9	Bear right (south) at the V in the road.
89.3	2.4	Entering Willow Springs Wash. Begin stratigraphic descent through alluvial-plain facies equivalent with Kf-3 through Kf-8. See van den Bergh (1995) and van den Bergh and Sprague (1995) for an attempt at correlating parasequence sets into the alluvial-plain facies.
90.2	0.9	Little dug-out building on left side of road is one of several relicts left from an old mine in the A-coal zone. The A-coal zone achieves its greatest thickness in this area and to the south.
90.8	0.6	STOP 6. Willow Springs Wash/Indian Canyon: sequence stratigraphy and depositional environments of Kf-1 and Kf-2 (fig. 11).

Kf-2 is found on the north side of Willow Spring Wash, at its mouth. The landward edge of the marine facies of Kf-2 is present in the same area, a short distance east of a large channel cut into Kf-1 called the "County Line channel" (Anderson, 1991). Thickening of the unit toward

the northeast onto the point that lies north of the mouth of the wash occurs rapidly, surprisingly so since the amount of overall climbing of Kf-2 from here to where it passes beyond the seaward edge of Kf-1 is relatively small. It is possible that the rapid thickening of Kf-2 is related to truncation by eroding channels. The landward pinchout of the marine facies is cut by a shale-filled channel, possibly of tidal origin. The original depositional limit of Kf-2 marine facies is likely farther to the west. The seaward extent of Kf-2 has not yet been determined, but it probably is present in the Molen Reef area about 30 miles (48 km) to the northeast. Along the east-facing cliffs, about 0.5 mile (0.8 km) north of Willow Springs Wash, the top of Kf-2 has been eroded and replaced by predominantly fine-grained deposits, some of which include "inclined heterolithics" indicative of channel deposition. This scour may be related to the areally more restricted scour that is present near the pinchout. The facies content of this shoreline unit is a wave-modified coast, probably a strand plain.

Indian Canyon, south of Willow Springs Wash, contains excellent exposures of Kf-1. Kf-1 is divided into four mappable units, Kf-1-Indian Canyon-a through d (Kf-1-IC-a through d), which display a forward-stepping arrangement. The transgressive (or "flooding") surfaces that separate the parasequences are overlain, at least in part, by mudstone units that may act as permeability barriers between sandstone bodies. Rocks in these units contain prodeltaic; lower, middle, and upper shoreface; foreshore; and fluvial-dominated delta-front deposits.



Figure 11. The "County Line channel" (view to the east) of Kf-1 in the Willow Springs Wash area at Stop 6 (mile 90.8). The channel is very late Kf-1 aged but older than the upper portion of the sub-A coal. The channel is about 60 feet (18 m) thick where it cuts into the uppermost parasequence of Kf-1.

91.1	0.3	View of Indian Canyon to the west.
91.5	0.4	View of Henry Mountains to the south.
92.2	0.7	Junction of Mussentuchit and Last Chance Roads. Bear right towards Last Chance. View to the north of Kf-2 (on the south-facing side of Willow Springs Wash). Here one can see an important trend in the seaward-stepping Kf-2 of the Ferron Sandstone. Note the thickening and increase in sandy facies in Kf-2 from west to east. This trend is readily observable in the Willow Springs Wash, and Quitcupah to Molen Reef areas. There is a corresponding east to west increase in the presence of "cannibalization" of delta-front sandstones by meanderbelt and distributary systems. These phenomena could be explained by a migrating flexure line of subsidence with time from west to east. West of the flexure line the basin is being uplifted, while east of the line the basin subsides. This creates more accommodation space on the east and increased cannibalization of previously deposited delta-front units on the west. This localized and subtle subsidence is superimposed onto a general sea-level rise through Kf-2 deposition.
96.2	4.0	Limestone Cliffs. The type section of Kf-LC is at Last Chance Creek and to the north into the next canyon. The shoreline unit, together with overlying Kf-1 (non-marine facies), forms vertical cliffs approximately 200 feet (60 m) high. Kf-LC dis-

96.6 0.4

98.3 1.7

111.9 13.6

145.7 33.8

MILEAGE
Cumulative Interval

0.0 0.0

33.8 33.8

42.2 8.4

44.6 2.4

plays inclined bedsets that appear to onlap or possibly downlap against a surface that may represent a paleotopographic high, resulting in very rapid seaward thinning to a feather edge. The high may represent the upthrown side of a down-to-the-west fault that was active during Ferron deposition. A problem with this interpretation is that the thick section represented by Kf-LC can be mapped as having a north-west-southeast trend based on limited subsurface data, whereas faults that formed along the eastern hinge of the foredeep would be expected to have a north-south orientation. No contemporaneous channel deposits have yet been identified.

Last Chance anticline. Descend through the Cretaceous Cedar Mountain Formation, and Jurassic Morrison, Summerville, Curtis, Entrada, and Carmel Formations. A minor amount of gas was produced from fractured zones in the Triassic Moenkopi Formation along the crest of the structure. Note the northwest-trending dike on the west side of the road.

Turn around in center of Last Chance anticline and return to I-70.

Junction with I-70. Turn west onto I-70 towards Salina.

Enter Salina. End of Day 1.

ROAD LOG

Second Day

Leave Salina east on I-70.

Junction of I-70 with Utah Highway 10.

Ranch Exit 97. Leave I-70. Turn left (north), crossing I-70. Return west-bound I-70 towards Salina.

Ivie Creek Amphitheater. Turn off I-70, driving down slight embankment. We will begin our day hike into the Ivie Creek amphitheater and lower canyon areas. Moderate to strenuous climbing will be required over the 2.5 mile (4.0 km) hike. Cross fence that runs along I-70 and proceed down steep embankment. Cross Ivie Creek and climb slight embankment on the north side. Proceed along trail

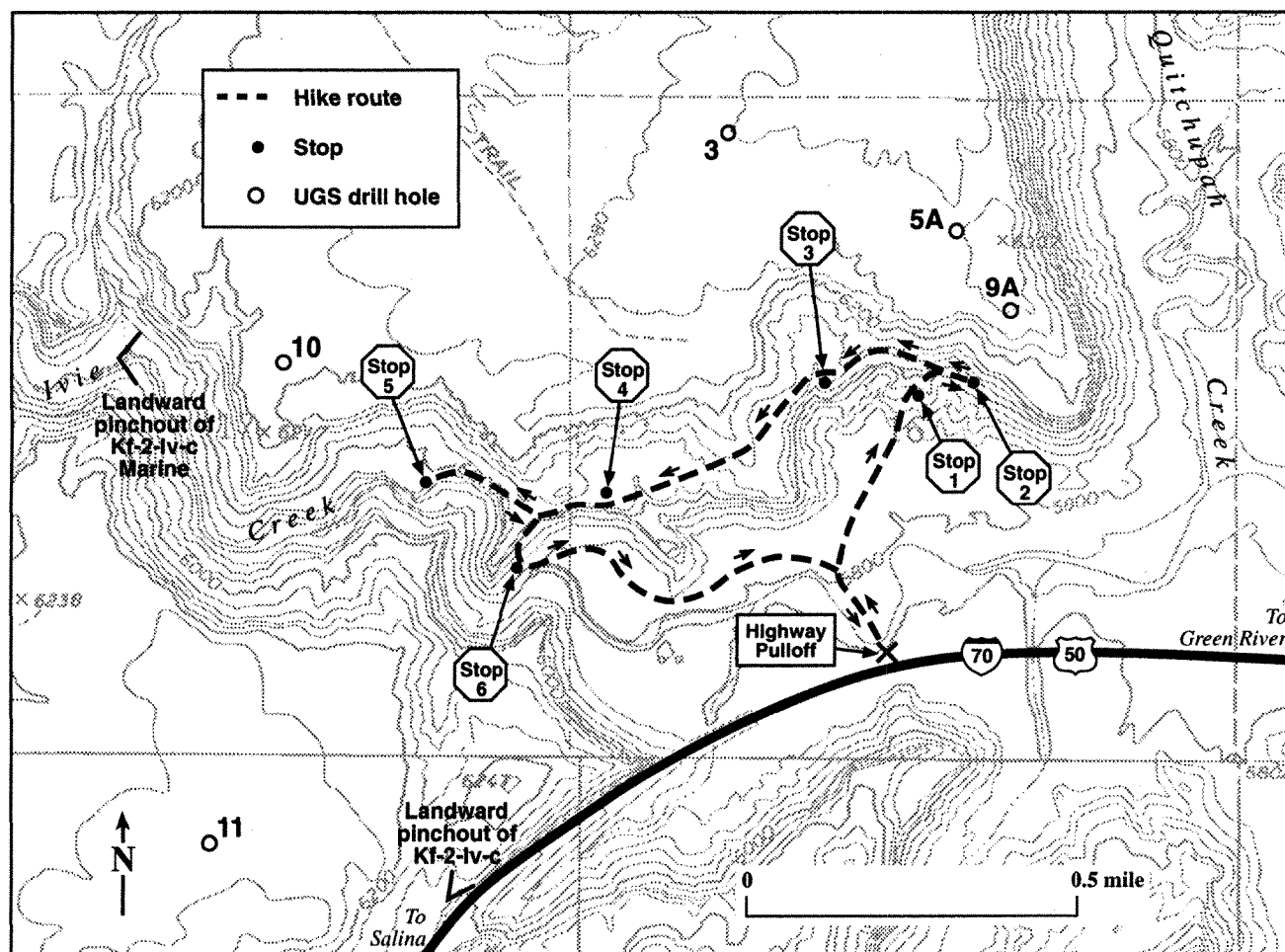


Figure 12. Index map to the Ivie Creek area showing topography, hike route, and stops. Base map from U.S. Geological Survey Mesa Butte and Walker Flats 7.5' topographic maps; contour interval is 40 feet (12 m).

towards the Ivie Creek amphitheater to the northwest following the map in fig. 12 to the base of Kf-1-Iv-a. Begin ascending up a steep slope in the Tununk Shale following the measured section on fig. 13.

IVIE CREEK HIKE—STOP 1: Climoform Facies of Kf-1-Iv-a

The clinoform section of Kf-1-Iv-a (fig. 9) is classified into four facies: clinoform proximal (cp), clinoform medial (cm), clinoform distal (cd), and clinoform cap (cc). Facies cp, cm, and cd are assigned to clinoforms only, and facies cc is a capping facies above the clinoforms (fig. 14). The cc facies is the result of reworking the tops of the clinoforms and the addition of new sediment.

Facies cp is mostly fine- to medium-grained sandstone. The chief sedimentary structure is low-angle cross-stratifi-

cation with minor horizontal and trough cross-stratification and rare hummocky bedding. The facies is dominantly thick to medium bedded, well to moderately indurated, with permeabilities ranging from 2 to 600 millidarcies (mD) and a mean of about 10 mD. The inclination of bed boundaries is generally greater than 10° . This facies is interpreted to be the highest energy and most proximal to the sediment input point. The steep inclinations are interpreted to represent deposition into a relatively localized deep area in an open bay environment. The dominance of low-angle cross-stratification with inclinations within the bed or clinoforms in an up-depositional dip direction indicates the influence of on-shore wave energy.

Facies cm is dominantly sandstone with about 5 percent shale. The sandstone is primarily fine-grained with slightly more fine- to very-fine-grained than fine- to medium-grained. Horizontal beds dominate with some rippled,

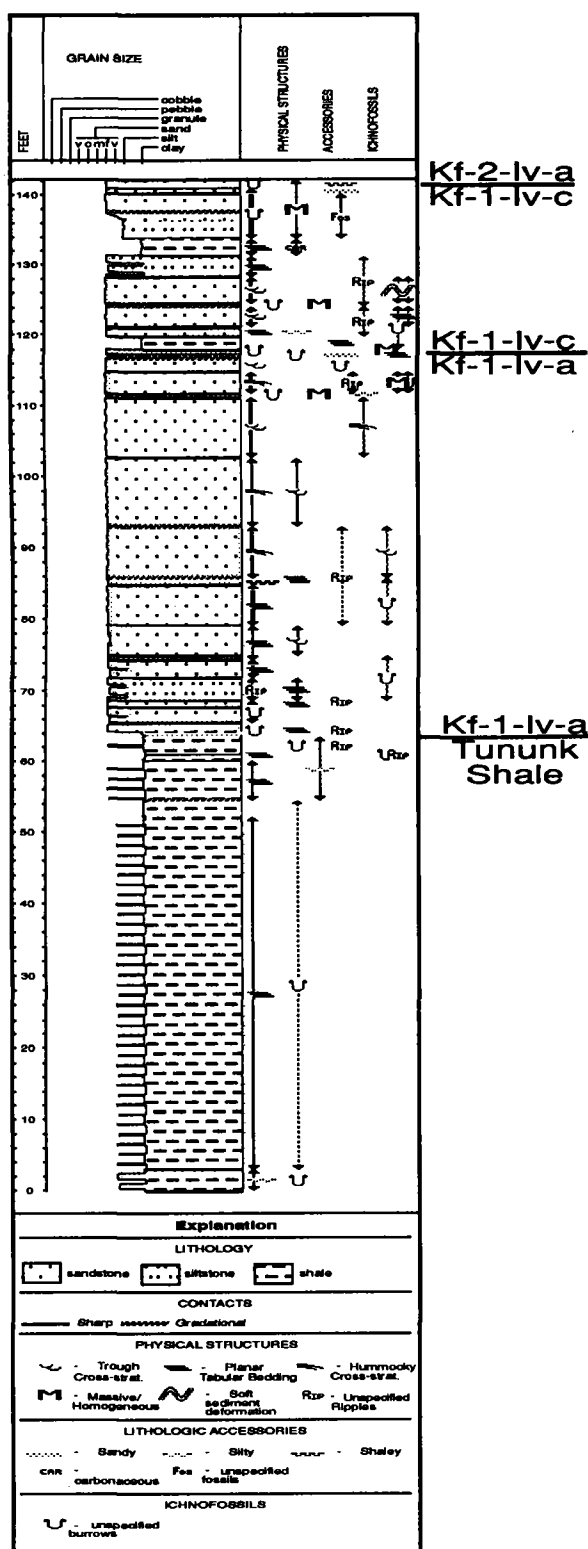


Figure 13. Stratigraphic section from the Ivie Creek amphitheater of Kf-1 (originally at a scale of 1 inch = 10 feet [2.54 cm = 3 m]) showing lithology, nature of contacts, sedimentary structures, ichnofossils, and parasequence designations.

trough and low-angle cross-stratification. Bed thicknesses range from laminated to very thick, but most are medium. The beds are generally well to moderately indurated, but are occasionally friable. The permeability values range from non-detectable to 100 mD with the mean about 3 mD. Inclination on the clinoform boundaries is between 2 and 10°. Facies cm is generally transitional between facies cp and cd, but occasionally is present at the erosional truncation or offlapping boundary of the clinoforms, with no visible connection to facies cp.

Facies cd is sandstone (sometimes silty) with about 10 percent shale. The sandstone grain size is dominantly fine- to very-fine-grained, with considerable variation. Sedimentary structures in this facies are chiefly horizontal laminations and ripples in medium to thin beds. The beds range from well indurated to friable. Average facies cd permeability is just at the instrument detection limit of 2 mD, but ranges up to 80 mD. This facies is gradational with facies cm and represents the deepest water and lowest energy deposition within the clinoform. It can be traced distally into prodelta to offshore facies.

Facies cc consists of very-fine- to fine-grained, thick- to medium-bedded sandstone. The beds are horizontal, with some trough and low-angle cross-stratification. Burrows and other trace fossils are rare. The sandstone is mostly well indurated, with permeabilities ranging from non-detectable to 100 mD with a mean of about 2 mD. This facies is present stratigraphically above the truncated clinoforms near the top of the parasequence and where bed boundaries show little to no inclination. The cc facies is interpreted to represent an eroded and reworked delta top.

Figure 8, the paleogeographic interpretation, represents the third step of the five depositional time steps of Kf-1-iv-a. The main delta lobe was located to the east and north-east. That delta lobe allowed a protected embayment to develop in the northwest part of the Ivie Creek area. The clinoforms represent deposition into the embayment fed by river channels from the southeast.

IVIE CREEK HIKE—STOP 2: Bounding Surfaces of Kf-1-iv-a and Depositional Environments of Kf-1-iv-c

Fluid-flow communication likely occurs between clinoforms (or parasequences) where shales are absent due to erosion or non-deposition. Porosity and permeability values, dependent on facies distribution, vary laterally and vertically within a clinoform. Bounding surfaces between clinoforms designated proximal or medial facies contain two common lithologic elements: (1) finer-grained, poorer cemented, and less resistant lithology than the overlying and underlying units, and (2) laminations of carbonaceous material which are consistently poorly cemented and become planes of

weakness which are expressed in the recessive outcrops of the bounding surfaces. Most of the bedding in the bounding surfaces is horizontal to slightly irregular. On occasion clearly recognizable wave-ripple laminations are found along with some flaser bedding. Often some portion of the bounding surface contains gypsum veinlets.

Bounding surfaces found associated with a proximal-to-proximal facies contact are generally somewhat thinner than those associated with a medial-to-medial facies contact. Lithologically, the contact in the proximal facies is sandier and thinner, but where the bounding surface is fairly thick (>0.30 feet [10 cm]) it shows an increase in finer-grained rocks. The amount of silt and shale within the bounding surface is related more to the thickness of the surface than the over- and underlying facies designations. The distal facies in the clinoforms are all similar in permeability and essentially act as strong baffles or barriers to flow.

Kf-1-Iv-c is capped by unidirectional, trough-cross-bedded sandstone. Above the cross-bedded sandstone are 10 to 15 feet (3–6 m) of bay-fill deposits. These deposits consist of carbonaceous mudstone; thin, rippled-to-bioturbated sandstone and siltstone; fossiliferous mudstone to sandstone; oyster coquina; and ash-rich coal. Although not mapped, the upper portion of this bay to coastal-plain interval is related younger marine progradations or parasequences found north and east of the Ivie Creek area.

IVIE CREEK HIKE—STOP 3: Sequence Stratigraphy and Depositional Environments of Kf-2

The base of Kf-2-Iv-a consists of interbedded sandstones and shales in prodelta to lower shoreface environments. In some places along the basal contact of the parasequence a thin (1 foot [0.3 m]) bed of transgressive deposits is present. Kf-2-Iv-a shoals to middle shoreface. The flooding surface and parasequence boundary is difficult to recognize because there is no offset in facies. The overlying Kf-2-Iv-b is also middle shoreface. Kf-2-Iv-a becomes thin and unrecognizable a short distance to the east. Kf-2-Iv-b exhibits gently seaward inclined beds which are very conspicuous when viewed east along the outcrop. The parasequence has at least two sub-cycles of grain size coarsening and bed thickening upward. These units are intensely bioturbated.

Kf-2-Iv-c is separated from the underlying Kf-2-Iv-b by a siltstone to shale interval which varies in thickness across the Ivie Creek area. Generally the entire parasequence fines from west to east. In the Ivie Creek amphitheater, Kf-2-Iv-c is interpreted as a bay-fill deposit (although it is devoid of body fossils). At the top of the sequence is a thin, medium-grained carbonaceous sandstone which may represent the migration of a low-energy beach (foreshore de-

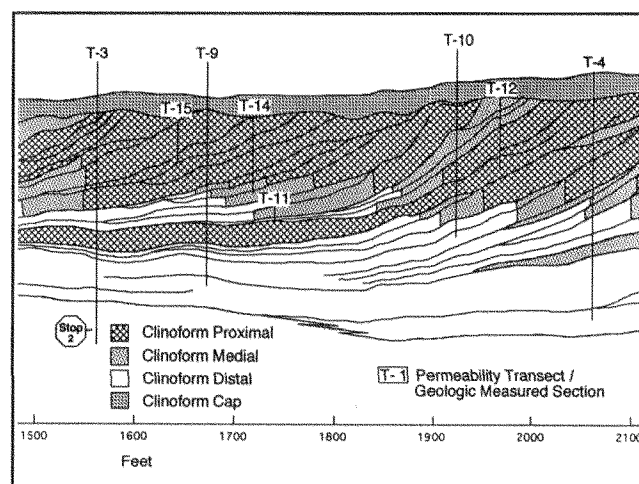


Figure 14. Scaled cross section, oriented west to east, showing clinoform facies assigned to Kf-1-Iv-a from the Ivie Creek amphitheater based on a portion of the interpreted photomosaic. Vertical lines represent permeability transect and measured section locations.

posits) across the bay fill prior to capping by coastal-plain deposits and deposition of the overlying A-coal zone (which is locally burned).

IVIE CREEK HIKE—STOP 4: Lateral Facies Changes in Kf-2

Kf-2-Iv-a is thicker here than at our last stop. It consists of a thin sequence of lower shoreface heterolithics overlain by about 28 feet (8.5 m) of middle-shoreface deposits.

Kf-2-Iv-b consists of horizontally bedded, silty sandstone at the base and unidirectional, trough-cross-bedded sandstone toward the top. In a road cut along I-70 and in Ivie Creek Canyon, this unit displays trough sets which become horizontally bedded in a down-dip direction (east). These deposits are interpreted as mouth-bar deposits.

The type area of Kf-2-Iv-c is the mouth of Ivie Creek Canyon. This unit undoubtedly warrants designation as a parasequence inasmuch as the associated transgressive surface is clearly recognizable both in Ivie Creek Canyon and to the south in the I-70 roadcut. The landward pinchout of the marine facies of Kf-2-Iv-c is found northwest of this stop (see fig. 12) and trends just slightly east of south toward I-70. The shoreline sandstone unit displays some interesting and unusual changes at the mouth of Ivie Creek Canyon, changing over about 300 feet (90 m) from a strongly wave-modified shoreface unit to a much lower wave energy unit that contains mud interbeds and finer sand, and that has a silvery-gray color on outcrop. This change suggests a change from a coast directly facing the sea to one that was

sheltered from wave energy. The facies content of this shore-line unit is a wave-modified coast, probably shoreface in the proximal part, transforming to a low-wave-energy bay. There is evidence for bay-head deltas and tidal channels feeding the bay to the northeast, in Quitcupah Canyon.

IVIE CREEK HIKE—STOP 5: Shoreface Deposition of Kf-2-Iv-a, b and c

Kf-2-Iv-a is exposed in the vertical cliff at the base of Kf-2. At this location, a distributary channel deposit has cut into the upper half of the shoreface deposits. The coarser (medium-grained) channel is easy to distinguish from the darker-colored shoreface deposits.

Kf-2-Iv-b (fig. 15) is dominated by unidirectional, trough-cross-bedded sandstone of the mouth-bar complex which continues farther up the canyon and is present in core from the UGS drill hole No. 11 0.5 mile (0.8 km) to the southwest. This stop offers an opportunity to walk through Kf-2-Iv-b and c.

Kf-2-Iv-c forms the 10-foot (3.1-m) cliff at the top of the alcove. Excellent upper-shoreface facies are exposed. The top of the unit is rooted by the overlying coastal-plain vegetation. Root casts are commonly visible at the top of this unit. Just a few tens-of-feet up the canyon from the stop, there is a thin, but well developed, carbonaceous shale at the top of Kf-2-Iv-b, with the flooding surface for Kf-2-Iv-c immediately above.

IVIE CREEK HIKE—STOP 6: Distributary Channels and Rotated Blocks in Kf-1

Kf-1-Iv-a now lies several tens-of-feet below the parasequence boundary. Recall that it filled an embayment and was sourced from the south to the southeast. Kf-1-Iv-c has thickened dramatically from our first stop. Here it is anomalously thick due to large slump features or rotated blocks. Failure of the rotated blocks is consistently toward the north to northwest, the direction that the delta lobe appears to have prograded. The abundance of rotated blocks, which are relatively rare entities elsewhere in the Ferron, in this particular area may be related to a zone of flexure. Tilting toward the northwest may have encouraged failure of the delta-front. Rotated blocks are also present in the lowest parasequence of Kf-2 in the Coal Cliffs south of Miller Canyon and in the lower part of Muddy Creek Canyon.

Kf-1-Iv-c has onlapped Kf-1-Iv-a. It represents a slightly younger episode of progradation filling space that Kf-1-Iv-a delta left unfilled, likely due to avulsion of the sediment source.

On return to the vehicles, note the cross-sectional view of a channel in Kf-1-Iv-c on the second point east of here.

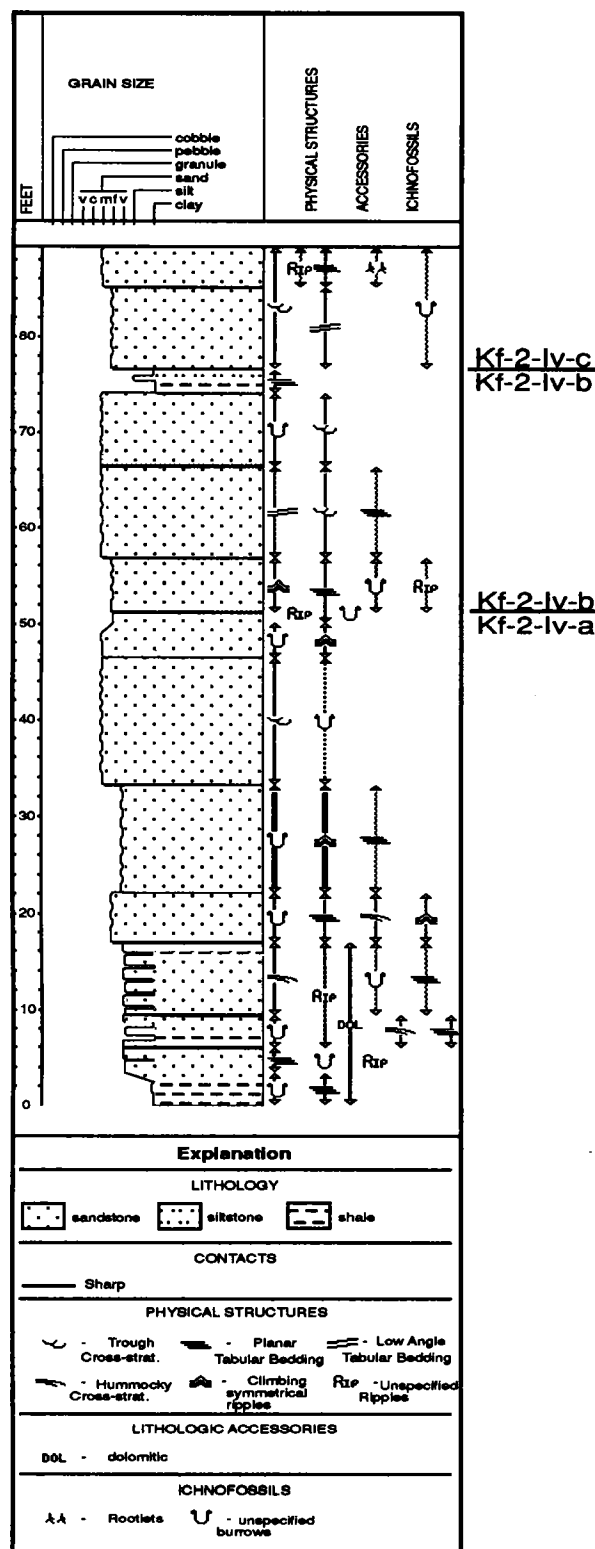


Figure 15. Stratigraphic section from Ivie Creek Canyon of Kf-1 and Kf-2 (originally at a scale of 1 inch = 10 feet [2.54 cm = 3 m]) showing lithology, nature of contacts, sedimentary structures, ichnofossils, and parasequence designations.

End of Day 2. Return to vehicles. Go westbound on I-70 to junction with Utah Highway 10. Return to Salt Lake City via Price on U.S. Highway 6.

ACKNOWLEDGMENTS

This research is part of an ongoing Utah Geological Survey project entitled *Geological and Petrophysical Characterization of the Ferron Sandstone for 3-D Simulation of a Fluvial-deltaic Reservoir*, M.L. Allison, Principal Investigator. The project is being funded by the U.S. Department of Energy (DOE) under the Geoscience/Engineering Reservoir Characterization Program of the DOE National Petroleum Technology Office, Tulsa, Oklahoma, contract number DE-AC22-93BC14896. The Contracting Officer's Representative is Robert Lemmon.

We thank the Mobil Exploration/Producing Technical Center and Amoco Production Company for their technical and financial support of the project. We also thank the following individuals and organizations for their technical contributions to this work: R.L. Bon, Brigitte Hucka, D.A. Sprinkel, D.E. Tabet, Kevin McClure, Jim Parker, K.A. Waite, S.N. Sommer, R.D. Adams, and M.D. Laine of the Utah Geological Survey, Salt Lake City, UT; M.A. Chan, C.B. Forster, Richard Jarrard, Ann Mattson, and S.H. Snelgrove of the University of Utah, Salt Lake City, UT; J.A. Dewey, Jr., and T.H. Morris of Brigham Young University, Provo, UT; J.V. Koebbe of Utah State University, Logan, UT; Don Best, Bruce Welton, F.M. Wright III of Mobil Exploration/Producing Technical Center, Dallas, TX; and R.L. Chambers, Chandra Rai, and Carl Sondergeld of Amoco Production Company, Tulsa, OK.

Finally, we thank Paul K. Link, Idaho State University, James G. Garrison, Jr. and T.C.V. van den Bergh, The Ferron Group Consultants, L.L.C., and Bryce T. Tripp and Mike Hylland, Utah Geological Survey, for their careful review and constructive criticism of the manuscript.

REFERENCES CITED

- Adams, R.D., 1995, The Cretaceous Ferron Sandstone of east-central Utah: a tale of three different morphologies for deltaic parasequences [abs.]: American Association of Petroleum Geologists Bulletin, v. 79, no. 6, p. 914.
- Adams, R.D., Chidsey, T.C., Jr., and Laine, M.D., 1995a, Integrated multi-disciplinary reservoir characterization of a deltaic system-1: architecture and facies of the Cretaceous-age Ferron Sandstone, east-central Utah [abs.]: 1995 Annual Convention of the American Association of Petroleum Geologists, Official Program, p. 1A.
- Adams, R.D., Snelgrove, S.H., and Forster, C.B., 1995b, A methodology for obtaining detailed geologic descriptions to constrain 3-D reservoir fluid-flow simulation models in delta-front facies [abs.]: American Association of Petroleum Geologists Bulletin, v. 79, no. 6, p. 914.
- Allison, M.L., 1995, Geological and petrophysical characterization of the Ferron Sandstone for 3-D simulation of a fluvial-deltaic reservoir—annual report for the period September 29, 1993 to September 29, 1994: U.S. Department of Energy, DOE/BC/14896-6, 49 p.
- Anderson, P.B., 1991, Comparison of Cretaceous landward pinch-outs of nearshore sandstones: wave- versus river-dominated deltas, east-central Utah, in Chidsey, T.C., Jr., editor, *Geology of east-central Utah*: Utah Geological Association Publication 19, p. 283–299.
- Anderson, P.B., 1993, Stratigraphic and sedimentologic characteristics of the lower portion of the Ferron Sandstone Member of the Mancos Shale along a portion of Muddy Creek, Emery County, Utah [abs.]: American Association of Petroleum Geologists Bulletin, v. 77, no. 8, p. 1441.
- Anderson, P.B., and Ryer, T.A., 1995, Proposed revisions to parasequence-set nomenclature of the Upper Cretaceous Ferron Sandstone Member of the Mancos Shale [abs.]: American Association of Petroleum Geologists Bulletin, v. 79, no. 6, p. 914–915.
- Anderson, P.B., Ryer, T.A., and Chidsey, T.C., Jr., 1996, Ferron Sandstone—stratigraphy and reservoir analogs, east-central Utah [abs.]: American Association of Petroleum Geologists Bulletin, v. 80, no. 6, p. 965.
- Barton, M.D., 1997, Sequence stratigraphic relationships within the Ferron Sandstone, central Utah [abs.]: American Association of Petroleum Geologists Annual Convention, Program with Abstracts, p. A8–A9.
- Barton, M.D., and Angle, E.S., 1995, Comparative anatomy and petrophysical property structure of seaward- and landward-stepping deltaic reservoir analogs, Ferron Sandstone, Utah: Gas Research Institute Topical Report GRI—95/0167, 59 p.
- Bunnell, M.D., 1991, Field symposium road log—Fremont Junction to Price, in Chidsey, T.C., Jr., editor, *Geology of east-central Utah*: Utah Geological Association Publication 19, p. 377–381.
- Chidsey, T.C., Jr., 1995, Geological and petrophysical characterization of the Ferron Sandstone in Utah, for 3-D simulation of a fluvial-deltaic reservoir [abs.]: American Association of Petroleum Geologists Bulletin, v. 79, no. 6, p. 916.
- Chidsey, T.C., Jr., and Allison, M.L., 1996, Geological and petrophysical characterization of the Ferron Sandstone for 3-D simulation of a fluvial-deltaic reservoir—annual report for the period October 1, 1994 to September 30, 1995: U.S. Department of Energy, DOE/BC/14896-13, 104 p.
- Chidsey, T.C., Jr., 1997, Geological and petrophysical characterization of the Ferron Sandstone for 3-D simulation of a fluvial-deltaic reservoir—annual report for the period October 1, 1995 to September 30, 1996: U.S. Department of Energy, in press.
- Cotter, Edward, 1975a, Deltaic deposits in the Upper Cretaceous Ferron Sandstone, Utah, in Broussard, M.L.S., editor, *Deltas, models for exploration*: Houston Geological Society, p. 471–484.
- Cotter, Edward, 1975b, Late Cretaceous sedimentation in a low-energy coastal zone: the Ferron Sandstone of Utah: *Journal of Sedimentary Petrology*, v. 45, p. 15–41.
- Dewey, J.A., Jr., Morris, T.H., and Ryer, T.A., 1995, Constraining reservoir models of fluvial- vs. wave-dominated delta-front sandstones through high resolution and high density sequence stratigraphic analysis, Ferron Sandstone, Utah [abs.]: American Association of Petroleum Geologists Bulletin, v. 79, no. 6, p. 917.
- Gardner, M.H., 1991, Siliciclastic facies architecture in foreland basin clastic wedges—field guide to the Ferron Sandstone Member of the Mancos Shale, east-central Utah: Boulder, Colorado School of Mines, unpublished report, 35 p.
- Gardner, M.H., 1993, Sequence stratigraphy of the Ferron Sandstone (Turonian) of east-central Utah: Boulder, Colorado School of Mines Ph.D. dissertation, 406 p.
- Gardner, M.H., 1995, The stratigraphic hierarchy and tectonic history of the mid-Cretaceous foreland basin of central Utah, in Dorobek, S.L., and Ross, G.M., editors, *Stratigraphic evolution of foreland basins*:

- SEPM (Society for Sedimentary Geology) Special Publication No. 52, p. 283–303.
- Gustason, E.R., 1993, Facies architectural analysis of progradational parasequence sets, upper coal-bearing Ferron Sandstone, central Utah: implications for reservoir description [abs.]. American Association of Petroleum Geologists Bulletin, v. 77, no. 8, p. 1450.
- Hucka, B.P., Sommer, S.N., Sprinkel, D.A., and Tabet, D.E., 1995a, Ferron Sandstone drill-hole database, Ferron Creek to Last Chance Creek, Emery and Sevier Counties, Utah. Utah Geological Survey Open-File Report 317, 1130 p., 9 pl.
- Hucka, B.P., Sommer, S.N., Sprinkel, D.A., and Tabet, D.E., 1995b, Ferron Sandstone drill-hole strip logs, Ferron Creek to Last Chance Creek, Emery and Sevier Counties, Utah: Utah Geological Survey Open-File Report 331, 1417 p., 2 volumes.
- Lupton, C.T., 1916, Geology and coal resources of Castle Valley in Carbon, Emery, and Sevier Counties, Utah. U.S. Geological Survey Bulletin 628, 88 p.
- Mattson, Ann, and Chan, M.A., 1996, Facies relationships and statistical measures for reservoir heterogeneities in the Cretaceous Ferron Sandstone, central Utah [abs.]: American Association of Petroleum Geologists Annual Convention, Program with Abstracts, p. A93.
- Rigby, J.K., Hintze, L.F., and Welsh, S.L., 1974, Geologic guide to the northwestern Colorado Plateau. Provo, Utah, Brigham Young University Geology Studies, v. 21, pt. 2, p. 79–93.
- Ryer, T.A., 1981, Deltaic coals of Ferron Sandstone Member of Mancos Shale: predictive model for Cretaceous coal-bearing strata of western interior. American Association of Petroleum Geologists Bulletin, v. 65, no. 11, p. 2323–2340.
- Ryer, T.A., 1982, Possible eustatic control on the location of Utah Cretaceous coal fields, in Gurgel, K.D., editor, Proceedings of the 5th symposium on the geology of Rocky Mountain coal. Utah Geological and Mineralogical Survey Bulletin 118, p. 89–93.
- Ryer, T.A., 1993, The Upper Cretaceous Ferron Sandstone of central Utah: an overview [abs.]. American Association of Petroleum Geologists Bulletin, v. 77, no. 8, p. 1459.
- Ryer, T.A., and Langer, A.W., 1980, Thickness change involved in the peat-to-coal transformation for a bituminous coal of Cretaceous age in central Utah. Journal of Sedimentary Petrography, v. 50, no. 3, p. 987–992.
- Ryer, T.A., and McPhillips, Maureen, 1983, Early Late Cretaceous paleogeography of east-central Utah, in Reynolds, W.M., and Dolly, E.D., editors, Mesozoic paleogeography of the west-central United States: SEPM (Society of Sedimentary Geology), Rocky Mountain Section, Rocky Mountain Paleogeography Symposium 2, p. 253–272.
- Ryer, T.A., and Lovekin, J.R., 1986, The Upper Cretaceous Vernal delta of Utah—depositional or paleotectonic feature?, in Peterson, J.A., editor, Paleotectonics and sedimentation in the Rocky Mountain region, United States: American Association of Petroleum Geologists, Memoir 41, p. 497–510.
- Ryer, T.A., and Anderson, P.B., 1995, Parasequence sets, parasequences, facies distributions, and depositional history of the Upper Cretaceous Ferron deltaic clastic wedge, Utah [abs.]. American Association of Petroleum Geologists Bulletin, v. 79, no. 6, p. 924.
- Ryer, T.A., Dewey, J.A., Jr., and Morris, T.H., 1995, Distinguishing allocyclic and autocyclic causes of parasequence-level cyclicity—lessons from deltaic strata of the Upper Cretaceous Ferron Sandstone, central Utah [abs.]: American Association of Petroleum Geologists Bulletin, v. 79, no. 6, p. 924.
- Snelgrove, S.H., Forster, C.B., and Koebe, J.V., 1995, Integrated multidisciplinary reservoir characterization of a deltaic system-2. developing a petrophysical model for reservoir simulation using data from the Ferron Sandstone, Utah [abs.]. 1995 Annual Convention of the American Association of Petroleum Geologists, Official Program, p. 90–91A.
- Snelgrove, S.H., Forster, C.B., Mattson, Ann, and Chan, M.A., 1996, Impact of facies architecture and distribution on fluid flow: examples from the Cretaceous Ferron Sandstone, east-central Utah [abs.]. American Association of Petroleum Geologists Annual Convention, Program with Abstracts, p. A132.
- van den Bergh, T.C.V., 1995, Facies architecture and sedimentology of the Ferron Sandstone Member of the Mancos Shale, Willow Springs Wash, east-central Utah. Madison, University of Wisconsin M.S. thesis, 255 p.
- van den Bergh, T.C.V., and Sprague, A.R., 1995, The control of high-frequency sequences on the distribution of shoreline and fluvial reservoir facies: an example from the Ferron Sandstone, Utah [abs.]. 1995 Annual Convention of the American Association of Petroleum Geologists, Official Program, p. 99A.
- Van Wagoner, J.C., Mitchum, R.M., Campion, K.M., and Rahmanian, V.D., 1990, Siliciclastic sequence stratigraphy in well-logs, cores, and outcrop. American Association of Petroleum Geologists Methods in Exploration Series 7, p. 1–55.
- Williams, G.D., and Stelck, C.R., 1975, Speculation on the Cretaceous paleogeography of North America, in Caldwell, W.G.E., editor, The Cretaceous System in the western interior of North America. Geological Association of Canada Special Paper 13, p. 1–20.

Depositional Sequence Stratigraphy and Architecture of the Cretaceous Ferron Sandstone: Implications for Coal and Coalbed Methane Resources—A Field Excursion

JAMES R. GARRISON, JR.

T.C.V. VAN DEN BERGH

The Ferron Group Consultants, L.L.C., P.O. Box 117, Emery, Utah 84522

CHARLES E. BARKER

United States Geological Survey, P.O. Box 25046, Denver, Colorado 80225

DAVID E. TABET

Utah Geological Survey, P.O. Box 146100, Salt Lake City, Utah 84109

ABSTRACT

This Field Excursion will visit outcrops of the fluvial-deltaic Upper Cretaceous (Turonian) Ferron Sandstone Member of the Mancos Shale, known as the Last Chance delta or Upper Ferron Sandstone. This field guide and the field stops will outline the architecture and depositional sequence stratigraphy of the Upper Ferron Sandstone clastic wedge and explore the stratigraphic positions and compositions of major *coal zones*. The implications of the architecture and stratigraphy of the Ferron fluvial-deltaic complex for coal and coalbed methane resources will be discussed.

Early works suggested that the southwesterly derived deltaic deposits of the the upper Ferron Sandstone clastic wedge were a Type-2 third-order depositional sequence, informally called the Ferron Sequence. These works suggested that the Ferron Sequence is separated by a type-2 sequence boundary from the underlying 3rd-order Hyatti Sequence, which has its sediment source from the northwest. Within the 3rd-order depositional sequence, the deltaic events of the Ferron clastic wedge, recognized as parasequence sets, appear to be stacked into progradational, aggradational, and retrogradational patterns reflecting a generally decreasing sediment supply during an overall slow sea-level rise. The architecture of both near-marine facies and non-marine fluvial facies exhibit well defined trends in response to this decrease in available sediment.

Recent studies have concluded that, unless coincident with a depositional sequence boundary, regionally extensive *coal zones* occur at the tops of the parasequence sets within the Ferron clastic wedge. These *coal zones* consist of coal seams and their laterally equivalent fissile carbonaceous shales, mudstones, and siltstones, paleosols, and flood plain mudstones. Although the compositions of coal zones vary along depositional dip, the presence of these laterally extensive stratigraphic horizons, above parasequence sets, provides a means of correlating and defining the tops of depositional parasequence sets in both near-marine and non-marine parts of fluvial-deltaic depositional sequences. Ongoing field studies, based on this concept of *coal zone* stratigraphy, and detailed stratigraphic mapping, have documented the existence of at least 12 parasequence sets within the Last Chance delta clastic wedge. These parasequence sets appear to form four high frequency, 4th-order depositional sequences. The dramatic erosional unconformities, associated with these 4th-order sequence boundaries, indicate that there was up to 20–30 m of erosion, signifying locally substantial base-level drops. These base-level drops were accompanied by a basinward shift in paleo-shorelines by as much as 5–7 km. These 4th-order Upper Ferron Sequences are superimposed on the 3rd-order sea-level rise event and the 3rd-order, sediment supply/accommodation space driven, stratigraphic architecture of the Upper Ferron Sandstone. The fluvial deltaic architecture shows little response to these 4th-order sea-level events.

Coal zones generally thicken landward relative to the mean position of the landward pinch-out of the underlying parasequence set, but after some distance landward, they decrease in thickness. *Coal zones* also generally thin seaward relative to the mean position of the landward pinch-out of the underlying parasequence set. The coal is thickest in the region between this landward pinch-out and the position of maximum zone thickness. Data indicate that the proportion of coal in the *coal zone* decreases progressively landward from the landward pinch-out. The effects of differential compaction and differences in original pre-peat swamp topography have the effect of adding perturbations to the general trends. These coal zone systematics have major impact on approaches to exploration and production, and the resource assessment of both coal and coalbed methane.

INTRODUCTION

This Field Excursion is conducted in the northwestern portion of the Colorado Plateau in East-central Utah (fig. 1). Here uplift and erosion of the broad north-northeast-trending anticlinal structure of the San Rafael Swell along the northwestern margin of the Colorado Plateau exposes Cretaceous rocks. The focus of this Field Excursion will be the outcrops of the fluvial-deltaic Upper Cretaceous (Turonian) Ferron Sandstone Member of the Mancos Shale (fig. 2).

This field guide is organized in a fashion as to provide the field trip participant, and future workers in the Ferron Sandstone, with a comprehensive database and detailed field trip guide. A general introduction to the geology and stratigraphy of the Ferron Sandstone is presented and the major studies, that have contributed to our general understanding of the stratigraphy of the Ferron Sandstone, have been discussed to provide a general background. Any omissions of previous works are due to unintentional oversights. This field guide has at its core, the recent and ongoing studies of Garrison and van den Bergh (e.g., van den Bergh, 1995; Garrison and van den Bergh, 1996; 1997; van den Bergh and Garrison, 1996). The results of these studies, up to the time of the printing of this guidebook, are compiled and are included below in a short paper.

A detailed road log, through the outcrop belt of the Ferron Sandstone, is provided below. Each day of the two day field trip has its own road log. Each of the road logs starts and end in Price, Utah. The road logs attempt to provide the reader with geological, geographical, and cultural information, in hopes that the excursion through the Ferron Sandstone outcrops in the Castle Valley will both enjoyable and informative. The detailed discussions of the geology of each days field trip stops are presented separately from the road logs. They can be found immediately following each day's road log. This is done, first, to make it easier for the reader to follow the road log without interruptions, and secondly, to make it more easy to obtain the key points and background geology for each field trip stops. In order to preserve continuity and to have both the paper of Garrison and van den Bergh and the field trip stop descriptions able to stand alone, the reader may find some information, pre-

sented by Garrison and van den Bergh, reiterated in the field trip stop descriptions.

Energy Resources in Fluvial-deltaic Reservoirs

Fluvial-deltaic sandstones, such as the Ferron Sandstone, combined with their related strand-plain deposits, make up an estimated 45% of world's oil and gas reservoirs. The Ferron Sandstone produces natural gas; cumulative production exceeds 128 BCF (Laine and Staley, 1991), with a cumulative production of 8.8 MMCF from the Ferron Gas Field alone. In addition, the coals of the Ferron Sandstone have been targeted for coalbed methane production, resulting in a cumulative production of over 30 BCF of coalbed methane.

Most of the worlds coal reserves occur in fluvial-deltaic facies associations, such as the Ferron Sandstone. The Ferron Sandstone coals are analogous to, and similar in occurrence to, the coals of many coal fields in the eastern United States, Europe, Asia, and Australia. The Upper Ferron Sandstone of the Emery Coal Field has itself produced as much as 600,000 tons/year of bituminous B rank coal. Total cumulative coal production from the Emery Coal Field exceeds 9.5 million tons (Jahanbani, 1996). It is estimated that the Emery Coal Field has reserves in excess of 2.15 billion tons (Doelling, 1972). The Ferron Sandstone is but one of several formations in the Cretaceous of Central Utah to produce coal. Estimates are that total coal production exceeds 22 million tons/year in the Emery, Book Cliffs, and Wasatch Plateau Coal Fields of Central Utah (Semborski, 1991).

Coal Correlation and Geometry as a Tool in the Energy Industry

In fluvial-deltaic facies associations, coals are ubiquitous, although many times discontinuous, lithostratigraphic horizons. There is a natural tendency to connect together these compact, lithologically unique beds in outcrop and subsurface correlations. In the coal mining and the petroleum industries, performing subsurface coal correlations is an every day event. Even after years of industry experience, many subsurface correlations can still be problematic. This

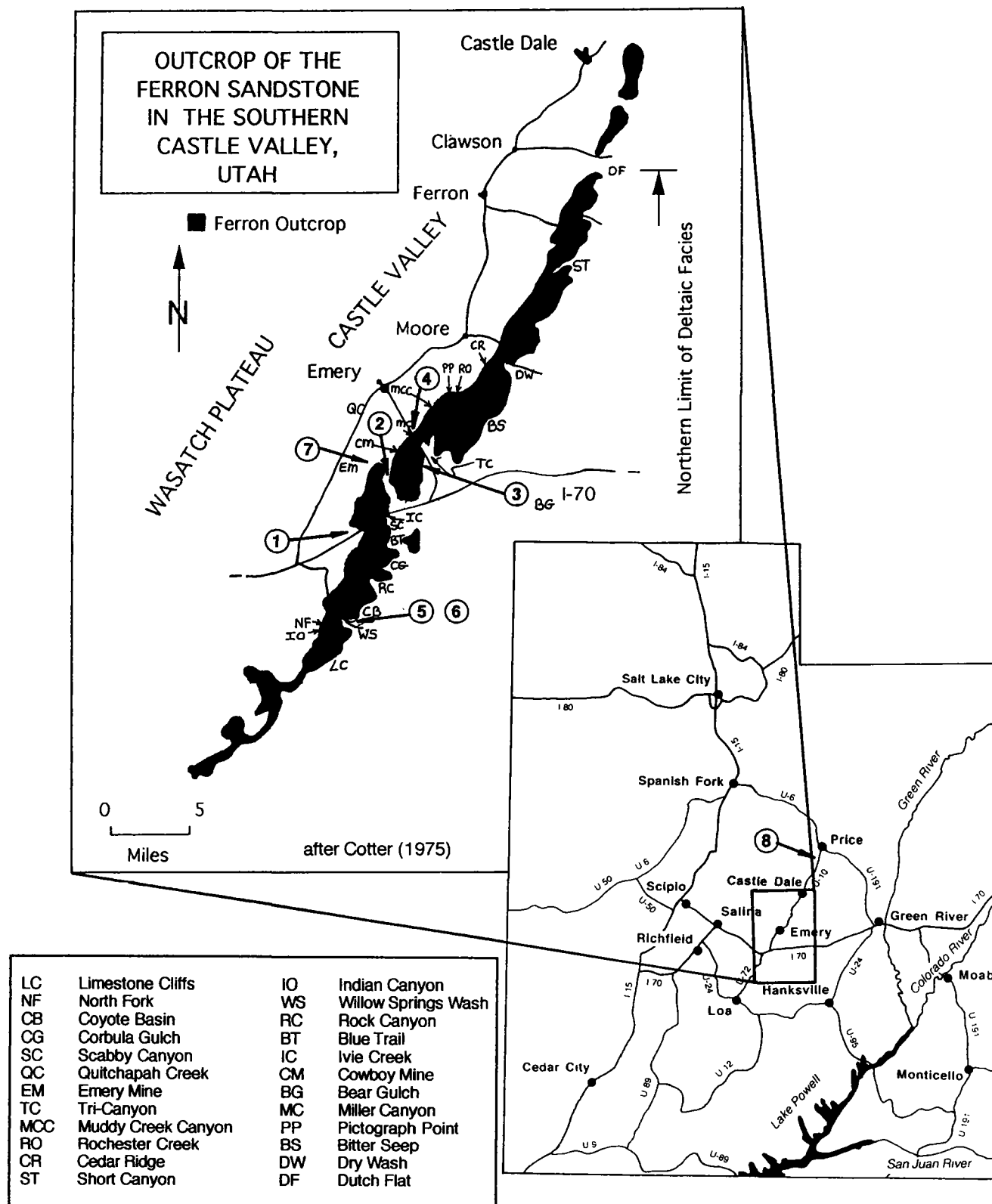


Figure 1. Location map for Ferron Sandstone outcrop belt and field trip stops.

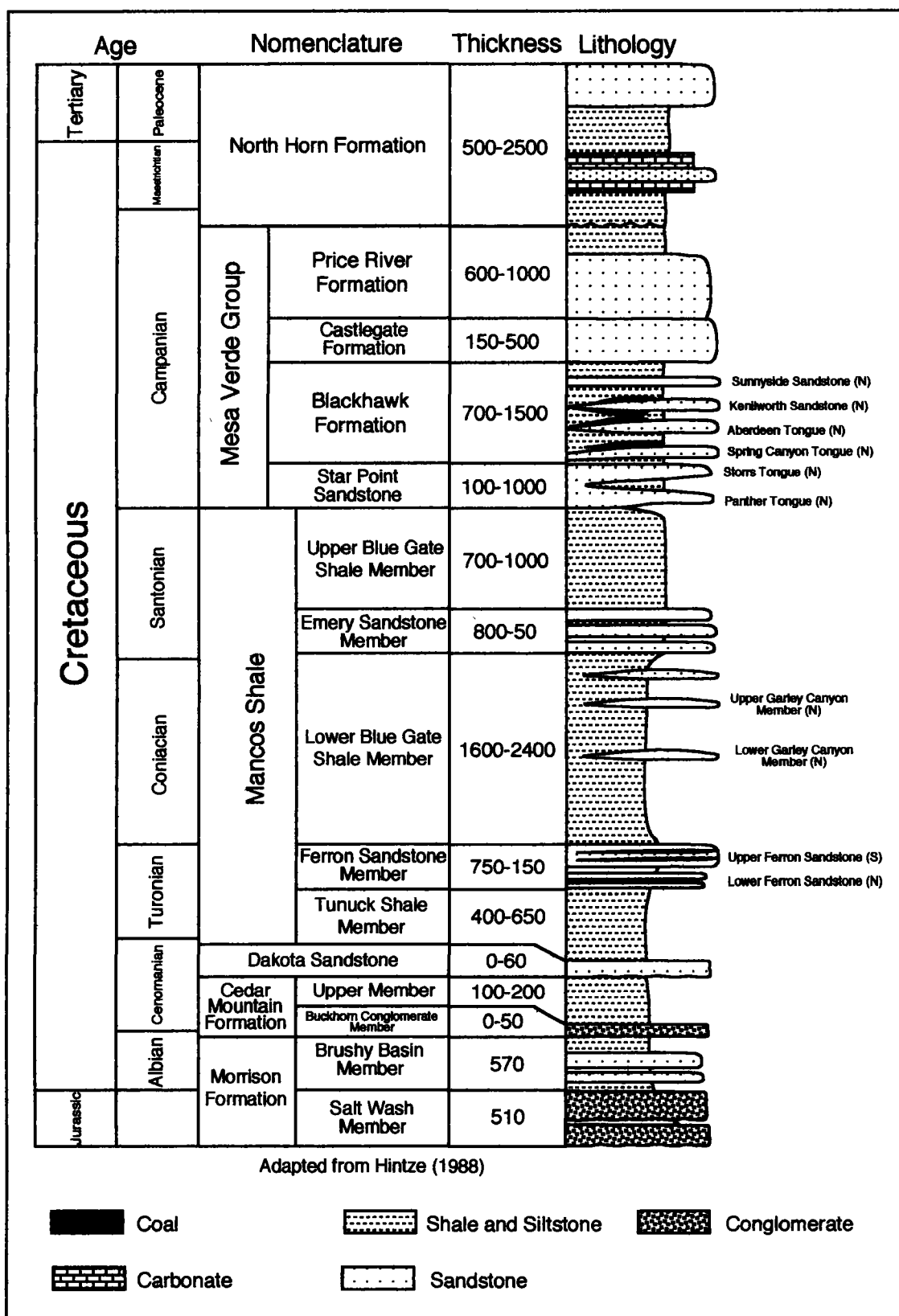


Figure 2. Stratigraphic column for the Cretaceous of the Castle Valley.

uncertainty introduces risk into exploration and production decisions. The desire to reduce this risk drives geologists to continue to investigate and to seek improved methodologies for making reliable subsurface correlations.

There appears to be a genetic relationship existing between the geometries of major coal beds and the geometries of the associated near-marine sediments in fluvial-deltaic deposits (e.g., see Ryer, 1981; Cross, 1988; Hamilton and Tadros, 1994). Numerous authors have proposed theories to utilize these relationships in lithostratigraphic, genetic sequence stratigraphic, depositional sequence stratigraphic, and/or regression/transgression sequence stratigraphic correlations (e.g., see Ryer, 1981; Cross, 1988; Hamilton and Tadros, 1994; Aitken, 1994; Ryer et al., 1980; Garrison and van den Bergh, 1996).

Garrison and van den Bergh (1996) outlined, in a case study within the Upper Ferron Sandstone, stratigraphic relationships existing between the geometries of major coal beds and the geometries of the associated near-marine and non-marine sediments in Ferron fluvial-deltaic deposits. They describe this approach as *coal zone* stratigraphy and outline its use in depositional sequence stratigraphy.

This field excursion will examine the use of *coal zone* stratigraphy in high-resolution depositional sequence stratigraphic correlations of the Upper Ferron Sandstone. The stratigraphic positions and compositions of the Ferron coal zones will be discussed, in the context of this stratigraphy. The implications of this stratigraphy for coal and hydrocarbon exploration and production will also be addressed.

GENERAL GEOLOGY AND STRATIGRAPHY OF THE FERRON SANDSTONE

Introduction

The Upper Cretaceous (Turonian) Ferron Sandstone Member of the Mancos Shale is one of several eastward thinning clastic wedges that prograded into the Mancos Sea along the western margin of the Interior Cretaceous Seaway, between 89 and 90 million years ago (Gardner, 1992). The Ferron deltaic complex was deposited into the Mancos Sea in response to the abundant supply of sediments shed from the thrust-faulted and uplifted Sevier Orogenic belt located to the west in southeastern Nevada, western Utah, and southern Idaho. It reaches a thickness of over 1100 feet in the western area beneath the Wasatch Plateau and extends over 10,500 square kilometers (Tripp, 1989). The Ferron Sandstone is exposed along the approximately 170 kilometer length of the northeasterly trending outcrop belt.

The Ferron Sandstone can be divided into two distinct clastic wedges (Ryer, 1981). The lower portion of the Ferron Sandstone is a thin, northerly derived storm- and wave-dominated shoreline/deltaic complex, informally called the Vernal delta. The upper portion of the Ferron Sandstone is

a younger, thicker, and more north-northeasterly prograding deltaic complex, informally called the Last Chance delta. The Last Chance deltaic complex is exposed along the outcrop belt generally parallel to the deltaic progradational direction. There is almost a complete 92 km long dip section exposure of the deltaic complex. The width of the outcrops of the Ferron Sandstone perpendicular to the trend of the outcrop belt is generally less than about 5 km, thus allowing very little opportunity to examine the deltaic deposits in the strike direction (Ryer, 1981) (fig. 1). In this discussion, only the upper clastic wedge of the Ferron Sandstone known as the Ferron Last Chance delta complex or the Upper Ferron Sandstone (Ryer, 1981) will be addressed, unless otherwise noted.

Stratigraphy

Ryer and McPhillips (1983) recognized that the Ferron deltaic complex was composed of sediments deposited during a series of transgressions and regressions of the Cretaceous shoreline. Ryer (1981; 1982) recognized five deltaic cycles within the Last Chance deltaic complex of the southern Ferron Sandstone outcrop belt. These delta-front sandstones were referred to as sandstones 1–5. Ryer (1981; 1982) noted that the delta-front sandstone 2 had both a seaward and landward limit displaced further seaward than delta-front sandstone 1 and that delta-front sandstones 3–5 each have seaward limits displaced successively landward. In a subsurface well-log study, Ryer and McPhillips (1983) identified delta-front sandstones 1–5 in the subsurface beneath the Castle Valley and the Wasatch Plateau. Subsequent work by Gardner (1992; 1993) and Ryer (1991) led to the identification of two more, stratigraphically higher, delta cycles in the outcrop belt, referred to as 6–7; both have seaward limits displaced successively landward. The Ferron Sandstone was subdivided into 7 major deltaic events (Gardner, 1992; 1993). Gardner also suggested that an eighth delta-front sandstone occurred in the subsurface further south. Gardner's eighth, subsurface, deltaic unit will not be discussed in this paper. Recent works have subsequently delineated an additional eighth delta-front sandstone in the outcrop belt.

Major coal beds occur within the Ferron sandstone complex and generally mark the top of the deltaic events. The coal nomenclature was first developed by Lupton (1916) and retained by Ryer (1981; 1982) and Gardner (1993). These coal beds can be easily correlated through the Ferron delta-front complex and can be further correlated as discontinuous zones of coal and carbonaceous shale into the distributary channel dominated delta-plain setting (Garrison and van den Bergh, 1996). Many of the major coal beds within the Ferron Sandstone contain one or more layers of kaolinitic/bentonitic material representing altered volcanic ash

falls (Ryer et. al., 1980). The coal beds together with altered volcanic ash layers can be generally used as chronostratigraphic indicators.

Sequence Stratigraphy—Historical Development

Gardner (1992; 1993) examined these deltaic events and placed them into a sequence stratigraphic framework. He recognized the upper portion of the Ferron Sandstone to be a Type-2 third-order depositional sequence, called the Ferron Sequence. A Type-2 sequence boundary is physically expressed by a downward shift in coastal onlap, onlap of overlying strata, and subaerial exposure with minor erosional truncation at the top or base of the progradational, parasequence set (Van Wagoner et. al., 1990). The southwesterly derived deltaic deposits of the 3rd-order Ferron Sequence contains *Scaphites ferronensis* and is separated by a type-2 sequence boundary from the underlying 3rd-order Hyatti Sequence, which contains the ammonite *P. hyatti* (Gardner, 1992). The Hyatti Sequence has its sediment source from the northwest (Gardner, 1993). Gardner (1993) places the sequence boundary at the base of the Upper Ferron Sandstone above the Hyatti condensed section. Ryer (1994) suggested that the fluvial-deltaic sandstones of the lower Ferron Sandstone (i.e., the Hyatti Sequence) probably formed in response to a dominantly eustatic sea level change. Leithold (1994) also suggested that the Hyatti Sequence (i.e., Lower Ferron Sandstone and its correlative siltstones and shales of the Tununk Member of the Mancos Shale) was formed as a result of a high frequency (i.e., 3rd-order) eustatic sea level change superimposed on the tectonically induced 2nd-order Greenhorn sea level cycle. Leithold (1994) also suggested that the Lower Ferron Sandstone, of the Hyatti Sequence, probably formed during the regressive phase of the Greenhorn sea level cycle (i.e., at the point of maximum sea level regression). Ryer (1994) postulated that the Upper Ferron Sandstone (i.e., the Ferron Sequence) probably formed in response to an increase in sediment supply associated with increased tectonic activity in the Sevier orogenic belt, during a period of slow sea level rise (i.e. during a 3rd-order slow sea level rise). These 3rd-order cycles are postulated to be on the order of 400,000 years in duration (Leithold, 1994).

Leithold (1994) hypothesized that the higher frequency Greenhorn events (i.e., parasequence sets and parasequences) are probably associated with local autocyclic events, although many of these events appear to be more basin-wide in extent and thus, may be associated with climatic changes or Malankovitch cycles. van den Bergh and Sprague (1995) and van den Bergh (1995) first discussed the possibility of additional high frequency (i.e., 4th-order) sequences within the 3rd-order Ferron Sequence deltaic complex.

Gardner (1992; 1993) described the individual deltaic events, within the 3rd-order Ferron Sequence, as genetic sequences (Galloway, 1989). Recent workers have described them as depositional parasequence sets (e.g., van den Bergh, 1995; Anderson and Ryer, 1995; Ryer and Anderson, 1995; Garrison and van den Bergh, 1996). After examining the seaward and landward limits of the delta-front complexes, Gardner (1993) recognized that genetic sequences 1–3 successively stepped seaward recording an overall regressive event and genetic sequences 4–7 recorded a relative transgression, with genetic sequences 4–5 being aggradational and genetic sequences 6–7 back-stepping sharply landward. Although described as depositional parasequence sets, the stacking pattern of the delta cycles was later confirmed by Ryer and Anderson (1995). van den Bergh and Sprague (1995) postulated that these parasequence sets may be grouped into high-frequency 4th-order depositional sequences within Gardner's 3rd-order Ferron Sequence.

Coals, where preserved within the Ferron Sandstone, generally occur below the flooding surface at the top of each of the delta cycle or parasequence sets (e.g., see Garrison and van den Bergh, 1996). Garrison and van den Bergh (1997) have noted that in a few instances, that in addition a transgressive lag or a high-order depositional sequence boundary may occur at the top of a parasequence set. Based on the Ferron *coal zone* stratigraphy and detailed stratigraphic mapping, Garrison and van den Bergh (1996; 1997) have subsequently documented the existence of at least 12 parasequence sets (i.e., including single hierarchically equivalent parasequences) which form four high frequency, 4th-order depositional sequences (fig.3). These 4th-order events are superimposed on the slow 3rd-order sea-level rise event discussed by Gardner (1993) and Leithold (1994). The work of Garrison and van den Bergh (1997) suggests that the 3 stratigraphically lowest parasequence sets, within the Ferron clastic wedge, may actually belong to the underlying 3rd-order Hyatti Sequence. Widespread condensed sections lie stratigraphically above (Garrison and van den Bergh, 1997) and below (Gardner, 1993) the Upper Ferron Sandstone clastic wedge.

COAL ZONE AND HIGH-RESOLUTION DEPOSITIONAL SEQUENCE STRATIGRAPHY AND ARCHITECTURE OF THE UPPER FERRON SANDSTONE

James R. Garrison, Jr. and T.C.V. van den Bergh

Introduction

In the petroleum industry, performing subsurface correlations is an every day event. Uncertainty in subsurface correlations introduces risk into exploration and/or production management decisions. The desire to reduce this risk drives

geoscientists to continue to investigate and to seek improved methodologies for making reliable subsurface correlations.

Coals are intuitively excellent stratigraphic correlation horizons because they are easily recognizable in outcrop, core, and on logs, they tend to be laterally extensive, and generally chronostratigraphic markers. In fluvial-deltaic facies associations, coal seams are ubiquitous, although many times discontinuous, lithostratigraphic horizons. There is an intuitive tendency to connect together these compact, lithologically unique beds in outcrop and subsurface correlation exercises.

There appears to be a clear genetic relationship between the geometries of major coal beds and the geometries of the associated near-marine sediments in fluvial-deltaic deposits. Numerous authors have proposed theories to utilize these relationships in lithostratigraphic, genetic sequence stratigraphic, depositional sequence stratigraphic, and/or regression/transgression sequence stratigraphic correlations (e.g., see Cross, 1988; Hamilton and Tadros, 1994; Ryer, 1981; Aitken and Flint 1994, 1995, van den Bergh, 1995; Garrison and van den Bergh, 1996). This paper details the high-resolution depositional sequence stratigraphy of the Upper Ferron Sandstone and outlines the ideas for the use of *coal zone* stratigraphy as a tool in high-resolution depositional sequence stratigraphic correlations, as proposed by Garrison and van den Bergh (1996).

Coal zones—An Extension of Coal Seam Stratigraphy

Flint et al., (1995), Aitken and Flint (1995), Gastaldo et al., (1993), Garrison and van den Bergh (1996) and van den Bergh (1995) have examined coal stratigraphy in a depositional sequence stratigraphic context. Aitken (1994) pointed out that in many situations coals may become thin and laterally restricted, commonly becoming poorly developed, with carbonaceous mudstones, shales, and siltstone and paleosols becoming more prevalent. The observation that coal seams, in the Ferron Sandstone, are commonly associated with carbonaceous siltstone and shales and paleosols, has suggested to the authors that *coal zones* (i.e. coals and their lateral equivalents) may prove useful tools in sequence stratigraphic correlations in fluvial-deltaic systems.

Garrison and van den Bergh (1996) define *coal zones* as coal seams and their laterally equivalent fissile carbonaceous mudstones, shales and siltstones, paleosols (e.g., rooted horizons), and flood plain mudstones. It should be noted that a *coal zone* may, vertically or laterally, consist of any combination of these components. This concept of *coal zones* has evolved as an outgrowth of the challenge of correlating coal horizons from within the lower delta plain/near-marine transition landward into the delta plain/alluvial plain environments. It is well known that lower delta plain coals are generally laterally extensive and thin, with

variable geometry, associated with back barrier environments, while coals in the upper delta plain to alluvial plain become thicker, more elongate, and associated with lacustrine and fluvial deposition systems (e.g., Fielding, 1985). This paper extends the well documented coal seam stratigraphy, as discussed above, to more non-marine, continental environments. Garrison and van den Bergh (1996) explain where these *coal zones* reside in the shoaling upward facies tracts outlined by Van Wagoner et. al. (1990) and developed a methodology for using *coal zones* in high resolution depositional sequence stratigraphy.

In the study of Garrison and van den Bergh (1996), a model was proposed in which peat accumulations and their laterally equivalent delta plain/alluvial plain facies associations, occur, generally time synchronously, in a variety of depositional situations ranging from back barrier (near-marine) peat swamps (i.e., generating true coal seams as defined by Hamilton and Tadros (1994) and Ryer, (1981)), to local to sub-regional ephemeral organic-rich swamp/lacustrine environments to very localized abandoned fluvial channel settings. All of these organic-rich peat or organic-rich mud accumulations are time synchronous, although not necessarily connected in space, either in elevation or geographic proximity. Ye (1995) also describes rooted paleosols that can also be correlated, for many kilometers, in fluvial flood-plain settings. This "South Louisiana" bayou/swamp model is most common in temperate to tropical delta plain and distal alluvial plain settings. Ryer (1981), McCabe (1993), Shanley and McCabe (1993), Cross (1988), and Vail (1987) have also discussed the occurrences of coal bearing strata in relation to their stratigraphic positions within a fluvial-deltaic sequence and hypothesized that the thickest accumulations of coal occur in areas landward of aggradational or landward-stepping shorelines.

The *coal zone* stratigraphic model has been successfully tested in a 3 km strike cross-section of the delta plain/alluvial plain facies association of the Ferron Sandstone. This *coal zone* correlation has also been further tested by constructing of a 40 km dip section, both north and south of the strike section, in the delta plain/alluvial plain to near-marine facies associations. It has been clearly demonstrated that coal seams occurring above near-marine parasequence sets are transitional into *coal zones* as they are traced landward into the non-marine facies associations (van den Bergh, 1995; Garrison and van den Bergh, 1996).

A Case Study in the Upper Ferron Sandstone

The Upper Cretaceous Ferron Sandstone Member of the Mancos Shale accumulated during late Turonian time as a series of river- and storm-dominated deltaic depositional episodes (e.g., see Ryer, 1981). Offshore marine, delta-front, delta-plain, and alluvial-plain depositional facies are

recognized within the Ferron delta complex. Ryer and McPhillips (1983) recognized that the Ferron deltaic complex was composed of sediments deposited during a series of transgressions and regressions of the Cretaceous shoreline of the Mancos Sea. The upper clastic wedge of the Ferron Sandstone, known as the Last Chance delta, can be subdivided into 7 major deltaic events (Ryer, 1991). Gardner (1993) described these deltaic events as genetic sequences. Recent workers have described them as parasequence sets (e.g., van den Bergh, 1995; Anderson and Ryer, 1995; Garrison and van den Bergh, 1996; 1997). Major coal beds occur within the Ferron Sandstone complex and, generally, mark the top of parasequence sets (van den Bergh, 1995; Garrison and van den Bergh, 1996). The coal nomenclature was first developed by Lupton (1916) and retained by Ryer (1981) and Gardner (1993). These coal beds can be easily correlated through the Ferron delta-front complex. Most of the major coal beds within the Ferron Sandstone contain one or more layers of kaolinitic/bentonitic material representing altered volcanic ash falls (Ryer et. al., 1980; Garrison and van den Bergh, 1996). The coals together with altered volcanic ash layers can be used as time line indicators.

The studies of Garrison and van den Bergh (1996; 1997) resulted in the construction of a short 3 km strike cross-section in Willow Springs Wash, Willow Springs Quadrangle, to document the uses of *coal zones* as tools for delineating parasequence sets in non-marine sections, and in the construction of a 40 km long sub-regional dip cross-section from the Limestone Cliffs, north of Last Chance Creek, to Dry Wash, in Willow Springs, Walker Flat, Mesa Butte, Emery East, and Short Canyon Quadrangles to test the *coal zone* stratigraphy model. The strike cross-section is based on 11 measured sections, seven of which are detailed sedimentological measured sections and four are geometric (i.e., only thicknesses of lithologic units are recorded with grain-size and sedimentary structures generalized). The dip cross-section is a projected 40 km long section based on 45 measured sections, five of which are geometric, and one core. The emphasis in the construction of these cross-sections was the application of *coal zone* stratigraphy and its relationship to the architecture and stacking patterns of parasequences and parasequence sets in a depositional sequence stratigraphic framework. Parasequence sets were delineated, and where possible, parasequences were broken out. The nature of the upper boundaries of parasequences and parasequence sets was determined.

The original delta cycle and/or genetic sequence and/or depositional sequence nomenclature (e.g., cycles 1–7, genetic sequences 1–7, and parasequence sets 1–7) is so prevalent in the literature (e.g., Ryer, 1991; Gardner, 1993; Ryer and Anderson, 1995; and Garrison and van den Bergh, 1996), that the authors have chosen to retain this numeric scheme in this study, although more than seven events have been

identified by the authors. How this will be accomplished is described below. For example, multiple parasequences identified within the original delta cycle 2 will be consecutively denoted as Parasequences 2a, 2b, 2c, etc. (Parasequence denoted as upper case). Furthermore, multiple parasequence sets identified within delta cycle 2 will be consecutively denoted as Parasequence Sets 2A, 2B, 2C, etc. (Parasequence Set denoted as upper case). This convention will retain the connection to the original Ferron nomenclature and make discussions of the newer depositional sequence stratigraphy easier. The only exception to this scheme is that the oldest identified parasequence in Parasequence Set 1 is given the non-sequential, designation of Parasequence 1z. This was done, in part, because its entire dip length has not yet been quantified in the studies of Garrison and van den Bergh (1996).

Ferron Sandstone Depositional Sequence Stratigraphy

These detailed cross-sections have delineated 12 parasequence sets within the Upper Ferron Sandstone (fig. 3). In the cross-sections, 12 near-marine parasequences have been identified within Ferron Parasequence Set 1 (denoted 1z, 1a–1k); 4 occur within Ferron Parasequence Set 2A (denoted 2a–2d). Parasequence Set 2B contains only Parasequence 2e. Parasequence Set 2C contains 5 parasequences (denoted 2f–2j). Parasequence Set 3 contains only two parasequences. Both Parasequence Sets 4A and 4B contains only one parasequence. Parasequence Set 5A contains 2 parasequences and Set 5B contains only one. Parasequence Set 6 contains one parasequence. Parasequence Set 7 contains 4 parasequences. Parasequence Set 8 contains two parasequences. The single parasequences of Parasequence Sets 2B, 4A, 4B, 5B, and 6 have been given hierarchical equivalence to a parasequence set. Parasequence Sets 3–8 are represented along the Ferron Sandstone outcrop belt as dominantly delta plain facies associations (fluvial channel belts, crevasse splays, delta plain mudstones, and carbonaceous shale/coals). Fluvial channel belts have width/thickness that varies as a function of parasequence set stacking pattern (van den Bergh and Garrison, 1996). These systematics are honored in the *coal zone* stratigraphy and parasequence set delineations.

The 12 parasequence sets form four high frequency, 4th-order depositional sequences (denoted FS1–4) (fig. 3). The lowest 4th-order sequence FS1 consists of three parasequence sets. FS2 also consists of three parasequence sets. FS3 consists of two parasequence sets and FS4 consists of four parasequence sets. In general, the 4th-order depositional sequences consist of progradational and/or aggradational parasequence sets, with the upper-most, highstand (back-stepped) parasequence set lying stratigraphically above a transgressive lag deposit. The upper boundaries of

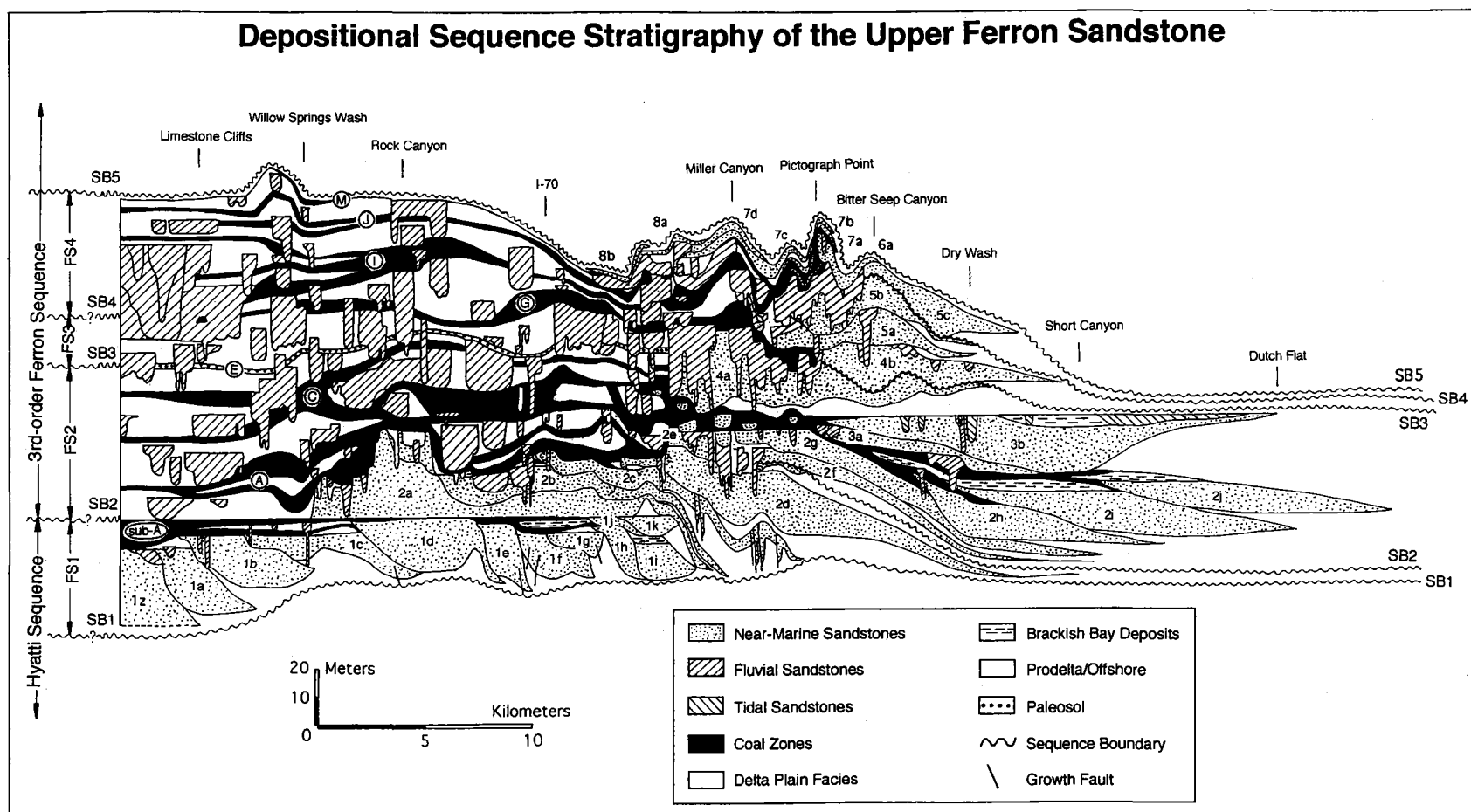


Figure 3. Cross-section showing the depositional sequence stratigraphy of the Upper Ferron Sandstone. Between Limestone Cliffs and the Emery Mine the datum is the top of the sub-A coal zone; from the Emery Mine to Pictograph Point the datum is the base of the composite A-C coal zone; from Pictograph Point to Dry Wash the datum is the top of the C coal zone/base of the transgressive lag at the top of Parasequence Set 3; north of Dry Wash the datum is the top of Parasequence Set 3.

parasequence sets, when not coincident with sequence boundaries, are *coal zones*.

The upper boundaries of 4th-order depositional sequences FS1, FS2, and FS3, are marked by regionally extensive erosional unconformities produced by major fluvial events that record major basinward shifts in depositional facies. It appears that erosion along these sequence boundary surfaces has removed most, if not all, of any previously deposited coals. The up-dip correlative surface of the upper boundary of FS2 is an extensive rooted zone in the non-marine part of the section. The up-dip correlative surfaces of FS1 and FS3 are still problematic. The lower boundary of FS1 is immediately above the Hyatti condensed section (Gardner, 1993) suggesting that it is actually a correlative conformity/condensed section boundary in this part of the basin. The upper boundary of FS4 is below a concretion-bearing condensed section a few m above the uppermost sandstones of FS4. Based on this interpretation, FS1 should probably be assigned to the 3rd-order Hyatti Sequence of Gardner (1993) and FS2, FS3, and FS4 assigned to the 3rd-order Ferron Sequence of Gardner (1993). FS1 would be the 4th-order highstand depositional sequence of the 3rd-order Hyatti Sequence. FS2 and FS3 would be the 4th-order progradational to aggradational sequences of the 3rd-order Ferron Sequence (i.e., representing a shelf-margin systems tract) and FS4 is the 4th-order transgressive depositional sequence of the Ferron Sequence. The 4th-order highstand sequence of the Ferron Sequence is not located in the study area, but is only represented by condensed section sediments.

Seaward-Stepping Parasequence Sets

In the context of the larger scale 3rd-order Ferron Sequence defined by Gardner (1992; 1993), each of the delta cycles represented by Ferron Parasequence Sets 1, 2A–2C, and 3 progressively step seaward. The landward pinch-out of the near-marine sandstones (i.e., location of paleo-shorelines) of each younger parasequence set is progressive further down-dip. Internally, within each of these parasequence sets, the parasequences themselves exhibit a progradational, seaward-stepping stacking pattern. *Coal zones* typically occur at or near the top of these depositional parasequence sets, with the thickest portion of the *coal zones* occurring near the landward pinch-out of the near-marine delta-front sandstones of the depositional parasequence sets. The sub-A *coal zone* caps Ferron Parasequence Set 1; the A *coal zone* caps Parasequence Set 2; the C *coal zone* caps Parasequence Set 3. It is common for these *coal zones* to split near the top of a depositional parasequence set.

Parasequence Set 1

Ferron Parasequence Set 1 contains at least 12 river-dominated, fluvial-deltaic parasequences (denoted 1z, 1a–1k),

that exhibit a seaward-stepping stacking pattern (fig. 3). Within Parasequence Set 1, the landward pinch-out of the near marine facies of each successively younger parasequence steps seaward by an average of about 2–5 km, relative to the landward pinch-out of the near marine facies of immediately underlying parasequence. The near-marine sandstones of Parasequence Set 1 extend at least 27 km in the dip direction.

The near-marine parasequences in Ferron Parasequences Set 1 exhibit both vertical and lateral facies changes from (1) stream mouth bar (SMB), to (2) proximal delta front (pDF), to (3) distal delta front (dDF), to (4) prodelta (PD) (figs. 4 and 5). Both proximal and distal delta front deposits, as denoted here, represent subdivisions of the distal bar facies of Ryer (1981). Distributary channels (DC) and delta plain (DP) facies associations are commonly present as well. Distal prodelta/shelf slumping, indicating instability as a result of rapid deposition, is common. Contorted bedding, flame structures, escape burrows, and the cannibalizing of distal stream mouth bar by proximal stream mouth bar (or distributary) channels also suggests generally a rapid rate of deposition (van den Bergh, 1995). In general, Parasequence Set 1 delta front deposits exhibit little to mild evidence of wave influence. They locally exhibit poorly developed hummocky stratification and only rare bi-directional ripple stratification.

Parasequences 1z–1d appear to represent a series of delta lobes prograding seaward in a northeasterly direction (25°–40° azimuth), each of which progressively steps seaward and rises stratigraphically relative to the immediately underlying parasequence. The outcrop belt is approximately along the depositional dip direction. The landward pinch-out of the near marine facies, of each successively younger parasequence, steps seaward by an average of about 2–5 km, relative to the landward pinch-out of the near marine facies of immediately underlying parasequence. The near-marine facies of Parasequences 1a, 1b, 1c, and 1d are approximately 4.9 km, 6.3 km, 8.4 km, and 7.5 km, in dip length, respectively, and maximum thicknesses are 24 m, 20 m, 10 m, and 17 m, respectively. Parasequence 1c is a composite delta with 2–3 mouth bars. Parasequences 1e, 1f, 1g, and 1i appear to have formed in response to the northwesterly (310°–335° azimuth) progradation of very small, river-dominated sub-delta lobes. The outcrop belt cuts these parasequences in a strike-oblique direction. Parasequences 1e, 1f, 1g, and 1i are approximately 2.9 km, 3.7 km, 2.7 km, and 2.5 km in strike width, respectively, and the maximum thicknesses are 22 m, 17 m, 9 m, and 13 m, respectively. Parasequence 1f appears to be a composite delta with two mouth bars. Parasequences 1h and 1k appear to represent small delta lobes prograding seaward in a northeasterly direction. Parasequence 1k pinches out into a split of the sub-A *coal zone*. The dip lengths of 1h and 1k are approxi-



Figure 4. Photograph of the Upper Ferron Sandstone Parasequence Set 1 at Ivie Creek/I-70 outcrop.

mately 2.5 km and 2.4 km and maximum thicknesses are 15 m and 7 m, respectively.

Parasequence 1j, occurs within a split in the sub-A *coal zone*, and is represented in the outcrop belt as a brackish water bay mudstone, to the south near I-70, and as a small 2.9 km, 3 m thick delta front sandstone body, to the north in Quitchapah Creek Canyon.

In the Limestone Cliffs, the sub-A *coal zone* is approximately 15 m thick and splits into two components denoted sub-A1 and sub-A2. The sub-A1 *coal zone* disappears in Coyote Basin and the Sub-A2 *coal zone* disappears in Rock Canyon. A *coal zone* stratigraphically equivalent to the Sub-A2 reappears in Blue Trail Canyon and splits into two components near I-70, where they are designated the sub-A3 and sub-A4. The sub-A3 and sub-A4 section of the sub-A *coal zone* extends some 8.5 km, from Blue Trail Canyon to North Quitchapah Creek. The total dip length for the sub-A *coal zone* is at least 27 km. In the Limestone Cliffs, the sub-A2 *coal zone* contains a very well-developed tonstein. This sub-A2 tonstein has not been identified further down-dip.

Parasequence Sets 2A, 2B, and 2C

Parasequence Set 2A contains 4 wave-modified, river-dominated parasequences (2a–2d), that exhibit a seaward-stepping stacking pattern (fig. 3). The near-marine sandstones of Parasequence Set 2A extend about 36 km in the dip direction. Parasequence 2e is hierarchically equivalent to a parasequence set and is placed in Parasequence Set

2B. Parasequence Set 2B is severely truncated by sequence boundary erosion, such that its true extent cannot be ascertained. Parasequence Set 2C contains 5 parasequences (2f–2j). The near-marine sandstones of Parasequence Set 2C extend about 29 km in the dip direction.

The near-marine parasequences in Ferron Parasequence Set 2A, 2B, and 2C all exhibit both vertical and lateral facies changes from (1) stream mouth bar and reworked stream mouth bar (frequently preserved as upper shoreface deposits (USF)), to (2) reworked delta front (pDF and dDF) (frequently preserved as middle (MSF) and lower shoreface (LSF) deposits), to (3) prodelta (figs. 6 and 7). South of Willow Springs Wash, distributary channels and delta plain facies associations are present as well. In general, Parasequence Set 2 stream mouth bar and distal bar (i.e., pDF and dDF) deposits exhibit evidence of moderate wave influence. The stream mouth bar deposits are frequently moderately burrowed (ichnofacies *Skolithos*) and may exhibit well-developed trough and herringbone stratification. The distal bar deposits are frequently moderately burrowed (ichnofacies *Skolithos* and *Cruziana*), but exhibit well-developed hummocky and planar stratification and bi-directional ripple-stratification (van den Bergh, 1995).

Parasequences 2a and 2b appear to represent large wave influenced, river-dominated delta lobes prograding seaward in a northeasterly direction. South of I-70, Parasequence 2a progrades northeast (034° azimuth) (van den Bergh, 1995). In the vicinity of I-70 and Ivie Creek, Parasequence 2a progrades northeast (025° azimuth). Parasequence 2b is actually

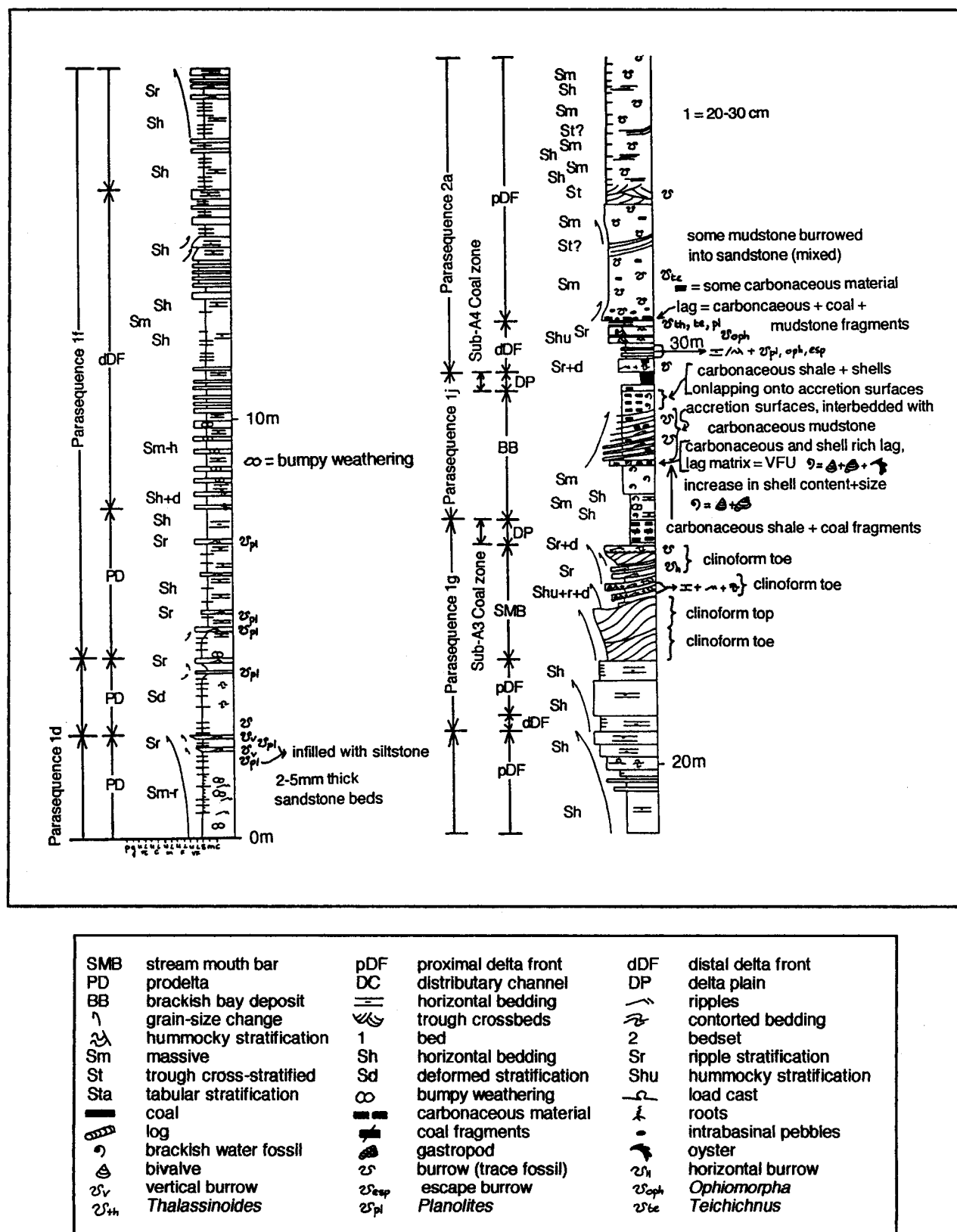


Figure 5. Measured section through the Upper Ferron Sandstone Parasequence Set 1 at the I-70 roadcut.

a composite delta lobe with a more easterly progradation direction. In the vicinity of Scabby Canyon and I-70, Parasequence 2b progrades northeast (045° azimuth). The landward pinch-out of the near-marine facies of Parasequence 2b steps seaward 3.5 km, relative to the landward pinch-out of the near-marine facies of the immediately underlying Parasequences 2a. Near-marine Parasequence 2c appears to be a deltaic lobe prograding northeast (025° azimuth) into a quiet brackish-water bay. The landward pinch-out of near-marine facies of Parasequence 2c occurs almost 7.5 km seaward of the landward pinch-out of the underlying Parasequence 2b. Parasequence 2d is a major delta lobe prograding northeast (050° azimuth). The landward pinch-out of Parasequence 2d steps seaward almost 2.7 km from the pinch-out of Parasequence 2c. There is slight stratigraphic rise associated with each seaward step. The near-marine facies of Parasequences 2a, 2b, 2c, and 2d are approximately 18.0 km, 15.1 km, 11.4 km, and 24.0 km in dip length, respectively and maximum thicknesses are 31 m, 16 m, 10 m, and 19 m, respectively.

Parasequence 2e has its landward pinch-out, in Quitchapah Creek Canyon, about 0.5 km seaward from the pinch-out of Parasequence 2d. In Bear Gulch, Parasequence 2e lies upon a highly bioturbated transgressive lag deposit. This transgressive lag deposit can be traced over 3 km northward into Muddy Creek Canyon, where it goes into the subsurface. Parasequence 2e has a very small stream mouth bar deposit and for much of its length. In Muddy Creek Canyon, it has distal delta front and prodelta facies lying stratigraphically above the stream mouth bar deposits of Parasequence 2d, suggesting a slight back-stepping relative to Parasequence 2d. Based on these observations, Parasequence 2e has been assigned to the stratigraphically higher Parasequence Set 2B. Due to severe degrees of erosional truncation by overlying fluvial deposits, it cannot be determined whether additional parasequences existed in Parasequence Set 2B prior to Parasequence Set 2C fluvial erosion.

From North Quitchapah Creek Canyon, near the Emery Mine, to Muddy Creek Canyon, Parasequence Set 2C consists of a major fluvial channel belt complex that incises up to 25 m deep into Parasequence 2A and 2B. South of I-70, this incision is represented only as an erosional unconformity, with up to 30 m of relief, as most of the sediment was by-passed some 5 km seaward to the northeast. This fluvial system marks a basinward shift of 3 km and a substantial base level fall. The wave-modified, river dominated, near-marine sandstones of Parasequence 2C, represented by Parasequences 2f, 2g, 2h, 2i, and 2j have their landward pinch-outs in South Muddy Creek Canyon, Muddy Creek Canyon, north of Bitter Seep Wash on the Molen Reef, Dry Wash, and near Short Canyon, respectively. Parasequences 2f and 2g are near vertically stacked. Parasequences 2h, 2i,

and 2j represent seaward steps of 6.7 km, 1.2 km, and 7.5 km respectively. The near-marine facies of Parasequences 2f, 2g, 2h, 2i, and 2j are approximately 16.2 km, 16.8 km, 11.6 km, 16.7 km, and 13.3 km in dip length, respectively and maximum thicknesses are 8 m, 10 m, 13 m, 15 m, and 11 m, respectively. Locally, in the Miller Canyon area, the upper part of Parasequence Set 2C contains small laterally restricted flood tidal delta deposits. These deposits are intimately associated with the A coal zone.

Parasequence Set 2C is capped by the A coal zone (fig. 3). In Blue Trail Canyon, the A coal zone splits into three components denoted A1, A2, and A3; the A1 coal zone disappears near I-70; only the A2 and A3 coal zones can be seen in Quitchapah Creek Canyon. In the region from just south of Bear Gulch to Muddy Creek, the A coal zone lies conformably below the C coal zone. The A coal zone extends over 40 km, from the Limestone Cliffs to just north of Dry Wash. Most of the coal deposited at the top of Parasequence Sets 2A and 2B was probably subsequently removed by erosion and is now represented only by the unconformity between FS1 and FS2. This will be discussed in more detail below.

Parasequence Set 3

Parasequence Set 3 contains 2 wave-modified, river-dominated parasequences, that exhibit an aggradational to seaward-stepping stacking pattern (fig. 3). The near-marine sandstones of Parasequence Set 3 extend about 22 km in the dip direction. Parasequence Set 3 contains 2 parasequences, denoted Parasequences 3a and 3b. In the southern half of the outcrop belt, Parasequence Set 3 is represented by non-marine delta plain facies associations composed of delta plain mudstones, large distributary channel belts, crevasse splay sandstones, over-bank deposits, and carbonaceous shales and siltstones.

The near-marine parasequences in Ferron Parasequence Set 3 exhibit both vertical and lateral facies changes from (1) stream mouth bar and reworked stream mouth bar (frequently preserved as upper shoreface deposits (USF)), to (2) reworked delta front (pDF and dDF) (frequently preserved as middle (MSF) and lower shoreface (LSF) deposits), to (3) prodelta. From Cedar Ridge Canyon to Dry Wash, Parasequence Set 3 also contains tidal inlet and channel deposits.

Parasequences 3a and 3b represent delta lobes with a general east-northeastern progradational direction (075° azimuth). This paleoshoreline is much north-south oriented (approximately 345° azimuth) than that of underlying and overlying parasequence sets. Parasequence 3a and 3b have near-marine facies that are 10.8 km and 20.8 km in dip length, respectively, and maximum thicknesses of 5 m and



Figure 6. Photograph of the Upper Ferron Sandstone Parasequence Set 2A at the I-70 roadcut.

16 m, respectively. Parasequence 3b steps seaward less 1 km relative to Parasequence 3a. Parasequence 3a steps landward 13 km relative to the youngest parasequence in Parasequence Set 2C.

Parasequence Set 3 is capped by the *C coal zone*. The *C coal zone* extends over 35 km from the Limestone Cliffs to its seaward pinch-out in Cedar Ridge Canyon. In Willow Springs Wash, the *C coal zone* splits into two components denoted C1 and C2; the *C2 coal zone* appears to not be present further down-dip than north Quitchapah Creek; the *C1 coal zone* locally splits into two components near Rock Canyon, but merges at Blue Trail Canyon and splits again at Ivie Creek, but merges again just south of Bear Gulch. The *C coal zone* has multiple tonstein layers. The *C2 coal zone* tonstein can be traced from Ivie Creek to its pinch-out in north Quitchapah Creek. The thickest tonstein in the *C1 coal zone* can be traced from Corbula Gulch, just south of Blue Trail, northward to northern portions of Muddy Creek, near Pictograph Point. Numerous smaller tonsteins can also be correlated from north of I-70 to Muddy Creek.

Aggradational Parasequence Sets

In the context of the larger scale 3rd-order Ferron Sequence defined by Gardner (1993), the delta cycles represented by Ferron Parasequence Sets 4A–4B and 5A–5B are essentially vertically stacked (i.e., aggradational) (fig. 3). In the southern 25 km of the outcrop belt, Parasequence Sets 4A, 4B, 5A, and 5B are represented by non-marine delta plain facies associations composed of delta plain mudstones, large distributary channel belts, crevasse splay sandstones, over-bank deposits, and carbonaceous shales and siltstones. *Coal zones* occur at or near the top of Parasequence Sets 4B and 5B, with the thickest portion of the *coal zones* occurring near the landward pinch-out of the near-marine delta-front sandstones. Parasequence Set 4B is capped by the *G coal zone* and Parasequence Set 5B is capped by the *I coal zone*. The near-marine facies of Parasequence Set 4A and 5A are sub-regionally bounded above by erosional unconformities representing 4th-order depositional sequence boundaries.

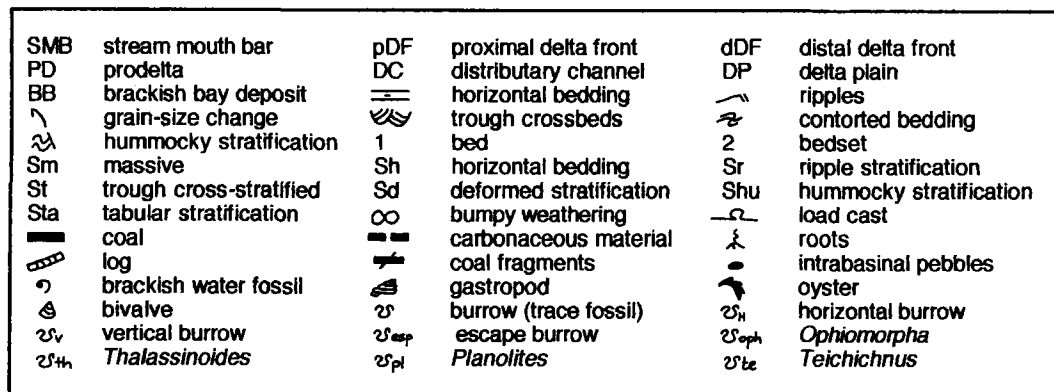


Figure 7. Measured section through the Upper Ferron Sandstone Parasequence Set 2A at the I-70 roadcut.

Parasequence Set 4A and 4B

Parasequence Sets 4A and 4B appears to contain only one parasequence (fig.3). The near-marine facies of the single parasequence in each Parasequence Sets 4A and 4B represent wave-dominated, wave-reworked delta front deposits. Near-marine facies of the parasequences in Parasequence 4a is 15.0 km, and the maximum thickness is approximately 28 m. Near-marine facies of the Parasequences 4b, in Parasequence Set 4B, is 11.2 km in dip length with a maximum thicknesses of approximately 20 m. The near-marine facies of both parasequences exhibit vertical and lateral facies changes from (1) stream mouth bar and reworked stream mouth bar (frequently preserved as upper shoreface deposits (USF)), to (2) reworked delta front (pDF and dDF) (frequently preserved as middle (MSF) and lower shoreface (LSF) deposits), to (3) prodelta. The stream mouth bar and reworked stream mouth bar deposits contain trough and herringbone stratification and frequently contain the ichnofossil *Ophiomorpha*. The reworked delta front deposits (pDF and dDF) contain hummocky, planar, and ripple cross-stratification and frequently the ichnofossils *Ophiomorpha*, *Teichichnus*, *Chondrites*, *Cylindrichnus*, *Arenicolites*, *Diplocraterion*, and *Thalassinoides*.

In Miller Canyon, Parasequence 4a of Parasequence Set 4A rests on a transgressive lag deposit. This deposit reworks the upper part of the C coal zone and exhibits extreme bioturbation. This transgressive deposit can be traced northward over 13 km to Dry Wash. The paleoshoreline of the near-marine facies of Parasequence 4a shifts landward approximately 7 km relative to the paleoshoreline of underlying Parasequence 3b. In Miller Canyon and southward into Bear Gulch, there is approximately 20 m of erosional relief developed on Parasequence Set 4A, as fluvial channel belts of Parasequence Set 4B scour down into the underlying parasequence (fig 8). The paleoshoreline of the near-marine facies of Parasequence Set 4B shifts basinward some 7 km relative to the paleoshoreline of Parasequence Set 4A and is accompanied by at least 32 m of erosion. This change in shoreline position and baselevel and the development of the erosional unconformity indicate that the boundary between Parasequence Sets 4A and 4B is the sequence boundary between 4th-order depositional sequences FS2 and FS3. In the non-marine part of the Parasequence Set 4A, south of Bear Gulch, Parasequence Set 4A is capped by a very laterally extensive rooted zone (designated the E Rooted Zone). This rooted zone can be traced from just north of Last Chance Creek northward to just south of Bear Gulch, where it is correlative with the erosional unconformity between Parasequence Set 4A and 4B cropping out in Bear Gulch and Miller Canyon.

The G coal zone caps Ferron Parasequence Set 4B. South of Indian Canyon, in the Limestone Cliffs, the G coal

zone is completely scoured out by distributary channel belts and does not occur further south than Mussentuchit Wash. Curiously, the G coal zone does not split within the study area. The G coal zone extends over 27 km from its erosional limit in the Limestone Cliffs to its seaward limit north of Bitter Seep Canyon.

Parasequence Set 5A and 5B

Parasequence Set 5A is a progradational to aggradational set containing two parasequences (fig. 3). The near-marine facies of the parasequences in each Parasequence Sets 5A and 5B represent wave-dominated, wave-reworked delta front deposits. They all exhibit both vertical and lateral facies changes from (1) stream mouth bar and reworked stream mouth bar (frequently preserved as upper shoreface deposits (USF)), to (2) reworked delta front (pDF and dDF) (frequently preserved as middle (MSF) and lower shoreface (LSF) deposits), to (3) prodelta. The stream mouth bar and reworked stream mouth bar deposits contain trough stratification and frequently contain *Ophiomorpha*. The reworked delta front deposits (pDF and dDF) contain hummocky, planar, and ripple cross-stratification and are commonly contain the ichnofossils *Ophiomorpha* and *Thalassinoides* and occasionally *Skolithos*.

The landward pinchout of Parasequence 5b is truncated by fluvial channels of Parasequence Set 5B, but can be located to within 1 km. This erosion makes estimates of maximum length and thickness problematic. Near-marine facies of the Parasequences 5a, and 5b, in Parasequence Set 5A, are approximately 10.4 km, and 9.6 km in dip length, respectively, and maximum thicknesses are approximately 14 m, and 15 m, respectively. The estimated overall dip length of Parasequence Set 5A is approximately 11 km with a maximum thickness of approximately 33 m. The near-marine facies of the Parasequence 5c, in Parasequence Set 5B, is 8.5 km in dip length and has a maximum thickness of 16 m.

Parasequence Set 5A backsteps landward about 2.2 km, from the position of the landward pinch-out of Parasequence Set 4B. From the southern goosenecks of Muddy Creek Canyon to Picture Flats, the top of Parasequence Set 5A has from 10 to 20 m of erosional relief developed, as fluvial channel belts of Parasequence Set 5B scour down into the underlying parasequence set. This represents a basinward shift of at least 3 km. Within progradational to aggradational Parasequence Set 5A, Parasequence 5b steps seaward 0.7 km, relative to the underlying Parasequences 5a.

The I coal zone caps Ferron Parasequence Set 5B. South of Indian Canyon, in the Limestone Cliffs, the I coal zones are completely scoured out by distributary channel belts and does not occur further south than Mussentuchit Wash.

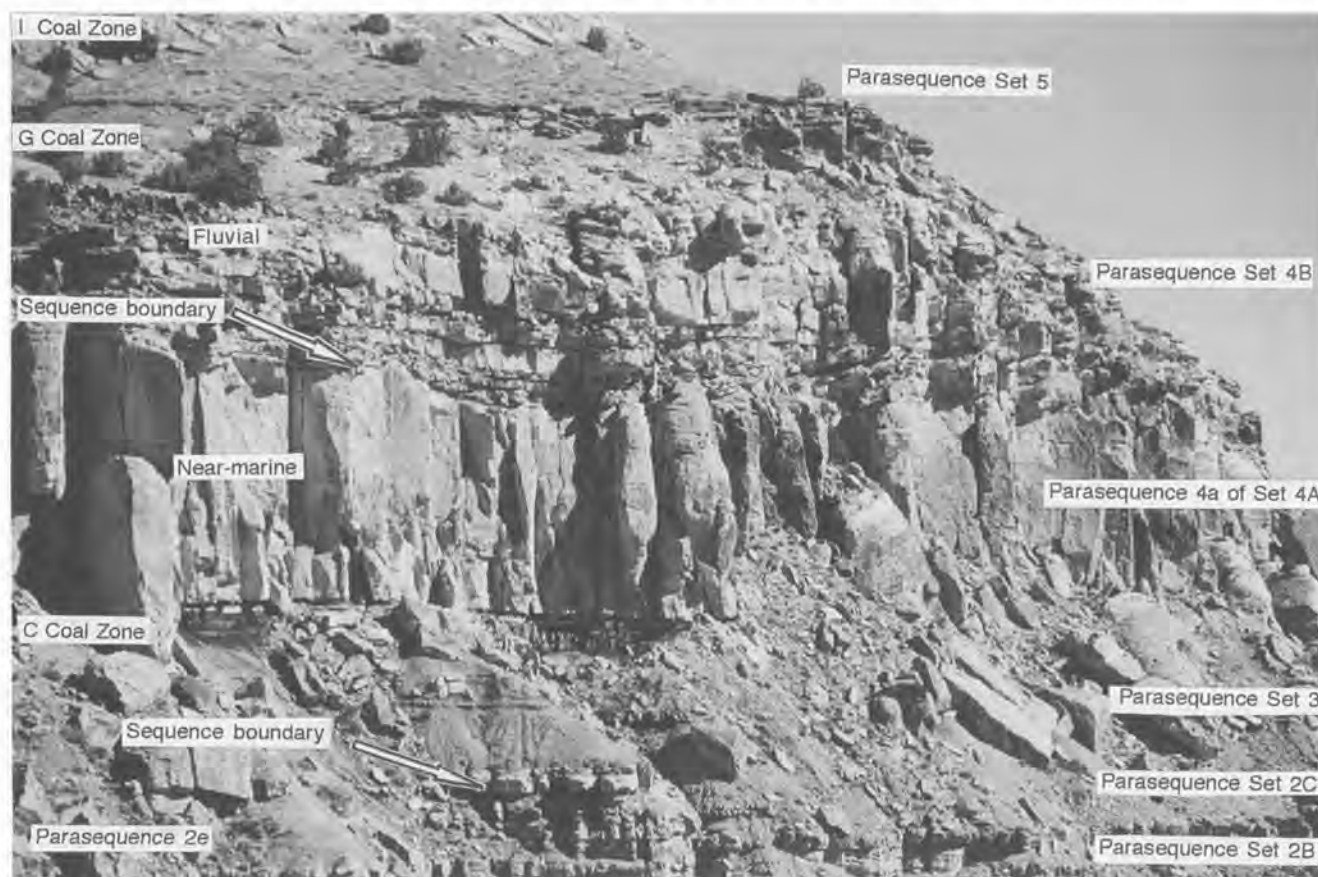


Figure 8. Photograph showing the sequence boundary separating Upper Ferron Parasequence Sets 4A and 4B in Bear Gulch.

South of Coyote Basin, the I coal zone splits into three zones, denoted as the I₁, I₂, and I₃ coal zones.

Landward-Stepping Parasequence Sets

Ferron Parasequence Sets 6, 7, and 8 each progressively step landward, relative to the older, underlying parasequence sets (Gardner, 1993) (fig. 3). Along most of the outcrop belt, Parasequence Sets 6, 7, and 8 are represented by delta plain facies associations composed of delta plain mudstones, wide distributary channel belts, crevasse splay sandstones, over-bank deposits, and carbonaceous shales and siltstones. Parasequence Sets 6, 7, and 8 contain one, four, and two parasequences, respectively. The near-marine facies of the parasequences in each Parasequence Sets 6, 7, and 8 represent a wave-dominated, wave-reworked delta front deposit. They all exhibit both vertical and lateral facies changes from (1) stream mouth bar and reworked stream mouth bar (frequently preserved as upper shoreface deposits (USF)), to (2) reworked delta front (pDF and dDF) (frequently preserved as middle (MSF) and lower shoreface (LSF) deposits), to (3) prodelta. The stream mouth bar and

reworked stream mouth bar deposits contain trough stratification and frequently contain *Ophiomorpha* and *Arenicolites*. The reworked delta front deposits (pDF and dDF) contain hummocky, planar, and ripple cross-stratification and commonly contain the ichnofossils *Ophiomorpha* and *Thalassinoides*. Locally, the base of Parasequence Set 7, resting on the J coal zone, contains the trace fossils *Teichichnus*, *Thalassinoides*, *Planolites*, and *Rhizocorallium*.

Near-marine facies of Parasequence Sets 6, 7, and 8 are approximately 2.8 km, 6.7 km, and 5.4 km, in dip length, respectively. The thicknesses of the near-marine facies of the Parasequence Sets 6, 7, and 8 are 6 m, 8 m, and 7 m, respectively. Parasequence 6a of Parasequence Set 6 is 2.8 km in dip length and has a maximum thickness of 6.4 m. Parasequence 6a backsteps 2 km relative to Parasequence Set 5B. Parasequences 7a, 7b, 7c, and 7d of Parasequence Set 7 are 1.3 km, 2.4 km, 3.2 km, and 3.8 km in dip length and have maximum thicknesses of 3.6 m, 2.1 m, 8.5 m, and 3.6 m, respectively. Parasequence Set 7 is a retrogradational parasequence set with the near-marine facies of Parasequence 7d back-stepped landward 2.9 km, relative to Para-

sequence 7c. Parasequence 7c backsteps 1.4 km landward, relative to Parasequence 7b and Parasequence Set 7b backsteps 1.7 km landward, relative to 7a. Parasequence 7a steps landward 0.2 km, relative to Parasequence Set 6. Parasequences 8a and 8b of Parasequence Set 8 are 2.8 km and 3.4 km in dip length and have maximum thicknesses of 3.2 m and 3.4 m, respectively. Parasequence Set 8 is a retrogradational parasequence set with the near-marine facies of Parasequence 8b back-stepped landward 2.0 km, relative to Parasequence 8a. Between south Quitchapah Creek and the Emery Mine, Parasequence 8 is separated from Parasequence Set 7 by a extra-basinal pebble lag. The pebbles range from 1 cm up to 10 cm in length and are found nowhere else in the Upper Ferron Sandstone. In some areas, these pebbles are found floating throughout the near-marine facies of Parasequence Set 8.

Coal zones occur at or near the top of these depositional Parasequence Sets 6 and 7. The *J coal zone* caps Ferron Parasequence Set 6; the *M coal zone* caps Ferron Parasequence Set 7. The *M coal zone* capping Parasequence Set 7 is only exposed from North Fork Canyon to Willow Springs Wash and from Ivie Creek to south Quitchapah Creek Canyon. North of Willow Springs Wash, the top of Parasequence Set 7 is represented only as a burrowed transgressive surface; the burrows are marine *Thalassinoides* belonging to the *Skolithos* ichnofacies. South of North Fork Canyon the surface is rooted and is burrowed by non-marine *Scoyenia*. In the Muddy Creek Canyon area, Parasequence Set 7 is capped by a thin shale interval containing septarian nodules. Parasequence Set 8 is locally capped by lag of oyster fragments and a thin shale interval containing septarian nodules.

Architectural Systematics of Near-Marine Facies

A plot of dip length versus thickness for Ferron Parasequence Sets and Parasequences is shown in figure 9. Examining the dimensions of parasequence sets and parasequences, clear trends can be discerned. When classified according to their delta cycle stacking arrangement in the 3rd-order Ferron Sequence (Gardner, 1993), the total near-marine facies of the parasequence sets occupy distinct fields on the plot of dip length versus thickness. The 3rd-order seaward-stepping Parasequence Sets 1, 2A–2C, and 3 have mean dip lengths of 24 km with mean thicknesses of 24 m; the mean aspect ratio (i.e., length/thickness) is 1180. The 3rd-order aggradational Parasequence Sets 4A–4B and 5A–5B have mean dip lengths of 11 km with mean thicknesses of 24 m; the mean aspect ratio is 490. The 3rd-order landward-stepping Parasequence Sets 6, 7, and 8 have mean dip lengths of 5 km with mean thicknesses of 7 m; the mean aspect ratio is 682. This suggests that the general trend in 3rd-order delta cycle evolution within the Ferron Sequence

(Gardner, 1993) is one of first seaward-stepping of thick, long parasequence sets, followed by the aggradation of thick, short parasequence sets, and finally followed by the back-stepping of thin, short parasequence sets. When considered in the context of the slow 3rd-order sea-level rise, this overall trend can be explained by a systematic decrease in sediment supply. In the seaward-stepping parasequence sets, sediment supply is large relative to available accommodation space, resulting in substantial seaward-stepping (i.e., progradation) of the deltas. Very early in this period (i.e., Parasequence Set 1 time), the deltas were extremely river dominated, with little wave-reworking. Later, there is an increase in the degree of wave-reworking, but still an abundance of sediment for major seaward progradation. Midway through the Ferron deposition (i.e. the aggradational phase of the 3rd-order cycle), sediment supply declined. This, coupled with substantial wave reworking slowed the seaward progradation, allowing aggradation of several delta cycles. In the final phase (i.e., during the back-stepping phase of Ferron deposition), sediment supply decreased dramatically resulting in small retrogradational deltas and a retreat of the paleoshorelines. These well defined trends suggest that the 4th-order depositional sequence events, described above, are superimposed on the 3rd-order sediment supply/accommodation space driven trends and that the superimposed 4th-order internal stacking patterns have little overall geometrical effects.

Examination of the dip length and thickness systematics, at the parasequence scale, reveals groupings based on the degree of wave-reworking (fig. 9). In particular, in the seaward-stepping phase of the 3rd-order cycle where both river-dominated parasequences and wave-reworked parasequences occur, the effects of degree of wave-reworking is very evident. In the very river-dominated Parasequence Set 1, the average near-marine facies of the parasequences is 15 m thick and 5.4 km long, with a mean aspect ratio of 400. The strike dimensions of parasequences suggest that these deltas had dip length/strike width aspect ratios near 1.8. These systematics are reasonable in light of the typical morphology and avulsion frequency exhibited by river-dominated deltas. The river-dominated, but wave-reworked near-marine facies of parasequences of Parasequence Sets 2A, 2C, and 3 are similar in thickness, with a mean thickness of 15 m, but have substantially longer dip lengths, averaging 15.9 km, and higher aspect ratios (e.g., mean aspect ratio is 1124). The length and thickness systematics of the parasequences belonging to the 3rd-order aggradational phase of Ferron deposition are somewhat thinner than the wave-reworked seaward-stepping deltas (i.e. mean thickness is 19 m), and shorter in dip length (i.e., mean dip length is 11 km); mean aspect ratio is 602. This decrease in progradational length reflects the overprint of a declining sediment supply, as discussed above. The parasequences

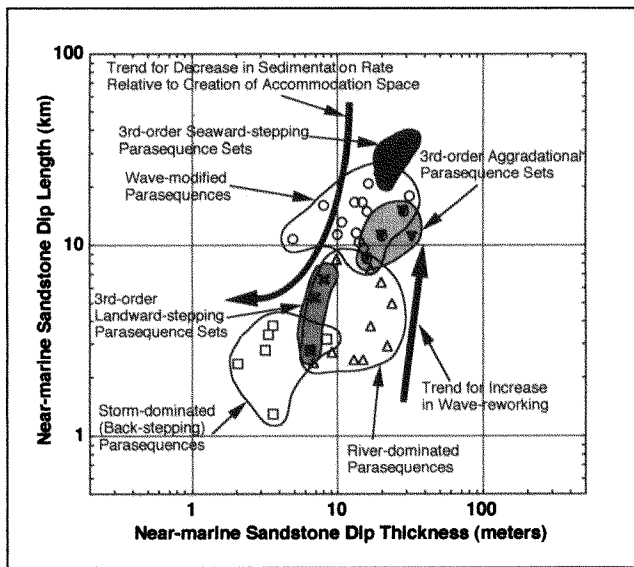


Figure 9. Plot of dip length versus thickness for Upper Ferron Sandstone Parasequence Sets and Parasequences.

belonging to the back-stepping phase of Ferron deposition have lengths and thickness that appear to be mainly controlled by the continued, but dramatic, decrease in sediment supply. They are shorter in dip length, with mean lengths of only 2.8 km, and are thin, with mean thicknesses of only 4 m, resulting in a mean aspect ratio of 754.

It is clear from these dimensional data that the volume of sediment progressively decreased throughout Ferron deltaic deposition. No relationship can be found with the positions of parasequences or parasequence sets within the higher frequency 4th-order sequences. Therefore, it can be assumed that the effects of the 4th-order sea-level fluctuations were over-shadowed by the overwhelming effects of a constantly varying sediment supply.

Architectural Systematics of Non-marine Channel Belt Sandstones

A favorable strike outcrop section that exposes almost the complete delta plain facies association of the Ferron Sandstone stratigraphic interval is located in Willow Springs Wash, Willow Springs Quadrangle, Emery and Sevier Counties (fig. 1). Outcrop studies to quantify the sizes and shapes of Ferron Sandstone fluvial channel belts were conducted by the authors in Willow Springs Wash, along both the north and south canyon walls (van den Bergh, 1995; van den Bergh and Garrison, 1996). These data represent the majority of the data for the following discussion and subsequent statistical analyses. Barton (1994) and Lowry and Jacobsen (1993) acquired data for some fluvial channel belts farther north

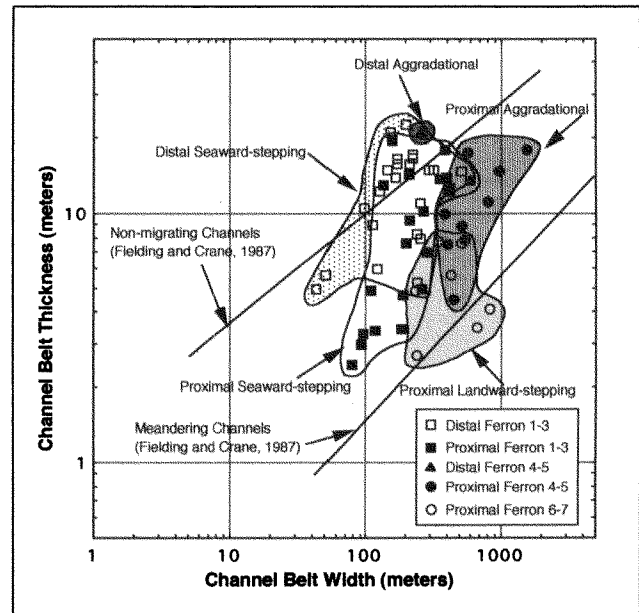


Figure 10. Plot of thickness versus width of Upper Ferron Sandstone channel belts.

from Willow Springs Wash; this data is also included in the following analysis.

Examination of the channels belts in Willow Springs Wash reveals clear differences in channel belt internal and external architecture as a function of channel position within the stacking arrangement in the 3rd-order Ferron Sequence (fig. 10). The fluvial channel belts of seaward-stepping parasequence sets are generally laterally restricted and multi-storied with channel filling elements (i.e., macroforms and/or barforms) generally stacked vertically within the channel belt boundaries. The fluvial channel belts of aggradational parasequence sets are generally quite laterally extensive and multi-storied with channel filling elements generally stacked en echelon laterally within the channel belt boundaries. The fluvial channel belts of landward-stepping parasequence sets are laterally extensive and sheet-like with channel filling elements generally stacked vertically within the channel belt boundaries.

The proximal seaward-stepping fluvial channel belts (i.e., those channel belt cross-sections that are located near the upper delta plain and adjoining the alluvial plain) in Willow Springs Wash have a bimodal thickness distribution ranging in thickness from 2.4 m to 20.1 m with thicknesses between 3–5 m and 12–14 m being most common. Their widths range from 77 m to 580 m, with widths near 90–220 and 360–430 m being most common. The width/thickness aspect ratios range from 7.8 to 52.9, with an average of 29.5 (fig. 10). The distal distributary channel belts (i.e., those near the paleoshoreline) are generally narrower and thicker

than the proximal channel belts with widths ranging from 43 m to 510 m, averaging 195 m, and thicknesses ranging from 4.9 m to 22.9 m, with thickness of 5–9 and 15–18 m being most common. The aspect ratios of the distal distributary channel belts are also much less than those of the proximal channel belts ranging from 7.1 to 45.5, averaging 16.6. This change in size and shape of the seaward-stepping distributary channel belts is consistent with the change in channel morphology resulting from river bifurcation.

The proximal aggradational distributary channel belts in Willow Springs Wash have a bimodal thickness distribution ranging in thickness from 4.6 m to 18.3 m, with thicknesses between 8–11 m and 17–18 m being most common. Their widths range from 380 m to 1448 m, with widths near 380–580 m being most common. The width/thickness aspect ratios range from 31.9 to 97.4, with an average of 57.2 (fig. 10). The distal distributary channel belt, reported by Barton (1994) at Cedar Ridge, is generally narrower and thicker than the proximal channel belts with a width of 255 m, and a thickness of 21.3 m. The aspect ratio of 12.0 for the distal distributary channel belt at Bitter Seep Canyon is also much less than those of the proximal channel belts. This change in size and shape of the aggradational fluvial channel belts is consistent with the change in channel morphology resulting from river bifurcation. The proximal aggradational fluvial channel belts in Willow Springs Wash are generally much wider than the seaward-stepping channel belts, while the thicknesses are generally slightly greater; aspect ratios of the aggradational fluvial channel belts are a factor of two higher than those of the proximal channel belts.

The proximal landward stepping fluvial channel belts in Willow Springs Wash have a thickness distribution ranging in thickness from 2.7 m to 7.9 m, averaging 5 m in thickness. Their widths are uniformly distributed from 228 m to 809 m. The width/thickness aspect ratios range from 43.8 to 195.0, with aspect ratios near 65–90 and 185–195 being most common (fig. 10). The landward-stepping channel belts in Willow Springs Wash are similar in width to the proximal channel belts, but generally much wider than the seaward-stepping channel belts; these channel belts are generally thinner than either the aggradational or seaward-stepping channel belts; aspect ratios of the landward-stepping fluvial channel belts are generally higher than those of the aggradational and seaward-stepping channel belts.

The aspect ratio distributions for the individual channel fill elements within the fluvial channel belts, are similar, regardless of position within the deltaic stacking pattern, suggesting that only channel belt internal stacking patterns vary between the fluvial channel belts within the Ferron seaward-stepping, aggradational, and landward-stepping stacking pattern. The proximal channel belt fill elements are generally thicker and wider than the distal channel belt

fill elements. This change in size of the distal fluvial channel belt macroforms is also consistent with the change in channel morphology resulting from river bifurcation.

The channel belts, in context of their position within the Ferron stacking pattern, exhibit clear differences in channel belt internal and external architecture as a function of stacking pattern. Channel belts evolve through the spectrum from supplying the purely river-dominated to the lobate wave-dominated to the strand/beach type strongly wave-dominated deltaic systems. As they move from river-dominated, seaward-stepping deltaic systems to more wave-dominated aggradational systems, they change from multi-storied belts with channel fill elements stacked vertically within the channel belt boundaries to increasingly wider and quite laterally extensive multi-storied channel belts with channel fill elements generally stacked in echelon laterally within the channel belt boundaries. As the deltas begin to step landward during strong (relative) transgressions, the channel belt morphology responds by becoming thinner and narrower, yet still quite laterally extensive.

Lithologic Composition of Coal Zones

Analysis of the *coal zone* thicknesses and compositions obtained from detailed measured sections has allowed some quantification of *coal zone* systematics as a function of dip length along the Ferron delta cycles (i.e., parasequence sets). Choosing an appropriate datum, with respect to which systematics are to be examined is difficult and problematic. One might choose the landward pinch-out of the near-marine facies of a parasequence set, or the landward pinch-out of the stratigraphically highest parasequence in the parasequence set, or the mean paleoshoreline position for the parasequence set, or the mean position of the paleoshoreline of the highest parasequence in the parasequence set. In this paper, the *coal zone* systematics are examined as a function of position along the dip cross-section of Garrison and van den Bergh (1996; 1997) (fig. 1), but the details of the *coal zones* are discussed in terms of the general architecture of the underlying parasequence set. In this analysis, the coal seam and *coal zone* thicknesses are the sums of all coal seams and *coal zone* thicknesses of all splits of the *coal zone* at the sampling location. The total *coal zone* thickness is the sum of the thicknesses of the coal seams, the carbonaceous shales, mudstones, and siltstones, tonsteins, paleosols, and delta plain mudstones and siltstones included within the coal zone.

Coal zones generally thicken landward relative to the mean position of the landward pinch-out of the underlying parasequence set, but after some distance landward, they decrease in thickness. This can be seen well in a plot of *coal zone* thickness and coal thickness versus distance for the C

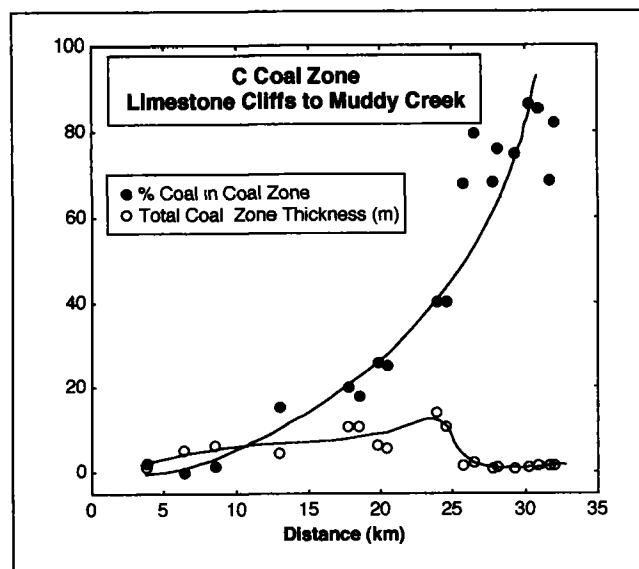


Figure 11. Thickness profile of Upper Ferron C coal zone along its dip length.

coal zone, from Limestone Cliffs to Muddy Creek Canyon (fig. 11). In this plot, the C coal zone progressively increases in thickness in a landward direction until it reaches a maximum thickness of 13.8 m, at Cowboy Mine Canyon, about 6 km landward of the approximate projected position of the landward pinch-out of Parasequence 3a in Parasequence Set 3; further south the zone continually decreases in thickness. The coal is thickest in the region between this landward pinch-out and the position of maximum zone thickness. The data indicate that the proportion of coal in the coal zone decreases progressively landward from the landward pinch-out of Parasequence Set 3 (fig. 11). The balance of the coal zone is composed of carbonaceous shale and mudstone; with tonstein and delta plain mudstone and siltstone occurring as minor constituents.

Coal zones generally thin seaward relative to the mean position of the landward pinch-out of the underlying parasequence set. This is particularly well shown in the data for the sub-A coal zone (fig. 12). The landward extent of the sub-A coal zone cannot be determined because it occurs south of the Ferron outcrop belt. Therefore, the outcrops of the sub-A are seaward of the landward pinch-out of the oldest near-marine rocks of Parasequence Set 1. The sub-A coal zone appears to have two distinct parts, the southern most part is composed of the sub-A1 and sub-A2 splits and overlies Parasequences 1z–1d, and the northern part consists of the sub-A3 and sub-A4 splits and overlies Parasequences 1e–1k. The composite sub-A1+A2 portion of the sub-A coal zone decreases dramatically in thickness in a

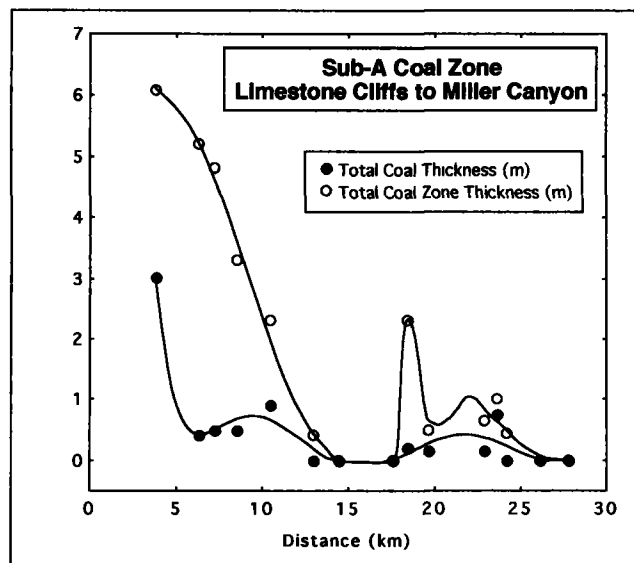


Figure 12. Thickness profile of Upper Ferron sub-A coal zone along its dip length.

seaward direction, from 6.1 m in the Limestone Cliffs to 0.5 m in Rock Canyon, before pinching out in Corbula Gulch. The composite sub-A3+A4 portion of the sub-A coal zone also decreases dramatically in thickness in a seaward direction, from 2.4 m in Scabby Canyon to 0.5 m in north Quitchapah Creek Canyon, before pinching out near Bear Gulch. These systematics suggest that the sub-A should actually be divided into 2 distinct coal zones. Examining composite sub-A1+A2 coal thickness, in light of the position of the near-marine pinch-out of Parasequence 1d, in Coyote Basin, it appears that the coals become thicker just landward of this position. The same is true of the composite sub-A3+A4 coal thickness, where it becomes thicker near the landward pinch-out of Parasequence 1k in Quitchapah Creek Canyon.

The effects of differential compaction and differences in original pre-peat swamp topography have the effect of adding perturbations to the general trends discussed above. The A coal zone illustrates this particularly well (fig. 13). Almost the entire A coal zone is exposed in the outcrop belt from Limestone Cliffs, where it is only 0.7 m thick, to its seaward pinch-out just north of Dry Wash. In Dry Wash, the A coal zone is 1.9 m thick and contains 0.45 m of coal. This zone represents the seaward extension of the A coal zone. The A coal zone has its minimum thicknesses near its landward limit and then again as it approaches its seaward limit. The most notable feature of the A coal zone is that it does not thicken to a maximum and then thin seaward, but has at least 4 distinct maxima. The A coal zone has its thick-

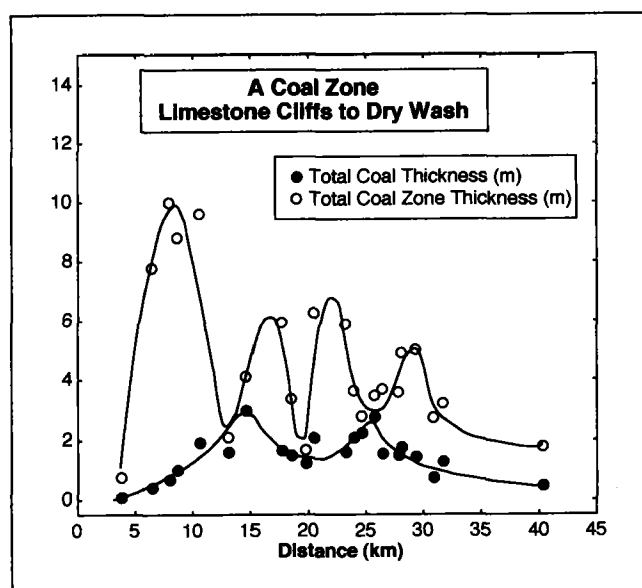


Figure 13. Thickness profile of Upper Ferron A coal zone along its dip length.

est accumulations just south of Coyote Basin (8.8 m thick) and just north of Ivie Creek and Quitchapah Creek Canyon (6.4 m thick). In the vicinity of Rock Canyon and Corbula Gulch and at I-70, the A coal zone appears to be abnormally thin. The coal is thickest in the area near Rock Canyon and to the north in Quitchapah Creek Canyon. In the vicinities of Rock Canyon and I-70, the A coal zone is composed of about 75% coal. The compaction of the coal zone (i.e., the original peat accumulation) was greater in these areas than in Coyote Basin, where it is composed of 20% coal, 56% carbonaceous shale, and 24% interlayered delta plain mudstones, and north of Ivie Creek area, where it is composed of 58% coal, 17% carbonaceous shale, and 25% delta plain mudstones. The A coal zone appears to be associated with the landward pinch-out of Parasequence Set 2C, because, except for a small A coal "split" between South Blue Trail Canyon and I-70, the A coal zone lies above the erosional unconformity on Parasequence Sets 2A and 2B, marking the sequence boundary between FS1 and FS2. Most of the older coals associated with Parasequence Sets 2A and 2B must have been removed by erosion. The only exceptions may be in the area south of Willow Springs Wash, where the zone becomes extremely thick, and in the area immediately south of I-70.

Altered Volcanic Ash Layers in Coal Zones (Tonsteins)

In the Ferron Sandstone, coal zones frequently contain volcanic ash layers (Ryer et al., 1980; Garrison and van den

Bergh, 1996). These volcanic ash horizons are characterized as laterally continuous kaolinitic claystone partings called "tonsteins" (Williamson, 1970). These tonsteins are greenish-white to gray in color and contain kaolinite booklets, beta quartz, volcanic K-feldspars, Fe-oxide and Ti-oxide minerals, and zircons (fig. 14) (van den Bergh, 1995). Tonsteins have been found in all major coal zones in the Ferron Sandstone (Garrison and van den Bergh, 1997). Many coal zones contain multiple tonstein layers. The tonsteins associated with these coal zones document near time synchronicity of the coal zone horizons, but splits in coal zones clearly indicate significant time represented by these deposits.

In the 7 Ferron Sandstone coal zones, 13 distinct tonsteins have been identified. In the Limestone Cliffs, the sub-A2 coal zone contains a very well-developed tonstein. This sub-A2 tonstein has not been identified further down-dip. Both the A1 and A2 splits of the A coal zone contain tonstein layers. The tonstein in the A1 coal zone extends as far up-dip as the Limestone Cliffs and as far down-dip as Blue Trail Canyon. The tonstein in the A2 coal zone has been identified in Coyote Basin and at I-70/Ivie Creek. North of I-70, the A2 coal zone contains two tonsteins that can be traced northward to at least Bear Gulch. North of I-70, the C coal zone contains at least 2 tonsteins and occasionally up to four tonsteins. The thickest tonstein in the C coal zone has been traced from Corbula Gulch to Muddy Creek Canyon, a distance of over 16 km. No tonsteins have been identified in the C coal zone south of Corbula Gulch. A tonstein occurs in the G coal zone from Willow Springs Wash to Muddy Creek. A tonstein was identified in the I coal zone from Rock Canyon to Bear Gulch. The J coal zone contain a tonstein from Willow Springs Wash to Rochester Creek, a distance of about 23 km. From the South Goose-necks of Muddy Creek to Rochester Creek, the J coal zone also contain an additional tonstein layer. A tonstein has been identified in the discontinuous M coal zone in Willow Springs Wash and in Coal Wash, north of Ivie Creek.

Landward and seaward of near-marine pinch-outs of parasequence sets, preservation potential of volcanic ash layers decreases dramatically, as illustrated well by the sub-A1-A2 and C coal zones. The southern most 15 km of the C coal zone, in the outcrop belt, is devoid of tonstein. From Corbula Gulch to I-70 only a single tonstein is present in the C coal zone, in Bear Gulch four tonsteins are assigned to the C coal zone, in Miller Canyon 3 tonsteins occur, and about 4 km north of Miller Canyon, near Pictograph Point, where the C coal zone goes into the subsurface, it still contains 2 tonsteins. This is approximately 20 km landward of the seaward pinch-out of Parasequence Set 3. The composite sub-A1-A2 coal zone is devoid of tonstein seaward from the Limestone Cliffs to its seaward limit in Rock Canyon, a distance of over 8 km.

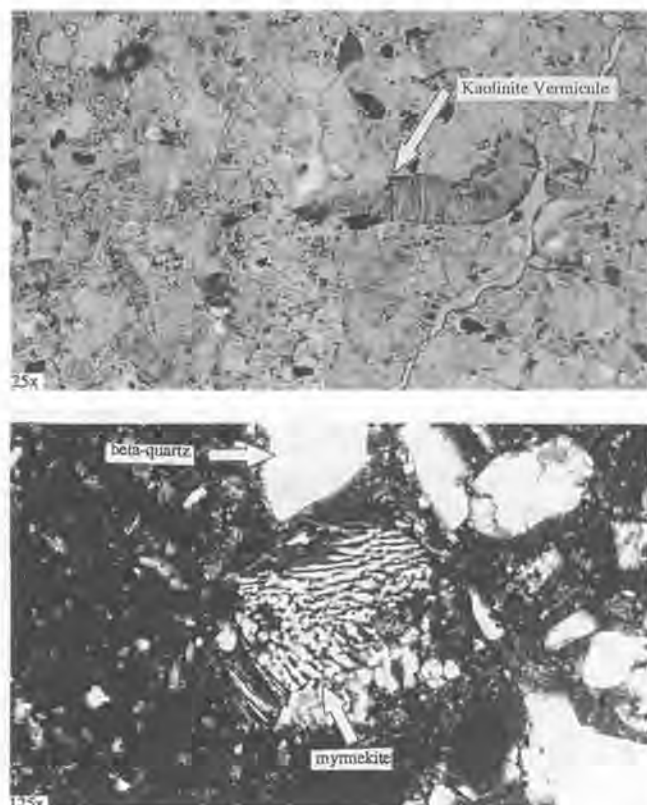


Figure 14. Photomicrographs of tonsteins within the A coal zone (top) and the J coal zone (bottom).

Depositional Sequence Stratigraphic History of the Last Chance Delta

Based on radiometric age dates of Obradovich (1991) and ammonioidea and inoceramadae faunal zonation, Gardner (1992) suggested that the Upper Turonian Ferron Sandstone Last Chance Delta was deposited between 89.8 and 88.8 m.y.b.p. During this period, the eustatic sea-level curves indicate a slow 2nd-order sea-level fall event, upon which are superimposed two 3rd-order sea-level cycles (Gardner, 1992). The tectonic activity in the Sevier orogenic belt was relative quite during this period, although a period of foreland basin expansion was occurring (Gardner, 1992). Based on the geochronology and faunal zone correlations, Gardner (1992) developed a relative sea-level curve for Central Utah and hypothesized that tectonic subsidence, coupled with the eustatic events, produced a local slow 3rd-order sea-level rise event in Central Utah during the Upper Turonian. The 3rd-order Ferron Sequence was deposited during this slow Upper Turonian 3rd-order sea-level rise.

Based on the geochronology and the sea-level curve developed by Gardner (1992), it is possible to speculate on the timing and durations of the depositional episodes occurring within the Ferron clastic wedge. The earliest deposi-

tion of Ferron Parasequence Set 1 occurred during the beginning of this slow sea-level rise, near 89.8 m.y.b.p. The youngest parasequence set of the outcrop belt, Parasequence Set 8, was deposited in earliest Coniacian time at about 88.8 m.y.b.p., while the local relative sea-level was still rising. Ryer (1994) suggested that this sea-level rise event was accompanied by an increase in sediment supply from the Sevier Orogenic Belt. The available stratigraphic and architectural data, for both near-marine and non-marine facies, as quantified by Garrison and van den Bergh (1996; 1997) and van den Bergh and Garrison (1996), indicate that, when taken in the context of 3rd-order deltaic parasequence set stacking patterns, the over-all Ferron Sandstone Last Chance Deltaic deposition is controlled by sediment supply. This is also confirmed by the calculations of Gardner (1992), in which he demonstrated that the total volume of sediment progressively decreased during each successive depositional episode. The increased sediment supply, in the early stages of deltaic development, resulted in a volume of sediment that exceeded the available accommodation space, with subsequent deltaic events stepping seaward at a dramatic rate. During each successive deltaic cycle, less sediment was available, resulting in aggradation and eventual back-stepping of the final delta cycles (i.e. transgression), as the sediment supply could no longer keep pace with the rise in relative sea-level.

The 4th-order Upper Ferron Sequences FS1-FS4 are superimposed on the 3rd-order sea-level rise event and the 3rd-order stratigraphic architecture of the Ferron Sandstone. The dramatic erosional unconformities associated with the sequence boundaries at the tops of Upper Ferron Sequences FS1, FS2, and FS3, indicate that there was up to 20–30 m of erosion, signifying locally substantial base-level drops. These base-level drops were accompanied by a basinward shift in paleoshorelines by as much as 5–7 km.

The internal architecture of the 4th-order depositional sequences FS1–FS4, of the Ferron clastic wedge (fig. 3), also reflect the progressive change in the ratio of sediment supply to available accommodation space. 4th-order sequence FS1, formed during a period in which available sediment supply was much greater than available accommodation space. It has an internal architecture dominated by progradational parasequence sets. The transgressive phase is probably only represented by the transgressive lag deposit. The highstand parasequence set is poorly developed. 4th-order sequence FS2 formed during a period in which available sediment was initially greater than available accommodation space, but later became more balanced. It has an internal architecture consisting of a progradational parasequence set overlain by an aggradational parasequence set. A transgressive lag is well developed and is overlain by a well-developed highstand parasequence set. 4th-order sequence FS3 developed during a period when

sediment supply was balanced with the rate of development of accommodation space. Its internal architecture is dominated by aggradational parasequences. The oldest parasequence set consists of a single parasequence overlain by a poorly developed transgressive lag deposit. The highstand parasequence set is slightly progradational to aggradational. 4th-order sequence FS4 developed during a period when the sediment supply was waning and could not keep up with the development of accommodation space. Its internal architecture is dominated by retrogradational (back-stepping) parasequence sets. The oldest parasequence set consists of a single (slightly progradational to aggradational) parasequence (i.e. its dip length is consistent with older aggradational parasequences). The transgressive phase is represented by retrogradational (back-stepping) parasequence sets. A transgressive lag is not apparently developed. A highstand parasequence set was either apparently not developed or has not been identified within the outcrop belt.

As stated above, FS1 actually belongs to the Hyatti Sequence and FS2, FS3, and FS4 belong to the Ferron Sequence. FS1 would be the 4th-order highstand sequence of the 3rd-order Hyatti Sequence. The lower boundary of FS1 is immediately above the Hyatti condensed section (Gardner, 1993) suggesting that it is actually a "correlative conformity/condensed section boundary" in this part of the basin. FS2 and FS3 would be the 4th-order progradational to aggradational sequences of the 3rd-order Ferron Sequence and FS4 is the 4th-order transgressive sequence of the Ferron Sequence. The upper boundary of FS4 is a below a concretion-bearing condensed section a few m above the uppermost sandstones of FS4, suggesting that the 4th-order highstand sequence of the Ferron Sequence is not located in the study area, but is only represented by condensed section sediments. On balance, these 4th-order events are most easily explained as forming as a result of small, rapid, sea-level fall and rise events. These events are superimposed on the overall 3rd-order patterns of the Upper Ferron Last Chance Delta, as described by Gardner (1992; 1993).

Within the clastic wedges of the Cretaceous interior seaway, conglomerates can mark major basinwide unconformities (Ryer, 1994). Within the Upper Ferron Sandstone only two major occurrences of extrabasinal pebble and conglomeratic lags have been identified. The channel belts of Ferron Parasequence Set 4B contain extrabasinal pebbles with a maximum long dimension of up to 4 cm. Extrabasinal pebbles (up to 15 cm) occur at the base of, and occasionally floating within, Ferron Parasequence 8a. The pebbles, in both Parasequence Sets 4B and 8 are quartzite, chert, sandstone, siltstone, volcanic-derived lithics, and large, rounded K-feldspar crystals. The pebbles, within Parasequence Set 4B, appear to occur in response to base-level drop during

sequence boundary development. The pebbles in Parasequence Set 8 may be related to sedimentological events that are correlative with the events that produced the Calico Beds of southern Utah and the Coalville Conglomerate of Northern Utah (e.g. see Ryer, 1994).

Based on stratigraphic data (Garrison and van den Bergh, 1996; 1997) and faunal zonations (Gardner, 1992), the Upper Ferron 4th-order Sequences would have each been deposited over about a 250,000 year period. The individual depositional events that produced the parasequences within the Upper Ferron Sandstone, would have been deposited over, on average, about a 20,000–30,000 year period. It is estimated that the parasequence sets within the Upper Ferron Sandstone, would have been deposited, on average, during a 60,000–100,000 year period of time. The duration of the Upper Ferron 4th-order depositional sequence events is similar to the duration of older 3rd-order events within the Tununk Shale (i.e., the Woolgari and Hyatti Sequences), observed by Leithold (1994). The duration of the depositional episodes that resulted in the Upper Ferron Parasequences and Parasequence Sets is similar to the 20,000–100,000 year durations postulated for 4th-order events in the Tununk Shale (Leithold, 1994).

DAY 1 ROAD LOG

Int. Miles	Cum. Miles	
0.0	0.0	Leave parking lot of Holiday Inn in Price, Utah. Travel east on Utah Highways 6 and 191.
0.6	0.6	Price River.
0.7	1.3	Exit 241. Junction with Utah Highway 10. Travel south on Utah Highway 10 through Huntington, Castle Dale, Ferron and Emery to Fremont Junction.
1.5	2.8	Industrial Park. The Book Cliffs can be seen to the north. The reddish coal burns are in the Blackhawk Formation that overlies ledges of Star Point Formation and the Aberdeen Tongue (fig. 2).
0.5	3.3	Four Mile Hill. The Blue Gate Shale in the road cut contains thin sandstone lenses probably representing small channels.
0.6	3.9	Junction with Ridge Road. Continue south on Utah Highway 10. To the southeast, Cedar Mountain and the San Rafael Swell can be seen. Cedar Mountain is capped by the Lower Cretaceous Buckhorn Conglomerate Member of the Cedar Mountain Formation (fig. 2).
1.0	4.9	Miller Creek.

0.5	5.4	Junction with Stake Farm Road on east. Continue south on Utah Highway 10. To the west, the northwest dipping Garley Canyon Sandstone can be seen (fig. 2). Pump jacks and well heads of the Drunkards Wash Coalbed Methane Field can be seen in the foreground to the west.	1.7	17.4	South junction with Utah Highway 155. Continue south on Utah Highway 10. Utah 155 provides access to the Cleveland-Lloyd Dinosaur Quarry. The Cleveland-Lloyd Dinosaur Quarry is managed by the BLM. More than 12,000 bones from at least 70 dinosaurs representing 14 species, including two previously unknown species, have been recovered.
0.9	6.3	Pinnacle Peak. A pinnacle of Blue Gate Shale.	1.2	18.6	Huntington Creek. Huntington Creek is a major tributary of the San Rafael River that dissects the San Rafael Swell.
0.3	6.6	Junction with Utah Highway 122 to the west. Continue north on Utah Highway 10. The Plateau Coal Mine is visible to the west on the Wasatch escarpment. The first prominent cliff former on the Wasatch escarpment is the Panther Tongue of the Star Point Formation (fig. 2).	0.4	19.0	Junction with Utah Highway 31 to the west. Continue south on Utah Highway 10.
0.4	7.0	Road cut in Blue Gate Shale. Note the sandy nature of the upper part of the outcrop.	1.0	20.0	Huntington. Huntington (pop. 1875, elev. 5791 feet) was established in 1879 by Elias Cox. Proceed south on Utah Highway 10.
0.4	7.4	Emery-Carbon County Line. Enter Carbon County.	1.0	21.0	Junction with north road to Lawrence. Continue north on Utah Highway 10.
0.3	7.7	Road cut in Blue Gate Shale. Note the sandy nature of the Blue Gate Shale and the thin sandstone lenses that are about 1 foot thick and 30–40 feet wide.	0.7	21.7	Five Mile Wash Bridge. Prominent topographic feature on the western skyline is Red Point. The lower slope of the Wasatch escarpment is the Blue Gate Shale, overlying the Emery Sandstone at the base of the escarpment. The three sandstone benches overlying the shale are the Panther, Storrs, and Spring Canyon Tongues of the Star Point and Blackhawk Formations. The Spring Canyon Tongue and the overlying Blackhawk Formation are reddish in color due to coal burns in the Blackhawk Formation (fig. 2).
0.4	8.1	Broad Valley Wash.			
1.3	9.4	Road cut in Blue Gate Shale.			
0.2	9.6	Washboard Wash.			
0.1	9.7	Road cut exposes small lamprophyre dike cut by a small thrust fault.			
0.2	9.9	North junction with Utah Highway 155 to Cleveland (pop. 498). Cleveland was established in 1885 by Samuel Alger and Henry Oviatt (Geary, 1996). Continue south on Utah Highway 10.	1.3	23.0	Wilberg Wash. Junction with south road to Lawrence (pop. 80, elev. 5652 feet). Lawrence was established in 1885 (Geary, 1996). Continue south on Utah Highway 10.
1.7	11.6	Wildcat Draw.			
0.5	12.1	Road cut in Blue Gate Shale. Trail to the west up the steeply sloping Poison Spring Bench. The Hiawatha Coal Mine is at the head of Poison Spring Bench.	1.3	24.3	Junction with Utah Highway 29 to the west to Joe's Valley Reservoir. Continue south on Utah Highway 10.
0.4	12.5	Top of Hill. View of Castle Valley with Wasatch Plateau to the west and the Book Cliffs to the north and northeast and Cedar Mountain to the east. Low outcrops of the reddish Jurassic Morrison Formation can be seen in the middle ground (fig. 2).	2.0	26.3	Junction with the Old Spanish Trail to the east. Continue south on Utah Highway 10.
			0.5	26.8	Roadcut through dark gray Blue Gate Shale, containing no sand or silt.
0.8	13.3	Potter Wash. To the west the Panther Tongue is well exposed on the Wasatch escarpment.	0.9	27.7	100 East Street in Castle Dale. Castle Dale, Utah (pop. 1707, elev. 5600 ft) was originally settled in 1877 by Orange Seely. Castle Dale lies in the central part of the Castle Valley located between the Wasatch Plateau to the west and the San Rafael
2.4	15.7	Huntington International Airport on the east.			

		Swell to the east and is the county seat of Emery County. Proceed south on Utah Highway 10 through the Castle Valley.			which is overlain by the cliff-forming Star Point Sandstone. The Star Point Sandstone is overlain by the coal-bearing Blackhawk Formation. The Castlegate Member of the Price River Formation caps the escarpment. Nelson Mountain (9070 feet) is the highest peak along the escarpment.
0.4	28.1	Cottonwood Creek. Cottonwood Creek is a major tributary of the San Rafael River.			
2.0	30.1	Hunter Power Plant. The power plant is fueled by local coal.			
0.6	30.7	Junction with Utah 57 on right to Orangeville (pop. 1459, elev. 5772 ft). Orangeville, named after Orange Seely, was established in 1880 (Geary, 1996). Continue on Utah Highway 10.	0.2	39.2	Ferron Gas Field. West of the highway, the pumping unit of the Pan American Ferron Unit 3 well within the Ferron Gas Field (10,022 ft TD) can be seen. This well produced over 36,000 bbl oil from the Permian Kaibab Formation and over 10 BCF gas from the Ferron Sandstone and the Kaibab Formation.
1.5	32.2	Old Rest Area in Rock Canyon Flat. On the right, cliffs exposing the Cretaceous age Mesaverde Group can be seen. The Blackhawk Formation overlies the cliff-forming Star Point Sandstone mid-way up the escarpment. The escarpment is capped by the Castlegate Member of the Price River Formation (fig. 2). The lower part of the Star Point Formation become more sandy as the correlative Panther and Storrs Tongue Members are developed. The "reddish" area marking a coal burn is on the uppermost Spring Canyon Tongue Member of the Blackhawk Formation.	2.2	41.4	Top of Hill. Roads cuts expose the Blue Gate Shale Member of the Mancos Shale. Note the lack of sandstone, siltstone, or concretions in the Blue Gate Member.
			1.1	42.5	Junction with old Utah Highway 10 to Moore (pop. 6, elev. 6269 feet). Moore, originally named Rochester, was established about 1903 (Geary, 1996). To the west, Youngs Peak (9005 feet) is the high peak along the Wasatch escarpment. Continue south on Utah Highway 10.
2.0	34.2	Junction with Main Street of Clawson (pop. 151, elev. 5950 feet). Continue on Utah Highway 10.	1.3	43.8	View of Dry Wash to the east. Dry Wash is formed by a major drainage that dissects the western limb of the San Rafael swell, a prominent north-south trending anticlinal structure, and exposes sandstones of the Upper Ferron Sandstone Member of the Mancos Shale. The Upper Ferron Sandstone (figs. 1 and 2) in this area is represented by the the more distal near-marine sandstones of the Last Chance Delta complex. Coal deposition was very minimal in this portion of the Upper Ferron Sandstone. Only the A coal zone remains in this northern portion of the outcrop belt.
0.7	34.9	South access road to Clawson. Continue on Utah Highway 10.			
1.1	36.0	"Castles" within the Blue Gate Shale along the Castle Valley. These "castles" are held up by thin sandstone tongues of the Garley Canyon Sandstone, can be seen in the foreground to the west and southwest. The Emery Sandstone can also be seen, in the background, up Garley Canyon. Note the down thrown fault block up the canyon, demarking the Joe's Valley fault system.			
1.8	37.8	Ferron (pop. 1606 and elev. 5934 feet). Ferron was established in 1880 by Abram Conover (Geary, 1996).	2.7	46.5	The town of Moore is visible in the foreground, to the east. In the foreground, the western limb of the anticlinal San Rafael Swell containing outcrops of the Upper Ferron Sandstone, can be seen dipping westward, while the eastern skyline is dominated by the distant peak-forming outcrops of Jurassic Navajo Sandstone.
0.6	38.4	Ferron Creek. Ferron Creek is a major tributary of the San Rafael River.			
0.6	39.0	Ferron Creek Drainage. View to the west, toward Ferron Canyon, that dissects the Wasatch Plateau escarpment, showing the units of the Upper Cretaceous Mesaverde Group. The Blue Gate Shale is the slope-former near the base of the escarpment,	1.6	48.1	South road to Moore and to the "Rochester Panel" Fremont Indian rock art site. A

		replica of the rock art panel is on display at the Museum of the San Rafael. Continue on Utah Highway 10.			a graben system that is manifest as a saddle in the mountains to the north.
0.3	48.4	Muddy Creek. One of the three major drainages that dissects the San Rafael Swell. It provides drinking and irrigation water for both Moore and Emery. At its confluence with the Fremont River near Hanksville, they become the Dirty Devil River which flows into the Colorado River near Hites Crossing at Lake Powell.	1.1	59.3	Junction with paved road, to the east, to the Hidden Valley Coal Mine. The mine, currently owned by Consol, has been reclaimed. The Hidden Valley Mine is in the Ferron A <i>coal zone</i> .
			1.2	60.5	Northern limit of Miocene basalt boulder field. These boulders were fluvially transported from Miocene basalt flows to the southwest.
0.4	48.8	Camp Muddy Creek Monument. From 1885–1888, early settlers, led by Heber Petty and Casper Christensen, dug a 1200 foot long tunnel through the Blue Gate Shale to bring waters from Muddy Creek to supply the settlement of Emery.	1.7	62.2	Junction with BLM access road to the east of Utah Highway 10. This road follows part of the historic Spanish Trail, a major trading route that wound through Utah, New Mexico, Arizona, Nevada, and California during the period from 1800–1850. Portions of the trail were first penetrated by Juan Maria de Rivera in 1765, and late in 1776 by Padres Dominquez and Escalante.
2.0	50.8	In the middle ground to the east, Miller Canyon can be seen cutting through the Molen Reef, a topographic escarpment whose western slopes are defined by the anticlinal San Rafael Swell. The Molen Reef rises almost 1,000 feet above the desert floor. In the background through the gap of Miller Canyon, the peaks of the Henry Mountains can be seen. The highest peak on the skyline to the south is Mount Hilgard (elev. 11,527 feet) in the Wasatch Mountains south of I-70.	0.5	62.7	Sandstone cliffs on the west side of Utah Highway 10 are formed by the Emery Sandstone Member of the Mancos Shale. The Emery Sandstone is another fluvial-deltaic wedge that prograded eastward into the Mancos Sea and is 3–4 million years younger than the Ferron Sandstone deltaic complex (fig. 2).
0.2	51.0	Junction with 300 East Street to Miller Canyon road and Interstate-70. Continue south on Utah Highway 10.	0.9	63.6	Fremont Junction. Proceed under the overpass to the south side of I-70 and immediately turn left onto the east-bound entrance ramp. Proceed east onto I-70.
0.3	51.3	Emery (pop. 300, elev. 6250 ft). Emery was established in 1884 by Samuel Williams. Rest Area on the west side of Utah Highway 10.	0.6	64.2	Road cuts expose the Blue Gate Shale Member of the Mancos Shale.
			1.7	65.9	To the north and northwest, the skyline is dominated by the Wasatch Plateau. The Castle Valley lies to the east of the plateau and is floored by the Mancos Shale. The northeastern skyline is Coal Cliffs outcrops of the fluvial-deltaic Ferron Sandstone. Note the gently westward dipping western limb of the north-south trending anticlinal San Rafael Swell.
4.0	55.3	Junction with road to Emery Coal Mine. The mine, inactive since about 1990, is owned by Consolidation Coal Company (Consol). Continue south on Utah Highway 10.			
1.0	56.3	Sevier-Emery County Line. Enter Sevier County. Coal beds can be seen in the Blackhawk Formation in the Wasatch Plateau escarpment to the west.	0.9	66.8	Sevier-Emery County Line. Enter Emery County and continue east on I-70.
0.3	56.6	Junction with BLM access road to the east. In the middle ground to the east the Emery Coal Mine can be seen at the confluence of Quitchapah Creek and Christiansen Wash.	1.1	67.9	To the south of the highway, a Ferron Parasequence Set 5 channel belt occurs within a split in the I <i>coal zone</i> . <i>Coal zones</i> such as this occur at the tops of parasequence sets within the Upper Ferron Sandstone. Splits such as seen here are common in the <i>coal zones</i> . Note
1.6	58.2	To the west, the Joe's Valley fault system can be seen veering off to the north. In this area, the fault system has developed			

		the accretionary surfaces within the channel complex and the mud-filled channel margin on the west side of the channel. Continue east on I-70 through the Ferron Sandstone outcrops.			sub-A (sub-A3 and sub-A4) <i>coal zone</i> . separate these two parasequence sets. Parasequence Set 2A is capped by the A <i>coal zone</i> . Ferron Parasequence Set 3 is chiefly represented by the C <i>coal zone</i> .
0.8	68.7	On the north side of I-70 near Mile Marker 94, the C <i>coal zone</i> . is well exposed and consists of several coal seams, layers of carbonaceous shale, delta plain mudstones and siltstones, and volcanic ash (tonstein).	0.0	74.6	Carefully pull back onto I-70 and proceed west.
			2.7	77.3	Sevier-Emery County Line. Enter Sevier County.
			2.8	80.1	Exit I-70 to north at exit 89. Stop sign at junction of I-70 exit ramp to Utah Highway 10. Turn north onto Utah Highway 10 and proceed north to Emery.
0.1	68.8	On the south side of I-70, the upper split of the A2 <i>coal zone</i> . is very well exposed and contains a thick white tonstein layer. Continue east on I-70 descending through the massive cliffs of Upper Ferron Parasequence Set 2A near-marine sandstones and the more mud-rich delta-front sandstones of Upper Ferron Parasequence Set 1. The gray shale underlying the Ferron Sandstone is the Tununk Shale Member of the Mancos Shale.	12.6	92.7	Junction with 300 East Street in Emery. Turn south and proceed south down 300 East Street.
			0.8	93.5	Junction with Miller Canyon Road on east side of 300 East Street. Proceed south on 300 East Street. Leave paved road and continue on dirt road south. Miller Canyon can be seen to the east cutting through the Coal Cliffs and Molen Reef to the southeast.
2.2	71.0	Ivie Creek Canyon. Note the slope-forming gray Tununk Shale exposed in the mesas to the south of the highway. The Coal Cliffs can be seen to the north of the highway. Mesa Butte is the high butte to the south of the highway. The amphitheater at the mouth of Ivie Creek Canyon exposes the near-marine rocks of Ferron Parasequence Sets 1 and 2.	1.0	94.5	Junction with Emery County Road to east. Continue south on dirt road.
			0.6	95.1	Cattle guard. Junction with Cowboy Mesa County Road. Turn east on the County Road and proceed up the dip slope of Cowboy Mesa. Cowboy Mesa, expressed as the gently sloping topographic feature in the middle ground, is the west side of the topographic Molen Reef and marks the western limb of the San Rafael Swell, in this area.
0.6	71.6	Turn right off I-70 at exit 97. Intersect the north-south Ranch Road, turn north, and cross over I-70. Where the Ranch Road intersects the I-70 entrance ramp, turn west and proceed west onto I-70.	0.7	95.8	Christiansen Wash. Continue on County Road up the dip slope of Cowboy Mesa. The low sandstone outcrop to the north of the road is the retrogradational (back-stepping) near-marine facies of Ferron Parasequence Set 7.
2.2	73.8	Mouth of Quitchapah Creek Canyon is located to the north of I-70. The mouth of Blue Trail Canyon can be seen on the south side of I-70 to the southeast. Note the intense red color of the canyon walls, to the north, due to coal burns in the A and C <i>coal zones</i> .	1.1	96.9	Cattle guard.
			0.5	97.4	Intersection with jeep trail to the south. Turn south and continue along Cowboy Mesa. The sandstone ridges to the east of the road are fluvial channel belts of Ferron Parasequence Sets 5A and 5B.
0.8	74.6	STOP 1: I-70 Road Cut at Ivie Creek (fig 1). (no facilities). Pull off I-70 on the north side of the highway, midway up the narrow road cut. The massive cliffs of the road cut expose the sand-rich Upper Ferron Parasequence Set 2A near-marine sandstones and more mud-rich delta-front sandstones of Upper Ferron Parasequence Set 1 (figs.3, 4 and 6). Two splits of the	0.7	98.1	Cowboy Mine Canyon. Intersection with jeep trail to east and west. Turn east and proceed up switchback, on jeep trail across Cowboy Mesa.
			0.4	98.5	Intersection with jeep trail to west. Turn west onto jeep trail and proceed along the south side of Cowboy Mine Canyon.

0.9	99.4	STOP 2: Overlook of Quitchapah Creek Canyon (fig 1). (no facilities).			through Ferron, Castle Dale, and Huntington and back to Price.
0.0	99.4	Retrace road back to Cowboy Mesa County Road.	49.7	160.8	Junction of Utah Highway 10 with Utah Highways 6 and 191. Turn west onto Utah Highways 6 and 191.
2.0	101.4	Junction of jeep trail with Cowboy Mesa County Road. Turn east onto Cowboy Mesa County Road and proceed up the dip slope of Cowboy Mesa.	1.3	162.1	Pull into parking lot of the Holiday Inn in Price.
0.3	101.7	Junction with jeep trail to the north. Turn north on jeep trail to Bear Gulch.			
DAY 1 STOPS					
Stop 1: I-70 Road Cut at Ivie Creek					
0.1	101.8	STOP 3: Bear Gulch (fig 1). (no facilities).	Vertical Sedimentology and Architecture of the Near-Marine facies of Ferron River-Dominated Parasequence Set 1 and Wave-modified Parasequence Set 2A		
0.0	101.8	Retrace road back to Cowboy Mesa County Road.	The road cut of I-70 through the Ivie Creek Bench, near Mile Marker 94, and the canyon incised by Ivie Creek, near Mile Marker 95, provide excellent 3-D exposures of Upper Ferron Parasequence Sets 1 and 2A (figs. 3, 4, 5, 6, and 7). Ferron Parasequence Set 1 is strongly river-dominated. Parasequence Set 2A is also river-dominated, but it exhibits evidence of substantial wave reworking.		
0.1	101.9	Intersection of jeep trail with Cowboy Mesa County Road. Turn west onto Cowboy Mesa County Road and proceed down the dip slope of Cowboy Mesa.	Ferron Parasequence Set 1 contains at least 12 river-dominated, fluvial-deltaic parasequences. The near-marine parasequences in Ferron Parasequences Set 1 exhibit both vertical and lateral facies changes from (1) stream mouth bar (SMB) to, (2) proximal delta front (pDF) to, (3) distal delta front (ddf) to, (4) prodelta (PD) (fig.5). Distributary channels (DC) and delta plain (DP) facies associations are commonly present as well. Distal prodelta/shelf slumping, indicating instability as a result of rapid deposition, is common. In general, Parasequence Set 1 delta front deposits exhibit little to mild evidence of wave influence. The high proportions of shale present in the near-marine facies of the parasequences within Parasequence Set 1, are characteristic of river-dominated delta front deposits.		
2.7	104.6	Junction with Emery County Road. Turn north on County Road and proceed north.	At the I-70 road-cut and along Ivie Creek, Parasequences 1e, 1f, 1g, and 1j are exposed. Parasequences 1e-f are represented by distal bar delta front deposits consisting of steeply dipping (310°–335° azimuth) prograding clinoforms (fig. 4). These clinoforms average about 3 m thick at their thickest part. Parasequence 1g also exhibits dipping, prograding clinoforms, although these clinoforms are of a much smaller scale (<1.5 m). The uppermost parasequence (Parasequence 1j) occurs within a split in the sub-A coal zone, and is represented at this outcrop as a thick succession of brackish water mudstones, containing fragments of gastropods and molluscs, as well as crevasse splay deposits. A selected portion of a measured section from I-70 showing Parasequences 1f, 1g, and 1j is shown in figure 5.		
0.6	105.2	Junction with Emery County Road to the east. Turn east and proceed east along County Road.	Ferron Parasequence Set 2A contains 4 wave-modified, river dominated, fluvial-deltaic parasequences (denoted as		
0.7	105.9	Junction with paved Miller Canyon Road. Turn southeast on Miller Canyon Road and proceed.			
1.0	106.9	Cattle guard. Enter Miller Canyon and descend along paved road. The massive sandstone outcrops are fluvial channel belt sandstones of Ferron Parasequence Sets 5A and 5B.			
0.3	107.2	Midway up the canyon walls, outcrops of the Ferron <i>G Coal zone</i> can be seen. In Miller Canyon, the <i>G coal zone</i> is dominantly carbonaceous shale and contains only three thin coal seams.			
0.2	107.4	On the east side of the Canyon, near the base of the cliffs, a small mine shaft into the <i>C coal zone</i> can be seen. Whitish-gray tonstein layers can be seen in this 2.6 m thick coal seam.			
0.1	107.5	STOP 4: Miller Canyon (fig 1). (no facilities).			
0.0	107.5	Pull back on Miller Canyon Road and proceed on paved road northwest back to Emery.			
2.8	110.3	Junction with Emery 300 East Street. Turn north on 300 East Street and proceed.			
0.8	111.1	Junction with Utah Highway 10. Turn east and proceed along Highway 10			

2a–2d). The near-marine facies of these parasequences exhibit both vertical and lateral facies changes (1) stream mouth bar and reworked stream mouth bar (frequently preserved as upper shoreface deposits (USF)), to (2) reworked delta front (pDF and dDF) (frequently preserved as middle (MSF) and lower shoreface (LSF) deposits), to (3) prodelta (figs. 6 and 7). The mouth bar deposits exhibit well-developed trough stratification. The distal bar deposits are moderately burrowed (*Ophiomorpha*, *Teichichnus*, and *Thalassinoides*) and locally exhibit well-developed hummocky stratification and planar stratification.

Figure 6 is a photograph of an outcrop of Parasequence Set 2A at I-70 showing Parasequences 2a, 2b, and 2c. A selected portion of a measured section at the I-70 roadcut showing Parasequences 2a, 2b, and 2c is shown in figure 7. The low proportion of shale present in Parasequences 2a and 2b, at I-70, is characteristic of wave reworked distal bar deposits in Parasequence Set 2A. Parasequence 2c occurs between the A1 and A2 coal zones.

Composition and Stratigraphic Positions of the Ferron Sub-A, A, and C Coal Zones

Coal zones have been defined by Garrison and van den Bergh (1996) as coal seams and their laterally equivalent carbonaceous shales and siltstones, carbonaceous rich mudstones and siltstones, paleosols, rooted horizons, and inter-layered flood plain mudstones and siltstones. The sub-A coal zone caps Ferron Parasequence Set 1; the A coal zone caps Ferron Parasequence Set 2; the C coal zone caps Ferron Parasequence Set 3. At I-70, the delta plain facies association of Parasequence Set 3 overlies the A coal zone (fig. 3). At the I-70 road cut, Parasequence Set 3 is composed dominantly of the C coal zone.

The sub-A coal zone splits into two components near I-70, where they are designated the sub-A₃ and sub-A₄, which are 0.6 m and 0.3 m thick, respectively. The A coal zone splits into two components denoted A₁ and A₂; the A₁ coal zone disappears near I-70; the A₂ coal zone splits into two components near Corbula Gulch, denoted A₂ and A₃, and are well exposed at I-70. The A₂ and A₃ coal zones are 2.5 m and 0.6 m thick at I-70, respectively and are separated by a small mud-filled fluvial channel. The C coal zone splits into two components denoted C₁ and C₂; the C₂ coal zone pinches out at Blue Trail Canyon and is not present at I-70. A selected portion of a measured section from I-70 showing the nature and composition of the 6.3 m thick C₁ coal zone is shown in figure 15. The C coal zone is composed of 26% coal, 7% carbonaceous shale, 19% mudstone, 44% delta plain sandstones and siltstones, and 4% tonstein.

Within coal zones, coal seams themselves are rarely homogeneous and can generally be sub-divided into dis-

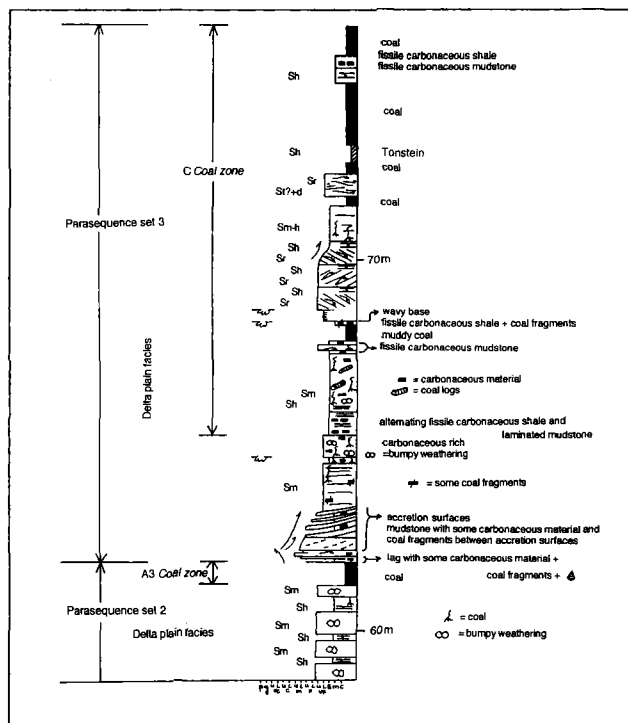


Figure 15. Measured section through the Upper Ferron C coal zone at the I-70 roadcut. Symbols and nomenclature defined as in figure 5.

tinct lithological sections. A distinct lithologic subdivision of a coal seam that has a uniform character is called a ply or coal lithotype. A lithotype that can be correlated through a seam over large lateral distance is defined as a coal facies. Figure 16 shows the lithotype (i.e., coal brightness) profiles of the A₂ coal zone and the C₁ coal zone at I-70.

In the Ferron Sandstone, coal zones frequently contain volcanic ash layers. These volcanic ash horizons are characterized as laterally continuous kaolinitic claystone partings called "tonsteins." Some whitish tonstein layers are almost completely kaolinized, while the other more grayish tonsteins are dominantly bentonitic and contain a full suite of volcanic minerals such as beta quartz, volcanic K-feldspars, Fe-oxide and Ti-oxide minerals, and zircons (fig. 14) (van den Bergh, 1995). The tonsteins associated with the Ferron Sandstone coal zones may represent time lines within the coal zone horizons. Splits in coal zones and multiple tonstein layers clearly indicate significant time represented by these coal zone deposits.

Tonsteins have been found in all major coal zones in the Ferron Sandstone (Garrison and van den Bergh, 1997). Many coal zones contain multiple tonstein layers. At I-70, the sub-A coal zone is devoid of tonstein layers, but further south in the Limestone Cliffs, it contains a very well-devel-

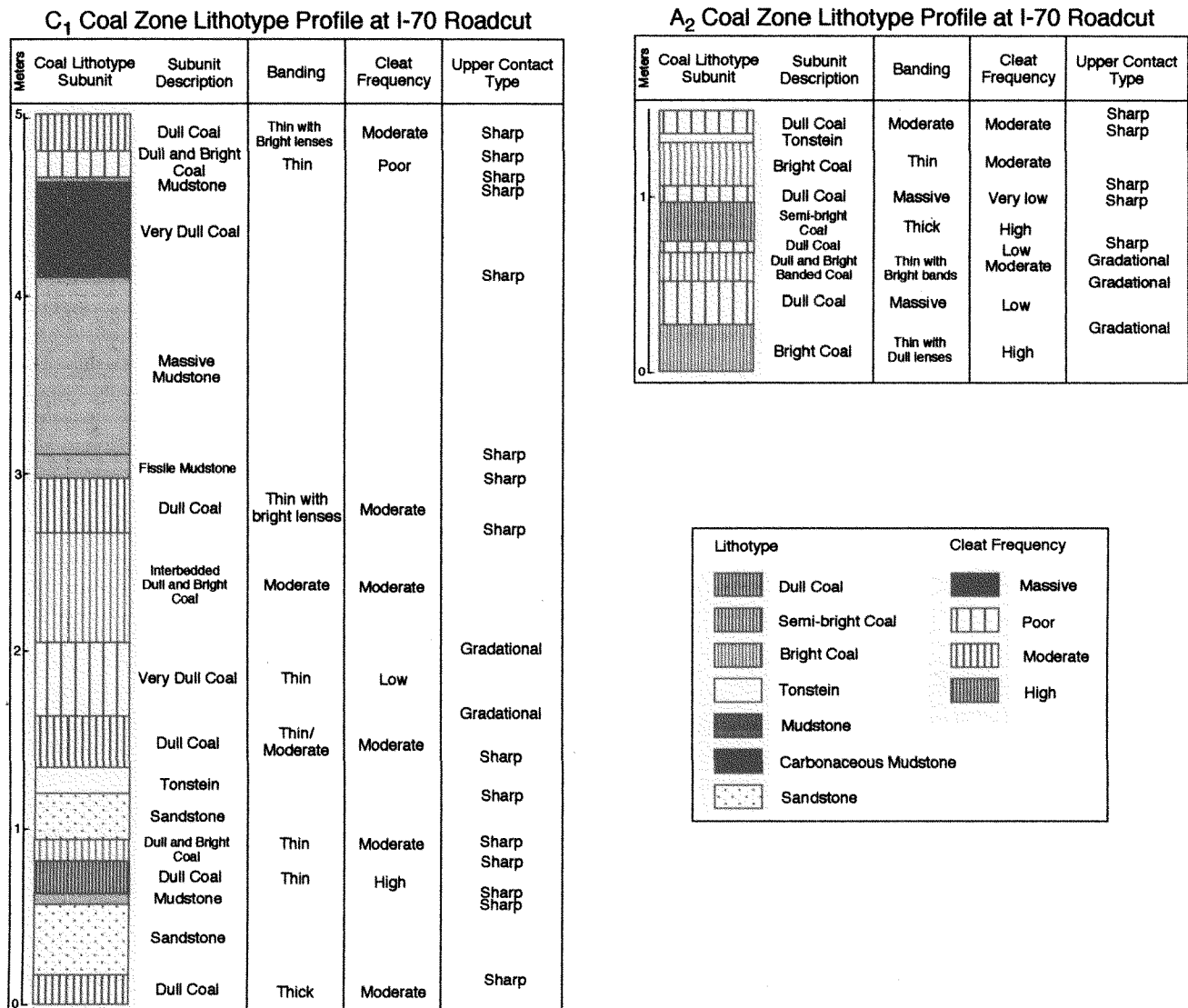


Figure 16. Lithotype profiles of the A₂ and C₁ coal zones at the I-70 roadcut.

oped tonstein. At I-70, the A₂ coal zone contains a 5 cm thick tonstein layer. The tonstein in the A₁ coal zone is not preserved at I-70, but it can be found just south of I-70 and can be traced to the Limestone Cliffs. North of I-70, the A₂ coal zone contains two tonsteins that can be traced northward to at least Bear Gulch. At I-70, the C coal zone contains a 23 m thick tonstein. North of I-70, the C coal zone contains at least two tonsteins. In some areas, north of I-70, the C coal zone contains up to four distinct tonsteins. Frequently these tonsteins show evidence of reworking. No tonsteins have been identified in the C coal zone south of Corbula Gulch. Tonsteins are generally preserved at, and seaward of the landward pinch-outs of the near-marine deltaic sands. As tonsteins are traced landward of near-

marine pinch-outs, preservation potential decreased dramatically.

Key Concepts of Stop 1:

- The river-dominated, near-marine facies of Ferron Parasequences 1e, 1f, and 1g exhibit a vertical shoaling upward sedimentary profile and contain high proportions of shale. The vertical stacking pattern of Parasequence Set 1, indicates that each successively younger parasequence steps seaward (i.e., is progradational), relative to the underlying parasequence.
- The river-dominated, but wave-modified, near-marine facies of Ferron Parasequences 2a, 2b, and

2c, of Parasequence Set 2A, exhibit a vertical shoaling upward sedimentary profile and are extremely sand-rich. Parasequence Set 2A is a progradational (seaward-stepping) parasequence set.

- *Coal zones* are lithologically complex and are composed of coal seams, carbonaceous shales and siltstones, carbonaceous rich mudstones and siltstones, paleosols, rooted horizons, and interlayered flood plain mudstones and siltstones. *Coal zones* occur at the tops of parasequence sets. *Coal zones* frequently split into multiple zones.
- Coal facies are distinct, uniform, lithologic subdivisions of a coal seam that can be correlated through a seam over large lateral distance.
- *Coal zones* frequently contain altered volcanic ash layers called "tonsteins." Tonsteins tend to be preserved at and seaward of the landward pinch-outs of the delta front sands. As tonsteins are traced landward of near-marine pinch-outs, preservation potential decreases dramatically.

Stop 2: Quitchapah Creek Canyon

Lateral (Dip Section) Stacking and Architecture of the Near-Marine facies of Ferron River-Dominated Parasequence Set 1 and Wave-modified Parasequence Sets 2A and 2B

The canyon incised by Quitchapah Creek provides excellent 2-D, dip section, exposures of Upper Ferron Parasequence Sets 1, 2A, and 2B (fig.3). Ferron Parasequence Set 1 contains at least 12 river-dominated, fluvial-deltaic parasequences, that exhibit a seaward-stepping stacking pattern. In Quitchapah Creek Canyon, elements of 6 of these parasequence can be seen (Parasequences 1f–1k). In general, each successively younger parasequence steps seaward by an average of 2–5 km. The near-marine sandstones of Parasequence Set 1 extend at least 27 km in the dip direction.

Ferron Parasequences 1e, 1f, 1g, and 1i formed in response to the progradation of very small, river-dominated sub-delta lobes prograding in a northwesterly direction (310°–335° azimuth). Parasequences 1e, 1f, 1g, and 1i are approximately 2.9 km, 3.7 km, 2.5 km, and 3.2 km in strike width, respectively, and the maximum thicknesses are 22 m, 17 m, 10 m, and 13 m, respectively. Parasequence 1h and 1k appear to represent small delta lobes prograding in a northeasterly direction. Their dip lengths are approximately 2.5 km and 2.6 km and maximum thicknesses are 15 m and 6 m, respectively. Parasequence 1j, occurring with a split in the sub-A *coal zone*, is represented in the outcrop belt as a brackish water bay mudstone, to the south at I-70, and a small 2.92 km, 3 m thick delta front sandstone body

occurs in Quitchapah Creek Canyon. Parasequence 1k can be seen pinching out into a split of the sub-A *coal zone*.

Parasequence Set 2A contains 4 river-dominated, wave-modified parasequences, that exhibit a seaward-stepping stacking pattern (Parasequences 2a–2d). All 4 can be seen in Quitchapah Creek Canyon. The near-marine sandstones of Parasequence Set 2A extend about 36 km in the dip direction. Parasequence 2e of Parasequence Set 2B is also exposed in Quitchapah Creek Canyon. The true extend of Parasequence 2e cannot be determined due to erosional truncation by fluvial channels in the overlying Parasequence Set. Parasequence 2e is hierarchically equivalent to a parasequence set and is placed in Parasequence Set 2B.

Parasequences 2a and 2b appear to represent large wave influenced, river-dominated delta lobes prograding seaward in a northeasterly direction. Parasequences 2a, 2b, 2c, and 2d all progrades northeast with azimuths of 025°, 045°, 025°, and 050°, respectively. The near-marine facies of Parasequences 2a, 2b, 2c, and 2d are approximately 18.0 km, 15.1 km, 11.4 km, and 24.0 km in dip length, respectively and maximum thicknesses are 31 m, 16 m, 10 m, and 19 m, respectively. The landward pinch-out of the near-marine facies of Parasequence 2b steps seaward 3.5 km, relative to the landward pinch-out of the near-marine facies of the immediately underlying Parasequences 2a. The landward pinch-out of near-marine facies of Parasequence 2c occurs almost 7.5 km seaward of the landward pinch-out of the underlying Parasequence 2b. The landward pinch-out of Parasequence 2d steps seaward almost 2.7 km from the pinch-out of Parasequence 2c. The landward pinch-out of Parasequence 2e steps seaward only about 0.5 km from the pinch-out of Parasequence 2d.

Although their compositions may vary laterally and they may split into multiple components, *coal zones* occur at the tops of parasequence sets. When they are not present at the tops of parasequence sets, it is due to the development of erosional unconformities associated with high-order sequence boundaries. This is well illustrated in Quitchapah Creek Canyon. In Quitchapah Creek Canyon, Parasequence Set 1 is capped by the sub-A (sub-A3 and sub-A4) *coal zone*. The sub-A3 and sub-A4 section of the sub-A *coal zone* extends some 8.5 km, from Blue Trail Canyon to North Quitchapah Creek. The total dip length for the sub-A *coal zone* is at least 27 km. In Quitchapah Creek Canyon, Parasequence Set 2 is capped by the A (A2 and A3) *coal zone*. The A *coal zone* extends over 40 km, from the Limestone Cliffs to north of Dry Wash. In Quitchapah Creek Canyon, the reddish coloring of the outcrop is due to a coal burn in the C *coal zone*. The C *coal zone* splits in the southern part of Quitchapah Creek Canyon and become one zone again in the northern part of Quitchapah Creek Canyon. The C *coal zone* extends over 34 km, from the Limestone Cliffs to just south of Dry Wash.

Key Concepts of Stop 2:

- The river-dominated, near-marine facies of Ferron Parasequences 1e, 1f, 1g, 1h, and 1i exhibit a down dip stacking pattern, within Parasequence Set 1, indicating that each successively younger parasequence steps seaward (i.e., is progradational), relative to the underlying parasequence.
- The river-dominated, but wave-modified, near-marine facies of Ferron Parasequences 2a, 2b, 2c and 2d, of Parasequence Set 2A, exhibit a progradational (seaward-stepping) down dip pattern.
- *Coal zones* are quite laterally extensive. The lateral dip section extend of the sub-A *coal zone* is over 27 km. The sub-A3 and sub-A4 section of the sub-A *coal zone* extends 8.5 km. The lateral dip section extends of the A and C *coal zones* are at least 40 km and 34 km, respectively.
- *Coal zone* compositions vary laterally and frequently they may split into multiple components. Within the Ferron clastic wedge, *coal zones* occur at the tops of parasequence sets. When they are not present at the tops of parasequence sets, it is due to the development of erosional unconformities associated with high-order sequence boundaries.

Stop 3: Bear Gulch

Depositional Sequence Stratigraphy and Sedimentology of the Near-Marine facies of Ferron Parasequence Sets 2A, 2B, 2C and Parasequence Sets 4A and 4B and the Nature of the Sequence Boundaries above Ferron 4th-order Sequences FS1 and FS2

The small north-south trending canyon of Bear Gulch exposes near-marine facies of Parasequence Sets 2A, 2B, 3, and 4A and non-marine facies associations of Parasequence Sets 4B, 5, and 6 (fig. 3). The sequence boundaries between FS1 and FS2 (i.e., SB1) and between FS2 and FS3 (i.e., SB2) are both well exposed in this canyon. Parasequences 1i and 1k, of Parasequence Set 1, pinch-out at the bottom of the southern end of the canyon of Bear Gulch.

The canyon exposes the seaward portions of parasequences 2a and 2b and more proximal portions of Parasequences 2c and 2d of Parasequence Set 2A. In this outcrop, the small back-stepped Parasequence 2e of Parasequence Set 2B can be seen sitting on a yellowish, highly bioturbated, transgressive lag deposit that overlies Parasequence 2d. This transgressive lag deposit can be traced over 5 km northward into Muddy Creek Canyon. Parasequence 2e has a very small mouth bar deposit and for much of its length, it has distal bar delta front facies lying strati-

graphically above the mouth bar deposits of Parasequence 2d suggesting a slight back-stepping relative to Parasequence 2d. Parasequence 2e is almost completely scoured out by the fluvial channel belts of the overlying Parasequence Set 2C. This is best seen near the northwestern end of the canyon of Bear Gulch to Miller Canyon and on into Muddy Creek Canyon. In some areas, this surface represents over 25 m of erosion into Parasequence Set 2A and 2B. This erosional surface can be identified in outcrops from Coyote Basin to Muddy Creek Canyon, representing a distance of over 18 km. Based on the back-stepped nature of Parasequence Set 2B, lying immediately below this surface, and the regional extent of the erosional surface between Parasequence Sets 2B and 2C, this erosional surface has been interpreted to represent the sequence boundary between Ferron 4th-order Sequences FS1 and FS2. Parasequence Sets 1, 2A, and 2B have been assigned to Ferron 4th-order Sequence FS1 and Parasequences 2C, 3, and 4A have been assigned to Ferron 4th-order Sequence FS2.

In Bear Gulch, the upper part of Parasequence Set 2C, capped by the stacked A and C *coal zones*, is represented by a laterally restricted, flood tidal delta. This unit can be traced to the south of Bear Gulch only about 0.9 km and pinches out into the C *coal zone* on the western canyon wall of Bear Gulch. A correlative unit crops out again in Miller Canyon. These small flood tidal deltas crop out about 1 km landward of the associated shoreline near-marine facies, *sensu stricto*, of Parasequence 2g. This small near-marine unit rests on a thin, 30 cm thick, section of the A *coal zone*. The A *coal zone* pinches out 16 km northward of Bear Gulch, just north of Dry Wash. The flood tidal delta deposit of Parasequence Set 2C, exposed in Bear Gulch, is represented by a sand-rich middle to upper shoreface facies that is trough and herringbone cross-stratified and contains abundant *Ophiomorpha* burrows in the upper part and *Thalassinoides* burrows in the lower part.

Parasequence Set 4A is represented, in the outcrops of Bear Gulch, by the reworked stream mouth bar/upper shoreface and reworked proximal delta front/middle shoreface facies of Parasequence 4a. Parasequence 4a rests on the C *coal zone* and has a bioturbated base with sand-filled *Thalassinoides* burrows extending into the underlying C *coal zone*. Large wood fragments can also be seen in the base above the C *coal zone*. The lower part of Parasequence 4a is sand-rich, with horizontal to massive bedding, and is pervasively burrowed, containing *Thalassinoides* and *Teichichnus*, with occasional *Ophiomorpha* burrows. The upper part of Parasequence 4a is sand-rich, with trough cross-stratification, and contains pervasive *Ophiomorpha*. The upper surface of Parasequence 4a is scoured by the fluvial channel belts of Parasequence Set 4B (fig. 8). There is up to 20 m of erosion of Parasequence Set 4A by the fluvial

facies of Parasequence Set 4B. In the non-marine part of the Parasequence Set 4A, south of Bear Gulch, Parasequence Set 4A is capped by a very laterally extensive rooted zone (designated the E Rooted Zone). This rooted zone can be traced from just north of Last Chance Creek northward to just south of Bear Gulch, where it is correlative with the erosional unconformity between Parasequence 4A and 4B cropping out from Bear Gulch to Miller Canyon to Muddy Creek (i.e. over 5 km). The paleoshoreline of the near-marine facies of Parasequence 4B shifts basinward some 7 km relative to the paleoshoreline of Parasequence 4A and is accompanied by at least 20 m of erosion. Northward in Miller Canyon, Parasequence 4A lies on a thick transgressive lag deposit, that is represented in Bear Gulch by only the *Thalassinoides* bioturbation of the upper part of the *C coal zone*. This lag can be traced 13 km north to Dry Wash. This change in shoreline position and baselevel and the development of an erosional unconformity indicate that the boundary between 4A and 4B is the sequence boundary between FS2 and FS3. Parasequence Sets 4B and 5A are assigned to Ferron 4th-order Sequence FS3.

Volcanic Ash Layers and Composition of the C Coal Zone

In Bear Gulch, the A and C *coal zones* are stacked into 5.9 m thick composite *coal zone* composed of 60% coal, 28% carbonaceous shale, 3% mudstone, and 9% tonstein. The coal lithotype profile is shown in figure 17. Based on tonstein regional correlations, the lower 3.7 m has been assigned to the A *coal zone*. The C *coal zone* is 2.2 m thick and is composed of 80% coal, 20% tonstein. A coal zone is composed of 42% coal, 45% carbonaceous shale, 10% mudstone and sandstone, and 3% tonstein. The composite A and C *coal zone*, in Bear Gulch, contains 5 tonsteins. The upper four tonsteins have been assigned to the C *coal zone* and the lower tonstein to the A *coal zone*. The uppermost tonstein in the C *coal zone* is a 5 cm thick impure tonstein, suggesting mixing of volcanic material with other terrigenous material. The thickest tonstein in the C *coal zone* is 30 cm thick. Below this thick tonstein is a tonstein doublet. The uppermost tonstein doublet is 3 cm thick and the lower is 5 cm thick. The thick, upper tonstein of the C *coal zone* can be traced over 13 km, from Miller Canyon southward (i.e., landward) to Corbula Gulch, south of Blue Trail Canyon, where it is 40 cm thick. There are no tonsteins preserved in the C *coal zone* further south than Corbula Gulch. Tonsteins correlative with the tonstein doublet can be traced as far south as Cowboy Mine Canyon and as far north as Miller Canyon. The tonstein in the A *coal zone* is 10 cm thick. This A *coal zone* tonstein can be correlated as far south as I-70 and as far north as Pictograph Point at the confluence of Muddy Creek and Rochester Creek.

C Coal Zone Lithotype Profile in Bear Gulch

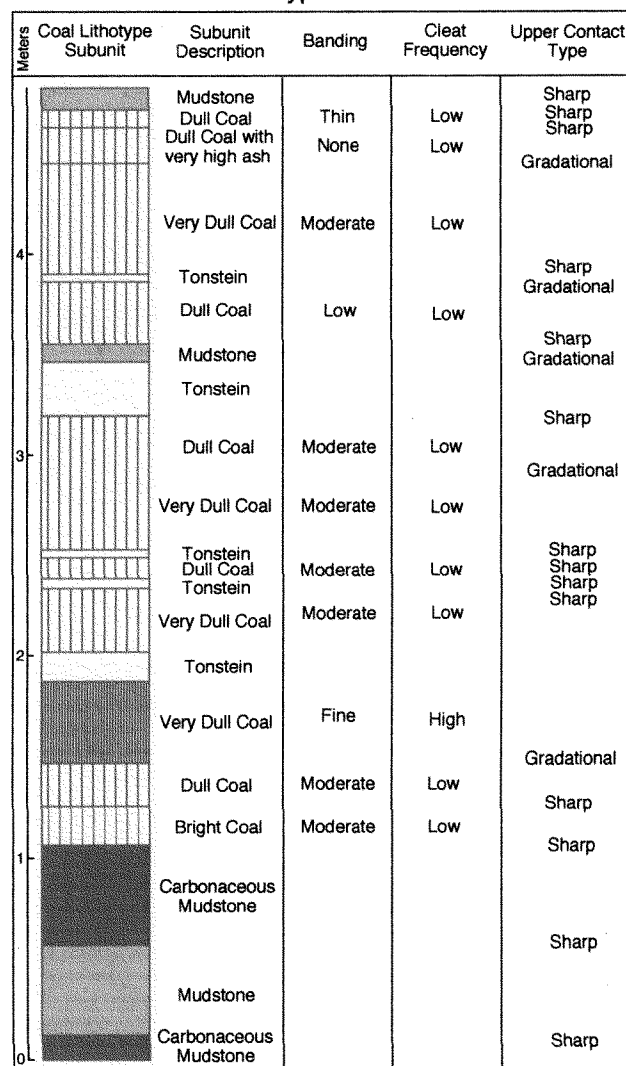


Figure 17. Lithotype profile of the A and C composite coal zone at Bear Gulch.

Coals such as those exposed within the A-C *coal zone* at Bear Gulch consist of microscopically identifiable organic substances formed from the initial plant materials and altered plant materials within the peat accumulation (i.e., cell wall material, spores, resins, cuticles, and fossil charcoals). These organic substances are called macerals. There are three basic maceral groups called vitrinite, liptinite, and inertinite. Vitrinites are generally derived from plant cell wall or woody material. Liptinites are derived from spores, cuticles, and resins. The inertinites represent fossil charcoal material and other oxidized, inert plant debris. The abundance and distribution of these macerals in coal seams is controlled by the original peat composition, as well as both

pre-burial history. The maceral compositions have been compiled for coal seams from the Ferron Sandstone C and I coal zones (Sommer et al., 1991; Crowley et al., 1989). The Ferron C coal has a complex composition due to the presence of thick, laterally extensive altered volcanic ash layers (tonsteins) (Crowley et al., 1989). Sampling above and below tonsteins produced two distinct maceral compositions (figure 18). The C coal samples taken immediately below tonsteins (Group B) have a higher percentage of inertinite (range = 31–50% and mean = 38%) relative to vitrinite (range = 45–65% and mean = 57%), while samples taken immediately above tonsteins (Group A) have a higher percentage of vitrinite (range = 72–89 and mean = 80%) relative to inertinite (range = 5.7–21.0 and mean = 14.6%). Liptinites remain fairly constant between the two groups, with means of 5.3% and 5.4%, respectively. Desmocollinite, telenite, and detrocollinite are the dominant vitrinite group macerals. Semifusinite, fusinite, and inertodetrinite are the dominant inertinite group macerals. Resinite, exsudatinites, and fluorinites are the dominant liptinite group macerals. Four samples taken from below tonsteins fall within Group A. Crowley et al., (1989) suggested that precursor peats formed in well drained environments until volcanic ash layers created impermeable zones and caused waters in the peat swamp to pond. Well drained, oxidizing initial conditions were favorable for the formation of degradofusinites, while poorly drained, more nutrient-rich conditions, following an ashfall, would be more conducive to the preservation of vitrinite.

Key Concepts of Stop 3:

- The sequence boundary between Ferron 4th-order Sequences FS1 and FS2 is represented, in Bear Gulch, as an erosional unconformity between the near-marine facies of Parasequence Set 2B and fluvial channel belt facies of Parasequence Set 2C. This sequence boundary can be traced over 18 km and exhibits up to 25 m of erosional relief. The back-stepped Parasequence 2e of Set 2B lies on a bioturbated transgressive lag deposit that can be traced over 3 km northward.
- The sequence boundaries between Ferron 4th-order Sequences FS2 and FS3 is represented, in Bear Gulch, as an erosional unconformity between the near-marine facies of Parasequence Set 4A and fluvial channel belt facies of Parasequence Set 4B. This sequence boundary can be traced over 5 km and exhibits up to 20 m of erosional relief.
- The A and C coal zones are stacked in Bear Gulch forming a thick composite zone containing 5 ton-

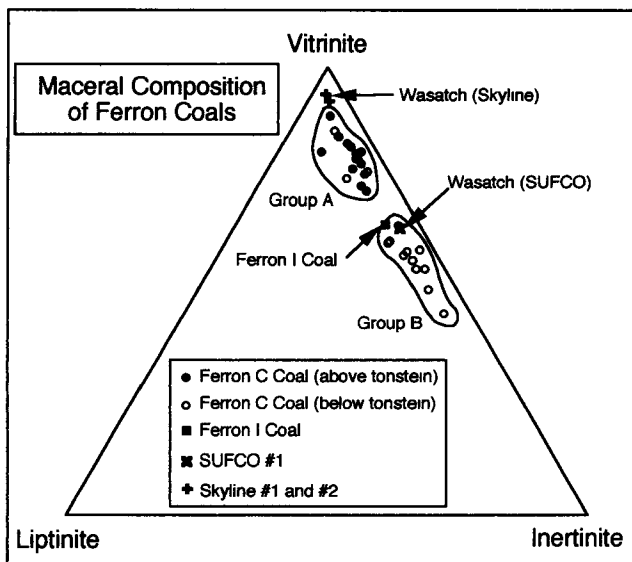


Figure 18. Ternary diagram showing the maceral composition of the Upper Ferron coal seams.

steins. The C coal zone is 2.2 m thick and contains 4 tonsteins, the thickest of which is 30 cm thick. This thick tonstein can be traced over 13 km. The lower 3.7 m of the composite zone and the lowest tonstein has been assigned to the A coal zone.

- Volcanic ash deposits alter the local environments within peat accumulations. These lead to variations in, and the alteration of, coal composition and coal quality.

Stop 4: Miller Canyon

Nature of the C Coal Zone to the Transgressive Lag Deposits of Parasequence Set 3 and the Near-Marine Sandstones of Parasequence Set 4A

The outcrops of Miller Canyon offer a final opportunity to examine the composition of the C coal zone and evaluate the variations in the C coal zone over a substantial distance along the Ferron outcrop belt. We have examined the C coal zone at two previous localities, I-70 and Bear Gulch. From I-70 to Miller Canyon, a down dip distance of over an 8 km has been traversed.

In Miller Canyon, the A and C coal zones are stacked together into a composite 6.2 m thick coal zone which is composed of 44% coal, 38% carbonaceous shale, 16% mudstone, and 6% tonstein. This coal zone is correlative with the exposures in Bear Gulch, therefore the lower 5.0 m of the zone is assigned to the A coal zone. The coal lithotype profile for the coal zone is shown in figure 19. The C coal

C Coal Zone Lithotype Profile in Miller Canyon

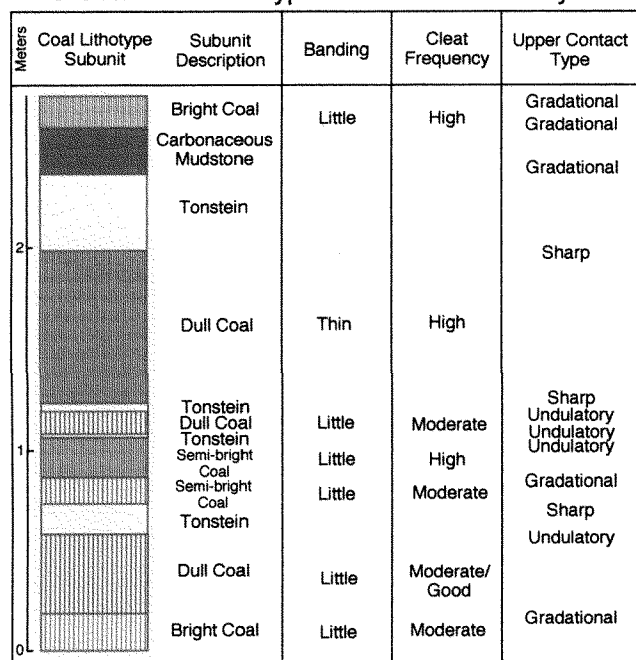


Figure 19. Lithotype profile of the A and C composite coal zone in Miller Canyon.

zone is composed of 76% coal and 24% tonstein. The A coal zone is composed of 35% coal, 42% carbonaceous shale, 20% mudstone, and 2% tonstein. The C coal zone, in Miller Canyon, contains three tonsteins. The thick tonstein seen in the C coal zone in Miller Canyon is the same tonstein examined in Bear Gulch and at the I-70 road cut. Recalling, at I-70 only a single tonstein was present, in Bear Gulch four tonsteins were present, and at this outcrop in Miller Canyon, only three tonsteins are present. About 4 km north of Miller Canyon, at Pictograph Point, where the C coal zone goes into the subsurface, the C coal tonsteins are still preserved. The lower tonstein in the composite A and C coal zone is assigned to the A coal zone.

The C coal zone is 6.3 m thick at I-70 and increases northward until it is 13.8 m thick in Quitchapah Creek Canyon and decreases again northward until it is 6.2 m thick in Miller Canyon. The percentage of the C coal zone that is coal varies from 26% at I-70 (1.6 m) to 40% in Quitchapah Creek Canyon (5.5 m) to 80% at Bear Gulch (1.8 m) to 76% in Miller Canyon (1.0 m). Figure 20 shows the lateral coal facies cross-section of the C coal from I-70 to Miller Canyon.

In Miller Canyon, prodelta deposits of Parasequence 4a of Parasequence Set 4A rests on a 2 m thick transgressive lag deposit. This lag deposit can be traced into Bear Gulch, where the reworked distal delta front facies lie on the feath-

ered up-dip end of the transgressive lag, and as far north as Dry Wash, a distance of 13 km. In Miller Canyon, this lag is a fine to medium grained, poorly sorted, fining-upward deposit that reworks the upper part of the C coal zone and exhibits extreme bioturbation. Abundant *Ophiomorpha*, *Thalassinoides*, and *Teichichnus* are present at the top of the lag deposit. This deposit represents the lag developed during the sea-level transgression prior to the development of the back-stepped deltaic deposits of Parasequence 4a of Parasequence Set 4A. The shoreline shifted landward by over 7 km.

Key Concepts of Stop 4:

- The C coal zone contains 2 tonsteins, the thickest of which is 30 cm thick. The thick tonstein can be traced over 18 km within the C coal zone.
- The C coal has lithofacies and tonsteins that can be correlated over a distance of at least 20 km.
- Parasequence 4a rests on a 2 m thick transgressive lag deposit. This deposit reworks the upper part of the C coal zone and exhibits extreme bioturbation. This lag was developed during the sea-level transgression prior to the development of the back-stepped deltaic deposits of Parasequence Set 4A.

DAY 2 ROAD LOG

Int. Miles	Cum. Miles	
0.0	0.0	Leave parking lot of Holiday Inn in Price, Utah. Travel east on Utah Highways 6 and 191.
1.3	1.3	Exit 241. Junction with Utah Highway 10. Travel south on Utah Highway 10 through Huntington, Castle Dale, Ferron and Emery to Fremont Junction.
62.1	63.4	Fremont Junction. Junction of Utah Highway 10 with I-70. Proceed under overpass under I-70 and continue south on unpaved Sevier County Road.
2.0	65.4	Junction with Dog Valley Coal Mine Road. Continue east on unpaved County Road.
0.8	66.2	Jeep trail to east of the County Road leads to Scabby Canyon, Blue Trail Canyon, Corbula Gulch, and Rock Canyon.
0.6	66.8	U.S.G.S. drill hole WS-22 is located on the east side of the road. In 1977, eight drill holes were put down in Willow Springs Quadrangle to evaluate and classify the federally owned coal resources

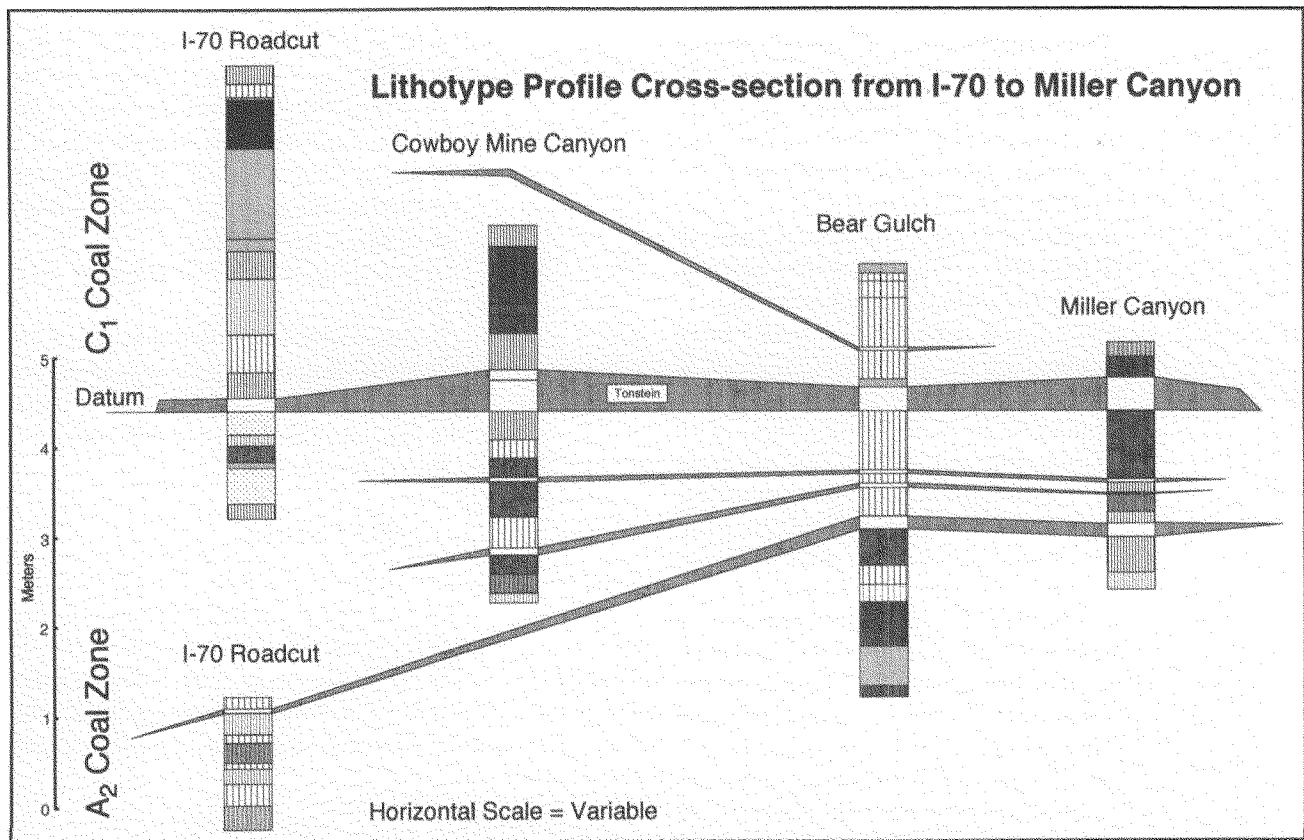


Figure 20. Lithotype profile cross-section of C coal zone from I-70 to Miller Canyon.

- and lands in the Emery Coal Field of the Upper Ferron Sandstone.
- 0.3 67.1 Jeep trail to the east of the County Road leads to Coyote Basin and Rock Canyon. A second jeep trail, up ahead a short distance, turns off to the west. U.S.G.S. drill hole WS-17 is located just north of this western jeep trail, about 0.5 miles west of the County Road.
- 0.6 67.7 Jeep trail to the east leads to the north canyon wall of Willow Springs Wash. Hills on the western skyline are formed of the Blue Gate Shale. Continue south on County Road.
- 0.2 67.9 Willow Spring Amphitheater. An outcrop of the Ferron Sandstone I coal zone can be seen on the south side of the County Road. Note the distributary channel belt of Ferron Parasequence Set 6 sitting on the I coal zone. Descend into Willow Springs Wash via County Road.
- 0.6 68.5 Willow Springs Wash. Note the small

coal mine developed (and abandoned) in the Ferron A coal zone. Small mining shacks can be seen on both sides of the County Road and the mine loading chute can be seen down in bottom of Willow Springs Wash on the south side of the County Road, just ahead.

- 0.1 68.6 **STOP 5: Willow Springs Wash South Canyon Wall** (fig.1). Pull off on the south side of the County Road. Walk through Willow Springs Wash and climb up onto the south canyon wall.
- 0.0 68.6 Return to vehicles and proceed east along County Road on north side of Willow Springs Wash.
- 0.6 69.2 **STOP 6: Willow Springs Wash North Canyon Wall and The County Line Channel** (fig.1). Turn into dirt road on the north side of the County Road. Climb up to the base of the County Line Channel.

0.0	69.2	Return along County Road to the west to the Junction with I-70 and Utah Highway 10.			Utah Highway 10 onto dirt road leading up to pump jack of the Utah 17-103 Coal-bed Methane well. These pump jacks are used to pump produced salt water to the surface, along with the produced gas. The water is then disposed of by pumping units that pump it back into the subsurface Navajo Sandstone.										
5.8	75.0	Fremont Junction. Junction of Utah Highway 10 with I-70. Proceed under overpass under I-70 and continue north on Utah Highway 10.													
4.3	79.3	Junction with paved road, to the east, to Hidden Valley Mine. The mine, currently owned by Consol, has been reclaimed.	0.0	137.4	Continue north on Utah Highway 10 to Price.										
3.0	82.3	Sevier-Emery County Line. Enter Emery County.	3.9	141.3	Junction with Utah Highways 6 and 191 in Price. Turn west onto Utah Highways 6 and 191 and continue northwest to Helper, Spanish Fork, and Salt Lake.										
1.0	83.3	Junction with road to Emery Coal Mine. Turn east onto Emery Coal Mine Road and proceed east toward Cowboy Mesa of the Molen Reef. Note the water pumping unit on the north side of the road. This unit is used by Consol to pump water from the Emery Mine Shafts 740 feet below. It is either used for irrigation or is held in holding ponds and then returned to Quitchapah Creek. This marks the northwestern extent of the underground Emery Mine.	0.0	113.6	End of Road Log.										
DAY 2 STOPS															
Note: Since the focus of the Day 2 Field Trip Stops will be petroleum and coal exploration and production oriented, the Day 2 Field Trip Stops will be discussed using the English units of feet, miles, and acres, in order to be consistent with current energy industry practice in the United States. The units of conversion for some of these units are given below:															
<table><tr><td>1 ft = 0.3048 meters</td><td>1 meter = 3.28 ft</td></tr><tr><td>1 mile = 1.609 km</td><td>1 km = 0.621 miles</td></tr><tr><td>1 acre = 43560 ft²</td><td>1 acre = 4049 m² = 0.004 km²</td></tr><tr><td>1 mi² = 640 acres</td><td>1 km² = 247 acres</td></tr><tr><td>40 acre well spacing = 1380 ft</td><td>40 acre well spacing = 421 meters</td></tr></table>						1 ft = 0.3048 meters	1 meter = 3.28 ft	1 mile = 1.609 km	1 km = 0.621 miles	1 acre = 43560 ft ²	1 acre = 4049 m ² = 0.004 km ²	1 mi ² = 640 acres	1 km ² = 247 acres	40 acre well spacing = 1380 ft	40 acre well spacing = 421 meters
1 ft = 0.3048 meters	1 meter = 3.28 ft														
1 mile = 1.609 km	1 km = 0.621 miles														
1 acre = 43560 ft ²	1 acre = 4049 m ² = 0.004 km ²														
1 mi ² = 640 acres	1 km ² = 247 acres														
40 acre well spacing = 1380 ft	40 acre well spacing = 421 meters														
1.3	84.6	Junction with paved County Road to Emery. Continue east on Emery Coal Mine Road.													
0.9	85.5	STOP 7: Emery Coal Mine (Consolidation Coal Company) (fig.1). Stop in front of Mine Office. The Emery Mine of Consolidation Coal Company (Consol) is the largest mine in the Emery Coal Field.													
0.0	85.5	Retrace route back to Utah Highway 10.													
2.2	87.7	Junction of Emery Coal Mine Road with Utah Highway 10. Turn north onto Utah Highway 10 and proceed north through the Castle Valley to Price via Castle Dale, Ferron and Emery.													
27.2	114.9	100 East Street in Castle Dale. Proceed north on Utah Highway 10 to Price via Huntington.													
20.3	135.2	Emery-Carbon County Line. Enter Carbon County.													
0.8	136.0	Junction with Utah Highway 122 to the west. Continue north on Utah Highway 10.													
1.2	137.2	Junction with Stake Farm Road on east. Continue north on Utah Highway 10.													
0.2	137.4	STOP 8: Drunkards Wash Coalbed Methane Field (River Gas of Utah and Texaco) (fig.1). Pull off to the west of													

Stop 5: Willow Springs Wash South Canyon Wall	
Fluvial and Distributary Channel Belt Geometry and Architecture as a Function of Depositional Parasequence Set Stacking Patterns	
The north and south canyon walls in Willow Springs Wash contains a strike outcrop section that exposes almost the complete delta plain facies association of Ferron Sandstone Parasequence Sets 2A-8 (fig.3). The lowermost cliff-forming units are the deltaic facies of Parasequences 1b and 1c. The delta plain facies association of Parasequence 1d also crops out. This canyon offers a superb opportunity to examine the geometry and architectural systematics of the non-marine delta plain facies of the Ferron parasequence sets, as a function of depositional parasequence and parasequence set stacking patterns.	
van den Bergh and Garrison (1996) have quantified the geometry and internal architecture of the fluvial channel belts exposed in the north and south canyon walls of Willow Springs Wash. They used the parasequence and parasequence set subdivisions of the Ferron Sandstone defined by Garrison and van den Bergh (1996; 1997) and	

Stop 5: Willow Springs Wash South Canyon Wall

Fluvial and Distributary Channel Belt Geometry and Architecture as a Function of Depositional Parasequence Set Stacking Patterns

The north and south canyon walls in Willow Springs Wash contains a strike outcrop section that exposes almost the complete delta plain facies association of Ferron Sandstone Parasequence Sets 2A-8 (fig.3). The lowermost cliff-forming units are the deltaic facies of Parasequences 1b and 1c. The delta plain facies association of Parasequence 1d also crops out. This canyon offers a superb opportunity to examine the geometry and architectural systematics of the non-marine delta plain facies of the Ferron parasequence sets, as a function of depositional parasequence and parasequence set stacking patterns.

van den Bergh and Garrison (1996) have quantified the geometry and internal architecture of the fluvial channel belts exposed in the north and south canyon walls of Willow Springs Wash. They used the parasequence and parasequence set subdivisions of the Ferron Sandstone defined by Garrison and van den Bergh (1996; 1997) and

classified the channel belts according to their stratigraphic position within the 3rd-order parasequence set stacking pattern, originally outlined by Gardner. The channel belts in Willow Springs Wash exhibit differences in geometry and internal and external architecture that can be correlated with 3rd-order depositional parasequence set stacking patterns, which can be related to sediment supply and accommodation space systematics (fig. 10).

The channel belts of 3rd-order Ferron Sequence seaward-stepping parasequence sets formed in river-dominated deltas, when the available sediment supply exceeded the available accommodation space. These are generally laterally restricted and multi-storied with channel filling elements (i.e., macroforms and/or barforms) that are generally stacked vertically within the channel belt boundaries. Thicknesses from 10–15 feet and 40–45 feet and widths from 300–700 feet and 1200–1400 feet are most common. Width/thickness aspect ratios range from 7.8–52.9 and average about 29.5. Channel belts bifurcate as they approach the paleoshoreline and become narrower, averaging 638 feet in width, with lower aspect ratios, averaging about 16.6.

The channel belts of 3rd-order Ferron Sequence aggradational parasequence sets that formed in more storm-dominated deltas, when the sediment supply was balanced with rate of development of accommodation space, are generally quite laterally extensive and multi-storied with channel filling elements generally stacked en echelon laterally within the channel belt boundaries. Their thicknesses range from 25–35 feet and 55–60 feet. Widths from 1250–1900 feet are most common. Aspect ratios range from 31.9–97.4 and average about 57.2. Channel belts closer to the paleoshoreline have aspect ratios averaging about 12.0.

The channel belts of 3rd-order Ferron Sequence backstepping parasequence sets, formed in wave-dominated deltas, when the available sediment supply was less than the available accommodation space. These channel belts are laterally extensive and sheet-like, with channel filling elements generally stacked vertically within the channel belt boundaries. They range in thickness from 9–27 feet and 749–2652 feet in width, with vertically stacked elements. Aspect ratios of 65–90 and 185–195 are most common.

There is not much evidence to suggest that local preserved sand body thickness (i.e., channel fill elements) changes significantly as a function of distance to the paleoshoreline. Data suggest that preserved channel fill elements do become thinner downstream, but the data are scattered. Therefore, the data would tend to indicate that the preserved thickness of channel fill elements is controlled by local sedimentation rates, which decrease slightly down stream. The modelling of Heller and Paola (1996) suggests that such a scenario would result in channel stacking patterns (i.e., thickness and interconnectedness) that are a function of the relationship of avulsion frequency and

sedimentation rate, but changes in stacking patterns downstream (i.e., along the dip direction of the alluvial/delta plain) are driven mainly by the rate of change of subsidence along the basin. Based on the modelling of Heller and Paola (1996), it appears that the driving force behind the development of different channel belt architectural styles can be attributed to changes in rate of sediment supply, with the relative rise in sea level being effectively constant and with regional avulsion frequency being also relatively constant.

The ratio of net sand thickness to gross stratigraphic thickness (net/gross), calculated for intervals within the Willow Spring Wash section, also vary as a function of 3rd-order deltaic stacking pattern. The overall Ferron Sandstone net/gross ratio, in Willow Springs Wash, ranges from 0.22 to 0.47, averaging 0.31. The net/gross ratios calculated for the seaward-stepping, aggradational, and landward-stepping intervals are 0.22 ± 0.08 (range = 0.09–0.33), 0.43 ± 0.18 (range = 0.14–0.65), and 0.32 ± 0.9 (range = 0.23–0.45), respectively. The aggradational interval has the largest net/gross ratios, reflecting the aggrading and lateral stacking of the channel belts. The seaward-stepping interval has the lowest net/gross reflecting the wide spacing of confined channel belts, in the river-dominated systems.

The probability of inter-well connectivity (i.e., the probability that two wells, at a specified well spacing, will penetrated the same lithologic unit), at typical 40 acre and 80 acre well spacings is also a strong function of position within the overall stacking pattern of the 3rd-order deltaic parasequence sets. In the seaward-stepping parasequence sets, the average width is 742 ± 412 feet. The probability of a channel belt extending between two wells spaced 40 acres apart is only about 10%, and there is very little probability at a 80 acre spacing. In the aggradational parasequence sets, the average width is 2045 ± 1101 feet. The probability of a channel belt extending between two wells spaced 40 acres apart is about 75%, and the probability at a 80 acre spacing is only about 22%. In the landward-stepping parasequence sets, the average width is 1499 ± 711 feet. The probability of a channel belt extending between two wells spaced 40 acres apart is about 50%, and the probability at a 80 acre spacing is less than 10%.

Key Concepts of Stop 5:

- The channels belts in Willow Springs Wash exhibit differences in geometry and internal and external architecture that can be correlated with 3rd-order depositional parasequence set stacking patterns, which are related to sediment supply and accommodation space systematics.
- Width/thickness aspect ratios for channel belts within 3rd-order seaward-stepping parasequence sets range from 7.8–52.9 and average about 29.5.

- Width/thickness aspect ratios for channel belts within 3rd-order aggradational parasequence sets range from 31.9–97.4 and average about 57.2.
- Aspect ratios of 65–90 and 185–195 are most common for channel belts within 3rd-order landward-stepping parasequence sets.
- Net/gross ratios, calculated for intervals within the Ferron Sandstone non-marine section, also vary as a function of 3rd-order deltaic stacking pattern.
- The probability of inter-well connectivity, at typical 40 acre and 80 acre well spacings, is also a strong function of position within the overall stacking pattern of the 3rd-order deltaic parasequence sets.

Stop 6: Willow Springs Wash North Canyon Wall and The County Line Channel

Internal Channel Belt Sedimentology and Architecture as a Function of Depositional Parasequence Set Stacking Patterns

The channel belts in Willow Springs Wash exhibit differences in internal sedimentology and architecture that can be correlated with 3rd-order depositional parasequence set stacking patterns, which can be related to sediment supply and accommodation space systematics. The channel belts of seaward-stepping parasequence sets are generally laterally restricted and multi-storied with channel filling elements (i.e., macroforms and/or barforms) generally stacked vertically within the channel belt boundaries. The channel belts of aggradational parasequence sets are generally quite laterally extensive and multi-storied with channel filling elements generally stacked en echelon laterally within the channel belt boundaries. The channel belts of landward-stepping parasequence sets are laterally extensive and sheet-like with channel filling elements generally stacked vertically within the channel belt boundaries.

The type channel belts for each of these architectural styles crop out in the north canyon wall. The County Line Channel, a Parasequence 1d (Parasequence Set 1) distributary channel belt, is excellently exposed in the lower cliffs of the north canyon wall of Willow Springs Wash (fig. 21). The Kokopelli Channel Belt, a Parasequence Set 4B channel belt, crops out mid-wall up the north canyon wall above the County Line Channel. The Caprock Channel, a Parasequence Set 7 channel belt caps the north canyon wall of Willow Springs Wash. This stop will focus on the internal sedimentology and architecture of the County Line Channel (fig. 22).

The County Line Channel, a Parasequence 1d distributary channel belt, trending 040°, is excellently exposed on

the north canyon wall of Willow Springs Wash. It has a meander wavelength of about 3 miles and a meander amplitude of only 0.6 miles. The County Line Channel bifurcates just south of Indian Canyon, resulting in a smaller channel belt, exposed further west in Willow Spring Wash. This smaller distributary, the Coal Miner's Channel, generally trending 360° north and has a meander wavelength of about 2 miles and an amplitude of only 0.2 miles. The County Line Channel feeds a mouth bar complex near the mouths of Coyote Basin and Rock Canyon. The County Line Channel is a 1243 feet wide and 60 feet thick distributary channel belt, with an aspect ratio of 20.7. It incises through the Sub-A1 *coal zone* into Parasequence 1c. The Coal Miner's Channel is 354 feet wide and 16.1 feet thick, resulting in an aspect ratio of 22.0. This smaller channel branch does not cut through the Sub-A1 *coal zone*.

The external geometry of the County Line Channel suggests that there are at least three stages in the development of the distributary channel belt morphology. Each stage preserves from 14–33 feet of sand and each stage becomes progressively wider and less confined than the previous stage. The lower five elements represent scour and fill elements deposited within a narrow 332 feet wide, confined channel. The preserved thickness of this first phase of the channel belt is approximately 33 feet, resulting in a width/thickness aspect ratio of 10.0. The second phase of channel development is recorded by the next seven higher channel fill elements, reflecting both cut and fill characteristics and lateral accretion structures. These channel fill elements were deposited in a much wider, yet confined channel 1120 feet wide. The preserved thickness of this second phase of the channel belt is approximately 22 feet, resulting in a width/thickness aspect ratio of 50.9. The final phase of the channel belt is dominated by lateral accretionary bedforms and bedsets, which interfinger with the laterally equivalent delta-plain facies associations. This channel fill event has well-developed levees and overbank facies. The preserved width and thickness of this phase are 1243 feet and 13.6 feet, respectively, resulting in of a width/thickness aspect ratio of 91.4.

The County Line Channel is composed of fourteen channel fill elements. The lower 5 elements are associated with the narrow, confined first stage of the channel belt development and represent major scour and fill events. The bounding surfaces of these channel fill elements are frequently delineated by thick clay pebble lag deposits. These channel fill elements are generally medium-lower to medium-upper grained sandstones that fine upward to medium-lower to fine-upper grained sandstones. They generally have large trough cross beds (i.e., >0.5 feet thick) near their bases, which change upward into faint large troughs and massive sandstones. The trough cross-beds decrease in

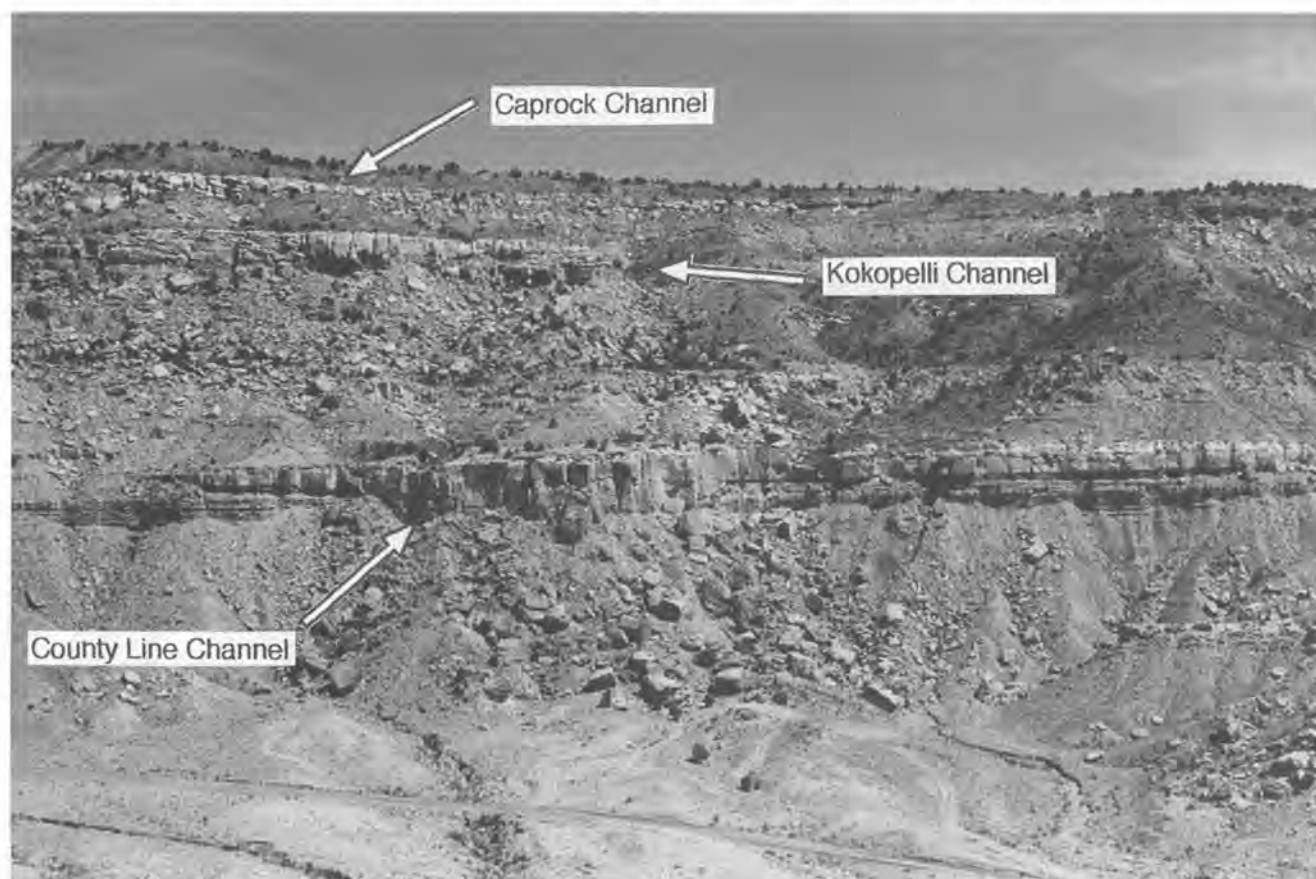


Figure 21. Photograph showing the County Line Channel in Willow Springs Wash. The channel belt is 1243 feet wide and 60 feet thick.

size upward (to < 0.3 feet thick). Occasionally, trough cross-beds near bounding surfaces are contorted. There are 7 channel fill elements in the second stage of the development of the County Line Channel. These channel fill elements are dominated by lateral accretion surfaces and bedforms. The bounding surfaces between these channel fill elements are frequently defined by bedding surfaces between major bedform domains or barforms. These channel fill elements are generally medium-lower to fine-upper grained and exhibit a general overall fining upward trend. These channel fill elements contain faint large trough cross-beds to massive, structureless sandstones that are transitional into smaller trough cross-beds and planar and wedge tabular cross-stratified beds that suggest a westward lateral migration. The upper two channel fill elements represent the final final phase of the development and preservation of the County Line Channel, and interfinger with delta-plain facies associations. These two channel fill elements are generally medium-lower to fine-upper sandstones. They exhibit large scale planar tabular cross-beds near the central portion of the channel, but exhibit small scale planar tabular

cross-beds, ripple cross-stratification, and climbing ripple cross-stratification near the top and laterally towards the channel margins.

The changes in the geometry and architecture of the County Line Channel are most easily explained as simple consequences of channel belt evolution as a result of normal delta progradation. The narrow confined first stage of channel fill (i.e., aspect ratio of 10) probably represents the channel belt at a position close to the paleoshoreline. The wider second stage of channel fill may represent the channel belt cross-section, some 1.4 miles from the paleoshoreline, after the delta front deposits prograded seaward about 0.8 miles (Garrison and van den Bergh, 1997). This change in position of the cross-section relative to the paleoshoreline is consistent with the change in width/thickness aspect ratio (i.e., 50.9), although the overall preserved channel belt aspect ratio was only 24.3. During the third stage of channel fill, the channel fill deposits had an aspect ratio of 91.4, although the overall preserved channel belt aspect ratio was only 20.7. The final channel fill and abandonment is probably a normal abandonment phase of the second stage.

County Line Channel Internal Architecture and Sedimentology

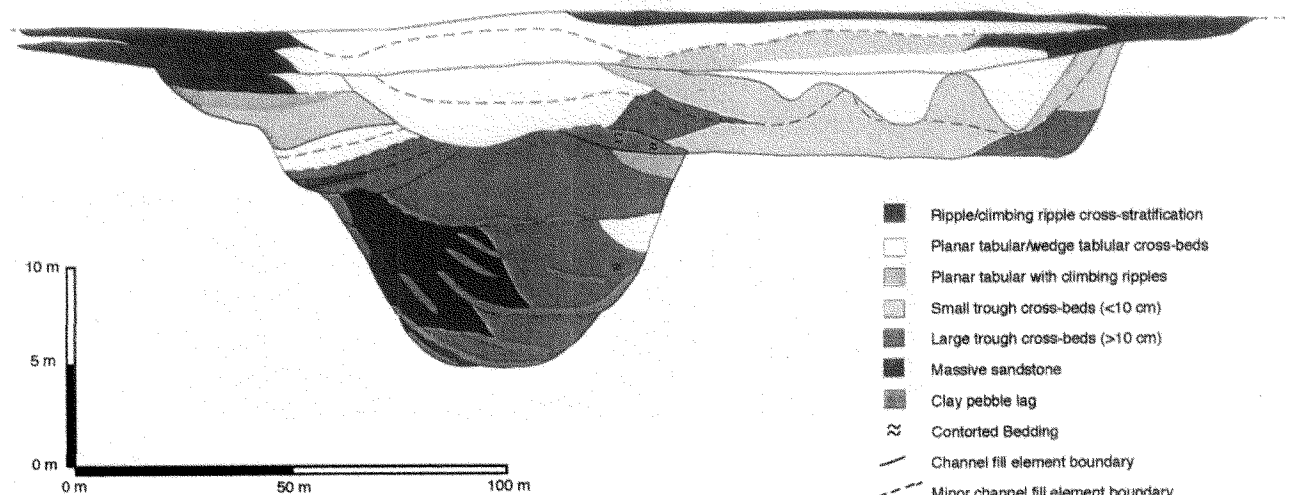


Figure 22. Schematic diagram showing the internal architecture and sedimentology of the County Line Channel.

Key Concepts of Stop 6:

- The channels belts in Willow Springs Wash exhibit differences in sedimentology and internal architecture that can be correlated with 3rd-order depositional parasequence set stacking patterns.
- The external geometry of the County Line Channel suggests that there are at least three stages in the development of the distributary channel belt morphology.
- The County Line Channel is composed of fourteen channel fill elements. The lower five channel fill elements represent major scour and fill events (1st stage). The overlying seven channel fill elements are dominated by lateral accretion sedimentary surfaces, structures, and bedforms (2nd stage). The upper two channel fill elements interfinger with the lateral delta-plain facies associations and represent the final stage of channel fill and abandonment.

Stop 7: Emery Coal Mine

The Emery Coal Field

The Emery Coal Field was originally defined from the surface exposures of coal in the Upper Cretaceous Ferron Sandstone Member of the Mancos Shale (Lupton, 1916) (i.e., Upper Ferron Sandstone). The surface exposures cover an area 25 miles long, from north to south and 2 to 10 miles from east to west along the Sevier-Emery County border

(fig. 23). This area lies about 45 miles southwest of Price, Utah, the nearest rail loadout. The field, as originally defined, is bounded on the east by an erosional escarpment and on the west by a fault zone (Doelling, 1972). Recently published drilling data show that similar thick coal beds also are present in the subsurface extending northward all the way to Price (Bunnell and Hollberg, 1992; Tabet et al., 1995) (i.e., Lower Ferron Sandstone). Thus, the northern boundary of the Emery Coal Field actually extends north-eastward beyond Price.

The coal of the Emery Coal Field, in the south, contains 13 coal seams, seven of which exceed 4 feet in thickness. Lupton (1916) gave the beds letter designations from A to M in ascending order of occurrence. Beds I and J are the most important, and the separation between them is minimal in many areas, resulting in a single seam up to 25 feet thick. The total net thickness of coal in the Ferron Sandstone reaches a maximum of nearly 60 feet in the southern part of the coal field, and is commonly 20 to 30 feet along the whole coal trend running northward past Price (Tablet et al., 1995).

The structure and stratigraphy of the coal field are favorable for mining. The coal beds strike northeasterly and dip to the west from 2° to 12°; most dips fall in the 4° to 7° range. Faulting is minor and presents little difficulty in mining or gas extraction. The overburden over 76 percent of the resources identified in the northern end of the field is less than 1,000 feet; very thin overburden in some areas creates surface mining possibilities (Doelling, 1972).

Original in-place resources for the southern part of the Emery Coal Field are estimated at 2.15 billion tons (Doelling and Smith, 1982) for all beds greater than 4 feet thick and under less than 3,000 feet of cover. Demonstrated resources make up 1.43 billion tons of the total, with the remainder falling in the hypothetical resource category. Cumulative coal production for the whole field through 1990 was 9.5 million tons (Jahanbani, 1996). Assuming a 40% recovery rate for both past and future underground mining, the Emery Coal Field's remaining recoverable coal resources are estimated to be 822 million tons. The use of surface mining to recover coal from areas with less than 100 feet of overburden would increase the recoverable resources in those areas.

Compositions of Upper Ferron Coals from the Emery Coal Field

Average proximate and ultimate compositional analyses for Upper Ferron Coals from the Emery Coal Field are summarized in Table 1 (Affolter et al., 1979; Hatch et al., 1979; Bunnell and Hollberg, 1991; Sommer et al., 1991). All analyses are reported in weight percent. Recent works indicate that the Upper Ferron coals are high volatile Bituminous B rank coals (Sommer et al., 1991; Tabet et al., 1995), although earlier studies by Doelling (1972) suggested high volatile Bituminous C rank coals. Vitrinite reflectance data from wells penetrating deep Ferron coals under the Wasatch Plateau indicate the coals gradually increase in rank to the west to high-volatile B bituminous (Tabet et al., 1995).

The most notable differences in the compositions of the Upper Ferron coals is their ash and sulfur contents. The ash content of the Ferron Coals ranges from 9.5% in the I Coal at the Emery Mine, to 29.4% in the J coal (Table 1). BTU content varies with ash content, ranging from 12690 BTU/lb, in the I coal, to 9480 BTU/lb, in the J coal. The sulfur content ranges from 0.6% in the I coal, up to 4.1% in the J coal (Table 1). With the exception of the I coal, the higher *coal zones* in the Upper Ferron Sandstone (i.e., the G, J, and the M) all have high ash and sulfur contents. The stratigraphically lower C coal also has a slightly higher ash and sulfur content than either the A and the I coals.

Figure 24 shows a ternary plot of the sulfur types for the Ferron coals. The A and I coals have a high weight percentage of organic sulfur, with pyritic sulfur being lowest; the G, J, and M are high in pyritic sulfur; the C coal appears to be intermediate between these two groups. Pyritic sulfur can be introduced after deposition. However, it is often early diagenetic and suggests continuing reducing conditions. Organic sulfur is generally introduced during deposition. The coals with the highest ash, total sulfur, and pyritic sulfur contents belong to transgressive phases of either the 3rd- or 4th-order depositional sequences; the coals with the

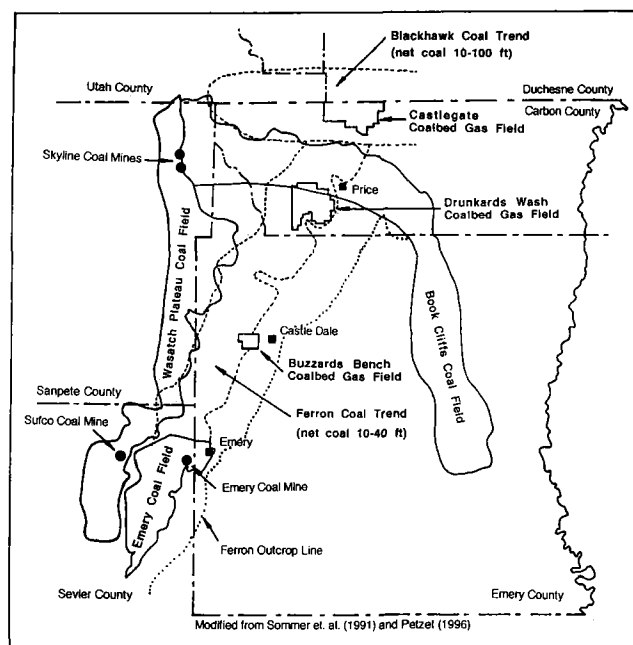


Figure 23. Location map for Emery, Bookcliffs, and Wasatch Coal Fields and the Ferron Coalbed Methane Play.

lowest ash and sulfur contents belong to parasequence sets that are either strongly aggradational or strongly progradational. Peterson et al., (1996) noted that coals formed from peats influenced by marine waters, generally have high sulfur contents. Such conditions are likely to occur during marine transgressions. These observations are consistent with the stratigraphic positions of the high sulfur Ferron coals.

Coal Mining at the Emery Mine

The Emery Mine, now operated by Consolidation Coal Company (Consol), produced coal from the Upper Ferron I coal zone. This was the largest and longest producing mine in the Emery Coal Field. The Browning Mine, the original underground mine in the canyon, was opened in 1910. The old Browning Mine has its portal about 200 m southeast of the current Emery Mine portal. The Browning Mine was abandoned when a major coal burn to the south was encountered. The portal was moved northwest and the current Emery Mine opened in 1945. In 1975, Consolidation Coal Company began operating the underground Emery Coal Mine. By the early 1980s, Consol employed up to 200 people, and was producing over 430,000 tons of coal per year. Total coal production exceeded 18 million tons. The mine extends about 1.4 miles underground to the northwest and reaches a depth of 740 feet. There are over 5 miles of conveyor belts. The main market for the Ferron I Coal from

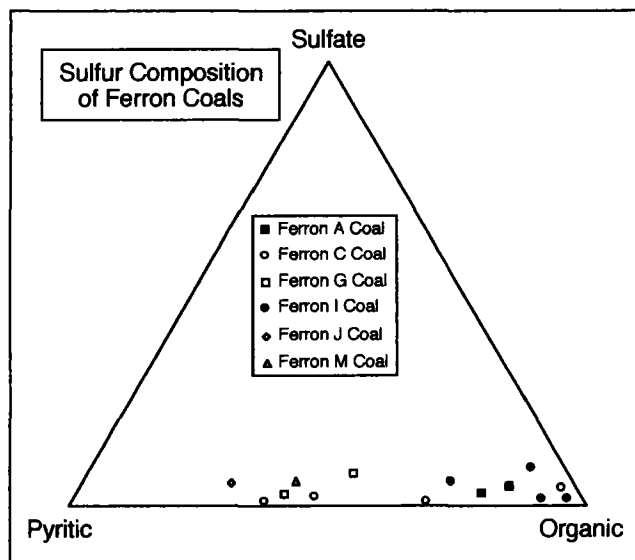


Figure 24. Ternary diagram showing composition of sulfur within the Upper Ferron coal seams.

the Emery Mine was the power plants scattered up the Castle Valley. In 1990, Consol ceased operations in the Emery Mine and by 1991, the mine was classified as inactive. In 1994, a small amount of coal was shipped from the stockpile. In 1995, Consol sealed the portals and limited maintenance to pumping water from the mine to prevent flooding. In 1996, the last coal from the Emery mine stockpile was shipped. The lack of railroad access and the high costs of trucking coal to the Castle Valley power plants contributed to the eventual closing of the Emery Mine.

At the Emery Mine, coal was produced from a 22 ft thick seam of coal within the Upper Ferron I coal zone. To the northwest the coal seam splits into two 10 ft thick seams. The I coal seam at the Emery Mine is low in ash (9.5%), with a BTU content of 12690 BTU/lb (dry-basis) (see Table 1). The sulfur content of the I coal seam is low (0.6%) and is dominantly organic sulfur, with only minor pyritic sulfur. The Emery Mine contains a moderate amount of free methane gas, and is considered by mining standards to be "gas-rich."

Key Concepts of Stop 7:

- The underground Emery Coal Mine of Consolidation Coal Company was the largest and most productive of the coal mines in the Emery Coal Field. It produced over 430,000 tons of coal per year from the Ferron I coal zone.
- At the mine, Ferron I coal seam is 22 feet thick and is the highest quality and thickest coal seam in the

Emery Coal Field, containing only 9.5% ash and producing 12690 BTU/lb.

- The Upper Ferron coals have ash contents that range from 9.5%, in the I Coal at the Emery Mine, to 29.4% in the J Coal. The sulfur content ranges from 0.6%, in the I coal, up to 4.1%, in the J coal

Stop 8: Drunkards Wash Coalbed Methane Field

Generation, Retention, and Production of Methane from Coal: Implications for the Ferron Coalbed Methane Play

Coal forms a unique hydrocarbon reservoir in that the hydraulic pressure typically maintains the gas in place rather than in a sealed porous reservoir like that found in conventional hydrocarbon reservoirs. Coal bed gas (CBG) is also unusual in that the coal itself is the source of the gas it stores. This gas is methane-rich and has a biogenic or thermogenic origin. Biogenic gas generation is restricted to shallow depth but this generation can occur both during early diagenesis and burial or late diagenesis and exhumation. Thermogenic gas generation typically caused by burial heating increases with coal rank. A coal of high volatile Bituminous B (hvBb) rank typically produces about 960 standard cubic feet/ton (SCF/ton) of methane (Choate et al., 1986).

Free gas is expelled from coal when the internally generated gas volume exceeds sorption capacity. The sorption capacity can also be filled by externally generated gas that migrates into the coal. Internally generated or migrating gas in excess of the sorption capacity continues through the coal and is not retained unless trapped. Thus, if a coal exists within a conventional gas trap, it is possible for the coal to retain gas above its apparent sorption capacity and become supersaturated with gas.

Coal maceral composition and ash content are also important internal coal bed controls on CBG content. There are three maceral groups found in coal. The Vitrinite group is formed from woody plant debris, the liptinite group is from waxy, resinous and oily components and the inertinite is from fossil charcoal as well as other altered and oxidized plants materials. Increasing vitrinite content enhances gas storage capacity and cleat (i.e., fractures in coal) permeability. Increasing liptinite content enhances gas generation but reduces storage capacity. Increasing inertinite content enhances matrix permeability but decreases gas generation but reduces storage capacity. Ash (mineral matter) has little storage capacity, reduces gas content in direct proportion to its abundance, and inhibits cleat formation.

Although coal porosity is high, matrix permeability is low, making cleat permeability an important control in commercial production. The capacity to hold and generate gas can

Table 1. Analyses of Ferron coals (all analyses reported air dried).

	U. Ferron A Coal	U. Ferron C Coal	U. Ferron G Coal	U. Ferron I Coal	U. Ferron J Coal	U. Ferron M Coal	L. Ferron Core	Ferron Henry Mts	Wasatch Skyline	Wasatch SUFCO
Volatile (wt%)	41.2	40.4	40.5	41.7	36.8	41.8	36.0	36.2	52.7	43.9
Fixed Carbon (wt%)	48.0	46.7	42.4	48.8	33.8	44.4	47.3	49.5	39.2	46.3
Ash (wt%)	10.9	12.9	17.2	9.5	29.4	13.8	17.1	14.3	8.1	9.9
H (wt%)	5.2	5.0	4.7	5.1	4.3	4.8	5.0	4.8	5.3	4.7
C (wt%)	71.0	68.1	63.8	71.6	52.9	66.0	68.2	65.7	72.8	71.7
N (wt%)	1.4	1.2	1.2	1.4	1.2	1.3	1.2	1.3	1.4	1.3
O (wt%)	10.9	11.2	10.0	12.5	8.3	10.6	7.9	11.8	12.0	12.1
S (wt%)	0.8	1.6	3.1	0.6	4.1	3.6	1.7	2.2	0.5	0.3
Sulfate S (wt%)	0.03	0.03	0.15	0.03	0.20	0.20	n.a.	n.a.	n.a.	n.a.
Pyritic S (wt%)	0.14	0.66	1.59	0.08	2.68	1.92	n.a.	n.a.	n.a.	n.a.
Organic S (wt%)	0.66	0.88	1.40	0.59	1.18	1.49	n.a.	n.a.	n.a.	n.a.
Btu/lb	12650	12150	11320	12690	9480	11810	12690	11550	12690	12440

be predicted using coal rank but coal seam permeability must be assessed in the field. In particular finding areas of enhanced production or high methane content are important to commercial production. Zones of high methane content formed by coal facies, partial exhumation and conventional gas traps are likely in the Ferron CBG Fairway.

Exploration for CBG generally ranges from 150 m to 2 km depth because: (1) at shallow depths, low hydraulic head causes the coal to retain little methane; and, (2) beyond 2 km, coal cleat is closed making commercial production difficult. The depth of burial in the Ferron CBG Fairway to the east of the Wasatch Plateau and west of the outcrop belt is generally ideal for CBG production.

Coalbed Methane Resources of the Ferron Sandstone Coalbed Methane Play

The Ferron Sandstone Coalbed Methane Play is a 6–10 mile wide by 80 mile long fairway (Tripp, 1989; Tabet et al., 1995) (fig. 23). The methane is produced from coal beds in the Lower Ferron Sandstone (Vernal Delta). The coals occur at attractive drilling depths ranging from under 1,000 feet to over 7,000 feet. Some gas desorption data have been collected from shallow coals of the Upper Ferron Sandstone, at the southern end of the coal field (Doelling et al., 1979), but these few, near-outcrop samples yielded only 0–16 standard ft³/ton (SCF/ton) methane. Only one gas content measurement for deep Ferron Sandstone coals has been released by companies currently exploring for gas. River Gas of Utah reports its initial core test well had in excess of 400 SCF/ton methane in a 36.7 foot thick coal interval (Lyle, 1991). If the entire Ferron coal play contains similar gas

contents, then in-place gas resources for the play could be as high as 9 TCF.

River Gas of Utah, Texaco, and Anadarko have been active in exploring and producing the coalbed methane from the Ferron play. The Ferron Sandstone CBM Play currently contains over 100 producing coalbed methane wells. In 1995, almost 4% of Utah's total gas production came from wells in the Ferron Sandstone CBM Play (Petzet, 1996). Cumulative production from the Ferron CBM play through October 1996 is approximately 30 BCF. Currently two fields are producing from the Ferron Sandstone CBM Play: the Drunkards Wash Field south of Price, Utah, operated by River Gas of Utah, and the Buzzards Bench Field at Orangeville, Utah, operated by Texaco.

Drunkards Wash Coalbed Methane Field

The Drunkards Wash Coalbed Methane Field is the largest field in the Ferron Sandstone CBM Play; it covers 120,000 acres and contains 89 producing wells on an 160 acre spacing (Lamarre and Burns, 1996). The wells have a classic coalbed methane negative decline curve with increasing gas rates as the reservoir pressure declines due to the production of water (Lamarre and Burns, 1996). These wells produce 43.7 MMCFD, averaging 491 MCFD/well. As of mid-1996, thirty of these wells had been producing for over 38 months and have an average of 692 MCFD/well (Lamarre and Burns, 1996). The daily water production is 16,500 bbl, averaging 185 BWPD/well. In 1995, the field produced 11 BCF of methane and 5.7 million bbl water. All wells are cased and hydraulically stimulated and most have pumping units to handle the large volume of produced salt water.

Salt water produced with the methane gas is disposed of by pumping units that pump the water into the subsurface Navajo Sandstone at a depth of 5500–6000 feet.

The typical depth for these wells is 1800–3400 feet. The total coal thickness within the field ranges from 4–48 ft, but averaging 24 ft (Lamarre and Burns, 1996). The coal occurs in from 3 to 6 distinct seams. The coal is high volatile Bituminous B (hvBb) coal. The hvBb rank of the Ferron coal is within the window of thermogenic gas generation, which typically produces about 960 SCF/ton of methane (Choate et al., 1986). This volume of gas is far more than the reported 440 SCF/ton of methane present in the Lower Ferron coals in the Drunkards Wash Field (Burns and Lamarre, 1996). The hvBb rank also suggests a sorption capacity of only 200 SCF/ton at their present burial depth of about 2,000 ft (Kim, 1977), suggesting the Ferron coals are supersaturated with gas. This amount of gas is higher than the coal rank and depth would suggest. The gas appears to be a combination of thermogenic and secondary biogenic gas (Lamarre and Burns, 1996). Canister desorption data and measured sorption isotherms suggest the coal is supersaturated with respect to gas at the initial measured reservoir pressures of 765 psi (Burns and Lamarre, 1996). Further, when wells are initially completed in these Ferron coals, gas can flow without stimulation, a signature of supersaturation. The excess gas in these marginally mature coals seems to come from Ferron coals themselves and perhaps other source rocks buried deeper in to the west. After generation, the gas apparently migrated into the conventional gas trap formed by the updip pinchout of coalbeds into the mudrocks at the Drunkards Wash field.

Key Concepts of Stop 8:

- The Ferron Sandstone Coalbed Methane Play is a 6–10 mile wide by 80 mile long fairway that has been estimated to contain as much as 9 TCF gas. Cumulative production from the Ferron CBM play, through October 1996 is approximately 30 BCF.
- The Drunkards Wash Coalbed Methane Field is the largest field in the Ferron Sandstone CBM Play; it contains 89 producing wells (1995). In 1995, the field produced 11 BCF of methane and 5.7 million bbl water.
- Salt water produced with the methane gas is disposed of by pumping units that pump the water into the subsurface Navajo Sandstone at a depth of 5500–6000 feet.

ACKNOWLEDGMENTS

Special thanks to Brenda Pierce, of the United States Geological Survey, and the Coal Geology Division of The

Geological Society of America for initiating and sponsoring this field trip and therefore making this publication possible. The Ferron Sandstone coal and depositional sequence stratigraphy research of Garrison and van den Bergh, of the Ferron Group Consultants, L.L.C., is supported in part by grants from Union Pacific Resources, Texaco, Arco, Anadarko, Amoco, Shell, and British Petroleum. The coal lithofacies and coalbed methane generation research of Barker is supported by the United States Geological Survey. The Utah coal and coalbed methane resource assessment research of Tabet is supported by the Utah Geological Survey of the State of Utah Department of Natural Resources. The Utah Geological Survey is gratefully acknowledged for granting Tabet permission to co-author this guidebook. The Ivie Creek photomosaic used in this paper is courtesy of T.A. Ryer. Special thanks to T.D. Burns of River Gas of Utah for arranging for the field stop at the Drunkards Wash Coalbed Methane Field. T.D. Burns of River Gas and R.A. Lamarre of Texaco provided background information on the Drunkards Wash Coalbed Methane Field. The assistance of S.R. Behling, of Consolidation Coal Company's Emery Mine, in arranging the field stop at the Emery Coal Mine is gratefully acknowledged. Many discussions of the Ferron Sandstone, over the years, with T.A. Ryer and P.B. Anderson form the background for this work. Discussions about the depositional sequence stratigraphy of the Ferron Sandstone with E.R. Gustason and K.W. Shanley proved invaluable. Reviews by Brenda Pierce, E.R. Gustason, and A. Pulham are gratefully acknowledged.

REFERENCES CITED

- Affolter, R.H., Hatch, J.R., and Ryer, T.A., 1979, Chemical analyses of coal and shale from the Ferron Sandstone Member of the Mancos Shale, Emery coal field, Emery County, Utah. U.S. Geological Survey Open-File Report 79-858, 36 p.
- Aitken, J.F., 1994, Utility of coal seams as genetic stratigraphic sequence boundaries in nonmarine basins: an example from the Gunnedah Basin, Australia: Discussion. *American Association of Petroleum Geologists Bulletin* v. 79, p. 1179–1181.
- Aitken, J.F., and Flint, S.S., 1994, High frequency sequences and the nature of incised valley fills in fluvial systems of the Breathitt Group (Pennsylvanian), Appalachian foreland basin, eastern Kentucky, in Dalrymple, R., Boyd, R., and Zaitlin, B., eds., *Incised valley systems: origin and sedimentary sequences*. Society of Economic Paleontologists and Mineralogists Special Publication 51, p. 353–368.
- Aitken, J.F., and Flint, S.S., 1995, The application of high resolution sequence stratigraphy to fluvial systems: a case study from the Upper Carboniferous Breathitt Group, eastern Kentucky, U.S.A. *Sedimentology* v. 42, p. 3–30.
- Anderson, P.B., and Ryer, T.A., 1995, Proposed revisions to parasequence set nomenclature of the Upper Cretaceous Ferron Sandstone Member of the Mancos Shale, Central, Utah (abs): American Association of Petroleum Geologists Rocky Mountain Section Meeting 1995, Reno, Nevada, American Association of Petroleum Geologists Bulletin v. 79, p. 914–915.
- Barton, M.D., 1994, Outcrop Characterization of Architecture and Permeability Structure in Fluvial-deltaic Sandstones, Cretaceous Ferron

- Sandstone, Utah [Ph.D. Dissertation]: The University of Texas at Austin, 260 p.
- Bunnell, M.D., and Hollberg, R.J., 1991, Coal beds of the Ferron Sandstone Member in northern Castle Valley, east-central Utah, in Chidsey, T.C., ed., *Geology of East-Central Utah*. Utah Geological Association Publication v. 19, p. 157–172.
- Burns, T.D., and LaMarre, R.A., 1996, Drunkards Wash Project: coalbed methane production from Ferron Coals in east-central Utah (Abs): American Association of Petroleum Geologists, Rocky Mountain Section Meeting, Billings, Montana, July, 1996. p. 4.
- Choate, R., McCord, J.P., and Rightmire, C.T., 1986, Assessment of natural gas from coalbeds by geologic characterization and production evaluation, in Rice, D.D., ed., *Oil and Gas Assessment—methods and applications*. American Association of Petroleum Geologists, p. 223–245.
- Cotter, E., 1975, Late Cretaceous sedimentation in a low energy coastal zone: the Ferron Sandstone of Utah. *Journal Sedimentary Petrology* v. 45, p. 669–685.
- Cross, T.A., 1988, Controls on coal distribution in transgressive-regressive cycles, Upper Cretaceous, Western Interior, U.S.A., in Wilson, C.K., Hastings, B.S., Kendall, C.G. St. C., Posamentier, H.W., Ross, C.A., and Van Wagoner, J.C., eds., *Sea level changes: an integrated approach: Society of Economic Paleontologists and Mineralogists Special Publication* 42, p. 371–380.
- Crowley, S.S., Stanton, R.W., and Ryer, T.A., 1989, The effects of volcanic ash on the maceral and chemical composition of the C coal bed, Emery Coal Field, Utah. *Organic Geochemistry* v. 14, p. 315–331.
- Doelling, H.H., 1972, Central Utah coal fields. Sevier-Sanpete, Wasatch Plateau, Book Cliffs, and Emery: Utah Geological and Mineralogical Survey Monograph 3, 572 p.
- Doelling, H.H., and Smith, M.R., 1982, Overview of Utah coal fields, in *Proceedings of the Fifth Symposium on the Geology of Rocky Mountain Coal 1982*. Utah Geological and Mineralogical Survey Bulletin v. 118, p. 1–26.
- Doelling, H.H., Smith, A.D., and Davis, F.H., 1979, Methane content of Utah coals. Utah Geological and Mineralogical Survey Special Study 49, p. 1–43.
- Fielding, C.R., 1985, Coal depositional models and the distinction between alluvial and delta plain environments. *Sedimentary Geology* v. 42, p. 41–48.
- Fielding, C.R., and Crane, R.C., 1987, An application of statistical modeling to the prediction of hydrocarbon recovery factors in fluvial reservoir sequences, in *Recent Developments in Fluvial Sedimentology*. Society of Economic Paleontologists and Mineralogists Special Publication 39, p. 321–327.
- Flint, S.S., Aitken, J.F., and Hampson, G., 1995, The application of sequence stratigraphy to coal-bearing coastal plain successions: implications for the U.K. Coal Measures, in Whateley, M., and Spears, D.A., eds., *European Coal Geology*. Geological Society Special Publication 82, p. 1–16.
- Galloway, W.E., 1989, Genetic stratigraphic sequences in basin analysis, I. architecture and genesis of flooding-surface bounded depositional units. *American Association of Petroleum Geologists Bulletin* v. 73, p. 125–142.
- Gardner, M.H., 1992, Sequence stratigraphy of the Ferron Sandstone, East-Central Utah, in Tyler, N., Barton, M.D., and Fisher, R.S., eds., *Architecture and Permeability Structure of Fluvial-deltaic Sandstones: A Field Guide to Selected Outcrops of the Ferron Sandstone, East-Central Utah: The University of Texas at Austin, Bureau of Economic Geology Guidebook*, p. 1–12.
- Gardner, M.H., 1993, Sequence stratigraphy of the Ferron Sandstone (Turonian) of East-Central Utah [Ph.D. Dissertation]: Colorado School of Mines, 406 p.
- Garrison, J.R., Jr., and van den Bergh, T.C.V., 1996, Coal zone stratigraphy—a new tool for high-resolution depositional sequence stratigraphy in near-marine to non-marine fluvial-deltaic facies associations. a case study from the Ferron Sandstone, East-central Utah: 1996 American Association of Petroleum Geologists Rocky Mountain Section Meeting—Billings, Montana, Expanded Abstracts Volume, Montana Geological Society, p. 31–36.
- Garrison, J.R., Jr., and van den Bergh, T.C.V., 1997, Depositional sequence stratigraphy and coal zone stratigraphy of the Upper Cretaceous (Turonian) Upper Ferron Sandstone, East-central Utah: G.S.A. 1997 Annual Meeting (in press).
- Gastaldo, R.A., Demko, T.M., and Liu, Y., 1993, Application of sequence and genetic stratigraphic concepts to Carboniferous coal-bearing strata. an example from the Black Warrior basin, USA: *Geologische Rundschau* v. 82, p. 212–222.
- Geary, E.A., 1996, A History of Emery County. Utah State Historical Society, Salt Lake City, 448 p.
- Hamilton, D.S., and Tadros, N.Z., 1994, Utility of coal seams as genetic stratigraphic sequence boundaries in nonmarine basins. an example from the Gunnedah Basin, Australia. *American Association of Petroleum Geologists Bulletin* v. 78, p. 267–286.
- Hatch, J.R., Affolter, R.H., and Law, B.E., 1979, Chemical analyses of coal from the Emery and Ferron Sandstone Members of the Mancos Shale Henry Mountains Field, Wayne and Garfield Counties, Utah. U.S. Geological Survey Open-File Report 79-1097, 24 p.
- Heller, P.L., and Paola, C., 1996, Downstream changes in alluvial architecture. an exploration of controls on channel-stacking patterns. *Journal of Sedimentary Research* v. 66, p. 297–306.
- Heward, A.P., 1978, Alluvial fan and lacustrine sediments from the Stephanian A and B (La Magdalena, Cínera-Matallana, and Sabero) coal fields, northern Spain. *Sedimentology* v. 25, p. 451–488.
- Hintze, L.F., 1988, Geologic History of Utah. Brigham Young University Geology Studies Special Publication 7, 202 p.
- Jahanbani, F.R., 1996, 1995 Annual review and forecast of Utah coal production and distribution. Utah Office of Energy Resource Planning, 26 p.
- Kim, S.C., 1977, Estimating methane content of bituminous coalbeds from adsorption data: U.S. Bureau of Mines, Report of Investigations 8245, 22 p.
- Lane, M.D., and Staley, D., 1993, Summary of oil and gas exploration and production in Carbon, Emery, and Sanpete Counties, East-central Utah, in Chidsey, T.C., ed., *Geology of East-Central Utah*. Utah Geological Association Publication 19, p. 227–235.
- Lamarre, R.A., and Burns, T.D., 1996, Drunkard's Wash Unit. Coalbed methane Production from Ferron coals in East-central Utah. 1996 American Association of Petroleum Geologists Rocky Mountain Section Meeting—Billings, Montana. American Association of Petroleum Geologists Bulletin v. 80.
- Lethold, E.L., 1994, Stratigraphical architecture at the muddy margin of the Cretaceous Western Interior Seaway, southern Utah: *Sedimentology* v. 41, p. 521–542.
- Lowry, P., and Jacobsen, T., 1993, Sedimentological and reservoir characteristics of a fluvial-dominated delta-front sequence. Ferron Sandstone Member (Turonian), East-Central Utah, in Ashton, M., ed., *Advances in Reservoir Geology*. Geological Society Special Publication 69, 81–103.
- Lupton, C.T., 1916, Geology and coal resources of Castle Valley in Carbon, Emery, and Sevier Counties, Utah. U.S. Geological Survey Bulletin v. 628, 88 p.
- Lyle, D., 1991, First well in Utah goal-gas program strikes pay on 92,000-acre Texaco farmout to River Gas. *Western Oil World*, v. 47, p. 8–9.
- McCabe, P.J., 1994, Depositional environments of coal and coal-bearing strata, in Rahmani, R.A., and Flores, R.M., eds., *Sedimentology of coal and coal-bearing sequences*. Special Publication of the International Association of Sedimentologists v. 7, p. 13–42.

- Peterson, H.I., Rosenberg, P., and Andsbjerg, J., 1996, Organic geochemistry in relation to the depositional environments of Middle Jurassic coal seams, Danish Central Graben, and implications for hydrocarbon generative potential. *American Association of Petroleum Geologists Bulletin* v. 80, p. 47–62.
- Petzet, G.A., 1996, Utah coalbed gas exploration poised for growth: *Oil and Gas Journal*, August 5, 1996, p. 54.
- Ryer, T.A., 1981, Deltaic coals of Ferron Sandstone Member of Mancos Shale: predictive model for Cretaceous coal-bearing strata of Western Interior. *American Association of Petroleum Geologists Bulletin* v. 65, p. 2323–2340.
- Ryer, T.A., 1982, Cross-section of the Ferron Sandstone Member of the Mancos Shale in the Emery Coal Field, Emery and Sevier Counties, Central Utah, U.S. Geological Survey Map MF-1357.
- Ryer, T.A., 1991, Stratigraphy, facies, and depositional history of the Ferron Sandstone in the canyon of Muddy Creek, East-Central Utah, in Chidsey, T.C., ed., *Geology of East-Central Utah*: Utah Geological Association Publication 19, p. 45–54.
- Ryer, T.A., 1994, Interplay of tectonics, eustasy, and sedimentation in the formation of Mid-Cretaceous clastic wedges, central and northern Rocky Mountain Regions. *Rocky Mountain Association of Geologists Unconformity Controls Symposium*, p. 35–44.
- Ryer, T.A., and McPhillips, M., 1983, Early Late Cretaceous paleogeography of east-central Utah, in Reynolds, M.W., and Dolly, E.D., eds., *Mesozoic paleogeography of west-central United States*: Society of Economic Paleontologists and Mineralogists Rocky Mountain Section, p. 253–272.
- Ryer, T.A., Phillips, R.E., Bohor, B.F., and Pollastro, R.M., 1980, Use of altered volcanic ash falls in stratigraphic studies of coal-bearing sequences. An example from the Upper Cretaceous Ferron Sandstone Member of the Mancos Shale in central Utah. *Geological Society of America Bulletin* v. 91, p. 579–586.
- Ryer, T.A., and Anderson, P.B., 1995, Parasequence sets, parasequences, facies distributions, and depositional history of the Upper Cretaceous Ferron Deltaic Clastic Wedge, Central Utah (abs). *American Association of Petroleum Geologists Rocky Mountain Section Meeting 1995*, Reno, Nevada, *American Association of Petroleum Geologists Bulletin* v. 79, p. 924.
- Semborski, J., 1991, History of coal mining in Carbon and Emery Counties, Utah 1870–1980, in Chidsey, T.C., ed., *Geology of East-Central Utah*: Utah Geological Association Publication v. 19, p. 149–156.
- Shanley, K.W., and McCabe, P.J., 1993, Alluvial architecture in a sequence stratigraphic framework: a case history from the Upper Cretaceous of southern Utah, U.S.A., in Flint, S., and Bryant, I., eds., *Quantitative modelling of clastic hydrocarbon reservoirs and outcrop analogues*: International Association of Sedimentologists Special Publication 15, p. 21–55.
- Sommer, S.N., Bodily, D.M., and Whitney, E.M., 1991, Characteristics of Utah coals in the University of Utah's coal sample bank, in Chidsey, T.C., ed., *Geology of East-Central Utah*: Utah Geological Association Publication 19, p. 199–209.
- Tabet, D.E., Hucka, B.P., and Sommer, S.N., 1995, Maps of total Ferron coal, depth to top, and vitrinite reflectance for the Ferron Sandstone Member of the Mancos Shale, central Utah: Utah Geological Survey Open-File Report 329, 1:250,000.
- Tripp, C.N., 1989, A Hydrocarbon Exploration Model for the Cretaceous Ferron Sandstone Member of the Mancos Shale, and the Dakota Group in the Wasatch Plateau and Castle Valley of East-Central Utah, with Emphasis on Post-1980 Subsurface Data: Utah Geological Survey Open-File Report 160, 81 p.
- Vail, P.R., 1987, Seismic stratigraphic interpretation procedure, in Bally, A.W., ed., *Atlas of Seismic Stratigraphy*. *American Association of Petroleum Geologists Studies in Geology* v. 27, p. 1–10.
- van den Bergh, T.C.V., 1995, *Facies Architecture and Sedimentology of the Ferron Sandstone Member of the Mancos Shale, Willow Springs Wash, East-central Utah* [M.S. Thesis] The University of Wisconsin, Madison, 255 p.
- van den Bergh, T.C.V., and Garrison, J.R., Jr., 1996, Channel belt architecture and geometry—a function of depositional parasequence set stacking pattern, Ferron Sandstone, East-central Utah: 1996 American Association of Petroleum Geologists Rocky Mountain Section Meeting—Billings, Montana, Expanded Abstracts Volume, Montana Geological Society, p. 37–42.
- van den Bergh, T.C.V., and Sprague, A.R., 1995, The control of high-frequency sequences on the distribution of shoreline and fluvial reservoir facies: an example from the Ferron Sandstone, Utah: 1995 American Association of Petroleum Geologists Annual Convention—Houston, TX.
- Van Wagoner, J.C., Mitchum, R.M., Campion, K.M., and Rahmanian, V.D., 1990, Siliciclastic sequence stratigraphy in well-logs, cores, and outcrop: *American Association of Petroleum Geologists Methods in Exploration Series* 7, p. 1–55.
- Williamson, I.A., 1970, Tonsteins—their nature, origins, and uses. *Mining Magazine* v. 122, p. 119–125 and p. 203–211.
- Ye, L., 1995, Paleosols in the Upper Guantao Formation (Miocene) of the Gudong Oil Field and their application to the correlation of fluvial deposits. *American Association of Petroleum Geologists Bulletin* v. 79, p. 981–988.

Extensional Faulting, Footwall Deformation and Plutonism in the Mineral Mountains, Southern Sevier Desert

DREW S. COLEMAN

*Department of Earth Sciences, 675 Commonwealth Avenue, Boston University,
Boston, Massachusetts 02215*

JOHN M. BARTLEY

*Department of Geology and Geophysics, 717 WBB, University of Utah,
Salt Lake City, Utah 84112*

J. DOUGLAS WALKER

*Department of Geology, 120 Lindley Hall, University of Kansas,
Lawrence, Kansas 66045*

DAVID E. PRICE

*Department of Geology and Geophysics, 717 WBB, University of Utah,
Salt Lake City, Utah 84112*

ANKE M. FRIEDRICH

*Department of Earth, Atmospheric and Planetary Sciences, Massachusetts
Institute of Technology, 54-1118, Cambridge, Massachusetts 02139*

ABSTRACT

Structural relations in the Mineral Mountains and surrounding area in southern Utah indicate that the major north-south striking Cenozoic normal faults in the region were tilted to their present gentle dips by either rolling-hinge style footwall uplift or domino style faulting. Field, geochronologic and thermochronologic data demonstrate that the main period of east-west directed extension along these normal faults occurred 6 to 7 Ma after peak magmatism. Thus, no direct link between magmatism, normal faulting and ductile deformation associated with normal faulting exists in the area. Prior to, and synchronous with, the main episode of east-west directed extension, several sets of northeast- to northwest-striking normal faults generated a series of east-west trending grabens throughout the region. The timing of formation of these grabens varies across the study area and overlaps with regional magmatism. We infer a large amount of slip along the Sevier Desert detachment fault which is the only structure north of the Mineral Mountains that could accommodate the extensional deformation documented there. This argues against the interpretation that the Sevier Desert reflector is the result of fortuitous alignment of a Mesozoic thrust fault and a Cenozoic unconformity. Tertiary extension disrupted Mesozoic thrust faults across the Mineral Mountains and surrounding ranges; however, new mapping provides a basis for regional correlation. We correlate the Wah Wah, Frisco and Antelope Mountain thrusts, and a sub-Antelope Mountain thrust with the Beaver Lake thrust and Dry Canyon/Tetons thrust zone.

INTRODUCTION

The common spatial and temporal association of magmatism and metamorphic core complexes suggests that a genetic relation exists between the two. The association of broadly coeval plutonic rocks with low-angle mylonitic detachment faults led Gans (1987), Lister and Baldwin (1993) and Parsons and Thompson (1993) to suggest direct links between magmatism, ductile deformation in core complexes, and the development of low-angle normal faults. In contrast, Axen et al., (1993) and Coleman et al., (in preparation) acknowledge the widespread importance of magmatism in extension, but find no consistent temporal or genetic link between magmatism and formation of extensional core complexes.

Another persistent debate regarding the origin of extensional core complexes is whether presently low-angle normal faults were active with shallow dips (e.g., Wernicke, 1981; Davis and Lister, 1988; Reynolds and Lister, 1990; Scott and Lister, 1992), or were active as moderately to steeply dipping normal faults that were subsequently tilted to shallow orientations (Proffett, 1977; Buck, 1988; Wernicke and Axen, 1988). Evaluating footwall deformation is difficult in core complexes that are dominated by young plutonic rocks that lack markers for reconstruction of structural geometries (e.g., Reynolds and Rehrig, 1980; Gans, 1987; Walker et al., 1990; Lister and Baldwin, 1993; Wright and Snoke, 1993; Coleman and Walker, 1994). The nature and amount of footwall deformation in such complexes has been examined indirectly using paleomagnetic and/or thermochronologic data (Holm et al., 1990; Hoisch and Simpson, 1993; John and Foster, 1993; Livaccari et al., 1993, 1995; Coleman and Walker, 1994; Coleman et al., in preparation). Furthermore, structures that directly record rebound kinematics in initially isotropic plutonic rocks are increasingly recognized (Bartley et al., 1990; Manning and Bartley, 1994; Axen et al., 1995).

The debate regarding the original orientation of low-angle detachment faults recently took on new life with the assertion that the reflector in west central Utah, previously interpreted as the Sevier Desert extensional detachment (MacDonald, 1976; Allmendinger et al., 1983; Von Tish et al., 1985), actually is defined by the coincidental alignment of a Mesozoic thrust fault and the sub-Tertiary unconformity (Anders and Christie-Blick, 1994). The Mineral Mountains in southwest Utah lie directly south of the Sevier Desert, and displacement across the Sevier Desert detachment is interpreted to be partially accommodated in this and adjacent basins and ranges (figs. 1 and 2; Price and Bartley, 1990; Coleman, 1991; Coleman and Walker, 1994; Price, in preparation). The Tertiary Mineral Mountains batholith, which forms the majority of the northern and central part of the range (Smith and Bruhn, 1984; Nielson et al., 1986;

Coleman, 1991; Coleman and Walker, 1992), lies in the footwall of the Cave Canyon detachment. The detachment and a klippe of its hanging wall are preserved in the southern part of the range (Nielson et al., 1986; Price and Bartley, 1990, 1992; Price, in preparation). The structural geology, petrology, geochronology and paleomagnetism of the Mineral Mountains and ranges to the west reveal the history of the Cave Canyon detachment and related faults, and provide insight into the amount and nature of crustal extension southward along strike from the Sevier Desert.

The principal aim of this trip is to examine what we have learned regarding the relationship between magmatism and extension in the Mineral Mountains. We will also examine field data bearing on the nature of footwall deformation and the amount of extension accommodated in the area. We present relevant results of field work in the Mineral Mountains and nearby Star Range, Beaver Lake Mountains and Wah Wah Mountains (figs. 1 and 2). We show evidence that magmatism and extension were not synchronous, but rather, that the main pulse of plutonism ended at least 6 Ma before the Cave Canyon detachment exhumed the plutonic complex (Coleman et al., in preparation). Furthermore, closely following the last episode of intrusive magmatism, unroofing of the plutonic complex by slip across the Cave Canyon detachment resulted in up to 90° of west-side-up tilting resulting in the present low-angle geometry of the fault (Price and Bartley, 1990, 1992; Coleman and Walker, 1994; Coleman et al., in preparation; Price, in preparation). Finally, restoration of mapped regional normal faults accounts for a minimum of 20 kilometers of east-west directed extension. Because no other structures that could accommodate this magnitude of slip are recognized to the north, these observations support the existence of, and large slip across, the Sevier Desert detachment.

An additional focus of our work in the Mineral Mountains region has been to document structural relations of the thrust faults in the area, including their overprinting by Cenozoic deformation, and to correlate the isolated exposures from range to range. Although severely disrupted by Tertiary extension, several thrust faults of regional significance are exposed in the area (figs. 1 and 2), including the Beaver Lake, Antelope Mountain, Pavant, and Frisco/Wah Wah thrusts. One of the aims of the field trip is to examine possible correlations amongst these structures.

MAP UNITS

Proterozoic Basement

Precambrian banded gneiss crops out on the western margin of the Mineral Mountains batholith (fig. 2, unit pC; Stop 1-5; Nielson et al., 1978; Sibbett and Nielson, 1980). Aleinikoff et al., (1987) report a U-Pb zircon age of 1716 ± 31 Ma and a Rb/Sr model age of 1750 Ma for the gneiss.

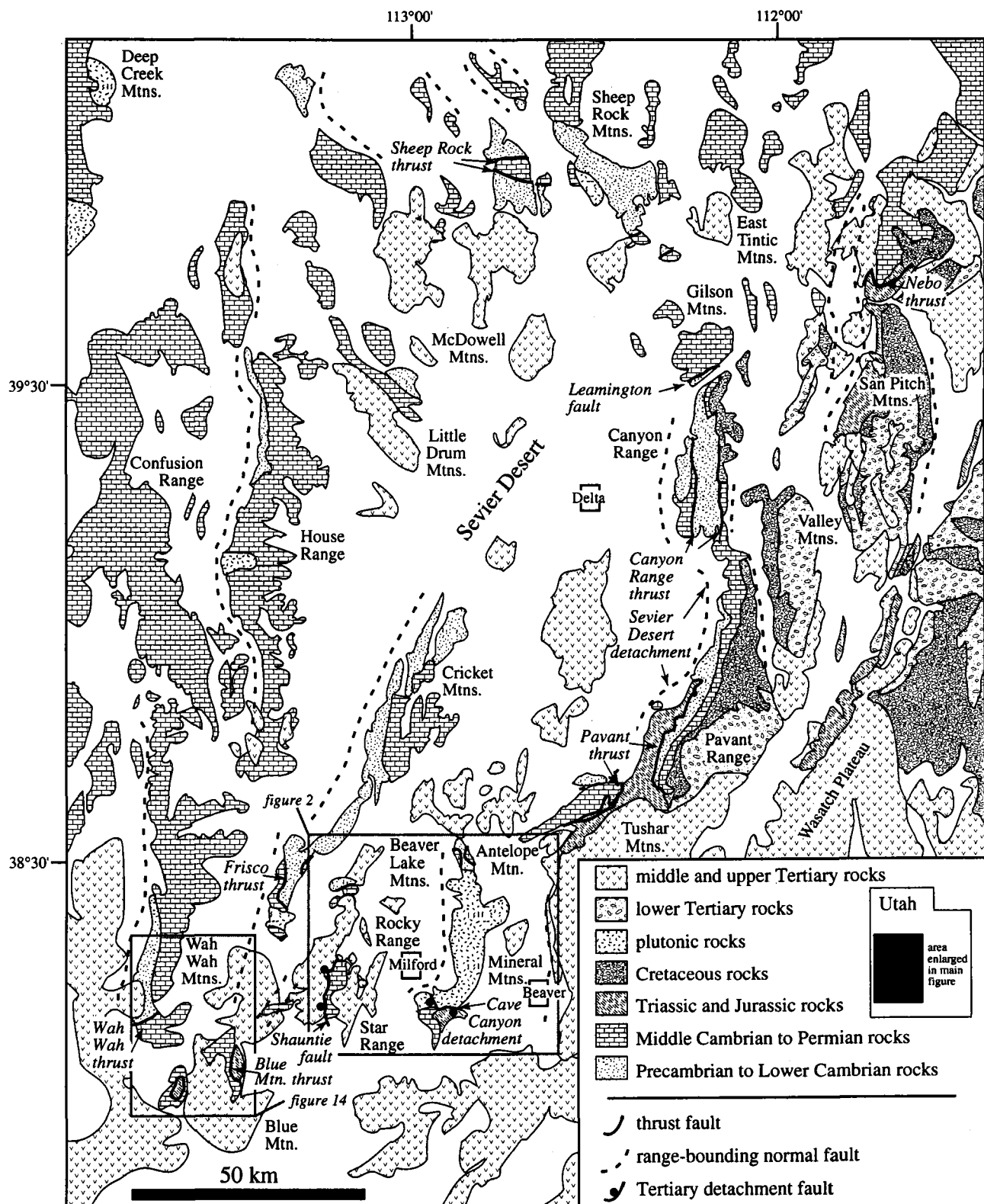


Figure 1. Simplified geologic map of southwestern Utah simplified after Hintze (1980) showing major thrust, normal and detachment faults. Locations of figures showing greater detail of the geology are also shown.

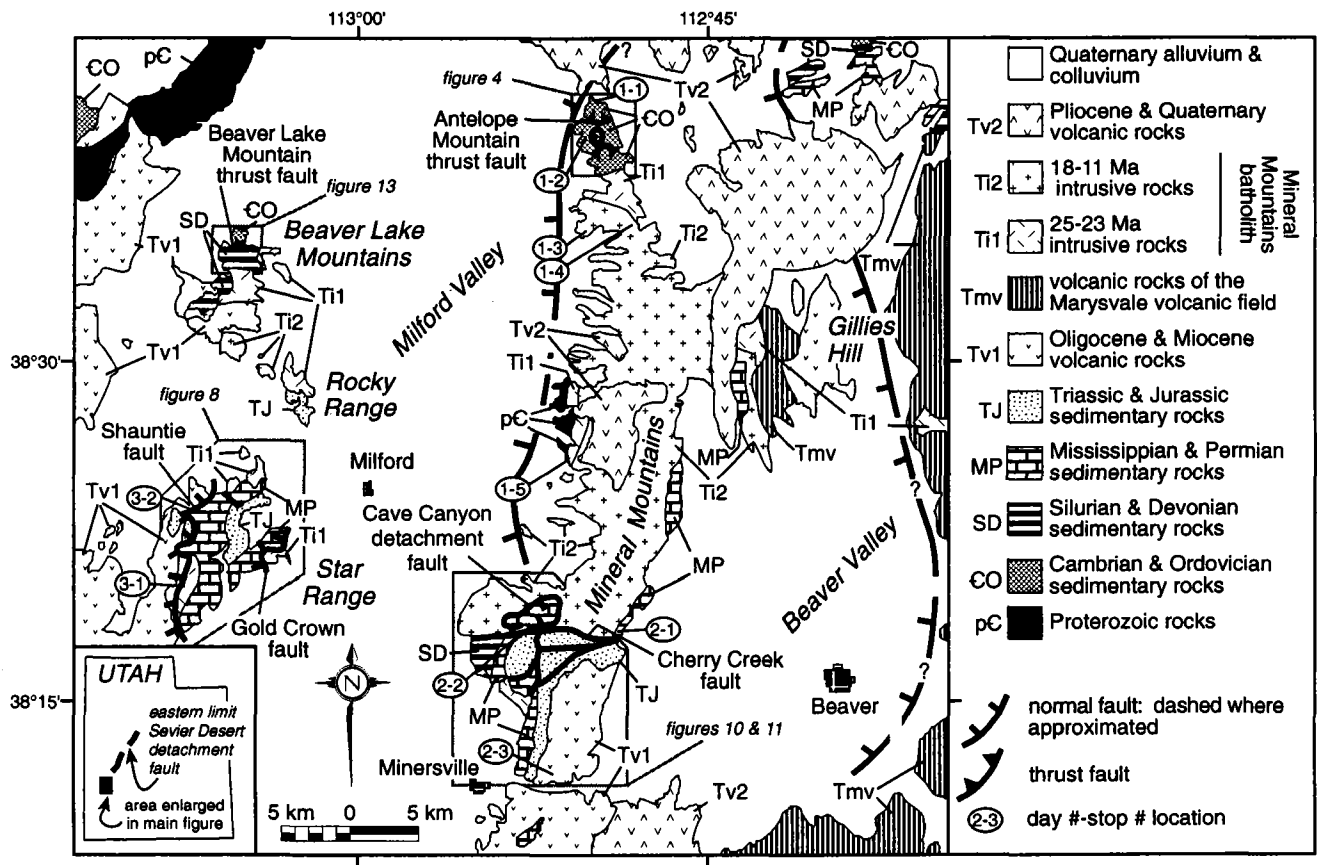


Figure 2. Simplified geologic map of the Mineral Mountains and surrounding ranges. Approximate field trip stop locations and areas of more detailed geologic map figures are shown. Geologic data from Hintze (1980), Coleman (1991), Price (in preparation) and this study. Modified after Coleman and Walker (1992).

Quartzite containing minor biotite, feldspar and chlorite occurs as inclusions within the Precambrian biotite gneiss and as xenoliths in the Mineral Mountains batholith (Nielson et al., 1978; Sibbett and Nielson, 1980; Coleman, 1991). Thin layers of sillimanite-K-feldspar schist also are found as inclusions in the batholith near exposures of the Precambrian biotite gneiss (Nielson et al., 1978; Sibbett and Nielson, 1980; Coleman, 1991). The quartzite and schist are assigned a Precambrian age because of their close association with the gneiss and high metamorphic grade; no known exposed Paleozoic wallrock experienced sillimanite zone metamorphism. Nielson et al., (1978) and Sibbett and Nielson (1980) interpreted the gneiss as a paragneiss on the basis of its field relations with the sillimanite schist and quartzite and the nature of banding within the unit.

Paleozoic-Mesozoic Rocks

Late Proterozoic to Mesozoic strata in the Mineral Mountains region represent the transition from the miogeocline to the craton inboard of a west-facing continental

margin (fig. 3). The area lies outside of the late Paleozoic Oquirrh basin of northern Utah and is sufficiently far from the ancient continental margin not to have recorded the Antler or Sonoma orogenies. It thus was tectonically quiescent from late Proterozoic time until initiation of the Sevier orogeny in latest Jurassic to early Cretaceous time when continental-margin facies were stacked, telescoped, and thrust toward the craton (Armstrong and Oriel, 1965; Armstrong, 1968; Heller et al., 1986; Royse, 1993; DeCelles et al., 1995).

Antelope Mountain

Stratified rocks of Cambrian and Cretaceous(?) age are exposed on Antelope Mountain at the northern end of the Mineral Mountains (fig. 2, unit CO; fig 4; Stops 1-1 and 1-2). Cambrian strata are part of the miogeocline sequence that is well described elsewhere (Hintze and Robison, 1975). Conglomerate of probable Cretaceous age, unrecognized prior to our mapping, is exposed in three outcrop areas bounded by faults and unconformities (fig. 4; Stop 1-2;

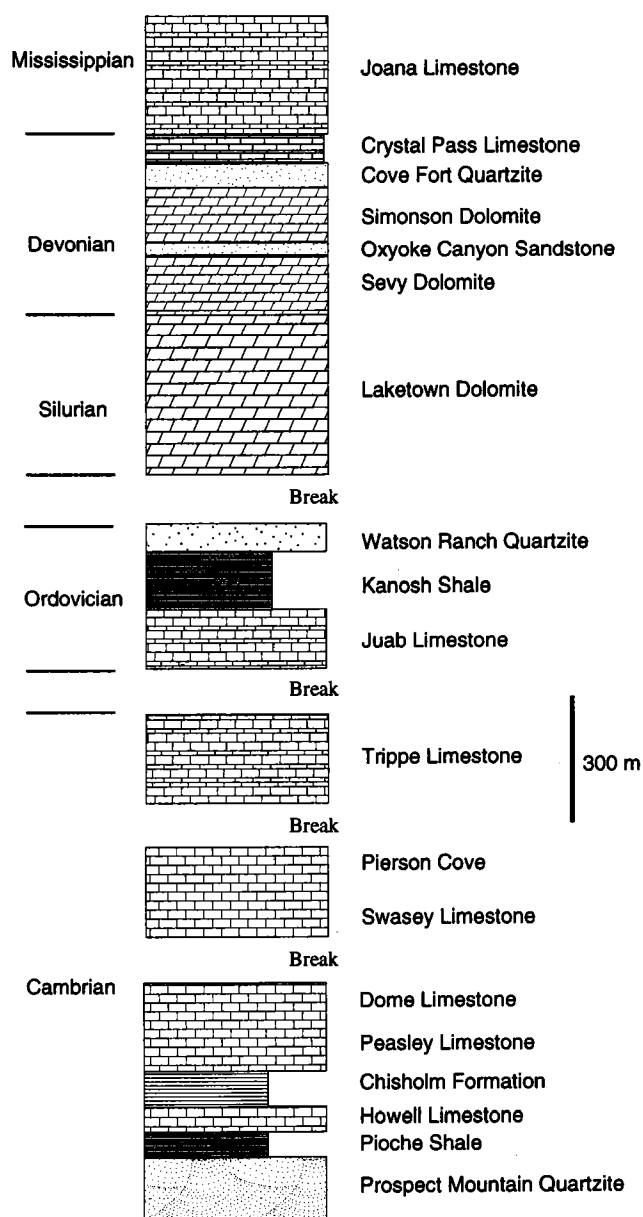


Figure 3. Generalized stratigraphic column for the Beaver Lake and Antelope Mountain areas. Unit assignments after Hintze and Robison (1975), Barosh (1960), and Lemmon and Morris (1984). Breaks in section correspond with faults within and between the two areas.

Walker and Bartley, 1991). The rocks consist of unfossiliferous, orange-weathering calcareous siltstone and conglomerate with subordinate quartz sandstone. Siltstone beds are typically thinly laminated (1 mm) and from 0.5 to 1 meter thick. Conglomerate beds are thick (1 to 5 m) and massively stratified. The conglomerate is mostly matrix-supported and the matrix consists of orange-weathering siltstone. Clasts include quartzite and carbonate rocks identical to

Cambrian strata in the hanging wall and footwall of the Antelope Mountain thrust. The basal contact of the conglomerate is an unconformity developed on progressively older Cambrian strata passing to the north. The upper contact is the Antelope Mountain thrust. We correlate these strata with the Cretaceous Indianola Group on the basis of their structural position and lithologic similarity to strata in the southern Pavant Range.

Central Mineral Mountains

Paleozoic rocks exposed in the central Mineral Mountains include recrystallized limestone and dolomite, and quartzite (fig. 2, unit MP; Crawford and Buranek, 1945; Earl, 1957; Condie, 1960; Nielson et al., 1978; Sibbett and Nielson, 1980; Coleman, 1991). Paleozoic sedimentary rocks immediately adjacent to the batholith are generally too metamorphosed to make definitive stratigraphic assignments; however, several workers have assigned ages and/or formation names to various parts of these metasedimentary rocks, and the reader is referred to the references cited above for more detailed descriptions.

Recognizable Paleozoic carbonate wallrocks in the Mineral Mountains include Mississippian Redwall Limestone and a dark colored dolomite that may be correlative with the Devonian Simonson Dolomite on the eastern side of the range (fig. 2; Stop 2-1; Crawford and Buranek, 1945; Sibbett and Nielson, 1980; Price, in preparation), and Permian Kaibab Limestone (Earl, 1957) on the western side. However, Sibbett and Nielson (1980) noted that the carbonate rocks on the western side of the batholith lack the chert nodules characteristic of the Kaibab Limestone, placing some doubt on the correlation made by Earl (1957).

Brown to gray schistose quartzite occurs as inclusions on the eastern side of the Mineral Mountains batholith, and in fault and depositional(?) contact with the carbonate rocks on the western side of the range (Nielson et al., 1978; Sibbett and Nielson, 1980; Coleman, 1991). This rock unit is assigned a Paleozoic age on the basis of the interpreted stratigraphic contact with rocks correlated with the Redwall Limestone (Crawford and Buranek, 1945; Nielson et al., 1978; Sibbett and Nielson, 1980) and may be equivalent to the Devonian Cove Fort Quartzite.

Southern Mineral Mountains and Star Range

Stratigraphic sections of pre-Cenozoic rocks exposed in the southern Mineral Mountains and in the Star Range across Milford Valley to the west are similar and therefore are treated together here (fig. 2, units SD, MP and TJ; fig. 5). The oldest exposed strata are assigned to the Devonian Simonson Dolomite based on the characteristic dark color and stromatoporoid fauna. The base of the section is everywhere either faulted, intruded, or concealed. The youngest pre-Cenozoic strata in the Star Range are assigned to the

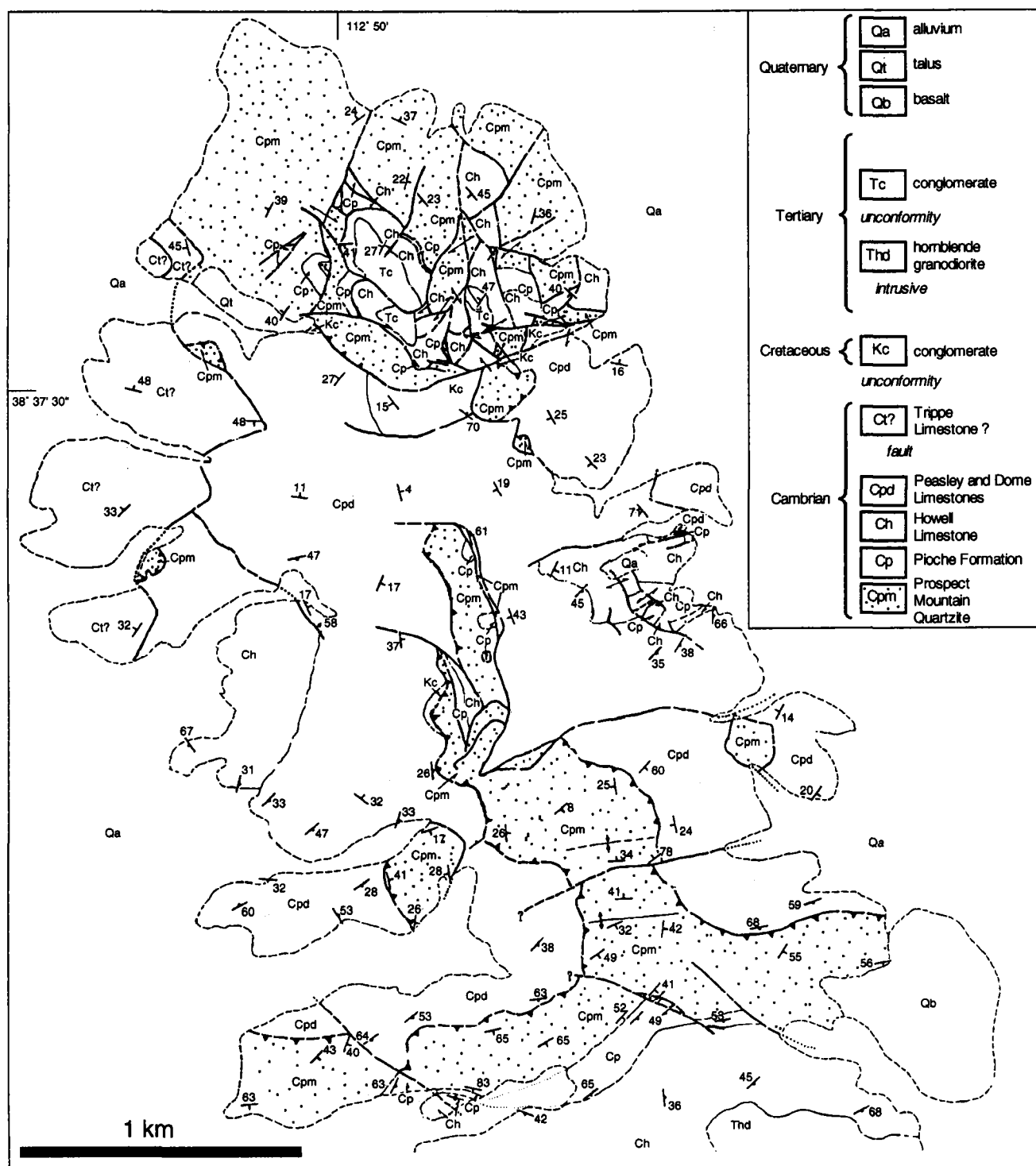


Figure 4. Geologic map of the Antelope Mountain area. The principal structure in this area is the Antelope Mountain thrust (see text for discussion). East-west trending folds in the footwall to the southern section of the Antelope Mountain thrust fault are attributed to synplutonic deformation. Mapping by J.D. Walker and J.M. Bartley.

Jurassic Navajo Sandstone, whereas the Mineral Mountains section locally includes overlying limestone assigned to the Jurassic Carmel Formation. The intervening upper Paleozoic through Triassic section is relatively thin and contains a larger proportion of quartzose clastic rocks and dolostone than miogeoclinal sections. As a result of this relatively cratonal character, most mapped formations are more readily correlated to the Colorado Plateau than to miogeoclinal sections (fig. 5 and compare to fig. 6).

Northern Beaver Lake Mountains

Stratified rocks of Cambrian to Mississippian age are present in the Beaver Lake Mountains (fig. 2 units CO and SD; fig. 3). The rocks are involved in a complex imbricate zone associated with the Beaver Lake thrust, intruded by mid-Tertiary granitoids, and dissected by normal faults; therefore the stratigraphy is fragmentary at best. Stratigraphic nomenclature that has been used for these rocks is a somewhat confusing patchwork of local names and names imported from Nevada and other parts of Utah. We have not attempted to resolve these problems, but use the unit designations of previous workers and names from the Wah Wah Mountains and southern Pavant Range (Barosh, 1960; Hintze, 1974; Abbott et al., 1983; Lemmon and Morris, 1984).

Southern Wah Wah Mountains

Late Proterozoic to Mesozoic strata are exposed as several inliers within the southern Wah Wah Mountains (figs. 6 and 7). Late Proterozoic strata consist mainly of quartzite and occur only in the Wah Wah thrust plate. Cambrian carbonate rocks of the Blue Mountain thrust plate include Upper Cambrian units that are not exposed elsewhere in the Mineral Mountains region. Ordovician to Mississippian carbonate strata are well exposed in several imbricate thrust slices; this section is similar to the section of the Beaver Lake Mountains with the exception of the Oxyoke Canyon Sandstone, which appears as a thin yellow siltstone layer. The upper part of the Mississippian section includes clastic sedimentary rocks that may represent the distal edge of the Antler foreland basin, which is otherwise unrecognized in rocks structurally below the Wah Wah-Canyon Range thrust plate. A relatively complete section of Middle Paleozoic rocks is only preserved in one of the thrust slices (Dry Canyon I thrust plate, Friedrich 1993; figs. 6 and 7). Individual sections appear to be thicker in this area than correlative strata in the Milford Valley area, consistent with a more open miogeoclinal setting.

Cenozoic Rocks

Volcanic Rocks

Tertiary volcanic rocks crop out throughout the Mineral Mountains (figs. 2 and 5; Stop 2-3). At the southern end of

the range the sequence includes Oligocene intermediate lava flows assigned to the andesite of the Shauntie Hills, ash-flow tuffs of the Oligocene Needles Range Group (fig. 2, unit Tv1; Best et al., 1989a), and latest Oligocene and early Miocene ash-flow tuffs and near-vent lava flows and volcanoclastic rocks of the Marysville Volcanic Field (fig. 2, unit Tmv; Bullion Canyon Volcanics and Mt. Dutton Formation; Steven et al., 1979). The andesite of the Shauntie Hills was correlated by Best and Grant (1987) with andesite in the Escalante Desert Formation of the Needles Range Group that has a stratigraphically bracketed age of 34–31 Ma. The youngest volcanic rocks exposed in the southern Mineral Mountains are 7.6 Ma basalt (Best et al., 1980).

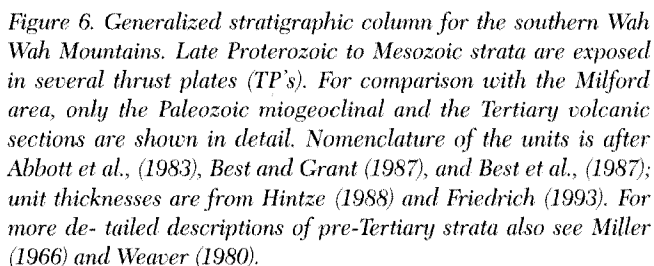
On the northeast side of the Mineral Mountains, the Gillies Hill rhyolite was deposited at approximately 9 Ma (fig. 2, unit Tv2; Evans and Steven, 1982), and on the west side of the range, the Corral Canyon rhyolite was deposited at approximately 8 Ma (Evans and Nash, 1978). Quaternary volcanic rocks occur throughout the Mineral Mountains (Nash, 1976; Nielson et al., 1978; Sibbett and Nielson, 1980; Crecraft et al., 1981; Nash and Crecraft, 1982). These rocks include ash-flow tuffs and obsidian lava flows in the central Mineral Mountains that were deposited contemporaneously with basalt lava flows in the northern Mineral Mountains between 0.8 and 0.5 Ma (fig. 2, unit Tv2; Lipman et al., 1978).

Volcanic rocks in the Star Range and Beaver Lake Mountains are Needles Range Group intermediate lavas assigned to the andesite of the Shauntie Hills and to the Horn Silver Andesite (fig. 2, unit Tv1; Stop 3-1; fig. 5). The volcanic section in the Wah Wah Mountains consists mainly of the Needles Range Group, and the bimodal early Miocene Blawn Formation (fig. 6).

Intrusive Rocks

Mineral Mountains. The largest area of the Mineral Mountains exposes a Tertiary batholith intruded between 25 and 11 Ma (Aleinikoff et al., 1987; Coleman and Walker, 1992). During this interval, there were three distinct episodes of magmatism, all characterized by coeval intrusion and mixing of mafic and felsic magmas (Coleman, 1991; Coleman and Walker, 1992; Coleman et al., in preparation). The first is preserved as mixed diorite and hornblende granodiorite (fig. 2, unit Ti1; Coleman, 1991). The second intrusive episode includes rocks ranging in composition from gabbro to high-silica granite and accounts for greater than 90% of the exposed batholith (fig. 2, unit Ti2). The final intrusive episode recorded is emplacement of rhyolite, basalt and mixed rhyolite-basalt dikes at 11 Ma (fig. 2, unit Ti2).

The northern and westernmost parts of the Mineral Mountains batholith comprise an Oligocene [U-Pb zircon age of 25 ± 4 Ma; (Aleinikoff et al., 1987)] resistant, light-



gray, coarse- to medium-grained hornblende granodiorite, that is easily recognized by the presence of large (up to 1 cm), euhedral hornblende phenocrysts (Nielson et al., 1978; Sibbett and Nielson, 1980; Coleman, 1991). The porphyry of Lincoln Gulch in the southern Mineral Mountains (small map area of unit Ti1 southwest of exposures of the Cave Canyon detachment fault, fig. 2) is distinguished from this hornblende granodiorite by the presence of phenocrysts of biotite and K-feldspar, but is considered part of this intrusive episode on the basis of a preliminary U-Pb zircon age of approximately 23 Ma (D. S. Coleman, work in progress). Similarly, isolated outcrops of 23 Ma syenite in the Gillies Hill area and the Tushar Mountains are considered part of this intrusive episode (fig. 2; Steven et al., 1979; Cunningham et al., 1982). Locally the hornblende granodiorite was migmatized during intrusion of 18 Ma magmas (Stop 1-4; Coleman, 1991; Coleman and Walker, 1992). The presence of sphene in the migmatites is critical for field differentiation between Precambrian and Miocene gneiss: no dated Precambrian units contain sphene. At the northern end of the batholith the Oligocene granodiorite intrudes Cambrian carbonates, and on the western side it intrudes Precambrian wall rocks (Stop 1-5).

The vast majority of exposed plutonic rocks in the Mineral Mountains include coarse-grained, biotite-hornblende quartz monzonite, porphyritic quartz monzonite and granite that are extensively mixed with a coeval, dated 18.2 Ma (U-Pb zircon) diorite (Stop 1-3; Coleman, 1991; Coleman and Walker, 1992; Coleman et al., in preparation). Mixing of diorite and more silicic magmas is interpreted to have generated the variation of composition and texture in these units; therefore, they are considered together here and referred to as a the 'main intrusive phase'. Field relations indicate that the youngest pluton in the main intrusive phase is a 17.5 Ma (U-Pb zircon; Coleman et al., in preparation) leucocratic, garnet granite that crops out at the crest of the range and along the eastern margin of the batholith. Other small intrusive bodies including hornblende gabbro and syenite, and microgranophyric dikes (Condie, 1960; Nielson et al., 1978; Sibbett and Nielson, 1980) are included in the 18.2 to 17.5 Ma intrusive event on the basis of field relations with dated units (Coleman, 1991; Coleman et al., in preparation). Magmas of the main intrusive phase intruded Oligocene hornblende granodiorite on the northern side of the batholith, and Precambrian and Paleozoic rocks on the western and eastern sides (Stops 1-4, 1-5 and 2-1; Nielson et al., 1978; Sibbett and Nielson, 1980; Coleman, 1991).

The last intrusive episode recorded in the Mineral Mountains is widespread emplacement of porphyritic rhyolite and basalt dikes (fig. 2, included in unit Ti2; Stops 1-4, 1-5 and 2-1; Nielson et al., 1978; Sibbett and Nielson, 1980; Nielson et al., 1986; Coleman, 1991). This suite of 11 Ma

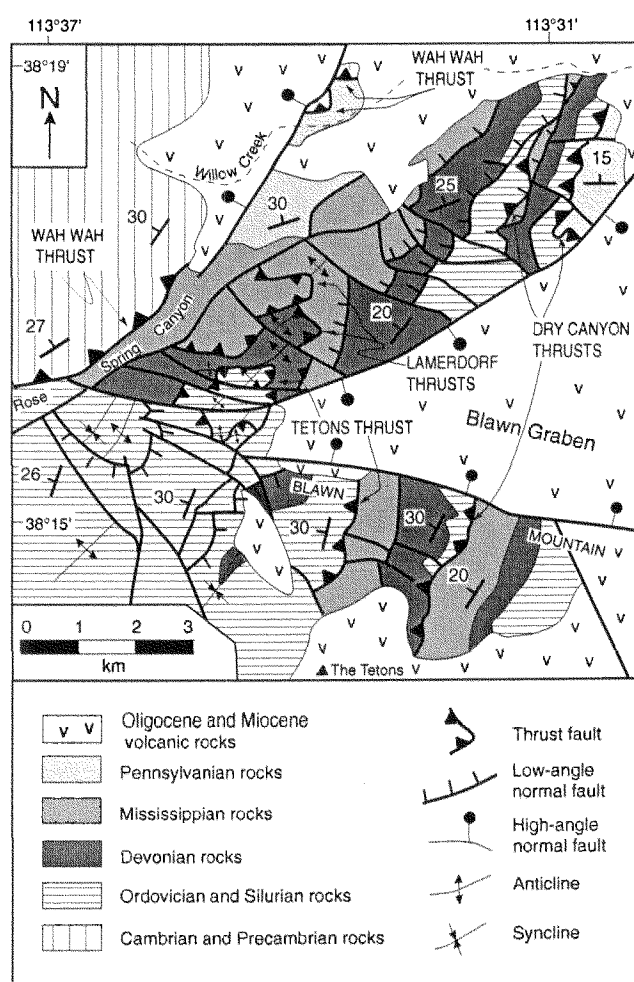


Figure 7. Simplified geologic map of the Rose Spring Canyon-Blawn Mountain area of the southern Wah Wah Mountains. See figure 14 for location. This figure shows the Wah Wah thrust and the backward-breaking imbricate thrusts in its footwall after Friedrich (1993). The Sevier thrusts and the oldest extensional faults are unconformably overlain by the basal volcanic rocks of the Oligocene Escalante Desert Formation.

(U-Pb zircon) dikes is correlative across the batholith and provides an important structural marker (Coleman and Walker, 1994). Although the dikes are mingled extensively, little mixing between the end members is evident.

Star Range. Rocks broadly resembling parts of the Mineral Mountains intrusive complex are exposed in small plutons scattered throughout the Star Range (fig. 2, unit Ti1; fig. 8). Their ages are not well established and, until these rocks are better studied, their relations to rocks in the Mineral Mountains remain unclear.

Three plutons or groups of plutons in the Star Range can be distinguished. A low spur extending from the east-central flank of the range is underlain by a relatively leucocratic

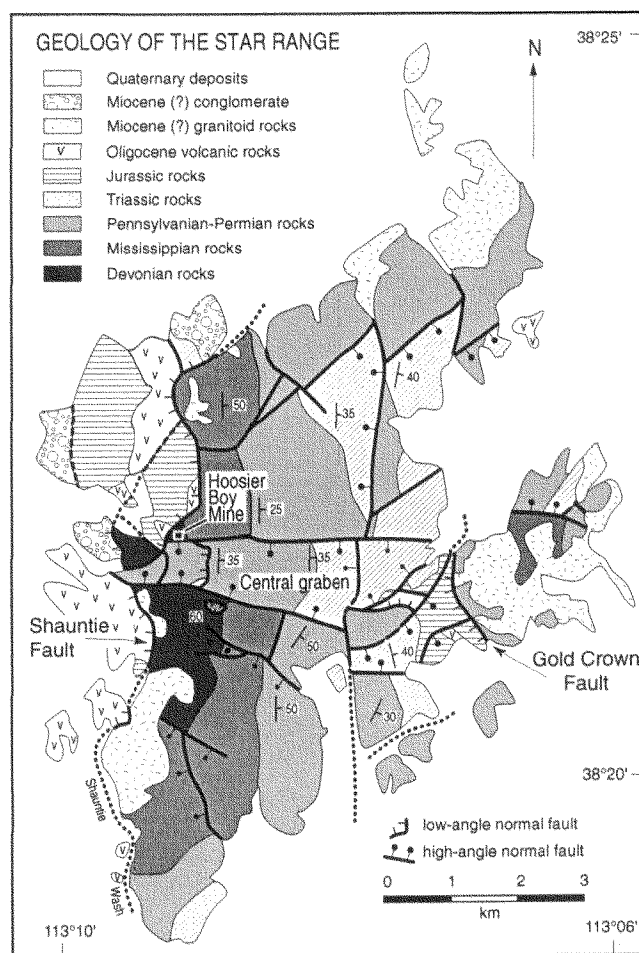


Figure 8. Geology of the Star Range simplified from Best et al., (1989a) and unpublished mapping by Bartley, Friedrich, Price and the 1990 University of Utah geology field class. Paleozoic-Mesozoic rocks that form the bulk of the range were interpreted to lie structurally above Mesozoic strata on the northwest flank along the Blue Mountain thrust. Our mapping indicates that the volcanic rocks deposited on these Mesozoic strata are juxtaposed with Paleozoic strata and the Miocene plutons that intrude them along a west-dipping, low angle normal fault (Shauntie fault). The Shauntie fault eliminates any need of, or evidence for, a thrust fault in the Star Range.

hornblende granodiorite pluton that intruded into upper Paleozoic and Triassic rocks. The exposures probably represent a cupola of a larger pluton that is continuous at depth because the intrusive contacts are highly irregular and rafts of wallrock are ubiquitous within the pluton. The northeastern third of the range provides exposures mainly of two plutonic rock types, porphyritic quartz monzonite which petrographically resembles the porphyry of Lincoln Gulch in the southern Mineral Mountains, containing large (up to 2 cm) K-feldspar phenocrysts, and mafic hornblende grano-

diorite to quartz diorite. Where exposed in mutual contact, these two rock types display clear magma-mixing textures. On the southwest flank of the range, a prominent leucogranite pluton forms the eastern wall of the canyon of Shauntie Wash. Early Miocene fission-track ages are reported from this pluton (Best et al., 1989b), but it is uncertain whether such ages record cooling after magmatic crystallization or later cooling related to unroofing.

Sedimentary Rocks

Mineral Mountains. Fine- to coarse-grained alluvium and colluvium occur throughout the Mineral Mountains. Alluvium generally comprises quartz and feldspar sand and gravel derived directly from weathering of the Tertiary plutonic units. Alluvium is apparently locally derived, and changes character (for example becomes darker near abundant diorite outcrop) with the locally dominant phase of the batholith.

Star Range. Some of the low hills on the west flank of the Star Range are underlain by a newly recognized Cenozoic rock unit that we informally call the conglomerate of the Hoosier Boy Mine (Stop 3-2). The hills had been mapped as Tertiary volcanic rocks (Best et al., 1989b) which is understandable because there are no outcrops and clasts in the float are mainly derived from the andesite of the Shauntie Hills. However, closer examination established the following points: (1) the clasts commonly are subangular to subrounded, indicating that they were transported from elsewhere rather than having weathered out of bedrock in situ; (2) although volcanic rocks predominate, clasts as large as 20 cm of fine-grained granitoid rocks are relatively common; (3) small clasts (< 8 cm) of Triassic sedimentary rocks, mainly red and green siltstone and fine-grained sandstone derived from the Chinle and Moenkopi formations, range from rare to moderately common. (4) Although immediately adjacent hills expose Paleozoic quartzite and carbonate rocks and Tertiary porphyritic quartz monzonite, no clast of these rock types has been found in areas underlain by the Hoosier Boy conglomerate. We interpret these observations to indicate that the Shauntie fault (see below) had not yet unroofed the adjacent Paleozoic and plutonic rocks when the Hoosier Boy conglomerate was deposited.

GEOLOGIC STRUCTURES

Geologic structures in the study area are typical of the Great Basin in that Mesozoic thrust faults are overprinted by Cenozoic extensional faults. Below we briefly summarize the structural geology in each of several areas we have studied in detail. Considerable emphasis is placed on the Mineral Mountains (including Antelope Mountain) which are the focus of this trip and where evidence for extensional

deformation and the timing relationship between extension and magmatism are well preserved.

Antelope Mountain

The principal structure on Antelope Mountain is the Antelope Mountain thrust (Stop 1-2; Liese, 1957; Whelan and Bowdler, 1979), which places Cambrian Prospect Mountain Quartzite over Cambrian Peasley/Dome Limestone and Cretaceous(?) conglomerate (fig. 4; Walker and Bartley, 1991). Although the actual thrust surface is not exposed, its location and attitude are tightly bracketed by outcrops. The thrust is folded into an open, east-plunging antiform. Tight folding of footwall rocks in the core of this antiform was synkinematic with contact metamorphism by the hornblende granodiorite intrusion and therefore we consider the folding to be related to emplacement of the Mineral Mountains batholith rather than to the Sevier orogeny.

The direction of emplacement of the Antelope Mountain thrust is uncertain, but its geometry is consistent with southeast vergence characteristic of the region. Footwall Cambrian rocks become stratigraphically higher to the south, but this relation is probably not related to ramping of the thrust because the intervening Cretaceous strata lie in angular unconformity on Cambrian footwall rocks. Thus, footwall rocks may have already dipped to the south before thrusting, and the footwall was deeply eroded by the time of deposition of the conglomerate. The cause of unroofing of the footwall probably was its elevation along a structurally lower thrust that we refer to as the sub-Antelope Mountain thrust. Considering the present distribution of the hanging wall, and assuming that the thrust climbs section at a moderate angle, displacement across the Antelope Mountain thrust must be at least 5 kilometers.

Tertiary structures at Antelope Mountain include map-scale folds and numerous moderate- to high-angle normal faults (fig. 4). The normal faults strike north or east and most have separations of tens to hundreds of meters. However, a north-striking fault zone on the western side of Antelope Mountain downdrops Middle Cambrian carbonate strata from the hanging wall of the Antelope Mountain thrust against footwall rocks (fig. 4, outcrops of Trippe(?) Limestone on far west side of Antelope Mountain). We know virtually nothing about either the Middle Cambrian stratigraphy or the internal structure of the Antelope Mountain thrust plate. Therefore, it is impossible to make a quantitative slip estimate for this fault zone.

Central Mineral Mountains

Because the central Mineral Mountains are underlain almost exclusively by massive granitoid plutons (fig. 2), the internal structure of this part of the range is difficult to recognize. Thin (less than 10 m) zones of cataclasite, ultracata-

clasite and mylonite which typically contain top-to-the-west shear-sense indicators are found throughout the main intrusive phase. The cataclastic-mylonitic foliation defines a broad north-south trending antiform across the range which Coleman (1991) interpreted to reflect folding of the range-forming block.

Range-scale folding is corroborated by structural orientations and paleomagnetic data from Paleozoic wallrocks and late Miocene dikes, and by the cooling history of the batholith. Rhyolite porphyry and basalt dikes in the northern (Stop 1-4) and western (Stop 1-5) Mineral Mountains consistently have nearly vertical dips and intrude nearly horizontal strata cut by nearly horizontal thrust faults. Dikes of the same swarm in the eastern part of the batholith (Stop 2-1) dip gently and intrude nearly vertical strata cut by nearly vertical thrust faults (Sibbett and Nielson, 1980; Coleman, 1991; Coleman and Walker, 1994). Paleomagnetism of the dikes and the rocks they intrude (both plutonic and wallrocks) supports the interpretation that the dikes were emplaced with subvertical dips and are variably tilted across the range up to a maximum of approximately 90° of west-side-up tilt on the east side of the range (fig. 9; Coleman et al., in preparation). Cooling dates ($^{40}\text{Ar}/^{39}\text{Ar}$ and fission-track) for the main intrusive phase are older on the east side of the batholith relative to those on the west side, consistent with rapid west-side-up tilt of the batholith after approximately 10 million years ago (Evans and Nielson, 1982; Coleman et al., in preparation).

Southern Mineral Mountains

The southern Mineral Mountains can be divided into three structural domains, from north to south: the Harkley Mountain domain, the Guyo graben, and the Yellow Mountain domain (fig. 10).

Harkley Mountain domain. The Harkley Mountain domain lies north of the Cherry Creek fault and includes exposures of the Cave Canyon detachment fault (fig. 11, map and section A-A'; Stop 2-2) which places steeply dipping upper Paleozoic rocks in its hanging wall upon the Mineral Mountains intrusive complex in the footwall (Nielson et al., 1986; Price, in preparation). Slip across the Cave Canyon detachment formed up to 100 meters of protocataclasite and cataclasite derived from footwall plutonic rocks. Extensional faulting and the intrusion of a small 11 Ma rhyolite porphyry pluton severely disrupted bedding in the hanging wall rocks.

Two adjacent fault surfaces mapped within the Harkley Mountain domain are interpreted to be eastern and western segments of the Cave Canyon detachment (fig. 11, section A-A'; Price, in preparation). The eastern segment undulates gently and the fault surface can be measured directly to be subhorizontal. The western segment dips 11° to 18°

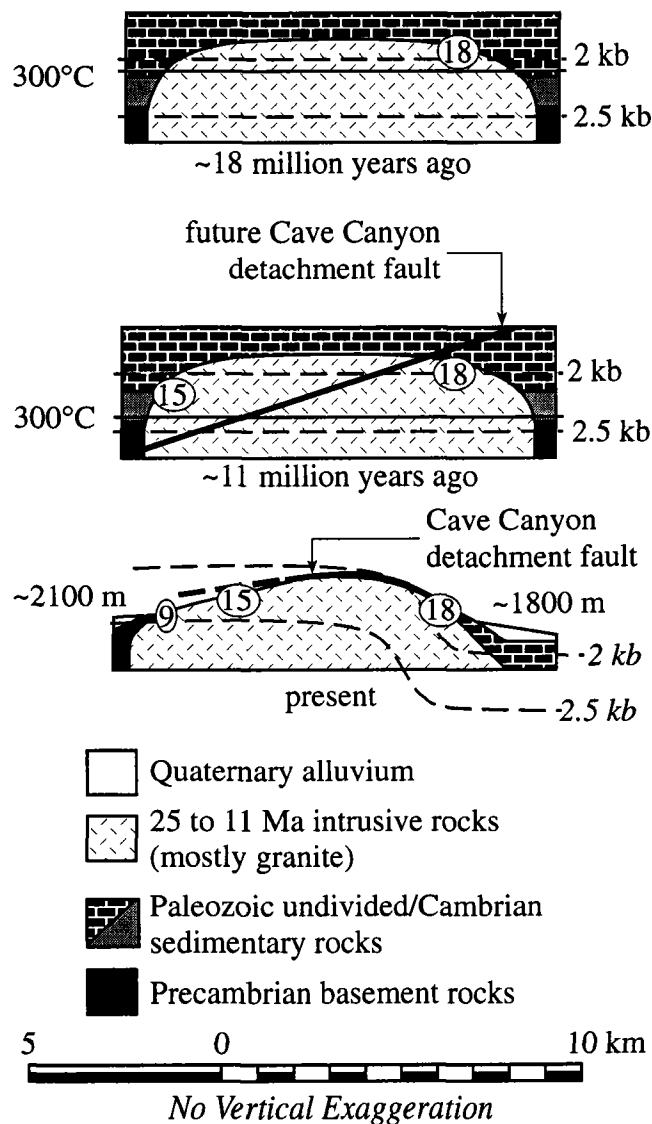


Figure 9. Cooling and deformational history of the Mineral Mountains batholith inferred from structural, thermochronologic and paleomagnetic data. Isobars are pressure estimates made using Al-in-hornblende barometry (Coleman, 1991). Numbers in white ellipses are biotite $^{40}\text{Ar}/^{39}\text{Ar}$ cooling dates in millions of years. We infer static cooling of the batholith between 18 and 11 Ma. By 18 Ma, the rocks of the main intrusive phase emplaced into Pennsylvanian strata had cooled below the 300°C isotherm. By 11 Ma, the 300°C isotherm had not reached the level where the batholith intrudes Proterozoic rocks. All of the exposed rocks had cooled below the 300°C isotherm by 9 Ma, following uplift and deformation of the batholith. Uplift was accompanied by tilting of the rocks on what is now the east side of the exposed batholith resulting in exposure of the shallowest levels of the batholith on the east and the deepest level of the batholith on the west. Uplifted and deformed isobars (indicated by italics) are shown in the last frame. Modified from Coleman et al., (in preparation).

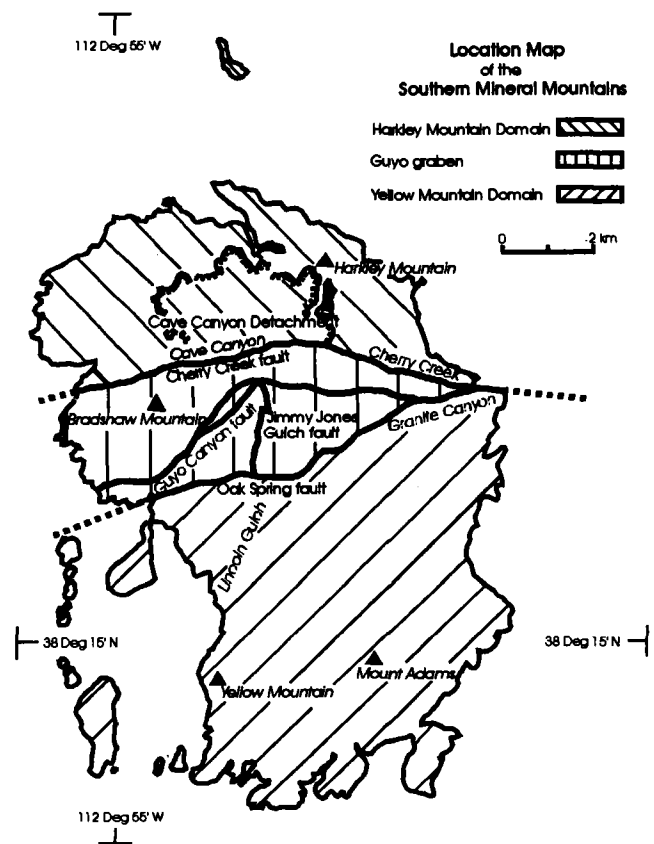


Figure 10. Structural domain map of the southern Mineral Mountains. See text for discussion.

west as determined by three-point solutions. Hanging wall rocks of the western segment were entirely removed by erosion such that the fault zone is recognized only as a layer of silicified cataclasite that caps a series of west-plunging ridges and is identical to that beneath the eastern segment. East- and north-striking high-angle faults cut both segments of the Cave Canyon detachment. Mapping did not reveal a direct spatial or temporal link between the two segments of the detachment fault (Price, in preparation).

Nielson et al., (1986) report that Tertiary rhyolite porphyry intrusions correlative with 11 Ma rhyolite porphyry dikes elsewhere in the Mineral Mountains (Coleman and Walker, 1994) cut the Cave Canyon detachment. However, detailed remapping revealed that the Cave Canyon detachment cuts all intrusive phases, including the Tertiary rhyolite porphyry, along its eastern segment. Whereas all earlier phases of the batholith are strongly cataclasized, however, the Tertiary rhyolite porphyry is scarcely deformed where it intrudes the cataclasite. This relation suggests that most of the displacement along the eastern segment of the detachment may have occurred before 11 Ma (Price and Bartley,

1992; Price, in preparation). Relations between Tertiary rhyolite dikes and the cataclasite along the western segment of the detachment are unknown.

Slip across the Cave Canyon detachment cannot be measured directly because no contacts or piercing points can be correlated from hanging wall to footwall. However, Paleozoic strata can be used to estimate the minimum separation. Wallrocks in the Beaver View Mine area (Stop 2-1) include dark dolomite lithologically resembling Devonian Simonson Dolomite, which is older than any rock currently exposed in the hanging wall of the Cave Canyon detachment in the Harkley Mountain domain. At least 9 kilometers of top-to-the-west slip across the Cave Canyon detachment is required to transport hanging wall Simonson Dolomite westward to a position stratigraphically below the younger hanging wall strata that are preserved (fig. 11, section B-B'; Price, in preparation).

Guyo graben. South of the Harkley Mountain domain is the east-west trending Guyo graben, which is defined by three broadly east-striking high-angle faults (the Cherry Creek, Oak Spring and Guyo Canyon faults) linked by several north- and northwest-striking faults (fig. 10). The northern margin of the graben is the Cherry Creek fault, an east-west striking, sub-vertical fault that places Paleozoic through Tertiary stratified rocks against both hanging wall and footwall rocks of the Cave Canyon detachment (fig. 11, map and section D-D'). The Oak Spring fault forms the southern margin of the Guyo graben and is interpreted to be non-planar and steeply dipping (fig. 11, section D-D'). Separation of rock units across the Oak Spring fault ranges from 300 to 600 meters down-on-the-north.

Running northeast to southwest within the Guyo graben is the non-planar south-dipping Guyo Canyon fault. This fault splays from the Cherry Creek fault near the eastern edge of the Mineral Mountains and converges with the Oak Spring fault at the western edge of the range. Dip separation across the Guyo Canyon fault is approximately 1500 to 1700 meters along much of its length. However, the fault rapidly loses separation in the western half of Guyo Canyon where it splays into several small faults. Many southwest-dipping faults cross from Guyo Canyon to Cave Canyon (fig. 11) and appear to transfer some of this displacement from the Guyo Canyon fault to the Cherry Creek fault. The remainder of the displacement is accommodated by a south-east-plunging fold east of Bradshaw Mountain.

Field relations between normal faults in the Guyo graben domain imply that all of the faults were active contemporaneously (Price, in preparation). The many small faults that splay off of the Guyo Canyon fault both cut and are cut by the north-south striking faults that link the Guyo Canyon fault to the Oak Spring fault. Nearly all of the north- and northeast-striking faults bridge between pairs of east-striking faults and do not cross them. Furthermore, there are no

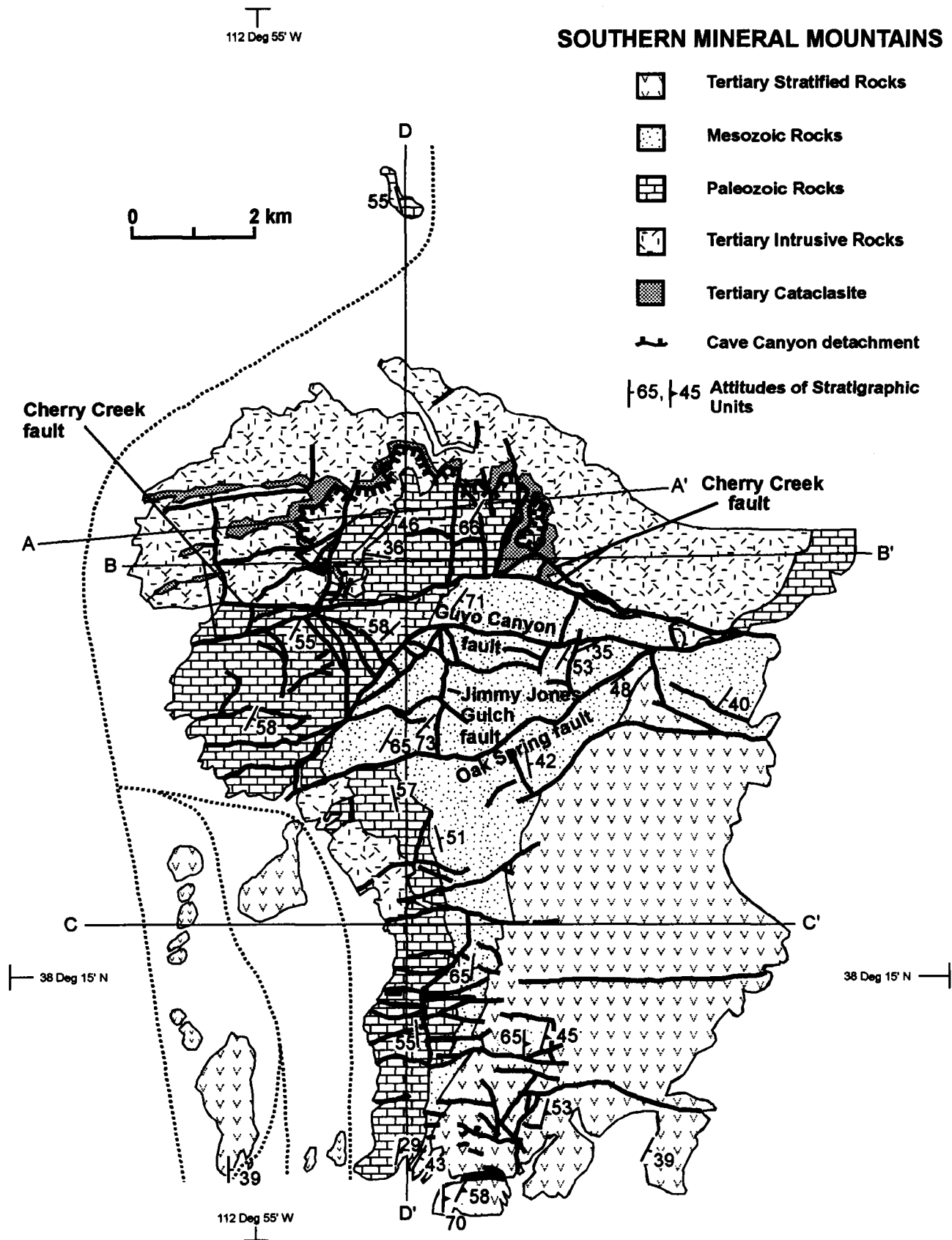
offset continuations of north-striking faults across the east-striking faults.

The location of the Cave Canyon detachment within the Guyo graben domain is uncertain. Its location depends on the nature of the Cherry Creek fault (fig. 12), which may represent a lateral ramp at which the Cave Canyon detachment either could step upward or downward, or it may be a younger fault that cuts and offsets the Cave Canyon detachment. It is also possible that the Cave Canyon detachment terminates at its southern end against the Cherry Creek fault and is not present in the Guyo graben domain (Price, in preparation). Present data do not permit confident selection between these alternatives, although the difficulty of matching rocks and structures across the Cherry Creek fault tends to argue against its interpretation as a younger fault.

Yellow Mountain domain. The Yellow Mountain domain extends from the Oak Spring fault on the north to Minersville Canyon on the south (fig. 10). The domain may be divided into three north-trending fault blocks defined by two inferred north-striking, west-dipping normal faults. However, the western and central blocks are exposed only in scattered low outcrops in the alluvial fan west of the range, and little is known about their structure because of poor exposure and low relief.

The eastern block of the Yellow Mountain domain forms the southern end of the Mineral Mountains and contains several interrelated sets of faults cutting Paleozoic through Tertiary strata. East-striking faults are linked with north-striking and predominantly west-dipping normal faults. The east-striking normal faults cut and offset the north-striking stratigraphic contacts and accommodate minor north-south extension (approximately 500 m, based on the cumulative heave of these faults in fig. 11, section D-D'). Neither east- or north-striking faults consistently cut the other, suggesting that, as in the Guyo graben, both fault sets were active at the same time (Price, in preparation).

Mapped north-striking faults in the Yellow Mountain domain repeat the Oligocene welded tuff sequence at the southern end of the range. These ash-flow tuffs terminate to the north against an east-striking fault north of Mt. Adams, here called the Mt. Adams fault (fig. 11). The outcrop width of andesite of the Shauntie Hills changes abruptly across this fault. The broad area underlain by andesite of the Shauntie Hills north of the Mt. Adams fault is unlikely to reflect an abrupt northward increase in stratigraphic thickness because the change occurs across a fault that equally affects the younger volcanic section. Therefore, cryptic west-dipping normal faults are hypothesized to repeat the andesite of the Shauntie Hills to the north of the Mt. Adams fault (fig. 11, Section C-C'). Thus, the Mt. Adams fault is interpreted to relay displacements between these two sets of north-striking domino-style normal faults.



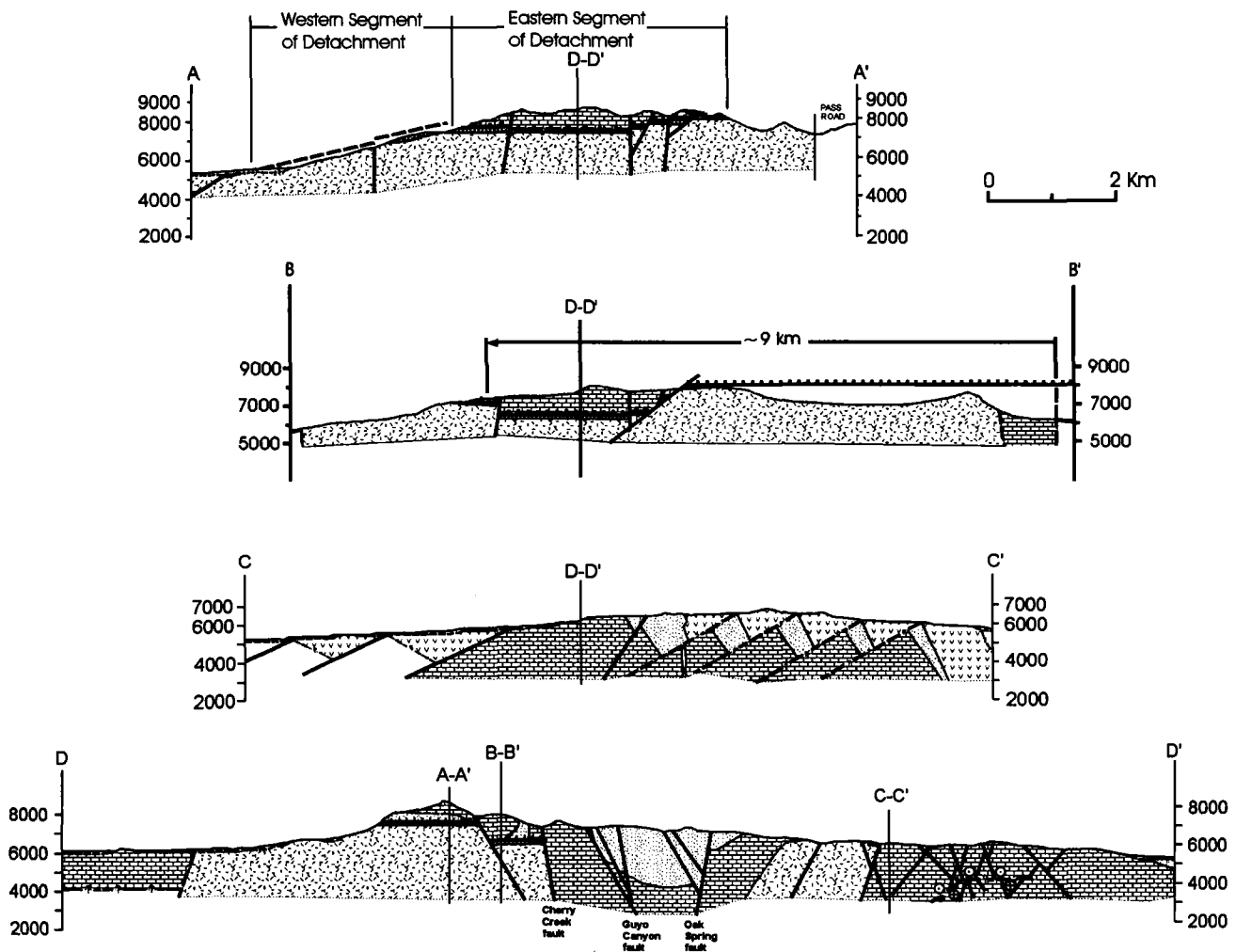


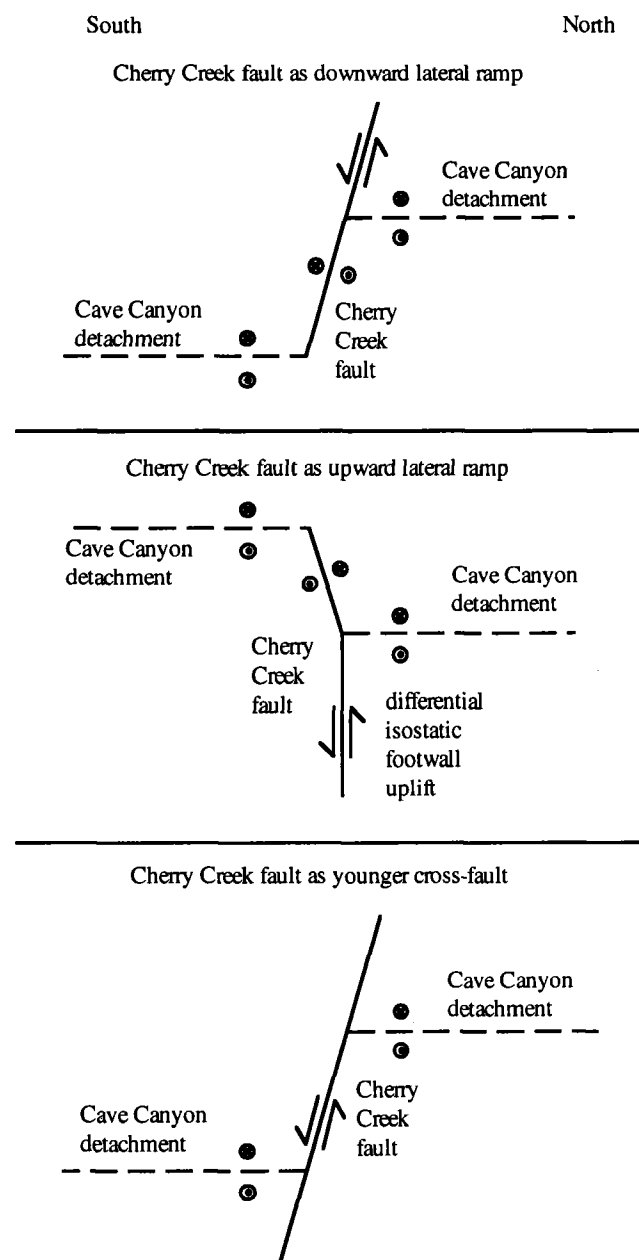
Figure 11. Simplified geologic map and cross-sections of the southern Mineral Mountains. Locations of cross sections are shown. Patterns on cross sections are the same as those shown on map. Mapping by D. Price.

The Yellow Mountain domain contains the only evidence in the area for pre-intrusive faulting. The 23 Ma porphyry of Lincoln Gulch cuts a west-dipping normal fault near the northeast corner of its exposure. Also, an angular unconformity between the three oldest ash-flow tuffs exposed in the southern Mineral Mountains (31 to 27 Ma) and the 26 Ma Isom Formation (Best and Grant, 1987) is suggested by a systematic dip discordance. Mean dips are 69° in the older ash-flow tuffs and 52° in the Isom Formation, whereas attitude data from individual fault blocks are discordant by from 9° to 25° (Stop 2-3). It is possible that the fault cut by the Lincoln porphyry reflects deformation related to tilting at 27 to 26 Ma, and may be related to the intrusion of the 25 ± 4 Ma granodiorite or collapse following eruption at 27 Ma of the Three Creeks tuff member of the Bullion Canyon Volcanics.

Faulting and tilting of the Tertiary section in the Yellow Mountain domain largely postdates the magmatic peak, however, and the amount of tilting varies throughout the domain. Tilting and erosion after deposition of the Tertiary Mt. Dutton Formation (approximately 21 Ma; Machette et al., 1984) formed a paleovalley in which quartz sandstone was deposited. Dip discordance indicates approximately 15° of eastward tilt between deposition of the Mt. Dutton Formation and the undated quartz sandstone. A basalt flow dated at 7.6 Ma (K-Ar whole-rock, Best et al., 1980) unconformably overlies the sandstone and dips 12° east (three-point solution on its basal contact). This indicates approximately 20 to 30° of further eastward tilt before 7.6 Ma and approximately 12° since 7.6 Ma. Bedding dips elsewhere in the domain record as little as 10° of tilt between 21 and 7.6 Ma and as much as 40° of tilt after 7.6 Ma.

Beaver Lake Mountains

The Beaver Lake thrust places Cambrian Prospect Mountain Quartzite on Mississippian Joana Limestone with two intervening horses of Cambrian rocks (fig. 13; Lemmon and Morris, 1984). Footwall rocks comprise Cambrian to Mississippian strata. The hanging wall consists of Prospect Mountain Quartzite passing up section into Dome Limestone. These rocks are probably in sequence with Cambrian-Ordovician Notch Peak Limestone exposed directly below the Frisco thrust in the adjacent San Francisco Mountains (fig. 1; Lemmon and Morris, 1984).



The Beaver Lake Mountains are cut by numerous moderate- to high-angle Tertiary faults in widely varying orientations (fig. 13). The faults generally have small stratal separations. More significant Tertiary deformation is present, however, near the contact with the hornblende granodiorite (fig. 2, unit T1). Here, Paleozoic carbonate rocks are contact-metamorphosed to the point that a formation assignment is generally impossible, and contain a steep foliation subparallel to the intrusive contact. The contact aureole locally contains recognizable Middle Cambrian silty limestone that clearly is out of place relative to the Siluro-Devonian dolostones adjacent to the contact aureole. We interpret these Cambrian rocks to have reached their present position as a result of synmetamorphic shearing in the contact aureole. This steep structural zone corresponds directly to the steep southern limb of the Tertiary antiform adjacent to the same pluton on Antelope Mountain to the east across Milford Valley. This correlation suggests that shearing was pluton-side down and that the Cambrian rocks were derived from the Beaver Lake thrust sheet. Similar wallrock-pluton relations described elsewhere in the western United States are interpreted to result from sinking of plutons following a density increase associated with crystallization (Glazner, 1994; Glazner and Miller, 1996).

Star Range

The Star Range is composed of several fault-bounded blocks containing mainly east-dipping strata. Although faults of virtually every strike are present, four main faults define

Figure 12. Possible geometries of the Cherry Creek fault as shown in simplified north-south cross sections approximately along the line D-D' in figure 9. Arrows show direction of movement of the Cherry Creek fault (solid); circles with dots and X's show motion of the Cave Canyon detachment (dashed) out of, and into, the page, respectively. The first two frames show the Cherry Creek fault as a lateral ramp along the Cave Canyon detachment. We regard the second possibility (a south-side-up lateral ramp) as unlikely because the rocks exposed south of the Cherry Creek fault are unlike footwall rocks exposed elsewhere in the Mineral Mountains. However, the same basic geometry would result if the Cherry Creek fault is a tear fault that transfers the Cave Canyon detachment to the west. The final frame shows the Cherry Creek fault as a younger, cross-cutting, down-on-the-south structure. An additional possibility (not explicitly shown) is that the Cherry Creek fault is a tear fault that separates two distinct sets of fault blocks. In this case, the Cave Canyon detachment terminates against the Cherry Creek fault at its southern end. Existing data do not establish direction of motion across the Cherry Creek fault or the relative ages of the Cherry Creek fault and the Cave Canyon detachment. Therefore, we are unable to determine which of these possibilities is most likely.

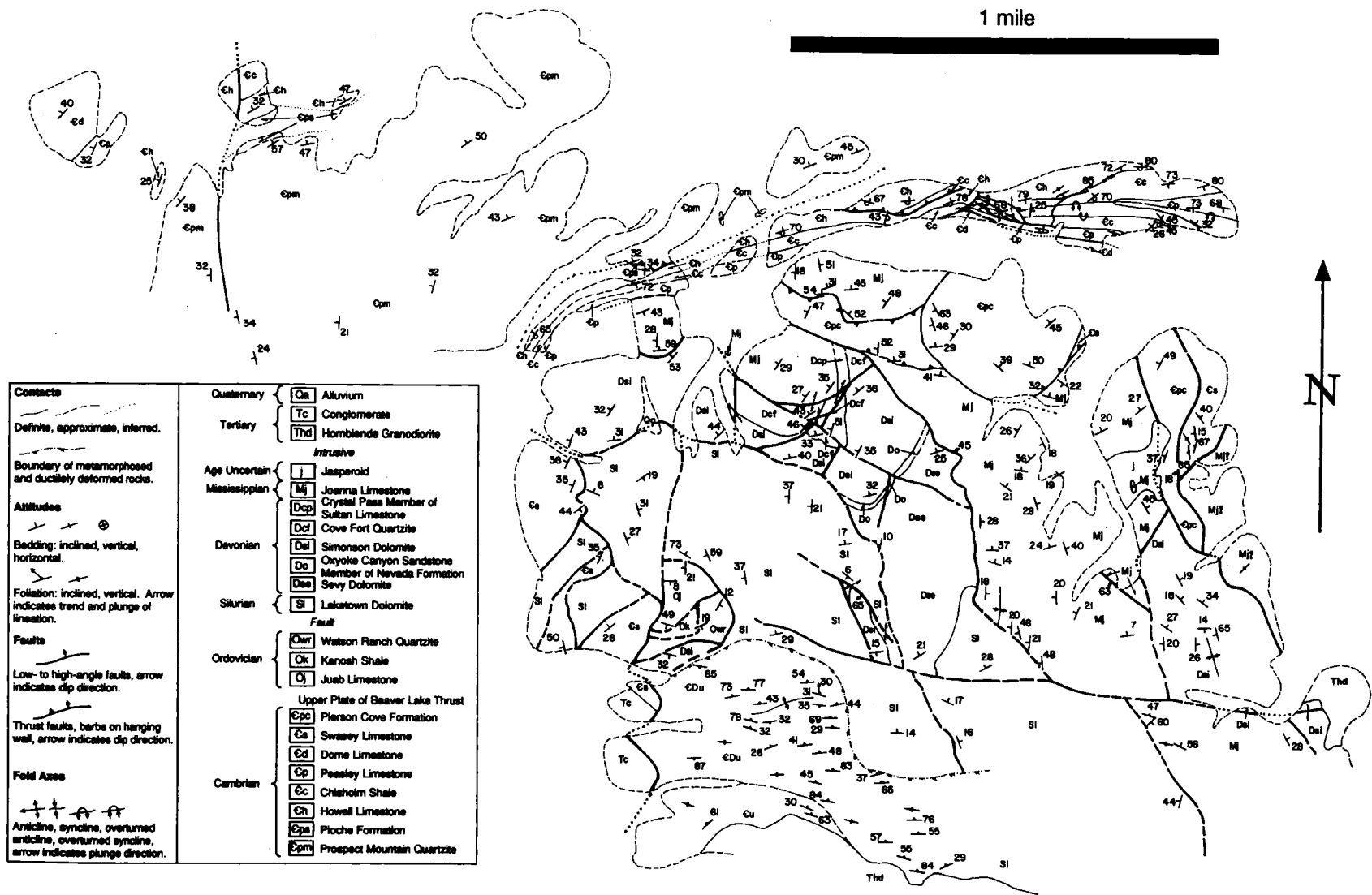


Figure 13. Geologic map of the Beaver Lake Mountain area. The Beaver Lake thrust and associated deformational features are well exposed in the northern part of the map area. Mapping by J.D. Walker and J.M. Bartley.

the overall structure. Two are west-dipping normal faults that we name the Shauntie fault and the Gold Crown fault, for mines located along their traces (figs. 2 and 8). The other two are east-striking normal faults that define what we call the Central graben.

The Shauntie fault is best exposed along Shauntie Wash (Stop 3-1), where it places a hanging wall of Jurassic Navajo Sandstone and 31 to 34 Ma andesite of the Shauntie Hills on the Miocene(?) Shauntie leucogranite pluton and its Paleozoic wallrocks. Horseshoes of unmetamorphosed Paleozoic and Triassic sedimentary rocks are found locally along the fault, which dips 20 to 35° west. The fault was not recognized in previous mapping (Best et al., 1989b) but its presence is clearly demonstrated by (1) cataclasis along the contact and (2) the lack of contact metamorphism of rocks in the hanging wall adjacent to the leucogranite pluton, which has an extensive contact aureole elsewhere adjacent to its intrusive contacts.

A klippe of Mississippian rocks similar to that to be examined at Stop 3-1 rests on Devonian strata at the crest of the Star Range. The underlying fault dips very gently westward (approximately 5°). The klippe may represent a horse emplaced along a splay of the Shauntie fault, now isolated 1 kilometer from the main fault trace by erosion. This would imply that the overall dip of the Shauntie fault was quite low.

In the northwestern Star Range, Jurassic Navajo Sandstone and Oligocene Shauntie andesite are exposed across a narrow valley from Paleozoic carbonate rocks containing Tertiary granitoid intrusions. This relation matches that across the Shauntie fault but previously was interpreted to represent a window through the Blue Mountain thrust (Best et al., 1989b); that is, the alluvium was inferred to conceal an east-dipping thrust that emplaced the Paleozoic strata on the Navajo Sandstone. The andesite of the Shauntie Hills and Tertiary intrusions thus were interpreted to post-date juxtaposition of the Mesozoic and Paleozoic rocks. We reject this interpretation for at least four reasons.

1. The map pattern can be explained by continuing the Shauntie fault northward into this area. An unexposed thrust for which there is no other evidence therefore is not required.
2. Paleozoic rocks in the Star Range are relatively cratonal and resemble parautochthonous rocks in the southern Mineral Mountains. These rocks therefore are unlikely to have been carried above the Blue Mountain thrust which carries more miogeoclinal facies.
3. The andesite of the Shauntie Hills lies on the Navajo Sandstone along an irregular erosion surface as little as a few hundred meters from exposures of coarse-grained quartz monzonite intruded into Mississippian carbonate rocks. No intrusions are found on the

west side of the valley and no volcanic rocks are found on the east side. This is a remarkable coincidence if juxtaposition of Paleozoic and Mesozoic rocks predated formation of any of the igneous rocks and the igneous rocks were emplaced in their present relative locations, as is required by the thrust interpretation.

4. The Hoosier Boy conglomerate was deposited on Tertiary volcanic and Mesozoic sedimentary rocks and mainly contains clasts derived from these units. It nowhere contains clasts of Paleozoic rocks, which in the thrust interpretation must have been exposed before Mesozoic rocks of the thrust window could have been. If the Paleozoic rocks structurally overlie the Mesozoic rocks, it is difficult to imagine how Paleozoic clasts could have been prevented from being incorporated in the Hoosier Boy conglomerate to which they are immediately adjacent.

Relations 3 and 4 are readily explained by the Shauntie normal fault. The hanging wall rocks were emplaced from an original location on the east side of the Star Range, providing suitable sources for the clast types in the Hoosier Boy conglomerate. Both the Paleozoic rocks and Tertiary intrusions in the western Star Range were unroofed by the Shauntie fault only after the plutons were emplaced in their Paleozoic wallrocks and after the Shauntie andesite and Hoosier Boy conglomerate were deposited. We therefore regard the entire Star Range to be composed of rocks that were parautochthonous relative to the Sevier fold-thrust belt.

The poorly exposed Gold Crown fault on the east side of the Star Range accomplished a very similar juxtaposition to the Shauntie fault. The hornblende granodiorite pluton on the east side of the range intruded and extensively contact metamorphosed Paleozoic and Triassic wallrocks, yet has an abrupt contact on its west side with unmetamorphosed Jurassic (and very locally Tertiary volcanic) strata. The geometry of the fault is not well defined by surface exposures, and the wall rocks of the pluton are highly faulted and can only locally be assigned to a particular formation. Therefore, the characteristics of the Gold Crown fault are less well determined than the Shauntie fault, but their mutual similarities suggest that they are part of a system of domino-style faults with similar slip magnitudes.

The main structure within the north-trending fault block between the Shauntie and Gold Crown faults is the Central graben, an east-trending graben bounded by nonrotational normal faults that dip toward each other at about 60° (fig. 8). The graben is roughly symmetrical with each bounding fault accommodating 1.0 to 1.5 kilometers of apparent throw, but apparent throw varies greatly along the graben owing to effects of intersecting faults both within the graben and

outside of it. The age of the Central graben cannot be determined directly. However, smaller east-striking normal faults subparallel to the southern bounding fault are cut by the Shauntie leucogranite pluton, which clearly is cut by the Shauntie fault. Therefore, we infer that the Central graben is older than the Shauntie fault.

Intersections of the Central graben with the Shauntie and Gold Crown faults are complex and incompletely understood. The simple graben geometry breaks down eastward into a plexus of variably oriented normal faults. Combined with the poor exposure of the Gold Crown fault itself, it is difficult to draw any clear conclusion about the chronology and kinematics of faults in this area. Relations at the westward intersection with the Shauntie fault are more clear-cut, however. Although the Central graben is believed to be older than the Shauntie fault, the Shauntie fault appears offset by the bounding faults of the Central graben (fig. 8). However, the sense of separation is the reverse of what would result if the Central graben cut the Shauntie fault: the Shauntie fault trace should be offset eastward, yet is offset to the west. We therefore interpret the offset to indicate that the bounding faults of the Central graben were propagation barriers to the Shauntie fault (e.g., Bartley et al., 1992), resulting in lateral stepping of the Shauntie fault and partial reactivation of the Central graben faults when the Shauntie fault intersected them.

Southern Wah Wah Mountains

The southern Wah Wah Mountains are the only area in western Utah where several Sevier thrust faults are exposed within a single range (figs. 7 and 14). Therefore, although the field trip makes no stops in the Wah Wah Mountains, they provide key insights into the geometrical evolution of the Sevier thrust system discussed here. The thrusts include the Blue Mountain thrust and the overlying Wah Wah thrust system, which comprises a complex imbricate thrust zone including, in ascending order in the nomenclature of Friedrich (1993), the Dry Canyon I and II thrusts, the Lamerdorf thrusts, the Tetons thrust, and the Wah Wah thrust (fig. 7).

The Wah Wah thrust is the largest-displacement thrust in southwestern Utah with minimum slip estimated by Friedrich (1993) at 38 kilometers. The Wah Wah and all other thrusts above the Dry Canyon I thrust each behead pre-existing thrusts or thrust-related folds in their footwalls, implying that the Wah Wah thrust system is internally backward-breaking with structurally higher thrusts emplaced after lower ones. Final emplacement of the Wah Wah thrust, however, was followed by forward propagation of the main Sevier decollement to form a new frontal ramp at the Blue Mountain thrust (Fillmore, 1991).

The Sevier thrusts in the southern Wah Wah Mountains are cut by at least four sets of faults; the oldest and

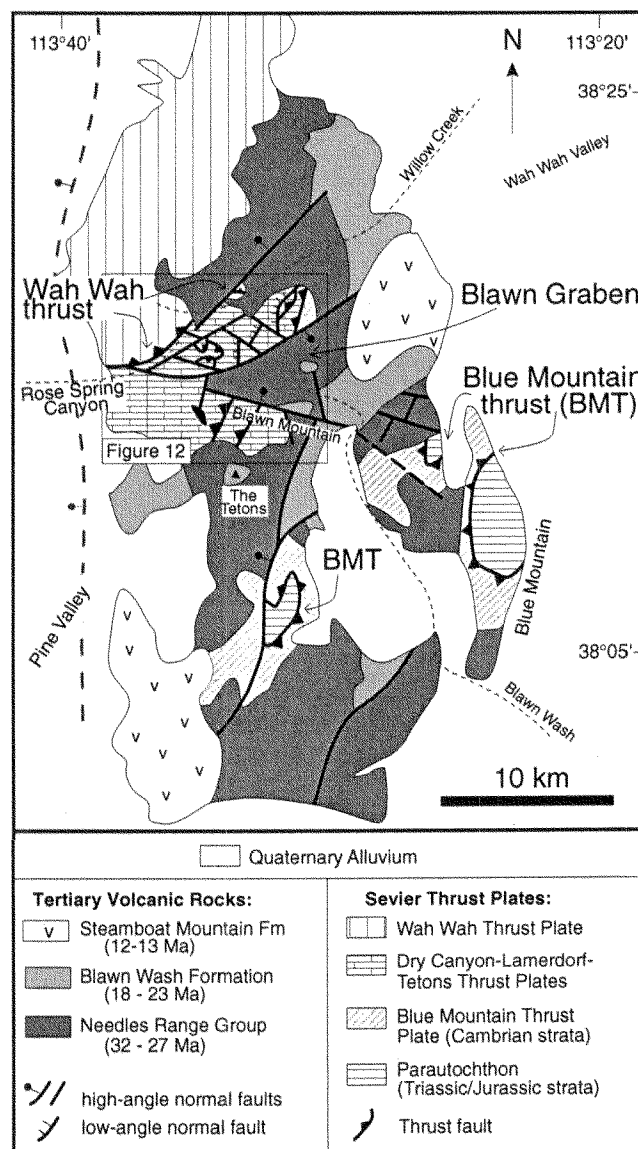


Figure 14. Tectonic map of the southern Wah Wah Mountains simplified from Weaver (1980), Abbott et al., (1983), Best et al., (1987b), and Friedrich (1993). This figure shows all levels of the frontal Sevier thrust belt and the timing relationships between extensional faulting and Oligocene to middle Miocene volcanism.

youngest fault sets have significant displacements and are discussed here (figs. 7 and 14). The oldest set of faults comprises southeast- and northwest-dipping low- to high-angle normal faults with a minimum cumulative heave of 650 meters (Friedrich, 1993; fig. 7). These faults are unconformably overlain by basal volcanic strata of the Oligocene Escalante Desert Formation and are the only known significant prevolcanic extensional faults in southwestern Utah (Friedrich and Bartley, 1992). The youngest fault set com-

prises northeast- and east-striking high-angle normal faults of the Blawn graben which juxtapose volcanic rocks of the Miocene Blawn Formation against Paleozoic rocks with a stratigraphic separation increasing eastward from 300 meters to at least 1700 meters (figs. 7 and 14). The Blawn graben broadly geometrically resembles the Central graben of the Star Range and lies roughly on trend with it.

DISCUSSION AND CONCLUSIONS

There are four key questions we would like to address on this trip: (1) How are mapped thrust faults correlated across the Mineral Mountains region? (2) What is the regional relation between extension and magmatism? (3) What is the origin of low-angle extensional faults in the Mineral Mountains area? (4) What is the minimum amount of east-west directed extension in the Mineral Mountains area and how is this extension accommodated in the Sevier Desert to the north? We address each of these separately below.

Correlation of Mesozoic thrusts

The Wah Wah and Frisco thrusts were correlated by several previous workers (Miller, 1966; Armstrong, 1968; Morris, 1983; figs. 1 and 15). These thrusts form the base of the structurally highest major tectonic element in the Sevier thrust belt of western Utah, which is a regionally extensive allochthon of miogeoclinal strata that underlies most of the ranges of west-central Utah (fig. 15, Canyon Range-Wah Wah allochthon; Hintze, 1963, 1980; Armstrong, 1968). In the Wah Wah Mountains, an extremely complex imbricate stack underlies the Wah Wah thrust (fig. 7). We correlate the Beaver Lake thrust (fig. 13) with this zone of imbricate thrusts between the Pavant and Wah Wah thrusts on the basis of similarities in style, although older rocks are involved at the present level of exposure in the Beaver Lake Mountains. Continuation of the Blue Mountain thrust to the east is uncertain. It is not exposed in the Star Range which is interpreted to expose only parautochthonous strata (fig. 8). It may correlate with a possible thrust in the Rocky Range (fig. 2) because this thrust apparently juxtaposes Cambrian rocks with Triassic strata (Welsh, 1973).

We correlate the sub-Antelope Mountain thrust with the Beaver Lake thrust and Dry Canyon/Tetons thrust zone. This correlation is based on structural style and stratigraphy: at this position the thrust belt contains numerous imbrications and major horses. Our interpretation is consistent with correlation of the Antelope Mountain thrust with the Frisco/Wah Wah thrusts. These segments carry similar types of rocks and comprise the highest thrusts in these segments. We are unable to make a one-to-one correlation of the Blue Mountain, Dry Canyon, or Tetons thrusts. This difficulty is probably due to the tendency of these imbricate and complex faults to change character along strike.

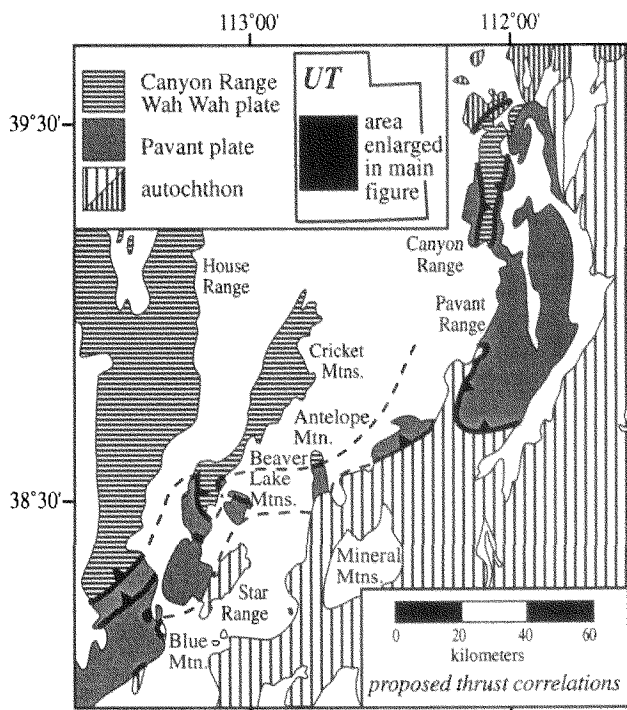


Figure 15. Correlation of thrusts and allochthons in the Milford area.

Correlation Between Extension and Magmatism

Extensional deformation in the Mineral Mountains area can be divided into north-south- and east-west-directed extension. Although mapping indicates that these two episodes of extension are partly contemporaneous in the southern Mineral Mountains, elsewhere in the area (as in the Basin and Range province in general [Axen et al., 1993]), development of east-trending grabens predates the main episode of north-striking Basin and Range faulting. Furthermore, throughout the area (and including the southern Mineral Mountains) development of north-trending detachment faults significantly post-dates the main period of magmatism.

It is tempting to interpret the east-trending grabens in the southern Mineral Mountains (Guyo graben; figs. 10 and 11), Star Range (Central graben; fig. 8) and Wah Wah Mountains (Blawn graben; fig. 14) to record a single event. In particular, tectonic models proposed by Bartley (1989) and Gans (1990), in which synmagmatic north-south extension is triggered by active spreading across the east-trending mid-Tertiary volcanic belt, predict such structures to have formed during the magmatic peak. However, timing relations in the study area do not consistently support this interpretation. The Central graben of the Star Range appears to date from before about 21 Ma and could have formed by

this mechanism. The Blawn graben, however, appears to be younger than 20 Ma although older than north-striking faults related to the main phase of Basin and Range extension (Friedrich, 1993). The Guyo graben in the southern Mineral Mountains appears to have developed contemporaneously with late Miocene north-striking normal faults (Price, in preparation). Although it is possible that the bounding faults of the Blawn and Guyo grabens were established earlier, there is no evidence that specifically suggests such an interpretation. The east-trending grabens thus have variable relations to regional magmatism and their tectonic significance remains obscure.

Evidence for ages of the large north-striking normal faults indicates that they are everywhere younger than early Miocene plutons. This is particularly clear in the case of the Mineral Mountains, where cross-cutting relations, thermochronology of lower-plate rocks, and paleomagnetic results combine to indicate that major extension began shortly before 11 Ma and mostly occurred after 11 Ma (Price and Bartley, 1992; Coleman and Walker, 1994; Coleman et al., in preparation; Price, in preparation). In contrast, the overwhelming majority of igneous rocks in the region formed in the period from about 32 Ma to 17 Ma. In the Star Range, cataclasis of rocks along the Shauntie fault and a lack of contact metamorphism across the fault indicate that the intrusive rocks had cooled significantly prior to deformation. Therefore, the main period of magmatism preceded the main period of crustal extension by several million years (Best and Christiansen, 1991), a relation that must be accommodated in physical models for crustal extension. For instance, it seems unlikely that Basin and Range extension in this area was either directly triggered or localized, or that trajectories of active faults were modified, by thermo-mechanical effects of the magmatism.

Origin of Presently Shallow Dips of Extensional Faults

The largest Cenozoic normal faults in the Mineral Mountains area strike north and dip to the west. Geometrical data concerning low-angle faults among this group consistently support their origins as steeper faults that were tilted to their present gentle dips by the isostatic rolling-hinge (Buck, 1988; Wernicke and Axen, 1988) or domino (Proffett, 1977) mechanisms. Locally, both isostatic rebound and tilting above structurally deeper faults may have contributed to the present geometry of faults.

The footwall to the Cave Canyon detachment preserves abundant evidence for deformation associated with isostatic rebound. Most notably, footwall rocks, deformation zones within footwall rocks and the Cave Canyon detachment are all folded in to a broad antiform across the Mineral Mountains (fig. 9). Maximum estimates of tilt are up to 90° on the far east side of the exposed batholith (Coleman and Walker,

1994; Coleman et al., in preparation). Price and Bartley (1992) and Price (in preparation) conclude that active segments of the Cave Canyon detachment were progressively abandoned as the footwall was tilted: currently active range-bounding faults on the far western side of the range dip steeply (Barker, 1986), whereas the western and eastern segments of the Cave Canyon detachment dip approximately 20° and 0°, respectively. Post-extensional tilting and isostatic uplift of the footwall block may have been localized by the Mineral Mountains batholith because there is no evidence for similar magnitudes of tilt at the breakaway zone for extension on the adjacent Colorado Plateau (Coleman et al., in preparation).

In addition to isostatic rebound, both the Cave Canyon detachment and other low-angle faults may have been, in part, tilted to their present orientation by domino-style normal faulting. Coleman and Walker (1994) concluded that up to 45° tilt of the Cave Canyon detachment and its footwall may have been accommodated by motion along the structurally deeper Beaver Valley fault (fig. 2). However, Price (in preparation) calls the existence of a separate Beaver Valley fault into question. Continued work in the region will help address these different interpretations. Regardless of the geometrical relations in the Mineral Mountains, we interpret the Shauntie and Gold Crown faults as a pair of domino-style faults.

The Magnitude of Regional Extension and Implications for Extension in the Sevier Desert

The absolute magnitude of extensional deformation across the Mineral Mountains region is difficult to measure due to limited exposure of hanging wall rocks and uncertainty in subsurface geology. However, it is possible to put broad minimum and maximum estimates on the amount of extension. Therefore, we frame this discussion in terms of limiting estimates: What is the bare minimum demanded by the geology? What is the maximum credible amount? Where in between these extremes is the real answer most likely to lie?

The minimum estimate for extension must account for (1) observed extension within ranges that did not contribute to forming the modern basins, and (2) formation of modern basins. Because the Cave Canyon detachment, Shauntie and Gold Crown faults do not appear to be correlative, displacements across them have to be additive. Separation across the Cave Canyon detachment is probably best understood and is at least 9 kilometers on the basis of restoring the Devonian Simonson Dolomite adjacent to correlative rocks in the footwall (Price, in preparation). This separation translates into an extension estimate of 4.5 to 8 kilometers assuming a fault with an initial dip of 60° to 30°, subsequently tilted to a horizontal orientation. Separation across

the Shauntie fault is less certain due to structural complications in the footwall and poor exposure of the hanging wall, but is approximately 4 to 5 kilometers based on separation of Jurassic strata across the fault. The Shauntie fault presently dips around 20° W and footwall strata dip about 40° E, indicating an initial fault dip of 60° and 40° of stratal tilt, which imply about 2 kilometers of extension. Because the juxtaposition of rocks across the Gold Crown fault is similar to that across the Shauntie fault (hanging wall of Navajo Sandstone and Tertiary volcanic rocks rests on a footwall composed of a Tertiary pluton intruded into Paleozoic carbonate rocks), we assume a similar amount of extension across the Gold Crown fault. Therefore, minimum extension across the ranges without opening any valleys is about 9 kilometers.

Estimates of minimum and maximum extension across the Beaver and Milford valleys are even more difficult to make than estimates of extension within adjacent ranges. To produce the observed basins in Beaver and Milford valleys, a bare minimum estimate of 1 kilometer extension across each is necessary assuming they are bounded by high-angle normal faults as shown by geophysical investigations (Smith and Bruhn, 1984; Barker, 1986).

A maximum estimate of extension across Beaver Valley (and part of the Mineral Mountains) is 10–15 kilometers on the basis of a match between a syenite/andesite (Ti1/Tmv) contact repeated across the Beaver Valley fault (fig. 2; Coleman, 1991). Walker and Bartley (1991) estimate a maximum of 30 kilometers of extension across Milford Valley on the basis of thrust correlations. This estimate is consistent with matching Tertiary intrusive/carbonate contacts (Ti1/CO-SD) between Antelope Mountain and the Beaver Lake Mountains (fig. 2). These estimates yield a minimum of about 11 kilometers and a maximum of about 40 kilometers of extension along a 40 kilometer line from the Colorado Plateau to the Shauntie Hills (the Shauntie Hills lie immediately west of the Shauntie fault on fig. 1).

The actual amount of extension across the Mineral Mountains region probably lies between these two extreme estimates. An approach to getting a somewhat less conservative minimum is to assume that faults similar to those exposed in the Mineral Mountains and Star Range exist under the adjacent valleys, too; we regard this as still conservative because the very existence of the valleys implies greater extension there than in the intervening ranges. The two ranges are each about 10 kilometers wide and each exposes one or more faults that accomplish 4 to 5 kilometers of extension. If the exposed faults represent a relatively uniform array of domino-style faults across the area, this implies 60 to 100% extension across a 40 kilometer transect, or 15 to 20 kilometers of total displacement. Assuming that the valleys exist because extension is more concentrated there than in

the ranges, 20 kilometers of extension across the transect appears to be a reasonable minimum.

Any amount of extension between the Colorado Plateau and the Shauntie Hills must be either accommodated in the Sevier Desert along the Sevier Desert detachment to the north, or transferred to the west at the northern end of the Mineral Mountains along an unrecognized structure (fig. 1). Estimates of extension across the Sevier Desert detachment (20–60 kilometers; Allmendinger et al., 1983; Von Tish et al., 1985; Coogan and DeCelles, 1996) agree well with minimum and maximum estimates for extension in the Mineral Mountains region. This observation, combined with new data supporting extension in the Sevier Desert (Otton, 1995; Coogan and DeCelles, 1996, Linn et al., in review) and the lack of a suitable structure to transfer extensional deformation elsewhere, favor the interpretation that extension is accommodated within the Sevier Desert. Therefore, we favor the interpretation of the Sevier Desert reflector as a regionally significant detachment fault over other interpretations.

ROAD LOG

The road log starts in Beaver Utah each day of the trip. The reader is referred to figure 16 for a simplified road map of the field trip area.

START DAY 1

0.0	0.0	South Beaver entrance to I-15 at highway mile 109. Travel north. Look west to Mineral Mountains. Note high, craggy Granite Peak. Look east to Tushar Mountains.
3.1	3.1	Highway mile 112. North Beaver exit. Continue north.
8.9	12.0	Highway mile 120. Look northwest to Gillies Hill, east to Tushar Mountains.
2.5	14.5	Highway mile 123. Road cuts through Gillies Hill rhyolite
7.0	21.5	Highway Mile 130. Quaternary basalt flows west of I-15.
3.0	24.5	Highway mile 133. The Tushar Mountains are due east, Dog Valley lies to the north and the Pavant Range north of Dog Valley. Rocks in Dog Valley comprise an autochthonous Paleozoic section that is approximately horizontal. Allochthonous Paleozoic rocks crop out north of Dog Valley.
2.0	26.5	Exit 135 at historic Cove Fort.
0.1	26.6	Left on well graded Black Rock Road over I-15 continuing west. Low hills of Quaternary basalt.

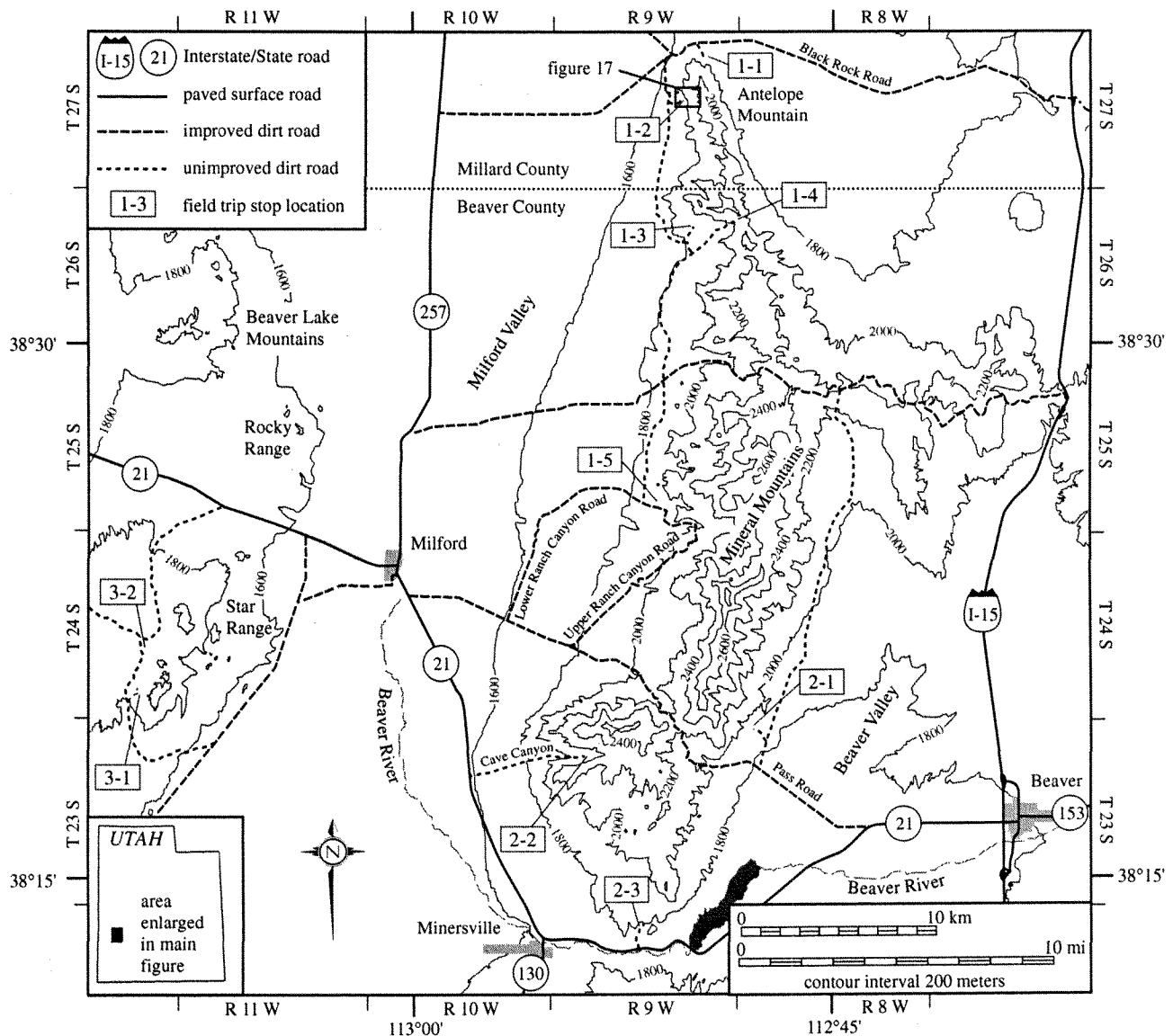


Figure 16. Road map for field trip. At many localities along the western side of the Mineral Mountains, there are complex intersections of unimproved dirt roads and it is recommended that you refer to appropriate U.S.G.S. 7.5 minute quadrangle maps. Topography and roads from U.S.G.S. Beaver, Wah Wah Mts. North and Wah Wah Mts. South 1:100 000, 30 X 60 minute quadrangle maps.

1.2	27.8	Cattle guard.	0.5	40.5
2.9	30.7	Cattle guard.		
1.2	31.9	Top of hill. View to west-northwest is pass between Paleozoic section of Antelope Mountain to the north and plutons to the south. Note vertical dikes of rhyolite porphyry cutting plutonic rocks.		
1.5	33.4	Fork, stay right.		
1.2	34.6	Cattle guard.		
5.4	40.0	Turn left on road at green gate and follow fence line.		

STOP 1-1. Overview of the Sevier Desert and the Beaver and Milford Valley area.

Park on float of the Prospect Mountain quartzite (fig. 4). Look north for a view of the Sevier Desert and the Canyon Range. The Cricket Mountains are to the northwest and the House Range is in the distant northwest. Here we have an overview of the Sevier Desert to the north. The Sevier Desert is underlain by a significant seismic reflector that is interpreted

variably as a detachment fault (e.g., Allmendinger et al., 1983; Von Tish et al., 1985) and an unconformity (Anders and Christie-Blick, 1994). According to the detachment model, the House Range and Cricket Mountains restore to a preextensional position 28 to 38 kilometers to the east of their current location (Sharp, 1984). The model of Anders and Christie-Blick (1994) predicts little or no offset across the Sevier Desert basin.

The view south is outcrop of Cambrian Prospect Mountain quartzite in the hanging wall of Antelope Mountain thrust. Looking to the south the Mineral Mountains are bounded by Beaver Valley to the east and Milford Valley to the west. Mapped faults and subsurface imaging of high-angle normal faults account for significant extension across the region. Our principal goal during this trip will be to examine the style of that extensional deformation and place some limits on the amount of extension. Somehow, that extension needs to be accommodated north of the Mineral Mountains. Two possibilities for this accommodation are an east-west trending strike slip fault zone or extension in the Sevier Desert.

0.5	41.0	Return to main road north of Antelope Mountain.
2.9	43.9	Take left fork toward Milford.
2.1	46.0	Left on road in small patch of sage and continue generally east toward range (this is a very tough intersection to find).
1.1	47.1	Gate through fence.
0.4	47.5	Left on road that continues east to the range.
0.6	48.1	STOP 1-2. The Antelope Mountain thrust fault and underlying Cretaceous(?) conglomerate.

Park where road gets bad, then walk up poor road and continue up wash to east-southeast (figs. 4 and 17). We will be walking up approximately 1000 feet through somewhat metamorphosed Cambrian Howell Limestone. The most altered rocks are at the start of the climb. The Antelope Mountain thrust fault is marked by the prominent ledge of Prospect Mountain Quartzite. Just below the quartzite are numerous exposures of conglomerate

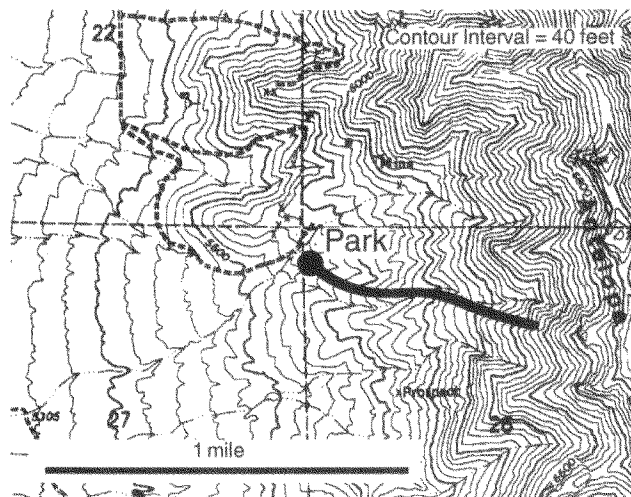


Figure 17. Topographic map showing exact location of outcrop for Stop 1-2.

and siltstone presumably unconformably resting on the Howell Limestone. The relations at this stop indicate that the footwall rocks were uplifted, eroded down to the Howell Limestone, and subsequently overthrust by the Antelope Mountain thrust. The Antelope Mountain thrust fault has a consistently shallow-dipping orientation.

0.6	48.7	Return to road and continue south.
0.5	49.2	Gate through fence.
2.0	51.2	Intersection with road on left. View east-southeast of spectacular mixed 18 Ma granite and diorite. Continue south along range front.
1.2	52.4	Left at T-intersection. In 50 feet turn hard to the right and continue south along the range front.
0.7	53.1	Bear left at fork.
0.4	53.5	Gate through fence. Immediately after gate take left on road to the north.

1.0 54.5 OPTIONAL STOP 1-3. Magma mixing during the 18 Ma intrusive event.

Park and walk west to outcrops of granite and diorite. Spectacular features resulting from mixing of magmas during the 18 Ma main intrusive event can be viewed on the hill past fence to the west. This mixing generates a regional variation in the composition of the diorite from diorite to granodiorite. The regional variation in the main intrusive phase composition

steeply dipping and yield Miocene expected paleomagnetic poles.

East of this stop, the batholith comprises well mixed diorite and granite of the 18 Ma intrusive event. To the south and east, Granite Peak (9580' and the Milford Needle (9582') expose 18 Ma granite, and are the highest points in the range. The high flat peaks immediately east of this location comprise Quaternary rhyolite lava domes. These are the source of the abundant obsidian float throughout the range. Geothermal activity at the Roosevelt Hot Springs, that we passed on the way to this location, attests to continued magmatic activity in the area.

0.6	71.2	Reverse direction. At intersection, continue toward Milford Valley on the Ranch Canyon Road.
1.1	72.3	Cattle guard.
6.7	79.0	Bear right toward Milford. This is the intersection with the Pass Road.
2.9	81.9	Cattle guard and start of pavement.
0.5	82.4	Turn left on Route 21 and return to Beaver (approximately 30 miles).

END DAY ONE

START DAY TWO

0.0	0.0	Start mileage at junction of highways 21 and 160. Continue west on 21 (Center Street) in downtown Beaver.
0.5	0.5	Underpass of I-15.
4.4	4.9	Exit right, and continue west on Pass Road into Mineral Mountains.
4.3	9.2	Turn right, and continue north along range front.
1.0	10.2	Turn left and continue west toward range.

0.5	10.7	STOP 2-1. Steeply dipping wallrocks and horizontal 11 Ma dikes of the southeast part of the batholith.
-----	------	---

Park and proceed west on road over ridge. Walk to where road ends in wash and continue 100 meters up the wash to outcrops of Paleozoic carbonate and rhyolite porphyry. Climb to the top of the hill on the south side of the wash. The batholith here dominantly comprises 18 Ma quartz monzonite and granite, and 11 Ma rhyolite porphyry and basalt dikes. The dikes are correlative with vertical rhyolite porphyry and basalt dikes seen at Pin-

nacle Pass (Stop 1-3). The view to the south shows the steeply dipping carbonate rocks (Mississippian Redwall Limestone[?]/Devonian Simonson Dolomite[?]) that comprise the eastern wall rocks of the batholith. To the north, the carbonate rocks are cut by a (presently) steeply dipping thrust fault that is locally intruded by a rhyolite porphyry dike (Sibbett and Nielson, 1980). This is the only steeply dipping dike in this part of the Mineral Mountains (although it is difficult to discern the orientation of some dikes such as the one that caps this hill). Looking to the west, a basalt/rhyolite porphyry dike pair with near horizontal dips can be seen about three-quarters of the way up the side of the range. Horizontal rhyolite porphyry dikes are also evident above and west of the carbonate rocks looking south. The most accessible horizontal dikes crop out at the bottom of the wash we parked in, several kilometers west and up the side of the mountain. Paleomagnetic analysis of the horizontal dikes, the steeply dipping dike intruded along the fault, and the Paleozoic carbonate rocks all suggest that the rocks experienced up to 90° of west-side-up tilt (Coleman et al., in preparation). Thus, the dikes and the wall rock of the batholith are orthogonal to each other as they are at Pinnacle Pass; however, all are tilted approximately 90° relative to their orientations on the north and west sides of the batholith. We interpret this tilt to be the result of footwall uplift in response to denudation along the Cave Canyon detachment fault that we will examine at the next stop.

0.5	11.2	Turn around and proceed back to Pass Road. Turn right on range front road.
0.9	12.1	Bear right onto Pass Road (continuing west).
4.0	16.1	Road cut through dated 11 Ma rhyolite porphyry dike.
0.3	16.4	Cattle guard at Soldier's Pass.
3.5	19.9	Cattle guard.
1.4	21.3	Merge with Upper Ranch Canyon road. Continue down and to the west.
2.2	23.5	Merge with Lower Ranch Canyon road. Continue down and to the west.
3.0	26.5	Cattle guard and pavement begins.

- 0.5 27.0 Junction with Route 21, turn left continuing southeast toward Minersville.
- 6.5 33.5 Left onto Cave Canyon road. Road takes an immediate sharp right turn.
- 0.1 33.6 Cattle guard and road turns east toward range.
- 2.1 35.7 View of cataclasite capping hills north of the road.
- 0.5 36.2 **STOP 2-2. The Cave Canyon detachment fault.**

Descend into Cave Canyon Wash and park. Walk approximately 1 mile east up Cave Canyon. The road starts in the canyon bottom, climbs onto the south slope, and then crosses back to the north slope just a little above the canyon bottom. When the road has crossed exposures of foliated granodiorite and rocks to the north have changed from intrusive rocks to Paleozoic carbonate rocks, look for the remains of a road on the left (difficult to find). Follow this road to the north approximately 0.5 mile and climb about 700 feet to the eastern end of cliff-forming outcrops with a subhorizontal top surface.

The Cave Canyon detachment fault is exposed as the top surface of these cliffs (fig. 11 map and section A-A'). Paleozoic rocks in the hanging wall were transported a minimum of approximately 9 kilometers to the west. Proto-cataclasite and cataclasite are exposed in the cliff walls. Evidence of magma mixing can be seen within the proto-cataclasite. The cliffs terminate eastward against one of the late-stage, high-angle faults that cut the detachment. To the west, exposures of the cataclasite of the western segment of the detachment can be seen on the crests of west-plunging ridges. The Cherry Creek fault, exposed in the bottom of Cave Canyon, juxtaposes both the hanging wall and footwall rocks of the Cave Canyon detachment on the north against the Paleozoic through Tertiary stratified section to the south.

- 2.6 38.8 Reverse direction and return to route 21. Turn left continuing southeast toward Minersville.
- 5.9 44.7 Junction of 21 and 130 at Minersville, continue east toward Beaver.
- 3.2 47.9 Turn left off 21 on gravel road continuing north into low hills.

0.7 48.6 **STOP 2-3. Tilted rocks in the hanging wall of the Cave Canyon detachment fault.**

Walk approximately 1.2 miles west (crossing a approximately 300' high ridge) to the base of the volcanic section. A Cretaceous-Tertiary(?) conglomerate unconformably overlies the Triassic Moenkopi Formation at the sub-Tertiary unconformity. Walk eastward up-section through the volcanic units (fig. 5). The lower three ash-flow tuff units dip more steeply (approximately 70°) than the overlying Isom Formation (approximately 50°), although the amount of differential tilt varies between fault blocks. The traverse crosses an uninterrupted section into the Oligocene-Miocene Mount Dutton Formation, and then two fault blocks which repeat the section from the Three Creeks tuff member of the Bullion Canyon Volcanics to the Mount Dutton Formation.

- 0.7 49.3 Reverse direction and continue back to Route 21. Turn left on 21 continuing east toward Beaver.
- 2.8 52.1 Minersville State Park on left.
- 6.5 58.6 Pass Road junction, stay on 21.
- 4.4 63.0 I-15 underpass.
- 0.5 63.5 Junction of 21 and 160—main street of Beaver.

END DAY TWO

START DAY THREE

- 0.0 0.0 Start mileage at junction of highways 21 and 160. Continue west on 21 (Center Street) in downtown Beaver.
- 0.5 0.5 Underpass of I-15.
- 4.4 4.9 Junction with Pass Road.
- 6.5 11.4 Minersville State Park on right.
- 6.0 17.4 Junction 21 and 130 in Minersville. Stay on 21 toward Milford.
- 5.9 23.3 Junction with Cave Canyon Road. Continue on 21 northwest to Milford.
- 6.5 29.8 Junction with Pass Road. Continue on 21.
- 0.7 30.5 Railroad crossing. Bear right on 21 and immediately turn left on 500 S Street and continue to the west.
- 0.5 31.0 End of road, turn left continuing south.
- 0.4 31.4 Turn right at intersection just before pavement ends. Golf course on right.
- 0.3 31.7 Pavement ends.
- 0.7 32.4 Cattle guard.

0.4	32.8	Bear left at fork.
1.5	34.3	Bear left to follow powerline road.
1.4	35.7	Cattle guard.
1.9	37.6	Gold Crown mine west of road.
1.2	38.8	Cattle guard.
1.6	40.4	Leave powerline road, turn right on road continuing west to Star Range.
1.4	41.8	Cattle guard.
1.3	43.1	Fork, stay to right.
1.4	44.5	Fork, bear right.

0.7 45.2 **STOP 3-1. Geology of the Shauntie fault.**

Stop between small hill (with klippe) and main range (fig. 8). Cross the wash and ascend the lower slopes of the reddish hill to the west. This hill is underlain mainly by altered and brecciated andesite of the Shauntie Hills, but its lower slopes on the east and south sides are Shauntie leucogranite. Ascending toward the contact, the leucogranite becomes progressively cataclasized, indicating that the contact is a fault rather than intrusive. This is the Shauntie fault, which is not well exposed here but dips about 30° west based on its intersection with topography. Return across the wash and ascend the slope to the south. Capping ridge are outcrops of dark gray Mississippian Monte Cristo Limestone. The limestone is shattered and silicified. The underlying leucogranite is again progressively cataclasized ascending toward the contact. Where the contact intersects a roadcut on the near side of the ridge, a zone of fault gouge several tens of centimeters thick is present. These relations are in stark contrast with intrusive contacts between the granite and limestone near the crest of the range, where the granite becomes vuggy and contains patches of pegmatite, and the dark limestone is bleached white and marmorized. We interpret the klippe here to be a horse along the Shauntie low-angle normal fault.

0.7	45.9	Reverse direction and return to last fork. Make a sharp right turn and continue north.
-----	------	--

2.2 48.1 **STOP 3-2. Geology of the Shauntie fault and the Hoosier Boy conglomerate.**

Top of pass with Hoosier Boy conglomerate. Shauntie fault and Central graben

of the Star Range. The intersection of the Shauntie fault with the southern bounding fault of the Central graben is located near where the road turns left at the top of a steep hill and leaves the Shauntie Wash, heading west. The graben-bounding fault appears to be the younger than the Shauntie fault because it apparently truncates the Shauntie fault. However, as noted in the foregoing article, cross-cutting relations with the Shauntie leucogranite suggest the opposite age relation and the Shauntie fault here is offset in the incorrect sense for such an interpretation. Therefore, the trajectory of the Shauntie fault may have been deflected where it intersected the Central graben when propagating northward, here reactivating a short segment of the graben-bounding fault as part of the Shauntie fault.

0.3	48.4	Continue northward. At intersection turn right.
3.9	52.3	Bear right at fork.
2.4	54.7	Intersection with Route 21. Turn right and continue east toward Milford.
6.1	60.8	Main street, Milford. Right to return to Beaver, left to Salt Lake City.

ACKNOWLEDGMENTS

Supported by National Science Foundation grant EAR-8904007 to J. D. W. and EAR-8904329 awarded to J. M. B. and Geological Society of America and Sigma Xi grants to D. S. C. and D. E. P. and grants from CENEX and AAPG to D. E. P. Thanks to P. Price for assistance in data analysis and preparation of figures. The manuscript was greatly improved by reviews from Gary Axen, Myron Best, Paul Link and Gautam Mitra. We thank R.L. Bruhn and W.P. Nash for many helpful discussions, and S.E. Coleman for assistance in mapping and sample collection.

REFERENCES CITED

- Abbott, J.T., Best, M.G., and Morris, H.T., 1983, Geologic map and cross sections of the Pine Grove-Blawn Mountain area, Beaver County, Utah: U.S. Geological Survey Miscellaneous Investigations Map I-1479, scale 1:24,000.
- Aleinikoff, J.N., Nielson, D.L., Hedge, C.E., and Evans, S.H., 1987, Geochronology of Precambrian and Oligocene rocks in the Mineral Mountains, south-central Utah. U.S. Geological Survey Bulletin 1622, p. 1-12.
- Allmendinger, R.W., Sharp, J.W., Von Tish, D., Serpa, L., Brown, L., Kaufman, S., and Oliver, J., 1983, Cenozoic and Mesozoic structure of the eastern Basin and Range province, Utah, from COCORP seismic-reflection data: v. 11, p. 532-536.

- Anders, M.H., and Christie-Blick, N., 1994, Is the Sevier Desert reflection of west-central Utah a normal fault? *Geology*, v. 22, p. 771–774.
- Armstrong, R.L., 1968, Sevier orogenic belt in Nevada and Utah. *Geological Society of America Bulletin*, v. 79, p. 429–458.
- Armstrong, F.C., and Oriel, S.S., 1965, Tectonic development of the Idaho-Wyoming thrust belt. *American Association of Petroleum Geologists Bulletin*, v. 49, p. 1847–1866.
- Axen, G.J., Taylor, W.J., and Bartley, J.M., 1993, Space-time patterns of the onset of extension and magmatism, southern Great Basin, Nevada, Utah, and California: *Geological Society of America Bulletin*, v. 105, p. 56–76.
- Axen, G.J., Bartley, J.M., and Selverstone, J., 1995, Structural expression of a rolling hinge in the footwall of the Brenner Line normal fault, eastern Alps. *Tectonics*, v. 14, p. 1380–1392.
- Barker, C.A., 1986, Upper-crustal structure of the Milford Valley and Roosevelt Hot Springs, Utah region, by modeling of seismic refraction and reflection data [M.S. thesis]: University of Utah, 101 p.
- Barosh, P.J., 1960, Beaver Lake Mountains, Beaver County, Utah: *Utah Geological and Mineral Survey Bulletin*, v. 68, 89 pp.
- Bartley, J.M., 1989, Changing Tertiary extension directions in the Dry Lake Valley area, Nevada, and a possible tectonic model, in Garside, L.J., and Shaddrick, D.R., eds., *Compressional and extensional structural styles in the northern Basin and Range*. Nevada Petroleum Society, Seminar Proceedings, p. 35–39.
- Bartley, J.M., Fletcher, J.M., and Glazner, A.F., 1990, Tertiary extension and contraction of lower-plate rocks in the central Mojave metamorphic core complex, southern California: *Tectonics*, v. 9, p. 521–534.
- Bartley, J.M., Taylor, W.J., and Lux, D.R., 1992, Blue Ribbon volcanic rift in southeastern Nevada and its effects on Basin and Range fault segmentation: *Geological Society of America Abstracts with Programs*, v. 24, p. 2.
- Best, M.G., McKee, E.H., and Damon, P.E., 1980, Space-time-composition pattern of late Cenozoic mafic volcanism, southwestern Utah and adjoining areas: *American Journal of Science*, v. 280, p. 1035–1050.
- Best, M.G., and Grant, S.K., 1987, Stratigraphy of the volcanic Oligocene Needles Range Group in southwestern Utah and eastern Nevada. U.S. Geological Survey, Professional Paper 1433-A, p. 3–28.
- Best, M.G., Mehnert, H.H., Keith, J.D., and Naeser, C.W., 1987, Oligocene and Miocene Volcanic Rocks in the central Pioche-Marysville Igneous Belt, western Utah and eastern Nevada. U.S. Geological Survey, Professional Paper 1433-B, p. 29–47.
- Best, M.G., Christiansen, E.C., and Blank, R.H., Jr., 1989a, Oligocene caldera complex and calc-alkaline tuffs and lavas of the Indian Peak volcanic field, Nevada, Utah: *Geological Society of America Bulletin*, v. 101, p. 1076–1090.
- Best, M.G., Lemmon, D.W., and Morris, H.T., 1989b, Geologic map of the Milford Quadrangle and east half of the Frisco Quadrangle, Beaver County, Utah: U.S. Geological Survey, Miscellaneous Investigations, Map I-1904, scale 1:50,000.
- Best, M.G., and Christiansen, E.H., 1991, Limited extension during peak Tertiary volcanism, Great Basin of Nevada and Utah. *Journal of Geophysical Research*, v. 96, p. 13509–13528.
- Buck, R.W., 1988, Flexural rotation of normal faults: *Tectonics*, v. 7, p. 959–973.
- Coleman, D.S., 1991, Geology of the Mineral Mountains Batholith, Utah [Ph.D. thesis]. University of Kansas, 219 p.
- Coleman, D.S., and Walker, J.D., 1992, Generation of juvenile granitic crust during continental extension. *Journal of Geophysical Research*, v. 92, p. 11011–11024.
- Coleman, D.S., and Walker, J.D., 1994, Modes of tilting during extensional core complex development: *Science*, v. 263, p. 215–218.
- Coleman, D.S., Geissman, J.W., Walker, J.D., and Hodges, K.V., in preparation, Paleomagnetic and thermochronologic evidence for footwall tilt during extensional core complex development.
- Condie, K.C., 1960, Petrogenesis of the Mineral Range Pluton, Southwestern Utah [MA thesis]: University of Utah, 99 p.
- Coogan, J.C., and DeCelles, P.G., 1996, Extensional collapse along the Sevier Desert reflection, northern Sevier Desert Basin, western United States: *Geology*, v. 24, p. 933–936.
- Crawford, A.L., and Buranek, A.M., 1945, Tungsten deposits of the Mineral Range, Beaver County, Utah. Department of Mining and Metallurgical Research (University of Utah State Eng. Exp. Station) Bulletin, v. 25, 48 p.
- Crecraft, H.R., Nash, W.P., and Evans, S.H., 1981, Late Cenozoic volcanism at Twin Peaks, Utah: *Geology and petrology. Journal of Geophysical Research*, v. 86, p. 10303–10320.
- Cunningham, C.G., Ludwig, K.R., Naeser, C.W., Weiland, E.K., Mehnert, H.H., Steven, T.A., and Rasmussen, J.D., 1982, Geochronology of hydrothermal uranium deposits and associated igneous rocks in the eastern source area of the Mount Belknap volcanics, Marysville, Utah. *Economic Geology*, v. 77, p. 453–463.
- Davis, G.A., and Lister, G.S., 1988, Detachment faulting in continental extension: Perspectives from the Southwestern U.S. Cordillera, in Clark, S.P., Burchfiel, B.C., and Suppe, J., eds., *Processes in Continental Lithospheric Deformation: Special Paper: Boulder, Geological Society of America Special Paper*, p. 133–159.
- DeCelles, P.G., Lawton, T.F., and Mitra, G., 1995, Thrust timing, growth of structural culminations, and synorogenic sedimentation in the type Sevier orogenic belt, western United States: *Geology*, v. 23, p. 699–702.
- Earl, F.N., 1957, Geology of the Central Mineral Range [Ph.D. thesis]: University of Utah, 112 p.
- Evans, S.H., and Nash, W.P., 1978, Quaternary rhyolite from the Mineral Mountains, Utah, U.S.A.: Salt Lake City, University of Utah, Department of Geology and Geophysics, 59 p.
- Evans, S.H., and Nielson, D.L., 1982, Thermal and tectonic history of the Mineral Mountains intrusive complex: *Geothermal Resources Council Transactions*, v. 6, p. 15–18.
- Evans, S.H., and Steven, T.A., 1982, Rhyolites in the Gillies Hill-Woodtick Hill area, Beaver County, Utah: *Geological Society of America Bulletin*, v. 93, p. 1131–1141.
- Fillmore, R.P., 1991, Tectonic influence on sedimentation in the southern Sevier foreland, Iron Spring Formation (Upper Cretaceous), southwestern Utah, in Nations, J.D., and Eaton, J.G., eds., *Stratigraphy, depositional environments, and sedimentary tectonics of the western margin, Cretaceous Western Interior Seaway*. Geological Society of America Memoir 260, p. 9–24.
- Friedrich, A.M., 1993, Analysis of the Mesozoic Wah Wah thrust system with Cenozoic extensional overprint, southwestern Utah [M.S. thesis]: University of Utah, 112 p.
- Friedrich, A.M., and Bartley, J.M., 1992, Geometry of the Wah Wah thrust zone, southern Wah Wah Mountains, SW Utah. *Geological Society of America Abstracts with Programs*, v. 24, p. 12.
- Gans, P.B., 1987, An open-system, two-layer crustal stretching model for the eastern Great Basin. *Tectonics*, v. 6, p. 1–12.
- Gans, P.B., 1990, Space-time patterns of Cenozoic N-S extension, N-S shortening, E-W extension, and magmatism in the Basin and Range province: Evidence for active rifting: *Geological Society of America Abstracts with Programs*, v. 22, p. 24.
- Glazner, A.F., 1994, Foundering of mafic plutons and density stratification of continental crust. *Geology*, v. 22, p. 435–438.
- Glazner, A.F., and Miller, D.M., 1996, Post-emplacement sinking of plutons: *Geological Society of America Abstracts with Programs*, v. 28, p. 69.
- Heller, P.L., Bowdler, S.S., Chambers, H.P., Coogan, J.C., Hagen, E.S., Shuster, M.W., Winslow, N.S., and Lawton, T.F., 1986, Time of initial thrusting in the Sevier Orogenic belt, Idaho-Wyoming and Utah. v. 14, p. 388–391.

- Hintze, L.F., 1963, Geologic map of southwestern Utah. Utah State Land Board, scale 1:250,000.
- Hintze, L.F., 1974, Preliminary geologic map of the Wah Wah Summit quadrangle, Millard and Beaver Counties, Utah. United States Geological Survey Misc. Field Studies Map MF-637, scale 1:48,000.
- Hintze, L.F., 1980, Geologic map of Utah. Utah Geological and Mineral Survey, scale 1:500,000.
- Hintze, L.F., 1988, Geologic History of Utah, Brigham Young University Geology Studies Special Publication 7, 202 p.
- Hintze, L.F., and Robison, R.A., 1975, Middle Cambrian stratigraphy of the House, Wah Wah, and adjacent ranges in western Utah: Geological Society of America Bulletin, v. 86, p. 881-891.
- Hoisch, T.D., and Simpson, C., 1993, Rise and tilt of metamorphic rocks in the lower plate of a detachment fault in the Funeral Mountains, Death Valley, California: Journal of Geophysical Research, v. 98, p. 6805-6827.
- Holm, D.K., Geissman, J.W., and Lux, D.R., 1990, Paleomagnetic and Ar-Ar constraints on Tertiary uplift of the Black Mountains, Death Valley region, California. EOS, Transactions American Geophysical Union, v. 71, p. 1298.
- John, B.E., and Foster, D.A., 1993, Structural and thermal constraints on the initiation angle of detachment faulting in the southern Basin and Range. The Chemehuevi Mountains case study. Geological Society of America Bulletin, v. 105, p. 1091-1108.
- Lemmon, D.M., and Morris, H.T., 1984, Geologic map of the Beaver Lake Mountains Quadrangle, Millard and Beaver Counties, Utah. U.S. Geological Survey Map I-1572, scale 1:48,000.
- Liese, H.C., 1957, Geology of the northern Mineral Range, Millard and Beaver counties, Utah [unpublished Master's thesis]: Salt Lake City, University of Utah, 88 pp.
- Linn, J.K., Walker, J.D., and Stockli, D.F., in review, Timing of tectonic denudation of the Canyon Range, west-central Utah in response to footwall uplift of the Sevier Desert detachment. Geology.
- Lipman, P.W., Rowley, P.D., Mehnert, H.H., Evans, S.H.J., Nash, W.P., and Brown, F.H., 1978, Pleistocene rhyolite of the Mineral Range, Utah. Geothermal and archaeological significance. United States Geological Survey Journal of Research, v. 6, p. 133-147.
- Lister, G.S., and Baldwin, S.L., 1993, Plutonism and the origin of metamorphic core complexes. Geology, v. 21, p. 607-610.
- Livaccari, R.F., Geissman, J.W., and Reynolds, S.J., 1993, Paleomagnetic evidence for large-magnitude, low-angle normal faulting in a metamorphic core complex. Nature, v. 361, p. 56-59.
- Livaccari, R.F., Geissman, J.W., and Reynolds, S.J., 1995, Large-magnitude extensional deformation in the South Mountains metamorphic core complex, Arizona. Evaluation with paleomagnetism. Geological Society of America Bulletin, v. 8, p. 877-894.
- Machette, M.N., Steven, T.A., Cunningham, C.G., and Anderson, J.J., 1984, Geologic map of the Beaver Quadrangle, Beaver and Piute Counties, Utah. U.S. Geological Survey, Miscellaneous Investigations, Map I-1520, scale 1:50,000.
- MacDonald, R.E., 1976, Tertiary tectonics and sedimentary rocks along the transition. Basin and Range province to plateau and thrust belt province, Utah, in Hill, J.G., ed., Symposium on the Geology of the Cordilleran Hinge. Denver, Rocky Mountain Association of Geologists, p. 281-317.
- Manning, A.H., and Bartley, J.M., 1994, Postmylonitic deformation in the Raft River metamorphic core complex, northwestern Utah: Evidence of a rolling hinge. Tectonics, v. 13, p. 596-612.
- Miller, G.M., 1966, Structure and stratigraphy of southern part of Wah Wah Mountains, southwest Utah. American Association of Petroleum Geologists Bulletin, v. 50, p. 858-900.
- Morris, H.T., 1983, Interrelations of thrust and transcurrent faults in the central Sevier orogenic belt near Leamington, Utah. Geological Society of America, Memoir 157, p. 75-81.
- Nash, W.P., 1976, Petrology of Quaternary volcanics of the Roosevelt KGRA, and adjoining area, Utah. Salt Lake City, University of Utah Publications Board, 102 p.
- Nash, W.P., and Crecraft, H.R., 1982, Evolution of the Quaternary magmatic system, Mineral Mountains, Utah. Interpretations from chemical and experimental modeling, University of Utah, Department of Geology and Geophysics, 50 p.
- Nielson, D.L., Sibbett, B.S., McKinney, D.B., Hulen, J.B., Moore, J.N., and Samberg, S.M., 1978, Geology of Roosevelt Hot Springs KGRA, Beaver County, Utah. Salt Lake City, Earth Science Laboratory, University of Utah Research Institute, 120 p.
- Nielson, D.L., Evans, S.H., and Sibbett, B.S., 1986, Magmatic, structural, and hydrothermal evolution of the Mineral Mountains intrusive complex, Utah. Geological Society of America Bulletin, v. 97, p. 765-777.
- Ottom, J.K., 1995, Western frontal fault of the Canyon Range. Is it the breakaway zone of the Sevier Desert detachment? Geology, v. 23, p. 547-550.
- Parsons, T., and Thompson, G.A., 1993, Does magmatism influence low-angle normal faulting? Geology, v. 21, p. 247-250.
- Price, D.E., in preparation, Timing, magnitude, and three-dimensional structure of detachment-related extension, Mineral Mountains, Utah [M.S. thesis]: University of Utah.
- Price, D.E., and Bartley, J.M., 1990, Low- and high-angle faulting, southern Mineral Mountains, southwestern Utah: Geological Society of America Abstracts with Programs, v. 22, p. 76.
- Price, D.E., and Bartley, J.M., 1992, Three-dimensional extensional structure of the southern Mineral Mountains, southwestern Utah. Geological Society of America Rocky Mountain Section Abstracts with Programs, v. 24, p. 58.
- Proffett, J.M.J., 1977, Cenozoic geology of the Yerington District, Nevada, and implications for the nature and origin of Basin and Range faulting. Geological Society of America Bulletin, v. 88, p. 247-266.
- Reynolds, S.J., and Lister, G.S., 1990, Folding of mylonitic zones in Cordilleran metamorphic core complexes. Evidence from near the mylonitic front. Geology, v. 18, p. 216-219.
- Reynolds, S.J., and Rehrig, W.A., 1980, Mid-Tertiary plutonism and mylonitization, South Mountains, central Arizona, in Crittenden, M.D.J., Coney, P.J., and Davis, G.H., eds., Cordilleran Metamorphic Core Complexes: Boulder, Geological Society of America Memoir 153, p. 159-175.
- Royse, F., Jr., 1993, Case of the phantom foredeep. Early Cretaceous in west-central Utah. Geology, v. 21, p. 133-136.
- Scott, R.J., and Lister, G.S., 1992, Detachment faults. Evidence for a low-angle origin. Geology, v. 20, p. 833-836.
- Sharp, J.W., 1984, West-central Utah: palinspastically restored sections constrained by COCORP seismic reflection data [M.S. thesis] Cornell University, 60 p.
- Sibbett, B.S., and Nielson, D.L., 1980, Geology of the central Mineral Mountains, Beaver County, Utah. Salt Lake City, Utah University Research Institute, Earth Sciences Laboratory Report no. 33, 42 p.
- Smith, R.B., and Bruhn, R.L., 1984, Intraplate extensional tectonics of the eastern Basin-Range. inferences on structural style from seismic reflection data, regional tectonics, and thermal-mechanical models of brittle-ductile deformation. Journal of Geophysical Research, v. 89, p. 5733-5762.
- Steven, T.A., Cunningham, C.G., Naeser, C.W., and Mehnert, H.H., 1979, Revised stratigraphy and radiometric ages of volcanic rocks and mineral deposits in the Marysvale area, west-central Utah. 40 p.
- Von Tish, D.B., Allmendinger, R.W., and Sharp, J.W., 1985, History of Cenozoic extension in central Sevier Desert, west-central Utah, from COCORP seismic reflection data. American Association of Petroleum Geologists Bulletin, v. 69, p. 1077-1087.
- Walker, J.D., and Bartley, J.M., 1991, New thrust fault relations in the Beaver Lake Mountains, southwestern Utah, and regional correlation

- of Sevier thrusts: Geological Society of America Abstracts with Programs, v. 23, p. 107.
- Walker, J.D., Bartley, J.M., and Glazner, A.F., 1990, Large-magnitude extension in the central Mojave Desert. Implications for Paleozoic to Tertiary paleogeography and tectonics. *Journal of Geophysical Research*, v. 95, p. 557–569.
- Weaver, C.L., 1980, Geology of the Blue Mountain Quadrangle, Beaver and Iron Counties, Utah: Brigham Young University Geology Studies, v. 27, p. 116–132.
- Welsh, J.E., 1973, Geology of the Beaver Lake Mountains, Beaver County, Utah: Utah Geological Association Publication 3, p. 49–53.
- Whelan, J., and Bowdler, J., 1979, Geology of the Antelope Springs quadrangle Millard County, Utah: *Utah Geology*, v. 6, p. 81–85.
- Wernicke, B., 1981, Low-angle normal faults in the Basin and Range Province: Nappe tectonics in an extending orogen: *Nature*, v. 291, p. 645–648.
- Wernicke, B.P., and Axen, G.J., 1988, On the role of isostasy in the evolution of normal fault systems: *Geology*, v. 19, p. 848–851.
- Wright, J.E., and Snoke, A.W., 1993, *Tertiary magmatism and mylonitization in the Ruby-East Humboldt metamorphic core complex, northeastern Nevada: U-Pb geochronology and Sr, Nd, and Pb isotope geochemistry*. Geological Society of America Bulletin, v. 105, p. 935–952.

Neotectonics, fault segmentation, and seismic hazards along the Hurricane fault in Utah and Arizona: An overview of environmental factors in an actively extending region

MEG E. STEWART

Dames & Moore, One Blue Hill Plaza, Suite 530, Pearl River, New York 10965

WANDA J. TAYLOR

University of Nevada, Las Vegas, Department of Geoscience, 4505 Maryland Pkwy, Las Vegas, Nevada 89154

PHILIP A. PEARTHREE

Arizona State Geological Survey, 416 W. Congress St., Tucson, Arizona 45701

BARRY J. SOLOMON

Utah Geological Survey, P.O. Box 146100, Salt Lake City, Utah 84114-6100

HUGH A. HURLOW

Utah Geological Survey, P.O. Box 146100, Salt Lake City, Utah 84114-6100

ABSTRACT

Long normal fault zones are in, and form the eastern boundary of, the transition zone between the Colorado Plateau and highly extended Basin and Range physiographic provinces. Seismicity in the transition zone of southwestern Utah and northwestern Arizona is believed to be influenced by earthquake rupture segment boundaries. Two geometric fault segment boundaries are identified on the active Hurricane fault. Fault geometry, scarp morphology, structures, and changes in amount of offset are used to define the boundaries. The seismic-risk implication of defining earthquake rupture segments and boundaries is significant in southwestern Utah, a region experiencing rapid population growth. The 1992 St. George M 5.8 earthquake probably occurred on the Hurricane fault, triggering a large and damaging landslide and other seismic hazards. Isolated Quaternary fault scarps are observed along the Hurricane fault. These fault scarps indicate that the fault is active, although no historical surface ruptures have occurred.

INTRODUCTION

The transition zone between the Basin and Range and Colorado Plateau physiographic provinces (fig. 1) displays tectonic features common to both provinces. In southwestern Utah and northwestern Arizona the zone is transected by four long normal fault zones—Toroweap-Sevier, Hurricane, Washington, and Gunlock-Grand Wash—each greater than 100 km long. The transition zone is an ideal location to study normal faulting. Important data may be obliterated by multiple-overprinting-faulting events in more highly extended regions such as the Basin and Range, but the tran-

sition zone experienced less strain and shows a higher degree of data preservation.

Within the Basin and Range Province and the transition zone, ongoing extension is typically accommodated by seismically active, long normal fault zones. Through detailed studies, long normal faults can be divided into geometric fault segments differentiated by faulting history, geometry, and seismicity. Boundaries separating segments are significant because they may be the sites of significant strain, may impede earthquake-rupture propagation, and may influence earthquake locations (e.g., Schwartz and Coppersmith, 1984;

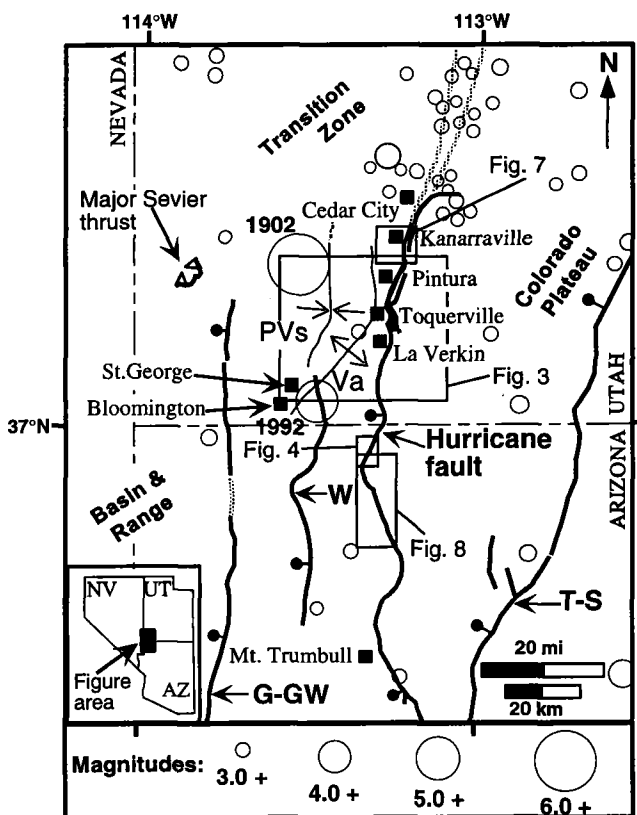


Figure 1. Locations of major faults in southwestern Utah and northwestern Arizona (ball and bar on downthrown side of normal faults; teeth on upper plate of thrust faults; stippled where concealed): G-GW = Gunlock-Grand Wash fault, W = Washington fault, and T-S = Toroweap-Sevier fault. Historical earthquakes are indicated with open circles, major earthquakes of 1902 and 1992 are labeled (modified from Bausch and Brumbaugh, 1994). The major folds are: PVs = Pine Valley syncline, Va = Virgin anticline. Major thrust is the Sevier-age Square Top Mountain thrust. Locations of Figures 3, 4, 7, and 8 along the Hurricane fault are outlined. Structural data compiled from Hintze (1980) and Reynolds (1988).

King, 1986; Bruhn et al., 1987; Bruhn et al., 1990; Susong et al., 1990; Crone and Haller, 1991; dePolo et al., 1991; Machette et al., 1991; Zhang et al., 1991; Janecke, 1993; Evans and Langrock, 1994). Segment boundaries may be defined based on a variety of data or concepts. In this paper a geometric segment boundary is defined as a zone across which a fault markedly changes strike and, in the case of a normal fault, forms a bend that is convex toward the hanging wall. An earthquake rupture segment boundary is defined as a location or zone where earthquakes repeatedly initiate or terminate, and thus, also restricts the locations of fault scarps. A segment boundary may be a geometric boundary, an earthquake rupture boundary or both. Identification of

geometric segments and boundaries is critical for seismic-hazard analysis because segment length provides an estimate of the maximum rupture length during an earthquake and can be used to estimate paleoearthquake magnitudes. We examine two geometric segment boundaries of the Hurricane fault (Stewart and Taylor, 1996; Taylor and Stewart, in review), but fault geometry (Hintze, 1980) indicates that additional geometric segment boundaries probably exist (cf., Taylor and Stewart, in review).

Typical of the Basin and Range province, evaluation of seismic hazards in southwestern Utah and northwestern Arizona is complicated by the apparent contradiction between the moderate level of historical seismicity and the existence of long fault zones with Quaternary scarps. Although the region has experienced earthquakes ranging up to M 6.3 (fig. 1), geologic evidence, such as fault scarps and amount of Quaternary displacement, indicates that the potential exists for much larger (magnitude 7+) earthquakes. The Hurricane fault and other major late Cenozoic normal faults that cut the western margin of the Colorado Plateau in this region have substantial Quaternary displacement. Documented fault scarps on the Hurricane fault point to the recency of movement (Menges and Pearthree, 1983; Anderson and Christenson, 1989; Stewart and Taylor, 1996). It is difficult to effectively integrate this geologic evidence into seismic-hazard analyses, however, because very little is known about the size and timing of Holocene and late Pleistocene surface ruptures or the length of geometric fault segments that might rupture in individual large earthquakes.

Seismic and other geological hazards in southwestern Utah and northwestern Arizona are important because of their potential impact on the significant and rapidly growing population. The region includes one of the fastest growing areas in Utah, the St. George Basin (see Lund, this volume). Significant seismic hazards posed to the region by the Hurricane fault are discussed here. In the following paper Lund (this volume) discusses other geological hazards including problem soil and rock, landslides, shallow ground water, and flooding.

The field trip associated with this paper will follow the Hurricane fault for approximately 60 km along strike (see Stewart et al., field trip log, this volume). The paper and field trip proceed from south to north discussing and observing structures and kinematics associated with the fault. Two geometric segment boundaries and their associated seismic-hazard implications will be observed and discussed. Evidence for these geometric segment boundaries includes fault geometry, slip direction or kinematic considerations, scarp morphology, changes in amount of offset around the fault bend, and fault zone complexity. These boundaries may be earthquake rupture boundaries. Documented fault scarps on the Hurricane fault are not common, especially in Utah; this trip will visit known scarps in three locations. We

will also examine the landslide in Springdale, Utah, triggered by the September 2, 1992, St. George earthquake, probably generated by movement on the Hurricane fault. Shortening structures predating the Hurricane fault and a synextensional basin will be discussed and observed at the New Harmony and Kanarraville Basins. The Toquerville fold, a synextensional footwall flexure will be discussed.

GEOLOGIC BACKGROUND

The Hurricane fault represents the youngest period of deformation in southwestern Utah and northwestern Arizona (Dobbin, 1939; Cook, 1957; Anderson and Christenson, 1989). It is a 250-km-long, north-south striking, high-angle, down-to-the-west normal fault that, in exposures, cuts Paleozoic, Mesozoic and Cenozoic rocks. The Paleozoic and Mesozoic rocks (fig. 2) predate all exposed deformation in the region (Armstrong, 1968). Thrust faults of the Sevier orogenic belt cut the area west and northwest of the Hurricane fault and Pine Valley Mountains during the Cretaceous, moderately folding older rocks in front of the thrust belt to form the Virgin anticline and the Pine Valley syncline (fig. 1) (Armstrong, 1968; Cowan and Bruhn, 1992).

Southwestern Utah and northwestern Arizona underwent a period of tectonic quiescence during the early and middle Tertiary (Cook, 1957) followed by magmatism and extension. Volcanism began about 33 million years ago just north of the Pine Valley Mountains and migrated southward through time (e.g., Rowley et al., 1979; Best and Grant, 1987; Best et al., 1989). Between ~20 and 22 million years ago the Pine Valley laccolith and other intrusions were emplaced (Armstrong, 1963; Nelson et al., 1992). Extension began in the Oligocene north of the Pine Valley Mountains and continued through the Miocene into the Quaternary near the Pine Valley Mountains and the Hurricane fault (Gardner, 1941; Cook, 1952, 1957; Mackin, 1960; Taylor and Bartley, 1992; Axen et al., 1993).

Volcanism accompanied extension on normal faulting in the transition zone. Small-volume basalt flows and cinder cones exist throughout southwestern Utah (fig. 3). Best et al., (1980) dated flow rocks near Hurricane, Utah, between 0.289 and 1.7 Ma using the K-Ar method. Sanchez (1995) used $^{40}\text{Ar}/^{39}\text{Ar}$ to date flows near Hurricane, Utah, at between 353 ± 45 ka and 258 ± 24 ka (a period of at least 100,000 years.)

Chronology of faulting

Long normal faults in this region, including the Hurricane, Toroweap-Sevier, Grand Wash, and Washington fault zones (fig. 1), have varying amounts of Quaternary displacement. The late Quaternary behavior of these faults has been investigated on a reconnaissance basis (Menges and Pearthree, 1983; Pearthree et al., 1983; Anderson and Christenson,

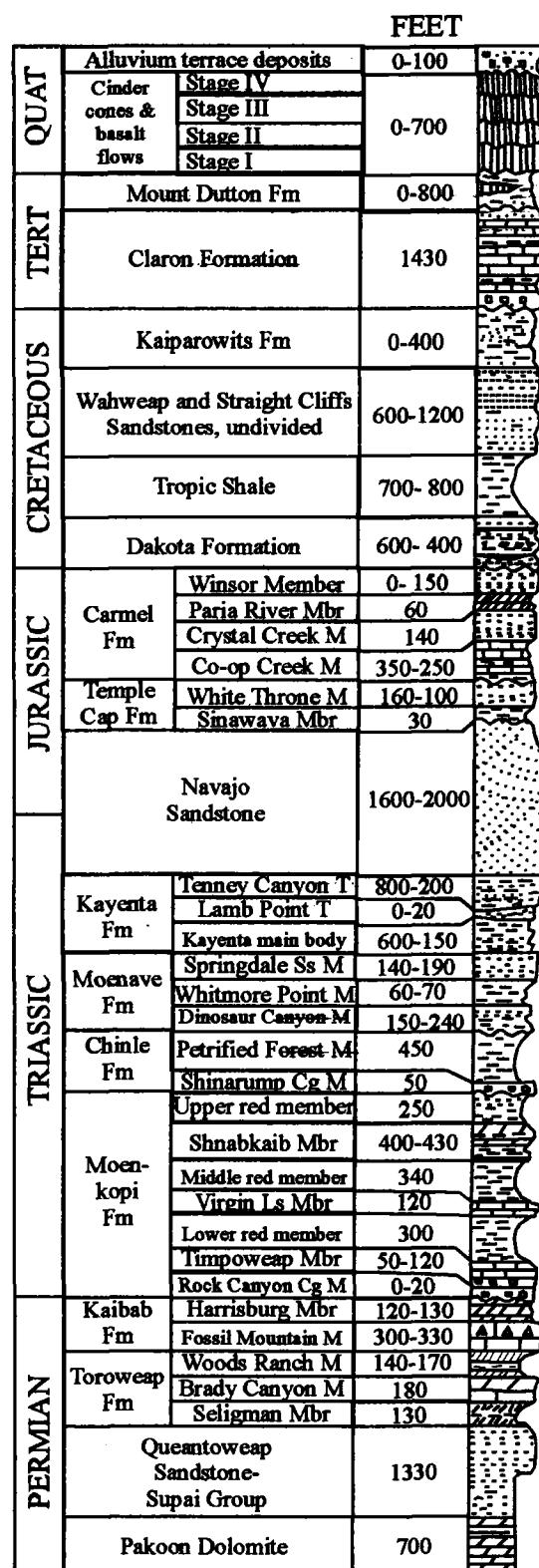


Figure 2. Stratigraphic column from the Zion Park—Cedar Breaks area in Utah; modified from Hintze (1980) and (1988) and Stokes (1986).

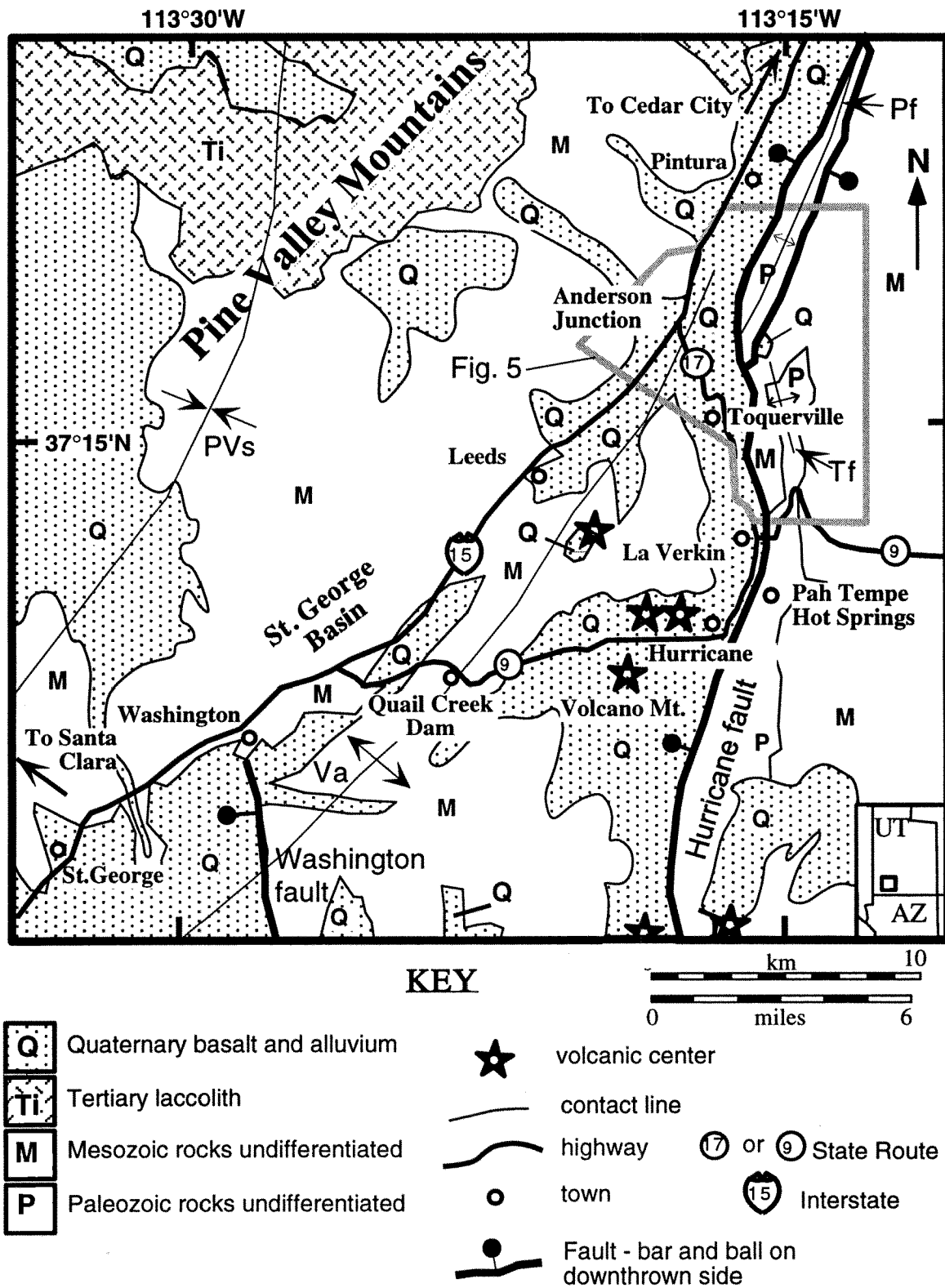


Figure 3. Location map of St. George Basin, surrounding communities, and highways. Folds discussed in text: PVs = Pine Valley syncline, Va = Virgin anticline, Pf = Pintura fold, Tf = Toquerville fold. Area of Figure 5 is outlined by dark stipple. Geology modified from Hintze (1963) and (1980).

1989; W.J. Taylor, unpublished mapping; H.A. Hurlow, unpublished mapping). Portions of the Hurricane fault (Stewart and Taylor, 1996) and Toroweap fault (Jackson, 1990) have also been studied in more detail. However, the age of youngest surface rupture, the frequency of ruptures, the amount of displacement per rupture, and the length of recent ruptures on most of these faults are poorly constrained at this time. Here we discuss the faulting history for that portion of the Hurricane fault that we will visit on the field trip.

It is unclear when movement first began along the Hurricane fault. Based on structural and stratigraphic relations some geologists suggest an initiation age of Miocene (Gardner, 1941; Averitt, 1964; Hamblin, 1970; Stewart and Taylor, 1996), or contemporaneously with laccolith emplacement (Cook, 1957). Others suggest Pliocene or Pleistocene initial movement for some sections of the fault (Anderson and Mehnert, 1979; Anderson and Christenson, 1989).

Fault scarps are evident in several places along the Hurricane fault in Arizona. Near the Utah-Arizona border Menges and Pearthree (1983) documented fault scarps up to 20 m high cutting steep alluvial fans at the base of the Hurricane Cliffs (fig. 4). Many of the scarps are large enough to be the result of several surface-faulting events. Holocene rupture may have occurred along part of the Hurricane fault, based on smaller scarps found on Holocene (?) deposits at one location just south of the Arizona-Utah border (Menges and Pearthree, 1983; Pearthree et al., 1983), but this age has not been demonstrated definitively. Fault scarps exist at a number of localities along the fault zone north of Mt. Trumbull, Arizona. These scarps range in height from about 4 to 25 m, with estimated vertical displacements of 1 to 10 m (Pearthree, unpublished data). In Whitmore Canyon near the Colorado River, the Hurricane fault probably ruptured in the early Holocene to latest Pleistocene based on analyses of fault scarps found there (Pearthree et al., 1983).

Near Toquerville, Utah, unconsolidated Quaternary alluvium is offset at three places along the Hurricane fault. Two scarps are exposed along the northern Ash Creek geometric fault segment (fig. 5) where they displace an alluvial deposit, but the precise age of the deposit is unknown. The largest fault scarp is 6 m high and the other is 3 m high. Bucknam and Anderson's (1979) maximum scarp height-slope angle technique provides a crude age approximation for the scarps of between 1,000 and 15,000 yr old (Stewart and Taylor, 1996). The third exposure of offset Quaternary sediment is along the Anderson Junction segment (fig. 5), where a gravel of unknown age in a stream channel is cut by two fault strands that crop out 3 m apart, but no scarps are present. As much as 3 m of stratigraphic separation was measured along the strand that dips 60°W; 1.2 m of stratigraphic separation was measured along the other strand, which is oriented N12°W, 73°W. The displaced deposits are

older than the most recent sedimentation in the area. The age of faulting is unknown and may represent a single or multiple events.

Quaternary displacement on the Hurricane fault near Toquerville, Utah, is shown by 450 m of stratigraphic separation of the top of undated Quaternary basalt (fig. 6; Stewart and Taylor, 1996). This basalt is geochemically similar to the 353 ± 45 ka basalt of Sanchez (1995). Prior to basalt extrusion, stratigraphic separation across the Hurricane fault ranges from 1740 to 2070 m in this area based on the location of Permian to Jurassic units in the footwall and their inferred locations in the hanging wall. Assuming a relatively constant strain rate, it is possible to back-calculate an estimated time of initial fault movement on this section of the Hurricane fault as Late Miocene to early Pleistocene.

Near the New Harmony and Kanarraville basins (fig. 7), stratigraphic and structural relations indicate that the Hurricane Cliffs and the presently observable slip on the Hurricane fault developed after about 1 million years ago (Anderson and Mehnert, 1979). The Kanarraville basin began forming in Late Pliocene or Quaternary time due to normal displacement on the Hurricane fault (H.A. Hurlow, unpublished mapping).

STRUCTURAL GEOLOGY

Total stratigraphic separation along the Hurricane fault (measured on Permian to Jurassic units directly along the fault) generally increases from south to north (Gardner, 1941). Near the southern tip line, south of the Grand Canyon, less than 61 m of stratigraphic separation is documented (Hamblin, 1970). Total stratigraphic separation is 450 m at the Grand Canyon (Hamblin, 1970), about 900 m in Arizona 30 km south of the Utah border, and 2070 m near Toquerville, Utah (Stewart and Taylor, 1996).

Stewart and Taylor (1996) identified a geometric segment boundary along the Hurricane fault near Toquerville, Utah, at an abrupt change in fault strike. Taylor and Stewart (in review) identified another geometric segment boundary in northwestern Arizona, marked by a large change in strike. The nature and history of these geometric fault segments and segment boundaries are important to understand because they have significant implications for seismic-hazard evaluation.

Hurricane fault near the Utah-Arizona state line

A prominent geometric fault bend exposed near the Utah-Arizona state line (Taylor and Stewart, in review) is interpreted as a geometric segment boundary based on fault geometry, changes in the amount of offset around the bend, changes in Quaternary fault scarps around the bend, and the presence of a small mafic intrusion at the bend. The strike of the fault changes about 40° from approximately

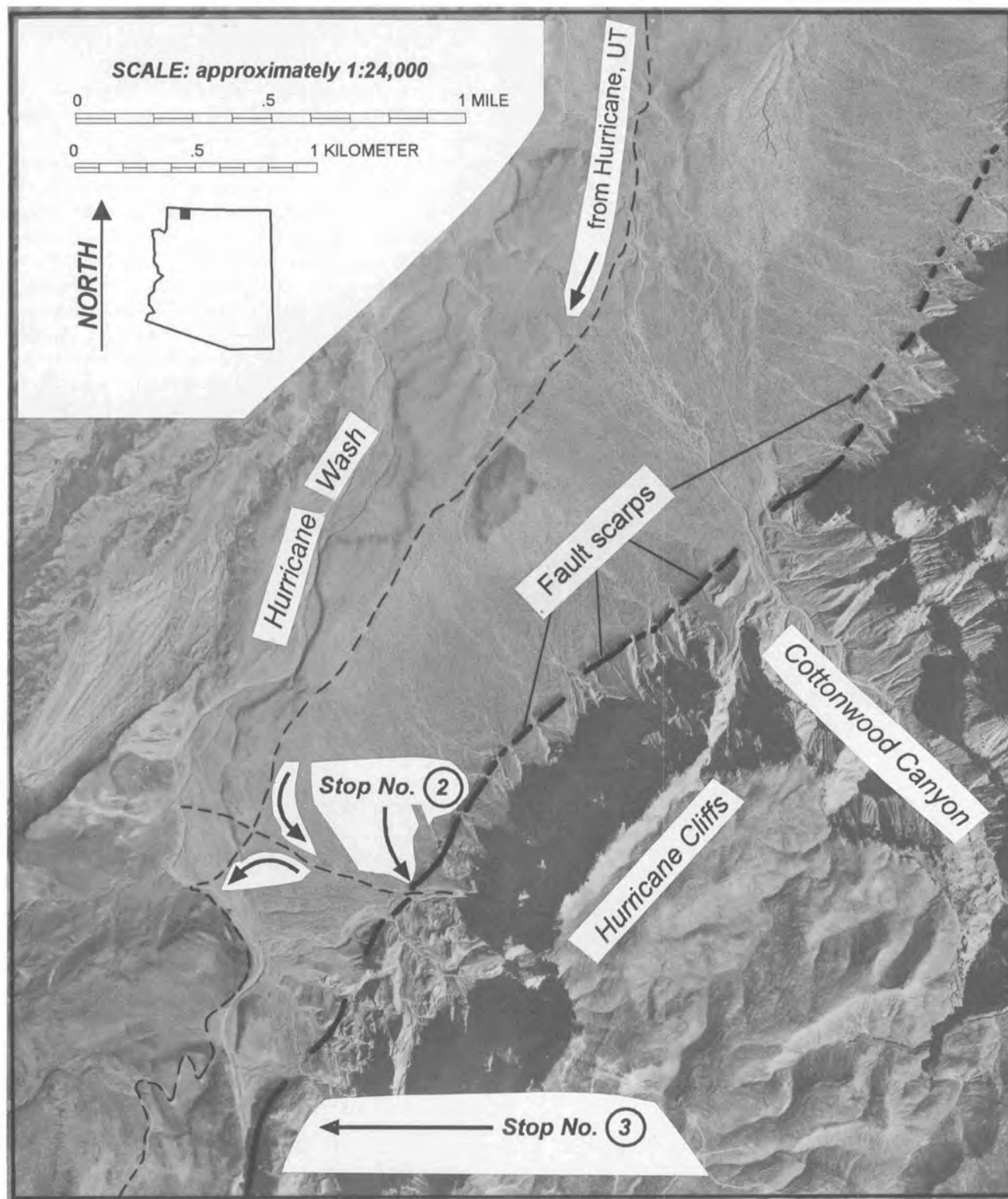


Figure 4. Annotated aerial photograph (scale 1:24,000) of a portion of the Hurricane fault south of the Utah-Arizona border (see Figure 1 for approximate location). Fault scarps are highlighted with bold lines on the footwall block. Gravel roads are shown with dashed lines, and the field trip route is shown with arrows.

N20°E north of the bend to N15–20°W south of it (fig. 8). This prominent bend also has strongly curved and asymmetric reentrant segments on either side of it. The southern segment is longer than the northern segment.

Stratigraphic separation, throw and heave measured on Permian and Mesozoic units decrease markedly from north to south across the fault bend (for definitions of these terms see figure 9). In addition, north of the fault bend the hanging wall basin is areally small, but south of the bend an areally much larger basin is present.

Footwall structures also change at the fault bend. Gentle to open folds and a few normal faults crop out south of the bend. The folds tend to continue for only 1 to 4 km along trend and generally parallel the Hurricane fault, thus they appear to be related to movement along the Hurricane fault. North of the bend only small stratigraphic separation normal faults are present. This change in footwall structures suggests that the change in fault geometry influenced the type of footwall deformation near the Hurricane fault.

Fault scarps in Quaternary deposits of approximately the same age (Billingsley, 1992b) crop out both north and south of the bend, but appear to be lacking in the area of maximum curvature. The fault scarps north of the bend are distinctly higher than those south of the bend. We interpret these data to suggest that the fault bend may be an earthquake rupture barrier.

Basalt. The Quaternary (?) igneous rocks near the apex of the large, sharp bend just south of the Utah-Arizona state line include mafic flow rocks and a small pluton that intrudes them (fig. 8). The presence of these rocks suggest that the Hurricane fault was active and that the segments north and south of the segment boundary were linked prior to emplacement of the igneous. The outcrop pattern of the flows shows that they thin away from the fault, but lie near the fault in the area of maximum fault curvature. This pattern suggests that the flows may have ponded in a topographic low created by the fault. For a topographic low or basin to exist at the bend apex, the two segments must have overlapped or been linked so that the fault(s) was able to down drop the hanging wall at the segment boundary. No evidence for along strike overlap of faults or fault segments exists in this area, so it appears that the two segments linked and the throughgoing fault downdropped the basin in which the basalt ponded.

The composition and mineralogy of the flows and pluton suggest that they may be related. The flows are fine grained and contain plagioclase and olivine phenocrysts. The pluton or plug also has plagioclase and olivine phenocrysts, but is granular and medium to coarse grained. Maureen Stuart (unpublished data from UNLV XRF laboratory, 1995) analyzed samples from four flows and the small intrusion that crops out just west of the bend for major and trace element contents. They are all subalkaline tholeiitic basalt (cf., Irvine

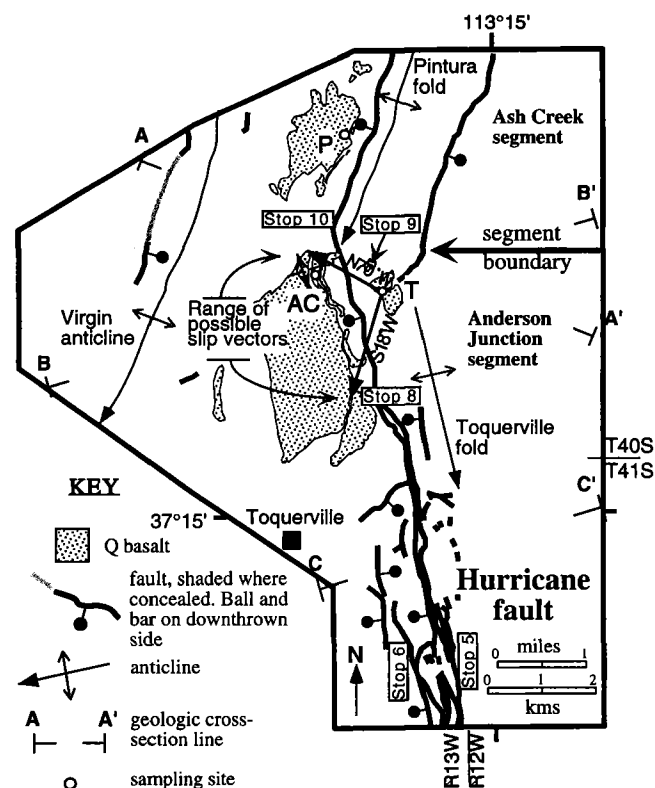
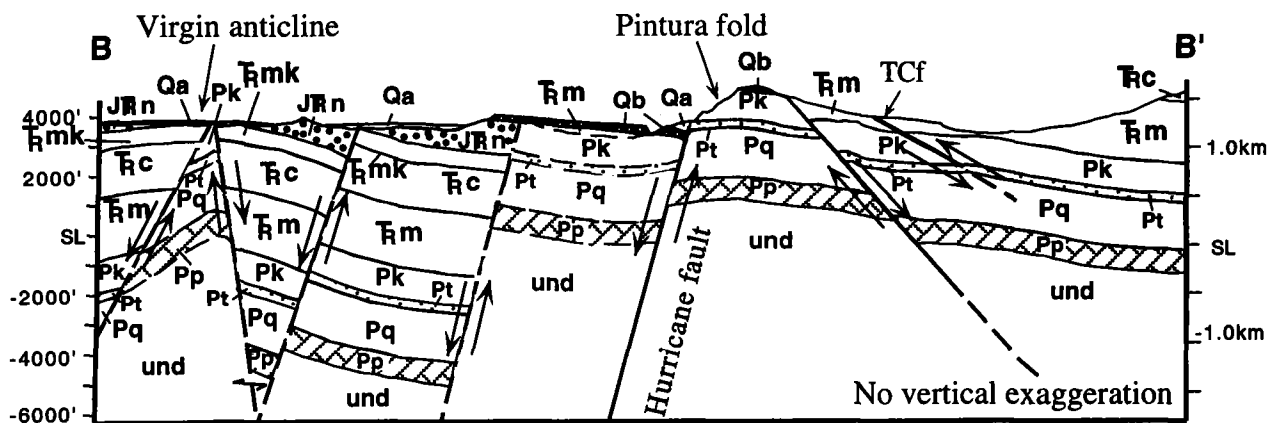
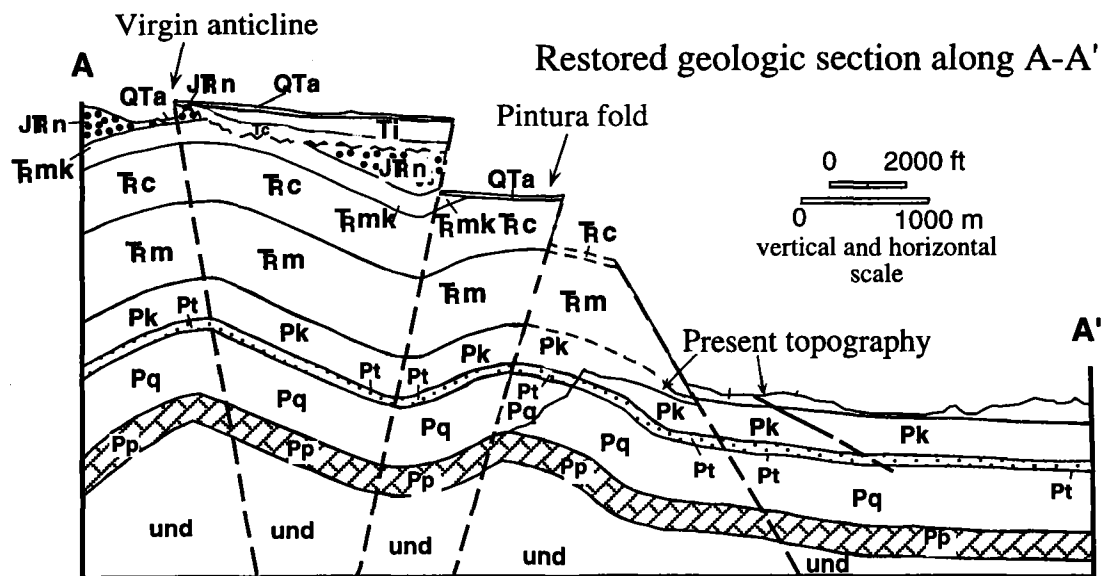
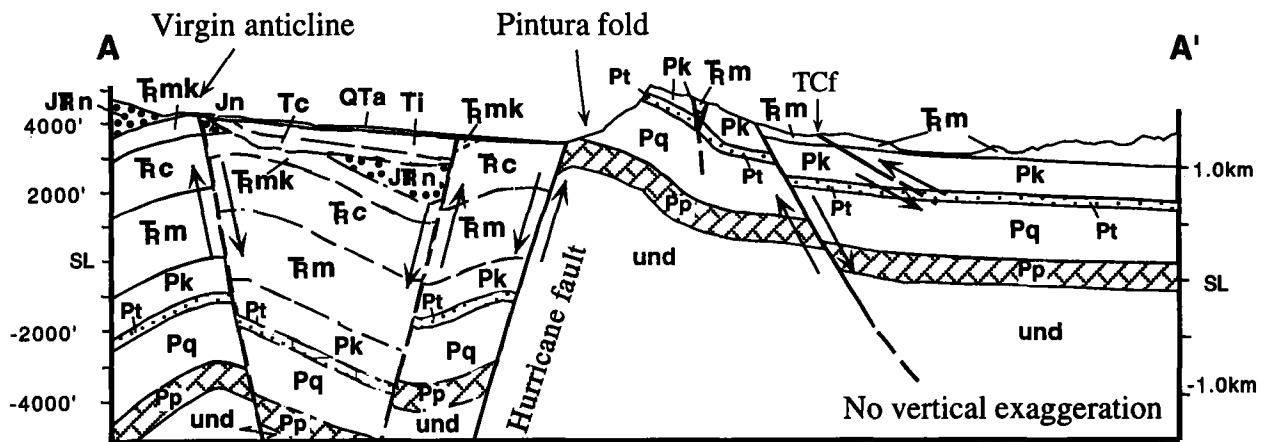


Figure 5. Simplified structure map of area near Toquerville, Utah. Basalt fields are stippled. Cross-section locations A-A' to C-C' are shown constructed on Figure 6. Open circles with letters adjacent (T = Toquerville, P = Pintura, or AC = Ash Creek) indicate where basalt sections were sampled. A range of possible slip vectors is shown between 73°, N70°W and 75°, S18°W, determined from correlating geochemically identical basalt in the hanging wall and footwall (sites T and AC) and assuming the basalt field is laterally homogeneous. Field trip stops 5, 6, 8, 9, and 10 are labeled.

and Baragar, 1971; Le Bas et al., 1986). Stuart also found that (1) the samples have an Ocean Island Basalt (OIB) pattern on a Spider diagram, but have slightly lower elemental abundances which is consistent with Pliocene and younger basalts in the transition zone, and (2) the incompatible element ratios (Nb/Ba vs. Rb/Sr and Nb/Ba vs. Zr/Y) show narrow ranges. These similarities between the flows and pluton suggest a possible genetic relationship between the flows and the intrusion. However, the small number of samples analyzed requires the hypothesis to be tested further.

The intrusion and flows were emplaced after initiation of movement along the Hurricane fault because they lie on Triassic rocks which were eroded off the footwall prior to the emplacement of different, but similar-aged basalt on the footwall. The basalt has not been dated. The assumption of a similar age for all the basalts is based on the fact that they are all surficial deposits, and chemically and miner-



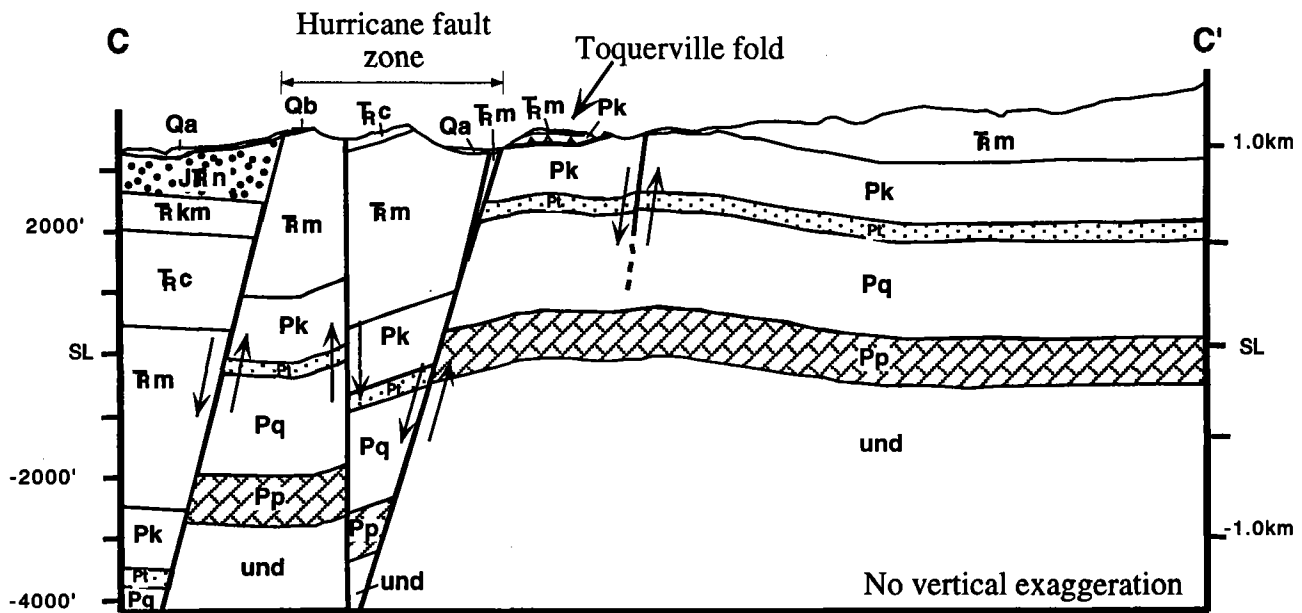


Figure 6. Geological cross sections along A-A' to C-C' from Figure 5. Cross-section A-A' is also drawn restored. Faults shown are drawn with relative motion arrows; dashed faults indicate geometrically required assumed faults. TCf = Taylor Creek thrust fault. Unit explanation: Qa = Quaternary alluvium and colluvium, QTa = Quaternary-Tertiary alluvium, weakly consolidated, Qb = Quaternary basalt, Ti = Tertiary monzodiorite, Tc = Tertiary Claron Fm., JTrn = Jurassic-Triassic Navajo Sandstone, Trmk = Triassic Kayenta Fm. and Moenave Fm., Trc = Triassic Chinle Fm., Trm = Triassic Moenkopi Fm. undifferentiated, Pk = Permian Kaibab Fm., Pt = Permian Toroweap Fm., Pq = Permian Queatoweap Fm., Pp = Permian Pakoon Dolomite, und = undifferentiated Paleozoic rocks and basement. These units are shown on Figure 2, however, relative thicknesses of units in cross-sections are derived from detailed mapping of area in Figure 5 (Schramm, 1994).

alogically similar basalt flows in the region are all Pliocene or younger (eg., Best et al., 1980; Sanchez, 1995). However, whether the intrusion has been cut by the Hurricane fault remains equivocal.

The intrusion suggests the possibility, at this location, of a non-conservative segment boundary (a boundary along which the slip vector and line the formed where the segments intersect are not parallel, and thus, space is generated or destroyed). In the situation where fault slip on different geometric segments is of different ages or magnitudes, space may be generated in the hanging wall. Space may be persistently created, resulting in extension or space-filling intrusions, or destroyed, resulting in folds or reverse faults as rocks are moved across a non-planar surface. The mismatch in the shapes of the hanging wall and footwall results in local strain near the geometric boundary which is then also a kinematic boundary that may impede rupture propagation, forming an earthquake rupture segment boundary.

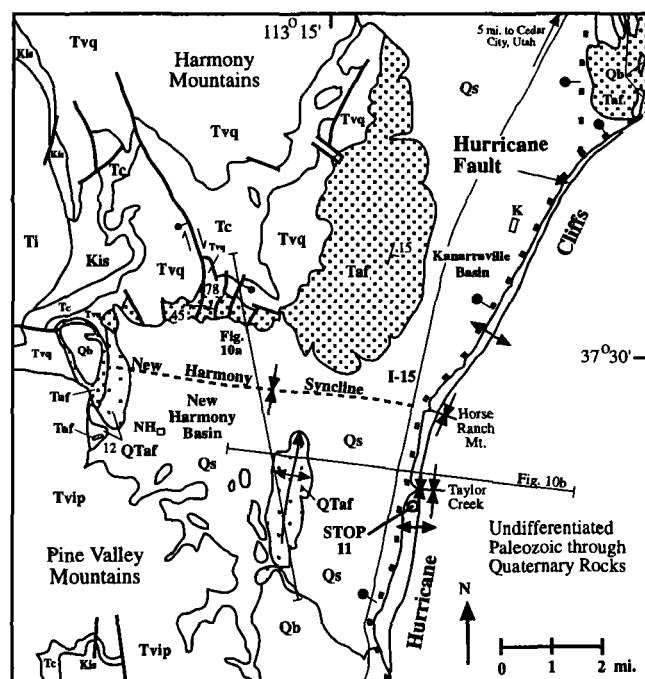
Stratigraphic Separation. Variations in the amount of offset across a fault bend suggest that different numbers or sizes of earthquakes or slip events occurred on opposite sides of it. Therefore, where significant differences in total throw or stratigraphic separation along the fault occur across

a bend, the geometric bend is likely to be an earthquake rupture boundary.

Detailed geologic mapping allows calculation of the stratigraphic separation, throw and heave across the Hurricane fault (fig. 9; Billingsley, 1992a, 1992b, 1993; W.J. Taylor, unpublished data). The calculated stratigraphic separations, throws and heaves are shown in figure 9 for the locations shown on figure 8. The stratigraphic separation, throw and heave, as measured from cross sections directly along the fault, markedly increase from south to north across this geometric bend suggesting that it has been an earthquake rupture barrier for some of the earthquakes and related slip along the fault.

Hurricane fault near Toquerville, Utah

Near Toquerville, Utah, a large change in fault strike ($\sim 34^\circ$ from N13°W to N21°E) marks the boundary between two geometric fault segments (Stewart and Taylor, 1996) (fig. 5). Based strictly on map view (Hintze, 1980) the segment north of the boundary (Ash Creek segment) is at least 24 km long and the segment south of the boundary (Anderson Junction segment) is between 19 and 45 km long (Stewart and Taylor, 1996). These estimates are straight line distance



- (a)
- Normal fault (dotted where concealed)
 - Dextral-normal fault
 - Line of cross section in Figure 10
 - Anticline axial trace showing plunge of hinge
 - Syncline axial trace showing plunge of hinge (dotted where concealed)
 - Strike and dip of bedding

measurements and may need to be refined with detailed mapping to the north and south of the segment boundary and Toquerville study area. The Ash Creek segment is characterized by a single surface trace and a few fault scarps in alluvium, whereas the Anderson Junction segment has multiple fault strands and no clear fault scarps, although offset of unconsolidated sediments of unknown age is observed. Apparent differences in Quaternary fault scarp patterns suggest that the two segments may have different slip histories to the north and south of the geometric bend and may be an earthquake rupture boundary. A small-scale, hanging wall anticline mapped in Quaternary basalt near the large change in fault strike on the Hurricane fault and normal to the fault is further evidence for the existence of a geometric segment boundary (Scott et al., 1994; Schlische, 1993) (fig. 5).

Basalt correlation. Undated Quaternary basalt is present in the hanging wall and footwall of the Hurricane fault

Age	Formation	Symbol	Thickness (ft)	Lithology
Quaternary	Quaternary sediments	Qs	0-1500	
	Quaternary basalt	Qb	0-500	
	Alluvial-fan deposits	QTaf	25-150	
Pliocene	Upper Member	Taf	0-700	
Miocene	Alluvial-fan deposits	Taf	0-450	
	Middle Member	Taf	0-350	
	Lower Member	Taf	0-350	
19 Ma	Racer Canyon Tuff	not shown	0-30	
21 Ma	Pine Valley monzonite & latite	Tvip	1000	
22 Ma	Stoddard Mt. intrusion	Tis		
23 Ma	Quichapa Group	Tvq	1000	
24 Ma				
Eocene-Oligocene	Claron Formation	Tc	700-1000	
Cretaceous	Iron Springs Formation	Kis	3800	

(b)

Figure 7. Simplified geologic map and lithologic column for the New Harmony and Kanarrville basins and adjacent areas. (a) Geologic map, based on Cook (1960), Grant (1995), and Hurlow (in press). NH is town of New Harmony, K is town of Kanarrville. Field trip stop 11 is labeled near Taylor Creek. (b) Lithologic column, based on same sources as geologic map.

(fig. 5). Stewart and Taylor (1996) conducted whole-rock trace element analysis to correlate flow rocks across the fault. Samples were collected from stratigraphic intervals from each of the three sites: one location in a paleochannel in the footwall (site T), and two locations in the hanging wall (sites AC and P; fig. 5). Trace-element data reveal striking positive correlations between flows at different stratigraphic intervals. However, the lowest flow at T and AC exhibit clear grouping in trace element plots suggesting that they relate genetically. From these data, Stewart and Taylor (1996) inferred a range of slip vectors for the fault, from 73°, N70° W to 75°, S18° W.

Stratigraphic separation. Near Toquerville, Utah, total normal stratigraphic separation measured directly along the Hurricane fault on Permian to Jurassic units ranges from 2070 m along A-A' to 1740 m along C-C' (fig. 6). A local northward increase in stratigraphic separation across the geometric segment boundary is observed.

Sense of slip. Movement on the Hurricane fault in the Quaternary is dominantly dip slip. Evidence for dip slip includes: (1) stratigraphic separation of geochemically identical Quaternary basalt flows in the footwall and hanging wall and the suggested slip vector (fig. 5); (2) rakes of slickenlines between vertical and 74° (Kurie, 1966; Schramm, 1994); (3) earthquake rake ($-89^\circ \pm 14^\circ$) from the 1992 St. George earthquake (Lay et al., 1994); and (4) slip direction

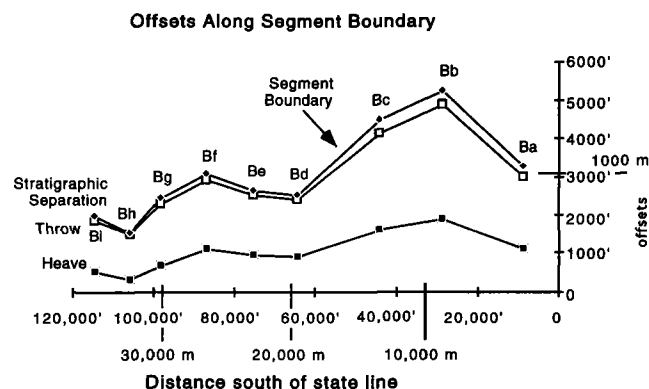
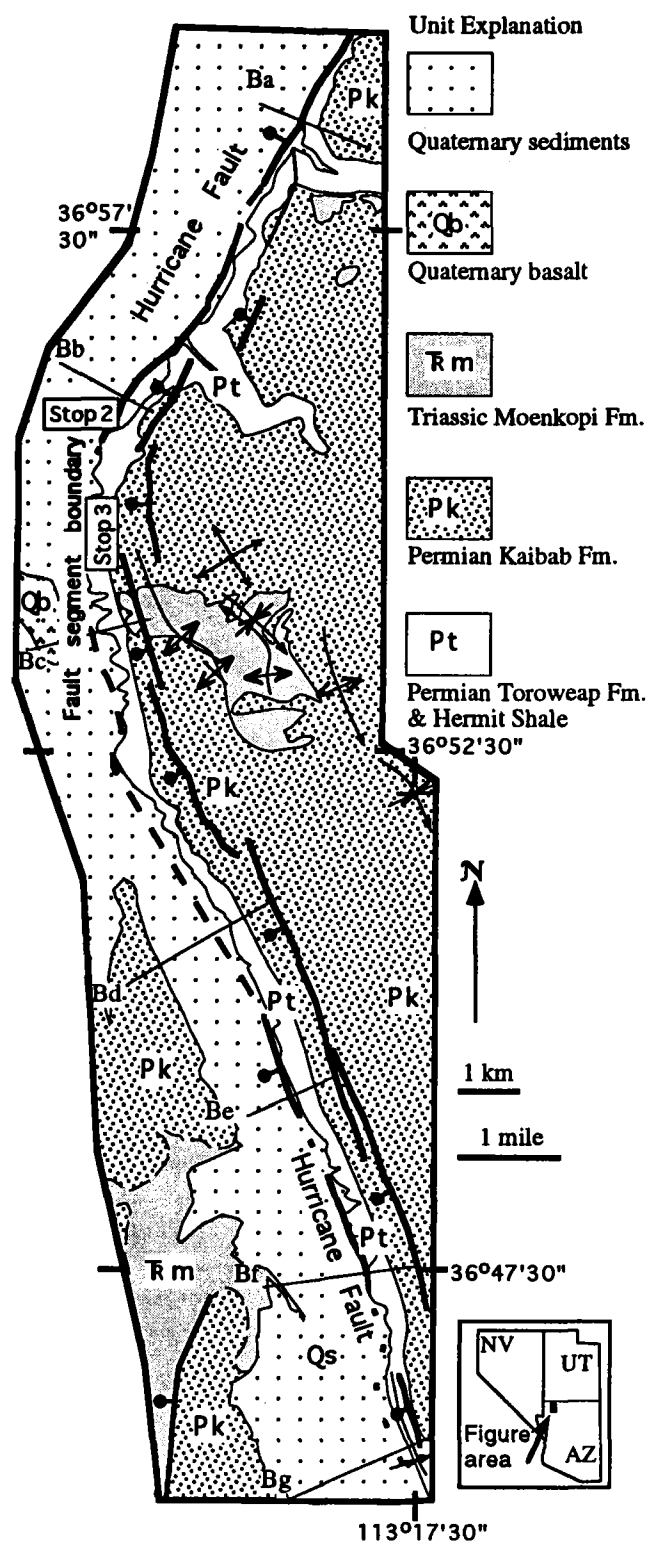


Figure 9. This graph shows the total stratigraphic separation, throw, and heave across the Hurricane fault in the vicinity of the geometric segment boundary (Fig. 8). Stratigraphic separation is the distance measured along the fault between a unit boundary in the hanging wall and the same unit boundary in the footwall. The throw is the vertical component of offset. The heave is the horizontal component of offset. All stratigraphic separations, throws and heaves shown here were measured on Permian to Jurassic units. Little to no variation in these measures was found among Permian to Jurassic units. The marked change in these parameters along the south side of the geometric bend supports the interpretation that this location is a behavioral or earthquake rupture segment boundary and that equal numbers or sizes of earthquakes did not occur to the north (right) and south (left) of the bend.

Figure 8. Simplified geologic map of area surrounding the fault segment boundary in Arizona based on geologic mapping of the Gyp Pocket and Rock Canyon 7.5' quadrangles by Billingsley (1992a, 1992b, 1993) and W. J. Taylor (unpublished mapping). Lines labeled Ba through Bg show locations where the stratigraphic separation, heave and throw were calculated as shown on Figure 9. Line Bh lies 2332 m south along the fault from line Bg. Line Bi lies 4952 m south of line Bg. Stop 2 of the field trip is located near line Bb and Stop 3 is near line Bc. Conventional symbols are used for faults and folds.

of N75–85°W from dip analysis on syndeformational basalt using the technique of Scott et al., (1994) (Stewart and Taylor, 1996). This slip direction agrees with the calculated stress field data for the transition zone of S78°E–N78°W \pm 21° (Zoback and Zoback, 1980; Arabasz and Julander, 1986). Relative motion on the Ash Creek segment is purely dip-slip, and on the Anderson Junction segment is dominantly dip-slip with a small dextral slip component (fig. 5).

The pre-Quaternary normal sense of movement on the Hurricane fault near Toquerville, Utah, is inferred from downdropped Jurassic-Triassic Navajo Sandstone in the hanging wall of the fault relative to Permian Kaibab Formation in the footwall (fig. 2). Our evidence neither supports nor refutes strike-slip or reverse motion along the Hurricane fault prior to the Quaternary (cf., Moody and Hill, 1956; Lovejoy, 1964; Anderson and Barnhard, 1993a).

Hurricane fault—New Harmony and Kanarraville Basins

The structural evolution of the New Harmony and Kanarraville basins, two relatively small Tertiary-Quaternary depositional centers in southwestern Utah (fig. 7), illustrates aspects of Neogene-Quaternary deformation in the Colorado Plateau—Basin and Range transition zone and aspects of the early history of the Hurricane fault. The New Harmony basin is underlain by a late Tertiary syncline formed by north-northeast to south-southwest shortening that was coeval with regional east-west crustal extension (Anderson and Barnhard, 1993a, 1993b; Hurlow, 1996). The Kanarraville basin is interpreted to have formed during Quaternary normal slip on the Hurricane fault.

Geologic setting. The New Harmony and Kanarraville basins lie between Miocene volcanic deposits to the west and the Hurricane Cliffs, which comprise the footwall of the Hurricane fault, to the east (fig. 7). The 40-km² New Harmony basin trends west-northwest, perpendicular to the Hurricane fault and Kanarraville basin. The Kanarraville basin is north and east of the New Harmony basin and has approximately the same surface area, but has a long, narrow form that trends north-northeast.

The New Harmony basin is filled with Quaternary alluvial-fan sediments deposited on a folded and faulted sequence of Miocene to Pliocene (?) volcanoclastic alluvial-fan deposits (Taf; fig. 7). These fan deposits were derived from volcanic rocks to the west and were deposited over an area larger than the New Harmony basin (fig. 7; Anderson and Mehnert, 1979).

This alluvial-fan unit (Taf) is divided into three informal members based on reconnaissance field work and local detailed mapping (H.A. Hurlow, unpublished mapping). The lower member is tan to gray, planar-bedded, cemented

diamictite, breccia, tuffaceous sandstone, and siltstone. Clasts are derived chiefly from the Miocene Quichapa Group, and the Stoddard Mountain and Pine Valley intrusions. This member is 107 m thick and is interbedded at its base with a white crystal tuff that P.D. Rowley of the U.S. Geological Survey (personal communication, 1996) correlates with the Racer Canyon tuff, which yielded a K-Ar date of 19 Ma (Rowley et al., 1979).

The middle member is ~135 m of predominantly poorly to laminar-bedded orange-tan tuffaceous siltstone with local conglomerate beds containing clasts of white biotite-feldspar crystal tuff. This member strongly resembles units northwest and west of the Pine Valley Mountains mapped as Muddy Creek Formation (Cook, 1960; Hintze et al., 1994).

The upper member is unconsolidated boulder gravel that is about 210 m thick. Clasts include Miocene volcanic and plutonic rocks and late Paleozoic through Tertiary sedimentary rocks exposed to the northwest and west. This unit is the “clastic debris” described by Anderson and Mehnert (1979) in both the hanging wall and footwall of the Hurricane fault.

A sequence of alluvial-fan deposits (QTaf), derived entirely from the Pine Valley laccolith and related volcanic rocks to the west, overlies unit Taf. Units Taf and QTaf were not distinguished by previous geologists (Cook, 1960; Grant, 1995), but their differentiation is crucial to deciphering the structural evolution of the New Harmony and Kanarraville basins. The pediment surface over which unit QTaf debris flows were transported and deposited slopes toward the southeast away from the Pine Valley Mountains. The pediment surface is now incised by modern drainages in the foothills of the Pine Valley Mountains, suggesting a Pleistocene age for unit QTaf deposits.

Structural geometry and evolution. The New Harmony syncline is defined by opposing dips of unit Taf on the north and southwest margins of the New Harmony basin (figs. 7 and 10a). In the southern Harmony Mountains, unit Taf dips moderately to steeply south and is overturned adjacent to a north-striking dextral-normal fault (fig. 7). In the same area the stratigraphically lower Quichapa Group and Claron Formation are also steeply dipping to overturned, but a tight anticline north of the syncline returns these units to moderate southward dips (fig. 10a). The Quichapa Group and Claron Formation are cut by numerous minor north- and east-striking normal, dextral-normal, and reverse faults, the majority of which are not shown in figures 7 and 10. The New Harmony syncline is interpreted to reflect north-northeast–south-southwest horizontal crustal shortening. Units QTaf and Qs are not deformed by the New Harmony syncline, nor are they cut by local faults that cut the fold.

The New Harmony syncline is exposed in the lower Hurricane Cliffs where it is expressed in cliff-forming exposures of Permian Kaibab Formation below Horse Ranch

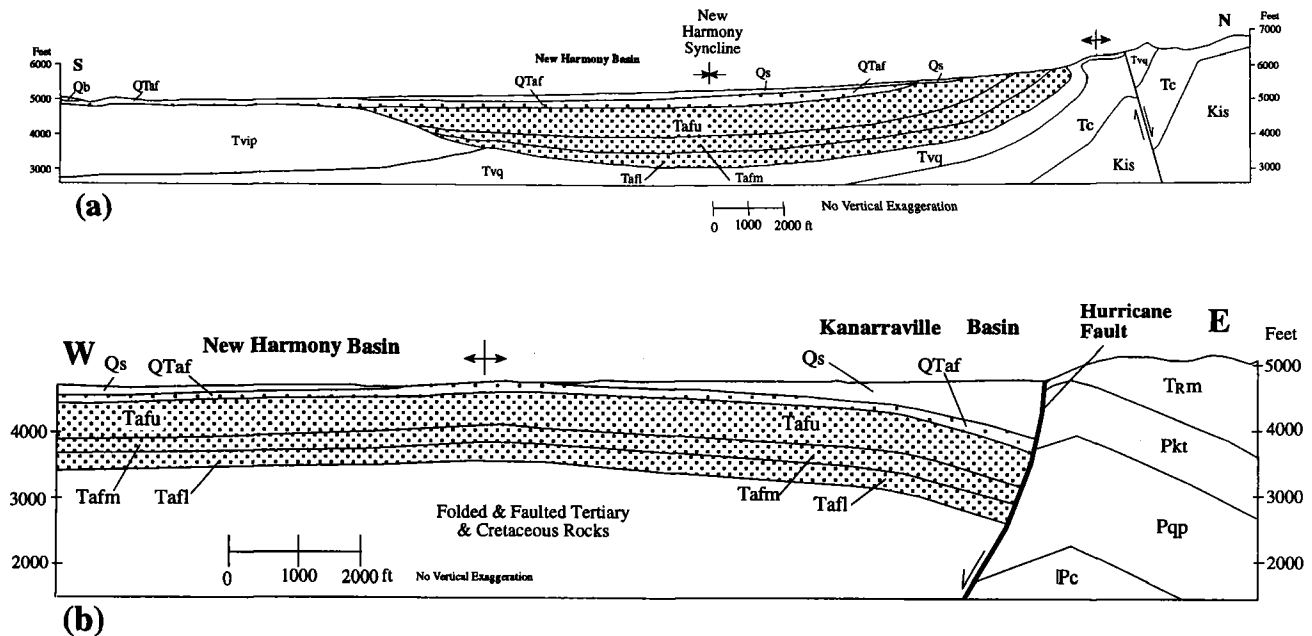


Figure 10. Geologic cross sections; locations shown in Figure 7. Scale is larger than in Figure 7. Units east of Hurricane fault not shown in Figure 7: TRm = Moenkopi Formation; Pkt = Kaibab Limestone and Toroweap Formation; Pqp = Queantoweap Sandstone and Pakoon Formation; and lPc = Callville Limestone.

Mountain. Another east-trending syncline is exposed along Taylor Creek at the entrance to the Kolob Canyons section of Zion National Park. These east-trending synclines re-fold a north-trending Sevier-age anticline, the Pintura fold (see below), exposed in the Hurricane footwall (fig. 7).

Unit QTaf is exposed along a north-trending ridge that divides the New Harmony and Kanarraville basins (fig. 7). This ridge is interpreted as an anticline related to reverse drag in the hanging wall of the Hurricane fault (fig. 10b).

The Kanarraville basin is adjacent and parallel to the Hurricane fault and is interpreted as a synextensional basin. Quaternary sediments are interpreted to have a wedge-shaped geometry reflecting infilling of the structural depression that formed in response to reverse drag in the hanging wall of the Hurricane fault (fig. 10b).

Discussion. Deformation of late Tertiary and Quaternary units in the New Harmony and Kanarraville basins suggests the following structural chronology:

1. North-south horizontal crustal shortening during Neogene time, manifested by the New Harmony syncline and east-west folds in the Hurricane Cliffs. The age of folding is not tightly constrained because the age of the upper member of unit Taf and its timing relative to the folding are unclear. The most likely time of folding is Late Miocene to Pliocene. The New Harmony syncline did not likely form in rela-

- tion to a segment boundary or along-strike displacement gradient (Schlische, 1995) on the Hurricane fault because: (a) the Hurricane fault lacks apparent geometric segment boundaries at either end of the New Harmony basin; (b) the New Harmony basin is larger, has a different shape, and extends farther away from the Hurricane fault than examples cited by Schlische (1995); and (c) the displacement-gradient model does not explain the extreme tightness and overturning of the synclinal and adjacent anticlinal hinges (fig. 10a). Instead, the New Harmony syncline is interpreted to reflect north-south crustal shortening associated with major, regional east-west crustal extension in the Basin and Range Province, as outlined by Anderson and Barnhard (1993a, 1993b). This extension was accommodated in the New Harmony basin area by normal faults west of the trace of the present Hurricane fault (Hurlow, in press).
2. Faulting on a complex system of north- and east-striking normal and reverse faults deformed the New Harmony syncline but may also have been partly coeval with it.
3. The Kanarraville basin is a synextensional basin that began forming in Late Pliocene or Quaternary time due to normal displacement on the Hurricane fault based on stratigraphic and structural relationships.

Major regional folds

The Virgin anticline and the Pintura fold are large regional structures that have been documented for decades (Dobbin, 1939; Gardner, 1941; Gregory and Williams, 1947; Neighbor, 1952; Cook, 1957; Cook and Hardman, 1967; Anderson and Mehnert, 1979; Hintze, 1986; Blank and Kucks, 1989). Parts of these two anticlines and the Toquerville fold were mapped at a scale of 1:12,000 near Toquerville, Utah (Schramm, 1994). A discussion of the anticlines is critical for the understanding of the Hurricane fault. The folds are identified in cross sections and in outcrop and help to constrain the timing of motion on the Hurricane fault to post-Sevier folding.

Virgin anticline. The Virgin anticline (figs. 1 and 3) extends 45 km along strike (Hintze, 1980) in the hanging wall of the Hurricane fault. The anticline involves the Triassic Chinle and the Moenkopi Formations near Quail Creek Reservoir and the Jurassic-Triassic Navajo Sandstone (fig. 2) at the northern limit of the fold near Toquerville, Utah (Dobbin, 1939). Regionally, the Virgin anticline has double plunges, both exposed near Hurricane, Utah.

The anticline is upright, gently plunging, and open. The fold axis orientation locally near Toquerville, Utah, is 5° , $S21^{\circ}W$ (figs. 6 and 11). Beds in the western limb of the Virgin anticline strike from N-S to $N50^{\circ}E$ and dip from 10° to $30^{\circ}W$. Beds in the eastern limb of the anticline strike from $N12^{\circ}E$ to $N35^{\circ}E$ and dip from $10^{\circ}E$ near the hinge to $41^{\circ}E$ on the limb.

Pintura fold. Another anticline extends about 23 km along strike in the Hurricane fault footwall (fig. 5; Anderson and Mehnert, 1979). This anticline is referred to by some geologists as the Kanarra fold (i.e., Gregory and Williams, 1947; Anderson and Mehnert, 1979) and by others (i.e., Gardner, 1941; Neighbor, 1952) as the Pintura fold. The latter term is used here because of the fold's proximity to the town of Pintura, Utah.

The Pintura fold is an upright, gently plunging to horizontal, open anticline. The fold axis is oriented 8° , $S24^{\circ}W$ (fig. 11). Permian rocks of the Pakoon, Queantoweap, Toroweap and Kaibab Formations are exposed in the fold near Toquerville, Utah (fig. 2). The eastern limb of the fold contains beds that dip from 10° to $41^{\circ}E$ and strike between $N12^{\circ}E$ and $N35^{\circ}E$. The western limb of the fold contains beds that strike from $N10^{\circ}E$ to $N42^{\circ}E$ and dip from $14^{\circ}W$ near the hinge to $75^{\circ}W$ close to the Hurricane fault (fig. 11). Beds in the western limb of the Pintura fold may dip more steeply because of drag along the Hurricane fault (Schramm, 1994).

Toquerville fold. The Toquerville fold (Lovejoy, 1964) is a gently-plunging upright anticline that roughly parallels the strike, and lies within the footwall of the Hurricane fault (figs. 5 and 6, cross section C-C'). The fold, about 4-

km long, is exposed in the Permian Kaibab Formation and the Triassic Moenkopi Formation. The attitude of the fold axis is 8° , $S13^{\circ}E$ (fig. 11). Beds in the western limb of the fold dip from $11^{\circ}W$ to $35^{\circ}W$ and strike from $N10^{\circ}W$ to $N34^{\circ}W$. Beds in the eastern limb strike between $N18^{\circ}W$ and $N52^{\circ}E$ and dip from $10^{\circ}E$ near the axis to $36^{\circ}E$ away from the axis.

Discussion. The Virgin anticline, the Pintura fold, and the Toquerville fold involve Paleozoic and Mesozoic rocks. Both the Virgin anticline and the Pintura fold generally parallel regional structures related to Sevier compression (cf., Armstrong, 1968), and thus, are interpreted to be Sevier-age structures (Stewart and Taylor, 1996). The term Sevier is used here to indicate Mesozoic to Paleogene deformation that pre-dates Neogene extension and movement on the Hurricane fault. The Virgin anticline and Pintura fold are connected by a syncline (fig. 6, restored A-A' cross section) that is evident in Bouguer gravity anomaly data (Cook and Hardman, 1967) and was mapped by Hamblin (1965) along strike to the south. These two anticlines and the syncline have similar wavelengths of about 10 km. The Virgin anticline and the syncline apparently parallel each other for at least 65 km along trend (Cook and Hardman, 1967).

Near Toquerville the Hurricane fault truncates the Pintura fold (fig. 5). Further to the south the Virgin anticline is cut by the Washington fault (fig. 1), a regionally-related normal fault (Dobbin, 1939; Hamblin, 1970) that parallels the Hurricane fault. These cross-cutting relationships indicate that these folds are older than the regional normal faults, consistent with a Sevier age.

The Toquerville fold, like the Pintura fold, is within the footwall of the Hurricane fault. The axial trends of the Toquerville fold and the Pintura fold are not parallel to each other, and thus, the anticlines appear to be unrelated genetically (fig. 11). The trend of the Toquerville fold axis does not parallel regional Sevier structures (cf., Armstrong, 1968), suggesting it is not a Sevier-age fold. The Toquerville and Pintura folds occur near fault sections with different strikes and have fold axes that parallel the strike of the fault, criteria required for extension-related footwall flexure. One or both of these folds could be footwall folding caused by isostatic rebound of the footwall or lithospheric flexure (Buck, 1988; Wernicke and Axen, 1988). However, as has already been interpreted, the Pintura fold is an older, pre-extensional structure. The Toquerville fold could be related to flexure of the footwall due to the initial break of, and movement along, the Hurricane fault. With footwall flexure due to isostatic rebound, rotation can occur by motion of vertical footwall shear zones (Wernicke and Axen, 1988). In lithospheric flexure, normal faults are affected by anelastic behavior of the upper crust and the footwall bends in response (Buck, 1988). The Pintura fold, existing prior to faulting,

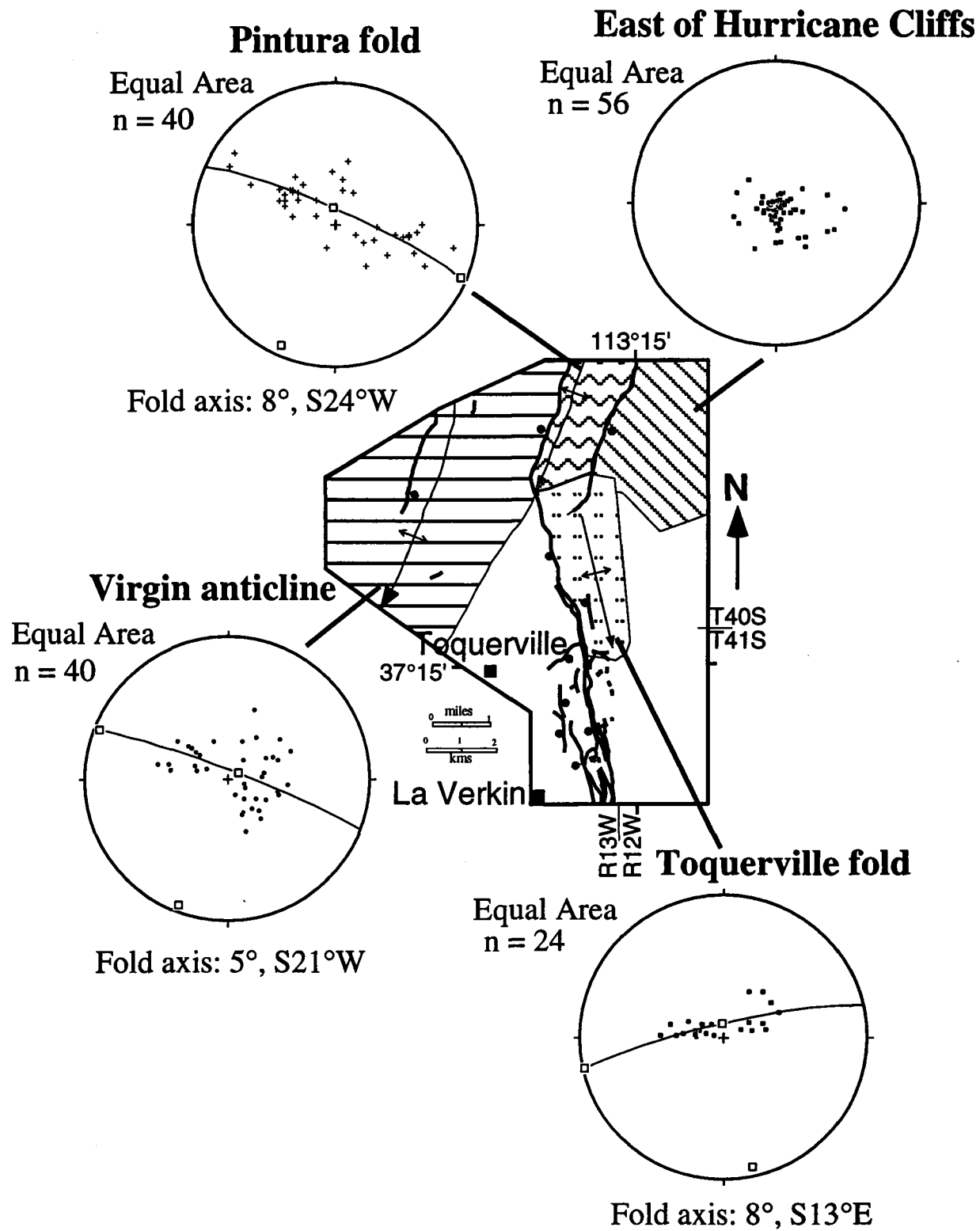


Figure 11. Map showing domains within the area of Figure 5 (marked with differing patterns) where attitudes were collected, and the equal area stereoplots of poles to bedding for domains. Great circles through the poles picked by the Bingham axial distribution analysis using Stereonet by R.W. Allmendinger.

may have been modified by footwall flexure but it is difficult if not impossible to determine if this is the case with the available data.

HISTORICAL SEISMICITY AND SEISMIC HAZARDS IN SOUTHWESTERN UTAH AND NORTHWESTERN ARIZONA

Historical seismic activity has been sufficient in southwestern Utah and northwestern Arizona to suggest a seismic hazard, but there have been no large, surface-rupturing earthquakes. Historical seismicity in the area generally has been diffuse, with several concentrations of activity and a few moderately large earthquakes (fig. 1). At least 20 earthquakes greater than M 4.0 occurred during this century in southwestern Utah and northwestern Arizona (Christenson and Nava, 1992).

The Hurricane fault lies near the southern end of the Intermountain Seismic Belt (ISB), a zone of relatively high seismic activity that extends from Montana to southern Utah and Nevada, and northern Arizona (Smith and Sbar, 1974; Smith and Arabasz, 1991). In southern Utah, the ISB coincides with the transition zone. The ISB is broad and poorly defined in southern Utah, and seismic activity diminishes substantially from northwestern to central and southern Arizona. Thus, the transition between the relatively active northern Basin and Range and the relatively inactive southern Basin and Range occurs in northwestern Arizona.

The historical record of seismic activity includes older earthquakes located primarily by felt reports (Arabasz and McKee, 1979; Dubois et al., 1982) and younger, instrumentally located events. Prior to establishment of a statewide seismic network by the University of Utah in 1962, epicentral locations and magnitude estimates were approximate. The detection threshold for earthquakes in southern Utah subsequently decreased to about M 2.5 around 1980 (Nava et al., 1990). The Arizona Earthquake Information Center (AEIC) at Northern Arizona University maintains a regional seismic network in northern Arizona, but AEIC coverage is limited in northwestern Arizona.

The epicenters of the two largest historical earthquakes in this region are located west of the west-dipping Hurricane fault (fig. 1). The largest event was a M 6.3 earthquake near Pine Valley, Utah, in 1902. This earthquake caused moderately severe damage in the epicentral region. The second largest earthquake was M 5.8 and occurred southeast of St. George, Utah, on September 2, 1992 (Arabasz et al., 1992b; Pechmann et al., 1992). The St. George earthquake had no foreshocks and only two aftershocks of $M \geq 2.0$. Hypocenters of 40 microaftershocks, constrained by data from portable seismographs operated by the University of Utah Seismograph Stations, define the fault plane of the St. George earthquake. The epicenter was located ~ 15 km

west of the Hurricane fault (Pechmann et al., 1992; Lay et al., 1994), the hypocenter depth is ~ 15 km, and the preferred fault plane dips west at about 45° ; thus, it projects to the surface approximately at the trace of the Hurricane fault. The locations of these earthquakes raises the intriguing possibility that the 1992 event, and possibly the 1902 event, actually involved limited rupture on the Hurricane fault (Pechmann et al., 1992). No surface rupture has been documented for either the Pine Valley or St. George earthquakes (Black, et al., 1995).

Earthquake swarms are relatively common in southwestern Utah. Two moderate events ($M \sim 5$) occurred within a swarm near Cedar City in 1942. Other swarms occurred in 1971 in the Cedar City-Parowan Valley and in 1980–81, when two separate clusters of seismicity were recorded on each side of the Hurricane fault near Kanarrville (Arabasz and Smith, 1981; Richins et al., 1981). A swarm of more than 60 earthquakes occurred on the Hurricane fault near Cedar City, Utah, on June 28–29, 1992; the largest registered M 4.1 (Arabasz et al., 1992a). This swarm occurred within an hour of the Landers, California, M 7.3 earthquake, 490 km southwest of Cedar City (Hill et al., 1993).

The largest historical earthquake in northwestern Arizona was the 1959 Fredonia earthquake ($M \sim 5.7$; Dubois et al., 1982). Since 1987, the northwestern quarter of Arizona has been quite seismically active. More than 40 events with $M > 2.5$ occurred, including the 1993 M 5.4 Cataract Creek earthquake located between Flagstaff and the Grand Canyon (Bausch and Brumbaugh, 1994).

Regional seismic hazards

Assessing seismic hazards is particularly important in southwestern Utah and northwestern Arizona because of the current population and construction boom. Zion National Park and the western part of Grand Canyon National Park also could experience damage from large earthquakes. Interstate 15, one of the major north-south transportation corridors of the Intermountain region, crosses southwestern Utah and northwestern Arizona and closely parallels the northern 40 km of the Hurricane fault.

A variety of potential earthquake-related hazards are recognized in southwestern Utah and northwestern Arizona (Christenson and Nava, 1992). Damage to structures as a result of strong ground shaking is likely the greatest hazard posed by large earthquakes in this region. The largest historical earthquakes have caused moderate to substantial damage to structures, and the potential exists for much larger earthquakes. A number of ancillary hazardous processes could occur as well, including surface displacement along the fault rupture, liquefaction along perennial streams like the Virgin River, rock falls, landslides, and flooding from dam failure (Christenson and Nava, 1992).

The potential for damage resulting from earthquakes in a region may be considered on a probabilistic basis. Probabilistic assessments typically depend on analysis of the historical seismic record, sometimes utilizing available information on late Quaternary fault behavior as well, to estimate the frequency of earthquakes of various magnitudes. Key data for such analyses are the frequency-magnitude relationship for the region, and if fault data are included, the locations of faults that are likely sources for large earthquakes. As was noted earlier, the frequency and size of large earthquakes in southwestern Utah and northwestern Arizona are poorly constrained. Probabilistic assessments of seismic hazard in this region suggest that it is moderate, with peak ground accelerations of <0.2 g that have a ten percent chance of exceedence in 50 years (Algermissen et al., 1990). The area lies within seismic zone 2B of the Uniform Building Code. Incorporation of the Hurricane and Toroweap-Sevier faults as discrete seismic sources in probabilistic analyses increases acceleration values, especially if longer intervals are considered (Euge et al., 1992; Bausch and Brumbaugh, 1994).

Seismic hazards caused by the 1992 St. George, Utah, earthquake

Ground shaking and slope failures were the dominant geologic effects of the 1992 St. George earthquake (Black et al., 1995). Ground shaking caused damage to buildings in Hurricane, La Verkin, Washington, St. George, and other communities (fig. 1). A destructive landslide in the town of Springdale destroyed three homes and forced the temporary evacuation of condominiums and businesses around the periphery of the slide. Numerous rock falls throughout the region caused minor damage. The earthquake also produced liquefaction along the Virgin River, changes to the springs at Dixie Hot Springs, and water-level fluctuations at the Quail Creek Main Dam (fig. 3). Carey (1995) estimated total earthquake losses from direct damage, response costs, and lost property values at about \$1 million.

Ground shaking. Ground shaking is typically the most widespread and damaging earthquake hazard, but the region experienced relatively little damage from ground shaking during the 1992 earthquake. The maximum Modified Mercalli intensity (MMI) of the St. George earthquake was a weak VII in the Hurricane-Toquerville-Virgin area with a strong VI MMI for the epicentral region near St. George (Olig, 1995) (fig. 12). Many older, unreinforced masonry buildings showed minor structural damage in the area of maximum intensity, but cracked chimneys and fallen plaster were the predominant damage in St. George. Pechmann et al., (1995) estimated a moderate to high stress drop associated with the main shock, with a minimum value of 25 bars. Neither this stress drop nor the radiation pattern pre-

dicted from the earthquake location and mechanism provided them with any simple explanation for the relative lack of damage in St. George. Only one strong-motion record of the earthquake was obtained, but it was from Cedar City, 72 km north of the epicenter. Susan Olig (verbal communication reported in Black et al., 1995) used the empirical relation of Campbell (1987) to estimate a peak horizontal acceleration of about 0.2 g for St. George.

Slope failures. The most dramatic geologic effect of the St. George earthquake was the triggering of the 14 million m^3 Springdale landslide (Black et al., 1995) (fig. 13). This landslide, the largest of two landslides in Springdale resulting from the earthquake, is a complex block slide that likely involves both rotational and translational elements. The slide measures roughly 490 m from the main scarp to the toe, with a width of about 1,100 m and a surface area of about 40 hectares. The landslide has a clearly defined main scarp dipping 57 to 77° that is 8–15 m high along most of its length, as well as numerous fissures and minor scarps that form a broken topography within the slide mass. These scarps and fissures indicate that the landslide likely moved in several coherent blocks. Smaller discrete landslides also developed on the oversteepened toe. The basal slide plane is in the Petrified Forest Member of the upper Triassic Chinle Formation. The landslide involved this unit, the overlying Dinosaur Canyon Member of the lower Jurassic Moenave Formation (fig. 2), and a surficial cap of colluvium.

Detailed geologic mapping of the Springdale area (Solomon, 1996a), part of a comprehensive study of geologic hazards conducted in response to the Springdale landslide, shows that ancient landslide deposits are common in the area. The Springdale landslide is only one of 69 mapped slope failures in the 41 km^2 Springdale area (Solomon, 1996b). The largest of these landslides is the Pleistocene Eagle Crags landslide which, with a volume of about 140 million m^3 (Shroder, 1971), is an order of magnitude larger than the Springdale landslide. However, the Springdale landslide is particularly significant because its distance from the earthquake epicenter, 44 km, far exceeds the farthest distance, 18 km, at which similar landslides have been triggered in earthquakes of the same magnitude worldwide (Jibson and Harp, 1996).

At least part of the hillside that moved as a result of the St. George earthquake had been moving within the past few decades. Hamilton (1984) monitored a portion of the slope from August 1974 to June 1975 and documented 3.3 cm of movement over 9 months. Dynamic analysis of the landslide by Jibson and Harp (1996) using Newmark's (1965) method yielded maximum predicted coseismic displacements of about 1–8 cm, which is supported by eyewitness accounts of small coseismic displacement followed, after several minutes, by catastrophic failure over a 10-hour period. Jibson and Harp (1996) attribute movement of the Spring-

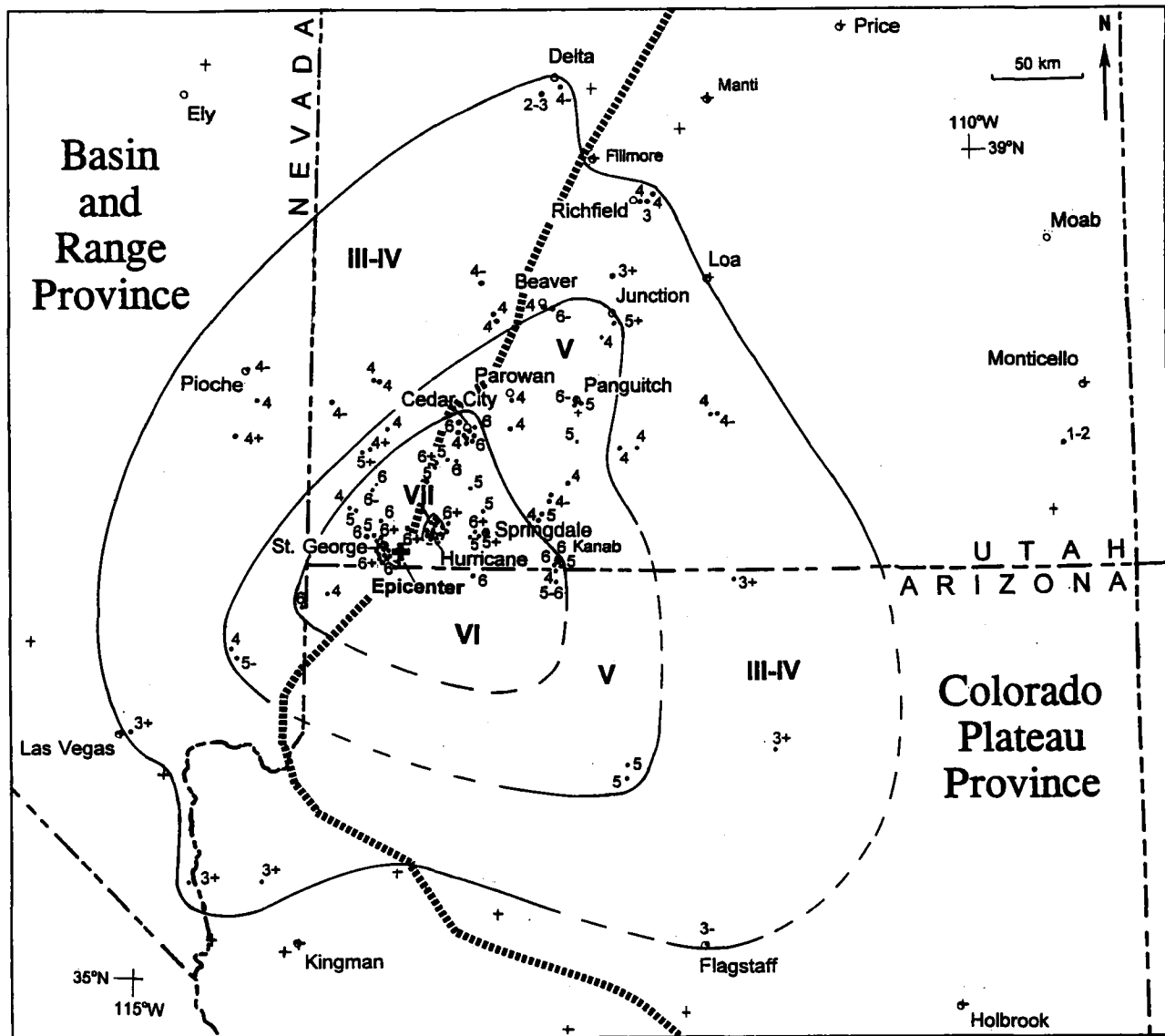


Figure 12. Preliminary isoseismal map for the M_L 5.8 September 2, 1992, St. George earthquake (from Olig, 1995). The map was developed from observations at 242 sites (not all are shown). Preliminary intensities from 85 sites were provided by the National Earthquake Information Center. Sites where shaking was felt are marked by solid circles with a number (given in Arabic numerals) for the intensity assigned (where sites are clustered a single label for the predominant intensity is given); crosses mark sites where shaking was not felt. Location of the epicenter is marked by a bold cross (epicenter obscures 5 sites of intensity VI). Isoseismal lines are dashed where poorly constrained.

dale landslide to a less stable geometry of the failed slope in an area of headward broadening of the Virgin River Canyon. The unstable slope configuration was susceptible to seismically triggered movement, and the catastrophic failure following small coseismic displacement was most likely the result of the time-dependent deformation behavior of plastic clays in the Petrified Forest Member (fig. 2). According to Jibson and Harp (1996), such behavior retards the deformation response of such clay to the brief, high-frequency

stresses induced by seismic shaking. Stress relief is achieved through post-seismic deformation analogous to viscous creep, and the resultant reduction in shear strength along the pre-existing slip surface rendered the slide statically unstable.

Rock falls. Black et al., (1995) report numerous rock falls resulting from the St. George earthquake. Rock falls occurred along the steep cliffs above the Virgin River west of Springdale, in the Hurricane Cliffs along the Hurricane fault, and in St. George along the Red Hills and West Black Ridge. In



Figure 13. Aerial view of the Springdale landslide (from Black et al., 1995). Utah Highway 9 is at the bottom; short arrows show the main scarp of the landslide, long arrows indicate three houses damaged, medium arrow locates an abandoned water tank, and dashed line outlines landslide toe.

most cases, the rock falls either occurred in uninhabited areas without resultant damage, or fell onto roads and were quickly cleared away. Rock falls damaged a truck, a car, a wall, footpaths, and irrigation lines in southwestern Utah. Numerous fresh rock-fall scars, probably from rock falls caused by the earthquake, occur in cliffs of the Triassic Moenkopi Formation near the Arizona border.

Liquefaction. Liquefaction features observed by Black et al., (1995) were lateral spreads, sand blows, and caved stream banks in alluvium along the Virgin River from 2 km south of Bloomington to 6 km west of Hurricane (fig. 3). Involved sediment was poorly graded channel sands, commonly covered by thin overbank deposits of silt and clay. The largest lateral spread extended along the river for 60 m and perpendicular to the river for 20 m. The largest sand blow was 50 cm in diameter. Black et al., (1995) compared measurements from 17 lateral-spread features to calculated liquefaction severity index (LSI) values in the area affected by the earthquake. The LSI expresses the potential maxi-

mum magnitude of differential deformation resulting from liquefaction of susceptible soils (Youd and Perkins, 1987). Probabilistic values of LSI in Utah are related to earthquake magnitude and distance from the earthquake source by an equation developed by Mabey and Youd (1989). Measured deformation at sites nearest the earthquake epicenter was generally less than corresponding LSI values, but calculated LSI values more closely predicted measured displacements at greater distances.

Hydrologic effects. Everitt (1992) described changes in the hydrology of Dixie Hot Springs at Pah Tempe Resort, 3 km north of Hurricane along the Hurricane fault (fig. 3). The spring water is probably heated by a high geothermal gradient resulting from Quaternary volcanic activity, flows through joints and faults of small displacement, and issues from cavities in the Kaibab Formation near the Virgin River (Mundorf, 1970). Combined spring flow in 1966 was 328.4 m³/sec, with a temperature ranging from 37.8–42.2°C (Mundorf, 1970). Following the St. George earthquake, flow from

the springs decreased dramatically, water emerged from new sources at a lower elevation and closer to the river, and flow ceased at springs more than 0.3 m above the river. Everitt (1992) credits these changes to fracturing of barriers between the aquifer and river bed, creating new outlets at lower elevations and causing water levels to drop below the elevation of the resort.

Borgione (1995) documented earthquake-induced changes in pore-pressure in the embankment and foundation measured in piezometers at the Quail Creek Main Dam, 8 km west of Hurricane (fig. 3). The dam is a zoned earthfill embankment, with the dam axis roughly parallel to the strike of beds in the Triassic Moenkopi Formation which dip downstream along the southeast flank of the Virgin anticline. Water-level fluctuations along the dam's embankment and abutments ranged from a rise of nearly 1.5 m to a drop of nearly 5.2 m immediately after the earthquake. However, none of the design parameters of the dam were exceeded and the dam was considered safe for continued operation.

SUMMARY AND CONCLUSIONS

The 250-km long Hurricane fault in southwestern Utah and northwestern Arizona is segmented. Identification of earthquake rupture segment boundaries is critical for seismic-hazard analysis. Two geometric segment boundaries have been identified in the northern 60 km of the Hurricane fault, which may correspond to rupture segment boundaries. One geometric segment boundary, near the Utah-Arizona state line, was identified on the basis of fault geometry, changes in the amount of stratigraphic separation across the fault bend, fault scarp morphology, and a small mafic intrusion that crops out at the bend (Taylor and Stewart, in review). The other fault segment boundary, near Toquerville, Utah, was identified using fault geometry, fault scarp morphology, slip direction, and shortening structures near the bend (Stewart and Taylor, 1996).

Shortening structures are associated with extensional faulting on the Hurricane fault. Neogene north-south crustal shortening was interpreted from deformation of late Tertiary and Quaternary sediments in the New Harmony basin where a syncline formed adjacent to the Hurricane fault. The Toquerville fold, a footwall structure near Toquerville, Utah, is related to footwall flexure following initial faulting on the Hurricane fault. In addition, a small anticline that

folds Quaternary basalt in the hanging wall of the fault and perpendicular to a fault bend was used to identify a geometric segment boundary (Stewart and Taylor, 1996).

A few short, isolated Quaternary fault scarps are present along the Hurricane fault. Scarps as high as 20 m near the Utah-Arizona border suggest multiple faulting events. Near the geometric segment boundary near Toquerville, two fault scarps, 6 and 3 m high, are formed in Quaternary (?) alluvium and bedrock north of the boundary. South of the boundary no scarps exist, but offset in a Quaternary (?) gravel deposit was observed in a stream channel. These fault scarps and the offset alluvium show that the Hurricane fault is active, although no historical surface ruptures have occurred.

Further suggestive evidence that the Hurricane fault is active is the 1992 St. George M 5.8 earthquake as well as other moderate earthquakes and earthquake swarms in the region. Moderate earthquakes occur with enough frequency to render a seismic risk in this rapidly growing portion of Utah. Seismic hazards such as ground shaking, slope failures, rock falls, liquefaction, and ground-water level changes resulted from the St. George earthquake and these hazards remain.

ACKNOWLEDGMENTS

We gratefully acknowledge financial support provided from the following institutions: Geological Society of America, Sigma Xi Grants-in-Aid, the University of Nevada Las Vegas Graduate Student Association, the Business and Professional Women's Foundation Career Advancement program, the University of Nevada Las Vegas Geoscience Department Scroungers Scholarship to Stewart (formerly Schramm), and the University of Nevada Las Vegas-National Science Foundation Women in Science program (Cooperative Agreement OSR-9353227) to Stewart and Taylor; a University of Nevada, Las Vegas Grant and Fellowships Committee Research Grant to Taylor. Pearthree would like to thank Chris Menges of the U.S. Geological Survey, who introduced him to the Hurricane fault and the Arizona Strip. Thorough reviews of the manuscripts and road log were kindly provided by Gary Christenson, Ben Everitt, Kimm Harty, Paul Link, and Susan Olig.

References for this paper are provided after the field trip log in the Combined References.

Geologic hazards in the region of the Hurricane fault

WILLIAM R. LUND

*Utah Geological Survey, Southern Utah University, Box 9053,
Cedar City, Utah 84720*

ABSTRACT

Complex geology and variable topography along the 250-kilometer-long Hurricane fault in northwestern Arizona and southwestern Utah combine to create natural conditions that can present a potential danger to life and property. Geologic hazards are of particular concern in southwestern Utah, where the St. George Basin and Interstate-15 corridor north to Cedar City are one of Utah's fastest growing areas. Lying directly west of the Hurricane fault and within the Basin and Range–Colorado Plateau transition zone, this region exhibits geologic characteristics of both physiographic provinces. Long, potentially active, normal-slip faults displace a generally continuous stratigraphic section of mostly east-dipping late Paleozoic to Cretaceous sedimentary rocks unconformably overlain by Tertiary to Holocene sedimentary and igneous rocks and unconsolidated basin-fill deposits. Geologic hazards (exclusive of earthquake hazards) of principal concern in the region include problem soil and rock, landslides, shallow ground water, and flooding.

Geologic materials susceptible to volumetric change, collapse, and subsidence in southwestern Utah include: expansive soil and rock, collapse-prone soil, gypsum and gypsiferous soil, soluble carbonate rocks, and soil and rock subject to piping and other ground collapse. Expansive soil and rock are widespread throughout the region. The Petrified Forest Member of the Chinle Formation is especially prone to large volume changes with variations in moisture content. Collapse-prone soils are common in areas of Cedar City underlain by alluvial-fan material derived from the Moenkopi and Chinle Formations in the nearby Hurricane Cliffs. Gypsiferous soil and rock are subject to dissolution which can damage foundations and create sinkholes. The principal formations in the region affected by dissolution of carbonate are the Kaibab and Toroweap Formations; both formations have developed sinkholes where crossed by perennial streams. Soil piping is common in southwestern Utah where it has damaged roads, canal embankments, and water-retention structures. Several unexplained sinkholes near the town of Hurricane possibly are the result of collapse of subsurface volcanic features.

Geologic formations associated with slope failures along or near the Hurricane fault include rocks of both Mesozoic and Tertiary age. Numerous landslides are present in these materials along the Hurricane Cliffs, and the Petrified Forest Member of the Chinle Formation is commonly associated with slope failures where it crops out in the St. George Basin. Steep slopes and numerous areas of exposed bedrock make rock fall a hazard in the St. George Basin. Debris flows and debris floods in narrow canyons and on alluvial fans often accompany intense summer cloudburst thunderstorms.

Flooded basements and foundation problems associated with shallow ground water are common on benches north of the Santa Clara River in the city of Santa Clara. Stream flooding is the most frequently occurring and destructive geologic hazard in southwestern Utah. Since the 1850s, there have been three major riverine (regional) floods and more than 300 damaging flash floods. Although a variety of flood control measures have been implemented, continued rapid growth in the region is again increasing vulnerability to flood hazards.

Site-specific studies to evaluate geologic hazards and identify hazard-reduction measures are recommended prior to construction to reduce the need for costly repair, maintenance, or replacement of improperly placed or protected facilities.

INTRODUCTION

The geology along the nearly 250-km-long Hurricane fault is both complex and variable. Geologic units range from Paleozoic sedimentary rocks to late Quaternary basalt flows and unconsolidated Holocene basin-fill deposits. The topography along the fault is similarly variable, ranging from nearly flat valley bottoms and plateaus to steep cliffs and deep canyons. As expected in such diverse terrain, natural conditions commonly exist that present a risk or potential danger to life and property. However, only in southwestern Utah near the northern end of the Hurricane fault is the population sufficient to make geologic hazards a significant concern. As a companion paper to the preceding one (Stewart et al., this volume), this report provides an overview of geologic hazards, exclusive of seismic hazards, affecting communities near the Hurricane fault. A number of figures from Stewart et al., (this volume) are referred to in this paper; therefore, the figures in both papers are numbered consecutively. The principal geologic hazards present include: problem soil and rock, landslides, shallow ground water, and flooding.

The St. George Basin and the Interstate-15 (I-15) corridor north to Cedar City (fig. 1) lie immediately west of the Hurricane fault and are one of Utah's fastest growing areas. In 1970, Washington and Iron Counties, Utah's two southwestern most counties, had populations of 10,270 and 10,780, respectively (Utah Governor's Office of Planning and Budget, 1996). Bureau of Census population estimates for July 1, 1994 place the population of those counties at 66,125 and 24,426, respectively. About 55,000 people live in and around St. George, a popular resort and retirement community. Although growth in Cedar City has been less rapid (1996 estimated population 24,000), the arrival of several new industries, continued expansion as a center of local and state government, and conversion of Southern Utah University from college to university status has produced significant new development there as well.

SETTING AND GENERAL GEOLOGY

St. George and the surrounding communities of Washington and Santa Clara lie within the St. George Basin (fig. 3). The basin is a fault block within a broad system of faults that forms a transition zone between the Colorado Plateau and Basin and Range physiographic provinces in extreme southwestern Utah. The basin has been downdropped 1,800–2,400 m along the Hurricane fault to the east and is bounded on the west by the Grand Wash fault (fig. 1). I-15 enters the basin from the Virgin River Gorge to the southwest and departs along Ash Creek to the northeast through a narrow gap between the Hurricane Cliffs (footwall of the Hurricane fault) and the Pine Valley Mountains (fig. 3). The interstate parallels the Hurricane Cliffs for another approximately 40 km to Cedar City. At Cedar City, the Hurricane

Cliffs form the boundary between the Colorado Plateau and the Basin and Range physiographic provinces.

Bedrock in the St. George Basin consists of Permian, Triassic, and Jurassic sedimentary rocks that include limestone, sandstone, siltstone, shale, conglomerate, and gypsum (fig. 2). Upper Jurassic, Cretaceous, and lower Tertiary rocks found to the north in the Pine Valley Mountains have been eroded from the basin, but upper Tertiary and Quaternary basalts and thin, discontinuous deposits of unconsolidated Quaternary clay, silt, sand, and gravel are present. The basalts flowed down paleostream channels. Subsequent erosion of the surrounding sedimentary rocks has inverted the topography, and the basalt flows now cap long, narrow, south-trending ridges. Sedimentary rocks in the St. George Basin dip gently (5–10°) to the northeast except in the vicinity of the Virgin anticline (see Stewart et al., this volume), which trends northeasterly through the basin east and south of St. George. The anticline is a broad, generally symmetrical fold with maximum flank dips of 25 to 30° to the southeast and northwest. Several north-south-striking normal faults are present north of St. George and in the Washington area. The most prominent of these is the Washington fault (fig. 1; Earth Science Associates, 1982; Anderson and Christenson, 1989).

The Hurricane Cliffs bound the St. George Basin on the east and continue northward past the towns of Hurricane, La Verkin, and Toquerville to where Ash Creek enters the basin from the north (fig. 3). Bedrock exposed along the cliffs consists of Permian, Triassic, and Jurassic sedimentary rocks including limestone, sandstone, gypsiferous mudstone, shale, and conglomerate capped locally by Quaternary basalt flows. The basalt flows are displaced down to the west across the Hurricane fault (Hamblin, 1963; Stewart and Taylor, 1996) and overlie the Jurassic Navajo Sandstone, which crops out over a broad area in the St. George Basin between the Hurricane Cliffs and the Virgin anticline. At Ash Creek, Permian and Triassic sedimentary rocks, locally capped by Quaternary basalt, form the Hurricane Cliffs east of I-15. Intrusive igneous rocks and basalt (the same flow found east of I-15 downdropped across the Hurricane fault) are west of the freeway along the flanks of the Pine Valley Mountains. At the top of the canyon of Ash Creek, I-15 enters the south end of Cedar Valley and follows the Hurricane Cliffs to Cedar City. Cedar Valley is a typical basin-and-range valley, downdropped along bordering faults (chiefly the Hurricane fault to the east) and filled with unconsolidated and semi-consolidated Quaternary basin-fill deposits.

Cedar City lies at the base of the Hurricane Cliffs, mostly on alluvial-fan material deposited by Coal Creek, which drains from the cliffs. More recent development has extended west of I-15 into the Cross Hollow Hills and north onto the Fiddlers Canyon alluvial fan. The Cross Hollow Hills are underlain chiefly by Miocene to Pliocene fanlom-

erate and Pleistocene basalt (Averitt and Threet, 1973). The Fiddlers Canyon fan consists of a coarse mixture of gravel, cobbles, and boulders deposited where Fiddlers Creek issues from the Hurricane Cliffs. Bedrock exposed in the Hurricane Cliffs east of Cedar City consists of a steeply east-dipping to locally overturned sequence of faulted and folded Lower Triassic to Upper Cretaceous sedimentary units including limestone, shale, mudstone, siltstone, sandstone, and minor conglomerate (Averitt and Threet, 1973; fig. 2).

GEOLOGIC HAZARDS

Geologic hazards (exclusive of earthquake hazards) of principal concern in the region include problem soil and rock, landslides, shallow ground water, and flooding.

Problem Soil and Rock

Geologic materials susceptible to volumetric changes, collapse, and subsidence are common in southwestern Utah. Particularly troublesome are (1) expansive soil and rock, (2) collapsible soil, (3) gypsum and gypsiferous soil, (4) limestone karst, and (5) soil piping and other ground collapse.

Expansive Soil and Rock. Expansive soil and rock is the most common problem deposit in southwestern Utah (Mulvey, 1992). The Triassic Chinle and Moenkopi Formations and the Cretaceous Dakota and Tropic Formations (fig. 2) are clay-rich and are the chief sources of expansive material in the region. The most common clay mineral associated with these deposits is montmorillonite, which expands and contracts with changes in moisture content.

Expansive deposits are extensive in the St. George Basin where the Petrified Forest Member of the Chinle Formation (locally known as the "blue clay") crops out. Cracking of walls and foundations has occurred in buildings in Santa Clara (fig. 14), and in Washington and the southern part of St. George. Expansive clays are also present in the Shnabkaib Member of the Moenkopi Formation. A housing development recently constructed on this unit in the Washington area will bear watching in the future for evidence of soil problems. The Chinle, Moenkopi, Tropic, and Dakota Formations all crop out in the Hurricane Cliffs east of Cedar City, but little development has taken place there, so expansive soils are not a widespread problem in the Cedar City area.

Collapsible Soil. Hydrocompaction, the phenomenon of subsidence in collapse-prone soil, occurs in loose, dry, low density materials that decrease in volume when saturated for the first time following deposition (Costa and Baker, 1981). Alluvial fans containing debris-flow deposits consisting of 10 to 15 percent clay are the most common environment for collapse-prone soils.



Figure 14. Cracks in the wall of a home on the Santa Clara Bench caused by expansion of the underlying Petrified Forest Member of the Chinle Formation.

Collapse-prone soils are widely distributed throughout those areas of Cedar City underlain by alluvial fans that have fine-grained sedimentary rocks in their drainage basins. Measured collapse strains of 5 to 15 percent are common in these fan deposits (Rollins et al., 1992). The Triassic Moenkopi and Chinle Formations, which crop out extensively along the Hurricane Cliffs east of town and in Coal Canyon, account for much of the collapsible soil material in Cedar City. Collapse-induced settlements have damaged many structures in Cedar City, and settlements became so great (up to 1.8 m) in 1977 on the northeast side of town that 14 homes had to be removed from their foundations and moved to new locations (Kaliser, 1978a). Collapsible soils have also been reported near the Hurricane airport, where Kaliser (1978b) documented as much as 1.6 m of subsidence.

Gypsiferous Soil and Rock. Gypsum is a primary component of some rocks and the soils derived from them. Gypsiferous deposits are subject to settlement caused by dissolution of the gypsum which creates a loss of internal structure and volume (Mulvey, 1992). Gypsiferous soils are common in southwestern Utah, particularly along the base of the Hurricane Cliffs and in parts of St. George. The Shnabkaib Member of the Moenkopi Formation and the Carmel Formation are the principal gypsum-bearing rock units in the area (fig. 2). Dissolution of gypsum can damage foundations, and create sinkholes. The January 1, 1989, catastrophic failure of the Quail Creek dike (fig. 15) located on the crest of the Virgin anticline about 22 km northeast of St. George was in part attributed to piping caused by dissolution of gypsum in the bedrock of the dike foundation. The unit involved was the Shnabkaib Member of the Moenkopi Formation, which post-failure investigation showed to be as much as 50 percent gypsum in some places beneath the dike (Gourley, 1992).



Figure 15. Quail Creek dike failure, January 1, 1989; dike was constructed across axial trace of the Virgin anticline on the gypsum-rich Shnabkaib Member of the Moenkopi Formation (photo credit, Ben Everitt, Utah Division of Water Resources). Location shown on Figure 3.

Strongly cemented gypsum layers in unconsolidated deposits in the shallow subsurface commonly mark the water table and locally form a confining layer causing artesian conditions in the St. George area (Christenson, 1992). The layer, locally termed "water rock," may have been deposited as shallow ground water evaporated in soil voids. The extent of the "water rock" has not been determined, but this layer has been encountered at shallow depths in many places in the St. George area. Changes in ground-water conditions may result in local dissolution of the layer and eventual subsidence.

Gypsum is also an inherently weak material which can deform or fail when loaded with the weight of a structure. In addition, when dissolved in water, gypsum forms sulfuric acid and sulphate which react with certain types of cement and weaken foundations (Bell, 1983).

Limestone Karst. Karst features are caused by ground- and surface-water dissolution of carbonate rocks, chiefly limestone and dolomite. The Kaibab and Toroweap Formations (fig. 2), which crop out in several areas along and near the Hurricane fault, are the principal carbonate rock units affected by dissolution in southwestern Utah. Due to the area's dry climate, most of the karst features are probably relict and related to wetter climates during the Pleistocene, although dissolution may be presently occurring where limestone crops out along the Virgin River and its tributaries. In the spring of 1985, a large, open sinkhole appeared in the bed of the Virgin River just downstream from a new diversion dam in Timpoweap Canyon (fig. 16) and swallowed the entire flow of the river for several months. The water captured by the sinkhole recharged the fractured limestone aquifer and almost immediately caused changes in discharge, temperature, and chemistry at springs located at the mouth



Figure 16. In 1985, a sinkhole in the Toroweap Formation opened suddenly in the bed of the Virgin River and swallowed the entire flow of the river for several months. The sinkhole is now behind an earthen dike on the south side of the river (shadow area at the base of the canyon wall).

of the canyon nearly three miles downstream (Everitt and Einert, 1994). In July 1996, a small gravel- and cobble-filled sinkhole developed in the channel of La Verkin Creek where the stream crosses the Kaibab Formation. An estimated 85 L/sec of flow disappeared into the sinkhole (Lund, 1996). A small coffer dam and pipeline were constructed to divert the stream around the sink area.

Soil Piping and Other Ground Collapse. Soil piping, removal of material by subsurface flow of water, is a common phenomenon in southwestern Utah. Soil piping forms open voids and subsurface cavities into which overlying material may collapse. The three prerequisites for piping are: a susceptible deposit, usually fine-grained alluvium or poorly cemented sedimentary rock (claystone, siltstone); subsurface flow of water; and a free face for the exit of seepage water and entrained sediment. In arid areas such as southwestern Utah, piping is an important process in the headward extension of gullies, which may intersect and damage roads. Piping has also affected canal embankments and water-retention structures constructed of fine-grained material near St. George (Christenson and Deen, 1983).

Several sinkholes of undetermined origin have opened over time in the vicinity of the town of Hurricane (Solomon, 1993). Although never investigated in detail because they have not damaged or threatened structures or roads, all have been in unconsolidated alluvium near outcrops of Miocene to Quaternary basalt flows, suggesting that the sinkholes result from the collapse of buried volcanic structures (e.g., lava tubes, blowholes). The most recent sinkhole opened in January 1993, about four months after the September 1992, M_L 5.8, St. George earthquake (Christenson, 1995). The sinkhole, which was 6 m wide and 4 m deep, probably opened in response to the collapse at depth



Figure 17. Truman Drive landslide on the south side of the Santa Clara Bench; failure occurred in the Petrified Forest Member of the Chinle Formation.

of a volcanic feature affected by earthquake ground shaking (Solomon, 1993).

Landslides

Landslides, including rock falls, large slump-type failures, debris and earthflows, and debris slides are common in southwestern Utah (Harty, 1992). Along the Hurricane fault, the geologic formations most commonly associated with slope failures are the Triassic Moenkopi and Chinle Formations, the Cretaceous Tropic and Dakota Formations, and the Tertiary Claron Formation (fig. 2). In Iron County, numerous landslides in these formations are located along and just east of the Hurricane Cliffs. Two examples are the Green Hollow and Square Mountain landslides located about 3.2 and 6.4 km, respectively, south of Cedar City. These large, complex, prehistoric landslides are failures in the Dakota Formation and involve approximately 221 and 36 million m³ of material, respectively (Harty, 1992). The landslides likely failed in the late Pleistocene under wetter climatic conditions, but the Green Hollow landslide has produced historical earth and debris flows. A housing development has been approved on this landslide and several large homes have been constructed there.

Landslides in the St. George area are predominantly in the Petrified Forest Member of the Chinle Formation (Harty, 1992). A high clay content and low shear strength make the Petrified Forest Member (blue clay) prone to failure. Slumps in this unit have damaged roads, canals, and utility lines. In 1992, a reactivation of a failure in the Petrified Forest Member where it crops out along the south edge of Santa Clara damaged a utility line and removed most of the backyard of a home at the top of the bench (Lowe, 1992; fig. 17).

Many steep slopes and areas of exposed bedrock make rock fall a prevalent hazard in the St. George Basin (fig. 18),



Figure 18. Rock-fall hazard in Bloomington area in southern St. George.

as was demonstrated in 1984 when a large boulder rolled down the east side of West Black Ridge narrowly missing an office building. Studies by a geological consultant and the Utah Geological Survey (Christenson, 1985) identified numerous other unstable boulders on the slope and led to a modification of the slope and construction of a catch fence to better protect the building.

Debris flows may occur during the summer months in southwestern Utah canyons and on alluvial fans at their mouths. They typically develop in response to intense cloud-burst thunder storms of short duration. For that reason, debris flows and associated flash floods are almost impossible to predict and present a significant hazard for back-country travel.

Shallow Ground Water

Shallow ground water can flood basements, septic-tank soil-absorption systems, and other subsurface structures and may reduce foundation stability by decreasing soil bearing strength and increasing liquefaction susceptibility during earthquakes (Christenson, 1992). Shallow ground water at depths of less than 3 m is found in unconsolidated deposits along river flood plains and adjacent lowlands in the St. George Basin. Ground-water levels fluctuate seasonally and annually in response to precipitation and stream flow. A very irregular shallow water table is found beneath St. George resulting from suballuvial discharge from bedrock aquifers (Christenson and Deen, 1983). Development in Santa Clara has been especially troubled by shallow ground-water problems. There, on terraces above the Santa Clara River, flooded basements are common as are foundation problems associated with expansion of the Petrified Forest Member of the Chinle Formation in response to wetting by ground water. Paleotopography on the Chinle Formation, now buried by several feet of fluvial gravel and sandy



Figure 19. Damage caused by a flash flood in July 1989 in the Fiddlers Canyon area of Cedar City (photo credit, Kimm Harty, Utah Geological Survey).

colian deposits, channels the ground water toward some areas and away from others. As a result, ground-water problems are irregularly distributed across the terrace. Except for a narrow zone along the flood plain of Coal Creek, shallow ground water is not a significant hazard in Cedar City.

Flooding

Stream flooding is the most frequently occurring and destructive geologic hazard in southwestern Utah (Lund, 1992). The high flood hazard results from the complex interaction of the area's rugged topography and seasonal weather patterns that bring moisture to the state. Two types of stream flooding typically occur in the region: riverine floods and flash floods. Riverine floods are usually regional in nature, last for several hours or days, and have return periods of 25 to more than 100 years. They commonly result from the rapid melt of the winter snowpack or from periods of prolonged heavy rainfall. Flash floods result from thunderstorm cloudbursts. They are localized, quickly reach a maximum flow, and then just as quickly diminish. Return periods for flash floods are erratic, ranging from a few hours to decades or longer for a particular drainage. Both types of flooding have caused extensive damage in the St. George and Cedar City areas.

Three major riverine floods have affected southwestern Utah since the area was settled in the 1850s. They occurred in 1966, 1983, and 1984. The 1966 flood resulted from an intense three-day rainstorm that produced record peak flows on the Virgin River (Butler and Mundorff, 1970). The flood

caused \$1.4 million (1966 dollars) damage to facilities and farm land, and remains the largest historical natural flood on the Virgin River. The 1983 and 1984 floods occurred in response to the rapid melting of maximum-of-record and greater-than-average snowpacks respectively. Both were statewide events that affected drainages throughout Utah. The occurrence of two major floods in successive years, each with an estimated return period of 25 to 100 years, demonstrates the unpredictable nature of riverine flooding.

Flash floods are by definition sudden, intense, and localized. The first recorded flash flood in southwestern Utah was on Coal Creek in Cedar City on September 3, 1853, when a "tremendous flood carried away bridges and dams, brought immense quantities of boulders and rocks into town, and did extensive damage to the iron works" (Woolley, 1946). Since then, over 300 damaging flash floods have been reported in southern Utah, and many towns such as Cedar City, St. George, and Santa Clara have experienced repeated flooding (Woolley, 1946; Butler and Marsell, 1972; Utah Division of Comprehensive Emergency Management, 1981).

In recent years, many communities have implemented various kinds of flood-control measures to eliminate or reduce the risk from flash floods. However, as rapid growth continues, development is outpacing these protective measures. Cedar City provides a good example; since 1853 extensive measures have been taken to control floods on Coal Creek. However, in the 1980s Cedar City expanded to the northeast onto alluvial-fan surfaces at the base of the Hurricane Cliffs. In July 1989, an afternoon thunderstorm over the cliffs produced approximately 2 cm of rain in 30 minutes (Harty, 1990). The resulting flood from canyons in the cliff advanced across the fan surface damaging residences and businesses, and burying parked cars (fig. 19).

SUMMARY AND RECOMMENDATIONS

Southwestern Utah, particularly in and around St. George and Cedar City, is one of the fastest growing regions of Utah. In addition to seismic hazards associated with the Hurricane and other potentially active Quaternary faults (see Stewart et al., this volume), development in the area may be adversely affected by problem soil and rock, landslides, shallow ground water, and flooding. Site-specific studies to evaluate hazards and identify hazard-reduction measures are recommended prior to construction in areas subject to geologic hazards (Christenson and Deen, 1983; Christenson, 1992). Initial planning and engineering to avoid or mitigate adverse geologic conditions can greatly reduce the need for costly repair, maintenance, or replacement of improperly placed or inadequately engineered structures.

References for this paper are provided after the field trip log in the Combined References.

Field Guide to Neotectonics, fault segmentation, and seismic hazards along the Hurricane fault in southwestern Utah and northwestern Arizona

MEG E. STEWART

Dames & Moore, One Blue Hill Plaza, Suite 530, Pearl River, New York 10965

WANDA J. TAYLOR

Department of Geoscience, University of Nevada, Las Vegas, 4505 Maryland Pkwy, Las Vegas, Nevada 89154

PHILIP A. PEARTHREE

Arizona State Geological Survey, 416 W. Congress St., Tucson, Arizona 45701

BARRY J. SOLOMON

HUGH A. HURLow

Utah Geological Survey, P.O. Box 146100, Salt Lake City, Utah 84114-6100

INTRODUCTION

This road log provides an overview of structures associated with the Hurricane fault from near the Arizona-Utah state line to Kanarrville, Utah. Stewart et al., (this volume) describe the general geologic background for this trip. Stops include Quaternary fault scarps, the landslide triggered by the 1992 St. George earthquake, and two fault segment boundaries. Shortening structures related to extension on the Hurricane fault will be visited. To conserve space, the figures and references for this road log are combined with Stewart et al., (this volume) and Lund (this volume). The field trip stops for this road log are shown in figure 20.

ROAD LOG

Day 0. Travel from Las Vegas to Hurricane, Utah

Log of Travel associated with the Hurricane fault GSA field trip

Incre- mental Mileage	Total Mileage
-----------------------------	------------------

0	0	Leave UNLV Geoscience Building and drive west on Harmon.
0.6	0.6	Continue straight (west) through the stop light at Harmon and Swenson.

0.1	0.7	At stop light at Paradise and Harmon turn right (north) onto Paradise.
0.4	1.1	At stop light at Flamingo and Paradise turn left (west) onto Flamingo. Continue straight (west) through lights along Flamingo past Las Vegas Boulevard ("The Strip").
1.5	2.6	Turn right (north) at ramp onto I-15 north.
8.2	10.8	The Cheyenne exit, a landmark only.
0.2	11.0	At 10:00 see the Las Vegas Range on the right (east) and Sheep Range on the left (west). The Sheep Range contains the Gass Peak thrust plate, a part of the Mesozoic Sevier orogenic belt (Longwell et al., 1965; Armstrong, 1968). The Las Vegas Range contains the Gass Peak thrust footwall. The Gass Peak thrust is exposed near the topographically low area that separates the two ranges (Longwell et al., 1965).
5.1	16.1	At ~2:00, are Frenchman and Sunrise Mountains. A Quaternary fault lies along the east side of Frenchman Mountain. These mountains contain Precambrian rocks on the east side, the Great Unconformity that separates Proterozoic and Paleozoic rocks and most of the Paleozoic stratigraphic section in this region. The

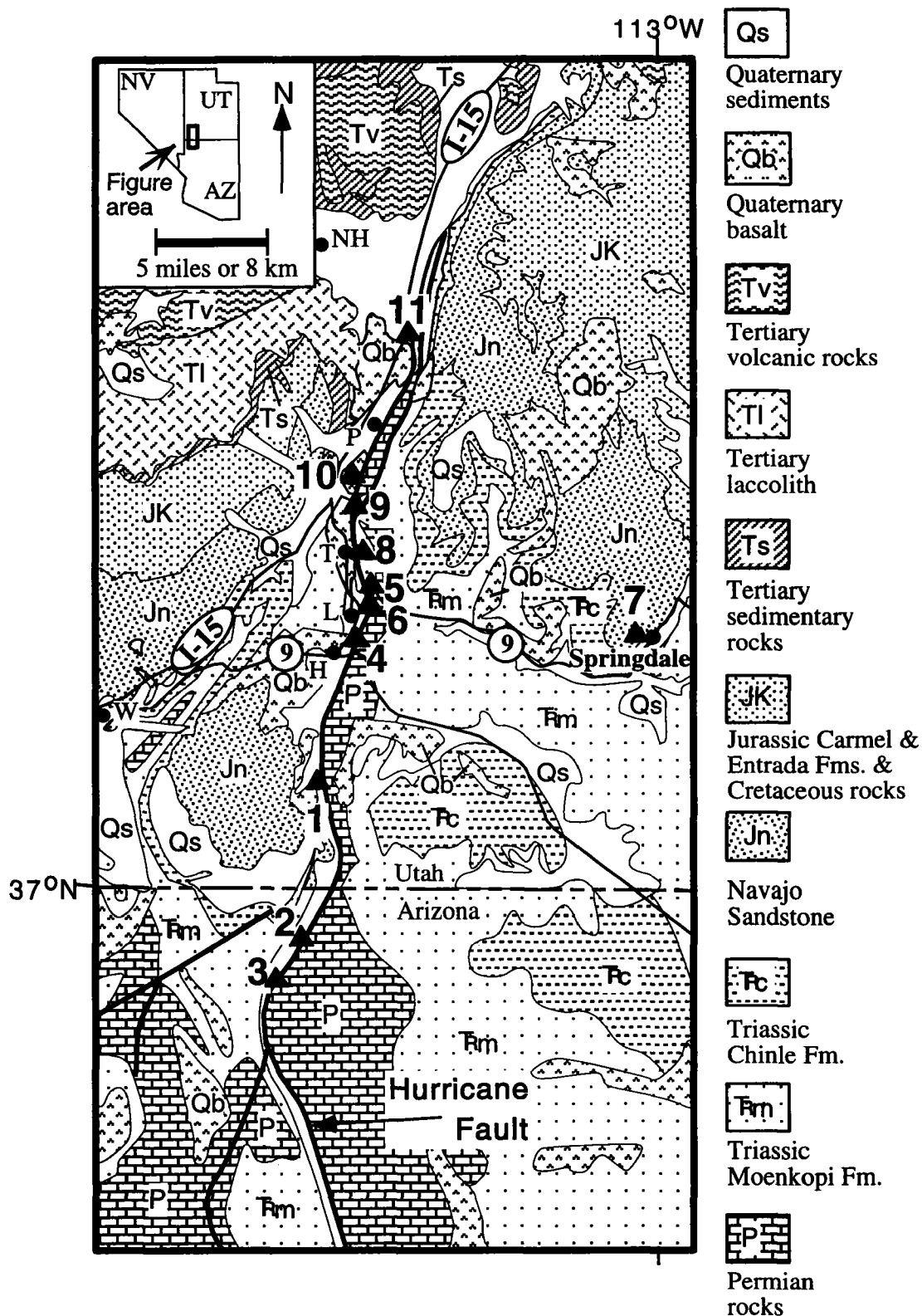


Figure 20. Field trip stop locations are shown on this map by triangles and labeled with stop numbers. Map is modified from Hintze (1980) and Reynolds (1988). Corrections of discrepancies between those two geological maps are generalized. Most faults are not shown. Towns, shown by a solid circle, are: H = Hurricane, L = La Verkin, NH = New Harmony, P = Pintura, T = Toquerville, and W = Washington.

		rocks dip moderately to steeply to the east; the tilting is a result of Cenozoic extension. The rocks in Frenchman and Sunrise Mountains are thought to have been formerly continuous with rocks near the Nevada–Arizona state line and have been transported to their present position during Cenozoic extension and strike-slip faulting.	3.2	44.3	At 2:00 between the highway and the bedrock is a small bluff at the edge of the alluvial fans. The bluff is the scarp of the California Wash fault continuing to the south along the west side of the North Muddy and Muddy Mountains.
9.5	25.6	Straight ahead and on the right are the Dry Lake Mountains. These mountains consist dominantly of the Bird Spring Formation which may range from Mississippian to Permian in age, but is mostly Pennsylvanian.	3.0	47.3	Looking toward the northeast and the Mormon Mountains at ~11:00 the alluvial fan is broken by bluffs along the west and southwest side. Above the bluff is an old alluvial surface called Mormon Mesa which is capped by a well-developed thick layer of caliche.
1.1	26.7	On the left (north) side of I-15 is the Chemical Lime plant and open-pit mine. The nearly horizontal cylinders are the kilns in which the lime is produced. The process involves heating the limestone to a high temperature using crushed coal blown into the kilns. This procedure drives off volatiles such as water and other impurities from the limestone.	8.3	55.6	The red-brown sedimentary rocks surrounding the small towns of Glendale and Moapa are dominantly Tertiary basin-fill deposits, mostly conglomerate, sandstone and siltstone.
			14.8	70.4	Here the highway crosses a surface that is equivalent in elevation to Mormon Mesa, and thus, possibly is similar in age.
			5.2	75.6	Enter Mesquite basin or valley. This basin contains some of the thickest (~10 km) basin-fill deposits in Nevada. The mountains straight ahead and on the right (southeast) are the Virgin Mountains. The Frenchman Mountain block is thought to have lain near the south end of these mountains prior to Cenozoic extension. The alluvial fans are well developed and protrude westward from the range. Some of these fans are dissected. The ends of the fan are cut by the Virgin River which runs through the topographic low.
10.4	37.1	The mountains on the right at ~3:00 are the Muddy Mountains. The lower mountains to the left (north) are the North Muddy Mountains.			
		Along the west side of these ranges is a young fault, called the California Wash fault (Bohannon, 1983a, W.J. Taylor, unpublished data). In good light the scarp along the fault can be seen from I-15. The scarp is approximately west facing.			
		In the Muddy Mountains the Muddy Mountain thrust, another fault of the Sevier orogenic belt, is exposed (Longwell, 1922, 1928; Bohannon, 1983a, 1983b). The North Muddy Mountains expose large folds and small thrusts also related to the Mesozoic Sevier orogenic belt (Longwell et al., 1965; Armstrong, 1968; Bohannon 1983a, 1983b).	19.4	94.0	Cross Arizona state line.
			6.7	100.7	The mountains straight ahead and to the north are the Beaver Dam Mountains. The obvious light colored, white and orange, sandstone exposed nearly straight ahead is the Permian Queantoweap Sandstone (Hintze, 1986).
4.0	41.1	The Mormon Mountains lie at ~11:00. The high peak on the right (south) end of the range is called Moapa Peak.			The highway crossing the Beaver Dam Mountains at ~10:00 is a state highway that cuts through the Cenozoic Castle Cliffs detachment fault (Axen et al., 1990).
		The Mesozoic Mormon thrust and Tertiary Mormon Peak detachment are exposed in the Mormon Mountains (Axen et al., 1990). The north–south part of the dome or arch that is typical of detachment terranes is visible in the topography from this vantage point.	5.9	106.6	Near here the Interstate enters the Virgin River gorge. At the near (west) end of the gorge two strands of the range-bounding fault are exposed on the right (south). The rocks near one strand are brightly colored purple and yellow from alteration along the fault. The other strand lies further west.

		In the gorge most of the Paleozoic stratigraphic section is exposed (Hintze, 1986). A small fault block at the west end comprises middle to upper Paleozoic rocks (Hintze, 1986). A short distance into the gorge (0.5–0.75 miles) many small stratigraphic separation normal faults are visible in the road cut.	1.3	142.3	Take exit 16 onto Utah Highway 9 to Hurricane, heading east. Turn right (east) at bottom of off-ramp.
			0.7	143.0	In the road cut on the left (north) side of the road, a syncline is exposed in Mesozoic rocks.
			0.7	143.7	Quaternary volcano at 1:00.
1.1	107.7	From here to the east, the highway passes by Cambrian through Permian rocks. The green shales exposed near here lie within the Cambrian section.	0.4	144.1	Straight ahead is the Virgin anticline. The beds on the right dip east; the beds on the left dip west. Follow these beds toward the dam on Quail Lake and they become more gently dipping. Continuing along, the fold hinge zone can be seen to the left over the top of the dam. Some small stratigraphic separation faults cut the fold hinge zone.
3.7	111.4	This orange sandstone is the Permian Queantoweap Sandstone. Many small stratigraphic separation faults are exposed in the road cut. This sandstone crops out in much of the upper part of the gorge and is overlain by the Permian Toroweap Formation. The Toroweap Formation forms the cliffs above the sandstone straight ahead.	1.3	145.4	The hinge zone of the anticline is to the left. A former version of this dam failed in 1989 when foundation problems caused dam failure and a flood (Lund, this volume). The flood water from the failure caused a large amount of scouring which is visible in this area.
8.6	120.0	The chert-rich carbonate exposed near the sign that says "Black Rock Road 1 mile" is the Permian Kaibab Limestone. From here to the Hurricane fault lies the transition zone between the Basin and Range Province to the west and the Colorado Plateau to the east. The Colorado Plateau can be seen straight ahead in the distance, on the skyline.			The Shinarump Conglomerate crops out near the road in a short distance.
		The transition zone is marked by small ridges, most of which are fault bounded. The fault blocks are dominantly east-tilted Mesozoic rocks.	1.2	146.6	On the right (east) is a basalt flow filling a paleochannel cut in the Triassic Moenkopi Formation.
3.4	126.8	To the east-northeast at 10:00 lie the Pine Valley Mountains. The upper part of these mountains is underlain by the Tertiary Pine Valley laccolith (Cook, 1957). Between the vehicle and the Pine Valley Mountains is a black surface which is the top of a young basalt that flowed down a surface that slopes toward the vehicle.	3.3	149.9	On the right (south) is the Quaternary volcano, Volcano Mountain. $^{40}\text{Ar}/^{39}\text{Ar}$ data from one flow erupted from this volcano are not of high quality; Sanchez (1995) was only able to conclude that flow had a maximum age of 270 ± 50 ka. To visit the volcano, turn right here and travel through this new subdivision.
0.7	127.5	Cross state line into Utah.	0.3	150.2	At ~10:00, north of the highway, is a polycyclic (multiple eruption) volcano. The cliffs straight ahead as well as toward 2:00 and 10:00 are the Hurricane Cliffs which are the Hurricane fault line scarp.
3.6	131.1	On top of the red-brown colored ridge straight ahead and to the north (left) the resistant cap rock is the Shinarump Conglomerate, the lowest member of the Triassic Chinle Formation. A short distance ahead is a road cut through the Shinarump Conglomerate.	1.9	152.1	Turn right (south) onto 700 W.
			0.05	152.15	Turn left (east) into Super 8 Motel parking lot, Hurricane, Utah.
			Day 1.		Examine a fault segment boundary in Arizona and the Anderson Junction fault segment.
9.9	141.0	At ~10:00 in the road cut, a basalt flow fills a paleochannel in the Mesozoic red beds.	0.0	0.0	Leaving Super 8. Turn left (south) on 700 W.
			0.3	0.3	Stop at stop sign, then proceed ~straight across small bridge.

- | | | | | | |
|-----|-----|---|------|-------|---|
| 0.1 | 0.4 | The Hurricane Cliffs are on the left (east) and straight ahead. | | | cause the flow conforms to the topography showing that it flowed down the cliff. The cliffs are about 300 m high here and the flow ends about 150 m down the cliff which suggests that at least one half of the total scarp height may have formed prior to eruption of the flow at about 200–300 ka ago. |
| 1.7 | 2.1 | Stay on the same paved road and follow it to the right (west) around curve. Continue around curves and stay on this paved road. | | | |
| 4.3 | 6.4 | Cross cattle guard. Road becomes dirt. Go straight, which is the left fork. | | | |
| 0.7 | 7.1 | Stop 1. Lava Cascade. This stop is on The Divide, UT, 7.5' quadrangle, Secs. 3 & 4, T.43S, R.13W. To the left (east) at ~10:00 is a lava cascade. A dark-colored lava flow is exposed where it flowed down the upper part of the Hurricane Cliffs. The flow ends part way down the cliff. The source of the basalt flow is a volcanic center exposed on the plateau east of the Hurricane Cliffs (Sanchez, 1995). | 0.8 | 7.9 | |
| | | The rock is fine grained, black in color, and contains small olivine phenocrysts. It is a basanite with less than 46% silica (Sanchez, 1995). | 0.7 | 8.6 | Cross cattle guard. |
| | | This lava flow falls into the Stage IV flows of Hamblin (1970). According to this classification scheme, Stage IV flows are young and were deposited in the present drainage system, the surface features are only slightly modified and the associated cinder cones are well preserved. Older flows belonging to Stages I (oldest), II and III were erupted onto older, topographically higher surfaces. | 2.0 | 10.6 | Continue straight south (left fork). The right fork goes to an exposure of dinosaur tracks and historic Fort Pearce. |
| | | The rock in the lava cascade has not been dated radiometrically, but the geomorphic-type stage dates can be used in combination with radiometric dates to estimate the age of the lava flow. Another Stage IV flow that was erupted from Volcano Mountain (seen along Utah Highway 9 west of Hurricane) was dated by Sanchez (1995) at 258 ± 24 ka using $^{40}\text{Ar}/^{39}\text{Ar}$. A Stage II flow in Hurricane Valley yielded a 353 ± 45 ka $^{40}\text{Ar}/^{39}\text{Ar}$ date (Sanchez, 1995). According to Sanchez, the dated flow has the same chemistry as the flow that is exposed in the Hurricane Cliffs, above other Stage II flows exposed in Hurricane Valley. | 0.7 | 11.3 | Cross cattle guard. |
| | | | 0.55 | 11.85 | On the right (east), the unconformity between Mesozoic and Quaternary deposits is exposed in the wash. |
| | | | 1.15 | 13.0 | Cross cattle guard. |
| | | | 0.1 | 13.1 | Quaternary (?) basalt is visible on the rounded hills and in the butte straight ahead. |
| | | | 2.2 | 15.3 | Pass the trail head for the Honeymoon Trail on the left (east) where there is a nice fault exposure (Hamblin, 1970). |
| | | | 1.7 | 17.0 | Cross wash and drive over outcrops of sandstone; continue to the left (east). |
| | | | 0.3 | 17.3 | Continue on left fork. Straight ahead (southeast) are the Hurricane Cliffs. The cliffs contain mostly Permian formations such as the Kaibab Formation, Toroweap Formation, and Hermit Shale. |
| | | | 0.4 | 17.7 | To the left (east), a high-angle fault cuts through the footwall of the Hurricane fault. It is most easily seen by the offset of one of the thick beds in the cliffs. |
| | | | 1.0 | 18.7 | At ~11:00 is a large canyon called Cottonwood Canyon. Rocks exposed on the right are Moenkopi Formation overlain by Quaternary (?) basalt. |
| | | | 0.9 | 19.6 | Continue straight (south) through the fence. Remember to leave the gate as you found it, either open or closed. |
| | | | | | Stop 2. Fault scarps along the Hurricane fault. Turn left on steep road beneath powerline. Continue up the road about |

500 m if it is passable. If not, hike up road toward the Hurricane Cliffs until you reach the prominent fault scarp on the north side of the road.

This stop is in the Rock Canyon 7.5' quadrangle, Mohave County, Arizona, Sec. 27, T. 41 N., R. 10 W. It is located at the southern end of a 7-km-long portion of the Hurricane fault where relatively low fault scarps formed in Quaternary deposits and bedrock are common along the base of the Hurricane Cliffs. It is just north of the prominent bend in the Hurricane fault that is discussed at Stop 3 (fig. 4). Between the town of Hurricane, Utah, and the Arizona border, the Hurricane Cliffs are composed almost entirely of the resistant rocks of the Kaibab and Toroweap formations. Along this section south of the Arizona border, the lower slopes of the fault escarpment are formed in rocks of the Supai Group, which generally are less resistant to erosion than the rocks of the overlying formations. Because of the erodibility of the Supai Group rocks, the steeper upper portions of the Cliffs have retreated by varying amounts from the principal Hurricane fault zone.

The relatively low fault scarps evident at this stop apparently record late to latest Quaternary displacement on this section of the Hurricane fault system. The scarp at this locality is typical of the scarps along this section of the fault. The scarp is high (~25 m) and steep (maximum slope of 35°). The scarp is formed on a steeply sloping landform colluvial/alluvial surface that mantles the lower part of the cliffs. The colluvial/alluvial deposits are typically quite thin (a few meters thick or less) over a bedrock erosion surface on the upthrown side of the fault. The scarp is formed in these deposits and bedrock, so the bedrock may exert some influence on scarp morphology and degradation rates. Reasonably well-developed calcic soils are developed in the faulted colluvial/alluvial deposits, suggesting that they are of late(?) Pleistocene age. The alluvium exposed immediately downslope of this fault scarp may be correlative with the colluvium/alluvium above the scarp, or it

may be younger alluvium derived from the scarp and adjacent drainages. Based on the size of the scarps, they almost certainly record multiple late Quaternary fault ruptures. The age of the youngest rupture on this section of the fault is not well constrained, but young terrace and alluvial-fan deposits are unfaulted.

No alluvial fault scarps are obvious in the area of the major bend along the Hurricane fault immediately south of Stop 2 (discussed in Stop 3). Relatively low scarps exist at many places along the base of the Hurricane Cliffs on the Shivwitz Plateau south of this locality. None of these scarps are as high or as steep as the scarp observed at Stop 2.

Continue along same road (center fork) to next stop. In a short distance along the center fork is another sign that says Temple Trail.

0.3 19.9
At wash. If driving two-wheel drive or low-clearance vehicle stop here for Stop 3. Otherwise continue along this road another 1.8 miles.

Stop 3. Segment boundary on the Hurricane fault. This is the southernmost stop on the Hurricane fault on the field trip. At this stop in the Rock Canyon 7.5' quadrangle (Secs. 26, 27, & 34, T.41S, R.10W), northern Mohave County, Arizona, a relatively abrupt bend in the trace of the Hurricane fault parallels the visible bend in the cliffs which lie to the east and south. We will walk along the Hurricane fault in the northern part of the bend and examine the fault geometry and Quaternary deposits which include older alluvium, talus, recent alluvium, mafic volcanic rocks, and a small mafic intrusion.

Taylor and Stewart (in review) suggest that the large bend, convex toward the hanging wall, bend in the Hurricane fault in this area is a geometric segment boundary (cf., Crone and Haller, 1991; dePolo et al., 1991). Several pieces of information support this interpretation. (1) The fault bends and changes strike from approximately N20°E north of the bend to N15–20°W south of the bend. We will walk along the NNE-striking fault

section and view the area of maximum curvature (fig. 8). (2) The total stratigraphic separation decreases toward the bend both from the north and from the south (fig. 9). We will see an artifact of this change in the elevation of the Triassic Chinle Formation in the hanging wall relative to the Paleozoic units in the footwall (described below). The elevation of the Chinle Formation is higher near the inflection point of the bend than along the fault sections to the north and south which corresponds to a decrease in stratigraphic separation at the bend. (3) A Quaternary(?) basaltic intrusion and basalt field near the apex of the bend suggest the possibility of non-conservative slip in the hanging wall near the segment boundary zone. Non-conservation of space suggests that the slip direction, magnitude and/or timing of movement is not constant on the fault sections around or on either side of the bend. (4) The footwall structures near the bend change from dominantly gentle to open folds and a few normal faults south of the bend to small stratigraphic separation normal faults north of the bend (Billingsley, 1992; W.J. Taylor, unpublished mapping). These differences in structural style imply a kinematic change at the bend. (5) In addition, fault scarps in Quaternary deposits crop out both north and south of the bend, but appear to be lacking in the area of maximum curvature. We saw scarps north of the bend at stop 2 and will note the lack of scarps in this area. This change in the Quaternary fault scarps suggests the possibility that this geometric barrier may also be a behavioral or paleoseismic barrier as well, if the Quaternary deposits are of similar ages (King, 1986).

The Paleozoic units exposed in the cliff near here lie in the footwall of the Hurricane fault. Recognition and identification of these units is critical in determining the total stratigraphic separation on the fault segments north and south of this bend as well as at the bend. The units are, from lowest to highest, the Permian Esplanade Sandstone which is a red, white or tan sandstone near the base of the cliffs; the Permian Hermit Shale which is

a red, brown and white siltstone to sandstone; the Permian Toroweap Formation that contains three members: a lower unit of interbedded gray, yellow and brown sandstone, siltstone and dolomite (Seligman Member); a middle gray limestone cliff (Brady Canyon Member); and an upper gypsiferous unit of gray siltstone and light-red siltstone to sandstone (Woods Ranch Member); and near the top of the cliffs, the Permian Kaibab Formation with a lower gray cherty limestone (Fossil Mountain Member) and an upper red and gray unit of interbedded limestone, sandstone and siltstone with white gypsum. More complete descriptions of these units are available with the quadrangle map for this area (Billingsley, 1992) and in Sorauf and Billingsley (1991).

Along the base of the Hurricane Cliffs and in the hanging wall a variety of Quaternary deposits are exposed. These deposits lack scarps near the apex of the bend, but they or similar deposits are faulted on the segments to the north and south of the bend. The sedimentary deposits include small alluvial fans, talus, alluvium, landslide deposits, colluvium, and gravel terraces. Many of these deposits are the debris slope and wash slope facies associated with the degradation of the escarpment associated with the Hurricane fault. The igneous deposits include mafic lava flow rocks and a small pluton that intrudes them. The hill to the west is composed of mafic extrusives and contains at least four distinct flows that are separated by agglomerate. The flows are fine grained and contain varying amounts of plagioclase and olivine phenocrysts. The pluton or plug also has plagioclase and olivine phenocrysts, but is granular and medium to coarse grained. Maureen Stuart (unpublished data from UNLV XRF laboratory, 1995) analyzed samples from the four flows and the plug for major and trace element contents and they are all subalkaline tholeiitic basalt (cf., Irvine and Baragar, 1971; Le Bas et al., 1986).

Turn around and follow same route to Utah Highway 9.

Cross under the power lines.

Pass through fence.

3.9	23.8
0.9	24.7

2.4	27.1	On the hill at ~10:00 are purple, red-brown, and tan layers. The tan unit is the Shinarump Conglomerate. The unit below it is the Moenkopi Formation.				Springs. This stop is on the Hurricane, UT, 7.5' quadrangle, SW1/4, Sec. 25, T.41S, R.13W. At this stop the Anderson Junction segment of the Hurricane fault consists of at least two fault strands. Both strands offset the young basalt at the top of the section, much of which contains well-developed columnar joints. On the south side of the canyon, the block between the two fault strands has been steeply tilted (~60–80°W), causing a large angle across the unconformity between the Cenozoic basalt and the Mesozoic rocks in the block. Note that in the footwall the angle across the unconformity at the base of the basalt is small (i.e., the unconformity is only slightly angular), but that all of the Mesozoic units are missing, probably due to erosion of the uplifted footwall prior to basalt emplacement.
4.35	31.45	Cross cattle guard. The lava cascade is visible from here.				A group of springs, Dixie Hot Spring, flows into the Virgin River just upstream from the parking lot. The spring temperatures are about 100–120°F. The combined flow from these springs decreased after the 1992 St. George earthquake (Stewart et al., this volume). Everitt (1992) suggests that flow from springs was diverted following the earthquake and attributes these new discharge points to the fracturing of hydrologic barriers between the aquifer and the river bed which resulted in a drop in water levels.
1.45	32.9	Cross cattle guard.				Turn around and return to Utah Highway 9.
1.9	34.8	Turn to Optional Stop at dinosaur tracks. To go to dinosaur tracks and Fort Pearce use the following directions. At 2.0 miles Cross cattle guard. At 3.4 miles Cross cattle guard and continue straight. At 0.7 miles Straight ahead (north) the purple outcrops are the Chinle Formation. In the topographically low area toward the vehicle from those exposures, is a yellow-tan exposure of the Shinarump Conglomerate. At 0.5 miles Turn right and follow small dirt road to dinosaur tracks at this intersection. Park in parking area at the end of the road and then hike along the trail to the dinosaur tracks. At 1.6 miles Cross cattle guard At 0.4 miles Dirt road to the left here leads to Fort Pearce. Return along same route to field trip route.				Turn right (north) back onto the highway and cross the Virgin River.
0.7	35.5	Cross cattle guard.				The town of La Verkin.
0.8	36.3	To the left (east) at ~10:00 is the lava cascade.	0.3	45.1		Turn right (east) staying on Utah Highway 9 and head toward Springdale.
0.7	37.0	Cross cattle guard. Road becomes paved. Go straight.	1.0	46.1		Slickenlines and slickensides on a fault surface that is a strand of the Hurricane fault are exposed to the right (east). Rounding the curve in the road to the right, the Hurricane fault can be seen toward the left (north).
4.3	41.3	Follow this same paved road to left (north) around curve and continue along it.	0.6	46.7		Turn left (north) onto a dirt road that passes a shooting range in a short distance on the right.
1.7	43.0	The Hurricane Cliffs are on the right (east).	1.4	48.1		
0.1	43.1	Cross small bridge and stop at stop sign, then proceed straight.				
0.3	43.4	Pass Super 8 Motel on 700 W and turn right (east) onto Utah Highway 9 at stop sign.	0.4	48.5		
0.15	43.55	Follow road around curve to left (north).				
0.95	44.5	Turn right onto Enchanted Way, the lane into Pah Tempe Resort.				
			0.5	49.0		Stop 5. The Hurricane fault zone, Anderson Junction segment. Drive along dirt road toward the northwest. This road is
0.3	44.8	Optional Stop 4. The Hurricane fault at Pah Tempe Resort near Dixie Hot				

rather rugged and not maintained. Once parked, walk toward the west to the eastern margin of the Hurricane fault zone. The stop is on the Hurricane, UT, 7.5' quadrangle, SE1/4, SE1/4, Sec. 12, T.41S, R.13W.

The vans are parked on the footwall of the Hurricane fault. Here the fault is a zone 1.5 km wide and multiple normal fault strands can be seen (fig. 6, cross section C-C'). These multiple normal fault strands are one line of evidence that this section of the fault is a distinct fault segment and differs from the fault segment north of a segment boundary to be discussed in Stop 10. Permian Kaibab Formation crops out in the footwall. Different members of the Triassic Moenkopi Formation lie within the hanging wall and are displaced along synthetic and antithetic faults. The yellow to tan-colored unit is the Timpoweap Member which is a fine-grained limestone and shale that breaks in platy fragments. The red unit is the Lower Red Member which is composed of finely-laminated mudstone to thin beds of sandstone.

The close hill to the west at ~11:00 is capped with the Virgin Limestone Member of the Moenkopi Formation. This member comprises interbedded limestone, sandstone, and siltstone and is typically yellow-tan to light gray.

- | | | |
|-----|------|--|
| 0.5 | 49.5 | Return to Utah Highway 9. Turn right and head west. |
| 2.0 | 51.5 | Turn right at Utah Highway 17 in La Verkin. |
| 0.4 | 51.9 | Turn right at road with a white office trailer (unnamed street). This is an entrance to a gravel pit and is private property; permission to drive through should be obtained prior to entry. |

- | | | |
|------|-------|---|
| 0.25 | 52.15 | Stop 6. Gravel/conglomerate offset by the Hurricane fault along the Anderson Junction segment. Follow road around and park near a part of the road that is constructed on a large ~9 ft diameter metal tunnel. Walk down from road towards the east and then follow a dry stream bed ~0.25 miles. This stop is on the Hurricane, UT, 7.5' quadrangle, NE1/4, SW1/4, Sec. 13, T.41S, R.13W. |
|------|-------|---|

In a small, scoured canyon is an exposure of Quaternary gravel with a small amount of stratigraphic separation along two fault strands about 3 m apart. The gravel can be correlated across the fault. This reddish gravel is a basin deposit that accumulated in the depression adjacent to and formed by the Hurricane fault. The red color is likely derived from weathered red members of the Moenkopi Formation. The age of this gravel is unknown, but it is older than the most recent sedimentation in the area. About 3 m of stratigraphic separation is observed on the 60°W dipping fault strand and 1.2 m of offset is measured on the 73°W strand. No fault scarp exists. Lack of an escarpment may be related to two reasons: (1) the age of the offset is so old that the scarp was eroded away or (2) the bedrock unit is the nonresistant Moenkopi Formation which may be less likely to form scarps than other less erodible formations. Either way, exposures such as this are uncommon along the Hurricane fault, but that should change as more geologists continue detailed mapping along the fault.

This stratigraphic separation of Quaternary gravel is another piece of evidence that this is a unique fault segment. As is typical of adjacent fault segments on normal faults, faulting history varies between the Anderson Junction segment and the Ash Creek segment in that no fault scarps are present on the Anderson Junction segment, although the Quaternary gravel is offset. Stop 10 will discuss two fault scarps on the Ash Creek segment.

Walk back to vans.

- | | | |
|------|-------|--|
| 0.25 | 52.4 | Return to Utah Highway 17. Turn left (south) and continue going south on Utah Highway 9. |
| 2.1 | 54.5 | Cross Virgin River. |
| 1.9 | 56.4 | Turn left (south) onto 700 W near the Chevron station in Hurricane. |
| 0.05 | 56.45 | Turn left (east) into Super 8 Motel parking lot. |

Day 2.

Examination of the Springdale landslide, the Anderson Junction and Ash Creek fault segments and folds in the New Harmony and Kanarraville basins.

Incre- mental Mileage	Total Mileage				
			0.6	20.1	To the right (east) is the Johnson Mountain landslide, another large Pleistocene slope failure in the Petrified Forest Member.
0.0	0.0	Leave Super 8 Motel on 700 W, Hurricane, Utah.	1.4	21.5	The road up lower Zion Canyon lies between the massive cliffs of Navajo Sandstone in Zion National Park. Mt. Kinesava is to the left (west) and The Watchman is to the right (east).
0.15	0.15	Follow road around curve to the left (north).			
0.95	1.1	Pass Enchanted Way, the lane into Pah Tempe Resort.			
1.0	2.1	The town of La Verkin.			
0.6	2.7	Turn right (east) staying on Utah Highway 9 at this intersection between Highway 9 (right) and Highway 17 (straight). Continue toward Springdale.	1.2	22.7	Stop 7. Springdale landslide. This stop is on the St. George, UT, 30 x 60' quadrangle, at Secs. 26 & 27, T.41S, R.10W. Park at the landslide toe on the dirt road to the left (west) of the highway. The Springdale landslide lies at the juncture between the wide, lower Zion Canyon and narrow, upper Zion Canyon. The catastrophic failure of the landslide, although seismically induced by the 1992 St. George earthquake, is related to the normal process of headward broadening of the canyon as the river entrenches and encounters the Petrified Forest Member. Older landslide debris is found on the Pleistocene alluvial terrace overlooking the Springdale landslide (fig. 13). The Springdale landslide is a complex block slide with its basal slide plane in the Petrified Forest Member and its main scarp in the overlying Dinosaur Canyon Member of the Jurassic Moenave Formation (fig. 2). Note the numerous fissures and minor scarps that form a broken topography within the slide mass.
4.2	6.9	Hurricane Mesa on the left (north), site of U.S. Air Force supersonic research facility. Almost complete section of Triassic Moenkopi Formation is exposed in cliff face, capped by resistant ledge of Shinarump Member, Triassic Chinle Formation.			
2.1	9.0	The town of Virgin.			
1.6	10.6	Westernmost exposure of the Pleistocene Crater Hill basalt, capping mesas to the left (north) of the road for the next 5.1 miles. The Crater Hill cinder cone is 3 miles to the northeast.			
5.1	15.7	Cross Coalpits Wash. Easternmost exposure of the Crater Hill basalt unconformably overlies the Pleistocene Parunuweap Formation on west side of wash. The town of Grafton is to the right (south) of the road.			
0.5	16.2	Parunuweap Formation, with basalt boulders, unconformably overlying Moenkopi Formation in roadcut on the left (north).			
1.0	17.2	Sand and gravel pit in Holocene Orderville gravel, across Virgin River flood plain to the right (south).	20.0	42.7	At intersection between Utah Highways 9 and 17 (near RV park) turn right (north) and continue along Highway 17.
0.6	17.8	The town of Rockville, named for rock-fall debris derived from the Shinarump Member capping the Rockville Bench to the left (north) of the road.	1.1	43.8	On the left is basalt unconformably overlying Tertiary (?) alluvial or fluvial deposits.
1.7	19.5	As the road curves left (northeast) into lower Zion Canyon, erosional remnants of the Jurassic-Triassic Navajo Sandstone are visible to the right (south). The remnants, known as Eagle Crag, stand at the head of a Pleistocene to Holocene landslide, one of the largest in Utah. Failure was due to downcutting of the East Fork of the Virgin River into the Chinle Formation, Petrified Forest Member.	2.3	46.1	The town of Toquerville. At ~2:00 a large convex-toward-the-hanging-wall bend in the Hurricane fault is visible as the fault curves west around a footwall block.
			0.8	46.9	Turn right (east) onto a small road, Spring Drive, just before (south of) the bridge over Ash Creek.
					Continue straight across cattle guard. At 10:00, the contact between the carbonate cliffs on the east and the dark colored basalt on the west is the Hurricane fault.

		The basalt lies in the hangingwall. High on the cliff, in the Hurricane fault footwall, is a paleochannel filled with basalt.	0.4	50.4	of the Moenkopi Formation. Look down to the right (southeast), and see the small thrust fault again.
0.25	47.15	Take the right fork on the dirt road.			
0.1	47.25	Optional Stop 8. Hurricane fault, Anderson Junction segment, near a gravel quarry. The Hurricane fault is exposed both to the north and south of here. To the north is the fault segment boundary. Along this dirt road are slickenline exposures on Permian Kaibab Formation. This is the Pintura, UT, quadrangle, SW1/4, NW1/4, Sec. 36, T.40S, R.13W.	1.0	51.4	Stop 9. Top of the Hurricane Cliffs. Drive up to the radio tower, shown as 'radio facility' on the Pintura, UT, 7.5' quadrangle, SE1/4, SE1/4, Sec. 23, T.40S, R.13W.
		Continue uphill along this road and road curves and heads south along the fault strand.			We are essentially at a fault segment boundary marked by a large bend in the Hurricane fault. The strike of the fault is N13°W to the south (right) along the Ash Creek fault segment and N21°E to the north (left) along the Anderson Junction segment. The local southward decrease in stratigraphic separation is marked across this segment boundary (fig. 6) and is indicative of a boundary that has been a persistent barrier to slip (King, 1986).
0.7	47.95	The view to the south from here is along the Hurricane Cliffs.			
0.65	48.6	Straight ahead is basalt unconformably overlying Mesozoic rocks.			The Quaternary basalt in the footwall of the fault is undated but is assumed to be between 0.3 and 1.1 million years old from dated geochemically similar nearby rocks (Best et al., 1980, Sanchez, 1995).
0.1	48.7	Small dirt road to right leads to a former oil or gas well site which is at ~2:00. The flat lying rocks in the distance are part of the Colorado Plateau and are in the footwall of the Hurricane fault.			The fault has 450 m of stratigraphic separation on the basalt (fig. 6). In the footwall basalt flowed onto Permian Kaibab Formation and in the hanging wall the basalt overlies Jurassic-Triassic Navajo Sandstone (fig. 2). Thus, it is apparent that the Hurricane fault existed as a normal fault prior to basalt flows. Based on observed relatively similar basalt thicknesses in the hanging wall and footwall, it appears that at the time of the basalt flows, there was very little to no fault escarpment.
0.8	49.5	The hills to the right (east) contain the red-white-red stripes of the Moenkopi Formation which is capped by the resistant tan-colored Shinarump Conglomerate Member which is overlain by the upper part of the Triassic Chinle Formation.			
0.025	49.52	Down the hill among the light-colored rocks, a small stratigraphic separation thrust fault is visible, which is the southern exposure of the Taylor Creek fault (Lovejoy, 1964; fig. 6, cross sections A-A' and B-B'). There is 15 m of stratigraphic separation of the Virgin Limestone Member of the Triassic Moenkopi Formation and the average orientation is N15°E, 30°E. Farther north near Zion National Park, the Taylor Creek thrust fault has more than 600 m of vertical and 760 m of horizontal displacement (Kurie, 1966).			
0.225	49.75	To continue to the top of the ridge, take the left (west) fork.			Geochemically identical basalt lies directly below this outcrop and a slip vector was determined to range from 73°, N70°W to 75°, S18°W (fig. 5; Stewart and Taylor, 1996).
0.05	49.8	To the right (~north) a high-angle fault is exposed. Kaibab Formation is in the footwall and Moenkopi Formation is in the hanging wall.	0.1	51.5	To the west are the Pine Valley Mountains. The Virgin anticline (fig. 11) is exposed in the valley (although this fold is not visible from this vantage). Turn around and return along same route to Utah Highway 17.
			0.8	52.3	Pass fork on left (east) and continue along dirt road.
			0.95	53.25	Pass road on east or left (T intersection).
0.2	50.0	The red mudstone unit that we are driving through is the Upper Red Member			The hill straight ahead (west) contains Moenkopi Formation capped by Shinarump Conglomerate in the tilted block.

1.05	54.3	Cross cattle guard and continue south-west.			nary-Tertiary gravel is an unconsolidated alluvial deposit containing well-rounded boulders shed from west-to-east from the Pine Valley laccolith to the west, as well as cobbles of well-rounded light gray fossiliferous limestone, chert, bedded yellow and brown quartzite, sandstone (Navajo), and clasts of Claron Formation. This unit is of unknown age but is older than the most recent alluvium in the area. The offset Quaternary-Tertiary gravel here is a different composition than the offset sediment at Stop 6 and the morphology of the two sites is noticeably distinct. At this stop scarps have formed in alluvium and bedrock because the bedrock comprises the resistant Pakoon Dolomite and Queantoweap Formation.
0.6	54.9	Turn right (north) off Spring Drive back onto Utah Highway 17 and immediately cross bridge over Ash Creek.			To the north along the Ash Creek fault segment, the Hurricane fault is a single surface trace (fig. 6, cross section A-A'). Compare this to the section of the fault at Stop 5, where the fault is a complex zone of multiple fault strands.
1.5	56.4	The hill on the left (west) is Jurassic-Triassic Navajo Sandstone. On the right (east), Quaternary (?) basalt is exposed. Both of these units lie in the hanging wall of the Hurricane fault.			Return along same route to stop sign.
0.8	57.2	The small, somewhat conical hill at ~10:00 is intrusive rocks, probably related to the Pine Valley laccolith exposed in the Pine Valley Mountains to the west.			Turn right (west) at stop sign and in a very short distance turn right onto the on ramp for I-15 N.
0.4	57.6	Take right fork and shortly thereafter take right turn. Just after taking the corner, the Pintura fold is visible in the footwall of the Hurricane fault folding the Permian Pakoon Dolomite, Queantoweap Sandstone, Toroweap Formation, and Kaibab Formation. The Pintura fold is a Mesozoic Sevier Orogeny-related fold and is truncated by the Hurricane fault (fig. 11).			On the west side of I-15 north of Exit 36 is Ash Creek Reservoir, which was completed in 1960 in conjunction with construction of the Interstate. The natural abutments are highly fractured Quaternary basalt, and consequently the reservoir is permeable and loses water. Poor dam construction caused collapse of the road above the dam in 1969, the first time the reservoir approached its capacity. As a result, the State Engineer imposed water-level restrictions on the reservoir and the spillway was subsequently lowered.
0.45	58.05	Turn right (~east) toward Hurricane fault.			Take Exit 40 (east) to the Kolob Canyons section of Zion National Park. Continue past the Visitor's Center into the park.
1.0	59.05	Stop 10. Fault scarps along Ash Creek segment. The road turns into dirt and then into sand. Park in sandy dune deposit. Note: the road is private property and permission to drive through must be obtained prior to entry. Walk ~ 0.25 mile to the northeast to two fault scarps in Quaternary-Tertiary alluvium that are next to each other. This stop is on the Pintura, UT, quadrangle, middle of Sec. 23, T.40S, R.13W. The two fault scarps are formed in Quaternary-Tertiary deposits and bedrock. The larger fault scarp has a scarp slope of 30° and a scarp height of 6 m; the smaller scarp has a slope of 15° and is 3 m high; both are down-to-the-west. Scarp slopes were measured from the angle made by the horizontal surface in the footwall of the scarp to the middle of the steep face of the scarp slope using the technique of Bucknam and Anderson (1979). A thin layer of the Quaternary-Tertiary gravel is in the upthrown side of the fault and in the downthrown side the gravel is thicker and overlain by colluvium derived from the Hurricane Cliffs to the east. The Quater-	1.85	60.9	
			9.5	70.4	
			12.6	83.0	
			13.7	97.1	Stop 11. New Harmony and Kanarraville Basins. Park on the wide paved shoulder of the road just past a 90° curve (road bends from north to east). Walk west back to the curve and cross the guard rail to a flat, relatively open area

west of the road. This stop is on the St. George, UT, 30 x 60' quadrangle, Sec. 26, T.38S, R.12W.

View west is of the New Harmony basin, flanked by the Pine Valley Mountains on the south and west, and by the Harmony Mountains on the north. The Pine Valley Mountains are underlain by the 21 Ma Pine Valley laccolith and associated volcanic rocks. The steep, rounded peak visible due west is another Miocene intrusion. The Harmony Mountains are underlain by Miocene Quichapa Group volcanic rocks above Tertiary Claron Formation.

Miocene-Pliocene (?) volcanoclastic debris-flow deposits (unit Taf, fig. 7), are exposed on the south flank of the Harmony Mountains. The lower member of unit Taf dips moderately to steeply south towards the basin and is locally overturned. Highly faulted and locally overturned strata of the Quichapa Group and Claron Formation are exposed north of unit Taf. This faulting and tilting is in the hinge area of a tight, east-west trending anticline that is paired with the New Harmony syncline, whose axis lies to the south below unfolded Quaternary deposits (fig. 7). The folding is attributed to Neogene extension-normal shortening in the Basin and Range-Colorado Plateau transition zone and predated the modern expression of the Hurricane fault.

The wooded, north-trending, low ridge west of I-15 is composed of debris-flow deposits derived from the Pine Valley Mountains (unit QTaf, fig. 7). This ridge is interpreted as a gentle anticline related to rollover in the hanging wall of the Hurricane fault. We are standing on the footwall of the Hurricane fault, and the fault trace lies along the sharp break in topography at the base of the Hurricane Cliffs.

View to the north and northeast is of the Kanarrville basin, which trends northeast parallel to the Hurricane fault and is bounded on the west by the Harmony Mountains. Unit Taf forms two subtle, east-dipping hogbacks (lower and upper members) in the eastern foothills of the Harmony Mountains.

Return to vans. Just east of the parking area on the south side of the road, a steeply dipping normal fault juxtaposes Quaternary (?) colluvium, probably derived from the Lower red member of the Triassic Moenkopi Formation, with the Timpoweap Member of the Moenkopi. Farther east, another normal fault juxtaposes the Timpoweap and Lower red member of the Moenkopi. These normal faults are interpreted as subsidiary faults to the Hurricane fault. Normal faults are also exposed along Taylor Creek just east of the Hurricane fault trace and are accessible by hiking down the steep ravine from the overview site.

Return to I-15 and proceed north.

Continue along I-15 to Salt Lake City, Utah.

End of trip

COMBINED REFERENCES

- Algermissen, S.T., Perkins, D.M., Thenhaus, P.C., Hanson, S.L., and Bender, B.L., 1990, Probabilistic earthquake acceleration and velocity maps for the United States and Puerto Rico: U.S. Geological Survey Map MF-2120, scale 1:750,000
- Anderson, R.E., and Barnhard, T.P., 1993a, Aspects of three-dimensional strain at the margin of the extensional orogen, Virgin River depression area, Nevada, Utah, and Arizona. *Geological Society of America Bulletin*, v. 105, p. 1019–1052.
- Anderson, R.E., and Barnhard, T.P., 1993b, Heterogeneous Neogene strain and its bearing on horizontal extension and vertical contraction at the margin of the extensional orogen, Mormon Mountains area, Nevada and Utah: *U.S. Geological Survey Bulletin* 2111, 43 p
- Anderson, R.E., and Christenson, G.E., 1989, Quaternary faults, folds, and selected volcanic features in the Cedar City 1° x 2° quadrangle, Utah. *Utah Geological and Mineral Survey Miscellaneous Publication* 89-6, 29 p.
- Anderson, R.E., and Mehnert, H.H., 1979, Reinterpretation of the history of the Hurricane fault in Utah, in Newman, G.W., and Goode, H.D., eds., 1979 Basin and Range Symposium: Rocky Mountain Association of Geologists, p. 145–165
- Arabasz, W.J., Nava, S.J., and Pechmann, J.C., 1992a, Earthquakes near Cedar City, Utah, June 28–29, 1992. *University of Utah Seismograph Stations, Preliminary Earthquake Report*, 5 p
- Arabasz, W.J., Pechmann, J.C., and Nava, S.J., 1992b, The St. George (Washington County), Utah, earthquake of September 2, 1992. *University of Utah Seismograph Stations, Preliminary Earthquake Report*, 6 p.
- Arabasz, W.J., and Julander, D.R., 1986, Geometry of seismically active faults and crustal deformation within the Basin and Range-Colorado Plateau transition of Utah, in Mayer, L., ed., *Extensional tectonics of the southwestern United States—A perspective on processes and kinematics*: Geological Society of America Special Paper 208, p. 43–74.
- Arabasz, W.J., and Smith, R.B., 1981, Earthquake prediction in the Intermountain Seismic Belt—An intraplate extension regime, in Simpson, D.W., and Richards, P.G., eds., *Earthquake prediction: An international*

- al review: American Geophysical Union, Maurice Ewing Series 4, p. 238–258.
- Arabasz, W.J., and McKee, M.E., 1979, Utah earthquake catalog 1850–June 1962, in Arabasz, W.J., Smith, R.B., and Richins, W.D., eds., *Earthquake studies in Utah 1850 to 1978* Salt Lake City, University of Utah Seismograph Stations Special Publication, p. 423–432.
- Armstrong, R.L., 1963, K-Ar ages of volcanics in southwestern Utah and adjacent Nevada, in *Guidebook to geology of southwestern Utah*. Inter-mountain Association of Petroleum Geologists Annual Field Conference Guidebook, p. 79–80.
- Armstrong, R.L., 1968, Sevier orogenic belt in Nevada and Utah: *Geological Society of America Bulletin*, v. 79, p. 429–458.
- Averitt, P., 1964, Table of post Cretaceous geologic events along the Hurricane fault near Cedar City, Iron County, Utah: *Geological Society of America Bulletin*, v. 75, p. 901–908.
- Averitt, P., and Threet, R.L., 1973, Geologic map of the Cedar City quadrangle, Iron County, Utah: U.S. Geological Survey Geologic Quadrangle Map GQ-1120, scale 1:24,000.
- Axen, G.J., Taylor, W.J., and Bartley, J.M., 1993, Space-time patterns and tectonic controls of Tertiary extension and magmatism in the Great Basin of the western United States. *Geological Society of America Bulletin*, v. 105, p. 56–76.
- Axen, G.J., Wernicke, B.P., Skelly, M.F., and Taylor, W.J., 1990, Mesozoic and Cenozoic tectonics of the Sevier thrust belt in the Virgin Valley area, southern Nevada, in Wernicke, B.P., ed., *Basin and Range extensional tectonics near the latitude of Las Vegas, Nevada*: Boulder, Colorado, Geological Society of America Memoir 176, p. 123–153.
- Bausch, D.B., and Brumbaugh, D.S., 1994, Seismic hazards in Arizona: Arizona ground shaking intensity and 100-year acceleration contour maps: Unpublished report to the Arizona Division of Emergency Management and FEMA/NEHRP, 49 p., 2 maps, scale 1:1,000,000.
- Bell, F.G., 1983, *Engineering properties of soil and rock* London, Butterworths, 149 p.
- Best, M.G., Christiansen, E.H., and Blank, R.H., Jr., 1989, Oligocene caldera complex and calc-alkaline tuffs and lavas of the Indian Peak volcanic field, Nevada and Utah. *Geological Society of America Bulletin*, v. 101, p. 1076–1090.
- Best, M.G., and Grant, S.K., 1987, Stratigraphy of the volcanic Oligocene Needles Range Group in southwestern Utah: U.S. Geological Survey Professional Paper 1433-A, p. 3–28.
- Best, M.G., McKee, E.H., and Damon, P.E., 1980, Space-time-composition patterns of late Cenozoic mafic volcanism, southwestern Utah and adjoining areas: *American Journal of Science*, v. 280, p. 1035–1050.
- Billingsley, G.H., 1992a, Geologic map of the Gyp Pocket quadrangle, northern Mojave County, Arizona: U.S. Geological Survey Open-File Report 92-412, scale 1:24,000.
- Billingsley, G.H., 1992b, Geologic map of the Rock Canyon quadrangle, northern Mohave County, Arizona. U.S. Geological Survey Open-File Report 92-449, scale 1:24,000.
- Billingsley, G.H., 1993, Geologic map of the Grandstand quadrangle, northern Mohave County, Arizona: U.S. Geological Survey Open-File Report 93-588, scale 1:24,000.
- Black, B.D., Mulvey, W.E., Lowe, M., and Solomon, B.J., 1995, Geologic effects, in Christenson, G.E., ed., *The September 2, 1992 ML 5.8 St. George earthquake*, Washington County, Utah: Utah Geological Survey Circular 88, p. 2–11.
- Blank, H.R., Jr., and Kucks, R.P., 1989, Preliminary aeromagnetic, gravity, and generalized geologic maps of the USGS Basin and Range–Colorado Plateau transition zone study area in southwestern Utah, southeastern Nevada, and northwestern Arizona (the “BARCO” project). U.S. Geological Survey Open-File Report 89-432, 16 p.
- Bohannon, R.G., 1983a, Geologic map, tectonic map, and structure sections of the Muddy and northern Black Mountains, Clark County, Nevada. U.S. Geological Survey Miscellaneous Investigations Map I-1406, scale 1:62,500.
- Bohannon, R.G., 1983b, Mesozoic and Cenozoic tectonic development of the Muddy, North Muddy, and northern Black Mountains, Clark County, Nevada, in Miller, D.M., Todd, V.R., and Howard, K.A., eds., *Tectonic and stratigraphic studies in the eastern Great Basin* Boulder, Colorado, Geological Society of America Memoir 157, p. 125–148.
- Borgione, J., 1995, Impacts on dams, in Christenson, G.E., ed., *The September 2, 1992 ML 5.8 St. George earthquake*, Washington County, Utah: Utah Geological Survey Circular 88, p. 31–34.
- Bruhn, R.L., Gibling, P.R., and Parry, W.T., 1987, Rupture characteristics of normal faults: An example from the Wasatch fault zone, Utah, in Coward, M.P., Dewey, J.F., and Hancock, P.L., eds., *Continental extensional tectonics*. Geological Society Special Publication No. 28, p. 337–353.
- Bruhn, R.L., Yonkee, W.A., and Parry, W.T., 1990, Structural and fluid-chemical properties of seismogenic normal faults. *Tectonophysics*, v. 175, p. 139–157.
- Buck, W.R., 1988, Flexural rotation of normal faults. *Tectonics*, v. 7, p. 959–974.
- Bucknam, R.C., and Anderson, R.E., 1979, Estimation of fault-scarp ages from a scarp-height-slope-angle relationship. *Geology*, v. 7, p. 11–14.
- Butler, E., and Marsell, R.E., 1972, Developing a state water plan—cloud-burst floods in Utah, 1939–1969. Utah Division of Water Resources and U.S. Geological Survey Cooperative Investigation Report Number 11, 103 p.
- Butler, E., and Mundorff, J.C., 1970, Floods of December 1966 in southwestern Utah. U.S. Geological Survey Water-Supply Paper 1870-A, 40 p.
- Campbell, K.W., 1987, Predicting strong ground motion in Utah, in Gori, P.L., and Hays, W.W., eds., *Assessment of regional earthquake hazards and risk along the Wasatch Front*, Utah: U.S. Geological Survey Open-File Report 87-585, p. L-1–90.
- Carey, R., 1995, Estimated economic losses, in Christenson, G.E., ed., *The September 2, 1992 ML 5.8 St. George earthquake*, Washington County, Utah: Utah Geological Survey Circular 88, p. 40.
- Christenson, G.E., 1985, Rock-fall hazard, West Black Ridge, St. George, Utah, in Harty, K.M., ed., *Technical reports for 1984, Site Investigation Section*. Utah Geological and Mineral Survey Report of Investigation 198, p. 282–289.
- Christenson, G.E., 1992, Geologic hazards of the St. George area, Washington County, Utah, in Harty, K.M., ed., *Engineering and environmental geology of southwestern Utah*. Utah Geological Association Publication 21, Field Symposium, p. 99–108.
- Christenson, G.E., editor, 1995, *The September 2, 1992, ML 5.8 St. George earthquake*, Washington County, Utah: Utah Geological Survey Circular 88, 41 p.
- Christenson, G.E., and Deen, R.D., 1983, Engineering geology of the St. George area, Washington County, Utah. *Utah Geological and Mineral Survey Special Studies* 58, 32 p.
- Christenson, G.E., and Nava, S.J., 1992, Earthquake hazards of southwestern Utah, in Harty, K.M., ed., *Engineering and environmental geology of southwestern Utah*. Utah Geological Association Publication 21, Field Symposium, p. 123–138.
- Cook, E.F., 1952, Geology of the Pine Valley Mountains, a preliminary note: *Guidebook to the Geology of Utah*, Utah Geological and Mineralogical Survey, n. 7, p. 92–100.
- Cook, E.F., 1957, Geology of the Pine Valley Mountains, Utah. *Utah Geological and Mineralogical Survey Bulletin* 58, 111 p.
- Cook, E.F., 1960, Geologic atlas of Utah, Washington County: *Utah Geological and Mineral Survey Bulletin* 70, 119 p.
- Cook, K.L., and Hardman, E., 1967, Regional gravity survey of the Hurricane fault area and Iron Springs district, Utah: *Geological Society of America Bulletin*, v. 78, p. 1063–1076.

- Costa, J.E., and Baker, V.R., 1981, *Surficial geology, building with the earth*: New York, John Wiley and Sons, 498 p.
- Cowan, D.S., and Bruhn, R.L., 1992, Late Jurassic to early Late Cretaceous geology of the U.S. Cordillera, in Burchfiel, B.C., Lipman, P.W., and Zoback, M.L., eds., *The Cordilleran orogen: Conterminous U.S.* [Boulder, Colorado,] The Geological Society of America, *Decade of North American Geology*, v. G3, p. 169–204.
- Crone, A.J., and Haller, K.M., 1991, Segmentation and coseismic behavior of Basin and Range normal faults; examples from east-central Idaho and southwestern Montana, U.S.A. *Journal of Structural Geology*, v. 13, p. 151–164.
- dePolo, C.M., Clark, D.G., Slemmons, D.B., and Ramelli, A.R., 1991, Historical surface faulting in the Basin and Range Province, western North America. Implications for fault segmentation. *Journal of Structural Geology*, v. 13, p. 123–136.
- Dobbin, C.E., 1939, Geologic structure of St. George district Washington County, Utah: *American Association of Petroleum Geologists Bulletin*, v. 23, p. 121–144.
- Dubois, S.M., Smith, A.W., Nye, N.K., and Nowak, T.A., 1982, Arizona earthquakes, 1776–1980. Arizona Bureau of Geology and Mineral Technical Bulletin 193, 456 p.
- Earth Science Associates, 1982, Seismic safety investigation of eight SCS dams in southwestern Utah: Palo Alto, California, unpublished consultant's report to the U.S. Soil Conservation Service, Portland, Oregon, 2 volumes, variously paginated.
- Euge, K.M., Schell, B.A., and Lam, I.P., 1992, Development of seismic acceleration contour maps for Arizona. Unpublished report no. AZ92-344, Arizona Department of Transportation, 327 p., 5 maps, scale 1:1,000,000.
- Evans, J.P., and Langrock, H., 1994, Structural analysis of the Brigham City-Weber segment boundary zone, Wasatch normal fault, Utah: Implications for fault growth and structure. *Pageoph*, v. 142, p. 663–685.
- Everitt, B., 1992, Inspection of Pah Tempe Spring, October 10, 1992. Unpublished memorandum, Utah Division of Water Resources, 2 p.
- Everitt, B., and Einert, M., 1994, The 1985 slug test of Pah Tempe Springs, Washington County, Utah, in Blackett, R.E., and Moore, J.N., eds., *Cenozoic geology and geothermal systems of southwestern Utah*. Utah Geological Association Publication 23, p. 189–194.
- Gardner, L.S., 1941, The Hurricane fault in southwestern Utah and northwestern Arizona. *American Journal of Science*, v. 239, p. 241–260.
- Gourley, C., 1992, Geological aspects of the Quail Creek dike failure, in Harty, K.M., ed., *Engineering and environmental geology of southwestern Utah*. Utah Geological Association Publication 21, p. 17–38.
- Grant, S.K., 1995, Geologic map of the New Harmony quadrangle, Washington County, Utah. Utah Geological Survey Miscellaneous Publication 95-2, 32 p., 1 plate, scale 1:24,000.
- Gregory, H.E., and Williams, N.C., 1947, Zion National Monument. *Geological Society of America Bulletin*, v. 58, p. 211–244.
- Hamblin, W.K., 1970, Late Cenozoic basalt flows of the western Grand Canyon, in Hamblin, W.K., and Best, M.G., eds., *The western Grand Canyon district*. Utah Geological Society Guidebook to the Geology of Utah, v. 23, p. 21–37.
- Hamblin, W.K., 1965, Origin of “reverse drag” on the downthrown side of normal faults: *Geological Society of America Bulletin*, v. 76, p. 1145–1164.
- Hamblin, W.K., 1963, Late Cenozoic basalts of the St. George Basin, in *Geology of southwestern Utah*. Intermountain Association of Petroleum Geologists Guidebook 12th Annual Field Conference, p. 84–89.
- Hamilton, W.L., 1984, The sculpturing of Zion. Springdale, Utah, Zion Natural History Association, 132 p.
- Harty, K.M., 1990, Field reconnaissance of the effects of the July 31, 1989, storm and flood on Cedar City and the Cedar Canyon landslide, Iron County, Utah, in Black, B.D., ed., *Technical reports for 1988–1989, Applied Geology Program*. Utah Geological and Mineral Survey Report of Investigation 220, p. 118–121.
- Harty, K.M., 1992, Landslide distribution and hazards in southwestern Utah, in Harty, K.M., ed., *Engineering and environmental geology of southwestern Utah*: Utah Geological Association Publication 21, p. 109–118.
- Hill, D.P., and 30 others, 1993, Seismicity remotely triggered by the magnitude 7.3 Landers, California, earthquake: *Science*, v. 260, p. 1617–1623.
- Hintze, L.F., 1963, Geologic map of southwestern Utah. Provo, Brigham Young University, Department of Geology, scale 1:250,000.
- Hintze, L.F., 1980, Geologic map of Utah. Utah Geological and Mineral Survey, scale 1:500,000.
- Hintze, L.F., 1986, Stratigraphy and structure of the Beaver Dam Mountains, southwestern Utah, in Griffen, D., and Phillips, W.R., eds., *Thrusting and extensional structures and mineralization in the Beaver Dam Mountains, southwestern Utah*. Utah Geological Association Publication 15, p. 1–36.
- Hintze, L.F., 1988, Geologic history of Utah. Provo, Brigham Young University Studies Special Publication 7, 202 p.
- Hintze, L.F., Anderson, R.E., and Embree, G.F., 1994, Geologic map of the Motoqua and Gunlock quadrangles, Washington County, Utah. U.S. Geological Survey Miscellaneous Investigation Series Map I-2427, scale 1:24,000.
- Hurlow, H.A., in press, The geology of the central Virgin River basin, southwestern Utah, and its relation to ground-water conditions. Utah Geological Survey Special Study.
- Hurlow, H.A., 1996, Contraction, extension, and strike-slip faulting in the Colorado Plateau-Basin and Range transition zone. Neogene-Quaternary tectonic evolution of the New Harmony and Kanarrville basins, southwest Utah. *Geological Society of America Abstracts with Programs*, v. 28, n. 7, p. A449.
- Irvine, T.N., and Baragar, W.R.A., 1971, A guide to chemical classification of the common volcanic rocks. *Canadian Journal of Earth Sciences*, v. 8, p. 523–548.
- Jackson, G.W., 1990, Tectonic geomorphology of the Toroweap fault, western Grand Canyon, Arizona: Implications for transgression of faulting on the Colorado Plateau: Arizona Geological Survey Open-File Report 90-4, 67 p. scale 1:24,000.
- Janecke, S.U., 1993, Structures in segment boundary zones of the Lost River and Lemhi faults, east-central Idaho. *Journal of Geophysical Research*, v. 98, p. 16,223–16,238.
- Jibson, R.W., and Harp, E.L., 1996, The Springdale, Utah, landslide—An extraordinary event. *Environmental & Engineering Geoscience*, v. 2, n. 2, p. 137–150.
- Kalser, B.N., 1978a, Ground subsidence in Cedar City, Utah. Utah Geological and Mineral Survey Report of Investigation 124, 130 p.
- Kalser, B.N., 1978b, Field reconnaissance of proposed Hurricane airport site. Utah Geological and Mineral Survey unpublished letter to Mr. Dan Nelson, State Department of Transportation, Planning Division, 1 p.
- King, G.C.P., 1986, Speculations on the geometry of the initiation and termination processes of earthquake rupture and its relation to morphology and geological structure. *Pure and Applied Geophysics*, v. 124, p. 567–585.
- Kurze, A.E., 1966, Recurrent structural disturbance of the Colorado Plateau margin near Zion National Park, Utah: *Geological Society of America Bulletin*, v. 77, p. 867–872.
- Lay, T., Ammon, C.J., Velasco, A.V., Ritsema, J., Wallace, T.C., and Patton, H.J., 1994, Near-real time seismology. Rapid analysis of earthquake faulting: *GSA Today*, v. 4, n. 5, p. 129–134.
- Le Bas, M.J., Le Maitre, R.W., Streckeisen, A., and Zanettin, B., 1986, A chemical classification of volcanic rocks based on the total alkali-silica diagram. *Journal of Petrology*, v. 27, p. 745–750.

- Longwell, C.R., 1922, Muddy Mountain overthrust in southeastern Nevada *Journal of Geology*, v. 30, p. 63–72.
- Longwell, C.R., 1928, Geology of the Muddy Mountains, Nevada with a section through the Virgin Range to the Grand Wash Cliffs, Arizona. U.S. Geological Survey Bulletin 798.
- Longwell, C.R., Pampeyan, E.H., Bowyer, B., and Roberts, R.J., 1965, Geology and mineral deposits of Clark County, Nevada; Nevada Bureau of Mines and Geology Bulletin 62, 218 pp.
- Lovejoy, E.M.P., 1964, The Hurricane fault zone, and the Cedar Pocket Canyon-Shebit-Gunlock fault complex, southwestern Utah and northwestern Arizona: [Ph.D. Thesis] University of Arizona, 195 p.
- Lowe, M., 1992, The 1992 Truman Drive landslide, Santa Clara, Washington County, Utah, in Harty, K.M., ed., Engineering and environmental geology of southwestern Utah. Utah Geological Association Publication 21, p. 119–122.
- Lund, W.R., 1996, La Verkin Creek sinkhole investigation, Washington County, Utah. Utah Geological Survey Technical Report 96-30, 5 p.
- Lund, W.R., 1992, Flooding in southwestern Utah, in Harty, K.M., ed., Engineering and environmental geology of southwestern Utah: Utah Geological Association Publication 21, p. 159–164.
- Mabey, M.A., and Youd, T.L., 1989, Liquefaction severity index maps of the state of Utah, in Watters, R.J., ed., Engineering geology and geotechnical engineering. Rotterdam, A.A. Balkema, Proceedings of the 25th Symposium on Engineering Geology and Geotechnical Engineering, p. 305–312.
- Machette, M.N., Personius, S.F., Nelson, A.R., Schwartz, D.P., and Lund, W.R., 1991, The Wasatch fault zone, Utah—segmentation and history of Holocene earthquakes *Journal of Structural Geology*, v. 13, p. 137–149.
- Mackin, J.H., 1960, Structural significance of Tertiary volcanic rocks in southwestern Utah. *American Journal of Science*, v. 258, p. 81–131.
- Menges, C.M., and Pearthree, P.A., 1983, Map of neotectonic (latest Pliocene-Quaternary) deformation in Arizona: Arizona Bureau of Geology and Mineral Technology Open-File Report 83-22, 15 p.
- Moody, J.D., and Hill, M.J., 1956, Wrench-fault tectonics. *Bulletin of the Geological Society of America*, v. 67, p. 1207–1246.
- Mulvey, 1992, Engineering geologic problems caused by soil and rock in southwestern Utah, in Harty, K.M., ed., Engineering and environmental geology of southwestern Utah: Utah Geological Association Publication 21, p. 139–144.
- Mundorf, J.C., 1970, Major thermal springs of Utah. Utah Geological and Mineralogical Survey Water-Resources Bulletin 13, 60 p.
- Nava, S.J., Pechmann, J.C., Arabasz, W.L., Brown, E.D., Hall, L.L., Oehmich, P.J., McPherson, E., and Whipp, J.K., 1990, Earthquake catalog for the Utah region—January 1, 1986 to December 31, 1988: Salt Lake City, University of Utah Seismograph Stations Special Publication, 96 p.
- Neighbor, F., 1952, Geology of the Pintura structure, Washington County, Utah: Guidebook to the Geology of Utah, Utah Geological Society, n. 7, p. 79–80.
- Nelson, S.T., Davidson, J.P., and Sullivan, K.R., 1992, New age determinations of central Colorado Plateau laccoliths, Utah. Recognizing disturbed K-Ar systematics and re-evaluating tectonomagmatic relationships. *Geological Society of America Bulletin*, v. 104, p. 1547–1560.
- Newmark, N.M., 1965, Effects of earthquakes on dams and embankments. *Geotechnique*, v. 15, n. 2, p. 139–160.
- Olig, S.S., 1995, Ground shaking and modified Mercalli intensities, in Christenson, G.E., ed., The September 2, 1992 ML 5.8 St George earthquake, Washington County, Utah. Utah Geological Survey Circular 88, p. 12–20.
- Pearthree, P.A., Menges, C.M., and Mayer, L., 1983, Distribution, recurrence and possible tectonic implications of late Quaternary faulting in Arizona: Arizona Bureau of Geology and Mineral Technical Bulletin OFR 83-20, 36 p.
- Pechmann, J.C., Arabasz, W.J., and Nava, S.J., 1995, Seismology, in Christenson, G.E., ed., The September 2, 1992 ML 5.8 St George earthquake, Washington County, Utah. Utah Geological Survey Circular 88, p. 1.
- Pechmann, J.C., Arabasz, W.L., and Nava, S.J., 1992, The St George, Utah, earthquake of September 2, 1992. A normal-faulting earthquake with very weak aftershock activity. *EOS (Transactions, American Geophysical Union)*, v. 73, p. 399.
- Reynolds, S.J., 1988, Geologic map of Arizona: Arizona Geological Survey, scale 1:1,000,000.
- Richins, W.D., Zandt, G., and Arabasz, W.J., 1981, Swarm seismicity along the Hurricane fault zone during 1980–1981: A typical example for SW Utah. *EOS (Transactions, American Geophysical Union)*, v. 62, n. 45, p. 966.
- Rollins, K.M., Williams, T., Bleazard, R., and Owens, R.L., 1992, Identification, characterization, and mapping of collapsible soils in southwestern Utah, in Harty, K.M., ed., Engineering and environmental geology of southwestern Utah. Utah Geological Association Publication 21, p. 145–158.
- Rowley, P.D., Steven, T.A., Anderson, J.J., and Cunningham, C.G., 1979, Cenozoic stratigraphic and structural framework of southwestern Utah: U.S. Geological Survey Professional Paper 1149, 22 p.
- Sanchez, A., 1995, Mafic volcanism in the Colorado Plateau/Basin-and-Range transition zone, Hurricane, Utah. [Master's Thesis] University of Nevada, Las Vegas, 92 p.
- Schlische, R.W., 1995, Geometry and origin of fault-related folds in extensional settings: American Association of Petroleum Geologists Bulletin, v. 79, n. 11, p. 1661–1678.
- Schlische, R.W., 1993, Anatomy and evolution of the Triassic-Jurassic continental rift system, eastern North America. *Tectonics*, v. 12, p. 1026–1042.
- Schramm, M.E., 1994, Structural analysis of the Hurricane fault in the transition zone between the Basin and Range Province and the Colorado Plateau, Washington County, Utah. [Master's Thesis] University of Nevada, Las Vegas, 90 p.
- Schwartz, D.P., and Coppersmith, K.J., 1984, Fault behavior and characteristic earthquakes: Examples from the Wasatch and San Andreas fault zones. *Journal of Geophysical Research*, v. 89, n. B7, p. 5,681–5,698.
- Scott, D.L., Braun, J., and Etheridge, M.A., 1994, Dip analysis as a tool for estimating regional kinematics in extensional terranes. *Journal of Structural Geology*, v. 16, p. 393–401.
- Shroder, J.F., Jr., 1971, Landslides of Utah. Utah Geological and Mineralogical Survey Bulletin 90, 51 p.
- Smith, R.B., and Arabasz, W.J., 1991, Seismicity of the Intermountain seismic belt, in Slemmons, D.B., Engdahl, E.R., Zoback, M.D., and Blackwell, D.D., eds., Neotectonics of North America. [Boulder, Colorado] Geological Society of America, *Decade of North American Geology Map Volume 1*, p. 185–228.
- Smith, R.B., and Sbar, M.L., 1974, Contemporary tectonics and seismicity of the western United States with emphasis on the Intermountain seismic belt. *Geological Society of America Bulletin*, v. 85, p. 1205–1218.
- Solomon, B.J., 1996a, Engineering geologic map folio, Springdale, Washington County, Utah. Utah Geological Survey Open-File Report 340, scale 1:14,400.
- Solomon, B.J., 1996b, Landslide hazards of Springdale, near Zion National Park, Washington County, Utah. *Geological Society of America Abstracts with Programs*, v. 28, n. 4, p. 38–39.
- Solomon, B.J., 1993, Hurricane sinkhole—documentation of phone conversation: Utah Geological Survey unpublished information, 12 p.
- Sorauf, J.E., and Billingsley, G.H., 1991, Members of the Toroweap and Kaibab Formations, Lower Permian, northern Arizona and southwestern Utah. *Rocky Mountain Geologist*, v. 28, p. 9–24.

- Stewart, M.E., and Taylor, W.J., 1996, Structural analysis and fault segment boundary identification along the Hurricane fault in southwestern Utah. *Journal of Structural Geology*, v. 18, p. 1017–1029.
- Stokes, W.L., 1986, *Geology of Utah*. Utah Museum of Natural History, University of Utah Geol. and Mineral Survey, Dept. of Natural Resources, 280 p.
- Susong, D.D., Janecke, S.U., and Bruhn, R.L., 1990, Structure of a fault segment boundary in the Lost River fault zone, Idaho, and possible effect on the 1983 Borah Peak earthquake rupture. *Bulletin of the Seismological Society of America*, v. 80, p. 57–68.
- Taylor, W.J., and Bartley, J.M., 1992, Prevolcanic extensional breakaway fault and its geologic implications for eastern Nevada and western Utah. *Geological Society of America Bulletin*, v. 104, p. 255–266.
- Taylor, W.J., and Stewart, M.E., in review, Definition of fault segments from bedrock data: Segmentation of the Hurricane fault, southwestern Utah and northern Arizona: *Bulletin of the Seismological Society of America*.
- Utah Division of Comprehensive Emergency Management, 1981, *History of Utah floods, 1847–1981. Floodplain Management Status Report*.
- Utah Governor's Office of Planning and Budget, 1996, *Utah demographic and economic analysis—Washington and Iron Counties: Contact <www.gvinfo.state.ut.us>*.
- Wernicke, B., and Axen, G.J., 1988, On the role of isostasy in the evolution of normal fault systems: *Geology*, v. 16, p. 848–851.
- Wooley, R.R., 1946, *Cloudburst floods in Utah, 1850–1938*. U.S. Geological Survey Water-Supply Paper 994, 128 p.
- Youd, T.L., and Perkins, D.M., 1987, Mapping of liquefaction severity index. *Journal of Geotechnical Engineering*, v. 113, p. 1374–1392.
- Zhang, P., Slemmons, D.B., and Mao, F., 1991, Geometric pattern, rupture termination and fault segmentation of the Dixie Valley–Pleasant Valley active normal fault system, Nevada, U.S.A.: *Journal of Structural Geology*, v. 13, p. 165–176.
- Zoback, M.L., and Zoback, M.D., 1980, State of stress in the conterminous United States: *Journal of Geophysical Research*, v. 85, p. 6113–6156.

Fault-related Rocks of the Wasatch Normal Fault

JAMES P. EVANS

*Department of Geology, Utah State University
4505 University Boulevard, Logan, Utah 84322-4505*

W. ADOLPH YONKEE

*Department of Geosciences, Weber State University
2507 University Circle, Ogden, Utah 84408-2507*

WILLIAM T. PARRY

RONALD L. BRUHN

*Department of Geology & Geophysics, University of Utah
717 W.C. Browning Building, Salt Lake City, Utah 84112-1183*

ABSTRACT

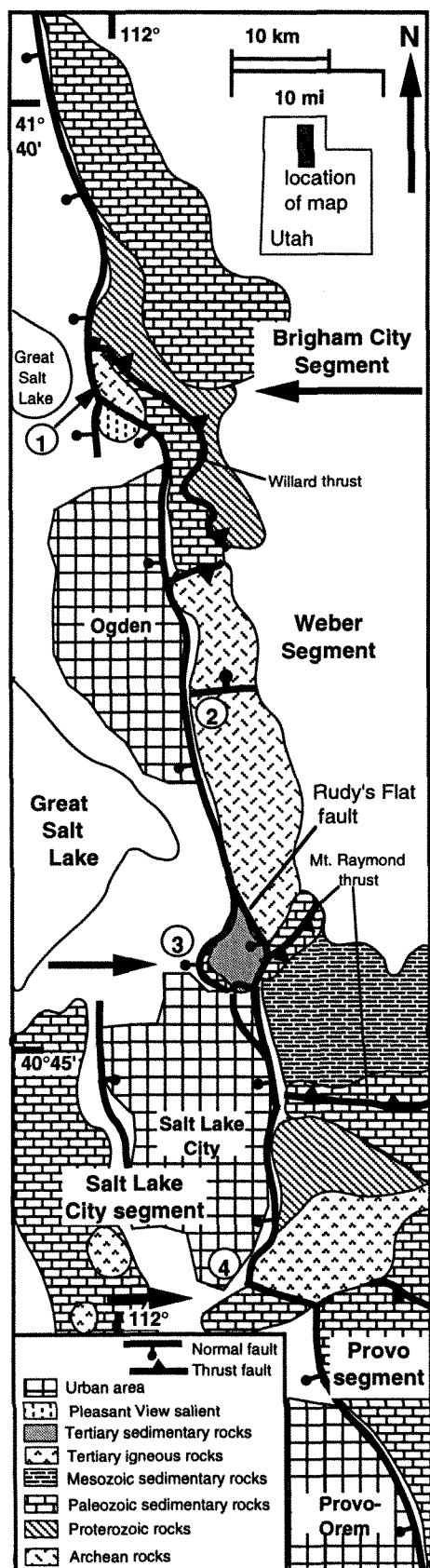
The Wasatch normal fault is a 370 km long fault zone composed of 10 segments which marks the physiographic boundary between the Basin & Range and Colorado Plateau/Rocky Mountains. Four to eleven km of slip along the Brigham City, Weber, and Salt Lake City segments has resulted in exhumation of numerous fault-related structures which record deformation mechanisms, geochemistry, temperatures, and fluid compositions present during faulting. Deformed Archean rocks at the southern tip of the Brigham City segment (Stop 1) and Oligocene Cottonwood Stock rocks Salt Lake City segment (Stop 4) record an evolution from deep level reaction softening and plastic deformation at $T \simeq 300\text{--}350^\circ\text{C}$ shallow-level to brittle faulting and cataclasis. Fluid inclusion data from rocks at the southern end of the Salt Lake City segment suggest pore fluid pressure varied from hydrostatic to lithostatic, which suggests P_f may reflect the seismic cycle. The distribution of chlorite-phyllonites and breccias, and subsequent brittle damage zone rocks, indicate the main slip surfaces of the Wasatch fault are enclosed in a weaker, more permeable region of hydrothermally altered and deformed rocks.

The orientation and distribution of structures at the localities also demonstrate the structure of faults at depth near fault bends and segment boundaries. Small fault data at the southern end of the Brigham City segment (Stop 1) are consistent with a $S70^\circ\text{W}$ plunging bedrock ridge, with slip complexly distributed across the ridge. Cross faults which intersect the Wasatch fault on the Weber segment (Stop 2) shows on a small scale how slip is distributed in a displacement transfer zone, where non-plane strain exists. The southern tip of the Salt Lake City segment also forms a southwest plunging bedrock ridge where numerous small faults accommodate slip across the segment boundary.

INTRODUCTION

The Wasatch fault zone of northern and central Utah (fig. 1) is one of the most thoroughly studied normal fault zones in the world, both in terms of paleoseismological studies (Schwartz and Coppersmith, 1984; Personius, 1990; Machette et al., 1991, 1992; Machette, 1992; Personius and Scott, 1992; Nelson and Personius, 1993; Hecker, 1993; McCalpin and Nishenko, 1996) and in terms of the characterization of the deformed bedrock in the footwall of the fault (Pack, 1926; Gilbert, 1928; Marsell, 1964, 1969; Parry

and Bruhn, 1986, 1987, 1990; Bruhn et al., 1987, 1990, 1992, 1994; Parry et al., 1988; Evans and Langrock, 1994). Numerous field trips along the fault have examined neotectonic features (e.g., Marsell, 1964; Machette, 1988; Nelson, 1988), but few modern field trips have focused on the nature of bedrock deformation and its use in interpreting the processes active along the fault. This field trip will visit localities along the Wasatch fault where detailed field mapping, structural petrography, geochemistry, geochronology, and modelling have focused on the style and distribution of



deformation adjacent to the fault, and where inferences regarding fluid flow and mechanical properties adjacent to the fault can be made.

GEOLOGIC SETTING

The Wasatch fault has long been recognized as a major fault which marks the eastern physiographic limit of the Basin and Range Province (Gilbert, 1890, 1928; Eardley, 1939). The fault is approximately 370 km long, and consists of 10 fault segments which extend from southern Idaho to central Utah (Gilbert, 1928; Swan et al., 1980; Machette et al., 1991, 1992). The segments are defined by Holocene slip histories as determined from trenching studies and on the basis of detailed mapping along the fault zone. Prominent topographic salients, where the mountains protrude westward and are underlain by bedrock, coincide with many of the segment boundaries (Machette et al., 1992; Wheeler and Krystinik, 1992). Gilbert (1928) was apparently the first to recognize and describe the salients that mark the boundaries between the Brigham City, Weber, Salt Lake City, and Provo segments (fig. 1), which are the focus of the stops described in this field guide. These bedrock salients may be rupture barriers between segments for long periods of time (Wheeler and Krystinik, 1992; Cowie and Scholz, 1992) and thus record deformation over a large time span of the fault.

The fault cuts a wide variety of rock types and structures along its entire trace (Eardley, 1944; Baker, 1964; Crittenden, 1965a, b; Hintze, 1980; Crittenden and Sorensen, 1985a, b; Bryant, 1990; Personius, 1990; Personius and Scott, 1992; Machette, 1992; Nelson and Personius, 1993). The Wasatch fault is superimposed on complex Cretaceous thrusts and folds of the Sevier fold and thrust belt (Eardley, 1944; Crittenden, 1974; Royse et al., 1975; Zoback, 1983; Smith and Bruhn, 1984; Yonkee et al., 1992; Arabasz et al., 1992). The major thrust structures are, from south to north, the Charleston-Mt. Nebo, Absaroska, and Willard thrusts and the imbricate stack of thrusts in the Ogden duplex (Schirmer, 1988; Yonkee, 1992). These thrust sheets have been cut by the Wasatch fault, exposing Late Archean through Jurassic rocks in the footwall.

Motion on the Wasatch fault zone may have started as early as 17.6 ± 0.7 U.C. Ma, based on a K-Ar date on hydrothermal sericite on rocks at the southern tip of the

Figure 1. Generalized geologic map of the Wasatch Front. Numbers indicate stops for this trip. The large arrows indicate the location of segment boundaries. Geology from Davis (1983, 1985), Personius (1990); Nelson and Personius (1993), Bryant (1990), and Personius and Scott (1993).

Salt Lake City segment where the fault cuts the Cottonwood stock (Parry et al., 1988). Apatite fission track ages of 9.6 to 8.2 my (Parry et al., 1988), and apatite fission track uplift rates of 0.4 mm/year for the past 10 million years (Naeser et al., 1983), suggest that rapid uplift along the central Wasatch fault began about 10 million years ago. Bryant et al., (1989) show that sedimentation rates in basins west of the Wasatch fault increased significantly at 10–12 million years ago, suggesting the onset of rapid slip along normal faults in the area began at that time.

Geophysical characterization of the region (Zoback, 1983; Mabey, 1992) shows that the basins in the hanging walls of the fault segments vary in thickness, and that numerous geophysical anomalies trend at high angles to the segments at or near segment boundaries. Gravity modelling suggests basin fill sequences are 1.2 to 3.8 km thick. Basin form is variable, with inferred maximum thicknesses of basin-fill roughly correlative with the centers of segments (Zoback, 1983; Mabey, 1992).

Historical seismicity in the area has been characterized by small to moderate events scattered throughout the hanging wall and footwall of the fault (Zoback, 1983; Arabasz and Julander, 1986; Arabasz et al., 1978, 1992). Locations of earthquakes in the area tend to be clustered at the northern and southern ends of the entire fault zone (Arabasz et al., 1992, their fig. 17; Pechman, 1992) with notable gaps on the Weber and Salt Lake City segments. Earthquakes on or near the Wasatch fault have been small, whereas the paleoseismologic data show that the fault segments are capable of M 7–7.5 earthquakes (see Machette et al., 1992 for a complete discussion of paleoseismological analyses of the Wasatch fault).

On this trip, we will travel to exposures of bedrock in the footwall of the Wasatch normal fault and examine evidence for deformation and fluid-rock interactions along the fault. These exposures reflect deformation at greenschist grade to shallow levels, and may record deformation for most of the fault history. We will first travel north to the bedrock salient known as the Pleasant View salient (stop 1), where Archean-Early Proterozoic rocks are in the footwall of the Wasatch normal fault. We then examine structures near Ogden in Paleozoic rocks (stop 2), shallow level deformation at the Beck Street Spur (Stop 3), and conclude with an examination of deformation of the Oligocene Little Cottonwood stock (stop 4).

Road Log

0.0		Depart the Salt Palace. Drive south on West Temple. Turn west on 1st South.
0.3	0.3	Turn right (north) on 2nd West.
2.7	3.0	Monroc Sand and Gravel quarries. The road veers around the western end of the

Beck Street salient at the northern end of the Salt Lake City. We will return to this site for Stop 3.

Merge with I-15.

View to east of basement rocks of Late Archean-Early Proterozoic Farmington Canyon Complex (Eardley and Hatch, 1940; Bryant, 1984, 1988) which lie on the steeply dipping eastern limb of a basement-cored anticline. "B" on hill slope to the east is at the Bonneville level of Lake Bonneville. Antelope Island visible to the northwest consists of Precambrian basement and gently dipping sedimentary cover rocks that lie on the western limb of a basement-cored anticline (Yonkee, 1992).

Quaternary landslide complex is visible to east.

Junction with U.S. Highway 89. Continue heading north on I-15.

Bumpy terrain in golf course to east is part of a lateral spread deposit that may have formed by ground failure during past earthquakes (Pashley and Wiggins, 1972).

View of Antelope Island to west.

The highway passes along the western (distal) edge of the Weber delta which was built out into ancient Lake Bonneville.

Descend onto alluvial deposits of Weber River.

View to the east shows the Willard and Ogden thrust systems, which display complex lateral ramps and branching of thrusts in the Wasatch Range. Details of this region are presented in Link et al., (1985, 1990; and Yonkee, 1992; Yonkee et al., this volume).

We are in the hanging wall of the Weber segment of the Wasatch normal fault, which last ruptured about 0.5 ka (Machette et al., 1989, 1992). Net displacement across the Wasatch fault zone in the Ogden area probably exceeds 5 km, and a deep hanging wall basin is filled with Miocene and younger deposits underlies the area to the west.

A view to the northeast from here shows the prominent shorelines of the Provo and Bonneville levels of Lake Bonneville, which are cut by younger alluvial fan and debris flow deposits

- sourced in the steep canyons beneath Ben Lomond Peak.
- 9.8 46.4 Exit 354. Take the exit and continue north on US 89.
- 1.5 47.9 Turn right onto the gravel road to the gravel pit owned by Jack B. Parsons Co. Note: This is a private road.
- 0.75 48.6 Turn left onto the road which is parallel to a canal. We are traversing the Pleasant View salient, which Gilbert (1928) first recognized as a bedrock-cored horse, mantled by deposits of Lake Bonneville.
- 1.1 49.7 Cross an outwash channel on the alluvial fan emanating from Pearson's Canyon. These debris flow channels were active in 1983 and 1984, and coarse material deposited during this event is on both sides of the road. Pearson's Canyon is at the 40° bend in the Wasatch fault (figs. 2, 3), which lies at the western margin of the bedrock to the east (Personius, 1990; Crittenden and Sorensen, 1985a). The scarp height south of Pearson's Canyon is 32 m, with an estimated offset of an alluvial fan surface of 19 m (Personius, 1990).
- 0.8 50.5 A concrete bridge crosses the canal. Turn onto the bridge, and follow the dirt track to the end (approximately 0.2 miles). Park.
- Stop 1. We are on the apex of the Holmes Canyon alluvial fan, which is an active region of coarse debris deposition (figs. 2, 3). Personius (1990) shows a scarp height of 22 m, and an offset of 18.5 m on the top of the alluvial fan surface here. Immediately to the east are exposures of deformed bedrock adjacent to the Wasatch fault.

We will examine fault-related rocks at the southern end of the Brigham City segment, in the Pleasant view salient. The Brigham City segment has a surface trace length of 40 km (Personius, 1990) and trends roughly north-south, except at the southern end of the segment, where it bends sharply to a N40°W trend (fig. 2) (Personius, 1990). The southern tip of the Brigham City segment overlaps the northern Weber segment by approximately 1.5 km at a 1 km left step here (Machette et al., 1991, 1992).

The Farmington Canyon Complex comprises the crystalline "basement" for the northern part of the Wasatch fault (Bryant, 1988), and is exposed in the footwall throughout the southern third of the Brigham City segment (fig. 2; Crittenden and Sorensen, 1985a,b; Personius, 1990). Rocks

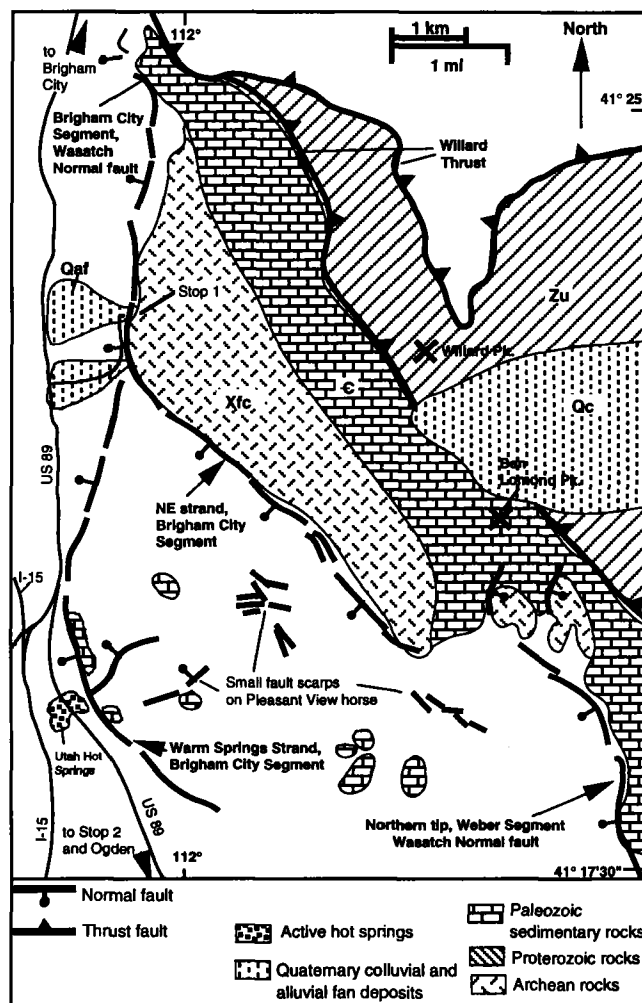


Figure 2. Detailed map of the southern termination of the Brigham City segment of the Wasatch Fault Zone. Bold lines indicate fault traces. The salient is formed by a left step between the Brigham City and Weber segments, and a western fault strand which bounds the Pleasant View horse. XFC—Farmington Canyon Complex; —Cambrian rocks; Zu—undifferentiated Proterozoic rocks in the hanging wall of the Willard thrust; Qc—Colluvium; Qaf—Alluvial fans. Unshaded region west of the Wasatch Fault is Lake Bonneville sediments. Geology from Crittenden and Sorensen (1985a, b); Personius (1990).

of the Farmington Canyon Complex are equigranular quartz-feldspar-biotite-hornblende gneiss. Foliation is defined by 1–10 cm mineral banding, and aligned micas and hornblende grains. Hanging-wall units of the Brigham City segment consist of Quaternary lacustrine sediments along the north-trending part of the segment (Personius, 1990) and a horse of Cambrian sedimentary rocks of the Pleasant View salient (Gilbert, 1928; Crittenden and Sorensen, 1985b).

The horse is bounded on the northeast by the northwest-striking strand of the Brigham City segment. On its west

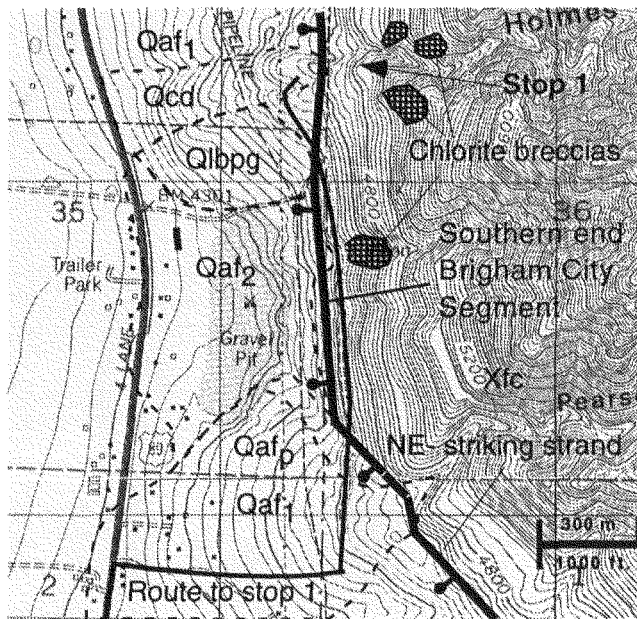


Figure 3. Detailed map of stop 1 geology. The fault trace corresponds closely with the Provo shoreline. At the mouth of Holmes Canyon, an alluvial fan is out by a scarp 22 m high, and an offset of 18 m. Chlorite breccias are indicated. Key to deposits on the hanging wall: Qafp—alluvial fan from Provo-level time (ca 1–3 14000 yrs b.p.); Qaf₁, Qaf₂—alluvial fans younger than Provo-level; Qlbpq—lacustrine near-shore grand deposits; Qcd—Debris flow deposits. Base map from Willard, Utah 7.5 minute quadrangle; geology from Personius, 1990; Evans and Langrock, 1994.

side the horse is bounded by an inferred southward continuation of the north-trending part of the Brigham City segment, termed the Hot Springs strand (fig. 2) (Gilbert, 1928; Crittenden and Sorensen, 1985b; Personius, 1990). Dip-slip displacement on the NW strand of the Brigham City segment is ~1.7 km, based on reconstruction of footwall and hanging-wall strata (Crittenden and Sorensen, 1985b). NE- and NW-striking Quaternary fault scarps cut the horse, and are especially numerous near the southern tip of the Brigham City segment (Personius, 1990).

Based on cross-cutting relationships, mesoscopic structures, and microstructures, we (Evans and Langrock, 1994) identify three major types of fault-related rocks and mesoscopic faults developed in the Farmington Canyon Complex adjacent to the Wasatch fault zone, and these faults are the focus of this stop. From oldest to youngest, these fault-related rocks are: (1) green and brown chlorite breccias and phyllonites, (2) planar, fretted “purple and brown weathered” fault surfaces, and (3) maroon and purple, highly polished, planar striated fault surfaces.

1. Chlorite breccias and phyllonites form an irregularly shaped, narrow north-trending band in the footwall

of the north-trending part of the Brigham City segment (fig. 3). Phyllonites are characterized by millimeter to centimeter thick, 20°–40° west-dipping foliation defined by chlorite-quartz layers (fig. 4). Down-to-the west motion is indicated by locally developed S-C fabrics developed at outcrop and thin-section scales (fig. 5a). Chlorite breccias consist of random-fabric zones which dip 30°–50° west in the immediate footwall of the Brigham City segment. The chlorite breccias comprise the majority of the chlorite zones.

Microstructures in the phyllonites consist of dynamically recrystallized quartz which forms elongated bands parallel to foliation (fig. 5a), and muscovite-chlorite which exhibit interlayer kinking and basal slip. Few feldspar grains remain in the phyllonite, and altered feldspars lie at the edges of the phyllonites.

The shallow dip of foliation of the phyllonites and their similarity to phyllonites and chlorite breccias in the footwall of the Salt Lake City segment (Bruhn et al., 1987; Parry and Bruhn, 1986; Stop 4 of this trip) is consistent with these rocks representing Wasatch fault-related rocks that formed at depth and have been uplifted in the footwall. However, unlike the fault-related rocks developed in Eocene-Oligocene quartz monzonites on the Salt Lake City segment (Bruhn et al., 1987), Farmington Canyon Complex rocks may also record Sevier contractional deformation (Yonkee, 1992).

2. Brown and purple fault surfaces are characterized by crescent-shaped, strike-parallel fractures, pits, and pockmarks that cut phyllonites, chlorite breccias, and the otherwise undeformed Farmington Canyon Complex protolith gneiss. Fretted, purple and brown weathered faults are planar to slightly curved, and the zone of deformation associated with a single surface is 1–10 cm thick. The fretwork faults are found in a broad zone adjacent to the north and NW-trending parts of the Wasatch fault, and their density appears to decrease east and northeast away from the trace of the Wasatch fault. Slickenlines are rare and tool marks and grooves are uncommon on these faults. Strike-parallel fractures inclined by 20°–40° to the fault surfaces resemble tensile or crescent fractures (Petit, 1987), which indicate down-to-the west motion.

Microstructures of the fretted purple weathered faults record fracture, frictional slip, and cataclasis (fig. 5b). Iron-oxide mineralization commonly fills fractures and thin cataclasite zones, suggesting at least limited fluid flow during development of these faults. Zones of distributed cataclasis are up to 10

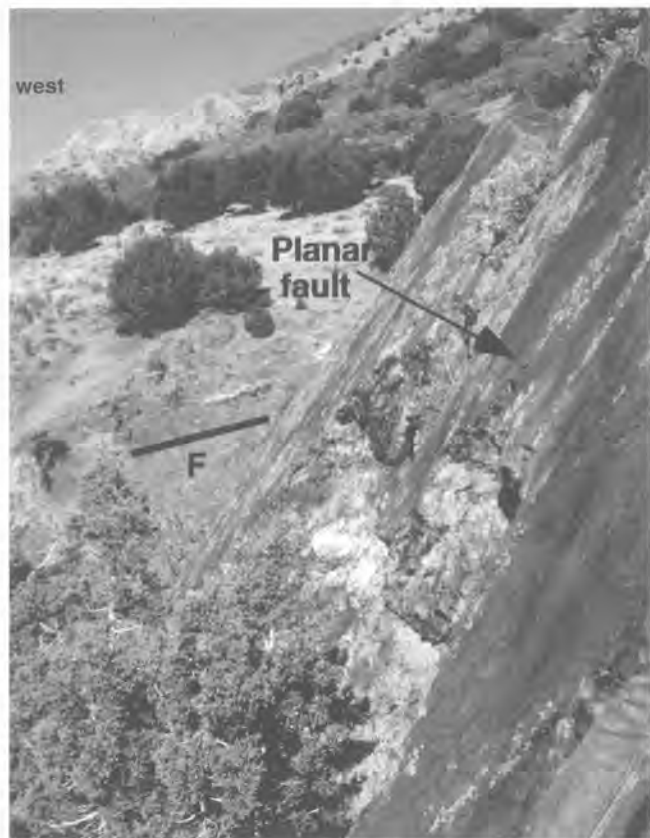


Figure 4. Outcrop photo of a younger, purple-weathered, planar fault surface in foreground dipping approximately 55° west, with 20° west-dipping chlorite phyllonites in the background (line S indicates dip of foliation). Trace of Wasatch fault is approximately 15 m to the west (left) of this view. View is to the north, from south-side of Holmes Canyon at stop 1. Wasatch Range is in the background.

- cm thick, and the fault-related rocks are all random-fabric cataclasesites.
3. The most striking mesoscopic faults at Stop 1 are west-dipping, maroon and purple, highly polished, planar faults. These faults are distributed throughout the study area, cut the phyllonites, chlorite breccias, and fretted faults, and their density decreases away from the trace of the Wasatch fault. The highly polished surfaces commonly have tool marks and grooves, some of which are curved, which record asperity ploughing and slip of the hanging wall in a down-to-the west sense. The fault surfaces are commonly only several millimeters thick.

Microstructures of the highly polished surfaces and related rocks indicate purely brittle deformation. Rocks adjacent to the narrow slip surfaces exhibit intra- and intergranular fracture, and very narrow zones of cataclasis (fig.

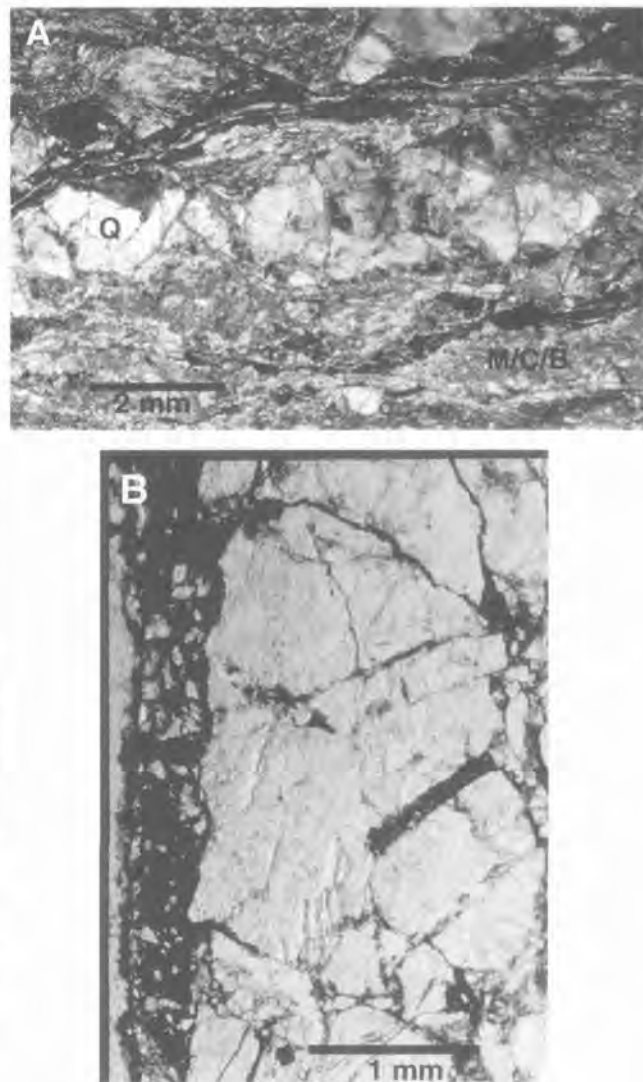


Figure 5. Photomicrographs of thin sections of samples at stop 1. A. Plastically deformed chlorite-muscovite phyllonite with west-dipping foliation developed in the footwall of the Wasatch fault at stop 1. Q-fractured quartz grain with some plastic deformation evident; M/C/B-Muxorite-Chlorite-Biotite. Cross-polarized light view. B. Plane-polarized light view of the narrow, highly polished faults superposed on fretted fault network. The narrow polished fault zone is approximately 0.2 mm wide at left side of photo, and consists of very fine grained hematite (crystallinity determined by x-ray diffraction). The network of fractures are due to brittle deformation related to the fretted faults, and consists of intergranular fractures filled with hematite and microcataclasis.

5b). The narrow slip horizons consist of very fine-grained hematite, usually in sharp contact with adjacent cataclastically deformed gneiss. Scant evidence from loose float blocks, and from several in-place hematite veins suggests

these faults may have first initiated as hematite-filled veins or coated fractures, and evolved into polished, planar surfaces.

The extreme polish of the mineralized surfaces and the microstructures may indicate extremely fast rates of slip on these surfaces (Grocott, 1981), which could represent seismic slip at several km depth, where confining pressures were large enough to maintain surface contact during a slip event. Conversely, these highly polished surfaces may represent aseismic creep (Power and Tullis, 1992), making a unique interpretation of slip rate for the highly polished surfaces difficult.

The orientations, spatial distributions, and characteristics of the three fault types represent an evolution from deep-level reaction softening and plastic deformation exhibited in the phyllonites and chlorite breccias to zones of cataclasis represented by the fretted purple-weathered faults and the polished planar faults. Phyllonites and chlorite breccias are restricted to the north-trending part of the Brigham City segment, which suggests deeper levels of the fault zone were exhumed there, or that more recent slip has stepped into the footwall on the northwest-striking strand, cutting out fault rocks from deeper levels.

Kinematic analyses of small fault populations in the footwall of the Brigham City segment constrain the orientations and relative magnitudes of principal stresses, and help examine the geometry of deformation in the footwall. We examined (Evans and Langrock, 1994) fault slip data for dominant clusters in slip directions and fault orientations and mean fault plane solutions, and inverted the fault data for principal stress orientations using the method of Gephart (1990a,b). Orientations of small faults on standard lower hemisphere stereograms (fig. 6) and kinematic analysis provide a first-order estimate of the orientation best-fit fault planes and a fast estimate of the orientations of the maximum and minimum principal stresses using the seismological convention for *P* and *T* axes. The stereograms and fault kinematic analyses show that along the north-striking trace, strikes of small faults roughly parallel the strike of the Wasatch fault zone.

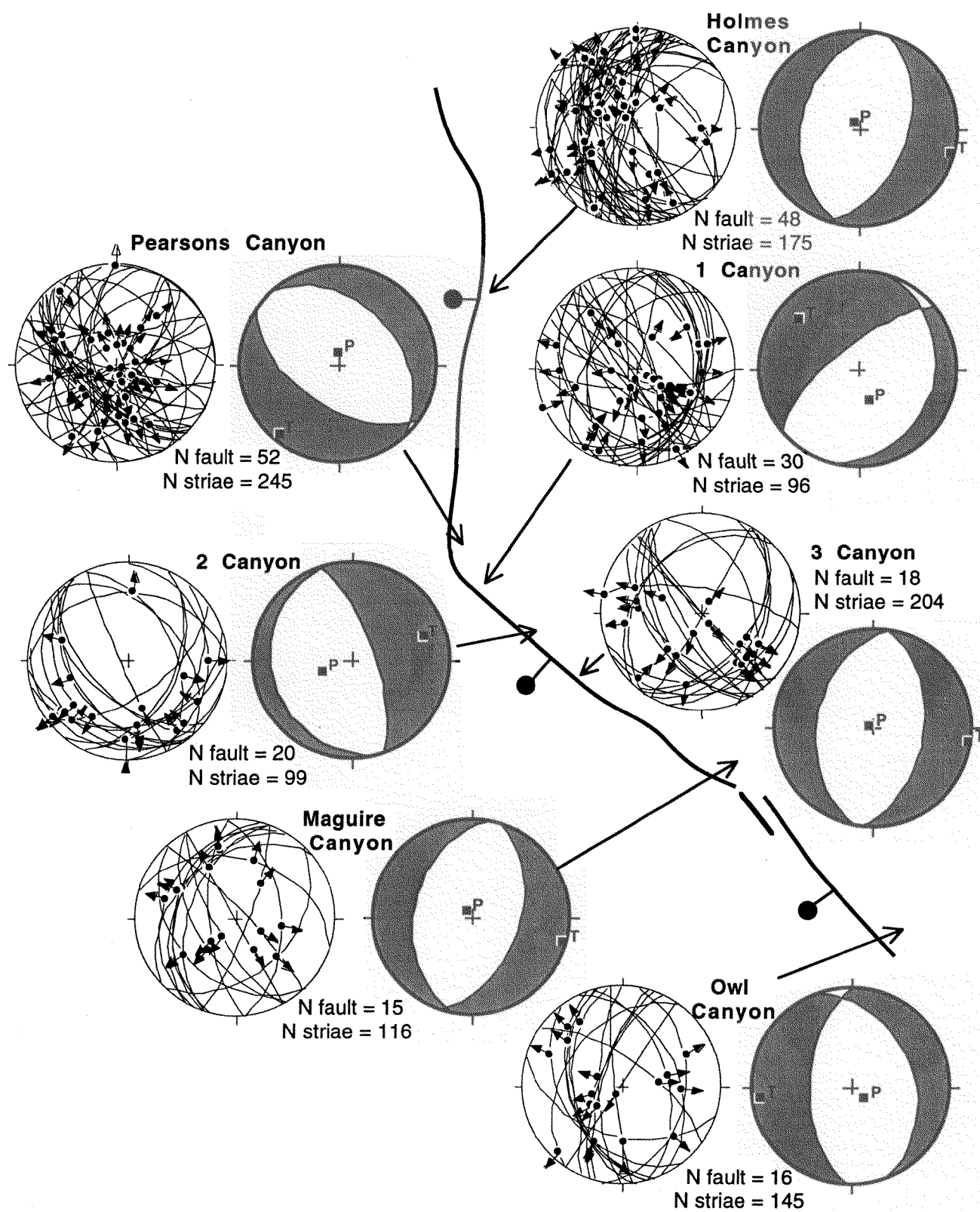
In the corner region and along the northern part of the northwest-striking strand of the Brigham City segment, the small faults strike northwest or northeast and slickenlines indicate slip occurred down-to the WNW, WSW, or south. Small oblique-slip components of both senses exist for most of the faults. The fault plane and slickenline data indicate oblique-slip motion generally on two sets of faults and non-plane strain behavior of these portions of the fault whereas the pseudo-nodal plane solutions yield nearly pure normal slip. The mean slip vectors along the NW-striking strand form a crude N70°W striking girdle distribution. This suggests that while fault slip occurred along faults of several orientations, including some at high angles to the main

trace of the fault, slip was restricted to a NW-striking band of deformation.

The kinematic and stress inversion analyses of the small faults, along with the mapping of the hanging wall horse (Personius, 1990) indicate that the segment boundary zone is a broad region of complex footwall and hanging-wall deformation. The different orientations of faults and slip vectors in the footwall, as well as the multiple orientations of faults in the Pleasant View horse (fig. 2) (Personius, 1990), may represent changes in the orientations of principal stresses over space or time, or represent non-plane strain behavior at the end of the fault segment (Scholz, 1990; Cowie and Scholz, 1992).

If the zone of deformation we observe is the result of fault tip damage, we would expect to see a similar, older damaged zone in the footwall to the north. The absence of a knot of complex faulting adjacent to the north-striking segment may be explained by several hypotheses: a) The damaged zone near the fault tip there may have been smaller, and was obliterated by later faulting, b) much of the damage occurred in the hanging wall, c) little damage occurred ahead of the relatively "cleanly" propagating shorter, north-striking fault segment, whereas the present Brigham City segment has developed a broad damaged zone at the fault tip due to encountering a structural complexity, or d) stresses on the fault changed over time.

- | | | |
|---------|------|---|
| 2.9 | 53.4 | Return to Highway 89 driving southward, the canal and returning through the gravel pit. Drive south on Highway 89 toward Ogden. |
| 1.6 | 55.0 | The road skirts Cambrian Tintic quartzites to the east, and hot springs emanating from the Wasatch fault to the west. |
| 7.8 | 61.2 | Highway 89 intersects with Washington Blvd in Ogden. Merge south. The rocks in the mountains to the east consist of thrustured Archean-Early Proterozoic basement and Cambrian strata in the Ogden Duplex (Schirmer, 1988; Yonkee, 1992). |
| 1.0 | 62.2 | Intersection with 12th South (Highway 39). Turn left (east). |
| 1.2 | 63.4 | Intersection with Harrison Blvd. turn right (south). We are driving up to the Provo-level delta of Lake Bonneville. |
| 1.0 | 64.4 | Intersection with 2100 South. Turn left (east). |
| 1.0 | 65.4 | Drive east to the trail head at the end of the street (fig. 7). |
| Stop 2. | | Stop 2 is located along the Weber segment near a small fault bend that was first described by Gilbert (1928). This area contains a northern fault and southern |



fault that both place Cambrian Tintic Quartzite against Quaternary unconsolidated deposits, and an east-striking cross fault that connects the two main faults, forming a composite cross-fault-intersection structure (fig. 7). The northern, southern, and cross faults are divided into approximately planar sections, but in detail, sections display roughness at a range of smaller scales, including crude ridges and troughs subparallel to slip directions. Sections of the northern fault dip 40 to 50° west and have west- to southwest-trending slip lineations. Sections of the southern fault also dip moderately westward and have west- to southwest-trending slip lineations. The cross fault dips steeply south, connects the northern and southern faults, which displays a 100 m left step along the cross fault. The cross fault and associated secondary faults have varying combinations of normal and sinistral slip, and displacement decreases to the east where the cross fault (C) continues into the footwall of the main faults. The northern fault (N) forms a bend along the intersection with the cross fault, and a fault-bounded bedrock wedge (S) is developed where the southern fault branches near the cross-fault intersection (fig. 7). Sections around the northern bend define an approximately cylindrical geometry of the fault, and slip directions diverge slightly around the bend. The change in slip directions, development of complex secondary faults near the cross fault, and formation of the bedrock wedge probably record displacement transfer and non-plane strain in the region connecting the northern and southern faults.

Figure 6. Lower hemisphere equal-area plots which depict the orientations of fault planes and slickenlines at seven localities along the Brigham City-Weber segment boundary zone. Kinematic solutions of the data give orientations of the nodal planes and mean compressional (P) axes and extensional (T) axes. Numbers indicate groups of data referred to in text. Open symbols indicate mean slip vectors.

Small faults across the bend can be interpreted to be due to east-west extension despite the variable slip vector orientations. From Evans and Langrock (1994).

Although some differences exist, the geometry and kinematics of this small-scale structure are similar to those in the boundary between the Salt Lake City and Provo segments (see stop 4), indicating that cross-fault-intersection structures may be important at a variety of scales. East-striking cross faults of varying trace length and displacement are widespread along parts of the Wasatch fault (fig. 1). Timing of slip on these faults is uncertain; some may have initiated during Mesozoic thrusting and been reactivated during Cenozoic extension, and others may be directly related to Cenozoic extension. Here the cross fault probably overlapped with early development of the northern and southern faults that cut bedrock, but these faults have not been active during the Holocene when near-surface faulting in the Wasatch fault zone shifted westward within surficial deposits. Some intersections with larger cross faults may develop into rupture boundaries (as between the Salt Lake City and Provo segments, stop 4), depending partly on the scaling and geometric relations between faults. Some intersections may affect, but not stop, rupture propagation, and some intersections may have no significant affect on ruptures. Both situations probably occurred here during recent episodes of faulting.

1.0	66.4	Return to Harrison Blvd. Turn right (south). As we drive south, we traverse the top of the Provo-level delta. The surface trace of the Wasatch fault in this area is marked by a single scarp 10–34 m high (Nelson and Personius, 1993).
2.6	69.0	Pashley & Wiggins (1972) and Nelson & Personius (1993) interpret the hummocky terrain on the left to mark a sequence of lateral spread and landslide deposits.
1.7	70.7	Road merges with Highway 89. Turn left (east). We descend to the Weber River flood plain.
13.4	84.1	Highway 89 merges with I-15 south bound. The surface trace of the Wasatch fault along this stretch splits into 2 or 3 scarps. Approximately 4.3 miles north of I-15 lies the site of the Kaysville trench, one of the first paleoseismology trenches in the Great Basin (Swan et al., 1980;

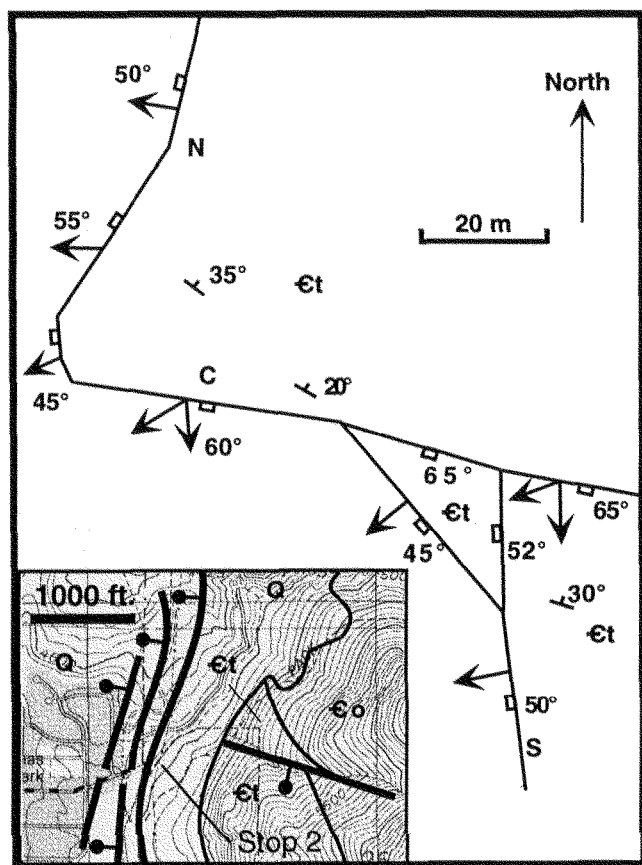


Figure 7. Generalized geologic map of composite cross-fault intersection structure at Stop 2, Ogden, Utah. Strike and dip of approximately planar fault sections and average slip directions are indicated. Units are: Ct—Cambrian Tintic Quartzite; Co—Cambrian Ophir Formation; and Q—Quaternary lacustrine, colluvial, and alluvial fan deposits. Dashed line indicates field trip route.

The Salt Lake City segment of the Wasatch fault zone is about 35 km long and consists of several approximately planar sections, each 3 to 12 km in length, that meet along fault bends and branches (fig. 1; Bruhn et al., 1987; Persenius and Scott, 1992). Estimated dips range from 30 to 60°. Paleostress analyses along the Salt Lake City segment have indicated a subhorizontal minimum compressive stress trending between 230 and 250°, consistent with west to southwest-trending normal to oblique slip along the fault sections (Bruhn et al., 1987; Yonkee and Bruhn, unpublished data).

The Salt Lake City salient, a complexly faulted and partly buried west-southwest-trending ridge of Tertiary and Paleozoic bedrock (Van Horn, 1982; Van Horn and Crittenden, 1987), forms the northern boundary of the Salt Lake City segment. Gravity and drill hole data indicate that the bedrock ridge continues westward into the Salt Lake Valley (Zoback, 1983), and a diffuse belt of epicenters of small earthquakes lies above this ridge. The Salt Lake City salient is a non-conservative barrier that separates the Weber and Salt Lake City segments (Schwartz and Coppersmith, 1984; Machette et al., 1991). The salient is largely covered by gently east-dipping Tertiary clastic and volcanoclastic deposits and these deposits are separated from Precambrian bedrock and steeply dipping Paleozoic rocks by the Rudys Flat fault along the eastern boundary of the salient. This west-dipping normal fault is "scoop-shaped" and varies in strike from northwest to northeast. The interior of the salient contains several north- to northwest-striking synthetic and antithetic normal faults, and several northeast-striking faults. The salient is partly bounded on the south by the west-northwest-striking Virginia Street fault. The north-striking Warm Springs fault separates Paleozoic and Tertiary bedrock from Quaternary deposits along the western margin of the salient (fig. 8) (Gilbert, 1928; Marsell, 1964, 1969; Scott, 1988). This fault appears to bend around the salient and a northeast-striking branch bounds the northwestern margin of the salient. A possible fault branch also continues north of the salient (Van Horn, 1982). The southern extent of the Warm Springs fault is uncertain, and this fault may be en echelon or merge with the main part of the Salt Lake City segment.

The Warm Springs fault dips 40 to 80° west within the MONROC quarries, and places southeast-dipping beds of Mississippian limestone in the footwall against Quaternary deposits in the hanging wall (fig. 8) (Marsell, 1969; Paulis and Smith, 1980). Deposits of Lake Bonneville are offset by 10 to 15 m across the fault, probably recording multiple slip events (Gilbert, 1928; Marsell, 1964). Fault surfaces display two dominant sets of slickenlines, a west-southwest-trending set and an older west-northwest-trending set (Paulis and Smith, 1980). Fault surfaces also display undulations

McCalpin & Nishenko, 1996). The last rupture on this segment was approximately 900 years ago, and 5 events dating back to 6400 years b.p. are recorded on the Weber segment (McCalpin & Nishenko, 1996).

- | | | |
|---------|------|---|
| 1.0 | 95.1 | Highway 89 exit. Get off I-15. |
| 2.7 | 97.8 | Continue south on Highway 89 past the Monroc Gravel Plant, and pull off in the industrial area on east side of street. Stop 3. |
| Stop 3. | | Tectonics of the Warm Springs fault zone and Salt Lake City segment of the Wasatch fault zone. Stop at pull out approximately 0.5 miles south of MONROC headquarters. |

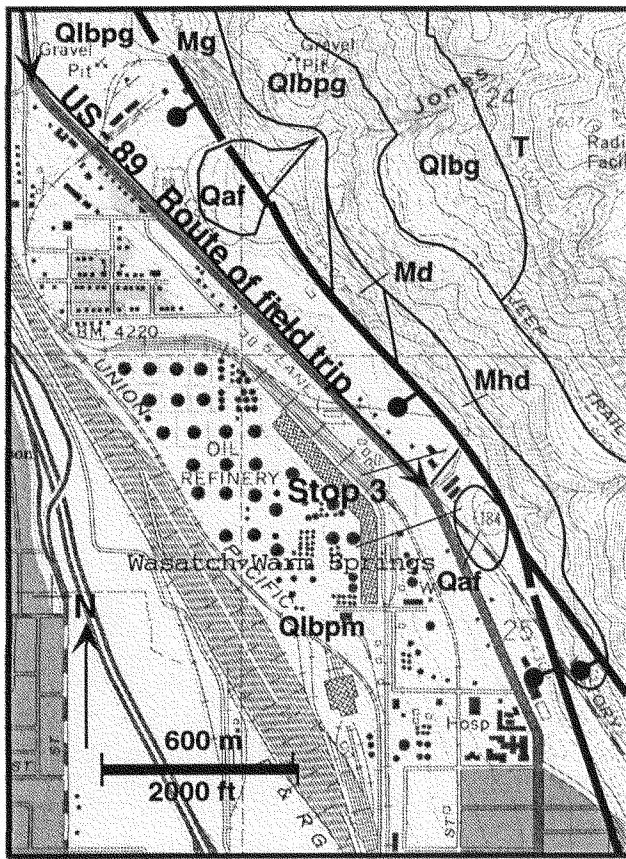


Figure 8. Geologic map of the Warm Springs section of the Wasatch fault at stop 3. Paleozoic carbonates are in the footwall here, and are overlain by Tertiary sediments and Lake Bonneville deposits. Mg—Gardison Formation; Md—Deseret Limestone; Mhd—Hamburg/Dunct Formations; T—Tertiary sediments; Qlbpg—lacustrine gravels of undifferentiated lake cycles; Qlb—Bonneville-stage lacustrine gravels; Qlbpm—Fine-grained lacustrine sediments; Qaf—alluvial fan deposits.

with wavelengths and amplitudes of millimeters to meters. Most undulations are aligned subparallel to slickenlines which are oriented approximately down the dip of the fault.

Pavlis and Smith (1980) show that slickenline data reflect dip slip displacement, with 3 or 4 events recorded by tool marks on the limestones. Photomicrographs of the fine-grained carbonate that forms a carapace have cataclastically deformed limestone grains entrained in the carbonate (fig. 9). The carbonate has a crude layering in thin section and outcrop. Ridges with crests parallel to dip and faint strike suggest the carbonate was explaced during faulting.

- 1.4 99.2 Drive south on Highway 89 to 5th North. Turn right (west). Proceed 0.5 miles to I-15, and return to I-15 south bound. As we travel southward along the Salt Lake

Valley, views of the geology of the Wasatch Range to the east are clear. The Wasatch Range east of the University of Utah (look for the U on the mountain front) to several miles south of Parleys Canyon consists of northeast trending folds in Triassic and Jurassic strata (Crittenden, 1965b; Van Horn and Crittenden, 1987; Bryant, 1990). These folds lie in the hanging wall of the east-striking, north-dipping Mt. Raymond thrust which intersects the mountain front due east of exit 304. South of the thrust, Cambrian and Proterozoic sedimentary rocks can be seen along the mountain front. At exit 298, we are due east of Little Cottonwood Canyon, which roughly coincides with the northern boundary of the Eocene Little Cottonwood Stock. Little Cottonwood Canyon was glaciated during the Pleistocene, and lateral moraines at the mouth of the Canyon are cut by the Wasatch fault, forming spectacular fault scarps depicted in many texts.

- 17 116.2 Exit 297 for Highway 71 (12,300 South). Get off I-15 and head east on Highway 71.
- 1.1 117.3 Turn right on 700 East. Drive 1 block, and turn east on the continuation of 12300 South (fig. 10).
- 1.9 119.2 Paved road ends. Turn right onto the gravel road.
- 0.8 120.0 Pull off road and park. Stop 4: Cherry Creek Canyon (fig. 10).

Stop 4.

Boundary between the Salt Lake City and Provo segments. Park along the side of the gravel road. Discussion of large-scale kinematics and short hike to observe nature of fault zone. Four features in this area are noteworthy: (1) kinematics of fault segments in the boundary are important in controlling rupture nucleation and propagation; (2) deeper levels of the fault zone were complex, up to several hundred meters wide, and consisted of anastomosing minor faults; (3) hydrothermal alteration and fluid-pressure fluctuations were important in evolution of the fault zone; and (4) the intensity and nature of alteration and fracturing produced changes in physical properties of the fault zone.

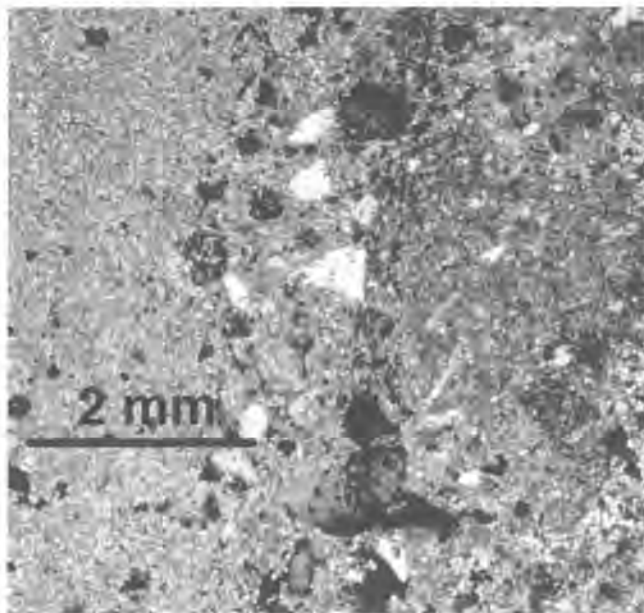


Figure 9. Cross-polarized light photomicrograph of the carbonate carapace formed along the Warm Springs portion of the Wasatch fault at stop 3, Beck Street locality. Before recent excavations the 1–4 cm thick, spelean calcite, was distributed across a large portion of the fault surface, and exhibited elongation undulations which have long axes oriented down-dip, and have faint down-dip lineations. This thin section exhibits a foliation parallel to the fault (vertical in this view). Small angular carbonate fragments from the footwall are entrained in the calcite, and appear to be the result of fragmentation during faulting, which were subsequently suspended in the calcite. This relationship suggests that carbonate-rich fluids have emplaced shortly after fragmentation.

Stop 4 is near a complex boundary between the Salt Lake City and Provo segments where the main fault zone curves around the base of the Wasatch Mountains (fig. 10; Schwartz and Coppersmith, 1984; Bruhn et al., 1987; Bruhn et al., 1990). Faulting in this area may have initiated by 17 Ma based on a K-Ar date of hydrothermal sericite (Parry and Bruhn, 1986). Apatite fission track ages record onset of rapid uplift and erosion by 10 Ma, with an ongoing average vertical displacement rate from 0.5 to 0.8 mm/yr (Evans et al., 1985; Kowallis et al., 1990). Total vertical displacement is greater than 11 km (Parry and Bruhn, 1986). Within the boundary, the two main segments display several bends and a ~6 km left step along an E-striking cross fault, which continues into the footwall as the Deer Creek fault. A complexly deformed bedrock ridge lies above the subsurface projection of the boundary within the hanging wall to the southwest in the Traverse Mountains. The boundary marks a change in rupture history between the Salt Lake City and Provo segments and its subsurface projection corresponds to a region of diffuse, historic microseismic activity, includ-

ing a $M_L=5$ earthquake in 1991 (Pechman, 1992), indicating that the boundary is important in nucleating and stopping ruptures at a range of scales. The fault zone cuts and deforms the Little Cottonwood granitic stock and well-exposed uplifted fault rock provides an excellent opportunity to examine the nature of deformation and fluid-rock interaction that occurred at deeper levels near the base of the seismogenic layer around the boundary.

At a megascopic scale, the segments are divided into crudely planar sections that vary systematically in orientation around the boundary (fig. 10), although in detail, fault sections display roughness at a variety of scales. Average slip directions also vary systematically around the boundary, but are locally variable along associated minor faults. The Salt Lake City segment is divided into four sections that define an approximately cylindrical bend with an axis plunging 25° toward 230° (S1–S4). Strikes of the sections vary from NE to NW, dips decrease from 45° to 25° around the bend, and trends of slip directions vary from W to WSW (fig. 11). The Deer Creek cross fault is divided into three sections (D1–D3) that dip 25° SW to 35° S and link the two main segments. Average slip directions plunge gently SW, but slip lineations on associated minor faults display large variations. Overall, slip directions diverge slightly around the bend in the Salt Lake City segment and along the Deer Creek fault, with complex deformation along minor faults in the boundary accommodating displacement transfer. WSW-striking normal faults that bound a fractured bedrock ridge in the hanging wall form a roughly conical structure parallel to and above the boundary axis, and accommodate both SW and NW extension. The northern part of the Provo segment is divided into 2 sections (P1 and P2) that dip moderately W to SW and have WSW-trending slip directions.

Observed slip directions for fault networks at different scales provide a record of “average” paleostress tensors, although in detail the stress field was spatially and temporally variable. Average slip directions for the main fault sections are consistent with a best-fit regional stress tensor having a steeply W-plunging σ_1 axis, a gently NNW-SSE-plunging σ_2 axis, a gently ENE–WSW-plunging σ_3 axis, and a stress magnitude ratio ϕ of 0.5 (fig. 11) (where $\phi = \sigma_1 - \sigma_3 / \sigma_2 - \sigma_3$), where $\sigma_1 > \sigma_2 > \sigma_3$ are the principal stresses. These values are similar to results obtained by Gibler (1986) for fault networks along the Salt Lake City segment. The regional σ_3 axis is subparallel to the trend of the boundary axis, but slip directions for individual faults diverge slightly around the boundary. Slip directions on minor faults within domains around the boundary display more complicated patterns. Domains away from the boundary have estimated local stress tensors similar to the regional tensor, but local stress tensors for domains within the boundary have lower values of ϕ and greater variations in

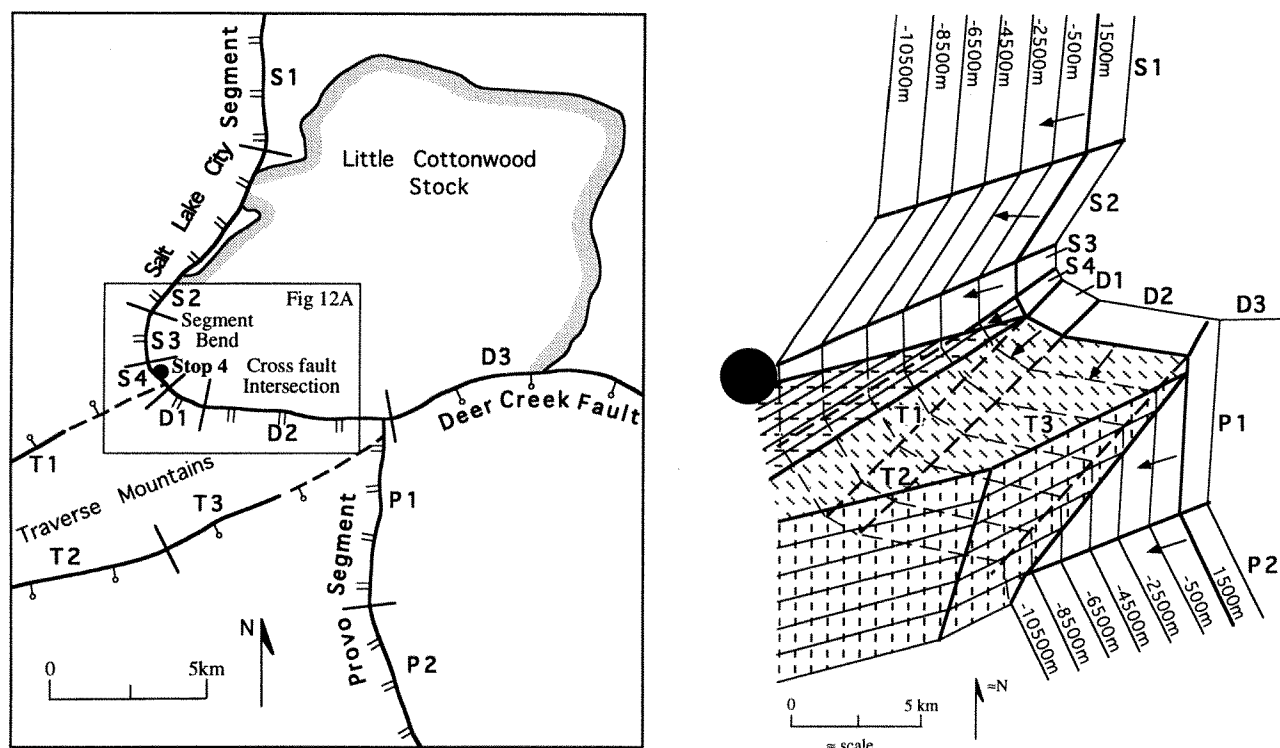


Figure 10. A. Index map of the large-scale structure of the Wasatch fault at a composite segment-bend, cross-fault-interaction boundary near stop 4. The Salt Lake and Provo segments and Deer Creek fault are divided into approximately planar fault sections labeled S1 to S4, P1 to P2, and D1 to D3. Major hanging wall faults that bound the Traverse Mountains are labeled T1 to T3. Location of figure 12A indicated.

B. Perspective view down and to NE of large-scale geometry of fault sections. Structure contours indicated and location of 1991 ML ~5 earthquake focus shown by solid circle. Average slip directions, indicated by arrows, diverge slightly around the boundary. Sections labeled same as in part A.

the trends of σ_3 axes. The decrease in ϕ for minor fault networks within the boundary may be related to divergence of slip vectors on the main fault sections around the bend, resulting in non-plane strain with components of both SW and NW extension. Also, individual minor faults in the boundary display large variations in slip directions, reflecting non-plane strain and temporal variations in stress, which may be partly related to complex deformation near rupture tips and intersecting fault sections.

The intensity of deformation and alteration varies with structural position within the fault zone and boundary (fig. 12; Yonkee and Bruhn, 1990; Bruhn et al., 1994). Relatively undeformed and unaltered footwall granite away from the fault, referred to as zone 0, is cut by widely spaced (average spacing > 1 m), relatively long (average trace lengths > 1 m), fractures (fig. 9). The fractures form simple networks consisting of steeply dipping and subhorizontal sets, and some fractures display limited alteration and minor extension or shear. Footwall granite grades upward into a transition zone of heterogeneously deformed and altered rock, with a preserved thickness that varies from about 20 m to > 200 m

within the boundary (fig. 12b). The lower part of the transition zone, referred to as zone 1, is cut by closer spaced (dm-scale average spacing) fractures that display more intersections, mutual truncation, and offset compared to footwall granite in zone 0 (figs. 12c, 13b). The upper, more deformed part of the transition zone, referred to as zone 2, is characterized by complex, anastomosing networks of closely spaced (cm-scale average spacing) fractures and minor faults (figs. 12c, 13c). Most trace lengths are less than 1 m, reflecting continued mutual offset and truncation of fracture and faults that display numerous intersections. Widespread veins are generally steeply dipping, display evidence for repeated cracking and sealing events, and produce locally significant dilation and horizontal extension, although some veins are activated as minor faults with both reverse and normal slip. The transition zone grades upward into a slip zone (zone 3) composed of discontinuous lenses of breccia, finely comminuted cataclasite, highly altered and partly recrystallized phyllonite, and large striated slip surfaces (fig. 12c). The slip zone has a preserved thickness generally < 10 m, but its total thickness is uncertain due to

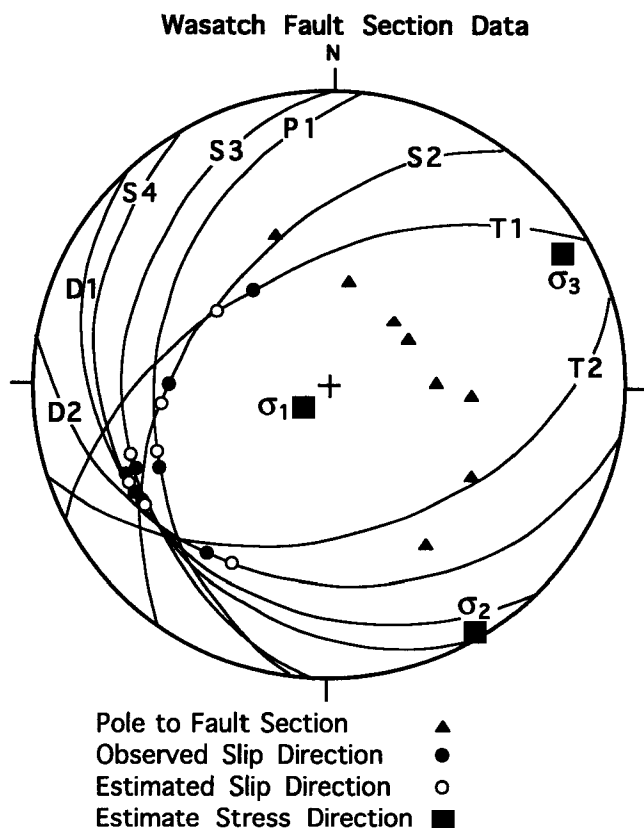


Figure 11. Equal area stereogram showing geometric relations of major structures. Average fault sections shown by great circles, poles to fault sections shown by triangles, observed average slip directions indicated by solid circles, and estimated average slip directions from stress inversion indicated by open circles. Principal stress directions estimated from stress inversion shown by squares. See figure 10A for explanation of fault section labels.

truncation by major slip surfaces. A phyllonitic fabric, defined by stretched quartz grains, fractured and boudinaged feldspar grains, and preferred orientation of altered mica aggregates is locally developed and overprinted by fractures, carbonate- and zeolite-filled veins, and cataclastic zones. Veins of partly altered and recrystallized pseudotachylite both cross cut and are deformed by the phyllonitic fabric, recording overlapping plastic flow and brittle faulting during generation of large earthquakes (Yonkee and Bruhn, 1990). Some large slip surfaces also have associated ultracataclasite dikes that are injected into adjacent wall rock.

Changes in fracture networks are evident along our hike across the fault zone. At point 4-1 in the lower part of the transition zone (fig. 12a), the network includes: (1) a dominant set of relatively long, close-spaced, moderately W-dipping, shear fractures parallel to the main fault zone; (2) a set of shorter, variably spaced, steeply dipping, hybrid frac-

tures that connect set 1 fractures; (3) a set of steeply dipping, hybrid and extensional cross fractures that strike at high angles to the main fault zone; and (4) other locally developed sets (fig. 12c). At point 4-2 in the middle part of the transition zone, the fracture network is broadly similar, but fracture intensity increases, additional sets are locally developed, and alteration is more widespread (fig. 13b). Some fractures, including the dominant set of shear fractures (set 1), show evidence of episodic dilation with precipitation of quartz veins during periods of high fluid pressure. Some veins were deformed during later shearing, recording repeated episodes of tensile and shear fracturing, fluid influx, and sealing. Continuing southwest in the upper part of the transition zone, the fracture network is very complex, with multiple sets of mutually offset, closely spaced fractures. The geometry of the fracture network varies over short distances within the boundary and includes synthetic normal faults and shear fractures, antithetic faults and shear fractures, steeply dipping hybrid fractures and veins that are locally activated as faults, cross fractures with varying slip directions, other local fracture sets, and random, curvilinear fractures (fig. 13e). Different slip directions on fractures and faults of varying orientation and the sinuous nature of many faults results in mutual offset and interlocking, and may lead to geometric hardening.

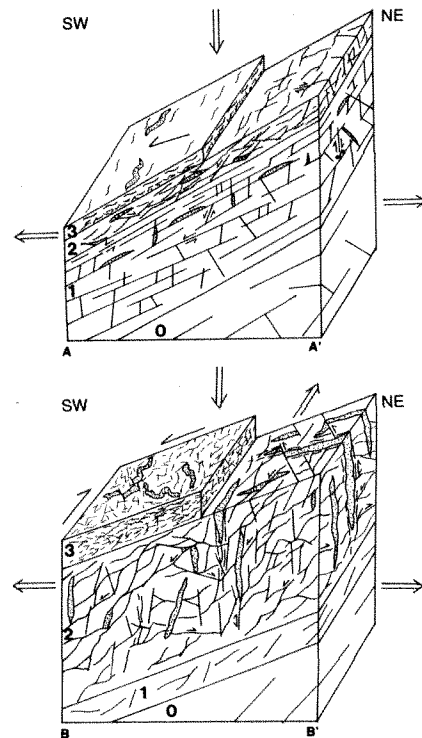
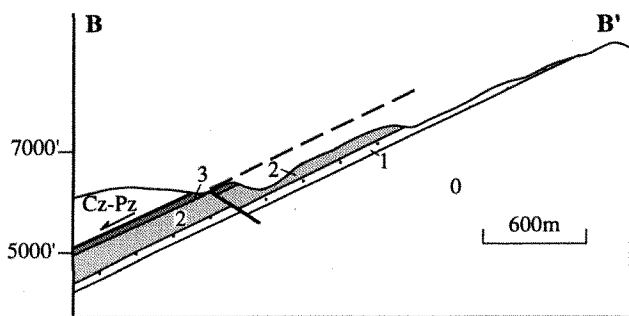
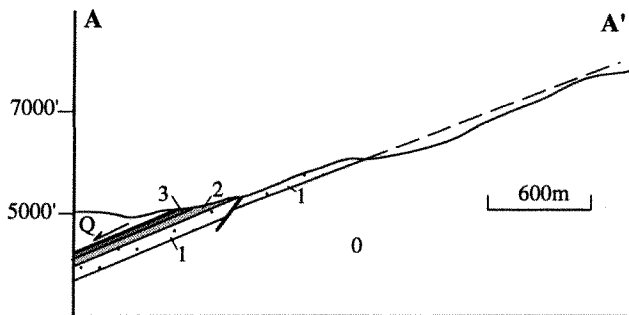
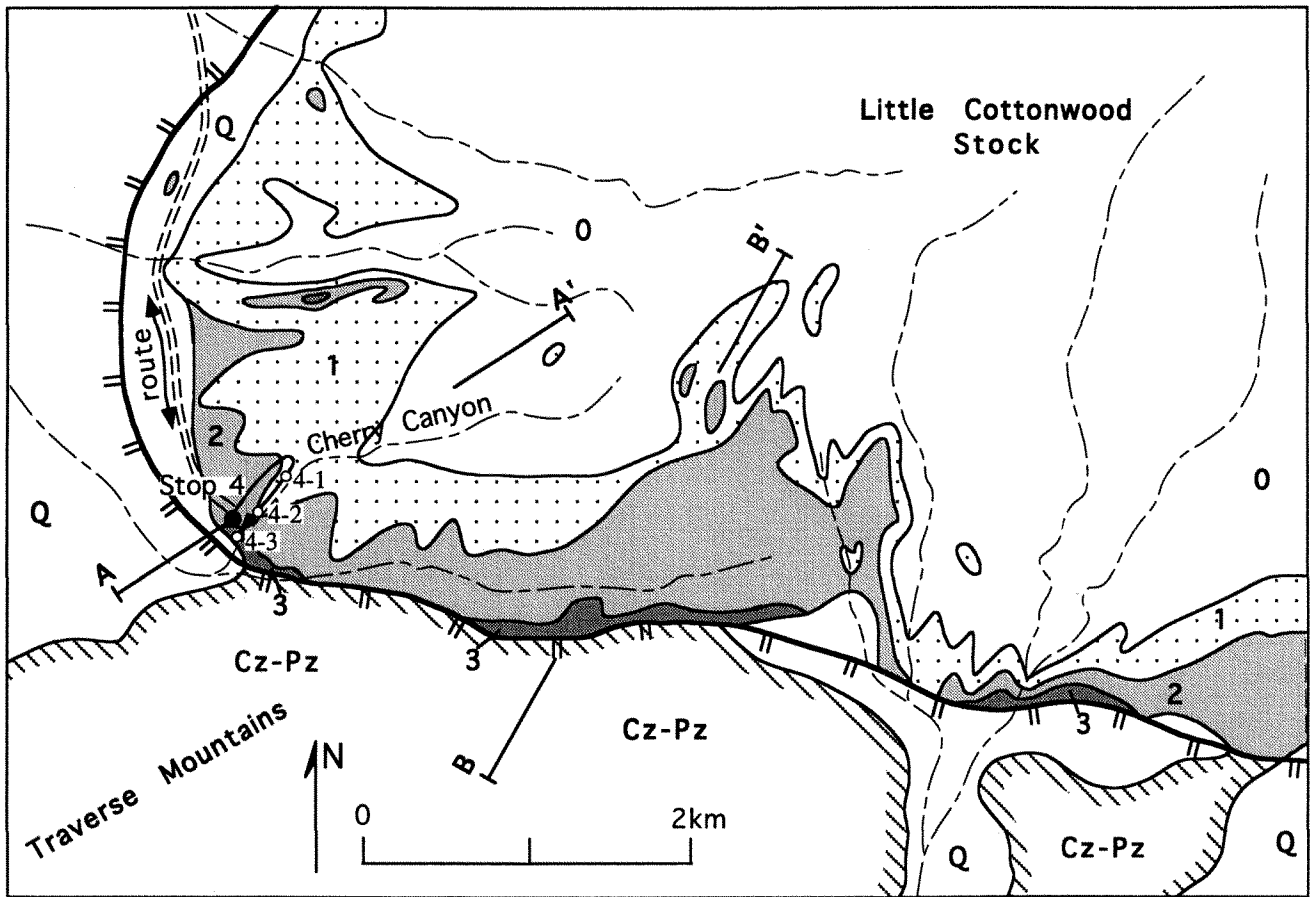
At point 4-3 in the slip zone, cataclasite and phyllonite are intensely deformed and altered, and locally cut by large slip surfaces, although most mesoscopic fractures are difficult to trace due to truncation, healing and sealing, and pervasive microcracking. Rare, variably deformed pseudotachylite veins occur within both cataclasite and phyllonite.

Hydrothermal alteration in the transition zone is concentrated along fracture, vein, and microcrack networks, and alteration is widespread in the slip zone, especially in phyllonite. Two main alteration assemblages are present:

Figure 12. A. Generalized geologic map of area around stop 4. Route of hike and sites indicated. Units are: zone 0—undeformed granitic rock of footwall; zone 1—lower, less deformed part of transition zone; zone 2—upper, more deformed part of transition zone; zone 3—slip zone of highly deformed phyllonite and cataclasite; Q—undivided Quaternary deposits; Pz-Cz—undivided Paleozoic to Cenozoic rocks in hanging wall.

B. Cross sections A-A' and B-B' illustrating variations in thickness of fault zones within the boundary. Section B-B' within the middle part of the boundary has a thick, complexly deformed zone 2 interval. See part A for locations of section lines.

C. Schematic block diagrams A-A' and B-B' illustrating styles of fracture networks within the boundary. Veins indicated by stippled pattern, phyllonite by short wiggly lines, and cataclasite by short dashed lines.



abilities related to fractures are greater in the transition zone compared to the footwall granite and range from on the order of 10^{-12} to 10^{-14} m² at high fluid pressures to 10^{-16} to 10^{-18} m² at low fluid pressures, reflecting a non-linear dependence of aperture on effective normal stress (Bruhn et al., 1994). In detail, permeability is anisotropic, and estimated permeability tensors in the transition zone have long axes at low angles to the main fault zone. Sealing and healing episodically closed fractures such that actual permeabilities may have been lower, particularly during inter-seismic periods. Permeability of the slip zone is uncertain. Estimated elastic moduli related to fractures decrease from the footwall into the transition zone, and are between 10 and 40% of intact rock. Elastic moduli are difficult to estimate within the slip zone due to pervasive fracturing and micro-cracking. Note that reduced moduli also result in reduced seismic velocities in the fault zone.

This ends the trip. Retrace the route to 12,300 South, return to I-15, and the Salt Palace. Thank you.

REFERENCES CITED

- Allmendinger, R.W., Marrett, R.A., and Cladouhos, T., 1992, Faultkin, a Program for analyzing fault slip data for the Macintosh computer. Copyrighted software.
- Arabasz, W.J., and Julander, D.R., 1986, Geometry of seismically active faults and crustal deformation within the Basin and Range-Colorado Plateau transition, in Mayer, L., ed., *Extensional tectonics of the southwestern United States. A perspective on processes and kinematics*, Geological Society of America Special Paper 208, p. 43–74.
- Arabasz, W.J., Pechmann, J.C., and Brown, E.D., 1992, Observational seismology and the evaluation of earthquake hazards and risk in the Wasatch Front area, Utah, in Gori, P.L., and Hays, W.W., eds., *Assessment of regional earthquake hazards and risk along the Wasatch Front, Utah*. U.S. Geological Survey Professional Paper 1500-D, 36 pp.
- Arabasz, W.J., Smith, R.B., and Richins, W.D., 1978, Earthquake studies along the Wasatch front, Utah. Network monitoring, seismicity, and seismic hazards, in Arabasz, W.J., Smith, R.B., and Richins, W.D., eds., *Earthquake studies in Utah, 1850–1978*, p. 253–285.
- Baker, A.A., 1964, *Geology of the Orem quadrangle, Utah*, U.S. Geological Survey Map GQ-241.
- Bruhn, R.L., Gibler, P.R., and Parry, W.T., 1987, Rupture characteristics of normal faults: an example from the Wasatch fault zone, Utah, in Coward, M.P., Dewey, J.F., and Hancock, P.L., eds., *Continental Extensional Tectonics*. Geological Society of London Special Publication 28, p. 337–353.
- Bruhn, R.L., Gibler, P.R., Houghton, W., and Parry, W.T., 1992, Structure of the Salt Lake segment, Wasatch normal fault zone. Implications for rupture propagation during normal faulting, in Gori, P.L., and Hays, W.W., eds., *Assessment of regional earthquake hazards and risk along the Wasatch Front, Utah*. U.S. Geological Survey Professional Paper 1500-H, 25 p.
- Bruhn, R.L., Lee, J.-J., and Yonkee, W.A., 1990a, Structural properties of the American Fork, Provo, and part of the Spanish Fork subsegments, Wasatch normal fault zone, Utah. Utah Geological Survey Open-File Report 186, 43 pp.
- Bruhn, R.L., Yonkee, W.A., and Parry, W.T., 1990b, Structural and fluid-chemical properties of seismogenic normal faults: Tectonophysics, v. 175, p. 139–157.
- Bruhn, R.L., Parry, W.T., Yonkee, W.A., and Thompson, T., 1994, Fracturing and hydrothermal alteration in normal fault zones. *Pure and Applied Geophysics*, v. 142, p. 609–643.
- Bryant, B., 1984, Reconnaissance geologic map of the Precambrian Farmington Canyon complex and the surrounding rocks in the Wasatch Mountains between Ogden and Bountiful, Utah. U.S. Geological Survey Miscellaneous Investigations Series Map I-1447, scale 1:50,000.
- Bryant, B., 1988, *Geology of the Farmington Canyon Complex, Wasatch Mountains, Utah*: U.S. Geological Survey Professional Paper 1476, 54 p.
- Bryant, B., 1990, *Geologic map of the Salt Lake City 30' x 60' quadrangle, north-central Utah, and Uinta County, Wyoming*: U.S. Geological Survey Miscellaneous Investigations Series Map I-1944, scale 1:100,000.
- Bryant, B., Naeser, C.W., Marvin, R.F., and Mehnert, H.H., 1989, Ages of Late Paleogene and Neogene tuffs and the beginning of rapid regional extension, eastern boundary of the Basin and Range Province near Salt Lake City, Utah: U.S. Geological Survey Bulletin 1787, 37 p.
- Buss, W.R., and Peterson, D., 1964, The Wasatch Fault in Weber and Davis Counties, Utah, in Marsell, R.E., ed., *The Wasatch Fault zone in north central Utah*, Guidebook to the Geology of Utah #18, Utah Geological Survey, p. 51–52.
- Cowie, P.A., and Scholz, C.H., 1992, Growth of the faults by accumulation of seismic slip. *Journal of Geophysical Research*, v. 97, p. 11,085–11,095.
- Crittenden, M.D., Jr., 1965a, *Geology of the Draper quadrangle, Utah*. U.S. Geological Survey Map GQ-377, scale 1:24,000.
- Crittenden, M.D., Jr., 1965b, *Geologic map of the Sugar House quadrangle: U.S. Geological Survey Map GQ-380*, scale 1:24,000.
- Crittenden, M.D., Jr., and Sorensen, M.L., 1985a, *Geologic map of the Mantua quadrangle and part of the Willard quadrangle, Box Elder, Weber, and Cache Counties, Utah*. U.S. Geological Survey Map I-1605, scale 1:24,000.
- Crittenden, M.D., Jr., and Sorensen, M.L., 1985b, *Geologic map of the North Ogden quadrangle and part of the Ogden and Plain City quadrangles, Box Elder and Weber Counties, Utah*. U.S. Geological Survey Map I-1606, scale 1:24,000.
- Davis, F.D., 1983, *Geologic map of the central Wasatch Front, Utah*. Utah Geological and Mineral Survey Map 54-A, scale 1:100,000.
- Davis, F.D., 1985, *Geology of the northern Wasatch front: Utah Geological and Mineral Survey Map 53-A*, 2 sheets, scale 1:100,000.
- Eardley, A.J., 1939, Structure of the Wasatch-Great Basin region: *Geological Society of America Bulletin*, v. 50, p. 1277–1310.
- Eardley, A.J., 1944, *Geology of the north-central Wasatch mountains, Utah: Bulletin of Geological Society of America*, v. 55, p. 819–894.
- Eardley, A.J., and Hatch, R.A., 1940, Precambrian crystalline rocks of north-central Utah. *Journal of Geology*, v. 48, p. 58–72.
- Evans, J.P., and Langrock, H., 1994, Structural analysis of the Brigham City-Weber Segment boundary zone, Wasatch normal fault, Utah: Implications for fault growth and structure: *Pure and Applied Geophysics*, v. 142, p. 663–684.
- Evans, S.H., Parry, W.T., and Bruhn, R.L., 1985, Thermal, mechanical, and chemical history of Wasatch fault cataclasite and phyllonite, Traverse Mountains area, Salt Lake City, Utah. From K/Ar and fission track measurements. U.S. Geological Survey Open-File Report 86-31, p. 410–415.
- Gephart, J.W., 1990a, Stress and the direction of slip on faults: *Tectonics*, v. 9, p. 845–858.
- Gephart, J.W., 1990b, FMSI: A Fortran program for inverting fault/slip-sense and earthquake focal mechanism data to obtain the regional stress tensor: *Computers and Geosciences*, v. 16, p. 953–989.
- Gilbert, G.K., 1890, *Lake Bonneville*: U.S. Geological Survey Monograph 1, 438 p.
- Gilbert, G.K., 1928, *Studies of Basin-Range structure*: U.S. Geological Survey Professional Paper 153, 89 p.

- Grocott, J., 1981, Fracture geometry of pseudotachylite generation. A study of shear fractures formed during seismic events. *Journal of Structural Geology*, v. 3, p. 169–178.
- Hecker, S., 1993, Quaternary tectonics of Utah with emphasis on earthquake-hazard characterization. *Utah Geological Survey Bulletin*, v. 127, 157 pp.
- Hintze, L.E., 1980, Geologic map of Utah. *Utah Geological and Mineral Survey Map A-2*, scale 1:500,000.
- Kowallis, B.J., Ferguson, J., and Jorgensen, G.J., 1990, Uplift along the Salt Lake segment of the Wasatch Fault from apatite and zircon fission track dating in the Little Cottonwood Stock, in Durrani, S.A., and Benton, E.V., eds., *Proceedings of the 6th International Fission Track Dating Workshop*, Nuclear Tracks and Radiation Measurements 17, Pergamon, Oxford, p. 325–329.
- Link, P.K., Crook, S.R., and Chidsey, T.C., Jr., 1985, Hinterland structure, paleozoic stratigraphy and duplexes of the Willard thrust system, Bannock, Wellsville and Wasatch ranges, southeastern Idaho and northern Utah, in Kerns, G.L., and Kerns, R.L., Jr., eds., *Orogenic Patterns and Stratigraphy of North-Central Utah and Southeastern Idaho*, Utah Geological Association Publication 14, p. 314–328.
- Link, P.K., and Smith, C.H., 1992, Late Proterozoic and Early Cambrian stratigraphy, paleobiology, and tectonics: Northern Utah and southeastern Idaho, in Wilson, J.R., eds., *Field Guide to Geologic Excursions in Utah and Adjacent Areas of Nevada, Idaho, and Wyoming*, Utah Geological Survey Miscellaneous Publication 92-3, p. 461–481.
- Mabey, D.R., 1992, Subsurface geology along the Wasatch Fault area, Utah, in Gori, P.L., and Hays, W.W., eds., *Assessment of regional earthquake hazards and risks along the Wasatch Front*, Utah: U.S. Geological Survey Professional Paper 1500-C, 16 p.
- Machette, M.N., 1988, In the footsteps of G.K. Gilbert—Lake Bonneville and neotectonics of the eastern Basin and Range Province. *Utah Geological and Mineral Survey Miscellaneous Publication 88-1*, 120 pp.
- Machette, M.N., 1992, Surficial geologic map along the Wasatch fault zone in the eastern part of the Utah Valley, Utah County, and parts of Salt Lake and Juab Counties, Utah. *U.S. Geological Survey Miscellaneous Investigations Series Map I-2095*, scale 1:50,000.
- Machette, M.N., Personius, S.F., Nelson, A.R., Schwartz, D.P., and Lund, W.R., 1991, The Wasatch fault zone, Utah. Segmentation and history of Holocene earthquakes. *Journal of Structural Geology*, v. 13, p. 137–149.
- Machette, M.N., Personius, S.F., Nelson, A.R., Schwartz, D.P., and Lund, W.R., 1989, Segmentation models and Holocene movement history of the Wasatch fault zone, Utah, in Schwartz, D.P., and Sibson, R.H., eds., *Proceedings of Conference XLV—Fault segmentation and controls on rupture initiation and termination*: U.S. Geological Survey Open-File Report 89-315, p. 229–245.
- Machette, M.N., Personius, S.F., and Nelson, A.R., 1992, Paleoseismology of the Wasatch fault zone—A summary of recent investigations, conclusions, and interpretations, in Gori, P.L., and Hays, W.W., eds., *Assessing regional earthquake hazards and risk along the Wasatch Front*, Utah. *U.S. Geological Survey Professional Paper 1500-A*, p. A1–A71.
- Marsell, R.E., 1964, The Wasatch Fault in Salt Lake County, Utah, in Marsell, R.E., ed., *The Wasatch Fault zone in north central Utah*, Guidebook to the Geology of Utah #18, Utah Geological Survey, p. 31–50.
- Marsell, R.E., 1969, The Wasatch Fault zone in north central Utah, in *Guidebook of northern Utah*, Utah Geological and Mineralogical Survey Bulletin 82, p. 124–129.
- McCalpin, J.P., and Nishenko, S.P., 1996, Holocene paleoseismicity, temporal clustering, and probabilities of future large ($M > 7$) earthquakes on the Wasatch fault zone, Utah. *Journal of Geophysical Research*, v. 101, p. 6233–6253.
- Naeser, C.W., Bryant, B., Crittenden, M.D., Jr., and Sorensen, M.L., 1983, Fission-track ages of apatite in the Wasatch Mountains, Utah. an uplift study, in Miller, D.M., Todd, V.R., and Howard, K.A., eds., *Tectonic and stratigraphic studies in the eastern Great Basin*. Geological Society of America Memoir 157, p. 29–36.
- Nelson, A.R., 1988, The northern part of the Weber segment of the Wasatch fault zone near Ogden, Utah, in Machette, M.N., ed., *In the Footsteps of G.K. Gilbert—Lake Bonneville and Neotectonics of the Eastern Basin and Range Province*. Utah Geological and Mineral Survey Miscellaneous Publication 88-1, p. 33–37.
- Nelson, A.R., and Personius, S.F., 1993, Surficial geologic map of the Weber segment, Wasatch fault zone, Weber and Davis Counties, Utah. *U.S. Geological Survey Map I-2199*, scale 1:50,000.
- Oda, M., Hatsuyama, Y., and Ohnishi, Y., 1987, Numerical experiments on permeability tensor and its application to jointed granite at the Stripa Mine, Sweden. *Journal of Geophysical Research*, v. 92, p. 8037–8048.
- Oda, M., 1986, An equivalent continuum model for coupled stress and fluid flow analysis in jointed rock masses. *Water Resources Research*, v. 22, p. 1845–1856.
- O'Connell, R.J., and Budiansky, B., 1974, Seismic velocities in saturated and dry cracked solids. *Journal of Geophysical Research*, v. 79, p. 5412–5426.
- Pack, F.J., 1926, New discoveries relating to the Wasatch fault. *American Journal of Science*, v. 27, p. 399–410.
- Parry, W.T., and Bruhn, R.L., 1986, Pore fluid and seismogenic characteristics of fault rock at depth on the Wasatch fault, Utah. *Journal of Geophysical Research*, v. 91, p. 730–744.
- Parry, W.T., and Bruhn, R.L., 1987, Fluid inclusion evidence for minimum 11 km vertical offset on the Wasatch fault, Utah. *Geology*, v. 15, p. 67–70.
- Parry, W.T., and Bruhn, R.L., 1990, Fluid pressure transients on seismogenic normal faults. *Tectonophysics*, v. 179, p. 335–344.
- Parry, W.T., Wilson, P.N., and Bruhn, R.L., 1988, Pore fluid chemistry and chemical reactions on the Wasatch normal fault, Utah. *Geochimica et Cosmochimica Acta*, v. 52, p. 2053–2063.
- Pashley, E.F., Jr., and Wiggins, R.A., 1972, Landslides of the northern Wasatch Front, in *Environmental geology of the Wasatch Front*, 1971. Salt Lake City, Utah, Utah Geological Association Publication 1, p. K1–K16.
- Pavlis, T.L., Serpa, L.F., and Keener, C., 1993, Roles of seismogenic processes in fault-rock development, an example from Death Valley, California. *Geology*, v. 21, p. 267–270.
- Pavlis, T.L., and Smith, R.B., 1980, Slip vectors from faults near Salt Lake City from Quaternary displacement and seismicity, in Arabasz, W.J., Smith, R.B., and Richins, W.D., eds., *Earthquake Studies in Utah*: Salt Lake City, Utah, University of Utah, p. 378–382.
- Pechmann, J.C., 1992, Focal mechanism and seismotectonic setting, in *The March 16, 1992 M 4.2 Western Traverse Mountains Earthquake*, Salt Lake County, Utah. Utah Geological Survey, Open-File Report 255, p. 3–7.
- Personius, S.F., 1990, Surficial geologic map of the Brigham City segment and adjacent parts of the Weber and Collinston segments, Wasatch fault zone, Box Elder and Weber Counties, Utah. *U.S. Geological Survey Map I-1979*, scale 1:50,000.
- Personius, S.F., and Scott, W.E., 1992, Surficial geologic map of the Salt Lake City segment and parts of adjacent segments of the Wasatch fault zone, Davis, Salt Lake, and Utah Counties, Utah: *U.S. Geological Survey Miscellaneous Investigations Series Map I-2106*, scale 1:50,000.
- Petit, J.P., 1987, Criteria for the sense of movement on fault surfaces in brittle rocks: *Journal of Structural Geology*, v. 9, p. 597–608.
- Power, W.L., and Tullis, T.E., 1992, The contact between opposing fault surfaces at Dixie Valley, Nevada, and implications for fault mechanics. *Journal of Geophysical Research*, v. 97, p. 15425–15435.
- Royse, F., Warner, M.A., and Reese, D.L., 1975, Thrust belt structural geometry and related stratigraphic problems, Wyoming-Idaho-northern

- Utah, in Boyland, D.W., ed., *Deep drilling frontiers of the central Rocky Mountains*: Rocky Mountain Association of Geologists, p. 41–54.
- Schirmer, T.W., 1988, Structural analysis using thrust fault hanging-wall sequence diagrams: Ogden duplex, Wasatch Range, Utah: *American Association of Petroleum Geologists Bulletin*, v. 72, p. 573–585.
- Scholz, C.H., 1990, *The mechanics of earthquakes and faulting*: Cambridge University Press, 439 pp.
- Schwartz, D.P., and Coppersmith, K.J., 1984, Fault behavior and characteristic earthquakes—Example from the Wasatch and San Andreas fault zones: *Journal of Geophysical Research*, v. 89, p. 5681–5698.
- Scott, W.E., 1988, G.K. Gilbert's observations of post-Bonneville movement along the Warm Springs Fault, Salt Lake City, Utah, in Machette, C., ed., *In the footsteps of G.K. Gilbert—Lake Bonneville and neotectonics of the eastern Basin and Range Province*: Utah Geological and Mineral Survey Miscellaneous Publication 88-1, p. 44–46.
- Smith, R.B., and Bruhn, R.L., 1984, Intraplate extensional tectonics of the eastern Basin-Range: Inferences on structural style from seismic reflection data, regional geophysics and thermal-mechanical models of brittle-ductile deformation: *Journal of Geophysical Research*, v. 87, p. 5733–5762.
- Swan, F.H., III, Schwartz, D.P., and Cluff, L.S., 1980, Recurrence of moderate to large magnitude earthquakes produced by surface faulting on the Wasatch fault zone, Utah: *Bulletin of the Seismological Society of America*, v. 70, p. 1431–1462.
- Van Horn, R., 1982, Surficial geologic map of the Salt Lake City North quadrangle, Davis and Salt Lake Counties, Utah: U.S. Geological Survey Miscellaneous Investigations Map I-1404, scale 1:24,000.
- Van Horn, R., and Crittenden, M.D., Jr., 1988, Map showing surficial units and bedrock geology of the Fort Douglas quadrangle and parts of the Mountain Dell and Salt Lake City North quadrangles, Davis, Salt Lake, and Morgan Counties, Utah. U.S. Geological Survey Miscellaneous Investigations Map I-1762, scale 1:24,000.
- Wheeler, R.L., and Krystinik, K.B., 1992, Persistent and nonpersistent segmentation of the Wasatch fault zone, Utah: Statistical analysis for evaluation of seismic hazard: U.S. Geological Survey Professional Paper 1500-B.
- Yonkee, W.A., 1992, Basement-cover relations, Sevier orogenic belt, northern Utah: *Geological Society of America Bulletin*, v. 104, p. 280–302.
- Yonkee, W.A., and Bruhn, R.L., 1990, Geometry and mechanics of a structural boundary, Wasatch fault zone, Utah, in Bruhn, R.L., Lee, J., and Yonkee, W.A., eds., *Structural properties of the American Fork, Provo, and Spanish Fork subsegments, Wasatch normal fault zone, Utah*: Utah Geological and Mineral Survey Open-File Report 186, 50 p.
- Yonkee, W.A., Evans, J.P., and DeCelles, P.G., 1992, Mesozoic tectonics of the northern Wasatch Range, Utah, in Wilson, J.R., ed., *Field guide to geologic excursions in Utah and adjacent areas of Nevada, Idaho, and Wyoming*: Utah Geological Survey Miscellaneous Publication 92-3, p. 429–460.
- Zoback, M.L., 1983, Structure and Cenozoic tectonism along the Wasatch fault zone, in Miller, D.M., Todd, V.R., and Howard K.A., eds., *Tectonic and stratigraphic studies in the eastern Great Basin*: Geological Society of America Memoir 157, p. 3–27.

Geologic Hazards of the Wasatch Front, Utah

MICHAEL D. HYLLAND

BILL D. BLACK

MIKE LOWE

Utah Geological Survey, P.O. Box 146100, Salt Lake City, Utah 84114-6100

ABSTRACT

The results of recent and ongoing research into six significant geologic hazards of the Wasatch Front region will be summarized on this field trip, including: (1) surface fault rupture on the Salt Lake City segment of the Wasatch fault zone; (2) seismic site response in the Salt Lake Valley, including ground shaking and liquefaction; (3) liquefaction-induced landsliding at the Farmington Siding landslide complex; (4) lake flooding along the shores of Great Salt Lake; (5) debris-flow deposition on alluvial fans at the base of the Wasatch Range; and (6) landsliding in the Ogden area. The trip will provide an opportunity to discuss the scientific, engineering, and administrative aspects involved in geologic-hazard evaluation in this rapidly growing region.

INTRODUCTION

Situated at the eastern margin of the Basin and Range physiographic province, the Wasatch Front is subject to a variety of geologic hazards due to a unique combination of geologic, topographic, and climatic conditions. The Wasatch Front occupies a series of north-trending valleys at the foot of the western slope of the Wasatch Range (fig. 1). The mountains rise steeply as much as 7,100 feet (2,165 m) above the valley floor, reaching elevations near 12,000 feet (3,660 m) above sea level. This impressive relief is the result of ongoing uplift along the Wasatch fault zone, a major intraplate tectonic boundary which is the longest active normal-slip fault zone in the United States and one of several fault zones in the region considered capable of producing large earthquakes that could generate strong ground shaking, surface fault rupture, and seismically induced liquefaction and landslides.

In the winter, frontal storms traveling east from the Pacific Ocean encounter the Wasatch Range and produce heavy snowfall in the mountains. Snow avalanches are common and present a significant, widespread hazard. Freeze-thaw cycles in steep exposures of fractured rock produce rock falls. Rapid melting of a lingering snowpack periodically results in slope failures, debris flows, and stream and alluvial-fan flooding. Convective storms in the spring and late summer also contribute to these hazards.

Great Salt Lake, the remnant of Pleistocene Lake Bonneville, forms the western boundary of the northern Wasatch Front. Because the lake occupies a closed basin within the internally draining Great Basin, it is subject to climate-induced fluctuations that may cause flooding in areas along

and near its gently sloping shores. A seiche hazard also exists because of the regional earthquake hazard. Furthermore, thick deposits of soft, fine-grained lacustrine sediment from repeated cycles of deep-water lakes that inundated the valleys could amplify earthquake ground motions, and loose, saturated sands are potentially liquefiable.

This field trip provides an opportunity to observe and discuss six of the most significant types of geologic hazards of the Wasatch Front. These include (1) surface fault rupture on the Salt Lake City segment of the Wasatch fault zone; (2) seismic site response in the Salt Lake Valley, including ground shaking and liquefaction; (3) liquefaction-induced landsliding at the Farmington Siding landslide complex; (4) lake flooding along the shores of Great Salt Lake; (5) debris-flow deposition on alluvial fans at the base of the Wasatch Range; and (6) landsliding in the Ogden area. These topics are discussed in the following six sections, which in turn are followed by a road log that describes the field-trip route. The route and stop locations are shown on figures 25 through 27.

FIELD TRIP STOP NO. 1

Bill D. Black, Leader

Mouth of Little Cottonwood Canyon,

Wasatch Boulevard and 9800 South; see Figure 25.

PALEOSEISMIC STUDIES ON THE SALT LAKE CITY SEGMENT OF THE WASATCH FAULT ZONE

The Wasatch fault zone is one of the longest and most active normal-slip faults in the world. Situated near the

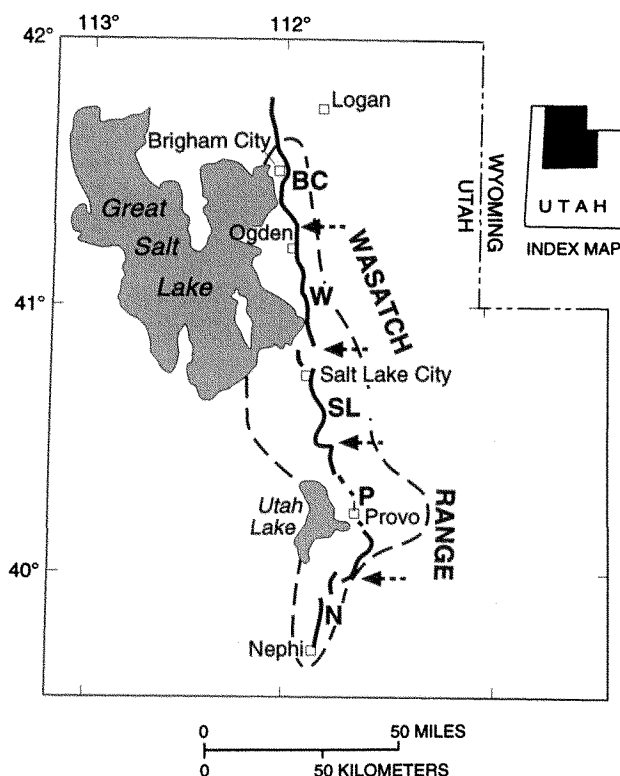


Figure 1. Generalized area of the Wasatch Front (dashed line). Central five segments of the Wasatch fault zone shown by heavy line with arrows indicating segment boundaries (modified from Machette et al., 1992): BC = Brigham City, W = Weber, SL = Salt Lake City, P = Provo, N = Nephi.

center of the Intermountain seismic belt (Smith and Sbar, 1974; Smith and Arabasz, 1991), a north-trending zone of historical seismicity that extends from northern Arizona to central Montana, the fault zone extends 213 miles (343 km) along the western base of the Wasatch Range from south-eastern Idaho to north-central Utah (Machette et al., 1992) and comprises 10 independent, seismogenic segments (Schwartz and Coppersmith, 1984; Machette et al., 1992). Results of numerous trenching studies indicate that the central five segments (Brigham City, Weber, Salt Lake City, Provo, Nephi) (fig. 1) each have generated three or more surface-faulting earthquakes in the past 6,000 years.

The Salt Lake City segment of the Wasatch fault zone trends through the densely populated Salt Lake Valley, extending 29 miles (46 km) from the Traverse Mountains on the south to the Salt Lake salient on the north (fig. 2). The fault segment displays abundant evidence for multiple surface-faulting earthquakes during Holocene time (Schwartz and Coppersmith, 1984), and thus it poses a significant seismic risk to people living in the Salt Lake City metropolitan area. The Holocene chronology of surface-faulting earth-

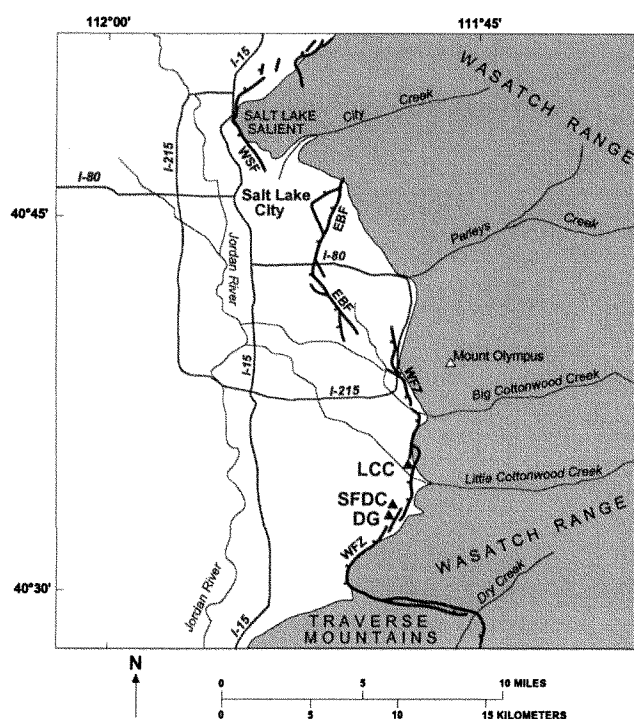


Figure 2. Salt Lake City segment of the Wasatch fault zone (WFZ) and locations of the Little Cottonwood Canyon (LCC), South Fork Dry Creek (SFDC), and Dry Gulch (DG) trench sites. WSF = Warm Springs fault, EBF = East Bench fault.

quakes has been determined through fault-trenching studies at Little Cottonwood Canyon in 1979, South Fork Dry Creek in 1985 and 1994, and Dry Gulch in 1991.

Little Cottonwood Canyon (1979)

The first paleoseismic investigation of the Salt Lake City segment was at Little Cottonwood Canyon in 1979 (fig. 2) by Woodward-Clyde Consultants, under contract to the U.S. Geological Survey (USGS) (Swan et al., 1981). The fault zone at this site is defined by a prominent west-facing main scarp that splays northward into three sub-parallel scarps and an east-facing antithetic scarp. South of the site, the fault zone forms a wide, deep graben as it traverses moraines near the mouth of the canyon (fig. 3).

Four trenches were excavated across the scarps at Little Cottonwood Canyon, exposing evidence for two surface-faulting earthquakes. Radiocarbon dating of detrital charcoal showed the older earthquake occurred shortly before 8,000 to 9,000 years ago. However, no material suitable for radiocarbon dating was found to constrain the timing of the younger event. Based on scarp profiling and stratigraphic evidence in the trenches, Swan et al., (1981) calculated a recurrence interval of 2,200 years and an average net slip per event of 6 feet (2 m).



Figure 3. Wasatch fault zone at the mouth of Little Cottonwood Canyon. A. Aerial view, looking east, of fault scarps (arrows) cutting upper Pleistocene moraine and alluvial deposits. B. South view of fault scarps (in shadow) cutting Bells Canyon moraine (large arrow on Fig. 3A). Residential development in foreground occupies a graben along the fault zone.

South Fork Dry Creek (1985)

The Utah Geological Survey (UGS), in cooperation with the USGS, conducted a paleoseismic investigation at South Fork Dry Creek (fig. 2) in 1985 (Lund and Schwartz, 1987; Schwartz and Lund, 1988). The fault zone at South Fork Dry Creek consists of six sub-parallel, west-dipping main fault scarps and a single east-dipping antithetic scarp (Personius and Scott, 1992). Four trenches were excavated across three of the main scarps, but access restrictions precluded trenching all of the scarps.

Two trenches each exposed evidence for two surface-faulting earthquakes. The other two trenches each exposed evidence for one surface-faulting earthquake, but no material suitable for radiocarbon dating was found in these trenches. Radiocarbon age estimates indicated that the earthquakes occurred (1) shortly after 1,100 to 1,800 years ago, and (2) shortly after 5,500 to 6,000 years ago. Based on

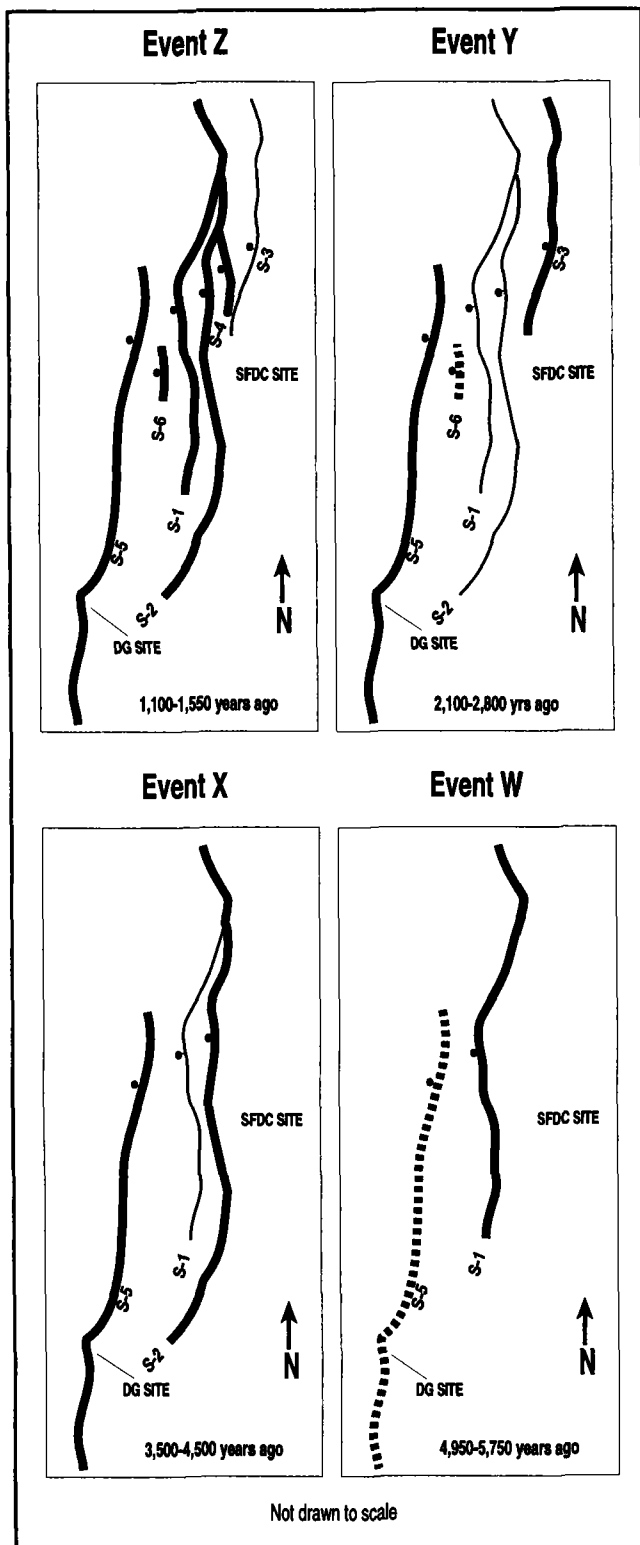
this information, Schwartz and Lund (1988) estimated a recurrence interval of 3,000 to 5,000 years. However, they acknowledged uncertainty regarding the paleoseismic history of the Salt Lake City segment, and cautioned that a true paleoseismic history could be developed only if information is obtained for every scarp at a site.

Dry Gulch (1991–92)

The incomplete nature of the Salt Lake City segment's earthquake history was demonstrated in 1991, when a non-research trench was excavated by a local consultant across the fault zone at Dry Gulch (fig. 2). Detailed geologic mapping by Personius and Scott (1992) shows the scarp at Dry Gulch extends northward to South Fork Dry Creek. However, this scarp was not trenched in 1985. The UGS inspected the Dry Gulch trench and found evidence for two surface-faulting earthquakes (Lund, 1992; Black et al., 1996). Radiocarbon dating indicated the earthquakes occurred: (1) roughly 1,600 years ago, which coincided with timing for the most recent event at South Fork Dry Creek; and (2) shortly after 2,400 years ago, which did not correspond to any previously known event. This newly discovered event showed that at least three (rather than two) surface-faulting earthquakes have occurred in the past 6,000 years, and at least four events (rather than three) in the past 8,000–9,000 years. Based on timing for the additional event, Lund (1992) calculated a surface-faulting recurrence interval of $2,150 \pm 400$ years for the past 6,000 years.

South Fork Dry Creek (1994)

In 1994, the UGS excavated five new trenches across fault scarps at South Fork Dry Creek to complete the investigation started there in 1985 (Black et al., 1996). With these additional trenches, all fault scarps at South Fork Dry Creek have now been trenched. The new trenches exposed evidence for one to four surface-faulting earthquakes, and documented a previously unrecognized earthquake (event X) which increased to four the total number of events on the Salt Lake City segment in the past 6,000 years. Radiocarbon age estimates show these earthquakes occurred: (1) shortly after 1,100–1,550 years ago (event Z), (2) shortly after 2,100–2,800 years ago (event Y), (3) shortly after 3,500–4,500 years ago (event X), and (4) shortly after 4,950–5,750 years ago (event W). Net slip per event could not be calculated, but earthquake timing combined with the age and cumulative offset of a debris-flow levee along South Fork Dry Creek suggests it is likely in the range of 5 to 8 feet (1.5–2.5 m), which is similar to that determined by Swan et al., (1981) at Little Cottonwood Canyon. Events W through Z show a varying pattern of surface rupture (fig. 4), indicating that in a wide fault zone containing many fault traces, subsequent earthquakes do not always rupture every trace.



Based on mean elapsed times between events W through Z, Black et al., (1996) calculated a new recurrence interval for surface faulting in the past 6,000 years of $1,350 \pm 200$ years (fig. 5). Elapsed time since event Z (about 1,300 years) is close to the new shorter recurrence interval and within the assigned range of uncertainty, suggesting risk for a future surface-faulting earthquake is higher than previously thought. However, more work is needed to characterize the surface-faulting history of the Salt Lake City segment in early Holocene time and refine the recurrence interval.

FIELD TRIP STOP NO. 2

Michael D. Hylland, Leader
Salt Lake Valley overlook from Wasatch Boulevard
at Pete's Rock; see Figure 25.

SEISMIC SITE RESPONSE IN THE SALT LAKE VALLEY

The Salt Lake Valley is a deep, sediment-filled structural basin formed by basin-and-range extensional block faulting. The combined thickness of unconsolidated Quaternary and semi-consolidated Tertiary basin-fill deposits locally exceeds 3,300 feet (1,000 m) (Zoback, 1983; Mabey, 1992). Quaternary deposits are dominated by lacustrine sediments deposited by repeated cycles of deep-water lakes during the Pleistocene. Coarse-grained Lake Bonneville shore facies consisting of sand and gravel are present along the margins of the Salt Lake Valley up to an elevation of about 5,180 feet (1,580 m), whereas deep-water facies consisting of clay, silt, and fine sand predominate toward the center of the valley (fig. 6). Post-Lake Bonneville materials include alluvial, flood-plain, and flood-plain/delta deposits.

The lateral and vertical variability of Quaternary deposits in the Salt Lake Valley results in a wide range of potential earthquake-induced ground motions. Furthermore, the presence of loose, sandy soils and shallow ground water makes many areas susceptible to liquefaction.

Earthquake Ground Shaking

Historical Seismicity and Building Damage

The Salt Lake Valley occasionally experiences ground shaking from earthquakes within and beyond the Wasatch

Figure 4. Pattern of surface rupture at the South Fork Dry Creek (SFDC) and Dry Gulch (DG) sites. Main scarps (S-1 through S-6) known to have been active during surface-faulting earthquakes on the Salt Lake City segment in the past 6,000 years are shown by heavy solid lines; scarps possibly active are shown by heavy dashed lines.

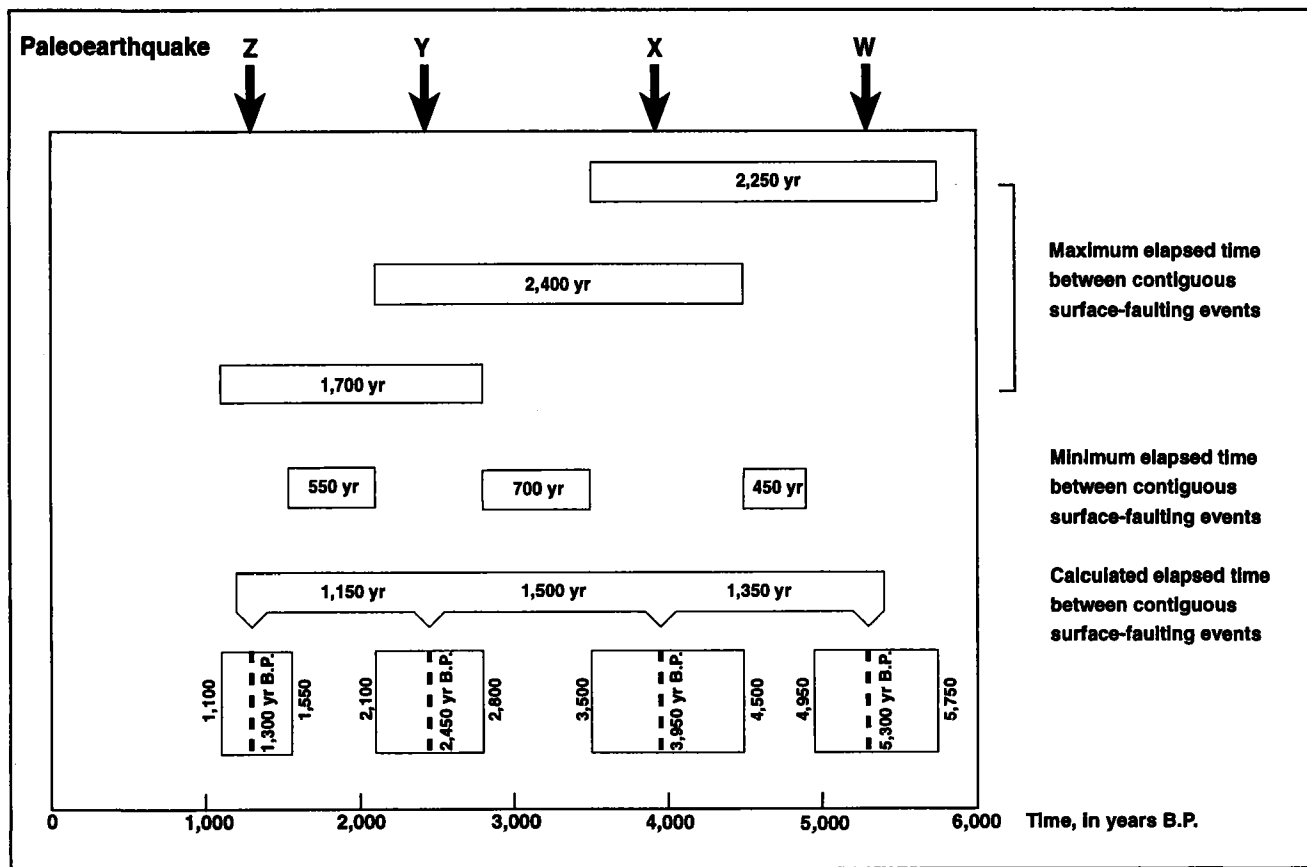


Figure 5. Timing of surface-faulting earthquakes on the Salt Lake City segment in the past 6,000 years.

Front region. Oaks (1987) summarized the effects of six moderate to large earthquakes (M_L 5.0 to 6.6) that produced ground shaking in the Salt Lake City area. These earthquakes occurred between 1909 and 1962 and resulted in damage consisting of toppled chimneys, cracked walls and windows, broken gas and water mains, and seiches on Great Salt Lake. The 1934 Hansel Valley earthquake, which produced surface rupture on the Hansel Valley fault at the north end of Great Salt Lake, generated the strongest ground shaking in the Salt Lake Valley in historical times. This earthquake had a maximum Modified Mercalli intensity of VIII in the Salt Lake City area and produced several long-period effects. Newspaper accounts described statues that shifted on the towers of the Salt Lake City and County Building and the LDS Salt Lake Temple, as well as adjacent six- and ten-story downtown buildings that swayed and battered against each other.

The Salt Lake Valley is in Uniform Building Code (UBC) seismic zone 3. Much of the development in the valley was originally constructed prior to implementation of the UBC seismic provisions. Many existing structures are being up-

graded or retrofit, however, and some new structures are being built to seismic zone 4 standards. A well-known project is the seismic retrofit of the Salt Lake City and County Building. Several earthquakes have caused damage, primarily masonry cracking, to this historic landmark, which was originally constructed between 1892 and 1894. During the 1934 Hansel Valley earthquake, 2.5 tons of mechanical clock equipment fell from the 12-story clock tower and "crashed down through the building" (Kaliser, 1971), and ground shaking from the 1983 Borah Peak, Idaho earthquake (M_S 7.3) caused extensive masonry cracking. Concerns over the possibility of severe structural damage associated with near-field strong ground shaking prompted Salt Lake City to commission a study to determine the need for seismic strengthening of city buildings. The resulting upgrade of the City and County Building included structural reinforcement and base isolation designed for a ground acceleration of 0.2 g (Prudon, 1990). The retrofit was completed in 1989 at a cost of \$30 million, and was the world's first application of seismic base isolation in the restoration of an historic structure (Bailey and Allen, 1988).

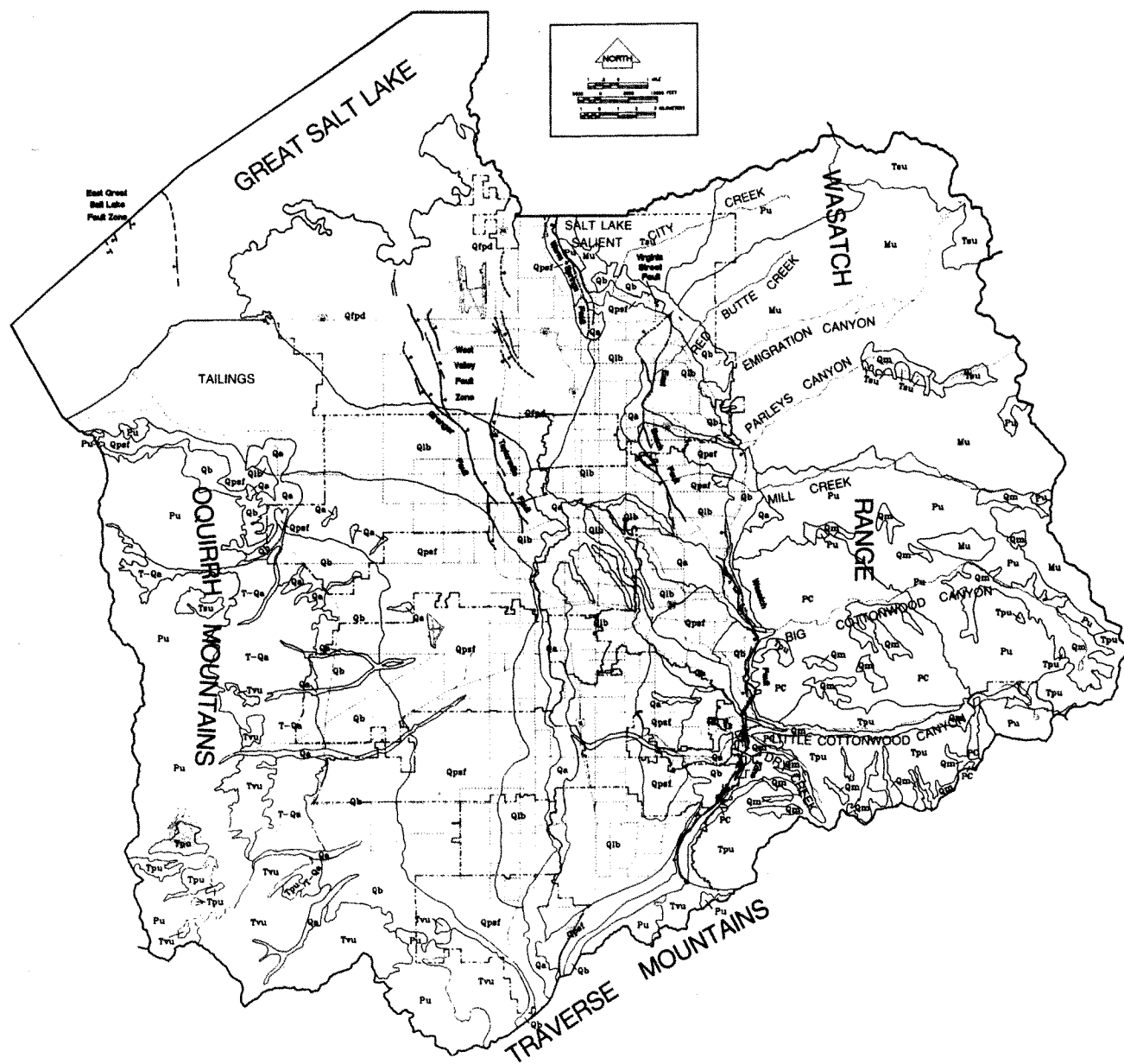


Figure 6. Generalized geologic map of the Salt Lake Valley (from Lund, 1990).

Ground-Motion Levels

Utah has few strong-motion accelerographs and meaningful earthquake records, so quantitative estimates of ground shaking are made using data from other areas, particularly California. However, federal, state, and private entities presently operate 20 three-component strong-motion accelerographs in the Salt Lake Valley, including eight instruments deployed in the last two years. Although statewide coverage still is relatively sparse, the new instruments increase the likelihood of measuring actual ground

motions during future earthquakes, especially in the Wasatch Front area.

National probabilistic seismic-risk maps indicate that, for a 50-year exposure time, peak ground accelerations (PGA) at rock sites around the Salt Lake Valley have a 10 percent probability of exceeding 0.20 to 0.30 g (Algermissen et al., 1990; Building Seismic Safety Council, 1994). However, unconsolidated surficial deposits and basin effects could amplify earthquake ground motions, producing even higher accelerations at soil sites. Youngs et al., (1987) indi-

EXPLANATION**DESCRIPTION OF MAP UNITS****Quaternary and Recent Deposits:**

Qa	Alluvial Deposits — <i>Stream alluvium, existing and abandoned flood plains, alluvial fans, and local mudflows.</i>
Qfpd	Flood-plain and Delta Complex — <i>Chiefly fine-grained and poorly drained sediments; includes deposits from the Jordan River and Great Salt Lake.</i>
Qm	Glacial Moraines and Talus — <i>Moraines, till, and outwash deposits consisting of unsorted mixtures of clay, silt, sand, gravel, and boulders; talus accumulations at the base of steep slopes or cliffs.</i>
Qib	Provo-level and Younger Lake Bottom Sediments — <i>Clays, silts, sands, and locally offshore sand bars.</i>
Qpsf	Provo-level and Younger Shore Facies — <i>Chiefly sand and gravel in beach deposits, bars, spits, and deltas.</i>
Qb	Bonneville-level Shore Facies — <i>Chiefly sand and gravel in beach deposits, bars, spits, and deltas.</i>
T-Qa	Harkers Alluvium — <i>Unconsolidated and poorly sorted boulders, gravel, sand, silt, and clay deposited in pre-Lake Bonneville alluvial fans.</i>
Tsu	Tertiary Sedimentary Rock Units, <i>undifferentiated.</i>
Tvu	Tertiary Volcanic Rock Units, <i>undifferentiated.</i>
Tpu	Tertiary Plutonic Rock Units, <i>undifferentiated.</i>
Mu	Mesozoic Rock Units, <i>undifferentiated.</i>
Pu	Paleozoic Rock Units, <i>undifferentiated.</i>
PE	Precambrian Rock Units, <i>undifferentiated.</i>

MAP SYMBOLS


Contact Between Units.



Suspected or Known Quaternary Faults — Dashed where approximately located, dotted where concealed, queried where suspected; Bar and Ball on downthrown side.

cate the PGA with a 10 percent probability of being exceeded in 50 years could be as high as 0.35 g at soil sites in the northern part of the Salt Lake Valley (fig. 7).

Ground-motion monitoring of Nevada Test Site nuclear tests confirmed amplifications of weak motions in the frequency range of engineering significance (0.2- to 0.7-second periods) in the Salt Lake Valley (Hays and King, 1984; Tinsley et al., 1991). The largest amplifications (in some cases greater than 10x) were in central valley areas and were attributed to deep, soft soil conditions. Recent studies along Interstate 15 identified areas underlain by significant thick-

nesses of soft clay having shear-wave velocities lower than average soft-soil shear-wave velocities in the San Francisco Bay area (Rollins and Gerber, 1995). Theoretical studies of stronger motions have also indicated the potential for significant amplifications, particularly of short-period motions, in areas around the edge of the valley having characteristics similar to where amplification was observed in the 1994 Northridge earthquake in California (Rollins and Adan, 1994). These amplifications are associated with shallow, stiff soil conditions (Adan and Rollins, 1993; Wong and Silva, 1993). Three-dimensional elastic-wave-propagation modeling indicates basin effects could produce significant amplification of low-frequency ground motions at sites over the deepest parts of the basin (Olsen et al., 1995).

Site-specific studies are helping to refine ground-shaking estimates in various parts of the Salt Lake Valley relative to estimates based on the existing regional maps. These studies include probabilistic ground-motion modeling for Kennecott Utah Copper Corp.'s Magna tailings impoundment (Wong et al., 1995) and the Interstate 15 reconstruction project (Dames & Moore, 1996). Also, a cooperative study by the UGS and Brigham Young University beginning in 1997 will result in a site-response map of the Salt Lake Valley that can be used in future probabilistic ground-shaking estimates.

The issue of appropriate ground-motion design levels for structures in the Wasatch Front region is complicated by long recurrence intervals (10^2 to 10^3 yr) for large earthquakes (see Machette et al., 1991). In other seismically active areas such as California, the probabilistic PGA does not continue to increase appreciably at long exposure times because crustal strain is dissipated by relatively frequent large earthquakes (fig. 8). In contrast, the infrequency of large earthquakes in the Wasatch Front region allows crustal strain to continue building over long periods of time, resulting in probabilistic PGAs associated with long exposure times being significantly greater than those associated with shorter exposure times.

Liquefaction

Much of the Salt Lake Valley is underlain at shallow depths by unconsolidated lacustrine and alluvial sand, silt, and clay, and has shallow ground water. The combination of soil gradation and density and shallow ground water results in extensive areas that are susceptible to liquefaction-induced ground failure (Anderson et al., 1986).

Anderson et al., (1986) mapped much of the Salt Lake Valley as having a moderate to high liquefaction potential (fig. 9) based on soil liquefaction susceptibility as determined from geotechnical parameters, calculated critical accelerations, and earthquake magnitude exceedance probability. Although prehistoric liquefaction-induced ground

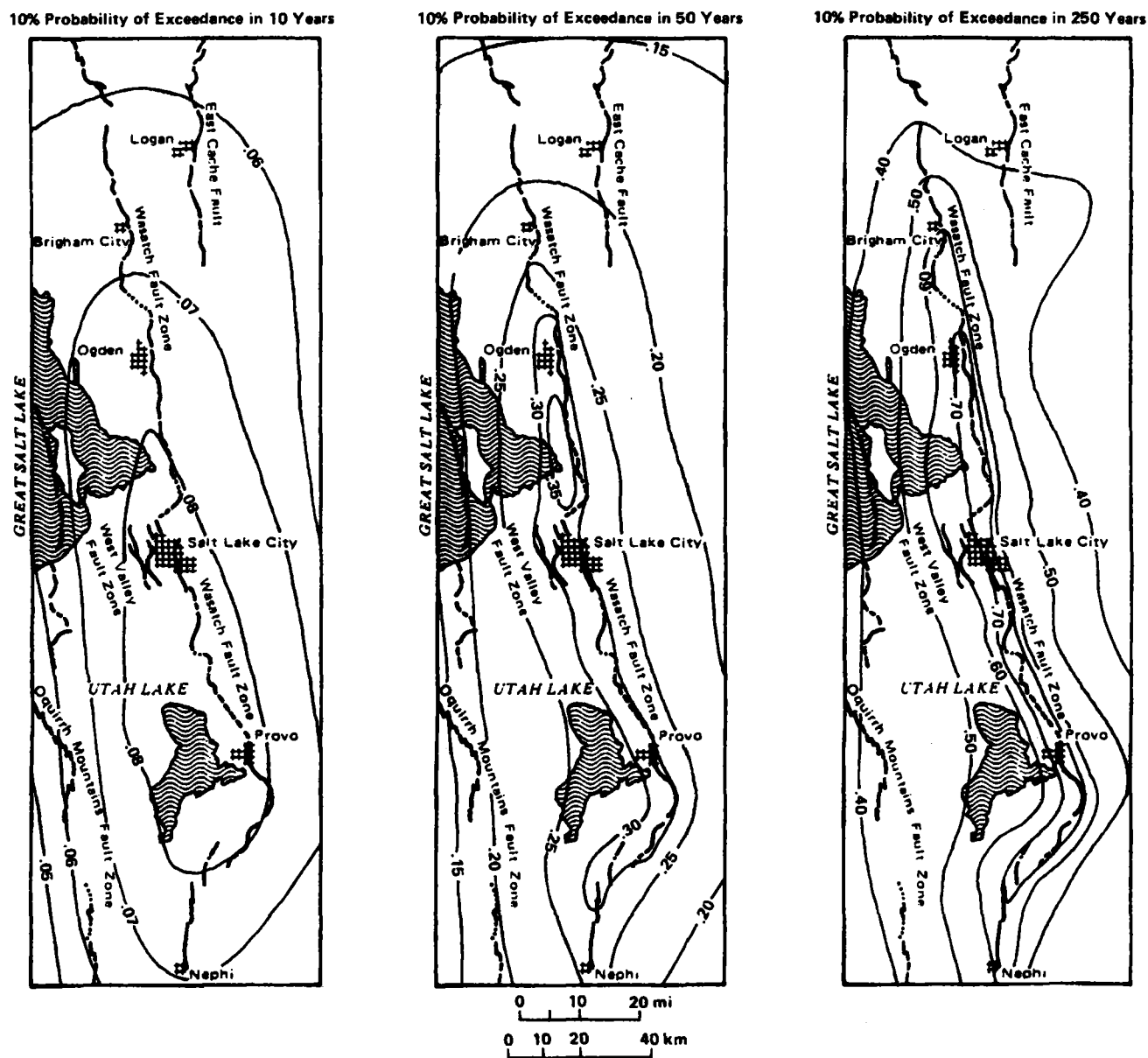


Figure 7. Contours of peak ground acceleration on soil sites with 10 percent probability of being exceeded in 10 years, 50 years, and 250 years (after Youngs et al., 1987).

failure has been verified in numerous excavations throughout the valley (Gill, 1987), many studies in areas mapped as having a high liquefaction potential have demonstrated moderate to very low liquefaction susceptibility based on an absence of sandy sediments, the presence of dense deposits, or the presence of undeformed Lake Bonneville sediments older than 10,000 years (Keaton and Anderson, 1995). More site-specific engineering-geologic information is needed to refine and update the existing liquefaction-potential maps.

FIELD TRIP STOP NO. 3

Michael D. Hylland, Leader
Corner of 1525 West and 675 North,
west of Farmington; see Figure 26.

THE LIQUEFACTION-INDUCED FARMINGTON SIDING LANDSLIDE COMPLEX

The prehistoric Farmington Siding landslide complex, about 15 miles (25 km) north of Salt Lake City, comprises

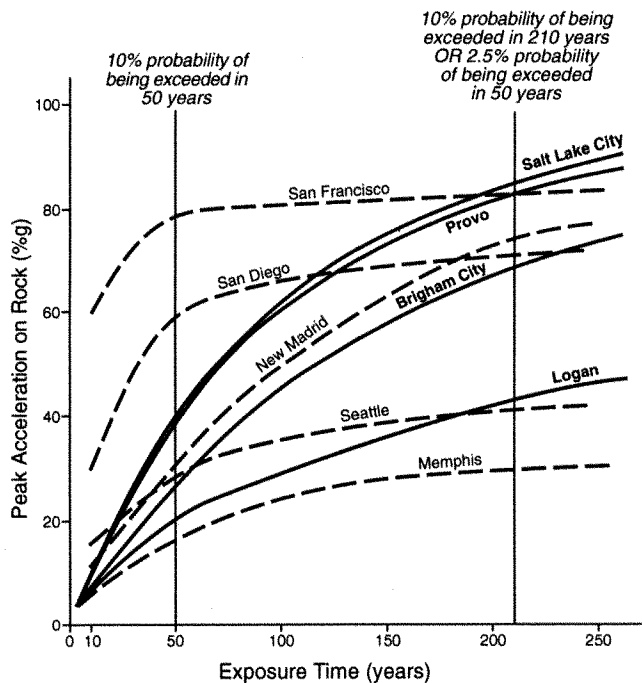


Figure 8. Plot of accelerations on rock with a 10 percent probability of being exceeded during various time periods (from Olig, 1991). Dashed curves are from Algermissen (1988) and solid curves were calculated from results of Youngs et al., (1987).

some of the largest landslides triggered by earthquakes in the United States. The landslide complex covers an area of approximately 7.5 square miles (19.5 km²) and is one of thirteen late Pleistocene/Holocene features along the Wasatch Front mapped by previous investigators as possible liquefaction-induced lateral spreads (Van Horn, 1975; Miller, 1980; Anderson et al., 1982; Nelson and Personius, 1993). Detailed discussions and results of recent investigations of the landslide complex are presented in Harty et al., (1993), Hylland and Lowe (1995), Lowe et al., (1995), Hylland (1996), and Hylland and Lowe (in press).

Geology and Geomorphology

The Farmington Siding landslide complex is in a gently sloping area underlain at shallow depths primarily by fine-grained, stratified, late Pleistocene to Holocene lacustrine deposits of Lake Bonneville and Great Salt Lake (fig. 10). Ground slopes within the landslide complex range from about 0.4 to 0.8 percent. Unfailed slopes adjacent to the complex range from about 1 to 2 percent along the flanks and 6 to 11 percent in the crown area. The deposits involved in landsliding consist of interbedded, laterally discontinuous layers of clayey to sandy silt, well-sorted fine sand to silty sand, and minor clay and gravel. The crown is underlain by Lake Bonneville sand and silt deposits and is

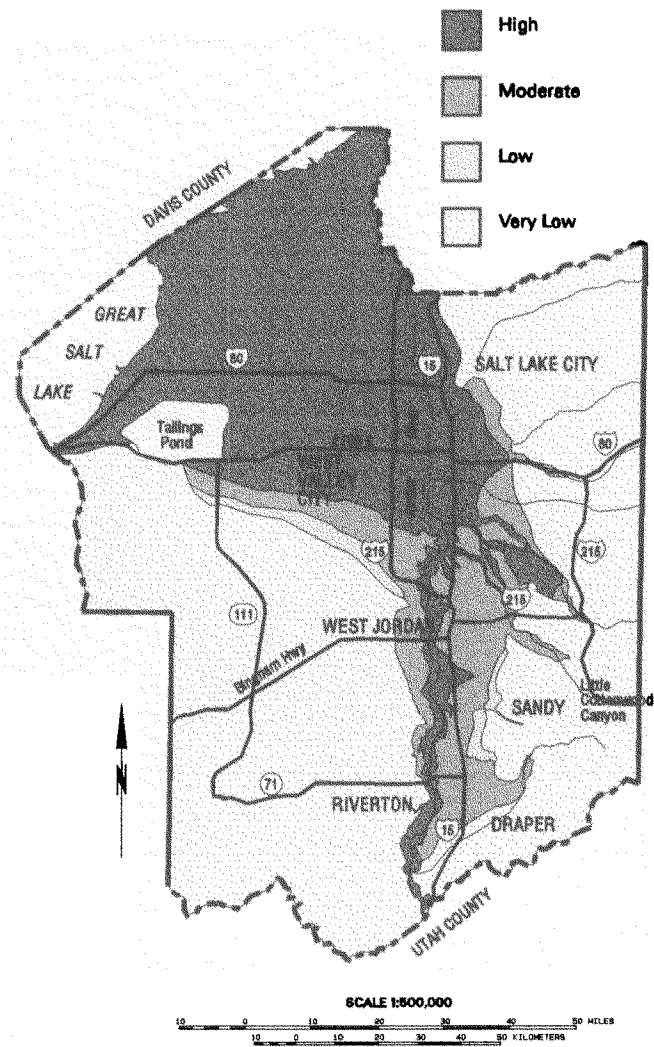


Figure 9. Liquefaction-potential map of the Salt Lake Valley (after Anderson et al., 1986).

at an elevation of about 4,400 feet (1,342 m) in the vicinity of the city of Farmington. The toe may have been encountered beneath Great Salt Lake during a drilling project in Farmington Bay to test foundation conditions for a proposed water-storage reservoir (Everitt, 1991).

The landslide deposits can be grouped in two age categories relative to the age of the Gilbert shoreline complex, which formed between 10,900 and 10,300 years ago (Currey, 1990). The northern part of the landslide complex truncates the Gilbert shoreline (Van Horn, 1975), indicating major post-Gilbert movement. However, the Gilbert shoreline can be traced across the southern part of the landslide complex (Anderson et al., 1982; Harty et al., 1993), indicating pre-Gilbert movement in this part of the complex.

Geomorphic features include scarps, hummocks, closed depressions, and transverse lineaments. Well-preserved

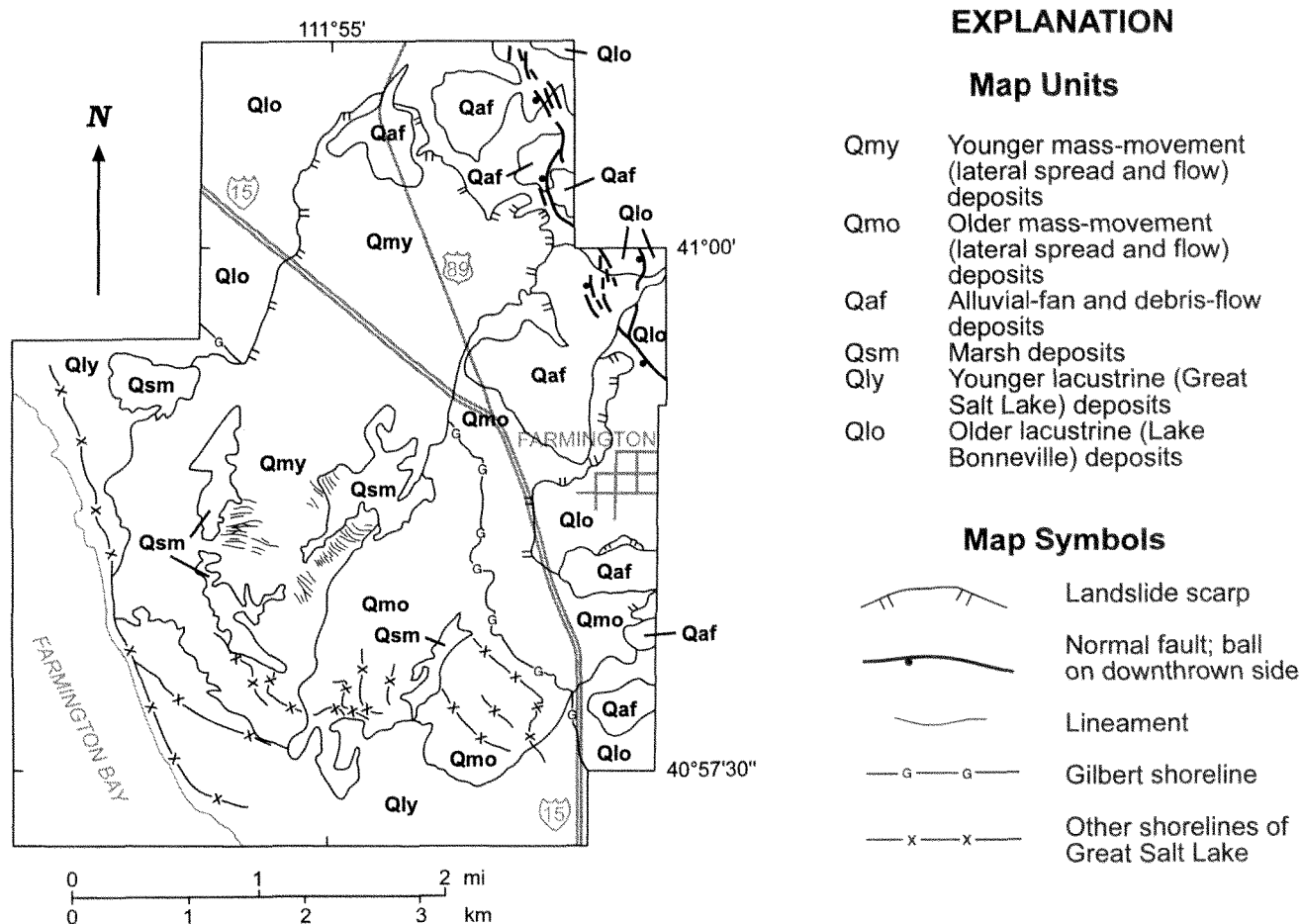


Figure 10. Simplified geologic map of the Farmington Siding landslide complex (modified from Harty et al., 1993).

lateral and main scarps in the northern part of the complex range in height from about 10 to 40 feet (3 to 12 m). Hummocks and closed depressions are present over most of the complex, but are more common in the northern part (fig. 11). Hummocks on the northern part are morphologically distinct, having as much as about 20 feet (6 m) of relief and lateral dimensions locally exceeding 1,000 feet. Hummocks on the southern part are morphologically subtle, generally having less than about 6 feet (2 m) of relief. Subtle transverse lineaments are present in the central part of the complex. Subsurface deformation of lacustrine deposits includes inclined strata, gentle to strong folding, and both low- and high-angle faulting. Small sand dikes are present locally, some of which were injected along fault planes (fig. 12).

Geotechnical Properties and Slope-Failure Mechanism

Soil grain-size distribution, standard-penetration resistance, and ground-water depth noted on logs of geotechnical boreholes (Anderson et al., 1982) indicate liquefiable

deposits in the shallow subsurface beneath the landslide complex. Miller et al., (1981) drilled three boreholes in an attempt to correlate beds beneath and adjacent to the landslide complex. Using these and Anderson et al.'s data, Hylland and Lowe (1995) interpret a possible landslide failure zone that occurs within a depth range of 14 to 40 feet (4–12 m). This zone locally corresponds to the contact between a relatively dense transgressive lacustrine sequence consisting of nearshore sand and gravel deposited during the early part of the Bonneville paleolake cycle, or possibly pre-Bonneville alluvium, and overlying loose/soft, offshore, fine-grained sediment subsequently deposited in deeper water.

Landsliding probably occurred as a combination of lateral spread and flow (Hylland and Lowe, 1995). The transverse lineaments near the middle of the complex may represent regressive lake shorelines (Lowe et al., 1995), but Hylland and Lowe (1995) believe the pattern and relative age of the lineaments indicate they represent infilled ground cracks associated with lateral spread. By excavating trenches



Figure 11. Aerial view of hummocky landslide terrain on the northern part of the Farmington Siding landslide complex. Hummocks appear as light-colored patches.

across hummock flanks and adjacent ground in the northern part of the complex, Harty et al., (1993) determined the hummocks are relatively intact "islands" of lacustrine strata surrounded by liquefied sand which resulted from flow failure. Other evidence for flow failure includes the existence of a landslide main scarp up to 40 feet (12 m) high; the overall negative relief in the head region of the complex, indicating evacuation of a large volume of material; and the overall positive relief in the distal region of the complex, indicating deposition of landslide material.

Landslide Timing and Seismic Considerations

Relative timing information and limiting radiocarbon soil ages indicate at least three, and possibly four, landslide events (fig. 13). Hylland and Lowe (1995) considered the timing of these landslide events within the context of paleoclimatic and lacustrine fluctuations, and observed that landsliding was associated with climate-induced highstands of Great Salt Lake. The apparent correspondence between landslide events and lacustrine highstands suggests that landsliding may have occurred under conditions of relatively high soil pore-water pressures, and possibly increased artesian pressures, associated with rising lake and groundwater levels.

Many features (for example, evidence of lateral spread, flow failure of gentle slopes, sand dikes, deposits susceptible to liquefaction, and proximity to faults with recurrent Holocene activity) indicate landsliding was likely triggered by strong earthquake ground shaking. Numerous fault studies (Machette et al., 1987; Schwartz et al., 1988; Personius, 1990; Forman et al., 1991; Lund et al., 1991; McCalpin and Forman, 1994; Black et al., 1996) constrain the timing of prehistoric surface-faulting earthquakes on the active segments of the Wasatch fault zone; comparison of the results of these



Figure 12. Liquefied sand (arrow) injected along fault plane in trench exposure of thin-bedded lacustrine deposits. Trowel for scale.

studies with the timing of landslide events indicates a close correspondence between landsliding and certain earthquakes (fig. 14). Within uncertainty limits, surface-faulting earthquakes on the Brigham City segment coincide with all four possible landslide events. Surface-faulting earthquakes on the Weber, Salt Lake City, and Provo segments also coincide with the more recent landslide events. Earthquake chronologies for these segments generally do not extend beyond 7,000 years ago, so unrecognized and/or undated earthquakes on these segments may also correspond to the earlier landslide events.

Hylland and Lowe (in press) used a variety of deterministic analyses to evaluate the relative likelihood of large-scale liquefaction-induced landsliding being triggered by earthquakes on various source zones, including: (1) empirical earthquake magnitude-distance relations, (2) comparison of expected peak horizontal ground accelerations with calculated critical accelerations, (3) liquefaction severity index, and (4) estimated Newmark landslide displacements. All of these analyses indicate that widespread liquefaction-induced ground failure involving significant lateral displacements is most likely associated with large earthquakes on the nearby Weber segment of the Wasatch fault zone.

At least two large earthquakes have occurred on the Weber segment that apparently do not coincide with land-

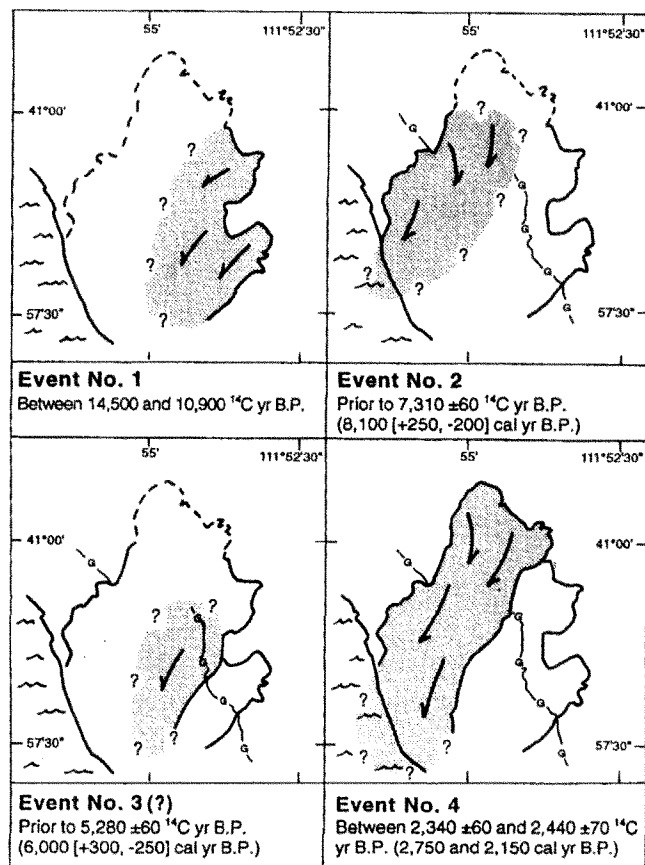


Figure 13. Timing and generalized areas (shaded) of landsliding within the Farmington Siding landslide complex. Arrows show speculated direction of movement; "G" indicates Gilbert shoreline.

slide events. Either geologic and hydrologic conditions at the time of these earthquakes were such that little or no slope movement occurred, or evidence for landsliding has not yet been observed. Because present lake and groundwater levels are relatively low, the likelihood of liquefaction-induced landsliding may be somewhat less than at other times during the Holocene. However, a higher potential for landsliding would exist if the area experienced strong ground shaking during a time of increased soil pore-water pressures associated with abnormally high groundwater levels.

FIELD TRIP STOP NO. 4

Bill D. Black, Leader

Buffalo Point on Antelope Island; see Figure 26.

FLOOD HAZARD FROM GREAT SALT LAKE

Great Salt Lake is located in the Great Salt Lake basin of northwestern Utah (fig. 15), and presents unique geologic

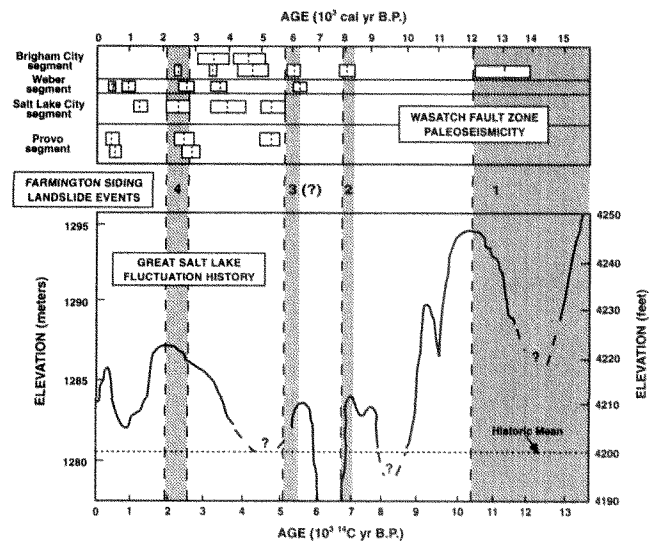


Figure 14. Comparison of the timing of landslide events within the Farmington Siding landslide complex (shaded areas) with Wasatch fault zone paleoseismicity (top) and Great Salt Lake fluctuations (bottom) (modified from Hylland and Lowe, 1995). Dashed lines limiting ages. Paleoseismic data summarized from Machette et al., (1987), Schwartz et al., (1988), Personius (1990), Forman et al., (1991), Lund et al., (1991), McCalpin and Forman (1994), Black et al., (1996), and McCalpin and Nishenko (1996). Great Salt Lake hydrograph after Murchison (1989).

hazards and engineering-geology problems to development. Flooding from lake rises and seiches are the greatest hazards, and flooding historically has caused millions of dollars in damage. Rising lake levels between 1983–1985 from above-normal precipitation caused \$240 million damage.

Fluctuating water levels are a particular problem along lakes which, like Great Salt Lake, have no natural outlet. Lake-level fluctuations occur daily, seasonally, and on a long-term basis. Natural factors causing fluctuations include precipitation, evaporation, runoff, ground water, aquatic growth, and wind; human factors include dredging, diversions, consumptive use, and regulation by engineered works (Federal Emergency Management Agency, 1985).

Daily fluctuations are commonly caused by strong winds, which produce oscillations in the main body of the lake (seiches). Seiches may also be caused by earthquakes. However, unlike long-term and seasonal fluctuations, daily fluctuations do not result from changes in the amount of water in the lake. Seasonal fluctuations reflect the annual hydrologic cycle. Great Salt Lake levels gradually rise in the spring in response to snow-melt runoff, increased precipitation, and warmer temperatures, until the lake level peaks in early summer (Atwood and Mabey, 1985; Federal Emergency Management Agency, 1985). As the amount of water flowing into the lake becomes less than the amount of water

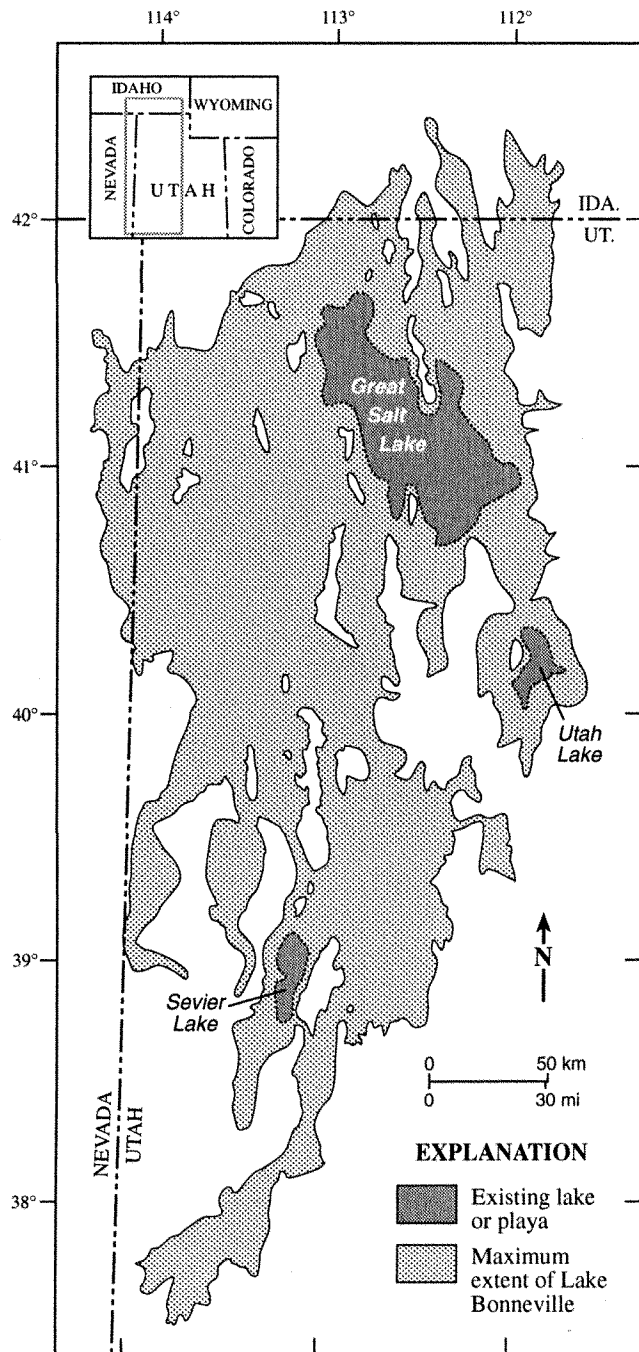


Figure 15. Location of Great Salt Lake and maximum extent of Pleistocene Lake Bonneville (modified from Currey et al., 1984).

removed by evaporation, lake levels drop to winter minima. Great Salt Lake levels fluctuate on average 2 feet (0.6 m) between winter low and summer high. Long-term fluctuations result from persistent low or high water-supply conditions, and lake levels are highly sensitive to minor precipi-

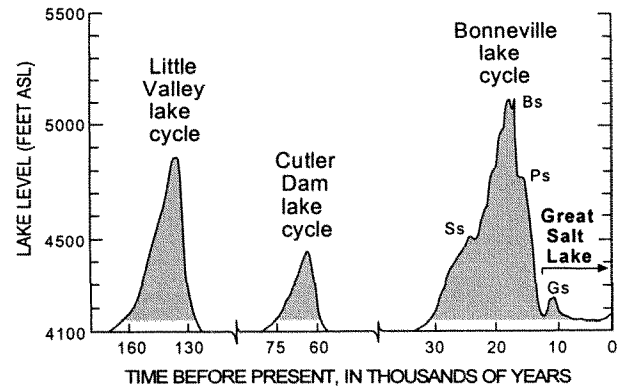


Figure 16. Hydrograph of probable lake levels in the Great Salt Lake basin for the past 150,000 years (modified from Currey and Oviatt, 1985; Machette et al., 1987). Ss = Stansbury shoreline, Bs = Bonneville shoreline, Ps = Provo shoreline, Gs = Gilbert shoreline.

tation, inflow, and evaporation variations. Long-term climatic trends play a major role in determining lake levels, as do diversion and consumptive use of water sources by man. Fluctuations in Great Salt Lake have a profound effect on the surface area of the lake because of the flatness of the lake basin. Extreme low or high lake levels are likely to persist even after the factors which caused them have changed.

Lake History and Flood Hazard

Lakes have occupied the Bonneville basin several times over the past several million years. Water levels in lakes such as Lake Bonneville and Great Salt Lake have oscillated with great elevation differences between highstands and lowstands (fig. 16). Lake Bonneville reached a maximum elevation (Bonneville shoreline) of 5,092 feet (1,552 m) around 15,000 years ago, and receded to a post-Bonneville lowstand after about 13,000 years ago (Currey and Oviatt, 1985). In the Salt Lake Valley, the elevation of the Bonneville shoreline varies from 5,161 to 5,216 feet (1,573 to 1,590 m) (Van Horn, 1972; Currey, 1982), due to a combination of isostatic rebound as the lake lowered and post-lake faulting (Miller, 1980). Isostatic rebound was generally greater near the center of the Bonneville basin than at the edges of the basin where water depths were shallower. Great Salt Lake reached a Holocene highstand of approximately 4,221 feet (1,287 m) between about 2,500 and 1,400 years ago (Currey et al., 1988; Murchison, 1989). A late pre-historic highstand of Great Salt Lake was at 4,215 feet (1,286 m) sometime during the 1600s (Murchison, 1989; Currey, 1990).

Although no significant diurnal tides occur on Great Salt Lake, wind seiches are common. Such seiches develop on the main body of the lake in response to strong winds from

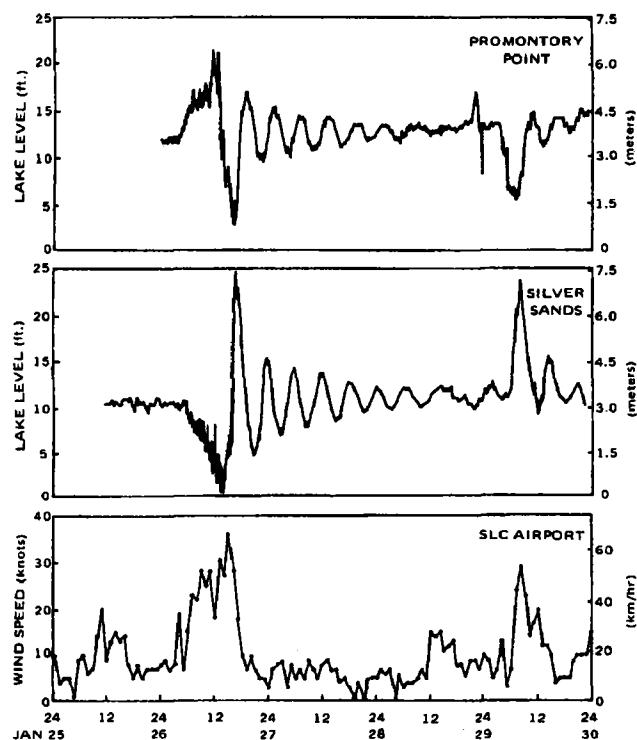


Figure 17. Great Salt Lake seiche hydrographs for Promontory Point (north) and Silver Sands (south), and wind speed at the Salt Lake City International Airport, showing wind seiches over a five-day period (from Lin and Wang, 1978).

the south or west. A major wind seiche commonly needs wind velocities in excess of 10 knots (18.5 km/hr) (Lin and Wang, 1978). Sustained, strong south winds cause the water level to decline in the south and increase in the north (wind setup). When the wind velocity drops, water levels try to reach equilibrium. These wind-induced oscillations have a fundamental period of about 6 hours and seiching lasts about 2 days (fig. 17; Atwood et al., 1990). During this time, up to 2 feet (0.6 m) of flooding may occur along the south shore.

Great Salt Lake levels go through a seasonal cycle, waxing in spring or early summer in response to spring runoff, and waning in the fall at the end of the period of high evaporation (fig. 18). The maximum seasonal lake rise (measured in 1983) is 5 feet (1.5 m), and the maximum seasonal lake decline (measured in 1988) is 3 feet (0.9 m) (Atwood et al., 1990; Atwood and Mabey, 1995). Seasonal fluctuations are largely controlled by weather and are difficult to predict, but generally do not present a direct threat to life due to their slow rate of rise (maximum of about 1 inch per day [2.5 cm/day]).

Historical water levels in Great Salt Lake have also fluctuated over the long term (fig. 18). Until mid-1986, the his-

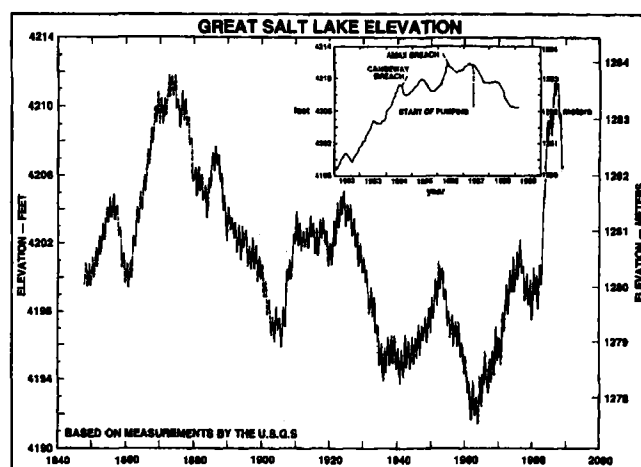


Figure 18. Hydrograph of Great Salt Lake. Elevations before 1875 are estimated from traditional accounts (from Atwood et al., 1990).

torical high of Great Salt Lake was 4,211.5 feet (1,283.6 m) (Arnow and Stephens, 1990), which was reached in the early 1870s (Gilbert, 1890). The lake dropped slowly from its high in the 1870s, reaching an historical low of 4,191.35 feet (1,277.46 m) in 1963. Above-average precipitation in the 1980s caused Great Salt Lake to attain a new historical high of 4,211.85 feet (1,283.71 m) in June 1986 (Arnow and Stephens, 1990) and April 1987 (USGS records). This lake-level rise caused damage to structures and other property along the shoreline and within the lake. The cost to Salt Lake County for flooding at lake elevations greater than 4,212 feet (1,284 m) is believed to be in the millions of dollars (Atwood et al., 1990). If the lake rises to 4,217 feet (1,285 m), potential additional costs could exceed \$3 billion (Steffen, 1986).

Flood Mitigation

The rapid rise of Great Salt Lake between 1982 and 1986 doubled the lake volume and increased its surface area by nearly 500,000 acres (Atwood et al., 1990). Flooding associated with the lake rise caused more than \$240 million damage to facilities within and adjacent to the lake (Austin, 1988). The Southern Pacific Railroad causeway divided the lake into two unequal areas of different elevations: the north arm and the main Great Salt Lake. Most of the inflow was to the main Great Salt Lake. The causeway was breached in 1984, reducing the elevation of the main Great Salt Lake by about 8 inches (20 cm) and increasing the elevation of the north arm by about 16 inches (40 cm). However, the lake continued to rise and peaked (at its historical high) two years later.

In response to flooding, the Utah State Legislature authorized a study of potential lake-level control measures

(Utah Division of Water Resources, 1984). Pumping excess water into the shallow desert basin west of Great Salt Lake was the only measure that could be implemented quickly enough to provide flood-damage relief. Thus, construction began in 1986 on the West Desert Pumping Project (Atwood et al., 1990). By the end of 1988 2.05 million acre-feet (2.52 billion m^3) of water had been pumped from Great Salt Lake (James Palmer, written communication, 1989). The lake dropped 5.4 feet (1.6 m) by the end of 1988 due to a combination of pumping, evaporation, and decreased inflow from two drier than average years. The pumps are kept in reserve for future lake rises.

FIELD TRIP STOP NO. 5

Mike Lowe, Leader

*Turn-out along North Ogden Canyon Road
east of North Ogden; see Figure 27.*

CAMERON COVE DEBRIS FLOW, NORTH OGDEN

A debris flow from an unnamed canyon deposited material on an alluvial fan in North Ogden (fig. 19) on September 7, 1991, damaging seven houses in the Cameron Cove subdivision (Mulvey and Lowe, 1991, 1994; Lowe et al., 1992). Over the 24-hour period prior to the debris-flow event, rainfall in the North Ogden area ranged from 2.5 to 8.4 inches (6.4 to 21.3 cm) (Brenda Graham, National Weather Service, verbal communication, 1991). This rain-storm set a new state record for a 24-hour period, and was estimated to be equivalent to a 1,000-year storm. Runoff from the storm was concentrated in channels on Tintic Quartzite cliffs at the head of the canyon and formed waterfalls which cascaded several hundred feet to talus slopes at the base of the cliffs. The runoff mobilized talus and other debris in and near tributary channels at the base of the cliffs, initiating debris flows. As the tributary flows moved downstream and combined with the main channel, additional channel material was incorporated into the debris flow. The flow exited the canyon mouth and traveled down an alluvial fan for a distance of about 1,300 feet (400 m), damaging the houses (Mulvey and Lowe, 1991).

An examination of the main and tributary channels indicated that channel material, from the base of the cliffs to the mouth of the canyon, had been incorporated into the debris flow (Mulvey and Lowe, 1991). Depth of scour in the main channel averaged 5 to 6 feet (1.5 to 1.8 m), and was as much as 17 feet (5 m) locally. Soils on drainage-basin slopes did not appear to have contributed much material to the flow except from an area of limited extent near the base of the cliffs where grasses were absent, cobbles were left standing on soil pedestals, and small rills were present. This was the only place damaged by a wildfire in 1990 that



Figure 19. Aerial view, looking northeast, of the September 7, 1991 Cameron Cove debris flow in North Ogden (photo taken in August 1996).

noticeably contributed sediment to the debris flow. Mulvey and Lowe (1991) concluded that sediment contribution from the burned area was low because of rapid revegetation of oakbrush, woody plants, and grasses.

Mulvey and Lowe (1991, 1994) observed that much debris remained in and along the main and tributary channels after the debris-flow event. Considerable debris was trapped behind several natural dams composed of large boulders. In many places along the channel, side slopes had been destabilized by scour and undercutting of channel banks. Mulvey and Lowe (1991) were not able to accurately estimate the volume of debris still in the channel, but they believed that enough debris remained in the channel that another large debris-flow event from the drainage basin was possible.

The volume of the debris-flow deposit was about 25,728 cubic yards (19,553 m^3) (Mulvey and Lowe, 1991). Using the Pacific Southwest Inter-Agency Committee (PSIAC) (1968) Sediment Yield Rating Model, Lowe et al., (1990) estimated an average annual post-fire sediment yield of approximately 387 cubic yards (294 m^3) per year from



Figure 20. View, looking southwest, from near the apex of the alluvial fan above the Cameron Cove subdivision showing levees from past debris flows (modified from Mulvey and Lowe, 1994).

slopes within the drainage basin. The large difference between the PSIAC estimate and the actual volume of the debris flow supports Mulvey and Lowe's (1991) field observation that a small percentage of the total volume of debris was derived from the slopes and that the 1990 fire was not a significant cause of the debris flow. The majority of debris-flow material in the 1991 event was derived from scour of stream channels and talus on slopes immediately below the cliffs.

Relative Hazard

Future debris flows from the unnamed canyon are inevitable. Levees from prehistoric debris flows are present on the steep, active alluvial fan at the mouth of the canyon (fig. 20), indicating the 1991 debris flow was not a geologically unusual event for this canyon, but instead is part of the alluvial-fan-building process (Mulvey and Lowe, 1991). Ridd and Kaliser (1978) recognized that the alluvial fan is active, and mapped relative flood-hazard zones on the fan. Lowe (Weber County Planning Commission, 1988; Lowe, 1990) mapped debris-flow hazards as part of a comprehensive evaluation of geologic hazards in Weber County and placed the alluvial fan in a debris-flow-hazard special-study zone. The Cameron Cove subdivision was approved prior to completion of these geologic-hazard studies. The Ridd and Kaliser (1978) study led to enactment of a hazard ordinance regulating development on alluvial fans in the City of North Ogden where the Cameron Cove subdivision is located.

In spite of the existence of these geologic-hazard studies and ordinance, homeowners and North Ogden City officials were apparently unaware that flooding and debris-flow hazards existed in the Cameron Cove subdivision (Mulvey and Lowe, 1994). North Ogden City was named in a lawsuit brought by the owner of the home most severely dam-

aged by the 1991 debris flow (Dennis Shupe, North Ogden City Manager, verbal communication, 1992). The lawsuit alleged that North Ogden City was negligent for not mitigating the debris-flow hazard on the alluvial fan after the hazard was identified by geologic studies (Mulvey and Lowe, 1994). The case judge ruled that the city could not be sued due to governmental immunity. The homeowner has subsequently erected a debris wall that can be seen along the eastern edge of the subdivision. Because no major sediment deposition has occurred on the alluvial fan since 1991, stream channels in the canyon above still contain debris that could be mobilized and incorporated into another large debris flow. Debris flows will likely be deposited again on the alluvial fan, and houses within the Cameron Cove subdivision remain at risk until a long-term, permanent solution to the problem is implemented.

FIELD TRIP STOP NO. 6

Mike Lowe, Leader

Rainbow Gardens parking lot, Ogden; see Figure 27.

RAINBOW IMPORTS LANDSLIDE, OGDEN

The Rainbow Imports landslide, near the mouth of Ogden Canyon in Weber County, is part of the Ogden River landslide complex of Pashley and Wiggins (1972). Vandre and Lowe (1995) delineated four domains within this landslide complex (fig. 21), each characterized by unique combinations of topography, ground-water conditions, soil properties, and movement mechanisms. They named the easternmost domain the frontage trough. After Pashley and Wiggins (1972), Vandre and Lowe (1995) referred to two other landslide domains, which include topographic reentrants, as the eastern amphitheater and western amphitheater. The fourth domain, the Rainbow Imports landslide, is along the eastern margin of the eastern amphitheater (figs. 21 and 22) and is the most active of the landslide domains. The landslide was named after the Rainbow Imports (now Rainbow Gardens) commercial development north of the landslide.

Geology

The Wasatch Range east of the Ogden River landslide complex is characterized by a lower section of near-vertical cliffs, consisting predominantly of Precambrian Farmington Canyon Complex granitic gneiss and Cambrian Tintic quartzite, and an upper section of more gently sloping mountainous terrain consisting predominantly of Paleozoic sedimentary rocks (Crittenden and Sorensen, 1985; Yonkee and Lowe, in preparation). Below 5,200 feet (1,585 m) in elevation, bedrock is generally covered by Lake Bonneville lacustrine sediments, or by post-Lake Bonneville alluvial-fan deposits. The bench area south of the landslide complex

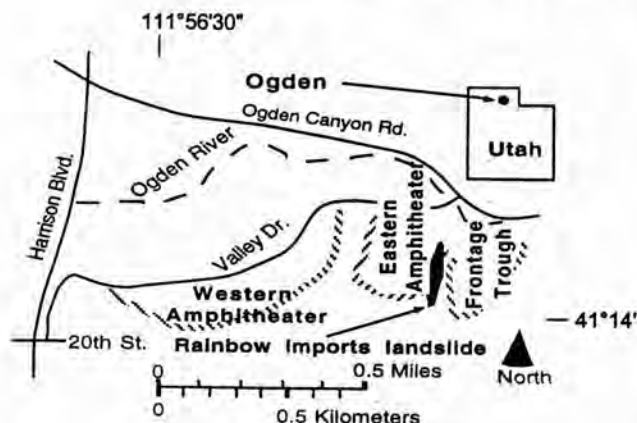


Figure 21. Landslide domains within the Ogden River landslide complex, and location of the Rainbow Imports landslide (from Vandre and Lowe, 1995).



Figure 22. Aerial view, looking south, of the eastern amphitheater of the Ogden River landslide complex. Rainbow Imports landslide indicated by arrow. Photo taken August 1996.

is the Provo-level delta of the Ogden and Weber Rivers and consists of gravel, sand, and silt deposited as Lake Bonneville occupied and then regressed from the Provo shoreline after about 14,000 years ago (Oviatt et al., 1992). The deltaic deposits overlie fine-grained, cyclically bedded sand, silt, and clay deposited during the earlier transgressional phase of Lake Bonneville.

Several ephemeral streams flow westward from the Wasatch Range and have deposited various ages of alluvial fans onto the delta. The four drainages between the Ogden River and Taylor Canyon, about 1.5 miles (2.4 km) south of the landslide complex, are ephemeral with catchment areas of less than 0.5 square mile (1.3 km²). Taylor Canyon Creek has a much larger catchment area of about 2 square miles (5.2 km²) and may be a significant source of recharge to ground water in the Lake Bonneville deposits at the landslide (Vandre and Lowe, 1995).

The Weber segment of the Wasatch fault zone offsets Lake Bonneville and alluvial-fan deposits along the eastern margin of the deltaic bench. Paleoseismic trenching studies of the Weber segment on the deltaic bench just north of the Ogden River show evidence of three to four surface-faulting events during the past 6,000 to 7,000 years (Nelson and Personius, 1993). Most of the fault scarps in the vicinity of the Ogden River landslide complex are west-facing, valley-side-down scarps. An antithetic, east-facing, mountain-side-down scarp is also present on the delta south of the Ogden River landslide complex, and this fault terminates along the eastern margin of the Rainbow Imports landslide (Yonkee and Lowe, in preparation). Two large conical depressions, probably sinkholes, along the base of the westernmost west-facing fault scarp (fig. 23) may be evidence of northward ground-water flow along the Wasatch fault zone.

The Ogden River incised and eroded laterally into the deltaic and lacustrine deposits at the mouth of Ogden Canyon as Lake Bonneville regressed from the Provo shoreline, leaving steep bluffs (Lowe et al., 1992) and depositing fluvial sand and gravel between the bluffs. The Ogden River landslide complex is along the erosional bluffs south of the Ogden River. All landslides in the complex are below about 4,710 feet (1,435 m) in elevation (Vandre and Lowe, 1995).

Movement History

The Rainbow Imports landslide initiated on March 9, 1987, damaging a steel transmission tower (fig. 24) causing a loss of power to much of Ogden's east bench area (Kaliser, 1987). Additional movement occurred on either the night of March 9 or early in the morning of March 10. Kaliser (1987) attributed the movement to soil saturation from melting snow and ice. Landsliding occurred again during April 1988 and February 1992. These landslide events involved mostly earth flows, and landslide activity generally stopped within a week or two.

The landslide moved again in early March 1994 (fig. 24) (Delta Geotechnical Consultants, 1994). Movement again involved mostly earth flows; however, the main scarp continuously retreated after the earth flows ceased. The main scarp of the landslide retreated an additional 50 feet (15 m) southward between April and August 1994, and two homes south of the landslide were removed in October 1994 due to concerns caused by the retreating main scarp (Vandre and Lowe, 1995). The main scarp had retreated southward an additional 15 to 20 feet (4 to 6 m) by April 1995. The overall slope of the main scarp during April 1995 was approximately 80 percent, with the top 15 to 20 feet (4 to 6 m) nearly vertical (Vandre and Lowe, 1995).



Figure 23. Sinkholes along a normal fault crossing the frontage trough, Ogden River landslide complex.

Vandre and Lowe (1995) estimated the width of historical landsliding to be approximately 50 yards (45 m). From 1987 to 1990, most of the movement involved sandy landslide debris. From 1990 to 1994, movement involved mostly deltaic and lacustrine deposits that had not previously been disturbed by landsliding (Vandre and Lowe, 1995). The volume of landslide material was about 25,000 cubic yards (19,000 m³) between 1987 and 1990 and about 50,000 cubic yards (38,000 m³) between 1990 and 1994.

Vandre and Lowe (1995) noted two springs discharging in the landslide area near the contact between the regressive deltaic and transgressive lacustrine deposits. They projected the top of the 1990 main scarp to be slightly below the elevation of the springs. A fault trace was noted in the 1994 main-scarp area; water moving northward along the Wasatch fault zone may have contributed to the spring flow.

Movement Mechanisms

SHB AGRA (1994) noted different soil movement mechanisms in different areas of the Rainbow Imports landslide. Vandre and Lowe (1995) refer to these areas as the undercut, erosion, and deposition zones.

The approximately 90-foot- (27 m) high main scarp is the undercut zone. The overall slope of this area was very steep with the finer grained soil layers generating near-vertical faces and the granular soils raveling to their angle of repose (Vandre and Lowe, 1995). The main soil movement mechanism in this area is collapse due to undercutting of fine-grained layers in response to wind and water erosion, and raveling of granular soils.

The erosion zone is the area immediately downslope from the undercut zone. The erosion zone's vertical extent was approximately 50 feet (15 m) with side scarps on the order of 20 to 30 feet (6–9 m) high (Vandre and Lowe, 1995). Soil movement in this zone was primarily erosion caused by



Figure 24. Rainbow Imports landslide in 1987 (A) and 1994 (B).

runoff from springs discharging at the top of the zone, and earth flows.

The deposition zone is below the erosion zone. The ground slope at the top of this zone is 25 to 30 percent, but lower in the zone is 20 percent or less (Vandre and Lowe, 1995). Soil deposition is caused by decreases in slope and spreading out of flowing water due to lack of confinement.

Potential for Additional Movement

Conditions contributing to slope failure at the Rainbow Imports landslide include the presence of: (1) slopes steeper than 60 to 70 percent which are subject to undercutting and raveling, (2) soils prone to erosion by wind and water, (3) ground water in close proximity to the contact between the deltaic and lacustrine deposits, and (4) saturated sandy soils which have the potential to undergo liquefaction. Due to these conditions, a high potential for future movement exists (Vandre and Lowe, 1995). The most significant landslide hazard is to homes south of the present main scarp.

The Rainbow Imports landslide will continue to retreat southward into the delta as the main scarp is undermined by erosion, flow slides, and/or raveling of the sand and gravel in the scarp. The rate of main-scarp retreat cannot be pre-

dicted. The time needed to reach stability may be 10, 50, or 100 years or more, and Vandre and Lowe (1995) expect the rate of main-scarp retreat to decrease as its slope decreases. Major earthquakes will likely accelerate the raveling of the main scarp, possibly causing liquefaction of the saturated sands deposited in the erosion zone, thereby causing liquefaction-induced slope failures and more erosion and undercutting. Runoff over the main scarp may accelerate the rate of retreat (Vandre and Lowe, 1995).

ROAD LOG

The following road log describes the route of the field trip and indicates selected geologic features and other points of interest. Space limitations preclude reference to many sites and features along the route, however, and the reader is encouraged to consult guidebooks for previous geologic field trips along the Wasatch Front (for example, Utah Geological Association, 1971; Gurgel, 1983; Machette, 1988; Lowe et al., 1992; Horns et al., 1995) for additional information.

Mileage		
0.0		The field trip departs from the Salt Palace Convention Center at 100 South West Temple in Salt Lake City (fig. 25); proceed SOUTH on WEST TEMPLE.
0.4	(0.4)	Turn LEFT (EAST) on 400 SOUTH.
0.7	(0.3)	Turn RIGHT (SOUTH) on STATE STREET.
3.5	(2.8)	Turn LEFT (EAST) onto I-80 eastbound; follow signs for I-215, SOUTH BELT ROUTE, at the mouth of Parleys Canyon. Rocks exposed in the vicinity of Parleys Canyon consist of folded Mesozoic strata.
10.0	(6.5)	On the left (east) side of the freeway, residences along the upper margins of Olympus Cove are periodically affected by rock falls. The prominent peak rising above the southern part of Olympus Cove is Mt. Olympus, the north face of which is a dip slope of Cambrian Tintic Quartzite (Crittenden, 1965a).
13.0	(3.0)	Take EXIT 6 (6200 SOUTH), turn LEFT (SOUTHEAST) under freeway, proceed up hill and continue SOUTH on WASATCH BOULEVARD.
14.0	(1.0)	Active sand and gravel mining operations on the left (east) side of the road in outwash-fan/delta-complex sediments (Scott, 1981; Personius and Scott, 1992).
14.9	(0.9)	Mouth of Big Cottonwood Canyon. Rocks exposed at the mouth of the canyon con-



Figure 25. Route of field trip showing stops 1 and 2. Base from USGS Salt Lake City 30 X 60 minute quadrangle.

- sist of quartzite, shale, and siltstone of the Precambrian Big Cottonwood Formation locally intruded by quartz monzonite of the Tertiary Little Cottonwood stock (Crittenden, 1965b).
- 17.0 (2.1) Turn RIGHT (SOUTH) and continue on WASATCH BOULEVARD; the road is in a graben bounded by scarps of the main trace of the Wasatch fault zone on the left (east) and an antithetic fault on the right (west) (Scott and Shroba, 1985; Personius and Scott, 1992).
- 18.1 (1.1) Turn RIGHT (WEST) on 9800 SOUTH, then RIGHT (SOUTH) into large vacant lot near the mouth of Little Cottonwood Canyon for **STOP 1** (fig. 25) and discussion of **PALEOSEISMIC STUDIES ON THE SALT LAKE CITY SEGMENT OF THE WASATCH FAULT ZONE**. From here, Wasatch fault zone scarps can be seen to the southeast cutting the Pine-dale-aged Bells Canyon moraine.
- Retrace route to NORTH on WASATCH BOULEVARD.
- 22.6 (4.5) Turn RIGHT (EAST) at traffic light and continue NORTH on WASATCH BOULEVARD.
- 23.3 (0.7) New golf course on the left (west) side of the road is in a reclaimed sand and gravel pit in Lake Bonneville regressive-phase deltaic deposits (Personius and Scott, 1992).
- 24.1 (0.8) Park at Pete's Rock, an outcrop of Precambrian Mutual Formation quartzite (Crittenden, 1965a) and local climbing area, for **STOP 2** (fig. 25) and discussion of **SEISMIC SITE RESPONSE IN THE SALT LAKE VALLEY**. This stop provides an overlook of the Salt Lake Valley with views from left (south) to right (north) of the Traverse Mountains, Oquirrh Mountains and Bingham open-pit mine, Great Salt Lake and Antelope Island, downtown Salt Lake City, and the Salt Lake salient.
- Continue NORTH on WASATCH BOULEVARD.
- 27.5 (3.4) At 3300 SOUTH, continue NORTH on I-215 and follow signs for FOOTHILL DRIVE.
- 32.0 (4.5) University of Utah campus. FOOTHILL DRIVE turns to the LEFT (WEST) and becomes 500 SOUTH.
- 32.7 (0.7) Robert L. Rice Stadium on the right (south) will be the locale for the opening and closing ceremonies of the 2002 Winter Olympics. Foundation excavations for the stadium, as well as the George S. Eccles Tennis Center on the south side of 500 South, revealed evidence of faulting in pre-Bonneville alluvial-fan deposits.
- 33.2 (0.5) 500 SOUTH turns to the RIGHT (NORTH) to descend a hill formed by the scarp of the East Bench fault. At the base of the scarp, the road turns to the LEFT (WEST) and becomes 400 SOUTH.
- 34.5 (1.3) At the intersection of 400 SOUTH and 200 EAST, the Salt Lake City and County Building is on the left. The seismic retrofit of this historic building is summarized above in the discussion for field-trip stop 2.
- 35.2 (0.7) Turn RIGHT (NORTH) on 300 WEST.
- 37.0 (1.8) 300 WEST becomes BECK STREET. Several hot springs occur in this area along the Warm Springs fault at the base of the slope to the right (east).
- 38.5 (1.5) Active quarry operations on the right (east) side of the road in Paleozoic carbonates. Crushed stone is produced here for use in aggregate and other engineering applications. A faulted Holocene alluvial fan observed here by G.K. Gilbert (1890) has been removed by quarrying; striated bedrock in the footwall of the fault is now exposed at the base of the slope.
- 39.4 (0.9) Continue NORTH on I-15. The Bonneville and Provo shorelines of Lake Bonneville are well exposed near the base of the Wasatch Range on the right (east). The Bonneville shoreline marks the highest level reached by Lake Bonneville around 15,000 years ago (Currey and Oviatt, 1985); the Provo shoreline is a regressive shoreline about 350 feet (107 m) below the Bonneville shoreline. Several of the canyons on the west slope of the Wasatch Range between Bountiful and Farmington have produced damaging and, in some cases, fatal debris flows and floods. Notable debris flows occurred in the 1920s, 1930s, and 1983. Debris flows during the 1920s and 1930s were primarily generated by overland erosion during summer cloudburst storms (Woolley, 1946; Butler and Marsell, 1972; Keaton, 1988),

whereas debris flows during the spring of 1983 were mobilized from landslides caused by rapid melting of an unusually thick snowpack (Wieczorek et al., 1983, 1989).

- 49.7 (10.3) Take EXIT 325 (LAGOON DRIVE-FARMINGTON) and bear RIGHT to continue NORTH on 200 WEST.
- 50.6 (0.9) Turn LEFT (WEST) on STATE STREET (U.S. 227). Cross over freeway, pass new Davis County Criminal Justice Complex on the left (south), which is near the center of the prehistoric Farmington Siding landslide complex.
- 52.1 (1.5) Turn RIGHT (NORTH) on 1525 WEST. Note hummocky landslide terrain in this area.
- 52.7 (0.6) Park near the intersection of 1525 WEST and 675 NORTH in hummocky landslide terrain for **STOP 3** (fig. 26) and discussion of **THE LIQUEFACTION-**

INDUCED FARMINGTON SIDING LANDSLIDE COMPLEX.

Continue WEST on 675 NORTH.

Turn RIGHT (EAST) on SHEPARD LANE and cross over freeway. The golf course was constructed on naturally hummocky landslide terrain; the clubhouse and parking lot (on the left [north]) are at the top of the landslide main scarp.

Turn RIGHT (SOUTH) on U.S. 89.

Turn RIGHT (WEST) onto I-15 NORTH-BOUND.

Take EXIT 335 (SYRACUSE).

Turn LEFT (WEST) on ANTELOPE DRIVE (UTAH 108). Proceed WEST, following signs for Syracuse and Antelope Island.

Antelope Island State Park fee station. The causeway that provides vehicle access to Antelope Island was completely submerged by high lake levels in 1985. The

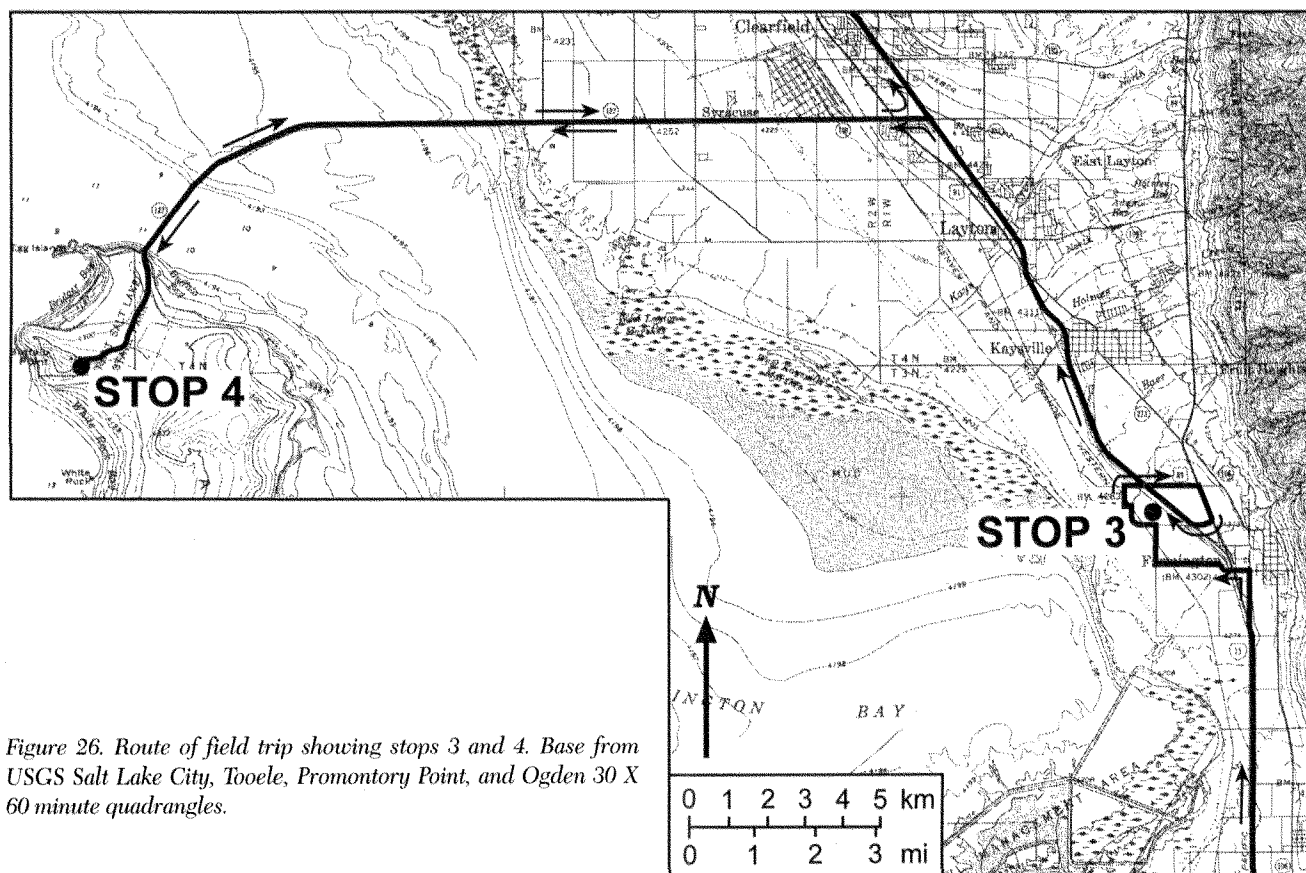


Figure 26. Route of field trip showing stops 3 and 4. Base from USGS Salt Lake City, Tooele, Promontory Point, and Ogden 30 X 60 minute quadrangles.

island was inaccessible to the public until Davis County rebuilt the causeway in 1993.

77.4 (6.8) Bear LEFT (SOUTHWEST) and follow paved road to Buffalo Point.

79.8 (2.4) Stop at Buffalo Point for **STOP 4** (fig. 26), discussion of **FLOOD HAZARD FROM GREAT SALT LAKE**, and lunch. Antelope Island has excellent exposures of Lake Bonneville and Great Salt Lake shorelines. Because of isostatic rebound, the elevation of the Bonneville shoreline is as much as 150 feet (45 m) higher on Antelope Island than at the margins of the Bonneville basin (Doelling et al., 1988).

Retrace route to I-15.

95.6 (15.8) Turn LEFT (NORTH) onto I-15 NORTH-BOUND.

111.6 (16.0) Take EXIT 352 (PLAIN CITY-NORTH OGDEN) and turn RIGHT (EAST) on 2700 NORTH. View to the left (north) of Ben Lomond Peak. Rocks exposed on the south flank of the mountain consist of quartz monzonite gneiss of the Lower Proterozoic Farmington Canyon Complex overlain by a thrust-fault-repeated sequence of Cambrian marine strata (Critenden and Sorensen, 1985). The prominent escarpment on the alluvial fan at the base of the mountain marks the Bonneville shoreline.

112.8 (1.2) Turn RIGHT (SOUTH) on U.S. 89.

112.9 (0.1) Turn LEFT (EAST) on UTAH 235 (2550 NORTH). The road between the freeway exit and Washington Boulevard crosses landslide deposits of the prehistoric liquefaction-induced North Ogden landslide complex (Miller, 1980; Personius, 1990; Harty et al., 1993).

114.7 (1.8) Turn LEFT (NORTH) on WASHINGTON BOULEVARD.

114.8 (0.1) Turn RIGHT (EAST) on 2600 NORTH.

115.8 (1.0) Turn LEFT (NORTH) on 1050 EAST.

116.5 (0.7) Turn RIGHT (EAST) on 3100 NORTH (NORTH OGDEN CANYON ROAD).

117.1 (0.6) Debris flow in 1991 exited canyon mouth on the left (north), crossed the road, and deposited material in the residential subdivision at the base of the alluvial fan.

117.3 (0.2) Park in turn-out on the right side of the road for **STOP 5** (fig. 27) and discussion of the **CAMERON COVE DEBRIS**



Figure 27. Route of field trip showing stops 5 and 6. Base from USGS Promontory Point and Ogden 30 X 60 minute quadrangles.

FLOW. View to the west of the 1991 debris-flow deposit on the alluvial fan.

Retrace route to WASHINGTON BOULEVARD.

119.9 (2.6) Turn LEFT (SOUTH) on WASHINGTON BOULEVARD.

124.0 (4.1) Turn LEFT (EAST) on 12TH STREET.

125.2 (1.2) Continue straight at the traffic light where 12TH STREET becomes UTAH 39.

126.2 (1.0) Turn RIGHT (WEST) on VALLEY DRIVE and then LEFT (SOUTH) into the Rainbow Gardens parking lot, located in the eastern amphitheater of the Ogden River landslide complex, for **STOP 6** (fig. 27) and discussion of the **RAINBOW IMPORTS LANDSLIDE**. The landslide is on the bluff south of the parking lot.

Continue WEST on VALLEY DRIVE. Landslides within the Ogden River landslide complex are on the left (south). At the golf course, the road crosses landslide toe deposits.

- 127.3 (1.1) Cross HARRISON BOULEVARD and continue WEST on 20TH STREET. Follow signs for I-15.
- 130.7 (3.4) Turn LEFT (SOUTH) onto I-15 SOUTHBOUND and return to Salt Palace Convention Center.

REFERENCES CITED

- Adan, S.M., and Rollins, K.M., 1993, Damage potential index mapping for Salt Lake Valley, Utah: Utah Geological Survey Miscellaneous Publication 93-4, 64 p.
- Algermissen, S.T., 1988, Earthquake hazard and risk assessment—Some applications to problems of earthquake insurance, in Hays, W.W., ed., Workshop on "Earthquake Risk—Needs of the Insurance Industry": U.S. Geological Survey Open-File Report 88-669, p. 9-39.
- Algermissen, S.T., Perkins, D.M., Thenhaus, P.C., Hanson, S.L., and Bender, B.L., 1990, Probabilistic earthquake acceleration and velocity maps for the United States and Puerto Rico: U.S. Geological Survey Miscellaneous Field Studies Map MF-2120, scale 1:7,500,000.
- Anderson, L.R., Keaton, J.R., Aubrey, K., and Ellis, S.J., 1982, Liquefaction potential map for Davis County, Utah: Logan, Utah State University Department of Civil and Environmental Engineering and Dames & Moore Consulting Engineers, final technical report for the U.S. Geological Survey, 50 p. (published as Utah Geological Survey Contract Report 94-7).
- Anderson, L.R., Keaton, J.R., Spitzley, J.E., and Allen, A.C., 1986, Liquefaction potential map for Salt Lake County, Utah: Logan, Utah State University Department of Civil and Environmental Engineering and Dames & Moore Consulting Engineers, final technical report for the U.S. Geological Survey, 48 p. (published as Utah Geological Survey Contract Report 94-9).
- Arnou, T., and Stephens, D., 1990, Hydrological characteristics of the Great Salt Lake, Utah—1847-1986. U.S. Geological Survey Water-Supply Paper 2332, 32 p.
- Atwood, G., and Mabey, D.R., 1995, Flooding hazards associated with Great Salt Lake, in Lund, W.R., ed., Environmental and engineering geology of the Wasatch Front region. Utah Geological Association Publication 24, p. 483-493.
- Atwood, G., Mabey, D.R., and Lund, W.R., 1990, The Great Salt Lake—A hazardous neighbor, in Lund, W.R., ed., Engineering geology of the Salt Lake City metropolitan area, Utah: Utah Geological and Mineral Survey Bulletin 126, p. 54-58.
- Austin, L.H., 1988, Problems and management alternatives related to the rising level of Great Salt Lake, in Proceedings 6th International Water Resources Association World Congress on Water Resources: Ottawa, Canada, International Water Resources Association.
- Bailey, J.S., and Allen, E.W., 1988, Massive resistance: Civil Engineering, v. 58, no. 9, p. 52-55.
- Black, B.D., Lund, W.R., Schwartz, D.P., Gill, H.E., and Mayes, B.H., 1996, Paleoseismic investigation on the Salt Lake City segment of the Wasatch fault zone at the South Fork Dry Creek and Dry Gulch sites, Salt Lake County, Utah, in Lund, W.R., ed., Paleoseismology of Utah, Volume 7: Utah Geological Survey Special Study 92, 22 p.
- Building Seismic Safety Council, 1994, NEHRP recommended provisions for seismic regulations for new buildings: Washington, D.C., Federal Emergency Management Agency Publications 222A (Part 1—Provisions, 290 p.) and 223A (Part 2—Commentary, 335 p.).
- Butler, E., and Marsell, R.E., 1972, Cloudburst floods in Utah, 1939-69: Utah Department of Natural Resources, Division of Water Resources, Cooperative Investigations Report No. 11, 103 p.
- Crittenden, Jr., M.D., 1965a, Geology of the Sugar House quadrangle, Salt Lake County, Utah: U.S. Geological Survey Geologic Quadrangle Map GQ-380, scale 1:24,000.
- Crittenden, Jr., M.D., 1965b, Geology of the Draper quadrangle, Utah: U.S. Geological Survey Geologic Quadrangle Map GQ-377, scale 1:24,000.
- Crittenden, Jr., M.D., and Sorensen, M.L., 1985, Geologic map of the North Ogden quadrangle and part of the Ogden and Plain City quadrangles, Box Elder and Weber Counties, Utah: U.S. Geological Survey Miscellaneous Investigations Series Map I-1606, scale 1:24,000.
- Currey, D.R., 1982, Lake Bonneville—Selected features of relevance to neotectonic analysis. U.S. Geological Survey Open-File Report 82-1070, 30 p.
- Currey, D.R., 1990, Quaternary paleolakes in the evolution of semidesert basins, with special emphasis on Lake Bonneville and the Great Basin, U.S.A.: Palaeogeography, Palaeoclimatology, Palaeoecology, v. 76, p. 189-214.
- Currey, D.R., Atwood, G., and Mabey, D.R., 1984, Major levels of Great Salt Lake and Lake Bonneville: Utah Geological and Mineral Survey Map 73, scale 1:750,000.
- Currey, D.R., Berry, M.S., Douglass, G.E., Merola, J.A., Murchison, S.B., and Ridd, M.K., 1988, The highest Holocene stage of Great Salt Lake, Utah [abs.]: Geological Society of America Abstracts with Programs, v. 20, no. 6, p. 411.
- Currey, D.R., and Oviatt, C.G., 1985, Durations, average rates, and probable causes of Lake Bonneville expansions, still-stands, and contractions during the last deep-lake cycle, 32,000 to 10,000 years ago, in Kay, P.A., and Diaz, H.F., eds., Problems of and prospects for predicting Great Salt Lake levels—Proceedings of a NOAA Conference, March 26-28, 1985: Salt Lake City, University of Utah, Center for Public Affairs and Administration, p. 9-24.
- Dames & Moore, 1996, Final report, seismic hazard analysis of the I-15 corridor, 10600 South to 500 North, Salt Lake County, Utah: Seattle and Salt Lake City, unpublished consultant's report, variously paginated.
- Delta Geotechnical Consultants, 1994, Preliminary assessment, Ogden Canyon landslide, Ogden, Utah: Salt Lake City, unpublished consultant's report, 3 p.
- Doelling, H.H., Willis, G.C., Jensen, M.E., Hecker, S., Case, W.F., and Hand, J.S., 1988, Geology of Antelope Island, Davis County, Utah: Utah Geological and Mineral Survey Open-File Release 144, 82 p.
- Everitt, B., 1991, Stratigraphy of eastern Farmington Bay: Utah Geological and Mineral Survey, Survey Notes, v. 24, no. 3, p. 27-29.
- Federal Emergency Management Agency, 1985, Reducing losses in high risk flood hazard areas—A guidebook for local officials: Federal Emergency Management Agency Publication No. 116, 225 p.
- Forman, S.L., Nelson, A.R., and McCalpin, J.P., 1991, Thermoluminescence dating of fault-scarp-derived colluvium—deciphering the timing of paleoearthquakes on the Weber segment of the Wasatch fault zone, north central Utah: Journal of Geophysical Research, v. 96, no. B1, p. 595-605.
- Gilbert, G.K., 1890, Lake Bonneville: U.S. Geological Survey Monograph 1, 438 p.
- Gill, H.E., 1987, Utah Geological and Mineral Survey excavation inspection program—A tool for earthquake hazard recognition in Utah, in Gori, P.L., and Hays, W.W., eds., Assessment of regional earthquake hazards and risk along the Wasatch Front, Utah, Volume II: U.S. Geological Survey Open-File Report 87-585, p. U1-U19.

- Gurgel, K.D., ed., 1983, *Geologic excursions in neotectonics and engineering geology in Utah*, Geological Society of America Guidebook—Part IV. Utah Geological and Mineral Survey Special Studies 62, 109 p.
- Harty, K.M., Lowe, M., and Christenson, G.E., 1993, Hazard potential and paleoseismic implications of liquefaction-induced landslides along the Wasatch Front, Utah. Utah Geological Survey, unpublished Final Technical Report for the U.S. Geological Survey, 57 p.
- Hays, W.W., and King, K.W., 1984, The ground-shaking hazard along the Wasatch fault zone, Utah, in Hays, W.W., and Gori, P.L., eds., A workshop on "Evaluation of regional and urban earthquake hazards and risk in Utah". U.S. Geological Survey Open-File Report 84-763, p. 133-147.
- Horns, D., Evenstad, N., Amodt, L., Atwood, G., Black, B.D., Hylland, M., Keaton, J.R., Lund, W.R., Rollins, K., and Vandre, B., 1995, Environmental and engineering geology of the Wasatch Front region, 1995 Utah Geological Association Field Conference, September 23, 1995, road log, in Lund, W.R., ed., *Environmental and engineering geology of the Wasatch Front region*: Utah Geological Association Publication 24, p. 533-541.
- Hylland, M.D., 1996, Paleoseismic analysis of the liquefaction-induced Farmington Siding landslide complex, Wasatch Front, Utah [abs.]. Geological Society of America Abstracts with Programs, v. 28, no. 7, p. A-157.
- Hylland, M.D., and Lowe, M., 1995, Hazard potential, failure type, and timing of liquefaction-induced landsliding in the Farmington Siding landslide complex, Wasatch Front, Utah. Utah Geological Survey Open-File Report 332, 47 p.
- Hylland, M.D., and Lowe, M., in press, Characteristics, timing, and hazard potential of liquefaction-induced landsliding in the Farmington Siding landslide complex, Wasatch Front, Utah. Utah Geological Survey Special Study.
- Kaliser, B.N., 1971, *Engineering geology of the City and County Building, Salt Lake City, Utah*. Utah Geological and Mineralogical Survey Special Studies 38, 10 p.
- Kaliser, B.N., 1987, Rainbow Gardens landslide of March 9, 1987, Weber County: Utah Geological Survey, unpublished memorandum, 2 p.
- Keaton, J.R., 1988, A probabilistic model for hazards related to sedimentation processes on alluvial fans in Davis County, Utah: College Station, Texas A&M University, 441 p.
- Keaton, J.R., and Anderson, L.R., 1995, Mapping liquefaction hazards in the Wasatch Front region—Opportunities and limitations, in Lund, W.R., ed., *Environmental and engineering geology of the Wasatch Front region*. Utah Geological Association Publication 24, p. 453-468.
- Lin, A., and Wang, P., 1978, Wind tides of the Great Salt Lake. Utah Geological and Mineral Survey, Utah Geology, v. 5, no. 1, p. 17-25.
- Lowe, M., 1990, Geologic hazards and land-use planning—Background, explanation, and guidelines for development in Weber County in designated special study areas. Utah Geological and Mineral Survey Open-File Report 197, 70 p.
- Lowe, M., Black, B.D., Harty, K.M., Keaton, J.R., Mulvey, W.E., Pashley, Jr., E.F., and Williams, S.R., 1992, Geologic hazards of the Ogden area, Utah, in Wilson, J.R., ed., *Field guide to geologic excursions in Utah and adjacent areas of Nevada, Idaho, and Wyoming*: Utah Geological Survey Miscellaneous Publication 92-3, p. 231-285.
- Lowe, M., Harty, K.M., and Hylland, M.D., 1995, Geomorphology and failure history of the earthquake-induced Farmington Siding landslide complex, Davis County, Utah, in Lund, W.R., ed., *Environmental and engineering geology of the Wasatch Front region*. Utah Geological Association Publication 24, p. 205-219.
- Lowe, M., Harty, K.M., and Rasely, R.C., 1990, Reconnaissance of area burned by wild fire northeast of North Ogden and evaluation of potential sediment yield. Utah Geological and Mineral Survey, unpublished memorandum to Dennis R. Shupe, North Ogden City Administrator, 5 p.
- Lund, W.R., ed., 1990, *Engineering geology of the Salt Lake City metropolitan area*, Utah. Utah Geological and Mineral Survey (in conjunction with the Association of Engineering Geologists) Bulletin 126, 66 p.
- Lund, W.R., 1992, New information on the timing of earthquakes on the Salt Lake City segment of the Wasatch fault zone—Implications for increased earthquake hazard along the central Wasatch Front: Utah Geological Survey, Wasatch Front Forum, v. 8, no. 3, p. 12-13.
- Lund, W.R., and Schwartz, D.P., 1987, Fault behavior and earthquake recurrence at the Dry Creek site, Salt Lake City segment, Wasatch fault zone, Utah [abs.]. Geological Society of America Abstracts with Programs, v. 19, no. 5, p. 317.
- Lund, W.R., Schwartz, D.P., Mulvey, W.E., Budding, K.E., and Black, B.D., 1991, Fault behavior and earthquake recurrence on the Provo segment of the Wasatch fault zone at Mapleton, Utah County, Utah. Utah Geological and Mineral Survey Special Studies 75, 41 p.
- Mabey, D.R., 1992, Subsurface geology along the Wasatch Front, in Gori, P.L., and Hays, W.W., eds., *Assessment of regional earthquake hazards and risk along the Wasatch Front, Utah*. U.S. Geological Survey Professional Paper 1500-A-J, p. C1-C16.
- Machette, M.N., ed., 1988, *In the footsteps of G.K. Gilbert—Lake Bonneville and neotectonics of the eastern Basin and Range Province*, Geological Society of America Guidebook for Field Trip Twelve. Utah Geological and Mineral Survey Miscellaneous Publication 88-1, 120 p.
- Machette, M.N., Personius, S.F., and Nelson, A.R., 1987, Quaternary geology along the Wasatch fault zone—Segmentation, recent investigations, and preliminary conclusions, in Gori, P.L., and Hays, W.W., eds., *Assessment of regional earthquake hazards and risk along the Wasatch Front, Utah*. U.S. Geological Survey Open-File Report 87-585, p. A1-A72.
- Machette, M.N., Personius, S.F., and Nelson, A.R., 1992, Paleoseismology of the Wasatch fault zone—A summary of recent investigations, interpretations, and conclusions, in Gori, P.L., and Hays, W.W., eds., *Assessment of regional earthquake hazards and risk along the Wasatch Front, Utah*: U.S. Geological Survey Professional Paper 1500, p. A1-A71.
- Machette, M.N., Personius, S.F., Nelson, A.R., Schwartz, D.P., and Lund, W.R., 1991, The Wasatch fault zone, Utah—Segmentation and history of Holocene earthquakes. *Journal of Structural Geology*, v. 13, no. 2, p. 137-149.
- McCalpin, J., and Forman, S.L., 1994, Assessing the paleoseismic activity of the Brigham City segment, Wasatch fault zone, Utah—Site of the next major earthquake on the Wasatch Front? Utah State University and Byrd Polar Research Institute, unpublished Final Technical Report for the U.S. Geological Survey, 19 p.
- McCalpin, J.P., and Nishenko, S.P., 1996, Holocene paleoseismicity, temporal clustering, and probabilities of future large ($M > 7$) earthquakes on the Wasatch fault zone, Utah. *Journal of Geophysical Research*, v. 101, no. B3, p. 6233-6253.
- Miller, R.D., 1980, Surficial geologic map along part of the Wasatch Front, Salt Lake Valley, Utah. U.S. Geological Survey Miscellaneous Field Studies Map MF-1198, scale 1:100,000, 13 p. pamphlet.
- Miller, R.D., Olsen, H.W., Erickson, G.S., Miller, C.H., and Odum, J.K., 1981, Basic data report of selected samples collected from six test holes at five sites in the Great Salt Lake and Utah Lake valleys, Utah. U.S. Geological Survey Open-File Report 81-179, 49 p.
- Mulvey, W.E., and Lowe, M., 1991, Cameron Cove subdivision debris flow, North Ogden, Utah, in Mayes, B.H., compiler, *Technical reports for 1990-1991, Applied Geology Program*. Utah Geological Survey Report of Investigation 222, p. 186-191.
- Mulvey, W.E., and Lowe, M., 1994, 1991 Cameron Cove subdivision debris flow, North Ogden, Utah, U.S.A.. *Proceedings of the 1992 Arid West Flood Plain Managers Conference*, p. 117-123.

- Murchison, S.B., 1989, Fluctuation history of Great Salt Lake, Utah, during the last 13,000 years. Salt Lake City, University of Utah, Ph.D. thesis, 137 p.
- Nelson, A.R., and Personius, S.F., 1993, Surficial geologic map of the Weber segment, Wasatch fault zone, Weber and Davis Counties, Utah. U.S. Geological Survey Miscellaneous Investigations Series Map I-2199, 22 p. pamphlet, scale 1:50,000.
- Oaks, S.D., 1987, Effects of six damaging earthquakes in Salt Lake City, Utah, in Gori, P.L., and Hays, W.W., eds., Assessment of regional earthquake hazards and risk along the Wasatch Front, Utah, Volume II. U.S. Geological Survey Open-File Report 87-585, p. P1-P95.
- Olig, S.S., 1991, Earthquake ground shaking in Utah. Utah Geological and Mineral Survey, Survey Notes, v. 24, no. 3, p. 20-25.
- Olsen, K.B., Pechmann, J.C., and Schuster, G.T., 1995, Simulation of 3D elastic wave propagation in the Salt Lake basin: *Bulletin of the Seismological Society of America*, v. 85, no. 6, p. 1688-1710.
- Oviatt, C.G., Curry, D.R., and Sack, D., 1992, Radiocarbon chronology of Lake Bonneville, eastern Great Basin, U.S.A.: *Palaeogeography, Palaeoclimatology, Palaeoecology*, v. 99, p. 225-241.
- Pacific Southwest Inter-Agency Committee, 1968, Report on factors affecting sediment yield in the Pacific Southwest area and selection and evaluation of measures for reduction of erosion and sediment yield: Report of the Water Management Subcommittee, 10 p.
- Pashley, E.F., Jr., and Wiggins, R.A., 1972, Landslides of the northern Wasatch Front, in *Environmental geology of the Wasatch Front*, 1971: Utah Geological Association Publication 1, p. K1-K16.
- Personius, S.F., 1990, Surficial geologic map of the Brigham City segment and adjacent parts of the Weber and Collinston segments, Wasatch fault zone, Box Elder and Weber Counties, Utah. U.S. Geological Survey Miscellaneous Investigations Map I-1979, scale 1:50,000.
- Personius, S.F., and Scott, W.E., 1992, Surficial geologic map of the Salt Lake City segment and parts of adjacent segments of the Wasatch fault zone, Davis, Salt Lake, and Utah Counties, Utah. U.S. Geological Survey Miscellaneous Investigation Series Map I-2106, scale 1:50,000.
- Prudon, T.H.M., 1990, The seismic retrofit of the City & County Building in Salt Lake City—A case study of the application of base isolation to a historic building, in *The City and County Building*, Salt Lake City, Utah—Earthquake risks and the architectural landmark. Salt Lake City Corporation, Proceedings from the International Seismic Isolation/Historic Preservation Symposium, May 11-14, 1988, variously paginated.
- Ridd, M.K., and Kaliser, B.N., 1978, North Ogden sensitive area study. Salt Lake City, unpublished report to North Ogden Planning Commission, 124 p.
- Rollins, K.M., and Adan, S.M., 1994, Soil response in the Salt Lake Basin Salt Lake City, EERI Wasatch Front Seismic Risk Regional Seminar, Seminar 2—Earthquake Research and Mitigation, p. 3-1 to 3-22.
- Rollins, K.M., and Gerber, T.M., 1995, Seismic ground response at two bridge sites on soft-deep soils along Interstate 15 in the Salt Lake Valley, Utah. Provo, Brigham Young University, unpublished Interim Report for the Utah Department of Transportation, 116 p.
- Schwartz, D.P., and Coppersmith, K.J., 1984, Fault behavior and characteristic earthquakes—Examples from the Wasatch and San Andreas fault zones: *Journal of Geophysical Research*, v. 89, no. B7, p. 5681-5698.
- Schwartz, D.P., and Lund, W.R., 1988, Paleoseismicity and earthquake recurrence at Little Cottonwood Canyon, Wasatch fault zone, Utah, in Machette, M.N., ed., In the footsteps of G.K. Gilbert—Lake Bonneville and neotectonics of the eastern Basin and Range Province. Utah Geological and Mineral Survey Miscellaneous Publication 88-1, p. 82-85.
- Schwartz, D.P., Lund, W.R., Mulvey, W.E., and Budding, K.E., 1988, New paleoseismicity data and implications for space-time clustering of large earthquakes on the Wasatch fault zone, Utah [abs.]. *Seismological Research Letters*, v. 59, no. 1, p. 15.
- Scott, W.E., 1981, Field-trip guide to the Quaternary stratigraphy and faulting in the area north of the mouth of Big Cottonwood Canyon, Salt Lake County, Utah. U.S. Geological Survey Open-File Report 81-773, 12 p.
- Scott, W.E., and Shroba, R.R., 1985, Surficial geologic map of an area along the Wasatch fault zone in the Salt Lake Valley, Utah. U.S. Geological Survey Open-File Report 85-448, scale 1:24,000.
- SHB AGRA, 1994, Report, geotechnical evaluation, effect of proposed demolition of residences at 1846 and 1850 East and 1950 South Street on stability of active landslide in the Ogden River landslide complex, Ogden, Utah: Salt Lake City, unpublished consultant's report, 8 p.
- Smith, R.B., and Arabasz, W.J., 1991, Seismicity of the Intermountain seismic belt, in Slemmons, D.B., Engdahl, I.R., Zoback, M.L., and Blackwell, D.D., eds., *Neotectonics of North America: Geological Society of America Decade Map Volume 1*, p. 185-228.
- Smith, R.B., and Sbar, M.L., 1974, Contemporary tectonics and seismicity of the western United States with emphasis on the Intermountain seismic belt. *Bulletin of the Geological Society of America*, v. 85, p. 1205-1218.
- Steffen, C.C., 1986, Economic impact of flooding on the Great Salt Lake. Speech presented to the Natural Resources Law Forum, J. Reuben Clark Law School, Brigham Young University, Provo, Utah, October 3, 1986, 14 p.
- Swan, F.H., III, Hanson, K.L., Schwartz, D.P., and Black, J.H., 1981, Study of earthquake recurrence intervals on the Wasatch fault at the Little Cottonwood Canyon site, Utah. U.S. Geological Survey Open-File Report 81-450, 30 p.
- Tinsley, J.C., King, K.W., Trumm, D.A., Carver, D.L., and Williams, Robert, 1991, Geologic aspects of shear-wave velocity and relative ground response in Salt Lake Valley, Utah, in McCalpin, J.P., ed., *Proceedings of the 27th Symposium on Engineering Geology and Geotechnical Engineering*. Logan, Utah State University, p. 25-1 to 25-9.
- Utah Division of Water Resources, 1984, Great Salt Lake—Summary of technical investigations for water level control alterations. Utah Department of Natural Resources unpublished report, variously paginated.
- Utah Geological Association, 1971, *Environmental Geology of the Wasatch Front*, 1971. Utah Geological Association Publication 1, variously paginated.
- Van Horn, Richard, 1972, Surficial geologic map of the Sugar House quadrangle, Salt Lake County, Utah. U.S. Geological Survey Miscellaneous Geologic Investigations Map I-766-A, scale 1:24,000.
- Van Horn, R., 1975, Largest known landslide of its type in the United States—A failure by lateral spreading in Davis County, Utah. *Utah Geology*, v. 2, no. 1, p. 83-87.
- Vandre, B.C., and Lowe, M., 1995, The Rainbow Imports landslide—A window for looking at landslide mechanisms within the Ogden River landslide complex, Weber County, Utah, in Lund, W.R., ed., *Environmental and engineering geology of the Wasatch Front region*: Utah Geological Association Publication 24, p. 137-156.
- Weber County Planning Commission, 1988, *Geologic hazards and land-use planning—Background, explanation, and guidelines for development in designated geologic hazards special study areas as required in Weber County ordinances*. Ogden, unpublished Weber County Planning Commission report and maps, 69 p., scale 1:24,000.
- Wieczorek, G.F., Ellen, S., Lips, E.W., Cannon, S.H., and Short, D.N., 1983, Potential for debris flow and debris flood along the Wasatch Front between Salt Lake City and Willard, Utah, and measures for their mitigation: U.S. Geological Survey Open-File Report 83-635, 45 p.
- Wieczorek, G.F., Lips, E.W., and Ellen, S.D., 1989, Debris flows and hyper-concentrated floods along the Wasatch Front, Utah, 1983 and 1984: *Bulletin of the Association of Engineering Geologists*, v. 26, no. 2, p. 191-208.

- Wong, I., Olig, S., Green, R., Moriwaki, Y., Abrahamson, N., Baures, D., Silva, W., Somerville, P., Davidson, D., Pilz, J., and Dunne, B., 1995, Seismic hazard evaluation of the Magna tailings impoundment, *in* Lund, W.R., ed., Environmental and engineering geology of the Wasatch Front region: Utah Geological Association Publication 24, p. 95–110
- Wong, I.G., and Silva, W.J., 1993, Site-specific strong ground motion estimates for Salt Lake Valley, Utah: Utah Geological Survey Miscellaneous Publication 93-9, 34 p.
- Woolley, R.R., 1946, Cloudburst floods in Utah, 1850–1938. U.S. Geological Survey Water-Supply Paper 994, 128 p.
- Yonkee, W.A., and Lowe, M., in preparation, Geologic map of the Ogden quadrangle, Utah. Utah Geological Survey Map, scale 1:24,000.
- Youngs, R.R., Swan, F.H., Power, M.S., Schwartz, D.P., and Green, R.K., 1987, Probabilistic analysis of earthquake ground shaking hazard along the Wasatch Front, Utah, *in* Gori, P.L., and Hays, W.W., eds., Assessment of regional earthquake hazards and risk along the Wasatch Front, Utah, Volume II. U.S. Geological Survey Open-File Report 87-585, p. M1–M110.
- Zoback, M.L., 1983, Structure and Cenozoic tectonism along the Wasatch fault zone, Utah, *in* Miller, D.M., Todd, V.R., and Howard, K.A., eds., Tectonic and stratigraphic studies in the eastern Great Basin: Geological Society of America Memoir 157, p. 3–28

Bedrock Geology of Snyderville Basin: Structural Geology Techniques Applied to Understanding the Hydrogeology of a Rapidly Developing Region, Summit County, Utah

KELLY E. KEIGHLEY

Geology Department., Utah State University, Logan, Utah 84322-4505

W. ADOLPH YONKEE

Department of Geosciences, Weber State University, Ogden, Utah 84408

FRANK X. ASHLAND

Utah Geological Survey, Salt Lake City, Utah 84114-6100

JAMES P. EVANS

Department of Geology, Utah State University, Logan, Utah 84322-4505

ABSTRACT

The availability of ground water is a problem for many communities throughout the west. As these communities continue to experience growth, the initial allocation of ground water supplies proves inadequate and may force restrictions on existing, and future, development plans. Much of this new growth relies on ground water supplies extracted from fractured bedrock aquifers. An example of a community faced with this problem is western Summit County, near Park City, Utah. This area has experienced significant water shortages coupled with a 50% growth rate in the past 10–15 years. Recent housing development rests directly on complexly deformed Triassic to Jurassic sedimentary rocks in the hanging wall of the Mount Raymond-Absaroka thrust system. The primary fractured bedrock aquifers are the Nugget Sandstone, and limestones in the Thaynes and Twin Creek Formations. Ground water production and management strategies can be improved if the geometry of the structures and the flow properties of the fractured and folded bedrock can be established. We characterize the structures that may influence ground water flow at two sites: the Pinebrook and Summit Park subdivisions, which demonstrate abrupt changes (less than 1 mi/1.6 km) within the hydrogeologic systems. Geologic mapping at scales of 1:4500 (Pinebrook) and 1:9600 (Summit Park), scanline fracture mapping at the outcrop scale, geologic cross sections, water well data, and structural analysis, provides a clearer picture of the hydrogeologic setting of the aquifers in this region, and has been used to successfully site wells. In the Pinebrook area, the dominate map-scale structures of the area is the Twomile Canyon anticline, a faulted box-like to conical anticline. Widely variable bedding orientations suggest that the fold is segmented and is non-cylindrical and conical on the western limb with a fold axis that plunges to the northwest and also to the southeast, and forms a box-type fold between the middle and eastern limbs with a fold axis that plunges to the northeast. The fold is cut by several faults including the Toll Canyon fault, which we interpret as a west-directed folded hanging-wall splay off the east-directed Mt. Raymond thrust. These complex geometries may be due to at least two phases of deformation. Results from outcrop analyses show that the fractured bedrock aquifers are lithologically heterogeneous, anisotropic, and compartmentalized. Two exposures of the Toll Canyon fault show that even though the fault cores may be thin, extensive damage zones develop in the Nugget Sandstone and Thaynes Limestone, and shale smears form in the Triassic shales. The damaged zones may be regions of enhanced fracture permeability, whereas the shale smears act as flow barriers. The orientation, density, and hydrogeologic characteristics for predominate fracture sets vary within meters.

In the Summit Park area, chronic water shortages required new wells to be sited in the northeast-plunging Summit Park anticline. The anticline experienced two phases of folding and at least one episode of faulting. Structural analysis of the fold defined the geometry of the structure, and a down plunge projection along the fold hinge was used to estimate the location of the Nugget Sandstone at a depth of 700 ft (213 m). The crestal region of the anticline was drilled in order to intercept regions of higher fracture density in the fold. The test well penetrated the Nugget Sandstone at 698 ft depth, and two production wells with long-term yields of 120 and 180 gpm completed. One well in the Sliderock Member (Twin Creek Formation) experiences seasonal fluctuations whereas production in the Nugget sandstone has only subdued seasonal variations, suggesting the Nugget may have great storage.

Complex structures work against the typical basin yield approach for water budgets, therefore, water supply estimates may benefit from detailed studies within local areas. The results of this study demonstrate how traditional structural analysis may be used as an integral component of ground water resource evaluation and management in regions developed on deformed sedimentary bedrock aquifers.

INTRODUCTION

Growth in the Park City area of western Summit County, Utah (fig. 1), has exceeded 5% per year during the past five years (fig. 2). This rate is expected to continue since Park City will host several events for the 2002 Winter Olympics, and as the area expands to a year-round "bedrock bedroom" community only 32 km/20 mi from Salt Lake City. The majority of this growth lies within the Snyderville basin, a physiographic basin bounded on the west, north, and south sides by high ridges of the Wasatch Range, and on the east by low hills underlain by Tertiary Keetley volcanic rocks. Two principle drainages, Silver Creek and East Canyon-Kimball Creek, flow from south to north and ultimately drain into the Weber River (fig. 1). Ground water flow occurs through complexly folded and fractured bedrock and discontinuous, thin unconsolidated valley-fill deposits, with most new development relying heavily on the fractured bedrock aquifers for municipal water supplies (Ashland et al., 1996).

The increased water supply demands associated with dramatic growth necessitated a basin-wide hydrogeologic study (Ashland et al., 1996) which identifies the likely key hydrostratigraphic units and their future water resource potential. That report was part of a comprehensive evaluation of the ground water resources of the area conducted by the Utah Geological Survey and U.S. Geological Survey, Water Resource Division, for the Utah Division of Water Rights and local water developers.

This field trip presents the results of integrating structural geologic analysis with hydrogeology in a small region, and provides examples of how this integration assists management and development of local ground water resources from fractured bedrock aquifers. Two development sites within the Snyderville basin will be discussed: the Pinebrook and Summit Park subdivisions (fig. 1). These sites depend on water supplies from fractured Mesozoic sedi-

mentary bedrock aquifers (Ashland et al., 1996). Even though the Pinebrook and Summit Park subdivisions are within 1 mile (1.6 km) of each other, the aquifer characteristics and consequent well yields between them are highly variable. The Summit Park area, which consists of approximately 200 single-family homes, experienced water shortages in the 1980s and further development there is limited by available water. At present, the Pinebrook area transfers water shares to Summit Park and consists of at least 700 single family homes, and 300 multiple family dwellings, and a small community services area (Dan Schofield, Gorgoza Water Co., pers.comm., 1996).

Based on a regional analysis of Snyderville basin, Ashland et al., (1996) suggest that at least 16 discrete structural and stratigraphic ground water compartments exist that may influence local water well production and the prediction of sustainable yields. This interpretation supports the need for detailed geologic studies within the proposed compartments to assess future ground water resources in this region.

In this trip, we will provide a regional overview of the physiography, geology, and development history of the area, and we will then visit localities which provide examples of the geometry of the folds, faults, and fractures which influence ground water flow.

GEOLOGIC SETTING

Stratigraphy

Figure 3 summarizes the stratigraphy of the Snyderville basin and the units within Summit Park and Pinebrook. Rocks exposed in the study area include the Triassic Thaynes and Ankareh Formations, the Jurassic Nugget Sandstone, the Jurassic Twin Creek Limestone, and minor amounts of Quaternary alluvium. Knowledge of stratigraphy is vital in recognizing the distribution of productive versus non-productive (confining) units within the hydrogeologic system.

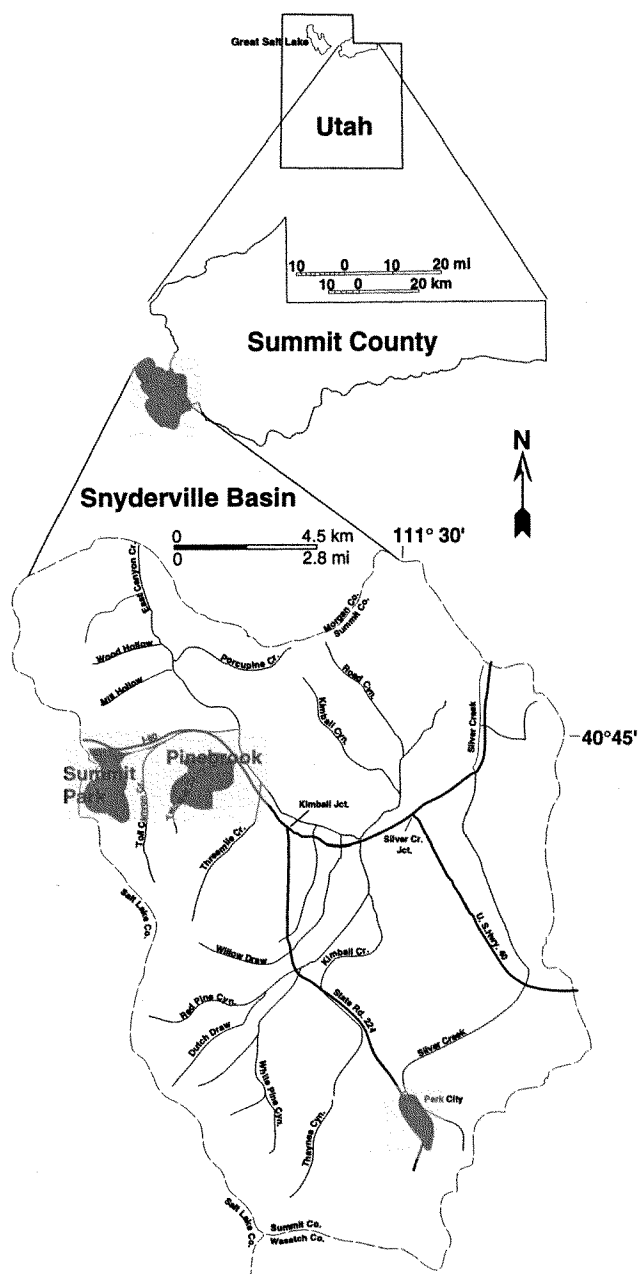


Figure 1. Geographic location map of the Snyderville hydrologic basin, and the Pinebrook and Summit Park subdivisions in western Summit County, Utah (modified from Ashland et al., 1996, and the USGS Salt Lake City 30 x 60 minute quadrangle).

The Thaynes Formation (Tt) is comprised of thin- to thick-bedded, greenish-brown to brown, light-gray, pale-red, and ocher, fine-grained, limy sandstone and siltstone interbedded with olive green to dull-red shale and thick bedded, light gray, fine grained, fossiliferous limestone (Crittenden et al., 1966; Bromfield and Crittenden, 1971). Boutwell (1912) and Barnes and Simos (1968) described a

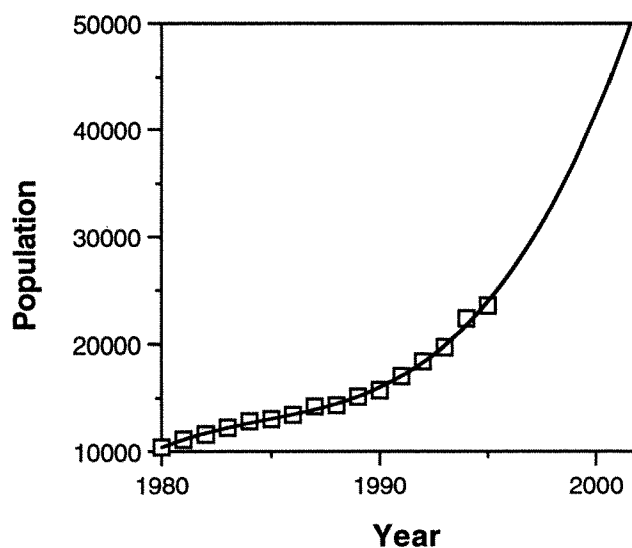


Figure 2. Population of Summit County. Growth at the current rates would result in a five-fold increase in population between 1980 and 2002. Source of data through 1995: Department of Planning and Analysis, 1997.

Mid-Red Shale unit that separates the Thaynes into upper and lower members of nearly equal thickness. The Thaynes Formation in this area is between 335 to 475 m (1,100 and 1,500 ft) thick (Bromfield, 1968).

The Ankareh Formation consists of the lower Mahogany Member (T_{am}), the middle Gartra Grit Member (T_{ag}), and the upper member (T_{au}). The Mahogany Member consists of approximately 305 m (1000 ft) of reddish-brown and pinkish-brown, locally ripple-laminated to finely-laminated, fine-grained sandstone and siltstone, purplish mudstone, and a few thin limestone beds. The Gartra Grit Member is composed of white, pinkish-white, and pale-purple massive, cross-bedded, coarse-grained to pebbly, strongly silica cemented sandstone grading to a deep maroon to dark purple, coarse-grained to pebbly, poorly cemented sandstone near the uppermost contact. Thickness ranges for this formation are between 75 to 200 feet in the Pinebrook subdivision study area. The upper member includes moderate-red, grayish-red, and grayish-purple mudstone and fine-grained sandstone and is gradational with the underlying Gartra Grit Member. This unit is very poorly exposed within the study area and approximate thicknesses range between 69 to 275 m (225 to 900 ft) (Bromfield, 1968; Bromfield and Crittenden, 1971).

The Jurassic rocks consist of the Nugget Sandstone (Jn) and the Twin Creek Limestone (Jtc). The Nugget Sandstone is a salmon colored, fine- to medium-grained, medium to thick bedded, internally finely cross-bedded sandstone. The Nugget Sandstone is about 244 m (800 ft) thick in the



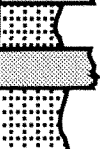
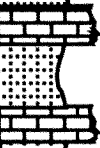

Age	Formation		Thickness m (feet)	Graphic log	Hydrostratigraphy		
Jurassic	Twin Creek Limestone	Giraffe Creek Mbr.	853 (2800)		<div>SGWC</div> <div>confining beds</div> <div>SGWC</div> <div>confining beds</div> <div>SGWC</div> <div>confining beds</div>		
		Leeds Creek Mbr.					
		Watton Canyon Mbr.					
		Boundary Ridge Mbr.					
		Rich Mbr.					
		Sliderock Mbr.					
		Gypsum Springs Mbr.					
Triassic	Nugget Sandstone		396 (1300)		SGWC		
	Ankareh Fm.	upper Mbr.	213 (700)		confining beds		
		Gartra Grit Mbr.	30 (100)		SGWC		
		Mahogany Mbr.	274 (900)		confining beds		
	Thaynes Fm.		~ 580 (1900)		SGWC		
	Woodside Shale		122 (400)		confining beds		

Figure 3. Stratigraphy and hydrostratigraphy of the Pinebrook and Summit Park subdivisions, Summit County, Utah (modified from Hintze (1988) and Ashland (1996)).

Park City area, and approximately 475 m (1,500 ft) thick in the Summit Park and Pinebrook areas (Jarvis and Yonkee, unpublished report, 1993).

The Twin Creek Limestone contains seven members: the Gypsum Spring, Sliderock, Rich, Boundary Ridge, Watton Canyon, Leeds Creek, and Giraffe Creek. The basal Gypsum Spring Member is a gypsiferous, red to reddish-brown clayey siltstone and silty claystone containing local blocks of gray to pink limestone. The upper members of the Twin Creek Limestone in the Snyderville basin area are primarily olive-drab-weathering, gray, oolitic, finely crystalline, and clayey to silty (micritic) limestone. The Twin Creek is about 792 m (2,600 ft) in the Summit Park study area (Crittenden et al., 1966; Hintze, 1988; Imlay, 1967; Jarvis and Yonkee, unpublished report, 1993).

Ashland et al., (1996) established a preliminary hydrostratigraphy of the layered rock units in the study area (fig. 3). They propose that stratigraphic ground water compartments (SGWCs) consisting of fractured limestone and sandstone are separated by confining shaly beds which may have local hydraulic conductivities approaching those of unfractured rock. This separation of permeable fractured

rock units by poorly permeable confining beds is evidence of stratigraphic compartmentalization.

Important aquifers (SGWCs) in the study region include the two limestone units of the Thaynes Formation, the Nugget Sandstone, the Rich and Leeds Creek Members of the Twin Creek Limestone, and potentially the Gartra Grit Member of the Ankareh Formation (Ashland et al., 1996). The confining beds or units that likely inhibit ground water flow include the Mid Red shale unit of the Thaynes Formation, the lower part of the Mahogany Member and the upper member of the Ankareh Formation, and the Gypsum Spring and Boundary Ridge Members of the Twin Creek Formation.

Structure

Crittenden et al., (1966) mapped the Summit Park and Pinebrook areas which are also included in the 1:100,000 scale map of Bryant (1990). The dominant structure in this region is the northeast striking Mount Raymond thrust (fig. 4), which carries Pennsylvanian through Cretaceous rocks in its hanging wall (Crittenden et al., 1966; Bryant, 1990).

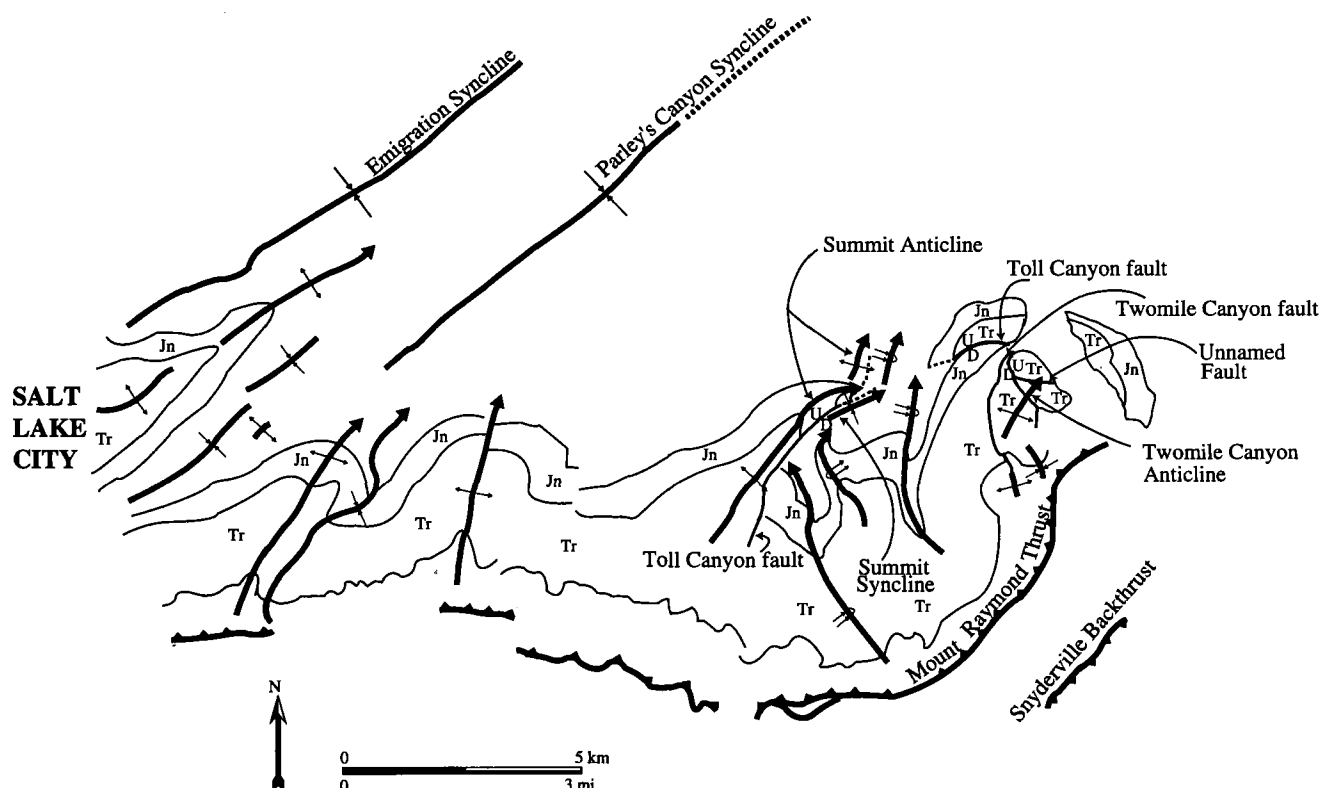


Figure 4. Regional fold train in Triassic (Tr = Thaynes and Ankareh Formations) and Jurassic (Jn = Nugget Sandstone) rocks in hanging-wall of Mount Raymond thrust (modified from Bryant, 1990; Ashland et al., 1996; Jarvis and Yonkee, 1993; Crittenden, et al., 1996). Macroscopic faults and folds present within study areas are noted.

The traditional interpretation of the thrust is that the sinuous trace, interpreted on the basis of a small thrust in the Snyderville basin, reflects folding of the thrust plane (Crittenden, 1974; Crittenden et al., 1966; Bradley and Bruhn, 1988; Bryant, 1990; Yonkee et al., 1992). In contrast, Lamerson (1982) and recent mapping for Mobil Oil by McBride (pers. comm., 1996), suggests the thrust has a relatively straight strike across the area, eliminating the need for post-thrust folding. The Mount Raymond thrust plane dips gently north (fig. 5), and appears to be a smoothly undulating surface that records northward tilting but little or no folding of the thrust plane.

Rocks in the hanging wall of the MRT are cut by a series of imbricate thrusts and folded within a fold train that extends for 20 km (13 mi) west of Park City (fig. 4; Bryant, 1990). The folds trend northeast to northwest, plunge between 5° to 72°, and are expressed in Triassic and Jurassic rocks with open to close box-like geometries. First-phase folds (referred to as F1) consist of a series of smaller-scale anticlines and synclines with generally north to northeast plunging fold axes, including the Summit Park anticline, the Toll Canyon syncline, and the Twomile Anticline examined here. These folds developed above detachments with-

in Pennsylvanian to Triassic strata, are locally associated with moderate to high angle reverse faults, and formed during an early phase of shortening. An early spaced cleavage (referred to as S1), defined by spaced seams of clay-rich material, is widely developed within the Twin Creek Formation. S1 is subparallel to F1 fold axes and strongly fanned about F1 folds, indicating that cleavage formed during initial shortening. Second-phase folds (referred to as F2) consist of larger-scale anticlines and synclines with gently east-northeast plunging fold axes, including the Parley's Canyon syncline and adjacent Spring Creek anticline and Emigration Canyon syncline. A weakly developed second cleavage (referred to as S2) formed during F2 folding. F2 folds may correlate with a series of folds exposed further north that formed during large-scale slip on the Crawford thrust (Yonkee and others, this volume) development of the Uinta-Cottonwood arch, or during Medicine Butte, and Absaroka thrust systems.

The structures of interest on this trip are the informally named, Summit Park anticline and syncline, the Toll Canyon syncline, the Twomile Canyon anticline, and the Toll Canyon and Twomile Canyon faults (fig. 4). We believe that understanding the aquifer and confining layer geometries

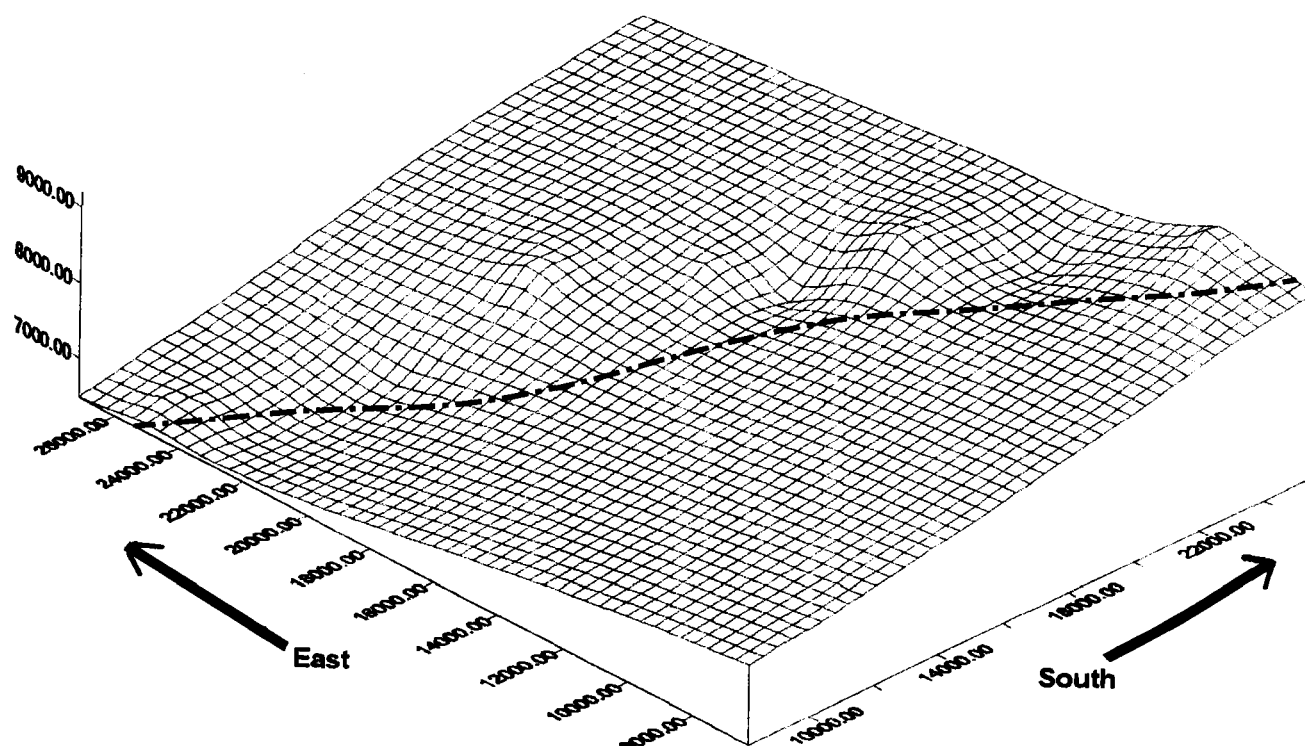


Figure 5. View to the southeast of the best-fit surface (in grids) of the Mt. Raymond thrust. Surface is a minimum curvature surface calculated from digitized points along the thrust trace (dashed line) using SURFER software. Gentle north dip of a smooth surface is suggested by the data. Coordinates are in feet from a datum on the Park City West quadrangle. Vertical scale is in feet above sea level.

are important for ground water resource management and development in this region.

Data Collection and Methods

Geologic mapping and structural analysis at a scale of 1:4500 were completed over an approximately 6 km² (2.25 mi²) area to characterize the geometry of the Twomile Canyon anticline and macroscopic faults within the Pinebrook subdivision. Fracture systems in the sedimentary bedrock were characterized by using a modified version of the scan-line technique (LaPointe and Hudson, 1985). Geologic mapping and cross-sections at a scale of 1:9600 were completed as part of a well siting and well head protection plan for the Summit Park subdivision conducted by Weston Engineering in 1994–95.

ROAD LOG

elapsed total
mileage mileage

0	0.0	Start trip from Salt Palace.
0.3	0.3	(approx) Travel south from the Salt Palace
	(approx)	until a left (east) turn can be made. Down-
		town construction alters this.

0.3	0.6	Turn right (south) onto State Street. Travel south to I-80.
3.2	3.8	Turn left (east) onto I-80 east bound.
1.4	5.2	Cross approximate trace of western splay of WFZ which has Holocene fault scarps. The East Bench fault forms prominent scarps along the 9th–11th East area in Salt Lake City (Personius and Scott, 1993). View to southeast of central part of the Wasatch Range. The steep slope of Mount Olympus consists of Tintic Quartzite in the footwall of the Mount Raymond thrust. Precambrian Big Cottonwood Formation and basement rock of the Little Willow Series core the Cottonwood arch to the south. Oligocene granite and quartz monzonite intrusions locally cut the crest of the arch.
2.2	7.4	Junction with Interstate 215. Continue west on I-80.
0.6	8.0	Cross approximate trace of eastern splay of WFZ along base of mountains.
1.1	9.1	Fractured and faulted sandstone beds of

		Nugget Sandstone are exposed in road cut. A locally faulted contact between Nug- get Sandstone and Sliderock and Gyp- sum Spring Members of the Twin Creek Limestone is exposed to the northeast. Heading northeast on I-80 we will be cutting obliquely across the SSE limb and hinge zone of the Parleys Canyon syncline, a major ENE trending F2 fold, and also across a series of smaller scale, N- to NE-trending F1 folds developed in Triassic to Jurassic strata above de- tachments in Permo-Pennsylvanian strata (fig. 4).	2.4	18.3	out further north toward the hinge of the Parleys Canyon syncline. Parleys Summit. Red siltstone and sand- stone beds of Preuss Formation dip NNW in road cuts. This information also con- tains salt-bearing intervals, and appears to have formed an important regional decollement during Cretaceous thrusting (Yonkee et al., this volume).
			0.9	18.2	Road cut in micrite beds of Twin Creek Formation. Summit Park is to southwest.
			2.3	20.5	Pass exit to Jeremy Ranch. Sandstone beds of Nugget Formation exposed in the quarry to the west lie within the northwest limb of the hanging-wall ramp anticline which is discussed in stops 1 and 4.
0.6	9.7	Argillaceous, fine-grained limestone of the Rich Member of the Twin Creek Lime- stone is exposed in roadcuts, and is de- formed by spaced cleavage, multiple vein arrays, and minor faults. An early, strong- ly developed, N- to NE-striking, steeply dipping cleavage is associated with F1 minor folds and early layer-parallel short- ening. A later, weakly developed, ENE- striking, gently dipping cleavage is asso- ciated with the Parleys Canyon syncline (see Yonkee et al., this volume, for details).	1.0	21.5	Junction with Utah Highway 224 from Park City. Exit I-80. Turn right (south) on Highway 224. Travel 1 block to traffic light, turn right.
			0.1	21.6	Turn right at the traffic light. Travel 1 block, and turn right onto the frontage road. Proceed north along the frontage road.
			1.0	22.6	Hi-Ute Ranch on left. The hills north across the freeway are underlain by northeast dipping Triassic and Jurassic rocks in the hanging wall of the Mount Raymond thrust.
0.7	10.4	Overpass. Complex folds are developed in the Watton Canyon Member of the Twin Creek Limestone, and spaced cleav- age is strongly fanned about the folds.	1.0	23.6	Junction with Pinebrook Drive—Entrance to Pinebrook Development. Turn left.
1.6	12.0	Ranch exit. Argillaceous to silty limestone beds are cut by minor fault zones in road cut to northwest. Cores of minor faults contain scaly, clay-rich material that may form impermeable barriers to ground water flow.	0.35	24.0	Turn right.
			0.1	24.1	Turn left. Proceed along Pinebrook Road.
			1.6	25.7	Sharp bend in street. Veer left (south).
			0.35	30.0	Hair pin bend in street. Veer north.
			0.4	30.4	Road bends west. Stop 1.
2.0	14.0	Mountain Dell exit. The ENE-plunging Spring Canyon anticline is exposed to the NNW (Crittenden, 1965). The anticline is cored by faulted Triassic rocks, and may continue northeast into the frontal anti- cline of the Crawford thrust sheet. Conglomerate beds exposed to the north along East Canyon may display progres- sive unconformities above the underlying tighter Parleys Canyon syncline and Spring Canyon anticline, recording most- ly Late Cretaceous development of F2 folds (Mullens, 1971).			
1.9	15.9	Lambs Canyon exit. NNW-dipping sand- stone and conglomerate beds of the Cre- taceous Kelvin and Frontier Formation crop			

Stop 1. Pinebrook Overview

The Pinebrook subdivision (figs. 1 and 6) is an excellent example of the extensive "bedrock community" development that is occurring within western Summit County and the Park City area. Pinebrook includes the southeast half of section 10 south through the east half of section 15, to the southern half of section 11 and south through section 14, T.1.S. R.3.E., Park City West 7.5 min quad.), bounded on the west by Summit Park and Timberline subdivisions and by I-80 to the north. The development boundaries are also Pinebrook's water rights boundaries. Pinebrook is intriguing because its wells are more productive than those in surrounding communities, it contains abundant high-quality bedrock exposures, and the structures are poorly understood.

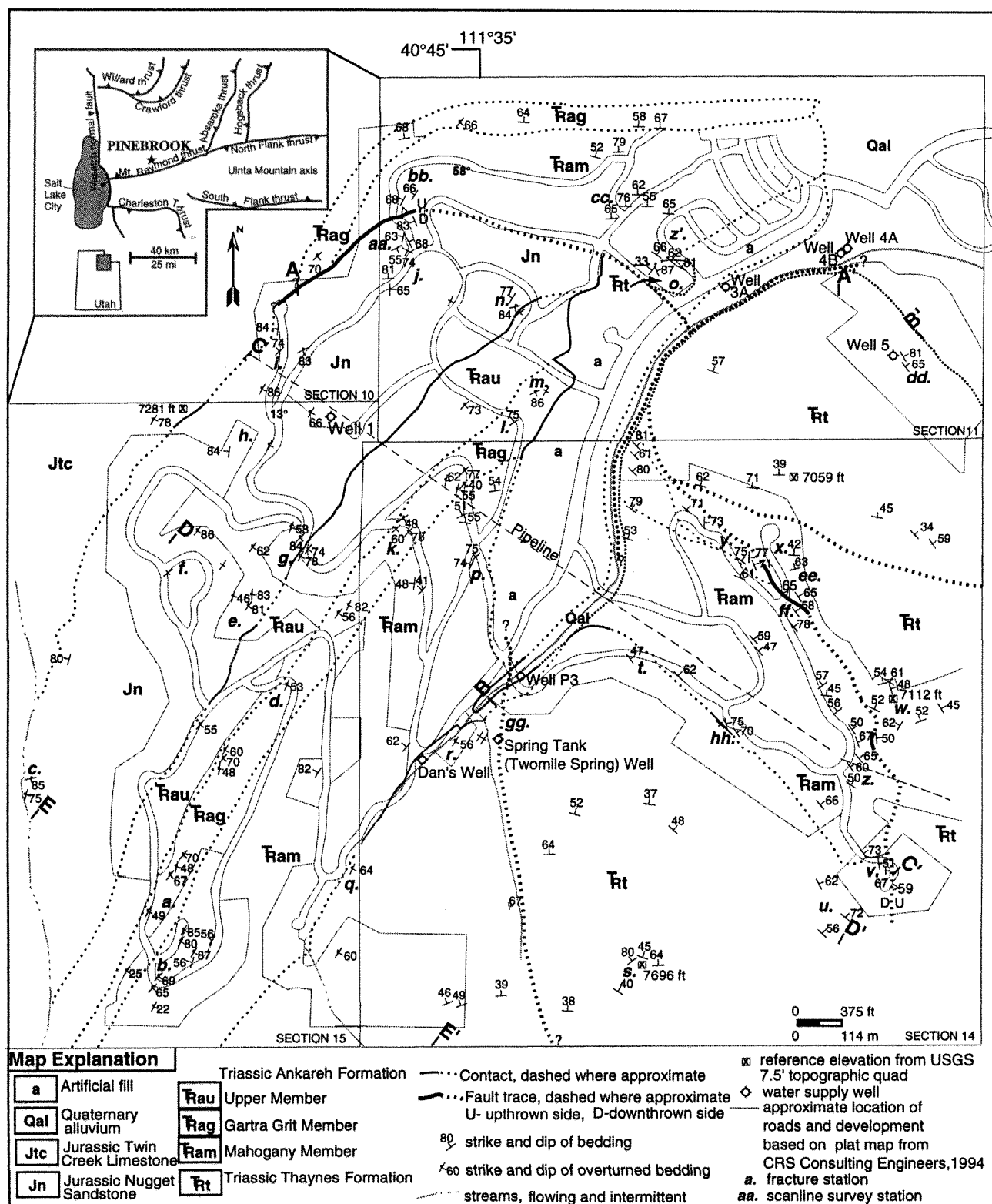


Figure 6. Location, regional geologic setting, geologic map and development of the Pinebrook subdivision area in western Summit County, near Park City, Utah. Field mapping was completed in sections 10, 11, 14, 15; T1S, R3E using the USGS Park City West quadrangle.

Table 1. Summary of Hydrogeology for Pinebrook Wells
(CRS Consulting Engineer's Inc., 1995; Gorgoza Mutual Water Company, oral comm., 1997)

Well # / Name	Formation Penetrated (see Figure 6)	Well Depth (feet)	Well Yield (gpm)	Description
1	Nugget Sandstone	710	40–175	Seasonal production fluctuations common
3A	Thaynes Formation	305	150–200	High turbidity, low usage; 7/97 yield @ 80 gpm
4A	Thaynes Formation	500	300	85 feet of alluvium; 7/97 yield @ 240 gpm
4B	Thaynes Formation	1200	1000	Thaynes at 535 feet; artesian flow March–June
5	Thaynes Formation	500	—	Not in use 7/97
6	Thaynes Formation	1100	300	Deepened from 800 ft (6/96)
Spring Tank (Twomile Spring)	Thaynes Formation	—	60–240	Natural spring; 7/97 yield @ 195 gpm
Dan's Well	Thaynes Formation	750	125–200	Seasonal production fluctuations common

This setting provides an excellent opportunity to use structural analysis at various scales to understand the subsurface structure and its relation to the hydrogeologic system.

Structural and Hydrogeological Setting

Fractured bedrock units include the Triassic Thaynes and Ankareh Formations and the Jurassic Nugget Sandstone (fig. 3). The Thaynes Formation and Nugget Sandstone provide Pinebrook with its' water supply (refer to Table 1 for well information and fig. 6 for well locations). Average production rates for wells in these aquifers range from 40–1000 gpm, with higher average yields associated with increased annual precipitation (Gorgoza Mutual Water Co., oral comm., 1996). These formations lie within a hanging wall ramp-anticline, referred to as the Twomile Canyon anticline (figs 4 and 6) after Ashland et al., (1996), of the Mount Raymond thrust (MRT). The nearest exposure of the MRT occurs approximately 3 km (1.9 mi) southeast of Pinebrook (fig. 4). This fold train consists of a series of gen-

erally north-northeast plunging folds that most likely developed with movement and/or re-activation on the MRT and/or related backthrusting. A second phase of east-northeast trending folds (F2) appears to have rotated some of the F1 folds, locally up to 40°–60°. Elsewhere, northwest plunging folds may have folded northeast plunging folds. Possible causes of the F2 folds include: (1) reactivation along the MRT or younger thrust systems, (2) slip on a lateral ramp, or (3) rotation related to uplift of the Uinta arch (Bradley and Bruhn, 1988; Bruhn et al., 1986; Bryant, 1990; Yonkee et al., 1992).

The other major structures in Pinebrook subdivision include high-angle faults (fig. 6) : (1) the Toll Canyon fault; (2) the Twomile Canyon fault, and (3) a previously unmapped fault, a possible splay from the Toll Canyon, in the northern section of the study area. The presence of these faults and the superposed folding within the study area complicate the interpretations of the structural and hydrogeological setting.

Regional hydrogeologic studies suggest that the aquifers in this area may be structurally (e.g. faults) and stratigraphically (e.g. Mid Red shale unit in the Thaynes Formation) compartmentalized (Ashland et al., 1996). Additional aquifer-test data will be needed to delineate and confirm the hydrogeologic compartments associated with the proposed geology for the Pinebrook and Summit Park subdivisions.

Structural Analysis

Structural analysis in the Pinebrook subdivision (fig. 7) are: (1) bedding attitudes are very scattered and do not conform to a single great-circle (interpret as a non-cylindrical fold if formed by one deformational event or evidence for refolding about a non-parallel fold axis); (2) cylindrical best-fit tests to the bed data generate an overall fold axis orientation of $55^{\circ}/038^{\circ}$ for the Twomile Canyon anticline (fig. 7a); and (3) a Kamb contour plot (fig. 7b) delineates four dip domains (Ia-steep to overturned SE dips; Ib-steep to overturned NW and SE dips; IIa-moderate to steep NE dips; and IIb-moderate-steep N-NE dips). The preferred fold geometry interpretation for these data is Interpretation A shown in figs 7c–e. Interpretation A suggests a partly non-cylindrical, northwest to southeast plunging conical fold (figs 7c. And 7d.) in the western portion of the study area that rotates into a cylindrical, north plunging box-like fold to the east (fig. 7e.). Another, less complex, fold geometry is Interpretation B shown in figs 7f–h. This interpretation assumes cylindrical folding and suggests a gently to moderately plunging, segmented box-like fold with three distinct axial surfaces: a. $282^{\circ}/14^{\circ}$ NW, b. $339^{\circ}/75^{\circ}$ NE, and c. $196^{\circ}/82^{\circ}$ NW.

The distribution of the predominate fracture trends present throughout the study area are shown in rose diagrams in fig. 8. These plots demonstrate the variation in fracture orientations within very short distances, as indicated by comparing the plots at each station with the station locations shown in fig. 6. The plots may be useful in determining flow directions throughout the Twomile Canyon anticline.

Turn vehicles around. Return down Pinebrook Road.

0.4	30.8	Hair pin in street.
0.35	31.1	Junction at hair pin. Veer right.
0.1	31.2	Dirt road to Spring Tank. Park here and walk to stop.

Stop 2. Spring Tank Outcrop

This site is situated at the Spring Tank (Twomile Spring) well shown in fig. 6. The Twomile Canyon fault, a north-striking, east-dipping to vertical reverse fault that cuts the

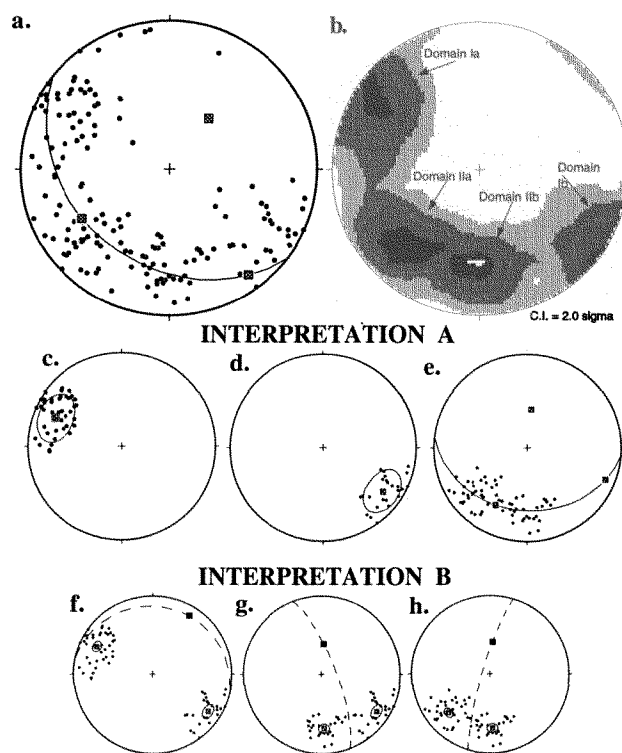


Figure 7. Fold analysis plots of bedding data in the Pinebrook subdivision, Summit County, Utah. a. Cylindrical fit to bedding plane poles generates a fold axis trend and plunge of $038^{\circ}/55^{\circ}$. b. Dip domains determined from Kamb contour of bedding plane poles and map relationships shown in fig. 6. Interpretation A: c. Conical fit to overturned western limb (Dip Domain Ia) generates a fold axis of $298^{\circ}/23^{\circ}$, half-apical angle of 18° ; d. Conical fit to northwest dipping to vertical, non-overturned limb (Dip Domain Ib) generates a fold axis of $126^{\circ}/21^{\circ}$, half-apical angle of 17° ; e. Cylindrical fit to north-dipping and north-east dipping limbs (Domains IIa and IIb) generates a fold axis of $005^{\circ}/56^{\circ}$. Interpretation B: f. Cylindrical fit to Domains Ia and Ib generates a fold axis of $032^{\circ}/13^{\circ}$; g. Cylindrical fit to Domains Ib and IIb generates a fold axis of $004^{\circ}/58^{\circ}$; h. Cylindrical fit to Domains IIa and IIb generates the same fold axis shown in e.

Thaynes Formation near the crest of the anticline, is inferred to pass just to the east of this site. The Twomile Spring well at this location, and Dan's well to the southwest, penetrate the Thaynes aquifer with yields between 125–300 gpm (Table 1). Spring discharge hydrographs and well logs suggest that ground water flow at this location is controlled by interconnected fractures (CRS Consulting Engineers, Inc., 1995).

The Thaynes Formation consists of interbedded limestones and shales, strikes northeast, and is nearly vertical at this location (figs 9a. and 9b). Fracture data was collected along vertical and horizontal scanlines through beds of

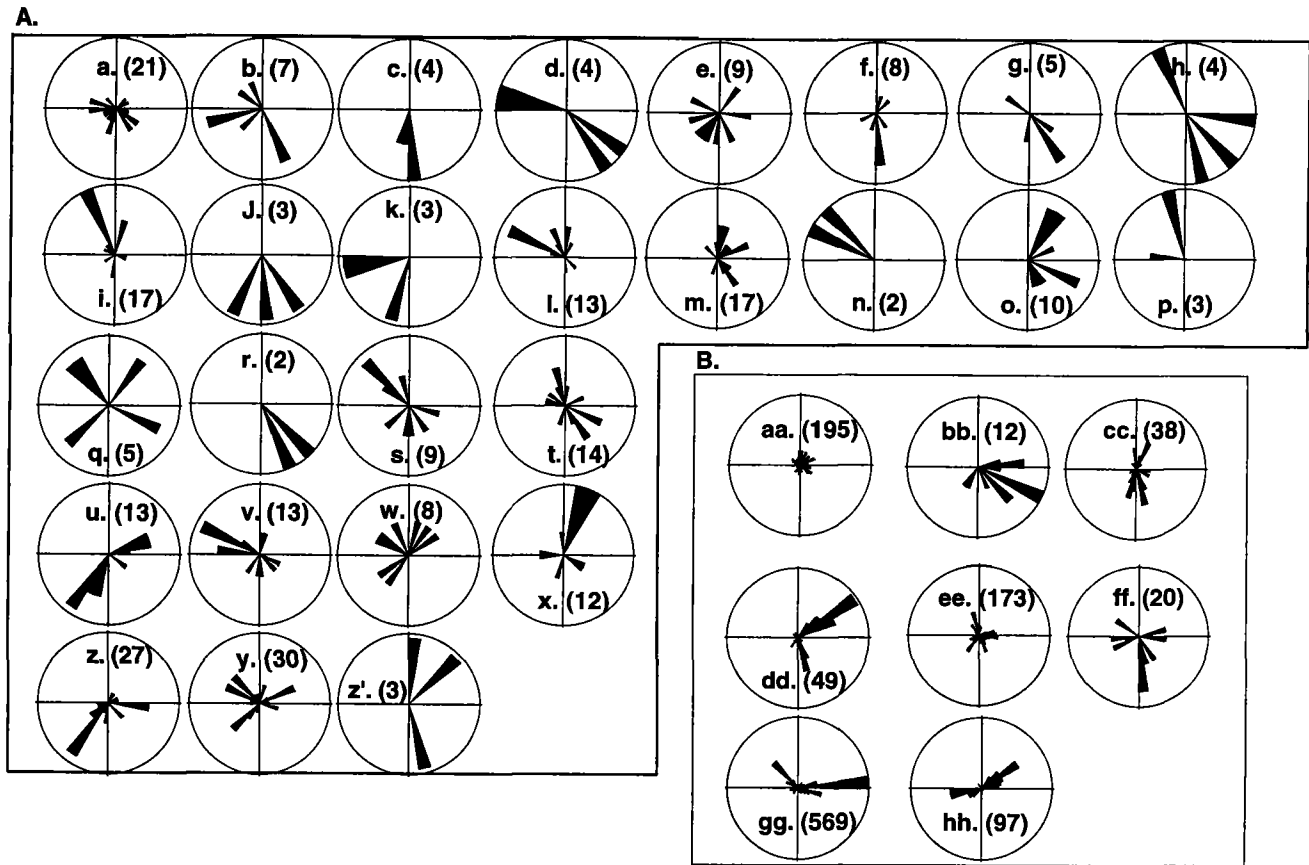


Figure 8. Equal area rose diagrams showing relative frequency of fracture trends for each of the stations located in fig. 6. Circle perimeters range between 25–50%. A. Major fracture sets observed at qualitative sampling stations. B. Results from detailed sampling methods using fracture scanline survey techniques at indicated stations.

varying thicknesses. The predominate fracture sets for thick, medium, and thin beds are highlighted in fig. 9a. Four main fracture sets and the fracture sets with small amounts of offset are observed on the stereonet plots (figs 9d., 9e., 9c.). Results from this analysis of the scanline data supports the sets determined qualitatively using the photograph in fig 9a. For each fracture set, the spacing increases with bed thickness, with the most common sets, the south-east-dipping joints (J2) and joints parallel to bedding (J1) present throughout the outcrop in the thick, medium, and thin beds.

0.4	31.6	Intersection with Big Spruce Way. Turn right.
0.3	31.9	Intersection with Tall Oaks Drive. Turn left.
0.3	32.2	Note complexly deformed Triassic Ankareh beds on left side of road.
0.2	32.4	Intersection with Tall Oaks Circle. Turn left and park. Stop 3.

Stop 3. Tall Oaks Circle—The Ecker Hill Fault

The Ecker Hill fault juxtaposes the Thaynes Formation and Mahogany Member of the Ankareh Formation. This fault may connect or splay off of the Toll Canyon fault in the western portion of the subdivision. The fault surface is undulatory with an average orientation of 305°/65° NE. Figure 10 is a geological map of the site plan view and structural geology of this site. A damage zone of intense fracturing extends for at least 3.5 m (11.5 ft) north of the fault into the Thaynes Formation, with 0.25 to 0.50 m (0.8 to 1.6 ft) of clay gouge adjacent to the fault core. The damage zone on the south side of the fault is represented by a 1 m (3 ft) thick clay smear in the lower Ankareh Formation (fig. 11). Filled veins, open fractures, and small faults extend for several meters north of the fault core and immediate damage zone in the Thaynes Formation. Based on these observations and the high clay content of the fault core, the fault may act as a combined conduit-barrier system as described by Caine et al., (1996). Ground water flow may be minimal

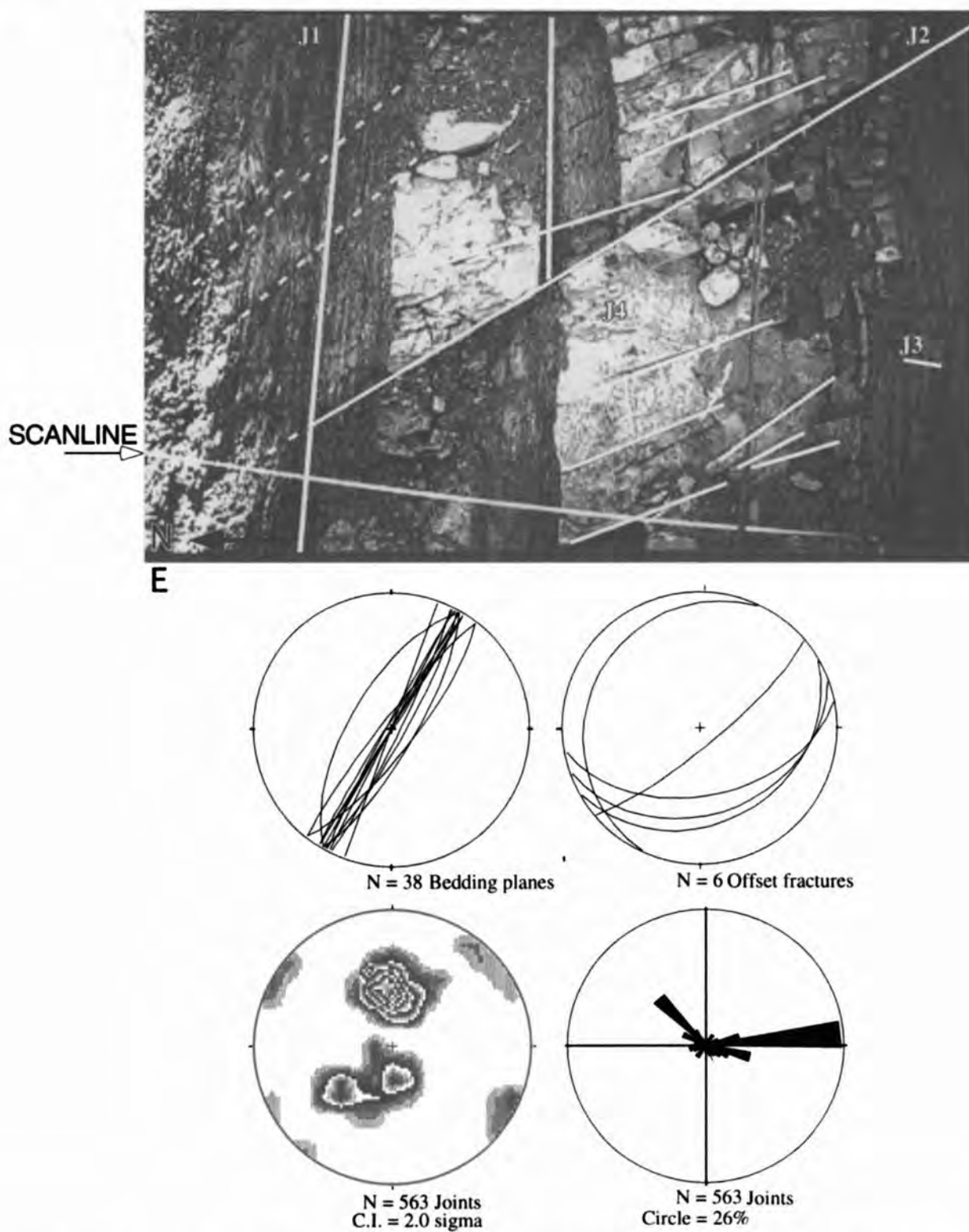


Figure 9. Structural analysis of the Spring Tank outcrop (station gg, in fig. 6). a. Major fracture sets are: i.) J1— $020^{\circ}-030^{\circ}/80^{\circ}-90^{\circ}$ SE; ii.) J2— $0.65^{\circ}-90^{\circ}/18^{\circ}-40^{\circ}$; iii.) J3— $105^{\circ}/33^{\circ}$ SW; iv.) J4— $315^{\circ}/35^{\circ}-45^{\circ}$. Scanline results: b. Average bedding at this outcrop is $030^{\circ}/90^{\circ}$. c. Orientation of fractures with offset; d. Poles to joint planes measured at scanlines; and e. Rose diagram of joint strike data further illustrates the dominant fracture sets at this location.

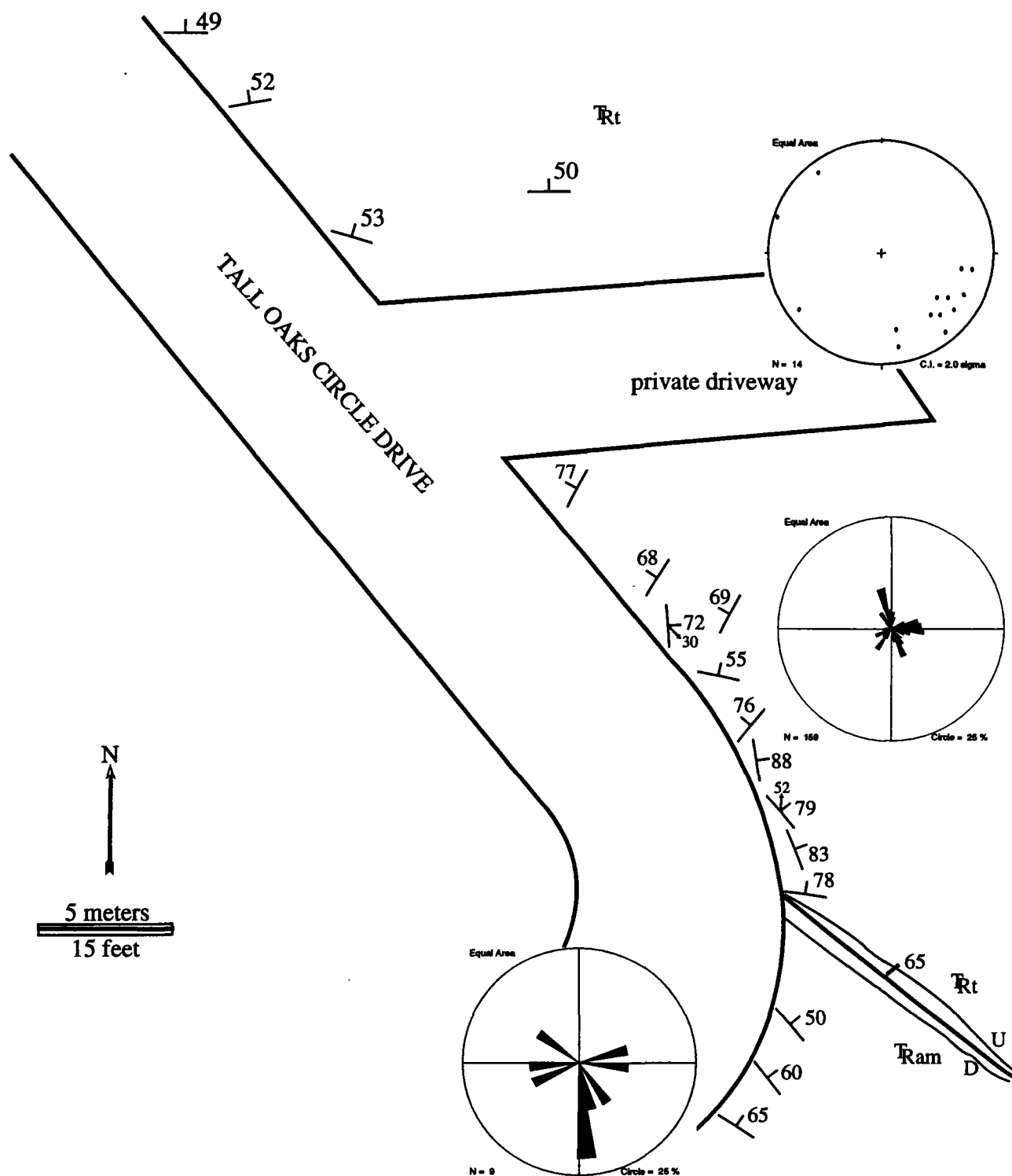


Figure 10. Map view of Tall Oaks Circle outcrop. Orientations of joints are plotted with Rose diagrams south of the fault within the Triassic Mahogany Member of the Ankareh Formation (T_{Ram}), and north of the fault in the Thaynes Formation (T_{Rt}). Poles to small planes in the Thaynes Formation are also shown. The main fault is the Toll Canyon fault (or related splay) outlined with the relative thicknesses of the gouge zones on either side of the fault.

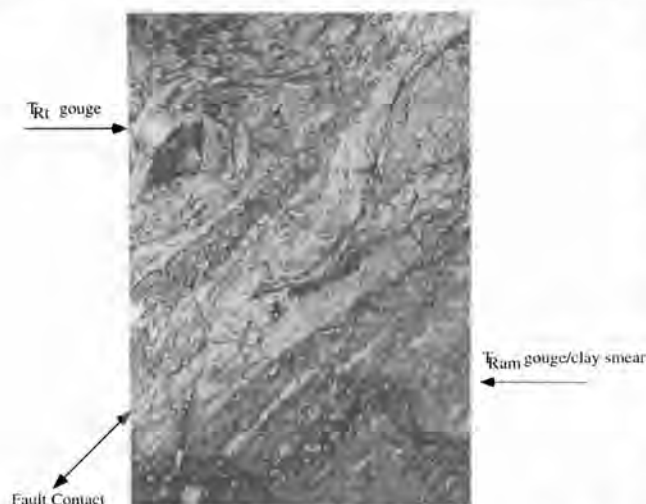


Figure 11. Gouge present at fault contact between the Thaynes Formation and Mahogany member, lower Ankareh Formation. Gouge zones in the Thaynes and Ankareh Formations are approximately 0.25 to 0.50 m (0.75–1.5 ft) and up to 1 m (3 ft) thick, respectively. Extent and pervasive fracturing within the damage zone coupled with the high clay content near the fault core suggest the Toll Canyon fault at this location acts as a conduit-barrier system (after Caine et al., 1996).

perpendicular to the fault within the immediate fault core and damage zone, but may increase to the north of the fault into the heavily fractured limestone beds. Flow to the south of the fault would most likely be parallel to bedding but the abundance of clay-fill within the fractures in the shaly unit would tend to impede flow.

Return to Pinebrook Road. (Note: An optional trip is to continue south to the end of Tall Oaks Drive, for overview of Winter Park Sports Park, Snyderville Basin, and Park City region.)

- | | | |
|------|------|--|
| 0.5 | 32.9 | Intersection with Big Spruce Way. Turn right. |
| 0.3 | 33.2 | Intersection with Pinebrook Drive. Turn right. |
| 0.3 | 33.5 | Turn left on Ecker Hill Drive. |
| 0.35 | 33.9 | Turn right on Stage Coach Drive. |
| 0.2 | 34.1 | Sunridge Drive intersection. Turn right and park for Stop 4. |

Stop 4. Nugget Sandstone at Sunridge-Toll Canyon fault

Pervasive fracturing and faulting of the Nugget Sandstone in the footwall of the Toll Canyon fault occurs at this location. The Toll Canyon fault contact was uncovered briefly during excavation of lot sr-43. The fault is inferred to

extend from this lot southwest through the gully north of sr-1, and to the east represented in fig. 6 by the approximate contact between the Nugget Sandstone and the Mahogany member of the Ankareh Formation. A damage zone at lot sr-1 characterized by pervasive fracturing and faulting of the Nugget Sandstone extends for at least 50 m (164 ft) to the south of the concealed Toll Canyon fault contact (fig. 13). Scanline data were collected at sr-43 and sr-1, but not at the fault contact because it was buried before detailed work was completed. The fault cores present throughout outcrops sr-43 and sr-1 are composed of brecciated sandstone and clay gouge, but are very thin 2–4 cm (0.8 to 1.6 in) average (fig. 14). Because of the nature of the damage zone, we suggest the Nugget Sandstone has enhanced permeability in this region and corresponds to a distributed conduit system as described by Caine et al., (1996). Other observations that suggest the Nugget Sandstone and the Toll Canyon fault form conduits at this location include: (1) during spring runoff flowing water occurs parallel, with seepage perpendicular, to the small faults at outcrops sr-1, sr-42, and sr-43; (2) pooling water was present into early summer at the sr-43 basement excavation; (3) builders have had to install pumps to divert water at the Sunridge lots identified on the map in fig. 12.

- | | | |
|------|------|--|
| 0.7 | 34.8 | Proceed on Sunridge Drive. The Ridge to the north is underlain by the Gartra Grit. Turn right on Gambel Drive. |
| 0.1 | 34.9 | Intersection with Boothill Drive. Turn right. |
| 0.1 | 35.0 | Intersection with Wagon Wheel Drive. Turn right. |
| 0.2 | 35.2 | Intersection with Pinebrook Road. Turn left. Return to Frontage Road. |
| 0.9 | 36.1 | Frontage Road. Turn left (northwest). |
| 2.4 | 38.5 | Exit from I-80. Begin to enter Summit Park Subdivision. Continue straight. |
| 0.4 | 38.9 | Road bends sharply south (left) |
| 0.2 | 39.1 | Road intersection. Turn sharply left. Continue on this road. |
| 0.75 | 39.9 | Road widens at outcrop of Jurassic Twin Creek Formation. Park here for Stop 5. |

Stop 5. Summit Park

Development in the Summit Park area, combined with large seasonal fluctuations in water production from existing wells, had led to water shortages in this area during the 1980s and early 1990s. Because of the need for more water, a test well siting program was initiated in 1993, and two final production wells were completed in 1996. Successful siting and completion of the wells illustrates the impor-

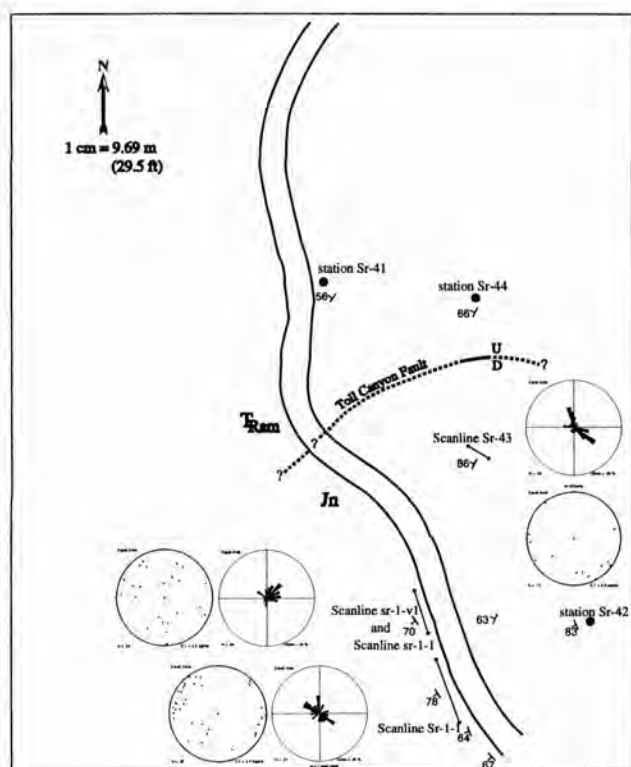


Figure 12. Sunridge outcrop site map. Rose diagram plots represent joint strikes and stereograms display poles to fault planes for data collected along each scanline.

tance of incorporating expertise from a variety of areas, including structural geology and hydrogeology. Pre-existing wells in this area had been completed in the complexly deformed Jurassic Twin Creek Limestone, but had only produced moderate amounts of water. Fractured sandstone of the underlying Jurassic Nugget Sandstone was selected as a likely target for a test well, but because of the complex structure and varying lithologies present in the area, detailed mapping and structural analysis were first undertaken. Here we discuss lithological and structural characteristics used to site the test well and briefly summarize completion of the production wells.

The main rock intervals of interest in the Summit Park area are the Nugget Sandstone and Twin Creek Limestone (figs. 3 and 15). The Nugget Sandstone consists of well sorted, variably cemented sandstone cut by widely to closely spaced fractures. Permeability is variable, being highest in areas of more intense fracturing and lowest in areas with silica cementation. The Twin Creek Limestone is divided into lithologically distinct members that have important controls on ground water flow. The basal Gypsum Spring Member consists mostly of mudstone and forms a ground-water compartment barrier with very low permeability per-



Figure 13. Photo of a portion of the Sunridge sr-1 outcrop showing location of scanline sr-2; a. represents location of fault core photo in figure 15.

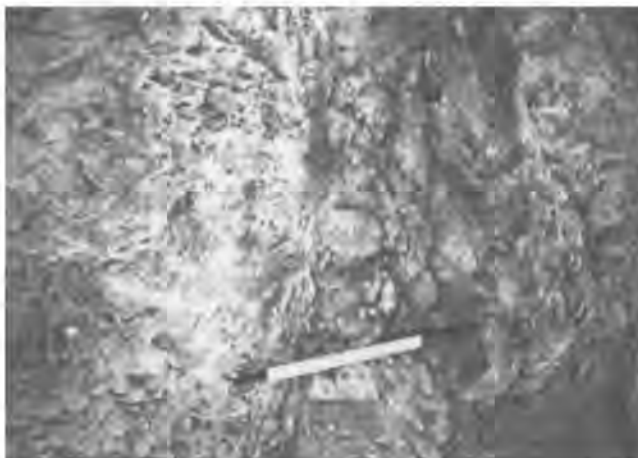
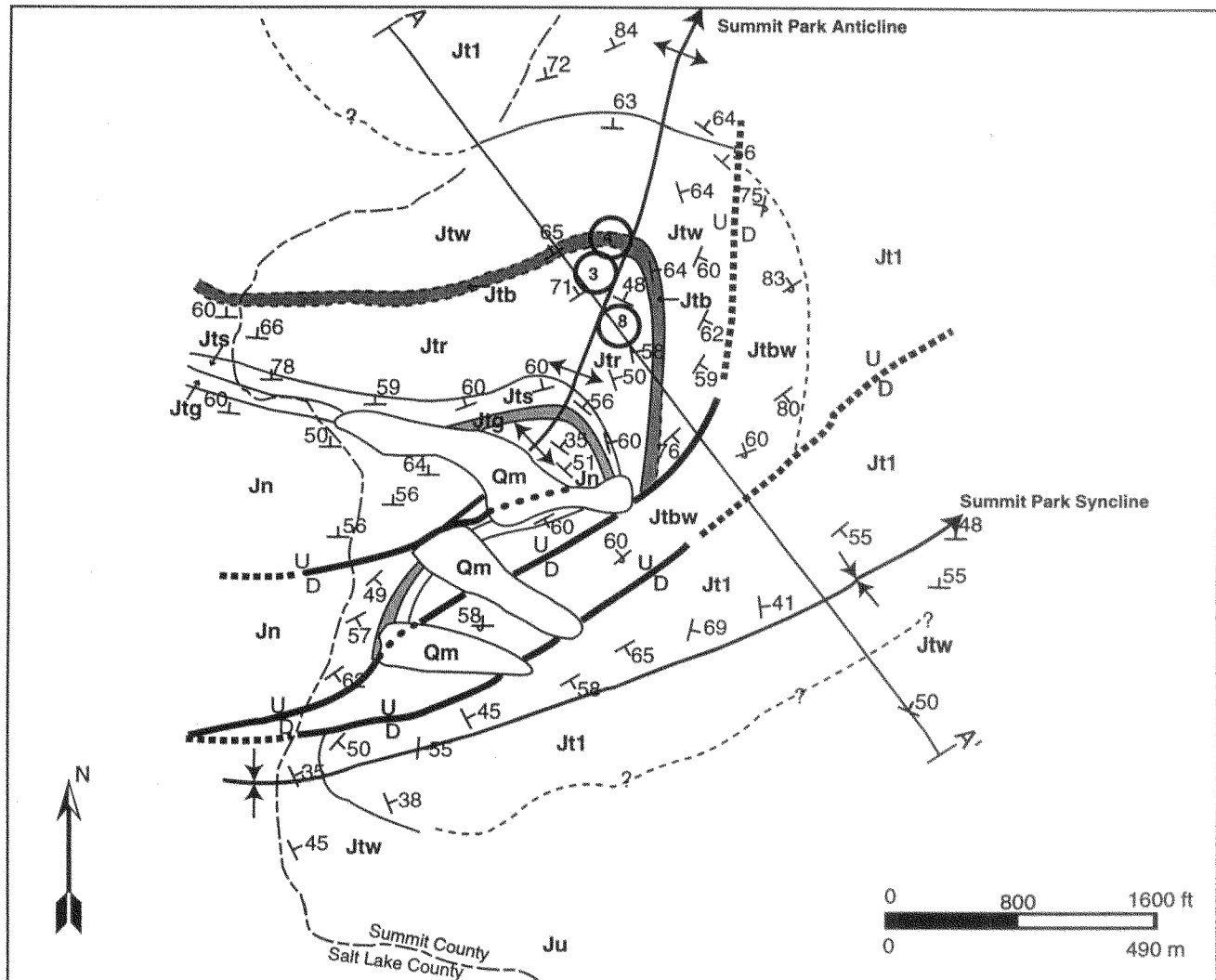


Figure 14. Fault at 6.32 meters along scan sr-1-2. Fault core composed of 2 centimeters of foliated clay with intense iron-oxide weathering. Damage zone extends from 5.9 meters to 6.55 meters. This fault is approximately 50 meters to the southeast from inferred Toll Canyon fault contact. The percentage of damage zone relative to fault core is high, suggesting a distributed conduit system as defined by Caine et al., (1996).

pendicular to bedding (Ashland et al., 1996). The overlying Sliderock Member consists mostly of thick-bedded, bioclastic to oolitic limestone that is moderately to strongly fractured, and probably has variably high permeability. The Rich Member consists of clayey to silty, fine-grained limestone that displays well developed spaced cleavage at high angles to bedding. Secondary fractures along cleavage seams are generally small and probably mostly closed at depth, suggesting overall low permeabilities. The Boundary Ridge Member includes thin-bedded silty limestone and mudstone that probably have very low permeabilities perpendicular to bedding and form another ground-water com-



Stratigraphy, Map, and Cross section Explanation

Quaternary	Qm	Qm - mass wasting and other deposits
	Jtu	Twin Creek Limestone undivided
Jurassic	Jt1	Leeds Creek Member
	Jtw	Watton Canyon Member
	Jtb	Boundary Ridge and Watton Canyon Members
	Jtr	Boundary Ridge Member
	Jts	Sliderock Member
	Jtg	Gypsum Spring Member
Triassic	Jn	Nugget Sandstone
	Tra	Ankareh Formation (on cross section only)

---	Contact, dashed where approximate dotted where concealed
U D	Fault trace, dashed where approximate dotted where concealed
↔	Axial trace of anticline, plunge of hinge indicated, location approximate
↕	Axial trace of syncline, plunge of hinge indicated, location approximate
45	Strike and dip of bedding
70	Strike and dip of overturned bedding
⚡	Area of complex deformation

Figure 15. Location, geologic map, and explanation of the Summit Park subdivision, western Summit County, Utah. Refer to fig. 16 for structures shown in cross-section A-A'.

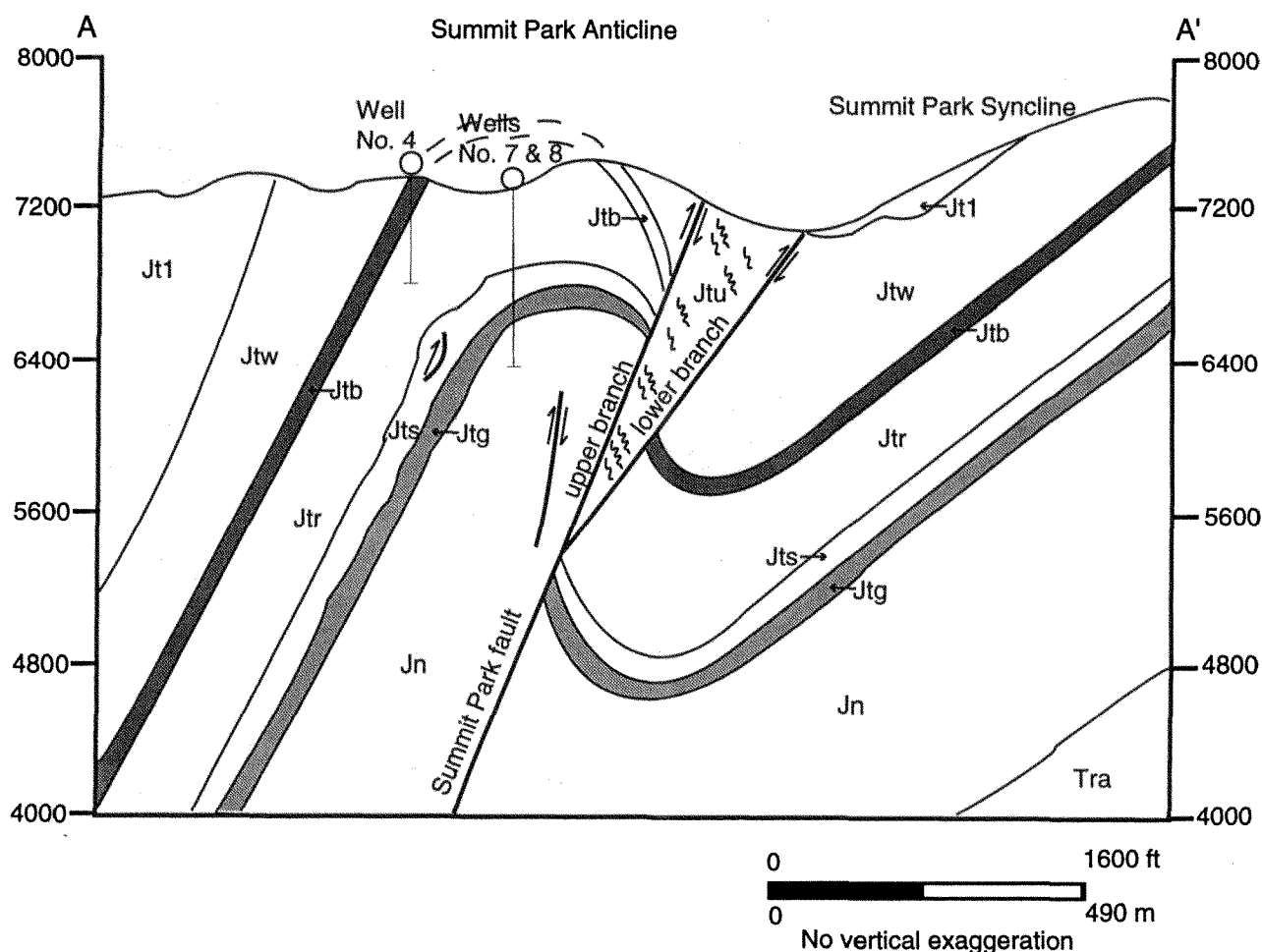


Figure 16. Geologic cross section A-A' through the Summit Park area.

partment barrier (Ashland et al., 1996). The Watton Canyon Member consists mostly of dense limestone cut by moderately to widely spaced, thicker cleavage seams. Longer, wider secondary fractures along these seams may be partly open at depth and some fractures may have undergone dissolution widening, resulting in overall moderate to high permeabilities. The Leeds Creek Member consists mostly of clayey to silty, fine-grained limestone that displays variably developed spaced cleavage and pencil fracturing, but most fractures are small and probably closed at depth resulting in overall low permeability.

The Summit Park area lies within complexly deformed rocks affected by F1 and F2 phases of folding and at least one phase of faulting (Crittenden and others, 1966; Bradley and Bruhn, 1988; Bryant, 1990; Yonkee and others, 1992; Jarvis and Yonkee, 1993; fig. 4). The dominant structural feature in the area is the Summit Park anticline. The anticline has a moderately southeast-dipping southeastern limb, a moderately north- to northwest-dipping northwestern limb,

and a complex hinge region that changes geometry with structural level (figs. 15 and 16). Within the Nugget Sandstone the two limbs are separated by a high angle fault along a sharp hinge; within the lower Twin Creek Limestone the fold is box-like with a central, planar hinge region; and in the upper Twin Creek Limestone a broad, rounded hinge region is marked by disharmonic minor folding and faulting. The fold is overall northeast plunging, but is non-cylindrical, being partly conical and also having a curvilinear hinge line. The anticline is bounded on the southeast by the Summit Park fault zone, which includes two branches that bound a complexly deformed, steeply southeast-dipping to overturned panel of rocks. The lower fault branch bounds the northwestern limb of the Summit syncline and dips steeply northwest. The upper fault branch bounds the southeastern limb of the anticline and curves slightly, probably reflecting a steeply dipping fault that changes strike and diverges upward from the lower branch. Although exact slip directions on the fault branches are unknown, both

faults probably have a significant component of top-to-the-southeast reverse slip. Geometric and spatial relations between the fault branches and anticline are consistent with a general model of fault propagation folding. A variety of small-scale deformation features are also present in the anticline hinge region. The Nugget Sandstone is cut by widely to closely spaced fractures, the Sliderock Member is locally faulted and thickened by minor folding, and the Rich Member displays vein arrays and well developed spaced cleavage at high angles to bedding.

Jarvis and Yonkee (1993) completed a report incorporating mapping and structural analysis, and proposed a test well site in the hinge region of the Summit Park anticline (figs. 15 and 16). This site was chosen based on access and estimated depths to fractured strata of the Nugget Sandstone in the subsurface. The Nugget Sandstone, as well as the Sliderock and Gypsum Spring Members, are exposed south of the test well site, and using the mapped location of the Nugget contact and an average apparent dip of 55° NE along the fold hinge, the estimated depth to the top of the Nugget was about 210 m (700 ft) at the proposed test well site. However, this estimate was somewhat problematical due to possible variations in bedding orientations from non-cylindrical folding and complex internal thickening in the hinge region.

The test well was drilled from 1994 to 1995 under the supervision of Weston Engineering. The well started in the Rich Member, drilled through fractured, permeable limestone of the Sliderock Member and impermeable mudstone of the Gypsum Spring Member, and encountered the top of the Nugget Sandstone at 698 feet (212 m). Initial pump tests indicated adequate water quality and quantity from both the Sliderock Member and Nugget Sandstone. Two final production wells were then drilled from 1995 to 1996 under the supervision of Weston Engineering, with well 7 cased through the Twin Creek Limestone and completed in the Nugget Sandstone and well 8 completed in the Sliderock Member (Weston Engineering, 1996). Pump tests indicated that well 7 could sustain a long-term yield of 180 gpm and well 8 could sustain a long-term yield of 120 gpm, and that pumping of each well did not produce drawdown in the adjacent well or in other nearby wells, probably indicating that the Nugget and Sliderock aquifers are separate and confined. Well 7 had a static water level of about 26 ft (8 m) below ground level that showed subdued seasonal fluctuations, whereas well 8 had a static water level between about 100 and 150 ft (30 and 45 m) below ground level that varied with seasonal variations in infiltration of rain and snowfall. These relations may reflect rapid recharge and low storage within fractured limestone of the Sliderock aquifer, versus greater storage within the Nugget aquifer, which has variable grain-scale porosity in addition to fractures.

The well locations were selected along the crest of the plunging Summit anticline partly because of the likelihood of finding through-going, high-angle extensional fractures in such a structural setting (Huntoon, 1993), and the occurrence of water yielding zones in the Nugget Sandstone and Sliderock Member appears to confirm the presence of such fractures. The setting of the wells also appears to confirm observations by Stone (1967) and Bruce (1988) that mudstone beds act as confining layers even where folded. Although the integrity of the Gypsum Spring Member as a confining interval appears to be preserved in this area, Bruce (1988) also indicated that regionally this member was locally broken during detachment faulting.

Turn vehicles around. Retrace route to I-80 on ramp.

0.75	40.6	Turn right at intersection
0.2	40.8	Turn right at bend.
0.4	41.2	Intersection with I-80 on ramp. Turn left. Take I-80 west bound to Salt Lake City.

End of trip.

REFERENCES CITED

- Ashland, F.X., Bishop, C E, Lowe, M., and Mayes, B.H., 1996. The Geology of the Snyderville Basin and its relation to groundwater conditions: Utah Geological Survey Open-File Report 337, 124 p.
- Barnes, M.P., and Simos, J.G., 1968, Ore deposits of the Park City district with a contribution on the Mayflower lode, in Rudge, J.D., editor, Ore deposits of the United States, 1933-1967. New York, American Institute of Mining, Metallurgical and Petroleum Engineers, p. 1102-1126.
- Boutwell, J.M., 1912, Geology and ore deposits of the Park City district, Utah: U.S. Geological Survey Professional Paper 77, 231 p.
- Bradley, M.D., and Bruhn, R.L., 1988, Structural interactions between the Uintah arch and the overthrust belt, north-central Utah; implications of strain trajectories and displacement modeling. Geological Society of America Memoir 171, p. 431-445.
- Bromfield, C.S., 1968, General geology of the Park City region, Utah. Utah Geological Society Guidebook to the Geology of Utah No. 22, p. 10-29.
- Bromfield, C.S., 1989, Gold deposits in the Park City mining district, Utah. U.S. Geological Survey Bulletin 1857-C, p. C14-C26.
- Bromfield, C.S., and Crittenden, M.D., Jr., 1971, Geologic map of the Park City East quadrangle, Summit and Wasatch Counties, Utah. U.S. Geological Survey Geologic Quadrangle Map GQ-852, scale 1:24,000.
- Bruce, C.L., 1988, Jurassic Twin Creek Formation—a fractured limestone reservoir in the overthrust belt, Wyoming and Utah: Carbonate Symposium, Rocky Mountain Association of Geologists, p. 105-120.
- Bruhn, R.L., Picard, M.D., Isby, J.S., 1986, Tectonics and sedimentology of Uinta Arch, western Uinta Mountains, and Uinta Basin, in Peterson, J.L., ed., Paleotectonics and Sedimentation in the Rocky Mountain Region, United States, American Association of Petroleum Geologists Memoir 41, p. 333-352.
- Bryant, B., 1990, Geologic map of the Salt Lake City 30' x 60' quadrangle, north-central Utah, and Uintah County, Wyoming: U.S. Geological Survey Map I-1944, scale 1:100,000.
- Bryant, B., 1992, Geologic and structure maps of the Salt Lake City 1° x 2° quadrangle, Utah and Wyoming: U.S. Geological Survey Miscellaneous Investigation Series Map I-1997, scale 1:125,000.

- Caine, J.S., Evans, J.P., and Forster, C.B., Fault zone architecture and permeability structure: *Geology*, v. 18, p. 1025–1028.
- Crittenden, M.D., Jr., 1965, Geologic map of the Sugar House quadrangle, Salt Lake County, Utah: U.S. Geological Survey Map GQ-380.
- Crittenden, M.D., Jr., 1974, Regional extent and age of thrusts near Rockport Reservoir and relation to possible exploration targets in northern Utah. *American Association of Petroleum Geologists Bulletin*, v. 58, no 12, p. 2428–2435.
- Crittenden, M.D., Jr., Calkins, F.C., and Sharp, B.J., 1966, *Geologic map of the Park City West quadrangle, Utah*: U.S. Geological Survey Geologic Quadrangle Map GQ-535, scale 1:24,000.
- CRS Consulting Engineers, Inc., 1995, Phase I Hydrogeologic Report for Gorgoza-Pinebrook Groundwater Sources, Salt Lake City, Utah, 24 p.
- Department of Planning and Analysis, 1997, Demographic and economic analysis report to the governor, www.gvinfo.state.ut.us/dea/erg97/tables.
- Granger, A.E., 1953, Stratigraphy of the Wasatch Range near Salt Lake City, Utah. *U.S. Geological Survey Circular*, 14 p.
- Hintze, L.F., 1988, Geologic history of Utah: *Brigham Young University Geology Studies, Special Publication 7*, 202 p.
- Huntoon, P.W., 1993, The influence of Laramide foreland structures on modern ground-water circulation in Wyoming artesian basins, in Snoke, A.W., Steidtmann, J.R., and Roberts, S.M., editors, *Geology of Wyoming: Geological Survey of Wyoming Memoir No. 5*, p. 756–789.
- Imlay, R.W., 1967, Twin Creek Limestone (Jurassic) in the western interior of the United States: *U.S. Geological Survey Professional Paper 540*, 105 p.
- Jarvis, T., and Yonkee, W.A., 1993, Summit Park and Timberline Water Special Service Districts test well siting program Laramie, Wyoming, unpublished technical memorandum, 10 p.
- Lamerson, P.R., 1982, The Fossil Basin area and its relationship to the Absaroka thrust fault system, in Powers, R.B., editor, *Geologic studies of the Cordilleran Thrust Belt, 1982* Denver, Colorado, Rocky Mountain Association of Geologists, p. 279–340.
- LaPointe, P.R., and Hudson, J.A., 1985, Characterization and interpretation of rock mass joint patterns, *Geological Society of America Special Paper 199*, 37 p.
- Mullens, T.E., 1971, Reconnaissance study of the Wasatch, Evanston, and Echo Canyon Formations in part of northern Utah: *U.S. Geological Survey Bulletin 1311-D*, p. 1–31.
- Personius, S.F., and Scott, W.E., 1993, Surficial geologic map of the Salt Lake City segment and parts of adjacent segments of the Wasatch fault zone, Davis, Salt Lake, and Utah counties, Utah. *U.S. Geological Survey Map I-2106*, scale 1:50,000.
- Stone, D.S., 1967, Accumulation theory, Big Horn Basin: *American Association of Petroleum Geologists Bulletin*, v. 51, p. 2056–2114.
- Weston Engineering, Inc., 1996, Final well report—Summit Park Water Special Service District Well No. 7 located in NW1/4NE1/4, section 16, T. 1 S., R. 3 E., Summit County, Utah: Park City, Utah, unpublished consultant's report, 13 p.
- Yonkee, W.A., Evans, J.P., and DeCelles, P.G., 1992, Mesozoic tectonics of the northern Wasatch Range, Utah: *Utah Geological Survey Miscellaneous Publication 92-3*, p. 429–460.

New explorations along the northern shores of Lake Bonneville¹

CHARLES G. (JACK) OVIATT

Department of Geology, Kansas State University, Manhattan, Kansas 66506

DAVID M. MILLER

U.S. Geological Survey, 345 Middlefield Road, Menlo Park, California 94025

ABSTRACT

This field trip begins in Salt Lake City and makes a clockwise circuit of Great Salt Lake, with primary objectives to observe stratigraphic and geomorphic records of Lake Bonneville. Stops include Stansbury Island, Puddle Valley, gravel pits at Lakeside and the south end of the Hogup Mountains, several stops in Curlew Valley and Hansel Valley, and a final stop at the north end of Great Salt Lake east of the Promontory Mountains. Stratigraphic observations at gravel-pit and natural exposures will be linked to interpretations of lake-level change, which were caused by climate change. Evidence of paleoseismic and volcanic activity will be discussed at several sites, and will be tied to the lacustrine stratigraphic record. The trip provides an overview of the history of Lake Bonneville and introduces participants to some new localities with excellent examples of Lake Bonneville landforms and stratigraphy.

INTRODUCTION

Objectives

The objectives of this trip are to (1) show key new localities along the northern shores of late Pleistocene Lake Bonneville in an area where unusually complete preservation of Lake Bonneville deposits and landforms provides new insights into the lake's evolution; (2) visit some classic sites; and (3) provide an overview of Lake Bonneville and selected Holocene lake features in the context of climate history and neotectonics. Lake Bonneville is one of the best studied late Pleistocene pluvial lakes and its record of waxing and waning is a powerful paleoclimate proxy. This paleoclimate record plays a fundamental role in paleoecology studies and serves as a benchmark for testing local, regional, and global climatic hypotheses. Geomorphic features of the lake serve as vital markers for recording neotectonic events because both age and paleohorizontal can be established with shoreline features. As a result, deposits and landforms of Lake Bonneville provide valuable clues for understanding Quaternary volcanism and faulting in north-west Utah. In addition, modern hazards, from flooding to

contamination and salt-water intrusion, are best understood within the context of the complete Holocene record of Great Salt Lake. Our approach will be to look at a number of Lake Bonneville features around Great Salt Lake, including at classic sites and newly discovered sites, and set this in the context of climate, neotectonic, and hazard themes.

Regional description

Lake Bonneville was the largest of numerous late Pleistocene pluvial lakes that formed in the Great Basin, a division of the Basin and Range physiographic province characterized by playas, lakes, and internally draining rivers in hydrologically closed basins interspersed with north-trending mountains that includes western Utah, most of Nevada, and parts of adjoining states. Although much of the northeastern part of the Great Basin was occupied by Lake Bonneville at its highstand (fig. 1), the Bonneville basin now is marked by mountains separated by wide arid valleys, and few perennial streams. The three broadest lowlands are Great Salt Lake, the Great Salt Lake Desert, and the Sevier Desert. Thresholds between these lowlands provided some

¹With a contribution by Dorothy Sack, Department of Geography, Ohio University, Athens, Ohio 45701.

With amino-acid results from Darrell Kaufman, Department of Geology, Utah State University, Logan, Utah 84322.

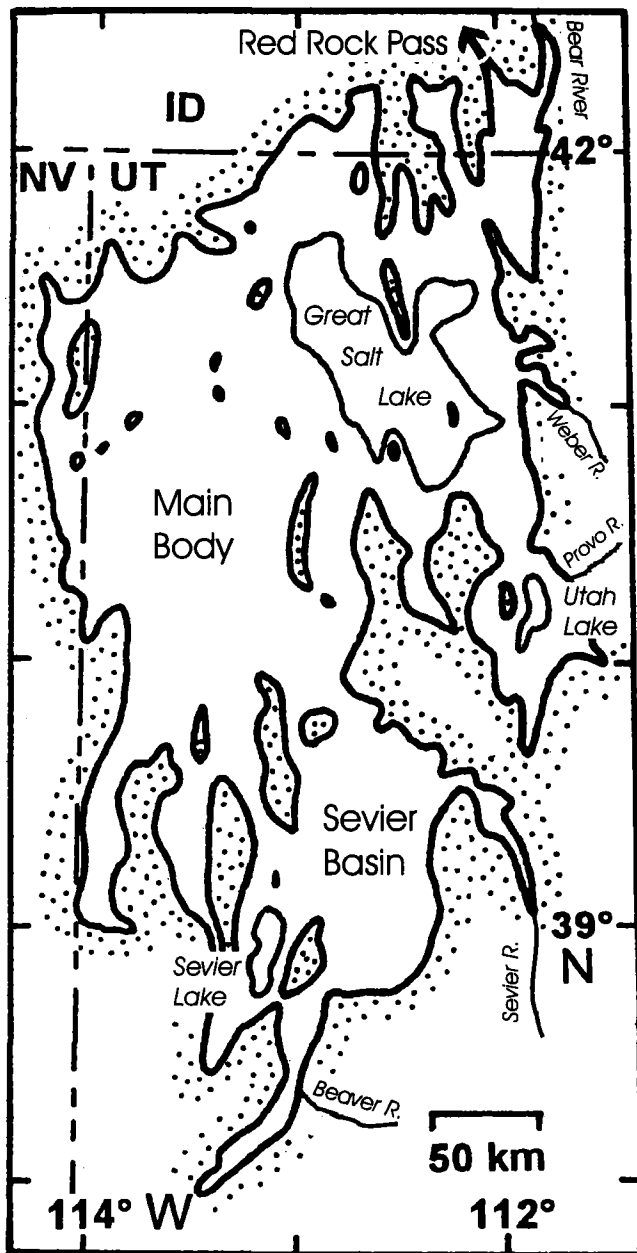


Figure 1. Map of Lake Bonneville at the Bonneville shoreline stage (15 ka).

controls on lake levels, but climatic factors provided the primary influence on the lake's budget of water influx and evaporation. Rivers on the eastern side of the basin contributed most of the water to the lake, because they drained the largest and highest mountains.

The topography of the northeastern part of the Great Basin was formed by normal faulting that created alternating uplifted and downthrown north-trending structural blocks, referred to as basins and ranges. This topography

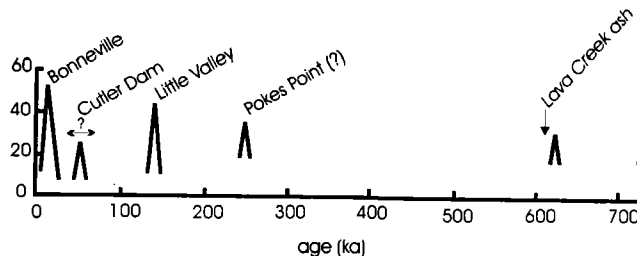


Figure 2. Major Quaternary lake cycles in the Bonneville basin (modified from Figure 3 of Machette and Scott, 1988), determined primarily from outcrop data.

started developing during the Pliocene or latest Miocene, about 5 to 7 Ma (Miller et al., 1992). Many of the ranges in northwestern Utah are bounded by normal faults that had Quaternary activity, and some have experienced Holocene activity (Christenson et al., 1987). The principal Holocene fault activity is along the Wasatch Front on the Wasatch fault (and related faults), but faults under Great Salt Lake and north of Great Salt Lake in and near Hansel Valley also ruptured during the Holocene. This western zone of recent faulting also contains Quaternary volcanoes (Miller et al., 1995), reinforcing the possibility that it is a zone of magmatism and rifting (Smith and Luedke, 1984) (see Stop 7 and fig. 24 below).

Late Cenozoic precursors to Lake Bonneville

The term Lake Bonneville is used here to refer to the last major late Pleistocene lake in the Bonneville basin, which existed between about 28 and 12 ka (Oviatt et al., 1992; Oviatt, 1997). Earlier Quaternary lake cycles have been documented in the basin (fig. 2), but Lake Bonneville and Holocene lakes are far better understood because the older lake deposits have been largely obliterated by erosion or buried by younger lake deposits and alluvium. Long cores of sediments from the floor of the Bonneville basin collected by A. J. Eardley and his colleagues during the 1950s and 1960s (Eardley and Gvosdetsky, 1960; Eardley et al., 1973) contain evidence of a number of pre-Bonneville Quaternary lakes that occupied the basin, although reexamination of these cores by Oviatt and R.S. Thompson (unpublished) indicates fewer major lake cycles than Eardley originally interpreted from the cores. On this field trip we will get a glimpse of deposits of several pre-Bonneville lake cycles (at the Lakeside gravel pit; Stop 3), but we will spend most of our time on deposits and landforms of Lake Bonneville.

Lake Bonneville studies

Although evidence of a greatly expanded lake was noted by the Spaniards Dominguez and Escalante in 1776, the

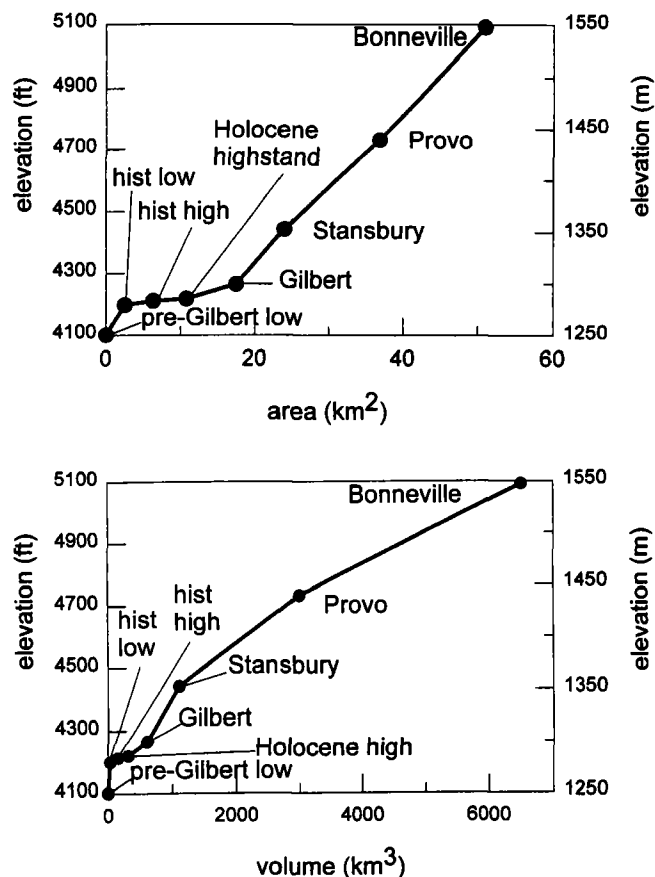


Figure 3. Graphs of surface area and volume vs. elevation in the Bonneville basin. Data from Currey (1990, Fig. 16). Data points are for shorelines of Lake Bonneville and for high and low stands of Great Salt Lake.

significance of shorelines far above the level of modern Great Salt Lake wasn't realized until Fremont and Stansbury explored the basin in the 1840s and 1850s (Sack, 1989). Other federally sponsored surveys during the late 1800s led to the masterful work of Grove Karl Gilbert, who named the ancient lake, Lake Bonneville, and spent many years studying its geology, geomorphology, and stratigraphy. USGS Monograph 1 (Gilbert, 1890) is the full report of Gilbert's studies and illustrates his amazing abilities as a scientist and observer.

Since the publication of Monograph 1 many people have studied Lake Bonneville, and ideas about its history have evolved considerably (see reviews by Machette and Scott (1988), and Sack (1989)). It is worth noting, however, that after more than a century, during which Gilbert's hypotheses have been repeatedly tested, many of his ideas and conclusions have withstood scrutiny and today stand as the solid framework of a robust body of knowledge about Lake Bonneville.

OVERVIEW OF LAKE BONNEVILLE

General Concepts

At its maximum about 15 ka, Lake Bonneville had a depth of over 300 m, a surface area of 51,000 km², and a volume of approximately 6500 km³ (fig. 3). It had numerous bays, arms, peninsulas, and islands. The large rivers that emptied into the lake along the high mountains to the east produced tremendous volumes of clastic sediment, which dominate the stratigraphic records in valleys along the mountain fronts (Lemons et al., 1996). Over most of the area of Lake Bonneville, however, where no rivers discharged sediment, the source of shorezone clastic sediment was alluvium and weathered bedrock on mountain flanks, and impressive constructional shoreline features, such as spits, barriers, and tombolos (some of which will be seen on this trip) were deposited. In distal areas where clastic input was small, the dominant fine-grained facies is marl.² Typically, coarser grain sizes were deposited close to shore where wave energy was high, and fine-grained facies (marl) were deposited offshore, but there are exceptions to these general rules that depend on local geomorphic controls. For instance, dropstones from shore ice or rootballs of rafted trees are common in certain settings of the marl, and some fine-grained sediments were deposited where wave energy was low and fine-clastic input was high.

A schematic stratigraphic column of a typical white marl section specific to a deep-water, or low-altitude, location is shown in fig. 4. At higher altitudes, early and late parts of the history are not represented. Refer to fig. 5 to place the stratigraphic units mentioned here in the chronology of Lake Bonneville. Coarse-grained littoral deposits at the base grade upward into sandy marl and laminated marl (early transgressive-phase and Stansbury marl), which grades upward into more massive marl (deposited during the deepest-water phases) that generally has a lower clastic content, and in many places is pink or dark green in color. The massive marl has an abrupt upper contact with a sandy laminated unit (the Bonneville flood unit) that in many places contains abundant reworked ostracodes. The sandy laminated unit

²Gilbert named one of the Lake Bonneville stratigraphic units the White Marl, and the fine-grained calcareous facies of the Bonneville Alloformation is still referred to informally as the white marl. On this field trip we will examine a number of exposures of the (stratigraphic unit) white marl, most of which will fit the definition of marl ("a soft, grayish to white, earthy or powdery, usually impure calcium carbonate precipitated on the bottoms of present-day freshwater lakes and ponds largely through the chemical action of aquatic plants... the calcium carbonate content may range from 90% to less than 30%" [Bates and Jackson, 1987]). In Lake Bonneville, marl was deposited even during the deepest stages, calcium carbonate was probably precipitated in the epilimnion, and minute crystals of calcite or aragonite settled to the lake bottom. In places the (stratigraphic unit) white marl contains over 80% calcium carbonate, but in other places it may consist of calcareous sand, depending on the local input of clastic debris.

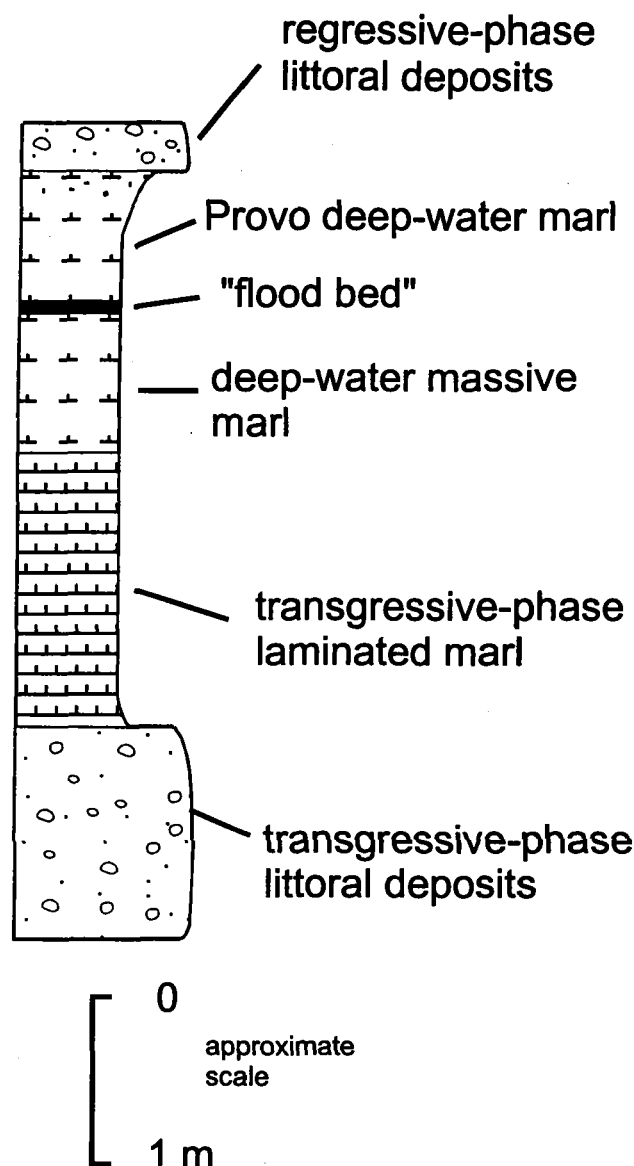


Figure 4. Generalized stratigraphic column of the white marl showing facies that are likely to be encountered at a low-elevation site in the main body of Lake Bonneville (modified from Oviatt et al., 1994, fig. 3). Typical ostracodes in the three main facies are as follows. Post-Bonneville flood (Provo deep-water marl): *Cytherissa lacustris*, *Candona caudata*, *Candona adunca*, *Limnocythere ceriotuberosa*, *Candona eriensis* (?); Deepest-water phase (deep-water massive marl): *Candona adunca*, *Limnocythere ceriotuberosa*, *Candona caudata*; Early transgressive phase (transgressive-phase laminated marl): *Limnocythere staplini*, *Candona caudata*. Ostracode abbreviations used in subsequent figures: **genus Candona**: *C. adunca* = Ca, *C. caudata* = Cc, *C. eriensis* = Ce, *C. decora* = Cd, *C. rawsoni* = Cr; **genus Limnocythere**: *L. staplini* = Ls, *L. ceriotuberosa* = Lc, *L. sappanensis* = Lsa; **genus Cytherissa**: *C. lacustris* = Cyl.

grades upward into another massive marl unit (deposited during the Provo stage and initial regression), which grades upward into coarse-grained sediments (of the final regression). Fossil ostracode faunas in these subunits of the white marl are distinctive (fig. 4), and are very helpful in intra-basin correlations (as the water chemistry changed with changes in lake volume and level, the ostracode assemblages changed [Forester, 1987; Thompson et al., 1990]). Marl chemistry (carbonate content, relative proportions of different carbonate minerals, oxygen and carbon isotopes) also varies systematically and will be discussed at several stops on the field trip. For instance, for marl precipitated during periods of relatively low lake level, the percentage of total carbonate, the aragonite/calcite ratio, and the relative values of oxygen and carbon isotopes are relatively high (Oviatt et al., 1994; Oviatt, 1997).

Some of the shorelines of Lake Bonneville have been mapped throughout the basin (Gilbert, 1890; Currey, 1982; Currey et al., 1984), but many shorelines do not have regional signatures, and can be mapped for only short distances along individual mountain fronts. Two of the mapped shorelines (Bonneville and Provo) are prominent because they formed during periods of overflow at the basin rim (near Red Rock Pass, Idaho), but other mapped shorelines (Pilot Valley, Stansbury, Gilbert) were not threshold controlled, and are difficult to confidently identify in many places. On this field trip we will observe good examples of all five of the above-mentioned shorelines, as well as numerous examples of unnamed shorelines.

As Gilbert (1890) noted, the major shorelines of Lake Bonneville are not horizontal on a regional scale, but are bowed upward in the interior of the basin—the Bonneville shoreline is 74 m higher in the Lakeside Mountains than at the basin rim (Red Rock Pass), and the Provo shoreline is bowed upward a maximum of 59 m (fig. 6). Gilbert correctly attributed the deformation to isostatic rebound following the removal of the Lake Bonneville water load, and subsequent work has refined Gilbert's shoreline mapping and the modeling of the isostatic response (see Crittenden, 1963; Currey, 1982; Bills and May, 1987).

History

Lake Bonneville began to rise from elevations similar to modern Great Salt Lake (~1280 m; 4200 ft) after about 28 ka (all ages discussed in this guidebook, except for historic dates, are in radiocarbon years B.P.) (fig. 5). The Pilot Valley shoreline, which was first mapped in the vicinity of Pilot Valley (Miller, 1990), was produced at about the level of the regressive-phase Gilbert shoreline sometime after 28 ka. The Pilot Valley shoreline is prominent in a number of areas in northwest Utah, but has not yet been mapped through-

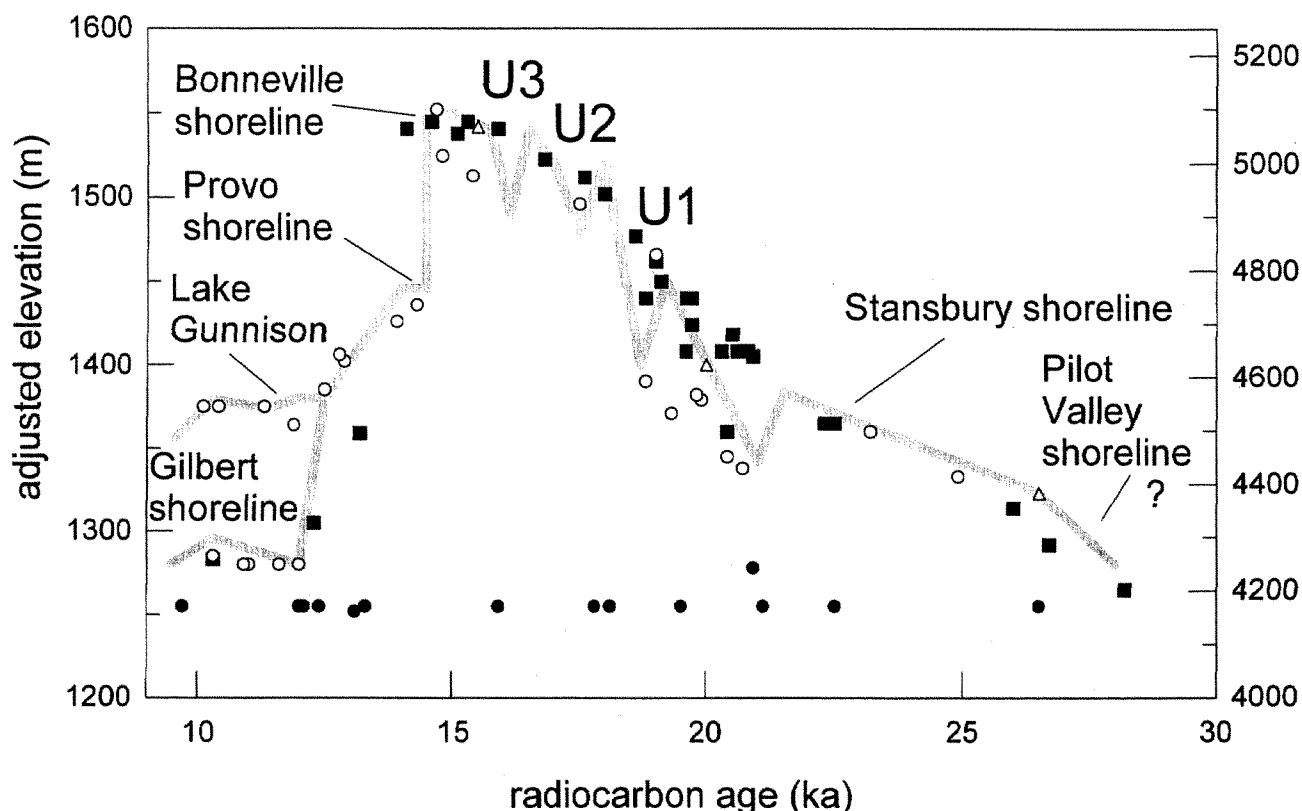


Figure 5. Lake Bonneville time-altitude curve modified from Oviatt et al., (1992, fig. 3) and Oviatt (1997, fig. 2). Elevations are adjusted for the effects of isostatic rebound in the basin (Oviatt et al., 1992), and ages are in radiocarbon years. Open circles are carbonate radiocarbon samples (shell, tufa), solid circles are disseminated organic carbon samples, solid squares are wood or charcoal samples, and open triangles are basaltic ashes. U1, U2, and U3 are unnamed transgressive-phase fluctuations.

out the Great Salt Lake basin. Lake Bonneville had reached an elevation of about 1340 m (4400 ft) by 26.5 ka (fig. 5). Later in the transgressive phase the lake experienced a series of fluctuations, each on the order of 30–50 m (Stansbury, U1, U2, U3), before reaching its highest stage at the Bonneville shoreline about 15 ka. The lake briefly overflowed (probably less than 500 yr) near Red Rock Pass, ID, as the Bonneville shoreline formed, catastrophically dropped about 100 m when the alluvial-fan threshold failed about 14.5 ka, then continued to overflow noncatastrophically at a new stable threshold during the formation of the Provo shoreline. During regression below the Provo shoreline the lake dropped past an intrabasin threshold, referred to as the Old River Bed threshold, and the lake was divided into two separate lakes, one in the Sevier Lake basin (Lake Gunnison), and one in the Great Salt Lake basin, which received overflow from the Sevier basin. The Gilbert shoreline formed in the Great Salt Lake basin during a moderate rise between 11 and 10 ka.

The Bonneville shoreline ranges widely in degree of development and preservation depending on local geomorphic controls, such as wave energy and direction, substrate resistance, slope, and sediment supply. The Provo shoreline is commonly the best developed, ~100 m (~330 ft) below the Bonneville. Provo and Stansbury shorelines are marked by prominent drapes of tufa and cemented beachrock, each with a marl “dump” below. The Gilbert shoreline is sporadically developed, and where present typically has a relatively fresh-looking appearance. The Pilot Valley shoreline is exposed sporadically across northern Utah at low elevations, and as the earliest regionally developed shoreline, is an important reference frame for measuring isostatic deformation.

Basaltic volcanic ash has been useful in Lake Bonneville stratigraphic studies (Oviatt and Nash, 1989; Miller et al., 1995). The Hansel Valley ash (discussed below) was erupted from an unidentified vent in northern Utah about 26.5 ka. Several other basaltic ashes (Pahvant Butte, Tabernacle Hill, and Pony Express) have been described in the Sevier Desert region in the southern part of the Bonneville basin.

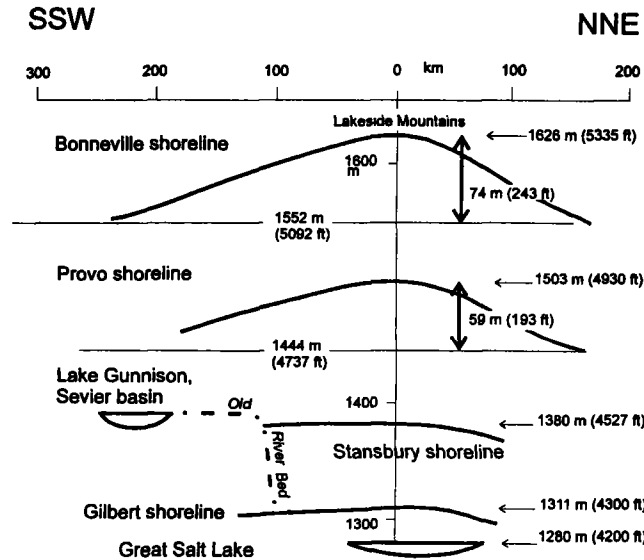


Figure 6. Isostatic rebound of Bonneville, Provo, Stansbury, and Gilbert shorelines. Modified from Currey (1990, fig. 13). The fine lines labeled 1552 m and 1444 m associated with the Bonneville and Provo shorelines, respectively, represent the unrebounded elevations of those shorelines. Lake Gunnison, in the Sevier basin, overflowed into the Great Salt Lake basin during the development of the Gilbert shoreline. The Lakeside Mountains are near the center of the Lake Bonneville water load, and therefore, the shorelines are rebounded the greatest amount in this area.

Unresolved questions

A number of questions about Lake Bonneville history are still being pursued. The transgression of Lake Bonneville, and all the falling-lake events (or regressions), such as the Stansbury, U1, U2, U3, the post-Provo regression, and the post-Gilbert regression, were caused by climate change in the basin. For most of its history the lake was hydrographically closed so that changes in lake level reflect shifts in the water budget of the basin. The Bonneville cycle as a whole was correlative with marine oxygen-isotope stage 2, and each of the major falling-lake events was correlative with the abrupt termination of an iceberg rafting event in which large quantities of debris were deposited on the floor of the North Atlantic Ocean (Oviatt, 1997). The iceberg-rafting events were associated with global climate changes (Bond and Lotti, 1995). Therefore, the Bonneville-basin water budget was sensitive to global climate change on time scales ranging from at least 10^5 to 10^3 yr. The rapid response of Great Salt Lake to El Niño forcing during the 1980s suggests that the basin has the potential to yield high-resolution (decadal?) paleoclimate records if complete, undisturbed sedimentary sequences can be identified and sampled. More work is needed (and underway) to help refine the timing

and magnitude of water-budget shifts during the late Pleistocene and Holocene.

Although the timing of the final regression of Lake Bonneville is known to have occurred between about 14 and 11 ka, the details of the regression are poorly understood because of the paucity of suitable datable materials in meaningful contexts. The isostatic response of the basin to loading and unloading is still being refined (Bills and May, 1987). For example, the altitude of the Gilbert shoreline varies from place to place in a way that is not easily predicted by isostatic models. It is higher on the northwestern edge of the basin (4260 ft [1298 m] from the Pilot Range along the Utah-Nevada stateline to Curlew Valley) than elsewhere along north shore (4250 ft; 1295 m).

Other unanswered questions include: (1) Where was the Hansel Valley ash eruptive center? See more discussion below—locating the vent is important in assessing regional geologic hazards. (2) The Pilot Valley shoreline (~4275 to 4295 ft; 1303–1309 m), which formed early in the transgressive phase, has not been studied in detail: was its development regional in extent, and what is its age and paleoclimatic significance? (3) Was the rise to Stansbury very rapid, and were there significant lake-level fluctuations between the time of eruption of the Hansel Valley ash and the Stansbury oscillation? (4) What is the origin of the double shorelines at the Provo level, and how did isostatic rebound immediately after the Bonneville Flood affect shoreline development at the Provo?

OVERVIEW OF GREAT SALT LAKE

Great Salt Lake is a shallow, highly saline lake in a hydrologically closed basin, which fluctuates largely as a result of climatic and human-induced influences (see Gwynn, 1980; and Arnow and Stephens, 1990). A pair of thresholds north and south of the Newfoundland Mountains control overflow to the Great Salt Lake Desert at ~4217 ft (1285 m) altitude (Currey et al., 1984). At the average historical lake level (4202 ft; 1280 m), maximum depth is roughly 35 ft (11 m) and areal extent is 1800 mi² (4600 km²) (Currey et al., 1984). The lake lies in an arid basin, and input is mainly from rivers draining mountains east of the lake. Principal stream inflow is from the Bear, Weber, and Jordan Rivers (fig. 9); this inflow is roughly double the direct contribution to the lake from precipitation. The shores of the lake typically have broad shallow mud flats that grade laterally to steeper areas, with the result that moderate lake-level fluctuations can produce either dramatic shoreline changes across the flats or very little shoreline change along steep slopes.

Prehistoric Great Salt Lake

The shoreline record that postdates the Gilbert-age lake deposits gives some information on major Holocene high-

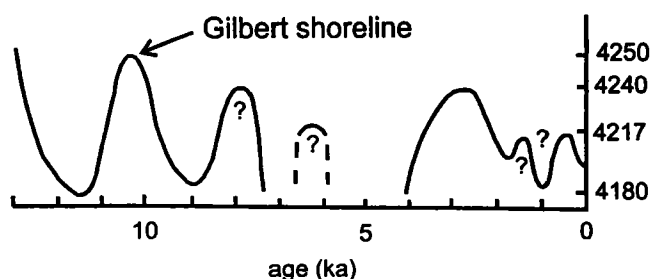


Figure 7. Holocene history of Great Salt Lake modified from Currey et al., (1984; see also Murchison, 1989).

stands of Great Salt Lake (fig. 7). At Locomotive Springs on the north shore of Great Salt Lake, a wave-cut notch at 4240 ft and a gravel beach at 4230 ft may be regressive shorelines of the Gilbert Stage but more likely are distinct Holocene lake highstands. A sand and gravel beach at 4218 ft rests on Holocene lake muds and represents one of the Holocene high stands of Great Salt Lake. Elsewhere along the north shore of Great Salt Lake 4240-ft and 4220-ft beaches are very common. Currey et al., (1988) described evidence that a 4221-ft shoreline formed between 2.5 and 2.0 ka. Some stands higher than the 4217-ft thresholds have taken place during the late Holocene, including the Little Ice Age highstand about 400 years ago (Currey et al., 1984). Atwood (1994) has been studying how the elevations of Great Salt Lake shorelines are affected by processes such as wind-generated lake-level changes, wind seiches, earthquake seiches, and diking or other human activities. An understanding of these geomorphic processes is important for accurate reconstructions of paleolake levels, and for assessing geologic hazards associated with rises in lake levels.

Historic lake levels

Great Salt Lake typically has 1- to 3-foot annual variation in lake level caused by seasonal variations in evaporation and influx. The hydrograph (fig. 8) for recordings at the southern end of the lake illustrates longer-term variation in lake levels, including the historic highs in the early 1870s, and in 1986–1987 (both rises reached almost to 4212 ft), and low in 1963 (4191 ft) (Mabey, 1986; Arnow and Stephens, 1990).

The Southern Pacific Railroad causeway bisecting the lake from Lakeside to Ogden artificially controls lake level. Most of the fresh water enters the south arm of the lake, and construction of the causeway in the 1950s, and modification in the 1980s, has caused lake levels in the northwest arm to be lower than in the south arm by several feet. In addition, the north arm has much higher salinity and slightly lower water levels. Several openings in the causeway

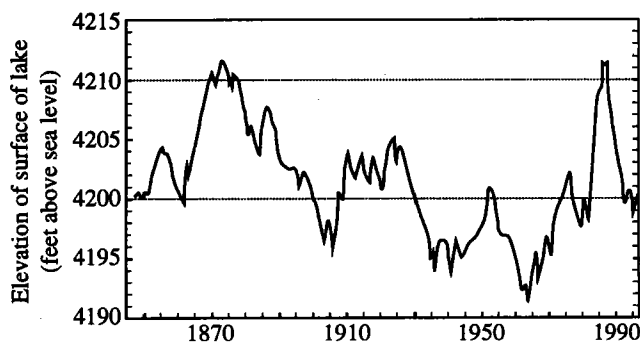


Figure 8. Historical fluctuations of the surface altitude of the southern part of Great Salt Lake. Data from the U.S. Geological Survey, 1996 Web Site.

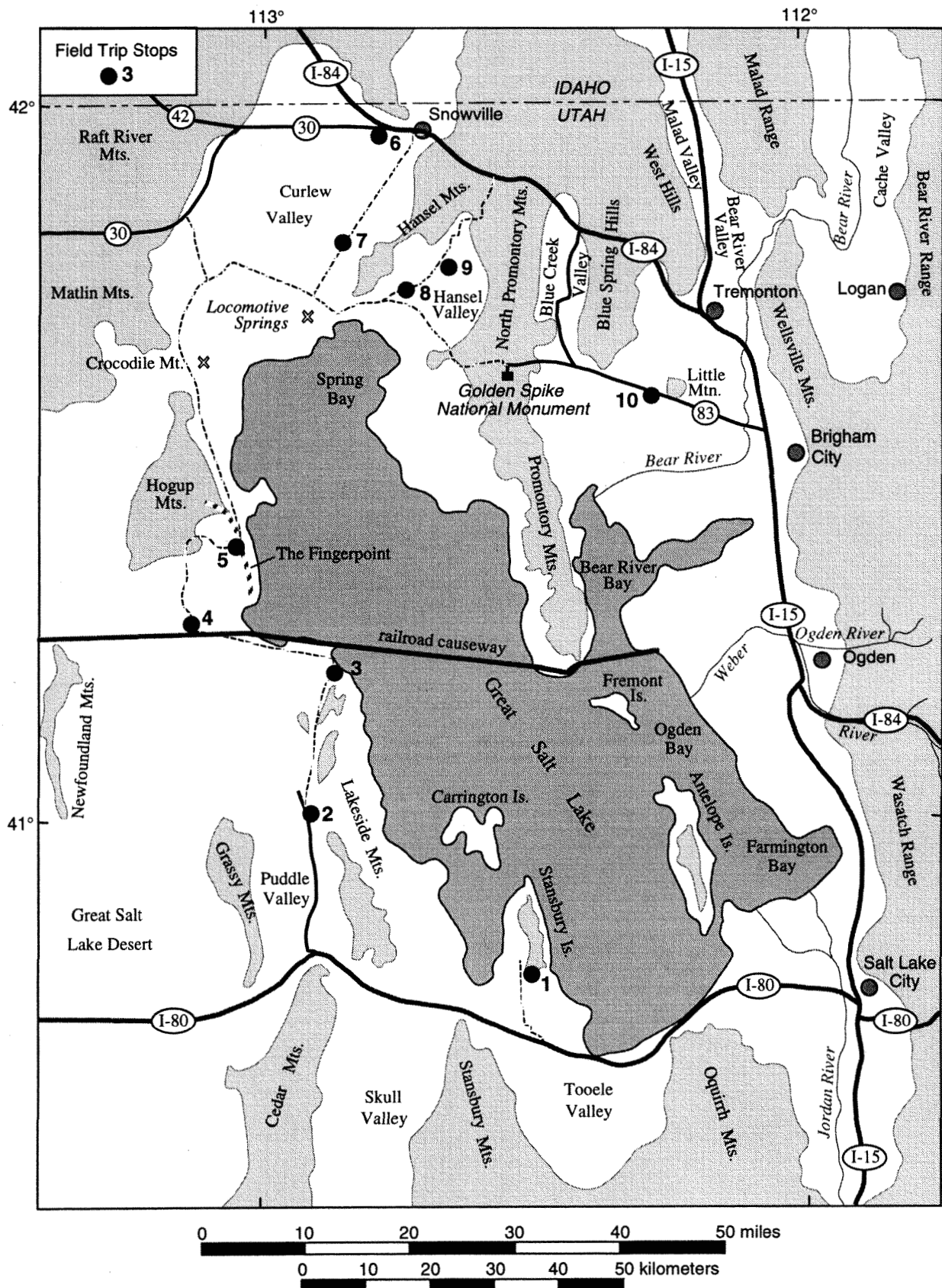
allow water from the south arm to flow to the north at the surface, although dense saline water from the north arm also flows southward through the causeway openings.

The high lake levels caused by floods of the 1980s were probably similar to the those of the 1870s, although the first lake-level gage was installed in 1875, so the pre-1875 levels are estimates (Mabey, 1986). In the 1980s, the lake rose rapidly during a five year period (1982–1986) from about 4200 ft to almost 4212 ft (reported as 4211.85 ft) during 1986, and then dropped just as rapidly to its present level. The rate of rise and fall during this flood event was greater than 2 ft per year, despite significant human water consumption. Similar rates for past recorded rises and declines in lake level demonstrate the rapidity with which lake levels change. Most population growth in the region took place during a time when the lake was below its average level, and the roads and buildings constructed at low altitudes and were considerably damaged during the lake rise of the 1980s. To help control the damaging effects of high lake levels, a pumping plant was constructed in the southern Hogup Mountains to pump water from the lake to shallow basins in the Great Salt Lake Desert, which together acted as a huge evaporation basin (U.S. Geological Survey, 1987). Pumping during 1987 flooded roughly 600 mi² (1700 km²) west of the Newfoundland Mountains.

Shorezone features

Oolitic sand is currently forming in shallow water around most of the margins of Great Salt Lake (Eardley, 1938; Gwynn and Murphy, 1980), except where clastic deposition and fresher water dominate near the deltas of the Bear and Jordan Rivers. In places, oolitic sand is reworked into eolian dunes at the shoreline.

We will observe or pass close to a number of springs and marshes at the margin of the lake on this field trip. Most notable will be the marshes at the Public Shooting Grounds



at the north end of Bear River Bay. The Bear, Weber, and Jordan Rivers have built deltas along the east shore of Great Salt Lake.

Ecology and contamination

Despite its high salinity, Great Salt Lake supports a healthy ecosystem. Typical organisms include bacteria, blue-green algae, diatoms, brine shrimp, brine flies, and other aquatic insects. The lake itself, and the springs, deltas, and marshes at the margin of the lake, support a diverse avifauna.

Restricted circulation in the lake, due both to natural causes such as shallowness and long islands, and also to artificial barriers such as causeways, has served to concentrate contaminants in parts of the lake. Effective mitigation of contamination relies on traditional hydrologic principals such as knowing paths and rates of water input and circulation, and also a detailed knowledge of the chemistry and physical attributes of water in different parts of the lake. The unique waters may provoke unusual reactions with contaminants.

FIELD TRIP GUIDE

This trip will start and end in Salt Lake City, and will circle Great Salt Lake in a clockwise direction (fig. 9). We will use highway mileage markers for locating features during travel along major routes such as Interstate freeways, and give odometer mileage for roads off the major routes. We reset mileage to zero after each stop. Elevations are given in feet throughout the guidebook because the USGS 7.5-minute topographic quadrangles and benchmarks are in feet, and it is easier not to convert to meters (metric equivalents are given in parentheses).

DAY 1

Travel west from Salt Lake City on I-80.

Mile 104. To the north, Saltair recreation park lies on the gently sloping shore of Great Salt Lake. It was built in the early 1980s as a partial replication of the historic Saltair park, and promptly flooded during the 1982 to 1986 rise of the lake. Despite attempts to dike around the building, it was damaged extensively. Water stood at least 5 ft deep at the building. Note how far the lake has now receded. Kennecott's copper smelter lies south of the freeway. Marshes

between the airport and Saltair are Holocene in age, and comprise part of the Jordan River tributary system.

Mile 93. In this vicinity both I-80 and the parallel railroad north of the highway were raised during the mid-1980s as the lake rapidly rose to its highstand of almost 4212 ft during the early summers of 1986 and 1987. Note fenceposts still partly submerged.

Mile 84. Exit here (Grantsville exit). Set mileage to zero at stop sign. Turn right (north) and follow paved road west and north through several bends.

- 0.5** Pavement ends. Cross railroad heading north.
- 4.2** Intersection; take left fork.
- 6.0** Crossroads. Turn right (east) and drive to floor of gravel pit. Shorelines are visible on the mountain facing us.

STOP 1. Stansbury shoreline on Stansbury Island.

We will examine exposures in Stansbury Gulch that show a section of the white marl and a wedge of tufa-cemented gravel that can be traced to the Stansbury shoreline. The exposures demonstrate that the Stansbury shoreline formed early in the lake history and that offshore stratigraphy can be linked to geomorphic features.

Cream-colored sandstone outcrops form the west ridge of the short, steep valley, and gray limestone, the east. The tufa-cemented prominent shoreline high on the sandstone outcrops is the Provo shoreline, and the fainter shoreline about half way between the gravel pit (at the base of the mountain) and the Provo shoreline is the Stansbury shoreline. Both shorelines also can be seen on the limestone ridge. Most gravel exposed in the gravel pit at the base of the mountain was deposited during the initial transgression of Lake Bonneville. In some parts of the gravel pit, the white marl can be seen overlying transgressive-phase gravel near the top of the exposure; the marl is overlain by a few meters of cobbles, which were deposited during the rapid regression of the lake. The white marl was truncated in most places during this regression event.

Walk up Stansbury Gulch to the northeast. A jeep track traverses the east side of the valley and may be drivable as far as a pit in the diatomaceous marl. The stratigraphy and geomorphology of Stansbury Gulch have been described in several previously published guidebooks (see Currey et al., 1983; Green and Currey, 1988). Two or three thin sand beds in the diatomaceous marl in the lower parts of the gully exposures can be traced up slope into thicker sand and then into a thick wedge of tufa-cemented gravel that is coincident with the Stansbury shoreline (fig. 10). A radiocarbon age of 20.7 ka (Currey et al., 1983) determined on gastropods collected from the sand at the lower end of the gravel wedge, in addition to the stratigraphic relationships, indicates that the Stansbury shoreline formed during the

Figure 9. Field trip stops and road route. Heavy lines are interstate highways; lighter lines are paved highways; dashed lines are graded gravel roads. Average shoreline for Great Salt Lake (4202 ft) is shown. Mountains (shaded) are outlined by the Provo shoreline. Adapted from Currey et al., (1984).

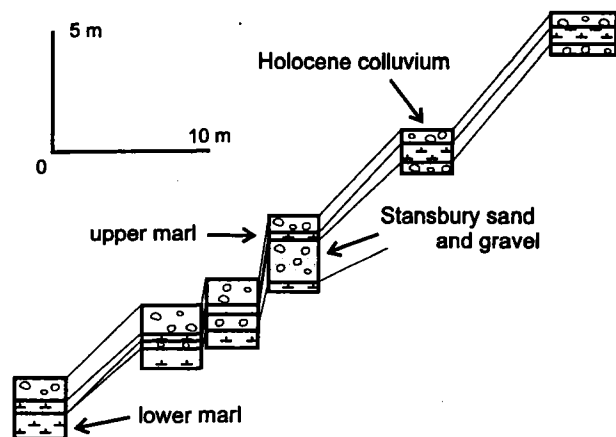


Figure 10. Stop 1—Schematic measured sections from the walls of the gully at Stansbury Gulch (modified from Currey et al., 1983, and Green and Currey, 1988). The sections are simplified into three main units: lower marl (below the Stansbury sand and gravel); Stansbury sand and gravel, including the thick tufa-cemented gravel; upper marl (which represents deep-water deposition between the time of development of the Stansbury shoreline and the regression below the Provo shoreline); and Holocene colluvium and debris flows. Two radiocarbon ages have been obtained from these sections: 20.7 ka on *Pyrgulopsis* (*Amnicola*) shells from the Stansbury sand; and 24.9 ka on fine-grained CaCO_3 from the lower marl (Green and Currey, 1988).

transgressive phase of Lake Bonneville during an oscillation in lake level. Stratigraphic and geomorphic interpretations from other locations in the Bonneville basin indicate that the total amplitude of the Stansbury oscillation was on the order of 45 to 50 m (150–165 ft) (Oviatt et al., 1990), although the evidence at Stansbury Gulch is insufficient in itself to demonstrate this.

The Stansbury oscillation is one of at least four major oscillations in lake level during the transgressive phase, each of which represents a significant change in water budget driven by climate change in the basin (fig. 5; Oviatt, 1997). For example, the Stansbury oscillation represented surface-area and water-volume changes of about 5000 km² and 1000 km³, or relative changes of 18 and 50%, respectively (Oviatt et al., 1990). The other transgressive-phase oscillations had similar magnitudes, and represent climate changes probably associated with shifts in the mean position of storm tracks, which in turn were possibly determined by changes in the size and shape of the Laurentide ice sheet (Oviatt, 1997).

Retrace route to I-80 and enter freeway headed *west*. Near this location the 1000-ft (300-m) deep Burmester core was taken in 1970 by A.J. Eardley and his colleagues (Eardley et al., 1973). Eardley et al., attempted to correlate their interpretations of the Burmester core with other records of

global climate change (European loess cycles and deep-sea records). However, a quick look at the core in 1993 convinced Oviatt and Bob Thompson (USGS) that Eardley et al., had missed the deposits of the deepest Quaternary lake in the basin (Lake Bonneville). That is, the white marl of Lake Bonneville is in the upper 6 ft of the core—an interval described by Eardley et al., as soil and interpreted as evidence of dry to shallow lake conditions. Therefore, in 1995 Oviatt and Thompson reexamined the Burmester core (and other cores taken by Eardley in the 1950s and 1960s) and concluded that the core contains a record of mudflat, eolian, and marsh sedimentation interspersed with a few units of marl deposited in deep lakes. The original paleomagnetic results, and recently obtained tephrochronology (Williams, 1994), provide age control for the past ~3.3 Ma. We concluded that there were only four major deep-lake cycles represented in the Burmester core, including Lake Bonneville, during the last 700 ka, in contrast to 17 deep-lake events interpreted by Eardley et al., (1973) for the same time interval. It is obvious that much more work needs to be done on the pre-Bonneville lacustrine history of the Bonneville basin.

Mile 81. Note the good view of the Bonneville, Provo, and Stansbury shorelines on the north end of the Stansbury Mountains, south of the freeway. The Provo shoreline is most prominent, and is draped by tufa-cemented beachrock.

Mile 77. Morton Salt plant on the right. Salt and other minerals extracted from Great Salt Lake brines are a key industry for the region.

Mile 62. Exit toward Lakeside. Reset mileage to zero at stop sign. Turn right and follow paved road toward Military area.

- 0.7 View over Puddle Valley, an internally-drained valley within the Bonneville basin. The two passes at the south end of Puddle Valley (one close by to the southeast and the other farther to the southwest where the freeway disappears over the horizon) are about 80 m below the Provo shoreline. The pass at the north end of the valley, which we will study at STOP 2, is lower.
- 4.6 Muddy marl outcrops are in the road cut; ostracodes indicate that the marl was deposited while Puddle Valley was inundated by Lake Bonneville.
- 4.9 Cross Lake Puddle shoreline. Currey (1980) noted and named this shoreline, which does not match regional shorelines of Lake Bonneville (see the contribution by Sack below).
- 8.9 Bonneville marl capped by eolian sand in exposures along the road.
- 13.1 Reduce speed as we approach a high mound with steep fronts north and west of the highway.

This is a mass of gravel (referred to by Sack [below] as an inflow feature or bar) that was emplaced into a lake in Puddle Valley. As the road climbs the gravel mound, note the steep southern front, and that the mound has an undulating surface, with swales filled by marl. The undulations are megaripple-like features, spaced 6 to 270 m apart. The marl is post-Stansbury in age, on the basis of ostracode studies.

- 14.4 Pass road on right to Wrathall Pass.
- 14.9 Turn right (east) on gravel road, pass under power lines.
- 15.1 Bear left to a gravel pit and pass sign "No trespassing-Government Property." Continue into pit and park on the left.

STOP 2. Stansbury oscillation and catastrophic inflow at Puddle Valley.

Lake Bonneville's Puddle Valley Connection

by

Dorothy Sack

Department of Geography, 122 Clippinger Labs
Ohio University, Athens, Ohio 45701

Puddle Valley is a 400-km² closed drainage basin located approximately 100 km west of Salt Lake City near the center of the Lake Bonneville basin. Its elevation ranges from 4317 ft (1316 m) on the valley floor to 6625 ft (2019 m) at the highest peak in the Lakeside Mountains, which form the valley's eastern boundary. Puddle Valley is completely surrounded by, that is, inset into, the Bonneville basin. For most of the last deep-lake cycle Puddle Valley was an integrated subbasin of Lake Bonneville and contained an arm of the great lake (Gilbert, 1890; Currey et al., 1984). Shoreline evidence reveals that an independent Lake Puddle (Currey, 1980) occupied the valley at least briefly after its re-isolation from Lake Bonneville (Sack, 1995), but today there is no naturally occurring perennial or intermittent surface water in the valley.

The lowest point on Puddle Valley's drainage divide lies in the unnamed pass through which the paved highway extends at the north end of the valley. The threshold has a modern elevation of about 4470 ft (1362 m), which is below the modern local elevations of all three major Lake Bonneville shorelines, the Bonneville (5330 ft; 1625 m), Provo (4925 ft; 1501 m), and Stansbury (~4530 ft; ~1380 m), and above the post-Bonneville Lake Puddle level 4390 ft (1338 m) (Currey, 1982; Sack, 1995). Puddle Valley became part of the Bonneville basin when Lake Bonneville spilled from the north over this threshold into Puddle Valley. The inflow event is marked in the pass by a 1.2-km long spillway that slopes to the south and by a distinctive landform, first noted

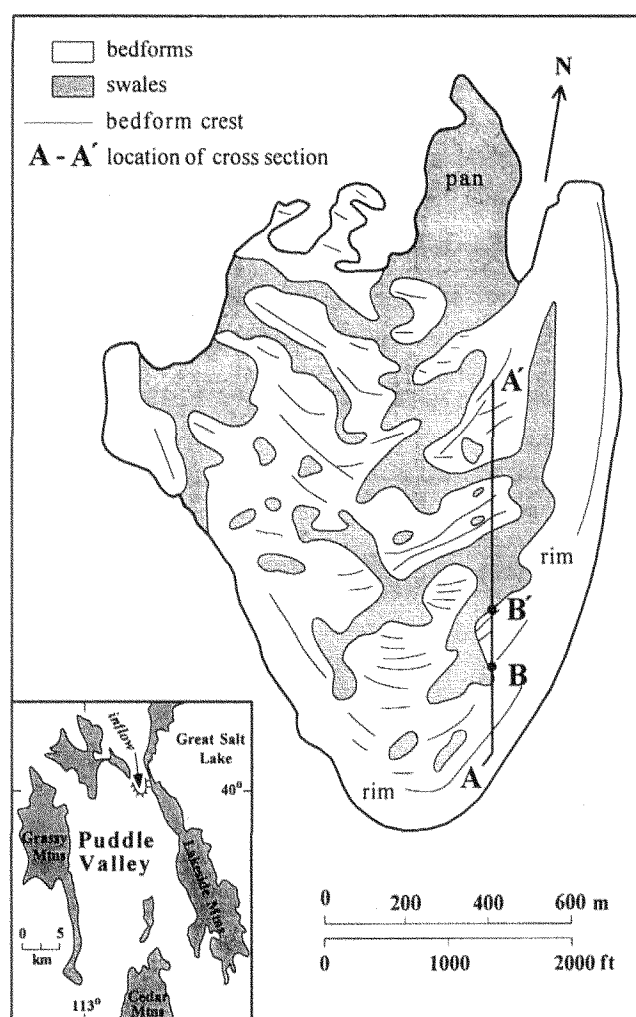


Figure 11. Planimetric map of the Puddle Valley inflow bar. The measured cross section from A-A' appears in figure 12.

by Currey (1980), that is preserved just beyond the end of the spillway in Puddle Valley.

The Lake Bonneville inflow feature in Puddle Valley is a large-scale, tongue-shaped bar on which are found giant current ripples (fig. 11). The gravel bar, which is 1.5 km long and up to 1.2 km wide, consists of a pan on the up-current side bordered by a continuous lateral and lee-side rim. Elevations range from 4400 ft (1341 m) at the distal base of the bar to 4450 ft (1357 m) at the crest of the highest bedform. Along the highway road cut, the moderately asymmetrical giant current ripples range in height from 0.2 to 5.2 m, in length from 6 to 271 m, and in vertical form index (L/H) from 15 to 71 (fig. 12). The ripples consist of gravel cross beds that dip 9° to 24° towards Puddle Valley. Clasts sampled from 14 sediment pits dug in the bedforms had an average A axis of 10 cm and the overall ten largest clasts

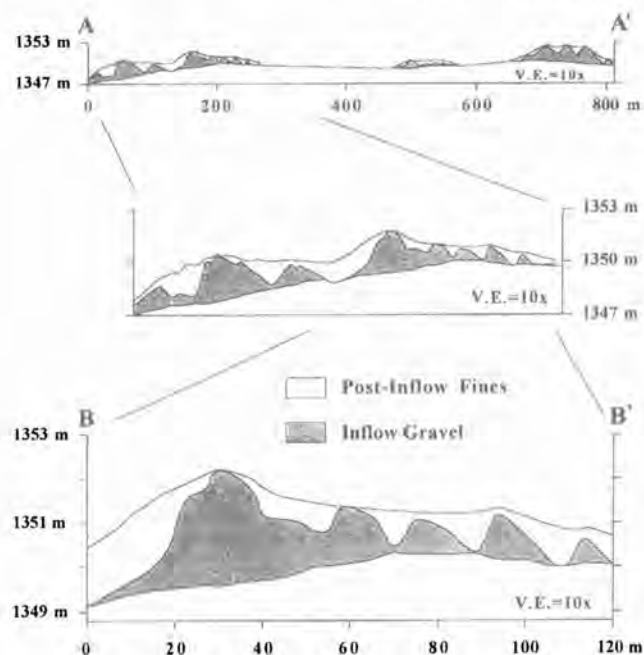


Figure 12. Measured cross section through giant current ripples on the Puddle Valley inflow bar.

had an average A axis of 35 cm. The surface of the bar complex is mantled with Lake Bonneville white marl, clastic lacustrine fine-grained sediments, and postlacustrine eolian sandy silt.

The dimensions of the giant current ripples, size of constituent clasts, and presence within the bedforms of rip-up fragments of pre-Bonneville lacustrine marl (R.M. Forester, 1992, pers. comm.), tufa, and beachrock indicate that inflow was a high-velocity event accompanied by sudden catastrophic failure of the threshold. Because evidence of the Stansbury shoreline complex, which formed between about 22 and 20 ka (Oviatt et al., 1992), is found in Puddle Valley (Sack, 1995), the valley must have become part of the Bonneville lake basin before Stansbury shoreline time. Using the Lake Bonneville hydrograph (fig. 5) and the Puddle Valley threshold elevation, corrected for postlake hydroisostatic rebound (Currey and Oviatt, 1985), it is estimated that Lake Bonneville spilled into Puddle Valley and created the inflow bar about 25.8 ka and that the two basins re-isolated no later than about 12.2 ka.

[end of contribution from D. Sack]

Marl exposed in the wall of the gravel pit east of the Puddle Valley threshold (fig. 13) is the upper, or post-Stansbury, marl as shown by the ostracode faunas. This indicates that the spits and barriers in the vicinity of the pass (fig. 14), on which the marl rests, are pre-Stansbury or Stansbury in



Figure 13. Photo of gravel pit exposure at stop 2 (east of Puddle Valley threshold).

age, and that the catastrophic inflow to Puddle Valley is also pre-Stansbury or Stansbury in age. Cross-bedded sand at the base of the exposure is overlain by about 65 cm (2 ft) of sandy marl. A carbonate hard ground in the upper part of the marl may mark the stratigraphic position of the Bonneville flood—marl and sand above this contact are coarser grained, and contain gastropods typical of Provo and post-Provo deposits (*Stagnicola* [formerly *Lymnaea*] and *Pyrgulopsis* [formerly *Annicola*]). A sample of gastropods collected from the sand directly above the marl yielded a radiocarbon age of 16,620 yr B.P. (Beta-100449). This apparent age, which is several thousand years older than expected, is inconsistent with the interpretation based on independent stratigraphic information (lithology, ostracodes, gastropods), and suggests that at least some of the dated gastropod shells were reworked from older deposits.

The hypothesis that some of the shells might be reworked is supported by amino acid analyses of a subsample of the gastropod shells. Darrell Kaufman (Utah State University, unpublished data) found potentially two different age groups of shells for each of the two genera. For instance, the average ratios of allosoleucine to isoleucine for a total of twelve analyses are: for *Stagnicola*, (group 1) 0.113 ± 0.001 , $n=2$ and (group 2) 0.133 ± 0.006 , $n=4$; and for *Pyrgulopsis*, (group 1) 0.149 ± 0.002 , $n=4$ and (group 2) 0.164 ± 0.004 , $n=2$. Reworking was likely a common process in Lake Bonneville, especially in certain environments during the regressive phase of the lake, or during smaller-scale fluctuations.

Return to the paved road, reset mileage to zero, and turn right (north).

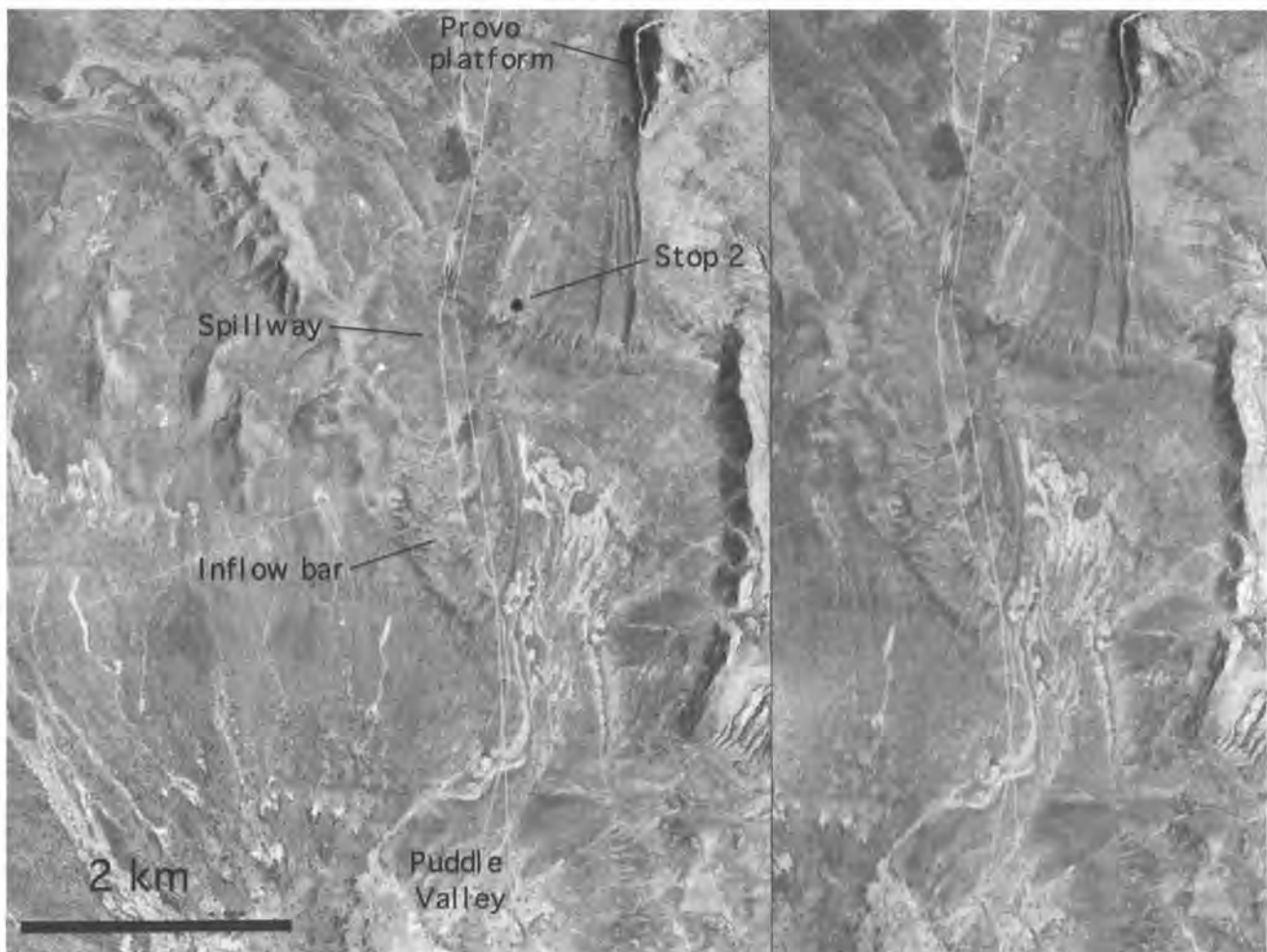


Figure 14. Stereo pair of Puddle Valley pass area. Aerial photographs were taken August 10, 1953.

- 0.5 Bear right on a gravel road. Paved road goes to military base.
- 7.5 The large tombolo on the skyline to the east is at an altitude between the Stansbury and Provo shorelines, just below the Provo.
- 8.4 Bear left at fork in road. Twin Hills (near Lakeside) lie in the distance to the north. Both have prominent Provo erosional platforms with sea stacks in their centers.
Homestead Knoll lies west of the road. Homestead and Cathedral caves, both in Homestead Knoll, have an important lacustrine and terrestrial record that is currently being studied by David Madsen (Utah Geological Survey) and colleagues.
- 12.9 Continue straight (north) on main road.
- 14.3 Turn right (east) on small gravel road toward pump house. Park about 150 ft past pump. Walk to edge of quarry (to the north).

STOP 3. Multiple barrier beaches at Lakeside quarry.

From the edge of the quarry, look east at the architecture and stratigraphy exposed at the east and south ends of the quarry where deposits of at least five lake cycles are exposed. The youngest of these is the Bonneville lake cycle, which is represented by a transgressive-phase gravel barrier overlain by the white marl. Underlying the Bonneville deposits is a sequence of at least four pre-Bonneville lacustrine units that are ripe for study (fig. 15).

Unit 1 is poorly exposed at the base of the east wall of the pit. It consists of coarse foreset gravel and minor carbonate mud that fills spaces between clasts. We know virtually nothing about the lake cycle created that it.

Unit 2 consists of horizontally bedded gravel that thickens to the south into foreset gravel of a barrier beach. On the lagoon side of the barrier, and exposed in a bench that trends west from the east wall of the pit, the barrier is conformably overlain by a marl unit that dips to the south (fig. 16). The



Figure 15. Photo of deposits on east wall of Lakeside gravel pit. Numbers refer to gravel units discussed in the text (under Stop 3).

marl is about 0.8 m thick, and grades upward into reworked lake deposits and lagoon fill about 1.5 m thick in which a calcic paleosol is developed. The paleosol is overlain by well sorted sand and gravel (unit 3?) of a younger lake cycle.

Ostracodes from the marl (fig. 16) suggest that the lake in which unit 2 was deposited may have reached a level no higher than levels equivalent to the Stansbury shoreline of Lake Bonneville. Only two species of ostracode are present in the unit-2 samples, *Limnocythere staplini*, and *Candona caudata* (?), and the assemblage is dominated by *L. staplini*. By comparison, this assemblage is found in the lower part of the Lake Bonneville marl, which was deposited before the lake reached the Stansbury shoreline. At lake levels higher than the Stansbury, the water chemistry changed, and other ostracodes begin to replace *L. staplini* (e.g., *L. ceriotuberosa*) (Forester, 1987; Thompson et al., 1990; Oviatt, unpublished data). Note that reconstructions of the Cutler Dam Lake cycle (~40–70 ka; fig. 2; Oviatt et al., 1987) suggest that it reached an elevation of no higher than about 4400 ft (1340 m), which is roughly the elevation of the low point of the Stansbury oscillation of Lake Bonneville. The highest level attained during the Little Valley Lake cycle (~150 ka) was an elevation between the Bonneville and Provo shorelines (of Lake Bonneville), and ostracode assemblages from marl of Little Valley age are more diverse (Oviatt, unpublished data). Therefore, the ostracodes in the unit-2 marl suggest that unit 2 was deposited in a relatively low pre-Bonneville lake, possibly of Cutler Dam age.

The lagoon sediments in which the paleosol is developed, and which overlie the unit-2 marl, can be traced to

the west across the floor of the pit, where they grade into silty lagoon fill that contains a white bed, 30–50 cm thick, of reworked fine-grained volcanic ash. Microprobe analyses of a sample of the ash suggest a correlation with one of the Mt. St. Helens ashes, which have been dated between ~40 ka and 150 ka (Mike Perkins, and Andrei Sarna-Wojcicki, personal communication, 1996). The possible correlates are a Mt. St. Helens C tephra, with a probable age between 40 and 50 ka, and another tephra from a core from Carp Lake, OR, with an age estimated between 75 and 125 ka.

Table 1 shows the results of amino acid analyses of ostracodes from the Lakeside unit-2 marl compared with results from deposits of known age in the Bonneville basin and elsewhere (analyses and data by Darrell Kaufman, Utah State University). The ostracode amino-acid data suggest a marl age older than Lake Bonneville (which is also clearly indicated by the overlying paleosol), and younger than the Little Valley lake cycle (about 150 ka; Scott et al., 1983). The amino acid ratios are similar to those for ostracodes from deposits of the Cutler Dam Alloformation, which was deposited sometime between 40 and 70 ka (figure 2; Oviatt et al., 1987). If the correlation with the Cutler Dam Alloformation is correct, the overlying paleosol is probably correlative with the Fielding Geosol (Oviatt et al., 1987). Further refinements to the basin-wide chronology of the Cutler Dam lake cycle, and tests of the hypothesis that unit 2 in the Lakeside gravel pit is Cutler Dam in age, are needed.

Units 3 and 4 are gravels that overlie unit 2 in the east wall of the pit, and also thicken to the south into foreset gravel. Each of the gravel units in the east wall, except unit 3, has a boulder or cobble lag at its top, which was probably

deposited by waves during the regressive phase of that lake cycle or during the transgressive phase of the succeeding lake cycle. A thin (~10 cm) fine-grained unit between units 3 and 2 may be composed of eolian silt. Units 3 and 4 have not been dated and nothing is known about the sizes of the lakes in which they were deposited.

Bonneville deposits (unit 5) at the top of the sequence also consist of horizontally bedded gravel in the east wall, but can be traced to the south into foreset gravel of a barrier beach. Although the gravel barrier has not been dated directly, it is near the right elevation (4300 ft; 1310 m) to be possibly equivalent to the transgressive-phase Pilot Valley shoreline. Most of the gravel barrier has been removed, but the Bonneville marl on the back (lagoon) side of the barrier is well exposed.

Ostracodes from the Bonneville marl in the Lakeside gravel pit permit correlations with typical white marl sections elsewhere in the Bonneville basin, and demonstrate that although the marl on the barrier is thin and sandy, it has some similarities with other marl sections. For instance, the ostracodes at the base of the section consist primarily of *Limnocythere staplini*, which is typical of pre-Stansbury marl (~25–~22 ka), and the ostracodes near the top of the section are typical of deep-water phases of Lake Bonneville (fig. 4). A thin carbonate crust about halfway up in the marl may represent the abrupt contact at the base of the Bonneville flood bed, and would therefore date to approximately 14.5 ka. However the crust probably formed long after deposition of the section; secondary carbonate precipitated at the contact between the less permeable sediments below, and the sandier, finely bedded marl above. We observed a similar carbonate crust at the Bonneville Flood contact at the Puddle Valley gravel pit. At the Lakeside gravel pit, however, the carbonate crust marks a level in the marl between deposits of approximately Stansbury age and deposits of Provo age, as determined from the ostracodes. Therefore, it appears that the massive marl deposited during the deepest-water phase of Lake Bonneville is missing from this section.

Return to gravel road, reset mileage to zero, and turn north.

- 0.3 Lakeside—Turn left along base of hill. Pass large quarry on left.
- 0.7 Turn right and cross railroad tracks.
- 0.8 Turn left parallel to railroad tracks. This road is *private property* and its use must be cleared with Southern Pacific Railroad.
- 11.7 Pump station and canal. This system was built in 1986 to pump flood water from Great Salt Lake westward to the Great Salt Lake Desert, where it would increase evaporation. The plan was successful in that it helped lower the lake faster



Figure 16. Photo of older marl (unit-2 marl) at Lakeside gravel pit. Ostracode samples are lettered (D = Ls, C = Ls, B = Cc, Ls, A = Ls, Cc). See figure 4 for explanation of abbreviations.

than it would have on its own. Reduced precipitation and increased evaporation, starting in 1987, further ensured the lake's decline to less destructive levels. Excellent exposures along the canal walls illustrate Holocene, Lake Bonneville, and pre-Bonneville deposits, as well as Miocene and Paleozoic strata and the faults affecting those older strata.

- 13.9 Bear right on dirt road.
- 14.1 Make acute right turn toward the north. BLM sign on the road reads: "Kelton 41 mi."
- 15.1 Stop along road where quarry edge on left is cut by gully.

STOP 4. Pilot Valley shoreline.

This long (6.2 km) narrow quarry, which was developed by the railroad in the early part of the 20th century to build the Lucin cutoff, beautifully displays a series of beach ridges that extend along the south flank of the Hogup Mountains (fig. 17). The beach gravels lie on loess and alluvium in which a paleosol is developed (exposed in three places in the west half of the quarry) and are overlain by Bonneville marl, and therefore are early transgressive Bonneville features. They represent the earliest regionally correlatable beaches of Lake Bonneville, informally termed the Pilot Valley shoreline by Miller (1990). Here and elsewhere, the shoreline is marked by a set of two to four beaches that climb from about 4275 to 4295 ft in altitude, with maximum development typically at 4285 ft.

Here we examine some gully exposures on the back (lagoon) side of a barrier where the white marl lies on beach

Table 1. Amino acid ratios for ostracodes (Candona and Limnocythere) from deposits of various ages. Analyses and data provided by Darrell Kaufman, Utah State University.

Lab No.*	Lake Cycle (age, ka)	Locality	Asp [†]	Glu [†]	Ala [†]	Ile [†]
<i>Candona</i> results:						
2030	post-Provo (12)	Fielding	0.196 ± 0.017 (2)	0.048 ± 0.007	0.075 ± 0.013	0.034 ± 0.012
2047	Bonneville (19)	Black Rock	0.275 ± 0.008 (10)	0.086 ± 0.005	0.172 ± 0.008	0.075 ± 0.008
2046	Bonneville (21)	Little Valley	0.300 ± 0.010 (10)	0.080 ± 0.007	0.184 ± 0.013	0.091 ± 0.015
2042	Bonneville (~25)	West Gully	0.299 ± 0.011 (9)	0.082 ± 0.009	0.194 ± 0.023	0.095 ± 0.014
2096	Bonneville (?)	Bear River	0.237 ± 0.005 (5)	0.062 ± 0.009	0.147 ± 0.005	0.075 ± 0.011
2041	Cutler Dam (~40?–70?)	West Gully	0.308 ± 0.025 (2)	0.125 ± —	0.361 ± 0.037	0.114 ± —
2095	Cutler Dam (~40?–70?)	Bear River	0.292 ± 0.015 (6)	0.079 ± 0.009	0.230 ± 0.029	0.099 ± 0.019
2036	unit-2 marl (age ?)	Lakeside	0.325 ± 0.038 (4)	0.106 ± 0.025	0.284 ± 0.062	0.096 ± 0.054
2032	— (~70)	Anna River, OR	0.304 ± 0.013 (9)	0.124 ± 0.017	0.223 ± 0.036	0.096 ± 0.014
2043	Little Valley (~150)	West Gully	0.481 ± 0.030 (8)	0.175 ± 0.015	0.424 ± 0.033	0.184 ± 0.039
2037	Little Valley (~150)	Little Valley	0.417 ± 0.010 (7)	0.194 ± 0.013	0.478 ± 0.021	0.233 ± 0.041
2056	— (~150 ka)	Anna River, OR	0.374 ± 0.012 (9)	0.160 ± 0.010	0.392 ± 0.024	0.271 ± 0.086
<i>Limnocythere</i> results:						
2103	Bonneville (~25)	West Gully	0.242 ± 0.006 (6)	0.043 ± 0.002	0.127 ± 0.002	0.024 ± 0.002
2101	Cutler Dam (~40?–70?)	West Gully	0.223 ± 0.012 (5)	0.066 ± 0.005	0.192 ± 0.013	0.026 ± 0.003
2148/49	unit-2 marl (age ?)	Lakeside	0.296 ± 0.040 (10)	0.092 ± 0.092	0.247 ± 0.070	0.037 ± 0.013
2102	Little Valley (~150)	West Gully	0.325 ± 0.015 (5)	0.103 ± 0.007	0.288 ± 0.010	0.061 ± 0.007
2107/50	Little Valley (~150)	Little Valley	0.359 ± 0.021 (10)	0.139 ± 0.019	0.388 ± 0.031	0.132 ± 0.039

*All samples were analyzed by Darrell Kaufman at the Amino Acid Geochronology Laboratory at Utah State University; therefore, each lab number has the prefix UAL-, e.g., UAL-2042. The samples were analyzed using a new reverse-phase HPLC procedure which is presented in Kaufman and Manley (in review)

[†]DL ratios and standard deviations for aspartic acid (Asp), glutamic acid (Glu), and alanine (Ala), the ratio value for isoleucine (Ile) is D-alloisoleucine L-isoleucine (alle/Ile). Numbers in parentheses indicate number of separate subsamples prepared from each sample. Each subsample was composed of 0.1–0.2 mg of ostracodes (10–40 individuals)

gravel. The marl represents most of the Bonneville lake history, as confirmed by stratigraphy and ostracode study (fig. 17). The marl is about 6 ft (2 m) thick, and overlies gravel and coarse oolitic sand of the barrier complex (fig. 17). Ostracodes from the marl permit correlations with other marl sections in the Bonneville basin. An abrupt contact overlain by sandy marl probably represents the Bonneville flood contact (based on its field appearance and the ostracode faunas).

Internal unconformities within the barrier-beach gravels may owe to overlapping beach development here. Figure 18 shows two well-developed beach ridges; stop 4 is in the lower one, which clearly predates the white marl. Stratigraphic relationships for the upper beach ridge are unclear (that is, exposures do not indicate whether the marl overlies it or underlies it), so it could be either a Pilot Valley, or Gilbert beach.

These gravel beaches are the earliest widely developed beaches recognized for Lake Bonneville, and have been

tracked across the northern Bonneville basin from Pilot Valley to the Rozel Hills (fig. 19). If they can be identified in other parts of the basin, they can serve as an important leveling marker because they formed so early in Lake Bonneville's history that little isostatic deflection should have taken place before their development.

Reset mileage to zero and continue on gravel road to the northwest.

- 0.9** Climb to crest of uppermost gravel beach of the Pilot Valley shoreline in this location; altitude is between 4285 and 4290 ft.
- 8.1** Cross Provo shoreline, expressed as two barrier beaches.
- 9.3** Cross tombolos below the Bonneville shoreline. The Bonneville is visible to the east and west of the tombolo. Tremendous Bonneville and Provo spits are visible to the north along the skyline.

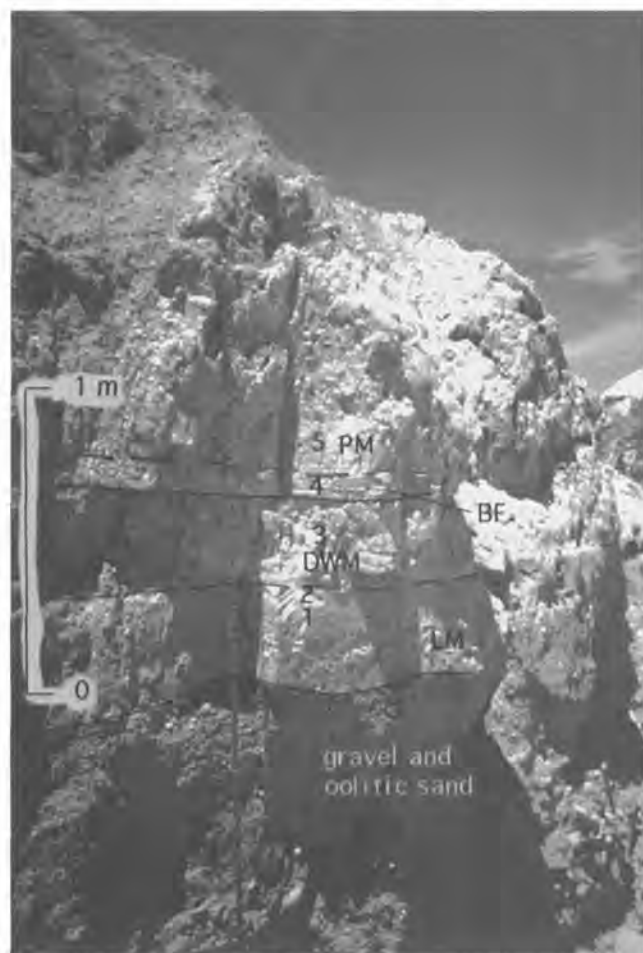


Figure 17. Photo of marl section at stop 4 (Pilot Valley shoreline). LM = laminated (transgressive) marl; DWM = deep-water marl; BF = Bonneville flood bed; PM = Provo marl. Ostracode samples are numbered (5 = Ca, Lc, 4 = Lc, Cc, Cd, Ca/c, 3 = Lc, Cc, 2 = Cc, Lc, Ls, 1 = Cc, Lc, Ls). See figure 4 for explanation of abbreviations.

These form the upper part of a feature called the Fingerprint, which we will cross after STOP 5.

- 9.4 Bear right at intersection.
- 9.6 Turn right on road to the Fingerprint and Kelton.
- 10.3 Cross Provo shoreline.
- 15.5 Park on right side of road after dropping down off the Gilbert beach. Walk southeast to the breach in the barrier beach.

STOP 5. Stratigraphy at the Gilbert shoreline (at the Fingerprint).

The exposure at stop 5 is a good contrast to the sequence at the Pilot Valley shoreline stop (stop 4). At stop 5, the white marl, which consists of a typical lithologic and ostra-



Figure 18. Area of Stop 4 shown on aerial photograph taken October 21, 1969. Small white arrows point to major gravel beaches. Linear gravel pit climbs northwestward from lower to upper beach. Area represented by photo is approximately 3.8 km wide.

code sequence, is overlain by gravel of a barrier beach indicating that the beach is regressive. The beach is interpreted as a local segment of the Gilbert shoreline because it has an appropriate elevation (4271 ft) and relative age (post-Bonneville). Gravel beneath the white marl at the Fingerprint stop is transgressive in age and approximately the same age as the Pilot Valley shoreline.

The white marl at this stop is somewhat different in appearance from the marl at other locations because it was deposited in a site that had considerable wave energy. Consequently the section overall is relatively sandy, and there are clean sand beds interspersed with the marl (figs. 20 and 21). We interpret the sand beds as turbidites, possibly generated by slumps off the large spits of the Fingerprint at higher elevations. Nevertheless, the ostracode sequence is easily correlated with that of other Bonneville sections (fig. 4).

Data on the total carbonate, carbonate mineralogy, and sand content of a short core collected at the outcrop are presented in fig. 21. Note the abrupt increase in aragonite above the Bonneville Flood contact. Also note that the

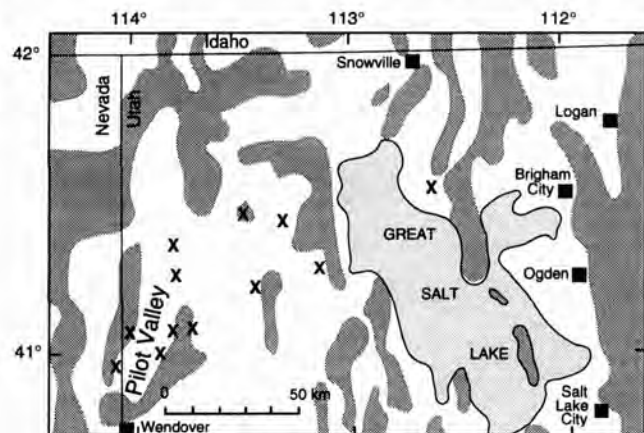


Figure 19. Map showing known localities of the Pilot Valley shoreline in NW Utah.

aragonite curve peaks after the total carbonate curve peaks. Similar trends have been noted in other white marl cores, including those described by Spencer et al., (1984) from the Great Salt Lake, who interpreted the rise in aragonite as having been caused by the increase in Mg/Ca ratio—Ca was quickly used up in the precipitation of carbonates as the lake evaporated to lower and lower levels at the end of the Bonneville regression.

Reset mileage to zero. We will drive to Utah Route 30 and then to Tremonton for the end of Day 1. Continue northeast on gravel road.

0.6 Crest of the Fingerprint. Continue north toward Kelton. The Fingerprint is a 9.5-mile long feature extending south from the Hogup Mountains as a series of platforms and beach ridges that represent every major shoreline of Lake Bonneville and many more local shorelines (fig. 22). Looking upslope along the Fingerprint, several huge gravel prominences mark spits and V-shaped barrier beaches that can be found by driving in that direction. Downslope, the Fingerprint extends southward to end in several recurved beaches, the lowest of which is the sand and gravel beach that formed during 1986–1987. Although some bedrock control for this enormous feature probably existed, the Fingerprint is composed entirely of gravel in surface exposures. This is one of the more impressive examples of enormous volumes of gravel transported by Lake Bonneville and its predecessors.

1.0 Bear right at fork in road.

3.1 Dolphin Island to the east is surrounded by mud flats. The high part of this island is com-



Figure 20. Photo of marl section at stop 5 (the Fingerprint). DWM = deep-water marl; BF = Bonneville flood bed; PM = Provo marl. The marl section is underlain by transgressive Bonneville gravel, and overlain by regressive gravel of the Gilbert shoreline.

posed of beachrock composed of cemented angular clasts of the Oquirrh Formation. Tails of lacustrine and eolian oolitic sand extend southward from the island.

16.6 Climb across a Gilbert barrier beach and across a large double tombolo connecting the mainland (Hogup Mountains) to an island (Crocodile Mountain).

23.2 The basalt-capped butte on the left is Table Mountain. The basalt is probably Pliocene (Miller et al., 1995).

24.2 Bear right (east) at the intersection.

26.8 Continue straight through crossroads. Kelton cemetery is on the right.

26.9 Townsite of Kelton. Bear left. Kelton was a major railroad depot on the original transcontinental railroad across the Great Salt Lake basin before the Lucin cutoff was built in 1904.

27.1 Continue straight at road junction. Follow signs to State Rte. 30.

30.1 Route 30. Turn right to Curlew Junction, turn right at Curlew Junction, and follow Rte. 30 to I-84 (16 miles). Follow I-84 east to Tremonton.

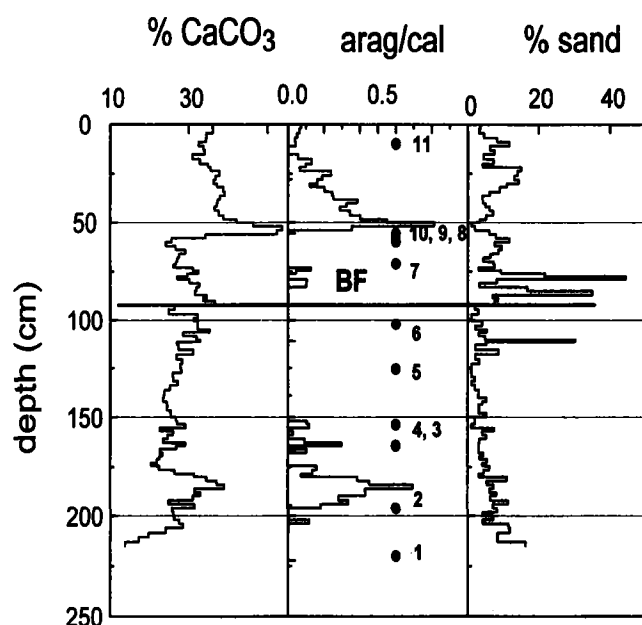


Figure 21. Lab data for a core through the marl section at stop 5. BF marks the base of the Bonneville flood bed in the core. Ostracode samples are numbered (11 = Lc, C. sp., 10 = Ca², Lc, 9 = Ca, Cc, Lc, Cyl, 8 = Ca, Lc, Cyl, 7 = Ca, Cc, Lc, 6 = Lc, Ca², 5 = Ca, Lc, 4 = Lc, Cc, Ca, Ls, 3 = Lc, C. sp., 2 = Lc, Cc, Ls, 1 = Cc, Ls). See figure 4 for explanation of abbreviations.

DAY 2

Travel west from Tremonton on I-84. We will cross several basins and ranges on the freeway, and then return eastward at lower altitudes nearer to Great Salt Lake.

Mile 37. Exposures of Lake Bonneville gravel in the large quarry pits on the north side of the freeway display the bewildering complexity of the beach gravels, including strongly cemented beds, and a variety of foresets and backsets. This gravel is probably mostly of Stansbury age.

Mile 34. Cross Provo shoreline as we climb the Blue Springs Hills. A barn is on the Provo platform on the north side of the freeway.

Mile 26. Cross Provo shoreline as we descend into Blue Creek Valley.

Mile 22. Cross Provo shoreline where it forms an extensive platform of sand and gravel in central Blue Creek Valley. Exposures near here, where Blue Creek gullied across the Provo barrier, display outstanding examples of rhythmically bedded near-shore sands, old alluvial units and paleosols, and a thick section of older (Little Valley lake cycle) marl.

Mile 18.3. Cross Bonneville shoreline.

Mile 17. Rattlesnake Pass. Black basalt K-Ar dated at 13.0 ± 0.3 Ma (unpublished USGS data) is exposed in the

roadcuts. Ahead about 1.5 miles, another roadcut exposes the same basalt flows. There, loess deposits lying on the basalt apparently are those that yielded middle Pleistocene rodent fossils (C.A. Repenning, oral communication., 1989). The loess contains several strongly developed calcic soil horizons. Normal faults at the west side of the roadcut displace basalt down to the west, and also cut a different (younger?) loess with less soil development.

Mile 16. A fault is well exposed on the north side of the freeway in the road cut. The fault places Miocene basalt against the late Paleozoic Oquirrh Formation.

Mile 13. Cross Bonneville shoreline.

Mile 9. Cross Provo shoreline as we descend into Curlew Valley.

Mile 5. Take exit and turn left (west) across the freeway. Set mileage to zero on overpass.

0.5 Turn left on small gravel road and through metal gate. (Permission required at Rose Ranch).

0.8 Proceed through corral.

0.9 Stop next to cut bank of gully on right. Walk about 100 ft west to a place to descend the bank to the gully floor, and east along the base of the wall to study the Lake Bonneville section.

STOP 6. Rose Ranch Section.

Exposures directly downstream from Rose Ranch Reservoir expose a complete Bonneville stratigraphic section at an elevation (4505 ft; 1373 m) close to the Stansbury shoreline. We will examine a section exposed near the north abutment of the dam where the base of the Bonneville section is not exposed. The base of the section can be seen by walking south across the dam to the south bank of Deep Creek, where a strongly developed calcic horizon, developed in loess, is exposed beneath the Bonneville sequence.

Ripple-laminated to massive fine sand at the base of the Bonneville section (fig. 23) is overlain by about 0.75 m of brown, blocky mud with oxidized root holes, probably deposited in deltaic or marsh environments in the estuary of Deep Creek as Lake Bonneville began to rise at the end of the Stansbury oscillation about 20 ka. The blocky mud is overlain by 1.4–0.75 m of laminated sandy marl, then 2.8–1.4 m of pink massive marl. A finely bedded sandy marl unit about 12 cm thick in the upper third of the massive marl may represent deposition during a fluctuation during the transgressive phase higher than the Stansbury shoreline (such as U1, fig. 5). An abrupt contact at the top of the massive marl is marked by pebbles and sand and overlain by white marl about 1.2 m thick. The modern soil is developed in this unit. We interpret the abrupt contact as the Bonneville flood contact based on its abruptness and on the appearance of the ostracode *Cytherissa lacustris* in the marl above it (fig. 4).

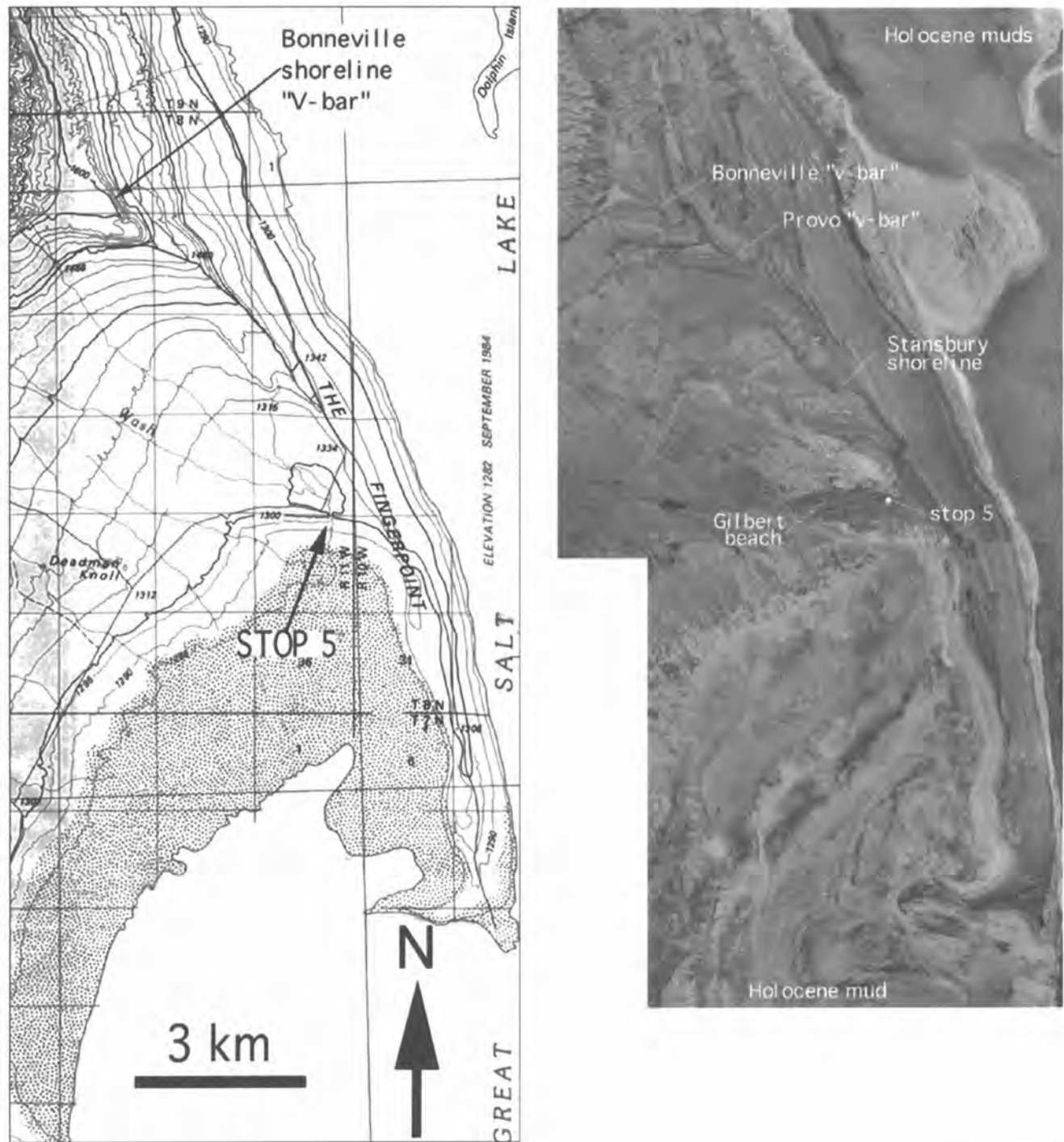


Figure 22. Map and aerial photographs of the Fingerpoint, showing roads and shorelines. Aerial photographs taken June 22, 1953. Map from U.S. Geological Survey 1:100,000-scale Newfoundland Mountains quadrangle, 1988. Contours in meters, interval 20 meters.



Figure 23. Photo of Rose Ranch marl section at stop 6. BBM = brown, blocky mud; LM = laminated (transgressive) marl; DWM = deep-water marl; BF(?) = possible Bonneville flood bed; PM(?) = possible Provo marl. Numbered ostracode samples (8 = Cc, Lc, Ce², 7 = Cyl, Cc/a, Cc, Lc, 6 = Lc, Ca, Cyl, 5 = Lc, Lsa, Cc/a, Ls, 4 = Ca, Lc, Cc, 3B = Ca, Lc, Cc, Ce², 3A = Ca, Lc, Cc, Ce², 2 = Ls, Cc, 1 = Cr, Ls). See figure 4 for explanation of abbreviations.

Here, and elsewhere in Curlew Valley, much of the marl section is preserved and locally exposed in gullies (Miller and Langrock, 1997a), an unusual occurrence in the Bonneville basin. A combination of factors probably led to this situation: (1) Deep Creek fed fine clastic material to the lake that led to fairly thick marl accumulations. (2) The low-gradient valley was not extensively eroded following lake withdrawal. (3) Deep Creek deeply entrenched the marl plains, and did not deposit appreciable sediment on the marl.

Return to vehicles and retrace route to I-84; enter freeway headed east.

Mile 7. Snowville exit. Exit the freeway and set mileage to zero at stop sign. Turn right (south) on paved road, then immediate right onto gravel road. Continue on main gravel road.

6.3 Proceed south past road to left.

9.6 View of Cedar Hill, a shield volcano about 1.2 million years old, on the west (Miller and Langrock, 1997b). On the east is Johnson Hill, etched by a prominent Provo shoreline. Johnson Hill lies between Curlew Valley and Sage Valley, a small internally-drained valley. Sage Valley drained abruptly, creating a small sand blanket projecting into Curlew Valley. Erosion caused by the rapid draining, apparently during the rapid regression from the Provo shoreline, truncated several shorelines.

13.2 Park on the barrier beach and look at the quarry on the west side of the road.

STOP 7. Stansbury shoreline and Quaternary volcanoes.

Barrier beach deposits form a prominent shoreline here and mark the upper Stansbury shorezone. A benchmark on the east side of the road on the beach crest is 4497 ft (1370 m). Structure within the barrier beach can be examined in the quarry walls on the west side of the road.

From at least 1.2 million years to 440,000 years ago basalt erupted intermittently to form the three shields along Curlew Valley just west of us, from Cedar Hill on the north to Locomotive Springs well to the south (fig. 24) (Miller and Langrock, 1997b). In addition, basaltic ash (the Hansel Valley ash) was erupted from an uncertain location west of Hansel Valley and probably in Curlew Valley, on the basis of chemical similarity with Curlew basalts and the location of the ejecta blanket (Miller et al., 1995). K-Ar ages for the shields are 1.16 ± 0.08 , 0.72 ± 0.15 , and 0.44 ± 0.10 Ma from north to south (Miller et al., 1995). The two northern shields retain summit collapse features, and individual flows can be traced down the flanks. The southern shield is small and may have been eroded more by waves of pluvial lakes; it shows only a flat summit that may once have been a crater. The Quaternary shield volcanoes of eastern Curlew Valley are similar in mineralogy and geochemistry but decrease systematically in age southward toward the Great Salt Lake, suggesting a progressive movement of an eruptive center with time, at a rate of about 2.1 cm/year. The recurrence of eruptions in this system is not well determined, but the volcanoes seem to have formed every 300,000 to 400,000 years. If the Hansel Valley ash is considered to be a minor event, the next large eruption is possible at any time (Miller et al., 1995) and may be located in Great Salt Lake. Such an eruption could severely impact the Wasatch Front population.

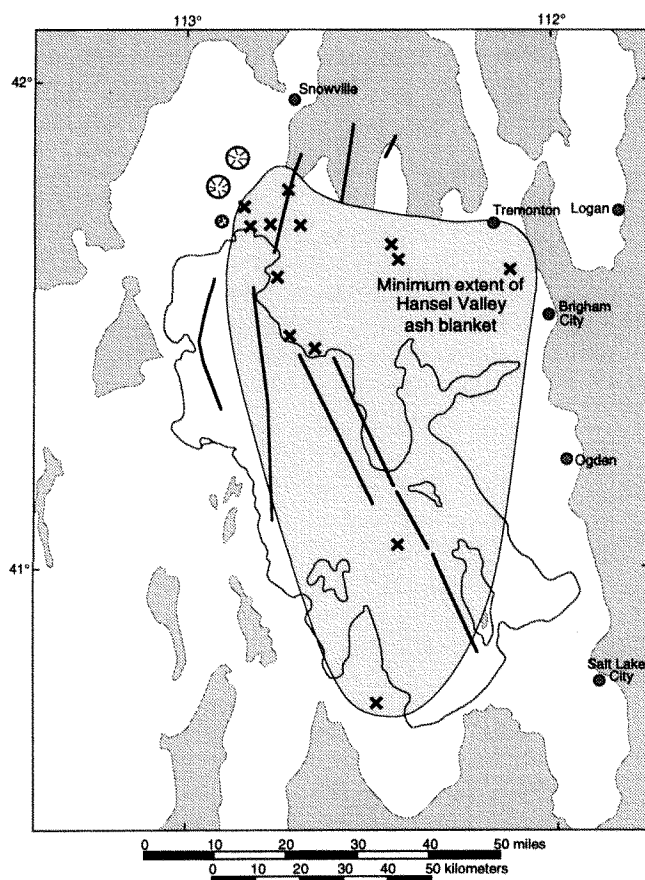


Figure 24. Selected volcanic features and faults of the Great Salt Lake area. X, Hansel Valley ash location. Volcanoes in Curlew Valley shown by circles with radiating lines. Faults shown are all Holocene.

The Hansel Valley ash has been identified in one exposure in eastern Curlew Valley and in roughly a dozen exposures to the east and southeast in Hansel and Blue Creek Valleys, the Rozel Hills, and at the Bear River (figs. 9 and 24). It also has been identified in cores from the south arm of Great Salt Lake (Spencer et al., 1984; Oviatt and Nash, 1989), and the Burmester core at the south margin of the lake. The explosive eruption that distributed the Hansel Valley ash likely was caused by interaction of magma with water in the near surface or at the surface. A source within water-charged lowlands of Curlew Valley or within Lake Bonneville is likely, but we have not yet discovered a tephra ring, coarse proximal deposits, or other indicators of the eruptive vent despite extensive field work. It is possible that the Hansel Valley ash eruption was triggered by the load of Lake Bonneville; several basaltic volcanoes in the Sevier Desert erupted into Lake Bonneville (Oviatt and Nash, 1989).

Reset mileage and proceed south on gravel road.

- 1.4 The shield volcano on the west is about 720 ka.
- 2.4 The low basalt hill to the east of the road is blanketed by Bonneville marl. The Hansel Valley ash is at the base of the marl.
- 5.0 Cross Gilbert shoreline. It is a low spit on the west that increases in prominence eastward toward Monument Point.
- 6.1 Turn left on gravel road just north of the old railroad grade. Locomotive Springs shield volcano (~440 ka) lies to the south (Miller and Langrock, 1997c).
- 8.2 Proceed across a Holocene Great Salt Lake barrier beach at about 4240 ft altitude. It postdates the Gilbert shoreline, but is otherwise undated.
- 10.3 Proceed past Monument Point (see Miller and Langrock, 1997d). By driving south toward Lone Rock, a good section of marl, including the Hansel Valley ash at the base, can be examined along wave-cut bluffs formed by Great Salt Lake during the highstands of 1986 and 1987.
- 14.1 Bear left at fork.
- 15.2 Climb onto Gilbert barrier beach from Gilbert erosional notch.
- 16.1 Gilbert barrier beach visible to south of road. Its crest is slightly above 4260 ft. To the east, it merges with the level of the road.
- 17.0 Stop on road.

STOP 8. Faulted Gilbert spit.

This stop is at a degraded scarp created by the 1934 Hansel Valley earthquake and previous faulting events. The Hansel Valley fault has displaced the surface of the Gilbert spit down to the east. The fault strikes slightly east of north, and its scarp is visible north of the road for some distance. In the mud flats south of the road, the mud was cracked and mud volcanoes formed in 1934, but only scattered evidence for the location of the fault can be seen now. The 1934 Hansel Valley earthquake is the only historic ground-rupturing seismic event in northern Utah, despite the highly active seismicity of this region (Christenson et al., 1987). Historic felt earthquakes include the magnitude 6 and larger events in Hansel Valley during 1909 and 1934 (Arabasz et al., 1994). Frequent smaller-magnitude earthquakes ($M < 4$) occur in broader zones in the area, including Blue Creek, Hansel, and Curlew Valleys, and northern Great Salt Lake and the Rozel Hills (Christenson et al., 1987).

The March 1934 magnitude 6.6 earthquake in Hansel Valley (Christenson et al., 1987) produced surface rupture along four zones, of which the zone where we stopped had as much as 20 inches of down-to-the-east offset. Some of the faults, including this one, show evidence for earlier dis-

placements (Robison and McCalpin, 1987). The earthquake caused severe damage in local towns and ranches, and it even caused damage in cities along the Wasatch Front. The evidence for repeat faulting at this location makes it clear that a threat for future earthquakes is real, but the pattern of recurrence is complex and not easily converted as a predictive tool. The recurrence interval *appears* to be several thousands of years.

Significant subsidence was noted by two types of studies following the 1934 earthquake. Adams (1938) compared by triangulation the nearby shoreline of Great Salt Lake in November 1934 to the shorelines surveyed by Captain Stansbury in 1850. Despite the lake being 6 feet lower in 1934 than in 1850, the shorelines overlapped. Adams concluded that about 4 feet of general subsidence of southern Hansel Valley took place between 1850 and 1934, with subsidence locally as great as 6 feet. Complications caused by causeways and dikes constructed after 1850 were not accounted for, but Adams showed that soundings and shorelines indicated little subsidence farther south in the lake. Adams (1938) also described the results of re-leveling the railroad grade across the mouth of Hansel Valley. Comparing 1911 and 1934 surveys, ground subsidence was 1.2 feet in lower Hansel Valley and could be identified to the west for 10 miles into Curlew Valley at diminished magnitude. These data suggest that only about one quarter of the 84-year subsidence record was produced during the Hansel Valley earthquake of 1934. A 1953 railroad levelling showed regional *uplift* of this same area west from the Hansel Valley fault (Bucknam, 1979).

Another potentially profitable approach for examining the neotectonic record would be to carefully level lake-shore features, such as the Gilbert spits, beaches, and abrasion platforms. Such a study could identify long-term subsidence and uplift relative to regionally established elevations for these features. A reconnaissance analysis of topographic data suggests that the west side of this fault is upthrown; elevations for the Gilbert spit and the 4240-ft shoreline to the east of the fault are consistent with regional values. Significant subsidence to the south, identified by comparing Great Salt Lake shorelines, may be a related but different manifestation of local tectonics. Careful study of shorelines since aerial photographs and satellite surveys began could address this problem over a time-span of several decades.

The Gilbert spit begins at about this location and extends to the east about two km. Wave energy from the southwest carried gravel northeast during the Gilbert lake's highstand to create this spit. As we drive east along the spit note the rapid drops of the surface to lower altitudes as we approach its terminus; these lower-altitude spits formed during regression from the Gilbert highstand or as other lake rises built onto the Gilbert spit. The 4240-ft shoreline is con-

structed along the front of the Gilbert spit in many places, and forms much of the end of the spit.

Reset mileage to zero and continue east.

2.4 Bear left at intersection. Elevation of the spit surface is 4242 ft here.

3.6 Stop along main road next to obscure road on right in greasewood plain. Take care not to drive in the greasewood; it destroys tires! Walk about 1 mile along this obscure road and continue into Hansel Valley Wash as road ends. The first half mile of the wash has been modified by bulldozer, but eventually the wash turns to its original northeasterly orientation. Proceed up this original wash several hundred feet until the marl section is about 3 m thick as exposed in walls on the east side of the gully.

STOP 9. Hansel Valley Wash.

This marl section is notable for several features, including: (1) its lateral continuity for several km along Hansel Valley, (2) presence of the Hansel Valley ash near the base, and (3) soft-sediment disruption of the marl, possibly induced by seismicity.

The Bonneville section at this stop is fairly complete because it was deposited on a low gradient valley floor at a relatively low elevation (4330 ft; 1320 m). Here we can observe the sequence of facies changes in the marl that can be seen at many similar sections around the basin. Coarse-grained deposits at the base of the section are interpreted as marking the initial transgression of Lake Bonneville (fig. 25). The coarse sand grades upward into blocky mud that contains oxidized root holes; we interpret this unit as having been deposited in a marsh or lagoon environment at the margin of the transgressing lake. Overlying the transgressive deposits is a sequence of laminated marl 3.2 ft (0.98 m) thick (early-transgressive and Stansbury), which grades upward into more massive, greenish gray to pink marl about 4 ft (1.3 m) thick (deep-water marl). The upper contact of the massive marl is abrupt and the overlying bed of ripple-laminated sand and sandy marl is about 0.4 ft (12 cm) thick (the Bonneville flood bed). Its upper contact is gradational into another massive marl (Provo marl), which coarsens upward and is disrupted in its upper part by modern soil development. Ostracodes and diatoms (fig. 25) support the interpretation of this sequence as a cycle, representing the transgression, deep water, and regression of Lake Bonneville.

One thing to speculate on at this section is the origin of the ripple-laminated beds in the Bonneville flood bed (the 12 cm thick bed between the two massive marls). Our interpretation is that during and immediately after the Bonneville flood, when lake level dropped catastrophically



Figure 25. Photo of Hansel Valley Wash marl section (stop 9). T = transgressive mud and sand; LM = laminated (transgressive) marl; DWM = deep-water marl; BF = Bonneville flood bed; PM = Provo marl. Lettered ostracode and diatom samples. Ostracode samples: W = Cyl, Ce, Ca, Lc, Lsa, V = Ce, Cc, Ca, Lc, U = Cc, Ce, Ca, LcLsa, T = Lc, Cc, Ca, Ce, S = Lc, Ls, Ca, Cc, R = Lc, Ca², Q = Lc, Ca, Cc, P = Ca, Lc, O = Ca, Lc, N = Ca, Lc, M = Lc, Ca, L = Lc, C sp., K = Lc, Cc, Ca, Cd, J = Lc, Cc, Ca, Cd, I = Lc, Cc, H = Lc, Cc, Ls, G = Cc, Ls, F = Cc, Ls, E = Ls, Cc, D = Ls, C sp., C = Ls, B = Ls, A = no ostracodes. See figure 4 for explanation of abbreviations. Diatoms from Hansel Valley Wash section identified by Platt Bradbury, May 27, 1992: W = *Cyclotella ocellata* (cold open water), V = *Synedra acus* (fresh open water), S. ulna, *Cyclotella ocellata*, C. caspia??, *Fragilaria brevistriata*, F. leptostauron, C-G = *Fragilaria brevistriata* (shallow, moderately saline water), F. construens v. subsalina, *Epithemia*, *Mastogloia*, *Navicula*, *Amphora*, *Surirella*, *Pinnularia*, others.

by about 100 m, vast areas of fine-grained lake-bottom sediments would have been stranded above lake level between the Bonneville and Provo shorelines. That sediment would have begun washing into the lake immediately after the flood (accounting for the thick marl and clastic deposits directly below the Provo shoreline throughout the basin, which we refer to as the Provo "dump" as per Don Currey), and provided a source for slumps and landslides that would have created turbidity currents on the lake bottom. In Hansel Valley, slumping of fine-grained sediments both above and below lake level might have been enhanced by earthquake activity.

Two cm above the base of the laminated marl is a thin (1 cm) bed of brown basaltic ash, which we have named the Hansel Valley ash (Miller et al., 1995) (formerly referred to as the "Thiokol ash" by Oviatt and Nash, 1989). We have found the Hansel Valley ash at many localities in northern Utah, including in the Burmester core at the south end of Great Salt Lake (Oviatt and Thompson, unpublished). At all known localities where the Hansel Valley ash has been found, including sediment cores from Great Salt Lake (Spencer et al., 1984), the ash bed is within a few centimeters of the base of the Bonneville section. A radiocarbon age of 26.5 ka for a core sample collected near the ash (Thompson et al., 1990) is the best available age for the eruption. Exposures in West Gully in Hansel Valley suggest that Lake Bonneville was close to an elevation of 4380 ft (1335 m) at the time the Hansel Valley ash was erupted. Despite extensive field efforts, we have not yet identified the source vent of the ash, but its chemistry is similar to that of basalts in the Curlew Valley area (Miller et al., 1995).

Note the common disrupted beds containing small faults and folds below and including the Hansel Valley ash. These features may have been caused by nearby small seismic events or larger distant events. Upstream several km, convoluted beds and hummocky cross-stratification are common in the section beneath the deep-water beds that lie below the flood bed. Robison and McCaipin (1987) suggested that these features indicate several local earthquakes, some of which displaced parts of the marl section in a tributary gully to Hansel Wash (referred to as West Gully).

Return to gravel road, set mileage to zero, and turn south.

- 0.9 Continue straight.
- 5.8 Pass shortcut on left.
- 6.5 Turn left on gravel road toward mud flat.
- 11.2 Double Gilbert barrier beach. Quarry pit on the right is in one of the beaches.
- 11.3 Continue straight. Route following the old railroad grade is to the right.
- 15.0 The Provo shoreline is expressed as wave-cut notches on both sides of the road.

- 16.4 Cross double Provo barrier beach. As in most places where the Provo shoreline is well exposed, it consists of two beaches about 10 ft different in altitude. Gilbert (1890) noted the double character of erosional segments of the Provo shoreline, but offered no explanation. Currey (Currey and Burr, 1988) has noted three or four steps in depositional Provo-shoreline segments at a number of locations around the basin, and suggests that landsliding and scour in the overflow threshold at Red Rock Pass, Idaho, complicated by ongoing isostatic rebound, controlled lake level throughout the basin during the development of the Provo shoreline. This hypothesis could be further tested by basin-wide mapping, careful geomorphic study, and surveying of the Provo shoreline.

The best available ages for the Provo shoreline suggest that it began forming after the Bonneville flood (14.5 ka), and that the lake overflowed at this level for 500 to 1000 years (Oviatt et al., 1992; Light and Kaufman, 1996). Overflow ceased and lake level began to drop rapidly between 14 and 13.5 ka.

- 18.4 Cross Bonneville barrier beach.
- 21.8 Intersection with paved road; *continue straight* on the paved road. Golden Spike National Monument, erected to commemorate the historic meeting of the transcontinental (Union and Central Pacific railroads), is to the right. We are driving along an unconformity cut into Miocene tuff during Pliocene time. Alluvial sediment on the tuff but beneath the Bonneville sediment yielded Pliocene fossils and volcanic ash (Nelson and Miller, 1990).
- 23.3 Transgressive-phase spits of Lake Bonneville are well exposed to the south, at the north end of the Promontory Mountains.
- 26.5 Junction; *continue straight*.
- 28.5 Junction with State Highway 83. Turn right toward Brigham City.
- 34.6 Stop on the right side of the road near exposures of red and brown sandy sediment of the marshes of Public Shooting Grounds.

STOP 10. Gilbert shoreline stratigraphy and chronology (Public Shooting Grounds).

At this stop we will briefly examine some exposures in roadcuts of sediments associated with the regression of Lake Bonneville and the transgression to the Gilbert shoreline. The road elevation is about 4230 ft (1289 m), for reference. The platform roughly at eye level throughout the

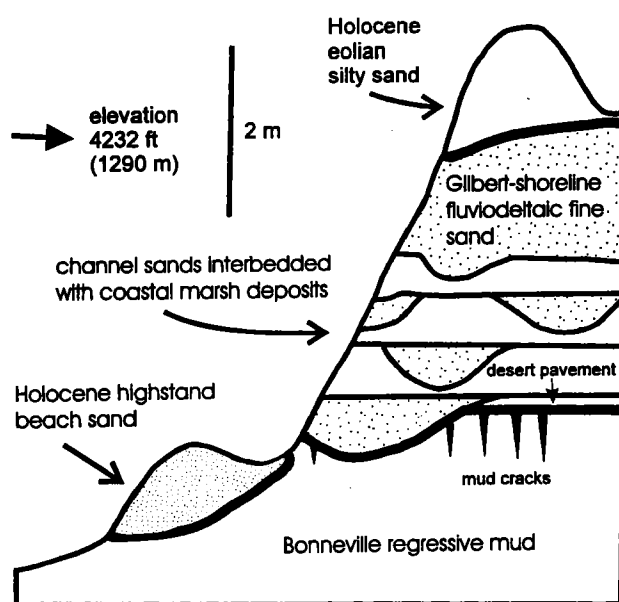


Figure 26. Generalized stratigraphy of road-cut exposures at the Public Shooting Grounds (stop 10). Modified from Currey (1990, fig. 15). Heavy lines represent unconformities. Radiocarbon ages of 10.9, 11.0, 11.6, and 12.0 have been obtained on samples of gastropods and organic-rich sediments from the channel sands and coastal marsh deposits, which were deposited prior to and during the Gilbert transgression (Currey, 1990).

marshes is a wave-cut surface left by the regression of the Gilbert lake. It is cut into a ~2-meter-thick deposit of lacustrine sand deposited by the Gilbert lake.

The general stratigraphic sequence in this area (fig. 26) has been described by Currey (1990). Reddish silty sediments at the base of the section are interpreted as late regressive-phase deposits of Lake Bonneville. These are overlain by gray, organic-rich mud and channel sands containing abundant molluscs, which have been dated at 11.9–10.9 ka (Miller et al., 1980; Currey, 1990). The organic-rich mud was probably deposited in a marsh environment, as suggested by the mollusk and ostracode faunas. Sand, interpreted as having been deposited during the transgression to the Gilbert shoreline (20 ft [6 m] above this site), overlies the marsh mud. The Gilbert shoreline was produced between 10.9 and 10.3 ka (Currey, 1990; Benson et al., 1992). All Holocene highstands of Great Salt Lake were lower than the Gilbert shoreline.

Reset mileage to zero and proceed east on Highway 83.

- 2.0 The Stansbury, Provo, and Bonneville shorelines are prominently displayed to the northeast on Little Mountain.
- 3.5 Putrid hot springs are common near the road as we drive along the base of Little Mountain. East

of Little Mountain, flats produced during the Gilbert regression merge with a broad, low-relief delta plain of the Bear River. East of the town of Corinne, the road drops to the modern flood plain of the Bear River. Bear River probably delivered the largest water and sediment influx to Lake Bonneville.

- 13.8 Turn left to enter I-15 southbound. Bonneville and Provo shorelines are visible to the east on the face of the Wellsville Mountains. A Gilbert-type delta graded to the Provo shoreline can be seen at the mouth of Box Elder Creek above Brigham City. Extensive quarries mark the delta.

Mile 358. On the east are good views of fault scarps cutting Holocene alluvial fans at the base of the Wasatch Mountains. This segment of the fault has undergone repeated Holocene rupture, but the youngest identified event is 3600 ± 500 years ago (Machette et al., 1991).

Mile 345. To the south is a view of the massive delta of the Weber River. It is composed mostly of silt and fine sand. The delta surface is about at the Provo shoreline.

Mile 340. Views to the west are of Great Salt Lake, Fremont Island, and Antelope Island. Hill Air Force Base lies on a delta surface to the east.

ACKNOWLEDGMENTS

We thank Peter Oviatt for field assistance, Andrei Sarna-Wojcicki, Bill Nash, and Mike Perkins for tephrochronology, Platt Bradbury for diatom identifications, Rick Forester for many discussions about ostracodes over the years, and Genevieve Atwood, Margie Chan, and Paul Link for helpful reviews of the manuscript.

REFERENCES CITED

- Adams, T.C., 1938, Land subsidence north of Great Salt Lake, Utah: Bulletin of the Seismological Society of America, v. 28, p. 65–70.
- Arabasz, W.J., Smith, R.B., Pechmann, J.C., and Nava, S.J., 1994, Regional seismic monitoring along the Wasatch front urban corridor and adjacent intermountain seismic belt, in Jacobson, M.L., compiler, National earthquake hazards reduction program, summaries of technical reports volume XXXV: U.S. Geological Survey Open-File Report 94-176, p. 3–4.
- Arnold, Ted, and Stephens, Doyle, 1990, Hydrologic characteristics of the Great Salt Lake, Utah: 1847–1986: U.S. Geological Survey Water-Supply Paper 2332, 32 p., map scale 1:125,000.
- Atwood, G., 1994, Geomorphology applied to flooding problems of closed-basin lakes . . . specifically Great Salt Lake, Utah: Geomorphology, v. 10, p. 197–219.
- Bates, R.L., and Jackson, J.A., 1987, Glossary of Geology: Third Edition: American Geological Institute, Alexandria, Virginia, 788 p.
- Benson, L.V., Currey, D.R., Lao, Y., and Hostetler, S., 1992, Lake-size variations in the Lahontan and Bonneville basins between 13,000 and 9000 ^{14}C yr B.P.: Palaeogeography, Palaeoclimatology, Palaeoecology, v. 95, p. 19–32.
- Bills, B.G., and May, G.M., 1987, Lake Bonneville: Constraints on lithospheric thickness and upper mantle viscosity from isostatic warping of Bonneville, Provo, and Gilbert stage shorelines: Journal of Geophysical Research, v. 92, p. 11,493–11,508.
- Bond, G.C., and Lotti, R., 1995, Iceberg discharges into the North Atlantic on millennial time scales during the last glaciation: Science v. 267, p. 1005–1010.
- Bucknam, R.C., 1979, Northwestern Utah seismotectonic studies: Summaries of Technical Reports, vol. VIII, U.S. Geological Survey, p. 72–74.
- Christenson, G.E., Harty, K.M., and Hecker, Suzanne, 1987, Quaternary faults and seismic hazards, western Utah, in, Kopp, R.S., and Cohenour, R.E., eds., Cenozoic geology of western Utah: Utah Geological Association Publication 16, p. 389–400.
- Crittenden, M.D., Jr., 1963, New data on the isostatic deformation of Lake Bonneville: U.S. Geological Survey Professional Paper 454-E, 31 p.
- Currey, D.R., 1980, Coastal geomorphology of Great Salt Lake and vicinity, in Gwynn, J.W., ed., Great Salt Lake: A scientific, historical, and economic overview: Utah Geological and Mineral Survey Bulletin 116, p. 69–82.
- Currey, D.R., 1982, Lake Bonneville: Selected features of relevance to neotectonic analysis: U.S. Geological Survey Open-File Report 82-1070, 31 p.
- Currey, D.R., 1990, Quaternary palaeolakes in the evolution of semidesert basins, with special emphasis on Lake Bonneville and the Great Basin, U.S.A.: Palaeogeography, Palaeoclimatology, Palaeoecology, v. 76, p. 189–214.
- Currey, D.R., and Oviatt, C.G., 1985, Durations, average rates, and probable causes of Lake Bonneville expansions, stillstands, and contractions during the last deep-lake cycle, 32,000 to 10,000 years ago, in Kay, P.A., and Diaz, H.F., eds., Problems of and Prospects for Predicting Great Salt Lake Levels: Salt Lake City, University of Utah Center for Public Affairs and Administration, p. 9–24.
- Currey, D.R., and Burr, T.N., 1988, Linear model of threshold-controlled shorelines of Lake Bonneville: Utah Geological and Mineral Survey Miscellaneous Publications 88-1, p. 104–110.
- Currey, D.R., Oviatt, C.G., and Plyler, G.B., 1983, Lake Bonneville stratigraphy, geomorphology, and isostatic deformation in west-central Utah: Utah Geological and Mineral Survey Special Studies, v. 62, p. 63–82.
- Currey, D.R., Atwood, G., and Mabey, D.R., 1984, Major levels of Great Salt Lake and Lake Bonneville: Utah Geological and Mineral Survey Map 73, scale 1:750,000.
- Currey, D.R., Berry, M.S., Douglass, G.S., Merola, J.A., Murchison, S.B., Ridd, M.K., Atwood, G., Bills, B.G., and Lambrechts, J.R., 1988, The highest Holocene stage of Great Salt Lake: Geological Society of America Abstracts with Programs, v. 20, p. 411.
- Eardley, A.J., 1938, Sediments of Great Salt Lake: American Association of Petroleum Geologists Bulletin, v. 22, p. 1305–1411.
- Eardley, A.J., and Gvostdetsky, V., 1960, Analysis of Pleistocene core from Great Salt Lake, Utah: Geological Society of America Bulletin, v. 71, p. 1323–1344.
- Eardley, A.J., Shuey, R.T., Gvostdetsky, V., Nash, W.P., Picard, M.D., Grey, D.C., and Kukla, G.J., 1973, Lake cycles in the Bonneville basin, Utah: Geological Society of America Bulletin, v. 84, p. 211–216.
- Forester, R.M., 1987, Late Quaternary paleoclimate records from lacustrine ostracodes, in Ruddiman, W.F. and Wright, H.E., Jr., eds., North America and adjacent oceans during the last deglaciation: Geological Society of America, Geology of North America K-3, p. 261–276.
- Green, S.A., and Currey, D.R., 1988, The Stansbury shoreline and other transgressive deposits of the Bonneville lake cycle: Utah Geological and Mineral Survey Miscellaneous Publication 88-1, p. 55–57.
- Gwynn, J.W., ed., 1980, Great Salt Lake: A scientific, historical, and economic overview: Utah Geological and Mineral Survey Bulletin 116, 400 p.

- Gwynn, J.W., and Murphy, P.J., 1980, Recent sediments of the Great Salt Lake basin: Utah Geological and Mineral Survey Bulletin 116, p. 83–96.
- Gilbert, G.K., 1890, Lake Bonneville: U.S. Geological Survey Monograph 1, 438 p.
- Kaufman, D.S., and Manley, W.F., in review, A new procedure for determining enantiomeric (DL) amino acid ratios in fossils using reverse phase liquid chromatography: Quaternary Science Reviews (Quaternary Geochronology)
- Lemons, D.R., Milligan, M.R., and Chan, M.A., 1996, Paleoclimatic implications of late Pleistocene sediment yield rates for the Bonneville basin, northern Utah: Palaeogeography, Palaeoclimatology, Palaeoecology, v. 123, p. 147–159.
- Light, Adam, and Kaufman, Darrell, 1996, Refinements to the radiocarbon shoreline chronology of Lake Bonneville, Great Basin, USA: EOS v. 77, No. 46, p. 304.
- Mabey, D.R., 1986, Notes on the historic high level of Great Salt Lake: Utah Geological Survey, Survey Notes, summer, 1986, p. 13–15.
- Machette, M.N., Personius, S.F., Nelson, A.R., Schwartz, D.P., and Lund, W.R., 1991, The Wasatch fault zone, Utah—segmentation and history of Holocene earthquakes: Journal of Structural Geology, v. 13, p. 137–149.
- Machette, M.N., and Scott, W.E., 1988, Field trip introduction: A brief review of research on lake cycles and neotectonics of the eastern Basin and Range Province: Utah Geological and Mineral Survey Miscellaneous Publication 88-1, p. 7–14.
- Miller, D.M., 1990, Geologic map of the Lucin 4 SW Quadrangle, Box Elder County, Utah: Utah Geological and Mineral Survey Map 130, 13 p., scale 1:24,000.
- Miller, D.M., Nakata, J.K., Sarna-Wojcicki, A., and Meyer, C.E., 1992, Neogene tectonic history of northern Utah revealed by depositional, magmatic, and structural features: Geological Society of America Abstracts with Programs, v. 24, no. 6, p. 53.
- Miller, D.M., Nakata, J.K., Oviatt, C.G., Nash, W.P., and Fiesinger, D.W., 1995, Pliocene and Quaternary volcanism in the northern Great Salt Lake area and inferred volcanic hazards, in Lund, W.R., ed., Environmental and Engineering geology of the Wasatch Front Region: Utah Geological Association Publication 24, p. 469–482.
- Miller, D.M., and Langrock, Holly, 1997a, Geologic map of the Monument Peak NE quadrangle, Box Elder County, Utah: Utah Geological Survey Open-File Map OFR 346.
- Miller, D.M., and Langrock, Holly, 1997b, Geologic map of the Monument Peak quadrangle, Box Elder County, Utah: Utah Geological Survey.
- Miller, D.M., and Langrock, Holly, 1997c, Geologic map of the Locomotive Springs quadrangle, Box Elder County, Utah: Utah Geological Survey Open-File Map OFR 349.
- Miller, D.M., and Langrock, Holly, 1997d, Geologic map of the Monument Point quadrangle, Box Elder County, Utah: Utah Geological Survey Open-File Map OFR 348.
- Miller, R.D., Van Horn, R., Scott, W.E., and Forester, R.M., 1980, Radiocarbon date supports concept of continuous low levels of Lake Bonneville since 11,000 yr B.P.: Geological Society of America Abstracts with Programs, v. 12, p. 297–298.
- Murchison, S.B., 1989, Fluctuation history of Great Salt Lake, Utah, during the last 13,000 years: Ph.D. thesis, University of Utah, Salt Lake City, 137 p.
- Nelson, M.G., and Miller, D.M., 1990, A Tertiary record of the giant marmot *Paenemarmota sawrockensis*, in northern Utah: Contributions to Geology, University of Wyoming, v. 28, p. 31–37.
- Oviatt, C.G., 1997, Lake Bonneville fluctuations and global climate change: Geology, v. 25, p. 155–158.
- Oviatt, C.G., McCoy, W.D., and Reider, R.G., 1987, Evidence for a shallow early or middle Wisconsin lake in the Bonneville basin, Utah: Quaternary Research, v. 27, p. 248–262.
- Oviatt, C.G., and Nash, W.P., 1989, Late Pleistocene basaltic ash and volcanic eruptions in the Bonneville basin, Utah: Geological Society of America Bulletin, v. 101, p. 292–303.
- Oviatt, C.G., Currey, D.R., and Miller, D.M., 1990, Age and paleoclimatic significance of the Stansbury shoreline of Lake Bonneville, northeastern Great Basin: Quaternary Research, v. 33, p. 291–305.
- Oviatt, C.G., Currey, D.R., and Sack, D., 1992, Radiocarbon chronology of Lake Bonneville, eastern Great Basin, USA: Palaeogeography, Palaeoclimatology, Palaeoecology, v. 99, p. 225–241.
- Oviatt, C.G., Habiger, G.D., and Hay, J.E., 1994, Variation in the composition of Lake Bonneville marl: A potential key to lake-level fluctuations and paleoclimate. Journal of Paleolimnology, v. 11, p. 19–30.
- Robison, R.M., and McCalpin, J.P., 1987, Surficial geology of Hansel Valley, Box Elder County, Utah, in Kopp, R.S., and Cohenour, R.E., eds., Cenozoic geology of western Utah: Utah Geological Association Publication 16, p. 335–349.
- Sack, D., 1989, Reconstructing the chronology of Lake Bonneville: An historical overview, in Tinkler, K.J., ed., History of geomorphology: Unwin Hyman, London, p. 223–256.
- Sack, D., 1995, The shoreline preservation index as a relative-age dating tool for late Pleistocene shorelines. An example from the Bonneville basin, U.S.A.: Earth Surface Processes and Landforms, v. 20, p. 363–377.
- Scott, W.E., McCoy, W.D., Shroba, R.R., and Rubin, M., 1983, Reinterpretation of the exposed record of the last two cycles of Lake Bonneville, western United States: Quaternary Research, v. 20, p. 261–285.
- Smith, R.B., and Luedke, R.G., 1984, Potentially active volcanic lineaments and loci in western conterminous United States, in Explosive volcanism: Inception, evolution, and hazards. Washington, D.C., National Academy Press, p. 47–66.
- Spencer, R.J., Baedeker, M.J., Eugster, H.P., Forester, R.M., Goldhaber, M.B., Jones, B.F., Kelts, K., McKenzie, J., Madsen, D.B., Rettig, S.L., Rubin, M., and Bowser, C.J., 1984, Great Salt Lake and precursors, Utah: The last 30,000 years. Contributions to Mineralogy and Petrology, v. 86, p. 321–334.
- Thompson, R.S., Toolin, L.J., Forester, R.M., and Spencer, R.J., 1990, Accelerator-mass spectrometer (AMS) radiocarbon dating of Pleistocene lake sediments in the Great Basin: Palaeogeography, Palaeoclimatology, Palaeoecology, v. 78, p. 301–313.
- U.S. Geological Survey, 1987, Great Salt Lake and Newfoundland evaporation basin. Experimental edition 1:250,000-scale satellite image map: U.S. Geological Survey, Denver, CO.
- Williams, S.K., 1994, Late Cenozoic tephrochronology of deep sediment cores from the Bonneville basin, northwest Utah: Geological Society of America Bulletin, v. 105, p. 1517–1530.

Quaternary Geology and Geomorphology, Northern Henry Mountains Region

BENJAMIN L. EVERITT

Utah Division of Water Resources, 1594 W. North Temple, Salt Lake City, Utah 84114-6201

ANDREW E. GODFREY

USDA Forest Service, Intermountain Region, 324 25th St., Ogden, Utah 84401

ROBERT S. ANDERSON

Department of Earth Sciences, University of California, Santa Cruz, California 95064

ALAN D. HOWARD

*Department of Environmental Sciences, University of Virginia,
Charlottesville, Virginia 22903*

PART 1—ROAD LOG

Ben Everitt and Andrew E. Godfrey

The following road log describes the Fremont River and the northern piedmont of the Henry Mountains. The field trip is designed to bring together summaries of current research from a variety of sources and place them in a historical and geologic context. Two broad subject areas of the geomorphology of the northern Henry Mountains region are presented in the road log and associated papers. One subject covers the history of the gravel deposits along the Fremont River and northward from Mount Ellen. The second includes some of the erosion processes of the Mancos Shale in the Upper Blue Hills Badlands.

Three papers describe erosion processes on the Mancos Shale. Dick, et.al., hypothesize that network geometry of small drainages exerts a significant control on a hydrograph's shape when flow is produced by high-intensity storms that are short relative to the rise time of the hydrograph. This is because tributary flows are short-lived and contribute to the trunk channel peaks that are preserved in the outflow hydrograph. For similar-sized but longer-duration storms they found that the hydrograph rises slowly, with smaller peaks that are not clearly preserved in the outflow hydrograph. Godfrey's paper on wind erosion showed that sudden gusts in southwest winds can produce short-lived pressure drops on the lee sides of southeast-trending ridges. The resulting pressure difference between the soil atmosphere and the air above can lift the surface crust to be blown away. Resulting landforms include hollows and notches near the top of the ridges, and northeast facing cliffs, some with shallow, closed depressions in front. Godfrey's 30-year

study of soil creep showed an average rate of 2.7 cm/yr on slopes averaging 35 degrees. Slope aspect did not appear to affect rates, but the upper meter or two moved at a significantly slower rate than lower portions of a slope. Winters with two or more consecutive days of at least 6 mm precipitation showed episodes of accelerated creep or shallow slumping.

Two papers discuss gravel deposits. Repka, et.al., dated terraces along the Fremont River using cosmogenic methods. They found age estimates of 60, 102, and 151 ka for the three most extensive terraces. This led then to the conclusion that the terraces were formed when there was a strong glacial source in the headwaters, and were abandoned when the sediment source shut off. In contrast, Godfrey's mapping of shoestring gravel deposits between Mount Ellen and the Fremont River suggests that random stream captures, rather than climate fluctuations, produced the various bench levels.

Everitt's observations, contained in the road log, show that alluvial fill in the Fremont-Dirty Devil river valley thins downstream from 80 feet below river level near Torrey, to 50 feet near Caineville, then thickens again to more than 100 feet at Hanksville. The thick alluvial fills, terraces, and buried canyons of the Fremont River system contain a record of the complex response of the river to the waxing and waning of Pleistocene glaciers in its headwaters, the changing precipitation regimes in its arid lower reaches, and the inconstant base level of the Colorado River to which it is tributary.

Observations by Everitt of the vegetation along the Fremont River flood plain show that the pioneer-dominated plant community has changed in relation to the introduction

of new species, and the evolution of the channel and its flood plain.

Day 1

Grass Valley summit to Hanksville

The trip proceeds south from Salina via Interstate 70, U.S. Highway 89, and Utah State Highway 24 (U-24). The route passes along the transition between the Basin-and-Range and Colorado Plateau structural provinces, crossing the Sevier and Paunsagunt Faults, two large down-to-the-west normal faults of Neogene age. The detailed log begins at Grass Valley summit, the divide between the Fremont River and the Sevier River. For additional information on the geology along the route, see Oaks, 1988.

Utah State Highway 24

Milepost 42— Summit at elevation 8385 feet; pass between Parker Mountain, to the south, and the Fish Lake Plateau to the north. This is the drainage divide between the Sevier River, tributary to the Great Basin, and the Fremont River, tributary to the Colorado. To the north at 9:00 on the summit of Fish Lake Plateau is the south end of the graben that contains Fish Lake. At 300 feet, it is one of the deepest natural lakes in Utah, and a source of the Fremont River. The north end of the lake is partly dammed by glacial moraine, suggesting that it could have been the source of Pleistocene glacial outburst floods on the Fremont.

In the near distance, the Fremont Valley cuts between two lava-capped plateaus, with summits near 11,000 feet: Thousand Lake Mountain to the left and Boulder Mountain to the right. The two northern peaks of the Henry Mountains are visible to the east in the far distance; Mt. Ellen to the left and Mt. Pennell to the right. The Henry Mountains were the last mountain system to be placed on the map of the United States. They were first described by G.K. Gilbert in his seminal work on geomorphology and igneous intrusions (Gilbert, 1877). Hunt, et.al. (1953) conducted the first detailed mapping of the Henry Mountains between 1935 and 1939 (Hunt, 1977).

Milepost 47— Road cut exposes bouldery lahar in the volcanics. The source of the volcanics, as well as some on Thousand Lake and

Boulder Mountains, is in the Marysvale calderas 35 miles to the west, showing that at least the earliest eruptions, dated at 23 million years (Mattox, 1991), predate offset on the Paunsagunt and Thousand Lakes Faults.

Begin descent into Rabbit Valley. Eastward across the valley is the west face of Thousand Lake Mountain, the escarpment of the Thousand Lake Fault, considered to be the western margin of the Colorado Plateau. Note the horizontal lava cap and the patches of the more resistant Triassic and Jurassic sandstones peeking through landslide-mantled slopes.

U-24 crosses a peculiar crescent-shaped valley. A large spring which emerges from the volcanic rock on the western margin feeds one of several fish-farming operations of the upper Fremont River.

Entering the town of Loa. Loa was named after the Hawaiian mountain, whose gently sloping flanks bear some resemblance to the volcanic slopes to the west and north. **At the south end of town, leave U-24 and continue south on Main Street.** Set odometer to zero.

End of pavement. Continue on graded county road.

Road forks, **TURN LEFT.**

Outcrop of welded Osiris Tuff whose joint blocks weather into large monoliths.

Regain pavement and cross the Fremont River. The river here leaves the valley, and continues south in a canyon cut into the north-eastward dipping volcanics. G.K. Gilbert recorded this feature in his field notes of July 12, 1875, and puzzled over whether the course was antecedent or superposed (Hunt, 1988, p. 34).

The road ascends the alluvial slope east of the river. Wayne Wonderland airport to the left. To the right is a small knoll underlain by horizontally bedded sand and gravel mapped as Pleistocene Fremont River terrace deposits by Smith, et. al. (1963). The sediment is similar to Tertiary gravel interbedded with the volcanics elsewhere in Rabbit Valley, and the hill is likely a remnant of Tertiary basin fill.

Junction with U-24; TURN RIGHT and continue southeast toward Bicknell.

Milepost 48—

Milepost 50—

Milepost 51—

Mile 0.8—

Mile 2.1—

Mile 2.7—

Mile 3.9—

Mile 5.0—

Mile 6.0—

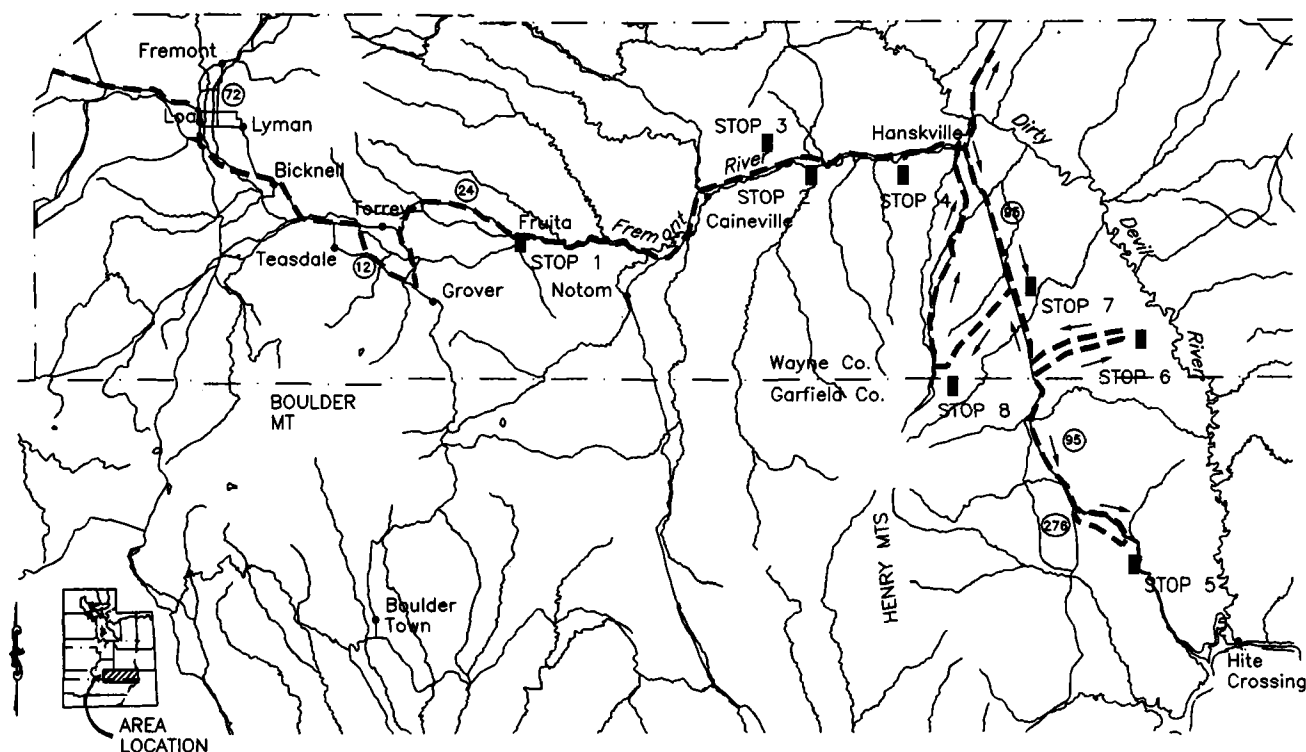


Figure 1. Map of field-trip route in area of Capitol Reef National Park and the Henry Mountains, with stops shown.

Milepost 59 on U-24—At 3:00 across the valley to the west is the mouth of the canyon by which the Fremont River returns to the valley. As the road turns eastward, the cliffs ahead expose horizontally bedded Triassic Wingate Sandstone. At the mouth of Sand Creek is a tilted block of Navajo Sandstone (Ss) within the Thousand Lake Fault zone.

Milepost 60—To the right, the Beard Oil Tanner #1-27 in 1990 penetrated the Carmel-Entrada Formation (Fm) at a depth of 730 feet beneath interbedded alluvium and volcanics. Offset of the Chinle Fm across this part of the Thousand Lake Fault is 2,500 feet. Faulting began in the early Miocene and continued through at least the Pliocene. There is no clear evidence for late Pleistocene or Holocene offset (Everitt, 1995). Enter Bicknell.

Milepost 62—To the south at 2:00, the Fremont River meanders through a broad marshy valley called the Bicknell Bottoms. The low gradient suggests ponding by either structural

Milepost 63—

Milepost 66—

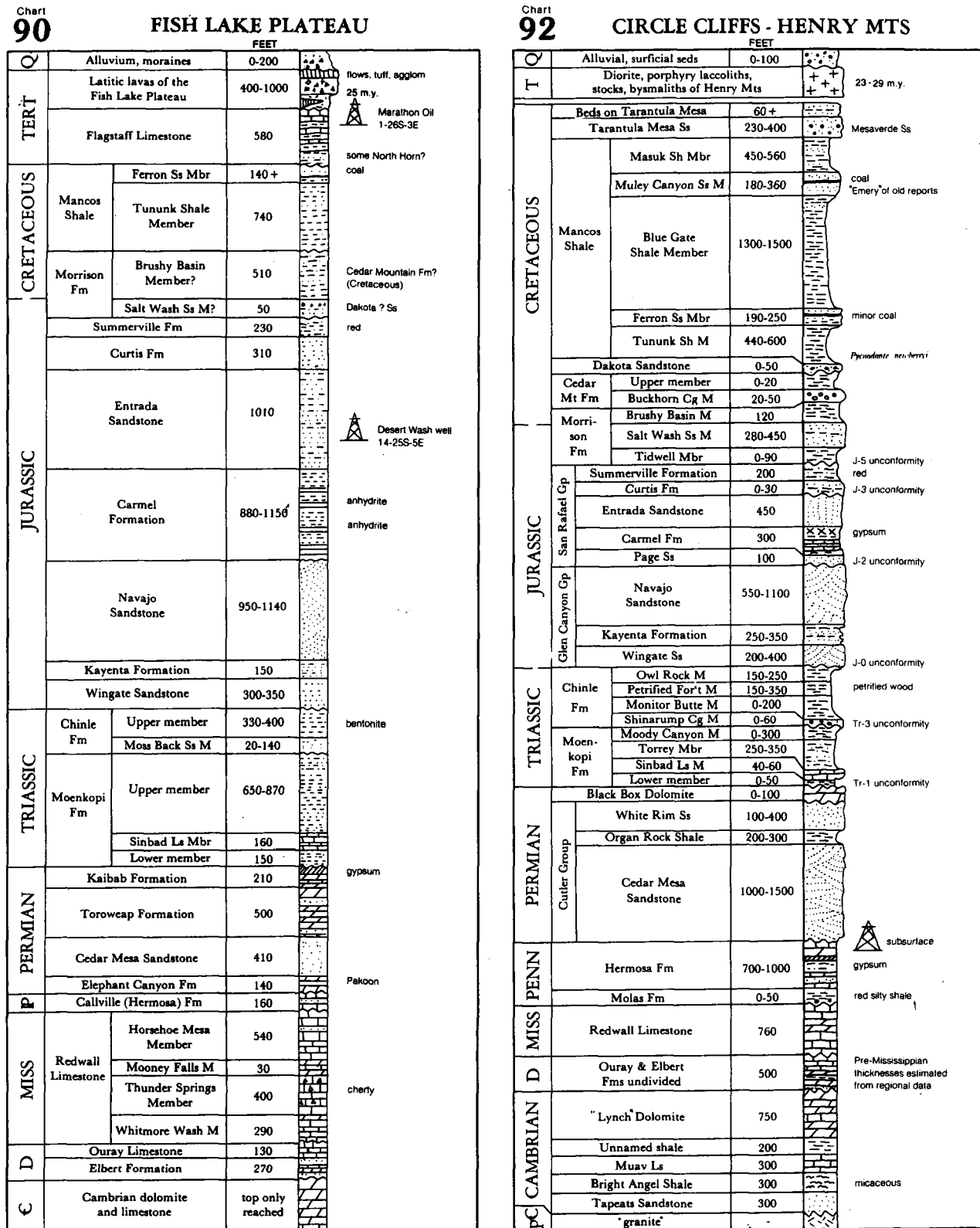
Milepost 67.5—

deformation or backwater from downstream glacial dams. Springs emerging from the toe of the volcanic slopes across the valley provide a year-round base flow of about 100 cfs.

Cross the Thousand Lake Fault and enter what G.K. Gilbert called the “Red Gate” (Hunt, 1988). The lower Triassic Moenkopi Formation is exposed at river level north of the river, forming red cliffs capped by the resistant Shinarump Member of the Chinle Fm (fig. 2). Notice how much larger the Fremont River is here than upstream from the Bicknell Bottoms.

Mt. Ellen in the distance at 1:00. The first well-defined gravel-capped river terraces are on the right.

Bridge over Fremont River. Drilling for a proposed dam in 1992 showed 35 feet of alluvial valley fill beneath the floodplain, with an inner buried canyon an additional 45' deep buried beneath the west valley margin (fig. 3).



from Hintze, 1988, Geologic History of Utah

Figure 2. Stratigraphic columns for Fish Lake Plateau and the Circle Cliffs-Henry Mountains area.

PROFILE OF FREMONT RIVER VALLEY AT TORREY DAM SITE

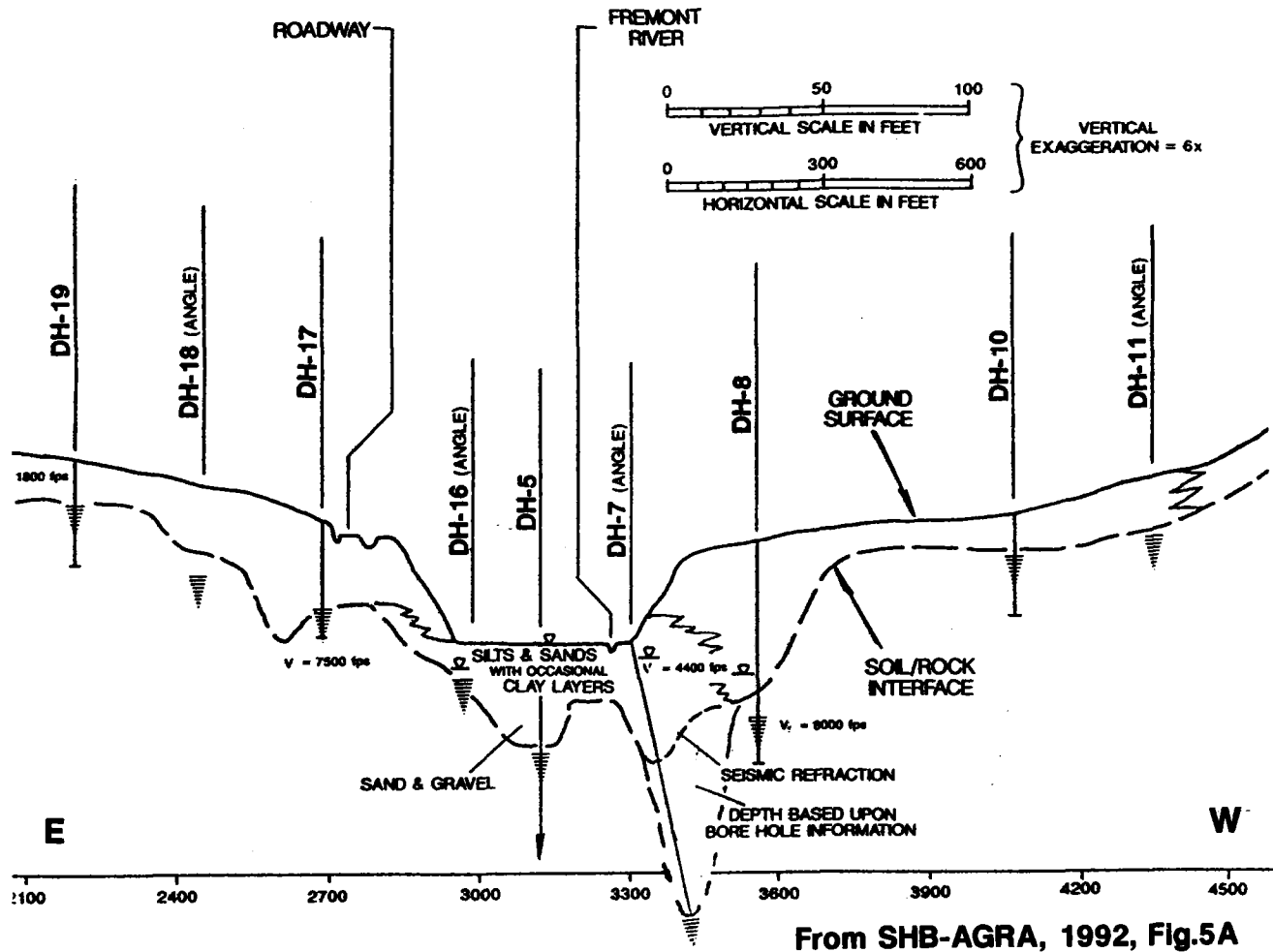


Figure 3. Profile of Fremont River valley at Torrey dam site.

- | | | | |
|-----------|--|-----------|--|
| | Continue through Torrey, and TURN RIGHT on 300 East, the first road past the post office. Set odometer to zero. | Mile 1.6— | Pleistocene valley fill exposed in road cut to the right. |
| Mile 1.0— | Descend into the Fremont valley through a cut in the Moenkopi Fm. | Mile 1.7— | Bedrock exposed to the left of the road separates the Holocene valley on the left from the Pleistocene valley ahead. |
| Mile 1.4— | Abandoned Garkane hydropower station and penstock is west across the valley behind the quarry. Ahead to the south, the narrows flanked by bedrock was studied as a potential dam site in 1987. The modern valley here is of latest Pleistocene or Holocene age (fig. 4). The Pleistocene valley lies to the south of the modern valley beneath the gravel terrace (Qat of Billingsley and others, 1987). | Mile 2.7— | TURN LEFT on County Road 3262. |
| | | Mile 3.7— | Road parallels the SE-trending Teasdale anticline, believed to be a Laramide (late Cretaceous to Eocene) structure. Moenkopi Fm crops out on the left. The ridge of fractured Navajo Ss on the right, now called the "Cockscomb," is Gilbert's "White Crag" (Hunt, 1988, p. 37). |
| | | Mile 4.7— | Road forks, BEAR RIGHT . |

- Mile 5.7— **TURN LEFT on U-12.** The lumpy, bouldery terrain is Flint and Denny's (1958) Carcass Creek Drift.
- Mile 6.4— The sloping surface is the glacial outwash fan of Fish Creek, graded to the Pleistocene Fremont River about 100 feet higher than the present river (Flint and Denny, 1958). Carcass Creek Drift, of possible Bull Lake age, is exposed beneath the outwash along the river. At this location, therefore, a glacier once dammed the Fremont River and pushed it northward.
- Mile 7.7— Bridge over Fremont River. The basal Sinbad Limestone Member of the Moenkopi Fm exposed in riverbed just downstream.
- Mile 10.2— **Return to U-24 at milepost 70. TURN RIGHT** toward Capitol Reef National Park.
- Milepost 74— Capitol Reef National Park boundary. The trip through the Park provides a traverse through the Mesozoic stratigraphic section (fig. 2).
- Milepost 75— SE-trending high angle fault and basalt dike parallels the highway to the left.
- Milepost 82— Highway returns to the Fremont River. **TURN RIGHT** to Park headquarters at Fruita.
- STOP 1:** Capitol Reef National Park Visitor Center. The relief model shows the interesting topographic features developed on the Water-pocket Fold, including superposed stream courses entrenched in sandstone canyons.
- Milepost 83— Entering the narrows of the Wingate Fm. The locally mild climate created by the narrow canyon favored development of fruit orchards, which are now operated by the Park as a reserve of classic varieties.
- Milepost 85— Navajo Ss at river level. Basalt boulders on two terrace levels. In 1960, the Utah Department of Transportation (UDOT) drilled three borings for Utah Highway 24 structure D235 over the Fremont River near Fruita (UDOT files). Bedrock was encountered at a maximum depth of 15 feet, 10 feet below river level. Because these borings do not provide a complete traverse across the valley, the maximum thickness of fill may be greater than 15 feet.
- Near Milepost 86. Navajo Ss penecontemporaneous deformation. The canyon meander cutoff on the right, and waterfall on the left were constructed by the Utah Department of Transportation during highway construction in the 1950's. Two terrace levels are capped by basalt boulder gravels.
- Near Milepost 87 and thereafter: Proceeding up-section through Carmel Fm, Entrada Ss, thin green Curtis Shale and the thinly bedded chocolate Summerville Fm, overlain unconformably in places by Pleistocene terrace gravel.
- Milepost 90— Salt Wash Sandstone Member of the Morrison Fm is overlain by the distinctive purple claystone of the Brushy Basin member. Two river terrace levels are present.
- Milepost 93— Highway enters strike valley in the Tununk Shale Member of the Mancos Fm. Eastward dip increases toward the Caineville monocline. Turnoff to the USGS gaging station "Fremont River near Caineville" on the left.
- Milepost 94— The dark gray Tununk directly overlies the green-gray shale of the Brushy Basin Member of the Morrison Fm. The usually intervening Dakota Ss is absent (fig. 2).
- Milepost 95— U-24 bridge over the Fremont River and the Caineville Diversion where the Caineville Irrigation Company takes its water. In 1980, investigation for an earthfill dam in the narrows just upstream showed the thickness of the alluvial valley fill to be 50 feet (Palmer-Wilding, 1981).
- Milepost 98— Highway bears right through the Caineville Reef, a hogback of Ferron Ss Member of the Mancos Fm folded upward on the steep western limb of the Henry Mountains structural basin. Return to the Fremont River valley at Caineville. A review of drillers' logs of water wells in the town of Caineville show bedrock at a maximum depth of 60 feet below terrace level, or about 45 to 50 feet below river level (Everitt, 1984).
- Milepost 100— The Fremont River valley passes between the escarpments of North and South Caineville Mesas, the "Blue Gate" of G.K. Gilbert (1877). At the axis of the Henry Mountains structural basin are about 2,000 feet of horizontally bedded Blue Gate Shale Member of the Mancos

TORREY (GARKANE) DAM SITE GEOLOGIC SKETCH

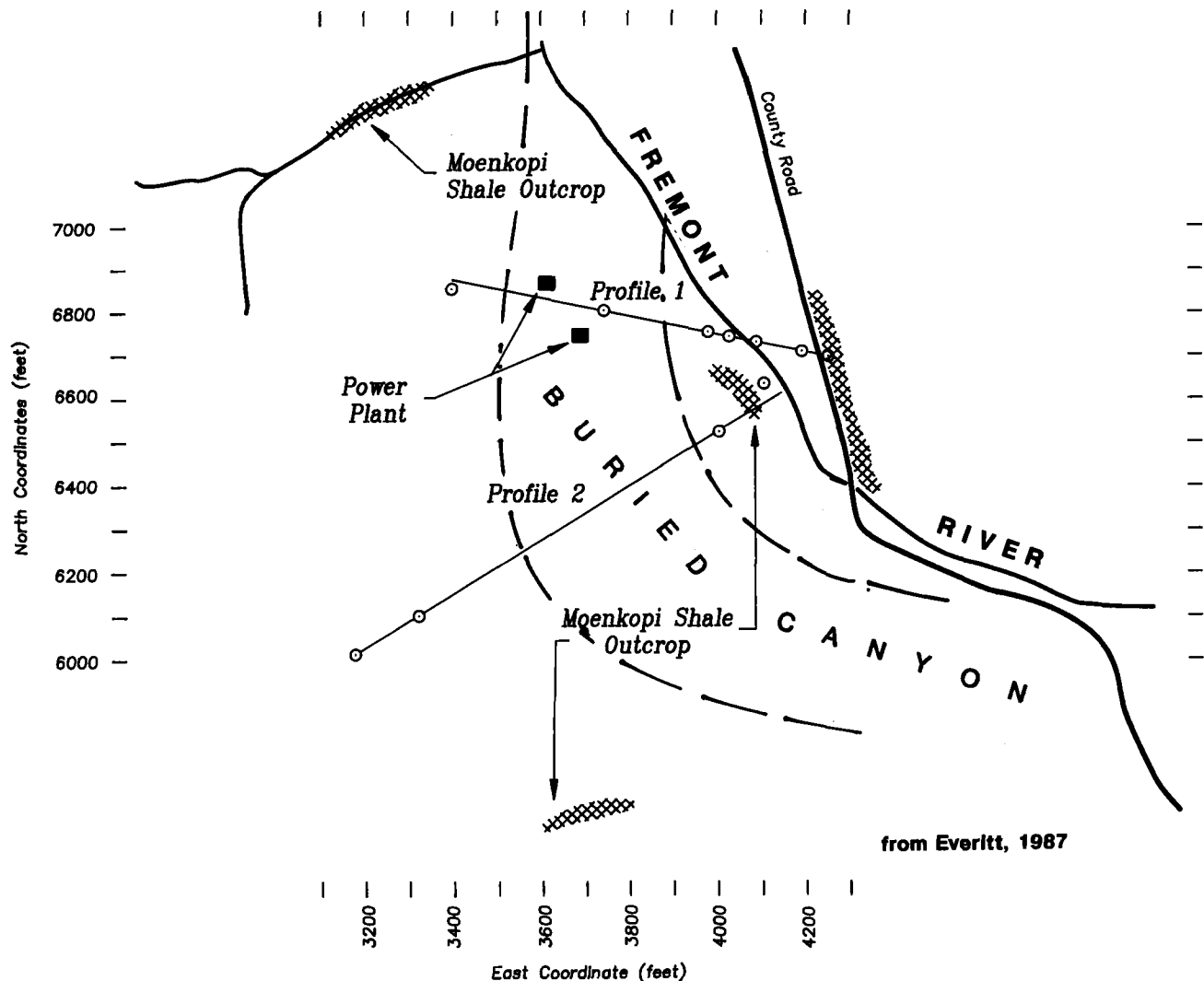


Figure 4. Torrey (Garkane) dam site geologic sketch.

- Fm, capped by the Emery Sandstone Member.
- Milepost 101*— Luna Mesa store; the butte ahead on the left is capped by Fremont River gravel, Howard's (1970) terrace 3a.
- Milepost 104*— To the left are asymmetrical ridges in the Blue Gate Shale, some with vertical faces on the northeast side. In 1876, G.K. Gilbert observed these, and postulated an aeolian origin (Hunt, 1988, p. 214).
- Milepost 105*— Ascend the dip slope of the Ferron Sandstone with outcrops of white and tan sandstone interbedded with coal. This marginally economic coal zone was open-

pit mined briefly in the 1980's at the Factory Butte coal mine about 15 miles along strike to the north.

Road junction. **TURN RIGHT** (south) on dirt road which climbs to the top of Howard's (1970) terrace 3a. Proceed 0.6 mile to overlook just past TV relay.

STOP 2: Overlook of the Fremont River valley, terrace levels, and the badlands around the Caineville mesas (Howard, Anderson, Godfrey). Drilling and seismic refraction traverses for a proposed dam on the Fremont River downstream from

BLUE VALLEY DAM SITE PROFILE 2, DRILL HOLES AND SHOT POINTS

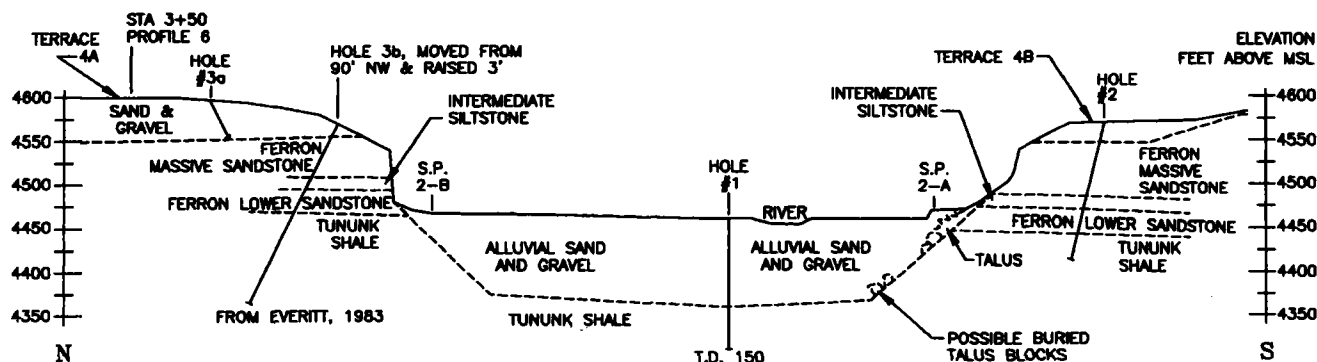


Figure 5. Geologic profile of Blue Valley dam site, with drill holes and shot points.

Caineville (Everitt, 1983) showed a thickness of 99 feet of alluvial fill beneath the flood plain (fig. 5). The site is in a canyon cut into the Ferron Sandstone Member of the Mancos Formation. The canyon rim is capped by gravel mapped as terrace levels 4a and 4b by Howard (1970). The extensive surface of terrace 4a conceals beneath it, to both the north and south of the modern canyon, filled canyons similar in width to the modern canyon, although not as deep.

Return 0.2 mile to test pits exposing soil profile of terrace 3a.

Return to Highway 24 and TURN LEFT (west) toward Caineville.

0.3 miles west of **Milepost 105**—East side of hill. **Turn off on track to right**, 0.2 mile to old highway, 0.5 mile to badlands. Or, as an alternate, turn off highway at mile 105.1 to the fluted wind towers at the dirt bike jamboree area.

STOP 3: Mancos Shale badlands and sites of wind erosion and soil creep (Godfrey); badlands modeling (Howard); and runoff monitoring (Anderson).

Return to U-24 and proceed east toward Hanksville.

Milepost 106.2—Highway descends the dugway through the Ferron Sandstone hogback and returns to the river valley. The Tununk Shale now at river level.

Milepost 108—The ghost town of Giles, abandoned in 1907, is across the river to the right. To the left between here and milepost 109 are the remains of an abandoned irrigation ditch with dead cottonwood trees along it. The trace of the canal is marked by pink silt from the Fremont River, which contrasts with the gray, residual soil of the Tununk.

Milepost 109—Blue Valley is a strike valley in the Tununk shale.

Milepost 110—Dakota Sandstone with interbedded coal ahead on the left. The basal Mancos consists of an oyster shell reef (*Gryphaea*) from 2 to 5 feet thick. (Possible stop, highway borrow pit on left.)

TURN RIGHT 0.2 mile past milepost 111 and proceed 0.1 mile on dirt track to abandoned well.

STOP 4: Fremont River flood plain and location of 1983 traverse of Fremont River flood plain and its vegetation (Everitt).

Milepost 111.5—Variegated shale of the Brushy Basin Member is at river level, capped by the Dakota Ss. Note the tilted slump block of Brushy Basin on the left.

Milepost 113—Extensive river terraces on the Brushy Basin are capped by Fremont River gravel. As the road goes over the rise, Howard's (1970) terrace 4b is on the right.

Milepost 114—Outcrops of Salt Wash Ss Member of the Morrison Fm are at river level ahead.

Milepost 115— Summerville Fm on the left, capped by the massive basal gypsum of the Morrison. Note the interbedded gypsum, with gypsum-filled fractures at various angles. The Fremont River on the right is aggrading above the Hanksville diversion dam, which has provided grade control since at least 1947.

Milepost 116— Fremont River bridge, entering Hanksville. In 1965, four borings were drilled here (structure F116, UDOT files). The deepest encountered bedrock beneath valley alluvium to a depth of 27 feet, 20 feet below river level. Because the bridge is near the south margin of the valley, this should be regarded as a minimum thickness of alluvial fill. A review of water wells in the town of Hanksville suggests a maximum of more than 100 feet of alluvial fill.

The highway is on a surface that is believed to have been the Fremont River flood plain at the time of settlement in the 1870's. During a series of floods beginning in the 1890's, the river cut the present channel 15 to 20 feet below the old flood plain (Hunt and others, 1953), and since about 1940 has been reconstructing a new floodplain at this lower level. North across the river at 9:00 is a little anticline in the Entrada Fm. The pinching out of beds at the top of the anticline indicates active folding during deposition.

END OF DAY 1

Day 2

Henry Mountains Piedmont near Hanksville

Begin at Hanksville and **proceed southeast on U-95** from milepost 0.

Milepost 1— The rolling, sandy country is underlain by the Entrada Fm. The Entrada forms sandstone pillars surrounded by moats.

Milepost 2.5— Highway bends left around a pediment remnant (Godfrey, 1969), an ancient channel of Bull Creek. The light gray gravel is diorite porphyry derived from the Henry Mountains. At 2:00 are the Henry Mountains. Mt. Ellen is the sharp peak on the right and Bull Mountain is the lower

sharp peak to its left. Modern Bull Creek flows northward from the basin between the two.

Three types of surfaces can be identified: (1) gravel-capped pediments, (2) alluvial fans, and (3) stripped benches on the resistant sandstones. The pediments and alluvial fans here slope north and east away from the mountains, whereas the stripped benches are west-facing dipslopes on resistant sandstone units. The entire area between the mountain front and the Fremont River is referred to as the "piedmont." A pediment is a primarily erosional segment of the piedmont where bedrock is beveled by running water, so that bedding is truncated. An alluvial fan is a depositional segment of the piedmont (Godfrey, 1969, p.3).

Mile 3.5—

The valley of Dry Valley Creek is a former course of Bull Creek into which Bull Creek was artificially diverted in the 1950's to keep it from flooding Hanksville.

Milepost 4—

On the left are four gravel-capped pediments radiating from the northern Henry Mountains.

Milepost 8—

To the east at 10:00 is Sorrell Butte, a pediment remnant capped by Bull Creek gravel, one of the oldest and highest remaining levels of the Henry Mountains pediments. It is flanked by radiating secondary pediments.

Milepost 10—

Sawmill Basin road on the right.

Mile 12.8—

Highway crosses Granite Wash which heads on the eastern slope of Bull Mountain. Coppice dunes (sand mounds of Everitt, 1980) are occupied by Brigham tea (*Ephedra torreyana*). Exposures in cross-section show that these are not traveling dunes, but layered accumulations of drift sand accreting with the growth of individual bushes.

Milepost 13—

Bull Mountain is at 3:00 (southwest). Hunt, et.al. (1953) classified it as a bysmalith—a laccolith (a floored, domed, igneous intrusion) with a faulted distal end. Note the sedimentary beds turned up around the base at the distal end, and the pattern of radiating fins on the summit. Garfield County line. To the west at 4:00 is a good view of Bull Mountain. In the foreground is a hogback of Summerville

Milepost 16—

- Fm capped by the Salt Wash Sandstone Member of the Morrison Fm. Beyond, at the base of Bull Mountain, is horizontally bedded Salt Wash Ss.
- Milepost 17—* Bridge over Poison Spring Wash. The road cuts through a pediment with a cap of porphyry gravel channeled into the underlying Entrada Fm.
- Milepost 21—* Mt. Pennell is at 2:30; Mt. Hillers at 2:00. The Little Rockies (Mts Holmes and Ellsworth) are in the distance at 1:00.
- Milepost 23—* Highway descends to the valley of North Wash. Henry Mountains gravel caps pediments on the Navajo Sandstone.
- Milepost 26—* Junction of Highway 276 to Bullfrog. Continue east on Highway 95 into the canyon of North Wash.
- Mile 29.5—* Contact of the Navajo Ss where with the underlying Kayenta Fm.
- STOP 5:** Alcoves formed at the Kayenta-Navajo contact by groundwater sapping (Howard).
- Return northward on U-95**, to just north of the Garfield/Wayne county line.
- Mile 15.7—* **TURN RIGHT** on graded road toward Burr Point, 11 miles.
- STOP 6:** Burr Point, and overlook of the Dirty Devil River Canyon. Review of Triassic stratigraphy, terrace formation, abandoned and filled canyons, and riparian vegetation (Howard, Everitt).
- Milepost 10—* Gravel pit on the right (east).
- STOP 7:** Gravel Pit with an exposure of a soil with a well developed gypsiferous carbonate horizon.
- Proceed north 0.2 mile on U-95 and **turn left** (southwest) on the Saw Mill Basin road. Set odometer to 0. Mt. Ellen is straight ahead. Bull Mountain is at 11:00. At the base of Bull Mountain are flat-lying sedimentary strata of the Salt Wash Member of the Morrison Fm. Just in front of and to the left of Mt. Ellen Peak is Horseshoe Basin, which is thought to be the source of some of the landslide debris around the north slopes of the range and the north side of Bull Mountain. At 1:00 is Table Mountain, one of the radiating laccoliths of the Ellen group.
- Mile 2.4—* Road climbs onto gravel-capped pediment surface.
- Mile 2.7—* Road forks: **BEAR LEFT** toward Granite Ranch.
- Mile 3.2—* View SSW toward the mouth of Bull Creek Canyon along a broken pediment surface, the Cottrell level of Godfrey (1969), to the few remnants of higher, older surfaces to the left. To the right is the head of a drainage in the process of eroding headward into the Cottrell pediment and slowly beheading it.
- Mile 5—* Road rises onto a higher sublevel within the Cottrell group of pediments. At 2:00 is a remnant of a higher ancient pediment at the Sorrell Butte level. This remnant is flanked by an apron of secondary pediments cut on the Mancos shale.
- Mile 5.8—* Road forks. **Take the jeep track to the RIGHT** and continue up the pediment surface. To the left across the draw is the apron of landslide debris at the foot of Bull Mountain, which appears to be graded to Horseshoe Basin.
- Mile 6.5—* The toe of the landslide with a group of large porphyry boulders with tafoni (cavernous weathering).
- STOP 8:** Pediment overview and review of erosion and deposition process (Godfrey). To the north is visible the general westward dip of the beds on the east limb of the Henry Mountains Basin and in the distance, the San Rafael Swell and the Book Cliffs. To the northeast is the canyon of the Dirty Devil River. If the day is clear, the LaSal Mountains may be visible 90 miles to the east.
- Proceed westward** across the pediment surface. Note the contrast between the rounded boulders in the pediment gravel and the angular and irregular boulders of the landslide.
- Mile 7.0—* Cross a small drainage, which exposes the pediment gravel in cut banks.
- Mile 7.4—* Rejoin the Sawmill Basin road and **TURN RIGHT** (north). The road descends from the Cottrell pediment onto the Fairview pediment. The modern channel of Bull Creek is to the left.
- Mile 8.0—* Proceed downstream along the Fairview pediment, which lies in a valley eroded

- into the Cottrell pediment. Remnants of the Cottrell pediment are on both sides of the lower, younger pediment. Exposures show 15 to 20 feet of gravel overlying Mancos Shale.
- Mile 9.0— To the right are badlands eroded in the Brushy Basin Member, with remnant caps of pediment gravel. Fairview Ranch is straight ahead.
- Mile 10.0— Road junction and Fairview Ranch. **Continue north toward Hanksville.**
- Mile 11.2— Proceed north on the Fairview pediment with outcrops of Brushy Basin Member poking through here and there.
- Mile 11.6— Adams Butte to the northwest at 10:00 is a remnant of Brushy Basin shale. Post-pediment slope retreat has formed a moat around the base of the butte.
- Mile 12.4— Cattle guard—we are now at the distal end of the local branch of the Fairview pediment. Distally thinner gravel forces groundwater to the surface here, leaving an efflorescence of thenardite: anhydrous sodium sulfate. A slightly higher, older branch of the Fairview pediment is at 2:00.
- Mile 13.0— Road rises on the dip slope of the Salt Wash Ss. The pink sandy soil is derived from the Entrada Fm. Drift sand forms coppice dunes occupied by Brigham tea.
- Mile 15.3— Road descends to the flood plain of Bull Creek. The gray, silty alluvium is derived largely from the Mancos Shale. The nearby arroyo with the young cottonwoods growing in the bottom is the active Dry Valley tributary of Bull Creek. In the distance to the northwest, old cottonwoods mark the course of the abandoned, pre-1950 Hanksville tributary. Although short, discontinuous sections of arroyo were present as early as 1850, the present continuously deep arroyo did not appear until after 1910 (Everitt, 1979).
- Mile 16.0— Bridge over the Dry Valley branch of Bull Creek.
- Mile 16.5— At 11:00 are bluffs formed by the Summerville Fm and capped by the basal gypsum of the Salt Wash Member of the Morrison.
- Mile 17.0— The greenish-gray marine shale is the Curtis Fm, which immediately underlies the Summerville.
- Mile 18.6—
- Mile 22.2—
- Milepost 118—
- Mile 119.5—
- Milepost 120—
- Milepost 122—
- Milepost 123—
- END OF LOG**—
- At 10:00 the Curtis unconformably overlies the Entrada, which is gently folded. Hanksville, and the junction of U-24 at milepost 117.
- Continue north on U-24.**
- Fremont River terraces here are capped with gravel mostly derived from Henry Mountains porphyry, transported northward by ancestral Bull Creek.
- Highway crosses the Dirty Devil River just downstream from the confluence of the two main branches. The Fremont River enters from the left (south) and Muddy Creek enters from the right (west). In 1973, five borings were drilled to investigate the bridge foundation (structure C656, UDOT files). The bridge abuts the north side of the valley. The thickness of alluvial fill increases southward from the north side of the valley to a maximum of 53 feet (50 feet below river level) at the south end of the bridge. Because the borings do not span the entire valley, this thickness should be regarded as a minimum.
- Road climbs to Airport Bench. Left at 9:00 are Factory Butte and the Caineville mesas, with the high plateaus in the distance.
- Castles of Entrada Ss on the left with basal moats formed by wind scour.
- Scenic turnout, optional stop. San Rafael Swell, distant left, is the steep east face of an asymmetrical anticline of Laramide age. The light-colored rock forming the principal hogback is the resistant Navajo Ss. View of Henry Mountains to the south and the high plateaus to the west.
- The route continues northward along the foot of the San Rafael Swell via U-24 to Interstate 70 and U.S. Highway 6, returning to Salt Lake City and the Basin-and-Range Province via Soldier Summit. For descriptions of geologic features, see Oaks, 1988; Laine, et al., 1991, and Rigby, 1976. For general historic information, see Midland Trail Association, 1916; and Van Cott, 1990.

Wind Erosion of Mancos Shale Badlands—Part 2

ANDREW E. GODFREY

INTRODUCTION

When G.K. Gilbert crossed the Mancos Shale badlands homeward bound on election day, 1876, he wrote in his notebook (Hunt, 1988, p. 214):

“There is a very curious phenomena (sic) of badlands across the river. At a score of places I can see them vertical on the NE side and sloping on the opposite. The prevailing wind must be from the side that has the slope. Can that in some way account for the phenomenon?”

Recent research by Godfrey (1997a) has determined that the phenomenon observed by Gilbert is caused by wind erosion. However, it is caused by vacuuming rather than by the tractional forces so well known in sand deserts.

The badlands are underlain by the Blue Gate Member of the Mancos Shale. Paralithic soils developed on this shale have a gypsum-cemented crust averaging 1.2 cm thick overlying randomly oriented silt- to sand-sized shale chips.

This area averages about 13 cm of precipitation a year.

THE PROCESS

Wind erosion of Mancos Shale badlands occurs only on the lee sides of ridges, not the windward side nor along flats when the soil crust is undisturbed. Preceding the passage of cold fronts, this area receives gusty southwest winds. There is an average of over ten such fronts a year, mainly during the months of March, April, and October.

Above the tops of the badland ridges the wind can explosively accelerate from about 7 ms^{-1} up to 22 ms^{-1} . This rapid acceleration of the wind causes a barometric-pressure drop that lasts one second or less. This pressure drop occurs on the upper portion of the lee slopes. The pressure

drop can be up to 1.27 mm Hg, but averages 0.76 mm Hg. This drop can be attributed to two factors: the Bernoulli effect and the expansion of a turbulent zone on the upper lee side of ridges that can be shown by tests with streamers and dust.

During the short-lived interval of local air-pressure decrease, the soil atmosphere below the crust remains at ambient levels. This pressure difference can produce a lifting force of as much as $1.7 \times 10^{-2}\text{N}$, nearly twice the unit force of gravity on the crust, which averages $0.88 \times 10^{-2}\text{N}$ and ranges from 0.62 to $1.5 \times 10^{-2}\text{N}$.

RESULTING FEATURES

This vacuuming process produces distinct erosional features on the lee sides of badland ridges. The smallest feature is the cavity left by the removal of a crustal polygon (fig. 6). Removal of the cemented crust exposes the underlying shale chips to be blown away later.

Continuation of the process forms micro-cirque features near the crests on the lee sides of ridges. Some have flat floors, in others the normal slope of about 40 degrees extends up to the vertical cliff (fig. 7). In the largest of these features, the downwind-facing cliff can attain a height of nearly 10 m.

A second feature that can be produced by the vacuuming process is a closed depression. These depressions are up to 1 m deep and 10 m in diameter (fig. 8). Some are at the bases of downwind-facing cliffs, others are near the crests of ridges. The floors of these depressions are smooth and flat, which suggests that they are being partially filled by sediment washed from surrounding slopes. These closed depressions are not formed by solution as there are no soluble rock types for several thousand feet stratigraphically beneath this area.



Figure 6. Removal of individual polygons of crust. The underlying soil of shale chips is exposed.



Figure 7. One of the micro-cirques along a ridge crest. The southwest winds blow from right to left. Cliff is about 1 m high.



Figure 8. Closed depression downwind of a cliff that has been breached by headward erosion of a micro-cirque. Wind direction is toward the camera. Note person for scale.

Long-term Measurements of Soil Creep Rates on Mancos Shale Badland Slopes—Part 3

ANDREW E. GODFREY

INTRODUCTION

Outcrops of Cretaceous Mancos Shale form a broad belt across the Colorado Plateau of southeastern Utah and southwestern Colorado. They are a major source of salinity and sediment to the Colorado River (Schumm and Gregory, 1986). Howard (1994a, b) used simulation models to argue that sediment production was limited by detachment rather than by transport.

This report summarizes a 30-year study conducted to determine the rate of downslope movement of surficial soil developed on the Mancos Shale near Caineville, Utah (Godfrey, 1997b). Other segments of the investigation, covering about a decade, studied the effects of aspect, slope position, seasonality, and depth of soil movement.

PROCEDURES

Seven sites were established. One was maintained for 30 years, and measured sporadically. Three were maintained for a decade and were measured mostly in June and November. Three others were maintained for almost seven years and were only measured at the beginning and end of the seven-year period.

Each site consisted of between 16 and 24 nails, 9 cm long, inserted vertically into the soil between benchmarks placed along the contour of the slope. Spacing of the nails was either 0.3 or 1.5 m. Benchmarks consisted of rods 1 m long driven vertically about two-thirds of a meter into the soil.

Measurements were made along the slope from a point directly below a string stretched between two benchmarks and the point where the nail met the soil surface. Average downslope distances and their standard deviations were then calculated for each measurement time at each site. These average distances were then plotted, and the linear regression computed to determine the average soil-movement rates.

RESULTS

The 30-year study showed an average downslope rate of 2.7 cm/yr on slopes averaging 35 degrees.

Data from one of the seasonally measured sites (see fig. 9) indicate several episodes of more rapid downslope movement. These steps occurred during the winters of 1985 and 1988, whereas smaller steps occurred during the winters of 1983 and 1991. Correlation of these episodes with precipitation records from the Hanksville weather station, 20 km to the east, indicates that the larger steps occurred during winters when there were two or more consecutive days of at least 6 mm of precipitation. The smaller steps occurred when the two consecutive days had between 2.5 and 6 mm of precipitation for the day with the lesser precipitation.

A Student's T test comparing movement rates on north- and south-facing slopes showed no significant difference in the populations at the 95 percent confidence level. The comparison was made for the period of five years before the north-facing site was disturbed.

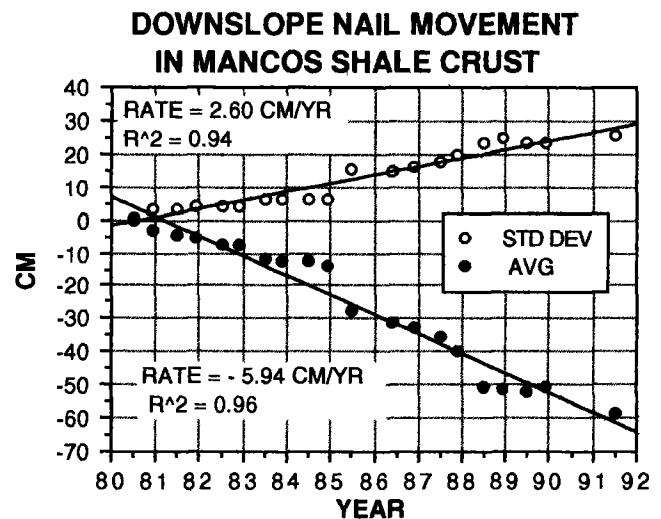


Figure 9. Graph from one of the study sites near Caineville, Utah. It shows the average downslope distances of 20 nails at the times of measurement and the standard deviations of those distances. Regression lines through both were used to determine their rates. Note that the standard deviation of the set of nails increases over time, which indicates increasing distances between higher and lower nails on the slope.

Slope position appears to be an important factor controlling movement rates, as indicated by the sites measured only at the beginning and end of a seven-year period. The site between 1 and 2 m below the ridge crest moved at an average rate of 0.7 cm/yr. At the same time, sites 5 and 10 m below the ridge crest moved at an average rate of 4.1 and 4.5 cm/yr. A Student's T test between the upper and middle sites indicated there were two separate populations at the 99 percent confidence level.

Figure 9 shows that the spread of the nails, as measured by the standard deviation, increases with time. For all the sites the rate of increase of the standard deviation is

between 35 and 46 percent of the average downslope distances the nails had moved at any given time. This spread of the nails indicates that downslope movement of the soil surface occurs as independent slices up to a few meters wide, with each slice moving independently. The relatively large spread in the distances the nails move helps explain why there is no significant difference in the rate of movement between north- and south-facing slopes.

The nails rotated in a downslope direction as they moved downslope. This indicates that a shallow surface layer of the soil is involved and that lower layers of the soil either are stable or move quite slowly.

Vegetation and Geomorphology on the Fremont River—Part 4

BEN EVERITT

INTRODUCTION

Dynamic sand-bed rivers such as the Fremont River of southern Utah provide a fruitful area for the study of the relationships among the variables of climate, hydrology, geomorphology and riparian vegetation. The changing survivorship of different pioneer species is recorded on flood bars of different ages.

PHYSIOGRAPHY

During the last century the Fremont River passed through an episode of arroyo cutting. Between 1896 and 1916 a series of floods gutted the valley, forming a wide braided channel which has destroyed most traces of the former narrow sinuous one (Wooley, 1946; Hunt, et.al., 1953; Graf, 1983; Webb, 1985). The present river is a product of the gradual shrinking of the channel and construction of a flood plain inset within the 1896 arroyo, mostly since 1940 (Everitt, 1995).

The valley floor and floodplain can be subdivided into physiographic units for the purposes of describing topography and vegetation. In figure 10, I have used the classification of Osterkamp and Hupp (1984, fig. 1). The *channel bed* (CB) carries the low flow, when there is any, and is wet most of the time. *Depositional bars* (DB) are ephemeral features in or adjacent to the channel bed, formed of newly deposited sediment, and unvegetated except by sparse annuals and seedlings. The Fremont presently has an *active channel shelf* (AS) which is a composite of many flood-deposited treads separated by steps and rising 0.9–1.2 meters above low water. The boundary between the channel shelf and the more horizontal surface of the *active flood plain* (FP) is a matter of judgement. The floodplain surface undulates between *flood bars* (FB) and *swales* (FS), with a relief of 0.3–0.6 meter. Behind the active flood plain are remnants of *terrace* (T), the flood plain abandoned in 1896. The terrace is about 3 meters above the active flood plain and separated from it by an erosional scarp. The substrate is friable fine sand with minor silt, with clay locally in the swales.

The relative area occupied by the various physiographic subdivisions of the flood plain has changed as the modern valley has evolved. The active flood plain with its bars and swales provides a variety of habitats for vegetation. It is mostly younger than about 1940 (Graf, 1983); the oldest woody plant found so far (tamarisk) dates from the 1950's (Everitt, 1995). The habitat available for colonization is evolving as the river evolves. The present flood plain is undoubtedly quite different from the braided channel of 1940, with respect to elevation, time subject to inundation, propensity to scour, stage versus velocity, and elevation above normal water table.

Graf (1983) presented a model of the Fremont River as one which alternates between two states: a process-dominated state, in which channel morphology is principally a function of discharge; and a form-dominated state, in which the geometry of channel and flood plain present more inertia, and exert feedback to the flow. The Fremont is evolving toward the form-dominated state. Floods have been smaller in recent years, due to either climatic effects or morphologic feedback, or a combination of the two. The channel is shrinking in width and meandering only slowly, continuing to provide new ground for colonization.

VEGETATION DESCRIPTION

The vegetation of the middle Fremont, as recorded in 1982 at the mile-post 111 traverse (fig. 10), is typical of the river between Caineville and Hanksville. Colonization by reed mats and seedlings of coyote willow and tamarisk begins on the active shelf (AS in fig. 10). Cottonwood probably appears here as well during favorable years. A row of cottonwood saplings to five meters in height occupies the proximal flood bar (FB) with some Russian olive, tamarisk, coyote willow, and rabbitbrush, with ground cover ranging from 30 to 50%. The cottonwood saplings belong to a single cohort which is dated to the early 1970's, and is probably a response to the late spring flood of 1973 (Everitt, 1995). The distal flood bar is occupied by tamarisk and rabbitbrush, with ground cover estimated at 60%. In the inter-

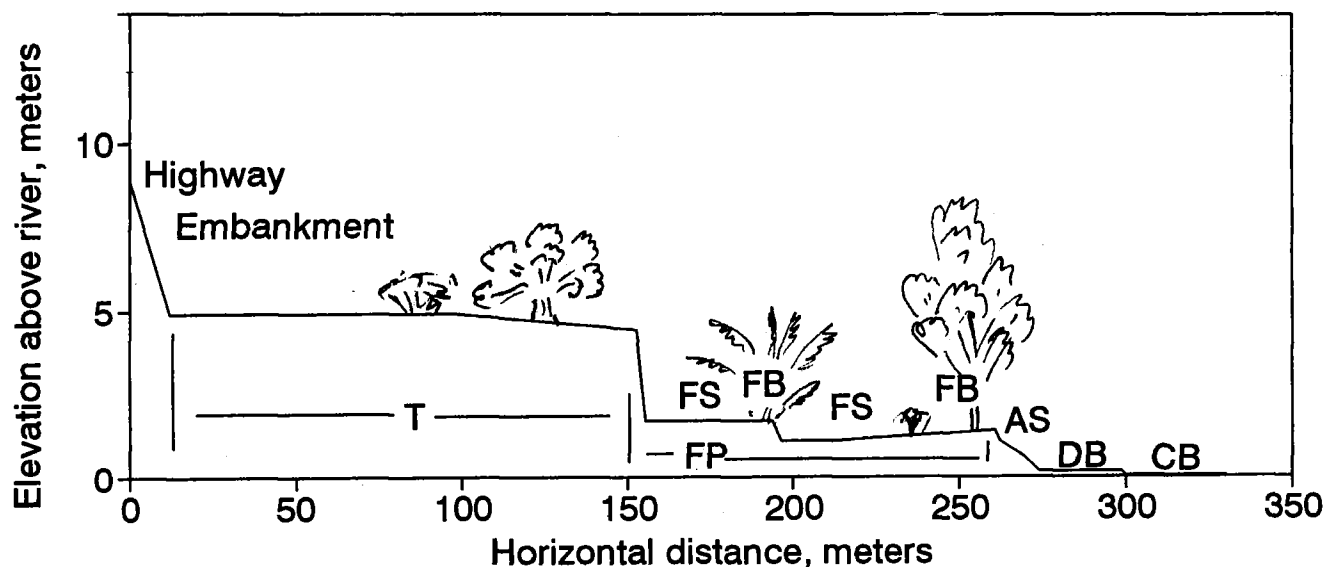


Figure 10. Pace and hand-level traverse of Fremont River Valley, running S 16 W from milepost 111, State Highway 24. The physiographic subdivisions of the valley floor are labeled with binomial initials: CB, channel bed; DB, depositional bar; AS, active channel shelf; FP, active flood plain; FB, flood bar; FS, floodplain swale; T, terrace—abandoned floodplain (from Everitt, 1995, Figure 4).

vening swales (FS) are rabbitbrush, tamarisk, four-wing saltbush, and Torrey seepweed to a lower density (10 to 20%). The dense fringe of tamarisk at the toe of the terrace is a widespread feature of the central Fremont, and indicates that tamarisk was the primary perennial pioneer species at the time the active channel margin began to retreat from the foot of the terrace.

The terrace (T) is occupied by four-wing saltbush and greasewood, with some old cottonwoods, many dead or dying. The absence of tamarisk shows that the terrace predates the introduction of tamarisk into the Fremont drainage.

CONCLUSION

The simple pioneer-dominated plant community of the Fremont River flood plain records a changing mix of species in response to changing habitat and the introduction of new species. Recorded in the transect at milepost 111 is the introduction of tamarisk (probably about 1940) and its subsequent decline; the resurgence of cottonwood in the 1970's, and a continuing gradual increase in Russian olive (Everitt, 1995).

Gravel Deposits North of Mount Ellen, Henry Mountains, Utah—Part 5

ANDREW E. GODFREY

INTRODUCTION

The piedmont north and northeast of Mount Ellen, northernmost of the Henry Mountains, is marked by fan-shaped gravel deposits of three streams. These deposits are the gravel-capped pediments of Gilbert (1880, p. 120–129), and Hunt, et.al. (1953, p. 189–195). From east to west the streams are Bull, Birch, and Nazer Creeks. A program of detailed mapping was undertaken to determine the history, mode of deposition, and controlling factors of these gravel deposits (Godfrey, 1969). This report presents a brief overview of the findings related to Bull Creek.

FINDINGS

A band of hummocky, boulder-strewn deposits separates Mt. Ellen's slopes from smooth-surfaced gravel deposits farther out. This band, containing boulders that range up to house size, is considered to be deposits of an Early Pleistocene debris avalanche (Godfrey, 1980).

Mapping of the smooth-surfaced gravel deposits showed they are a composite of discrete linear deposits extending from the mountain front to the Fremont-Dirty Devil river system. Figure 11 shows the directions of several paleo-courses of Bull Creek. Additional, minor routes are not shown. For Bull Creek there were at least 13 distinct gravel deposits representing different stream courses.

This investigation indicated that, in the piedmont north of the Henry Mountains, the development of a gravel bench is a repetitive process. It begins with gully erosion of some older piedmont landform. However, the critical factor is the gradient of streams tributary to main streams originating in the mountains. Unlike the more common case, where tributaries have steeper gradients than the main stem, tributary desert washes not draining igneous rocks have flatter gradients. These washes are eroding and transporting only fine-grained erosion products of sedimentary units exposed on the piedmont rather than the coarse products of the igneous mountain mass. This difference in gradients results in each tributary being at a lower elevation than the adjacent main stem at any point upstream from the junction.

Erosion of drainage divides, random lateral migration of mountain streams across their flood plains, and overflow of

a divide during a flood, can lead to the capture of the headwaters of a main stem stream by a nearby desert wash. With the diversion of the gravel-transporting stream, the valley of the desert wash changes from a locus of erosion to one of deposition. This change results in the steepening of the

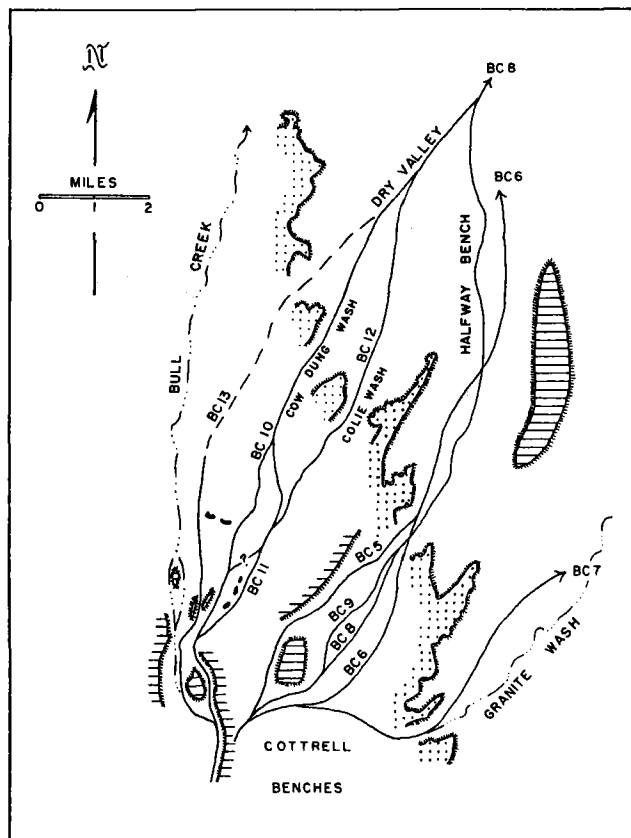


Figure 11. Sequential changes of ancestral Bull Creek interpreted from gravel deposits on the Cottrell and Fairview Benches. Higher numbers are younger deposits. Hatchers represent escarpments, stiples are on the dip slope of the Summerville Escarpment, horizontal rulings represent higher-standing gravel deposits, and black areas represent sandstone hills at or just above the level of the gravels. In general, the sequence shows a progressive headward capture of the main stream.

wash's gradient so the wash can transport the coarse gravel. Accompanying this steepening of gradient is a regrading of the point of capture into a smooth profile.

During burial of the former desert wash's valley, its floor can be smoothed by lateral planation. However, the linear nature of the mapped gravels indicates that this lateral planation is restricted to the already existing valley. There is little widening by the gravel-carrying streams, perhaps due to the steepness of the slopes in this area. Braided streams have distributed gravels over flood plains whose limits have been predetermined by the width of the pre-existing valley.

CONCLUSIONS

Detailed mapping of Bull Creek's gravel benches north of Mount Ellen showed that the apparent fan-shaped, gravel-capped pediments are a composite of several linear deposits, each representing an identifiable stream course at progressively lower levels. They fit Robert Oak's classification of a "shoestring" pediment (Oaks, personal communication). This is because the gravels were deposited in pre-existing val-

leys cut by desert washes. Lateral planation can occur within a valley, but widens it only slightly in areas of steep slopes.

The processes that form these gravel benches are not climatically controlled. There is not one set of conditions that causes erosion and another set that favors deposition. Both erosion and deposition can occur simultaneously. Desert washes with lower gradients erode valleys in the piedmont that are at lower elevations upstream from their confluences than the aggradational, higher-gradient, gravel-bearing main streams flowing out of the mountains (Rich, 1935). Capture occurs randomly when the main stream migrates to the edge of its valley where its interfluvium has been eroded away.

Relative relief between gravel benches is not necessarily an indicator of the time between the deposition of the benches. Instead, distance between capture point and downstream confluence, and the resistance of the rocks that a desert wash erodes through, are significant controls of relief.

Monitoring flash floods in the Upper Blue Hills Badlands, Southern Utah—Part 6

GREGORY S. DICK
ROBERT S. ANDERSON
DANIEL E. SAMPSON

*Department of Earth Sciences and Institute of Tectonics,
University of California, Santa Cruz, California 95064*

Why study badlands, or flash floods, or flash floods in badlands?

Badlands are intriguing for their unique and often desolate appearance and apparently rapid rates of change. These barren landscapes develop through intense fluvial dissection that produces steep hillslopes and high local relief (Bryan and Yair, 1982; Howard, 1994), and are most often found on easily eroded, "soft" bedrock (e.g., shales) in arid to semi-arid environments. Spot hillslope erosion rates in badlands on the order of mm/yr are among the highest measured in any landscape (Schumm, 1956; Schumm, 1964; Campbell, 1982). The short time scales during which badlands develop and their manageable spatial scales (e.g., area, relief) provide us with a geomorphic microcosm in which to study fluvially controlled landform evolution.

Because hillslopes erode quickly, maintenance of the rugged topography in the Upper Blue Hills (Blue Hills) requires high channel incision rates. The typical assumption is that the regolith and bedrock common in badlands are easily erodable, coupled with nearly impermeable regolith, leading to high runoff/rainfall ratios. High runoff appears to be needed to cause high rates of incision. While these shales are visibly quite friable, much existing work challenges the notion that badlands surfaces are simply impermeable "parking lots" (Schumm and Lusby, 1963; Lusby, 1979; Yair et al., 1980; Bryan et al., 1984). The heavily cracked and piped regolith in badlands is often highly permeable, with maximum potential infiltration rates on par with maximum rainfall intensities (~50–100 mm/hr). Yair et al., (1980), comparing experimental infiltration rates to rainfall records, conclude that surface flow in the Zin badlands of Israel is exceedingly rare under the present climate, and is produced only during extreme rainfall events. Apparently, only a few rainfall events produce surface flow in these landscapes under present climate conditions.

The combination of rapid channel erosion with apparently rare flow events poses an interesting problem: when

and how are these channels eroded? Are rare, large-magnitude rainfall events the only way, or can less frequent events accomplish much geomorphic work? To decipher this, we need documentation of the frequency and erosive power of flows in these channels, but little flow information is available for such small catchments. In fact, there are few measurements of flash floods in general, as they are rare and difficult to gauge accurately. However, the limited observations suggest they are quite different from that of perennial flows. They are typically highly turbulent, and carry extremely high suspended sediment loads relative to perennial flows of similar size (Reid and Frostick, 1987). Typical flash floods initiate with the passage of a small, steep-faced bore front, immediately followed by some flow recession. Thereafter, the hydrograph gradually rises to peak depth. The time to peak discharge is short, and decreases with increasing drainage area as the hydrograph front steepens downstream. Recession is typically rapid. Excellent discussions of flash floods are available (Hassan, 1990; Leopold and Miller, 1956; Reid and Frostick, 1987; Renard and Keppel, 1966; and Schick, 1988).

To learn how often erosive flows occur in the Blue Hills, we began actively (and accurately) monitoring channel flow and rainfall in the Upper Blue Hills in early summer 1994. Our aim is to address the following questions: (1) what is the hydraulic nature of the ephemeral flows in these channels, and what produces the observed characteristics?; and (2) what controls the frequency and magnitude of geomorphically significant flow events?

The Blue Hills Flash-Flood-Monitoring Project

The Upper Blue Hills badlands

The Upper Blue Hills badlands extend from the Henry Mountains to the south (Mt. Ellen, at 3510 m, is the highest peak in the Henry Mountains), to North Caineville Mesa and Factory Butte, just to the north and northeast. Channels

drain to the Fremont River, a tributary to the Colorado River. The blue-gray marine shales in the Blue Hills belong to the Blue Gate Member of the Cretaceous Mancos Shale, which floors roughly one-sixth of the upper Colorado River basin. The climate is arid: Hanksville, ~25 km east, receives an average of 12 ± 4 cm annual rainfall (period 1947–1992). Local convective thunderstorms occur during the summer, when the warm continental interior draws monsoonal winds off the Gulf of California. Frontal storms deliver low-intensity rainfall (and some snow in winter) during the remainder of the year.

The Blue Hills provide a stunning visual example of the intimate linkage between hillslopes and channels in fluvial landscapes. Drainage densities in the instrumented basin are high, exceeding 60 km/km^2 . Channels along the instrumented reach have slopes >0.01 , with frequent knickpoints up to ~1 m in relief in bedrock and alluvium, and alternate between short bedrock reaches and reaches covered with a thin (<0.5 m) alluvial mantle. The erosion of the channels is accomplished through: (1) direct, subaerial (perhaps salt expansion) weathering of the bedrock channel floor, with weathering products transported in flows; (2) disaggregation of the rock by water (drop a piece of the Mancos Fm in your water bottle!); (3) headward propagation of knickpoints throughout the badlands; and (4) some direct “plucking” of blocks and rock fragments from the bed which are likely later weathered or disassociated by water. The hills are evolving through a combination of diffusive rain-splash erosion along the ridge lines (note convexity and “smooth” look) where slope is gentle, and shallow (~few cm’s) landsliding on steeper hillslopes. The transition to landslide-dominated erosion is quite visible on the hillslopes, and typically occurs at slope angles of 35° – 40° . Hillslopes are rarely steeper than this, except where actively undercut by channel meanders. Steep hillslopes are maintained by incision of the adjacent channels. Such landslides transport a substantial quantity of material to the channels, where it is later transported by channeled flows and thereby helps generate the high sediment concentrations in flows from the Blue Hills. Erosion by overland flow (i.e., sheetflow) appears to be minimal, although there is evidence of regolith stripping by small mudflows in the rills.

The Blue Hills are evolving through headward channel incision likely initiated by rapid post-glacial incision of the Fremont River (Howard, 1970). This incision is recorded by the terraces now visible along the Fremont. The isolated, relatively smooth surfaces that cap the badlands here are inferred to be paleovalleys mantled with debris-flow material from the adjacent buttes; the debris-flows are perhaps most active during pluvial (glacial) episodes. These surfaces appear to grade to a Fremont River terrace, although correlating these remnant surfaces is tricky. Cosmogenic radio-

nuclide dating of the large remnant along the western edge of the monitored basin yields ages of ~18 kyr (unpubl. data, J.L. Repka). This age ties debris-flow deposition on this surface to the last glacial maximum. If this date records the approximate time of abandonment, the current relief of the monitored catchment implies average post-pluvial channel erosion rates up to ~2 mm/yr. This scenario of badland development through post-pluvial incision of a trunk stream is similar for badland development elsewhere in western North America (e.g., Bryan et al., 1987).

Hydrograph measurement technique

Because flash flows are turbulent, sediment-laden, rare, and rapidly varying, and because we needed a gauging technique that could operate without frequent maintenance, we developed an acoustic depth monitoring system, dubbed the EchoRanger. The acoustic sensors, which are based on Polaroid autofocus camera electronics, are hung below PVC supports, and “look” down on the channel floor. The sensors are connected and controlled by a Campbell Scientific CR10 datalogger located in watertight control boxes adjacent to the channel. These sensors obtain distance measurements to a reflector by measuring the travel time of an emitted pulse of sound, and can obtain distances as frequently as 8 Hz. Here, we operated them at 1 Hz. The recorded distance between the sensor and a reflective surface (either water or channel bottom) is converted to a flow depth, from field calibrations, after correcting for temperature.

We deployed four stations (A–D), each with two acoustic transducers, along the same channel, and one recording, tipping-bucket rain gauge at station B (fig. 12). Gauged basin sizes are from 0.88 km^2 to 1.03 km^2 (fig. 12). Rainfall was totaled at 1 minute intervals, and ambient temperature was recorded whenever depth readings were saved.

Recorded hydrographs

From summer 1994 to summer 1996, we have evidence for 11 flows in the monitored catchment. Seven of these events were relatively small (peaks $<0.15 \text{ m}^3/\text{s}$); only four flows exceeded $0.5 \text{ m}^3/\text{s}$. We focus here on the two hydrographs discussed in Dick et al., (1997).

Event A: September 20, 1994

On September 20, 1994, we witnessed a rainfall event that produced a small flow. The rain gauge recorded 4.8 mm during a period of 8 min, with intensities ranging from 15 to 76 mm/hr. Rills on hillslopes contained visible runoff within several minutes after rainfall began, especially following the highest rainfall intensity. The heavily cracked

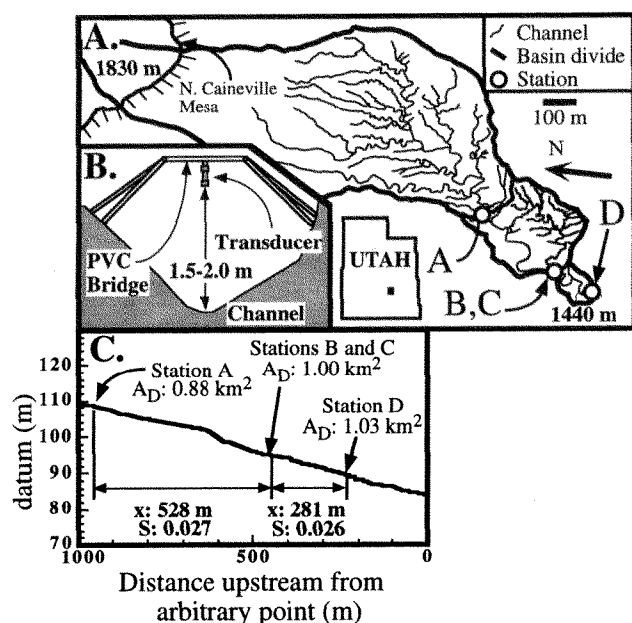


Figure 12. A: Drainage network and location of gauging stations. B: Schematic of acoustic-sensor installation. C: Profile of main channel through monitored area, with total drainage area (A_D) above each station, and horizontal distance (x) and average slope (s) between each station.

regolith did not seal during the rainfall, and we did not observe concentrated surface flow on undisturbed regolith. Depth of regolith wetting was up to a few centimeters. Surface failures ~5 cm deep occurring during the storm revealed a dry bedrock surface.

We measured flow depth and surface velocity manually at station B (fig. 13). Flow began ~5 min into the rainfall event, and gradually increased to several centimeters depth by rainfall completion. Two bores of several centimeters height passed ~9 and ~16 min after rainfall began. Surface velocity measurements ranged from 0.7 m/s (depth = 2.5 cm) to 1.9 m/s (depth = 7.0 cm). Standing waves were observed at depths ≥ 2.5 cm, evidence of near critical ($Fr \approx 1$) flow conditions (Knighton, 1984). Flow Reynolds numbers were $\leq 41,000$. Measured surface velocities yielded n values from 0.012 (depth = 7.5 cm) to 0.022 (depth = 2.5 cm).

The station A acoustic system recorded flow above the ~8 cm threshold (fig. 13). Depth at the remaining stations was below the recording thresholds (<10 cm). The hydrograph is complex: there were numerous rapid changes in depth that were large relative to the total depth. The average translation velocity of the rapid rise of flow level (a at A, a' at B, fig. 13) was ~1.8 m/s. The estimated runoff coefficient (total runoff/total rainfall) was ~0.01.

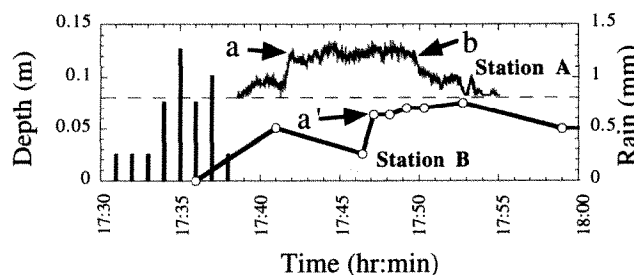


Figure 13. Event A hyetograph (bars) and hydrographs for stations A and B. Black line is 3 s running average of d measured every 1 s; gray line shows 1 s data. Scatter in the 1 s data is indicative of measurement error. Dashed line is recording threshold (~8 cm). Hand-held measurements at station B were made at times shown. We collected during any notable changes in flow, and the hydrograph between gauging points did not depart significantly (± 1 cm) from the line connecting the points. Average translation velocity for rapid rise in flow level, labeled a-a', was 1.8 m/s over 0.5 km reach between stations A and B. Note several distinct flow peaks of station A hydrograph, and rapid depth changes at a and b that are large relative to total depth.

Event B: September 29–30, 1994

On September 29–30, 1994, a rainfall event lasting 30 min and totaling 5.3 mm produced the deepest recorded flow (fig. 14). Rainfall intensities were low (<30 mm/hr). However, 3.0 mm of rain had fallen during the preceding 12 hr. Three stations recorded the resulting hydrograph (fig. 14).

At each station, depth increased rapidly, rising from below the recording threshold to ~15–20 cm in <5 min (fig. 14). This initial front advanced with an average velocity of 2.0 m/s from station A to B and 1.5 m/s from station B to D, and retained a height of ~20 cm. The rise time to the initial flow peak (a-a', fig. 14) shortened from ~5 min at station A to ~3 min at station D. The initial peak was followed by recession of several centimeters, and later by two primary flow peaks (b and c, fig. 14) presumably associated with individual rainfall maxima within the storm. Features identifiable in each hydrograph (a, b, and c, fig. 14) traveled with velocities of 1.2 to 2.2 m/s, increasing with flow depth. The time lag between the start of flow recording and peak flow was ~15 min at each station. Runoff coefficients were $\geq \sim 0.08$.

Controls on hydrograph shape and total runoff

Events A and B had different hydrograph characteristics. We suggest that this may reflect differences in rainfall delivery. In the event A hydrograph, produced by an intense thunderstorm (fig. 13), large depth changes (relative to total

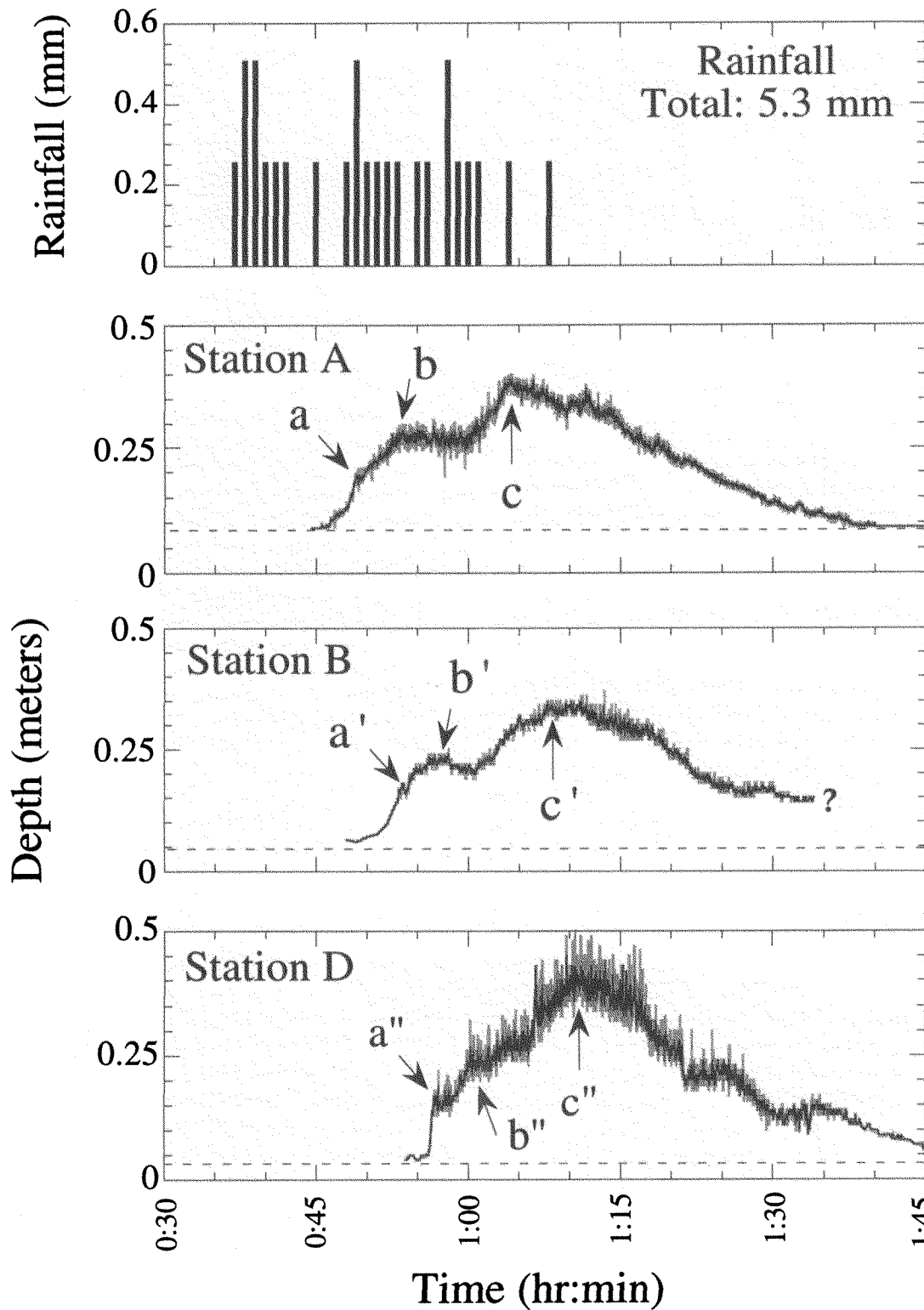


Figure 14. Event B hietograph (top graph) and hydrographs for stations A, B, and D. Dashed lines as in Figure 3. Large scatter in station D data arises from false triggering of sensor by splash. Note reduced rise time to initial hydrograph peak ($a-a'$) and overriding of $b-b'$ by peak $c-c''$ during hydrograph translation downchannel. Features a , b , and c are selected where hydrograph curvature is high. Average velocity (m/s) of hydrograph features: $a-a' = 2.0$, $b-b' = 1.9$, $c-c' = 2.2$, $a'-a'' = 1.5$, $b'-b'' = 1.2$, and $c'-c'' = 1.8$.

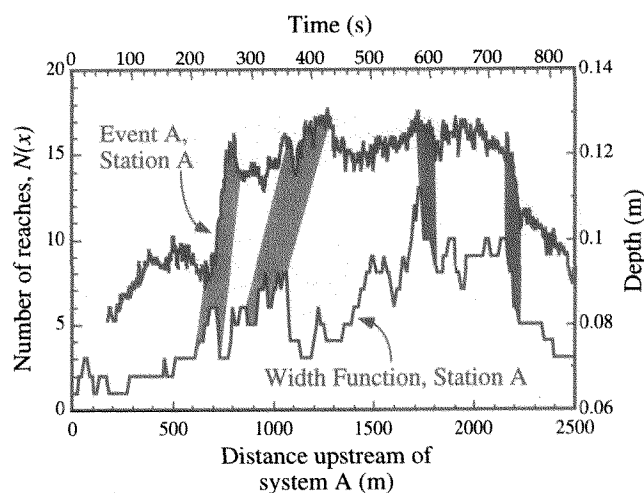


Figure 15. Comparison of event A, station A hydrograph (d vs. time) and the network width function (see text) for basin above station A. Gray boxes highlight similarities between the two curves.

depth) are frequent and occasionally rapid (a and b, fig. 13). Similar rapid depth fluctuations observed in other flash floods were suggested to be either “momentum waves” (Leopold and Miller, 1956), or an expression of the channel-network shape (e.g., Renard and Keppel, 1966). We compare the event A hydrograph to the graphical network width function, which is the sum of channel segments as function of distance above a point in the channel network (fig. 15; see Mesa and Mifflin, 1986, and Dick et al., 1997, for details). The event A hydrograph and the network width function are similar (fig. 15), which suggests that the hydrograph shape could reflect the network geometry. The only other recorded hydrograph produced by a high-intensity storm also looks similar to the width function, despite differences in the hyetograph (Dick, 1995). In contrast, the event B hydrograph is much smoother, lacks obvious features reflecting network shape, and is broadly similar in shape to the rainfall hyetograph. We hypothesize hydrograph shape is controlled by the network geometry when flow is produced by high-intensity storms that are short relative to the rise time of the hydrograph (e.g., event A). In such cases, overland and shallow subsurface flow produce rapid runoff; tributary flows are short-lived, and contribute peaks to the trunk channel that are preserved in the outflow hydrograph. For storms of similar size but longer duration (i.e., event B), tributary hydrographs rise more slowly, with smaller peaks that are not clearly preserved in the outflow hydrograph. We continue to collect data here to test these hypotheses.

A critical factor in runoff generation here is antecedent moisture. The difference in the two flow events we describe

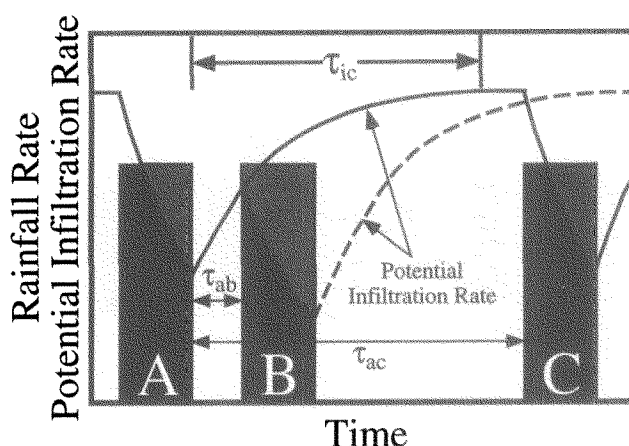


Figure 16. Schematic illustration of important antecedent-moisture time scales using three simplistic boxcar-shaped “storms” of equal intensity and duration (A, B, and C), shown as rainfall-intensity histories. Rainfall event A decreases potential regolith infiltration rate (solid line), so that eventually the constant rainfall intensity exceeds this rate, producing runoff (light gray area of rainfall boxes). Infiltration capacity begins to recover following completion of storm A. Full infiltration capacity recovers fully in time t_{ic} . Time between storms A and C, t_{ac} , is long enough ($t_{ic}/t_{ac} \leq 1$) for infiltration capacity to have fully recovered. Time between storms A and B, t_{ab} , is short ($t_{ic}/t_{ab} > 1$); the infiltration capacity has not recovered from previous wetting. Further decrease in infiltration rate (dashed line) during storm B allows production of much more runoff than equal-sized storms A and C.

here is a good model. The events had comparable total rainfall (4.8 mm in event A and 5.3 mm in event B), but, counterintuitively, the storm with lower intensity produced flow with maximum discharge and total energy expenditure an order of magnitude greater than event A, produced by a more intense storm (up to 76 mm/hr). The outstanding difference between the two events is the antecedent moisture condition: whereas no rain fell in the 9 days prior to event A, 3.0 mm fell intermittently during the 12 hr preceding event B. The reduced potential regolith infiltration rate allowed significant runoff production ($\geq 8\%$ total rainfall vs. $\sim 1\%$ in event A). In fact, of 33 rainfall events exceeding 0.5 mm total rainfall recorded in 1994 and 1995, only three produced flows with maximum discharges $>0.5 \text{ m}^3/\text{s}$. These three rainfall events, although not remarkable in total rainfall (1.2, 5.3, and 6.6 mm), were preceded by >3.0 mm rainfall during the previous 24 hr. The remaining 30 rainfall events occurred when rainfall was ≤ 1.8 mm during the preceding 24 hr, and produced little or no flow.

For antecedent moisture to be important, storms must occur within some time, t_{ic} , after a previous wetting event (fig. 16). This time scale reflects how quickly infiltration capacity is recovered through drying, which depends upon

regolith properties and weather (e.g., temperature, wind). We estimate τ_{ic} to be roughly 24 hr in the Upper Blue Hills. Because of this recovery time, we must know the full probability distribution of spacing between rain events to estimate flow frequency. The average time between storms (e.g., Schumm and Lusby, 1963) is not sufficient, because storms are not evenly spaced. For instance, the total energy

expenditure suggests that event B was geomorphically significant (Costa and O'Connor, 1995). The total rainfall for event B has a return period of ~ 1 yr. However, geomorphically important event B-type channel flows may occur at a quite different frequency dependent on storm-sequencing rather than rainfall recurrence interval.

Dating the Fremont River Terraces—Part 7

JAMES L. REPKA
ROBERT S. ANDERSON
GREG S. DICK

*Department of Earth Sciences and Institute for Tectonics,
University of California, Santa Cruz, California 95064*

ROBERT C. FINKEL
*Geosciences and Environmental Technology Division and Center for
Accelerator Mass Spectrometry, Lawrence Livermore National Laboratory,
Livermore, California 94550*

ABSTRACT

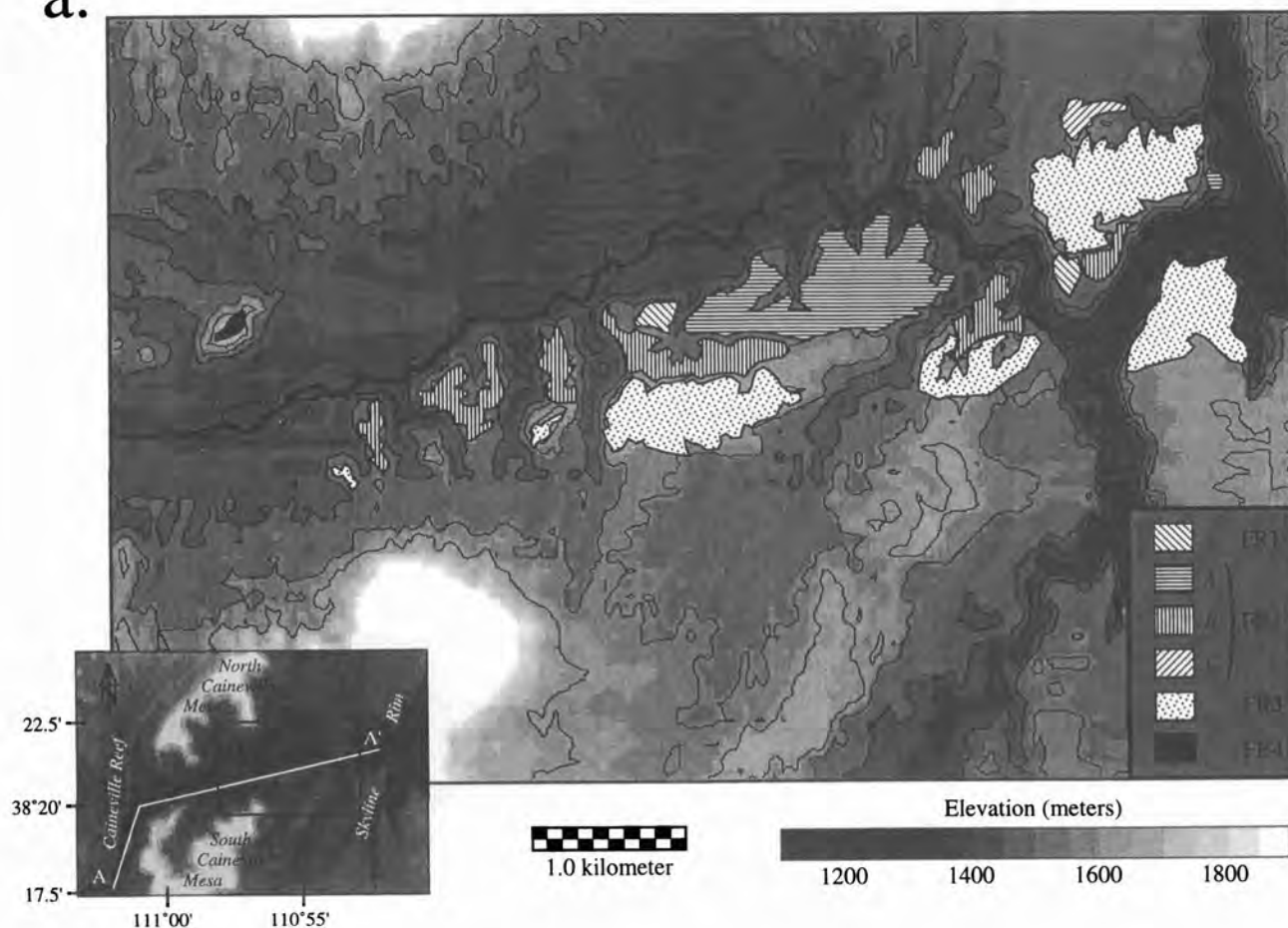
In many parts of the world, sequences of terraces that flank river drainages mark periods of stasis in the downcutting history of the river. Absolute dating of these terraces, in addition to yielding long-term incision rates, can clarify the role of climate in controlling river-drainage evolution and can establish the rates of pedogenic processes. Surface exposure dating using cosmogenic ^{10}Be and ^{26}Al would seem to be an ideal way to date such surfaces. However, the surfaces are composed of individual clasts, each with its own complex history of exposure and burial. Because the exposure age of a clast may be different than the exposure age of the surface, the stochastic nature of nuclide production in the clasts, both during their exhumation and transport to fluvial terraces as well as during post-depositional stirring, can result in neighboring clasts containing grossly different nuclide concentrations. We describe here a strategy for dealing with the problem of the stochastic nature of inheritance. First we study samples amalgamated from individual clasts in order to average the widely different exposure histories of each. Second, we measure samples from depth profiles to estimate the actual level of inheritance and to check for the possible importance of stirring.

The results of applying this technique to terraces along the Fremont River in southern Utah demonstrate that single clast ages are indeed more widely scattered than those of amalgamated samples and that samples amalgamated from 30 clasts represent the mean concentration quite well. Depth profiles consisting of several amalgamated samples show an exponential decline in concentration attributable to post-depositional nuclide production, and argue strongly against relative displacements of the clasts on these horizontal surfaces subsequent to deposition. Using the production rates of Nishiizumi et al., (1996) as adjusted for geographic latitude and for reassessment of the deglaciation age (Clark et al., 1995), our technique yields ^{10}Be age estimates of 60 ± 9 , 102 ± 16 and 151 ± 24 ka for the three most extensive terraces, corresponding to isotope stages 4, 5d and 6. Isotope stage 2 appears to be represented here by either a small group of isolated narrow surfaces or by the current flood plain of the Fremont River. These dates support a conceptual model in which the terraces formed when there was a strong glacial source of sediment within the headwaters, and were abandoned when the sediment source shut off. The mean inheritance is remarkably constant from terrace to terrace. Failure to correct for inheritance would yield dates several tens of thousands of years too old. Inheritance likely reflects primarily the mean exhumation rates in the headwaters, of order 30 m/Ma.

The channels of the Blue Hills badlands have as their base level the channel of the Fremont River (fig. 17). The numerous extensive terraces of the Fremont River attest to the lowering of this boundary condition through time. To begin to assess the history of this downcutting, and hence the

history of the baselevel forcing that was experienced by the adjacent badlands, we set out to establish the ages of these Fremont terraces. While these surfaces were mapped in detail by Howard (1970) in his thesis work, no absolute ages exist. As the headwaters of the Fremont have experienced

a.



b.

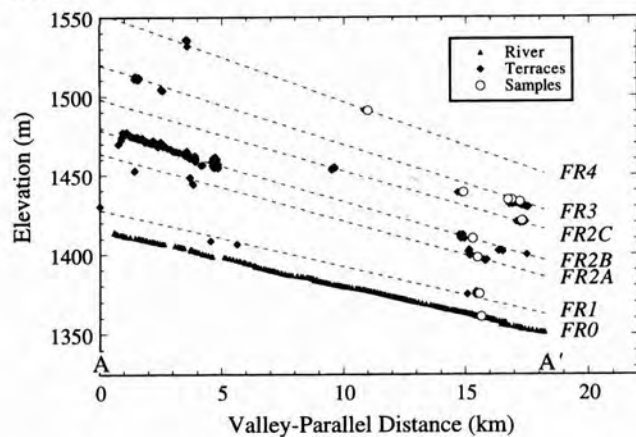


Figure 17. (a) Detailed topography adjacent to the Fremont River as it passes eastward through the gap between North and South Caineville Mesas. The sampled terraces are depicted. Note the isolated scraps of FR1 and FR4 surfaces, and the extensive preservation of FR2 and FR3 surfaces. (b) Valley-parallel longitudinal section of the terraces (diamonds) in the study area (A-A' from the inset map in Figure 17a), showing elevations relative to the modern Fremont River floodplain (triangles). Sampled sites are shown as open circles.

occasional glaciation (Flint and Denny, 1956), the sediment- and water-discharge histories from the headwaters should have seen large swings that result in downstream propagation of waves of aggradation followed by incision and abandonment of outwash terraces (e.g., Bull, 1991). The glacial deposits in the headwaters are not well dated. In addition, correlation to other glacial sequences within the western U.S., such as those in Wind River system (Howard, 1986), implicitly assumes the synchronicity of the responses to regional climate change. Absolute dates of these, and of other sequences of glacial outwash terraces in the western U.S., would allow testing of the conceptual model for the formation of such terraces, and would allow assessment of the degree to which these isolated alpine glacial systems responded in phase with one another and with continental ice sheets through the late Pleistocene glacial ages.

We have employed ^{10}Be and ^{26}Al , cosmogenic radionuclides produced *in situ* (see, for instance, Bierman, 1994; Cerling and Craig, 1994; Finkel and Suter, 1993; Lal, 1991; Nishiizumi et al., 1993) to date the most extensive of the surfaces exposed along the Fremont River as it passes between the Caineville Mesas (fig. 17). Cosmogenic radionuclides are produced by the energetic impacts of secondary particles produced by cosmic rays with near-surface materials, ^{10}Be largely from impacts with oxygen, and ^{26}Al largely from impacts with silicon. Quartz is an ideal target mineral because it contains two of the primary target elements and because its resistance to weathering allows it to retain the cosmogenic radionuclides. The half-lives of ^{10}Be (1.5 Ma) and ^{26}Al (0.7 Ma) make them appropriate candidates for dating surfaces throughout the Quaternary.

There is a down side, however. Because cosmogenic radionuclides are produced whenever a rock is within roughly 2 meters of the earth's surface, the cosmogenic radionuclide clock starts to tick well before a clast is embedded within its present deposit. It will have inherited radionuclides both during exhumation from a hillslope within the headwaters, and as it travels through the fluvial system, stopping here and there in the flood plain. Each clast will have its own individual history, reflecting the particular route it took to get to the final terrace site. All clasts will arrive with at least a few ticks on the cosmogenic clock. The trick is to see through this inheritance to extract the age of the surface. We have outlined a technique designed to do just this (Anderson et al., 1996): We show here our latest results, applied to the Fremont River terraces.

One possibility would be to analyze many clasts from the surface and to take the clast with the lowest concentration of radionuclides as having been emplaced with minimal inheritance. Its concentration could then be inverted for the time since emplacement on the surface, and know-

ing the production rate and the decay constant, one could back out the age of the surface. (Crudely, ignoring decay, the effective age is $T=N/P_0$, where N is the measured concentration of cosmogenic radionuclides, and P_0 is the surface production rate). Unfortunately, cosmogenic radionuclide analysis is both expensive and time consuming, making it difficult to analyze a sufficient number of individual clasts to map out the distribution of inheritance. Our initial experiments with single clasts demonstrate that the concentrations and hence effective ages are indeed widely spread (Repka et al., in press).

Our technique is based upon the following conceptual model of the geomorphic system (fig. 18): The depositional system was that of a braided outwash plain, and the deposit at the site we ultimately sample accumulated rapidly over time scales that are very short (probably 100s of years at the most) compared to the age of the terrace. Inheritance varies randomly from clast to clast because the exhumation rate within the basin is nonuniform, and because the transit times and burial depths during transit within the fluvial system vary. Abandonment of the terrace occurred as the river incised into the weak Mancos shale bedrock, presumably when sediment supply in the headwaters declined as the glacial system collapsed. Subsequent to abandonment, the surface of the terrace slowly aggraded with eolian dust to produce a loess blanket 10–20 cm thick. A desert pavement developed in which a monolayer of clasts remained atop the dust mantle (Wells et al., 1995). A soil developed in which gypsum and carbonate cements dominate, but actual turbation of the subsurface clasts was minimal. The distribution of lithologies of the clasts on the surface evolved as those most susceptible to weathering disintegrated. Locally derived sandstones and shales disintegrated rapidly, while quartzites derived from the middle Mesozoic outcrops 20–30 km upstream prove to be the most resistant (Billingsly et al., 1987).

Given this picture, which is developed from field observations of the Fremont terrace sequence, we can assume that the terrace deposit was rapidly emplaced and the depth history of any individual clast within the deposit can be well constrained, both by its present depth and the thickness of the eolian silt. We collect a series of samples from several discrete depths within the terrace gravel deposit, each sample consisting of several dozen quartzite clasts. Back in the lab we construct an amalgamated sample from each horizon, taking mass aliquots from each clast so that no single large clast dominates the signal at a particular horizon. If we have taken enough clasts, the cosmogenic radionuclide concentration of this sample therefore approximates the mean concentration of clasts at that depth. At the time of deposition the profile of mean concentration versus depth should be uniform and reflect the mean cos-

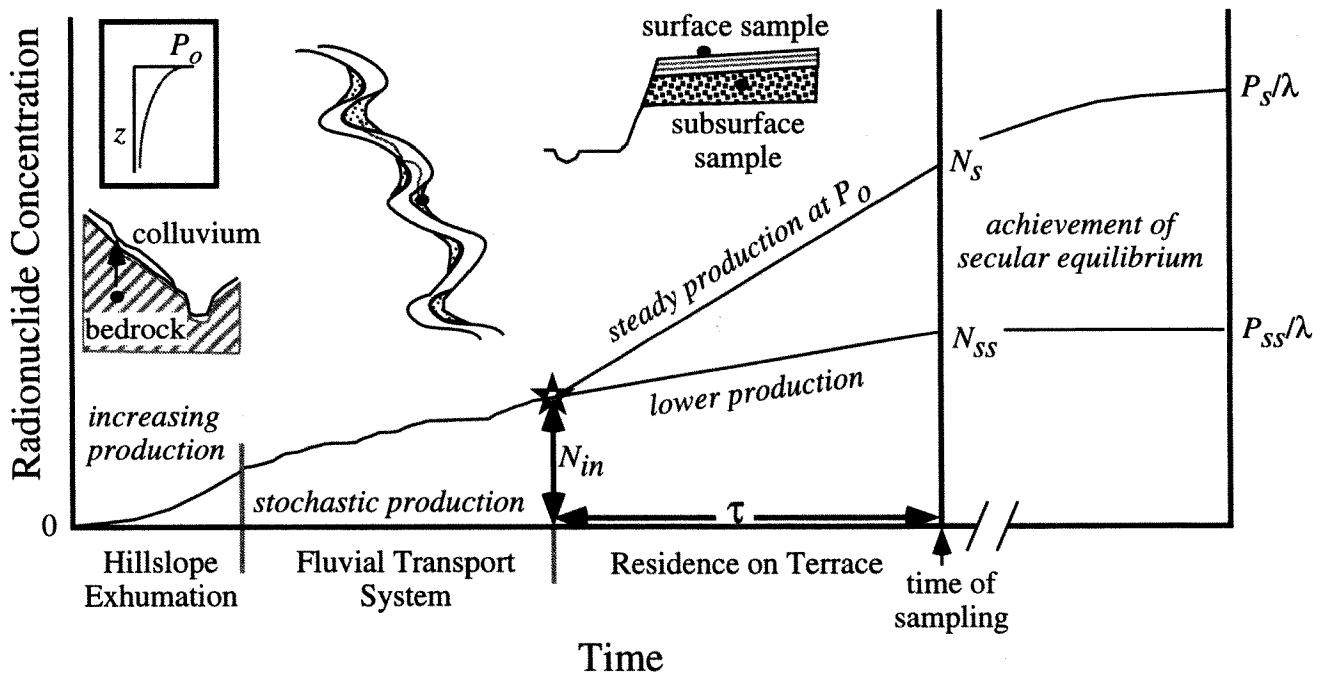


Figure 18. History of the cosmogenic radionuclide concentration of a hypothetical clast, following its transport history in hillslope and fluvial systems, and in its subsequent residence at its present site. Production rate is dictated by depth beneath the local surface, z , which falls off exponentially with depth (see inset). Exhumation on hillslope results in monotonic increase in concentration. Production history is stochastic within the fluvial system, when a clast travels between point bars and then is buried to differing depths. Evolution of concentration on final terrace site is shown for two possible burial depths, one on surface, other in subsurface. One scenario for surface clast is that it remains on the silt surface, in which case it always experiences the surface production rate, P_0 , and attains sampled concentration of N_s . The subsurface clast within underlying gravels (stippled) will undergo a lower production rate, and is sampled with concentration N_{ss} . Clasts on terraces much older than nuclide half lives attain secular equilibrium, with labeled concentrations. Amalgamated samples consisting of numerous clasts allow back-calculation of terrace age, τ , and of the mean inherited radionuclide concentration, N_{in} .

mogenic radionuclide inheritance of the clasts within the geomorphic delivery system. Because the production rate falls off exponentially with depth beneath the surface, and because the clasts have not moved relative to one another in the subsurface, we expect that the post-depositional cosmogenic radionuclide profile should look exponential. The sum of inherited cosmogenic radionuclides and post-depositional cosmogenic radionuclides should therefore produce an exponential profile that is simply shifted or offset.

The results on the Fremont terraces support the validity of our technique (fig. 19). Where we have generated full cosmogenic radionuclide profiles, these show the expected shifted exponential form, from which we can extract both the inheritance (from the shift) and the age of the surface (from the exponential). This broadly supports the series of assumptions we have made in the above conceptual model of the origin and evolution of these surfaces. The inheritance is large. Clasts arrive on the final terrace surface with effective ages up to several tens of thousands of years. This

implies that, without taking inheritance into account, age estimates based upon single clasts would be far too old. Using the latest published production rates for ^{10}Be (Nishiizumi et al., 1996), our technique yields estimates of the ages of the most prominent of the terraces to be 60 ± 9 ka, 102 ± 16 ka and 151 ± 24 ka, which correspond to benthonic-plankton isotope stages 4, 5d and early stage 6 (fig. 20). The ^{26}Al results yield similar age estimates.

We note that at this location there is no well expressed terrace that corresponds to isotope stage 2 (Last Glacial Maximum). There are two surfaces here that may represent isotope stage 2: One is a narrow, intermittent terrace 10 meters above the river (FR 1); our cosmogenic radionuclide results from this surface are inconsistent with those on other surfaces (fig. 19). This difference may reflect poor access to the subsurface in our sampling and/or a burial of the surface by colluvium from a higher terrace. It is also possible that the stage 2 glaciation is represented here by the current flood plain (FR0). In either case, the minor, narrow exposures

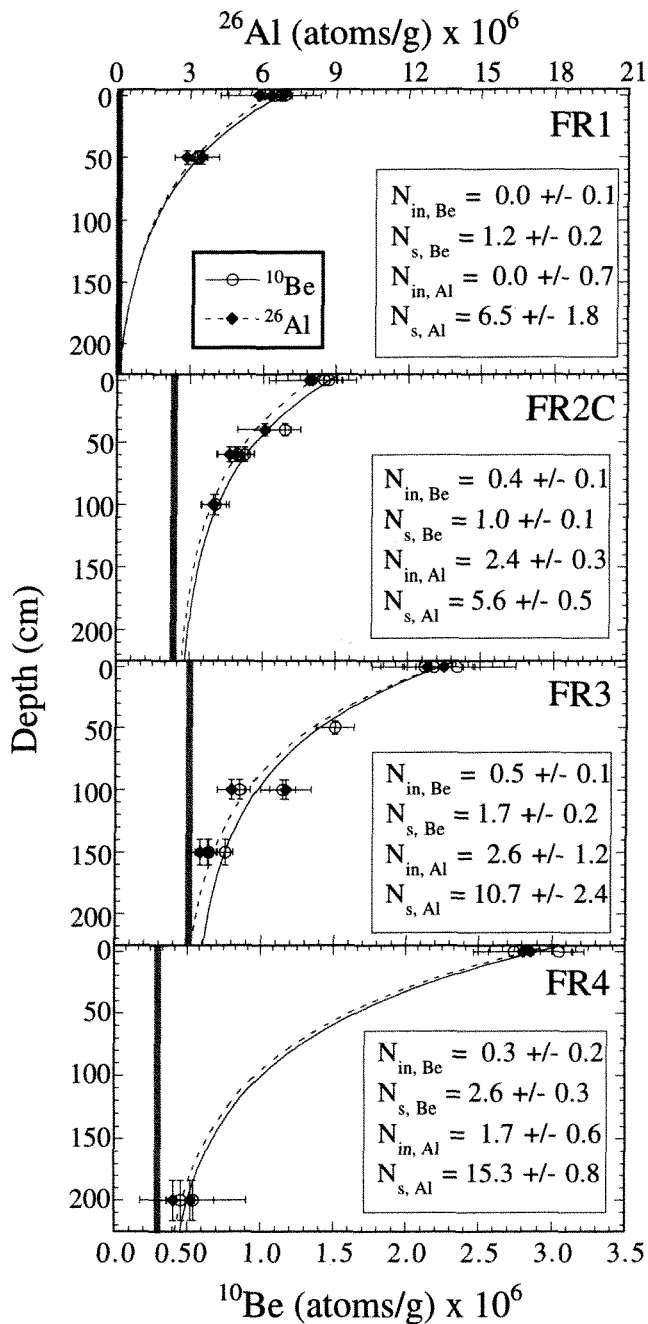


Figure 19. Plot of the full cosmogenic radionuclide concentration profiles for FR2C and FR3, and the amalgamated sample results used in the pairs techniques on all terraces. Note ^{26}Al (top axis) and ^{10}Be (bottom axis) are plotted on scales that differ by a factor of 6.0. Curves are fits to a shifted exponential with the length scale z^* fixed at 0.8 m (solid line ^{10}Be ; dashed ^{26}Al). The fits yield similar values of inheritance for FR2C, FR3 and FR4. Inheritance on FR1 appears to be minimal.

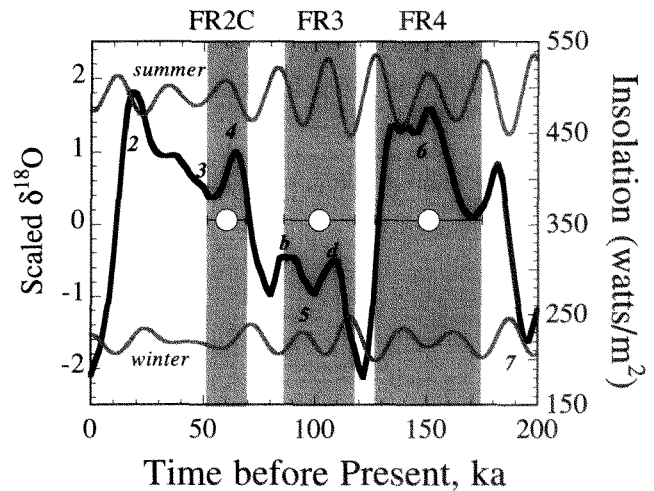


Figure 20. Age estimates of the three best dated terraces (FR2C, FR3, and FR4) shown against the last 250 ka of the normalized global $\delta^{18}\text{O}$ record (Imbrie et al., 1984); oxygen-isotope stages are numbered. The terrace ages (gray bars) were determined from production rates scaled to the Nishiizumi et al., (1996) calibrations, and post-depositional accumulations of cosmogenic radionuclides were constrained by fitting the concentration profiles shown in Figure 19. Also shown are the summer and winter insolation calculations of Berger and Loutre (1991) for 30°N . The terrace ages correspond roughly to global ice volume maxima in stages 4, 5d and 6, and to insolation histories of maxima in the summer and minima in the winter.

present in the area do not allow proper sampling with a sufficient degree of confidence in the results.

The terrace ages appear to support a glacial origin of the terrace gravels, and post-glacial abandonment of the surfaces. The previous assumption (Howard, 1986) that the largest two terraces correspond to the last glacial maximum and penultimate glaciations, by analogy with the Wind River sequence, must clearly be superseded by these absolute ages. That these small alpine systems apparently respond significantly to relatively minor global climate swings, as these results demonstrate for the Fremont, and as has been recently suggested for Sierran glacial systems (Phillips et al., 1996), makes regional correlations more difficult: One system is likely to respond more, or less, sensitively than another to the same fluctuations in regional climate.

COMBINED REFERENCES

Parts 1-5

- Billingsley, G.H., Huntoon, P.W., and Breed, W.J., 1987, Geologic map of Capitol Reef National Park and vicinity, Emery, Garfield, Millard and Wayne counties, Utah. Utah Geological and Mineral Survey, Map 87, 1.62.500.
- Everitt, B.L., 1979, The cutting of Bull Creek arroyo: Utah Geology, v. 6, No. 1, p. 39-44.
- Everitt, B.L., 1980, Vegetation and sediment migration in the Henry Mountains region, Utah, in Picard, 1980, p. 209-214.
- Everitt, B.L., 1983, Preliminary foundation investigation, Blue Valley Dam site, Lower Fremont River. Utah Division of Water Resources report, 18 p.
- Everitt, B.L., 1984, Potential for groundwater development in Caineville Utah Division of Water Resources memorandum, 4 p.
- Everitt, B.L., 1987, Torrey dam site seismic refraction survey, lower Fremont project: Utah Division of Water Resources memorandum, 3 p.
- Everitt, B.L., 1995a, Activity classification of the Thousand Lake Fault: Utah Division of Water Resources memorandum, 7 p.
- Everitt, B.L., 1995b, Hydrologic factors in regeneration of Fremont Cottonwood along the Fremont River, Utah: Amer. Geophysical Union, Geophysical Monograph 89, p. 197-208.
- Flint, R.F., and Denny, C.S., 1958, Quaternary geology of Boulder Mountain, Aquarius Plateau, Utah. U.S. Geological Survey Bulletin 1061-D, p. 103-164.
- Gilbert, G.K., 1877, report on the geology of the Henry Mountains (Utah): U.S. Geological and geographical Survey, Rocky Mountain Region (Powell), 160 p.
- Godfrey, A.E., 1969, Geologic history and processes of fan and pediment development in the northern Henry Mountains piedmont, Utah: Ph.D. dissertation (unpublished), the Johns Hopkins University, Baltimore, Maryland.
- Godfrey, 1980, Debris avalanche deposits north of Mount Ellen Henry Mountains Symposium, Utah Geological Association Publication 8, M. Dane Picard, Editor, pp. 171-176.
- Godfrey, 1997a, Wind erosion of Mancos Shale badland ridges by sudden drops in pressure: Earth Surface Processes and Landforms, v. 22, no. 4, p. 345-352.
- Godfrey, 1997b, Mass movement of Mancos Shale crust near Cameville, Utah: a 30-year record: Geografiska Annaler, no. 3.
- Graf, W.L., 1983, Downstream changes in stream power in the Henry Mountains, Utah. Annals, Assoc. Am. Geog. V. 73, No. 3, p. 373-387.
- Hintze, L.F., 1988, Geologic history of Utah: Brigham Young University Geology Studies, Special Publication 7.
- Howard, A.D., 1970, A study of processes and history in desert landforms near the Henry Mountains, Utah. Ph.D. dissertation (unpublished), The Johns Hopkins University, Baltimore, Maryland.
- Howard, Alan D., 1994a, Badlands in Abrahams, A.D., and Parsons, A.J., editors, Geomorphology of Desert Environments: Chapman and Hall, London, pp. 213-242.
- Howard, Alan D., 1994b, A detachment-limited model of drainage basin evolution: Water Resources Research, V. 30, p. 2261-2285.
- Hunt, C.B., Averitt, Paul, and Miller, R.L., 1953, Geology and geography of the Henry Mountains region, Utah. U.S. Geological Survey Professional Paper 228, 234 p.
- Hunt, C.B., 1977, Around the Henry Mountains with Charlie Hanks: Utah Geology, Vol. 4, no. 2, p. 95-104.
- Hunt, C.B., 1988, Geology of the Henry Mountains, Utah, as recorded in the notebooks of G.K. Gilbert, 1875-76: Geol. Soc. Am. Memoir 167, 229 p.
- Laine, M.D., Anderson, P.B., and Caputo, M.V., 1991, Field Symposium road log section I: Price to Green River, in Chidsey, Thomas C., ed., 1991, Geology of east-central Utah. Utah Geol. Association, Publication 19, p. 347-362.
- Mattox, S.R., 1991, Petrology, age, geochemistry, and correlation of the Tertiary volcanic rocks of the Awapa Plateau, Garfield, Piute, and Wayne Counties, Utah: Utah Geological Survey Misc. Publication 91-5, 46 p.
- Midland Trail Association, 1916, Midland trail tour guide: Midland Trail Log Book Company, Grand Junction (facsimile reprint 1969, Rio Grande Press).
- Oaks, Robert Q., 1988, Geology 350 fall field trip, Capitol Reef, Henry Mountains: Manuscript, Utah State University, 15 p.
- Osterkamp, W.R., and Hupp, C.R., 1984, Geomorphic and vegetative characteristics along three northern Virginia streams. Geol. Soc. Am. Bull., V. 95, p. 1093-1101.
- Palmer-Wilding, 1981, Preliminary design investigation, Cameville Dam, Lower Fremont River Report to Wayne County Water Conservancy District.
- Picard, M.D., (ed.), 1970, Henry Mountains Symposium: Utah Geological Association Publication 8, 388 p.
- Rich, J.L., 1935, Origin and evolution of rock fans and pediments. GSA Bull., v. 46, pp. 999-1024.
- Rigby, J.K., 1976, Field Guide, Northern Colorado Plateau. Kendall/Hunt, 207 p.
- Schumm, Stanley A., and Gregory, Daniel I., 1986, Diffuse-source salinity: Mancos Shale Terrain: Bureau of Land Management Technical note 373
- SHB AGRA, 1992, Engineering geology, geoseismic, and geotechnical study, proposed Torrey Dam and Reservoir. Report to Wayne County Water Conservancy District, SHB AGRA Job E90-2027.
- Smith, J.F., Jr., Huff, L.C., Hinrichs, E.N., and Luedke, R.G., 1963, Geology of the Capitol Reef area, Wayne and Garfield counties. U.S. Geological Survey Professional Paper 363, 102 p.
- Van Cott, J.W., 1990, Utah Place Names: University of Utah Press, 453 p.
- Webb, R.H., 1985, Late Holocene flooding on the Escalante River, South-central Utah PhD dissertation, University of Arizona, Tucson.
- Wooley, Ralf R., 1946, Cloudburst floods in Utah, 1850-1938. U.S. Geol. Surv. Water Supply Paper 994, 128 p.

Part 6

- Bryan, R.B., and Yair, A., 1982, Perspectives on studies of badland geomorphology, in Bryan, R.B., and Yair, A., eds., Badland geomorphology and piping: Norwich, Geo Books, p. 1-12.
- Bryan, R.B., Imeson, A.C., and Campbell, I.A., 1984, Solute release and sediment entrainment on microcatchments in the Dinosaur Park badlands, Alberta, Canada: Journal of Hydrology, v. 71, p. 79-106.
- Bryan, R.B., Campbell, I.A., and Yair, A., 1987, Postglacial geomorphic development of the Dinosaur Provincial Park badlands, Alberta. Canadian Journal of Earth Sciences, v. 24, p. 135-146.
- Campbell, I.A., 1982, Surface morphology and rates of change during a ten-year period in the Alberta badlands, in Bryan, R.B., and Yair, A., eds., Badland geomorphology and piping: Norwich, Geo Books, p. 221-238.
- Costa, J.E., and O'Connor, J.E., 1995, Geomorphically effective floods, in Costa, J.E., Miller, A.J., Potter, K.W., and Wilcock, P.R., eds., Natural and anthropogenic influences in fluvial geomorphology The Wolman volume. Geophysical Monograph 89: Washington, D.C., American Geophysical Union, p. 45-56.
- Dick, G.S., 1995, Documentation of flow in ephemeral channels, Upper Blue Hills, Utah [M.S. thesis]: Santa Cruz, University of California
- Dick, G.S., Anderson, R.S., and Sampson, D.E., 1997, Controls on flash flood magnitude and hydrograph shape, Upper Blue Hills badlands, Utah Geology, v. 25, p. 45-48.

- Hassan, M.A., 1990, Observations of desert flood bores: *Earth Surface Processes and Landforms*, v. 15, p. 481–485.
- Howard, A.D., 1970, A study of process and history in desert landforms near the Henry Mountains, Utah [Ph.D. dissertation]. Baltimore, Johns Hopkins University.
- Howard, A.D., 1994, Badlands, in Abrahams, A.D., and Parsons, A.J., eds., *Geomorphology of Desert Environments*: London, Chapman and Hall, p. 213–242.
- Knighton, D., 1984, *Fluvial forms and processes*: London, Edward Arnold, 218 p.
- Leopold, L.B., and Miller, J.P., 1956, Ephemeral streams—Hydraulic factors and their relation to the drainage net, U.S. Geological Survey Professional Paper 282-A, 37 p.
- Lusby, G.C., 1979, Effects of grazing on runoff and sediment yield from desert rangeland at Badger Wash in western Colorado, 1953–1973, Volume 34, U.S. Geological Survey Water-Supply Paper 1532-I, 34 p.
- Mesa, O.J., and Mifflin, E.R., 1986, On the relative role of hillslope and network geometry in hydrologic response, in Gupta, V.K., Rodriguez-Iturbe, I., and Wood, E.F., eds., *Scale problems in hydrology*: Dordrecht, Holland, D. Reidel, p. 1–17.
- Reid, I., and Frostick, L.E., 1987, Flow dynamics and suspended sediment properties in arid zone flash floods: *Hydrological Processes*, v. 1, p. 239–253.
- Renard, K.G., and Keppel, R.V., 1966, Hydrographs of ephemeral streams in the Southwest. American Society of Civil Engineers, *Journal of the Hydraulics Division*, v. 92, p. 33–52.
- Schick, A.P., 1988, Hydrologic Aspects of Floods in Extreme Arid Environments, in Baker, V.R., Kochel, R.C., and Patton, P.C., eds., *Flood Geomorphology*: New York, Wiley-Interscience, p. 189–204.
- Schumm, S.A., 1956, The role of creep and rainwash on the retreat of badland slopes: *American Journal of Science*, v. 254, p. 693–706.
- Schumm, S.A., 1964, Seasonal variation of erosion rates and processes on hillslopes in western Colorado: *Zeitschrift für Geomorphologie Supplement Band 5*, p. 215–238.
- Schumm, S.A., and Lusby, G.C., 1963, Seasonal variation of infiltration capacity and runoff on hillslopes in western Colorado. *Journal of Geophysical Research*, v. 68, p. 3655–3666.
- Yair, A., Lavee, H., Bryan, R.B., and Adar, E., 1980, Runoff and erosion processes and rates in the Zin Valley badlands, northern Negev, Israel: *Earth Surf. Process.*, v. 5, p. 205–225.
- Billingsly, G.H., Huntoon, P.W., and Breed, W.J., 1987, Geologic map of Capitol Reef National Park and vicinity, Emery, Garfield, Millard and Wayne Counties, Utah: Utah Geological and Mineral Survey, Salt Lake City, UT.
- Bull, W.B., 1991, *Geomorphic Responses to Climate Change*. Oxford University Press, New York City, N.Y., 352 pp.
- Cerling, T.E., and Craig, H., 1994, Geomorphology and in-situ cosmogenic isotopes: *Reviews of Earth and Planetary Sciences*, v. 22, p. 273–317.
- Clark, D.H., Bierman, P.R., and Larsen, P., 1995, Improving *in situ* cosmogenic chronometers: *Quaternary Research*, v. 44, p. 367–377.
- Finkel, R.C., and Suter, M., 1993, AMS in the earth sciences. *Technique and applications: Advances in Analytical Geochemistry*, p. 1–114.
- Flint, R.F., and Denny, C.S., 1956, *Quaternary Geology of Boulder Mountain, Aquarius Plateau, Utah*: U.S. Geological Survey Bulletin 1061-D, p. 103–164.
- Howard, A.D., 1970, Study of process and history in desert landforms near the Henry Mountains, Utah. Ph.D. thesis, Johns Hopkins University, Baltimore, MD, 198 pp.
- Howard, A.D., 1986, Quaternary landform evolution of the Dirty Devil River system, Utah: Geological Society of America Abstracts with Programs, v. 18, p. 641.
- Imbrie, J., Hays, J.D., Martinson, D.G., McIntyre, A., Mix, A.C., Morley, J.J., Pisias, N.G., Prell, W.L., and Shackleton, N.J., 1984, The orbital theory of Pleistocene climate: support from a revised chronology of the marine $\delta^{18}\text{O}$ record, in: Milankovitch and Climate: Understanding the Response to Astronomical Forcing, Part 1, Berger, A., Imbrie, J., Hays, J., Kukla, G., and Saltzman, B., eds., Reidel Publishing, Higham, MA, p. 269–305.
- Lal, D., 1991, Cosmic ray labeling of erosion surfaces: in situ nuclide production and erosion models. *Earth and Planetary Science Letters*, v. 104, p. 424–439.
- Nishiizumi, K., Kohl, C.P., Arnold, J.R., Dorn, R.I., Klein, J., Fink, D., Middleton, R., and Lal, D., 1993, Role of in situ cosmogenic nuclides ^{10}Be and ^{26}Al in the study of diverse geomorphic processes: *Earth Surface Processes*, v. 18, p. 407–425.
- Nishiizumi, K., Finkel, R.C., Klein, J., and Kohl, C.P., 1996, Cosmogenic production of ^7Be and ^{10}Be in water targets: *Journal of Geophysical Research*, v. 101, p. 22,225–22,232.
- Phillips, F., Zreda, M.G., Benson, L.V., Plummer, M.A., Elmore, D., and Sharma, P., 1996, Chronology for fluctuations in late Pleistocene Sierra Nevada glaciers and lakes: *Science*, v. 274, p. 749–751.
- Repka, J.L., Anderson, R.S., and Finkel, R.P., in press, Cosmogenic dating of fluvial terraces, Fremont River, Utah: *Earth and Planetary Science Letters*.
- Wells, S.G., McFadden, L.D., Poeths, J., and Olinger, C.T., 1995, Cosmogenic ^3He surface-exposure dating of stone pavements—Implications for landscape evolution in deserts: *Geology*, v. 23, p. 613–617.

Part 7

- Anderson, R.S., Repka, J.L., and Dick, G.S., 1996, Explicit treatment of inheritance in dating depositional surfaces using *in situ* ^{10}Be and ^{26}Al : *Geology*, v. 24, p. 47–51.
- Berger, A., and Loutre, M.F., 1991, Insolation values for the climate of the last 10 million of years: *Quaternary Sciences Review*, v. 10, p. 297–317.
- Bierman, P., 1994, Using *in situ* produced cosmogenic isotopes to estimate rates of landscape evolution: A review from the geomorphic perspective: *Journal of Geophysical Research-Solid Earth*, v. 99, p. 13,885–13,896.

PART TWO

MESOZOIC TO RECENT GEOLOGY OF UTAH

